

MECHANICAL DESIGN OF HEAT EXCHANGERS

AND PRESSURE VESSEL COMPONENTS

KRISHNA P. SINGH

Vice President of Engineering
Joseph Oat Corporation
Camden, NJ

and

ALAN I. SOLER

Professor of Mechanical Engineering
& Applied Mechanics
University of Pennsylvania
Philadelphia, PA

Springer-Verlag Berlin Heidelberg GmbH

المنارة للاستشارات

FIRST EDITION

Copyright © 1984 by Springer-Verlag Berlin Heidelberg

Originally published by Springer-Verlag Berlin Heidelberg New York Tokyo in 1984

All rights reserved by the publisher. This book, or parts thereof, may not be reproduced in any form without the written permission of the publisher.

Library of Congress Catalog No. 84-70460

Exclusive distribution rights outside
United States of America, Mexico and Canada
Springer-Verlag Berlin Heidelberg GmbH

ISBN 978-3-662-12443-7

ISBN 978-3-662-12441-3 (eBook)

DOI 10.1007/978-3-662-12441-3

المنارة للاستشارات

This book is dedicated to:

Our wives, Martha Singh and Debby Soler

for their patience, understanding and support,

and

the late **Dr. William G. Soler**, an English teacher who spent countless hours reading technical papers in order to comprehend his son's work.

PREFACE

A tubular heat exchanger exemplifies many aspects of the challenge in designing a pressure vessel. High or very low operating pressures and temperatures, combined with sharp temperature gradients, and large differences in the stiffnesses of adjoining parts, are amongst the legion of conditions that behoove the attention of the heat exchanger designer. Pitfalls in mechanical design may lead to a variety of operational problems, such as tube-to-tubesheet joint failure, flanged joint leakage, weld cracks, tube buckling, and flow induced vibration. Internal failures, such as pass partition bowing or weld rip-out, pass partition gasket rib blow-out, and impingement actuated tube end erosion are no less menacing. Designing to avoid such operational perils requires a thorough grounding in several disciplines of mechanics, and a broad understanding of the inter-relationship between the thermal and mechanical performance of heat exchangers. Yet, while there are a number of excellent books on heat exchanger thermal design, comparable effort in mechanical design has been non-existent. This apparent void has been filled by an assortment of national codes and industry standards, notably the "ASME Boiler and Pressure Vessel Code" and the "Standards of Tubular Exchanger Manufacturers Association." These documents, in conjunction with scattered publications, form the motley compendia of the heat exchanger designer's reference source. The subject matter clearly beckons a methodical and comprehensive treatment. This book is directed towards meeting this need.

Many of our readers have been witness to the profound changes that have occurred in recent years in heat exchanger design practice. Only two short decades ago, seismic analysis was an alien term to the heat exchanger trade. Words like "response spectrum", "flow induced vibration", "nozzle load induced vessel stresses", etc., held little kinship to the heat exchanger design technology. Today, these terms occupy a great deal of the designer's attention. A thorough grasp of the underlying concepts in flow induced vibration and seismic analysis, along with pressure vessel mechanical design and stress analysis techniques, is essential for developing cost effective and reliable designs. Successful troubleshooting of problems in operating units relies equally on an in-depth understanding of the fundamentals. Our object in this book is to present the necessary body of knowledge for heat exchanger design and operating problems-resolution in a logical and systematic manner.

The book begins with a comprehensive introduction to the physical details of tubular heat exchangers in Chapter 1, followed by an introduction

to the stress classification concept in Chapter 2. The following three chapters are devoted to bolted flange design with particular emphasis on devising means to improve joint reliability. Chapter 6 treats the so-called “boltless” flanges. The subject of tube-to-tubesheet joints is taken up in Chapter 7 wherein a method to predict the “optimal tube expansion” is presented. The subsequent four chapters deal with the tubesheets for various exchanger styles, viz. U-tube, fixed and floating head, double tubesheet, and rectangular tubesheets. Methods for complete stress analysis of tubesheets, with the aid of computer programs, are given. Additional topics of mechanical design/stress analysis covered are: flat cover (Chapter 12); heads (Chapter 13); U-tubes (Chapter 14); and expansion joints (Chapter 15). Chapter 16 is devoted to fostering an understanding of flow induced vibration in tube bundles; design methods to predict its incidence and design remedies to obviate its occurrence are presented.

The group of chapters from 17 through 20 deal with heat exchanger/pressure vessel support design and seismic analysis. Chapter 21 is intended to introduce the application of the “response spectrum” analysis technique to heat exchangers. Finally, Chapter 22 contains a brief resumé of operational and maintenance considerations in heat exchanger design.

Since much of the pressure vessel design theory requires some knowledge of plate and shell theory, a self contained treatment of this subject is given in Appendix A at the end of the text. Additional material, pertinent to a particular chapter, is presented in appendices at the end of each chapter.

Since many of the design/analysis techniques presented here require lengthy computations, sometimes impossible by manual means, suitable computer programs are provided in the text. The source listings of twenty-two (out of a total of twenty-seven computer codes), along with input instructions, are provided in the text. In order to avoid manual transfer of these codes, source codes (including the five codes not listed in the book) in more computer amenable form (such as tape, mini-disc, cards, etc.), can be obtained from the publisher separately.

This book is written with two audiences in mind. The practicing engineer, too harried to delve into the details of analysis, may principally use the computer codes with the remainder of the book serving as a reference source for design innovation ideas or for operational diagnostics work. A university student or a researcher seeking to obtain an exoteric (as opposed to esoteric) knowledge of the state-of-the-art in heat exchanger technology can concentrate on the theoretical developments. As such, this book can be used for teaching a senior/first year graduate level course in “heat exchangers” or “pressure vessel design technology”. We have made a concerted effort to bridge the gap between analytical methods and practical considerations.

Many men and women have contributed towards the successful conclusion of this effort which sometimes appeared to us to be never ending. From the Joseph Oat Corporation, M. J. Holtz, L. Ng, R. Shah, F. McAnany, deserve mention. The encouragement and support of Mr.

Maurice Holtz of the Joseph Oat Corporation, Dr. William S. Woodward of the Westinghouse Corporation, and Dr. Ramesh Shah of General Motors Corporation are also acknowledged. Mr. Xu Hong, of the Beijing Institute of Chemical Technology, contributed to the development of two of the computer codes during his term as a visiting researcher at the University of Pennsylvania. Ms. Nancy Moreland of the Joseph Oat Corporation pursued the task of word processing with unwavering zeal and fervor, and Mrs. Dolores Federico and Mr. John T. Sheridan, both of Sheridan Printing Company brought forth tireless effort to bring out the book in record time. We deeply appreciate their contributions.

Finally, we acknowledge the contributions of our Ph.D. thesis advisors, Dr. Burton Paul of the University of Pennsylvania, and Dr. Maurice A. Brull, of the Tel Aviv University. It was their original efforts which started both of us on the paths leading to the creation of this book.

K. P. SINGH
A. I. SOLER
Cherry Hill, New Jersey
February, 1984

TABLE OF CONTENTS

1. HEAT EXCHANGER CONSTRUCTION	
1.1 Introduction	1
1.2 Heat Exchanger Styles	2
1.3 Heat Exchanger Nomenclature	14
1.4 Heat Exchanger Internals	14
1.5 Tube Layout and Pitch	23
1.6 General Considerations in Pass Partition Arrangement	24
1.7 Impingement Protection	25
1.8 Designing for Thermal Transients	34
1.9 Interdependence of Thermal and Mechanical Design	37
1.10 Feedwater Heater Design	39
1.11 Codes and Standards	45
References	46
Appendix 1.A Typical Shell and Channel Arrangements and Parts Identification	47
2. STRESS CATEGORIES	
2.1 Introduction	57
2.2 Beam Strip Analogy	57
2.3 Primary and Secondary Stress	60
2.4 Stress Classification	62
2.5 General Comments	68
2.6 Stress Intensity	68
2.7 An Example of Gross Structural Discontinuity	69
2.8 Discontinuity Stresses at Head, Shell and Skirt Junction	72
Nomenclature	79
References	79
3. BOLTED FLANGE DESIGN	
3.1 Introduction	81
3.2 Bolted Flange Types	82
3.3 Flange Facings	83
3.4 Flange Facing Finish	86
3.5 Gaskets	87
3.6 Bolt Pre-Tensioning	95
3.7 Flange Sizing	99
3.8 Flange Moments	101
3.9 Circular Rings under Distributed Couples	102
3.10 Deformation of a Flanged Joint	104
3.11 Waters, Rossheim, Wesstrom and Williams' Method for Flange Design	108
3.11.1 Flange Ring (Element #1)	109
3.11.2 Taper Hub (Element #2)	112

3.11.3	Shell (Element #3)	118
3.11.4	Compatibility Between Shell and Hub	118
3.11.5	Compatibility Between Hub and Ring	120
3.11.6	Longitudinal Stress in the Hub	124
3.11.7	Longitudinal Stress in the Shell	124
3.11.8	Radial Stress in the Ring	125
3.11.9	Tangential Stress in the Ring	125
3.12	Computer Program FLANGE	126
3.13	Stress Analysis of the Welding Neck Flange	141
3.14	Controlled Compression Joint	144
	Nomenclature	151
	References	154
Appendix 3.A	Derivation of Polynominal Expressions for Hub Deflection (Eq. 3.11.20a)	156
Appendix 3.B	Schleicher Functions	158
4.	TUBESHEET SANDWICHED BETWEEN TWO FLANGES	
4.1	Introduction	161
4.2	The Structural Model	165
4.3	Tubesheet	166
4.4	Flange	170
4.5	Method of Solution	170
4.6	Leakage Area	176
4.7	Two Example Problems	178
4.7.1	Classical Three Element Joint	178
4.7.2	Controlled Metal-to-Metal Contact Joint	180
4.7.3	Observations	187
4.8	Computer Program TRIEL	188
4.8.1	Input Data for Program "TRIEL"	188
4.8.2	Two Flanges Bolted Together	204
4.8.3	Other Applications	204
	Nomenclature	204
	References	206
5.	BOLTED JOINTS WITH FULL FACE GASKETS	
5.1	Introduction	209
5.2	General Equations	210
5.3	Non-Linear Analytical Expressions Simulating Gasket Behavior	219
5.4	Simulation of Bolt Effects	223
5.5	Calculation of Flange Stress	225
5.6	Application of the Method	226
5.6.1	Gasketed Joint Model	227
5.6.2	Analysis of a Full Face Gasket-Two Element Joint	233
5.6.3	Analysis of Ring Gasketed Joint	235
5.6.4	Ring Gasketed Joint with Compression Stop	236

5.6.5	Analysis of Three Element Joint with Non-Symmetric Load and Geometry	237
5.7	Concluding Remarks	237
	Nomenclature	238
	References	239
Appendix 5.A	User Manual For Computer Code “GENFLANGE”	239
6.	JOINTS FOR HIGH PRESSURE CLOSURES	
6.1	Introduction and Standard Industry Designs	289
6.2	Wedge Seal Ring Closure	297
6.2.1	Joint Description	297
6.2.2	Analysis of Sealing Action	300
6.2.3	Disassembly Analysis	301
6.2.4	Sizing the Retainer Shoe	301
	Nomenclature	304
	References	305
7.	TUBE-TO-TUBESHEET JOINTS	
7.1	Joint Types	307
7.2	Expanding Method	307
7.3	Roller Expanding	308
7.4	Hydraulic Expansion	310
7.5	Impact Welding	311
7.6	Edge Welding	312
7.7	Butt Welding	315
7.8	Tube-to-Tubesheet Interface Pressure	315
7.8.1	Initial Expansion of the Tube	317
7.8.2	Loading of Tube and Tubesheet	319
7.8.3	Displacement in the Tubesheet	323
7.8.4	Unloading of the System	324
7.8.5	Tube Pull-Out Load	325
7.8.6	Computation of Residual Pressure	328
7.8.7	Re-Analysis of the Tube Rolling Problem Using the von Mises Yield Criteria	329
7.9	Ligament Temperature	329
7.9.1	Introduction	329
7.9.2	Analysis	330
7.9.3	Solution Procedure	335
7.9.4	Numerical Example—Computer Program LIGTEM	336
7.10	Tube Removal and Tube Plugging	342
	Nomenclature	345
	References	347
Appendix 7.A	Coefficients of [A] Matrix and {F} Vector	349

Appendix 7.B	Computer Code for Evaluation of Residual Roll Pressure Using Tresca Yield Condition . . .	350
Appendix 7.C	Tube-Tubesheet Joint Loading Including Thermal Effects	354
Appendix 7.D	User Manual and Computer Code for Tube Rolling Program GENROLL	368
8.	TUBESHEETS FOR U-TUBE HEAT EXCHANGERS	
8.1	Introduction	387
8.2	Analysis of Perforated Region	390
8.3	Analysis of Two Side Integral Construction	393
8.4	Analysis of One Side Integral, One Side Gasketed Construction	399
8.5	Analysis of Two Side Gasketed Construction	401
8.6	Tubesheet Stress Analysis	402
	Nomenclature	409
	References	411
Appendix 8.A	Computer Code "UTUBE"	412
9.	TUBESHEETS IN FIXED AND FLOATING HEAD HEAT EXCHANGERS	
9.1	Scope of Analysis	415
9.2	Effective Pressure on Tubesheet Due to the Tube Bundle	418
9.3	Analysis of a Perforated Circular Tubesheet	420
9.4	Analysis of an Unperforated Tubesheet Rim	424
9.5	Method of Solution and Computer Implementation	430
9.5.1	Differential Thermal Expansion Between the Shell and the Tubes	431
9.5.2	Sample Application of Analysis	435
9.6	Modifications for Floating Head Exchangers	439
9.7	Simplified Analysis of Stationary Tubesheet in an Integral or Floating Head Heat Exchanger	440
9.7.1	Evaluation of Integration Constants	444
9.7.2	Development of Expressions for Ring Rotation	447
9.7.3	Determination of Perforated Region Edge Force, Edge Moment, and Shell Axial Force	450
9.7.4	Computer Analysis	453
9.8	Reduction of Analysis to Simplified Form	461
9.9	Range of Application of the TEMA Bending Equations Given in Reference [9.1.1]	481
9.10	Closure	483
	Nomenclature	484
	References	488
Appendix 9.A	Solution of Coupled Plate Equations	489
Appendix 9.B	Computer Program FIXSHEET	490
9.B.1	Scope	490

	9.B.2 Input Data for FIXSHEET	491
Appendix 9.C	User Manual for Tubesheet Analysis Program FIXFLOAT and Source Listing	500
Appendix 9.D	Basic Computer Code for MICRO-FIXFLOAT for Simplified Calculation of Tubesheet Thickness	514
10.	SPECIAL TUBESHEET CONSTRUCTION— DOUBLE TUBESHEET	
	10.1 Introduction	517
	10.2 Formulation of the Double Tubesheet Equations	519
	10.3 Theoretical Analysis of Double Tubesheet Construction Using Plate Theory	520
	10.4 Solution of the Double Tubesheet Equations by Direct Integration and Application to a Selected Unit	528
	10.5 The Finite Element Method in Tubesheet Analysis	534
	10.6 Sample Results Using the Finite Element Method	536
	Nomenclature	539
	References	540
Appendix 10.A	User Manual for Double Tubesheet Analysis—Computer Code DOUBLESHEET	541
Appendix 10.B	Sample Input and Output Files for Example Problem of Section 10.4	561
11.	RECTANGULAR TUBESHEETS—APPLICATION TO SURFACE CONDENSERS	
	11.1 Introduction	565
	11.2 The Condenser Tubesheet Design Problem	565
	11.3 Introductory Remarks on Analysis of a Rectangular Tubesheet Using Beam Strips	570
	11.4 Analysis of a Single Beam Strip	575
	11.5 Development of Final Equations for Edge Displacements	581
	11.6 A Specific Application of the Multiple Beam Strip Method to Investigate the Effects of Tubesheet Geometric and Material Parameters	586
	11.7 Concluding Remarks	589
	Nomenclature	590
	References	591
Appendix 11.A	Coefficients of A-Matrix and B-Vector	591
12.	FLAT COVER	
	12.1 Introduction	593
	12.2 Conventional Design Formulas	596
	12.2.1 ASME Code	596
	12.2.2 TEMA Standards	597
	12.2.3 Heat Exchange Institute	597

12.3	Flange-Cover Interaction	598
12.3.1	Cover	598
12.3.2	Flange Ring	603
12.3.3	Interaction Relations	604
12.4	Cover and Flange Ring Stresses	608
12.5	Loss of Heat Duty Due to Flow Bypass	609
12.6	Thermal Performance of Two Tube Pass Heat Exchangers	610
12.7	Computer Program LAPCOV	612
12.7.1	Program Description	612
12.7.2	Example	612
12.8	Flat Cover Bolted to a Welding Neck Flange	614
	Nomenclature	622
	References	624
13.	PRESSURE VESSEL HEADS	
13.1	Introduction	625
13.2	Geometry of Shells of Revolution	626
13.3	Membrane Theory for Shells of Revolution	629
13.4	Stress Analysis of Membrane Shells under Internal Pressure	634
13.5	Physical Interpretation of N_{θ}	642
13.6	Derivation of ASME Code Formula for the Large End of a Reducer	647
13.7	Membrane Displacement	649
13.8	Evaluation of Discontinuity Effects	656
	Nomenclature	661
	References	662
14.	THERMAL STRESSES IN U-BENDS	
14.1	Introduction	663
14.2	Analysis	666
14.3	Method of Solution	672
14.4	An Example	674
14.5	Discussion	678
14.6	A Practical Design Formula	679
14.7	Computer Program UBAX	681
	Nomenclature	685
	References	686
	Appendix 14. A Elements of B-Matrix	687
15.	EXPANSION JOINTS	
15.1	Introduction	689
15.2	Types of Expansion Joints	690
15.3	Stiffness of "Formed Head" Type Joints	694
15.4	Stresses in the Expansion Joint	700

15.5	Finite Element Solution—Computer Program	
	FLANFLUE	707
15.6	Bellows Expansion Joint for Cylindrical Vessels	709
15.7	Bellows Expansion Joints for Rectangular Vessels	710
15.8	Fatigue Life.	713
	Nomenclature	716
	References.	716
	Appendix 15.A Computer Program EXJOINT.	718
	Appendix 15.B Computer Program EJMAREC	726
16.	FLOW INDUCED VIBRATION	
16.1	Introduction	735
16.2	Vibration Damage Patterns	736
16.3	Regions of Tube Failure	737
16.4	Vibration Mechanisms.	738
	16.4.1 Vortex Shedding.	738
	16.4.2 Fluid Elastic Excitation	740
	16.4.3 Jet Switching	747
	16.4.4 Acoustic Resonance	748
16.5	Fluid Inertia Model for Fluid-Elastic Instability.	749
	16.5.1 Fluid Inertia	749
	16.5.2 Stability Criterion	755
16.6	Natural Frequency.	756
	16.6.1 Basic Concepts	756
	16.6.2 Single Span Tube	757
	16.6.3 Multiple Span Tube	761
	16.6.4 Tube under Axial Load	762
	16.6.5 U-Bend Region.	764
16.7	Correlations for Vibration Prediction	768
	16.7.1 Fluid-Elastic Correlations	768
	16.7.2 Turbulent Buffeting Correlations	773
	16.7.3 Periodic Wake Shedding	777
	16.7.4 Acoustic Resonance Correlations	778
16.8	Effective Tube Mass	782
16.9	Damping.	788
	16.9.1 Classification	788
	16.9.2 Damping Coefficient	788
	16.9.3 Fluid Damping	792
	16.9.4 Damping Data	792
16.10	Cross Flow Velocity.	795
	16.10.1 Computer Models.	795
	16.10.2 Effective Velocity.	796
	16.10.3 Stream Analysis Method.	798
	16.10.4 Flow Distribution in the U-Bend Region.	800
16.11	Vibration Due to Parallel Flow	810

16.12	Ideas for Preventing Flow Induced Vibration Problems . .	813
16.12.1	Fluid Elastic Instabilities	813
16.12.2	Acoustic Resonance	820
16.13	Flow Induced Vibration Evaluation Procedure	823
	Nomenclature	830
	References	833
Appendix 16.A	Computer Program MULTSPAN	841
Appendix 16.B	Natural Frequency of U-Bends— Computer Program UVIB	851
Appendix 16.C	Computer Program UFLOW	856
17.	SUPPORT DESIGN AND EXTERNAL LOADS	
17.1	Introduction	861
17.2	Types of Supports—Design Data	861
17.3	Loadings	866
17.4	Analysis for External Loads	869
17.5	Stresses in Annular Ring Supports Due to Vertical Loads	871
17.6	Lug Design	879
17.7	Stresses in the Shell at Saddle Supports	881
17.8	Elementary Solution for Anchor Bolt Loads	886
17.8.1	Bolt Load Distribution in a Three Lug Support System	886
17.8.2	Foundation Response of Ring Type Supports Mounted on Rigid Foundations	889
	Nomenclature	891
	References	891
Appendix 17.A	Computer Program RINGSUP	892
18.	FOUR-LEG SUPPORTS FOR PRESSURE VESSELS	
18.1	Introduction	899
18.2	Problem Definition	902
18.3	Determination of the Most Vulnerable Direction of External Loading	903
18.4	Computation Procedure	909
18.5	An Example	909
18.6	Observations on the Optimization Method	910
18.7	Stress Limits	912
	Nomenclature	914
	References	914
Appendix 18.A	Multiple Loadings on the Pressure Vessel	915
Appendix 18.B	Computer Program FORLEG	916
19.	SADDLE MOUNTED EQUIPMENT	
19.1	Introduction	925
19.2	Determination of Support Reactions	928

19.3	Foundation Stresses	930
19.4	An Example	934
19.5	Bolt Load—Rigid Foundation	934
19.6	Computer Code HORSUP	937
19.7	Stress Limits for the Concrete Pedestal and Anchor Bolts	938
	Nomenclature	939
	References	940
20.	EXTERNAL LOADS ON VERTICALLY MOUNTED EQUIPMENT	
20.1	Introduction	947
20.2	Maximization of Support Reactions	949
20.3	Foundation Response	955
20.4	Computer Program “VERSUP”	960
	20.4.1 Overview of the Code	960
	20.4.2 Input Data for Program VERSUP	961
	Nomenclature	974
	References	974
	Appendix 20.A Partial Compression—Thick Ring Base	975
21.	RESPONSE SPECTRUM	
21.1	Introduction	979
21.2	Physical Meaning of Response Spectrum	979
21.3	Response of a Simple Oscillator to Seismic Motion	987
21.4	Application to Heat Exchanger Type Structures	991
21.5	An Example	996
21.6	System Response When the Natural Frequencies Are Closely Spaced	1000
21.7	System Response When Multi-Direction Seismic Loads Are Imposed	1001
21.8	Finite Element Method for Response Spectrum Analysis. .	1003
	Nomenclature	1004
	References	1005
22.	PRACTICAL CONSIDERATIONS IN HEAT EXCHANGER DESIGN AND USE	
22.1	Introduction	1007
22.2	Design for Maintenance.	1007
22.3	Selecting the Right Tube	1013
22.4	Handling	1013
22.5	Installation	1016
22.6	Operation	1016
22.7	Maintenance and Trouble Shooting	1018
	References	1019

APPENDIX A	Classical Plate and Shell Theory and its Application to Pressure Vessels	
A.1	Introduction	1021
A.2	Basic Elasticity Equations.	1021
A.3	Specialization to the Bending and Extension of Thin Walled Cylindrical Shells	1024
A.4	Some Applications of Thin Shell Theory Results.	1029
A.5	Specialization to Bending and Extension of Circular Plates.	1035
	Nomenclature.	1039
	References	1040

GLOSSARY OF COMPUTER PROGRAMS

HEADSKIRT (Chapter 2): Evaluation of discontinuity stresses at ellipsoidal head-shell-skirt junction.

FLANGE (Chapter 3) Flange analysis using Taylor Forge Method. 5 types of flange configurations: welding neck, slip on hubbed flange; lap joint; hubbed lap joint; and ring joint: Options: Given flange ring thickness computer flange stresses—or given stress limits determine flange ring thickness.

TRIEL (Chapter 4) Stress analysis of a three element flanged joint (tubesheet sandwiched between two flanges) in U-tube heat exchangers. The concept of flange-tubesheet contact outside of the bolt circle is included in the analysis (controlled metal-to-metal contact). A two element joint, or a bolted joint consisting of a flat cover and a welding neck flange, can also be analyzed. Stresses in all elements are predicted.

GENFLANGE (Chapter 5) Analysis of a two or three element bolted joint having gaskets too wide to be modelled as line elements. Full faced gaskets can be treated. Non-linear gasket stress strain curves are allowed. The gasket compression and decompression history is followed using an incremental solution technique. Joint leakage pressure as well as bolt and flange stress is computed. Effects of bolt overstress can be studied. Compression stops at different locations can be accommodated.

LIGTEM (Chapter 7) Prediction of temperature distribution in a tube wall and in a tubesheet ligament (through the thickness of the tubesheet) under specified thermal boundary conditions on the tubesheet surfaces, and on the tube inside surface.

TBROLL (Chapter 7) Fortran microcomputer code using CRT input and output and also printer hard copy. Evaluates residual roll pressures using Tresca Yield Condition.

GENROLL (Chapter 7) Elastic-Plastic analysis of tube rolling process and a single cycle of subsequent thermal loading. The von Mises Yield Condition is assumed without strain hardening. Large deformation effects are included. The code does an incremental analysis of loading, unloading, and subsequent thermal cycling. The tube-tubesheet interface pressure is traced throughout the problem. Arbitrary tube/tubesheet material combinations can be used.

UTUBE (Chapter 8) Interactive Microcomputer code written in BASIC for analysis of a tubesheet in a U-tube heat exchanger. The effect of unperforated rim is included in the model. Support conditions permitted are: integral construction both sides; one side integral, one side gasketed; and,

two side gasketed. The effect of different gasket radii on each side of the tubesheet as well as the effect of edge bolting is accommodated. Shell and channel stresses are also computed.

FIXSHEET (Chapter 9) Performs a complete stress analysis of two side integral tubesheets in fixed tubesheet heat exchangers. The two tubesheets are identical, and vertical and horizontal orientations are permitted. The effect of elevation in vertically mounted units, the pressure loss due to fluid flow, and quasi-static seismic acceleration effects along the tubesheet axis can be incorporated. Complete stress analysis of all portions of the unit are obtained. The unperforated rim of the tubesheets is treated by plate theory, so that there is no restriction on the width of the unperforated zone.

FIXFLOAT (Chapter 9) Program assumes heat exchanger symmetry so only one tubesheet need be modelled. Analysis of the tubesheet of fixed tubesheet exchangers, or the stationary tubesheet of a floating head unit can be carried out. The program computes stresses in all relevant portions of the exchanger for a given tubesheet thickness and unit geometry. Mechanical and thermal loads are included, and a thickness based on the TEMA formulas can also be determined. The unperforated rim is treated by ring theory and the tubesheet attachment to shell and channel can be two side integral, one side integral and one side gasketed, or two side gasketed construction. Bolt loading and different gasket radii on each side of the tubesheet can be accommodated.

MICROFIXFLOAT (Chapter 9) Interactive microcomputer BASIC code which uses the same basic theory as FIXFLOAT but utilizes additional data, input by user, from graphs to predict the tubesheet stress, tube load, and shell force.

PRESHEET* (Chapter 10) A pre-processor code to construct a finite element model for analysis of single and double tubesheets for U-tube construction or for fixed tubesheet exchangers. The pre-processor accepts a minimum of user supplied geometry and material data and constructs the necessary data file for a model with 310 node points and 270 elements. The data file created is usable directly by the finite element code AXISTRESS.

AXISTRESS* (Chapter 10) A 2-D elastic finite elements code for plane or axi-symmetric "finite element analysis."

POSTSHEET* (Chapter 10) A post-processor for analysis of single or double tubesheets. The code processes the results of an AXISTRESS analysis and presents the results in a form for easy checking of critical stress areas.

DOUBLESHEET (Chapter 11) Solves field equations for closely spaced double tubesheets under mechanical and thermal load. The tubesheets can be either simply supported or clamped. The tubesheets are modelled as thick

*Listing not given in the text

plates; the tubing between tubesheets is modelled by appropriate stiffness elements which reflect the effects of both bending and shear in the tubes. Stresses are computed for user specified radial locations in the tubesheet and in the tubes.

LAPCOV (Chapter 12) Responses of a Bolted Cover-Lap Joint Flange Under Seating and Pressurized Conditions. Metal to metal contact at any radius outside of the bolt circle is permitted.

UBAX (Chapter 14) Computes the bending and direct stresses in the tube overhang and U-bend regions due to a specified interleg differential thermal expansion, and an increase in U-bend radius due to a temperature rise. The code incorporates the effect of baffle restraint on U-tube thermal growth.

EXJOINT (Chapter 15) Stress and deformation analyses of expansion joints using an improved theoretical analysis of the classical Kopp and Sayre model.

EJMAREC (Chapter 15) Analysis of rectangular expansion joints using EJMA formulas.

FLANFLUE* (Chapter 15) Pre- and Post-Processor for a finite element analysis of a single convolution of an expansion joint. The codes are set up to construct a data file for AXISTRESS, and to present the results of the finite element analysis in a convenient form for checking stress in critical locations. The spring rate of the joint is computed based on the finite element results.

MULTSPAN (Chapter 16) Computes natural frequencies and mode shapes for a straight tube on multiple supports. The straight two ends are assumed built-in and N-1 intermediate supports can be located along the tube.

UVIB* (Chapter 16) Computes natural frequencies and mode shapes for the out-of-plane vibrations of tubes in the U-bend region.

UFLOW (Chapter 16) Computes the quantities needed to describe the flow field in the U-bend region of a heat exchanger. It is assumed that double-segmental baffles are present in the unit. The code computes the flow velocity for different tube layers at various radial locations.

RINGSUP (Chapter 17) Calculates the total membrane and bending stress at the junction of an annular ring type support and the barrel of a pressure vessel.

FORLEG (Chapter 18) Determines the orientation of horizontal force and overturning moment on a vertical unit with a four leg support structure that maximizes the stress in one of the support legs. This stress is then computed and all loads on the highly loaded leg are printed out for use in foundation design and for use in local stress analysis of the vessel.

HORSUP (Chapter 19) Analyzes a horizontal saddle mounted vessel subject to discrete nozzle loads at arbitrary locations and to seismic inertia

*Listing not given in the text

loads. The program computes the overturning moment and axial force at both supports and determines the maximum concrete pressure and bolt stress. The maximum support stress is also computed.

VERSUP (Chapter 20) The code determines the support reactions in a vertically mounted unit supported at two locations. Both supports can resist lateral loads and bending moments; only the bottom support resists torsion or vertical force. The magnitudes of nozzle loads, but not their sense of action, is assumed given. The code determines the sense of action of all components of nozzle loads so that each one of the reaction components is maximized in turn. These maximized reactions are combined with seismic g-loads to compute the maxi-max of each reaction component in turn. If the sense of action of all loads is specified, then no maxima are found.

Numbering Scheme for Equations, Tables, etc.; notes on arrangement of the text

All equations are labelled as “chapter number. section number. equation number.” For example, Eq. (3.10.4) means equation number 4 in section 10 of Chapter 3. Tables and references are also numbered in an identical manner. Appendices pertinent only to a particular chapter are labeled with the chapter number followed by an alphabetic appendix number (A, B, C in sequence). Equations, tables, etc. in appendices are labelled sequentially. For example, equation 16.A.1 is the first labelled equation in Appendix 16.A.

1. HEAT EXCHANGER CONSTRUCTION

1.1 INTRODUCTION

A wide range of industries – pharmaceutical, chemical, petrochemical, dairy, food, refrigeration, bio-chemical, fossil and nuclear power, etc. – utilize tubular heat exchangers. Exchangers have been given a variety of names depending on their heat transfer functions; viz. kettle reboiler, condenser, thermosiphon reboiler, regenerator, recuperator, blow-down heat exchanger, heating element, and so on. These names serve to identify the heat transfer function of the hardware, and in many cases, also conjure up the image of the shape and appearance of the unit. In most instances, thermal design considerations dictate the external appearance of the unit. Rating engineers recognize that boiling, partial or total condensation, highly viscous flows, etc., are considerations which may profoundly affect the desirable shape of the heat exchanger. Books covering thermal design of heat exchangers must labor through the maze of heat transfer conditions which might exist in an operating unit. The picture from the mechanical design viewpoint, however, is far more unified.

In essence, as a piece of mechanical hardware, a tubular heat exchanger consists of two intertwined pressure vessels. The inlet header, outlet header, inside of the tubes and the inlet/outlet nozzles define the domain of the pressure vessel commonly referred to as the “tubeside” chamber (Fig. 1.1.1). The remaining space in the heat exchanger between the shell and the tubes is the other pressure vessel, known as the “shellside” chamber. Two fluids at different temperatures enter the two pressure chambers, exchange heat across the tube walls through a combined conduction-convection mechanism, and then exit through the outlet nozzles. The central challenge in thermal design lies in effecting the desired amount of heat transfer with a minimum amount of tube surface while remaining within prescribed limits on pressure loss due to flow of the fluids in the two chambers. The arrangement of the flow of fluids in the two chambers is thus conceptualized in the process of thermal design. Subsequently, the mechanical design effort must contend with the problems arising from two integrally attached pressure vessels subject to different pressure and temperature fields. This has led to the evolution of several styles of heat exchanger construction which are reviewed briefly in the following so we can acquire an understanding of the relative merits of each type.

The internal anatomy of the tubular heat exchanger is also exposed in this chapter with particular reference to its effect on mechanical design. In

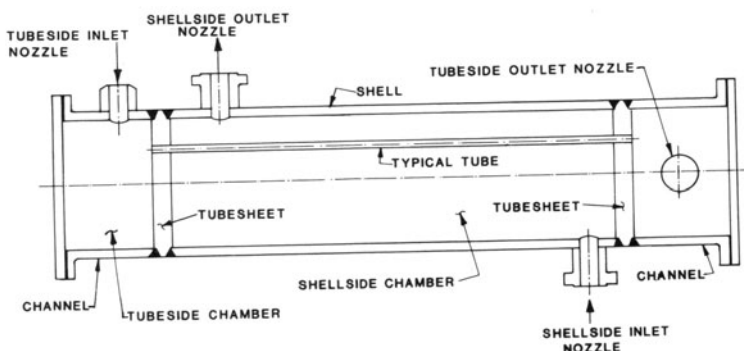


Fig. 1.1.1. Integral tubesheet head exchangers (through tube design).

addition, some unusual heat exchanger designs are discussed to help reinforce the understanding of the limitations of conventional designs. Our central goal in this chapter is to familiarize the reader with all essential details of heat exchanger construction, and to provide the building blocks on which in-depth treatment of subsequent chapters can be carried out without loss of continuity.

1.2 HEAT EXCHANGER STYLES

Heat exchanger construction styles may be broadly divided into three categories:

- (i) Fixed tubesheet
- (ii) U-tube
- (iii) Floating tubesheet

(i) Fixed Tubesheet Heat Exchanger

In this design, the straight tubes are fastened to tubesheets at their two extremities. The two tubesheets are welded to the two ends of the shell. Bonnet head, channel (with flat cover), or reducer type of headers may be provided at the two ends. For example, Fig. 1.1.1 shows a fixed tubesheet exchanger with integral channel type headers. In this construction, the tubesheet is welded to the shell and to the header at both ends. This is referred to as all-integral construction. In other variations the tubesheets may be welded to the shell but bolted to the headers; or one tubesheet may be integrally welded to both shell and header, while the other tubesheet is welded to the shell and bolted to the header. The header may be shaped in the form of a bonnet (see Chapter 13 for bonnet types), conical reducer, or cylindrical shell.* Figure 1.2.1 and Photograph 1.a show fixed tubesheet heat exchangers with removable headers and removable flat covers, respectively. In common terminology, a fixed tubesheet welded to the shell (or channel) is called “integral” with the shell (or the channel).

*In this text, we usually employ the terms “bonnet” and “channel” as generic notation for the header.

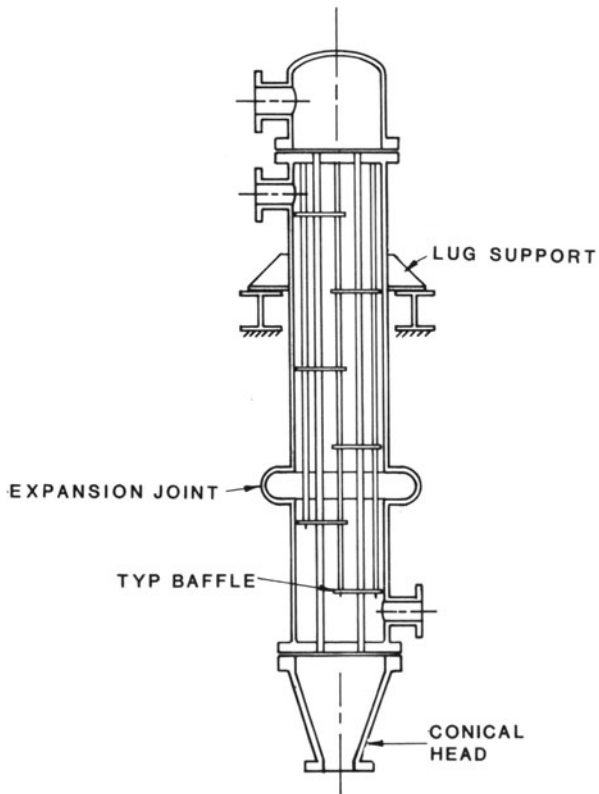
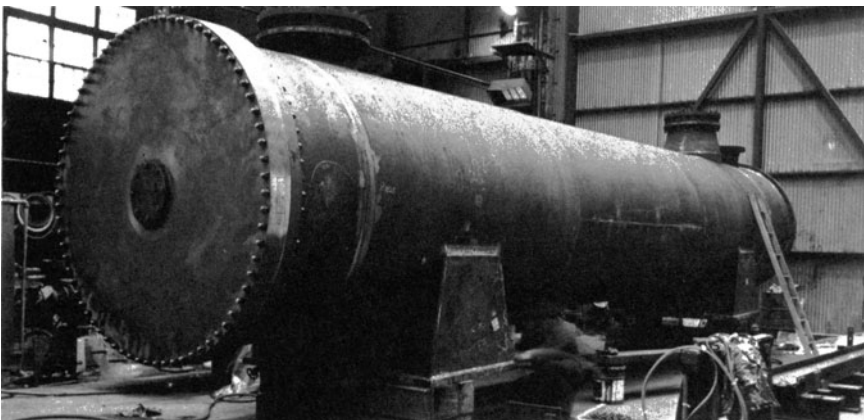


Fig. 1.2.1. Fixed tubesheet heat exchanger with removal headers (TEMA type BEM).



Photograph 1.a. Integral tubesheet heat exchanger with removable flat cover. (Courtesy Joseph Oat Corporation.)

It is unusual to make a fixed tubesheet exchanger where the tubesheets are bolted to the shell. This is due to the fact that the closure gasket cannot be replaced after the unit is tubed. In some rare commercial applications that require the use of weld incompatible materials for shell and tubesheet, pliable packings have been used in bolted shell to tubesheet designs. Such a construction is obviously limited to small units under benign pressure and temperature conditions. It is preferable to weld overlay the shell edge with a third material to which the tubesheet can be welded.

The decision as to whether a channel should be welded or bolted to the tubesheet must be made with due caution. Welded construction is usually cheaper if edge welding of the tubesheet, as shown in Fig. 1.1.1, is permitted. On the other hand, some design codes, such as the ASME Boiler and Pressure Vessel Code for Class 1 nuclear components, require radiographic butt welds at tubesheet to shell/channel junction. Butt welds imply that the tubesheet must be procured in the form of a forging with lateral extensions for welding. A forging is a relatively expensive product form, which along with the expense of radiography, may make the bolted alternative relatively economical. In general, however, welded construction means reduction in the cost of the equipment. Welded-in channels do, however, reduce the accessibility to the tube ends and therefore make internal tube cleaning, tube end plugging, tube replacement, etc., more difficult and time consuming. On the other hand, a bolted-in channel is "removable" only if its nozzles are also flanged, if any of the exchanger supports is not welded to it, and if the necessary physical space for its removal is available.

Bolted joints introduce potential locations of leakage during operation and therefore are viewed with disfavor in units operating under high pressures. The tubesheet is extended beyond the shell to act as a flange. Alternatively, the tubesheet is extended as a stub end, and a backing ring serves as the flange (Fig. 1.2.2). The latter construction is often employed where the tubesheet is made of any expensive alloy, and its weight is sought to be minimized.

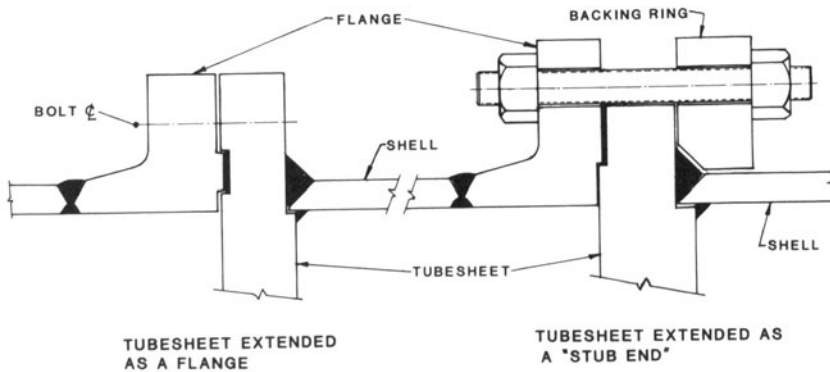


Fig. 1.2.2. Tubesheet to shell joint.

Fixed tubesheet construction is rather uncomplicated and economical and its advantages are many. It permits access to both tube ends; any leaky or failed tube can be individually plugged or replaced. Absence of bends in the tube secures the tube interior against localized foulant deposition. The interior of the tubes can be cleaned conveniently. Perhaps the only problem with fixed tubesheet construction is the axial thermal stress developed between the shell and the tubes. The differences in the temperature and coefficient of thermal expansion of the shell and tube materials may set up severe axial stresses in the tubes and the shell, precipitating possible buckling of the tubes, or failure of tube-to-tubesheet joints. To alleviate such problems, an expansion joint may be added to the shell as shown in Fig. 1.2.1. Details on the effect of an expansion joint on the fixed tubesheet design process are found in Chapter 9.

Fixed tubesheet construction is preferred for conditions of service where the temperature difference between the shellside and the tubeside fluids is small and where the inside of the tubes require frequent cleaning. From a mechanical design standpoint, this style exhibits some odd characteristics. For example, it is possible to have practical designs wherein the pressures in the tubeside and shellside chambers act additively to increase tube-to-tubesheet joint load in certain regions of the tubesheet. Thus, the standard practice of hydrostatically testing each chamber independently may not load the tubejoint to the operating condition pressure stresses making a hydrostatic test all but meaningless as a verification of safety factor. Industry standards such as TEMA [1.2.1, p. 10; 1.2.2] take note of such latent aspects of fixed tubesheet exchanger operation.

The addition of an expansion joint to alleviate thermal loads is not done without incurring negative features. The expansion joint increases the tubesheet thickness. It also provides bypass regions for the shellside fluid. It is often difficult to incorporate expansion joints in shells equipped with non-removable longitudinal baffles (Section 1.4).

(ii) U-Tube Heat Exchanger

The effect of axial expansion and contraction of the shell and the tube bundle is decoupled in this design. The tubes are bent into U-shapes and attached to the same tubesheet (Fig. 1.2.3; Photograph 1.b). Thus, the design dispenses with the second tubesheet and header, making it an economical construction. Unlike the fixed tubesheet design, the tube bundle can be made detachable from shell and channel to facilitate cleaning of the outer surface of the tubes. Cleaning of the internal surface of the tubes is, however, easier in the straight tube design.

The designer has wide latitude in deciding the degree to which the unit can be dismantled. The following combinations are available:

a. Tubesheet integral to both shell and channel: In this construction the channel usually has a removable flat cover to permit access to the tube ends. However, integrally welded hemispherical heads are employed in conditions

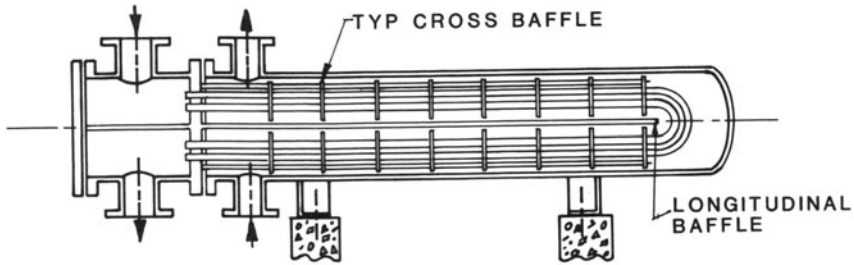


Fig. 1.2.3. Removable U-tube heat exchanger (TEMA type CFU).



Photograph 1.b. Four-tube pass, U-tube bundle. (Courtesy Joseph Oat Corporation.)

of high pressure and temperature. Figure 1.2.4 shows the schematic of a high pressure feedwater heater (used in the turbine cycle of power plants) equipped with non-removable shell and bonnet. The bonnet is, however, equipped with a manhole to permit access to the tubes.

Completely welded-in U-tube heat exchangers without manholes or other accessways have also been used in applications involving high operating pressures and extreme concern with joint leakage. The regenerative heat

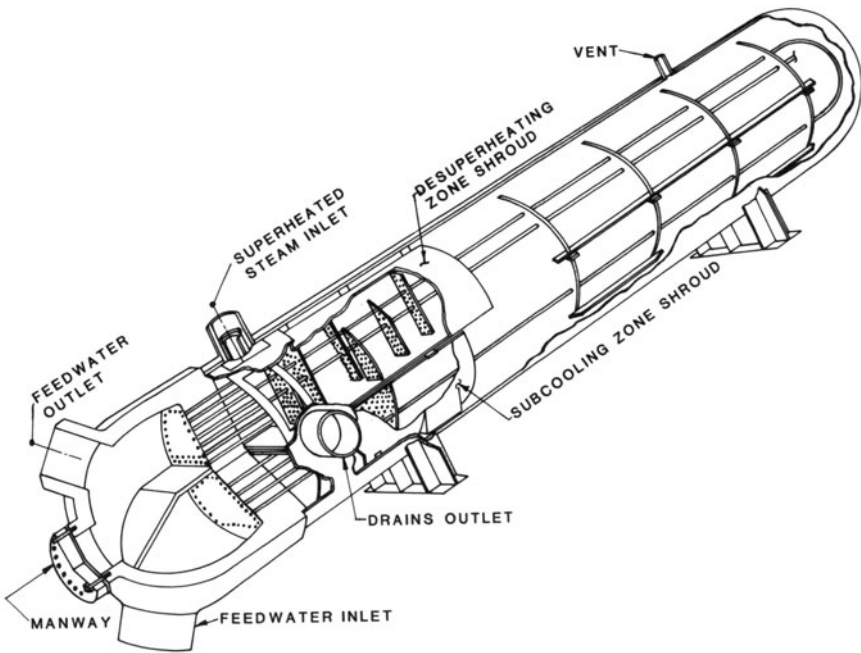


Fig. 1.2.4. Cutaway view of a three-zone horizontal feedwater heater.

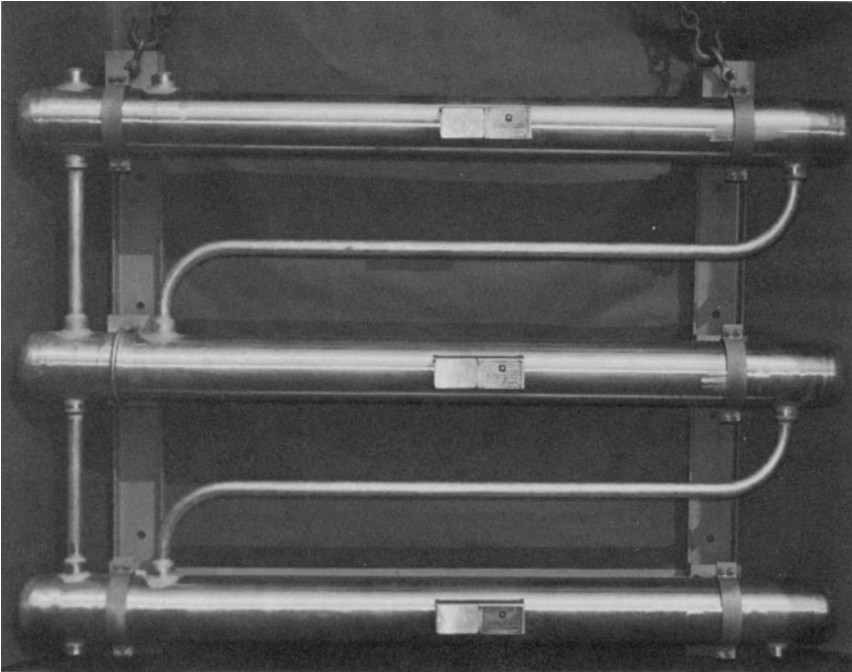
exchanger (Photograph 1.c) used to reheat the reactor coolant fluid in Westinghouse designed Pressurized Water Reactor plants is an example of such a unit.

b. Tubesheet integral to shell, bolted to channel: The bundle is not removable which negates a major benefit of U-tube design. The outside of the tubes is not accessible for mechanical cleaning, and any leaky tube must be plugged (cannot be removed).

This construction is employed if leakage of the shellside fluid is a safety concern, or if the shellside pressure is high enough to make the reliability of a shell-tubesheet bolted joint suspect. This design is also used when the shell longitudinal baffle must be welded to the tubesheet for thermal design considerations.

c. Tubesheet integral to channel, bolted to shell: This configuration, shown in Fig. 1.2.3, is quite common. Access to the tube ends is available through a removable cover. However, replacement of a worn tubesheet-shell flange gasket requires full length removal of the bundle—a time-consuming operation.

d. Tubesheet bolted to both shell and channel: This construction offers maximum disassembly capability. The bonnet is usually in the shape of a formed head. The tubesheet is sandwiched between the shell and tubeside flanges. The gaskets between the bonnet flange and tubesheet, and between the tubesheet and shell flange are seated by a common set of studs. This

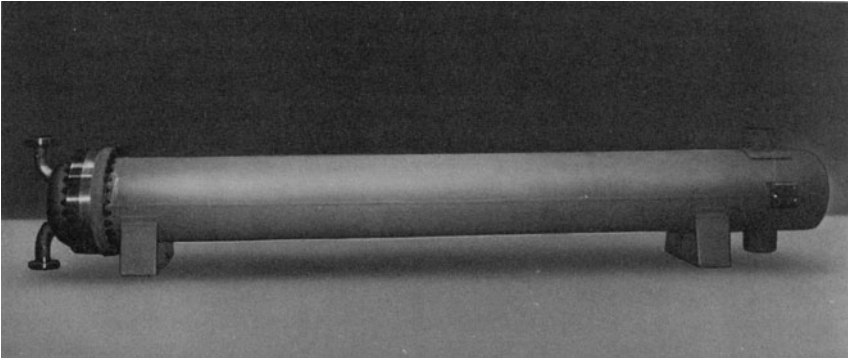


Photograph 1.c. Regenerative heat exchanger; three integrally welded U-tube heat exchangers interconnected with “flangeless” piping. (Courtesy Joseph Oat Corporation.)

bolted joint, consisting of two flanges and a tubesheet, is referred to as the “three-element joint” in the literature. Photograph 1.d shows such a joint used in a power plant heat exchanger. Since the same bolt pull is responsible for loading both gaskets, one gasket cannot be replaced without unloading the other. This is a negative factor since replacement of the bonnet side gasket is far easier than replacement of the shellside gasket. In order to avoid unloading the shellside gasket while replacing the gasket in the channel side, a fraction of the bolt holes (usually every fourth) in the tubesheet are made “tapped holes” instead of the usual “clearance holes.” The studs in the tapped tubesheet hole locations will not unload upon removal of the bonnet-side nut, thus maintaining a pre-load on the shell gasket upon removal of the bonnet.

In those cases where economy of design is the primary motive, the tubesheet outer diameter may be reduced such that it clears the inside of the bolt circle. In this case, the tubesheet rim merely provides the seating surface for the gaskets.

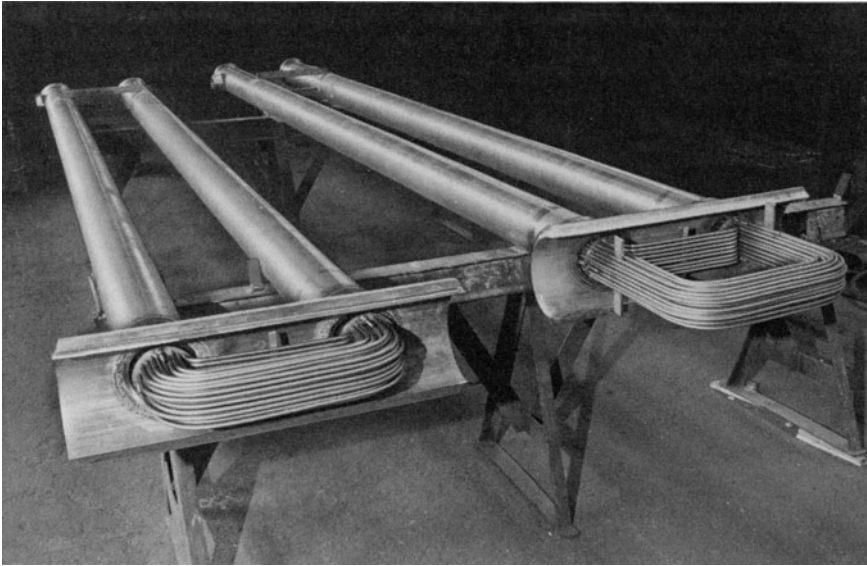
Offsetting the advantages are some problems with the U-tube design. The tubeside fluid must traverse the shell an even number of times (even number



Photograph 1.d. Horizontal letdown heat exchanger with a “three-element joint.”

of “tube passes”). This places a restriction on exchanger thermal design. The process of forming the U-bends thins the tube in the U-bend region requiring heavier gage tube to allow for this thinning [1.2.1, p. 23]. In addition to wall thinning, the tube section in the bend region also ovalizes, reducing its external pressure carrying capacity. The design codes recognize these effects and offer guidelines on tube gage selection [1.2.3, p. 915]. Cold working some tube materials makes them more susceptible to embrittlement and stress corrosion. U-bends of tubes are also more vulnerable to flow induced vibration [1.2.4]. The U-tube bundle geometry makes it impossible to pull out and replace leaky tubes in the bundle interior. Such tubes must be plugged and thus removed from heat transfer duty; unlike straight tube designs, one location of failure means two tube lengths are lost to heat transfer. The inside of the U-tube is also more difficult to clean compared to straight tubes. Finally, although U-tube design eliminates the differential expansion problem between shell and tubes, the problem of differential expansion between two legs of the U-tube remains. However, the issue of stresses in the U-bends due to unequal thermal growth of the two legs is problematic only in conditions involving large temperature differences [1.2.5]. Despite these shortcomings, the U-tube heat exchanger is the most popular style in use. In the power industry, U-tube design is almost exclusively used in feedwater heaters and in moisture separator reheaters. Steam generators in many pressurized water nuclear reactors are also of U-tube construction.

In addition to the standard U-tube designs depicted above, many hybrids of fixed and U-tube designs have been devised for particular applications. Photograph 1.e shows the “hair pin” design used as a regenerative heat exchanger in nuclear power plants. In this design, there are two tubesheets and the shell and tubes are in the form of broad U’s. In the photograph, the shoulder of the broad U’s is shown exposed. The unit is completed by welding on the other half of the transverse shell and the end caps.



Photograph 1.e. Hairpin “regenerative” heat exchanger under fabrication. (Courtesy Joseph Oat Corporation.)

(iii) Floating Tubesheet Heat Exchangers

In this class of designs, one of the two tubesheets is free to move axially as the tubes expand or contract. The bundle is removable from the shell. There are four main styles in use, namely:

- a. Outside packed floating head (TEMA type “P” head*).
- b. Floating head with backing device (TEMA type “S” head).
- c. Pull through floating head (TEMA type “T” head).
- d. Packed floating head with Lantern Ring (TEMA type “W” head).

a. Outside Packed Floating Head

Figures 1.2.5 and 3.1.1 show the outside packed floating head heat exchanger design. A packed stuffing box seals the shellside chamber while permitting the floating tubesheet to move back and forth. A “split ring” flange seals the back end of the tubeside chamber. Since the packing seals the shellside chamber against the atmosphere, any leakage does not cause mixing between the shell and the tubeside fluids.

Care should be exercised in designing the floating head cylindrical skirt. Designing the skirt merely as a cylindrical shell under internal pressure

*The designation of Tubular Exchanger Manufacturer’s Standards (TEMA) are explained in Section 1.3.

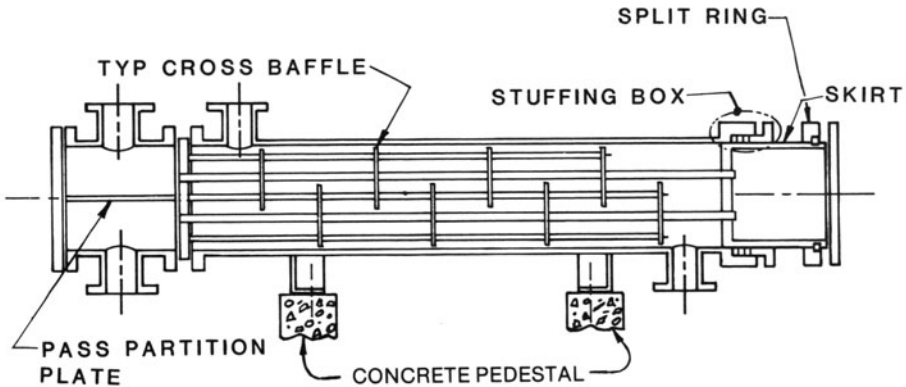


Fig. 1.2.5. Outside packed floating head heat exchanger (TEMA type AEP).

(tubeside pressure) is not sufficient since the external pressure of the packing may be the controlling load, especially if the shellside pressure exceeds the tubeside pressure. It is also to be recognized that the tubeside inlet and outlet nozzles must be located on the stationary header in the outside packed floating head heat exchanger. Therefore, this style is limited to an even number of tube passes.

It is necessary to protect the packing seating surface on the floating head from scratching while pulling the bundle out of the shell. For this reason, designers often require bundle runners in such units. The stationary tubesheet in the packed floating head design can be part of a three-element joint, or it may be truncated (shortened in diameter) in the manner shown in Fig. 1.2.5. The latter construction is cheaper, but removes the facility to unload bonnet and shellside gaskets independently of each other, as noted earlier in the context of U-tube exchangers.

The most serious drawback of this floating head design lies in the untubed outer annulus on the tubesheet. The outermost tubes must be inboard of the inside diameter of the floating tubesheet skirt. The outer diameter of the skirt must be less than the effective shell inside diameter (defined as the diameter of the largest perfectly straight cylinder that can be inscribed in the shell). This can mean as much as a 1½" wide untubed annulus between the tube bundle and the shell. This untubed region can cause significant flow bypass. Sealing strips utilized to force the flow into the bundle often precipitate flow induced vibration in outer periphery tubes. The reader is referred to Section 16.10 for further details on this matter.

b. Floating Head with Backing Device

This arrangement (Fig. 1.2.6) employs a split ring flange to bolt the tubesheet to the floating head. Leakage at the floating head joint causes

mixing of shell and tubeside fluids and is a drawback of this construction. A special test ring is required to seal the shellside chamber (Fig. 22.7.1) if it is to be pressurized with exposed tube ends to detect leaky tubes. The un-tubed annulus is also a concern in thermal design of this style of heat exchangers.

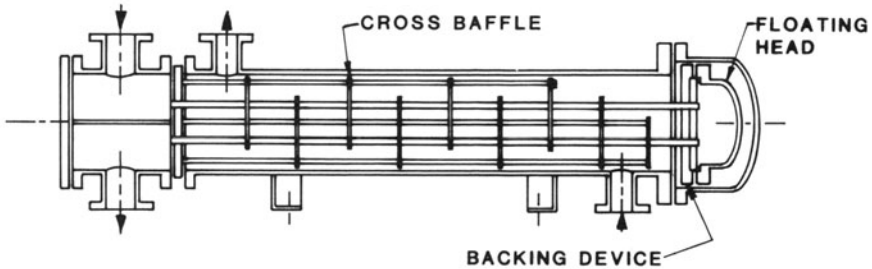


Fig. 1.2.6. Floating head heat exchanger with backing device (TEMA type AES).

c. Pull Through Floating Head

In the pull through floating head design, the tubesheet itself acts as the flange (Fig. 1.2.7). However, valuable surface on the outer rim of the tubesheet which would contain tubes, is lost to make room for the flange, forcing an increase in the shell diameter. This increases equipment cost and also leads to un-tubed annular voids in the shell which produce undesirable flow bypass. The design is utilized in those situations where an ample open space in the shellside is required for flow considerations, such as a kettle reboiler (Fig. 1.2.7).

d. Floating Head with Lantern Ring

Packed floating head with lantern ring, shown in Fig. 1.2.8, is another variation in the floating tubesheet design. Here the cylindrical edge surface of the tubesheet is machined to effect two separate seals for the shell and for the tubeside flanges. Vents in the lantern ring help locate any leak in the seals, and keep the leakage out of one joint from intruding into the other.

Floating tubesheet designs have found some application in the chemical and petrochemical industries where their relatively greater initial cost is offset by the accessibility to the tube ends for cleaning and repair.

In all of the design configurations discussed above, the tubesheet is the principal barrier between the two chambers. The joint between the tubesheet and the tubes is often the path of inter-chamber leakage. Designers resort to a “double tubesheet” configuration where mixing between the two flow streams is absolutely unacceptable for safety or for process dependent reasons. For example, if the shellside fluid polymerizes below a certain temperature, then separating the cold channel from the shell through a double tubesheet device may elevate the shellside tubesheet

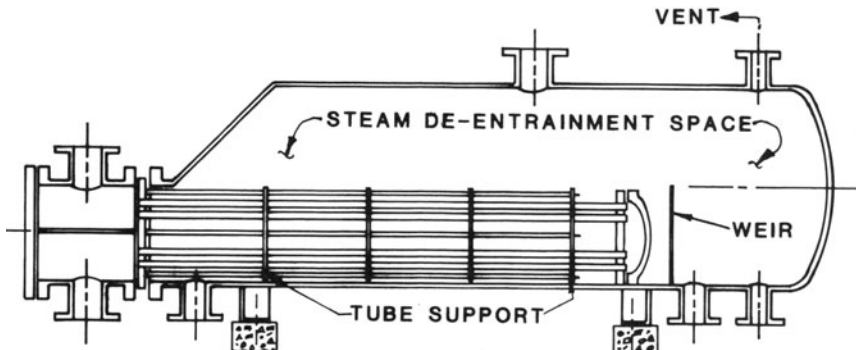


Fig. 1.2.7. Kettle reboiler; pull through floating head (TEMA Type AKT).

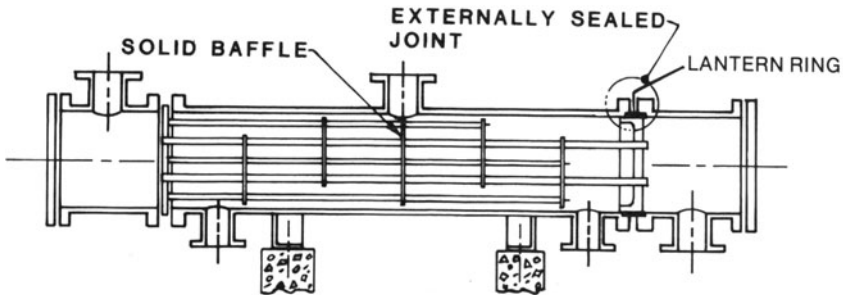


Fig. 1.2.8. Externally sealed floating head heat exchanger (TEMA type AEW).

temperature sufficiently to arrest the polymerization process. Double tubesheet design permits the tubesheets to be made from dissimilar materials. Figure 1.2.9 shows a double tubesheet heat exchanger with an outside packed floating head construction. We note that in double tubesheet construction, the tubesheet skirt extends inwards rather than outwards as in the standard outside packed design (Fig. 1.2.5). This is done

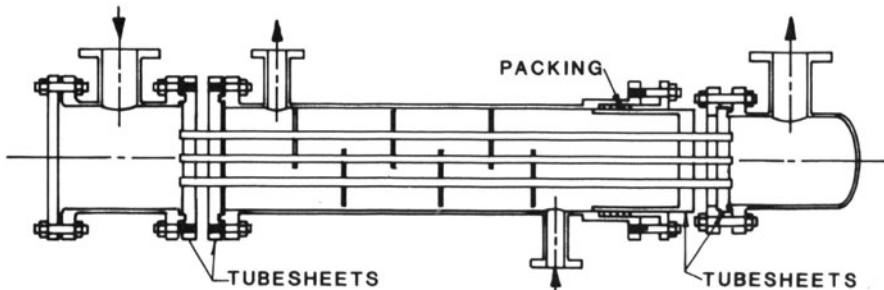


Fig. 1.2.9. Double tubesheet with outside packed floating head.

to minimize the tube surface area inactive in heat transfer (the portion of the tubes between the tubesheets). Double tubesheet design can also be employed with other heat exchanger styles. We note, however, that the reliability of the inner tubesheet-to-tube joint is suspect since the fastening of the joint in the inner tubesheet must be made remotely.

1.3 HEAT EXCHANGER NOMENCLATURE

The Standards of Tubular Exchanger Manufacturers Association (TEMA) give a succinct scheme for designating heat exchangers. Table 1.3.1 presents the TEMA notation. Three columns in Table 1.3.1 give alphabetic symbols for common front end (tubeside inlet header), shell, and rear end (tubeside return or outlet header) geometries. The designations for the front and rear headers help indicate the extent to which the unit can be disassembled. For example, an “A” type front head implies that the channel and channel cover can be detached from the heat exchanger either together or individually, furnishing complete access to tube-to-tubesheet joints. An “N” type channel provides somewhat restricted access to the tube ends since the channel is integrally welded to the tubesheet. The TEMA nomenclature does not address second level details, such as the number of tube passes, number of baffles and tie rods. Shellside flow arrangement is, however, indicated by the shell designation. For example, an “E” type shell implies that the shellside fluid traverses the shell length only once (one shell pass).

In addition to the alphabetic symbols, the nominal inside diameter and tube length are furnished to indicate the overall exchanger size. Thus a “Size 16-120 AEP” heat exchanger implies that the shell inside diameter is approximately 16”, and the tube length is approximately 120”. The header and shell arrangement corresponds to Fig. 1.2.5. For U-tube construction, the tube length is equal to the length of the straight leg (from tube end to the U-bend tangent line). In a kettle reboiler, where both port and kettle diameters are meaningful to the unit designs, both diameters can be reported in the unit designation.

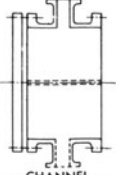
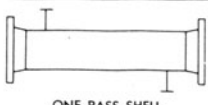
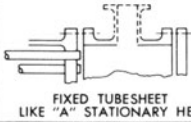
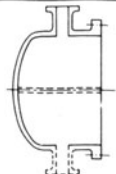
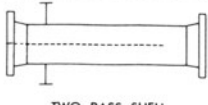
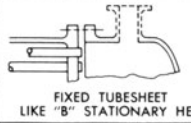
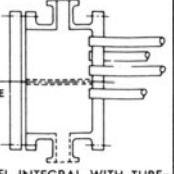
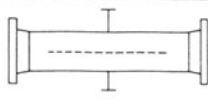
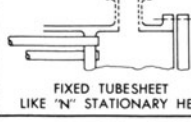
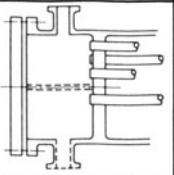
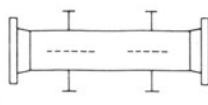
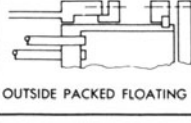
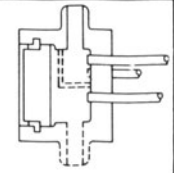
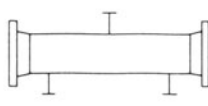
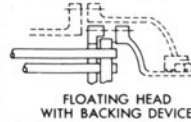
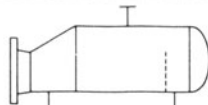
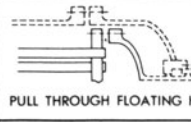
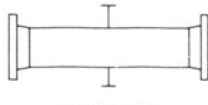
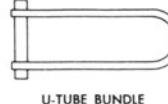
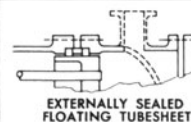
Recently, HEI standards for power plant heat exchangers [1.2.6] have proposed an alternate nomenclature. Appendix 1.A presents their notation scheme. This notation is yet to gain widespread popularity.

1.4 HEAT EXCHANGER INTERNALS

The parts list in Appendix 1.A helps explain the components that constitute the internals of a heat exchanger. The internals are required for thermal performance or for unit assembly. For example, the cross baffles shown in the preceding figures are required to guide the fluid flow of the shellside stream and to act as tube supports. The tie rods and spacers, on the other hand, are needed to position the baffles such that the tube bundle cage can be prepared and the tubesheet can be tubed conveniently. By and large, internals are not considered to support pressure or thermal loads. The

design codes treat them as non-pressure parts and hence beyond their purview. Providing guidelines for their sizing is left to the industry's own standards [1.2.1, 1.2.2, 1.2.6, 1.2.7, 1.2.8]. Nevertheless, many so-called "non-pressure parts" actively experience some pressure and thermal

Table 1.3.1. TEMA Nomenclature*

FRONT END STATIONARY HEAD TYPES		SHELL TYPES		REAR END HEAD TYPES	
A	 CHANNEL AND REMOVABLE COVER	E	 ONE PASS SHELL	L	 FIXED TUBESHEET LIKE "A" STATIONARY HEAD
B	 BONNET (INTEGRAL COVER)	F	 TWO PASS SHELL WITH LONGITUDINAL BAFFLE	M	 FIXED TUBESHEET LIKE "B" STATIONARY HEAD
C	 REMOVABLE TUBE BUNDLE ONLY CHANNEL INTEGRAL WITH TUBESHEET AND REMOVABLE COVER	G	 SPLIT FLOW	N	 FIXED TUBESHEET LIKE "N" STATIONARY HEAD
N	 CHANNEL INTEGRAL WITH TUBESHEET AND REMOVABLE COVER	H	 DOUBLE SPLIT FLOW	P	 OUTSIDE PACKED FLOATING HEAD
D	 SPECIAL HIGH PRESSURE CLOSURE	J	 DIVIDED FLOW	S	 FLOATING HEAD WITH BACKING DEVICE
		K	 KETTLE TYPE REBOILER	T	 PULL THROUGH FLOATING HEAD
		X	 CROSS FLOW	U	 U-TUBE BUNDLE
				W	 EXTERNALLY SEALED FLOATING TUBESHEET

*Reprinted by courtesy of Tubular Exchanger Manufacturers Association.

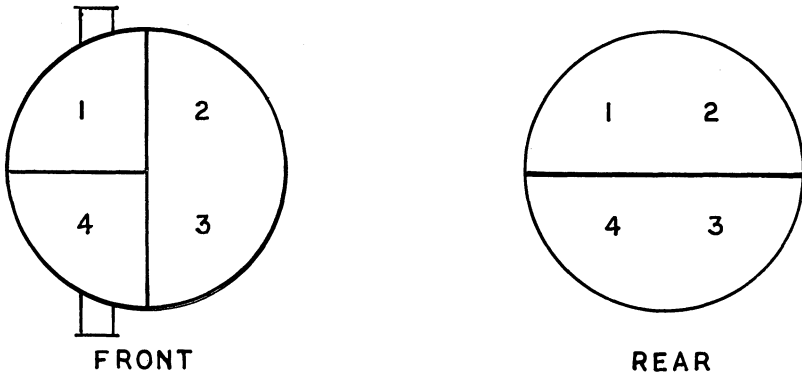
loadings, and it may be perilous to ignore their presence in designing the pressure parts. A brief description of the so-called non-pressure parts is given in the following to complete our exposition of the tubular heat exchanger geometry.

Tubeside pass partition plates: The number of tube passes is equal to the number of times the tubeside fluid traverses the length of the tubes. In multiple-tube pass heat exchangers, pass partitions are required in the inlet and outlet headers (in the outlet header only if the unit has more than two tube passes).

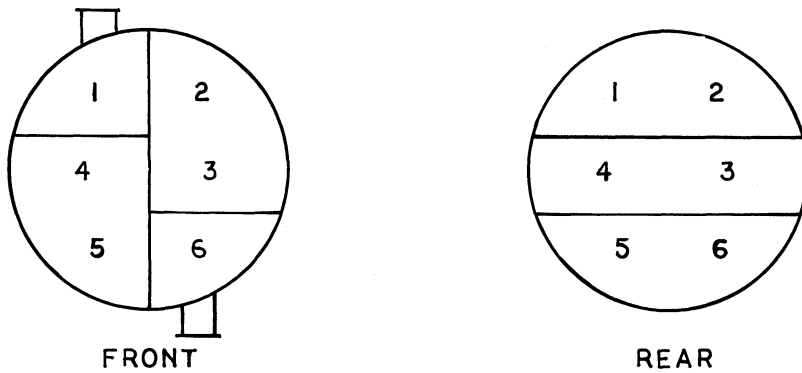
The arrangement of tubeside pass partitions in a multi-pass heat exchanger depends on the number of tube passes and tube bundle type. Figure 1.4.1 shows some typical pass partition arrangements for four-, six-, and eight-tube passes. While, in general, a wide variety of options in the arrangement of pass partitions exists, the choice is somewhat narrowed down for U-bundles. For example, the six-pass layout shown in Fig. 1.4.1.c cannot be used for U-tubes, since U-tube layout requires that each set of consecutive passes be mirror images of each other.

The arrangement of tubeside pass partitions profoundly affects the heat transfer and mechanical behavior of the heat exchangers. The tube bundle has “slits” in the plane of the tubeside pass partition plates, which can be conduits of flow bypass in the shellside stream if the shellside crossflow is aligned with the “slits”. The arrangement of tubeside passes largely determines the orientation of the tubeside nozzles, and (as we will observe later) also shellside nozzles. Photograph 1.f shows an eight-pass U-bundle (split flow shellside heat exchanger arranged in such a way that all nozzles point to within 30° of the vertical). The inter-relationship of the nozzle orientation to pass partition layout and cross baffle geometry will be discussed further after we introduce cross baffle shapes.

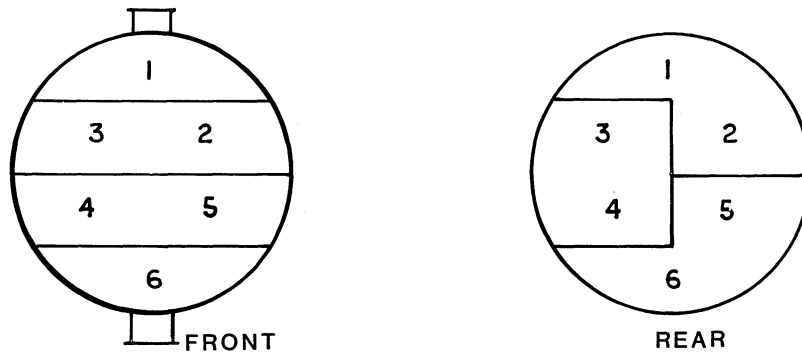
Figures 1.2.3 and 1.2.5 show two common tubeside pass partition plate attachment details. The pass partition plate is welded to the channel wall and to the tubesheet and gasketed to the cover in Fig. 1.2.3. In Fig. 1.2.5, the pass partition plate is gasketed to both the tubesheet and the cover. It is apparent that the radial expansion of the channel shell will be resisted by the pass partition plate. Furthermore, the pass partition plate itself is subject to a certain lateral pressure caused by the pressure loss of the in-tube fluid due to its flow. The pass partition plate must be sufficiently strong to withstand this lateral pressure without yielding. Furthermore, the gasket at the bolted joint must have “ribs” to seal the pass partition plate against the tubesheets or the cover, as the case may be. The bolt load must be sufficient to “seat” the “rib” in addition to seating the gasket ring. The operating pressure causes the cover/tubesheet to flex, thereby creating a crevice between the pass partition and the abutting member. This crevice becomes a short circuit path for the tubeside fluid (see Chapter 4, Fig. 4.1.3). Quantification of deflection induced leakage is discussed in Chapters 4 and 12. Where the inter-tube pass leakage due to cover deflection must be entirely eliminated, an internal pass partition chamber concept can be used. As illustrated in



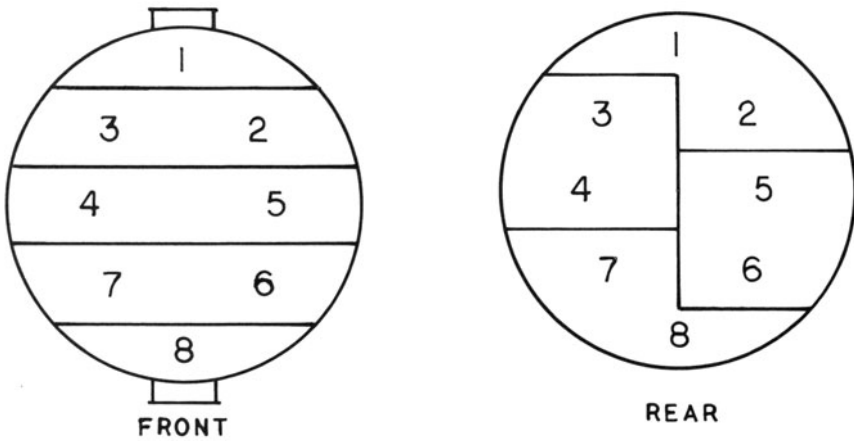
(a) FOUR TUBE PASS



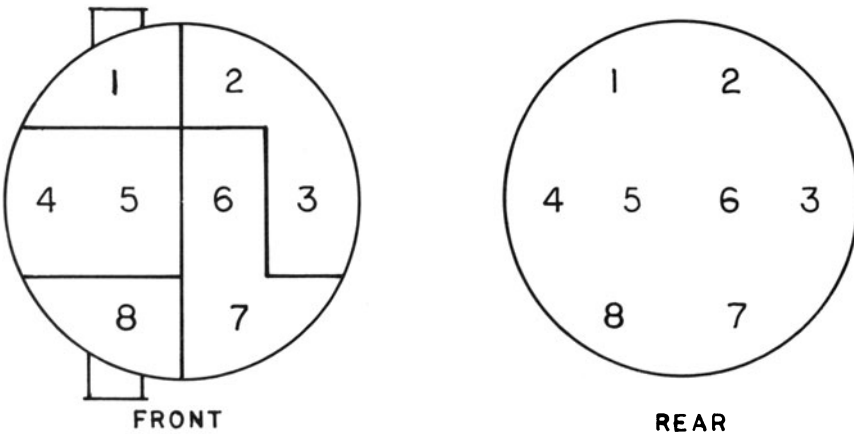
(b) SIX TUBE PASS



(c) SIX TUBE PASS (ALTERNATE STYLE)
(NOT SUITABLE FOR U-TUBE)



(d) EIGHT TUBE PASS (NON-U-TUBE LAYOUT)

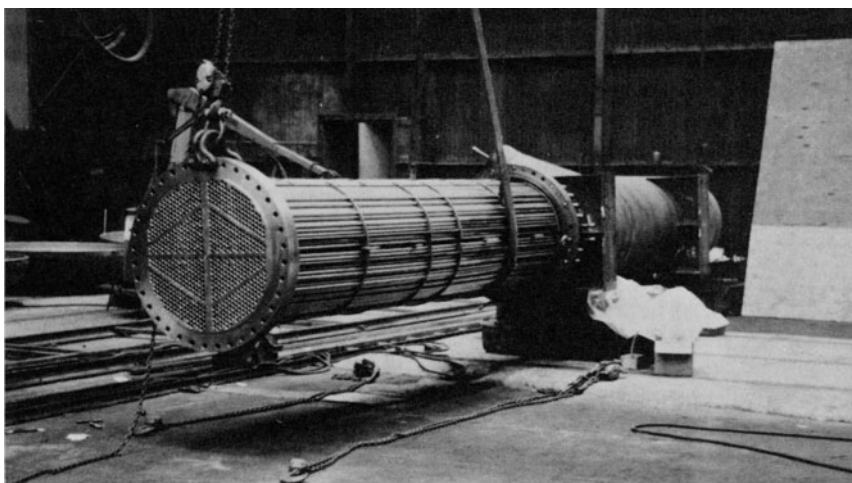


(e) EIGHT TUBE PASS

Fig. 1.4.1. Typical pass partition layout.

Fig. 1.4.2 for a two-tube pass design, the internal pass partition closure seals against the pass partition rib. The pressure drop from the inlet pass to the outlet pass acts to compress the cover plate gasket even further. The flat cover serves the sole function of pressure retention against the outside environment.

Shellside pass partition plates: The longitudinal pass partition plate (also called “longitudinal baffle”) in the shell is utilized to build multiple shell



Photograph 1.f. Eight-tube pass horizontal heat exchanger with pass partition arranged to provide “near vertical” (about 30° from vertical) nozzle connections.

passes* (Fig. 1.2.3). Its effect on the shellside chamber is similar to that of the tubeside plate on the tubeside chamber. It is desirable to weld the long edges of the shellside pass partition plate to the shell. However, it is not always possible to do so. For instance, if the U-bundle heat exchanger has two tube passes, as in Fig. 1.2.3, then welding the longitudinal pass partition plate would trap the tube bundle in the shell. In such cases, the pass partition plate is equipped with suitable edge seals to prevent leakage across the pass partition plate. Figure 1.4.3 shows a typical edge seal detail.

Heat exchangers are seldom designed with more than two shell passes, although units with as many as six passes have been successfully designed and fabricated. Photograph 1.g shows the tube bundle of a six-shell pass–twelve-tube pass heat exchanger.

Internal shrouds: Internal shrouds are used in some heat exchangers where the shellside fluid medium undergoes phase change. Figure 1.2.4 shows a feedwater heater which has three distinct zones – desuperheating, condensing and subcooling – for cooling the inlet stream. The desuperheating zone is separated from the condensing zone by a desuperheating zone shroud. Similarly, the “drain subcooling zone” is equipped with its own enclosure. These shrouds are subject to severe thermal stresses, and failure of their welds is known to be a major culprit behind heater failures in power plants.

Tube supports: The term baffle or tube support is used to indicate plates in the form of sector of a circle used to support tubes. In small condensers

*Number of shell passes is equal to the number of times the shellside fluid traverses the full length of the shell.

(condensation on the shellside) the baffles do little more than provide the tube support function. In single-phase flow conditions, however, the baffle cut and type play an important role in establishing the total shellside pressure loss and heat transfer coefficient. Figure 1.4.4 shows the so-called “single segmental baffles” with horizontal cuts in a single-pass shell. Figure 1.4.5 shows “double segmental baffles” with vertical cuts in a two-pass shell. Triple segmental baffles (Fig. 1.4.6) are used less frequently but are known to provide increased safety against flow-induced vibrations. Figure 1.4.7 shows an idealized rendering of the flow pattern in one-half of the shell equipped with triple segmental baffles.

In conventional heat exchangers, baffles and tube supports are not attached to the shell. However, in large surface condensers, they are welded to the side walls to help support the walls of the shell (usually rectangular in cross section). In-plane thermal growth of the baffles stresses the tubes, and can lead to their failure due to fatigue and wear.

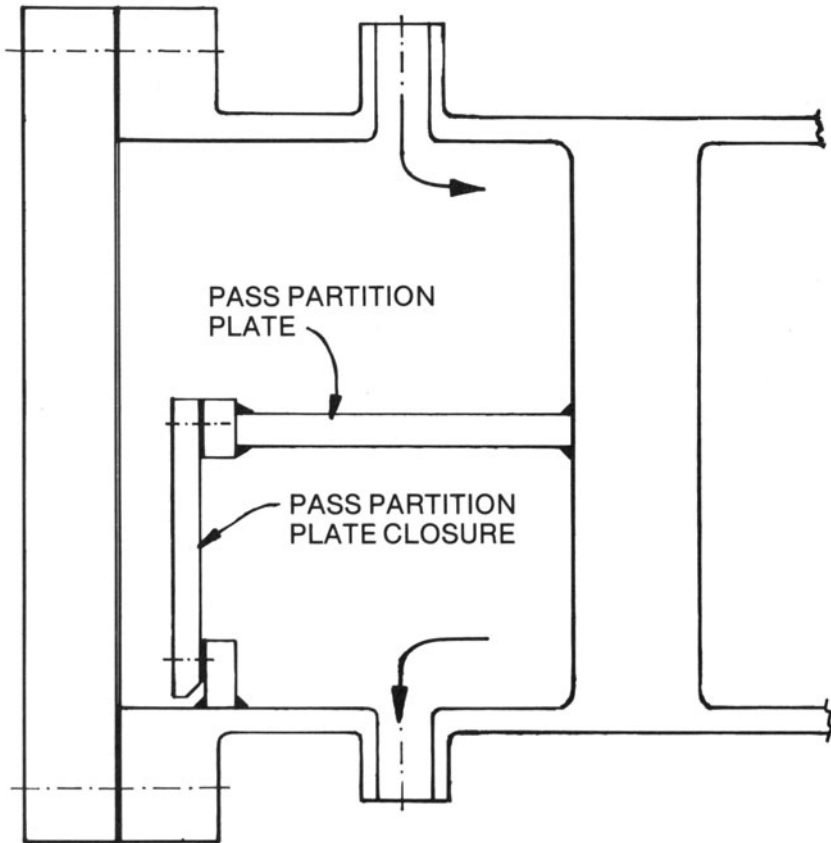


Fig. 1.4.2. Alternate pass partition arrangement (two pass).

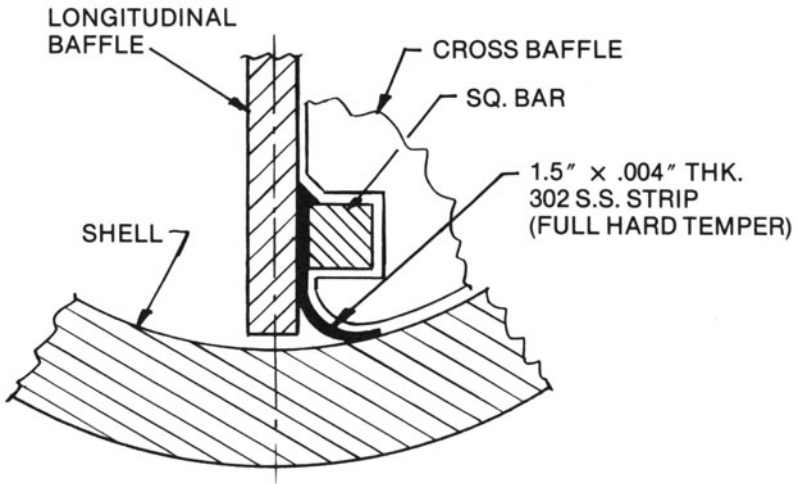
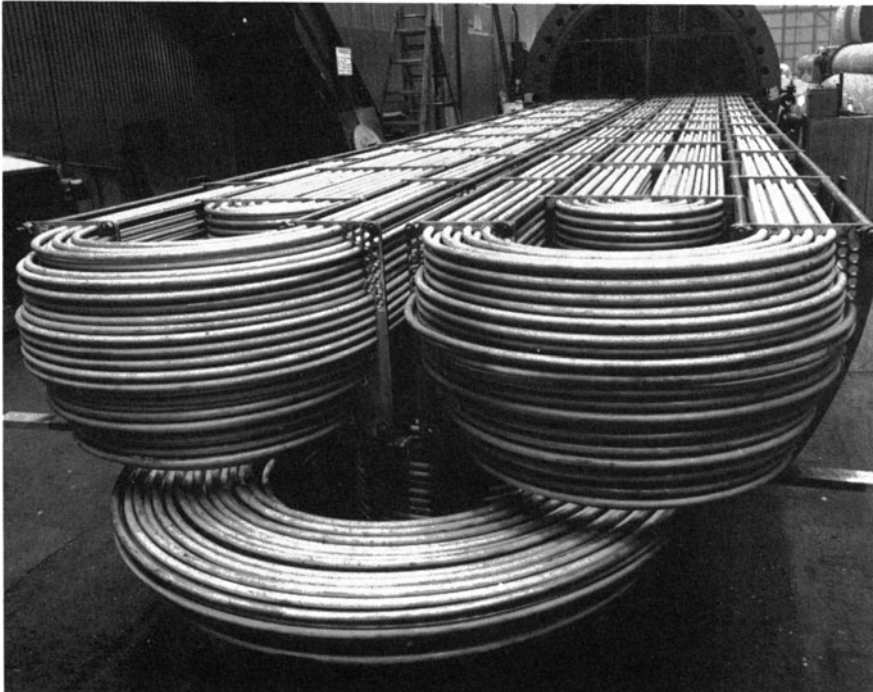


Fig. 1.4.3. Typical longitudinal baffle edge seal detail.



Photograph 1.g. Half-completed bundle of a six-shell pass, 12-tube pass heat exchanger. (Courtesy Joseph Oat Corporation.)

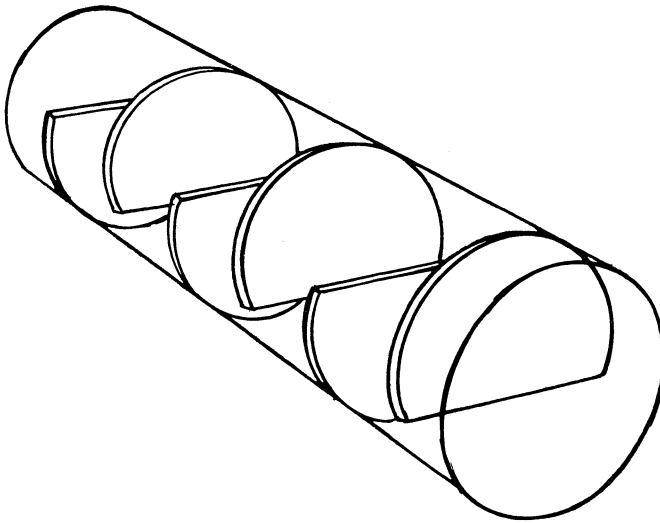


Fig. 1.4.4. Horizontal cut single segmental baffle layout.

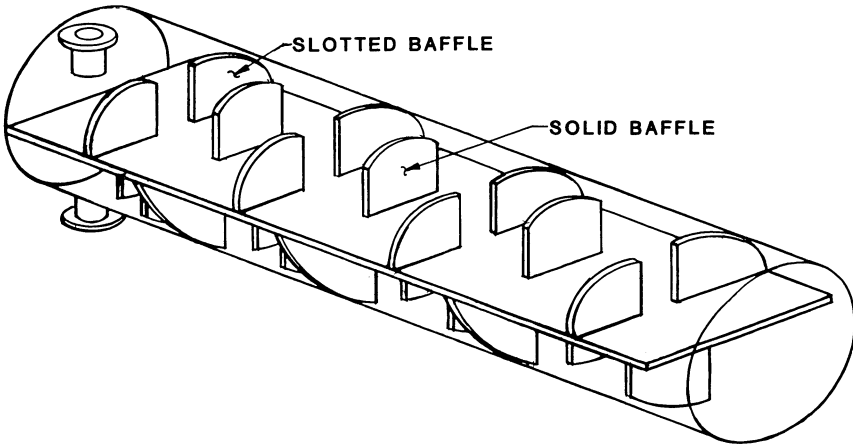


Fig. 1.4.5. Double segmental baffles.

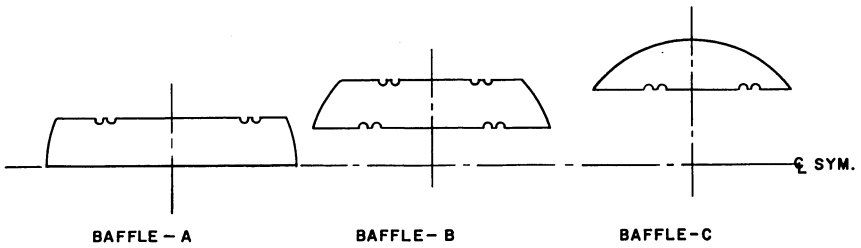


Fig. 1.4.6. Triple segmental baffle.

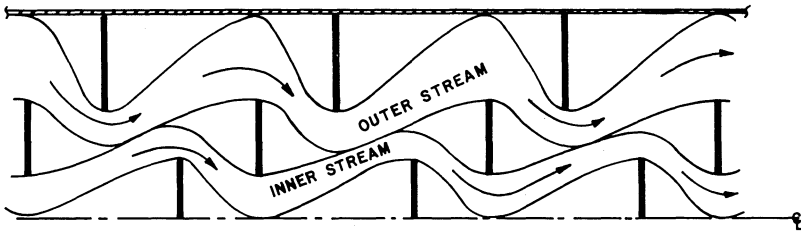


Fig. 1.4.7. Flow visualization in a triple segmental baffle heat exchanger.

1.5 TUBE LAYOUT AND PITCH

The common tube layout patterns are: (a) 30° or triangular, (b) 60° or rotated triangular, (c) 90° or square, (d) 45° or rotated square. Figure 1.5.1 shows the layout pitch, transverse pitch and longitudinal pitch for the different layout schemes. The relationship between the pitches and the gap *g* in the flow direction is defined in Table 1.5.1 for various layout angles.

Table 1.5.1. Pitches and gap in terms of layout pitch *P* and tube O.D. *d*₀

Layout Angle	<i>P_t</i>	<i>P_l</i>	<i>g</i>
30°	$2 P \cos 60^\circ$	$P \sin 60^\circ$	$P \sin 60^\circ - d_0$
60°	$2 P \cos 30^\circ$	$P \sin 30^\circ$	$P \sin 30^\circ - d_0$
90°	P	P	$P - d_0$
45°	$2 P \cos 45^\circ$	$P \sin 45^\circ$	$P \sin 45^\circ - d_0$

The orientation of baffle cuts determines the plane of flow of the shellside fluid. Since the baffle cuts are half-moons at the edges (Photograph 1.h) the gap *g* must be positive (preferably over 1/8") to avoid a ragged baffle cut edge. From Table 1.5.1 it is apparent that for a 60° layout, $P > 2d_0$ to meet this condition. This fact limits the use of 60°, and to some extent 45° layouts, in practical designs.

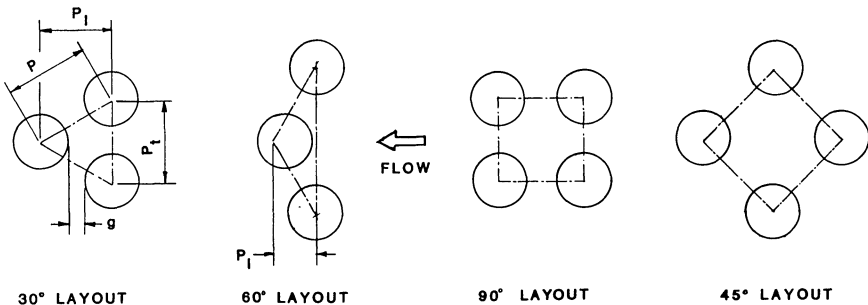
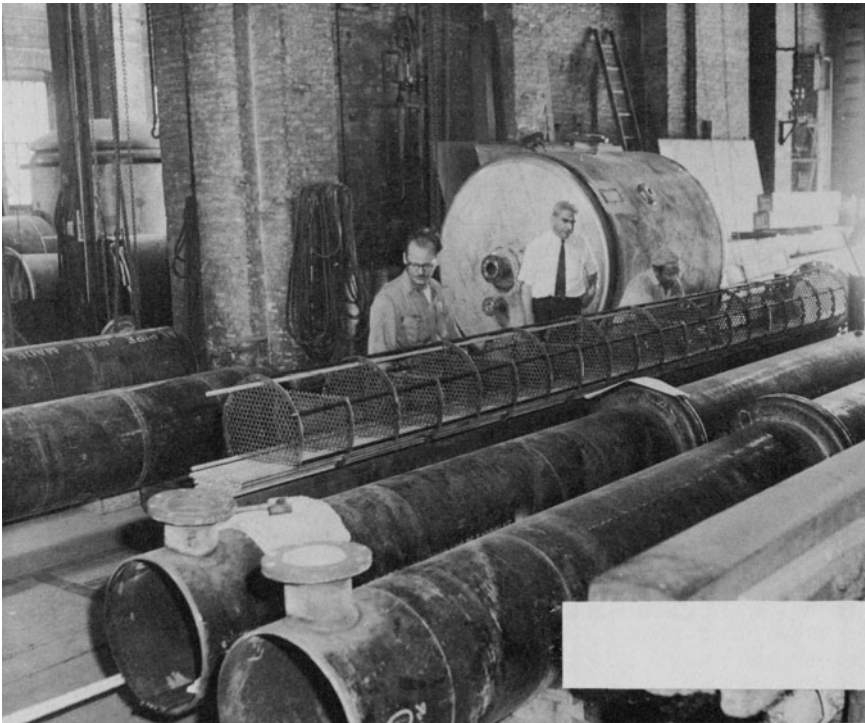


Fig. 1.5.1. Tube layout schemes.



Photograph 1.h. Views showing baffle cages and shells with expansion joints. (Courtesy Joseph Oat Corporation.)

Square and rotated square layouts permit convenient cleaning of the tube external surfaces. For this reason, they are widely used in the petrochemical and dairy industries where fouling of the tube surface is an endemic problem.

1.6 GENERAL CONSIDERATIONS IN PASS PARTITION ARRANGEMENT

It is apparent from the foregoing that the designer has several options in the selection of the pass partition arrangement scheme. The best arrangement depends on a number of factors which must be given due consideration in order to arrive at the optimum design. Some of these are:

(i) *Orientation of cross baffles with respect to the pass partition lanes:* The pass partitions should be arranged in such a manner that the plane of shellside flow is not aligned with the pass partition lanes. If pass partition lanes exist in two normal planes, then ones having the minimum lane width should be aligned with the shellside plane of flow. Rotating the cross baffles so that the flow plane is at 45° to both planes of the pass partition layout eliminates this source of shellside bypass entirely.

(ii) *Pass Partition arrangement to avoid severe thermal gradient in the tubesheet:* In multiple tube pass (more than two) exchangers involving a large temperature change of tubeside fluid, it is advisable to avoid arranging inlet and outlet passes contiguously. The temperature gradient across the pass partition rib in the tubesheet is directly proportional to the difference in the fluid temperatures in the two passes. Locating the inlet and outlet passes adjacent to each other maximizes the thermal gradient induced stress in the tubesheet.

(iii) *Pass Partition arrangement to minimize inter-pass leakage:* As mentioned before, the crevice formed between the pass partition plate and tubesheet (or flat cover), due to the lateral deflection of the latter, can derate the exchanger thermal performance. For a given crevice size, the rate of leakage depends on the pressure difference between the two adjacent passes. The pressure difference will be maximum between the inlet and outlet passes. This is another reason why inlet and outlet passes should be geographically separated by as much distance as possible (recall the pass placement in Fig. 1.4.1).

(iv) *Tubeside pass partition plate vs. shellside longitudinal baffle:* In designs utilizing a longitudinal baffle in the shell, it is obviously an efficient practice to align the tubeside diametral pass partition plate with the longitudinal baffle. This will minimize the loss of valuable tubed region to pass partition lanes.

1.7 IMPINGEMENT PROTECTION

The diameter of the piping leading to the shell inlet is selected to strike an optimum between pipe material cost and pumping costs. Usually, the flow velocity in the piping is on the order of 8 ft/sec for water (and other liquids) and 200 ft/sec for ambient condition steam and other vapors. Fluids, especially vapors, entering the shell in such a velocity range and impinging the front row tubes, can damage the tubes in front of the shell inlet. Tube wastage due to flow impingement may be due to erosive or vibration effects. Erosion is a mechanical action which is strongly dependent on the impact velocity of the fluid. The effect is particularly severe if the vapors or gases carry liquid droplets or particulate matter. Experiments suggest that the rate of erosion due to impact of liquid droplets varies roughly as the impact velocity raised to an exponent in the range of 2 to 5 [1.7.1]. As discussed in Chapter 16, vibration of long slender members, such as tubes, is also a strong function of the cross flow velocity. Therefore, any reduction in the velocity of fluid impinging on the tubes has a direct effect on retarding the rate of tube wastage.

A solution frequently advanced to prolong the heat exchanger life is to use heavy walled tubes in the shell inlet and outlet regions. This concept is based on the fact that the flow distributes itself into the bundle quite well after having crossed two or three rows of tubes.

One way to attack the root of the problem itself, namely the nozzle line velocity, is to employ a conical shaped nozzle. However, laboratory tests on expansion of incompressible fluids indicate that the efficiency of the conical expander plummets if the angle of expansion (included angle) exceeds 15° . The extent to which large expansion angles are effective in expanding the flow is not known. The mechanical efficiency of expansion has been studied by numerous investigators [1.7.2]. Table 1.7.1 shows the variation of the efficiency η of the conical expander (defined as the ratio of the actual pressure recovery to the ideal condition pressure recovery), as a function of the included angle and expander length. Since the plant design limits the nozzle length, the extent of velocity reduction attainable through the conical expander is quite modest, unless large expansion angles are used. However, as seen in Table 1.7.1, large expansion angles lead to severe pressure losses.

In Table 1.7.1, r_1 is the small diameter of the conical expander and l is its length. Therefore, the area ratio is given by:

$$\text{Area ratio} = 1 + 2 \frac{l}{r_1} \tan \gamma + \frac{l^2}{r_1^2} \tan^2 \gamma$$

The velocity distribution is also an important factor. The velocity distribution can become quite skewed if the inlet piping has bends in the proximity of the heat exchanger inlet. Flow straighteners (Fig. 1.7.1) at the nozzle inlet are found to be quite effective in eliminating rotational flow components and in improving the profile of the velocity field. An effective device to reduce the bundle penetration velocity is the use of an annular distributor. Figure 1.7.2 (Photograph 1.k) shows a typical distributor. The large shell is sized to provide the annular space for the fluid to spread out. Suitable slots are cut out in the shell to permit a uniformly diffused entry into the bundle. The main shell may be continuous or discontinuous. The latter arrangement, shown in Fig. 1.7.2, permits the (additional) use of the flow distributor dome as an expansion joint for absorbing axial movement of the shell.

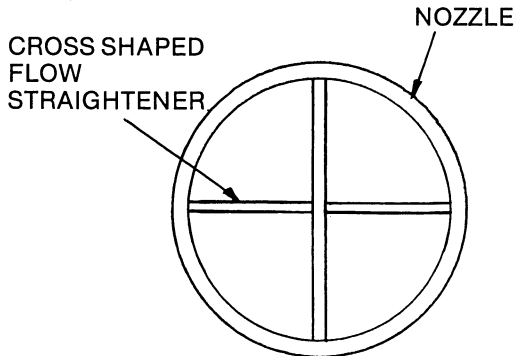


Fig. 1.7.1. Flow straightener.

Table 1.7.1. Performance of Conical Expanders (Water Flow)
[from Ref. 1.7.2]

2γ (degrees)	l/r_1	Area Ratio	η
2.0	16	1.63	0.74
2.0	32	2.43	0.77
4.0	4.0	1.30	0.83
4.0	8.0	1.64	0.81
4.0	16.0	2.43	0.80
4.0	32.0	4.48	0.82
8.0	4.0	1.64	0.81
8.0	8.0	2.43	0.77
8.0	16.0	4.48	0.79
8.0	26.8	8.27	0.81
15.8	2.0	1.64	0.67
15.8	4.0	2.43	0.58
15.8	8.0	4.48	0.57
15.8	13.4	8.27	0.60
31.2	2.0	2.43	0.40
31.2	4.0	4.48	0.36
31.2	6.7	8.27	0.36

Special design features may be required in units which handle large quantities of vapors and steam, and where the primary shellside heat transfer is by condensation. In such units, it may be advantageous to arrange the flow distributor such that the shellside fluid enters the entire span of the tube bundle in a uniform manner. Figure 1.7.3 shows a distribution arrangement for a two-zone vertical feedwater heater with mid-shell steam entry. The distributor system consists of two perforated plates with a small separation. The perforations in the two plates are laid out to prevent a direct normal "line of sight".

Some innovative designs have been developed to handle problems of impingement induced tube wastage. The Type "ES" (a tradename of Basco, Division of American Precision Industries) intercooler, which is used to cool compressed gases between compressor stages, is an example of such an innovative design. Photographs 1.i-1.j show some details of the patented "ES" intercooler. The tube bundle consists of a plate-fin surface which is covered on top and bottom by an integral shroud, forming a large horizontal flow passage. Hot gas enters a large inlet volume chamber which is formed by the shell and an internal welded partition plate. An annular plate divides the plenum into two distinct non-communicating inlet and outlet chambers. The gas is distributed over the shell length and flows in cross flow horizontally through the plate-fin core. The longitudinal seals between the bundle shroud and the shell internal partition plate inhibit any circumferential flow bypass. This design is characterized by low shell side pressure loss, high thermal effectiveness, flexible nozzle arrangements, and ease of tubeside maintenance while maintaining a removable bundle configuration.

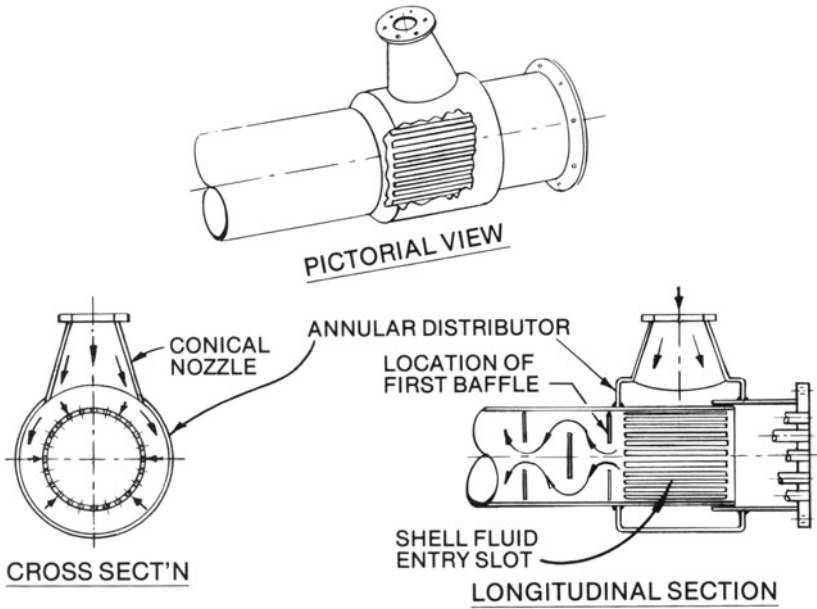
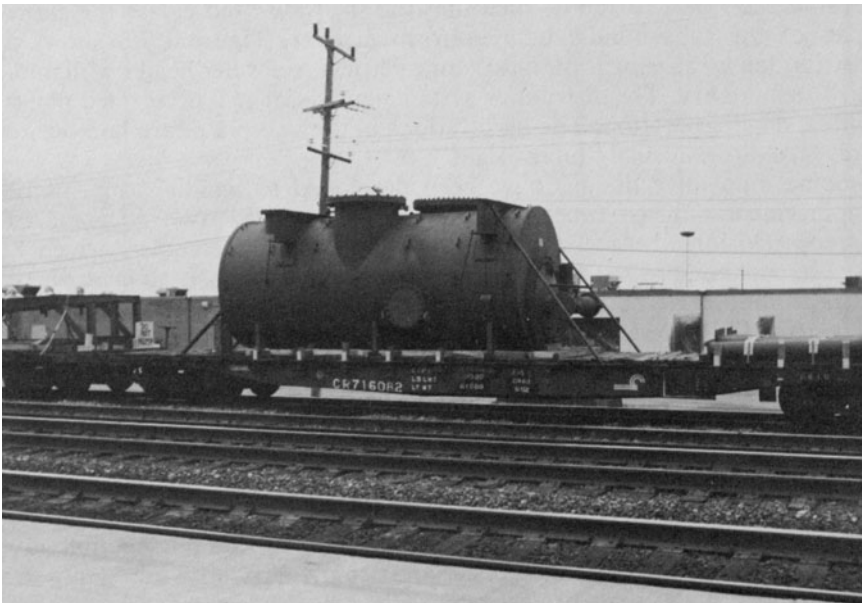
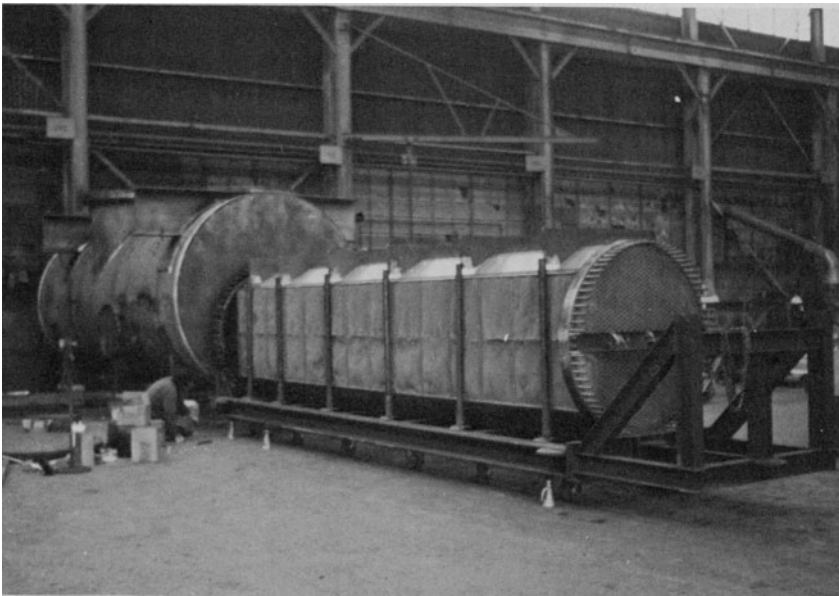


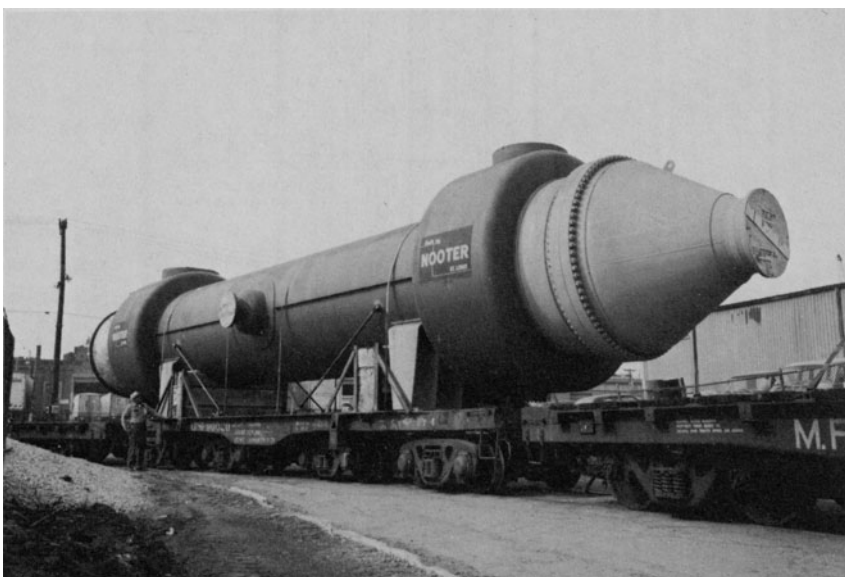
Fig. 1.7.2. A flow distributor concept.



Photograph 1.i. “ES” intercooler. (Courtesy Basco Division of American Precision Industries Inc.)



Photograph 1.j. Tube bundle and shell disassembled, “ES” intercooler. (Courtesy Basco Division of American Precision Industries Inc.)



Photograph 1.k. Heat exchanger with enlarged shells at nozzle entry and exit. (Courtesy Nooter Corporation, St. Louis, Missouri.)

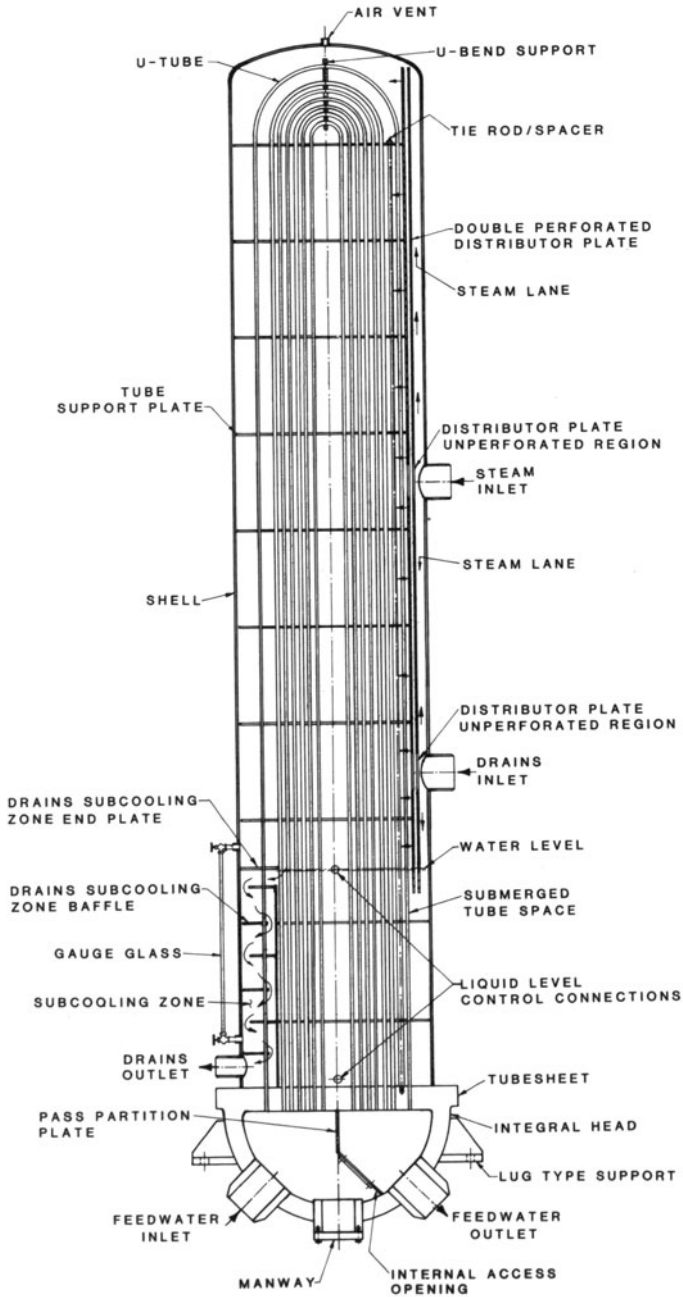


Fig. 1.7.3. Vertical feedwater heater with full length distributor: two-zone two-phase head down.

Added expense of fabrication, despite the distributor's merits, has limited its use in heat exchangers.

A cheaper, and somewhat less satisfactory alternative, is to use the so-called "impingement plate". In its simplest form, an impingement plate is a solid plate (usually of square or circular plane form) placed in the path of the impinging shellside stream (Fig. 1.7.4). The impingement plate is somewhat larger than the nozzle opening. An impingement plate actually reduces the bundle entrance area even though it protects the tubes directly underneath it. As a consequence the tubes just beyond the edge of the impingement plate (shown by darkened circles) may experience even higher flow. Despite its arguable usefulness in many applications, the impingement plate has been widely used in the industry. Industry standards have long recognized the destructive effects of unimpeded impingements of shellside fluid on the tube bundle. For example, the TEMA Standards [1.2.1] mandate impingement protection if the fluid is two phase or corrosive/erosive in nature. For other fluids the impingement protection requirement depends on the value of ρv^2 , where ρ is the local density of the shellside fluid and v is the nozzle line velocity. For non-corrosive, non-abrasive, single-phase fluids $\rho v^2 < 1500$; for a liquid at its boiling point and all other fluids, $\rho v^2 < 500$. If these inequalities are not satisfied, then TEMA mandates that impingement protection be provided. Standards for Feedwater Heaters [1.2.7] have similar empirical limits.

TEMA also places limits on the "shell entrance" and "bundle entrance" regions. The value of ρv^2 is required to be limited to 4000 in these areas. Shell entrance area is defined as the sum of frontal area A_F and lateral area A_L . Frontal area A_F is the flow area between the tubes within the projection of the nozzle bore. A_F is zero when a solid impingement plate is provided. A_L is the lateral (radial with respect to the nozzle axis) flow area available between the tube bundle and the shell. These areas are best calculated by making a bundle layout. However, if an impingement plate is present then A_L can be written in closed form, as shown below.

Circular Impingement Plate

The total lateral flow area, A_L , is given by

$$A_L = 4a \int_0^{\pi/2} [(r^2 - a^2 \sin^2 \theta)^{1/2} - h] d\theta \quad (1.7.1)$$

where a , h and r are impingement plate radius, plate height from shell centerline, and shell radius, respectively (Fig. 1.7.4). Integrating the above expression, and rearranging terms gives the required plate height h corresponding to a specified area A_L .

$$h = \frac{4ar E(m) - A_L}{2\pi a} \quad (1.7.2)$$

In the above expression $E(m)$ is the elliptic integral of the second kind, defined as

$$E(m) = \int_0^{\pi/2} (1 - m \sin^2 \theta)^{1/2} d\theta \tag{1.7.3}$$

where

$$m = \frac{a^2}{r^2} \tag{1.7.4}$$

$E(m)$ is tabulated as a function of m in mathematical handbooks. Figure 1.7.5 gives a plot of $E(m)$ as a function of a/r .

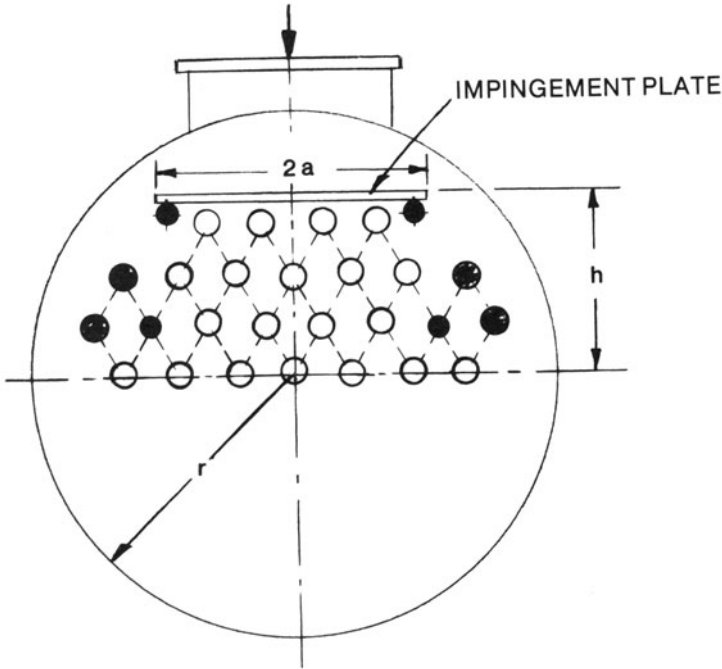


Fig. 1.7.4. Solid impingement plate.

Square Impingement Plate

The radial flow area A_L between the inside diameter of the shell at the nozzle I.D. and the impingement plate can be calculated using the above equations. However, the radial area available at the outer edge of the impingement plate may be smaller. The radial velocity vector is not normal to the surface of square cylinder formed by projecting the impingement plate to the inside surface of the shell except at the four lines of symmetry. The equivalent radial area is therefore

$$A_L = \int dA_L \cos\theta \tag{1.7.5}$$

where θ is the angle between the radial direction and normal to the surface

element dA_L . It can be shown [1.7.3] that this expression reduces to

$$A_L = 4a \left[\int_0^a \left[\frac{r^2 - y^2}{a^2 + y^2} \right]^{1/2} dy - h \int_0^a (a^2 + y^2)^{-1/2} dy \right] + 4a[(r^2 - a^2)^{1/2} - h] \int_0^a (a^2 + y^2)^{-1/2} dy \tag{1.7.6}$$

where $2a$ is equal to the side dimensions of the square impingement plate. Equation (1.7.6) yields

$$A_L = 4a \{ I + \ln(1 + \sqrt{2})[r^2 - a^2]^{1/2} - 2h \} \tag{1.7.7}$$

where

$$I = \int_0^a \left(\frac{r^2 - y^2}{a^2 + y^2} \right)^{1/2} dy \tag{1.7.8}$$

Figure 1.7.6 gives a plot of A_L/r^2 vs. h/r with a/r as the parameter.

An impingement plate is readily incorporated in so-called “no-tubes-in-window” designs without sacrificing any tubes in the bundle. In other designs, impingement plates require removal of tubes near the nozzle inlet. This has the effects of increasing shell diameter and cost of the hardware. The window space left out for impingement is also a path for internal flow bypass of the shellside fluid, which the thermal designer must contend with in development of the equipment design.

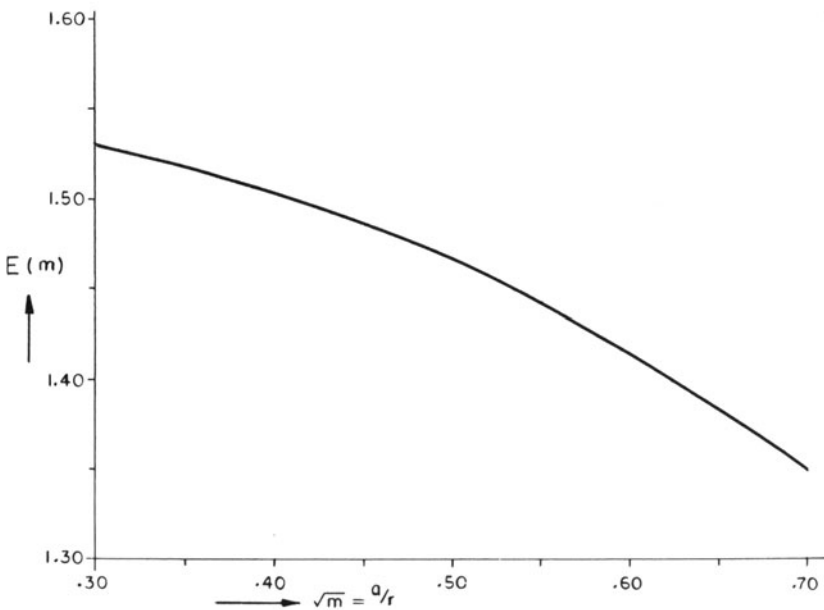


Fig. 1.7.5. $E(m)$ as a function of a/r .

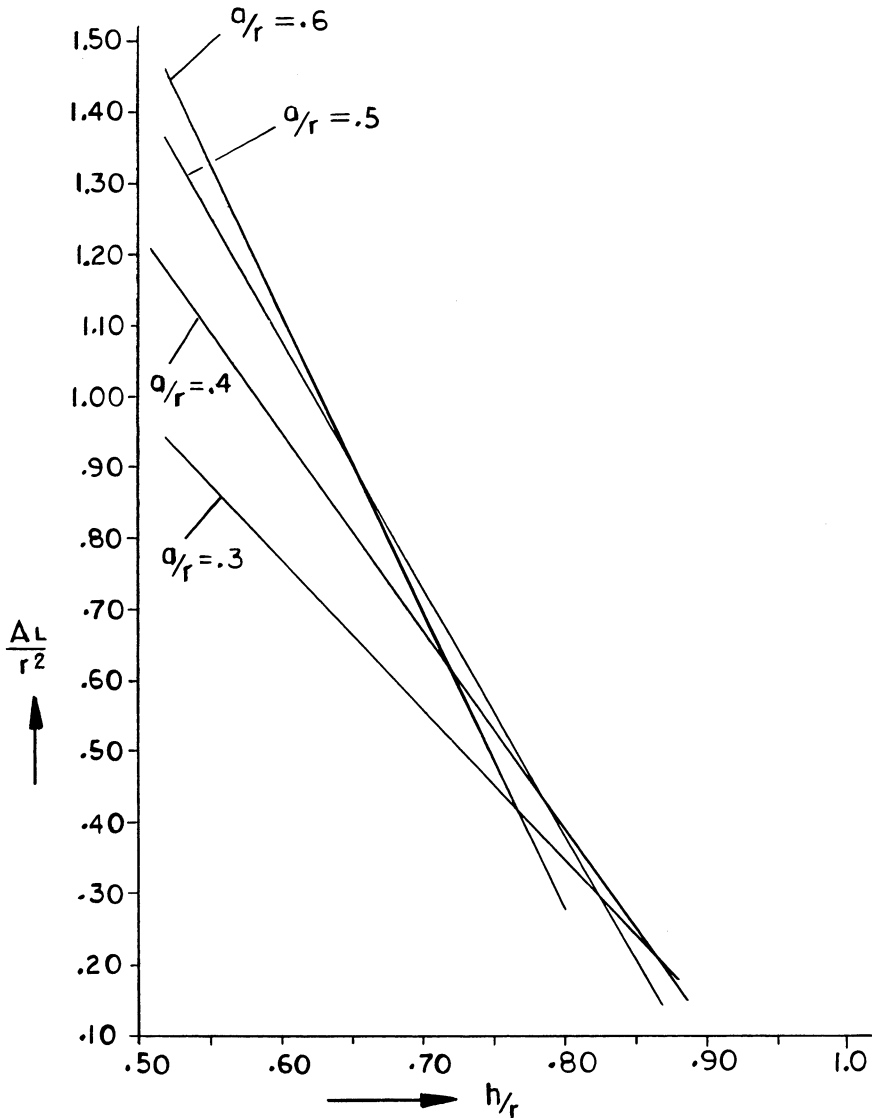


Fig. 1.7.6. Effective radial flow area for square impingement plate.

1.8 DESIGNING FOR THERMAL TRANSIENTS

Mechanical design of heat exchangers and pressure vessels typically involves determining the thickness of pressure parts for pressure loadings. The thickness of non-pressure parts such as baffles, tie rods, pass partition

plates, is determined by reference to the industry standards and the owner's Design Specification. The general trend in the industry is towards performing additional design checks for (mainly) local stresses at the vessel/nozzle interface due to transmitted loads from the interconnected piping and for stresses in the vessel due to postulated earthquake motions. Tall towers are also designed to withstand wind loads.

Safe and trouble-free operation of a heat exchanger depends to a large measure on the care and accuracy brought to bear on the Design Specification. A Design Specification which faithfully describes all significant operating conditions goes a long way towards ensuring reliable hardware. The most significant of the operating conditions are those involving unit start up and shutdown. Rapid fluctuation in the temperatures of the entering fluids is another source of potential trouble.

As will be discussed in Chapter 2, the stresses produced by temperature fluctuations are self-limiting in that failure from one thermal application is not to be expected. However, repeated cycling can cause the material to fail in fatigue. A notable exception to the above statement is the tube-to-tubesheet joint which, because of slenderness of the "leak path," may fail in even one application. The critical regions which behoove careful consideration of thermal transient conditions are:

(i) *Tube-to-tubesheet joint*: In fixed tubesheet heat exchangers, the tube-to-tubesheet joint loads can reach high values (Chapter 9). An expansion joint is sometimes incorporated to mitigate the effect of differential axial growth of the shell and tubes on the tube-to-tubesheet joint. In U-tube heat exchangers, the joint is not loaded as severely. Inner bends, however, can experience unacceptably high axial loads due to differential expansion between the two legs of the U. Multiple-tube pass fixed tubesheet heat exchangers, in general, warrant careful consideration of temperature change from pass to pass. The design standards base the calculations on *average* pass temperature. In reality, the loads in some tubes can be substantially higher.

(ii) *Tubesheet, shell, channel junction*: The tubesheet typically contains a perforated interior surrounded by a solid rim. The flow of tubeside fluid through the tubesheet coupled with the reduced metal mass of the perforated zone has the net effect of producing a temperature profile in the interior which is substantially different from the solid rim region. Variation in the temperature of the shellside fluid with time actuates changes in the metal temperature of the tubesheet. However, the perforated interior follows the fluid temperature variation much more closely than the outer rim due to the reduced thermal mass of the former. Different temperature change rates in the rim and in the interior of the tubesheet produce thermal stress variations.

The effect of pulsations in the tubeside fluid temperature is usually far more severe. The perforated interior follows the temperature of the tubeside fluid even more closely due to the extensive surface contact between the tubeside fluid and the tubesheet (over the lateral surface, and inside surface

of perforations). Thus the temperature ramps of the perforated region and the untubed region can be significantly different. The resulting pulsations in the stresses can cause fatigue failure of the metal in the perforated zone, or in the rim, depending on the geometric dimensions of the tubesheet. If the tubesheet is integrally welded to the channel and (or) the shell, then these junctions may emerge as the most vulnerable spots.

The remedy for the shellside transients is relatively simple. Placing a sacrificial liner plate on the shellside surface of the tubesheet would sufficiently insulate tubesheet metal from shellside fluid temperature ramps to alleviate fatigue concerns. Such a remedy is not readily applied to the channel side. An effective method is to make the rim as narrow as possible. A narrow rim is structurally less constraining to the interior. Moreover, it has less thermal capacitance. However, for reasons stated before, the rim for floating head construction can not be narrowed.

Where danger to the welded joints between the tubesheet and shell or channel exists due to thermal fatigue, consideration should be given to using a bolted joint instead. Alternatively, a radical procedure similar to the one illustrated by Fig. 1.8.1 may be used. Figure 1.8.1 shows the tubesheet-channel-shell joint for the heat exchanger of Photograph 1.e [1.8.1]. Here the tubesheet is made a segment of a spherical shell which introduces significant radial flexibility in the structure in the radial direction. The junction between the shell and the tubesheet also has a built-in expansion joint to reduce differential thermal expansion stresses. The “crotch” between the shell and the tubesheet further serves to produce a stagnant region with attendant low convective heat transfer coefficient. This further moderates the effect of shellside fluid transients.

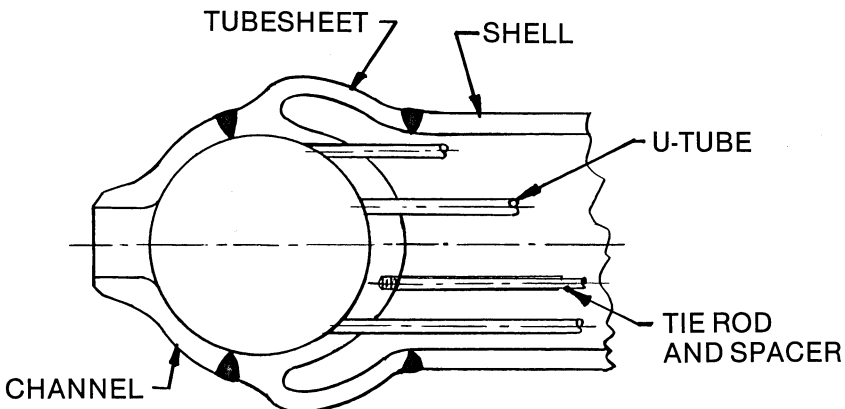


Fig. 1.8.1. Integral tubesheet for severe thermal transients.

(iii) *Flange joints*: Any region in the heat exchanger where significant metal mass is attached to thinner sections is a potential candidate for damage due to thermal transients. By virtue of their geometry, flanged

joints are prime locations for such problems. Use of a sacrificial liner sheet (thermal shield) is quite effective in such cases.

(iv) *Nozzle-shell/channel junctions*: The thermal transient problem in nozzle penetration locations arises from the following reason:

The sudden change in the geometric shape at the penetration produces high discontinuity stresses. Codes [1.8.2] and standards require that additional metal be added at the locations for reinforcement. This increases the local “thermal capacitance” of the shell. The flow velocity through the nozzle, on the other hand, is usually in the turbulent region. Therefore, any fluctuations in the fluid temperature changes the nozzle wall temperature much more rapidly than the shell wall temperature. The thermal stresses thus produced are magnified by the presence of the structural discontinuity.

Thermal sleeves have been used in combating the effects of nozzle thermal transients with success.

Except in certain simple axisymmetric situations, a proper analysis of thermal transients is only possible through a Finite Element Analysis procedure.* Despite widespread availability of Finite Element computer codes, such analyses have remained expensive to conduct. Consequently, many units which really require a thermal transient evaluation are designed without such analysis with predictable loss of reliability.

1.9 INTERDEPENDENCE OF THERMAL AND MECHANICAL DESIGN

Designers and fabricators of heat exchangers often treat thermal design and mechanical design as two discrete and separable functions. Such an approach runs the risk of producing “tunnel view” designs. The interaction between thermal and mechanical design considerations can be quite significant in some cases. A designer, alert to the mutual influence of mechanical and thermal designs, can often devise a superior design without incurring any additional hardware cost. Some examples given below illustrate the interdependence of thermal and mechanical designs.

(i) Thermal stresses in multiple-pass fixed tubesheet heat exchangers

It has been stated in Section 1.2 that thermal stresses in the tubes and in the shell are endemic to fixed tubesheet heat exchanger designs. In multiple-tube pass units, the thermal stresses are the highest in the tube bank associated with the inlet pass, and the lowest in the outlet pass. Arranging the tube passes such that the inlet pass is located in the central region of the tubesheet can alleviate axial tube thermal stresses and tube/tubesheet joint loads because of the local flexibility of the tubesheet. If the tubeside fluid is the heating medium then the tube thermal stresses will be generally compressive. We show in Chapter 16 that compressive axial stress lowers the

*The Finite Element Method is discussed briefly in the latter part of Chapter 10.

fundamental frequency of vibration of the tube, making it susceptible to flow-induced vibration at lower cross flow velocities. This reduction in the natural frequency can be counteracted by locating the inlet pass tube bank in the overlap region of the cross flow baffles. In the single segmental baffle construction, tubes in the overlap region have one-half of the span of those in the window region. Since the fundamental natural frequency of a tube is inversely proportional to the square of the unsupported span,* locating the most heavily loaded tubes in the overlap zone would secure them against flow-induced vibration. This arrangement can be accommodated in most shellside flow layouts without any loss in the indicators of the efficacy of heat transfer (such as the LMTD correction factor, or NTU).

Finally, since the shellside nozzle entry and exit regions have high associated velocities, the designer should arrange the tube pass partitions in such a manner that the tubes possessing lowest natural frequencies are located away from the inlet and outlet sectors.

(ii) Effect of flexing of the tubesheet

As discussed before, deflection of the tubesheet in unstayed designs (such as U-tube construction) can cause significant flow bypass. In Chapter 4 a method to quantify this bypass is given. However, if the shellside operating pressure exceeds the tubeside operating pressure ($p_s > p_t$), then the tubesheet would not flex away from the tubeside pass partition gasket ribs and the inter-pass leakage path would not develop. Although the assignment of flow streams to the shellside and tubeside is guided by a multitude of considerations, it is known that most designs are stream-symmetric; i.e., interchanging the two streams has no effect on the heat duty [1.9.1]. Thus, it may be feasible to eliminate tubeside interpass leakage by a suitable assignment of flow streams.

(iii) Effect of shell bypass stream on tube stress

Practical fabrication requires that the cross baffles be made slightly smaller than the shell to facilitate assembling of the tube bundle cage. This small baffle to shell diametral clearance provides a narrow annular cross section path through which a portion of the shellside fluid can bypass without any contact with the tube surface. This stream is referred to as the “E-stream” in the literature (refer to Section 16.10 for details). A large E-stream ensures that the shell metal temperature would approximate the shell fluid inlet temperature. On the other hand, a well mixed shellside flow (with non-existent E-stream) would produce shell metal temperatures close to the shellside fluid bulk temperature. In most cases, the former condition is undesirable because it produces higher axial tube load due to differential expansion between the shell and the tubes (Chapter 9).

*The reader is referred to Section 16.12 for a more comprehensive discussion of this matter.

(iv) Locating shellside nozzles in multiple pass heat exchangers

If we jump ahead for the moment and examine Fig. 4.1.1, we see a two-tube pass, one-shell pass heat exchanger. The shell inlet and outlet nozzles are located at the two extremities of the shell. We know from the heat transfer theory that switching the inlet and outlet nozzle locations has *negligible* effect on the heat duty. The effect of such a switch on the tubesheet stress field is not insignificant. The condition where the shell inlet is located near the tubesheet will produce the highest thermal gradient (Section 7.9) across the tubesheet. In units subject to thermal transients, and where tubesheet fatigue life is a concern, it is clearly preferable to locate the shell inlet nozzle at the far end.

(v) Split flow (TEMA Type G) shells

In many applications, a split flow shell design would produce a heat duty commensurate to an F-type shell. The split flow construction, however, may lead to a far less severe tube thermal stress field than the F-type shell. This fact should be explored in the design stage whenever the thermal stresses are high enough to impair equipment reliability.

The split flow design has the disadvantage of creating two nozzle penetrations at the same location in the shell. This may be unacceptable in certain cases where the nozzle loads on the shell are excessive and/or the shellside design pressure is very high. Fortunately, in many cases, displacing the nozzles in the axial direction, with respect to each other, can even augment the heat duty [1.9.2]!

The foregoing examples serve to illustrate the significance of an integrated approach to heat exchanger design which seeks to obtain the best symbiosis between thermal-hydraulic and structural considerations.

The full measure of interaction between mechanical and thermal designs is illustrated by considering a heat exchanger which performs condensation, and sensible cooling in vapor and liquid phases, all in the same shell. Exchangers of this type, used in power plants, are referred to as “feedwater heaters.” In the next section, we take up the design features of feedwater heaters to further elaborate on the preceding observations.

1.10 FEEDWATER HEATER DESIGN

Feedwater heaters are used in power generation plants to improve the thermodynamic efficiency of the Rankine cycle. The use of feedwater heaters increases the efficiency by as much as 50% in some power plants. As its name implies, the feedwater heater heats the boiler feedwater using the steam drawn from selected port locations in the steam turbine. The boiler feedwater is at a higher pressure than the heating steam, and it is nearly always the tubeside fluid. Most modern heaters are of U-tube construction. The heating steam may enter the heater in a superheated or saturated state. The steam is desuperheated, condensed and subcooled in the heat exchanger

before exiting the unit. Such an exchanger is referred to as a “three-zone” heater (Fig. 1.2.4). A “two-zone” heater may consist of desuperheating and condensing zones, or of condensing and subcooling zones. Since the heat transfer mechanisms of the three zones are quite different, it is frequently necessary to build each zone with its own “shroud”, and baffling scheme. Because of the diversity of the design imperatives in the three zones, the feedwater heater perhaps best epitomizes the interplay of the numerous factors governing heat exchanger design. We will briefly review some of the important considerations in the following:

(i) *Orientation*: Plant architect-engineers prefer to mount heat exchangers vertically because they take up less floor space. Conventional wisdom in power plant design holds that economizing in plant floor space minimizes the cost of building the plant. Equipment orientation, however, profoundly affects the heat transfer characteristics of exchangers involving phase change (e.g., condensation). In the case of feedwater heaters, the effect is even more far reaching. This is best explained after exposing the reader to the standard orientations; viz. (a) horizontal, (b) vertical, channel down, and (c) vertical, channel up.

The horizontal feedwater heater, equipped with a desuperheating zone and an integral drain cooler, is shown in Fig. 1.2.4. The tubeside inlet and outlet are arranged in such a manner that the feedwater temperature rise is countercurrent to the enthalpy loss of the heating medium. This requirement of countercurrency is a central requirement to the internal flow arrangement of the heater. The main design object in a heater is to elevate the temperature of the feedwater to the highest possible value. Whenever sensible heat transfer is involved, countercurrency is essential in achieving this objective.

The flow profiles in the condensing zone, however, are not as important from this viewpoint since the “Log Mean Temperature Correction Factor”—the best known index of performance—is unity (its maximum possible value) in this zone regardless of the flow arrangement. Therefore, the shell inlet nozzle in a heater containing a desuperheating zone must be located near the tubesheet. However, if the incoming steam is saturated and therefore undergoes no sensible cooling in the vapor state, then there is considerable latitude in locating the shell inlet nozzle. In order to promote even distribution of the saturated steam, designers prefer to locate the inlet nozzle near the mid-span, or more precisely at the “Thermal Centerline” of the heat exchanger. The “Thermal Centerline” [1.2.7, p. 6] divides the heater condensing surface into two parts producing equal heat duty. Figure 1.7.3 shows a vertical two-zone heater with mid-length steam entry. Erosion damage of the tubes due to impact of water droplets, entrained by the condensing steam, is the chief concern in the condensing zone. To avoid erosion induced tube wastage, designers should provide a large inlet plenum and flow distribution arrangement as discussed in Section 1.7.

The drains outlet nozzle must be located near the tubesheet to preserve countercurrency of flows, unless condensate subcooling is not performed in the unit.

Figure 1.10.1 shows a channel-down three-zone vertical feedwater heater. The integrity of the desuperheating shroud is very important in this type of construction, since intrusion of water from the inventory of water outside the desuperheating zone can severely harm the heat transfer rate in the desuperheating zone. Units which do not require a desuperheating zone must have a portion of the tube bank immersed in a relatively quiescent pool of water. This immersed tube surface is effectively lost to heat transfer.

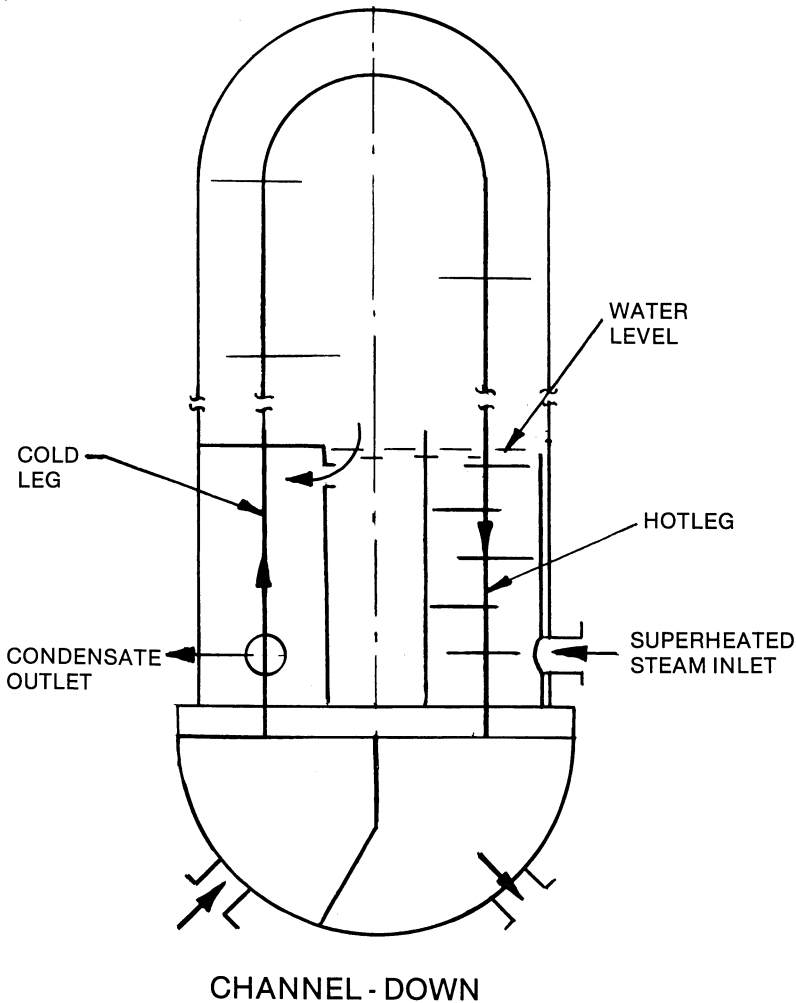


Fig. 1.10.1. Channel – down, three zone vertical feedwater heater.

The vertical channel-up heater (Fig. 1.10.2) does not suffer from this drawback. The water inventory is conveniently located in the U-bend region

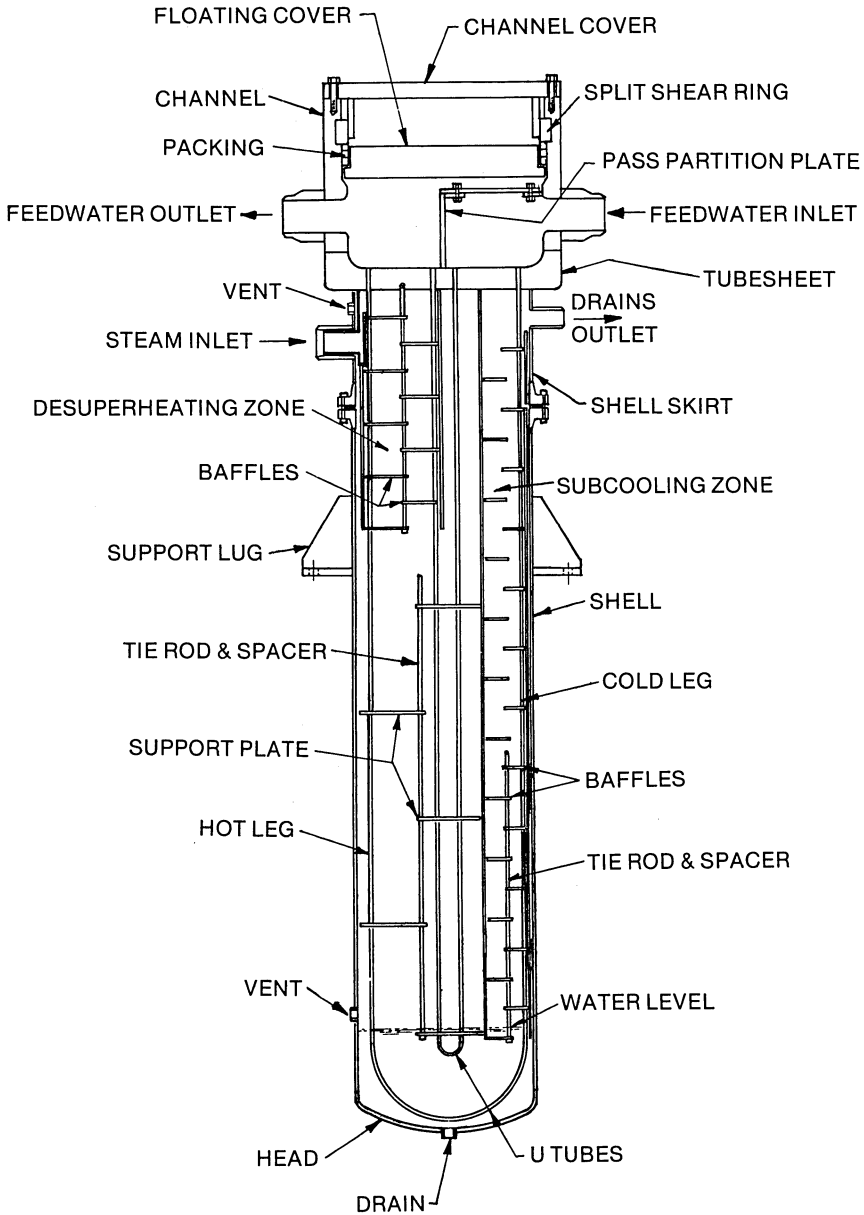


Fig. 1.10.2. Vertical feedwater heater three-zone two-pass channel up.

where high flow velocities are undesirable from a flow induced vibration standpoint (Chapter 16). The danger of flooding of the desuperheating zone does not exist. However, the piping must be routed to the top of the unit where the nozzle connections are located. For tube repair and cleaning purposes, a suitable well must be provided to remove the shell; alternatively, the header along with the tube bundle must be removed by raising from overhead. The channel-down unit lends itself to convenient shell removal from above.

Both vertical designs suffer from the drawback of providing too little space for condensate inventory. Since the steam consumption rate in the heater fluctuates with time, the rate of condensate formation can be quite rapid in heaters installed in the power generation plants used to “trim” the power supply to match demand. The drains removal rate from the heater depends on the instantaneous pressures in other connecting drain lines, and on the effectiveness of the drain level control valve. An inadequate inventory of condensate in the heater exposes the drain cooler to the hazard of steam intrusion should the level control not respond fast enough to rapid withdrawal of drains. The drop in the condensate level in a horizontal cooler is far more gradual since the bottom part of the entire shell length is available for condensate inventory. The control of condensate level in the heater is viewed as an important operational consideration in heater design. Most plant operators favor horizontal designs for this reason.

(ii) *Heater type*: Depending on the pressures of the steam and the feedwater, heaters are typified as (a) high pressure, (b) intermediate pressure, or (c) low pressure. The focus of mechanical and thermal design concerns is different depending on the heater type. In a high pressure heater, the pressure parts are quite thick. The most serious concern centers around the material failure due to thermal transients. There are numerous reported cases of tubesheet cracking in high pressure heaters [1.10.1].

Although present in all heater types, the danger of flashing of the condensate is particularly severe in low pressure heaters. Flashing of the condensate in the drain cooler is known to actuate rapid tube failure. Flashing can be caused by intrusion of steam into the drain cooler, by reheating of the condensate across the drain cooling shroud via conduction, or by a drop in the static pressure of the condensate. If the drop in static pressure, due to hydraulic losses or altitude change, is excessive, then the water temperature may exceed the coincident saturation temperature, resulting in flashing. The danger of flashing is particularly severe in channel-up designs where the condensate must “climb up” the drain cooler. The pressure-saturation temperature plots of water/steam in Figs. 1.10.3-4 illustrate the relative vulnerability of low pressure units to flashing. We note that the drop in saturation pressure corresponding to a two-degree drop in temperature is approximately 6 times in the 700-psi range compared to the 70-psi range. Therefore, the low pressure heater designer must consider the pressure-enthalpy variation of water in the drain cooler carefully.

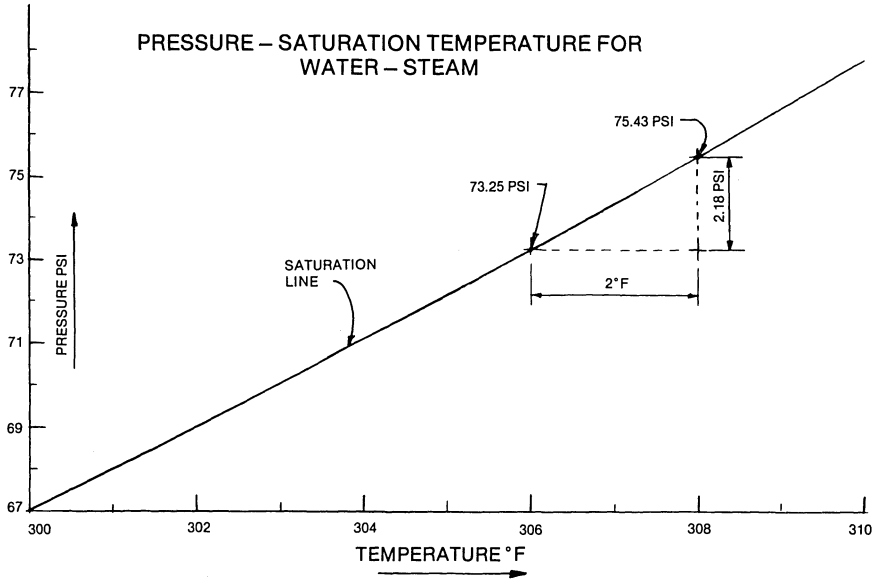


Fig. 1.10.3. Pressure-saturation temperature for water-steam.

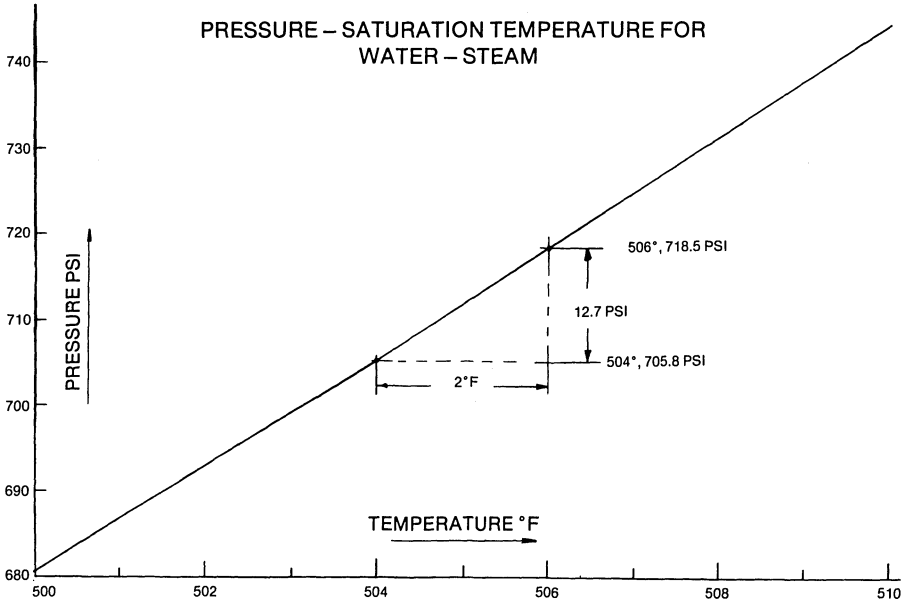


Fig. 1.10.4. Pressure-saturation-temperature for water-steam.

Efficient venting of non-condensibles is more vital in low pressure designs, since the heat transfer deterioration due to the presence of non-condensibles can be severe in the low pressure range of the steam.

The foregoing discussion is intended to provide an overview of the major issues and considerations in heater design. The reader is referred to the EPRI Workshop Proceedings [1.10.1] for a more detailed exposition of this subject. In the following chapters, all of our discussion of design methods are applicable to feedwater heaters.

1.11 CODES AND STANDARDS

A resumé of the codes and standards used in heat exchanger design and manufacturing is given in this section.

(i) TEMA Standards

The most widely used consensus standard for heat exchanger manufacture is the “Standards of Tubular Manufacturers Association” [1.2.1]; in short, the TEMA Standards. First published in 1941, this standard has evolved into something of an international document. Many countries have accorded it the status of their national codes. TEMA Standards specify three classes of construction, namely TEMA-R, TEMA-C and TEMA-B. The formulas for determining thicknesses are the same for all TEMA classes; however, empirical guidelines for sizing non-pressure part items vary. TEMA-R, which specifies the most rugged construction, is widely used in refinery service and nuclear power plant applications. TEMA-C and TEMA-B are used in other industries. TEMA-B has been promulgated as an American National Standard (ANSI B-78).

(ii) Heat Exchange Institute

Several groups of U.S. manufacturers under the umbrella name of the Heat Exchange Institute (HEI) publish standards for special classes of heat exchangers. HEI Standards for closed feedwater heaters [1.2.7] and surface condensers [1.2.8] are generally quoted for the design and manufacture of such equipment. The HEI standard for power plant heat exchangers, written during the heady days of commercial nuclear power, has not yet acquired the recognition and authority of its sister standards.

(iii) ASME Boiler and Pressure Vessel Codes

The ASME Code is published in eleven major sections. Section VIII, Div. 1 of the code, first published in 1914, is the premier document for pressure vessel design. This code contains formulas for determining the thickness of common pressure vessel shapes under pressure not exceeding 3000 psi. For higher pressures, complex shapes, or for conditions of service that warrant detailed stress analysis, the owner can specify Section VIII, Div. 2. Section III, Div. 1 of the code, presented in seven sub-sections, and one appendix is written specifically for pressure vessels in nuclear power plant service (Section III, Div. 2, pertains to reinforced concrete vessels).

In addition to the above, design codes, dealing with material specification (Section II), non-destructive examination (Section V), Welding Qualification (Section IX), and in-service inspection (Section XI) are required to complete the specification for fabrication and testing of pressure vessels. The ASME Codes have the force of law in the United States.

(iv) *ANSI Standards*

Several ANSI standards are frequently used to specify commercially available off-the-shelf items and standardized practice for welding, non-destructive testing, machining, etc.

- a. American Standard for Pipe Threads, ANSI B2.1.
- b. American Standard for Steel Pipe Flanges and Flanged Fittings, ANSI B16.5.
- c. American Standard for Steel Butt Welding Fittings, ANSI B16.9.
- d. American Standard for Steel Welded Fittings, ANSI B16.11.
- e. American Standard for Butt Welding Ends, ANSI B16.25.

(v) *“Manual of Steel Construction” by the American Institute of Steel Construction*

(vi) Surface Preparation and painting requirements are usually specified by the publication of the *“Structural Steel Painting Council.”*

Reference [1.11.1] reproduced in [1.11.2] contains a summary of the pressure vessel codes and standards used in European countries.

REFERENCES

- [1.2.1] “Standards of Tubular Exchanger Manufacturer’s Association,” 6th edition (1978).
- [1.2.2] “1982 Addenda to Standards of Tubular Exchanger Manufacturer’s Association” (1982).
- [1.2.3] “Boiler and Pressure Vessel Code, Section II, Part A,” The American Society of Mechanical Engineers; SA688, New York (1983).
- [1.2.4] Singh, K. P., “Predicting Flow Induced Vibrations in U-Bend Regions of Heat Exchangers: An Engineering Solution,” *Journal of the Franklin Institute*, Vol. 302, No. 2, pp. 195–205 (1976).
- [1.2.5] Singh, K. P., and Holtz, M., “On Thermal Expansion Induced Stresses in U-Bends of Shell and Tube Heat Exchanges,” *Trans. ASME, Journal of Engineering for Power*, Vol. 101, No. 4, pp. 643–649 (1979).
- [1.2.6] “Standards for Power Plant Heat Exchangers,” 1st edition, Heat Exchange Institute, Cleveland (1980).

- [1.2.7] "Standards for Closed Feedwater Heaters," 3rd edition, Heat Exchange Institute (1979).
- [1.2.8] "Standard for Surface Condensers," 7th edition, Heat Exchanger Institute (1978).
- [1.7.1] Ramamurthy, A. S., and Bhaskaran, P., "Velocity Exponent for Erosion and Noise Due to Cavitation," *Journal of Fluids Engineering*, Vol. 101, pp. 69-75 (1979).
- [1.7.2] McDonald, A. T., and Fox, R. W., "An Experimental Investigation of the Incompressible flow in Conical Diffusers," *Inter. J. Mechanical Science*, Vol. 8, No. 2, pp. 125-139 (1966).
- [1.7.3] Singh, K. P., "How to Locate Impingement Plates in Tubular Heat Exchangers," *Hydrocarbon Processing*, pp 147-149, October 1974.
- [1.8.1] Holtz, M., Singh, K. P., and Soler, A. I., "Heat Exchanger for Withstanding Cyclic Changes in Temperature," U.S. Patent #4,207,944 (1980).
- [1.8.2] "Boiler and Pressure Vessel Code, Section VIII, Div. 1," The American Society of Mechanical Engineers, New York (1983).
- [1.9.1] Singh, K. P., "On the Necessary Criteria for Stream-Symmetric Tubular Heat Exchanger Geometries," *Heat Transfer Engineering*, Vol. 3, No. 1 (1981).
- [1.9.2] Singh, K. P., and Holtz, M. J., "Generalization of the Split Flow Heat Exchanger Geometry for Enhanced Heat Transfer," AIChE Symposium Series No. 189, Vol. 75, pp. 219-226 (1979).
- [1.10.1] "Feedwater Heater-Workshop Proceedings," Electric Power Research Institute, WS-78-123, Palo Alto, California (1979).
- [1.11.1] Dallora, F., "European Pressure Vessel Codes," *Hydrocarbon Processing*, Vol. 50, No. 6, pp. 93-96 (June 1971).
- [1.11.2] Mahajan, K. K., "Design of Process Equipment," Pressure Vessel Handbook Publishing Company, Tulsa, Oklahoma, (1979).

APPENDIX 1.A*

TYPICAL SHELL AND CHANNEL ARRANGEMENTS AND EXCHANGER PARTS IDENTIFICATION

1.A.1 SCOPE

This appendix provides a detailed expression for describing the construction of a heat exchanger in accordance with the notation of the Heat Exchange Institute.

*This appendix is reproduced with minor changes with the courtesy of Heat Exchange Institute, Cleveland, Ohio.

1.A.2 GENERAL EXPRESSION

$$VWS_jYZ > V^1 W^2 S_j^3 Y^4 Z^5$$

This expression breaks down as follows:

- Term 1: V represents the front tube side closure
- Term 2: W represents the front tubesheet arrangement
- Term 3: S_j represents the shell side arrangement
- Term 4: Y represents the rear tubesheet arrangement
- Term 5: Z represents the rear tube side closure

1.A.3 PARAMETERS

The parameters for each term are described below:

1.A.3.1 Term 1: V (See Fig. 1.A.1)

- $V = B$ for an integral channel cover (Bonnet)
- $= C$ for a bolted channel cover
- $= R$ for a channel reducer

1.A.3.2 Term 2: W (See Fig. 1.A.2)

- $W = 1$ for a tubesheet which is gasketed (bolted) on both sides
- $= 2$ for a tubesheet which is integral (welded) on the tube side and gasketed (bolted) on the shell side
- $= 3$ for a tubesheet which is gasketed (bolted) on the tube side and integral (welded) on the shell side
- $= 4$ for a tubesheet which is integral (welded) on both sides

1.A.3.3 Term 3: S_j (See Fig. 1.A.3)

- S represents the shell
 - Subscript j represents the shell side arrangement
 - $j = 1$ for a one-pass shell
 - $= 2$ for a two-pass shell, etc.
 - $= d$ for a divided-flow shell
 - $= k$ for a kettle type
 - $= s$ for a splitflow shell
- If the exchanger contains a one-pass shell j need not be given.

1.A.3.4 Term 4: Y (see Figs. 1.A.2 and 1.A.4)

- $Y = 1, 2, 3, 4$ for the tubesheet arrangements described in Paragraph 1.A.3.2 above.
- $= 5$ for a tubesheet used with a pull-through floating head.
- $= 6$ for a tubesheet used with a floating head with a backing ring

- = 7 for a tubesheet used with an outside packed floating head
- = 8 for a tubesheet used with a packed floating tubesheet

1.A.3.5 Term 5: Z (See Figs. 1.A.1, 1.A.4, and 1.A.5)

- Z = B, C, R for the tube side closures described in Paragraph A.3.1 above.
- = F for a floating head
- = U for U-tubes

1.A.4 PARTS LIST

- | | |
|---|---------------------------------------|
| 1. Bolted Channel Cover | 21. Floating Head Flange |
| 2. Channel Cover Flange | 22. Floating Head |
| 3. Channel Cylinder | 23. Floating Head Split Backing Ring |
| 4. Integral Channel Head (Bonnet) | 24. Floating Head Gasket |
| 5. Channel Reducer | 25. Shell Rear Flange |
| 6. Channel Nozzle (Flanged or Weld End) | 26. Shell Cover Flange |
| 7. Channel Cover Gasket | 27. Shell Cover |
| 8. Channel Tubesheet Flange | 28. Shell Rear Gasket |
| 9. Stationary Tubesheet | 29. Packed Floating Head Cylinder |
| 10. Shell Tubesheet Flange | 30. Packed Floating Head Flange |
| 11. Channel Tubesheet Gasket | 31. Split Shear Ring |
| 12. Shell Tubesheet Gasket | 32. Packed Floating Head Cover |
| 13. Shell Cylinder | 33. Packed Floating Head Cover Gasket |
| 14. Shell Longitudinal Baffle | 34. Channel Packing Flange |
| 15. Shell Nozzle (Flanged or Weld End) | 35. Shell Packing Flange |
| 16. Shell Front Cylinder | 36. Packing Gland |
| 17. Shell Front Reducer | 37. Packing |
| 18. Shell Rear Reducer | 38. Lantern Ring |
| 19. Shell Rear Cylinder | 39. Tubes |
| 20. Floating Tubesheet | |

These parts are identified in Figs. 1.A.1-1.A.5, wherein the notation scheme is also illustrated.

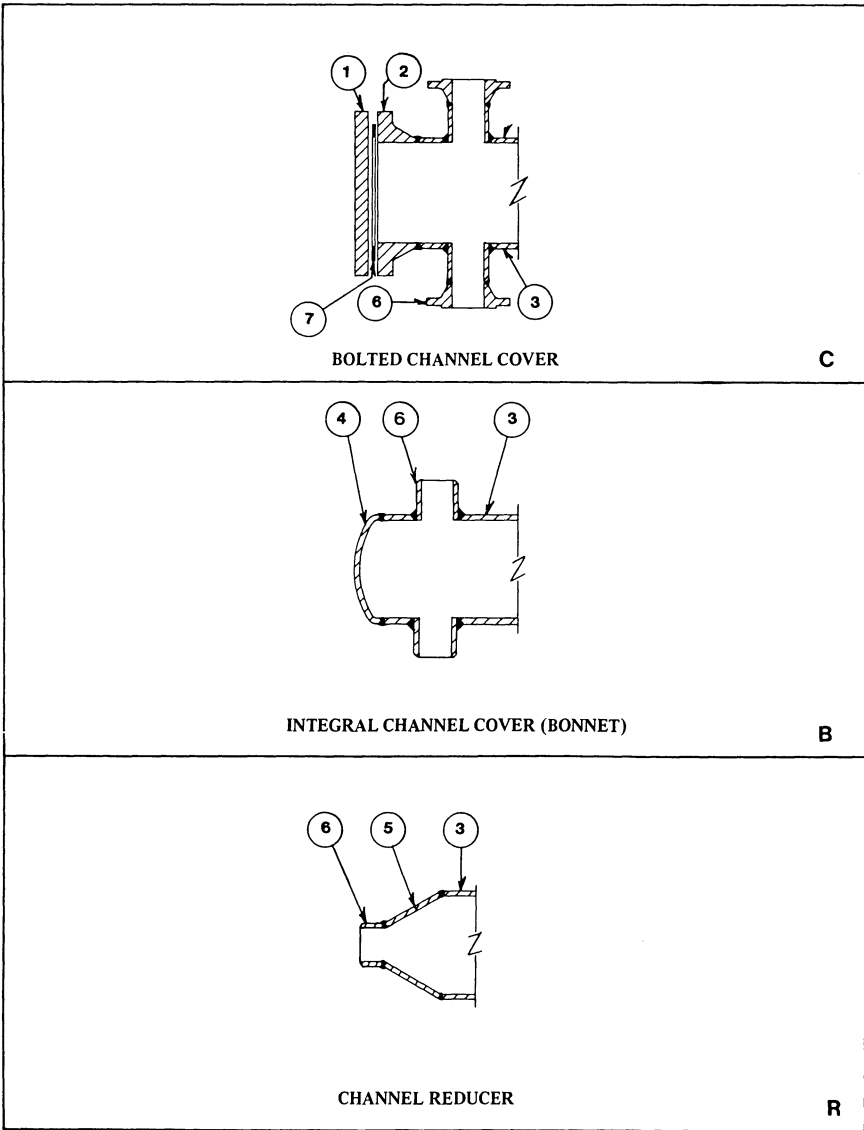


Fig. 1.A.1. Tube side closures (front and rear).

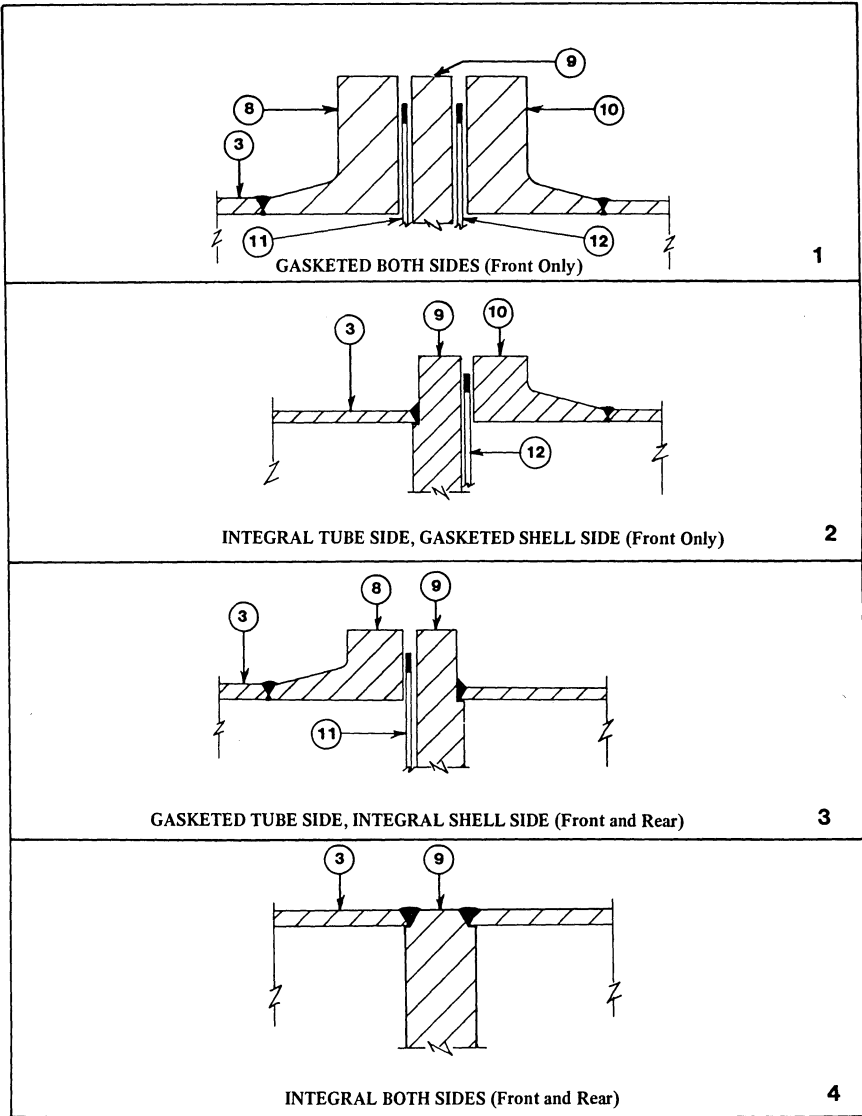


Fig. 1.A.2. Stationary tubesheet arrangements.

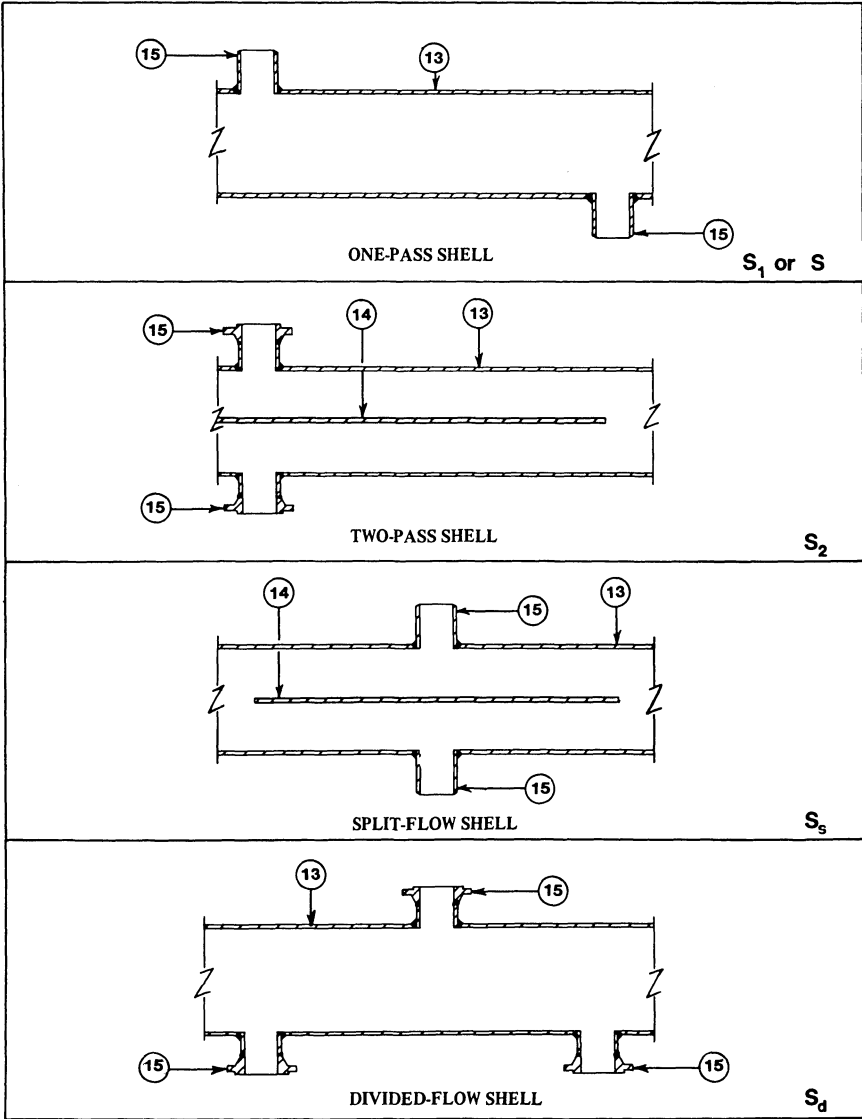


Fig. 1.A.3. Shell side arrangements.

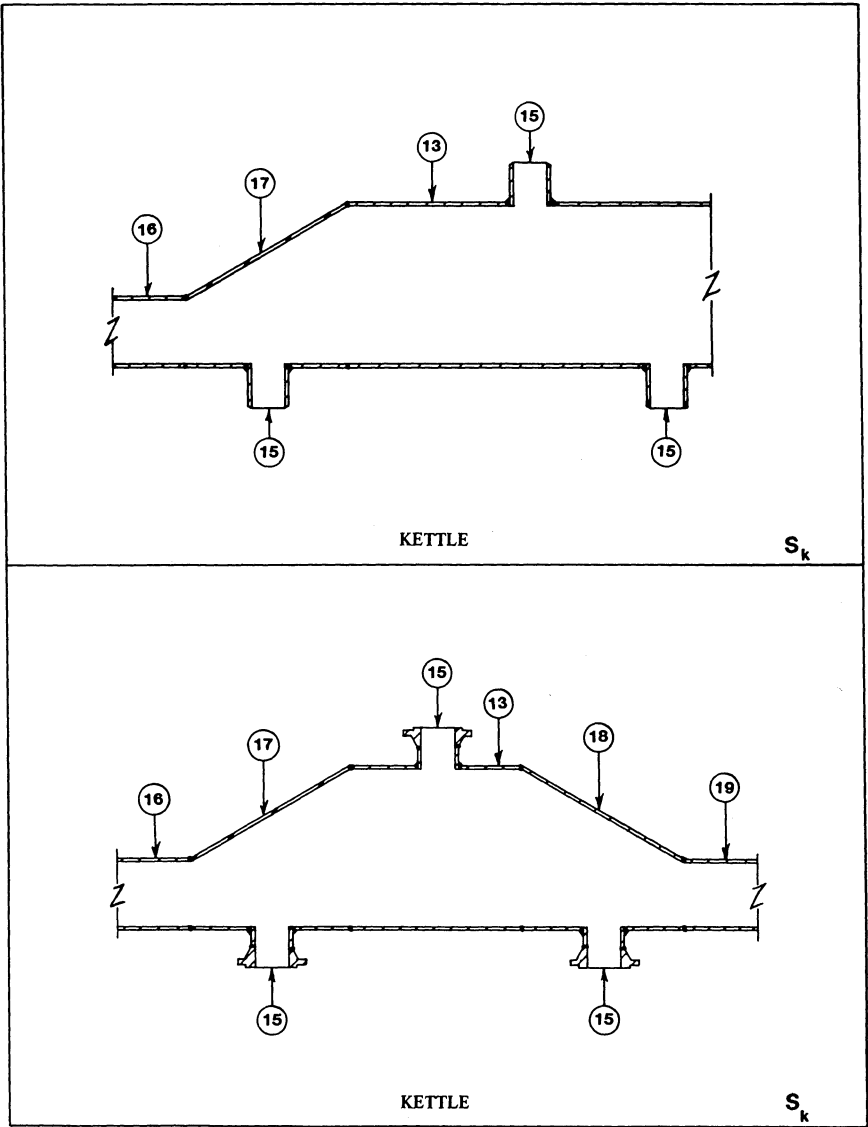


Fig. 1.A.3 (cont'd.). Shell side arrangements.

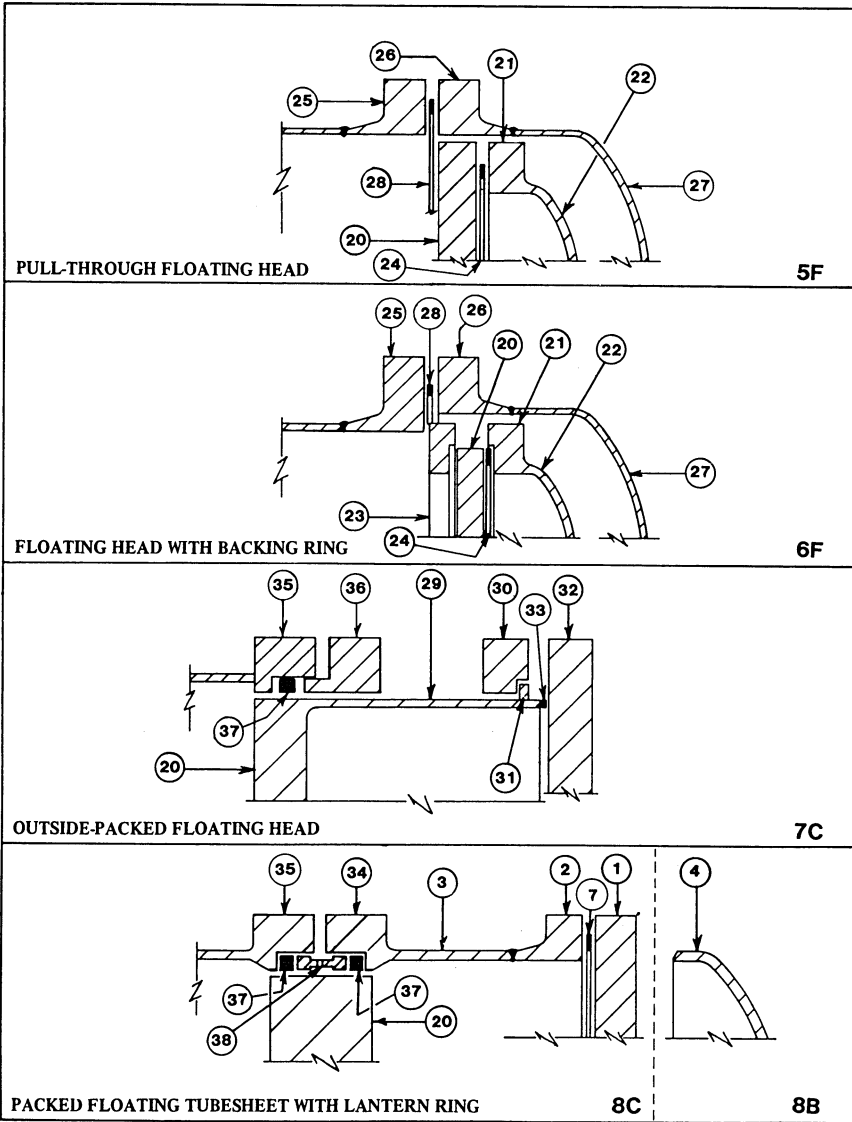


Fig. 1.A.4. Floating head and tubesheet arrangements (rear only).

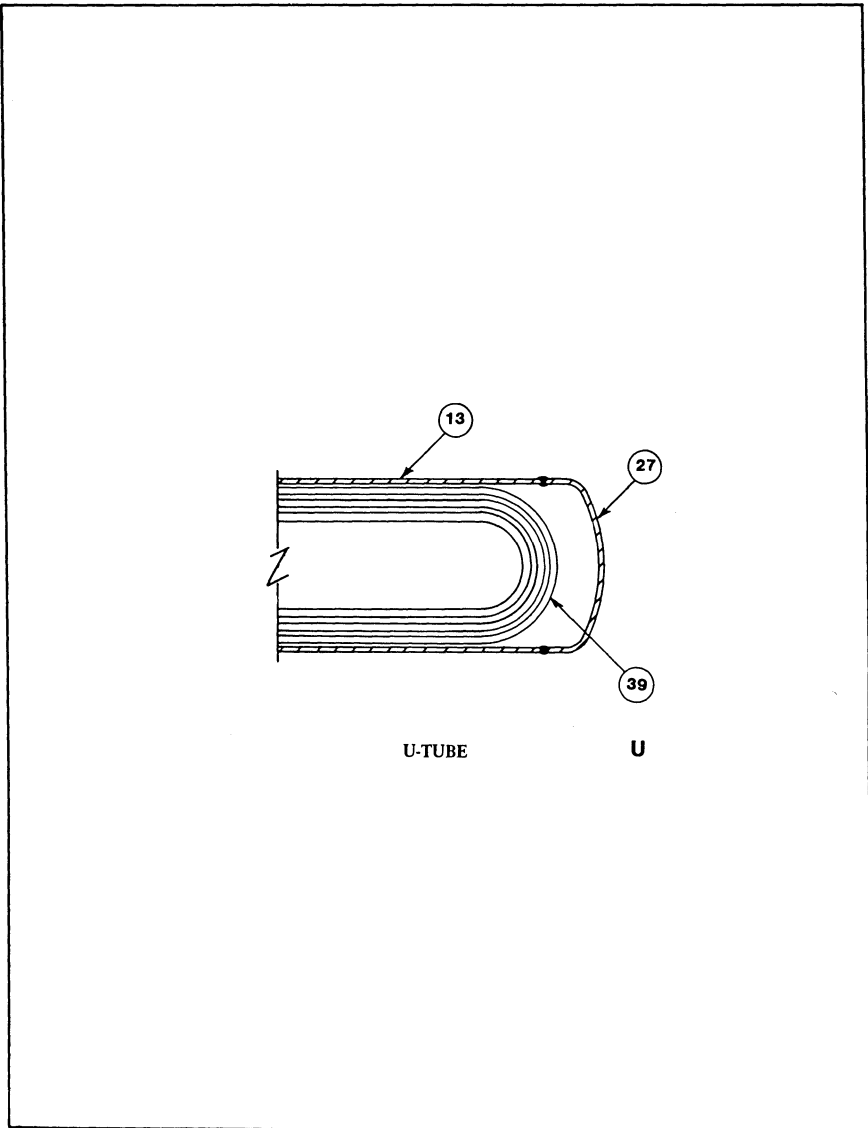


Fig. 1.A.5. U-Tube arrangement (rear only).

2. STRESS CATEGORIES

2.1 INTRODUCTION

In a general three-dimensional continuum, the state of stress at any material point is characterized by six components of the stress tensor.* With reference to a set of orthogonal axes, three of these stress components are normal stresses and the remaining three are shear stresses. Linear theory of elasticity shows us that by suitably choosing the coordinate axes, the shear stress components can be made to vanish, and the state of stress can be defined solely in terms of the three normal stresses, referred to as “principal stresses”. The corresponding coordinate axes are denoted as principal axes, and the planes formed by them are called principal planes.

In the evaluation of the stress field in heat exchangers and pressure vessels the problem is considerably simplified. Nearly all pressure retaining members in a heat exchanger are surfaces of revolution. The primary mechanical loading is pressure loading which is spatially uniform. With little accuracy loss, we can assume that the meridional, tangential, and through-thickness directions are principal directions. Since the thickness of a pressure vessel is small compared to its other characteristic dimensions, it is customary to view the major components of the stress distribution through the thickness as consisting of an “average quantity” plus a “linearly varying quantity”. Qualification of a pressure part is then made by comparing these quantities with specified stress limits. The reason for this approach is best understood by considering the deformation of a “beam type” structure beyond the elastic limit assuming a material stress-strain curve similar to that given in Fig. 2.1.1.

2.2 BEAM STRIP ANALOGY

We consider a long strip of unit width and thickness t . If the strip is subjected to an axial tensile load N , distributed uniformly over its cross section, then the state of uniaxial stress in the strip is defined by

$$\sigma = \frac{N}{t} \quad (2.2.1)$$

If N is allowed to increase, the value of the axial tensile stress σ rises in

*In exceptional cases involving body moments due to effects such as magnetism, nine components of the stress tensor are required to define the state of stress.

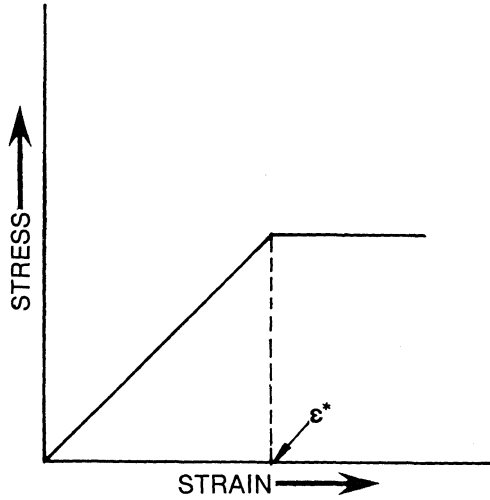


Fig. 2.1.1. Stress-strain curve for an elastic perfectly plastic material.

direct proportion to N until the yield strength of the material is reached. The load $N = N_y$, corresponding to the material yield strength σ_y , is the maximum load that the strip can withstand. An infinitesimally small increase in N beyond N_y will cause the strain to increase without limit, resulting in failure.

Next, we consider bending of this strip by two equal and opposite couples M applied at the two ends (Fig. 2.2.1a). From equilibrium, the moment at all locations is M . Assuming that plane sections remain plane (classical beam flexure theory) the longitudinal strain at a distance y from the centroidal axis is

$$\epsilon = \frac{y}{R}; |y| \leq t/2 \quad (2.2.2)$$

and

$$\epsilon_{\max} = \pm t/2R \text{ at } y = \pm t/2 \quad (2.2.3)$$

R is the radius of the arc of the centroidal plane of the deflected strip. If ϵ_{\max} is less than ϵ^* (Fig. 2.1.1) then the corresponding stress distribution is also linear, given by

$$\sigma = \frac{Ey}{R} \quad (2.2.4)$$

and equilibrium of the cross section yields

$$M = \int_{-t/2}^{t/2} \sigma y \, dy = \frac{Et^3}{12R} \quad (2.2.5)$$

Both strain and stress distributions are linear. From Eqs. (2.2.3) and (2.2.5), we have

$$\epsilon_{\max} = \frac{6M}{Et^2} \quad (2.2.6)$$

As M is increased, ϵ_{\max} increases, and the general shape of the through-thickness strain and stress distribution, resembles Fig. 2.2.1 (b) until ϵ_{\max} exceeds ϵ^* . When ϵ_{\max} reaches ϵ^* , the corresponding moment is

$$M_e = \frac{Et^2}{6} \epsilon^* \quad (2.2.7)$$

From the stress-strain curve we have

$$\begin{aligned} \sigma &= E\epsilon \text{ if } \epsilon \leq \epsilon^* \\ &= E\epsilon^* \text{ if } \epsilon > \epsilon^* \end{aligned} \quad (2.2.8)$$

Therefore, when the strain at the outer fibers reaches the elastic limit, any further increase in the moment results in the stress distribution of the shape shown in Fig. 2.2.1. (c). Notice the strain distribution still has to follow Eq. (2.2.2). As the moment is increased further, the flat portion of the stress diagram propagates inwards until, in the limit:

$$\begin{aligned} \sigma &= E\epsilon^* \text{ for } t/2 \geq y \geq 0 \\ &= -E\epsilon^* \text{ for } -t/2 \leq y \leq 0 \end{aligned} \quad (2.2.9)$$

At this point the external moment balanced by the internal stress distribution is:

$$M_p = E\epsilon^* \frac{t^2}{4} \quad (2.2.10)$$

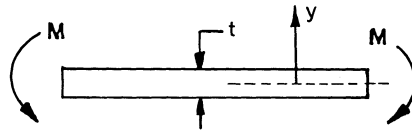
Comparing Eqs. (2.2.7) and (2.2.10) we observe that:

$$M_p = 1.5M_e \quad (2.2.11)$$

The moment M_p supported by a fully plastic rectangular section is 1.5 times the moment supported by the section when only the outer fibers reach the elastic limit. Since any attempt to increase M past M_p results in unlimited cross section rotation, M_p is the maximum moment that the beam strip can withstand. Thus, we conclude that for an elastic-perfectly plastic material that:

- The collapse axial force under a pure tension or compression load corresponds to the point when the axial stresses reach the yield point of the material.
- The collapse moment is $1\frac{1}{2}$ times the moment corresponding to which the maximum fiber stress reaches the yield point for the section of the strip considered.

Therefore it stands to reason that if the limit on the uniform stress is σ_0 , then the corresponding limit on a purely flexural stress should be $1.5 \sigma_0$. In reality, most materials workharden when strained beyond their elastic range, which makes the maximum moment that can be supported greater than $1.5 M_e$.



(a) STRIP UNDER END COUPLES

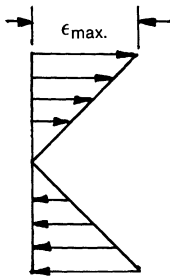
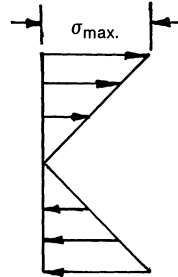
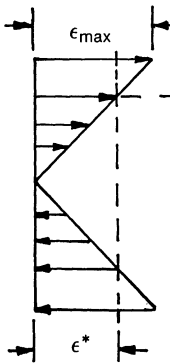
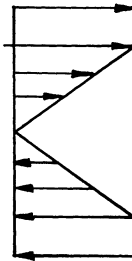
(b) STRAIN DISTRIBUTION
($\epsilon_{\max.} < \epsilon^*$)(b) STRESS DISTRIBUTION
($\epsilon_{\max.} < \epsilon^*$)(c) STRAIN DISTRIBUTION
($\epsilon_{\max.} > \epsilon^*$)(c) STRESS DISTRIBUTION
($\epsilon_{\max.} > \epsilon^*$)

Fig. 2.2.1. Pure bending of a beam strip.

2.3 PRIMARY AND SECONDARY STRESS

Stresses in pressure vessels can be divided into two broad categories: (i) primary; and (ii) secondary stress.

An essential attribute of a primary stress is that it is not self-limiting. We observed in the preceding section, with reference to an uniaxially loaded strip, that the strain grows indefinitely when the axial load reaches the value to produce the yield strain. If the material workhardens, then exceeding the yield point strain will not cause total collapse, but significant deformation would occur under small increases in applied force.

Primary stresses are caused by externally applied mechanical loads and are required to be in equilibrium with the external loads. Secondary stresses, on the other hand, arise solely to satisfy compatibility and are self-limiting in nature. They are not required to satisfy equilibrium. To illustrate, let us consider a bar of unit cross-sectional area and length l held between two rigid platens.

If the temperature of the bar is raised by an amount T , then the bar, in absence of the platens, would grow by an amount

$$\delta = \alpha T l \quad (2.3.1)$$

where α is the linear coefficient of expansion of the bar material. Since the platens are present, displacement compatibility requires that the rigid platens exert an axial force on the bar to compress it by the amount δ , producing a compressive strain $\epsilon = -\alpha T$. If the bar material follows the stress-strain curve of Fig. 2.1.1, and if $\epsilon > \epsilon^*$, then the bar will experience compressive yielding and develop an axial compressive force $N_y = E \epsilon^*$. ϵ can be permitted to become quite large compared to ϵ^* , but it is clear that no unbounded deformation results even though the yield load is reached. If, on the other hand, the load N_y was induced by a mechanical action, any attempt to load beyond N_y induces unbounded deformation.

In the above discussion we have tacitly assumed that the material is sufficiently ductile so that plastic strain can be many times the elastic limit strain without causing failure. The concept of primary and secondary loads is not meaningful in brittle materials.

The above example indicates that temperature differences in a structure produce secondary stresses. Another source of secondary stresses is the geometry of the structure itself. A simple example to illustrate this fact is shown in Fig. 2.3.1. Two shells of unequal sections are welded such that their midsurfaces are coaxial. When pressure is applied to the shell, the hoop stress and radial deflection are greater in the thinner shell as compared to the thicker shell, causing a mismatch at the girth seam. Thus there is a tendency for the material to try to separate at the girth seam. A structural geometry change which produces a mismatch of this nature is called a "gross structural discontinuity". Since the two shells cannot separate from each other, the deflection and slope at the weld seam must match. This induces a discontinuity moment M_0 and shear Q_0 . These discontinuity loads produce additional membrane (through-thickness) and bending stresses in the two shell segments which attenuate rapidly along the axes of the shells. Strictly speaking, all of the discontinuity stresses are generated to satisfy internal compatibility and therefore should be classified as secondary stress.

However, high membrane stresses distributed over the entire circumference and cross section, even though localized in the axial direction and self-limiting in nature, are a cause of concern. Design codes [2.3.1] place them in a special category of “local membrane stress”, and prescribe special limits on their permissible magnitude. Any discontinuity bending stresses, however, are treated as “secondary stresses”.

Further subdivisions among primary and secondary stresses are made by considering the degree of threat that a particular stress type poses to the pressure vessel. In the next section, the commonly used classification in the pressure vessel industry is described and explained with the aid of examples.

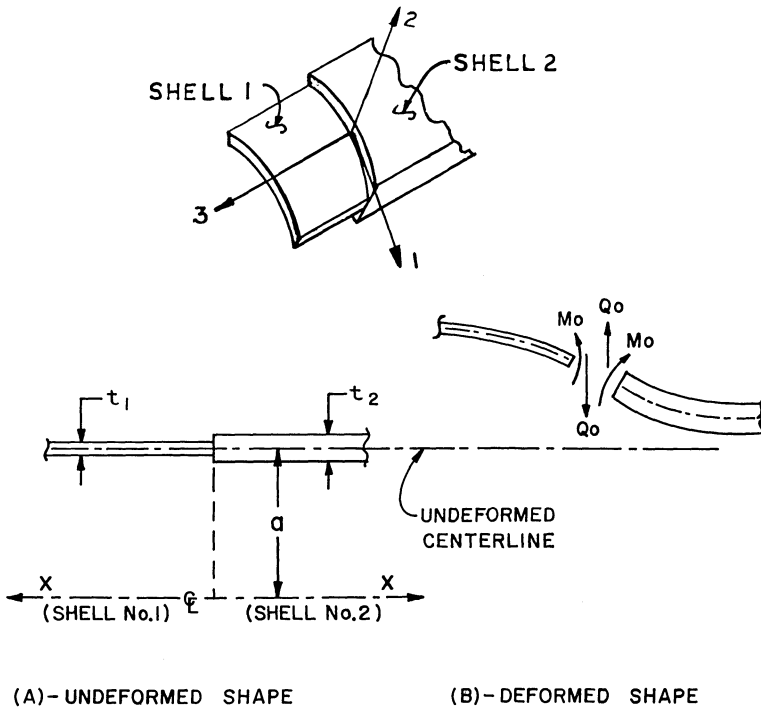


Fig. 2.3.1. Cylindrical shell under internal pressure.

2.4 STRESS CLASSIFICATION

In the design codes, stresses are classified into five types, namely

- (i) primary membrane stress, P_m
- (ii) primary bending stress, P_b
- (iii) local membrane stress, P_L
- (iv) secondary stress, Q
- (v) peak stress, F

(i) Primary Membrane Stress

The component of primary stress that is obtained by averaging the stress distribution through the thickness of the pressure vessel is referred to as the primary membrane stress. It is the most significant stress type. Design codes limit its value to the specified allowable material stress. An essential attribute of a primary membrane stress is that if the yield point is reached, causing the material to yield, a redistribution of stresses in the structure does not occur.

For example, let us consider a thick cylindrical shell of inner radius r_1 and outer radius r_2 , under internal pressure. The Lamé formulas [2.4.1] give the radial stress σ_r and tangential stress σ_t as a function of radius:

$$\sigma_t = \frac{pr_1^2}{r_2^2 - r_1^2} \left(\frac{r_2^2}{r^2} + 1 \right) \quad (2.4.1)$$

$$\sigma_r = \frac{-pr_1^2}{r_2^2 - r_1^2} \left(\frac{r_2^2}{r^2} - 1 \right) \quad (2.4.2)$$

where positive value of a stress means that it is tensile. The average value of σ_t , σ_{tm} , is obtained by integrating across the thickness of the vessel:

$$\sigma_{tm} = \frac{1}{(r_2 - r_1)} \int_{r_1}^{r_2} \sigma_t dr = \frac{pr_1}{r_2 - r_1} \quad (2.4.3)$$

We note that the expression for σ_{tm} derived above can be directly obtained by considering the overall equilibrium of a sector of the shell. This expression does not change even if plastic deformation occurs.

The radial stress varies from $-p$ at the inside surface to 0 at the outside surface. Strictly speaking, its average value across the thickness of the vessel is given by:

$$\sigma_{rm} = \frac{1}{\pi(r_2^2 - r_1^2)} \int_{r_1}^{r_2} 2\pi\sigma_r r dr \quad (2.4.4)$$

However, σ_{rm} is usually taken as the arithmetic mean of its value at $r=r_1$ and $r=r_2$; i.e., $\sigma_{rm} = -0.5 p$.

One important category of primary membrane stress arises in a heat exchanger or pressure vessel due to beam bending of the shell. Stresses are induced when the heat exchanger or pressure vessel is subject to external loadings which cause the shell to flex as a beam-type structure. The stresses vary across the entire cross section of the shell, with the entire thickness of the shell circumference located farthest from the neutral axis experiencing the maximum flexural stress. The stress is essentially constant through the shell thickness, and hence is considered as a membrane stress. It is arguable whether this stress should be treated as a primary membrane stress, since its maximum value is rather localized. Design codes [2.3.1], however, adopt the conservative approach and label this stress induced by gross bending as a primary membrane stress in the shell wall.

(ii) Primary Bending Stress

Primary bending stress is produced in certain regions of a pressure vessel to resist externally applied loads. In contrast to a cylindrical shell, certain structural shapes cannot resist external loadings without bending. The most notable example is the case of a flat cover bolted to a flange with a raised face gasket in such a manner that the end of the cover simulates a simple support. The bending stress in the cover, developed due to lateral pressure, reaches its maximum value at the outer fiber in the center of the cover:

$$\sigma_r = \sigma_t = \frac{3(3 + \nu)}{8} \frac{p a^2}{t^2} \quad (2.4.5)$$

where ν is the Poisson's ratio, p is the lateral pressure, t is the cover thickness and a is the cover radius. As discussed in the preceding section, since this stress varies linearly across the thickness, the metal is not in the plastic range except at the outer fiber when $\sigma_r = \sigma_t =$ yield stress for the material. As a result, the cover can support additional loading after the outer fibers have reached the yield point. For this reason, in some codes [2.3.1] the maximum allowable primary bending stress limit is set higher than the primary membrane stress limit. The formula for cover thickness in one of the most widely used pressure vessel codes [2.4.2] is, however, based on the primary bending stress being set equal to the material allowable stress.

Some other cases of primary bending stress are:

a. Bending stress in the crown of a torispherical head (Chapter 13) due to internal pressure.

b. Bending stress in the tubesheets averaged across the ligament. Since the holes in the tubesheet of heat exchangers are closely spaced, the overall plate-type bending stress varies linearly through the thickness of the tubesheet, but varies sharply across the ligament width due to stress intensification effects. Averaging the stress across the ligament width incorporates the integrated effect of the presence of perforations. Therefore, this stress is in the nature of a primary bending stress.

c. Bending stress in the cover (integrally welded to a shell) produced due to edge restraint (gross structural discontinuity). The edge discontinuity moment and shear produce a bending stress throughout the cover. Normally, if this edge moment is not counted on to satisfy the primary bending stress limit in the cover in the central region then the developed edge stress is classified as secondary. However, if the developed moment helps to reduce the central region stress, then the edge stress must be considered as primary. The rationale behind this dual classification is appreciated by recognizing that the bending stresses arising due to discontinuity reactions in shells are classified as secondary stresses and therefore, subject to higher stress limits. Consequently, if the secondary stresses reach values above yield, some plastic deformation in the shell edge occurs, diminishing the edge restraint applied by the shell on the cover. Satisfaction of the primary bending stress

limit in the central region of cover should not be dependent on this uncertain edge counteractive moment. If the edge restraint moment is counted on for reducing stress in the central portion of the cover, then the edge moment maximum value should be limited such that plastic strains at the shell-cover interface are not developed.

Similar remarks apply to the effects of edge restraint of the shell on an integrally welded tubesheet.

(iii) Local Membrane Stress

Local membrane stress can be caused by one of three possible sources.

- a. Geometric discontinuity in the structure
- b. Locally applied external load on the structure
- c. Load discontinuity in a structure

By definition a local membrane stress is a membrane type of stress limited to a small part of the structure. Typical examples of local membrane stress are:

a. Membrane stresses developed in the shell or the knuckle at the joint of a torispherical head to cylindrical shell. (See Chapter 13 for details.)

b. Stresses in the shell and the head due to a joint between a flat head and shell subject to internal pressure. It is to be noted that the in-plane load in the cover due to the edge restraint produces a uniform state of stress throughout the cover and would normally be considered a primary membrane stress. However, since its origin is in the internal reactions caused by geometric discontinuity rather than in support of an external loading, it is treated as a local membrane stress.

c. Local membrane stresses in the shell due to an axial thrust or bending moment at a nozzle connected to the shell.

Since a membrane stress is assigned to the local category if the stress region is localized, some definitions of a localized region are necessary. The ASME Code [2.3.1] gives the following rules for determining whether a local membrane stress qualifies as P_L .

a. The stressed region will be considered local if the distance, over which the membrane stress intensity exceeds $1.1 S_m$,* does not exceed $(rt)^{1/2}$, where r is the minimum mid-surface radius of curvature and t is the minimum thickness in the region considered.

b. Regions of local primary stress intensity involving axisymmetric membrane stress distributions which exceed $1.1 S_m$ shall not be closer in the meridional direction than $2.5(rt)^{1/2}$, where r is defined as average of r_1 and r_2 and t is defined as average of t_1 and t_2 ; t_1 and t_2 are the minimum thicknesses of each of the regions considered, and r_1 and r_2 are the minimum mid-surface radii of curvature of these two regions where the membrane stress intensity exceeds $1.1 S_m$.

*Stress intensity S_m is defined in Section 2.6.

c. Discrete regions of local primary membrane stress intensity, such as those resulting from concentrated loads acting on brackets, (where the membrane stress intensity exceeds $1.1 S_m$) shall be spaced so that there is no overlapping of the areas in which the membrane stress intensity exceeds $1.1 S_m$.

If the stress intensity being considered does not meet the applicable conditions, then it should be considered as a primary membrane stress with lower allowable limits.

(iv) Secondary Stress

Secondary stress is a normal or shear stress arising because of the constraint of adjacent material or by self constraint of the structure. The basic characteristic of a secondary stress is that it is self-limiting. In other words, local yielding or minor distortions can relieve the conditions which lead to the development of these stresses and limit their maximum value. Failure from one application of such a stress is not to be expected. Examples of secondary stresses are:

- a. Stresses developed due to differential thermal growth in the structure.
- b. Bending stress at a gross structural discontinuity.
- c. Non-uniform portion of stresses across the vessel wall in a shell subjected to internal pressure.

Since a thermal stress is a self-balancing stress produced by a non-uniform distribution of temperature or by different thermal coefficients of expansion, thermal stresses always belong to either the secondary or to the peak category. In order for a thermal stress to be qualified in the secondary category it has to actuate a distortion of the structure in which it occurs. Those thermal stresses which are very localized and are such that the differential expansion is almost completely suppressed do not belong to the secondary category. They are called peak stresses. A discussion of thermal stresses which belong to the peak category is given in the next section. We see that secondary stresses can be sub-divided into two major categories: those that are actuated by mechanical loads, and those that are actuated by temperature distribution. Some examples of load actuated secondary stresses are given below:

- a. Any linear component of the stress distribution through the thickness of a shell subject to internal pressure and located away from a structural discontinuity.
- b. Bending stress in a shell where it is connected to a head or to a flange.
- c. Bending stress in a shell or a head due to nozzle loads.
- d. Bending stress in the knuckle or shell at a head to shell joint.
- e. Bending stress in a flat head due to edge restraint posed by shell to head joint when the local bending stress in the shell exceeds the material yield point.

- f. Bending stresses in a nozzle at the nozzle-shell junction due to internal pressure.

Temperature actuated secondary stresses are also found extensively in a pressure vessel. Some examples are:

- a. Stresses caused by axial temperature variation in a shell.
- b. Bending and membrane stresses due to a temperature difference between shell and attached head.
- c. Differential thermal expansion stress (both membrane and bending components) between two adjoining parts of a structure such as nozzle to shell or shell to head.
- d. Equivalent linear stress due to a radial temperature distribution in any shape pressure vessel.

(v) Peak Stress

Peak stress is that increment of stress which adds to the uniform plus linear stresses. Peak stresses are added to the primary and secondary stress to give the total stress at a point. The basic characteristic of a peak stress is that it does not cause any noticeable distortion and is objectionable only as a possible source of a fatigue crack or fracture. A structure which is subject to peak stresses requires evaluation of these stresses only when a fatigue analysis of the structure is performed. Some typical examples of peak stresses due to thermal loads are:

- a. Thermal stress in the cladding of a tubesheet.
- b. Certain thermal stresses which may cause fatigue but not distortion. For example, the non-linear bending part of thermal stress across a cylinder wall.
- c. The non-linear stress at a local structure discontinuity, such as small nozzles and couplings attached to thin shells, caused by thermal mismatches.
- d. Surface stresses produced by a thermal shock.

All examples above belong to the temperature actuated category. Some examples of load actuated peak stresses for specific situations are given below:

- a. Additional stresses developed at the fillet between a nozzle to shell junction due to internal pressure or external loads.
- b. Peak stress in a ligament (uniform ligament pattern). Both the bending and membrane stresses in a typical ligament are evaluated by averaging the stresses across the width of the ligament. The peak stress is the additional stress above the membrane plus bending stress that is developed due to the stress concentration effect of the ligament.
- c. Bending and peak stresses near an isolated or atypical ligament.

2.5 GENERAL COMMENTS

Depending on the thoroughness of the analysis required in the design of a particular pressure vessel, one or many of the stress categories has to be calculated. The most important stress category is the primary membrane stress and most formula based designs entail evaluating the membrane stresses in the pressure vessel. However, some pressure vessel components resist pressure or external loads only through bending. Typically, these are plate type members such as flat heads, a blind flange in a nozzle, etc. These elements develop mainly primary bending stresses and the design formula for these members are based on the bending stress limitation. Somewhat less important are the local membrane stresses. These are evaluated whenever a higher level of confidence in the pressure vessel design is required. The most commonplace application of a local membrane stress calculation is in the evaluation of allowable nozzle loads at heat exchanger connections (see Chapter 17). An excellent discussion of stress classification and design categories is found in [2.5.1].

There are, however, stresses in a heat exchanger which transcend all categories described in the foregoing. The most notable is the tube joint stress. The importance of a sound tube-to-tubesheet joint is so vital to the performance of a heat exchanger that conservative limits [2.4.2] are placed on this load even though much of the joint load may develop from temperature differences. Similarly, buckling of tubes is another factor, especially in fixed tubesheet heat exchangers, which is not addressed by any of the stress categories. Another area of concern is the hoop stress developed in a torispherical or ellipsoidal (typically two-to-one major-to-minor diameter ratio of the generator ellipse) head. The stress is compressive near the equator of the head and in large diameter vessels, can cause “wrinkling” of the head in its knuckle region. Despite the fact that these special areas are not addressed by the stress categories discussed in the preceding sections, the scheme of dividing the stresses into well defined classifications described in the foregoing is found to be extremely valuable in conducting detailed stress analyses of pressure vessel components.

2.6 STRESS INTENSITY

Stress intensity is defined as the difference between the algebraically largest and smallest principal stresses at a point. From Mohr’s diagram of stresses, we recognize stress intensity to be twice the maximum shear stress. Some design codes [2.3.1] use the maximum shear stress theory, the so-called Tresca criterion, as the governing theory of failure. Since the membrane stress is, by definition, the averaged stress across a section; the membrane stress intensity really pertains to the section rather than to a point. It is evaluated by first computing the three principal membrane stresses and then determining the maximum algebraic difference.

2.7 AN EXAMPLE OF GROSS STRUCTURAL DISCONTINUITY

Evaluation of the stress field at gross structural discontinuities is essential for a complete stress analysis of a pressure vessel or a heat exchanger. We will encounter solutions of varied structural discontinuity problems throughout this work. The underlying concepts are introduced by treating the configuration of Fig. 2.3.1 in some detail.

Unequal Thickness Welded Cylinders

Consider two thin shells of thickness t_1 and t_2 respectively, under pressure p , welded together along the girth seam as shown in Fig. 2.3.1. The two ends of the closed pressure vessel are assumed to be at least $5(at_2)^{1/2}$ (assuming $t_2 > t_1$) from the junction. a is the common mid-surface radius of the two shells. The above restriction is imposed so that we may neglect the effects of the vessel ends (see our discussion of edge loading of a shell in Appendix A following Eq. (A.4.5)).

The membrane stress components in the two shells given by Lamé's formula are listed below (tensile stresses are considered positive).

	Shell No. 1 (thickness t_1)	Shell No. 2 (thickness t_2)
Hoop (tangential) membrane stress; σ_1 (direction No. 1)	$\frac{pa}{t_1}$	$\frac{pa}{t_2}$
Radial membrane stress (direction No. 2); σ_2	$\frac{-p}{2}$	$\frac{-p}{2}$
Longitudinal (meridional) membrane stress (direction No. 3); σ_3	$\frac{pa}{2t_1}$	$\frac{pa}{2t_2}$
Membrane stress intensity in 1-2 plane; $ \sigma_1 - \sigma_2 $	$\frac{pa}{t_1} + \frac{p}{2}$	$\frac{pa}{t_2} + \frac{p}{2}$
Membrane stress intensity in 1-3 plane; $ \sigma_1 - \sigma_3 $	$\frac{pa}{2t_1}$	$\frac{pa}{2t_2}$
Membrane stress intensity in 2-3 plane; $ \sigma_2 - \sigma_3 $	$\frac{pa}{2t_1} + \frac{p}{2}$	$\frac{pa}{2t_2} + \frac{p}{2}$

The membrane stress intensity in the 1-2 plane (radial plane) is the highest and hence is the controlling stress intensity.

The above stresses are valid in the region of the shell away from the ends and from the welded joint. At the welded joint location, the radial deflection w_i in the two shells ($i = 1, 2$), if the shells were free to expand freely, is computed as follows:

The circumferential strain is

$$\epsilon_\theta = \frac{w_i}{a} = \frac{1}{E} [\sigma_1 - \nu(\sigma_2 + \sigma_3)]$$

where E is the Young's modulus of the shells i and the deflection w_i is positive if directed away from the centerline of the shell (in the 2-directions in Fig. 2.3.1).

Substituting for σ_1 , σ_2 , and σ_3 we have

$$w_i = \frac{pa^2}{E_i t_i} \left[1 - \frac{\nu}{2} \left(\frac{t_i}{a} + 1 \right) \right]; \quad i=1,2 \quad (2.7.1)$$

Since the deflections of the two shells are different, discontinuity shear force Q_0 and moment M_0 are needed to establish displacement and slope continuity, when the actual system, including the welds, is considered.

Axisymmetric edge moment M and shear Q acting on the edge of shell of radius a , thickness t , (see Fig. 2.7.1) produce the following deflections and slopes (see Appendix A for derivation and note the direction changes for M and Q).

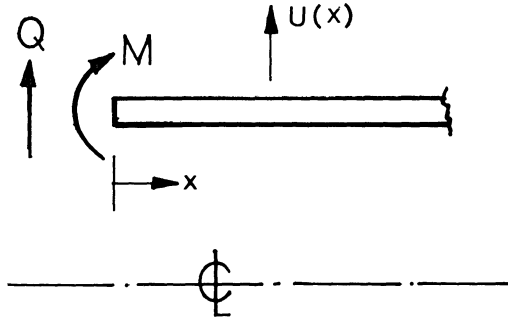


Fig. 2.7.1. Axisymmetrically edge loaded shell.

$$U(x) = \frac{1}{2\beta^3 D} [\beta M \psi(\beta x) + Q \lambda(\beta x)] \quad (a)$$

$$\frac{dU}{dx} = -\frac{1}{2\beta^2 D} [2\beta M \lambda(\beta x) + Q \phi(\beta x)] \quad (b) \quad (2.7.2)$$

$$\frac{d^2 U}{dx^2} = \frac{1}{\beta D} [\beta M \phi(\beta x) + Q \zeta(\beta x)] \quad (c)$$

where

$$\beta = \left[\frac{3(1-\nu^2)}{a^2 t^2} \right]^{0.25} \quad (d)$$

$$D = \frac{Et^3}{12(1-\nu^2)} \quad (e)$$

$U(x)$ is the radial deflection of the shell wall, and

$$\phi(\beta x) = e^{-\beta x} (\cos \beta x + \sin \beta x) \quad (a)$$

$$\psi(\beta x) = e^{-\beta x} (\cos \beta x - \sin \beta x) \quad (b) \quad (2.7.3)$$

$$\lambda(\beta x) = e^{-\beta x} \cos \beta x \quad (c)$$

$$\zeta(\beta x) = e^{-\beta x} \sin \beta x \quad (d)$$

Substituting β_i and D_i for β , and D , and Q_0 and M_0 (with proper signs) for Q and M , we obtain

$$U \Big|_{x=0, \text{Shell No. 1}} = \delta_1 = \frac{1}{2\beta_1^3 D_1} (\beta_1 M_0 - Q_0) \quad (a)$$

$$\frac{dU}{dx} \Big|_{x=0, \text{Shell No. 1}} = \alpha_1 = -\frac{1}{2\beta_1^2 D_1} (2\beta_1 M_0 - Q_0) \quad (b) \quad (2.7.4)$$

$$U \Big|_{x=0, \text{Shell No. 2}} = \delta_2 = \frac{1}{2\beta_2^3 D_2} (\beta_2 M_0 + Q_0) \quad (c)$$

$$\frac{dU}{dx} \Big|_{x=0, \text{Shell No. 2}} = \alpha_2 = -\frac{1}{2\beta_2^2 D_2} (2\beta_2 M_0 + Q_0) \quad (d)$$

Compatibility of displacement and slope at the junction requires:

$$\begin{aligned} w_1 + \delta_1 &= w_2 + \delta_2 \\ \alpha_1 &= -\alpha_2 \end{aligned}$$

The above equations enable determination of M_0 and Q_0 at the weld location.

Substituting for w_i , δ_i and α_i ($i = 1, 2$) from the above equations, and rearranging terms, we have

$$M_0 = C Q_0 \quad (a)$$

where

$$C = \frac{(1 - \rho)}{2(\beta_1 + \rho\beta_2)} \quad (b) \quad (2.7.5)$$

$$\rho = \frac{\beta_1^2 D_1}{\beta_2^2 D_2} \quad (c)$$

and

$$Q_0 = \frac{\frac{pa^2}{E} \left\{ \frac{1}{t_1} \left[1 - \frac{\nu}{2} \left(\frac{t_1}{a} + 1 \right) \right] - \frac{1}{t_2} \left[1 - \frac{\nu}{2} \left(\frac{t_2}{a} + 1 \right) \right] \right\}}{m_1(1 - C\beta_1) + m_2(1 + C\beta_2)} \quad (a) \quad (2.7.6)$$

where:

$$m_i = \frac{1}{2\beta_i^3 D_i}; \quad i = 1, 2 \quad (b)$$

Equations (2.7.5) and (2.7.6) define the discontinuity stress resultants M_0 and Q_0 . In keeping within the spirit of thin shell theory, $t_i/a + 1 \approx 1$ may be used in all of the above equations.

The additional stresses at the junction due to these discontinuity loads are

given below (setting $i = 1, 2$, gives respective values on the two sides of the junction).

Source	Type of Stress	Category	Magnitude
Q_0	Shear stress at mid-section in 1-3 plane. (Fig. 2.3.1)	Secondary	$\frac{3Q_0}{2t_i}$
M_0	Longitudinal bending stress at outer fibers in 1-3 plane.	Secondary	$\frac{6M_0}{t_i^2}$
M_0	Circumferential bending stress at outer fibers in 1-2 plane.	Secondary	$\nu 6M_0/t_i^2$
δ_i	Tangential stress (positive if tensile) in 1-2 plane.	Local Membrane	$\frac{E\delta_i}{a}$

These stresses are in addition to the primary membrane stresses computed before.

2.8 DISCONTINUITY STRESSES AT HEAD, SHELL AND SKIRT JUNCTION

As another illustration of a gross geometric discontinuity, let us consider the junction of a two-to-one ellipsoidal head, its straight flange which continues on as a channel of a heat exchanger, and a welded on skirt. This situation is encountered in vertical skirt mounted pressure vessels and heat exchangers, such as the one shown in Photograph 2.a.

For simplicity of analysis, it is assumed here that the support skirt joins the head at its junction with the shell. The three surfaces are labeled 1, 2, and 3, as shown in Fig. 2.8.1. t_i , M_i , and Q_i indicate the thickness, discontinuity moment and discontinuity shear, respectively, pertaining to element i . The shell is subjected to pressure p .

The expansion of the equatorial radius (radius of the junction) of the cylindrical shell (element #1) due to pressure p is given by Eq. (2.7.1) (and also developed in Chapter 13) as

$$\delta_1 = \frac{pa^2}{Et_1}(1 - 0.5\nu) \quad (2.8.1)$$

Similarly, the radial expansion of the equatorial radius of the ellipsoidal head (element #2) is

$$\delta_2 = -\frac{pa^2}{Et_2}(1 + 0.5\nu) \quad (2.8.2)$$



Photograph 2.a. Skirt mounted heat exchanger with a three-element joint (TEMA type BEU). (Courtesy Joseph Oat Corporation.)

Note that pressure causes a contraction of the head diameter if no restraint is present.

The third element, the skirt, is not pressurized, and therefore undergoes no membrane expansion. The magnitudes of Q_i and M_i are determined by requiring continuity of slope and deflection at the junction (equator). A reasonably accurate solution can be obtained by assuming that the edge displacement solution for the ellipsoid, due to axisymmetric moment and shear loads, is equal to that of a thin cylinder of equal thickness and radius.

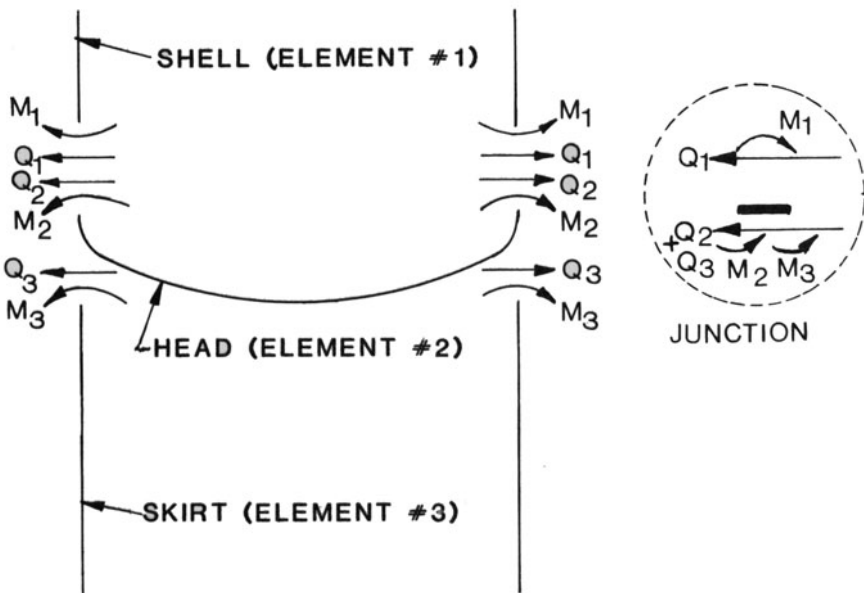


Fig. 2.8.1 Shell, head, and skirt shown as freebodies.

The expressions for radial displacement and edge slope due to edge loadings are found from the preceding section. By matching displacements and slopes at the equator between the three structural elements (junction of the three elements) four algebraic equations are obtained. Finally, a balance of edge shears and moments at the junction furnishes two additional equations (see Fig. 2.8.1):

$$-M_1 + M_2 + M_3 = 0 \quad (2.8.2)$$

$$Q_1 + Q_2 + Q_3 = 0 \quad (2.8.3)$$

Six algebraic equations are thus assembled to solve for six unknowns, namely M_i, Q_i ($i = 1, 2, 3$). These equations can be written in the matrix form

$$\begin{bmatrix} -\frac{1}{\chi_1} & -\frac{1}{\beta_1 \chi_1} & \frac{1}{\chi_2} & \frac{1}{\beta_2 \chi_2} & 0 & 0 \\ -\frac{1}{\chi_1} & -\frac{1}{\beta_1 \chi_1} & 0 & 0 & \frac{1}{\chi_3} & \frac{1}{\beta_3 \chi_3} \\ -\frac{2\beta_1}{\chi_1} & -\frac{1}{\chi_1} & -\frac{2\beta_2}{\chi_2} & -\frac{1}{\chi_2} & 0 & 0 \\ -\frac{2\beta_1}{\chi_1} & -\frac{1}{\chi_1} & 0 & 0 & \frac{-2\beta_3}{\chi_3} & -\frac{1}{\chi_3} \\ -1 & 0 & 1 & 0 & 1 & 0 \\ 0 & 1 & 0 & 1 & 0 & 1 \end{bmatrix} \begin{Bmatrix} M_1 \\ Q_1 \\ M_2 \\ Q_2 \\ M_3 \\ Q_3 \end{Bmatrix}$$

$$= \begin{Bmatrix} \delta_1 - \delta_2 \\ \delta_1 - \delta_3 \\ 0 \\ 0 \\ 0 \\ 0 \end{Bmatrix} \quad (2.8.4)$$

where $\chi_i = 2 \beta_i^2 D_i; i = 1, 2, 3$.

These equations are solved using a suitable Gaussian elimination scheme. Computer program HEADSKIRT listed in the following pages gives the necessary tool to perform the analysis.

Having determined the discontinuity reactions, the corresponding discontinuity stresses are found. The following relations are derived in Appendix A:

$$\begin{aligned}\sigma_{cm} &= \frac{EU(x)}{a} \\ \sigma_{lb} &= \pm \frac{6D}{t^2} \frac{d^2 U}{dx^2} \\ \sigma_{cb} &= \nu \sigma_{lb}\end{aligned}$$

where σ_{cm} is membrane stress, σ_{lb} , is longitudinal bending stress, and σ_{cb} is circumferential bending stress due to edge loads.

$U(x)$ and $d^2 U/dx^2$ are defined by Eqs. (2.7.2) with appropriate quantities replacing M , Q , t , β . For instance, to calculate stresses in element 1, replace M by M_1 , Q by Q_1 , t by t_1 , and β by β_1 .

These equations are computerized in the computer code "HEADSKIRT". The listing of "HEADSKIRT" is given in this section. The following terms define the input data:

Term	Mathematical Symbol	Fortran Symbol
Mean radius	a	U
Pressure	p	P
Thickness of element 1 (shell)	t_1	$T(1)$
Thickness of element 2 (head)	t_2	$T(2)$
Thickness of element 3 (skirt)	t_3	$T(3)$
Young's Modulus $\times 10^{-6}$	E	E
Poisson's Ratio	ν	PR

Example: Let us consider the junction of a shell, a 2:1 ellipsoidal head, and a skirt of mean radius 20" subject to an internal pressure 200 psi. The Young's Modulus and Poisson ratio of all materials are assumed to be 30×10^6 psi and 0.3, respectively. We consider two cases.

Case I: All three elements have equal thickness = 0.25".

Case II: $t_1 = t_2 = 0.25$ "; skirt thickness 0.001".

(Case II numerically simulates the condition of no skirt.)

The variations of σ_{cm} and σ_{lb} with x_i ($x_i = 0$ at the junction) are plotted in Fig. 2.8.2 for the shell, in Fig. 2.8.3 for the head, and in Fig. 2.8.4 for the skirt. σ_{cb} is not plotted since it bears a fixed ratio to σ_{lb} .

These plots clearly show the exponentially decaying nature of the stresses produced by edge loadings. The comparison between Cases I and II indicates the effect of the skirt.

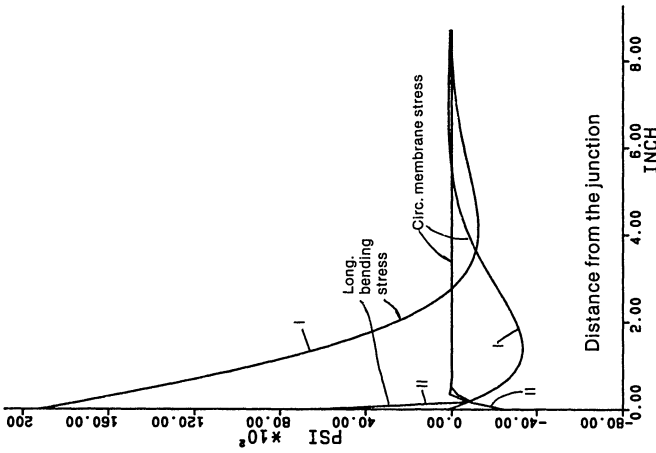


Fig. 2.8.4. Local stresses in the skirt due to edge loads.

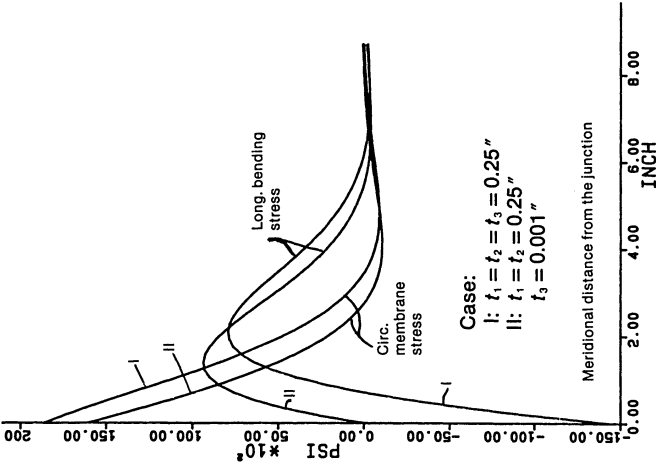


Fig. 2.8.3. Local stresses in the head due to internal pressure.

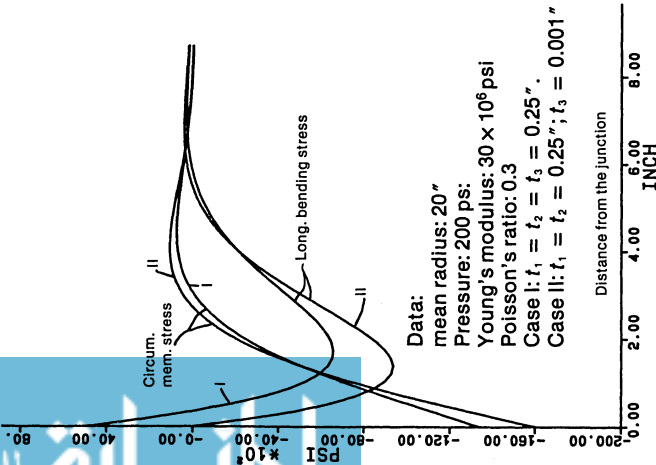


Fig. 2.8.2. Local stresses in the shell due to internal pressure.

In order to obtain the complete state of stress in the shell and the head, these discontinuity stresses should be added to the membrane stresses produced by pressure. The stresses in the skirt are only due to edge loadings, since there is no pressure in that element. The method of obtaining membrane stresses in pressure vessels is given in Chapter 13.

PROGRAM HEADSKIRT

```

DIMENSION A(6,6), B(6) , G(36), T(3),PSI(3), BETA(3)
  DIMENSION AM(3),AQ(3),SIGCM(3,60),SIGLB(3,60),SIGCB(3,60),XX(60)
  TH(X)= EXP(-X)*COS(X)
  ZETA(X)=EXP(-X)*SIN(X)
  R(X) = 1.0/X
1 ACCEPT  U, P,T(1),T(2), T(3) , E,PR
2 E= E*1.0E6
  WRITE(6,700)P,T(1),T(2), T(3) ,E,PR,U
  PR2= 1.-PR*PR
  DO 100 I=1,3
    BETA(I) = (3.*PR2/(( U*T(I))**2))**.25
100 PSI(I) = (BETA(I) **2) *E*(T(I)**3) /(6.*PR2)
    DEL1 =P*U*U*(1.-.5*PR) / (E*T(1))
    DEL2 = -P*U*U*(1.+ .5*PR) / (E*T(2))
    DEL3 = 0.
  DO 200 I=1,6
  DO 300 J=1,6
300 A(I,J) = 0.0
200 B(I) =0.0
  A(1,1) = R(PSI(1))
  A(1,2) = R( PSI(1)*BETA(1))
  A(1,3) = R(PSI(2))
  A(1,4) = R(PSI(2)*BETA(2))
  B(1) = DEL1-DEL2
C
  A(2,1) = A(1,1)
  A(2,2) = A(1,2)
  A(2,5) = R(PSI(3))
  A(2,6) = R(PSI(3) *BETA(3))
  B(2) = DEL1-DEL3
C
  A(3,1) = 2.*BETA(1) /PSI(1)
  A(3,2) = A(1,1)
  A(3,3) = -2.*BETA(2) /PSI(2)
  A(3,4) = -A(1,3)
C
  A(4,1) = A(3,1)
  A(4,2) = A(3,2)
  A(4,5) = -2.*BETA(3) /PSI(3)
  A(4,6) = -R(PSI(3))

```

```

C
  A(5,1) = -1.
  A(5,3) = -1.
  A(5,5) = -1.
C
  A(6,2) = 1.
  A(6,4) = -1.
  A(6,6) = -1.
C
  DO 400 J=1,6
  DO 410 I=1,6
  NDEX= (6*(J-1) +1)
  G(NDEX) = A(I,J)
410 CONTINUE
400 CONTINUE
  CALL SIMQ(G,B,6,KS)
  B(1) = - B(1)
  B(2) = -B(2)
  IF(KS .NE. 0) GOTO 1000
  WRITE(6,710) (B(I),I=1,6)
  DO 500 J=1,3
  AM(J) = B(2*J-1)
500 AQ(J) = B(2*J)
  ALIM=AMINI(BETA(1),BETA(2))
  XLIM=5./ALIM
  XINC = XLIM*.02
C
  DO 550 I=1,3
  DO 550 J=1,51
  X= XINC*(J-1)
  BX=XINC*(J-1)*BETA(I)
  SIGCM(I,J)=(2.*U*BETA(I)/T(I))*(BETA(I)*AM(I)*(TH(BX)-ZETA(BX)
  / )+AQ(I)*TH(BX))
  SIGLB(I,J)= (6./((BETA(I)*T(I)**2))* (BETA(I)*AM(I)*(TH(BX)+
  / ZETA(BX))+AQ(I)*ZETA(BX))
  SIGCB(I,J) = PR*SIGLB(I,J)
  XX(J)= X
550 CONTINUE
  DO 650 J=1,51
  WRITE(6,750)XX(J),((SIGCM(I,J),SIGCB(I,J),SIGLB(I,J)),I=1,3)
650 CONTINUE
750 FORMAT(10E13.4)
1001 STOP
1000 WRITE(6,720)
  STOP
700 FORMAT(1H1,5X,"P,T1,T2,T3=",4( F9.3)/,5X,"E,POISSON RATIO = ",
  1 3X,E11.4,3X,F6.4/, 5X, "A = ",
  2 3X,F10.4)
710 FORMAT(/,////,5X,"M1,Q1=",2E12.4,5X,"M2,Q2=",2E12.4,5X,"M3,Q3 =",
  1 2E12.4///)
720 FORMAT(5X,"EQUATIONS LINEARLY DEPENDENT")
  END

```

Note: Subroutine SIMQ is listed with computer program FLANGE in Chapter 3.

NOMENCLATURE

- M = Bending moment on section
 M_e = Bending moment to cause outer fiber to reach yield limit
 M_p = Plastic limit moment – Eq. (2.2.10)
 M, Q = Generic edge moment and shear
 N_y = Uniform load on structural section causing section yielding
 p = Internal pressure
 r_1, r_2 = Inner, outer radii of a thick-walled cylinder
 R = Radius of curvature
 S_m = Stress intensity
 $U(x)$ = Shell deflection shape due to edge loading – Eq. (2.7.2)
 w_i = Shell deflection, due to pressure, away from edges – Eq. (2.7.1)
 α = Coefficient of thermal expansion – Eq. (2.3.1)
 ϵ = Strain measure
 ϵ^* = Strain to cause yielding
 σ_{rm} = Average value of σ_r – Eq. (2.4.4)
 σ_t, σ_r = Tangential, radial stresses
 σ_{tm} = Average value of σ_t – Eq. (2.4.3)

REFERENCES

- [2.3.1] ASME Boiler and Pressure Vessel Code, Section III, Div. I, Sub-section NB (1983).
 [2.4.1] Seeley, F. B., and Smith, J. O., “Advanced Strength of Materials,” second edition, pp. 299–300, Wiley, New York (1965).
 [2.4.2] ASME Boiler and Pressure Vessel Code, Section VIII, Div. I (1983).
 [2.5.1] Burgreen, D., “Design Methods for Power Plant Structures,” 1st Edition, C.P. Press, N.Y., (1975).

3. BOLTED FLANGE DESIGN

3.1 INTRODUCTION

Pressure vessels require flanged joints to permit their disassembly, inspection and cleaning. Bolted joints are also utilized to alleviate stresses at sections where sharp temperature changes occur, such as the joint between tubeside and shellside chambers in a heat exchanger (Fig. 3.1.1). From a conceptual standpoint, flanged joints may be subdivided into two major categories.

- (i) Bolted joints
- (ii) Pressure-actuated joints

The so-called “bolted joint” is by far the most common type. Its underlying principle is, in essence, brute force. “Pressure actuated joints” find application in the higher pressure range, typically over 2000 psi. The main difference between these two joint types lies in the manner by which the pressure load is resisted and leak-tightness is achieved. In a bolted joint, pre-load in the bolt provides initial pre-stress in the gasket. Upon introduction of internal pressure, the normal surface load on the gasket drops. The objects in flange design are to ensure that the residual gasket load is sufficient to maintain the joint leak tight, and, to ensure that the stress levels in the flange during bolt pre-load, as well as during pressurization, do not exceed allowable values. Pressure actuated joints, on the other hand, exploit the header pressure force to compress and to seal the gasket. This chapter concentrates on the structural behavior of bolted joints. First, an outline of various types of flanges used in bolted joints is given, followed by a brief discussion on the significance of surface finish of

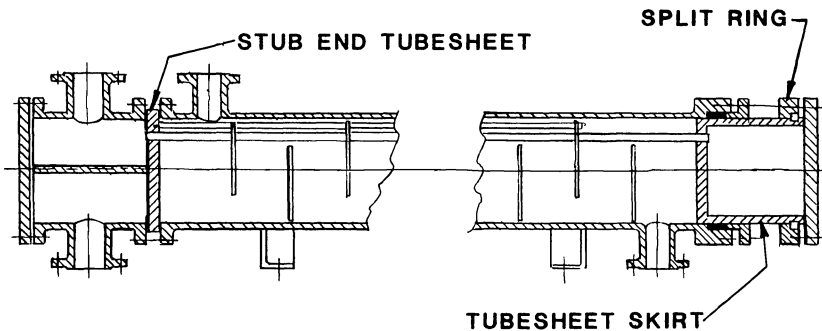


Fig. 3.1.1. Outside packed floating head heat exchanger.

flange facings, and of gasket characteristics on the joint performance. The concepts leading to the characterization of the sealing action of bolted joints are next developed. Conventional design methods and stress analysis procedures are also described. Similar concepts for pressure actuated closures are developed in Chapter 6.

3.2 BOLTED FLANGE TYPES

Bolted flanges may be subdivided into three major categories:

- (i) Ring flange (Fig. 3.2.1.a)
- (ii) Tapered hub (or welding neck) flange (Fig. 3.2.1.b)
- (iii) Lap-joint flange (Fig. 3.2.1.c)

The ring flange consists of an annular plate welded to the end of the

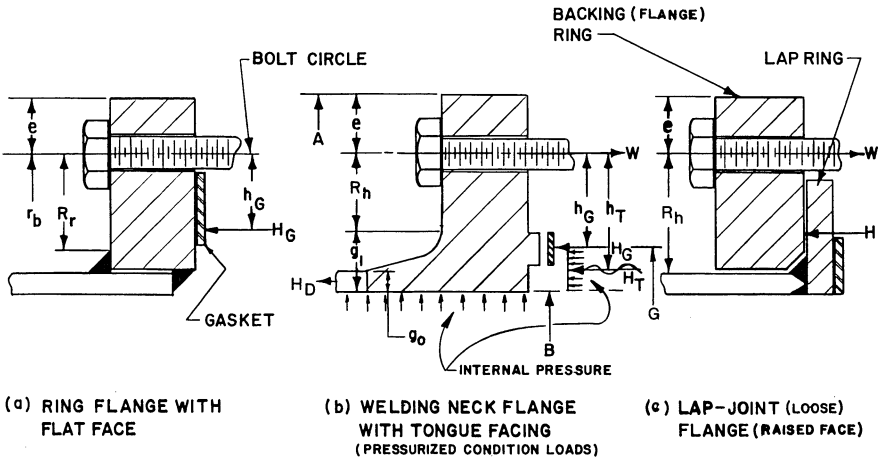


Fig. 3.2.1. Bolted flange types and typical facing details.

cylindrical shell. A number of equidistant bolt holes (conventionally, a multiple of 4) are drilled on a uniform pitch on a circle (known as the bolt circle). The gasket is confined inside the bolt circle. This joint is utilized in low to moderate pressure applications. If the pressure is quite low (less than 100 psi), wide gaskets which span the entire flange face (within and beyond the bolt circle) may be used. This construction is referred to as “full face gasket” design. A design method for flanges utilizing full face gaskets is presented in Chapter 5. The work in Chapter 5 also focuses on the effect of the non-linear material characteristics of the gasket.

The tapered hub flange is shown in Fig. 3.2.1.b. The annular ring is integral with a short tapered hub. The small end of the hub is butt welded to the cylindrical shell. This class of flange is widely utilized where reliability and safety are major concerns. Tapered hub flanges have been used in

pressures as high as 5000 psi, although the flange becomes massive and unwieldy as pressure and diameter increase. Pressure actuated closures become more cost effective at pressures over 2000 psi in shell diameters exceeding 20" .

The lap joint flange finds extensive use in low pressure piping and in pressure vessel construction where economy of construction is an important consideration. The backing ring, shown in Fig. 3.2.1.c, can be made from an inexpensive yet strong structural material (e.g., carbon steel), even though the internals of the pressure vessel including the "lap ring" may have to be made from expensive corrosion resistant alloys. Furthermore, lap joint construction facilitates alignment of bolt holes in matching rings in opposing pipe ends. In outside packed floating head heat exchangers, the flange at the rear end must be of the lap joint type. The backing ring shown in Fig. 3.1.1 is split into two or three segments to enable its removal before the tube bundle can be pulled through the shell. The backing ring can also contain a hub if added rigidity against rotation is desired.

Some "off-the-shelf" lap joint flange rings are equipped with hubs to increase their rotational stiffness. Such joints are referred to as "hubbed lap joints".

3.3 FLANGE FACINGS

The geometric detail of the flange surface on which the gasket sits is prepared to suit the gasket type, the kind of application, and the service conditions. The ability of a joint to maintain a seal depends on a complex interaction between a host of parameters, of which the gasket and facing details are perhaps the most important as well as the most intractable to analytical simulation. In the following, some common facing details and gasket types are described. The material presented here should provide the reader with the necessary background of the practical considerations in selecting flange facings.

Generally speaking, flange facings may be divided into four categories:

- (i) Unconfined and pre-stressed
- (ii) Semi-confined and pre-stressed
- (iii) Confined and pre-stressed
- (iv) Self-equalizing

(i) Unconfined and Pre-stressed

In this construction, the gasket is free to expand outwards as well as inwards when the bolt load is applied. The flange facing may be either flat (Fig. 3.2.1.a); or raised face (Fig. 3.2.1.c). The gasket ordinarily extends to the inner edge of the bolt line (within a certain tolerance) so that bolts may serve to center it. Flat faced designs are used in low pressure applications. Raised face designs are somewhat superior to the flat faced type, because the raised face protects the mating flange rings from contacting each other

at the outer edges when the joint is pulled up. Neither of the two facings provide protection against gasket blow-out.

(ii) Semi-Confined and Pre-stressed

The “male and female” joint shown in Fig. 3.3.1 is a typical example of a semi-confined joint. The gasket is protected from blow-out; however, no protection is offered against extrusion on the inside.

The semi-confined effect can also be produced in unconfined facing detail by equipping the gasket with a so-called “retainer ring”. The retainer ring may be on the outside, inside or both locations; the last arrangement simulates a fully confined joint.

(iii) Confined and Pre-stressed

This detail is utilized in operating conditions subject to pressure and temperature fluctuations. The tongue and groove joint (Fig. 3.3.2), the double step joint (Fig. 3.3.3), and the ring joint (Fig. 3.3.4) are typical examples of confined joints. These joints are generally preferable for cyclic applications. The machining must be quite precise such that the mating parts fit properly. The tongue (Fig. 3.3.2) is specially susceptible to damage during handling and hence, is usually made on the part which is easier to handle.

(iv) Self-equalizing

Self-equalizing facing detail relies on the deformation of the gasket during pressurization to effect the joint seal. Figure 3.3.5 shows typical facing details. Such gaskets are usually made from an elastomeric material, e.g., rubber, or from hollow tubular (metallic) elements.

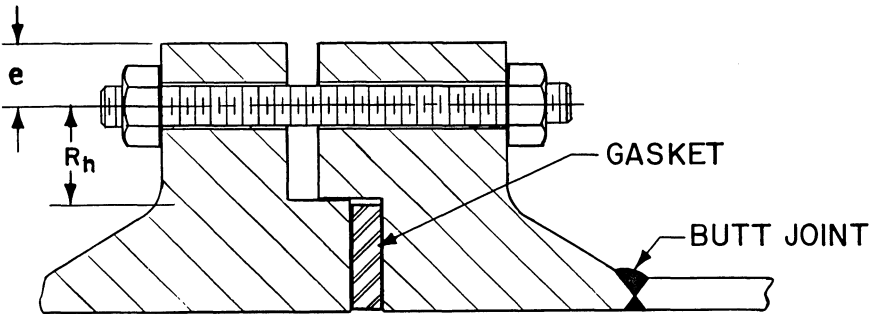


Fig. 3.3.1. Male and female joint (semi-confined).

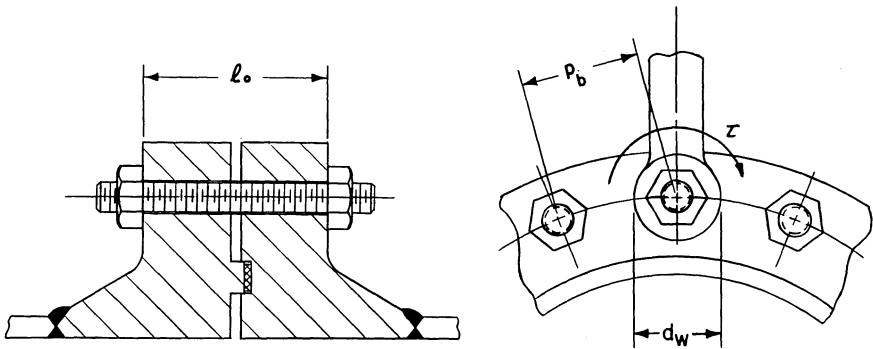


Fig. 3.3.2. Tongue and groove.

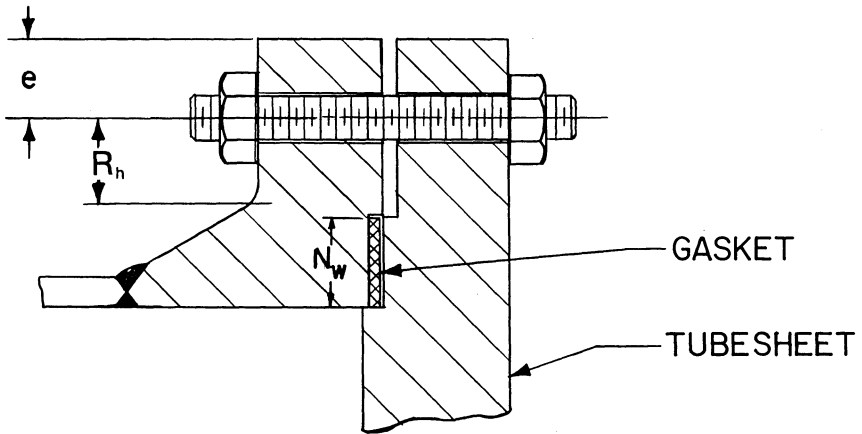


Fig. 3.3.3. Double step confined joint.

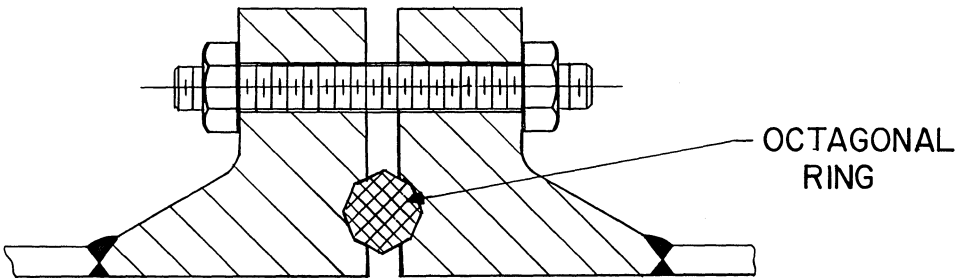
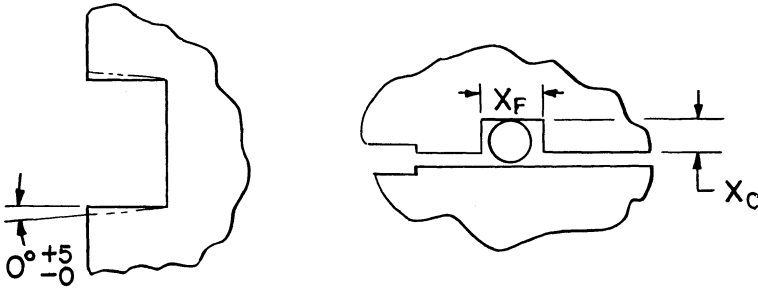


Fig. 3.3.4. Ring joint.



(a) ELASTOMER (b) METALLIC O-RING

Fig. 3.3.5. Self-energizing facings.

3.4 FLANGE FACING FINISH

The type and texture of surface finish play a major role in the sealworthiness of a flanged joint. The surface finish should have the correct quality (RMS or AA finish rating) and type. There are five distinct styles of surface finish which are commonly used in the industry to indicate the quality and type of finish. These are:

- (i) Rounded nose spiral finish
- (ii) Spiral serrated finish
- (iii) Concentric serrated finish
- (iv) Smooth finish
- (v) Cold water finish

(i) Rounded Nose or Stock Finish

The rounded nose or stock finish is a continuous spiral groove. For nominal sizes 12" and smaller, it can be generated by a 1/16" radius round nose tool at a feed of 1/32" per revolution. For sizes above 12", the tool nose radius is increased to 1/8" and the feed rate is increased to 3/64". This finish is mostly used with compressed asbestos, fiber, rubber and other organic gaskets. This finish is also referred to as "phonograph" finish.

(ii) Spiral Serrated

Continuous spiral groove is generated with a 90° included angle "V"-tool. The groove is 1/64" deep and the feed is 1/32" for all sizes.

(iii) Concentric Serrated

The groove cross section detail is identical to (ii); however, the groove is made in concentric circles.

(iv) Smooth Finish

A finish produced with no visible tool markings to the naked eye. Final dressing up, using an abrasive material such as emery paper, is necessary to obtain such a finish.

(v) Cold Water Finish

This refers to the surface with mirror-like appearance. It is produced by using a wide tool at high speeds. This finish is seldom used due to its excessive cost and fragility.

3.5 GASKETS

A gasket is the heart of a bolted joint. It is essentially an elasto-plastic material which is softer than the flange face. Under the application of a bolt load, the gasket deforms, and fills up the irregularities on the flange face. In this condition, the gasket is considered to be seated. It is shown in a later section that when pressure is introduced in the pressure vessel, the flanges separate by a small amount at the gasket location. The gasket should possess the resilience to maintain a sufficient residual surface pressure to keep the joint from leaking. These qualities of plastic compliance and resilience are difficult to build into the same material and therein lies the challenge to the manufacture of a successful gasket. Gaskets are made out of a myriad variety of materials. The ASME Codes [3.5.1-3] list some common types. Butcher [3.5.4] is another excellent source of information on this subject. The choice of the proper gasket material depends on operating conditions, on mechanical attributes of the flanged joint, and on metallurgical considerations. Some factors which should be considered in selecting the proper gasket material are described below:

Pressure

For a given pressure vessel diameter, the pressure determines the magnitude of the hydrostatic load that the bolts are required to resist. Therefore, the bolt load must at least exceed the hydrostatic load. In the seating condition (pre-load condition), this entire bolt load is borne by the gasket. The gasket must be strong enough to withstand the bolt pre-load without crushing or extruding out. Thus, soft materials, such as asbestos, organic fibers, etc., are ruled out for high pressure applications.

Temperature

Operating temperature of the fluid contained by the gasketed joint must be below the permissible temperature for non-metallic gasket materials. For example, an asbestos filled gasket is seldom used in joints in sustained contact with fluids over 800°F.

Corrosion

Oxidation, galvanic corrosion, dezincification, etc., are important considerations when selecting metallic gaskets.

Cyclic Conditions

Fluctuations in the internal pressure result in repeated loading and unloading of the gasket. Spiral wound, and hollow tubular gaskets are known to withstand such conditions quite well.

We now discuss some of the classical aspects of loading a ring gasketed joint. The structural behavior of the gasket is customarily expressed in terms of two quantities: the so-called minimum seating stress y and gasket factor m . The minimum seating stress is the surface pressure which must be exerted on the gasket to make its surface completely conformal with the flange facing profile. The required bolt load to seal the gasket is then given as

$$W_1 = \pi G b y \quad (3.5.1)$$

where G is the effective gasket diameter and b is the effective gasket width. Recognizing that the rotation of the flange ring causes non-uniform pressure distribution in the radial direction, the ASME codes [3.5.1–3] give algebraic expressions to define the effective gasket diameter G and the corresponding gasket effective width b . These semi-empirical formulas are, by now, well entrenched in the industry. Their success attests to their general validity, although the minimum seating stress y , based on the above referenced definition of G and b , has been the subject of much controversy and speculation [3.5.5–9].

When the joint is pressurized, the total bolt load, W_2 , must equal the pressure induced header load and the residual load acting on the gasket bearing area; i.e.

$$W_2 = \frac{\pi G^2 P}{4} + 2\pi b G m P \quad (3.5.2)$$

where P is the internal pressure. The integer 2 in the second term is essentially a factor of safety. The minimum value of m required to maintain the joint leak-tight is known as the “gasket factor” for the gasket material. According to the Code, a joint is leak tight if the surface pressure on the gasket (assuming it to be of width $2b$) is at least m times the internal pressure. Of course, “leak-tight” is an imprecise term. All gasketed joints lose pressurized fluid, even if the loss is at an immeasurably small rate. Experiments [3.5.6] show that the leakage rate Λ (gms/day) is related to the actual seating stress y_s ($\text{psi} \times 10^{-3}$) (based on width b) by a relationship of the form

$$\Lambda = K_1 y_s^{-n_1} \quad (3.5.3)$$

where the exponent n_1 is of the order of 10 for spiral wound gaskets.

Likewise, the leakage rate correlates with the calculated value of m by a similar relationship;

$$\Lambda = K_2 m^{-n_2} \quad (3.5.4)$$

where n_2 varies from 2 to 9 depending on the gasket material. The above relationships indicate that the greater the values of y_s and m , the lower the leakage rate Λ . This is, however, true only so long as the load is not so high as to crush or to extrude the gasket. Design codes [3.5.1–3] and gasket manufacturers' technical bulletins give recommended values for y and m . We should remember that these values are meaningful only if the flange facing finish is in accord with the finish required for the particular gasket being used.

Considerations become quite involved in applications where cyclic conditions are present. Pulsations in pressure cause the compressive load on the gasket to fluctuate. Therefore, the unloading and reloading moduli of the gasket become very important. Figure 3.5.1 shows a typical compression curve for a spiral wound gasket (stainless steel strips with compressed asbestos filler). Referring to this compression curve, the following observations warrant attention:

(i) Upon first loading and unloading, the uncompressed thickness of the gasket is less than its original thickness by over 25%. This implies that the bolt load after "hydrotest" will drop. To reestablish the bolt load to the required design value, the bolts must be retightened.

(ii) The "gasket recovery" δ_r , upon unloading is less than 0.014 inch. Therefore, the additional joint separation at the gasket location upon application of pressure, δ_s , must be less than δ_r if any residual force is to remain on the gasket surface. It is incumbent on the flange designer to ensure that the separation is sufficiently less than δ_r ; so that the required residual force on the gasket for leak tightness is retained.

(iii) The increase in load during the first compression is slow and non-linear with a "boss" in the middle of the curve. This boss is prevalent in spiral wound gaskets.

(iv) The stress (load) drops sharply during decompression, and rises sharply during recompression.

Experimental observations by Bazergui [3.5.7] indicate that if recompression is carried above the value reached during the first cycle, then the curve is resumed practically as if the intermediate loading-unloading loop had not occurred (Fig. 3.5.2). Bazergui conducted extensive testing of spiral wound gaskets made from stainless steel windings (0.007" thick) and asbestos filler; and correlated the data for the decompression modulus E_g , and gross area seating stress σ_g in terms of two parameters:

(i) Winding density, $\rho_w = \eta_w / N_w$; where η_w is number of turns, and N_w is gasket width (Fig. 3.5.3). The winding density varies from 30 to 70 turns/inch in commercial spiral wound gaskets.

(ii) Extent of initial gasket compressive strain; $\epsilon_g = \delta_c / t_g$; where t_g is initial gasket thickness. In this correlation, the modulus of decompression is defined as:

$$E_g = \frac{\Delta\sigma_g}{\Delta\epsilon_g} \tag{3.5.5}$$

where $\Delta\sigma_g$ is the drop in compression stress, based on the gross gasket bearing area, corresponding to a decompression of 0.003", and $\Delta\epsilon_g$ is

$$\Delta\epsilon_g = \frac{0.003}{t_g - \delta_c} \tag{3.5.6}$$

According to [3.5.7], the gross area seating stress σ_g is related to the strain ϵ_g during initial loading by:

$$\sigma_g = 47 \rho_w e^{(7.26 \epsilon_g)} \text{ (psi)}$$

and during the unloading, the decompression modulus is

$$E_g \times 10^{-6} = 0.00164 \frac{\sigma_g}{\rho_w} + 0.057 \text{ (psi)} \tag{3.5.7}$$

It is to be noted that the ASME code seating stress y is proportional to σ_g ;

$$y = \sigma_g \frac{N_w}{b}$$

Bazergui's gasket width N_w is the gross gasket width less winding bead height ($\approx 1/16''$) as shown in Fig. 3.5.3. Spiral wound gaskets are characterized by high values of y and decompression modulus E_g . Large E_g implies that the gasket decompression due to joint pressurization should be minimized.

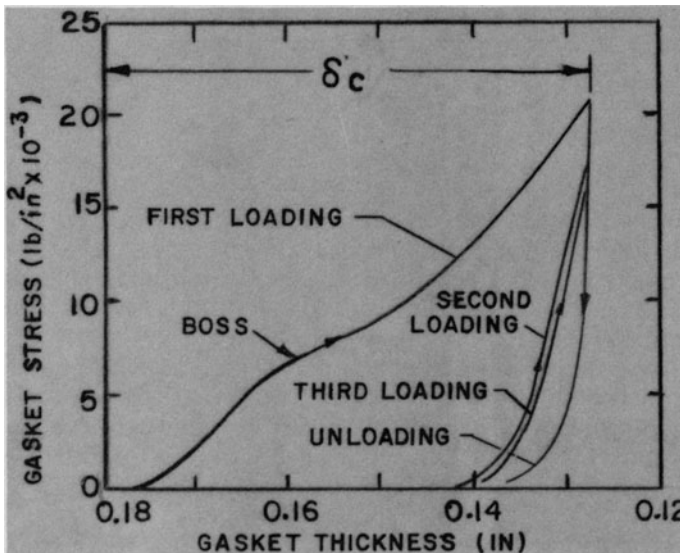


Fig. 3.5.1. Typical compression curve for spiral wound gasket.

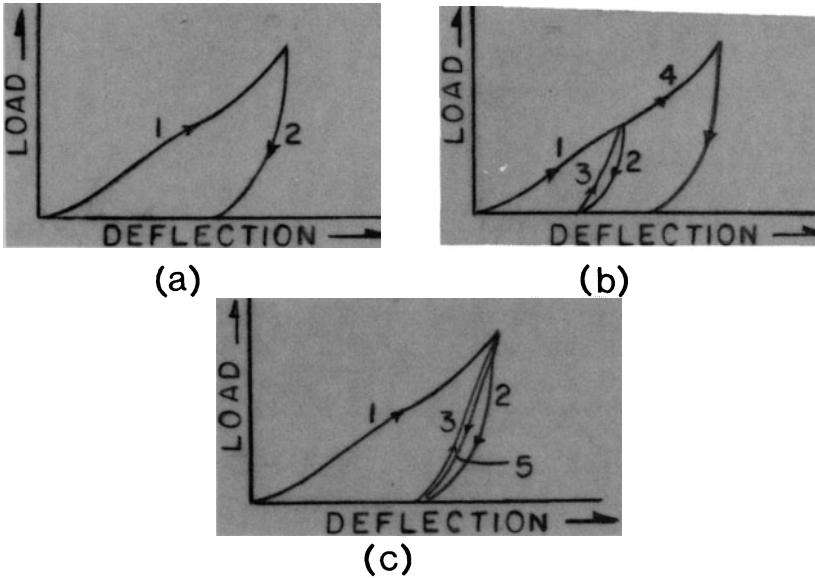


Fig. 3.5.2. Spiral wound gasket loading-reloading shapes.

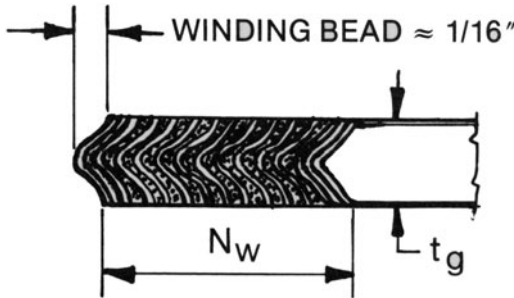


Fig. 3.5.3. Drawing of a spiral wound gasket.

Tightness Factor

As stated before, the minimum gasket seating stress y , and gasket seating factor m have been the subject of much disagreement and discussion [3.5.8-9] in the literature. Investigators generally agree, however, that y and m are somehow related. A systematic evaluation of the gasket characteristics by Bazergui and coworkers has provided some useful insight along with design data of practical use. Bazergui, et al. [3.5.10-11] proposed the term “tightness factor”, L_p , defined as the internal pressure required to produce unit leak rate from the joint. L_p correlates to P by a relationship of the form

$$L_p = P / (LR)^x$$

where P is the pressure (psi), and LR is leak rate in cubic cm/sec. The exponent x ranges from 0.58 to 0.64. By conducting tests on primarily spiral wound gaskets and correlating data, Bazergui observed that:

(i) When a new gasket is compressed for the first time, the surface stress σ_g to produce a required leak tightness factor L_p is substantially greater than the residual surface stress σ_g' required for L_p when the gasket is decompressed. This is illustrated schematically in Fig. 3.5.4 wherein the solid line represents the first compression cycle and the dotted lines represent decompression from stress levels corresponding to points B and C on the loading curve. Figure 3.5.4 shows that a seating stress equal to the ordinate AD is required to produce leak tightness equal to OD .

The required gasket surface stress is only DB' if the gasket is loaded to point B and then decompressed (by pressurizing the joint). The required surface stress is even lower (DC') if the gasket is originally compressed to point C .

Thus if σ_g corresponds to CF , then

$$y = \frac{(CF)N_w}{b}$$

and the corresponding gasket factor is given by

$$2bmP = (C'D)N_w$$

or

$$m = \frac{(C'D)N_w}{2bP}$$

Similarly, if σ_g (initial seating stress) is to the point B , then

$$y = \frac{(BE)N_w}{b}$$

and

$$m = \frac{(B'D)N_w}{2bP}$$

It is noted that y varies in an inverse manner to m . At the present time, unfortunately, leak tightness charts similar to Fig. 3.5.4 are not available for most gasket materials.

One effective means of reducing the joint separation, δ_s , is to employ the concept of "controlled compression." In this concept, we compress the gasket to a pre-determined thickness to develop the required pre-stress y . An additional increment of bolt load is then applied to produce a contact (metal-to-metal) load on a "land" region inside the bolt circle (Fig. 3.5.5). The axial force equilibrium (Eq. 3.5.1), now has an additional term:

$$W_1 = \pi b G y + R_c \quad (3.5.8)$$

R_c is the contact force on the "land". During pressurization, this contact force must be overcome by the header pressure before gasket unloading can initiate. In this manner the residual force on the gasket is increased and the range of fluctuation of the gasket residual force due to header force cycling

is reduced. The advantage of pre-loading the “land” is mathematically proved in Section 3.14.

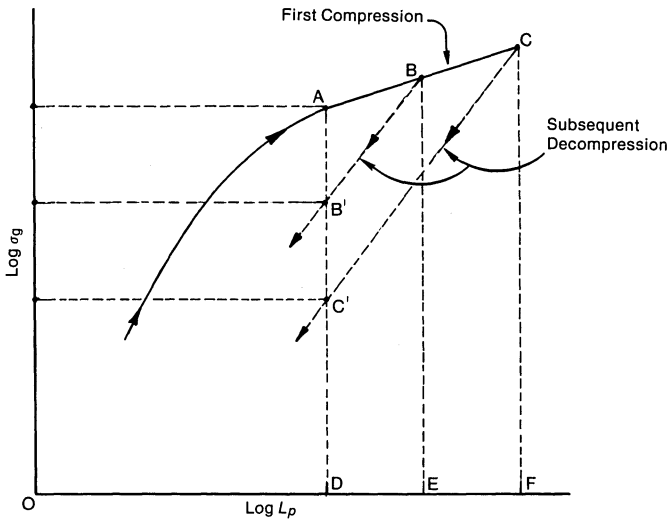


Fig. 3.5.4. Leak tightness vs. gasket surface stress during initial loading and unloading.

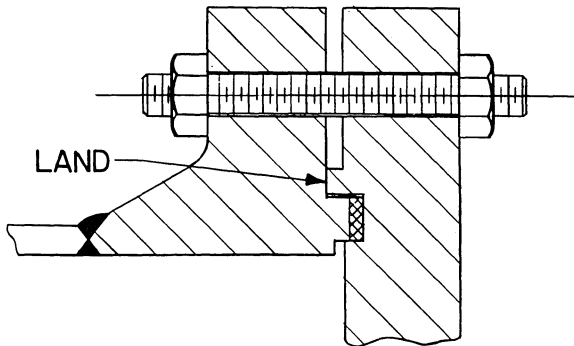


Fig. 3.5.5. Controlled compression joint.

In subsequent sections, the mechanics of the flanged joint is explored in some detail, and the implications of concepts such as controlled compression are analyzed in mathematical terms. It is, however, obvious that successful exploitation of such a concept hinges on the precise knowledge of the gasket loading/unloading curve. Unfortunately, such information is frequently not available.

Among self-equalizing gaskets, some reliable data on hollow metallic tubing can be found in the commercial literature. Tables 3.5.1 and 3.5.2 give excerpts of design data from ref. [3.5.12] for Inconel 718 tubing for 0.375", 0.5" and 0.625" O.D. tubing gaskets.

Table 3.5.1 Deflection and Springback of Inconel 718 O-Ring Gasket
(unlabeled data in parentheses are mm equivalents)

Load Force Unrestrained /linear inch →	.375" dia. × .0375" wall (9.5250 × 0.9525)		.500" dia. × .050" wall (12.700 × 1.2700)		.625" dia. × .0625" wall (15.8750 × 1.5875)						
	2500 lb/in(450 kg/cm)	Min. Spring Back .009(0.2286)	Deflection .030(0.7620)	2500 lb/in(450 kg/cm)	Min. Spring Back .013(0.3302)	Deflection .040(1.0160)	4000 lb/in(715 kg/cm)	Min. Spring Back .013(0.3302)	Deflection .050(1.2700)	Min. Spring Back .017(0.4318)	Deflection .062(1.5748)
Percentage 8%											
10%	.037(0.9398)	.009(0.2286)	.050(1.2700)	.013(0.3302)	.062(1.5748)	.017(0.4318)					
12%	.045(1.1430)	.009(0.2286)	.060(1.5240)	.013(0.3302)	.075(1.9050)	.017(0.4318)					
16%*	.060(1.5240)	.009(0.2286)	.080(2.0320)	.013(0.3302)	.100(2.5400)	.017(0.4318)					
17%	.064(1.6256)	.009(0.2286)	.085(2.1590)	.013(0.3302)	.106(2.6924)	.017(0.4318)					

*Optimum compression percentage.

Table 3.5.2. O-Ring and Groove Dimensions, inches (mm) (Fig. 3.3.5)

O Nominal Tubing O.D.	Nominal Tube Wall Thickness	X_c Groove Depth $\mp .005''$ (∓ 0.1270)	X_F Groove Width $\mp .010''$ (∓ 0.2540)
.375 (9.525)	.0375 (0.9525)	.300 (7.620)	.445 (11.303)
.500 (12.700)	.050 (1.2700)	.420 (10.668)	.645 (16.383)
.625 (15.875)	.0625 (1.5875)	.525 (13.335)	.780 (19.812)

3.6 BOLT PRE-TENSIONING

As stated earlier, pre-load in the bolts is required to pre-stress the gasket. This load can be developed in one of the following ways:

- (i) Thermal pre-tensioning
- (ii) Mechanical pre-tensioning
- (iii) Torque application

(i) Thermal Pre-Tensioning

Thermal pre-tensioning involves heating the stud to a pre-determined temperature, placing the nut in snug contact with flange faces, and subsequently allowing the stud to return to room temperature. For this purpose, an axial hole in the stud is drilled extending from one end to the point where the far end will be engaged in another nut (or into tapped holes in the flange). Electric heater rods are inserted in the axial slots. An approximate expression for computing the required temperature rise t_b , for a desired preload, can be derived as follows:

If we assume that the studs are raised to a temperature t_b above the ambient and that the end nuts are set in snug contact with flange faces, then the total axial force in the studs upon return to ambient temperature is given by:

$$W_1 = \frac{(\alpha_b t_b l_0 - \delta_1 - \delta_2) A_b' E_b n}{l_0} \quad (3.6.1)$$

where α_b , E_b , A_b' and l_0 denote the average coefficient of linear expansion of the stud material in the applicable temperature range, the Young's modulus, root area (Table 3.7.1), and free length of the stud, respectively, and n is the total number of bolts.

δ_1 and δ_2 denote the deflections of the mating flange rings at the bolt centerline location. Formulas to compute δ_1 and δ_2 in terms of δ_c , the compression of the gasket due to W_1 , are derived in a later section. δ_c is expressed in terms of the applied load by the gasket loading curve (such as Fig. 3.5.1). The required temperature rise to develop a certain bolt pre-load W_1 can be computed from Eq. (3.6.1) if the gasket loading diagram is

available, and if the appropriate equations for δ_1 and δ_2 are employed.

Caution should be observed in applying Eq. (3.6.1) if the bolt force is to be developed in more than one thermal step. As noted in the preceding section, the gasket unloading curve seldom follows the loading curve. Reheating the bolt in the second step may unload the gasket (Fig. 3.5.1) along a path different from its loading curve. The reloading during cooling of the bolt after the second heating may follow yet another curve. Unless the gasket loading, unloading and reloading characteristics are precisely known, it may be impossible to obtain the required pre-load accurately using a multiple heating-cooling procedure.

(ii) Mechanical Pre-Tensioning

As the name implies, mechanical pre-tensioning is accomplished by elongating the stud using a suitable stretch device, placing the end nuts in snug contact, and withdrawing the axial pull. The elongation is obtained using a hydraulic tensioner, such as the one shown in Fig. 3.6.1. As shown in this figure, the stud tensioner consists of a hydraulic cylinder, a stud puller bar, and a nut socket with turning mechanism.

If δ_i is the initial bolt elongation, then the final bolt preload is given by

$$W_1 = \frac{(\delta_i - \delta_1 - \delta_2)E_b A_b}{l_0} \quad (3.6.2)$$

where $A_b = nA'_b$ and δ_1 and δ_2 are functions of the applied load W_1 , flange stiffness and gasket compliance. The method to calculate δ_1 and δ_2 is given in a later section. Like thermal pre-tensioning, the simple formula for W_1 given above is not valid if the mechanical pre-tensioning is performed in more than one step.

(iii) Torque Application

This is the most common way of pre-stressing bolts. The nut is turned using a manual, pneumatic, or hydraulic wrench. The torque required to produce a preload F_{ax} in one bolt can be computed as follows:

Referring to Fig. 3.3.2, the required torque consists of three components, namely

- Torque τ_1 required to overcome friction between nut and flange interface.
- Torque τ_2 required to overcome friction between the turning nut and stud.
- Torque τ_3 required to propel the nut on the stud thread.

$$\tau = \tau_1 + \tau_2 + \tau_3 \quad (3.6.3)$$

We let d_i and d_o denote the inner and outer diameters of the annular bearing surface (see Table 3.7.1) of the nut.* Assuming uniform pressure p

*The cross section of the nut utilized in flanged joints is actually hexagonal. The bearing surface can be approximated by an annulus where the I.D. is the stud diameter and the O.D. is the dimension across the flat sides of the nut (Table 3.7.1).

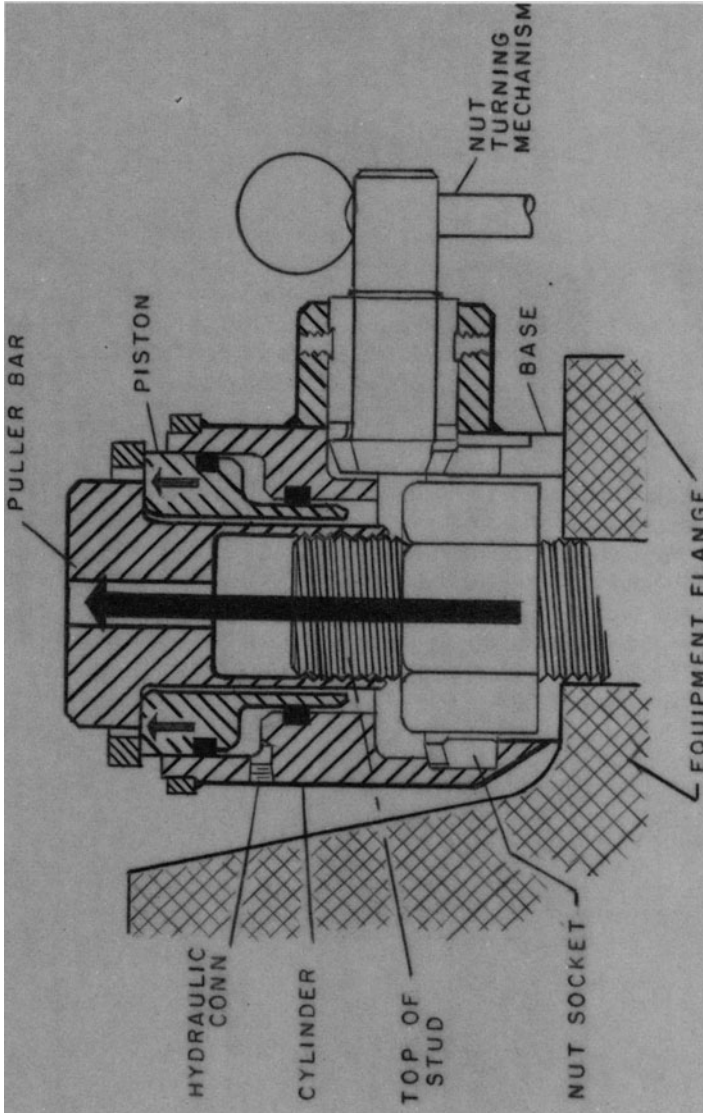


Fig. 3.6.1. Biach pre-tensioner.

= $4 F_{ax}/(\pi(d_o^2 - d_i^2))$ on this bearing surface, and a surface static coefficient of friction, μ_1 , we have:

$$\tau_1 = \frac{8F_{ax}\mu_1}{(d_o^2 - d_i^2)} \int_{0.5d_i}^{0.5d_o} r^2 dr$$

or

$$\tau_1 = \frac{F_{ax}\mu_1(d_o^3 - d_i^3)}{3(d_o^2 - d_i^2)}$$

or

$$\tau_1 = \frac{F_{ax}\mu_1(d_o^2 + d_i^2 + d_o d_i)}{3(d_o + d_i)} \quad (3.6.4)$$

The axial force F_{ax} gives rise to a bearing load between the nut and the thread, and hence to a friction load on the stud thread. τ_2 is given by calculating the moment due to the friction force between the nut and the stud thread. Assuming the coefficient of friction to be μ_2 ,

$$\tau_2 = \frac{\mu_2 F_{ax} d_p}{2 \cos \theta_t} \quad (3.6.5)$$

where d_p is the pitch diameter of the stud thread (Table 3.7.1) and θ_t is the angle of the thread helix, $\theta_t = \sin^{-1}(1/\pi d_p n_t)$. Finally, the torque required to propel the nut, τ_3 , can be computed by using the principle of conservation of energy. The work done by the external torque in turning the nut through one revolution must be equal to the work done against the axial force F_{ax} which is moved axially by $1/n_t$ unit of length in the process. n_t represents the number of threads per unit length in the bolt.

Hence:

$$2\pi\tau_3 = \frac{F_{ax}}{n_t}$$

or

$$\tau_3 = \frac{F_{ax}}{2\pi n_t} \quad (3.6.6)$$

Therefore, the torque required to turn the nut is given by:

$$\begin{aligned} \tau = \tau_1 + \tau_2 + \tau_3 &= \frac{F_{ax}\mu_1(d_o^2 + d_i^2 + d_i d_o)}{3(d_o + d_i)} \\ &+ \frac{\mu_2 F_{ax} d_p}{2 \cos \theta_t} + \frac{F_{ax}}{2\pi n_t} \end{aligned} \quad (3.6.7)$$

We emphasize that the above formula is, at best, a good estimate of the required torque. The coefficients of friction, μ_1 and μ_2 can vary widely depending on the material, surface finish, presence of lubricants, etc. The assumption of uniform pressure on nut/flange interfaces is simplistic, and rigorously speaking, incorrect.

Torquing is used to produce pre-tension in the bolt. But it also produces shear stress due to the torque τ_2 which is directly applied to the stud. For this reason, bolts subject to critical operating conditions are pre-stressed using one of the previously described pre-tensioning methods which do not induce shear stress in the bolt. Nevertheless, the majority of commercial heat exchangers and pressure vessel flanges are pre-stressed using the torquing method, presumably, due to its ease of application, economy, and a well established history of usage.

3.7 FLANGE SIZING

The geometric dimensions of a flange must be established before its stresses can be evaluated. Typically, the process of deciding the geometric details of the flange proceeds in the following order:

- (i) Select a flange type.
- (ii) Select facing detail and finish.
- (iii) Select a suitable gasket.
- (iv) Establish required bolting.
- (v) Determine bolt circle diameter and outer ring diameter. Choose appropriate hub dimensions (for hubbed flanges).
- (vi) Compute flange thickness to meet stipulated stress limits; or conversely, determine flange ring thickness for a given set of stress limits.

Steps (i)–(iii) have been discussed in some detail in the preceding sections. Empirical guidelines to complete steps (iv) and (v) are now described.

Required Bolt Cross-Sectional Area

The axial stress in the bolt should not exceed the allowable stress limit for its material of construction under both seating and pressurized conditions. Assuming all bolts to be uniformly loaded, the required total bolt root area A_b should be greater than or equal to the larger of A_{b1} and A_{b2} ; where:

$$A_{b1} = \frac{W_1}{S_{b1}}$$

$$A_{b2} = \frac{W_2}{S_{b2}} \quad (3.7.1)$$

Loads W_1 and W_2 are defined by Eqs. (3.5.1) and (3.5.2), and S_{b1} and S_{b2} are allowable bolt material stress limits at temperatures corresponding to seating (ambient) and to pressurized conditions, respectively.

The bolt area A_b is provided through n bolts arranged uniformly on the bolt circle. n is customarily an integral multiple of 4. Table 3.7.1 gives recommended bolt pitch p_b for a wide range of bolt sizes. The recommended radial offset R_h or R_r of the bolt circle, and edge distance e (Fig. 3.2.1) are also given in Table 3.7.1.

Table 3.7.1 Bolting Data*

THREADS			NUT DIMENSIONS (Heavy Hex)			MINIMUM FLANGE FACE DIMENSIONS					
Bolt Size d_B (inch)	No. of Threads n_t	Root Area A_b (in ²)	Pitch Diameter d_p (inch)	Across Flats d_o	Across Corners (inch)	Fig. 3.3.2 Bolt Spacing p_B (inch)	Fig. 3.2.1 Radial Distance R_R (inch)	Fig. 3.2.1 Radial Distance R_r (inch)	Fig. 3.3.3 Edge Distance e (inch)	Fig. 3.3.2 Wrench Diameter d_w (inch)	
1/2	13	0.126	.449	7/8	0.969	1 1/4	13/16	5/8	5/8	1 1/2	
5/8	11	0.202	.564	1 1/16	1.175	1 1/2	15/16	3/4	3/4	1 3/4	
3/4	10	0.302	.683	1 1/4	1.383	1 3/4	1 1/8	13/16	13/16	2 1/16	
7/8	9	0.419	.801	1 7/16	1.589	2 1/16	1 1/4	15/16	15/16	2 3/8	
1	8	0.551	.917	1 5/8	1.796	2 1/4	1 3/8	1 1/16	1 1/16	2 5/8	
1 1/8	8	0.728	1.042	1 13/16	2.002	2 1/2	1 1/2	1 1/8	1 1/8	2 7/8	
1 1/4	8	0.929	1.167	2	2.209	2 13/16	1 3/4	1 1/4	1 1/4	3 1/4	
1 3/8	8	1.155	1.292	2 3/16	2.416	3 1/16	1 7/8	1 3/8	1 3/8	3 1/2	
1 1/2	8	1.405	1.417	2 3/8	2.622	3 1/4	2	1 1/2	1 1/2	3 3/4	
1 5/8	8	1.680	1.542	2 9/16	2.828	3 1/2	2 1/8	1 5/8	1 5/8	4	
1 3/4	8	1.980	1.667	2 3/4	3.035	3 3/4	2 1/4	1 3/4	1 3/4	4 1/4	
1 7/8	8	2.304	1.792	2 15/16	3.242	4	2 3/8	1 7/8	1 7/8	4 1/2	
2	8	2.652	1.917	3 1/8	3.449	4 1/4	2 1/2	2	2	4 3/4	
2 1/4	8	3.423	2.166	3 1/2	3.862	4 3/4	2 3/4	2 1/4	2 1/4	5 1/4	
2 1/2	8	4.292	2.416	3 7/8	4.275	5 1/4	3 1/16	2 3/8	2 3/8	5 7/8	
2 3/4	8	5.259	2.666	4 1/4	4.688	5 3/4	3 3/8	2 5/8	2 5/8	6 1/2	
3	8	6.324	2.916	4 5/8	5.102	6 1/4	3 5/8	2 7/8	2 7/8	7	
3 1/4	8	7.487	3.166	5	5.515	6 5/8	3 3/4	3	3	7 1/4	
3 1/2	8	8.749	3.416	5 3/8	5.928	7 1/8	4 1/8	3 1/4	3 1/4	8	
3 3/4	8	10.108	3.666	5 3/4	6.341	7 5/8	4 7/16	3 1/2	3 1/2	8 5/8	
4	8	11.565	3.916	6 1/8	6.755	8 1/8	4 5/8	3 5/8	3 5/8	9	

*Adapted from Standards of Tubular Exchanger Manufacturers Association, Sixth Edition, printed with the permission of the publisher.

Establishing Important Radial Dimensions of Flange

The values given in Table 3.7.1 are sufficient to establish all in-plane dimensions of a ring or lap joint flange. However, the welding neck flange requires two additional decisions; namely the length and taper of the hub. As a rule, the hub is made as short as possible to economize the material cost of the flange. Shortening the hub, however, reduces the overall rigidity of the flange and makes radiographic or volumetric examination of the shell-to-hub butt joint (Fig. 3.3.1) less convenient, and consequently less precise. The (tangent) slope of the hub taper is usually selected in the range of 1/3 to 1/4. The slope directly affects the location where the maximum bending stress in the hub occurs.

3.8 FLANGE MOMENTS

As stated earlier, under the seating condition, the bolt pull W_1 is balanced by the axial compression load on the gasket in raised face designs (no metal-to-metal contact elsewhere on flange face). In a ring joint (Fig. 3.2.1a) or welding neck (Fig. 3.2.1b) design these two coaxial forces, at an offset h_G , generate a moment. This moment produces a stress field in the flange. To minimize stresses, it is advisable to minimize the offset h_G between these opposing forces. This is accomplished by placing the gasket as close to the bolt circle as is practically feasible. In the lap joint flange (Fig. 3.2.1c) the situation is somewhat different. The bolt pull induces a contact force between the lap ring and the flange ring. It is reasonable to assume that the rotation of the flange ring would push the resultant of the contact pressure towards the bolt center line. However, the design codes [3.5.1–3] require this resultant to be assumed at the mid-circumference of the nominal annular contact patch. It should be noted that any eccentricity between this contact force and gasket force resultant will produce a twisting moment on the lap ring. Sound engineering warrants that this moment be minimized or eliminated if possible.

Clearly, the axial load W_1 need not be limited by the minimum gasket seating stress (Eq. 3.5.1) specially if A_b is much greater than A_{b1} . Since the bolt tightening techniques can be quite imprecise, some codes require W_1 to be suitably increased wherever a possibility of overtightening exists.

When the joint is pressurized, the longitudinal pull on the header, H_d (Fig. 3.2.1b), alters the axial force equilibrium on the flange ring. The initial bolt load W_1 may change to a new load W_2 which may be viewed as resisting three discrete loads (Fig. 3.2.1b):

- (i) Axial load H_d due to hydrostatic force on the area bounded by the inside of flange diameter.
- (ii) Axial load H_T due to the pressure acting on the annular area between effective gasket diameter G and inside flange diameter B .
- (iii) Residual gasket load, H_G .

It is important to note that H_d is zero in those designs where the pressurization of the joint does not produce an axial pull in the shell. The shellside of the three-element flanged joint shown in Fig. 3.1.1 belongs to this category. Flange designers often overlook this important fact.

The four coaxial loads under the pressurized condition produce a circumferentially distributed moment which is readily computed by multiplying the opposing forces by their offsets and summing them. The design codes [3.5.1–3] give detailed procedures for computing the total moment. Replacing discretely spaced equal and opposite axial loads by resultant couples is an approximation which is justifiable as long as the flange ring can be structurally analyzed as a “ring” rather than as an “annular plate.” This assumption introduces small errors in commercial flange designs.

From the above discussion, we see that an understanding of the structural behavior of axisymmetrically loaded annular rings is essential in analyzing the mechanics of flange action.

3.9 CIRCULAR RINGS UNDER DISTRIBUTED COUPLES

We consider an elastic circular ring of mean radius r_m , radial width b_r , and thickness t_r , (Fig. 3.9.1) subject to a uniformly distributed couple m , per unit circumference at mean radius r_m . Due to axisymmetry, every cross section of the ring rotates in its own plane about its centroid through an angle θ_r . The physical state of strain in the ring can be visualized by noting that any point located to the right at distance y from the central plane in Fig. 3.9.1b will move in towards the center by an amount $y\theta_r$. This radially inwards motion reduces the circumference of the circle on which this point is located producing compressive stress. Similarly, a point located to the left of the plane of symmetry will experience tensile stress.

Figure 3.9.1c shows the equilibrium of a small sector of projected angle $d\alpha$. From symmetry, the internal moments M_t on the two cut-away sections of the sector must be equal. Requiring moment equilibrium between internal ring moments M_t and the total external moment due to m , yields:

$$2 \sin \frac{d\alpha}{2} M_t = m_r r_m d\alpha; \text{ or } M_t = m_r r_m \quad (3.9.1)$$

This bending moment M_t , acting on the ring cross section of area $b_r t_r$, produces a flexural stress distribution in the ring; the maximum magnitude of this stress occurs at the top or bottom surface. Referring to Fig. 3.9.1b, a point P located at coordinate (x,y) with respect to the origin of the centroidal planes of the ring cross section, moves radially outwards by an amount $y\theta_r$. Since the point P is located on a circle of radius $(r_m + x)$, the circumferential strain due to this radial movement is $y\theta_r/(r_m + x)$. Therefore, the circumferential stress S is

$$S = \frac{E_r y}{(r_m + x)} \theta_r \quad (3.9.2a)$$

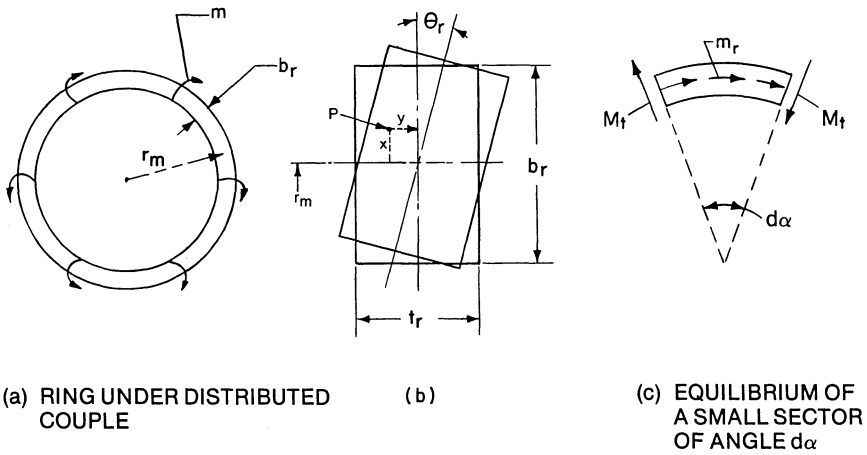


Fig. 3.9.1. Axisymmetric couple loading on a thin ring.

where E_r is the Young's modulus of the ring material.

The first moment of S about the $y=0$ axis must equal the internal moment M_t .

$$M_t = \int_{-0.5t_r}^{+0.5t_r} \int_{-0.5b_r}^{+0.5b_r} S y dx dy$$

Substitution for S from above and integrating yields

$$M_t = \frac{E_r t_r^3}{12} \theta_r \ln \bar{K}; \quad \bar{K} = \frac{1 + b_r/2r_m}{1 - b_r/2r_m} \tag{3.9.2b}$$

From Eq. (3.9.2a), we note that the maximum S will occur at $y = \pm 0.5t_r$ (either of the two lateral surfaces of the ring), and $x = -0.5b_r$; thus, the maximum stress is

$$S_{\max} = \frac{E_r t_r \theta_r}{2 \left(r_m - \frac{b_r}{2} \right)} \tag{3.9.2c}$$

Therefore

$$S_{\max} = \frac{6M_t}{t_r^2 \phi} \tag{3.9.2d}$$

where ϕ has the dimensions of length

$$\phi = r_m (1 - b_r/2r_m) \ln \frac{(1 + b_r/2r_m)}{(1 - b_r/2r_m)} \tag{3.9.3}$$

We note that assuming $b_r/2r_m$ small compared to unity leads to $\phi \approx b_r$. The rotation of the ring, θ_r , is obtained from Eq. (3.9.2b) by noting that $M_t = m_r r_m$:

$$\theta_r = \frac{12}{E_r t_r^3} \frac{(r_m m_r)}{\ln \bar{K}} \quad (3.9.4a)$$

We will use this equation again in Chapters 8 and 9. For our purposes herein, we can define I_r as the area moment of inertia of the ring cross section about its neutral axis (i.e., $I_r = b_r t_r^3 / 12$); then for $b_r / 2r_m < 1$, Eq. (3.9.4a) can be rewritten as

$$\theta_r = \frac{m_r r_m^2}{E_r I_r} \quad (3.9.4b)$$

Finally, from Eq. (3.9.2c) we note that

$$\theta_r \doteq 2S_{\max} r_m / E_r t_r \quad (3.9.5)$$

Equations (3.9.1), (3.9.2d), and (3.9.4) completely characterize the elastic behavior of the ring. It is noted that the cross section of the ring has been assumed to be non-deformable in the above derivation. The radial bending effect can be included in the analysis if Kirchoff's plate bending equations are used. This is discussed further in a later section. For our purposes, the foregoing relationships furnish the necessary tools to examine the essential characteristics of a bolted joint as long as one is willing to assume that the ring width b_r is much smaller than the ring I.D. and that t_r is of the same order as b_r .

3.10 DEFORMATION OF A FLANGED JOINT

To gain some insight into the mechanics of flange deformation, it is instructive to examine, in detail, the deformation characteristics of a bolted joint consisting of a pair of identical ring flanges. The connecting shells are assumed to be so thin that their contribution to the rigidity of their respective flanges can be neglected without much error. The connecting bolts are assumed to be of free length l_0 and cross-sectional area A_b . Under the seating condition the total bolt pre-load W_1 is balanced by an equal and opposite gasket reaction located at an offset h_G (Fig. 3.10.1). This produces, on each flange, an axisymmetric couple of magnitude

$$m_r = \frac{W_1 h_G}{2\pi r_m}$$

per unit circumference. r_m denotes the mean radius of the flange ring. Therefore, the rotation θ_r of each ring is given by Eq. (3.9.4) as

$$\theta_r = \frac{m_r r_m^2}{E_r I_r} = \frac{W_1 h_G r_m}{2\pi E_r I_r} \quad (3.10.1)$$

Figure 3.10.2 shows the pressurized joint. The gasket compression is reduced to H_G' , and the flange ring rotation acquires a new value θ_r' . The total header load H_p is assumed to act at a distance h_p from the bolt center line. Note that $H_p = H_d + H_T$ (recall Fig. 3.2.1b).

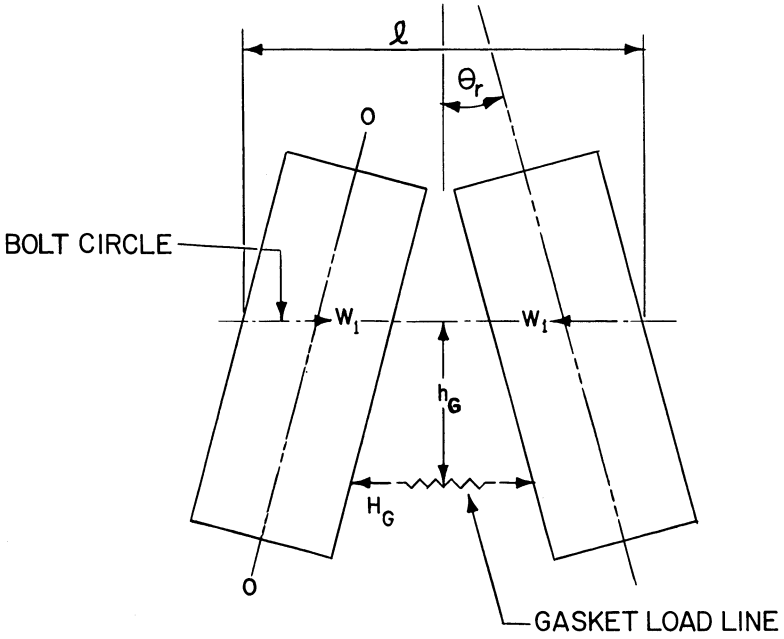


Fig. 3.10.1. Pair of ring flanges under seating condition.

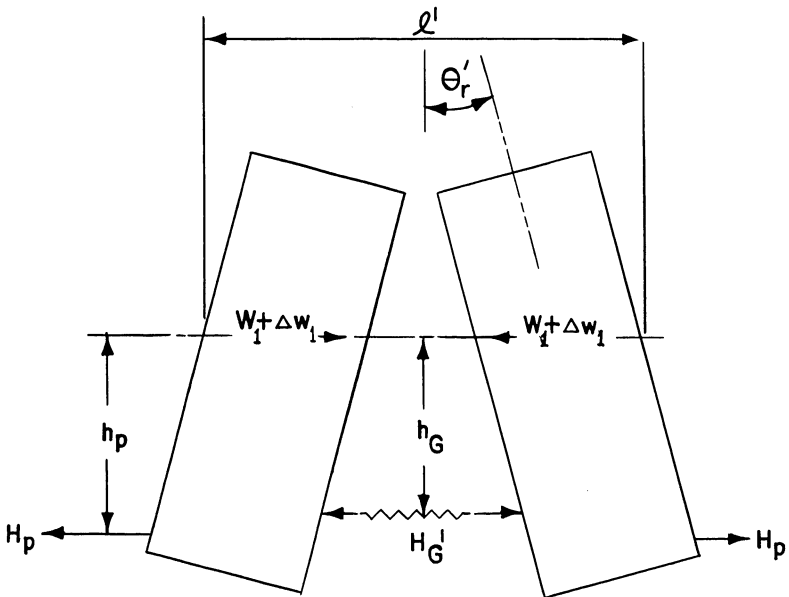


Fig. 3.10.2. Pair of ring flanges under pressurized condition.

Axial equilibrium now yields:

$$H_G' = W_1 + \Delta W_1 - H_p \quad (3.10.2)$$

where ΔW_1 is the increase in bolt load. As before, the relationship between ring rotation and applied moment yields:

$$\theta_r' = \frac{(H_G' h_G + H_p h_p) r_m}{2\pi E_r I_r}$$

or

$$\theta_r' = \frac{[(W_1 + \Delta W_1) h_G + H_p (h_p - h_G)] r_m}{2\pi E_r I_r} \quad (3.10.3)$$

Let K_b and K_G define the spring stiffnesses of the bolt and gasket (unloading modulus), respectively. Hence;

$$\Delta W_1 = K_b (l' - l) \quad (3.10.4a)$$

where

$$K_b = \frac{A_b E_b}{l_0} \quad (3.10.4b)$$

and l and l' are the bolt length during preloading and pressurized conditions, respectively. Referring to Figs. 3.10.1 and 3.10.2, the total relaxation of the gasket, δ_g , is given by

$$\delta_g = (l' - l) + 2(\theta_r' - \theta_r) h_G \quad (3.10.5)$$

Furthermore, since $H_G = W_1$, then

$$\delta_g = \frac{H_G - H_G'}{K_G} = \frac{H_p - \Delta W_1}{K_G} \quad (3.10.6)$$

In Eq. (3.10.5), substituting for δ_g from Eq. (3.10.6), θ_r and θ_r' from Eqs. (3.10.1) and (3.10.3), respectively, we have, after some manipulation,

$$\frac{\Delta W_1}{H_p} = \frac{1 - \frac{h_G (h_p - h_G) r_m K_G}{\pi E_r I_r}}{1 + \frac{K_G}{K_b} + \frac{h_G^2 K_G r_m}{\pi E_r I_r}} \quad (3.10.7)$$

Let

$$\frac{K_G}{K_b} = \alpha_1 \quad (a)$$

$$\frac{K_G r_m h_G^2}{\pi E_r I_r} = \alpha_2 \quad (b) \quad (3.10.8)$$

$$\frac{h_p - h_G}{h_G} = \alpha_3 \quad (c)$$

then:

$$\frac{\Delta W_1}{H_p} = \frac{1 - \alpha_2 \alpha_3}{1 + \alpha_1 + \alpha_2} \quad (3.10.9)$$

Equation (3.10.9) gives the fractional increase in bolt load with respect to the pressure load. It is noted that if:

$$\alpha_2 \alpha_3 > 1$$

then ΔW_1 will be negative. This is clearly undesirable since, from Eqs. (3.10.2) and (3.10.3), the drop in the gasket load is given by

$$\Delta H_G = H_G - H_G' = H_p - \Delta W_1$$

Thus, a negative ΔW_1 serves to increase ΔH_G , which may be written using Eqs. (3.10.8) and (3.10.9) as:

$$\Delta H_G = H_p \left[\frac{\alpha_1 + \alpha_2 + \alpha_2 \alpha_3}{\alpha_1 + \alpha_2 + 1} \right] \quad (3.10.10)$$

From the above equation it can be deduced that the design goal should be to minimize α_1 , α_2 , α_3 . Ideally, α_3 should be made zero; although in practical designs, this is usually not achievable. The following additional deductions from the above equations give useful guidelines in flange design:

a. Small α_1 is a desirable design goal. Thus a gasket of small unloading modulus is preferable to one with a larger modulus. However, there are manufacturing limitations on how small K_G can be made for a particular application. On the other hand, the bolt stiffness K_b usually can be increased substantially by increasing total bolt tensile stress area. *Thus, a flanged joint with a greater bolt cross-sectional area and lower pre-stress (to produce a given preload) is better than one with a smaller sectional area which is pre-stressed to a proportionately larger value.* Stiffness can also be increased by reducing bolt effective length l_0 . This can be accomplished by using tapped holes in one of the flanges instead of an end nut.

b. Reduction in α_2 can be accomplished by reducing h_G . Designers, however, try to minimize h_G to reduce flange moment. A further reduction is usually not feasible. Also, increasing the flange ring moment of inertia, I_r , decreases α_2 and hence helps increase ΔW_1 .

c. The results show clearly that large diameter flanges are harder to seal than small diameter units, since α_2 increases linearly with r_m .

We have deduced the above results from a simplified ring flange model. The behavior of more complex flange geometries, such as a tapered hub design, is more involved. Nevertheless, the qualitative remarks stated above give some valuable insight into all raised face external flange designs.

Example: To illustrate some of the concepts derived in this section, let us consider a ring flange 27" O.D. by 22" I.D., 3" thick, bolted to an identical flange with 24 bolts of 5/8" diameter. Assuming 25,000 psi pre-stress in bolts, we have $W_1 = 121,200$ lb. The flange ring moment of inertia, I_r is 5.63 in.⁴; and the material Young's modulus is 30×10^6 psi. We assume a gasket unloading modulus 8.08×10^6 lb/in. Finally $h_G = 1$ " and $h_p = 1.25$ ".

Results computed from Eqs. (3.10.7)-(3.10.10) for $K_b = 20.8 \times 10^6$ lb/in. (7" long bolt); and $K_g = 32.4 \times 10^6$ lb/in. are given below.

$(\times 10^{-6} \text{ lb/in.})$	α_1	α_2	α_3	$\Delta W_1/H_p$	$\Delta H_G/H_G$
20.8	0.39	0.19	0.25	0.60	0.40
32.4	0.25	0.19	0.25	0.66	0.34

We see that, in both cases, the increase in bolt load is a substantial fraction of the imposed pressure load. The fractional increase is greater for the stiffer bolt geometry.

3.11 WATERS, ROSSHEIM, WESSTROM AND WILLIAMS' METHOD FOR FLANGE DESIGN

Waters, et al. [3.11.1] are generally credited with having first developed a consistent treatment for tapered hub flanges. Reference [3.11.1] gives an abbreviated account of their analysis. Unabridged details were published in booklet form in 1949 by Taylor Forge & Pipe Works [3.11.2]. Their work has received widespread acceptance in the American pressure vessel industry. Even at this date, design rules for raised face flanges in the ASME Codes [3.5.1–3] are almost entirely based on this work. In view of its unarguable importance, we will present the analysis in the following in sufficient detail to enable the reader to obtain full appreciation of the approach and the method of analysis.

The freebody of the tapered hub flange to be analyzed herein is shown in Fig. 3.11.1. Waters, et al. sought to solve this problem in such a manner that the computations could be carried out manually with the aid of charts and tables. Accordingly, several assumptions were made to render this possible. The important assumptions are:

- (i) *Ring*: The flange ring is modelled as an annular plate; Kirchoff's plate bending equations are used to characterize its behavior. Why Waters, et al. did not use the simpler ring equations (Section 3.9) is not clear. Perhaps concern regarding accuracy in the small diameter range (when flange ring radial width to mean diameter can get as high as 0.4) prompted them to use the annular plate equations.
- (ii) *Bolts*: The bolt load is, of course, applied at discrete bolt locations. However, for the purpose of analysis, this load is assumed to be "smeared" uniformly over the bolt circle circumference.
- (iii) *Ring Moment*: The overturning moment due to non-concentricity of bolt load and gasket load is replaced by two equal and opposite forces W_{eq} at the inner and outer circumference of the ring such that the overall moment is unchanged. This assumption implies that the annular plate is narrow which makes it somewhat incongruous with the emphasis to model the flange ring using "plate" equations.
- (iv) Point 0 in Fig. 3.11.1 is assumed to have zero radial displacement. This assumption is made strictly for the sake of simplification.
- (v) *Hub*: The hub is modelled as a thin shell of varying thickness. The

inside radius r_1 of the hub is used interchangeably with the shell mean radius in the shell equations to simplify the analysis. Local pressure acting on the hub surface is neglected.

- (vi) *Shell*: The shell, like the hub, is assumed to be thin and local pressure on the shell wall is neglected. The shell is assumed to be sufficiently long such that the effect of edge loads P_0 and M_{h0} are not felt at the other extremity of the shell. (See our comments on shell boundary layer effects in Appendix A).

The anatomy of the flange as articulated above leads to a standard problem in stress analysis near geometric discontinuities (see Chapter 2). The object is to compute the discontinuity shear P_0 and moment M_{h0} at the shell/hub interface, and the shear P_1 and moment M_{h1} at the hub/ring interface due to the imposed load on the ring. This is done by writing the governing equations for each structural element, and requiring that the edge loadings take on values so as to maintain compatibility of geometry at the interface boundaries. We proceed to develop the structural relations for each element in a form suitable for algebraic manipulation. Detailed derivation of these relations from first principles is not given here. Readers interested in the background derivations should consult the references cited at appropriate locations in the text below. We have also provided, in Appendix A, some background on the development of the shell equations in order to give the interested reader some insight into the development of structural theories.

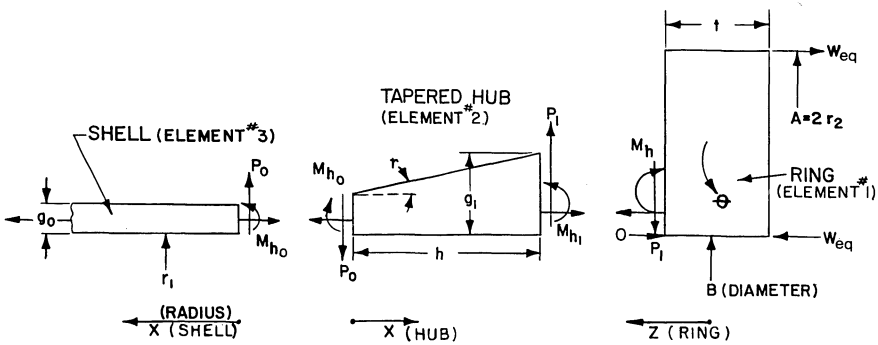


Fig. 3.11.1. Three element model of an integral tapered hub flange (seating condition).

3.11.1 Flange Ring (Element #1)

The governing differential equation for small deflection of an axisymmetrically loaded thin plate is given by the so-called Poisson-Kirchoff equation [3.11.3].

$$\frac{1}{r} \frac{d}{dr} \left\{ r \frac{d}{dr} \left[\left(\frac{1}{r} \frac{d}{dr} r \frac{dz}{dr} \right) \right] \right\} = \frac{q}{D} \quad (3.11.1)$$

where z denotes the lateral deflection of the plate in the direction of the applied load q . D is the flexural rigidity of the plate, defined as:

$$D = \frac{Et^3}{12(1-\nu^2)} \quad (3.11.2)$$

The solution of Eq. (3.11.1) consists of a homogeneous solution containing four undetermined constants of integration, and a particular solution which depends on the form of $q(r)$.

Thus, as shown in Appendix A and in Ref. [3.11.4], the general solution can be written as

$$z(r) = C_1 r^2 \ln r + C_2 r^2 + C_3 \ln r + C_4 + f(r) \quad (3.11.3)$$

where C_i ($i=1,2,3,4$) are constants of integration, and $f(r)$ is the particular solution appropriate to the given loading $q(r)$. The solutions for C_i are found by applying the appropriate boundary conditions. Having determined C_i and $f(r)$, the internal stress resultants are then found using the relations:

$$\begin{aligned} M_r &= D \left(\frac{d^2 z}{dr^2} + \frac{\nu}{r} \frac{dz}{dr} \right) \quad (a) \\ M_t &= D \left(\frac{1}{r} \frac{dz}{dr} + \nu \frac{d^2 z}{dr^2} \right) \quad (b) \\ Q &= -D \frac{d}{dr} \left[\frac{1}{r} \frac{d}{dr} \left(r \frac{dz}{dr} \right) \right] \\ &= -\frac{dM_r}{dr} + \frac{M_t - M_r}{r} \quad (c) \end{aligned} \quad (3.11.4)$$

In the foregoing equations, M_r , M_t , and Q denote the radial bending moment, tangential bending moment, and radial shear per unit length, respectively. The sign convention used here is shown in Fig. 3.11.2.

The four boundary conditions for the ring are:

At $r=r_2$, the radial bending moment is zero, i.e., $M_{r_2} = 0$.

At $r=r_2$, the shear Q_{r_2} is given by

$$Q_{r_2} = \frac{-W_{eq}}{2\pi r_2}$$

In order to fix the structure in space, the z direction deflection (axial movement) of one point must be specified. For convenience the deflection of point 0 in Fig. 3.11.1 is set equal to zero (3rd boundary condition). For the remaining boundary condition, let the slope of the ring at $r=r_1$ be given by θ , i.e.

$$\frac{dz}{dr} = \theta \text{ at } r=r_1$$

We emphasize here that θ is at present unknown. We will determine θ by requiring geometric compatibility of the ring with the adjoining structure.

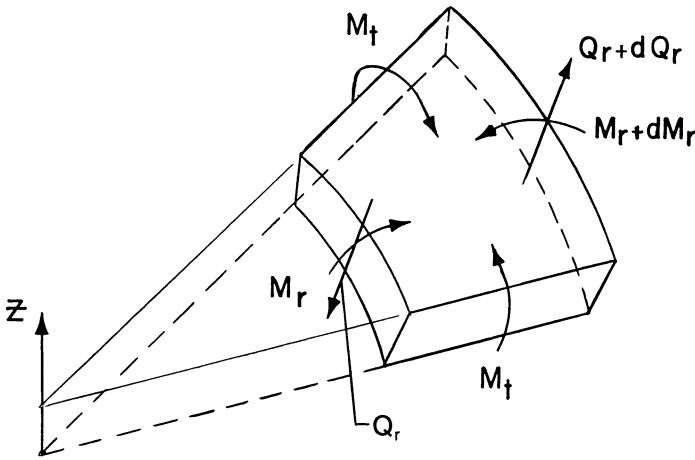


Fig. 3.11.2. Sign convention for stress resultants.

Finally, since there is no lateral loading on the ring (Fig. 3.11.1), (recall that the line load W_{eq} has been accounted for in the boundary condition) the function $f(r)$ is identically zero. We see that the assumption that W_{eq} acts at the ring boundary leads to the elimination of the particular solution in the plate solution.

The four constants of integration are evaluated using the above boundary conditions as follows:

$$C_1 = \frac{W_{eq}}{8\pi D}, \quad (a)$$

$$C_2 = \frac{-W_{eq}}{16\pi D} (2\ln r_1 + 1) - \frac{C_3}{2r_1^2} + \frac{\theta}{2r_1} \quad (b)$$

$$C_3 = \left\{ \frac{W_{eq}}{8\pi D} [2(1+\nu)\ln K + 2] + \frac{1+\nu}{r_1} \theta \right\} \times \left[\frac{r_2^2}{(1+\nu)K^2 + (1+\nu)} \right] \quad (c) \quad (3.11.5)$$

$$C_4 = -C_1 r_1^2 \ln r_1 - C_2 r_1^2 - C_3 \ln r_1 \quad (d)$$

where $K = A/B = r_2/r_1$

From Eqs. (3.11.4) and (3.11.3) the stress resultants are given as:

$$M_r = D \left[2C_1(1+\nu)\ln r + (3+\nu)C_1 + 2(1+\nu)C_2 - (1-\nu)\frac{C_3}{r^2} \right] \quad (a)$$

$$M_t = D \left[2C_1(1+\nu)\ln r + (3\nu+1)C_1 + 2(1+\nu)C_2 - (\nu-1)\frac{C_3}{r^2} \right] \quad (b)$$

$$(3.11.6)$$

Substituting, for C_i from above, and letting $r = r_1$ yields the values for the radial and for the tangential moments of the ring at the inner radius. After the necessary algebraic manipulations, the following results are obtained:

$$M_{r_1} = \frac{1-K^2}{\left(\frac{1+\nu}{1-\nu}\right)K^2+1} \left\{ (1+\nu) \frac{2D\theta}{B} + \frac{W_{eq}}{2\pi} \left[\frac{1}{2} + \left(\frac{1+\nu}{1-\nu}\right) \left(\frac{K^2}{K^2-1}\right) \ln K \right] \right\} \quad (a) \quad (3.11.7)$$

$$M_{t_1} = \frac{K^2+1}{(1-K^2)} M_{r_1} - \frac{W_{eq}}{2\pi} \left[\frac{(1-\nu)}{2} + (1+\nu) \left(\frac{K^2}{K^2-1}\right) \ln K \right] \quad (b)$$

where subscript 1 appended to the M_r and M_t indicates that they are evaluated at $r = r_1$, and $K = A/B$ (see Fig. 3.11.1).

We note that for a loose ring flange, $M_{r_1} = 0$. For this case Eq. (3.11.7a) gives the rotation θ and Eq. (3.11.7b) determines the tangential moment M_{t_1} . It can be shown that in the case of a loose ring flange, M_t reaches its maximum value at $r = r_1$. The maximum moment $M_{t(\max)}$ is given by:

$$\begin{aligned} M_{t(\max)} &= \frac{-W_{eq}}{2\pi} \left[\frac{(1-\nu)}{2} + (1+\nu) \left(\frac{K^2}{K^2-1}\right) \ln K \right] \\ &= \frac{-W_{eq}}{12} (K-1) Y = \frac{-W_{eq}(A-B)}{12B} Y = \frac{-M_{ext} Y}{6B} \end{aligned} \quad (3.11.8)$$

where Y is the well known "Y factor" in the ASME Codes [3.5.1,2,3]

$$Y = \frac{6}{\pi(K-1)} \left[\frac{(1-\nu)}{2} + (1+\nu) \frac{K^2}{(K^2-1)} \ln K \right] \quad (3.11.9)$$

and M_{ext} is the applied moment on the flange ring;

$$M_{ext} = \frac{W_{eq}(A-B)}{2}$$

3.11.2 Tapered Hub (Element #2)

The tapered hub is the second element shown in Fig. 3.11.1 which needs to be analyzed. Its thickness at the small end (joint to shell) is denoted by g_0 ; the thickness increases linearly to g_1 in a distance h . The "taper factor" of the hub is defined as

$$\alpha = \frac{g_1 - g_0}{g_0} \quad (3.11.10)$$

This dimensionless factor appears repeatedly in the course of the flange analysis. It should not be confused with the slope of the taper.

The hub is modelled using thin shell equations for axi-symmetric bending [3.11.3, p. 468]. As in the case of the flange ring, the deflection y_h is given

in terms of a fourth order linear differential equation with x as the independent coordinate (Fig. 3.11.1).

$$\frac{d^2}{dx^2} \left[g^3 \frac{d^2 y_h}{dx^2} \right] + \frac{12(1-\nu^2)g}{r_1^2} y_h = 0 \quad (3.11.11)$$

The r.h.s. is zero in the absence of any lateral loading. The inner radius r_1 is substituted in place of the mean radius to simplify analysis. The longitudinal moment M_h at any location is given by

$$M_h = D_h \frac{d^2 y_h}{dx^2} \quad (3.11.12)$$

where D_h is the shell flexural rigidity, defined as

$$D_h = \frac{Eg^3(x)}{12(1-\nu^2)} \quad (3.11.13)$$

Similarly, the radial shear P_h is defined as

$$P_h = \frac{-dM_h}{dx} \quad (3.11.14)$$

Equation (3.11.11) is cast into dimensionless form by redefining the dependent and independent variables as follows:

$$\xi = x/h \quad (a)$$

$$w = y_h/r_1 \quad (b) \quad (3.11.15)$$

Then we have:

$$\frac{d^2}{d\xi^2} \left[(1 + \alpha\xi)^3 \frac{d^2 w}{d\xi^2} \right] + \kappa(1 + \alpha\xi)w = 0 \quad (3.11.16)$$

$$M_h = \frac{Eg_0 h^2}{r_1 \kappa} (1 + \alpha\xi)^3 \frac{d^2 w}{d\xi^2} \quad (3.11.17)$$

where κ is referred to as the "hub modulus"

$$\kappa = \frac{12(1-\nu^2)h^4}{r_1^2 g_0^2} \quad (3.11.18)$$

κ will be encountered repeatedly in further analysis.

A similar expression for P_h is obtained using Eqs. (3.11.14) and (3.11.17)

$$P_h = \frac{-Eg_0 h}{r_1 \kappa} \left[(1 + \alpha\xi)^3 \frac{d^3 w}{d\xi^3} + 3\alpha(1 + \alpha\xi)^2 \frac{d^2 w}{d\xi^2} \right] \quad (3.11.19)$$

Equation (3.11.11) can be solved using standard procedures, and the solution may be obtained in terms of four undetermined constants (see, for example, Hildebrand [3.11.5]). The solution, as seen later, involves Bessel functions. A solution involving transcendental functions would thwart the objective of developing a manual computation procedure. For this reason, Waters, et al. devised an approximate solution. This approximate solution is constructed by assuming a certain polynomial function for w which is compatible with the boundary conditions, and which contains six undetermined parameters. Three of these parameters are evaluated by

requiring that the boundary conditions be satisfied. The other three parameters are evaluated by using energy principles. The potential energy of the hub, in terms of the assumed polynomial function for w , its derivatives, and the externally applied loads, is written out. The optimal values of the three floating parameters are those that make the potential energy function stationary [3.11.6]. Thus, the vanishing of the partial derivatives of the potential energy with respect to the three parameters gives three additional algebraic equations to determine them. Waters, et al. proposed the following sixth-order polynomial for w .

$$w = (1 - \xi)a_1 + \left(\xi - \frac{5}{2}\xi^2 + \frac{3}{2}\xi^3\right)a_2 + \left(\xi^4 - \frac{9}{5}\xi^5 + \frac{4}{5}\xi^6\right)a_3 - \left(\frac{5}{12}\xi - \frac{1}{2}\xi^2 + \frac{1}{12}\xi^4\right)A_0 - \left(\frac{1}{12}\xi - \frac{1}{12}\xi^4\right)A_1 - \left(\frac{1}{12}\xi - \frac{1}{6}\xi^3 + \frac{1}{12}\xi^4\right)B_0 \quad (3.11.20a)$$

The rationale for this polynomial function is given in Appendix 3.A. It should be added here that a higher (say seventh) order polynomial could have been selected. It would have merely required that the potential energy function be differentiated with respect to one additional parameter, resulting in one additional algebraic equations to be solved. Similarly, selecting a lower order polynomial would have reduced the number of equations. Waters, et al. settled on the sixth order by striking a compromise between the level of accuracy and the tedium of algebra.

From Eq. (3.11.20a) we have:

$$\begin{aligned} \frac{dw}{d\xi} = & -a_1 + a_2\left(1 - 10\xi^3 + \frac{15}{2}\xi^4\right) + a_3\left(4\xi^3 - 9\xi^4 + \frac{24}{5}\xi^5\right) \\ & - A_0\left(\frac{5}{12} - \xi + \frac{1}{3}\xi^3\right) - A_1\left(\frac{1}{12} - \frac{1}{3}\xi^3\right) \\ & - B_0\left(\frac{1}{12} - \frac{1}{2}\xi^2 + \frac{1}{3}\xi^3\right) \end{aligned} \quad (3.11.20b)$$

$$\begin{aligned} \frac{d^2w}{d\xi^2} = & a_2(-30\xi^2 + 30\xi^3) + a_3(12\xi^2 - 36\xi^3 + 24\xi^4) \\ & - A_0(\xi^2 - 1) + A_1\xi^2 - B_0(\xi^2 - \xi) \end{aligned} \quad (3.11.20c)$$

Substituting $\xi = 0$ and $\xi = 1$ in the above equations yields:

$$\begin{aligned} \left. \frac{d^2w}{d\xi^2} \right|_{\xi=0} & = A_0 \\ \left. \frac{d^2w}{d\xi^2} \right|_{\xi=1} & = A_1 \end{aligned} \quad (3.11.21)$$

Similarly, we have:

$$\left. \frac{d^3 w}{d\xi^3} \right|_{\xi=0} = B_0$$

Referring to Eq. (3.11.17) and Eq. (3.11.19), A_0 , A_1 and B_0 may be defined as “curvature factor at the small end”, “curvature factor at the large end”, and “shear factor at the small end”, respectively. Substituting for the derivatives of w in Eqs. (3.11.17) and (3.11.19) gives:

$$M_{h_0} = \frac{Eg_0 h^2}{r_1 \kappa} A_0 \quad (a)$$

$$M_{h_1} = \frac{(1 + \alpha)^3 Eg_0 h^2}{r_1 \kappa} A_1 \quad (b) \quad (3.11.22)$$

$$P_0 = \frac{-Eg_0 h}{r_1 \kappa} (3\alpha A_0 + B_0) \quad (c)$$

where the subscripts 0 and 1 on the quantities on the l.h.s. indicate that they are evaluated at $\xi=0$ and $\xi=1$, respectively. The above equations for the edge moments and shear will be needed to write moment and shear compatibility at the interfaces of the hub with the ring and with the shell. It should be noted that the edge moments and shear only involve three of the six parameters; a_1 , a_2 , and a_3 do not occur in these expressions. Thus linear equations arising from boundary compatibility will not involve a_1 , a_2 , and a_3 . This strategy is pivotal in reducing the equations to a form amenable to manual computations.

Minimization of Potential Energy

The potential energy function, Φ , is defined as

$$\Phi = U^* - \Gamma \quad (3.11.23)$$

where U^* is the strain energy due to deformation of the elastic body and Γ is the sum of the product of the external forces and their displacements. The strain energy of the hub is due to the curvature in the longitudinal plane produced by the longitudinal moment M_h and by the stretching of the hub centerline due to radial deflection y_h . The bending strain energy per unit circumference of the hub is given by

$$U_1 = \int_0^h \frac{M_h^2}{2D_h} dx$$

Substituting for D_h and M_h from Eqs. (3.11.12) and (3.11.13) and non-dimensionalizing as before we have:

$$U_1 = \frac{Eg_0 h}{2\kappa} \int_0^1 (1 + \alpha\xi)^3 \left[\frac{d^2 w}{d\xi^2} \right]^2 d\xi$$

The strain energy per unit circumference due to stretching of the mid-plane is given by:

$$U_2 = \int_0^h \frac{E y_h^2 g}{2 r_1^2} dx = \frac{E g_0 h}{2} \int_0^1 (1 + \alpha \xi) w^2 d\xi$$

Therefore, the net strain energy per unit circumference is given by:

$$U^* = U_1 + U_2 = \frac{E g_0 h}{2\kappa} \int_0^1 (1 + \alpha \xi)^3 \left[\frac{d^2 w}{d\xi^2} \right]^2 d\xi + \frac{E g_0 h}{2} \int_0^1 (1 + \alpha \xi) w^2 d\xi \quad (3.11.24)$$

The external forces sustaining displacement in the hub are P_0 , M_{h_0} , and M_{h_1} . Referring to Eq. (3.11.20) it is observed that $w=0$ at $\xi=1$, which satisfies the zero displacement condition assumed for point 0 (Fig. 3.11.1), and also implies that the shear P_1 does no work. Hence, we have, by using Eq. (3.11.22),

$$\Gamma = -M_{h_0} \frac{dy_h}{dx} \Big|_{x=0} + M_{h_1} \frac{dy_h}{dx} \Big|_{x=1} - P_0 y_h \Big|_{x=0} = \frac{E g_0 h}{\kappa} \left[(1 + \alpha)^3 A_1 \frac{dw}{d\xi} \Big|_{\xi=1} - A_0 \frac{dw}{d\xi} \Big|_{\xi=0} \right] + \frac{E g_0 h}{\kappa} (3\alpha A_0 + B_0) w \Big|_{\xi=0} \quad (3.11.25)$$

Substituting the derivatives of w in the above expressions, and performing the necessary integrations give expressions for U^* and Γ in terms of the six parameters A_0 , A_1 , B_0 , a_1 , a_2 and a_3 . The theorem of "minimum potential energy" requires that for w to most closely approximate the true solution, the partial derivatives of Φ with respect to a_i must vanish, i.e.,

$$\frac{\partial \Phi}{\partial a_i} = 0; \quad i = 1, 2, 3$$

The details of the algebra are quite cumbersome. The three resulting equations can be written in the form

$$\begin{aligned} c_{11} a_1 + c_{12} a_2 + c_{13} a_3 &= c_{14} A_0 + c_{15} A_1 + c_{16} B_0 \\ c_{21} a_1 + c_{22} a_2 + c_{23} a_3 &= c_{24} A_0 + c_{25} A_1 + c_{26} B_0 \\ c_{31} a_1 + c_{32} a_2 + c_{33} a_3 &= c_{34} A_0 + c_{35} A_1 + c_{36} B_0 \end{aligned} \quad (3.11.26)$$

The coefficients c_{ij} ($i = 1, 2, 3; j = 1, 2, \dots, 6$) are functions of only α and κ . These are defined as follows:

$$c_{11} = 1/3 + \alpha/12$$

$$c_{12} = 5/42 + 17\alpha/336$$

$$c_{13} = 1/210 + \alpha/360$$

$$c_{14} = 11/360 + 59\alpha/5040 + (1 + 3\alpha)/\kappa$$

$$c_{15} = 1/90 + 5\alpha/1008 - (1 + \alpha)^3/\kappa$$

$$c_{16} = 1/120 + 17\alpha/5040 + 1/\kappa$$

$$c_{21} = c_{12}$$

$$c_{22} = 215/2772 + 51\alpha/1232 + (60/7 + 225\alpha/14 + 75\alpha^2/7 + 5\alpha^3/2)/\kappa$$

$$c_{23} = 31/6930 + 128\alpha/45045 + (6/7 + 15\alpha/7 + 12\alpha^2/7 + 5\alpha^3/11)/\kappa$$

$$c_{24} = (533/30240) + 653\alpha/73920 + (1/2 + 33\alpha/14 + 39\alpha^2/28 + 25\alpha^3/84)/\kappa$$

$$c_{25} = 29/3780 + 3\alpha/704 - (1/2 + 33\alpha/14 + 81\alpha^2/28 + 13\alpha^3/12)/\kappa$$

$$c_{26} = 31/6048 + 1763\alpha/665280 + (1/2 + 6\alpha/7 + 15\alpha^2/28 + 5\alpha^3/42)/\kappa$$

$$c_{31} = c_{13}$$

$$c_{32} = c_{23}$$

$$c_{33} = 1/2925 + 71\alpha/300300 + (8/35 + 18\alpha/35 + 156\alpha^2/385 + 6\alpha^3/55)/\kappa$$

$$c_{34} = 761/831600 + 937\alpha/1663200 + (1/35 + 6\alpha/35 + 11\alpha^2/70 + 3\alpha^3/70)/\kappa$$

$$c_{35} = 197/415800 + 103\alpha/332640 - (1/35 + 6\alpha/35 + 17\alpha^2/70 + \alpha^3/10)/\kappa$$

$$c_{36} = 233/831600 + 97\alpha/554400 + (1/35 + 3\alpha/35 + \alpha^2/14 + 2\alpha^3/105)/\kappa$$

Using Cramer's rule [3.11.7], the three linear algebraic equations can be solved for a_i ($i = 1, 2, 3$) in terms of A_0 , A_1 , and B_0 .

We note that the determinant of the coefficient matrix in Eq. (3.11.26) is:

$$\zeta = c_{11}(c_{22}c_{33} - c_{23}c_{32}) - c_{21}(c_{12}c_{33} - c_{13}c_{32}) + c_{31}(c_{12}c_{23} - c_{22}c_{13})$$

Thus, the solution can be written formally as

$$\begin{aligned} a_1 &= \lambda_1 A_0 + \lambda_2 A_1 + \lambda_3 B_0 \\ a_2 &= \lambda_4 A_0 + \lambda_5 A_1 + \lambda_6 B_0 \\ a_3 &= \lambda_7 A_0 + \lambda_8 A_1 + \lambda_9 B_0 \end{aligned} \quad (3.11.27)$$

where

$$\lambda_i = \frac{1}{\zeta} \begin{vmatrix} c_{1(i+3)} & c_{12} & c_{13} \\ c_{2(i+3)} & c_{22} & c_{23} \\ c_{3(i+3)} & c_{32} & c_{33} \end{vmatrix}; \quad i = 1, 2, 3$$

$$\lambda_i = \frac{1}{\zeta} \begin{vmatrix} c_{11} & c_{1i} & c_{13} \\ c_{21} & c_{2i} & c_{23} \\ c_{31} & c_{3i} & c_{33} \end{vmatrix}; \quad i = 4, 5, 6$$

$$\lambda_i = \frac{1}{\zeta} \begin{vmatrix} c_{11} & c_{12} & c_{1(i-3)} \\ c_{21} & c_{22} & c_{2(i-3)} \\ c_{31} & c_{32} & c_{3(i-3)} \end{vmatrix}; \quad i = 7, 8, 9$$

Equation (3.11.27) gives a_1 , a_2 and a_3 as linear functions of the three parameters A_0 , B_0 , and A_1 . We recall that only the latter set occurs in the edge load expressions (Eq. 3.11.22). Furthermore, since the c_{ij} are only functions of α and κ , the λ_i 's become uniquely known if κ and α are specified. Since both κ and α depend entirely on the flange geometry and its material properties, it follows that the λ_i ($i = 1, 9$) are entirely known for a given flange.

At this point, save for the unknown edge conditions, the displacements and stress profile of the hub are completely characterized. We need similar relations for the shell (element #3 in Fig. 3.11.1) before the interface conditions can be applied.

3.11.3 Shell (Element #3)

Equation (3.11.11), for axisymmetric bending of thin shells by edge loadings which are symmetrical about the shell axis, simplifies if the shell thickness does not vary with x . The local x -coordinate for the shell is directed away from the hub with its origin located at hub-shell interface (see Fig. 3.11.1). Let y^* denote the radially outward deflection of shell; then Eq. (3.11.11) can be written as:

$$\frac{d^4 y^*}{dx^4} + \frac{12(1-\nu^2)}{g_0^2 r_1^2} y^* = 0 \quad (3.11.28)$$

The solution of this fourth order differential equation is given in terms of four constants of integration, C_5, C_6, C_7 and C_8 :

$$y^* = e^{-\beta x} (C_5 \sin \beta x + C_6 \cos \beta x) + e^{\beta x} (C_7 \sin \beta x + C_8 \cos \beta x) \quad (3.11.29)$$

where:

$$\beta = \left[\frac{3(1-\nu^2)}{r_1^2 g_0^2} \right]^{1/4} = \frac{(0.25\kappa)^{1/4}}{h} \quad (3.11.30a)$$

Since the shell is assumed to be infinitely long in the positive x -direction, a physically admissible solution requires that $C_7 = C_8 = 0$. The moment M_s and shear P_s at any location x are given by Eqs. (3.11.12)–(3.11.14) ($y_h \rightarrow y^*$), with the shell flexural rigidity D_s replacing D_h in the equations. D_s is defined in an identical manner to D_h .

$$D_s = \frac{E g_0^3}{12(1-\nu^2)} \quad (3.11.30b)$$

Differentiating Eq. (3.11.29), and substituting the moment and shear expressions gives P_s and M_s in terms of the undetermined constants C_5 and C_6 . If M_{h_0} and P_0 denote the moment and shear at $x = 0$, then it can be shown that (see Ref. 3.11.3, p. 469, or our Appendix A):

$$C_5 = \frac{-M_{h_0}}{2 \beta^2 D_s}$$

$$C_6 = \frac{1}{2 \beta^3 D_s} (P_0 + \beta M_{h_0})$$

In this manner, the deflection y^* is expressed solely in terms of the edge moment M_{h_0} and the edge shear P_0 . In particular, the edge deflection and slope (at $x = 0$) are given by:

$$y^* |_{x=0} = \frac{1}{2 \beta^3 D_s} (\beta M_{h_0} + P_0) = C_6 \quad (3.11.31)$$

$$\frac{dy^*}{dx} \Big|_{x=0} = \frac{-1}{2 \beta^2 D_s} (2 \beta M_{h_0} + P_0) = \beta (C_5 - C_6)$$

3.11.4 Compatibility Between Shell and Hub

The edge moment M_{h_0} and shear P_0 are assumed to be equal at the shell-

hub interface (Fig. 3.11.1). To maintain complete geometric compatibility, the slope and deflection at the interface must also be equal.

Referring to Eq. (3.11.20), deflection of the hub at $x = 0$ is:

$$w|_{x=0} = a_1$$

$$\text{or } y_h|_{x=0} = a_1 r_1 \quad (3.11.32a)$$

Substituting for a_1 from Eq. (3.11.27) we have:

$$y_h|_{x=0} = r_1 (\lambda_1 A_0 + \lambda_2 A_1 + \lambda_3 B_0) \quad (3.11.32b)$$

Similarly, the slope of the hub at $x = 0$ is

$$\left. \frac{dw}{d\xi} \right|_{x=0} = -a_1 + a_2 - \frac{5}{12} A_0 - \frac{1}{12} A_1 - \frac{1}{12} B_0$$

$$\begin{aligned} \text{or } \left. \frac{dy_h}{dx} \right|_{x=0} &= \frac{r_1}{h} A_0 \left(-\lambda_1 - \frac{5}{12} + \lambda_4 \right) + \frac{r_1}{h} A_1 \left(-\lambda_2 + \lambda_5 - \frac{1}{12} \right) \\ &+ \frac{r_1}{h} B_0 \left(-\lambda_3 + \lambda_6 - \frac{1}{12} \right) \end{aligned} \quad (3.11.33)$$

In the foregoing, a_i have been replaced by their r.h.s. equivalents from Eq. (3.11.27).

Geometric compatibility between the hub and shell requires

$$y^*|_{x=0} \text{ (Eq. 3.11.31)} = y_h|_{x=0} \text{ (Eq. 3.11.32)}$$

$$- \left. \frac{dy^*}{dx} \right|_{x=0} \text{ (Eq. 3.11.31)} = \left. \frac{dy_h}{dx} \right|_{x=0} \text{ (Eq. 3.11.33)}$$

Therefore, we obtain the two equations:

$$\begin{aligned} a_1 r_1 &= C_6 \\ \left(-a_1 + a_2 - \frac{5}{12} A_0 - \frac{1}{12} A_1 - \frac{1}{12} B_0 \right) r_1 / h &= \beta (C_6 - C_5) \end{aligned} \quad (3.11.34)$$

Using Eqs. (3.11.31–33), substituting for M_{h_0} and P_0 from Eq. (3.11.22), and rearranging terms, yields two equations involving A_0 , B_0 , A_1

$$\begin{aligned} \rho_{11} A_0 + \rho_{12} B_0 &= \lambda_2 A_1 \\ \rho_{21} A_0 + \rho_{22} B_0 &= - \left(\lambda_5 - \lambda_2 - \frac{1}{12} \right) A_1 \end{aligned}$$

where

$$\rho_{11} = \frac{0.5}{(0.25\kappa)^{1/2}} - \frac{3\alpha}{2(0.25\kappa)^{3/4}} - \lambda_1$$

$$\rho_{12} = -\lambda_3 - \frac{0.5}{(0.25\kappa)^{3/4}}$$

$$\rho_{21} = - (0.25\kappa)^{-0.25} + 1.5\alpha(0.25\kappa)^{-0.5} + \left(\lambda_4 - \lambda_1 - \frac{5}{12} \right)$$

$$\rho_{22} = \frac{(0.25\kappa)^{-1/2}}{2} + (\lambda_6 - \lambda_3 - 1/12)$$

Therefore:

$$A_0 = \frac{A_1}{\Delta} \left[\lambda_2 \rho_{22} + \left(\lambda_5 - \lambda_2 - \frac{1}{12} \right) \rho_{12} \right] \quad (3.11.35a)$$

$$B_0 = \frac{-A_1}{\Delta} \left[\rho_{11} \left(\lambda_5 - \lambda_2 - \frac{1}{12} \right) + \rho_{21} \lambda_2 \right] \quad (3.11.35b)$$

$$\Delta = \rho_{11} \rho_{22} - \rho_{12} \rho_{21} \quad (3.11.36)$$

Thus A_0 and B_0 are expressed in terms of A_1 and the two geometric parameters κ and α .

At this point in the analysis, a_1 , a_2 , and a_3 are expressed as linear combinations of A_0 , A_1 and B_0 (Eq. 3.11.27). Furthermore, A_0 and B_0 are expressed in terms of A_1 (Eq. 3.11.35). Thus, the expression for the hub deflection w (Eq. 3.11.20) is now expressed in terms of one parameter, A_1 .

3.11.5 Compatibility Between Hub and Ring

Geometric compatibility between the hub and ring requires that the displacement and slope at point 0 (Fig. 3.11.1) between the two bodies must match. Recall that point 0 has been assumed, a priori, to undergo zero displacement in the radial direction, and that the assumed displacement functions for the hub (Eq. 3.11.20) and the ring (by virtue of no stretching of the neutral axis and small deformation theory) automatically satisfy this condition. Continuity of slope, however, is not automatically satisfied. Therefore, we enforce the following condition:

$$\left. \frac{dz}{dr} \right|_{r=r_1} [\text{ring}] = \left. \frac{dy_h}{dx} \right|_{x=h} [\text{hub}]$$

or

$$\theta = \left. \frac{r_1}{h} \frac{dw}{d\xi} \right|_{\xi=1}$$

$$\frac{dw}{d\xi} \text{ is obtained from Eq. (3.11.20b).}$$

Thus, the ring rotation θ shown in Fig. 3.11.1 becomes

$$\theta = \frac{r_1}{h} \left(-a_1 - \frac{3}{2} a_2 - \frac{1}{5} a_3 + \frac{1}{4} A_0 + \frac{1}{4} A_1 + \frac{1}{12} B_0 \right) \quad (3.11.37a)$$

Equation (3.11.27) gives a_1 , a_2 and a_3 as linear combinations of A_0 , A_1 , and B_0 . Further, Eq. (3.11.35) gives A_0 and B_0 in terms of A_1 . Making these substitutions in the above equation, we have, in symbolic form:

$$\theta = \frac{r_1}{h} f_1(\kappa, \alpha) A_1 \quad (3.11.37b)$$

where $f_1(\kappa, \alpha)$ is an explicit function in the two geometric parameters κ and α .

Performing the required algebra, we can show that:

$$f_1(\kappa, \alpha) = \left[\frac{1}{\Delta} \left\{ \lambda_2 \rho_{22} + \left(\lambda_5 - \lambda_2 - \frac{1}{12} \right) \rho_{12} \right\} \left(-\lambda_1 - \frac{3}{2} \lambda_4 - \frac{1}{5} \lambda_7 + \frac{1}{4} \right) \right. \\ \left. + \left(-\lambda_2 - \frac{3}{2} \lambda_5 - \frac{1}{5} \lambda_8 + \frac{1}{4} \right) - \frac{1}{\Delta} \left\{ \rho_{11} \left(\lambda_5 - \lambda_2 - \frac{1}{12} \right) + \rho_{21} \lambda_2 \right\} \right. \\ \left. \left(-\lambda_3 - \frac{3}{2} \lambda_6 - \frac{1}{5} \lambda_9 + \frac{1}{12} \right) \right] \quad (3.11.38)$$

Let us define $V(\kappa, \alpha)$ as

$$V(\kappa, \alpha) = \frac{f_1(\kappa, \alpha)}{\left[\frac{3(1-\nu^2)}{\kappa} \right]^{1/4} (1+\alpha)^3} \quad (3.11.39)$$

We note that V is uniquely defined for a given set of values of κ and α (and Poisson's ratio ν).

Finally, moment continuity at the hub-ring interface implies that the ring is subject to a radial bending moment, at its central plane at radius $r = r_1$, given by:

$$M_{r_1} = M_{h_1} - \frac{P_1 t}{2} \quad (3.11.40)$$

where t is the ring thickness and P_1 is the interface shear. M_{r_1} and M_{h_1} are defined by Eqs. (3.11.7) and (3.11.22), respectively. An expression for P_1 in terms of A_1 and the geometric parameters κ and α , is required. This could be accomplished by using Eq. (3.11.19) which gives P in terms of derivatives of w . However, since the assumed function for w (Eq. 3.11.20) is an approximate one, the derivatives are likely to be even more in error. An equally expeditious, and more accurate procedure, used by Waters, et al., is to represent P as an integral of w . This is accomplished by writing the equilibrium relationship for the hub in the radial direction. If we consider a thin slice of the hub of thickness dx in the x -direction, the circumferential stress s due to the net shear dP can be shown to be given by:

$$s = \frac{r_1 dP}{g dx}$$

where g is the local thickness of the hub.

Since the circumferential strain in the slice is given by y_h/r_1 , we have

$$s = E y_h / r_1 = \frac{r_1 dP}{g dx}$$

or
$$dP = \frac{E y_h g}{r_1^2} dx$$

Integrating this expression between $x = 0$ and h yields

$$P_1 - P_0 = \frac{E}{r_1^2} \int_0^h g y_h dx = \frac{E g_0 h}{r_1} \int_0^1 w(1 + \alpha \xi) d\xi$$

Integrating and substituting for P_0 from Eq. (3.11.22) yields:

$$P_1 = \frac{E g_0 h}{r_1} \left[\left(\frac{1}{2} + \frac{\alpha}{6} \right) a_1 + \left(\frac{1}{4} + \frac{11\alpha}{84} \right) a_2 + \left(\frac{1}{70} + \frac{\alpha}{105} \right) a_3 - \left(\frac{7}{120} + \frac{\alpha}{36} + \frac{3\alpha}{\kappa} \right) A_0 - \left(\frac{1}{40} + \frac{\alpha}{72} \right) A_1 - \left(\frac{1}{60} + \frac{\alpha}{120} + \frac{1}{\kappa} \right) B_0 \right] \quad (3.11.41)$$

Proceeding as before, we replace a_1, a_2, a_3, A_0 and B_0 by functions of A_1, κ and α . Therefore, we have

$$P_1 = f_2(\kappa, \alpha) A_1 \frac{E g_0 h}{r_1} \quad (3.11.42)$$

For convenience, let us define F , such that:

$$F = \frac{-f_2(\kappa, \alpha)}{\left[\frac{\kappa}{3(1-\nu^2)} \right]^{1/4} \frac{(1+\alpha)^3}{\kappa}} \quad (3.11.43)$$

Returning now to Eq. (3.11.40), and substituting M_{r_1} and M_{h_1} and P_1 from Eqs. (3.11.7), (3.11.22) and (3.11.42) we have:

$$\begin{aligned} & \frac{(1-K^2)}{\left[\frac{(1+\nu)}{(1-\nu)} K^2 + 1 \right]} \left\{ (1+\nu) \frac{2D\theta}{B} + \frac{W_{eq}}{2\pi} \left[\frac{1}{2} + \frac{(1+\nu)}{(1-\nu)} \left(\frac{K^2}{K^2-1} \right) \ln K \right] \right\} \\ & = \frac{(1+\alpha)^3}{r_1 \kappa} E g_0 h^2 A_1 + \frac{t}{2} \left[\frac{\kappa}{3(1-\nu^2)} \right]^{1/4} \frac{(1+\alpha)^3}{\kappa} F A_1 \frac{E g_0 h}{r_1} \end{aligned}$$

Substituting for θ from Eqs. (3.11.37b), (3.11.39) and simplifying, yields

$$A_1 = - \left[\frac{K^2-1}{\frac{1+\nu}{1-\nu} K^2 + 1} \right] \left[\frac{B \kappa}{(1+\alpha)^3 E g_0 h^2} \right] \frac{W_{eq}}{4\pi} \cdot \frac{\left[\frac{1}{2} + \frac{1+\nu}{1-\nu} \left(\frac{K^2}{K^2-1} \right) \ln K \right]}{\left[1 + \frac{(t/g_0)F}{(B/g_0)^{1/2}} + \frac{[(1+\nu)(K^2-1)(t/g_0)^3]V}{\left(\frac{1+\nu}{1-\nu} K^2 + 1 \right) (B/g_0)^{1/2}} \right]} \quad (3.11.44)$$

At this point all unknowns, including A_1 and the interface loads, are defined in terms of the geometric parameters, the elastic constants, and the

applied loading, W_{eq} . We recall that the externally applied moment M_{ext} on the ring is defined after Eq. (3.11.9) as

$$M_{ext} = \frac{W_{eq}(A-B)}{2} \quad (3.11.45)$$

We can therefore eliminate W_{eq} from Eq. (3.11.44), and obtain

$$A_1 = -\frac{2(1-\nu^2)h^2}{E g_1^3 r_1} M X \quad (3.11.46)$$

where:

$$M = \frac{M_{ext}}{B} \quad (3.11.47)$$

and:

$$X = \frac{1}{\frac{1}{T} \left(1 + \frac{t/g_0}{(B/g_0)^{1/2}} F\right) + \frac{V}{U} \frac{(t/g_0)^3}{(B/g_0)^{1/2}}} \quad (a)$$

$$T = \frac{3K^2 \left(1 + \frac{2(1+\nu)}{(1-\nu)} \ln K\right) - 3}{\pi(K-1) \left[1 + \frac{(1+\nu)}{(1-\nu)} K^2\right]} \quad (b) \quad (3.11.48)$$

$$U = \frac{3K^2 \left(1 + 2 \frac{1+\nu}{1-\nu} \ln K\right) - 3}{\pi(1+\nu)(K^2-1)(K-1)} \quad (c)$$

All quantities of interest are now determined. For a given flange geometry and applied ring moment loading, M_{ext} , the solution for the displacement field for the three elements and their interface discontinuity moments and shears are computed by the following steps:

- (i) Evaluate basic quantities; $K = A/B$, α (Eq. 3.11.10), κ (Eq. 3.11.18).
- (ii) Compute c_{ij} ($i = 1,3; j = 1 \dots 6$), ζ , λ_i ($i = 1 \dots 9$) (Eq. 3.11.27), ρ_{ij} ($i, j = 1,2$) (Eq. 3.11.35) and Δ (Eq. 3.11.36).
- (iii) Evaluate $f_1(\kappa, \alpha)$ (Eq. 3.11.38) and then V (Eq. 3.11.39).
- (iv) Evaluate $f_2(\kappa, \alpha)$ using Eqs. (3.11.41–42) and then evaluate F (Eq. 3.11.43).
- (v) Determine the ring factors T , U (Eq. 3.11.48) and Y (Eq. 3.11.9).
- (vi) Determine X (Eq. 3.11.48a) and then A_1 (Eq. 3.11.46).
- (vii) Compute A_0 and B_0 (Eq. 3.11.35) and a_1 , a_2 and a_3 using Eq. (3.11.27).
- (viii) Compute the discontinuity longitudinal moments and shears from Eq. (3.11.22) and Eq. (3.11.42).

- (ix) Displacements, if required, can also readily be obtained. The hub displacement w follows from Eq. (3.11.20), and rotation of the flange ring at the inside radius follows from Eq. (3.11.37).

Having determined the internal stress resultants, the next step in the analysis is to compute the important stresses in the flange. The appropriate procedure for this, following Waters, et al. is given below.

3.11.6 Longitudinal Stress in the Hub

The longitudinal moment at the small and large ends of the hub are given by Eq. (3.11.22). The corresponding maximum longitudinal hub stresses follow from the classical thin shell theory:

$$\begin{aligned}\sigma_{h_0} &= \pm \frac{6M_{h_0}}{g_0^2} = \pm \frac{6Eh^2}{r_1 g_0 \kappa} A_0 \\ \sigma_{h_1} &= \pm \frac{6M_{h_1}}{g_1^2} = \pm \frac{6(1+\alpha)^3 E g_0 h^2 A_1}{r_1 \kappa g_1^2}\end{aligned}\quad (3.11.49)$$

where σ_{h_0} and σ_{h_1} are the longitudinal hub bending stresses at the small and large ends, respectively.

The equation for σ_{h_1} can be further simplified by substituting for A_1 from Eq. (3.11.46) and cancelling out terms:

$$\sigma_{h_1} = \mp \frac{X M}{g_1^2} \quad (3.11.50)$$

In design work, it is sufficient to evaluate σ_{h_0} and σ_{h_1} , and use the larger of the two as the limiting hub bending stress. Detailed parametric studies by Waters, et al. [3.11.1] indicate that the maximum hub stress is “nearly” always at one of the two extremities of the hub. Thus, if a stress magnification factor f is defined as

$$f = \text{Max}\left(1, \frac{\sigma_{h_0}}{\sigma_{h_1}}\right)$$

then the maximum hub stress is given by:

$$\sigma_h(\text{max}) = \frac{f M X}{g_1^2} \quad (3.11.51)$$

The detailed distribution for the longitudinal hub stress can be obtained by using Eq. (3.11.17), which gives:

$$\begin{aligned}\sigma_h = \pm \frac{6M_h}{g^2} &= \frac{6E g_0 h^2 (1+\alpha\xi)^3}{r_1 \kappa g_0^2 (1+\alpha\xi)^2} \frac{d^2 w}{d\xi^2} = \pm \frac{6E(1+\alpha\xi)h^2}{r_1 \kappa g_0} [30\xi^2(\xi-1)a_2 + \\ &+ 12\xi^2 a_3(1-3\xi+4\xi^2) + (1-\xi^2)A_0 + \xi^2 A_1 - B_0 \xi(\xi-1)]\end{aligned}\quad (3.11.52)$$

3.11.7 Longitudinal Stress in the Shell

The radial displacement of the shell as a function of x is given by Eq. (3.11.29) where the constants C_5 and C_6 are defined in the preceding

subsection 3.11.3. The longitudinal shell bending stress at location x is given by:

$$\sigma_x = \pm \frac{6D_s}{g_0^2} \frac{d^2 y^*}{dx^2} \quad (3.11.53)$$

where D_s is defined by Eq. (3.11.30b).

Waters, et al. found that $\sigma_{h(\max)}$ (Eq. 3.11.51) almost always exceeds σ_x for any value of x . In other words, the bending stress in the shell does not control the design of the flange.

3.11.8 Radial Stress in the Ring

The radial stress in the flange ring consists of two components: (i), the bending stress caused by the radial bending moment M_r ; and (ii) the membrane stress caused by the in-plane surface load P_1 on the inside diameter. P_1 is assumed to be uniformly distributed through the thickness t of the ring for the purpose of computing the membrane stress.

The bending stress at the inside diameter is given by:

$$\sigma_{rb} = \pm \frac{6M_{r_1}}{t^2}$$

Using Eqs. (3.11.40), (3.11.22) and (3.11.42) yields:

$$\sigma_{rb} = \pm \frac{6}{t^2} \left(M_{h_1} - \frac{P_1 t}{2} \right) = \pm \frac{6}{t^2} \left[\frac{(1 + \alpha)^3 E g_0 h^2 A_1}{r_1 \kappa} - \frac{t}{2} \frac{A_1 E g_0 h f_2}{r_1} \right]$$

Substituting for A_1 and simplifying yields:

$$\sigma_{rb} = \mp \frac{MX}{t^2} \left[1 + \frac{t/g_0}{(B/g_0)^{1/2}} F \right] \quad (3.11.54)$$

The membrane stress at the inside diameter is:

$$\sigma_{rm} = \frac{P_1}{t} = \frac{f_2(\kappa, \alpha) A_1 E g_0 h}{r_1 t}$$

Substituting for A_1 and f_2 , as before yields:

$$\sigma_{rm} = \frac{t/g_0}{3t^2(B/g_0)^{1/2}} MXF \quad (3.11.55)$$

Therefore, the maximum magnitude of the radial stress is

$$\begin{aligned} \sigma_r &= |\sigma_{rm}| + |\sigma_{rb}| \\ \sigma_r &= \frac{MX}{t^2} \left[1 + \frac{4}{3} \frac{t/g_0}{(B/g_0)^{1/2}} F \right] \end{aligned} \quad (3.11.56)$$

Waters, et al. shows that the maximum radial stress in the ring always occurs at the inside diameter.

3.11.9 Tangential Stress in the Ring

The tangential stress in the flange ring also consists of two components: (i), a bending stress due to the circumferential bending moment; and (ii), a

circumferential stress due to P_1 assumed to be applied at the inner circumference uniformly through the thickness.

The bending stress at the inner radius is

$$\sigma_{ib} = \pm \frac{6M_{r_1}}{t^2}$$

The expression for M_{r_1} (Eq. 3.11.7b) in conjunction with Eq. (3.11.8) and Eq. (3.11.9) gives:

$$\sigma_{ib} = \pm \frac{6}{t^2} \left[-Z M_{r_1} - \frac{W_{eq}(K-1)Y}{12} \right]$$

where:

$$Z = \frac{K^2 + 1}{K^2 - 1} \quad (3.11.57)$$

Substituting for W_{eq} from Eq. (3.11.45) and Eq. (3.11.47), we have:

$$\sigma_{ib} = \pm \frac{6}{t^2} \left[-Z M_{r_1} - \frac{MY}{6} \right] \quad (3.11.58)$$

Substituting for M_{r_1} in the manner of the preceding subsection, and simplifying we have:

$$\sigma_{ib} = \mp \left[\frac{MY}{t^2} - \frac{MXZ}{t^2} \left\{ 1 + \frac{t/g_0}{(B/g_0)^{1/2}} F \right\} \right] \quad (3.11.59)$$

The hoop stress due to stretching caused by P_1 acting at the inner circumference of the ring is given by the classical results for thick shells under internal pressure. At the inner radius, we have:

$$\sigma_{im} = - \frac{K^2 + 1}{K^2 - 1} \frac{P_1}{t}$$

Substituting for P_1 as before, we have:

$$\sigma_{im} = - \frac{t/g_0}{3t^2 (B/g_0)^{1/2}} Z M X F \quad (3.11.60)$$

Combining σ_{ib} and σ_{im} we have:

$$\sigma_t = (\sigma_{im} + \sigma_{ib})_{\max} = \frac{MY}{t^2} - \frac{MXZ}{t^2} \left[1 + \frac{4}{3} \frac{t/g_0}{(B/g_0)^{1/2}} F \right] \quad (3.11.61)$$

Waters, et al. concluded that the maximum tangential stress occurs at the inner diameter of the ring, and therefore evaluation of stresses at other locations in the ring is not required.

3.12 COMPUTER PROGRAM FLANGE

In the preceding section, a detailed exposition of the method of Waters, et al. (the so-called Taylor Forge Method) has been given. The apparent success of this work lies in the casting of the solution of a problem involving two locations of gross structural discontinuity into a series of algebraic expressions. The computational problems can be drastically reduced if the

function V (Eq. 3.11.39) and F (Eq. 3.11.43) are plotted for the practically significant range of α and κ , the latter treated as a parameter. Indeed, such charts were prepared by Waters and his co-workers [3.11.1], and appear in essentially unaltered form in codes and standards [3.5.1-3] to this day. In a computer program, however, it is more expedient to solve the algebraic equations directly. Computer program FLANGE, based on the method of Waters, et al. is described below. Prior to presenting its input data, it is useful to discuss its general attributes.

The program is arranged to accept the complete geometric details of the hubbed flange, the bolts and the gasket. The gasket seating stress y , factor m , flange and bolt material, nominal allowable stresses at ambient and design temperatures (temperature corresponding to the pressure loading) are also input to the program. Five types of flange configurations can be specified by the parameter MFLG (MFLG = 1, welding neck, MFLG = 2, slip-on hubbed flange, MFLG = 3, Lap Joint flange, MFLG = 4, hubbed Lap Joint flange; MFLG = 5, Ring Joint flange). The program can be operated in two modes:

(i) Flange ring thickness, THIK is specified—compute the maximum hub stress σ_h , maximum ring radial stress σ_r , and the maximum tangential ring stress σ_t .

(ii) Determine the flange ring thickness such that the following stress limits are satisfied under both seating and operating conditions [3.5.1-3]

$$\begin{aligned} \sigma_h &< 1.5S_a \\ \sigma_r, \sigma_t &< S_a \\ \text{Max} [0.5(\sigma_h + \sigma_t); 0.5(\sigma_h + \sigma_r)] &< S_a \end{aligned}$$

where S_a is the allowable flange material stress at the appropriate temperature.

The last two stress limits are in fact stress intensity limits. The quantities $1/2 (\sigma_h + \sigma_t)$ and $1/2 (\sigma_h + \sigma_r)$ represent upper bounds on the two largest stress intensities at the hub-ring junction. We observe that σ_h is a bending stress produced by discontinuity moment and shear; therefore, it is a secondary stress. The code, however, specifies a lower stress limit for the hub bending stress than for other secondary stresses for reasons of flange performance rather than flange safety. Control of the rotation of the flange is important for the joint sealing function. Allowing σ_h to attain values above the material yield point would cause permanent set in the hub and could adversely affect the sealworthiness of the joint.

The gasket seating load is computed for the specified gasket data. However, the seating phase axial load is taken as the average of the gasket seating load, and the axial bolt pull based on the nominal bolt allowable stress, as recommended in the design codes.

The operating load is computed in terms of its three constituent loads (Section 3.8) and the corresponding moment arms are calculated following the guidelines in the ASME Codes [3.5.1-3]. In this manner, the external moments for seating and operating conditions are determined. We recall

that since local pressure effects on the hub and in the shell have been neglected, the configuration loading is given solely by the value for W_{eq} .

To evaluate the flange factors F and V ; seven simultaneous linear equations (3.11.26)–(3.11.31), with M_{h_0} and P_0 replaced via Eq. (3.11.22), and (3.11.34) in seven unknowns, namely

$$\left(\frac{a_1}{A_1}\right), \left(\frac{a_2}{A_1}\right), \left(\frac{a_3}{A_1}\right), C_5, C_6, \left(\frac{A_0}{A_1}\right) \text{ and } \left(\frac{B_0}{A_1}\right)$$

are solved using Gaussian elimination.

Next, θ/A_1 follows directly from Eq. (3.11.37a) which in turn yields $f_1(\kappa, \alpha)$ via Eq. (3.11.37b). The factor V follows directly from Eq. (3.11.39). F is computed in a similar manner from Eq. (3.11.43). The number of simultaneous equations is reduced to five if MFLG = 2 or 3, since in these cases $A_0 = B_0 = 0$ (no shear or moment at the hub/shell interface). Having evaluated the factors F and V , the remaining quantities X , T , U , etc., follow directly. The hub stress intensification factor f is evaluated using empirical relations based on the original chart developed by Waters, et al. [3.11.1].

In addition to computerizing the theory presented in the preceding section, this program permits the user to specify the dimensions of an internal gasket containing the pass partition ribs and an outer ring. Where the pass partition ribs are directly attached to the main gasket, the outer ring dimensions of the rib gasket are set equal to zero. This feature permits incorporation of partition rib seating loads which may become significant in multiple pass units. Figure 3.12.1 shows both configurations. The required bolt load needed to seat the gasket then includes the additional load to seat the rib or the inner gasket.

Another useful feature available in the program is the capability to calculate the thickness of a flat cover bolted to the flange in accordance with TEMA rules (input data lines 6 and 7 in the program).

The design guide published by Gulf & Western (previously by Taylor Forge Company) suggests increasing the flange moment by the factor $(BS/BSN)^{1/2}$ whenever the actual bolt spacing BS is greater than the *normal* bolt spacing BSN . The normal bolt spacing BSN is defined as

$$BSN = 2 d_b + t$$

Computer program FLANGE includes the above correction factor on the flange moment. The most recent issue of the Taylor Forge design guide [3.12.1] gives other semi-empirical rules for considering the effect of bolt spacing on joint leakage. The program is listed after the input data described below.

Input Data: Eight lines of input data are required to run the program.

Line 1: Pressure and allowable stress data

Pressure; allowable flange material stress at design temperature; allowable flange material stress at ambient temperature; allowable bolt material stress at design temperature; allowable bolt material stress at ambient temperature.

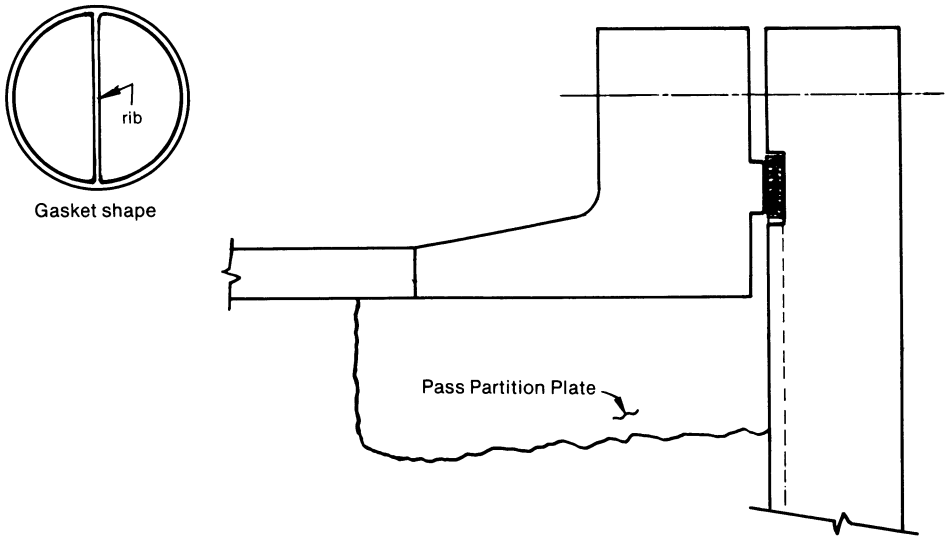


Fig. 3.12.1a. Conventional gasket with a diametral rib; tubesheet to channel flange joint.

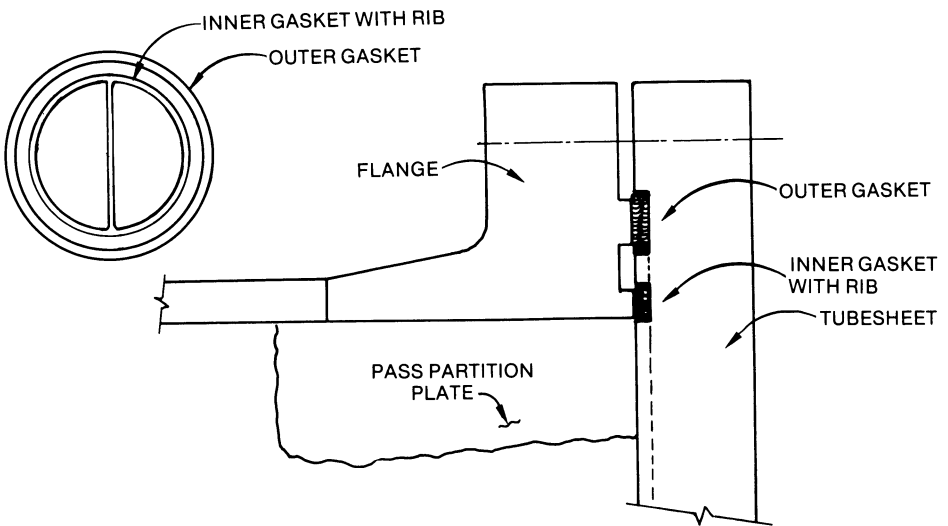


Fig. 3.12.1b. Double gasket arrangement for a tubesheet/flange joint.

Line 2: Gasket data

Gasket width, N ; gasket minimum seating stress y ; gasket factor m .

Line 3: Ring geometry data

Flange ring I.D. (B); Flange ring O.D. (A); Effective gasket diameter G ; Bolt circle diameter; Nominal bolt diameter; number of bolts; Flange type (1 = weld neck, 2 = slip-on, 3 = lap joint, 4 = unhubbed lap joint, 5 = slip on ring flange); IBT (specify 0 if the program should determine bolt diameter, 1 if bolt diameter is specified).

Line 4: Flange data

Shell thickness g_0 ; maximum hub thickness g ; hub length h ; flange ring thickness (specify 0 if the thickness is to be determined by the program).

Line 5: Rib and inner gasket data:

Total length of rib segments; rib width; inner ring width; effective ring diameter; rib design seating stress; inner ring design seating stress.

Line 6: Cover Calculation:

Input 1 if cover calculation is required, 0 if it is not required.

Line 7: Delete this line if 0 is entered in line 6; otherwise enter.

Cover material allowable stress at design temperature; cover material allowable stress at ambient temperature; mean cover gasket diameter.

Line 8:

Run again; input 1 for yes, 0 for no.

The program also prints out the required thickness if the flange were of the loose ring type. This information is strictly of advisory nature.

To illustrate the application of program FLANGE, we consider the design of a welding neck flange, defined by the following data:

Line 1: Pressure and allowable stress data

Pressure = 600 psi; flange material allowable stress at ambient and design temperatures = 17,500 psi; bolt material allowable stress at ambient and design temperatures = 35,000 psi.

Line 2: Gasket data

Gasket width = 0.75"; minimum seating stress = 9,000 psi; gasket factor = 3.

Line 3: Ring geometry data

Flange I.D. = 44.75"; O.D. = 53"; effective gasket diameter = 47.84"; bolt circle diameter = 50.5"; bolt nominal diameter = 1.25"; number of bolts = 52; flange type = 1; IBT = 1

Line 4: Flange data

Shell thickness = 0.88"; maximum hub thickness = 1.13"; hub length = 1.25"; THIK = 0.

Lines 5, 6 and 7 have all inputs = 0 (no inner ribs, no cover calculation required).

The program output is given in the pages following the program listing for this case, and the case where the ring thickness is specified and the corresponding stresses are required to be evaluated. This example problem will be used to illustrate the differences between the classical method of Waters et al. and modern stress analysis techniques.

PROGRAM FLANGE

```

COMMON YFLG, T,U,Z,E,D,SFC,SFA,      G1,B,GO,Q,MFLG,W
COMMON/ONE/FS
C   PROGRAM FOR CALCULATING THE THICKNESS OF HUBBED FLANGES AND THE
C   NECESSARY BOLTING BY THE METHOD OF SECTION 3.11
C   THREE TYPES OF HUBBED FLANGES MAY BE USED: 1=WELD NECK, 2=SLIP ON,
C   3=LAP JOINT.
DIMENSION BTD(25),BTS(25)
DATA BTD/.126,.202,.302,.419,.551,.728,.929,1.155,1.405,1.68,1.98,
+ 2.304,2.652,0.0,3.423,0.0,4.292,0.0,5.259,0.0,6.324/
1001 ACCEPT P,SFO,SFA,SB,SA
ACCEPT FN,Y,FMG
ACCEPT B,A,G,BC,BOLT, BN,  MFLG, IBT
ACCEPT GO,G1,Q,THIK
ACCEPT RL,FNR,FNC,GR,YRRIB,YRCIR
ACCEPT MCOVER
WRITE(6,19)P
19  FORMAT(1H1,6X,"DESIGN PRESSURE(PSI)=",F10.2)
WRITE(6,12)SFA,SFO,SA,SB
12  FORMAT(1H0,6X,"ALLOW.STRESSES(PSI)",/,25X,
+"AMBIENT TEMP.OF",20X,"DESIGN TEMP.OF"/7X,"FLANGE",12X,F10.2,25X,
+F10.2/7X,"BOLTING",11X,F10.2,25X,F10.2)
WRITE(6,13)B,A,G,BC,GO,G1,Q
13  FORMAT(1H0,6X,"FLANGE GEOMETRY DATA(INCH)"/7X,
+"INNER DIA-----=",F10.4,10X,"OUTER DIA-----=",F10.4/7X,
+"EFFECTIVE GASKET DIA=",F10.4,10X,"BOLT CIRCLE DIA--=",F10.4/7X,
+"SHELL THICKNESS-----=",F10.4,10X,"MAX HUB THICKNESS=",F10.4/7X,
+"LENGTH OF HUB-----=",F10.4)
WRITE(6,14)FN,Y,FMG
IF(FNR+FNC .LT. .0001) GOTO 315
WRITE(6,15) RL,FNR,FNC,GR,YRRIB,YRCIR
15  FORMAT( 7X, "RIBS + INNER GASKET DATA",/,7X, "TOTAL LENGTH OF"
+" RIB SEGMENTS (INCH) =",F10.1, /,7X, "RIB WIDTH ",9("----"),"=",
+ F10.4,/, 7X, "RING WIDTH ----- =",
+ F10.4,/,7X, "EFFECTIVE RING DIAMETER (INCH) ----- =",F10.3,/,
+ 7X, "DESIGN SEATING STRESS (RIB) (PSI)----- =",F10.0,/,

```

```

+ 7X, "DESIGN SEATING STRESS (RING) (PSI)---- =",F10.0,/)
14  FORMAT(1H0,6X,"GASKET DATA"/7X,"WIDTH(INCH)-----=",
+ F10.2/7X,"DESIGN SEATING STRESS(PSI)=" ,F10.0/7X,
+ "GASKET FACTOR-----=",F10.1,/)
315 GO TO (320,330,340,345,346),MFLG
320 WRITE (6,360)
360 FORMAT(7X,"FLANGE IS A WELD NECK",/)
GO TO 350

330 WRITE (6,370)
370 FORMAT(7X,"FLANGE IS A HUBBED SLIP ON")
GO TO 350

345 WRITE(6,375)
375 FORMAT(7X,"LAP JOINT FLANGE")
GO TO 350

340 WRITE (6,380)
380 FORMAT(7X,"FLANGE IS A HUBBED LAP JOINT")
GO TO 350

346 WRITE(6,385)
385 FORMAT (7X,"RING JOINT FLANGE",/)
350 BO=FN/2.
BG=BO
IF(BO.GT. .25) BG=SQRT(BO) *.5
BR=AMIN1(.5*FNC,.5*SQRT(.5*FNC))
WM2R=RL*FNR*YRRIB + GR*3.1416*BR *YRCIR
WM2G=BG*3.1416*G*Y
WRITE(6,356) WM2R,WM2G
356 FORMAT( 7X,"RIB AND INNER RING SEATING FORCE= ",F10.0,/,
+ 7X,"GASKET SEATING FORCE ----- =",F10.0,/)
WM2=WM2R+WM2G
HP=2.*BG*3.1416*G*FMG*P
H=(G*G*3.1416 * P)/4.
WM1 = HP+H
AM = AMAX1( WM2/SA, WM1/SB)
BDM = .5
DO 40 I= 1,21
BTS(I) = BDM
IF (BOLT +.000001 .GT. BTS(I) .AND. BCLT-.000001 .LT. BTS(1))
+NBT = I
BDM =BDM + .125
40 CONTINUE
IF (IBT .NE. 0) GO TO 78
400 DO 50 K=NBT,17
AB =BTD(K)*BN
IF(AB .GE. AM) GO TO 75
50 CONTINUE
60 WRITE (6,70)
70 FORMAT(" CALCULATION GONE AWRY ")
GO TO 1000
78 THEBLT = BTS(NBT)
AB = BTD(NBT) * BN
IF(AB+.0000001 .GT. AM) GO TO 80
WRITE (6,79)

```

```

79 FORMAT(" THE BCLT IS TOO SMALL ,CALCULATIONS TERMINATED "
GO TO 1000
75 THEBLT = BTS(K)
80 GASKET = AB*SA / (2.0*Y*3.14159*G)
IF(FN .GE. GASKET) GO TO 82
81 FORMAT(" FOR RAISED FACE, THE MIN. GASKET WIDTH =",
+F7.4,/)
WRITE(6,81) GASKET
82 WRITE(6,17) BN,THEBLT
17 FORMAT(1H0,6X,"BOLTING DATA"/7X,"NUMBER-----",F5.0/7X,
+"NOM DIA(INCH)=",F5.3 )
WRITE(6,85)AM,AB
85 FORMAT(1H0,5X,
+" THE NECESSARY TOTAL CROSS SECTIONAL AREA =",F9.4,/6X,
+" THE ACTUAL TOTAL CROSS SECTIONAL AREA-----",F9.4)

C IT IS NOT CONSIDERED THAT RIB FORCES CONTRIBUTE TO SEATING MOMENT
AM = AMAX1((WM2-YRRIB*RL*FNR) /SA ,WM1/SB)
W= .5*(AM+AB)*SA
C LOAD
HD = 3.14159*B*B*P/4.
HT=H-HD
C LEVER ARM
HDLA = (BC-B) * .5
IF(MFLG .EQ. 1) HDLA=HDLA-(G1/2.)
HGLA = (BC-G) * .5
HTLA = .5*((BC-B)/2. + HGLA)
IF(MFLG .EQ. 3 .OR. MFLG .EQ. 4)HTLA=HGLA
C MOMENT
890 CONTINUE
FM1 =((HD*HDLA)+(HP*HGLA)+(HT*HTLA))/B
FM11=FM1
FM2=(W* (BG*Y*HGLA + BR*YRCIR*.5*(BC-GR)))/(BG*Y +BR*YRCIR))/B
FM22 = FM2
FFM1 = B*FM1
FFM2 = B*FM2
WRITE(6,888) WM1,WM2,FFM1,FFM2
888 FORMAT(1H0,6X, "OPERATING LOAD=",F10.2/7X,"SEATING LOAD---=",
+F10.2/7X,"OPERATING MODE MOMENT=",E10.2/7X,
+"SEATING MODE MOMENT---=",E10.2/)
FK=A/B
ALOGK = ALOG10(FK)
YFLG=(((5.7169*FK*FK*ALOGK)/((FK**2)-1.0))+.66845)/(FK-1.0)
IF(MFLG .EQ. 4)GO TO 9998
IF(MFLG .EQ. 5)GO TO 9998
CALL FACT(F,V)
CALL FAC2(FS)
IF(MFLG .NE. 1)FS=1.0
WRITE(6,605)F,V,FS,W
605 FORMAT(1H0,6X,"INTEGRAL FLANGE FACTORS"/7X,"QUANTITY",10X,"
+FIG(APPENDIX11)",13X,"VALUE"/11X,"F",24X,"3240-2",18X,F10.5/11X,
+"V",24X,"3240-3",18X,F10.5/11X,"FS",23X,,"3240-6",18X,F10.5/11X,
+"H/HG",20X," - ",18X,F10.5/)

```

```

T=((FK*FK)*(1.0+(8.55246*ALGGK))-1.0)/((1.04720+ 1.9448 *(FK**2))
+*(FK-1.0))
U=(T*(1.0472+(1.9448*FK*FK)))/(1.36136*((FK*FK)-1.0))
Z= ((FK*FK)+1.0)/ ((FK**2)-1.0)
HO= SQRT(B*GO)
E=F/HO
D=U*HO*GO*GO/V
IF(THIK .LT. .0001) GO TO 120
INT = 2
CALL WELD(THIK,SCRD,INT,FM1,FM2)
GOTO 999
120 THK1= SQRT(FM1/(1.5*SFO))
THK2 = .95*THK1
INT=1
CALL WELD (THK1,SCRD1,INT,FM1,FM2)
DO 610 J=1,100
CHECK = (2.* THEBLT)+THK2
BSP = BC* 3.1416/BN
IF(BSP.LE.CHECK) GO TO 660
FM1=FM11*SQRT(BSP/CHECK)
FM2=FM22*SQRT(BSP/CHECK)
660 CALL WELD (THK2,SCRD2,INT,FM1,FM2)
IF(ABS(SCRD2) .LT. 5.0) GO TO 650
C ITERATION SCHEME
SLO=(SCRD2-SCRD1)/(THK2-THK1)
THK3=THK2-(SCRD2/SLO)
THK1=THK2
THK2=THK3
SCRD1 = SCR2
610 CONTINUE
615 WRITE (6,620)
620 FORMAT(" TRIAL WILL NOT CONVERGE, DO BY HAND")
GO TO 1000
650 INT = 2
CALL WELD (THK2,SCRD2,INT,FM1,FM2)
9998 THK1=SQRT(FM1*YFLG/SFO)
THK2=SQRT(FM2*YFLG/SFA)
BSP=BC*3.1416/BN
DO 9995 J=1,4
CHECK =AMIN1(BSP, 2.*THEBLT + AMAX1(THK1,THK2) )
THK1=((FM1*YFLG/SFO)**2 *(BSP/CHECK))**.25
THK2=((FM2*YFLG/SFA)**2 *(BSP/CHECK))**.25
9995 CONTINUE
WRITE(6,9997)THK1,THK2
9997 FORMAT(1H0,6X,"RING FLANGE THICKNESS(OPERATING MODE)=" ,F5.2
+/7X,"RING FLANGE THICKNESS(SEATING MODE)---",F5.2//)
999 IF(MCOVER.EQ. 0) GOTO 1000
ACCEPT SFO,SFA,G
HGLA=(BC-G)/2.
TCOV1=G*SQRT(.3*P/SFO + 1.78*WM1*HGLA/SFO/(G**3))
TCOV2=SQRT(1.78*FFM2/SFA/G)
TCOV3=(5.7*P*((G/100.)**4) + 2.*HGLA*AB*G/100./SQRT(THEBLT))**.333

```

```

WRITE(6,1202) TCOV1,TCOV2,TCOV3
1202 FORMAT(1H0,6X,"COVER CALCULATIONS"/7X,
+"OPERATING COVER THK=",F10.5,/7X,
+"GASKET SEATING THK=",F10.5,/7X,"TEMA MULTI-PASS THK=",F10.5,
+"CUBE ROOT(25.E6/E)")
1000 ACCEPT IRUN
IF(IRUN .EQ. 1) GO TO 1001
STOP
END
SUBROUTINE WELD (THK,SCRD,INT,FM1,FM2)
COMMON Y,T,U,Z,E,D,SFO,SFA, G1 , B,GO,H,MFLG,W
COMMON/ONE/FS
ALP = THK*E +1.0
BET = 1.3333*THK*E +1.0
GAM = ALP/T
DEL= (THK**3)/D
FLAM = GAM+ DEL
SHC = FS*FM1 /(FLAM*G1*G1*1.5)
SHCR = 1.5*SHC
SRC = BET*FM1/(FLAM*THK*THK)
STC = ((FM1*Y)/(THK**2))-(Z*SRC)
SGRC = .5*(SHCR+AMAX1(STC, SRC))
SHG = FS*FM2 /(FLAM*G1*G1*1.5)
SHGR = 1.5* SHG
SRG = BET*FM2/(FLAM*THK*THK)
STG = ((FM2*Y)/(THK**2))-(Z*SRG)
SGRG = .5*(SHGR+AMAX1(STG, SRG))
SCRC = AMAX1(SHC, SRC, STC, SGRC)
SCRG = AMAX1(SHG, SRG, STG, SGRG)
SCRD = AMAX1(SCRC-SFO, SCRG-SFA)
IF (INT .EQ. 1) GO TO 50
WRITE (6,10) THK,SHCR, SRC, STC, SGRC, SHGR, SRG, STG, SGRG
10 FORMAT(7X,"MIN.THK.OF HUBBED FLANGE=",F7.4,/ ,7X,
+"STRESSES" ,/ ,7X, "HUB" ,7X, "RADIAL" ,5X, "TANGENL" ,4X, "AVERAGE" ,
+/,14X, "CONDITIONS" ,/5X,4F10.2,/ ,13X, "GASKET LOADING" ,/5X,4F10.2)
50 RETURN
END
SUBROUTINE FAC2(F)
COMMON YFLG, T,U,Z,E,D,SFO,SFA, G1,C,GO,H,MFLG,W
XX= G1/GO
W=H/ SQRT(C*GO)
X=ALOG(XX)
TT=.25 - .12*W/.5
SLOPE = 2.00 +TT*W/.5
IF(W .GT. .5) SLOPE = 2.10 + .23*(W-.5)/.3
IF(W.GT. .8) SLOPE = 2.32 + .32*(W-.8)/ .2
YY = SLOPE* (X-W*(1.15 + .095*W- .020*W*W) )
F=AMAX1( 1.0,EXP(YY))
RETURN
END
SUBROUTINE FACT (F,V)
COMMON YFLG, T,U,Z,E,D,SFO,SFA, G1,C,GO,H,MFLG,W

```

```

DIMENSION A(7,7),B(7),G(49)
E=28.6E6
A1 =.01
N=7
DC 10 I=1,N
B(I) = 0.0
DO 10 J = 1,N
A(I,J) = 0.0

10 CONTINUE
IF(MFLG .NE. 1) N=5
R1 = C/2.
ALPHA =(G1-G0)/G0
PSI = 10.92*(H**4) / (R1*R1*G0*G0)
BETA = (2.73/(R1*R1*G0*G0))**.25
A(1,1) = .333333 + ALPHA /12.
A(1,2) = .1190476 + .0505952 * ALPHA
A(1,3) = .0047619 + ALPHA/360.
A(1,6) = -( .03055556 +59. *ALPHA/5040. + (1. + 3. *ALPHA)/PSI)
B(1) = (.01111111 +5. * ALPHA/1008. -((1.0 + ALPHA)**3)/PSI)*A1
A(1,7) =-(.00833333 + .003373015 * ALPHA + 1.0/PSI)
A(2,1) = A(1,2)
A(2,2) = .07756133 + .0413961*ALPHA + (60./7. + 225.*ALPHA/14.+
+75.*ALPHA*ALPHA/7. +5.*ALPHA**3/2.)/PSI
A(2,3) = 31./6930. + 128.*ALPHA/45045. + (6./7. + 15.*ALPHA/7.
++ 12.*ALPHA*ALPHA/7. + 5.*ALPHA**3/11.)/PSI
A(2,6) = -(533./30240. + 653. * ALPHA / 73920. +( .5 +33. *ALPHA
+/14. + 39.*ALPHA**2/28. + 25. * ALPHA**3/84.)/PSI)
B(2) = (29./3780. + 3.*ALPHA/704. -( .5 +33.*ALPHA/14. +
+81.*ALPHA**2/28. + 13.*ALPHA**3/12.)/PSI) * A1
A(2,7) = -(31./6048. + 1763.*ALPHA/665280. + (.5 +6.*ALPHA/7.
++15.*ALPHA**2/28. +5.*ALPHA**3/42.)/PSI)
A(3,1) = A(1,3)
A(3,2) = A(2,3)
A(3,3) = 1.0/2925. + 71.*ALPHA/300300. + (8./35. + 18.*ALPHA
+/35. + 156.*ALPHA**2/385. + 6. *ALPHA**3/55.)/PSI
A(3,6) = -(761./831600. +937.*ALPHA/1663200. + (1./35. +
+6.*ALPHA/35. + 11. *ALPHA**2/70. +3.*ALPHA**3/70.)/PSI)
B(3) =(197./415800. + 103.*ALPHA/332640.-(1./35. + 6.*ALPHA
+/35. + 17.*ALPHA*ALPHA/70. + .1*ALPHA**3)/PSI) *A1
A(3,7) = -(233./831600. + 97.*ALPHA/554400. + (1./35. + 3.*
+ALPHA/35. + ALPHA**2/14. + 2.0*ALPHA**3/105.)/PSI)
A(4,1) = R1
A(4,5) = -1.0
A(5,1) = -R1/H
A(5,2) = R1/H
A(5,7) = -.08333333333 * R1/H
A(5,6) = -.416666666 *R1/H
A(5,4) = -BETA
A(5,5) = -BETA
B(5) = .083333333*A1* R1/H
IF(MFLG .NE. 1) GO TO 444
A(6,6) = E*G0*H*H/R1/PSI

```

```

A(6,4) = -E*(G0**3) * (BETA**2)/ 5.46
A(7,7) = -E*G0*H/R1/PSI
A(7,6) = 3.0 * ALPHA * A(7,7)
A(7,4) = E*(G0**3) * (BETA**3)/ 5.46
A(7,5) = -A(7,4)
444 CONTINUE
DO 30 J=1,N
DO 30 I= 1,N
NDEX=(N*(J-1)+I)
G(NDEX)=A(I,J)
30 CONTINUE
CALL SIMQ(G,B,N,KS)
IF(KS.EQ.0) GO TO 100
WRITE(6,40)
40 FORMAT(5X,"EQUATIONS ARE NOT LINEARLY INDEPENDENT")
STOP
100 CONTINUE
C B(1) = A SUB 1
C B(2) = A SUB 2
C B(3) = A SUB 3
C B(4) = C5
C B(5) = C6
C B(6) = A0
C B(7) = B0
P1 = E*G0*H/R1* ((.5 + ALPHA/6.) * B(1) + (.25+11.*ALPHA/84.)
+B(2) + (1./70. + ALPHA/105.)*B(3) - (7./120. + ALPHA/36. +
+3.*ALPHA/PSI)*B(6) - (1./40. + ALPHA/72.)*A1 - (1./60. + ALPHA
+/120. + 1.0/PSI) * B(7) )
THETA =(-B(1)-1.5*B(2)-.2*B(3) + .25*B(6) + .25*A1 + .08333333*
+B(7)) * R1/H
F=-P1/A1/(E*G0*H/R1*2.0*H/SQRT(C*G0))*((1.0+ALPHA)**3)/PSI)
V= THETA /A1/(R1/H*SQRT(C*G0))/(2.*H)*(1.0+ALPHA)**3)
RETURN
END
SUBROUTINE SIMQ(A,B,N,KS)
DIMENSION A(49),B(7)

C
C FORWARD SOLUTION
C
TOL=0.0
KS=0
JJ=-N
DO 65 J=1,N
JY=J+1
JJ=JJ+N+1
BIGA=0
IT=JJ-J
DO 30 I=J,N

C
C SEARCH FOR MAXIMUM COEFFICIENT IN COLUMN
C
IJ=IT+I

```

```

IF (ABS(BIGA)-ABS(A(IJ))) 20,30,30
20 BIGA=A(IJ)
   IMAX=I
30 CONTINUE
C
C   TEST FOR PIVOT LESS THAN TOLERANCE (SINGULAR MATRIX)
C
IF (ABS(BIGA)-TOL) 35,35,40
35 KS=1
   RETURN
C
C   INTERCHANGE ROWS IF NECESSARY
C
40 I1=J+N*(J-2)
   IT=IMAX-J
   DO 50 K=J,N
     I1=I1+N
     I2=I1+IT
     SAVE=A(I1)
     A(I1)=A(I2)
     A(I2)=SAVE
C
C   DIVIDE EQUATION BY LEADING COEFFICIENT
C
50 A(I1)=A(I1)/BIGA
   SAVE=B(IMAX)
   B(IMAX)=B(J)
   B(J)=SAVE/BIGA
C
C   ELIMINATE NEXT VARIABLE
C
IF (J-N) 55,70,55
55 IQS=N*(J-1)
   DO 65 IX=JY,N
     IXJ=IQS+IX
     IT=J-IX
     DO 60 JX=JY,N
       IXJX=N*(JX-1)+IX
       JJX=IXJX+IT
60 A(IXJX)=A(IXJX)-(A(IXJ)*A(JJX))
65 B(IX)=B(IX)-(B(J)*A(IXJ))
C
C   BACK SOLUTION
C
70 NY=N-1
   IT=N*N
   DO 80 J=1,NY
     IA=IT-J
     IB=N-J
     IC=N
     DO 80 K=1,J

```

```

B(IB)=B(IB)-A(IA)*B(IC)
IA=IA-N
80 IC=IC-1
RETURN
END

```

Note: Subroutine SIMQ is adapted from the scientific subroutine package, system 360-CM-03X, by the Courtesy of the IBM Corporation, White Plains, New York.

```

OPTION I: DETERMINE RING THICKNESS

DESIGN PRESSURE(Psi)= 600.00
ALLOW.STRESSES(Psi)
      AMBIENT TEMP.OF          DESIGN TEMP.OF
FLANGE          17500.00      17500.00
BOLTING         35000.00      35000.00
FLANGE GEOMETRY DATA(INCH)
INNER DIA-----= 44.7500    OUTER DIA-----= 53.0000
EFFECTIVE GASKET DIA= 47.8400    BOLT CIRCLE DIA--= 50.5000
SHELL THICKNESS-----= .8800    MAX HUB THICKNESS= 1.1300
LENGTH OF HUB-----= 1.2500

GASKET DATA
WIDTH(INCH)-----= .75
DESIGN SEATING STRESS(Psi)= 9000.
GASKET FACTOR-----= 3.0

FLANGE IS A WELD NECK

RIB AND INNER RING SEATING FORCE= 0.
GASKET SEATING FORCE ----- = 414162.

BOLTING DATA
NUMBER-----= 52.
NOM DIA(INCH)=1.250
THE NECESSARY TOTAL CROSS SECTIONAL AREA = 35.5479
THE ACTUAL TOTAL CROSS SECTIONAL AREA-----= 48.3080
OPERATING LOAD=1244175.25
SEATING LOAD---= 414162.00
OPERATING MODE MOMENT= .27E+07
SEATING MODE MOMENT---= .20E+07

INTEGRAL FLANGE FACTORS
QUANTITY          FIG (APPENDIXI)†          VALUE
F                  3240-2                      .89791
V                  3240-3                      .45536
FS                 3240-6                      1.03680
H/HO              -                      .19919

MIN.THK.OF HUBBED FLANGE= 5.3986
STRESSES
HUB      RADIAL      TANGENL      AVERAGE
CONDITIONS
22960.23  1969.52  12042.41  17501.32
GASKET LOADING
16697.95  1432.34  8757.91  12727.93
RING FLANGE THICKNESS(OPERATING MODE)= 6.29
RING FLANGE THICKNESS(SEATING MODE)--= 5.37

```

+ REFERENCE (3.5.3)

OPTION 2: COMPUTE STRESSES FOR A GIVEN RING THICKNESS

DESIGN PRESSURE(P51)= 600.00

ALLOW.STRESSES(P51)

	AMBIENT TEMP.OF	DESIGN TEMP.OF
FLANGE	17500.00	17500.00
BOLTING	35000.00	35000.00

FLANGE GEOMETRY DATA(INCH)

INNER DIA-----=	44.7500	OUTER DIA-----=	53.0000
EFFECTIVE GASKET DIA=	47.8400	BOLT CIRCLE DIA--=	50.5000
SHELL THICKNESS-----=	.8800	MAX HUB THICKNESS=	1.1300
LENGTH OF HUB-----=	1.2500		

GASKET DATA

WIDTH(INCH)-----=	.75
DESIGN SEATING STRESS(P51)=	9000.
GASKET FACTOR-----=	3.0

FLANGE IS A WELD NECK

RIB AND INNER RING SEATING FORCE= 0.

GASKET SEATING FORCE ----- = 414162.

BOLTING DATA

NUMBER-----= 52.

NOM DIA(INCH)=1.250

THE NECESSARY TOTAL CROSS SECTIONAL AREA = 35.5479

THE ACTUAL TOTAL CROSS SECTIONAL AREA-----= 48.3080

OPERATING LOAD=1244175.25

SEATING LOAD--= 414162.00

OPERATING MODE MOMENT= .27E+07

SEATING MODE MOMENT--= .20E+07

INTEGRAL FLANGE FACTORS

QUANTITY	FIG(APPENDIX11)	VALUE
F	3240-2	.89791
V	3240-3	.45536
FS	3240-6	1.03680
H/HO	-	.19919

MIN.THK.OF HUBBED FLANGE= 6.0000

STRESSES

HUB	RADIAL CONDITIONS	TANGENL	AVERAGE
18728.39	1374.10	11063.99	14896.19
13620.32	999.32	8046.35	10833.34

+REFERENCE (3.5.3)

3.13 STRESS ANALYSIS OF THE WELDING NECK FLANGE

The method of Waters, et al. described in the preceding sections provides a complete stress analysis of a tapered hub flange. However, the assumptions made in the solution process have been subject to a great deal of critical inquiry [3.13.1-2]. Practical and experimental evidence suggests that flanges designed using this method are structurally safe; however, difficulty is frequently encountered in achieving leak tightness in large diameter flanges operating at high pressures. The simplified analysis for a pair of ring flanges (Section 3.10) points up the significance of bolt/gasket interaction effects on the stress level in the flange. Therefore, a stress analysis procedure which eliminates the important limitations of the Waters, et al. method can be a valuable design and analysis tool. The method proposed by Murray and Stuart [3.13.1] is quite adequate in these respects. A brief outline of this method is presented in the following. The reader is referred to Rose [3.13.2] for a lucid and concise presentation on this matter.

Assumptions:

- (i) The flange hub and shell are modelled by thin shell theory equations.
- (ii) The flange ring is modelled by ring theory rather than plate theory.
- (iii) Mean diameters of the shell and hub are assumed to be equal to the mean shell diameter.

The flange is composed of its three constituent elements, namely the shell, hub and ring. It is assumed here that the external loading consists of: (i), a circumferentially distributed radial couple of magnitude M_{ext} ; (ii), an axial force W on the shell; (iii), internal pressure p on all inside surfaces. The solution procedure consists again of writing the structural relationships for the three elements in terms of unknown constants, which are subsequently evaluated by imposing displacement and traction compatibility at element interfaces.

i. *Shell*: Referring to Fig. 3.13.1, the radial deflection (positive if directed away from the center) of a long thin shell subject to internal

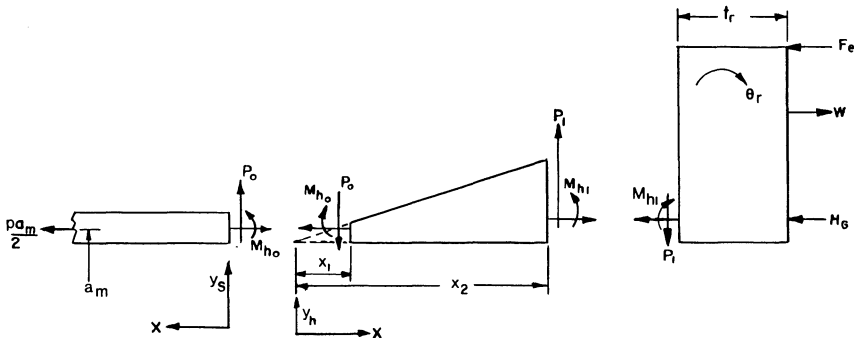


Fig. 3.13.1. Stress analysis model.

pressure p , and edge loads P_0 and M_{h_0} is given by (see Appendix A for derivation).

$$y_s = \frac{e^{-\beta x}}{2\beta^3 D_s} [\beta M_{h_0} (-\sin \beta x + \cos \beta x) + P_0 \cos \beta x] + \frac{p a_m^2}{E g_0} (1 - 0.5\nu) \quad (3.13.1)$$

where a_m is the mean shell diameter, and β and D_s are defined by replacing r_1 by a_m in Eq. (3.11.30). The last term in the above equation is due to the dilatation effect of internal pressure. It is to be noted that the term 0.5ν should be set equal to zero in designs where the longitudinal force $H = p a_m/2$ is absent (such as the shell flange in Fig. 3.1.1). Note here that in contrast with Waters analysis, the local pressure on the shell wall is included.

ii. *Hub*: For the hub, Murray and Stuart employ the solution for an axisymmetrically loaded thin cylindrical shell with linearly varying thickness. The radial displacement, y_h , (positive if directed away from the center) is expressed in terms of the longitudinal coordinate measured from the point of zero thickness. Thus, the thickness of the hub at the small end (equal to the shell thickness) is

$$g_0 = \gamma x_1 \quad (3.13.2)$$

where γ is the rate of taper. We have:

$$y_h = -x^{-1/2} [c_1 \psi_1'(\epsilon) + c_2 \psi_2'(\epsilon) + c_3 \psi_3'(\epsilon) + c_4 \psi_4'(\epsilon)] + \frac{p a_m^2}{E \gamma x} (1 - 0.5\nu) \quad (3.13.3)$$

where:

$$\epsilon = 2\rho x^{1/2} \quad (3.13.4)$$

and:

$$\rho = \left[\frac{12(1-\nu^2)}{\gamma^2 a_m^2} \right]^{1/4} \quad (3.13.5)$$

c_i ($i = 1-4$) are constants of integration and the ψ 's are the so called Schleicher functions, akin to the well known Kelvin functions. The series expansion for these functions is given in Appendix 3.B. The bending moment M_x and shear force P follow by successive differentiations of Eq. (3.13.3). We obtain:

$$P = -\frac{E \gamma^3 \rho^2 x^{1/2}}{24(1-\nu^2)} [c_1 S_2(\epsilon) + c_2 S_1(\epsilon) + c_3 S_4(\epsilon) + c_4 S_3(\epsilon)] \quad (3.13.6)$$

$$M_x = \frac{E \gamma^3 x^{1/2}}{48(1-\nu^2)} [c_1 S_5(\epsilon) - c_2 S_6(\epsilon) + c_3 S_7(\epsilon) - c_4 S_8(\epsilon)] + \frac{p a_m^2 \gamma^2}{6(1-\nu^2)} (1 - 0.5\nu) \quad (3.13.7)$$

The functions $S_i(\epsilon)$ are combinations of Schleicher functions and their derivatives. These are defined in Appendix 3.B.

We recognize that revolving the hub middle surface about the axis of revolution gives the frustum of a cone; therefore conical solutions [3.13.3–4] would have been more appropriate for this purpose. However, the error introduced due to the use of a tapered cylindrical shell assumption is negligible in most cases.

iii. *Ring*: Referring to Fig. 3.13.1, the flange ring is subject to a net radial couple M given by:

$$M = M_{ext} + \left(M_{h_1} - \frac{P_1 t_r}{2} \right) \left(\frac{r_m - a_m}{r_m} \right) \quad (3.13.8)$$

where M_{ext} is the external couple due to the combined effect of bolt pull, gasket reaction, and header pressure load and other effects (such as reaction due to any metal-to-metal contact F_e on an annular portion of the ring surface). The rotation of the centerline of the flange ring, θ_r , is given by (Eq. 3.9.4):

$$\theta_r = \frac{M r_m^2}{E_r I_r} \quad (3.13.9)$$

where:

r_m = mean ring radius

E_r = Young's modulus of the ring material

I_r = moment of inertia of the ring cross section

$$(I_r = b_r t_r^3 / 12)$$

The radial displacement of the ring centerline due to in-plane loads is given by:

$$w_{rm} = \left(p - \frac{P_1}{t_r} \right) \frac{r_m^2}{b_r E_r} \quad (3.13.10)$$

Thus, the radial displacement of the ring at its junction with the hub is given by:

$$w = w_{rm} + \frac{\theta_r t_r}{2} \quad (3.13.11)$$

By matching the displacement, slope, shear force, and bending moment at the two locations of discontinuity, eight linear algebraic equations are obtained, which may be written in subscript notation as:

$$\sum_{j=1}^8 m_{ij} c_j = n_i; \quad i = 1, 2, \dots, 8. \quad (3.13.12)$$

The unknown vector c_j consists of the four constants of integration in Eq. (3.13.3) and four discontinuity reactions with the notation,

$$c_5 = M_1, \quad c_6 = -P_0, \quad c_7 = M_2, \quad c_8 = -P_1$$

The non-zero element of m_{ij} and n_i are defined as follows:

$$m_{(2i-1)j} = \frac{2\rho}{\epsilon_i} \psi_j'(\epsilon_i); \quad i = 1, 2; \quad j = 1, 2, 3, 4$$

where

$$\epsilon_i = 2\rho x_i^{1/2}; \quad i = 1, 2$$

x_1 and x_2 are shown in Fig. 3.13.1 (hub end coordinates):

$$m_{15} = \frac{1}{2\beta^2 D_s} \quad m_{16} = \frac{-1}{2\beta^3 D_s}$$

$$m_{2ij} = (-1)^{j+1} \frac{4\rho^3}{\epsilon_i^3} S_j(\epsilon_i); \quad i = 1, 2; \quad j = 1, 2, 3, 4$$

$$m_{25} = \frac{1}{\beta D_s} \quad m_{26} = -m_{15}$$

$$m_{37} = \frac{6r_m^3}{E_r b_r t_r^2 a_m} \quad m_{38} = \frac{4r_m^2}{E_r b_r t_r}$$

$$m_{47} = \frac{-12r_m^2}{E_r b_r t_r^3} \quad m_{48} = \frac{-6r_m^2}{E_r b_r t_r^2}$$

$$m_{3+2i,j} = (-1)^{j+1} S_{4+j}(\epsilon_i); \quad i = 1, 2; \quad j = 1, 2, 3, 4$$

$$m_{55} = \frac{96\rho(1-\nu^2)}{E_r \gamma^3 \epsilon_1}$$

$$m_{4+2i,j} = S_{j+1}(\epsilon_i); \quad i = 1, 2; \quad j = 1, 3$$

$$m_{4+2i,j} = S_{j-1}(\epsilon_i); \quad i = 1, 2; \quad j = 2, 4$$

$$m_{66} = \frac{-48(1-\nu^2)}{E_r \gamma^3 \rho \epsilon_1} \quad m_{77} = \frac{96\rho(1-\nu^2)}{E_r \gamma^3 \epsilon_2}$$

$$m_{88} = \frac{-48(1-\nu^2)}{E_r \gamma^3 \rho \epsilon_2} \quad n_2 = \frac{p a_m^2 (1-0.5\nu)}{E_r \gamma x_1^2}$$

$$n_3 = \frac{p a_m^2 (1-0.5\nu)}{E_r \gamma x_2} - \frac{p r_m^2}{b_r E_r} - \frac{6r_m^2 M_{ext}}{E_r b_r t_r^2}$$

$$n_4 = \frac{-p a_m^2 (1-0.5\nu)}{E_r \gamma x_2^2} + \frac{12r_m^2 M_{ext}}{E_r b_r t_r^3}$$

$$n_{3+2i} = \frac{16p a_m^2 \rho (1-0.5\nu)}{E \gamma \epsilon_i}; \quad i = 1, 2$$

Equation (3.13.12) can be solved using a standard linear equation solver subroutine. Having determined the discontinuity moments and shears, the stress fields in the three elements are readily evaluated. The above equations are programmed in subroutine, FLG, which is utilized in Chapter 4 to perform a flange-tubesheet interaction analysis. The listing of FLG can be found in Section 4.8. We delay further discussion of this analysis until Chapter 4.

3.14 CONTROLLED COMPRESSION JOINT

In illustrating the deflection characteristics of a pair of identical ring

flanges (Section 3.10), we assumed that the bolt load was completely reacted by the gasket. In practical designs, it is advisable to provide protection against overcompressing the gasket, since in most joints the gasket will be crushed or extruded before the studs will fail in tension. However, in order to maintain a leak tight joint at the operating pressure, the bolts must be preloaded to such an extent that the bolt force exceeds the sum of the required gasket residual load and the header load. For an otherwise suitable gasket, such a magnitude of bolt preload may exceed its optimum "seating load." This difficulty can be overcome by using the concept of "controlled compression." This concept entails machining the mating flange faces in such a manner that the gasket can only be compressed to a preset value. Upon application of additional bolt preload, the two flanges develop metal-to-metal contact over a suitable region, henceforth referred to as the "land" (Fig. 3.5.5). The contact force generated on the land can significantly modify the deflection characteristics of the flange and its attributes of leak tightness. We will presently explore the merit of this concept by treating a pair of identical flanges in some detail.

It is noted that the moment on the flange ring *always* increases as the pressure is increased. This is because the load line of the pressure load is always farther than the effective gasket circle from the bolt load line. Therefore, the maximum ring stress corresponds to the condition of maximum pressure. The central design goal lies in selecting a land location and contact load in such a manner that the residual gasket load, H'_G , under *maximum* internal pressure, is maximized, while the corresponding ring rotational moment does not exceed the value for the standard geometry (treated in Section 3.10). Thus, our analysis will compare the performance of a ring flange with and without a controlled contact land. At the design pressure, the unit equipped with a contact land is required to develop an identical moment to the one without a land. When the condition of maximum pressure is reached, the load on the contact land should vanish, thus maximizing the residual gasket load. The initial bolt pull (under seating condition) is to be adjusted for each design in such a manner that the above requirements are met. The initial contact load on the land is another variable which can be suitably adjusted by machining the flange facings appropriately. With the problem formulated in this manner, we wish to compare the variation in gasket pressure and bolt load as the internal pressure in the joint is varied. To simplify the analysis, the gasket loading and unloading moduli are assumed to be equal to the same constant value of K_G .

Under the seating condition, axial force equilibrium yields (Fig. 3.14.1):

$$W_1 = H_G + H_c$$

where H_c is the contact load on the effective circle of the land region assumed to be located at an offset h_c from the bolt circle.

The rotation of the flange rings is given by Eq. (3.9.4):

$$\theta_r = \chi(H_G h_G + H_c h_c) \quad (3.14.1)$$

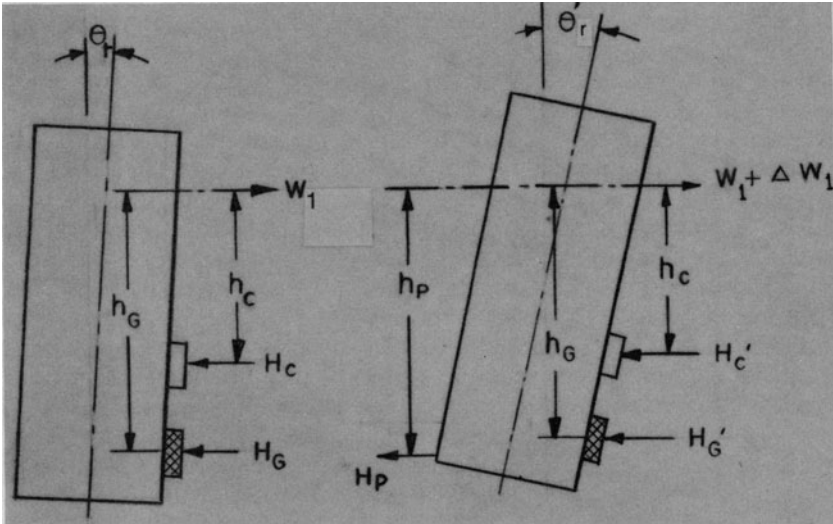


Fig. 3.14.1. Deflection of one pair of identical flanges.

where:

$$\chi = \frac{r_m}{2\pi E_r I_r} \quad (3.14.2)$$

As the internal pressure is applied, the bolt load, gasket compression load and contact load change. Let H'_G , H'_c and θ'_r represent the new gasket compression load, contact load and flange rotation (with reference to the undeformed condition), respectively. Referring to the ring moment-rotation relationship, we have:

$$\theta'_r = \chi (H_p h_p + H'_G h_G + H'_c h_c) \quad (3.14.3)$$

If $H'_c > 0$, i.e., contact at the land is not lost, then geometric compatibility at the land location requires:

$$\frac{\Delta W_1}{K_b} + 2(\theta'_r - \theta_r) h_c = 0$$

where ΔW_1 is the increase in the bolt load. Since $\Delta W_1 = H_p + H'_G + H'_c - H_G - H_c$, we have

$$\frac{H_p + H'_G + H'_c - H_G - H_c}{K_b} + 2\chi h_c (H_p h_p + H'_G h_G + H'_c h_c - H_G h_G - H_c h_c) = 0 \quad (3.14.4)$$

Let ΔH_c and ΔH_G denote the drops due to H_p in the contact load and gasket load respectively, i.e.

$$\begin{aligned}\Delta H_c &= H_c - H'_c \\ \Delta H_G &= H_G - H'_G\end{aligned}\quad (3.14.5)$$

Equation (3.14.4) yields:

$$\Delta H_c = \rho_2 H_p - \rho_1 \Delta H_G \quad (3.14.6)$$

where:

$$\begin{aligned}\rho_2 &= f(h_c, h_p) / f(h_c, h_c) \\ \rho_1 &= f(h_c, h_G) / f(h_c, h_c)\end{aligned}\quad (3.14.7)$$

The function f in the foregoing is defined as:

$$f(x, y) = \frac{1}{K_b} + 2\chi xy \quad (3.14.8)$$

Proceeding in a similar manner, geometric compatibility at the effective gasket circle gives:

$$\frac{\Delta H_G}{K_G} = \frac{H_p - \Delta H_c - \Delta H_G}{K_b} + 2\chi h_G (H_p h_p - \Delta H_G h_G - \Delta H_c h_c)$$

Substituting for ΔH_c from Eq. (3.14.6), and rearranging terms, we obtain:

$$\Delta H_G = \psi H_p \quad (3.14.9)$$

where

$$\psi = \frac{[f(h_p, h_G) - \rho_2 f(h_c, h_G)]}{\frac{1}{K_G} + f(h_G, h_G) - \rho_1 f(h_G, h_c)} \quad (3.14.10)$$

It is desirable to have $\psi < 1$, since the smaller the value of ψ , the smaller is the change in gasket compression load due to fluctuations in the internal pressure.

For a given contact preload H_c , contact at the land is lost at $H_p = H_p^{*\dagger}$. We have from Eq. (3.14.6):

$$\Delta H_c = H_c = \rho_2 H_p^* - \rho_1 \Delta H_G = \rho_2 H_p^* - \rho_1 \psi H_p^*$$

or

$$H_p^* = H_c / (\rho_2 - \psi \rho_1)$$

Let

$$\phi = \rho_2 - \psi \rho_1 \quad (3.14.11)$$

then

$$H_c = \phi H_p^* \quad (3.14.12)$$

[†] All quantities with * superscript imply that they pertain to the design pressure condition.

Equation (3.14.12) defines the required contact load at the land under the seating condition. If the pressure is further increased, an analysis analogous to the above yields:

$$\begin{aligned}\Delta H_G &= \rho_3 H_p - \rho_4 H_c \\ \rho_3 &= f(h_p, h_G) / \left[\frac{1}{K_G} + f(h_G, h_G) \right] \\ \rho_4 &= f(h_G, h_c) / \left[\frac{1}{K_G} + f(h_G, h_G) \right]\end{aligned}\quad (3.14.13)$$

The case for no contact at the land, i.e., $H_c = 0$, follows directly from Eq. (3.14.13). The expression for ΔH_G becomes:

$$\Delta H_G = \rho_3 H_p \quad (3.14.14)$$

We can now compare the controlled compression and uncontrolled compression designs under the condition that both develop identical gasket compression load, H_G^* , when the pressure load reaches H_p^* . Identical gasket compression load means that the bolt loads will be equal. The overturning couple and hence maximum ring stresses will also be equal.

Uncontrolled Compression:

$$\begin{aligned}H'_G &= H_G - \Delta H_G \\ &= H_G - \rho_3 H_p\end{aligned}$$

Therefore:

$$\begin{aligned}H_G^* &= H_G - \rho_3 H_p^* \\ H'_G &= H_G^* + \rho_3 (H_p^* - H_p)\end{aligned}\quad (3.14.15)$$

The bolt load under the seating condition is:

$$W_1 = H_G = H_G^* + \rho_3 H_p^* \quad (3.14.16)$$

Similarly the bolt load at H_p is given by:

$$\begin{aligned}W_1 + \Delta W_1 &= H'_G + H_p \\ &= H_G^* + \rho_3 H_p^* + (1 - \rho_3) H_p \\ &= W_1 + (1 - \rho_3) H_p\end{aligned}\quad (3.14.17)$$

Controlled Compression:

Gasket compression load at pressure load H_p is given by:

$$H'_G = H_G - \psi H_p; \quad H_p < H_p^*$$

From Eq. (3.14.9), $\Delta H_G = \psi H_p \rightarrow \Delta H_G^* = \psi H_p^*$

$$H'_G = H_G^* + \psi (H_p^* - H_p) \quad (3.14.18)$$

Similarly, the bolt load at the seating (unpressurized) condition is:

$$W_1 = H_G + H_c$$

or

$$W_1 = H_G^* + (\psi + \phi)H_p^* \tag{3.14.19}$$

The bolt load under the pressurized condition is:

$$W_1 + \Delta W_1 = W_1 - \Delta H_G - \Delta H_c + H_p$$

or

$$W_1 + \Delta W_1 = W_1 + (1 - \psi - \phi)H_p \tag{3.14.20}$$

Figure 3.14.2 shows a schematic representation of the residual gasket load and bolt load as a function of pressure loads for the two constructions. A qualitative comparison of the joint performance can be made by considering the numerical example of Section 3.10.

Table 3.14.1 gives the values of the bolt load and gasket load at the two end points and the slopes of the bolt load and gasket load lines for three conditions: (i) no land contact, (ii) land contact at $h_c = 0.75''$, and (iii) land contact at $h_c = -1''$.

The last case corresponds to metal-to-metal contact outboard of the bolt circle, whereas case (ii) pertains to contact loading between the gasket and bolt center lines.

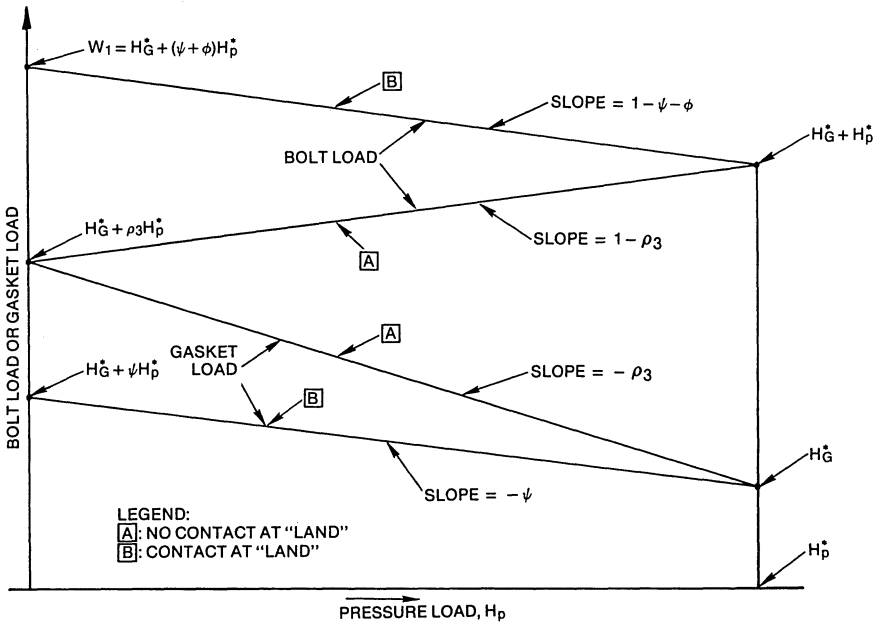


Fig. 3.14.2. Gasket load and bolt load plotted as a function of H_p .

Table 3.14.1

Case	Gasket Load		Bolt Load		Slope of load line
	At zero pressure	At H_p^*	At zero pressure	At H_p^*	
(i) (no contact)	$H_G^* + .395 H_p^*$	H_G^*	$H_G^* + .395 H_p^*$	$H_G^* + H_p^*$	0.605
(ii) $h_c = .75''$	$H_G^* + .0182 H_p^*$	H_G^*	$H_G^* + 1.138 H_p^*$	$H_G^* + H_p^*$	-0.138
(iii) $h_c = -1''$	$H_G^* + .377 H_p^*$	H_G^*	$H_G^* + .514 H_p^*$	$H_G^* + H_p^*$	0.486

Table 3.14.1 is constructed on the assumption that the contact load is set such that it vanishes as the pressure load reaches its maximum design value H_p^* . Thus, the final gasket pressure H_G^* and bolt load are the same in all cases, resulting in identical ring stress under the condition of maximum pressure. The gasket load at pressures below the design pressure varies in a markedly different manner for the three cases. The variation in gasket load is the minimum in case (ii), and maximum in case (i). This indicates that case (ii) best protects the gasket from deterioration due to frequent load variation caused by pressure changes in the pressure vessel. The initial gasket load ($H_p = 0$) is much less in case (ii) compared to the other cases. This is consistent with the seating requirements of soft and hollow metal (tubular) type gaskets. The designer should select the joint construction which yields the most compatible seating load for the gasket.

The bolt load increases for increasing H_p in cases (i) and (iii); and decreases in case (ii). The rate of variation of bolt load is also found to be most moderate in case (ii).

This example problem illustrates the relative merits of controlled and uncontrolled metal-to-metal contact constructions. The central objective in the design process is to select a joint design which produces maximum protection against leakage under the condition of maximum pressure, and protects the gasket from load cycling during pressure fluctuations. The concept of "controlled compression" appears to be an excellent vehicle towards such an objective.

The foregoing analysis treats a highly simplified structure, that of two identical bolted ring flanges. The analysis is much more involved when the bolted members are of more complicated variety (e.g., welding neck type) and dissimilar in construction.

In the next chapter we will present a detailed analysis of one such common construction in heat exchangers to illustrate the significance of the "controlled compression" concept.

NOMENCLATURE

- A = flange ring O.D.
- A_b = total root area of body bolts
- A'_b = root area of one bolt
- A_0 = hub curvature factor at small end
- A_{b_1}, A_{b_2} = required total bolt root area for seating and pressurized condition, respectively
- a_m = mean radius of shell (Fig. 3.13.1)
- A_1 = hub curvature factor at large end
- a_1, a_2, a_3 = coefficient in hub deflection equation (Eq. 3.11.20)
- B = flange ring I.D.
- B_0 = shear factor at small end
- b = effective gasket width (Eq. 3.5.1)
- b_r = radial width of ring

- c_{ij} = functions of α and κ (Eq. 3.11.26) ($i = 1,2,3$), ($j = 1,2,3,4,5,6$)
 C_i = constants of integration ($i = 1,2 \dots 8$)
 D = flexural rigidity of flange ring
 D_h = flexural rigidity of hub (Eq. 3.11.13)
 d_B = nominal bolt diameter
 d_i, d_o = inner and outer diameters of the nut bearing surface (Eq. 3.6.4)
 d_0 = dimension across flats in heavy hex nut (Table 3.7.1)
 d_p = pitch diameter (Table 3.7.1)
 d_w = wrench diameter (Fig. 3.3.2)
 E = Young's modulus of hubbed flange material
 E_b = Young's modulus of bolt material
 E_g = decompression modulus of gasket (Eq. 3.5.7)
 E_r = Young's modulus of ring material (Eq. 3.9.2a)
 e = minimum radial distance between bolt circle and O.D. of flange (Table 3.7.1)
 F = hub large end shear coefficient (Eq. 3.11.43)
 F_{ax} = axial load in one bolt
 f = hub stress magnification factor
 G = effective gasket diameter (Eq. 3.5.1)
 g = hub thickness at axial coordinate x (Fig. 3.11.1)
 g_0 = shell thickness (Fig. 3.11.1)
 g_1 = hub thickness at the large end (Fig. 3.11.1)
 H_d = end header load on the area bounded by flange inside diameter
 H_G = seating condition gasket load
 H'_G = residual gasket load under pressurized condition
 H_T = axial pressure load in the annulus between effective gasket diameter and flange I.D.
 H_c = contact load on the land under seating condition
 H_p = total header end load (Section 3.10)
 h = hub length
 h_G = gasket line offset from bolt circle
 h_p = moment arm of the header load H_p
 I_r = moment of inertia of flange ring cross section in Fig. 3.9.1b about the radial axis of symmetry ($y = 0$)
 K = flange ring O.D./I.D.
 K_b = bolt (spring) stiffness (Eq. 3.10.4b)
 K_g = spring stiffness of gasket in unloading
 K_1, K_2 = coefficients in the leakage rate equation (Eq. 3.5.3)
 l = effective bolt length under seating
 l' = effective bolt length under pressurized condition
 l_0 = free bolt length
 M_{ext} = total external moment on the flange ring (Section 3.11)

M_h = hub longitudinal bending moment at coordinate x (Fig. 3.11.1)

M_{h_0} = longitudinal moment per unit circumference at the small end of the hub

M_{h_1} = longitudinal moment per unit circumference at the large end of the hub

M_r = radial bending moment in flange ring

M_{r_1}, M_{r_2} = radial bending moment per unit circumference at the inside and outside radius of flange ring, respectively

M_s = shell longitudinal moment at coordinate x

M_t = tangential bending moment in flange ring

m = gasket factor (Eq. 3.5.2)

m_r = distributed couple per linear length of circumference (Fig. 3.9.1)

n = number of bolts on the bolt circle

N_w = gasket width (Fig. 3.3.3)

n_t = number of threads per inch (Table 3.7.1)

P = internal pressure in the flanged joint

P_h = radial shear in the hub (Eq. 3.11.14)

P_0 = shear at hub/shell junction (P_h at $\xi = 0$)

P_s = shell radial shear at coordinate x

P_1 = shear at hub/ring junction (P_h at $\xi = 1$)

p_b = circumferential bolt pitch (Table 3.7.1)

Q_r = radial shear in flange ring at radius r

R_h = minimum radial distance between bolt center line and outer hub diameter (Fig. 3.2.1b)

R_c = contact force on the land (Eq. 3.5.8)

R_r = minimum radial distance (Fig. 3.2.1a)

r_m = mean radius of circular ring

r_1 = inside radius of shell ($r_1 = 0.5B$)

r_2 = outside radius of flange ring

S_{max} = maximum flexural stress in the circular ring (Eq. 3.9.2)

t = flange ring thickness in Section 3.11

t_r = ring thickness (Fig. 3.9.1)

W_1 = total bolt load (seating condition)

W_{eq} = equivalent ring load in Water's, et al. model (Section 3.11)

y = ASME Code Seating Stress

y_h = radial deflection of the hub (positive if radially outwards)

α = hub taper factor

α_b = mean coefficient of linear thermal expansion of bolt material

β = shell attenuation coefficient (Eq. 3.11.30a)

ξ = hub coordinate, dimensionless

Δ = coefficient determinant (Eq. 3.11.36)

ΔW = increase in bolt load from seating to pressurized condition

ΔW_1 = increase in the bolt load due to joint pressurization

- δ_c = gasket compression under seating condition
 δ_g = gasket relaxation (Eq. 3.10.6)
 δ_i = initial bolt elongation due to mechanical pre-tensioning (Eq. 3.6.2)
 δ_1, δ_2 = a lateral deflection of the two mating flanges at bolt center line location
 δ_r = gasket recovery upon unloading
 δ_s = joint separation upon application of pressure
 γ = slope of hub (Fig. 3.11.1)
 ϕ = potential energy function for the hub (Eq. 3.11.23)
 κ = hub modulus (Eq. 3.11.18)
 $\lambda_1, \lambda_2, \lambda_3$ = functions of c_{ij}
 Λ = leakage rate (gm/day)
 μ_1, μ_2 = limiting static coefficient of friction between nut and flange surface and nut and stud surface, respectively (Section 3.6)
 ν = Poisson ratio of flange material
 θ = flange ring rotation at $r = r_1$
 θ_r = rotation of a narrow circular ring (Fig. 3.9.1)
 θ'_r = rotation of flange ring under pressurized condition
 η_w = number of turns in spiral wound gasket
 ρ_{ij} = function of κ and α
 σ_g = gross area seating stress
 $\sigma_{h_0}, \sigma_{h_1}$ = maximum hub longitudinal bending stress at small and large end, respectively
 τ = torque required to turn the nut on the flange face (Eq. 3.6.3)
 τ_1, τ_2, τ_3 = components of τ (Eq. 3.6.3)
 ζ = determinant of c -matrix

REFERENCES

- [3.5.1] ASME Boiler and Pressure Vessel Code, Section VIII, Division 1, The American Society of Mechanical Engineers, Appendix 2 (1983).
 [3.5.2] ASME Boiler and Pressure Vessel Code, Section VIII, Division 2, The American Society of Mechanical Engineers, Appendix 3 (1983).
 [3.5.3] ASME Boiler and Pressure Vessel Code, Section III, Division 1, The American Society of Mechanical Engineers, Appendices XI and XII (1983).
 [3.5.4] Butcher, H., "Industrial Sealing Technology," Wiley, New York (1979).
 [3.5.5] Rosshem, D. B., and Markl, A. R. C., "Gasket Loading Constants," Pressure Vessel and Piping Design, Collected

- Papers, 1927–1959, The American Society of Mechanical Engineers, p. 87 (1960).
- [3.5.6] Stevens-Guille, P. D., and Crago, W. A., “Application of Spiral Wound Gaskets for Leak Tight Joints,” *Journal of Pressure Vessel Technology*, Trans. ASME, Vol. 97, Series J, No. 1, pp. 29–33 (1975).
- [3.5.7] Bazergui, André, “Compressibility and Compliance of Spiral Wound Gaskets,” Third International Conference on Pressure Vessel Technology, Part I, pp. 183–191, The American Society of Mechanical Engineers (1977).
- [3.5.8] Discussion of [3.5.6] by H. D. Traut, and author’s reply, *Journal of Pressure Vessel Technology*, Trans. ASME, Vol. 97, Series J, No. 2, p. 142 (1975).
- [3.5.9] Discussion of [3.5.6] by K. P. Singh, and author’s reply, *Journal of Pressure Vessel Technology*, Trans. ASME, Vol. 98, Series J, No. 1, p. 81 (1976).
- [3.5.10] Raut, H. D., Bazergui, A., and Marchand, L., “Gasket Leakage Behaviour Trends,” Welding Reserach Council Bulletin No. 271, pp. 16–42 (October 1981).
- [3.5.11] Bazergui, A., and Payne, J. R., “Progress in Gasket Testing—Milestone Results,” 4th National Congress, Portland, Oregon, ASME 83-PVP-45.
- [3.5.12] Bulletin No. 721, United Aircraft Products, Seals Division, Dayton, Ohio (1972).
- [3.11.1] Waters, E. O., Westrom, D. B., Rossheim, D. B., and Williams, F. S. G., “Formulas for Stresses in Bolted Flanged Connections,” *Trans. of the ASME*, FSP-59-4, pp. 161–169 (1937).
- [3.11.2] Waters, E. O., Rossheim, D. B., Westrom, D. B., and Williams, F. S. F., “Development of General Formulas for Bolted Flanges,” Taylor Forge and Pipe Works, Chicago (1949).
- [3.11.3] Timoshenko, S. P., and Woinowsky-Krieger, S., “Theory of Plates and Shells,” McGraw-Hill, New York (1959).
- [3.11.4] Vinson, J. R., “Structural Mechanics: The Behaviour of Plates and Shells,” Wiley, New York (1974).
- [3.11.5] Hildebrand, F. B., “Advanced Calculus for Applications,” Prentice-Hall (1962).
- [3.11.6] Sokolnicoff, I. S., “Mathematical Theory of Elasticity,” 2nd edition, p. 382, McGraw-Hill, New York (1956).
- [3.11.7] Fox, L., “An Introduction to Numerical Linear Algebra,” Oxford University Press, p. 34 (1965).
- [3.11.8] Timoshenko, S. P., “Strength of Materials,” Vol. II, Chapter VI, 3rd edition, Van Nostrand (1958).
- [3.12.1] “Modern Flange Design,” Bulletin 502, Gulf and Western Co., Energy Products Group, Oak Brook, Illinois.
- [3.13.1] Murray, N. W., and Stuart, D. G., “Behavior of Large Taper Hub Flanges,” Proceedings Symposium Pressure Vessel Research

- Towards Better Design, Institute of Mechanical Engineers, United Kingdom, p. 133 (1961).
- [3.13.2] Rose, R. T., "Flanges" in "Stress Analysis of Pressure Vessels and Pressure Vessel Components," edited by S. S. Gill, pp. 290–297, Pergamon Press (1970).
- [3.13.3] Chou, I-Hui, "The Exact Solution of Stress Analysis of Truncated Conical Shells," Second International Conference on Pressure Vessel Technology: Design and Analysis, Part I, The American Society of Mechanical Engineers, pp. 105–114 (1973).
- [3.13.4] Flugge, W., "Stresses in Shells," Springer Verlag, New York, p. 373 (1967).

APPENDIX 3.A

DERIVATION OF THE POLYNOMIAL EXPRESSIONS FOR HUB DEFLECTION (Eq. 3.11.20a)

A polynomial expression for w in terms of ξ is sought which satisfies the following conditions:

$$\text{At } \xi = 0, \frac{d^2 w}{d\xi^2} = A_0, \text{ and } \frac{d^3 w}{d\xi^3} = B_0$$

$$\text{At } \xi = 1, w = 0, \text{ and } \frac{d^2 w}{d\xi^2} = A_1$$

where A_0 , B_0 and A_1 are specified quantities.

Let:

$$w = \sum_{i=0}^n k_i \xi^i \quad (3.A.1)$$

where k_i are the coefficients of the polynomial. If $n = 5$ is selected, then four coefficients can be determined in terms of the fifth by utilizing the four conditions mentioned above.

We note that:

$$\frac{dw}{d\xi} = \sum_{i=1}^{n-1} i k_i \xi^{(i-1)} \quad (3.A.2)$$

$$\frac{d^2 w}{d\xi^2} = \sum_{i=2}^{n-2} i(i-1)k_i \xi^{(i-2)}$$

Setting $n = 4$, and using the above conditions, we have:

$$k_1 = -k_0 - \frac{5}{12}A_0 - \frac{1}{12}B_0 - \frac{1}{12}A_1$$

$$k_2 = \frac{1}{2} A_0$$

$$k_3 = \frac{1}{6} B_0$$

$$k_4 = -\frac{1}{12} A_0 - \frac{1}{12} B_0 + \frac{1}{12} A_1$$

Thus the fourth-order polynomial expression for w becomes:

$$w^{(1)} = k_0(1 - \xi) - A_0 \left(\frac{5}{12} \xi - \frac{1}{2} \xi^2 + \frac{1}{12} \xi^4 \right) - \frac{1}{12} B_0 (\xi - 2\xi^3 + \xi^4) - \frac{1}{12} A_1 (\xi - \xi^4) \quad (3.A.3)$$

where k_0 is an adjustable parameter, and the superscript "1" indicates "first approximation" for w .

Two such additional adjustable parameters are required in the expression for w . In this manner, a total of 3 parameters will be available to be selected in such a way that w most closely approximates the true displacement field. In order to obtain the additional parameters, let us superpose on the above expression for w (Eq. 3.A.3), another 5-term polynomial starting with the first power of ξ , i.e.

$$w = w^{(1)} + P_2 \quad (3.A.4)$$

where:

$$P_2 = l_1 \xi + l_2 \xi^2 + l_3 \xi^3 + l_4 \xi^4 + l_5 \xi^5 \quad (3.A.5)$$

This expression for w should also satisfy the foregoing four conditions. However, since $w^{(1)}$ satisfies them identically, the polynomial with coefficients l must satisfy homogeneous conditions, i.e.

$$\text{At } \xi = 0, \frac{d^2 P_2}{d\xi^2} = 0, \frac{d^3 P_2}{d\xi^3} = 0$$

$$\text{At } \xi = 1, P_2 = 0, \frac{d^2 P_2}{d\xi^2} = 0$$

This gives:

$$l_2 = 0, l_3 = 0, l_4 = -\frac{5}{2} l_1, l_5 = \frac{3}{2} l_1$$

so that the polynomial P_2 is

$$P_2 = l_1 \left(\xi - \frac{5}{2} \xi^4 + \frac{3}{2} \xi^5 \right)$$

and we can write

$$w^{(2)} = w^{(1)} + l_1 \left(\xi - \frac{5}{2} \xi^4 + \frac{3}{2} \xi^5 \right) \quad (3.A.6)$$

where l_1 is the second adjustable parameter, and the superscript on w indicates that it is the second approximation. A third approximation for w is obtained by assuming an expression of the form:

$$w^{(3)} = w^{(2)} + P_3$$

where:

$$P_3 = m_2 \xi^2 + m_3 \xi^3 + m_4 \xi^4 + m_5 \xi^5 + m_6 \xi^6$$

Proceeding as before, we have:

$$m_2 = m_3 = 0, \quad m_5 = -\frac{9}{5}m_4, \quad m_6 = \frac{4}{5}m_4$$

$$P_3 = m_4 \left(\xi^4 - \frac{9}{5} \xi^5 + \frac{4}{5} \xi^6 \right) \quad (3.A.7)$$

Equations (3.A.3), (3.A.6) and (3.A.7) give the required polynomial in three parameters k_0 , l_1 , and m_4 . These are redesignated as a_0 , a_1 and a_2 , respectively, in the main text (Eq. 3.11.20a).

It should be noted that this process of generating additional parameters can be continued *ad infinitum*. However, each relaxable parameter implies that the expression for w will be optimized with respect to it. Therefore, a compromise between the level of accuracy and quantity of algebra has to be made. For Waters, et al. the optimal number was three.

APPENDIX 3.B

SCHLEICHER FUNCTIONS

The Schleicher functions used in Section 3.13 are directly related to Ber and Bei functions [3.11.5]. In the interest of completeness, their series expansions are given below

$$\psi_1(x) = ber(x) = \sum_{k=0}^{\infty} (-1)^k \frac{z^{4k}}{[(2k)!]^2}$$

where $z = 0.5x$

$$\psi_2(x) = -bei(x) = \sum (-1)^{k+1} \frac{z^{4k+2}}{[(2k+1)!]^2}$$

$$\psi_3(x) = 0.5\psi_1(x) - \frac{2}{\pi} [R_1(x) + \psi_2(x) \cdot \ln \beta z]$$

where $\beta = 1.78108$ and

$$R_1(x) = \sum_{k=0}^{\infty} (-1)^k \frac{S'_{2k+1}}{[(2k+1)!]^2} \cdot z^{4k+2}$$

$$S'_n = \sum_{j=1}^n \frac{1}{j}$$

$$\psi_4(x) = 0.5\psi_2(x) + \frac{2}{\pi} [R_2(x) + \psi_1(x) \cdot \ln \beta z]$$

where

$$R_2 = \sum_{k=0}^{\infty} (-1)^k \frac{(2k+2)S'_{2k+2}}{[(2k+2)!]^2} z^{4k+3}$$

Finally the S -functions are defined as follows:

$$S_1(x) = x\psi_2(x) - 2\psi_1'(x)$$

$$S_2(x) = x\psi_1(x) + 2\psi_2'(x)$$

$$S_3(x) = x\psi_4(x) - 2\psi_3'(x)$$

$$S_4(x) = x\psi_3(x) + 2\psi_4'(x)$$

$$S_5(x) = x^2\psi_2'(x) - 4x\psi_2(x) + 8\psi_1'(x)$$

$$S_6(x) = x^2\psi_1'(x) - 4x\psi_1(x) - 8\psi_2'(x)$$

$$S_7(x) = x^2\psi_4'(x) - 4x\psi_4(x) + 8\psi_3'(x)$$

$$S_8(x) = x^2\psi_3'(x) - 4x\psi_3(x) - 8\psi_4'(x)$$

For small values of x , the series for Schleicher functions converge rapidly. For large values ($x \geq 6$), asymptotic approximations given in Ref. [3.11.3, p. 496] are sufficiently accurate.

4. TUBESHEET SANDWICHED BETWEEN TWO FLANGES

4.1 INTRODUCTION

Three element bolted joints consisting of an unstayed tubesheet, sandwiched between two tapered hub flanges, find extensive use in the heat exchanger and pressure vessel industries. For example, removable bundle U-tube heat exchangers, denoted as “BEU” in the lexicon of the heat exchanger trade [4.1.1] utilize this joint detail (Fig. 4.1.1). Figure 3.1.1 shows another application of this joint in a “pull through externally packed” construction. In view of its widespread use, we focus our attention on this joint in some depth and present a technique for performing a detailed stress analysis. The need to evolve a comprehensive solution for this class of joints is particularly important, since a standard application of the code design methods may produce grossly erroneous results for the low pressure side flange. The 1983 issue of the ASME Code [4.1.2] recognizes the quirks in the structural behavior of such joints, but offers no detailed solution.

The motivation for a comprehensive stress analysis stems from structural as well as heat transfer considerations. This can be explained by referring to the heat exchanger of Fig. 4.1.1. As shown in Fig. 4.1.2, a set of common studs provide the necessary compression load on the two gaskets. The non-colinearity of the bolt line and gasket compression load line on each flange causes the flanges to rotate (in the plane of the paper in Fig. 4.1.3). Thus, under the prestressed condition (denoted as the “seating condition” in reference [4.1.2]), the flanges are subject to some rotation as indicated in Fig. 4.1.3. The tubesheet may also experience a net axisymmetric moment if the shell and channel gasket circles are not colinear. When the two chambers are pressurized (operating condition), the bending moment on the flanges increases further, causing the flanges to rotate even more. If the tubeside pressure significantly exceeds the shellside pressure then the deflected tubesheet surface will be concave to the tubeside chamber. Such a situation is quite common in nuclear installations. For example, in the Pressurized Water Reactor system, the exchangers used to transfer heat between the reactor cooling water circuit and the component cooling water circuit are subject to large differential pressures, since these independent circuits operate in quite different pressure ranges.

The crevice formed between the pass partition plate and tubesheet surface due to “cupping” of the tubesheet and inadequate spring-back of the pass

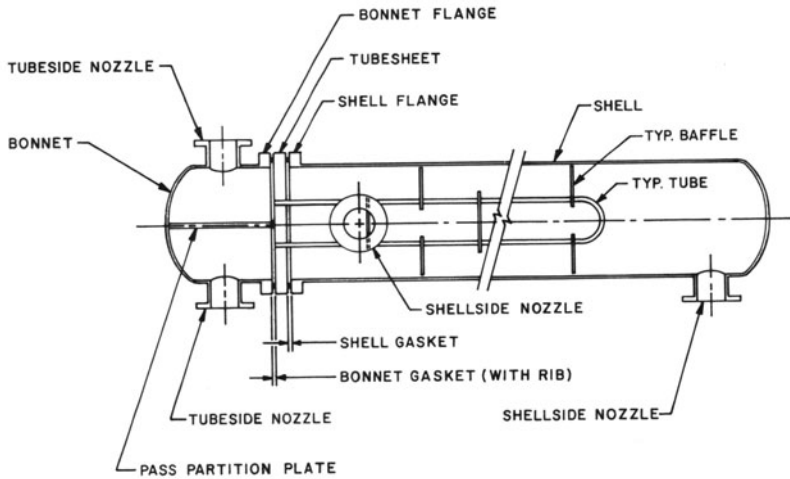


Fig. 4.1.1. Two tube pass removable bonnet heat exchangers.

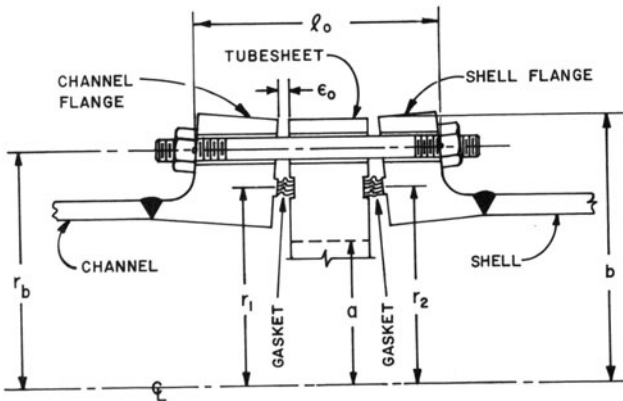


Fig. 4.1.2. Bolted joint under seating condition.

partition rib is quite small. However, the associated leakage stream (Fig. 4.1.3) can become significant in exchangers with high interpass pressure drops and multiple tube passes. This tubeside leakage stream is the counterpart of shellside baffle-to-shell bypass stream, designated as the E-stream by Tinker [4.1.3]. In addition in lowering the tubeside film coefficient, it also reduces the effective “Log Mean Temperature Difference (LMTD)”, thus derating the overall heat duty. The tubeside leakage stream is considered to be a veritable nuisance in those process applications where the in-exchanger tubeside fluid temperature is sought to be closely regulated. When a considerable leakage stream is present, the downstream gages are not really monitoring tubeside temperature since a portion of the flow has bypassed the tubes. Therefore, these downstream gages cannot be used to

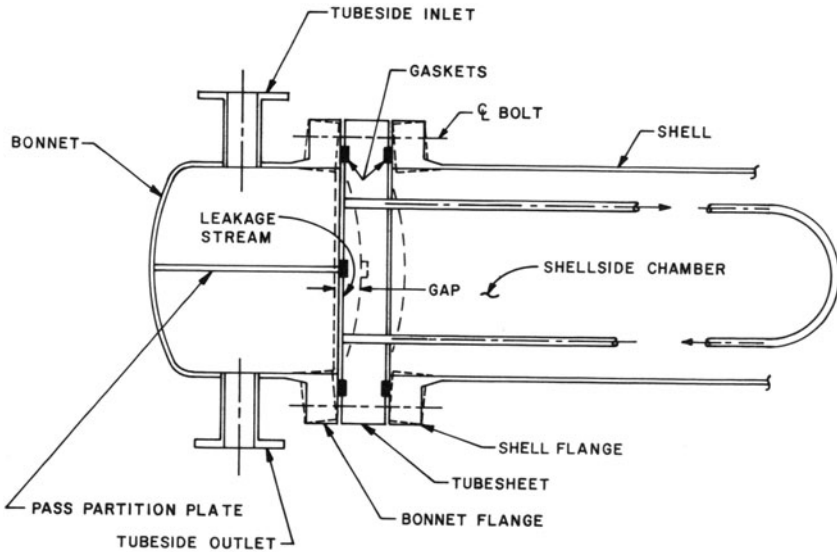
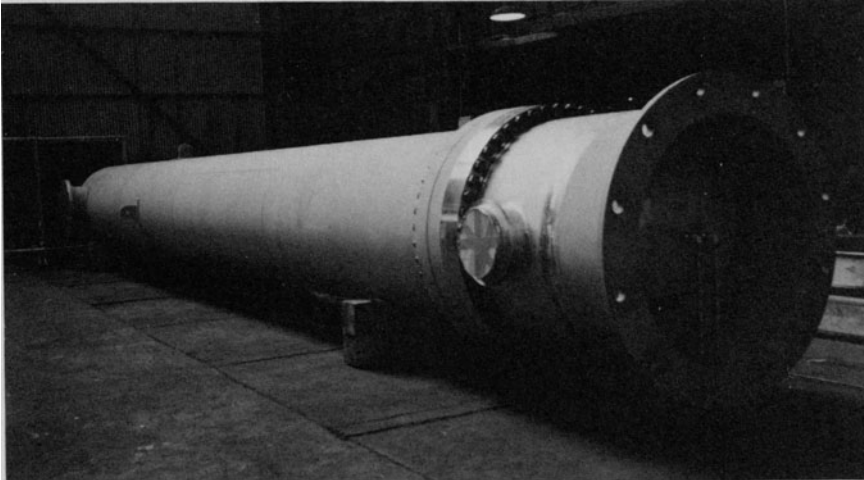


Fig. 4.1.3. Tubeside leakage mechanism in a bolted tubesheet joint.



Photograph 4.a. U-tube heat exchanger with two flanges sandwiching a tubesheet

reliably determine the tubeside temperature profile inside the heat exchanger. Furthermore, with the rapid recent advances in the quality of the correlations for the shellside film coefficient [4.1.4–5], previously unimportant imprecisions in tubeside heat transfer coefficient predictions are beginning to acquire added significance. Heuristic reasoning suggests that providing metal-to-metal contact at the outer edge between the bonnet

flange and the tubesheet would produce a counteracting moment on the tubesheet which would reduce its lateral deflection and, therefore, decrease the area available for the tubeside leakage stream. Metal-to-metal contact at the outer edge may be effected during the seating condition by suitably machining the flange faces so that contact occurs prior to reaching the specified bolt pre-stress. If contact is desired during pressurization, then a certain edge gap, ϵ_0 , may be prescribed under the seating condition (Fig. 4.1.2) which diminishes to zero and further develops an edge contact load as the internal joint pressure is applied. This latter case as will be referred to as a “controlled” MTM (metal-to-metal contact) condition.

The analysis to be presented here can be readily utilized for determining the “maximum allowable working pressure” for tubeside and shellside chambers. The “maximum allowable working pressure” is the highest pressure that all pressure parts in a pressure chamber can withstand without exceeding the relevant ASME Code stress limits.

The foregoing statements suggest the need for a convenient analysis tool which would enable rapid evaluation of the effect of flange/tubesheet facing detail, gasket material, available bolt pull, flange geometry (thickness, shape of hub, etc.), tubesheet thickness, etc., on the stress levels in the elements of the joint, and on the size of the inter-pass leakage area. The computer program that will be developed to meet the above goals should also permit analysis of more specialized joints such as flange-to-flange, flange-to-flat cover, etc. These design objectives are achieved by the solution procedure described in this chapter.

The solution procedure developed herein enables the study of the effect of variation of design variables (flange and tubesheet geometric details, bolt pre-stress, etc.), on the following principal quantities of interest:

- i. Change in bolt tensile stress due to joint pressurization
- ii. Residual bonnet and shell gasket surface pressures (ring gaskets only)
- iii. Maximum tubesheet stress
- iv. Bonnet flange hub and ring bending stresses
- v. Shell flange hub and ring bending stresses
- vi. Leakage area

Structural relations to characterize the behavior of tube sheet and flange type members are first outlined, and the solution procedure to determine their interaction is described. A typical numerical example is then utilized to demonstrate the usefulness and limitations of the “controlled MTM” concept. The computer program “TRIEL” based on this method is also presented.

Study of a typical “three element joint” presented in this chapter reveals some aspects of the joint behavior which are not apparent from a direct application of code rules. The most recent edition of the ASME Code [4.1.2, p. 412] recognizes the hidden peculiarities of the structural behavior of the “three element joint”.

As stated before, although the analysis described in this chapter focuses on the three element joint, solution for other cases, such as two bolted up flanges, or a flange bolted to a flat cover, can be obtained using TRIEL. The procedure for solving such specialization of the general solution is explained in Sections 4.8 and 12.8.

4.2 THE STRUCTURAL MODEL

Figure 4.1.2 shows the structural model of the bolted joint. The tubesheet is sandwiched between two flanges, which are henceforth referred to as the “Channel (Bonnet) Flange”, and “Shell Flange”, respectively. The bolts pass through clearance holes in the tubesheet. We assume that there are n bolts, each of root area A_b , prestressed to a certain known stress level, σ_0 . It is further assumed that the channel flange bears against the gasket on the tubesheet groove, and it may have an initial edge gap ϵ_0 under the “seating condition”,* or it may develop an edge contact load F_e . The edge gap ϵ_0 or edge contact load F_e are design options which can be easily adjusted in a joint assembly by properly machining the flange/tubesheet surface. The shell flange, however, is assumed to bear totally against the gasket, i.e., it does not make metal-to-metal contact during either the seating or the pressurized stage of joint loading.

The model is equally valid for the case where the shellside design pressure exceeds the tubeside pressure, and the designer seeks to evaluate the effect of “controlled metal-to-metal” contact in the shellside of the joint. The analysis is fully applicable once the terms “shellside” and “tubeside” are interchanged.

The formulation presented here assumes the contact load to be exerted at the outer edge (radius b). The case of a “land” at a radius, r_L , to produce controlled metal-to-metal contact (at radius r_L) can also be treated using this formulation by merely replacing the quantity b associated with F_e by r_L throughout the analysis. The effect of varying r_L is treated in Section 3.14. We fix r_L (equal to b) in the present analysis to reduce the number of parameters. This will help maintain our focus on the variables mentioned in the foregoing.

In Chapter 5, a parallel analysis of this problem is developed which treats gaskets of arbitrarily non-linear loading/unloading curves, and finite widths. The behavior of a joint containing full face gaskets and gaskets with controlled “MTM” can be studied by following the joint response to incremental increase (or decrease) of pressure. This time step analysis, however, is considerably more computation intensive than the one presented in this chapter.

As noted in Section 3.5, the mathematical model for the gasket presents the greatest problem. A typical spiral wound gasket possesses highly non-

*Used in Ref. [4.1.2] to indicate the condition of bolt prestress.

linear and non-conservative loading, unloading and reloading characteristics [4.2.1]. Furthermore, the minimum surface pressure on the gasket to maintain a leak-tight joint depends on a host of parameters, such as surface finish, groove clearance, gasket strip material, filler material, loading history, etc. Strictly speaking, if the stress-strain relationship of the gasket is known, then the “exact” pressure distribution on the gasket can be determined as a function of the rotation of the mating surfaces. Since the rotation of the mating flanges themselves will depend on the gasket surface pressure distribution, an iterative or incremental solution will have to be devised. Assuming that the gasket is narrow in the radial direction, we borrow the assumption of the ASME Code [4.1.3] that the gasket pressure resultant acts at the “effective gasket diameter”, irrespective of the flange rotations. However, the loading and unloading stiffnesses are allowed to be an arbitrary (known) function of the compression and decompression history. The case where the gasket is relatively wide, so that the gasket resultant force moves during the joint loading, is treated in the next chapter.

4.3 TUBESHEET

The tubesheet contains a perforated interior in which the tube holes are arranged in a geometric pattern on a specified pitch, P . Following the ASME Code [4.1.2], we define the outer radius a of the perforated interior as:

$$a = r_{\max} + \frac{P - h_p}{4} \quad (4.3.1)$$

where r_{\max} is the radius of the outermost tube center, and h_p is the ligament width. The ligament efficiency, η , of the perforations is defined as:

$$\eta = \frac{h_p}{P} \quad (4.3.2)$$

We note here that h_p may or may not incorporate some of the tube wall. We discuss the concept of effective ligament width further in the chapters dealing specifically with tubesheet design (Chapters 8 through 11).

It is well known [4.3.1, 2, 3] that the perforated region may be idealized as a homogeneous, isotropic plate with modified elastic constants. The modified elastic constants are given as function of η and the elastic constants of the plate material for any given tube layout pattern. Thus, the tubesheet is modeled as a composite plate consisting of two concentric circular plates bonded at the interface radius a . The inner plate is the perforated region, while the outer annular plate is the “untubed rim” which is loaded by pressure and gasket loads.

The following major assumptions are made to simplify modeling and analysis of the tubesheet:

- i. The resistance offered to the bending of the tubesheet by the tubes

due to their restraint at the baffle location is neglected. Gardner [4.3.4] has considered this effect and delineated its significance in practical design applications.

- ii. The strengthening effect of the pass partition lanes in the tubesheet is neglected.
- iii. The weakening effect of the bolt holes in the tubesheet is neglected.

A complete analysis of tubesheets for U-tube heat exchangers is found in Chapter 8. The discussion presented in this section, however, suffices for analyzing a “three element joint” in U-tube heat exchangers. We begin by treating the outer plate as an elastic ring. In Fig. 4.3.1, F_1 and F_2 denote the tubeside and shellside gasket reaction resultants, respectively. F_e denotes the potential edge contact load between the channel flange and the

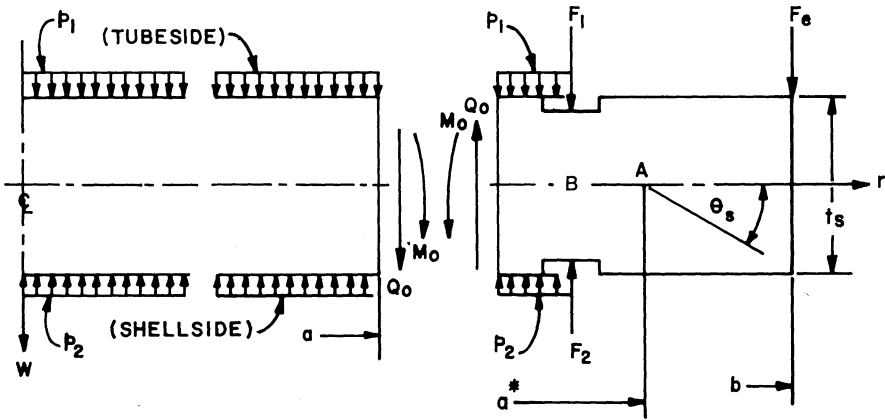


Fig. 4.3.1. Freebody of the tubesheet.

tubesheet. p_1 and p_2 are tubeside and shellside pressures, assumed to act up to radii r_1 and r_2 , respectively, where r_1 and r_2 are the effective gasket radii. The mean radius of the rim (point A in Fig. 4.3.1) is given by:

$$a^* = 0.5(a + b) \tag{4.3.3}$$

and the width of the ring h is given by:

$$h = (b - a) \tag{4.3.4}$$

Let the pressure difference across the tubesheet be defined as p ;

$$p = p_1 - p_2 \tag{4.3.5}$$

Then the shear force Q_0 at the rim-perforated plate interface follows from equilibrium:

$$Q_0 = -\frac{pa}{2} \tag{4.3.6}$$

Furthermore, the net ring moment about point A (positive if clockwise in the plane of the paper) is given by:

$$M = \frac{M_1 a}{a^*} + \frac{Q_0 h}{2a^*} - F_1(a^* - r_1) \frac{r_1}{a^*} + F_e(b - a^*) \frac{b}{a^*} \\ - \frac{p_1(r_1^2 - a^2)(2a^* - r_1 - a)}{4a^*} + F_2(a^* - r_2) \\ + \frac{p_2(r_2^2 - a^2)(2a^* - r_2 - a)}{4a^*} \quad (4.3.7)$$

Thus

$$a^* M = -(M_0 + \chi)a \quad (4.3.8)$$

where:

$$a\chi = -\frac{pa^2 h}{4} + F_1(a^* - r_1)r_1 - F_2(a^* - r_2)r_2 - F_e(b - a^*)b \\ + \frac{p_1(r_1^2 - a^2)(2a^* - r_1 - a)}{4} - \frac{p_2(r_2^2 - a^2)(2a^* - r_2 - a)}{4} \quad (4.3.9)$$

The rotation of the rim, θ_s , due to M , follows from elementary strength-of-materials theory [see Section 3.9]:

$$\theta_s = \frac{-12a^* a (M_0 + \chi)}{E_2 h t_s^3} \quad (4.3.10)$$

Next we set up the governing equations for the perforated interior modeled as an equivalent solid plate in the manner described before. The governing differential equation for axisymmetric deflection of circular plates is well known* [4.3.4]:

$$\left(\frac{d^2}{dr^2} + \frac{1}{r} \frac{d}{dr}\right) \left(\frac{d^2}{dr^2} + \frac{1}{r} \frac{d}{dr}\right) w = \frac{p}{D_1} \quad (4.3.11)$$

where the plate flexural rigidity is defined as:

$$D_1 = \frac{E_1 t_s^3}{12(1 - \nu_1^2)} \quad (4.3.12)$$

with E_1 , ν_1 representing the modified elastic constants.

The general solution of Eq. (4.3.11) is shown in Appendix A at the end of the text to be

$$w = \gamma_1 + \gamma_2 r^2 + \gamma_3 \ln r + \gamma_4 r^2 \ln r + \frac{pr^4}{64D_1} \quad (4.3.13)$$

*The circular plate equations utilized in this section have been derived from first principles in Appendix A.

where γ_i ($i = 1, 4$) are arbitrary constants of integration. For a solid plate (no hole in the center), finiteness of deflection and slope yield $\gamma_3 = \gamma_4 = 0$. γ_1 and γ_2 are determined by the boundary conditions. By appealing to continuity of slope, and traction (radial moment) at $r = a$, and performing the necessary algebra, the following results are derived:

$$\gamma_2 = \frac{-6a^*a(M_0 + \chi)}{E_2 h a_s^3} - \frac{pa^2}{32D_1} \quad (4.3.14)$$

$$M_0 = \frac{-1}{1 + \rho} \left(\rho \chi - \frac{pa^2}{8} \right) \quad (4.3.15)$$

where:

$$\rho = \frac{12a^*aD_1(1 + \nu_1)}{E_2 h a_s^3} \quad (4.3.16)$$

The details of matching conditions of slope and moment at $r=a$ are discussed fully in Chapter 8 where we deal specifically with the tubesheet analysis.

From Eq. (4.3.13), the deflection of the inside edge of the rim is

$$w_a = \gamma_1 + \gamma_2 a^2 + \frac{pa^4}{64D_1}$$

Therefore, the deflection of the tubesheet with respect to the inside edge of the rim is given by:

$$w^* = \gamma_2(r^2 - a^2) + \frac{P}{64D_1}(r^4 - a^4) \quad (4.3.17)$$

Similarly, the deflection of point B ($r=r_1$) with respect to the inside edge of the rim is $\theta_s(r_1 - a)$.

Thus, the deflection of the tubesheet at a radius r with respect to point B ($r = r_1$) is given by:

$$\begin{aligned} w &= -(r_1 - a)\theta_s + w^* & r \leq a \\ &= -(r_1 - r)\theta_s & r \geq a \end{aligned} \quad (4.3.18)$$

The radial bending moment M_r is given by:

$$\begin{aligned} M_r &= 2\gamma_2 D_1(1 + \nu_1) + \frac{(3 + \nu_1)pr^2}{16}; & r \leq a & \quad (a) \\ & & & \\ M_\theta &= 2\gamma_2 D_1(1 + \nu_1) + \frac{(1 + 3\nu_1)pr^2}{16}; & r \leq a & \quad (b) \end{aligned} \quad (4.3.19)$$

The maximum bending stress in the perforated plate, averaged across the ligament width, is given by [4.1.2]:

$$\sigma_t = \frac{k' 6M}{\eta t_s^2} \quad (4.3.20)$$

where k' is the “stress multiplier” given in Ref. [4.1.2] as a function of the radial to tangential stress ratio and M is the larger of the radial and circumferential bending moments.

4.4 FLANGE

The stress analysis method described in Section 3.13 is utilized to model shell and channel flanges. It was shown that the stress and displacement fields in a flange are completely described for given external moment M_{ext} and pressure p . To start, generic variables will be used without subscripts in this section. In later sections, wherever a distinction is necessary, subscripts 1 and 2 are appended to the variables to indicate the quantities pertaining to the channel and shell flanges, respectively. As noted previously, we assume that the shellside of the unit is the lower pressure side.

For a given bolt load B' per unit circumference, force equilibrium yields (Fig. 4.4.1):

$$r_b B' - b F_e - r F - \frac{p r^2}{2} = 0 \quad (4.4.1)$$

We assume that the edge contact load F_e is zero for the flange on the lower pressure side (shellside). The external moment on the flange ring M_{ext} (Eq. 3.13.8), per unit circumferential length at the bolt circle radius, is given by

$$M_{\text{ext}} = \frac{-F_e b (b - r_b)}{r_b} + \frac{F r}{r_b} (r_b - r) + \frac{p a'^2 d}{2 r_b} + \frac{p (r^2 - a'^2) (2 r_b - r - a')}{4 r_b} \quad (4.4.2)$$

Thus, if the bolt load B' , the edge contact load F_e , and the pressure p are specified, then the gasket linear pressure F follows from Eq. (4.4.1) and the external ring moment M_{ext} from Eq. (4.4.2). The solution procedure of Section 3.13 can then be used to evaluate the stress and displacement fields in the flange.

4.5 METHOD OF SOLUTION

The physical dimensions of the bolted joint and its elements are assumed to be known. The bolts, n in number of root area A_b each, are assumed to be pre-stressed to a desired value σ_0 . The object is to determine the service bolt stress σ , maximum hub and ring stresses in the bonnet and shell flanges, maximum stress in the tubesheet, and finally, the leakage areas formed by the deflection of the tubesheet and the bonnet flange when the channel and

shell chambers are subjected to pressures p_1 and p_2 , respectively. Within the framework of the available data, two design parameters can be varied; namely the pre-stress σ_0 , and the “initial edge gap” ϵ_0 , between the outer edges of the bonnet flange and the tubesheet, under the seating condition. ϵ_0 can be varied by properly machining the faces of the bonnet flange and/or the tubesheet beyond the gasket seating surface. The influence of these parameters on the aforementioned quantities of interest can now be examined.

The force equilibrium Eq. (4.4.1) for the bonnet flange during seating yields the lineal gasket force F_1^0 on the bonnet gasket*:

$$F_1^0 = \frac{n\sigma_0 A_b}{2\pi r_1} - \frac{bF_e^0}{r_1} \tag{4.5.1}$$

F_e^0 is the initial edge contact force per unit circumference. Note $F_e^0 = 0$ if the initial gap $\epsilon_0 > 0$. Equation (4.5.1) determines the lineal force on the bonnet gasket. The lineal compression force F_2^0 on the shell gasket follows from force equilibrium:

$$F_2^0 = \frac{n\sigma_0 A_b}{2\pi r_2} \tag{4.5.2}$$

The corresponding gasket compressed thicknesses under F_1^0 and F_2^0 are denoted by δ_1^0 and δ_2^0 , respectively.

Using the method described in Sections 3.13 and 4.3, the rotations of the bonnet flange θ_1^0 , shell flange θ_2^0 , and tubesheet θ_s can be determined (positive values of θ_1^0 , θ_2^0 imply a movement of the outer edge of the respective flange towards the tubesheet ring):

$$\begin{aligned} \theta_1^0 &= \xi_1(F_1^0, \sigma_0, F_e^0) \\ \theta_2^0 &= \xi_2(F_2^0, \sigma_0) \\ \theta_s^0 &= \xi_s(F_1^0, F_2^0, F_e^0) \end{aligned} \tag{4.5.3}$$

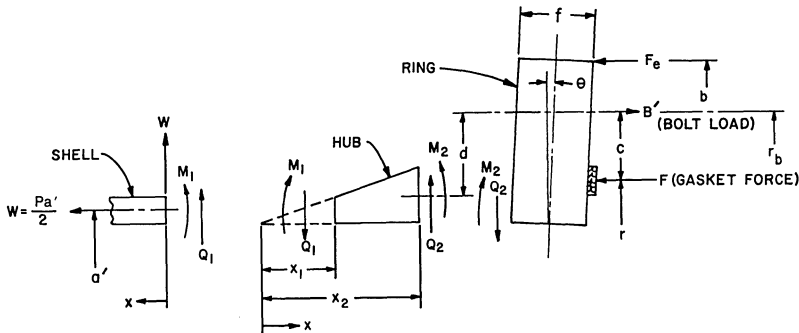


Fig. 4.4.1. Flange stress analysis model.

*Recall that we attach subscripts 1 and 2 wherever necessary to distinguish between the channel and the shellside of the unit.

The superscript “0” is appended to the quantities to indicate that these pertain to the seating condition. Thus the effective bolt length under the prestress condition l_0 (Fig. 4.1.2) is given by:

$$l_0 = s + f_1 \sec \theta_1^0 + f_2 \sec \theta_2^0 + t_s \sec \theta_s^0 - (r_b - r_1) \sin \theta_1^0 - (r_b - r_2) \sin \theta_2^0 + (r_2 - r_1) \sin \theta_s^0 + \delta_1^0 + \delta_2^0 \quad (4.5.4)$$

For small values of θ_1^0 , θ_2^0 and θ_s^0 , Eq. (4.5.4) can be further simplified:

$$l_0 = s + f_1 + f_2 + t_s + \delta_1^0 + \delta_2^0 - (r_b - r_1) \theta_1^0 + (r_2 - r_1) \theta_s^0 - (r_b - r_2) \theta_2^0 \quad (4.5.5)$$

where the term s represents the total effect of any difference between the joint thickness at the bolt center line and at the gasket locations.

Equation (4.5.5) defines the quantity l_0 . We further note that the initial edge gap ϵ_0 is given by:

$$\epsilon_0 = s_1 + \delta_1^0 - (b - r_1)(\theta_1^0 - \theta_s^0) \quad (4.5.6)$$

where s_1 represents the term due to the face machining of the mating elements. As stated before, ϵ_0 can be set equal to a small positive quantity (by adjusting s_1). Further, ϵ_0 can be zero, and an initial edge contact load F_e^0 may be developed on the channel flange-tubesheet outer edge. In short, the initial condition at the outer edge can be suitably prescribed. The object now is to investigate the behavior of the flanged joint and its constituent elements when the two chambers are pressurized. If σ and F_e denote the “correct” bolt stress and edge load, respectively, under this condition, then the channel gasket residual lineal force F_1 follows from force equilibrium (Eq. 4.4.1):

$$F_1 = \frac{n\sigma A_b}{2\pi r_1} - \frac{bF_e}{r_1} - \frac{p_1 r_1}{2} \quad (4.5.7)$$

Similarly, the residual lineal force F_2 on the shell gasket is given by:

$$F_2 = \frac{n\sigma A_b}{2\pi r_2} - \frac{p_2 r_2}{2} \quad (4.5.8)$$

Let δ_1 and δ_2 denote the channel and shell gasket thicknesses corresponding to F_1 and F_2 , respectively. The magnitudes of δ_1 and δ_2 depend on the gasket stiffness characteristics, as described in Chapter 3.

The solution procedure to determine σ and F_e , and other field quantities of interest consists of two major steps which may be stated as follows:

Step I: It is assumed a priori that there is no edge contact under the pressurized condition; i.e., $\epsilon_1 > 0$, and $F_e = 0$. The appropriate bolt stress σ , under this assumption, is calculated as follows:

- (a) Assume a value of σ and evaluate F_1 and F_2 using Eqs. (4.5.7) and

(4.5.8), respectively ($F_e = 0$ in Eq. (4.5.7)). We note that in the first step, $\sigma = \sigma_0$ is a natural choice.

- (b) Compute the bonnet flange ring rotation θ_1 , shell flange ring rotation θ_2 , and tubesheet rotation θ_s by computing the appropriate net ring moment and using relations between ring rotation and net ring moment:

$$\begin{aligned}\theta_1 &= \xi_1(F_1, \sigma, F_e) \\ \theta_2 &= \xi_2(F_2, \sigma) \\ \theta_s &= \xi_s(F_1, F_2)\end{aligned}\quad (4.5.9)$$

For example, θ_s follows from Eqs. (4.3.10), (4.3.9), (4.3.15), and (4.3.16).

- (c) Evaluate δ_1 and δ_2 , corresponding to F_1 and F_2 , using the gasket loading-unloading diagram.
 (d) The “effective length of the joint” l under this assumed condition is given by Eq. (4.5.5):

$$l = s + f_1 + f_2 + t_s + \delta_1 + \delta_2 - (r_b - r_1)\theta_1 + (r_2 - r_1)\theta_s - (r_b - r_2)\theta_2 \quad (4.5.10)$$

The “length of the joint” is defined as the distance between the back ends of the two flanges at the bolt circle radius.

- (e) Next, assume another value of σ (close to the value assumed in (a)), say σ' ; and, following the steps (a) through (d), compute the corresponding bolt length l' .
 (f) The “joint stiffness” K is then defined as:

$$K = \frac{\sigma - \sigma'}{l - l'} \quad (4.5.11)$$

- (g) The correct bolt stress is one for which the “joint length” and “bolt length” are equal. Let $(l_0 + \lambda)$ denote the correct value of bolt and joint lengths. The corresponding bolt stress is

$$\sigma_c = \sigma_0 + \lambda K_b$$

Since bolt stress σ corresponds to joint length l , the bolt stress corresponding to $l_0 + \lambda$ is

$$\sigma_c' = (l_0 + \lambda - l)K + \sigma$$

σ_c' must equal σ_c for convergence. Hence $\sigma_0 + \lambda K_b = \sigma + K(l_0 + \lambda - l)$

or

$$\lambda = \frac{K(l_0 - l) + \sigma - \sigma_0}{K_b - K} \quad (4.5.12)$$

where the bolt stiffness K_b is defined by:

$$K_b = \frac{E_b}{l_0} \tag{4.5.13}$$

Thus the corrected bolt stress, σ_c is given by:

$$\sigma_c = \sigma_0 + K_b \lambda \tag{4.5.14}$$

If the gaskets behave as (or are modeled as) linear springs, then Eq. (4.5.14) gives the correct bolt stress. If, however, the gasket load-deflection relationship is non-linear, then further iteration is necessary. In the latter case, σ is set equal to σ_c in step (a) above, and the procedure is repeated. Convergence is obtained when the assumed bolt stress σ (step a) equals the corrected stress σ_c (step g) within a prescribed tolerance.

We can describe qualitatively our procedure by referring to Fig. 4.5.1 which shows bolt stress σ plotted against joint length l and bolt length l_b . As σ increases, the joint length l decreases, while the bolt length l_b increases (linearly). The procedure in Step I simply provides a quantitative approach to finding the intersection of the two curves.

Having determined the correct bolt stress, σ , the remaining quantities of interest, such as θ_1 , θ_2 and θ_s follow from the ring rotation equations which are given symbolically in Eq. (4.5.9).

The edge gap ϵ_1 under the service condition can now be determined by writing

$$\epsilon_1 = \epsilon_0 + \delta_1 - \delta_1^0 - (b - r_1)(\theta_1 - \theta_s - \theta_1^0 + \theta_s^0) \tag{4.5.15}$$

where Eq. (4.5.6) determines ϵ_0 .

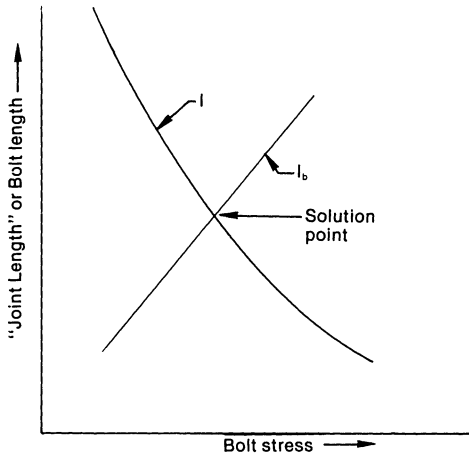


Fig. 4.5.1. Variation of bolt length and joint length with bolt stress.

If $\epsilon_1 > 0$ then the assumption for zero edge load made in the beginning is verified, and the results obtained above from Step I are established to be correct. However, if $\epsilon_1 < 0$, then the edge force F_e and corresponding bolt

stress σ have to be determined to satisfy the edge condition of zero penetration (i.e., $\epsilon_1 = 0$). The method to obtain this is described in Step II.

Step II: As determined above, the bolt stress σ may correspond to a negative edge gap ϵ_1 . We imagine now that the edge gap ϵ_1 is an implicit function of σ and F_e and that we will change the negative edge gap ϵ_1 by “adding” an increment $\Delta\epsilon_1$ obtained by a change in σ and F_e . Therefore, it (ϵ_1) is written symbolically as

$$\epsilon_1 = \beta_1(\sigma, F_e) \quad (4.5.16)$$

then

$$\epsilon_1 + \Delta\epsilon_1 = \epsilon_1 + \left. \frac{\partial\beta_1}{\partial\sigma} \right|_{\sigma} \Delta\sigma + \left. \frac{\partial\beta_1}{\partial F_e} \right|_{F_e=0} \Delta F_e \quad (4.5.17)$$

Since we wish to determine $\Delta\sigma$, ΔF_e to enforce the requirement that $\epsilon_1 + \Delta\epsilon_1 = 0$, then the incremental changes must satisfy the equation

$$\left. \frac{\partial\beta_1}{\partial\sigma} \right|_{\sigma} \Delta\sigma + \left. \frac{\partial\beta_1}{\partial F_e} \right|_{F_e=0} \Delta F_e = -\epsilon_1 \quad (4.5.18)$$

Similarly, the “joint length” l is an implicit function of σ and F_e (via Eqs. (4.5.9) and (4.5.10)). Hence:

$$l = \beta_2(\sigma, F_e) \quad (4.5.19)$$

The bolt length l_b corresponding to bolt stress σ is

$$l_b = \frac{(\sigma - \sigma_0)l_0}{E_b} + l_0 \quad (4.5.20)$$

Hence:

$$\tau = l - l_b = \beta_2(\sigma, F_e) - l_0 - \frac{(\sigma - \sigma_0)l_0}{E_b} \quad (4.5.21)$$

At the solution point, the joint length must equal the bolt length; i.e., $\tau = 0$.

Thus the increments in σ and F_e required to make τ zero must satisfy the equation:

$$-\tau = \left(\frac{\partial\beta_2}{\partial\sigma} - \frac{l_0}{E_b} \right) \Delta\sigma + \left. \frac{\partial\beta_2}{\partial F_e} \right|_{F_e=0} \Delta F_e \quad (4.5.22)$$

Equations (4.5.18) and (4.5.22) are solved for $\Delta\sigma$ and ΔF_e . Then the corrected value of σ and F_e are:

$$\sigma_c = \sigma + \Delta\sigma \quad (4.5.23)$$

$$F_e = \Delta F_e$$

If ϵ_1 and τ are zero (within a specified tolerance) corresponding to the

corrected values of bolt stress and edge load, then convergence is achieved. Otherwise, this process is repeated, until convergence is obtained. The rate of convergence depends on the non-linearity of the gasket stress-strain curve.

4.6 LEAKAGE AREA

The gasket ribs compressed by the pass partition plates relax when the tubesheet and the channel flange undergo additional rotations due to the effect of pressure loadings. The ribs, however, possess limited resilience, usually in the order of a few thousandths of an inch. If the channel pressure is sufficiently greater than the shellside pressure, then as stated before, a narrow gap between the pass partition plate and the gasket surface may be formed. The mathematical expressions to evaluate the leakage area and magnitude of the associated leakage stream are formulated in the following. We assume that the flange rotations and the tubesheet displacement have been determined for the seating condition and for the service condition.

It can be readily verified from Fig. 4.6.1 that the rib thickness under the seating condition at radius r is given by:

$$\begin{aligned} \Delta^0(r) &= \delta_1^0 + w^0(r) + (r_1 - r)\theta_1^0; \quad r \geq a'_1 - 0.5t_1 \\ &= \delta_1^0 + w^0(r) + (r_1 - a'_1 + 0.5t_1)\theta_1^0; \quad r \leq a'_1 - 0.5t_1 \end{aligned} \quad (4.6.1)$$

where $w^0(r)$ is the tubesheet deflection with respect to the gasket at $r=r_1$, and θ_1^0 is the rotation of the channel flange. These quantities are defined by

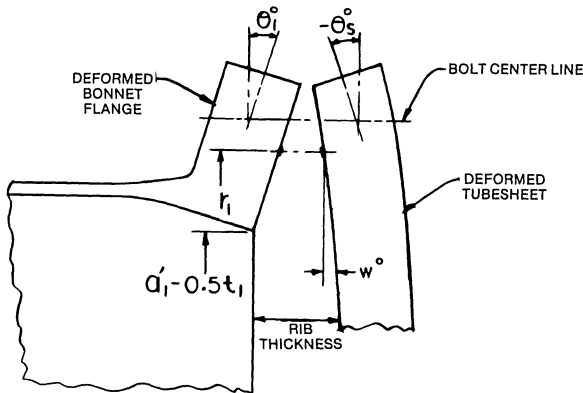


Fig. 4.6.1. Rib thickness under seating condition.

Eqs. (4.3.18) and (4.5.3), respectively. It is to be noted that the superscript "0" is appended to indicate that all these quantities are evaluated for the seating condition. The distance of the pass partition plate from the gasket rib seating surface, $\Delta(r)$ under the operating condition is also represented

by Eq. (4.6.1) with the superscript “0” deleted. Thus the net gap ζ at radius r is given by:

$$\begin{aligned}\zeta(r) &= \Delta(r) - \Delta^0(r) - \phi(r), \text{ if } \zeta > 0 \\ &= 0 \quad \quad \quad \text{if } \zeta < 0\end{aligned}\quad (4.6.2)$$

where $\phi(r)$ is the rib “spring back” at radius r . We note that ϕ is usually a rather complex, and often unknown, function of Δ^0 , rib width, filler material, etc.

Having established the gap width ζ as a function of r , the net gap area, A_L , under any pass partition plate is given by direct integration. Simpson’s formula for numerical quadrature [4.6.1] is found to yield quite accurate results with relatively few (11 to 21) nodal points.

Once the leakage area A_L is determined, the leakage rate Q_L is given by:

$$Q_L = V_L A_L' \quad (4.6.3)$$

where V_L is the bulk leakage velocity. V_L depends on the pressure drop across the gap, the shape of the flow constriction, etc. Its magnitude can be estimated as follows.

The total pressure drop across the pass partition lane may be viewed as consisting of three components, namely: (i) friction loss; (ii) contraction loss; and (iii) expansion loss. Thus;

$$\frac{\Delta P}{\rho} = \left[\frac{4f_F L}{D} + K_c + K_e \right] \frac{V_L^2}{2g} \quad (4.6.4)$$

where ρ is the density of the fluid, D is the characteristic gap dimension (maximum width) and L is the length of the constriction. For a tubesheet without pass partition grooves, L is equal to the pass partition plate thickness. f_F denotes the friction factor. Recognizing that the ratio of the constriction flow area to the channel flow area will be a very small quantity, the values of K_e and K_c can be defined by simple expressions. Kays [4.6.2] has shown that for high Reynolds number and for very small area ratio, the coefficient K_e approaches unity regardless of the shape of the gap. K_c may be approximately defined as:

$$K_c = \frac{1 - 2C_c + C_c^2(2K_d - 1)}{C_c^2} \quad (4.6.5)$$

where, for small area ratios, the jet area ratio C_c is equal to 0.6. Substituting for C_c in Eq. (4.6.5) yields:

$$K_c = 2K_d - 1.56 \quad (4.6.6)$$

The momentum distribution coefficient K_d is defined by a semi-empirical relationship [4.5.2] in terms of the friction factor f_F ; the relation is

$$K_d = 0.75(4f_F) + 0.024(4f_F)^{0.5} + 1 \quad (4.6.7)$$

Substituting for K_d in Eq. (4.6.6) yields for K_c , the result

$$K_c = 0.44 + 1.5(4f_F) + 0.048(4f_F)^{0.5} \quad (4.6.8)$$

Finally, the friction factor f may be estimated by the expression

$$f_F = 0.049\text{Re}^{-0.2} \quad (4.6.9)$$

where Re is the Reynolds number associated with the leakage stream. We note that since f_F and K_e in Eq. (4.6.4) depend on the flow velocity via the Reynolds number, the computation of V_L requires a trial-and-error procedure.

4.7 TWO EXAMPLE PROBLEMS

The aforementioned design procedure has been computerized for efficient design computation. The program is discussed in Section 4.8. Here we show application of the method to two joint configurations.

4.7.1 Classical Three Element Joint

Consider a typical two-pass U-tube heat exchanger designed in accordance with conventional codes. The flanges, shell and channel are designed using the ASME Code Method (Section 3.11) and the tubesheet is designed in accordance with the TEMA standards [4.1.1]. The following design data is relevant to the analysis (refer to Figs. 4.3.1, 4.4.1, to the necessary design equations in the previous sections, and to the nomenclature at the end of the chapter):

- (a) Channel flange: SA182-F304 material, $a_1' = 22.81''$, $\alpha_1 = 0.2$, $x_1 = 4.38''$, $x_2 = 5.63''$, $f_1 = 6''$, $b_1' = 4.13''$, $d_1 = 2.3125''$, $b = 26.5''$, $E_1' = 30 \times 10^6$ psi, $\nu_1' = 0.3$, $c_1 = 1.33''$, $t_1 = 0.88''$, $r_1 = 23.92''$. We note that this flange was used for illustration of the ASME Code Method in Section 3.11.
- (b) Shell flange: SA105 material, $a_2' = 22.81''$, $\alpha_2 = 0.22$, $x_1 = 1.69''$, $x_2 = 2.81''$, $f_2 = 4.75''$, $b_2' = 3.88''$, $d_2 = 2.3125''$, $E_2' = 30 \times 10^6$ psi, $\nu_2' = 0.3$, $c_2 = 1.33''$, $t_2 = 0.375''$, $r_2 = 23.92''$.
- (c) Bolts: $n = 52$, $A_b = 0.929$ sq. in., $r_b = 25.25''$. The bolt seating stress σ_0 is taken equal to 35,000 psi. Bolt material Young's modulus is 30×10^6 psi.
- (d) Tubesheet: SA515-Gr70, $a = 22.3''$, $E_1 = 6.4 \times 10^6$ psi, $\nu_1 = 0.39$, $E_2 = 29 \times 10^6$ psi, $\nu_2 = 0.3$. Allowable stress S for the tubesheet material = 16,940 psi.

The effective elastic constants E and ν are taken from the ASME Code [4.1.2] and are based on a ligament efficiency equal to 0.283. (0.6718" expanded) tube I.D. on 0.9375" pitch).

The TEMA [4.1.1] rule for calculating thickness (for TEMA R, C, or B)

for this tubesheet gives $t_s = 1.25 r_1 (p_1/S)^{1/2} = 5.625''$. The tubesheet will be assumed to be 5.625'' thick in both perforated and solid rim regions.

- (e) Gaskets: Both gaskets have an effective width of 0.354'', and are compressed to 0.125'' under the seating condition. The unloading stiffness is based on unloading the gasket linearly to zero stress in 0.01''. The rib relaxation range ϕ (Eq. 4.6.2) is also assumed to be 0.01''.
- (f) Miscellaneous: $p_1 = 600$ psi, or $p_2 = 150$ psi, $\Delta p = 20$ psi. Thickness of pass partition plate, $L = 0.5''$, $\rho = 62.4$ lb/ft³, $\mu = 0.517$ centipoise.

The solution procedure described in Sections 4.2–4.6, and implemented in the computer code TRIEL, yields a maximum tubesheet moment at $r = 0$, equal to 43,440 lb inch/inch. Using Eq. (4.3.20), the bending stress in the tubesheet is found to be 29,100 psi. This indicates that the TEMA designed tubesheet may be overstressed for this class of problems.

Table 4.7.1 gives the longitudinal hub stresses and tangential ring stresses in the channel and shell flanges for $\sigma_0 = 35,000$ psi using the Taylor Forge Method (ASME Code). The gasket seating stress y and gasket factor m used to quantify the gasket characteristics are assumed to be 9000 psi and 3, respectively. The longitudinal hub membrane stress due to internal pressure is purposely not included in the stress analysis results since the ASME Code Method does not include it. We note that for $\sigma_0 = 35,000$ psi, the channel flange stresses given by the Taylor Forge Method (ASME Code) are generally unconservative, but within a tolerable range of error.

The results for the shell flange, however, show a startling discrepancy between the two solutions. The results of the ASME Code calculation appear to be serious under-predictions. The reasons for this lie in the basic assumptions made in the Code flange design practice. The main cause of the discrepancy in the seating condition stresses is due to the ASME code sanctioned practice of computing the seating condition moment based on the average of the required gasket seating load and the available bolt load. It should be added here that the designer is urged to use the "full available bolt load" in computing the seating mode moments whenever the conditions so warrant. Unfortunately, this suggestion is generally unheeded in the industry, understandably for reasons of economy.

The aforementioned discrepancy under the pressurized condition is ascribed to a more fundamental reason. The ASME code assumes that the gasket surface pressure drops to m times the hydrostatic pressure under the pressurized condition. In a three element joint, this assumption may be completely untrue for the low pressure gasket (shellside). As a matter of fact, the shell gasket surface "residual" pressure may even exceed the seating condition pressure. This is demonstrated by numerical results later in this section.

Corresponding to $\sigma_0 = 35,000$ psi, the diametral leakage area A_L is computed to be 1.65 sq. in. Following the method given in Section 4.6, the

leakage velocity V_L is calculated to be approximately 40 ft/sec which yields a leakage rate equal to 0.11×10^6 pounds per hour. This leakage rate represents 6% of the total tubeside flow rate in the heat exchanger. The significance of a leakage ratio of this proportion should not be lost on a heat exchanger designer. Depending on the degree of co-currency of the heat exchanging media, traditionally measured by the so-called “temperature correction factor”, a leakage rate of this magnitude can drastically lower the effective log mean temperature difference, and affect the exchanger heat duty. Evidently, the quantity of the leakage as well as its damaging effect will be more aggravating in multiple tube pass exchangers containing several pass partition lanes.

Table 4.7.1. Comparison of ASME Code Method with Stress Analysis Method for a Three-Element Joint

Condition	Bolt stress	Channel Flange		Shell Flange		Method of Computation*
		Hub Long. bending	Flange ring	Hub Long. bending	Flange ring	
Seating Condition	35,000	16,580	6,360	31,030	15,690	I
Pressurized Condition	35,000	13,620	8,046	14,600	9,990	II
Seating Condition	38,470 [†]	21,900	12,090	34,920	20,050	I
Pressurized Condition	35,000 [†]	18,728	11,063	9,900	6,780	II

* Computation Method I means results are obtained using the stress analysis technique described in this chapter; more specifically, using computer program TRIEL. Computation Method II means the results are obtained using The ASME Code Method as programmed in the code FLANGE (Chapter 3).

† Recall that The ASME Code Method assumes that the bolt load remains unchanged when the joint is pressurized.

4.7.2 Controlled Metal-to-Metal Contact Joint

The foregoing observations illustrate the inherent weaknesses in the current formula-based design methods for flanges and tubesheets. We will next explore the relative advantages and disadvantages derived by allowing “controlled” metal-to-metal (MTM) contact, beyond the bolt circle, between the mating surfaces on the high pressure side (channel side). Physical reasoning suggests that the edge contact force generated by MTM will reduce the tubesheet deflection, maximum tubesheet stress, and also channel flange stress. Its effect on the residual bonnet gasket pressure, however, is not readily surmised. To derive the maximum benefit from the MTM condition on the high pressure side, the mating surfaces on the low pressure side (shell side) are assumed to be machined such as to preclude any metal-to-metal contact beyond the bolt circle.

To fix ideas, we investigate the impact of varying σ_0 and ϵ_0 (edge gap under the seating condition) on the following field quantities:

- (i) Service bolt stress σ , and edge load, F_e
- (ii) Residual bonnet and shell gasket pressures

- (iii) Tubesheet stress
- (iv) Channel flange hub and ring bending stresses
- (v) Shell flange hub and ring bending stresses
- (vi) Leakage area

(i) *Service bolt stress σ , and edge load F_e* : The computation of the service bolt stress is important in the calculation of the fatigue life of the bolts; this is especially true in the units subject to a high frequency and amplitude of fluctuations in their operating pressures. Figure 4.7.1 shows the variation of the bolt service stress with the bolt prestress for the example problem. Results for different values of the edge gap ϵ_0 are reported. It is observed that the service bolt stress σ may exceed the prestress σ_0 by over 20% for $\epsilon_0 = 0$. The increase is smaller for $\epsilon_0 > 0$, the minimum increase corresponds to the no "MTM" condition (not plotted in Fig. 4.7.1). The relationship between σ and σ_0 for a given ϵ_0 is almost linear. This linear result is, however, due to the piecewise linear gasket stiffness characteristics assumed in this problem.

These results indicate that the range of bolt axial stress variation is more severe for the controlled MTM condition than for the no edge contact condition.

(ii) *Residual bonnet and shell gasket pressures*: The residual gasket pressures are the key variables which determine the leakage potential.

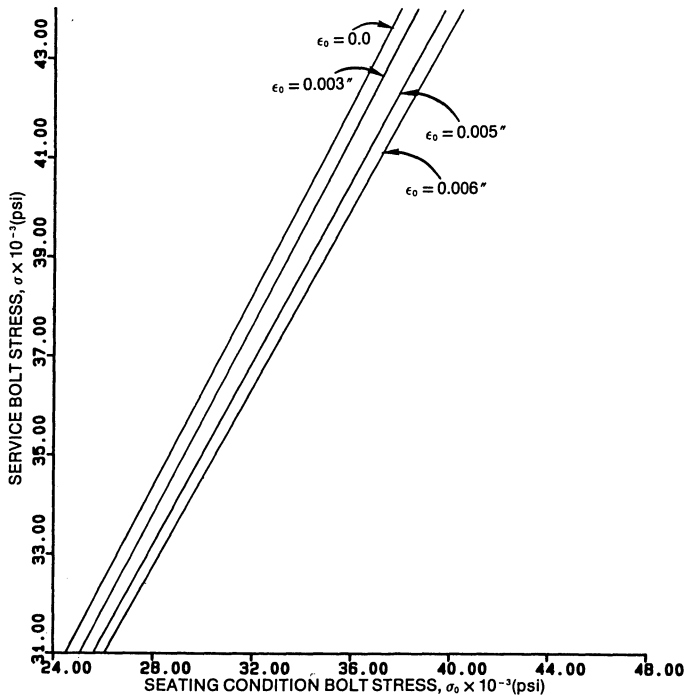


Fig. 4.7.1. Variation of σ with σ_0 for various ϵ_0 .

Figures 4.7.2 a, b show the bonnet gasket lineal force F_1 , and the shell gasket lineal force F_2 , respectively, plotted against the edge clearance ϵ_0 , with σ_0 as the parameter. F_1 is seen to decrease as the gap ϵ_0 is decreased, and F_1 asymptotically approaches the value corresponding to the “no-MTM” condition as ϵ_0 is increased. These asymptote values are denoted in Fig. 4.7.2 a,b. Thus the MTM condition reduces F_1 ; this is a disadvantage of the concept since F_1 directly affects the joint leakage. However, this decrease in F_1 can be mitigated if σ_0 is increased. F_2 , however, is a weak function of ϵ_0 . F_2 increases with decreasing ϵ_0 , and may indeed exceed the seating condition value, F_2^0 , in some cases. Thus, although there is no possibility of leakage past the shell gasket, there may be a possibility of crushing it due to excessive surface pressure, specially for high σ_0 and small ϵ_0 .

(iii) *Tubesheet*: The maximum moment in the tubesheet (equivalent plate) under the pressurized condition is always found to occur at the center ($r = 0$) in the example considered, indicating that the edge constraint provided by F_e is not strong enough to simulate a built-in edge condition. Figure 4.7.3 shows that the radial moment $M_{r(\max)}$ decreases rapidly in a linear manner with ϵ_0 . For $\sigma_0 = 35,000$ psi, the tubesheet maximum moment is reduced by approximately 20% from the no-MTM condition to the condition of zero edge gap, $\epsilon_0 = 0$. Increasing σ_0 is also seen to reduce $M_{r(\max)}$.

(iv) *Bonnet flange stresses*: The maximum longitudinal hub moment, M_h , and the ring tangential bending stress σ_r are plotted in Fig. 4.7.4 a,b for the pressurized condition. As witnessed in the case of the tubesheet, the bonnet flange stresses reduce rapidly with reduction in ϵ_0 . For $\sigma_0 = 35,000$ psi, the bonnet flange ring and hub stresses are reduced by nearly 25% and 36%, respectively, from the no-MTM condition to the zero edge gap condition ($\epsilon_0 = 0$). Increasing σ_0 , however, increases the flange stresses.

(v) *Shell flange stresses*: The shell flange hub moments, and ring stresses under the pressurized condition, are plotted in Fig. 4.7.5 a, b. These plots show that the shell flange stresses increase with decreasing ϵ_0 . However, the increase is moderate. For example, for $\sigma_0 = 35,000$ psi, the hub moment and ring stress increase by under 7% for $\epsilon_0 = 0$, over the no-MTM condition.

(vi) *Leakage Area*: The diametral leakage area is plotted in Fig. 4.7.6. A_L is seen to decrease rapidly with ϵ_0 . It reaches a minimum at $\epsilon_0 = 0$.

The foregoing observations are based on the numerical study of a typical bolted joint. Therefore, the conclusions are at best qualitative, since the joint response is strongly predicated on the physical dimensions of its elements, and the gasket stress-strain relationships. The inferences derived herein should not be construed to be of universal applicability, although they represent the typical behavior of bolted joints used in the current industrial practice. The important fact is that with the use of the computer to carry out the various computations, examination of the characteristics of any joint configuration becomes a routine design effort.

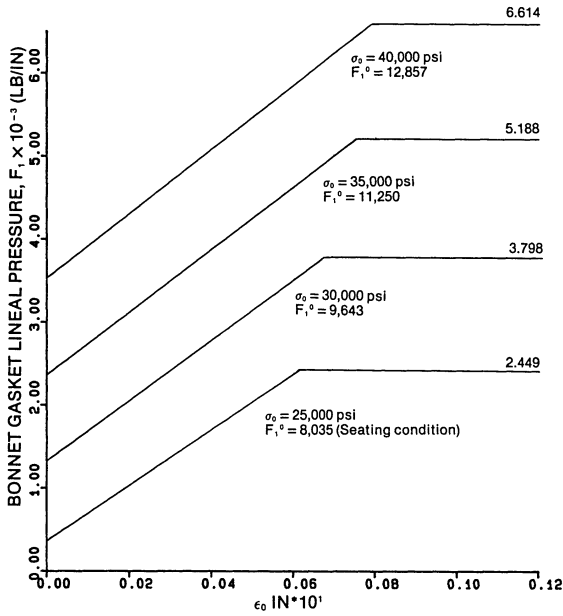


Fig. 4.7.2a. Variation of bonnet gasket residual pressure with edge clearance (pressurized condition) for various σ_0 .

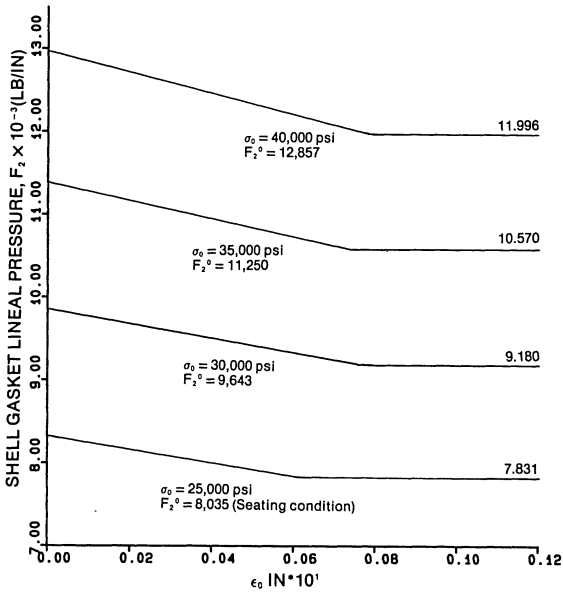


Fig. 4.7.2b. Variation of shell gasket residual pressure with edge clearance (pressurized condition) for various σ_0 .

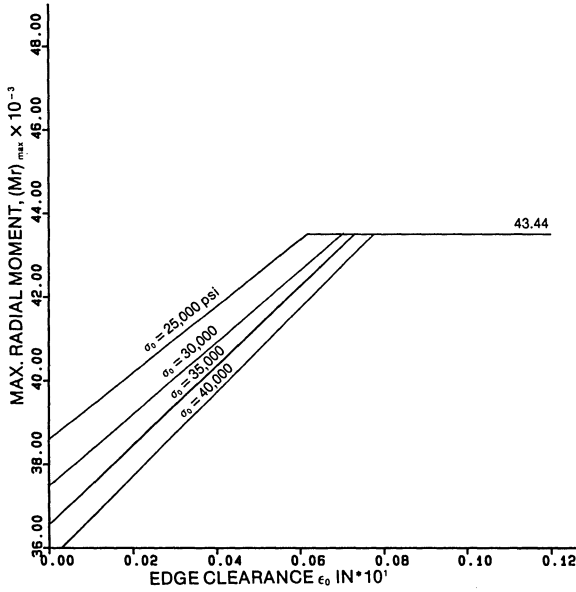


Fig. 4.7.3. Variation of maximum tubesheet moment (pressurized condition) with edge clearance for various σ_0 .

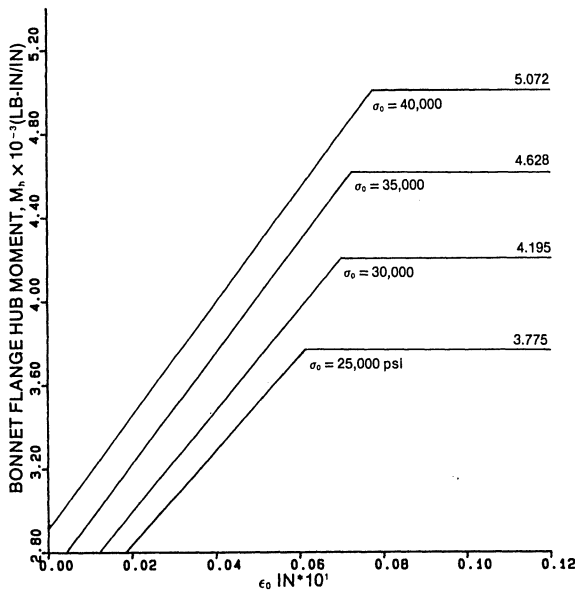


Fig. 4.7.4a. Variation of maximum bonnet hub longitudinal moment with edge clearance for various σ_0 .

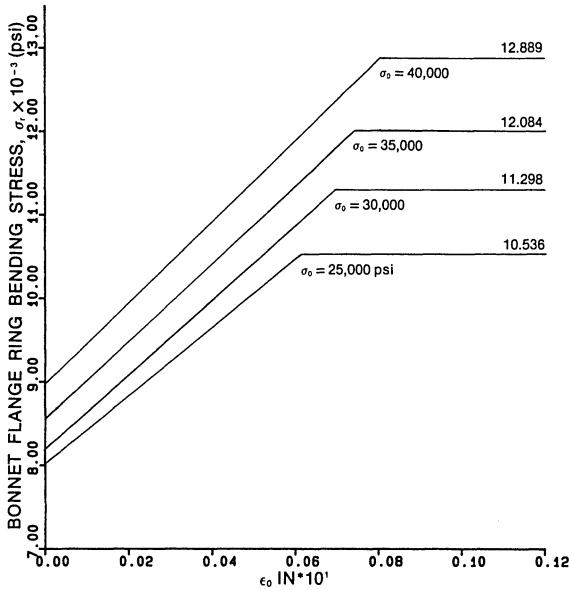


Fig. 4.7.4b. Variation of maximum bonnet flange ring bending stress with edge clearance for various σ_0 .

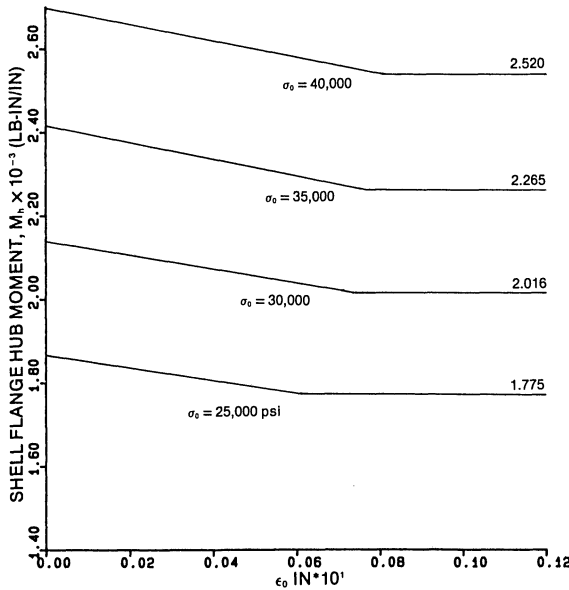


Fig. 4.7.5a. Variation of maximum shell hub longitudinal moment with edge clearance for various σ_0 .

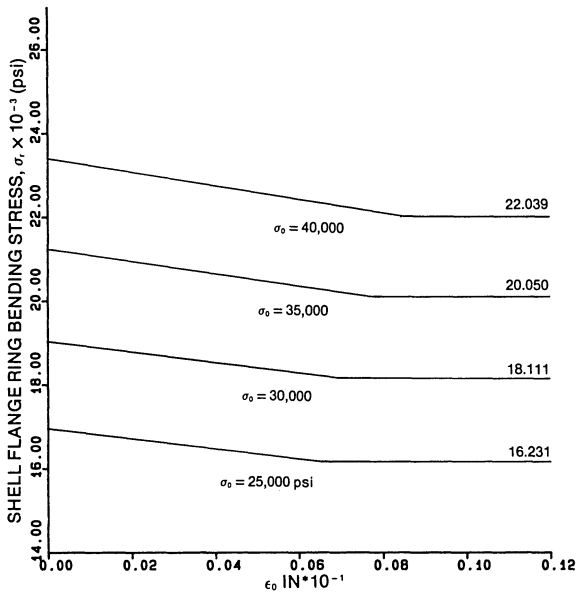


Fig. 4.7.5b. Variation of maximum shell flange ring bending stress with edge clearance for various σ_0 .

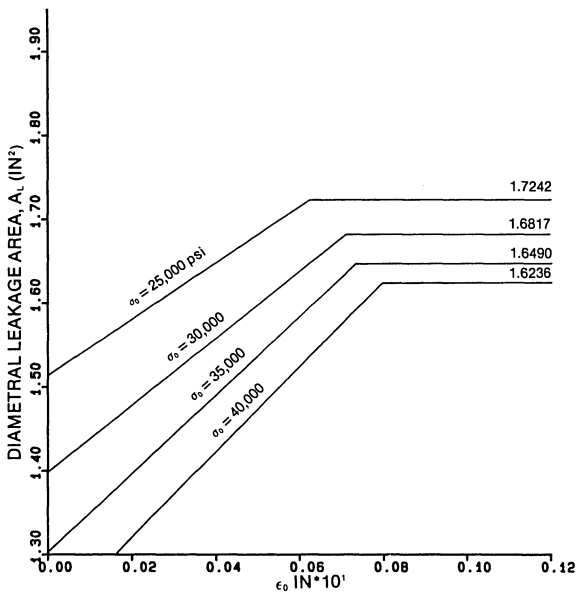


Fig. 4.7.6. Variation of diametral leakage area with edge clearance for various σ_0 .

4.7.3 Observations

The following main conclusions can be derived from the preceding example problem [4.7.1, 4.7.2].

- i. The tubeside leakage stream can be a cause of deterioration in the exchanger performance. In addition to lowering the tubeside film coefficient, it also drives down the effective Log Mean Temperature Difference (LMTD).
- ii. The flange for the low pressure chamber (shell side flange in our model) may be grossly overstressed if sized using the Taylor Forge Method (see Section 3.11).
- iii. The stresses in the high pressure side flange are also generally higher than those predicted by the ASME Code. The underdesign is more pronounced if higher (than customary) values of bolt prestress are assumed.
- iv. Increasing the bolt prestress increases the stresses in the flanged joint elements. It, however, has a minor effect in reducing the leakage area.

To alleviate the state of overstress in the flanged joints, and to reduce the leakage area, the concept of controlled metal-to-metal contact can be utilized [4.7.1–2]. Under the seating condition, a deliberate gap, ϵ_0 , between the bonnet flange (high pressure side) and tubesheet at their outer edge is prescribed. Upon pressurization, this gap diminishes. Depending on the gap size prescribed and on the applied pressures, this gap may diminish to zero, and an edge contact force may even be developed. This edge contact force exerts a counter moment on the tubesheet and on the channel flange, and thus reduces the stress levels in these members. By suitably adjusting ϵ_0 , the edge contact force may be generated at just the right stage of pressurization. The MTM condition, however, does reduce the bonnet gasket residual pressure. This deficiency can be overcome by employing a higher bolt prestress, or more bolts. The shell flange stresses, however, sustain a moderate increase as the bolt prestress is increased. The major gain is registered in drastically reducing the leakage area. The leakage area is found to be the minimum at $\epsilon_0 = 0$ in the sample problem studied.

In short, the concept of a “controlled” metal-to-metal contact beyond the bolt circle in conjunction with a high bolt prestress may be utilized to mitigate the tubeside interpass leakage and to reduce the stress levels in the bonnet flange and the tubesheet.

The main theme of the utilitarian aspects of the “MTM” concept for three element joints hinges on the fact that the channel pressure is much higher than the shell pressure, i.e., $p_1 \gg p_2$. However, if the converse is true ($p_2 > p_1$), then tubeside leakage is obviously not a problem. In this latter case, the motivation of the analyst will be to reduce tubesheet and shell flange stresses by examining “controlled” MTM between these two members. The analysis procedure will remain unchanged (with subscripts 1 and 2 now representing shellside and tubeside flange parameters, respectively).

4.8 COMPUTER PROGRAM ‘TRIEL’

Computer program TRIEL is based on the analysis for the three element joint presented in this chapter. The input data for this program is given below, followed by the listing of the computer program. The reader is referred to sub-sections 4.8.2, 4.8.3, and section 12.8 for other applications of this program.

4.8.1 Input Data for Program ‘TRIEL’

Input is in free field format.
 Line 1: Problem Heading (limited to 80 alphanumeric characters).

Line 2: Bolt data and run identification:

ITEM	Fortran Variable	Mathematical Symbol
Loading Option = 1 Seating Condition analysis only = 2 Run for seating and operation conditions	MCOND	-
Number of body bolts	N	n
Bolt pre-stress	SIG	σ_0
Root area per bolt	AROOT	A_b
Bolt circle radius	RB	r_b
Channel flange hub radial offset with respect to bolt circle	DSC	d_1
Shell flange hub offset with respect to bolt circle	DSS	d_2
Bolt material Young's Modulus	EB	E_b
Gasket data:		
Mean channel gasket radius	R ₁	r_1
Channel gasket effective (radial) width	ES1	-
Mean shell gasket radius	S ₁	-
Shell gasket effective (radial) width	GS1	-
Channel gasket loading stiffness	STIF1	-
Shell gasket loading stiffness	STIF2	-
Channel gasket thickness under seating condition	DEL1	δ_{10}
Shell gasket thickness under seating condition	DEL2	δ_2

Line 4 (Channel Flange) and Line 5 (Shell Flange) Data:

	Line 4 (Channel Flange)		Line 5 (Shell Flange)	
ITEM	Fortran Variable	Mathematical Symbol	Fortran Variable	Mathematical Symbol
Young's Modulus of the material	EC	E_1'	ES	E_2'
Mean Shell Radius	ASC	a_1'	ASS	a_2'
Hub slope	ALFAC	α_1	ALFAS	α_2
Distance of the small end from origin	XOC	x_1	XOS	x_1
Distance of the large end from origin	XHUBC	x_2	XHUBS	x_2
Shell thickness	TC	t_1	TS	t_2
Ring thickness	FC	f_1	FS	f_2
Line 6:				
Tubesheet data:			A	a
Interface radius			B	b
Outer radius			T	t
Tubesheet thickness			E1	E_1
Young's modulus of the equivalent plate for the perforated interior			E2	E_2
Young's modulus of tubesheet material			PR1	ν_1
Poisson ratio of equivalent plate			PR2	ν_2
Poisson ratio of tubesheet material				
Line 7:				
Loading data:			PC	p_1
Tubeside pressure			PS	p_2
Shellside pressure				
Line 8:				
Miscellaneous data:			UNLOAD	φ
Gasket unloading range			EPS0	ϵ_0
Edge separation under seating condition			FED	F_e
Edge contact load under seating condition ($= 0$ if $\epsilon_0 > 0$)				

PROGRAM TRIEL

```

C -----
C COMPUTES STRESSES AND DEFLECTIONS IN A THREE ELEMENT JOINT
C (TWO FLANGES AND TUBESHEET)
C -----
C FORTRAN VARIABLES:
C ***INPUT LIST : INPUT ALL DATA IN CONSISTENT UNITS***
C
C TITLE: TITLE FOR PROBLEM; ANY ALPHANUMERIC-80 CHARACTERS LONG
C
C ...FOR BOLT DATA...
C MCOND: LOADING OPTION; =1 FOR SEATING CONDITION ONLY,
C >1(SAY 2) FOR SEATING AND OPERATING CONDITONS
C N : NO. OF BOLTS
C SIG : INITIAL PRESTRESS IN BOLTS
C AROOT: ROOT AREA OF EACH BOLT
C RB : BOLT CIRCLE RADIUS
C DSC : OFFSET OF CHANNEL HUB CENTER W.R.T. BOLT CENTERLINE
C DSS : OFFSET OF SHELL HUB CENTER W.R.T. BOLT CENTERLINE
C EB : YOUNG'S MODULUS OF BOLT MATERIAL
C ...FOR GASKET DATA...
C R1 : EFFECTIVE CHANNEL GASKET RADIUS
C ES1 : EFFECTIVE GASKET WIDTH (CHANNEL SIDE)
C S1 : MEAN SHELL GASKET RADIUS
C GS1 : EFFECTIVE GASKET WIDTH (SHELL SIDE)
C STIF1: CHANNEL GASKET STIFFNESS
C STIF2: SHELL GASKET STIFFNESS
C DELC : THICKNESS OF CHANNEL GASKET UNDER SEATING CONDITION
C DELS : THICKNESS OF SHELL GASKET UNDER SEATING CONDITION
C ...FOR CHANNEL FLANGE DATA...
C EC : CHANNEL FLANGE YOUNG'S MODULUS
C ASC : CHANNEL MEAN RADIUS
C ALFAC: HUB SLOPE(CHANNEL)
C XOC : DISTANCE OF SMALL END FROM THE POINT OF ZERO THICKNESS
C XHUBC: DISTANCE OF LARGE END " " " " " "
C TC : CHANNEL THICKNESS
C FC : RING THICKNESS
C ..FOR SHELL FLANGE DATA...
C ES : SHELL FLANGE YOUNG'S MODULUS
C ASS : SHELL MEAN RADIUS
C ALFAS: HUB SLOPE(SHELL)
C XOS : DISTANCE OF SMALL END FROM THE POINT OF ZERO THICKNESS
C XHUBS: DISTANCE OF LARGE END " " " " " "
C TS : SHELL THICKNESS
C FS : RING THICKNESS
C ...FOR TUBESHEET DATA...
C A : INTERFACE RADIUS
C B : OUTER RADIUS
C T : TUBESHEET THICKNESS
C E1 : EQUIVALENT YOUNG'S MOD. OF PERFORATED REGION

```



```

C  E2 : YOUNG'S MOD. OF TUBESHEET MATERIAL
C  PR1 : EQUIVALENT POISSON'S RATIO OF PERFORATED REGION
C  PR2 : POISSON'S RATIO OF TUBESHEET MATERIAL
C  ...FOR PRESSURE DATA...
C  PC : TUBESIDE PRESSURE
C  PS : SHELLSIDE PRESSURE
C  ...FOR MISCELLANEOUS DATA...
C  UNLOAD:GASKET UNLOADING RANGE; ALSO A SENTINEL IF NEGATIVE
C  EPSO : EDGE SEPARATION IN SEATING CONDITION
C  FED : EDGE LOAD UNDER SEATING CONDITION
C  -----
C  OTHER PRINCIPAL VARIABLES:
C  BRC : CHANNEL FLANGE RING WIDTH
C  BRS : SHELL FLANGE RING WIDTH
C
C  CSC :RADIAL DISTANCE OF BOLT CENTER LINE FROM EFF. BONN. GSKT CIRCLE
C  CSS :RADIAL DISTANCE OF BOLT CENTER LINE FROM SHELL GSKT EFF. CIRCLE
C
C  -----
C  ***RESULTS HAVE UNITS CONSISTENT WITH THOSE OF INPUT DATA***
C  *****
C  DIMENSION DISP(20),GAP(20),RT(20),THICK(20),TITLE(20)
C  COMMON/KPS/JPAR
C  COMMON/MJH/DISP
C  COMMON/FOUR/CED
C  *****
C  ...STATEMENT FUNCTIONS...
C  FF(SIGMA,P,RAD,FEDGE)=(SIGMA*AROOT*N-3.14159*P*RAD*RAD)
C  1/(6.283185*RAD)-FEDGE*B/RAD
C  ELEN(TH1,TH2,THT,DEL1,DEL2)=FC+FS+T-CSC*TH1-CSS*TH2+
C  1(S1-R1)*THT+DEL1+DEL2
C  EPS(DEL,TH1,THT)=EPSO+DEL-DEL2-(CED+CSC)*(TH1-THT-TH1+THAT)
C  *****
C  ...SET THE FOLLOWING...
C  TOL = 100.
C  PRC = .3
C  PRS = .3
C  *****
C  ...GIVE HEADING FOR PROBLEM...
C  READ(5,5)(TITLE(I),I=1,20)
C  5 FORMAT(20A4)
C  ***INPUT DATA***
C  ...FOR BOLTS...
C  READ(5,*) MCOND,N,SIG,AROOT,RB,DSC,DSS,EB
C  ...FOR GASKET...
C  READ(5,*) R1,ES1,S1,GS1,STIF1,STIF2,DEL2,DELS
C  ...FOR CHANNEL FLANGE...
C  READ(5,*) EC,ASC,ALFAC,XOC,XHUBC,TC,FC
C  ...FOR SHELL FLANGE DATA
C  READ(5,*) ES,ASS,ALFAS,XOS,XHUBS,TS,FS
C  ...FOR TUBESHEET...
C  READ(5,*) A,B,T,E1,E2,PR1,PR2
C  ...FOR PRESSURES...

```

```

IF(MCOND .NE. 1) GO TO 40
PS = 0.0
PC = 0.0
GO TO 43
40 READ(5,*) PC,PS
43 CONTINUE
C   ...MISCELLANEOUS DATA...
1  READ(5,*) UNLOAD,EPSO,FED
C   ...SET SENTINEL FOR END OF RUN...
   IF(UNLOAD.LT.0.) GO TO 1001
C   *****
C   ...COMPUTE OTHER DIMENSIONS...
   CED = B-RB
   BRC = B-ASC+0.5*TC
   BRS = B-ASS+0.5*TS
   C = B-.5*BRC
   RMS=B-.5*BRS
   CSC = RB-R1
   CSS = RB-S1
C   *****
C   ...PRINT HEADING...
   WRITE(6,6) (TITLE(I),I=1,20)
6  FORMAT(1H1,5X,20A4)
C   ...PRINT INPUT DATA...
   WRITE(6,21) MCOND,N,SIG,AROOT,RB,DSC,DSS,EB,R1,ES1,S1,GS1,
+             STIF1,STIF2,DELC,DELS
21  FORMAT(1H0,15X,"*****INPUT DATA*****"/
+20X,"          BOLT DATA          "/
+6X,"LOADING OPTION ..... =",I10/
+6X,"NO. OF BOLTS ..... =",I10/
+6X,"BOLT PRESTRESS ..... =",F10.1/
+6X,"ROOT AREA PER BOLT ..... =",F10.3/
+6X,"BOLT CIRCLE RADIUS ..... =",F10.3/
+6X,"CHANNEL HUB CENTER OFFSET W.R.T BOLT CENTERLINE =",F10.4/
+6X,"SHELL HUB CENTER OFFSET W.R.T BOLT CENTERLINE . =",F10.4/
+6X,"YOUNG'S MODULUS OF BOLT MATERIAL ..... =",E10.3//
+20X,"          GASKET DATA          "/
+6X,"EFFECTIVE CHANNEL GASKET RADIUS ..... =",F10.3/
+6X,"EFFECTIVE CHANNEL GASKET WIDTH ..... =",F10.3/
+6X,"EFFECTIVE SHELL GASKET RADIUS ..... =",F10.3/
+6X,"EFFECTIVE SHELL GASKET WIDTH ..... =",F10.3/
+6X,"CHANNEL GASKET STIFFNESS..... =",E10.3/
+6X,"SHELL GASKET STIFFNESS ..... =",E10.3/
+6X,"CHANNEL GASKET THICKNESS UNDER SEATING CONDITION=",F10.3/
+6X,"SHELL GASKET THICKNESS UNDER SEATING CONDITION=",F10.3/)
   WRITE(6,22) EC,ES,ASC,ASS,ALFAC,ALFAS,XOC,XOS,XHUBC,XHUBS,
+             TC,TS,FC,FS
22  FORMAT(15X,"          CHANNEL AND SHELL FLANGE DATA   "/
+6X,"FLANGE YOUNG'S MODULUS : CHANNEL, SHELL ..... =",2E10.3/
+6X,"MEAN RADIUS :          CHANNEL, SHELL ..... =",2F10.3/
+6X,"HUB SLOPE :           CHANNEL, SHELL ..... =",2F10.3/
+6X,"DISTANCE OF SMALL END OF HUB FROM POINT OF "/

```

```

+6X,"ZERO THICKNESS : CHANNEL, SHELL ..... =" ,2F10.3/
+6X,"DISTANCE OF LARGE END OF HUB FROM POINT OF "/
+6X,"ZERO THICKNESS : CHANNEL, SHELL ..... =" ,2F10.3/
+6X,"THICKNESS : CHANNEL, SHELL ..... =" ,2F10.3/
+6X,"RING THICKNESS : CHANNEL, SHELL ..... =" ,2F10.3/)
WRITE(6,23) A,B,T,E1,E2,PR1,PR2,PC,PS,UNLOAD,EPSO,FED
23 FORMAT(20X,"_____TUBESHEET DATA _____"/
+6X,"INTERFACE RADIUS ..... =" ,F10.3/
+6X,"OUTER RADIUS ..... =" ,F10.3/
+6X,"THICKNESS ..... =" ,F10.3/
+6X,"EQUIVALENT YOUNG'S MOD. OF PERFORATED REGION .. =" ,E10.3/
+6X,"YOUNG'S MODULUS OF TUBESHEET MATERIAL ..... =" ,E10.3/
+6X,"EQUIVALENT POISSON'S RATIO OF PERFORATED REGION =" ,F10.3/
+6X,"POISSON'S RATIO OF TUBESHEET MATERIAL ..... =" ,F10.3//
+20X,"_____PRESSURES _____"/
+6X,"TUBESIDE PRESSURE ..... =" ,F10.1/
+6X,"SHELLSIDE PRESSURE ..... =" ,F10.1//
+20X,"_____MISCELLANEOUS DATA _____"/
+6X,"GASKET UNLOADING RANGE ..... =" ,F10.3/
+6X,"EGDE SEPARATION UNDER SEATING CONDITION ..... =" ,F10.3/
+6X,"EDGE LOAD UNDER SEATING CONDITION ..... =" ,F10.1//
+6X,"*****")

```

C

JPAR= 0

WRITE(6,6) (TITLE(I),I=1,20)

C CALCULATE ROTATION OF BONNET FLANGE

WRITE(6,51)

51 FORMAT(1H0,15X,"*****RESULTS*****"//

+21X,"++++++"//

+21X,"+++ SEATING CONDITION +++"/21X,"++++++"//)

WRITE(6,52)

52 FORMAT(1H0,5X,"(A) BONNET FLANGE"/10X,"=====")

45 FFCO = FF(SIG,0.,R1,FED)

CALL FLG(EC,PRC,ASC,0.0,ALFAC,XOC,XHUBC,TC,BRC,FC,CSC,FFCO

1 ,DSC,THA1,FED,RMC,RB)

C CALCULATE ROTATION OF SHELL FLANGE

WRITE(6,61)

61 FORMAT(1H0,5X,"(B) SHELL FLANGE"/10X,"=====")

FFSO = FF(SIG,0.,S1,0.)

CALL FLG(ES,PRS,ASS,0.,ALFAS,XOS,XHUBS,TS,BRS,FS,CSS,FFSO,DSS,

1 THA2,0.,RMS,RB)

C CALCULATE TUBESHEET ROTATION

CALL TSHEET(0.,0.,FFCO,FFSO,A,B,R1,S1,T,E1,E2,PR1,PR2,THAT,FED)

C COMPUTE SEATED GASKET THICKNESS

RCI = ASC-.5*TC

DELCO = (R1-RCI)*(THA1-THAT)+DELCO

WRITE(6,72).

72 FORMAT(1H0,10X,"THICKNESS PROFILE OF GASKET"/

+ 11X,"-----")

+ 11X," RADIUS",9X,"GASKET THICKNESS")

DO 70 I=1,11

RT(I) = (I-1)*.1*A

```

        THICK(I)= DELCO +DISP(I)
70      WRITE(6,71) RT(I),THICK(I)
71      FORMAT(2E20.6)
C      CALCULATE BOLT LENGTH FOR SEATING CONDITION
        ELO = ELEN(THA1,THA2,THAT,DELC,DELS)
        WRITE(6,62) ELO
62      FORMAT(1H0,5X,"SEATING CONDITION BOLT LENGTH=",F15.6)
C      ELO IS ORIGINAL BOLT LENGTH
C      COMPUTE OPERATING CONDITION LENGTH (BY ITERATION)
        IF(MCOND .EQ. 1) GO TO 1000
        I=0
        WRITE(6,81)
81      FORMAT(1H1,10X,"+++++++/
+11X,"+++PRESSURIZED CONDITION:UNCHANGED EDGE LOAD+++/"
+11X,"++++++/")
        AKB = EB/ELO
C      ESTABLISH PRELIMINARY K
        JPAR = 1
        SIGMA= .9*SIG
        FFC = FF(SIGMA,PC,R1,FED)
        FFS = FF(SIGMA,PS,S1,0.)
        CALL FLG (EC,PRC,ASC,PC,ALFAC,XOC,XHUBC,TC,BRC,FC,CSC,FFC,DSC,TH1,
/ FED,RMC,RB)
        CALL FLG(ES,PRS,ASS,PS,ALFAS,XOS,XHUBS,TS,BRS,FS,CSS,FFS,DSS,TH2,
/ O.,RMS,RB)
        CALL TSHEET(PC,PS,FFC,FFS,A,B,R1,S1,T,E1,E2,PR1,PR2,THT,FED)
        CALL GASKET(FFC,FFCO,UNLOAD,DELC,STIF1,ES1,DEL1)
        CALL GASKET(FFS,FFSO,UNLOAD,DELS,STIF2,GS1,DEL2)
        EL = ELEN(TH1,TH2,THT,DEL1,DEL2)
        FUNC = EPS(DEL1,TH1,THT)
        SIGMAP = SIGMA
        SIGMA = SIG
100     I= I+1
        IF (I .GT. 10) GO TO 1000
102     CONTINUE
        FFC = FF(SIGMA,PC,R1,FED)
        FFS = FF(SIGMA,PS,S1,0.)
        IF(JPAR.EQ.0) WRITE(6,52)
        CALL FLG (EC,PRC,ASC,PC,ALFAC,XOC,XHUBC,TC,BRC,FC,CSC,FFC,DSC,TH1,
+ FED,RMC,RB)
        IF(JPAR.EQ.0) WRITE(6,61)
        CALL FLG(ES,PRS,ASS,PS,ALFAS,XOS,XHUBS,TS,BRS,FS,CSS,FFS,DSS,TH2,
+ O.,RMS,RB)
        CALL TSHEET(PC,PS,FFC,FFS,A,B,R1,S1,T,E1,E2,PR1,PR2,THT,FED)
        CALL GASKET(FFC,FFCO,UNLOAD,DELC,STIF1,ES1,DEL1)
        CALL GASKET(FFS,FFSO,UNLOAD,DELS,STIF2,GS1,DEL2)
        IF(JPAR .NE. 0) GO TO 106

C
        DELCC = (R1-RCI)*(TH1-THT)+ DEL1
        WRITE(6,101)
101     FORMAT(1H0,18X,"GAP PROFILE"/19X,"-----/"
+ 12X,"RADIUS",15X,"GAP")

```

```

DO 105 J=1,11
GAP(J)= DELCC +DISP(J)-THICK(J)-.01
IF(GAP(J) .LT. 0.) GAP(J)=0.
WRITE(6,71) RT(J),GAP(J)
105 CONTINUE
CALL ALEAK(RCI,A,GAP)
106 IF(JPAR .EQ. 0) GO TO 875
C
ELL= ELEN(TH1,TH2,THT,DEL1,DEL2)
FUNCC= EPS(DEL1,TH1,THT)
AK = (SIGMA-SIGMAP)/(ELL-EL)
DELTA= (AK*(ELO-ELL)+SIGMA-SIG)/(AKB-AK)
EL = ELL
FUNC = FUNCC
SIGMAP = SIGMA
ELL = ELO+DELTA
SIGMA = SIG+AKB*DELTA
DEV=ABS((ELL-EL)/EL)*EB
IF(DEV-TOL)205,205,100
205 IF(FUNC.LE.0.) GO TO 875
JPAR=0
GO TO 102
875 CONTINUE
C DETERMINE IF THE EDGE GAP IS POSITIVE
IF(FUNC.GT.0. .AND. JPAR.EQ.0) GO TO 900
C OTHERWISE DETERMINE EDGE LOAD FED AND BOLT STRESS SIGMA
FEDP = .01*FFC+FED
220 WRITE(6,221)
221 FORMAT(1H0,15X,".....THERE IS EDGE CONTACT....."/)
SIGMAP = 1.01*SIGMA
C ESTIMATE DERIVATIVES
ITIME = 0
TAU = 0.
EL = ELL
225 ITIME = ITIME +1
FFC = FF(SIGMA,PC,R1,FEDP)
FFS = FF(SIGMA,PS,S1,0.)
JPAR = 1
CALL FLG (EC,PRC,ASC,PC,ALFAC,XOC,XHUBC,TC,BRC,FC,CSC,FFC,DSC,TH1,
+ FEDP,RMC,RB)
CALL FLG(ES,PRS,ASS,PS,ALFAS,XOS,XHUBS,TS,BRS,FS,CSS,FFS,DSS,TH2,
+ 0.,RMS,RB)
CALL TSHEET(PC,PS,FFC,FFS,A,B,R1,S1,T,E1,E2,PR1,PR2,THT,FEDP)
CALL GASKET(FFC,FFCO,UNLOAD,DELC,STIF1,ES1,DEL1)
CALL GASKET(FFS,FFSO,UNLOAD,DELS,STIF2,GS1,DEL2)
ELL= ELEN(TH1,TH2,THT,DEL1,DEL2)
FUNCC= EPS(DEL1,TH1,THT)
A12 = (FUNCC-FUNC)/(FEDP-FED)
A22 = (ELL-EL)/(FEDP-FED)
FFC = FF(SIGMAP,PC,R1,FED)
FFS = FF(SIGMAP,PS,S1,0.)
CALL FLG (EC,PRC,ASC,PC,ALFAC,XOC,XHUBC,TC,BRC,FC,CSC,FFC,DSC,TH1,

```

```

+ FED,RMC,RB)
CALL FLG(ES,PRS,ASS,PS,ALFAS,XOS,XHUBS,TS,BRS,FS,CSS,FFS,DSS,TH2,
+ O.,RMS,RB)
CALL TSHEET(PC,PS,FFC,FFS,A,B,R1,S1,T,E1,E2,PR1,PR2,THT,FED)
CALL GASKET(FFS,FFSO,UNLOAD,DELS,STIF2,GS1,DEL2)
CALL GASKET(FFC,FFCO,UNLOAD,DEL2,STIF1,ES1,DEL1)
ELL= ELEN(TH1,TH2,THT,DEL1,DEL2)
FUNCC= EPS(DEL1,TH1,THT)
A11 = (FUNCC-FUNC)/(SIGMAP-SIGMA)
A21 = ((ELL-EL)/(SIGMAP-SIGMA))- (EL/EB)
240 DETER = A11*A22 - A21*A12
DELSIG = (-FUNC*A22-TAU*A12)/DETER
DELF = (A21*FUNC +A11*TAU)/DETER
SIGMAC = SIGMA+DELSIG
FEDC = FED+DELF
FFC = FF(SIGMAC,PC,R1,FEDC)
FFS = FF(SIGMAC,PS,S1,O.)
250 CONTINUE
IF(JPAR.EQ.0) WRITE(6,52)
CALL FLG( EC,PRC,ASC,PC,ALFAC,XOC,XHUBC,TC,BRC,FC,CSC,FFC,DSC,TH1,
+ FEDC,RMC,RB)
IF(JPAR.EQ.0) WRITE(6,61)
CALL FLG(ES,PRS,ASS,PS,ALFAS,XOS,XHUBS,TS,BRS,FS,CSS,FFS,DSS,TH2,
+ O.,RMS,RB)
CALL TSHEET(PC,PS,FFC,FFS,A,B,R1,S1,T,E1,E2,PR1,PR2,THT,FEDC)
CALL GASKET(FFS,FFSO,UNLOAD,DELS,STIF2,GS1,DEL2)
CALL GASKET(FFC,FFCO,UNLOAD,DEL2,STIF1,ES1,DEL1)
FUNCC= EPS(DEL1,TH1,THT)
IF(JPAR .NE. 0) GO TO 306
DELCC = (R1-RC1)*(TH1-THT)+ DEL1
WRITE(6,101)
DO 305 J=1,11
GAP(J)= DELCC +DISP(J)-THICK(J)-.01
IF(GAP(J) .LT. 0.) GAP(J)=0.
WRITE(6,71) RT(J),GAP(J)
305 CONTINUE
CALL ALEAK(RC1,A,GAP)
306 CONTINUE
IF(JPAR .EQ. 0) GO TO 800
ELL= ELEN(TH1,TH2,THT,DEL1,DEL2)
ELLB = ELO +(SIGMAC-SIG)*ELO/EB
TAU = ELLB-ELL
DEV = ABS(AKB*TAU)
C WRITE(6,750) ITIME,ELL,EL,FUNCC,FUNC,SIGMA,SIGMAC
C 750 FORMAT(1HOI4,6E17.8)
DEVFUN = ABS(AKB*FUNCC)
IF(DEVFUN .LT. TOL .AND. DEV .LT. TOL) JPAR = 0
IF(JPAR .EQ.0) GO TO 250
EL = ELL
FUNC = FUNCC
SIGMA = SIGMAC
FED = FEDC

```

```

FEDP = FED*1.01
SIGMAP = 1.01*SIGMA
IF(ITIME .GT. 20) GO TO 1000
GO TO 225
800 WRITE(6,801) ELL,SIGMAC,FEDC,DEL1,FFC,DEL2,FFS
801 FORMAT(1H0,5X,"FINAL RESULTS ARE:"/6X,"BOLT LENGTH =",E15.8,
1 6X,"BOLT STRESS =",E12.5,6X,"CONTACT LOAD =",E12.5/6X,
2 "COMPRESSED BONNET GASKET THICKNESS =",E12.5,6X,
3 "COMPRESSED BONNET GASKET LOAD =",E12.5/6X,
4 "COMPRESSED SHELL GASKET THICKNESS =",E12.5,6X,
5 "COMPRESSED SHELL GASKET LOAD =",E12.5)
GO TO 1000
900 WRITE(6,901)
901 FORMAT(1H0,6X,".....NO EDGE CONTACT.....")
1000 GO TO 1
1001 STOP
END

C *****
C
SUBROUTINE TSHEET(P1,P2,F1,G1,A,B,R1,S1,T,E1,E2,PR1,PR2,THETA,FED)
C CALCULATES DEFLECTION PROFILE OF U TUBESHEET IN A 3 ELEMENT JOINT
DIMENSION DISP(20) , AMR(20)
COMMON/KPS/JPAR
COMMON/MJH/DISP
COMMON/FOUR/CED
AM(R) = -D1*2.*BETA*(1.+PR1) -P*R*R*(3.+PR1)/16.
W(R) = BETA*(R*R - A*A) + P*(R**4-A**4) /(64.*D1)
P = P1-P2
H = B-A
ASTR = .5*(B+A)
ZI = .25*P*A*H + (F1*(ASTR-R1)*R1-G1*(ASTR-S1)*S1+.25*(R1**2-A**2)*P1*
1 (2.*ASTR-R1-A)-.25*(S1**2-A**2)*P2*(2.*ASTR-S1-A)-FED*(B-ASTR)
1 *B)/A
D1 = E1*T**3 /(12.*(1.-PR1*PR1))
R0 = 12.*ASTR*D1*(1+PR1)/(E2*H*T**3)
AM0 = (R0*ZI - .125*P*A*A) /(1. + R0)
BETA = 6.*(AM0 -ZI) *ASTR/(E2*H*T**3) - (P*A*A/(32.*D1))
THETA = 12.*ASTR*A*(AM0-ZI) /(E2*H*T**3)
AMRI=AM0-ZI
IF(JPAR .EQ. 1) GO TO 95
WRITE(6,110) F1,G1
110 FORMAT(1H0,5X,"(C) TUBESHEET"/10X,"====="//
+6X,"BONNET SIDE UNIT GASKET FORCE =",F10.2/
+6X,"SHELL SIDE UNIT GASKET FORCE =",F10.2)
WRITE(6,120) THETA,AMRI
120 FORMAT(1H0,5X,"RING ROTATION = ",E10.4,5X,"RING MOMENT =",E10.2/)
WRITE(6,130)
130 FORMAT(1H0,8X,"DEFLECTION PROFILE OF TUBESHEET"/
+
9X,"-----"/
+6X,"RADIUS", 3X, "DISPLACEMENT", 3X, "RADIAL MOMENT")
DO 100 I=1,11
R= (I-1) *.1*A

```

```

DISP(I) = W(R)
AMR(I) = AM(R)
WRITE(6,30) R,DISP(I) , AMR(I)
100 CONTINUE
95  CONTINUE
30  FORMAT(1X,F10.2,2E15.4)
RETURN
END

C *****
C
SUBROUTINE GASKET(F,FO,UNLOAD,DELO,STIF,ES,DEL)
C LINEAR LOADING AND UNLOADING MODULI
IF(F .GT. FO) GO TO 20
AMOD = FO/(UNLOAD*ES)
DEL = DELO+(FO-F)/(AMOD*ES)
GO TO 30
20  DEL = DELO-(F-FO)/(STIF*ES)
30  RETURN
END

C *****
C
SUBROUTINE FLG(E,PR,AS,P,ALFA,X0,XHUB,T,BR,F,CS,FF,DS,THETA
1 ,FED,RM,RB)
DIMENSION A(8,8), B(8),G(64)
COMMON/ONE/S1,S2,S3,S4,S5,S6,S7,S8
COMMON/TWO/SI1,DSI1,SI2,DSI2,SI3,DSI3,SI4,DSI4
COMMON/THREE/B,PRES
COMMON/KPS/JPAR
COMMON/FOUR/CED
EPS(X) = 2.*RO*X**.5
C SHELL PARAMETERS
D= E*T**3/(12.*(1.-PR*PR))
BETA = (3.*(1.-PR*PR)/(AS*AS*T*T))**.25
RO =(12.*(1.-PR*PR) /((ALFA*ALFA*AS*AS))**.25
C INITIALIZE MATRIX ELEMMENTS
DO 100 I=1,8
B(I) = 0.
DO 100 J=1,8
100 A(I,J) =0.
C DEFINE MATRIX ELEMENTS
XA= EPS(X0)
CALL SERIES(XA,6)
A(1,1) = 2.*RO*DSI1/XA
A(1,2) = 2.*RO*DSI2/XA
A(1,3) = 2.*RO*DSI3/XA
A(1,4) = 2.*RO*DSI4/XA
A(1,5) = 1./(2.*BETA*BETA*D)
A(1,6) = -1./(2.*BETA**3*D)
A(2,1) = 4.*RO**3*S1/XA**3
A(2,2) = -4.*RO**3*S2/XA**3
A(2,3) = 4.*RO**3*S3/XA**3
A(2,4) = -4.*RO**3*S4/XA**3
A(2,5) = 1./(BETA*D)

```

```

A(2,6) = -A(1,5)
A(3,7) = ( 6.*RM*RM/(E*BR*F*F))*RM/(RB-DS)
A(3,8) = ( 4.*RM*RM/(E*BR*F))*RM/(RB-DS)
A(4,7) = ( -12.*RM**2/(E*BR*F**3))*RM/(RB-DS)
A(4,8) = ( -6.*RM*RM/(E*BR*F*F))*RM/(RB-DS)
A(5,1) = S5
A(5,2) = -S6
A(5,3) = S7
A(5,4) = -S8
A(5,5) = 96.*RO*(1.-PR*PR)/(E*ALFA**3*XA)
B(5) = 16.*P *AS*AS*RO*(1.-.5*PR)/(E*ALFA*XA)
A(6,1) = S2
A(6,2) = S1
A(6,3) = S4
A(6,4) = S3
A(6,6) = -48.*(1.-PR*PR)/(E*ALFA**3*RO*XA)
C  REDEFINE XA
   XA = EPS(XHUB)
   CALL SERIES(XA,6)
A(7,7) = 96.*RO*(1.-PR*PR)/(E*ALFA**3*XA)
A(8,8) = -48.*(1.-PR*PR)/(E*ALFA**3*RO*XA)
A(3,1) = 2.*RO*DSI1/XA
A(3,2) = 2.*RO*DSI2/XA
A(3,3) = 2.*RO*DSI3/XA
A(3,4) = 2.*RO*DSI4/XA
A(4,1) = 4.*RO**3*S1/XA**3
A(4,2) = -4.*RO**3*S2/XA**3
A(4,3) = 4.*RO**3*S3/XA**3
A(4,4) = -4.*RO**3*S4/XA**3
A(7,1) = S5
A(7,2) = -S6
A(7,3) = S7
A(7,4) = -S8
B(7) = 16.*P *AS*AS*RO*(1.-.5*PR)/(E*ALFA*XA)
A(8,1) = S2
A(8,2) = S1
A(8,3) = S4
A(8,4) = S3
PRES = P*AS*AS*(1.-.5*PR)/(E*ALFA)
B(2) = -PRES/(XO*XO)
C  ADD THE ANNULAR PRESSURE TERM TO GASKET LOAD
   AMEX=(FF*CS*(RB-CS)/RM)+.5*P*((RB-CS)**2-(RB-DS)**2)/RM
   1 -FED*CED*(RB+CED)/RM+(.5*P*AS*AS*DS/RM)
B(3) = (PRES/(XHUB)) - (P*RM*RM/(E*BR))
   1 -(6.*RM*RM* AMEX/(E*BR*F*F))
B(4) = -(PRES/(XHUB*XHUB)) +
   1 (12.*RM**2 *AMEX/(E*BR*F **3))
C  CONVERT A TO A COLUMN VECTOR
   DO 200 J=1,8
   DO 200 I=1,8
   200 G((J-1)*8+I) = A(I,J)
   CALL SIMQ(G,B,8,KS)

```

```

      IF(JPAR .EQ. 1) GO TO 95
      WRITE(6,20) BR,FF
20  FORMAT(6X,"RING WIDTH =",F10.3,5X,"GASKET LOAD =",F10.2////
      +10X,"SOLUTION FOR FLANGE CONSTANTS"/
      +6X,"-----")
      WRITE(6,250) (B(I),I=1,8)
250  FORMAT(6X,"C1=",E12.4,5X,"C2=",E12.4,/,6X,"C3=",E12.4,5X,
      +"C4=",E12.4,/,6X,"M0=",E12.4,5X,"Q0=",E12.4,/,6X,"M3=",E12.4,
      +5X,"Q3=",E12.4,/,6X,"-----"/)
      CALL HUB(RO,X0,XHUB,ALFA,AS,P,E,PR)
95  CONTINUE
      CALL RING(DS,F,BR,AS,THETA,AMEX,P,E,PR,RM,RB)
      RETURN
      END
C *****
C
      SUBROUTINE HUB(RO,X0,XHUB,ALFA,AS ,P,E,PR)
C COMPUTES DEFLECTION AND STRESSES IN THE HUB
      DIMENSION B(8)
      COMMON/ONE/S1,S2,S3,S4,S5,S6,S7,S8
      COMMON/TWO/SI1,DSI1,S12,DSI2,S13,DSI3,S14,DSI4
      COMMON/THREE/B,PRES
      EPS(X) = 2.*RO*X**.5
      WRITE(6,10)
10  FORMAT(1H0,20X,"HUB DEFLECTION AND STRESSES"/
      + 21X,"-----"/
      +4X,"LOCN OF POINT",2X,"DISPLACEMENT",5X,"ROTATION",
      +5X,"SHEAR FORCE",2X,"BENDING MOMENT",2X,"LONG.BEND. STRESS"/)
      XLEN = XHUB-X0
      DO 30 I=1,6
      X= X0+(I-1) *XLEN*.2
      ES = EPS(X)
      THIK=ALFA*X
      CALL SERIES(ES,6)
      DEFF = E*ALFA**3/(48.*(1.-PR*PR))
      DISP = ((B(1) *DSI1 + B(2) *DSI2 + B(3) *DSI3 + B(4)*DSI4)*X**(-.5
1 ))-(PRES/X)
      ROTN = ((B(1) *S1-B(2)*S2 + B(3)*S3 -B(4)*S4)* .5* 1.0/(X**1.5) )
1 + (PRES/(X*X))
      AMX = -DEFF*X**.5*(B(1)*S5 -B(2) *S6+B(3)*S7-B(4) *S8)
1 +P*AS*AS*ALFA*ALFA*(1-.5*PR)/(6.*(1.-PR*PR))
      QX = DEFF*2.*RO*RO*X**.5*(B(1)*S2 + B(2)*S1 +B(3)*S4 + B(4)*S3)
      BENSTR=6.*AMX/(THIK*THIK)
      WRITE(6,20) X,DISP,ROTN,QX,AMX,BENSTR
20  FORMAT(6E15.5)
30  CONTINUE
      RETURN
      END
C *****
C
      SUBROUTINE RING(DS,F,BR,AS,THETA,AMEX,P,E,PR,RM,RB)
      DIMENSION B(8)

```

```

C   COMPUTES STRESSES IN THE RING
      COMMON/THREE/B,PRES
      COMMON/KPS/JPAR
      W= P*AS*.5
      AM =( B(7) + B(8)*.5*F)*RM/(RB-DS)+AMEX
      THETA = 12.*RM*RM*AM/(E*BR*F**3)
      SIGTB = 6.*AM*RM/(BR*F*F)
      IF(JPAR .EQ. 1) GO TO 95
      WRITE(6,10) AM,THETA,SIGTB
10  FORMAT(1H0,/,6X,"TOTAL RING MOMENT = ",5X,E15.5,/,6X,"RING ",
+ "ROTATION = ",10X,E15.5,/,6X, "MAX CIR BENDING STRESS = ",E15.5,/)
95  CONTINUE
      RETURN
      END

```

```

C   *****
C

```

```

      SUBROUTINE ALEAK(RCI,A,GAP)
C   CALCULATES NET FLOW AREA AVAILABLE ACROSS A DIAMETRAL LINE
      DIMENSION GAP(20)
      H= .1*A
      SUM = 0.
      DO 10 I=2,8,2
10  SUM = SUM +4.*GAP(I)+2.*GAP(I+1)
      SUM = ((SUM+GAP(1)+GAP(11)+4.*GAP(10))*H/3.) +GAP(11)*(RCI-A)*.5
      SUM = SUM*2.
100 WRITE(6,100) SUM
      FORMAT(1H0,6X,".....DIAMETRAL LEAK AREA.....",E15.5)
      RETURN
      END

```

```

C   *****
C

```

```

      SUBROUTINE SERIES(X,NTERM)
      EXTERNAL ASUM,FCTL
      DIMENSION C(4,50) , R(4)
      COMMON/ONE/S1,S2,S3,S4,S5,S6,S7,S8
      COMMON/TWO/SI1,DSI1,SI2,DSI2,SI3,DSI3,SI4,DSI4
      PII= .392699
      IF(X .GT. 6.) GO TO 400
      XP= .5*X
      CALL BESSEL(X,BERO,BE1,BE10,BE11)
C   EVALUATE R FUNCTIONS
      DO 10 I=1,4
      R(I) = 0.
      DO 10 J=1,NTERM
10  C(I,J) =0.0
      DO 100 J=1,NTERM,2
      M=J-1
      FS= FCTL(2*M+1)
      FSS = FCTL(2*M+2)
      C(1,J) = (ASUM(2*M+1) -XP**4 *ASUM(2*M+3) )/((2*M+3)
1 * (2*M+2)**2)*(XP**(2*M+1)/FS)**2
      C(2,J) = (ASUM(2*M+2) -XP**4*ASUM(2*M+4) /

```

```

1 ((2*M+4) *(2*M+3)**2) *(XP**(2*M+2)/FSS)**2
  C(3,J) = ((ASUM(2*M+1) *(2*M+1)) - ASUM(2*M+3) *XP**4
1 /((2*M+3) *(2*M+2) **2) *(XP**(2*M+.5)/FS)**2
  C(4,J) = ((ASUM(2*M+2) *(2*M+2)) -ASUM(2*M+4)*XP**4
1 /((2*M+4)*(2*M+3) **2) *(XP**(2*M+1.5)/FSS)**2
100 CONTINUE
  DO 200 I=1,4
  DO 200 J=1,NTERM,2
200 R(I) = R(I) +C(I,J)
  S13= .5*BERO - .6366197*(R(1) -ALOG(XP*1.78108) *BEIO)
  S14 = -.5*BEIO + .6366197*(R(2) + ALOG(XP*1.78108)*BERO)
  DSI3 = .5*BER1 -.6366197 *(R(3) -BEI1*ALOG(XP*1.78108) -(BEIO/X ))
  DSI4 = -.5*BEI1 + .6366197 *(R(4) + BER1 *ALOG(1.78108*XP)
1 +(BERO/X))
  S11 = BERO
  DSI1 = BER1
  SI2 = -BEIO
  DSI2 =-BEI1
  GO TO 450
400 XS= .7071067*X
  FAC= 1./SQRT (6.283185 *X)
  ES= EXP(XS)
  ESI= EXP(-XS)
  S11 = FAC*ES*COS(XS-PII)
  SI2 =-FAC*ES*SIN(XS-PII)
  DSI1 = FAC*ES*COS(XS+PII)
  DSI2 = -FAC*ES*SIN(XS+PII)
  SI3 = 2.*FAC*ESI*SIN(XS+PII)
  SI4 = -2.*FAC*ESI*COS(XS+PII)
  DSI3 = -2.*FAC*ESI*SIN(XS-PII)
  DSI4 = 2.*FAC*ESI*COS(XS-PII)
450 CONTINUE
  S1 = X*SI2 -2.*DSI1
  S2= X*S11+2.* DSI2
  S3= X*SI4-2.* DSI3
  S4= X*SI3+2.* DSI4
  S5 = X*X*DSI2 - 4*X*SI2 + 8*DSI1
  S6 = X*X*DSI1 - 4*X*S11 - 8*DSI2
  S7 = X*X*DSI4 - 4*X*SI4 + 8*DSI3
  S8 = X*X*DSI3 - 4*X*SI4 - 8*DSI4
  RETURN
  END

```

```

C *****
C

```

```

SUBROUTINE BESSEL(XP,BERO,BER1,BEIO,BEI1)
DIMENSION G(4),A(4),B(4),C(4)
EXTERNAL CALC
X=XP*.5
X4=X**4
F=1.0
DO 100 J=1,4

```

```
100 G(J)=0.0
```

```

      DO 200 I=1,51,2
      K=I-1
      CALL CALC(K,A,F)
      F=F*(2*K+1)*(2*I)
      CALL CALC(I,B,F)
      DO 300 J=1,4
      C(J) =(X4**K)*(A(J)-X4* B(J))
300 G(J)=G(J)+C(J)
      DO 301 J=1,4
301 C(J)=ABS(C(J)/G(J))
      IF (AMAX1(C(1),C(2),C(3),C(4)) .LT. .00001) GO TO 400
200 F=F*(2*I+1)*(2*I+2)
400 BERO=G(1)
      BER1=-G(2)*(X**3)
      BEIO=G(3)*X*X
      BEII=G(4)*X
      RETURN
      END
C *****
C
      SUBROUTINE CALC(K,A,F)
      DIMENSION A(4)
      A(1)=1.0/(F*F)
      A(2) = 2.*(K+1)/ ((F*(2*K+1)*(2*K+2))**2 )
      A(3)=1.0/ ((F*(2*K+1))**2)
      A(4) =(2.* K+1)*A(3)
      RETURN
      END
C *****
      FUNCTION ASUM(N)
      ASUM =0.
      DO 10 I=1,N
10 ASUM = ASUM + 1./FLOAT(I)
      RETURN
      END
      FUNCTION FCTL(N)
C   COMPUTES FACTORIAL
      SUM = 1.0
      DO 10 I=1,N
10 SUM = SUM*I
      FCTL=SUM
      RETURN
      END

```

Note: Subroutine SIMQ used in this program is listed with program FLANGE in Chapter 3.

4.8.2 Two Flanges Bolted Together

Two flanges are often utilized to connect two piping runs. TRIEL can be used to compute the stress and deflection in these flanges by making the following provisions in the input data.

- (i) Input the geometric data for the two flanges by treating them as bonnet and shellside flanges, respectively.
- (ii) Set shell and tubeside pressures equal to the joint pressure.
- (iii) Specify the shellside and tubeside gasket effective widths equal to the joint gasket effective width. Specify their loading and unloading stiffness equal to twice the joint gasket loading and unloading stiffness, respectively.
- (iv) Set the tubesheet to be very thin (say, 0.1") and set the seating condition gap ϵ_0 large enough to simulate a raised face condition (no MTM condition).

Following the above procedure, the stress field in bolted raised face hubbed flanges can be found using computer program "TRIEL".

4.8.3 Other Applications

"TRIEL" can be used to analyze a bolted joint consisting of a flat cover and a welding neck flange. The appropriate input data provision to simulate such joints is described in Section 12.8.

Ring flanges wherein the flange ring is welded to the shell (Fig. 3.2.1.a), are a special case of tapered hub flanges with the hub slope $\alpha = 0$. To avoid computational difficulties, slope should be input as a very small quantity (say, $\alpha = 0.01$).

In the next chapter, the three element bolted joint is analyzed for the more general case of gaskets which are too wide to be modelled as narrow rings. In particular, the condition of full face gaskets with or without compression stops is treated. The gaskets are allowed to have non-linear loading and unloading properties. The gasket compression and decompression history is followed using an incremental technique. The solution process sacrifices speed for the ability to predict the entire gasket deformation history.

NOMENCLATURE

- a = Tubesheet interface radius
- a_i' = Mean radius of ($i = 1$, channel side; $1 = 2$, shell side)
- A_b = Root area of body bolts
- a^* = Mean radius of tubesheet rim
- A_L = Diametral leakage area, square inch
- A_L' = Leakage area under a pass partition plate
- B' = Bolt load per unit circumference

- b = Outer radius of the tubesheet and flanges
 b_i' = Width of channel ($i = 1$), and shell flange ($i = 2$) rings
 c_i = Radial distance between bolt centerline and gasket reaction line ($i = 1$), channel flange; ($i = 2$, shell flange)
 C_c = Jet area ratio
 D_i = Flexural rigidity of channel ($i = 1$), and shell ($i = 2$)
 d_i = Radial distance between bolt centerline and hub centerline at large end ($i = 1$, channel flange; $i = 2$, shell flange)
 E_1 = Equivalent Young's modulus of perforated tubesheet region
 E_2 = Young's modulus of tubesheet material
 E_i' = Young's modulus of channel ($i = 1$), and shell material ($i = 2$)
 E_b = Young's modulus of bolt material
 f_F = Fanning Friction factor
 f_i = Flange thickness ($i = 1$), channel; $i = 2$, shell)
 F_1 = Channel gasket surface pressure resultant
 F_2 = Shell gasket surface pressure resultant
 F_e = Edge contact load per unit circumference between the channel flange and tubesheet
 h_p = Ligament width
 h = Width of tubesheet untubed rim
 K = Joint stiffness
 K_b = Bolt stiffness
 k' = Stress multiplier
 K_c = Contraction loss coefficient
 K_d = Momentum distribution coefficient
 K_e = Expansion loss coefficient
 L = Pass partition plate thickness
 l_0 = Bolt length under prestress (unpressurized condition)
 m = Gasket factor
 M_0 = Radial bending moment at tubesheet interface radius a
 $M_{r\max}$ = Maximum radial bending moment in tubesheet
 M_{ext} = External ring moment (Eq. 4.4.2)
 M_h = Maximum longitudinal moment in the flange hub
 n = Number of bolts
 P = Tube layout pitch
 p = Net pressure on the tubesheet ($p = p_1 - p_2$)
 p_1 = Channel side pressure
 p_2 = Shell side pressure
 Q_0 = Shear force per unit circumference at the interface between the rim and the perforated interior (Eq. (4.3.6))
 R_e = Reynolds number
 r_1 = Effective channel gasket radius ($r_1 = r_b - c_1$)
 r_2 = Effective shell gasket radius ($r_2 = r_b - c_2$)
 r_b = Bolt circle radius
 r_{\max} = Radius of the outermost tube hole center in the tubesheet

- s = Term representing the cumulative contribution of machining of the bolted joint elements
 s_1 = Term representing the total contribution of machining of the channel flange-tubesheet mating surfaces
 t_i = Thickness of channel ($i = 1$) or shell ($i = 2$)
 t_s = Thickness of the tubesheet
 V_L = Leakage velocity
 $w(r)$ = Deflection of tubesheet with respect to $r = r_1$
 x_1, x_2 = Distance of small and large end of the hub from the point of zero thickness
 y = ASME Code gasket seating stress
 α = Slope of flange hub
 δ_i = Thickness of gasket ($i = 1$ channel side, $i = 2$, shell side)
 $\delta(r)$ = Thickness of channel gasket rib at radius r
 ΔP = Tubeside pressure drop across the pass partition lane
 ϵ_0 = Initial edge gap
 ϵ_1 = Edge gap between channel flange and tubesheet under pressurized condition
 $\phi(r)$ = Gasket spring-back at radius r
 η = Ligament efficiency
 μ = Tubeside fluid viscosity
 ν_1 = Poisson's ratio of perforated tubesheet region
 ν_2 = Poisson's ratio of tubesheet material
 ν_i' = Poisson's ratio of shell and channel materials, respectively ($i = 1, 2$)
 θ_i = Rotation of channel flange ring ($i = 1$) and shell flange ring ($i = 2$), respectively
 θ_s = Rotation of tubesheet rim
 ρ = Density of tubeside fluid
 σ = Service bolt stress
 σ_0 = Prestress (seating stress) in bolts
 σ_i = Maximum bending stress in the perforated plate
 σ_r = Flange ring bending stress
 $\zeta(r)$ = Gap at radius r

REFERENCES

- [4.1.1] "Standards of Tubular Manufacturers Association," 6th ed., TEMA, New York (1978).
 [4.1.2] "ASME Boiler and Pressure Vessel Code, Section VIII, Div. I, Appendix 2, The American Society of Mechanical Engineers, New York (1983).
 [4.1.3] Tinker, T. 1951. "Shell Side Characteristics of Shell and Tube Heat Exchangers". In *General Discussion of Heat Transfer*, Institute of Mechanical Engineers and ASME, pp. 97-116, London, England.

- [4.1.4] Taborek, J., "Design Methods for Heat Transfer Equipment – A Critical Survey of the State-of-Art," In *Heat Exchangers: Design and Theory Sourcebook*, Afgan, N., and Schlünder, E.V., eds., Scripta Book Company, pp. 45–74, Washington, D.C. (1974).
- [4.1.5] Singh, K. P., and Holtz, M., "A Method to Design Shell-side Pressure Drop Constrained Tubular Heat Exchangers," *Trans. ASME, Journal of Engineering for Power*, Vol. 99, Series A, No. 3, pp. 441–448 (1977).
- [4.2.1] Stevens-Guille, P. D., and Crago, W. A., "Application of Spiral Wound Gaskets for Leak-Tight Joints," *Journal of Pressure Vessel Technology*, *Trans. ASME*, Vol. 97, Series J, No. 1, pp. 29–33 Feb. 1975. See also Discussion by Singh, K. P., *Journal of Pressure Vessel Technology*, *Trans. ASME*, Vol. 98, Series J, No. 1, pp. 81–83 (Feb. 1976).
- [4.3.1] Slot, T., and O'Donnel, W. J., "Effective Elastic Constants for Thick Perforated Plates with Square and Triangular Penetration Patterns," *Pressure Vessel and Piping: Design and Analysis*, Vol. 2, ASME, pp. 1081–1101 (1972).
- [4.3.2] Sampson, R. C., "Photoelastic Analysis of Stresses in Perforated Material Subject to Tension or Bending," *Bettis Technical Review*, WAPD-BT-18 (April 1960).
- [4.3.3.] Soler, A. I., and Hill, W. S., "Effective Bending Properties for Stress Analysis of Rectangular Tubesheets," *Trans. ASME, Journal of Engineering for Power*, Vol. 99, No. 3, pp. 365–370 (July 1977).
- [4.3.4] Gardner, K. A., "Heat Exchanger Tubesheet Design – III U-Tube and Bayonet Tubesheets," *Journal of Applied Mechanics*, *Trans. ASME*, Vol. 27, No. 82, pp. 25–32 (1960).
- [4.6.1] Carnahan, B., Luther, H. A., and Wilkes, D. O., *Applied Numerical Methods*, pp. 71–75, New York, Wiley (1969).
- [4.6.2] Kays, W. M., 1950. "Loss Coefficients for Abrupt Changes in Flow Cross Section with Low Reynolds Number Flow in Single and Multiple Tube Systems," *Trans. ASME*, Vol. 72, pp. 1067–1074 (1950).
- [4.7.1] Singh, K. P., "Study of Bolted Joint Integrity and Inter-Tube-Pass Leakage in U-tube Heat Exchangers; Part II: Applications," *Trans. ASME, Journal of Engineering for Power*, Vol. 101, No. 1, pp. 9–15 (1979).
- [4.7.2] Singh, K. P., "Study of Bolted Joint Integrity and Inter-Tube-Pass Leakage in U-Tube Heat Exchangers: Part I: Analysis," *Trans. ASME, Journal of Engineering for Power*, Vol. 101, No. 1, pp. 16–22 (1979).

5. BOLTED JOINTS WITH FULL FACE GASKETS

5.1 INTRODUCTION

In the preceding two chapters, several topics concerned with flanges have been discussed. The previous analyses have considered the gasket as a lineal element located at a particular radial position. For the most part, the effect of non-linear gasket material behavior has been neglected in all previous analyses. This chapter focuses on development of an analysis method which can be applied to flanges with either full face gaskets or ring type gaskets. The proposed method also permits inclusion of non-linear gasket material behavior. The procedure assumes use of a computer to effect the solution; as such, the method may not be directly suitable for inclusion in any design code that is intended to supply simple formulas for the designer's use. However, we will show that it certainly has value as a design tool.

We have already noted that proper design of a flanged joint is not complete unless both structural integrity and joint leak tightness are assured. Most analyses used in practice tend to emphasize structural integrity (joint components are designed to experience preload and service stress levels below some specified value). It is generally inferred that maintenance of some preset stress level assures a leak-tight joint; however, there is no guaranteed relationship between flange stress level, bolt preload, and leak tightness since gasket material characteristics have an important effect. For example, we can demonstrate that a correct characterization of gasket material behavior is essential to the correct characterization of a bolted joint having full face gaskets.

In the previous chapter, the complete analysis of a circular flange with ring gasket-tubesheet-bolted joint connection was considered and we demonstrated how to predict service stresses in the various components as well as to predict deformations and residual pressure in the gasket region. A simplified ring type gasket model was adopted which modeled the gasket as a piecewise linear elastic spring with different spring rates for loading and unloading. We also assumed that the ring type gasket pressure force acted at a known, constant location on the flange.

This chapter focuses on a bolted flange joint sealed by either a full face gasket or a ring type gasket having a general non-linear loading and unloading behavior. We note that full face gaskets find their application in large, low pressure units with one of the most widely used applications in the rectangular shaped water box-tubesheet-condenser connection in power plants. A theory is developed for a three element joint connection having

two flanges and a spacer, together with a bolt and two gaskets with non-linear material behavior. Figure 5.1.1 shows the typical configuration studied; the bolted joint is sealed by full face gaskets having nonlinear material characteristics.

5.2 GENERAL EQUATIONS

In this section, we focus on the general analysis and algebra necessary to develop an approximate method of analyzing the joints in question. We discuss configurations of circular plan form common to large commercial heat exchangers; the formulation is, however, directly applicable to power plant condenser configurations of rectangular plan form. Figure 5.2.1 shows the overall geometry of one of the elements between two bolt locations. The flange section is assumed to be an annular section extending over the radial region $-a \leq x \leq b$.

Loading and geometric symmetry permits focusing only on the portion of the joint between two bolt holes. The gasket between any two elements is a thin nonlinear elastic layer; for the purposes of this simulation the gaskets are modelled as discrete springs with strain dependent spring rates. For full face gaskets, the discrete non-linear springs are positioned at known locations within the annular plate segment; for ring type gaskets, the discrete non-linear springs are concentrated near the desired radial location. The springs are positioned radially to model the compression behavior of a specified area of the gaskets between two bolt holes.

Because of the non-linear character of the gaskets, an incremental formulation for simulation of loading and unloading is suggested. In the following description, certain approximations to reduce algebraic complexity are introduced:

1. Circumferential variations of flange displacement and loading between bolt holes are neglected.
2. Only large diameter flanges are modelled such that $a + b \ll R_b$. R_b is the bolt circle radius.
3. The flange is modelled using ring theory.
4. In-plane (radial) movements are neglected.

The foregoing assumptions provide sufficient accuracy for design work; they may easily be lifted at the expense of formulation and computational complexity.

The complication in analyzing flanged joints accounting for a finite width gasket (having width comparable to the flange radial width L) stems from the non-linear loading, unloading, and reloading characteristics of the gasket material. When such a joint is pressurized, the separation and rotation of the flange rings produces wide variation in the distribution of the gasket surface pressure in the radial direction. Indeed, as the joint internal pressure is increased, one portion of the gasket may be loading (rising surface pressure) while another portion is unloading. The loading and

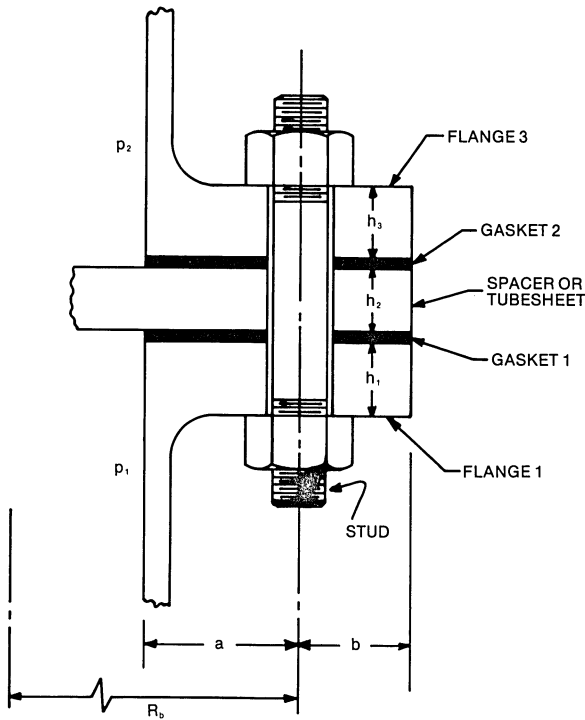


Fig. 5.1.1. Bolted joint with full face gaskets.

unloading of portions of the gasket may undergo several reversals as the joint pressure is increased. Different loading, unloading, and reloading gasket moduli require that the stress and deformation behavior of the joint be followed in a step-by-step manner as the joint is pre-loaded and then pressurized. This step-by-step analysis of the joint is the easiest way to keep track of the extent of the different loading and unloading regions of the gasket. The step-by-step solution method is also described as an “incremental” procedure.

The study of the joint behavior begins from the unstressed state. As the bolts are tightened (seating condition), the variations in the gasket surface compression and pressure distribution, and the flange and tubesheet rim rotation (in a three element joint) are computed for small increments of bolt pre-tension. At the end of the bolt pre-loading step, the deformation of the joint is thus completely characterized. Similarly, the process of joint pressurization is assumed to occur in an incremental manner. The variations in the gasket pressure distributions, and the kinematics of the joint elements are charted by computing the joint response for small increments of pressure rise. Therefore, it is natural to think in terms of stress and strain rates in formulating the governing equations. The required equations to

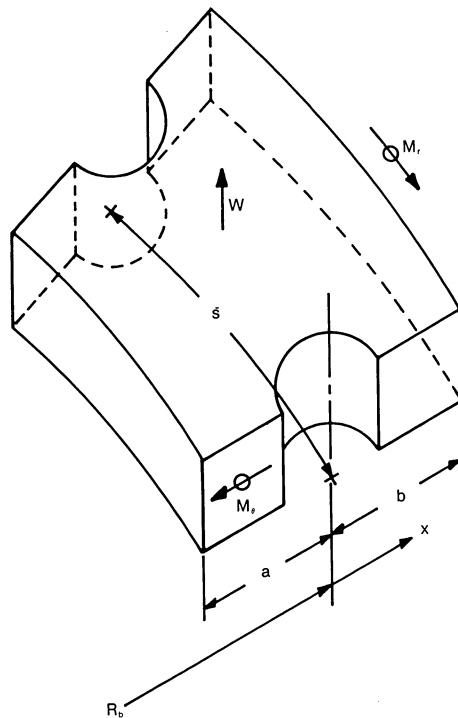


Fig. 5.2.1. Geometry of joint element between bolt holes showing positive directions of bending moments and displacements.

characterize the joint response can be written directly from equilibrium considerations of each element. It is, however, more convenient to utilize the principle of Minimum Potential Energy which has also been used in Section 3.11 to develop the tapered hub load-deformation equations. The potential energy of the flanged joint in Fig. 5.2.2 is defined as the sum of the strain energy of its flanges, tubesheet (if present), bolt, and gaskets, less the product of the external loads and their associated movements. The Theorem of Minimum Potential Energy states that of all candidate deformation states, consistent with the boundary and compatibility conditions in the joint, the one state which makes the potential energy a minimum will produce a stress field in equilibrium with the external loads. The external loads in the flanged joint are the bending moments and shear forces on the inner edge of the elements due to the presence of the remainder of the structure not modelled; e.g. the tubesheet interior to the middle element, or the shell or channel connected to the flanges.

The governing incremental equations for analyses are obtained by application of the Theorem of Minimum Potential Energy applied to the rate deformation variables of the problem. Since the problem being considered

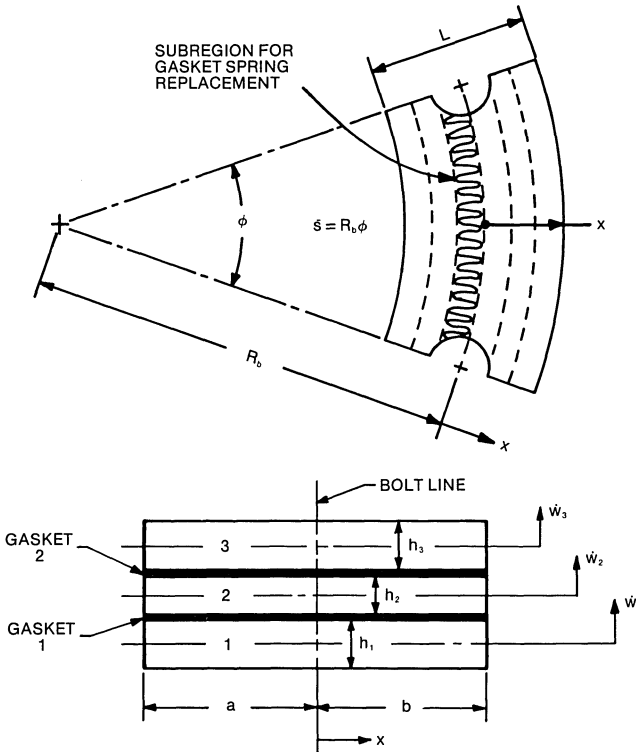


Fig. 5.2.2. Model of three element bolted joint.

assumes non-linearity only in the stress strain behavior of the gaskets, it is easily demonstrated that a deformation based variational principle carries directly over to a variational principle for incremental changes. Considering the three layer joint shown in Fig. 5.2.2, the following variational equation can be employed to obtain the equations governing incremental behavior of the joint.

$$\sum_{i=1}^3 \delta \bar{E}_i + \sum_{j=1}^2 \delta \bar{U}_j + \delta \bar{U}_b = \delta \bar{W}_e \tag{5.2.1}$$

In Eq. (5.2.1), δ is the variational operator.

It is not our intent to digress here on the theoretical foundations of the applications of energy principles to structural mechanics problems. For the interested reader, Refs. [5.2.1, 5.2.2] contain excellent presentations of variational principles in mechanics, and of application of these principles in incremental form. For our purposes in this chapter, we simply state that correct application of the variational principle results in balance of the rate of working of the internal incremental forces, with the rate of working of

the external forces applied to the joint. At this point, we accept Eq. (5.2.1) as a valid equation and proceed to develop an approximate analysis technique. The intent of our presentation here is to show that by starting from the energy principle and by making certain assumptions on the flange deformation pattern, we can evolve a set of linear algebraic equations to solve for the flange deformation parameters during each increment of loading and unloading. With the flange deformation pattern determined at all "times" during the cycle, it becomes a straightforward exercise to check gasket leakage, bolt load, and flange stress at all "times". Since the intent here is to develop a method which relies on machine computation, there is no need to pursue algebraic simplifications; we will show that the approximate analysis results in five linear algebraic equations, valid at each increment of the loading or unloading process, which are solvable on the computer for five unknown flange deformation parameters. The non-linear aspect of the problem is felt through the modification of the coefficients of these five equations at each stage in the process. This Section 5.2 develops the general equations. Section 5.3 provides a discussion of the simulation of non-linear gasket stress strain relations, while Sections 5.4 and 5.5 discuss bolt modelling and flange stress calculations. Section 5.6 presents some application of the modelling and analysis procedure to a typical configuration.

\bar{E}_i in Eq. (5.2.1), ($i=1,2,3$) represent incremental energy contributions from each elastic element (flanges or spacer), written in terms of incremental displacement variables. \bar{U}_j ($j=1,2$) are energy contributions from the discrete springs modelling the non-linear gaskets; \bar{U}_b is the incremental bolt strain energy, and \bar{W}_e is the incremental external work done by edge forces and internal pressure. Although the flange deformation certainly varies with both radial position and location between bolt holes, only the average value from the analysis is sought; therefore, as noted previously, all deformation rates are assumed independent of circumferential position ϕ in Fig. 5.2.2. Therefore, we can represent the deformation rate, normal to the gasket plane, for each flange or spacer, as

$$\dot{w}_i(x, \phi) = \dot{U}_i(x) \quad i=1,2,3 \quad (5.2.2)$$

We assume that the flange and spacer deformation rates are in the form

$$\dot{U}_i(x) = \dot{W}_i + f_i \dot{\theta}_i \quad (5.2.3)$$

where:

$$f_i(x) = (x+a) \quad (5.2.4)$$

The above choice for the deformation rates implies that \dot{W}_i is the lateral deformation rate of the i th element at $x = -a$, and $\dot{\theta}_i$ are the element cross section rotation rates at $x = -a$. Equations (5.2.3), (5.2.4) reflect our ring theory assumption that the flange cross section rotates like a rigid body.

Without loss of generality, we may fix one point in the joint assembly and measure all deformation relative to that point. We choose to fix the interior edge of element 2 against displacement so that

$$\dot{W}_2 = 0 \quad (5.2.5)$$

Thus, the deformation of the three element flanged joint is expressed in terms of the five quantities: $\dot{W}_1, \dot{\theta}_1$ for element one, $\dot{\theta}_2$ for element two, and $\dot{W}_3, \dot{\theta}_3$ for element three. These five unknowns will be concisely represented by the vector $\{\dot{Z}\}$ with elements $\dot{Z}_1 = \dot{W}_1, \dot{Z}_2 = \dot{\theta}_1, \dot{Z}_3 = \dot{\theta}_2, \dot{Z}_4 = \dot{W}_3,$ and $\dot{Z}_5 = \dot{\theta}_3.$

Assuming that all variations between bolt holes can be neglected, the incremental strain energy for the i th element of subtended angle ϕ is:

$$\bar{E}_i = \frac{D_i}{2} \int_{-a}^b \left\{ \left(\dot{U}_i'' + \frac{\dot{U}_i'}{R_b} \right)^2 - \frac{2(1-\nu)}{R_b} \dot{U}_i'' \dot{U}_i' \right\} dx \quad (5.2.6)$$

where

$$D_i = \frac{E\bar{s}h_i^2}{12(1-\nu_i^2)} \quad \dot{U}_i' = \frac{d\dot{U}_i}{dx}$$

Note that in our case, the ring theory assumption eliminates contributions from all but the second term in Eq. (5.2.6). \bar{s} is the circumferential arc length between adjacent bolt centers.

Referring to Fig. 5.2.2, we assume that the gaskets are subdivided into N annular subregions having plan-form area approximately $\bar{s}(1 + x/R_b)$ $(a + b)/N$. The loading and unloading behavior of the subregions of each gasket is characterized by a discrete spring with spring rate $K_m^{(i)}$ ($i = 1, 2$). Then the total contribution to Eq. (5.2.1) from the ensemble of gasket springs is:

$$\sum_{j=1}^2 \bar{U}_j = \sum_{m=1}^N \left\{ \frac{K_m^{(1)}}{2} [\dot{U}_2(x_m) - \dot{U}_1(x_m)]^2 + \frac{K_m^{(2)}}{2} [\dot{U}_3(x_m) - \dot{U}_2(x_m)]^2 \right\} \quad (5.2.7)$$

The spring rates $K_m^{(i)}$ are specified non-linear functions of the current gasket strain which represents the behavior of the particular gasket material.

The spring rates of the bolt in extension and bending are denoted as $K_b, K_\theta,$ respectively; the contribution from the bolts in Eq. (5.2.1) becomes:

$$\bar{U}_b = \frac{K_b}{2} [\dot{U}_3(0) - \dot{U}_1(0) + \Delta]^2 + \frac{K_\theta}{2} [\dot{U}_3'(0) - \dot{U}_1'(0)]^2 \quad (5.2.8)$$

Note that in Eq. (5.2.8) we assume that the bolt strain is explicitly dependent only on the characteristics of the two flanges and on the initial preload parameter Δ of the bolt. In the case of a two element joint $\dot{U}_3 \rightarrow \dot{U}_2.$

Finally, contributions to $\delta\dot{W}_e$ in Eq. (5.2.1) are considered. Since the flanges are attached to a shell and channel in the usual structural configuration, and since the intermediate element may represent a tubesheet, the free body being analyzed (Fig. 5.2.2) requires consideration of external shear and moment rates applied at the boundary edges $x = -a,$ as shown in

Fig. 5.2.3. If \dot{V}_i^* , \dot{M}_i^* , are the external rates, with units of force/length and force-length/length, respectively, then for $i = 1, 2, 3$:

$$\begin{aligned}\dot{V}_i^* &= C_{11}^{(i)} \dot{W}_i + C_{12}^{(i)} \dot{\theta}_i + C_{13}^{(i)} \dot{p}_i \\ \dot{M}_i^* &= C_{21}^{(i)} \dot{W}_i + C_{22}^{(i)} \dot{\theta}_i + C_{23}^{(i)} \dot{p}_i\end{aligned}\quad (5.2.9)$$

Note that because of our choice of reference point for measurement of deformation (recall Eq. (5.2.5)), $C_{11}^{(2)}$ will not enter into any subsequent analyses. Also, for element 2, the last terms are replaced by $C_{13}^{(2)} (\dot{p}_1 - \dot{p}_2)$, $C_{23}^{(2)} (\dot{p}_1 - \dot{p}_2)$, respectively. For element 3, $\dot{p}_3 = \dot{p}_2$.

In keeping with earlier assumptions, boundary loads are assumed to depend only on the average displacement and rotation. The term involving \dot{p}_i gives the contribution of any explicit dependence of the boundary forces on the local pressure rates.

The contribution of the term $\delta \bar{W}_e$ in Eq. (5.2.1) can now be written as follows:

$$\delta \bar{W}_e = \bar{s}(1 - a/R_b) \sum_{i=1}^3 (\dot{V}_i^* \delta \dot{W}_i + \dot{M}_i^* \delta \dot{\theta}_i) \quad (5.2.10)$$

The above general expressions for the various incremental terms are substituted into Eq. (5.2.1) with the form of $U_i(x)$ given by Eq. (5.2.2) used to explicitly evaluate the terms. For example,

$$\bar{E}_1 = \frac{D_1}{2} \int_{-a}^b (\dot{U}'_1/R_b)^2 dx = \frac{D_1}{2R_b^2} \dot{\theta}_1^2 L \quad (5.2.11)$$

so that

$$\delta \bar{E}_1 = D_1 \frac{L}{R_b^2} \dot{\theta}_1 \delta \dot{\theta}_1 \quad (5.2.12)$$

The contribution of the bolt strain energy increment is likewise computed as

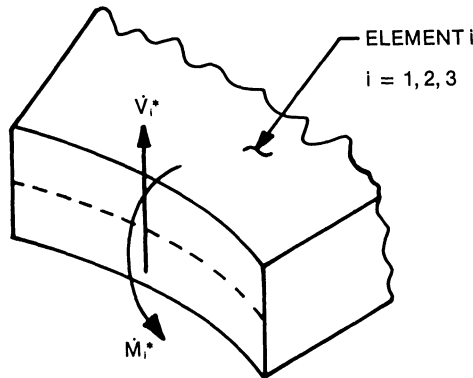


Fig. 5.2.3. Edge loading on element at $x = -a$.

$$\delta\bar{U}_b = K_b[\dot{W}_3 - \dot{W}_1 + a(\dot{\theta}_3 - \dot{\theta}_1) + \dot{\Delta}] \delta[\dot{W}_3 - \dot{W}_1 + a(\dot{\theta}_3 - \dot{\theta}_1)] \\ + K_\theta[\dot{\theta}_3 - \dot{\theta}_1] \delta[\dot{\theta}_3 - \dot{\theta}_1] \quad (5.2.13)$$

which can be rewritten in the form

$$\delta\bar{U}_b = \{K_b(\dot{W}_3 - \dot{W}_1 + a(\dot{\theta}_3 - \dot{\theta}_1) + \dot{\Delta})\} \delta\dot{W}_3 - \{K_b(\dot{W}_3 - \dot{W}_1 + a(\dot{\theta}_3 - \dot{\theta}_1) \\ + \dot{\Delta})\} \delta\dot{W}_1 + \{K_\theta(\dot{\theta}_3 - \dot{\theta}_1) + aK_b(\dot{W}_3 - \dot{W}_1 + a(\dot{\theta}_3 - \dot{\theta}_1) + \dot{\Delta})\} \delta\dot{\theta}_3 \\ - \{K_\theta(\dot{\theta}_3 - \dot{\theta}_1) + aK_b(\dot{W}_3 - \dot{W}_1 + a(\dot{\theta}_3 - \dot{\theta}_1) + \dot{\Delta})\} \delta\dot{\theta}_1 \quad (5.2.14)$$

or finally, as

$$\delta\bar{U}_b = \{K_b \dot{W}_1 + aK_b \dot{\theta}_1 - K_b \dot{W}_3 - aK_b \dot{\theta}_3 - K_b \dot{\Delta}\} \delta\dot{W}_1 \\ + \{aK_b \dot{W}_1 + (K_\theta + a^2 K_b) \dot{\theta}_1 - aK_b \dot{W}_3 - (K_\theta + a^2 K_b) \dot{\theta}_3 - aK_b \dot{\Delta}\} \delta\dot{\theta}_1 \\ + \{-K_b \dot{W}_1 - aK_b \dot{\theta}_1 + K_b \dot{W}_3 + aK_b \dot{\theta}_3 + K_b \dot{\Delta}\} \delta\dot{W}_3 \\ + \{-aK_b \dot{W}_1 - (K_\theta + a^2 K_b) \dot{\theta}_1 + aK_b \dot{W}_3 + (K_\theta + a^2 K_b) \dot{\theta}_3 + aK_b \dot{\Delta}\} \delta\dot{\theta}_3 \quad (5.2.15)$$

Expressing the incremental contributions from each gasket spring, and from the edge loads V_i^* , M_i^* , in a similar form, we can collect all of the contributions and write Eq. (5.2.1) in the general form

$$X_1 \delta\dot{W}_1 + X_2 \delta\dot{\theta}_1 + X_3 \delta\dot{\theta}_2 + X_4 \delta\dot{W}_3 + X_5 \delta\dot{\theta}_3 = 0 \quad (5.2.16)$$

In the case of a two element joint, the gasket springs $K_m^{(2)} = 0$, \dot{W}_3 , $\dot{\theta}_3$ are set to zero, and edge loads V_3^* , M_3^* are neglected.

Since the variations $\delta\dot{Z}_j$ are independent, Eq. (5.2.16) requires that $X_j = 0$ for all j , leading to linear algebraic equations for the rate coefficients of Eq. (5.2.3) in the symbolic form:

$$[\bar{a}]\{\dot{Z}\} = \{\dot{B}\} \quad (5.2.17)$$

The terms in the stiffness matrix $[\bar{a}]$ are functions of the current configuration, and the number of unknowns \dot{Z} in Eq. (5.2.17) is given by the expression $NU = 2i - 1$ where i is the number of elements in the joint. Equation (5.2.17) may be solved to find the flange deformation as a function of applied loadings by incorporation of a suitable incremental integration scheme to determine the configuration state at "time" $t + \Delta t$ (knowing the configuration state at "time" t). The use of "time" here represents a means of counting the number of increments to be taken to describe a given load and deformation history. At each point in the incremental process, the elements of the stiffness matrix $[\bar{a}]$ and of the vector $\{\dot{B}\}$ are computed using current values of the deformation and load parameters; Eq. (5.2.17) can then be solved for $\{\dot{Z}\}$, the current rates. The determined values of $\{\dot{Z}\}$ lead directly to evaluation of the new configuration at time $t + \Delta t$. For the usual flange, the loading consists initially of a specified bolt displacement rate $\dot{\Delta}$ to impose a given bolt preload after a number of increments. (The number of increments chosen depends on the non-linear character of the gaskets. It is desirable to choose small enough

increments so that the loading curves for the gaskets are accurately followed.) At the same time, the gasket springs acquire, in an incremental manner, compressive loading dependent on joint geometry. The second stage of the loading process imposes appropriate pressure increments on the various components, while holding the initial bolt preload constant until desired operating conditions are obtained, or until "failure" of a component occurs.

The expanded form of Eq. (5.2.17) is, for $i = 1, 2, \dots, 5$

$$\sum_{j=1}^5 \bar{a}_{ij} \dot{Z}_j = \dot{B}_i \quad (5.2.18)$$

where

$$Z_1 = W_1, Z_2 = \theta_1, Z_3 = \theta_2, Z_4 = W_3, Z_5 = \theta_3, \text{ and } a_{ij} = a_{ji}.$$

If we let $\bar{C}_{ij} = \bar{s}(1 - a/R_b)C_{ij}$, then the elements a_{ij} , \dot{B}_i are:

$$\begin{aligned} \bar{a}_{11} &= K_b + \Sigma K_m^{(1)} - \bar{C}_{11}^{(1)}; \quad \bar{a}_{12} = aK_b + \Sigma(x_m + a)K_m^{(1)} - \bar{C}_{12}^{(1)} \\ \bar{a}_{13} &= -\Sigma(x_m + a)K_m^{(1)} - \mu_2 aK_b; \quad \bar{a}_{14} = \mu_3 K_b \end{aligned} \quad (5.2.19)$$

$$\begin{aligned} \bar{a}_{15} &= -\mu_3 aK_b; \quad \dot{B}_1 = \dot{p}_1 \bar{C}_{13}^{(1)} + K_b \dot{\Delta} \\ \bar{a}_{22} &= D_1 L/R_b^2 - \bar{C}_{22}^{(1)} + K_\theta + a^2 K_b + \Sigma(x_m + a)^2 K_m^{(1)} \\ \bar{a}_{23} &= -\mu_2 (K_\theta + aK_b) - \Sigma(x_m + a)^2 K_m^{(1)} \end{aligned} \quad (5.2.20)$$

$$\begin{aligned} \bar{a}_{24} &= -\mu_3 aK_b; \quad \bar{a}_{25} = -\mu_3 (K_\theta + a^2 K_b) \\ \dot{B}_2 &= \dot{p}_1 \bar{C}_{23}^{(1)} + aK_b \dot{\Delta} \\ \bar{a}_{33} &= D_2 L/R_b^2 - \bar{C}_{22}^{(2)} + \mu_2 (K_\theta + a^2 K_b) + \Sigma(x_m + a)^2 (K_m^{(1)} + K_m^{(2)}) \\ \bar{a}_{34} &= -\Sigma(x_m + a)K_m^{(2)}; \quad \bar{a}_{35} = -\Sigma(x_m + a)^2 K_m^{(2)} \end{aligned} \quad (5.2.21)$$

$$\begin{aligned} \dot{B}_3 &= (\dot{p}_1 - \dot{p}_2) \bar{C}_{23}^{(2)} - \mu_2 aK_b \dot{\Delta} \\ \bar{a}_{44} &= \mu_3 K_b + \Sigma K_m^{(2)} - \bar{C}_{11}^{(3)} \\ \bar{a}_{45} &= \mu_3 aK_b + \Sigma(x_m + a)K_m^{(2)} - \bar{C}_{12}^{(3)} \end{aligned} \quad (5.2.22)$$

$$\begin{aligned} \dot{B}_4 &= \dot{p}_2 \bar{C}_{13}^{(3)} - \mu_3 K_b \dot{\Delta} \\ \bar{a}_{55} &= D_3 L/R_b^2 - \bar{C}_{22}^{(3)} + \mu_3 (K_\theta + a^2 K_b) + \Sigma(x_m + a)^2 K_m^{(2)} \\ \dot{B}_5 &= \dot{p}_2 \bar{C}_{23}^{(3)} - \mu_3 aK_b \dot{\Delta} \end{aligned} \quad (5.2.23)$$

In the above equations for a three element joint, $\mu_2 = 0$, $\mu_3 = 1$. For a two element joint, $\dot{p}_2 = 0$, $K_m^{(2)} = 0$, $\mu_2 = 1$, $\mu_3 = 0$. The proper setting of these parameters has the effect of reducing the five equations to a solution of three non-trivial equations for \dot{W}_1 , $\dot{\theta}_1$, $\dot{\theta}_2$ in a two element joint, and the effect of properly attaching the bolt to either elements 1 and 3, or to elements 1 and 2.

We point out that the final Eqs. (5.2.18) simply reflect overall equilibrium requirements for the various elements of the joint. The first

equation is force equilibrium for element 1, while the second equation is simply the fulfillment of the moment equilibrium requirement for element 1. The third equation is the moment equilibrium equation for element 2, while the remaining two equations ensure satisfaction of force and moment equilibrium requirements for element 3. No force equation is necessary for element 2 since we have already ensured satisfaction of this condition by fixing one point of the element against any displacement.

5.3 NON-LINEAR ANALYTICAL EXPRESSIONS SIMULATING GASKET BEHAVIOR

The previous incremental solution procedure assumes that each gasket spring, representing compressive behavior of a local region of the annular gasket, be represented by an incremental force-deformation rate expression having the form,

$$\dot{F}_j^{(i)} = K_j^{(i)} \dot{\delta}_{ij} \quad (5.3.1)$$

where $\dot{F}_j^{(i)}$ is the rate of change of gasket spring force and $\dot{\delta}_{ij}$ is the rate of change of gasket spring length. The i superscript refers to the gasket, and the subscript is the particular sub-region. If the spring is to be nonlinear, the spring rate $K_j^{(i)}$ is a function of the current local deformation δ_{ij} . The necessary one-dimensional rate parameter $K_j^{(i)}$ is developed by starting with a general stress strain law and matching with gasket test data. We assume the form

$$\sigma = \sigma(\epsilon) \quad (5.3.2)$$

so that if ($\dot{\quad}$) represents an incremental change, then:

$$\dot{\sigma} = \frac{\partial \sigma}{\partial \epsilon} \dot{\epsilon} \quad (5.3.3)$$

Therefore, if $\dot{F} = \dot{\sigma} A$, where A is the gasket sub-region area, and $\dot{\epsilon} = \dot{\delta}/t_g$, then a spring rate parameter K is:

$$K = \frac{\partial \sigma}{\partial \epsilon} \frac{A}{t_g} \quad (5.3.4)$$

where t_g is the undeformed gasket thickness.

The explicit form of the functional relationship in Eq. (5.3.2) depends on the gasket material. In the following, we indicate a method to develop suitable analytical functional forms for a rubber or an asbestos gasket. To simulate any gasket behavior, one needs only to establish $\partial\sigma/\partial\epsilon$ as a function of current strain by fitting an analytical representation to specific experimental data. Figure 5.3.1. shows test results obtained by loading and unloading a sheet of a typical neoprene material (1/8", durometer 35-45). During a single load-unload cycle, it appears that Eq. (5.3.2) is nicely fit to the experimental results by an exponential function during loading and by two straight lines during unloading. The approach here is to establish

appropriate analytical formulations for $\partial\sigma/\partial\epsilon$ containing sufficient parameters to enable duplication of any experimental gasket data with the simple Eq. (5.3.2). To that end, during loading in Fig. 5.3.1, the following equations are used to model the stress strain behavior of the gasket

$$\sigma = E\epsilon; \quad \epsilon \leq \epsilon_1$$

$$\sigma = \sigma_0 e^{\epsilon/\epsilon_1}; \quad \epsilon \geq \epsilon_1; \quad \epsilon_1 = \frac{\sigma_0}{E} e; \quad e = 2.718 \quad (5.3.5)$$

The parameters σ_0, E are chosen to fit the experimental data during the initial portion of the loading curve. A single non-linear analytical expression capable of closely approximating the two nearly straight lines in $\sigma-\epsilon$ space is suggested to simulate unloading behavior in Fig. 5.3.1. If we assume that unloading begins from a specified state of stress and strain σ_f, ϵ_f ; then during unloading, we propose using the stress strain relation:

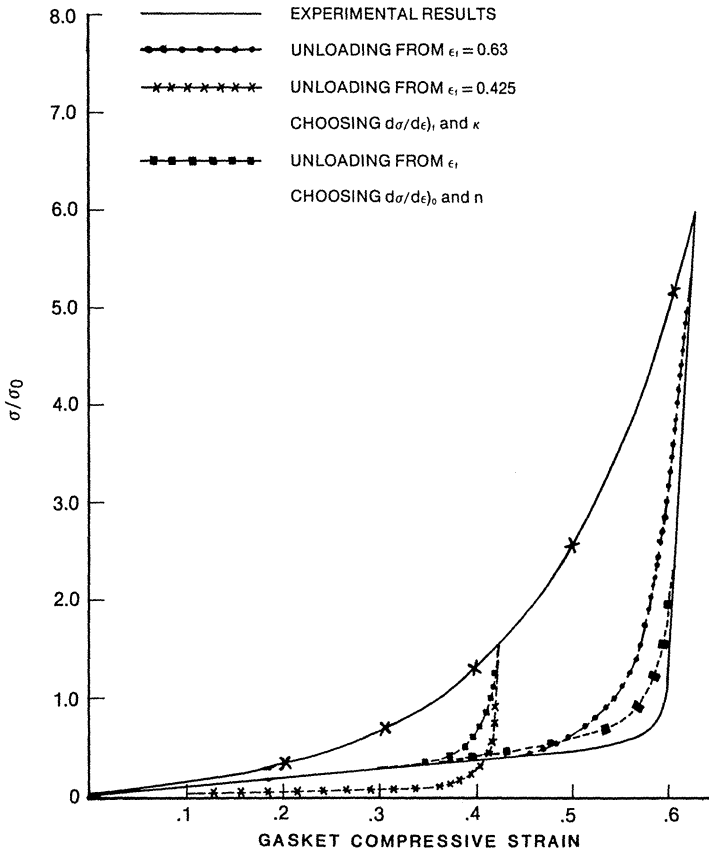


Fig. 5.3.1. Neoprene gasket stress strain relation (Experimental and Numerical Results).

$$\sigma = \frac{\sigma_f}{1 + \kappa} \left[\frac{\epsilon}{\epsilon_f} + \kappa \left(\frac{\epsilon}{\epsilon_f} \right)^n \right] \quad (5.3.6)$$

to simulate the gasket behavior. The stress strain curve slope during unloading is given as:

$$\frac{d\sigma}{d\epsilon} = \frac{\sigma_f}{\epsilon_f (1 + \kappa)} \left[1 + n\kappa \left(\frac{\epsilon}{\epsilon_f} \right)^{n-1} \right] \quad (5.3.7)$$

It remains to choose κ and n to fit the details of the particular unloading relationship. For example, we may directly match the data for:

$$d\sigma/d\epsilon)_{\epsilon \rightarrow 0}$$

by choosing the parameter κ to satisfy

$$\kappa = \frac{\sigma_f/\epsilon_f}{d\sigma/d\epsilon)_{\epsilon \rightarrow 0}} - 1 \quad (5.3.8)$$

The parameter n can then be chosen as a sufficiently large number to capture the details of the knee of the unloading stress strain data. Alternatively, evaluating Eq. (5.3.7) at the state σ_f, ϵ_f leads to an expression for n in terms of $\sigma_f, \epsilon_f, d\sigma/d\epsilon)_{\epsilon_f}$ and κ :

$$n = \frac{1}{\kappa} \left[\frac{d\sigma/d\epsilon)_{\epsilon_f} (1 + \kappa)}{\sigma_f/\epsilon_f} - 1 \right] \quad (5.3.9)$$

κ can be chosen from Eq. (5.3.8) or by attempting to match the stress level at the knee of the unloading curve using the approximate relationship

$$\sigma_{\text{knee}} \approx \sigma_f / (1 + \kappa) \quad (5.3.10)$$

The utility of any of the above approximations of course depends on the accuracy of fit to specific experimental data for gasket materials. It is likely that the above illustrative examples cannot reflect the gasket behavior during subsequent reloads. We should also note that many gasket materials indicate significant permanent set after a load cycle. The importance of the previous discussion is not to indicate that Eqs. (5.3.5)–(5.3.6) represent gasket behavior under all conditions; rather it is to indicate that it should always be possible to develop reasonably accurate models for the spring rate defined by Eq. (5.3.4) that reflect the important characteristics of the gasket behavior during the current load cycle. *This is extremely critical to the simulation of a joint with one or more full face gaskets, since during a single cycle at a given pressure, one portion of the gasket may be loading while another region may be experiencing unloading.*

To evaluate the calculation procedure for the gasket material whose behavior is reflected in Fig. 5.3.1, it is noted that the exponential behavior of the loading data of Fig. 5.3.1 is easily ascertained by a re-plot of the given data onto semi-log paper. An excellent fit of σ - ϵ data during loading above 100 psi is obtained using the exponential relationship:

$$\sigma = \sigma_0 e^{6.5\epsilon}; \quad \sigma_0 = 100 \text{ psi} \quad (5.3.11)$$

Then $\epsilon_1 = 0.154$ and

$$\sigma = E\epsilon; \quad E = 1765 \text{ psi for } \sigma \leq \sigma_0.$$

From the experimental data in Fig. 5.3.1, the unloading slope for small strain is estimated as:

$$d\sigma/d\epsilon)_{\epsilon \rightarrow 0} \cong 1091 \text{ psi} \quad (5.3.12)$$

If one considers unloading from the state $\sigma_f = 60 \sigma_0$, $\epsilon_f = 0.63$, then Eq. (5.3.8) yields $\kappa = 7.729$. If we choose $n = 30$, then the unloading stress strain curve given by Eq. (5.3.6) becomes:

$$\sigma = 687.36 \left[\frac{\epsilon}{0.63} + 7.729 \left(\frac{\epsilon}{0.63} \right)^{30} \right] \quad (5.3.13)$$

Figure 5.3.1. shows some simulation points computed using Eq. (5.3.13). The larger the value employed for n , the sharper the knee of the unloading curve becomes. However, the larger the value of n , the smaller the upper limit on increment step size becomes to retain good accuracy in any numerical solution. Using the same philosophy for choosing κ and examining unloading from the state $\sigma_f = 16\sigma_0$, $\epsilon_f = 0.425$, with $n = 30$ yields $\kappa = 2.451$ and the stress strain relation for unloading

$$\sigma = 463.68 \left[\frac{\epsilon}{0.425} + 2.451 \left(\frac{\epsilon}{0.425} \right)^{30} \right] \quad (5.3.14)$$

to be used for unloading from $\epsilon_f = 0.425$. Calculated points from Eq. (5.3.14) are also shown in Fig. 5.3.1.

Alternatively, one could choose $\kappa = 9$ based on an assumption of the ratio $\sigma_{\text{knee}}/\sigma_f$, and then evaluate n from Eq. (5.3.9). This avoids the need to evaluate $d\sigma/d\epsilon)_{\epsilon \rightarrow 0}$. Using the data from Fig. 5.3.1 and unloading from $\sigma_f = 60\sigma_0$, $\epsilon_f = 0.63$, then if one estimates the unloading slope at ϵ_f as:

$$d\sigma/d\epsilon)_{\epsilon = \epsilon_f} \cong 140,000 \text{ psi} \quad (5.3.15)$$

then Eq. (5.3.9) yields $n \approx 16.22$ and

$$\sigma = 600 \left[\frac{\epsilon}{0.63} + 9 \left(\frac{\epsilon}{0.63} \right)^{16.22} \right] \quad (5.3.16)$$

If unloading occurs from the point $\sigma_f = 16\sigma_0$, $\epsilon_f = 0.425$; then, using Eq. (5.3.15) for the unloading slope and $\kappa = 9$, Eq. (5.3.9) now gives $n \approx 41.21$ so that the stress strain relation becomes:

$$\sigma = 160 \left[\frac{\epsilon}{0.425} + 9 \left(\frac{\epsilon}{0.425} \right)^{41.21} \right] \quad (5.3.17)$$

Equations (5.3.16) and (5.3.17) are also shown on Fig. 5.3.1. For the data shown, the first approach for unloading seems to provide the best fit. The purpose of the above exercises simply illustrates that the choice of analytical representations for non-linear material behavior of the gaskets is certainly not unique. The analytical representation should reflect, in the simplest manner possible, the best efforts of the user to simulate the behavior of the real material as noted from the experimental data available. In any com-

puter simulation, the calculation of κ or n is done using the σ_f , ϵ_f results for each gasket spring when it begins to unload.

We must emphasize that the above relations give only variations on one suggested set of constitutive equations. Other gasket materials may require more complex representations to capture the essence of the non-linear behavior. *The key point, however, is that $\partial\sigma/\partial\epsilon$ is always obtained from experimental results and coded for computer modelling.*

To conclude this section, we note that an appropriate definition of gasket leakage at any location is

$$|F_m| \leq \bar{\mu} p A_m \quad (5.3.18)$$

where F_m is the current compressive gasket load in the discrete spring representing the gasket at location m , p is the current pressure (either p_1 or p_2), A_m is the gasket area at location m , and $\bar{\mu}$ is the gasket seating factor. For full face gaskets, we assume that joint failure due to leakage occurs when all gasket springs inboard of a specified location (either the bolt circle or the inboard edge of the bolt hole) satisfy Eq. (5.3.18). For a short, ring type gasket, inboard of the bolt circle, leakage occurs when all spring elements satisfy Eq. (5.3.18).

5.4 SIMULATION OF BOLT EFFECTS

The current stiffness matrix $[\bar{a}]$ needed to solve for the incremental deformation parameters at each stage in the unloading process, involves bolt spring rates K_b , K_θ (see Eq. (5.2.8)). The simplest idealization for the bolt in extension and bending suggests that if E_B , A_B , I_B , L_B are the Young's Modulus, bolt tensile area, bolt area moment of inertia, and effective bolt length, respectively, then K_b , K_θ have the form:

$$K_b = E_B A_B / L_B; \quad K_\theta = E_B I_B / L_B \quad (5.4.1)$$

As long as the bolt stress remains below yield, we consider that the above representation adequately models the effect of bolting on joint deformation behavior.

We note that many bolted flange joint analyses presume that the bolt acts only as a single tension-compression member, and that the bolt stress level remains essentially at its preload value during pressurization. In the analysis set forth in this chapter, the elementary effects of bolt bending are included; since this analysis is incremental in nature, the opportunity to examine effects of bolt overstress on integrity of the entire bolted joint configuration is provided. What is proposed in the following is a rudimentary simulation of overstress effects; by its very simplicity, however, it clearly demonstrates the weakening of the joint caused by bolt overstress. The representation of bolt overstress is based on the concept that as yielding of the bolt occurs (due to combined axial force and bending moment), the values for K_b , K_θ should be reduced from their initial elastic values given by Eq. (5.4.1). For the purposes of this model, we formulate a parameter α , a function of the

Equation (5.4.2) leads directly to the conclusion that in accordance with these assumptions, the spring rates should vanish when $\alpha = -0.412 M/M_y$. This completes the justification for Fig. 5.4.1 and provides a simple mechanism to study bolt yielding effects on flange deformation.

5.5 CALCULATION OF FLANGE STRESS

We have assumed that the i th flange element behaves as an elastic annular ring-like element and have neglected all circumferential variations between bolt holes. In keeping with the treatment of only large diameter flanges, the relations between average circumferential bending moment rates and average element deformation rates are:

$$\dot{M}_{\theta i}(x) \approx \frac{E h_i^3}{12 R_b} \frac{d\dot{U}_i}{dx} + \nu \dot{M}_{r i}(x) \quad (5.5.1)$$

Since the assumed form used for $\dot{U}_i(x)$ contains only the rigid body rotation component, $\dot{M}_{r i}(x)$ can only be computed by direct appeal to the equilibrium of the i th flange element. To illustrate the computation of $\dot{M}_{r i}(x)$ directly from equilibrium, consider the free body of a typical flange element shown in Fig. 5.5.1. Assuming that the flange is of sufficient diameter so that the replacement $\sin(\phi/2) \approx \phi/2$ is valid, then the bending moment $\dot{M}_r(\bar{x})$ at radial location \bar{x} can be obtained from the moment equation:

$$\begin{aligned} \bar{s} \left[\left(1 + \frac{\bar{x}}{R_b} \right) \dot{M}_r(\bar{x}) + \dot{M}^* \left(1 - \frac{a}{R_b} \right) - \left(1 - \frac{a}{R_b} \right) (\bar{x} + a) \dot{V}^* \right. \\ \left. - \frac{1}{R_b} \int_{-a}^{\bar{x}} \dot{M}_{\theta}(x) dx \right] + \sum_{i=1}^{NG} (\dot{G}_i - \dot{F}_i) (\bar{x} - XG(i)) - \dot{M}_b + \dot{T}_b \bar{x} = 0 \quad (5.5.2) \end{aligned}$$

where \dot{M}_b , \dot{T}_b only enter if $\bar{x} > 0$. G_i , F_i represent the equivalent gasket reactions discussed in Section 5.2. The integral containing $\dot{M}_{\theta}(x)$ is eliminated using Eq. (5.5.1) and yields:

$$\int_{-a}^{\bar{x}} \dot{M}_{\theta}(x) dx = \frac{E h^3}{12 R_b} [\dot{U}(\bar{x}) - \dot{U}(-a)] \quad (5.5.3)$$

where we have here neglected the Poisson's ratio effect for the purposes of evaluating the integral. Using Eq. (5.5.3) in Eq. (5.5.2) and solving for $\dot{M}_r = \bar{s} \dot{M}_r(\bar{x})$ yields

$$\begin{aligned} \left(1 + \frac{\bar{x}}{R_b} \right) \dot{M}_r = \sum_{i=1}^{NG} (\dot{F}_i - \dot{G}_i) (\bar{x} - XG(i)) + \dot{M}_b - \dot{T}_b \bar{x} + \left(1 - \frac{a}{R_b} \right) \bar{s} \dot{V}^* (\bar{x} + a) \\ + \frac{\bar{s} h_i^3}{12 R_b^2} E \{ \dot{U}(\bar{x}) - \dot{U}(-a) \} - \bar{s} \dot{M}^* (1 - a/R_b) \quad (5.5.4) \end{aligned}$$

$NG \leq N$ includes all gasket regions inboard of \bar{x} . The bolt force and

Equation (5.4.2) leads directly to the conclusion that in accordance with these assumptions, the spring rates should vanish when $\alpha = -0.412 M/M_y$. This completes the justification for Fig. 5.4.1 and provides a simple mechanism to study bolt yielding effects on flange deformation.

5.5 CALCULATION OF FLANGE STRESS

We have assumed that the i th flange element behaves as an elastic annular ring-like element and have neglected all circumferential variations between bolt holes. In keeping with the treatment of only large diameter flanges, the relations between average circumferential bending moment rates and average element deformation rates are:

$$\dot{M}_{\theta i}(x) \approx \frac{E h_i^3}{12 R_b} \frac{d\dot{U}_i}{dx} + \nu \dot{M}_{r i}(x) \quad (5.5.1)$$

Since the assumed form used for $\dot{U}_i(x)$ contains only the rigid body rotation component, $\dot{M}_{r i}(x)$ can only be computed by direct appeal to the equilibrium of the i th flange element. To illustrate the computation of $\dot{M}_{r i}(x)$ directly from equilibrium, consider the free body of a typical flange element shown in Fig. 5.5.1. Assuming that the flange is of sufficient diameter so that the replacement $\sin(\phi/2) \approx \phi/2$ is valid, then the bending moment $\dot{M}_r(\bar{x})$ at radial location \bar{x} can be obtained from the moment equation:

$$\begin{aligned} \bar{s} \left[\left(1 + \frac{\bar{x}}{R_b} \right) \dot{M}_r(\bar{x}) + \dot{M}^* \left(1 - \frac{a}{R_b} \right) - \left(1 - \frac{a}{R_b} \right) (\bar{x} + a) \dot{V}^* \right. \\ \left. - \frac{1}{R_b} \int_{-a}^{\bar{x}} \dot{M}_{\theta}(x) dx \right] + \sum_{i=1}^{NG} (\dot{G}_i - \dot{F}_i) (\bar{x} - XG(i)) - \dot{M}_b + \dot{T}_b \bar{x} = 0 \quad (5.5.2) \end{aligned}$$

where \dot{M}_b , \dot{T}_b only enter if $\bar{x} > 0$. G_i , F_i represent the equivalent gasket reactions discussed in Section 5.2. The integral containing $\dot{M}_{\theta}(x)$ is eliminated using Eq. (5.5.1) and yields:

$$\int_{-a}^{\bar{x}} \dot{M}_{\theta}(x) dx = \frac{E h^3}{12 R_b} [\dot{U}(\bar{x}) - \dot{U}(-a)] \quad (5.5.3)$$

where we have here neglected the Poisson's ratio effect for the purposes of evaluating the integral. Using Eq. (5.5.3) in Eq. (5.5.2) and solving for $\dot{M}_r = \bar{s} \dot{M}_r(\bar{x})$ yields

$$\begin{aligned} \left(1 + \frac{\bar{x}}{R_b} \right) \dot{M}_r = \sum_{i=1}^{NG} (\dot{F}_i - \dot{G}_i) (\bar{x} - XG(i)) + \dot{M}_b - \dot{T}_b \bar{x} + \left(1 - \frac{a}{R_b} \right) \bar{s} \dot{V}^* (\bar{x} + a) \\ + \frac{\bar{s} h_i^3}{12 R_b^2} E \{ \dot{U}(\bar{x}) - \dot{U}(-a) \} - \bar{s} \dot{M}^* (1 - a/R_b) \quad (5.5.4) \end{aligned}$$

$NG \leq N$ includes all gasket regions inboard of \bar{x} . The bolt force and

moment rates \dot{T}_b , \dot{M}_b , are included only if $\bar{x} > 0$. With $\dot{M}_r(x)$ computed using Eq. (5.5.4) and $\dot{M}_\theta(x)$ computed from Eq. (5.5.1), the bending stress increments at the extreme fiber of the flange are computed from the relations.

$$\dot{\sigma}_r(\bar{x}) = \frac{6 \dot{M}_r(\bar{x})}{\bar{s} t_i^2} ; \quad \dot{\sigma}_\theta(\bar{x}) = \frac{6 \dot{M}_\theta(\bar{x})}{t_i^2} \tag{5.5.5}$$

Note that $\dot{M}_r(\bar{x})$ has the units of lb.-in./sec., while M_θ has the units of lb.-in./(in.-sec).

An appropriate limiting flange stress criteria can be employed to qualify a given joint configuration.

5.6 APPLICATION OF THE METHOD

A computer code, based on the philosophy discussed in this chapter, and incorporating an incremental solution scheme, is easily developed. For a given joint configuration and a specified initial bolt direct tensile stress, the

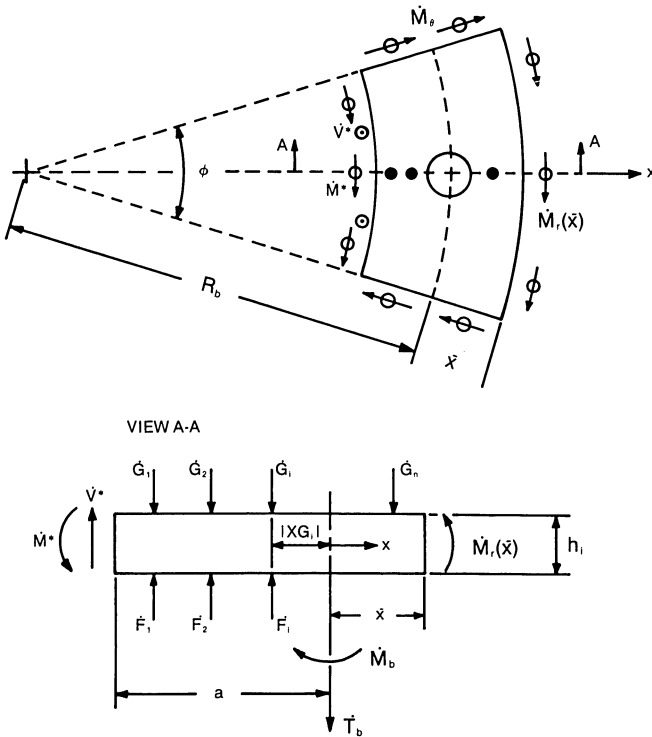


Fig. 5.5.1. Free body diagram used for calculation of $M_r(\bar{x})$.

preload stress distribution in both the gasket elements and in the flange elements is computed by incrementally applying the bolt preload. Subsequent to this initial stage, pressure increments are applied and the field equations updated after each step based on the current gasket strain at each location $XG(i)$. The solution proceeds until the desired pressure is reached, or until all of the gasket springs inboard of the bolt line experience leakage. A user's manual and a source listing of the code for a general three element flange joint is presented in Appendix 5.A. The complete equations for a two element symmetric joint, including some elastic plate effects, are presented in [5.4.1] along with some typical results. The computer code listed at the end of this chapter, for three element joints, and the additional numerical results presented in this text, have been developed during the course of a sponsored research program [5.4.2]. Note that the method set forth in this chapter simulates a single load cycle of pressure application; it should be a relatively straightforward task to extend the simulation to pressure cycling of the joint once reasonable relationships are developed for the gasket constitutive equations under repeated cycling. That extension is not, however, discussed here.

5.6.1 Gasketed Joint Model

To illustrate the application of the joint analysis method, we first consider a configuration for a two element symmetric joint (no spacer or tubesheet) connecting two pipes. The joint layout is shown in Fig. 5.6.1. The following data is used in the analysis.

Number of bolts	–	20
Bolt length	–	7.25"
Bolt diameter (nominal)	–	1.25"
Flange, bolt Young's Modulus	–	29×10^6 psi
a (Fig. 5.2.2)	–	3.125"
b (Fig. 5.2.2)	–	1.125"
Thickness of flanges $h_1 = h_2$	=	1.818"
Desired bolt pre-stress	–	4371 psi

Because of the many parameters involved in a flanged joint simulation, we will be quite detailed in our description of the model and in the development of the computer input; we do this to make it easier for the potential user to gain some insight into the applicability and utility of the computational model.

In the course of "building" a simulation input file, we need to choose the number of gasket springs, establish the bolt pre-stress level, determine the parameters that are used to model the edge forces and moments, establish the magnitude of the applied loading, quantify the non-linear properties of the gasket material, and decide on a gasket seating factor (i.e., the criteria for leakage). For the flange geometry just set forth, we will now go into

each of these items in turn and illustrate how a user can develop the necessary data for the input code.

Gasket Spring Assumptions

Our initial task is to choose the number of gasket springs to be used in the joint model. For a full face gasketed joint, we are guided by the joint dimensions; our goal here is simply to have the total gasket area between two bolt holes divided into roughly equal areas. For the full face joint to be examined here, we settle on a total of nine non-linear springs; six springs are positioned inboard of the bolt circle with the remaining three springs located outboard of the bolt circle. The geometric location of each spring is chosen by the code once the total number of springs and the number inboard of the bolt circle is input. Since we also plan to examine ring gasketed joints with non-linear gasket material properties, we mention that in the simulation of a ring gasket, the code assumes that three gasket springs are active, with positioning of the springs given in terms of the width of the ring and its location relative to the bolt circle.

Specification of Bolt Pre-stress

We assume the bolt stress to be $\sigma_{AV} = 4371.2$ psi. It is of interest to point

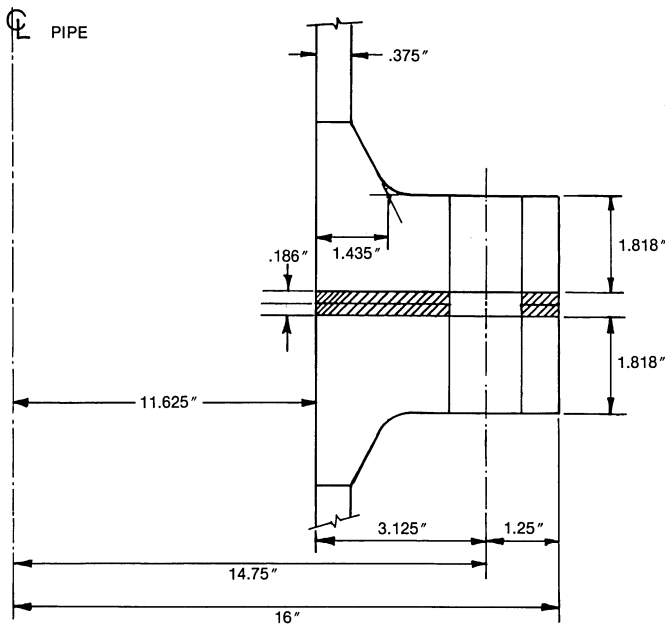


Fig. 5.6.1. Flange joint for sample calculation.

out that if we assume, for the moment, that both flanges are rigid (so that no rotation of the flange occurs during tightening), then the average gasket stress σ_g can be obtained from, the equation

$$\sigma_g A_G = N_B \sigma_{AV} A_B \quad (5.6.1)$$

A_G is the total gasket area and N_B is the number of bolts. If we neglect the bolt hole area in calculating A_g , we find that $\sigma_g \approx 214$ psi for the model shown in Fig. 5.6.1. While knowledge of this average gasket compressive pre-stress is not needed to exercise the computer simulation, if we assume that the gasket material of our analysis follows Fig. 5.6.2, then we see that less than 10% prestrain is imposed on this full face gasket, during the tightening phase, by the assumed initial bolt torque.

Specifications of Edge Forces and Moments

Continuing with the development of the numerical model, we next examine calculation of the parameters C_{ij} for the edge moments and forces given by Eq. (5.2.9). Referring to Fig. 5.6.1, which shows a two element symmetric joint, we see that the general equations for \dot{V}_i^* , \dot{M}_i^* , specialize to the simpler set

$$\begin{aligned} \dot{V}_1^* &= -\psi \dot{p}_1; & \dot{V}_2^* &= \psi \dot{p}_1 \\ \dot{M}_1^* &= -\beta \dot{\theta}_1 + \gamma \dot{p}_1; & \dot{M}_2^* &= -\beta \dot{\theta}_2 - \gamma \dot{p}_1 \end{aligned} \quad (5.6.2)$$

following the sign convention of Fig. 5.2.3. Here, β is a rotational stiffness parameter reflecting the rotational resistance of the adjacent hub and shell; ψ , γ are parameters which give the change in edge load due to a unit increment of applied pressure. The rotational resistance parameter β is estimated using some results developed in Chapter 3. It is shown there that the relation between hub rotation and the *total* external moment applied to a flanged joint is obtained by combining the following equations (here we use the notation of Chapter 3):

$$\begin{aligned} \phi &= \frac{r_1}{h} f_1(\kappa, \alpha) A_1; & \kappa &= \frac{12(1-\nu^2)h^4}{r_1^2 g_0^2} \\ |A_1| &= \frac{2(1-\nu^2)h^2}{Eg_1^3 r_1} MX \end{aligned} \quad (5.6.3)$$

$$f_1(\kappa, \alpha) = (1 + \alpha)^3 \left[\frac{3(1-\nu^2)}{\kappa} \right]^{1/4} V; \quad \alpha = \frac{g_1}{g_0} - 1$$

In the above, ϕ is the hub rotation at the attachment to the flange, M is the total flange moment, g_0 is the thickness of the attached pipe, g_1 is the hub thickness at the large end, h is the hub length, and r_1 is the inside radius of the hub. The parameters V and X can be obtained from results given in the Appendix on Flanges in the ASME Code, Section VIII, Division 1 or from

the formulas given in Chapter 3. Combining the above results, we obtain the relations

$$\frac{\phi}{M} = \sqrt{2} \frac{(1 - \nu^2) V X (1 + \alpha)^3}{E g_1^3} (r g_0)^{1/2} \quad (5.6.4)$$

We also show in Chapter 3 that the hub moment, M_H , at the large end of the hub, is related to M by Eqs. (3.11.49) and (3.11.50):

$$M = 6M_H / X \quad (5.6.5)$$

Therefore, defining a rotational spring rate K_ϕ by the equation

$$M_H / \phi = K_\phi \quad (5.6.6)$$

leads to the result

$$K_\phi = \frac{E g_1^3}{6\sqrt{2}(1 - \nu^2)} \frac{1}{V(1 + \alpha)^3 (r_1 g_0)^{1/2}} \quad (5.6.7)$$

For the joint at hand, $g_0 = 0.375''$, $g_1 = 1.435''$, $1 + \alpha = 3.83$, and we can determine that $V \approx 0.04$. This leads to a final value for K_ϕ as

$$K_\phi / E = 0.0816 \quad (5.6.8)$$

It is of interest to point out that for a shell having uniform thickness of $0.375''$, we would obtain $K_\phi / E = 0.0117$, while for a shell having uniform thickness $1.435''$, we would obtain $K_\phi / E = 0.1676$. Both of these shell estimates are easily calculated using classical thin shell theory (see main Appendix A) which yields the general formula

$$K_\phi / E = \frac{1.285}{\sqrt{Rt}} \frac{t^3}{6(1 - \nu)^2} \quad (5.6.9)$$

t and R are the shell thickness and mean radius, respectively. As expected, the hub effect leads to a rotational spring rate that is bounded by the two shell theory results. In the flange model under study here, we make the supposition that $|\beta| = K_\phi$ in Eq. (5.6.2). If we assume $E = 27 \times 10^6$ psi, then

$$\beta = 2.2032 \times 10^6 \text{ in. lb./in.}$$

Having determined the rotational resistance parameter β , we turn next to the evaluation of γ , ψ for our sample calculations. If we consider first the thrust due to the internal pressure p , then the flange edge load V^* has the form

$$V^* \approx pR_M / 2 \quad (5.6.10)$$

where R_M is the mean radius of the adjacent pipe wall. In addition to the edge force component due to pipe internal pressure, it is clear that a force can develop in the flange if the adjacent pipe imposes a gross bending moment M_f on the joint. For example, if we assume that at some given pipe pressure p_M , a gross moment M_M is applied to the joint, then at any arbitrary pipe pressure we have

$$M_f = \left(\frac{M_M}{p_M} \right) p \quad (5.6.11)$$

If we now calculate the circumferentially varying direct force in the pipe wall necessary to resist M_f , and if we set the maximum value of that force per unit circumferential length equal to an edge force acting on the flange, we obtain

$$\Delta V^* = \frac{M_F}{\pi R_M^2} = \frac{(M_M/p_m)}{\pi R_M^2} p \quad (5.6.12)$$

Restricting consideration to the portion of the flange where the total edge force per unit circumferential length that is explicitly due to pipe wall pressure is $V^* + \Delta V^*$, then a comparison with Eq. (5.6.2) suggests that

$$\psi = R_M/2 + \frac{(M_M/p_m)}{\pi R_M^2} \quad (5.6.13)$$

In the numerical results presented here, we will use the value of $\psi = 6.746$ in all simulations.

To complete the specifications of edge loading, we must determine the edge moment parameter γ in Eq. (5.6.2) giving the explicit local pressure dependence of the edge moment. We suggest here an admittedly approximate calculation procedure for this simulation of a pipe flange; however, the approximation should be conservative. If we consider a thin cylindrical shell under internal pressure and fixed against lateral deflection and rotation at the end, we find that the edge moment M_0 , and the edge shear Q_0 are given by the equations

$$\begin{aligned} |M_0| &= -\frac{p R_M^2 \beta^2 D}{E t} (2 - \nu); \quad D = Et^3/12(1 - \nu^2) \\ |Q_0| &= -2M_0\beta; \quad \beta = 1.2854/(R_M t)^{1/2} \end{aligned} \quad (5.6.14)$$

(See Eqs. (A.2.41) and (A.2.42) of Appendix A at the end of the text.) R_M , t are the mean shell radius and thickness, respectively. If the shell edge is at distance L_H from the centerline of the flange, then the moment applied to the flange may be conservatively estimated as

$$M^* = |M_0| - L_H |Q_0| = \gamma p \quad (5.6.15)$$

where

$$\gamma = \frac{\beta^2 R_M^2 t^2}{6(1 - \nu^2)} (1 - \nu/2)(1 + 2\beta L_H) \quad (5.6.16)$$

For the numerical results presented herein, we have used $\gamma = 7.0238 \text{ in.}^2$ in all of the studies; this value is obtained using $t = 0.375''$, $R_M = 12''$, $L_H = 4.182''$ in Eq. (5.6.16).

Gasket Material Property Parameters

The next set of data required for this joint analysis is the specification of

the gasket properties. Figure 5.6.2 shows the gasket stress strain data for the material. For the loading phase, the stress-strain data is simulated by a linear region, and two exponential regions. Figure 5.6.3 shows the loading region plotted on semi-log paper. In the first exponential loading region $\epsilon < 0.6$, we write

$$\sigma = \sigma_0 e^{\epsilon/\epsilon_0} \quad (5.6.17)$$

so that

$$\log \sigma = \log \sigma_0 + \frac{\epsilon}{\epsilon_0} \log e; \quad e = 2.718 \quad (5.6.18)$$

or

$$\log \sigma = A + B\epsilon \quad (5.6.19)$$

Using the data points $\sigma_1 = 848$ psi at $\epsilon_1 = 0.3$, and $\sigma_2 = 2520$ psi at $\epsilon_2 = 0.6$ yields $A = 2.455$, $B = 1.577$, so that $\epsilon_0 = \log e/B = 0.2754$, and $\sigma_0 = 10^A = 285.1$ psi. Therefore, for $0.2754 < \epsilon < 0.6$, we have

$$\frac{d\sigma}{d\epsilon} = \frac{\sigma}{\epsilon_0}; \quad \epsilon_0 = 0.2754 \quad (5.6.20)$$

For $\epsilon < 0.2754$, we have, from Eq. (5.3.5)

$$\frac{d\sigma}{d\epsilon} = E = \frac{\sigma_0}{\epsilon_0} e = 2813 \text{ psi} \quad (5.6.21)$$

Equation (5.6.17) is shown plotted in Fig. 5.6.2. Note that above $\epsilon = 0.6$, the stress strain equation does not follow the experimental loading curve. Returning to Fig. 5.6.3, we can construct a second exponential loading curve in the region $\epsilon > 0.6$ by using the data points $\epsilon_1 = 0.6$, $\sigma_1 = 2520$; $\epsilon_2 = 0.84$, $\sigma_2 = 19,600$. From Eq. (5.6.19), we obtain $A = 1.17426$, $B = 3.7119$ which yields $\sigma_0 = 14.937$ psi and $\epsilon = 0.1170$. While these parameters may not have the physical significance that they acquire in the first loading region, it suffices for our purposes here to note that for $\epsilon > 0.6$, the new values for σ_0 , ϵ_0 , when used in Eq. (5.6.17), give results that match the final part of the loading curve (see Fig. 5.6.2).

To match the unloading behavior indicated by Fig. 5.6.2, we use Eqs. (5.3.6), (5.3.7) with the parameters n and $d\sigma/d\epsilon)_{\epsilon=0}$ chosen as

$$n = 50; \quad d\sigma/d\epsilon)_{\epsilon=0} = 1276 \text{ psi} \quad (5.6.22)$$

Equation (5.3.6) is plotted on Fig. 5.6.2 using the chosen data; we see that a good fit to the unloading data is achieved.

Criteria for Joint Leakage

The test of leakage at a particular gasket location is a comparison between current pressure to be sealed and current pressure in the local gasket spring. The leakage criteria is set by the gasket seating factor $\bar{\mu}$ (see Eq. (5.3.18)). In all of the numerical examples to be examined here, we assume a

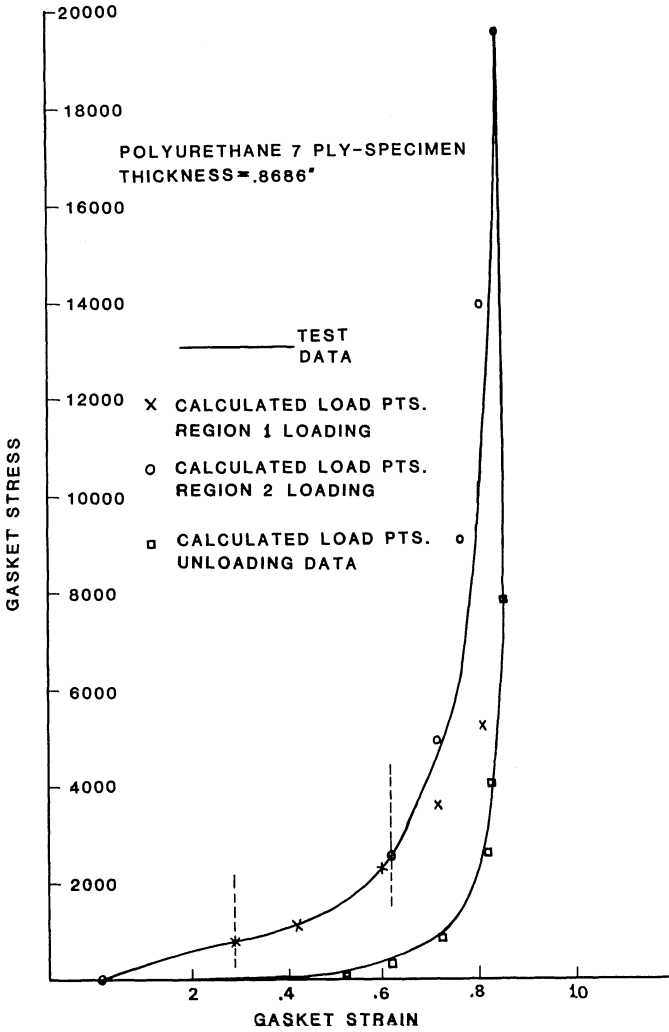


Fig. 5.6.2. Polyurethane gasket stress strain relation.

gasket factor $\bar{\mu} = 2.5$. We also assume that the weakening of the flange, due to the presence of bolt holes, can be simulated by a simple reduction of the flange Young's Modulus to 21×10^6 psi.

5.6.2 Analysis of a Full Face Gasket-Two Element Joint

Table 5.6.1 shows selected results obtained from computer analyses of the full face gasketed joint. In the studies shown in the table, we have simply varied the total thickness of the gasket separating the two flanges.



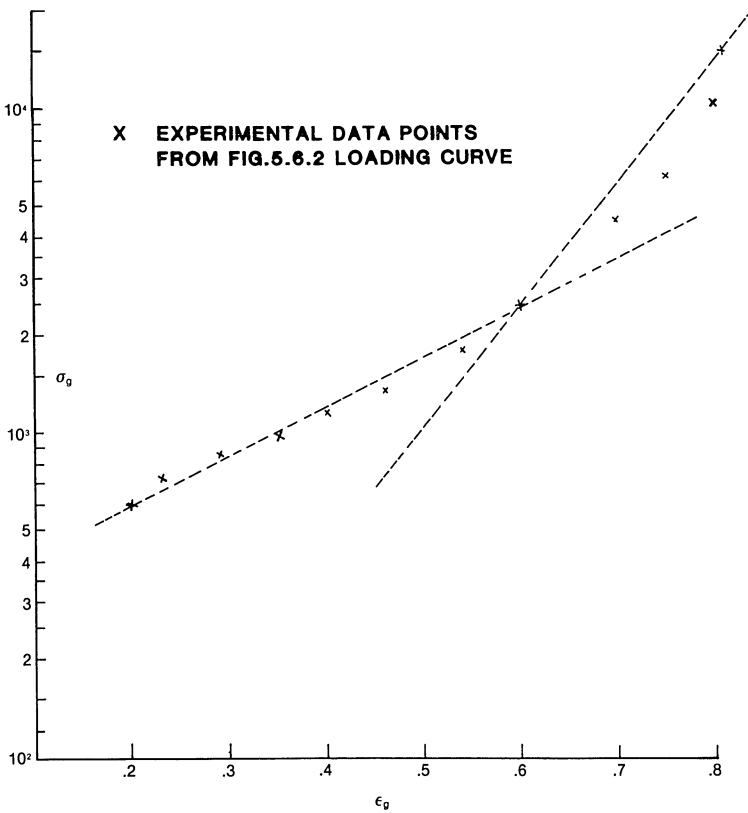


Fig. 5.6.3. Gasket loading $\sigma - \epsilon$ relations.

Table 5.6.1 Full Face Gasketed Joint Simulation-Effect of Gasket Thickness

Gasket Thickness (in.)	Actual Bolt Tensile Stress at Preload (psi)	Pressure at Joint Failure (psi)	Bolt Tensile Stress at Joint Failure (psi)
0.093	4425	38.0	4142.
0.186	4439	43.0	4299.
0.357	4405	48.0	4480.

We see that a slight increase in joint leak pressure can be obtained by increasing the thickness of the gasket.

Table 5.6.2 shows the distribution of gasket stress across the joint (9 gasket springs are used in this full face gasket model) for the 0.186" thick gasket at the end of the preload stage and at the point of joint failure due to leakage. We note that because of flange rotation during the preload stage and during the pressurization phase, the bolt experiences bending as well as direct tension. The maximum bolt stress after preload is 5837 psi, while the

same bolt stress increases to 6708 psi when all gaskets springs inboard of the bolt hole have leaked.

Table 5.6.2. Gasket Stress Distribution in Full Faced Gasketed Joint with Total Gasket Thickness = 0.186"

Gasket Spring	Stress after Preload	Stress After Leak @ 43 psi
1	197.4	78.9
2	202.4	84.4
3	207.5	92.3
4	212.6	106.0
5	217.6	133.4
6	222.8	189.27
7	227.2	229.2
8	231.3	236.2
9	235.3	243.2

5.6.3 Analysis of Ring Gasketed Joint

Our next example uses the same joint geometry of Fig. 5.6.1 but assumes that instead of a full face gasket, a ring gasket of radial width 0.625", with outer edge located 1.625" inboard of the bolt circle, is used to seal the joint. We assume the stress strain curve for the ring gasket material as given by Fig. 5.6.2, and a total gasket thickness of 0.357". All loading and edge support conditions remain the same as does the desired preload tensile stress and the gasket seating factor. Table 5.6.3 summarizes typical results obtained at the end of the preload stage, and Table 5.6.4 shows results at a pressure of 200 psi. The ring gasket is simulated by springs at locations 2, 3, and 4 (see Appendix 5.A).

Table 5.6.3. Ring Gasketed Joint at the End of Preload Stage Bolt Tensile Stress = 4379 psi

Gasket Spring	Gasket Strain	Gasket Stress (psi)
2	0.47735	1611.6
3	0.47830	1617.1
4	0.47925	1622.7

Table 5.6.4. Ring Gasketed Joint at Pressure = 200 psi Bolt Tensile Stress = 7209 psi

Gasket Spring	Gasket Strain	Gasket Stress (psi)
2	0.45539	673.8
3	0.45828	701.3
4	0.46117	734.4

We note that the reduced gasket area leads to a relatively high maximum gasket strain after preload (close to 48%); this is in contrast to the full face gasketed joint previously studied where it turns out that the maximum



gasket prestrain does not exceed 8%. If extrusion of the gasket is not a problem, a ring gasket is required in order to obtain higher joint service pressures for any specified preload bolt tension.

5.6.4 Ring Gasketed Joint with Compression Stop

We continue with our illustrative examples of the joint simulation code by investigating the effect of introducing a compression stop into the two element ring gasketed joint just discussed. The purpose of a compression stop is to limit the compressive strain in a ring gasket and to prevent extrusion of the gasket material. We use the computer model to investigate the effect of placing a compression stop just inboard of the bolt circle, at the inboard edge of the flange, and at a location outboard of the bolt circle (roughly midway between the bolt circle and the outer edge of the flange). The width of the compression stop is 0.375", and the effective length of the stop spring is taken as 4" (for the purpose of computing a stop spring constant). The stop is assumed to be effective only when the strain (based on the total gasket thickness) at the stop location exceeds $\epsilon_s = 0.193427$. Table 5.6.5 shows, for the three stop element locations, the gasket and stop element pressures during various phases of the load cycle.

Table 5.6.5. Effect of Compression Stop Location on Gasket Pressure

Stop Element Location	Maximum Pressures (psi)	Pressures at Pre-load (psi)	Pressures at Leakpoint	Location of Gasket or Stop
5 $p_{LEAK} = 78.9$ psi	305.6	231.0	159.2	2
	306.1	257.4	174.5	3
	306.6	290.3	197.0	4
	2152.0	2152.0	0.	5 (stop)
1 $p_{LEAK} = 111.8$ psi	2342.1	2342.1	0.	1 (stop)
	326.9	326.9	255.3	2
	330.8	330.8	267.0	3
	334.7	334.7	279.3	4
8 $p_{LEAK} = 57.9$ psi	312.8	312.8	138.8	2
	312.6	312.6	141.4	3
	312.5	312.5	144.5	4
	2711.4	2711.4	3417.0	8 (stop)

We note that the gasket spring locations are automatically numbered 1–10 in the ring gasket model. Location 1 is closest to the inside edge of the flange, location 5 is just inside the bolt circle, and locations 6–10 are outside the bolt circle. We also caution the user to employ a very small preloading step increment when the stop becomes active.

The results presented in Table 5.6.5 graphically demonstrate the effect of a stop element. In all cases, the bolt load at the end of preload is 4060 pounds. In the first case, with the stop located just inboard of the bolt circle, the ring gasket loads and then unloads somewhat as the flange rotates using the stop element as a pivot point. This loading and unloading of the

gasket during tightening will always occur if the stop is located between the ring gasket and the bolt circle. In the second case, the stop located at the inside edge of the flange permits continued loading of the gasket during the bolt tightening phase. During pressurization, the gasket experiences very little unloading until the stop element loses contact; once the stop becomes inactive, rapid unloading of the gasket occurs. Finally, for case 3 with the stop located outboard of the bolt line, we see that the stop continues to load during the pressurization phase and the gasket unloads more rapidly than in the initial cases.

5.6.5 Analyses of Three Element Joint with Non-Symmetric Load and Geometry

The computer model can be used to examine a three element joint with non-symmetries in the applied pressures p_1 and p_2 (Fig. 5.1.1), and in the edge rotational resistances C_{22} (Eq. (5.2.9)). We note here only that some results of typical simulations indicate that during the pressurization phase, portions of each gasket continue to load, unload, or may unload and then reload. The possibility of unloading and reloading does not appear in the case of a symmetric joint. Additional material on this subject may be found in Ref. [5.6.1].

5.7 CONCLUDING REMARKS

Our intent in this chapter has been to re-examine the analysis of bolted flange joints with the aim of including a more exact representation of non-linear gasket behavior. We do this primarily to present a method for analyzing joints with full face gaskets for both leak tightness and strength. We have demonstrated that the modelling technique lends itself to ring gaskets, with and without compression stops, with equal facility. The computerized design approach presented in this chapter offers the user a powerful new approach to the design of bolted flange connections. However, as with any new method, the application must be tempered with the use of good engineering judgement in both the modelling stage and in the interpretation of the results. We close by noting that none of the sample problems examined here have been subjected to loading sufficient to cause bolt yielding prior to leakage. The reader may find it of interest to use the computer code to examine the consequences of using a smaller bolt size and a higher preload. Some effects of bolt overstress have been illustrated in Ref. [5.4.1] which uses an earlier version of the source code presented here, restricted to two-element symmetric joints.

NOMENCLATURE

- \bar{a}_{ij} = Elements of matrix (Eqs. (5.2.19–23))
 a = Width of flange inboard of bolt circle
 b = Width of flange outboard of bolt circle
 A_B = Root area of bolt
 C_{ij} = Edge force and moment coefficients (Eq. (5.2.9))
 E_B, E = Young's Modulus of bolt, flange
 $\bar{E}_j, \bar{U}_j, \bar{U}_b, \bar{W}_e$ = Energy quantities given in Eq. (5.2.1)
 F_y = Force to cause full cross section bolt yield
 \dot{F}_i, \dot{G}_i = Gasket reactions (Fig. 5.5.1)
 h_i = Thickness of element
 I_B = Bolt area moments of inertia
 $K_m^{(j)}$ = Spring rates of gasket elements
 K_b = Bolt spring constant in extension
 K_θ = Bolt spring constant in bending
 L = Radial width of flange (Fig. 5.2.2)
 L_B = Effective bolt length for spring constant computation
 M_i^* = Edge moment acting on flange
 M_y = Bending moment necessary to cause first yield at outer fiber of bolt bending cross section
 $M_{\theta i}$ = Circumferential bending moment in flange (Eq. (5.5.1))
 $M_{r i}$ = Radial bending moment in flange (Eq. (5.5.2))
 N = Number of subregions for gasket subdivision
 N_B = Number of flange bolts
 NG = Summation variable in Eq. (5.5.4)
 p_1, p_2 = Pressures to be sealed by three-element joint (Fig. 5.1.1)
 R_b = Bolt circle radius
 \bar{s} = Circumferential distance between centers of adjacent bolt holes
 t_g = Gasket thickness
 $U(x)$ = Deformation pattern of flange
 V_i^* = Edge shear acting on flange
 \dot{W}_i = Velocity of inner edge of element
 x = Radial coordinate measured from bolt circle
 \dot{Z}_i = Elements of unknown vector
 α = Bolt inelastic parameter (Eq. (5.4.2))
 $\dot{\Delta}$ = Preloading displacement rate for bolt
 κ, n = Gasket stress strain unloading parameters (Eq. (5.3.6))
 ψ, β, γ = Parameters for sample problem (Eq. (5.6.2))
 σ = Gasket stress
 σ_0, ϵ_1 = Gasket stress strain loading parameters (Eq. (5.3.5))

- σ_f, ϵ_f = Maximum load point reached on gasket stress-strain curve
 σ_g = Average gasket pre-stress (Eq. (5.6.1))
 $\bar{\mu}$ = Gasket seating factor (Eq. (5.3.18))
 μ_2, μ_3 = Parameters introduced in Eqs. (5.2.19)–(5.2.23)
 ϕ = Angle defined in Fig. 5.2.2.
 $\dot{\theta}_i$ = Rotation rate of inner edge of flange

REFERENCES

- [5.2.1] Fung, Y. C., “Foundations of Solid Mechanics,” Prentice-Hall, N.J., Chapter 10 (1963).
 [5.2.2] Biot, Maurice A., “Mechanics of Incremental Deformations,” John Wiley, New York, Chapters 2, 3 and the Appendix, pp. 496–497 (1965).
 [5.4.1] Soler, A. I., “Analysis of Bolted Joints with Nonlinear Gasket Behavior,” *ASME Journal of Pressure Vessel Technology*, Vol. 102, pp. 249–256 (1980).
 [5.4.2] NSF Grant MEA-8120347, “Analysis and Design of Pressure Vessel Bolted Flanges with Non-linear Gasket Materials,” Aug. 1982–Jan. 1985, University of Pennsylvania.
 [5.6.1] Singh, K. P., and Soler, A. I., “HEXDES User Manual,” Arcurus Publishers, Cherry Hill, N.J. (1984).

APPENDIX 5.A

User Manual for “GENFLANGE” – A Computer Code for Analysis of Two or Three Element Bolted Flange Joints with Non-Linear Gasket Properties

All input is in free field format.

DATA READ IN FROM TERMINAL

- NR = Logical unit number for input data file
 NTST = 0 (full echo of input data in output file)
 = 1 (suppress printout of input data)
 NFL = Number of flange elements in joint to be analyzed (2 or 3)
 DSPEC = Step size multiplier at EPSE1, EPSE2 used during preload. If a compression stop is present in a ring gasket analysis, the preloading initial step size DDD can be changed to DDA = DSPEC*DDD when the compression stop strain is near the strain EPSE1 (or EPSE2) where stop action begins.

DATA READ IN FROM LUN NR, THE INPUT FILE**LINE 1**

HEDING — Any title for job—72 characters permitted

LINE 2

DB — bolt thread root diameter
 BL — effective bolt length for computing bolt spring rates
 EB — Young's Modulus of bolt material
 SIGMBY — bolt yield stress
 POIS1 — Poisson's ratio for flange material

LINE 3

EF1 — Young's Modulus of Flange 1 (including reduction for bolt hole perforation)
 HF1 — thickness of flange 1
 EF2 —
 HF2 — } Same as above for flanges 2 and 3
 EF3 —
 HF3 — }

LINE 4

A — width of flange inside bolt circle (refer to Fig. 5.1.1)
 B — width of flange outside bolt circle
 RB — radius of bolt circle (see Fig. 5.1.1)
 NG — number of gasket springs (≤ 12 for full face gaskets). Automatically set to 10 for ring gaskets.
 NING — number of gasket springs inside bolt circle (set to 5 for ring gaskets).
 NIT1 — number of iterations on simultaneous equation solver before program aborts = 2^{NIT1}

LINE 5

EG1 — linear elastic modulus of gasket springs for gasket 1 in initial loading region
 HG1 — thickness of gasket 1
 COEF1 — seating factor for gasket 1
 EPS11 — limiting strain for linear region for gasket 1

- EPSL1 — limiting strain for first exponential loading region for gasket 1
 EPS21 — loading parameter for second exponential loading region for gasket 1
 CN1 — parameter n for unloading curve of gasket 1
 DSDE01 — $d\sigma/d\epsilon$ at $\epsilon=0$ for gasket 1 unloading curve

For loading region of gasket 1

$$\begin{aligned}\frac{d\sigma}{d\epsilon} &= EG1 \quad \epsilon \leq EPS11 \\ &= \frac{\sigma}{EPS11} \quad EPS11 \leq \epsilon \leq EPSL1 \\ &= \frac{\sigma}{EPS21} \quad EPSL1 \leq \epsilon\end{aligned}$$

For unloading of gasket 1 from σ_f, ϵ_f

$$\frac{d\sigma}{d\epsilon} = \frac{\sigma_f/\epsilon_f}{1+K} [1 + nK(\epsilon/\epsilon_f)^{n-1}]$$

where $n = CN1$ and $K = \frac{\sigma_f/\epsilon_f}{DSDE01} - 1$

LINE 6

- EG2 —
 HG2 —
 COEF2 —
 EPS12 —
 EPSL2 —
 EPS22 —
 CN2 —
 DSDE02 —
- } Same parameters as on line 5 except for gasket 2.
 Note that for a two element joint, EG2 = 0 and
 EPS12 = 1.0 are set internally so that gasket 2
 has no effect.

LINE 7

- C1(1,1))
 C1(2,1))
 C1(1,2))
 C1(2,2))
 C1(1,3))
 C1(2,3))
- } edge load coefficients for flange element 1 (see Eq. (5.2.9))

LINE 8

Same data as line 7, except for flange element 2

LINE 9

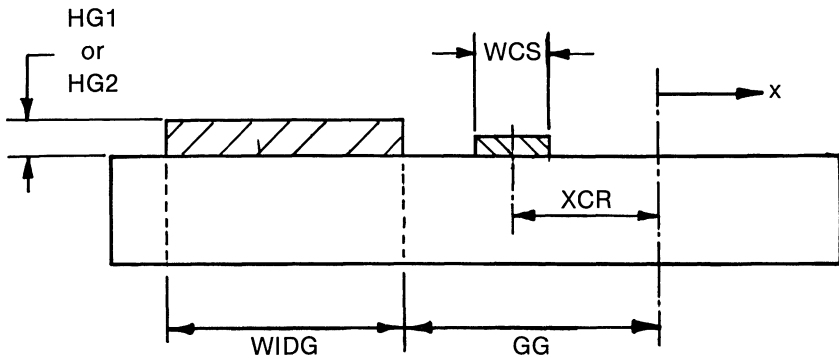
Same data as line 7, except for flange element 3

LINE 10

- NPMODE — 0
 P1MAX — desired maximum pressure for p_1 acting on gasket between elements 1 and 2
 P2MAX — desired maximum pressure for p_2 acting on gasket between elements 2 and 3 (note that for a two element joint, P2MAX will be internally set to zero)

LINE 11

- GAP10 — The initial gap between outer edge of flange 1 and flange 2
 GAP20 — The initial gap between outer edge of flange 2 and flange 3
 GG — The distance from bolt line to the outer edge of ring gasket
 WIDG — width of ring gasket

**LINE 12**

- IG = 0 (full face gasket)
 1 (full face gasket inboard of bolt circle)
 2 (ring gasket)
 KLEAK = 0 (assume leakage when all gasket springs inboard of bolt circle fail)
 = 1 (assume leakage when all gasket springs inboard of bolt hole edge fail)
 SIZE1 = preloading step printout increment—when total bolt stress $\geq N \cdot \text{SIZE1}$, printout will occur
 SIZE2 = pressure stage printout increment—when pressure $\geq N \cdot \text{SIZE2}$, printout will occur.

- N1 = printout options
 1—full output for flanges 1, 3 and gaskets 1, 2
 2—full output for flanges, limited gasket output
 3—full output for gaskets, limited flange output
 4—limited output for flanges and gaskets

LINE 13

- CCC — initial prestress of bolt (psi)
 SAFCB — allowable bolt stress
 = SAFCB * bolt yield stress. This parameter is for informational purposes only on output
 MATRIX = 0—no printouts of stiffness matrix and force vector
 = 1—printout displacement rate solutions
 = 2—printout matrix, force vectors, and displacement rates
 NW1 — logical unit number for job output

LINE 14

- DDD — preloading increment size (usually 0.001 or less so as to take a reasonable number of steps Δ during loading)

LINE 15

- PDD — pressure increment size, usually 0.5 psi or less. User should run convergence checks.

LINE 16

- IGAS — location of compression stop in ring gasket model = 1 or a number between 5 and 10. If IGAS = 21, no compression stop is modeled in a ring gasket analysis. Stops, when present, are in the same location for both gaskets.
 EGE1 — slope of stress strain curve in gasket 1
 EGE2 — slope of stress strain curve in gasket 2
 EPSE1 — strain at stop location when stop makes initial contact with flange element
 EPSE2 — strain at stop location when stop makes initial contact with gasket element
 *XCR — location of compression stop
 *WCS — width of compression stop
 HCS — height of compression stop used to compute effective E for stop

*See figure associated with data line 11. Note that effective E for compression stop is $E_{\text{eff}}^{(1)} = \text{EGE1} * \text{HG1} / \text{HCS}$, etc.

PROGRAM GENFLANGE

```

PROGRAM MAIN
C ANALYSIS OF THREE-ELEMENT BOLTED FLANGE JOINT WITH NONLINEAR GASKET.
C ----- OCT.1983 XU HONG & A.SOLER -----
C
C (1) FULL FACE GASKET OR RING TYPE GASKET;
C     FULL FACE GASKET IS REPRESENTED BY (NG.LE.12) GASKET SPRINGS;
C     RING TYPE GASKET IS REPRESENTED BY GASKET SPRINGS 2,3,4
C (2) CONSIDERING METAL TO METAL CONTACT FOR RING TYPE GASKET;
C     WITH RING GASKET COMPRESSION STOP PERMITTED
C (3) CONSIDERING GASKET LEAKAGE;
C (4) CONSIDERING BOLT STRENGTH (TENSION AND BENDING);
C (5) CONSIDERING FLANGE STRENGTH (BENDING);
      IMPLICIT DOUBLE PRECISION (A-H,O-Z)
      CHARACTER*4 HEDING(18)
      COMMON /AAA/AA(12,12),BB(12),BBF(12)
      COMMON /AAB/DB,BL,EB,SIGMBY
      COMMON /BBC/EF1,POIS1,HF1,SIGFY1,EF2,POIS2,HF2,SIGFY2,EF3,
&          POIS3,HF3,SIGFY3
      COMMON /CC/A,B,RB,NB,NG,NING,GG,WIDG,WL
      COMMON /DD/EG1,HG1,COEF1,EPS11,CN1,DSDE01
      COMMON /EE/EG2,HG2,COEF2,EPS12,CN2,DSDE02
      COMMON /FF/C1(2,3),C2(2,3),C3(2,3)
      COMMON /GG/BF1D,BF3D,P1MAX,P2MAX,BFO
      COMMON /HH/GAP1,GAP2,MTM1,MTM2,NYIELD,NSTOP
      COMMON /II/IG,KLEAK,NPMCDE,SIZE1,SIZE2,N1,CCC,SAFCB,MATRIX
      COMMON /KK/NNN,ISTG,KP,NW1
      COMMON /LAM/LAMDA1(12),LAMDA2(12),LOAD1(12),LOAD2(12)
      COMMON /MM/LAST1(12),LAST2(12),FEPS1(12),FEPS2(12)
      COMMON /OO/XG(12),AG(12)
      COMMON /EEP/MEPS1(12),MEPS2(12),EPS1(12),EPS2(12)
      COMMON /SIGF/SIGMF1(12),SIGMF2(12),SIGM1(12),SIGM2(12)
      COMMON/ESIG/ EPSF1(12),EPSF2(12)
      COMMON /QQ/GK1(12),GK2(12),GK1GK2(12)
      COMMON /RR/BKO,BRKO,BK,BRK,D,PRESIG,ALSIGB
      COMMON /SS/FI1,FI2,FI3
      COMMON /TT/P1,P2,P1D,P2D,DDA,DDAO,DSPEC
      COMMON /VV/W1(12),W2(12),W3(12),WA1,WA2,WA3,ROTA1,ROTA2,ROTA3
      COMMON /WW/BM,BF,BMTR1(21),BMTR3(21),BMTT1(21),BMTT3(21),
&          FG1F(12),FG3F(12)
      COMMON/ZZZ/EPS21,EPS22,EPSL1,EPSL2
      COMMON/XYZ/EGE1,EGE2,EPSE1,EPSE2,IGAS
      COMMON/RST/Z1,NFL,L2,L3
C
C     WRITE(6,*) 'INPUT NR,NTST,NFL,DSPEC
      READ(5,*)NR,NTST,NFL,DSPEC
C TO READ IN INPUT DATA.
      READ(NR,20) HEDING
20     FORMAT(18A4)
      READ(NR,*)DB,BL,EB,SIGMBY,POIS1
      READ(NR,*)EF1,HF1,EF2,HF2,EF3,HF3
      READ(NR,*)A,B,RB,NB,NG,NING,NIT1

```

```

      READ(NR,*)EG1,HG1,COEF1,EPS11,EP11,EP21,CN1,DSDE01
      READ(NR,*)EG2,HG2,COEF2,EPS12,EP12,EP22,CN2,DSDE02
C INPUT C1,C2,C3 IN SEQUENCE: C(1,1),C(2,1),C(1,2),C(2,2),C(1,3),C(2,3)
      READ(NR,*)C1
      READ(NR,*)C2
      READ(NR,*)C3
      READ(NR,*)NPMODE,P1MAX,P2MAX
      READ(NR,*)GAP10,GAP20,GG,WIDG
      READ(NR,*)IG,KLEAK,SIZE1,SIZE2,N1
      READ(NR,*)CCC,SAFCB,MATRIX,NW1
      READ(NR,*)DDD
      READ(NR,*)PDD
      READ(NR,*)IGAS,EGE1,EGE2,EPSE1,EPSE2,XCR,WCS,HCS
      WRITE(6,*)'PROGRAM IS RUNNING.....'
          IF(NFL.EQ.2)P2MAX=0.
          IF(NFL.EQ.2)EG2=0.
          IF(NFL.EQ.2)EPS12=1.
          IF(NFL.EQ.2)EP12=0.
          IF(NFL.EQ.2)EGE2=0.
          IF(NFL.EQ.2)EPSE2=0.
          POIS2=POIS1
          POIS3=POIS1
          IF(IG.NE.2) GO TO 50
C FOR RING TYPE GASKET,NG=10,NING=5,AND GASKET IS REPRESENTED
C BY 3 GASKET SPRINGS:2-ND,3-RD,4-TH SPRING.
      NG=10
      NING=5
50      CONTINUE
1000     IF(NTST.GE.1) GO TO 1091
C INPUT ECHO FROM OUTPUT FILE (LUN.=NW1).
      WRITE(NW1,20) HEDING
      WRITE(NW1,*)
      WRITE(NW1,*)'NUMBER OF FLANGES=',NFL
      WRITE(NW1,*)'***** INPUT DATA *****'
      WRITE(NW1,*)'DIAMETER OF BOLT,DB' =',DB,'(IN)
&'
      WRITE(NW1,*)'BOLT LENGTH,BL' =',BL,'(IN)
&'
      WRITE(NW1,*)'ELASTIC MODULUS OF BOLT,EB' =',EB,'(PSI
&)'
      WRITE(NW1,*)'YIELD STRESS OF BOLT,SIGMBY' =',SIGMBY,'
&(PSI)'
      WRITE(NW1,*)'NUMBER OF BOLTS,NB' =',NB
      WRITE(NW1,*)
      WRITE(NW1,*)'ELASTIC MODULUS OF FLANGE-1,EF1' =',EF1,'(PSI
&)'
      WRITE(NW1,*)'POISSON RATIO OF FLANGE-1,POIS1' =',POIS1
      WRITE(NW1,*)'THICKNESS OF FLANGE-1,HF1' =',HF1,'(IN)
&'
      WRITE(NW1,*)
      WRITE(NW1,*)'ELASTIC MODULUS OF FLANGE-2,EF2' =',EF2,'(PSI
&)'
      WRITE(NW1,*)'POISSON RATIO OF FLANGE-2,POIS2' =',POIS2

```

```

WRITE(NW1,*)'THICKNESS OF FLANGE-2,HF2                =','HF2','(IN)
&'
WRITE(NW1,*)
WRITE(NW1,*)'ELASTIC MODULUS OF FLANGE-3,EF3          =','EF3','(PSI
&)'
WRITE(NW1,*)'POISSON RATIO OF FLANGE-3,POIS3         =','POIS3
WRITE(NW1,*)'THICKNESS OF FLANGE-3,HF3              =','HF3','(IN)
&'
WRITE(NW1,*)
WRITE(NW1,*)'FLANGE GEOMETRY:'
WRITE(NW1,*)'  A=','A','(IN);  B=','B','(IN)''
WRITE(NW1,*)'RADIUS OF BOLT LINE,RB                  =','RB','(IN)''
WRITE(NW1,*)
WRITE(NW1,*)'GASKET PROPERTIES'
WRITE(NW1,*)'LINEAR ELASTIC MODULUS,EG1              =','EG1','(PSI
&)'
WRITE(NW1,*)'THICKNESS,HG1                            =','HG1','(IN)
&'
WRITE(NW1,*)'GASKET COEFFICIENT,COEF1                 =','COEF1
WRITE(NW1,*)'UNLOADING PARAMETERS N1,DSDE01=' ,CN1,DSDE01
WRITE(NW1,*)'CRITICAL STRAIN FOR NONLINEARITY,EPS11  =','EPS11
WRITE(NW1,*)'SECOND LOADING REGION INITIAL STRAIN EPSL1 ',EPSL1
WRITE(NW1,*)'SECOND LOADING REGION PARAMETER EPS21  ',EPS21
WRITE(NW1,*)'LINEAR ELASTIC MODULUS,EG2              =','EG2','(PSI
&)'
WRITE(NW1,*)'THICKNESS,HG2                            =','HG2','(IN)
&'
WRITE(NW1,*)'GASKET COEFFICIENT,COEF2                 =','COEF2
WRITE(NW1,*)'UNLOADING PARAMETERS N1,DSDE01=' ,CN1,DSDE01
WRITE(NW1,*)'CRITICAL STRAIN FOR NONLINEARITY,EPS12  =','EPS12
WRITE(NW1,*)'SECOND LOADING REGION INITIAL STRAIN EPSL2 ',EPSL2
WRITE(NW1,*)'SECOND LOADING REGION PARAMETER EPS22  ',EPS22
WRITE(NW1,*)
WRITE(NW1,*)'EXTERNAL EDGE FORCE AND MOMENT FACTORS:'
WRITE(NW1,*)'C1(1,1)=' ,C1(1,1),' C1(1,2)=' ,C1(1,2),' C1(1,3)=' ,C
&1(1,3)
WRITE(NW1,*)'C1(2,1)=' ,C1(2,1),' C1(2,2)=' ,C1(2,2),' C1(2,3)=' ,C
&1(2,3)
WRITE(NW1,*)'C2(1,1)=' ,C2(1,1),' C2(1,2)=' ,C2(1,2),' C2(1,3)=' ,C
&2(1,3)
WRITE(NW1,*)'C2(2,1)=' ,C2(2,1),' C2(2,2)=' ,C2(2,2),' C2(2,3)=' ,C
&2(2,3)
WRITE(NW1,*)'C3(1,1)=' ,C3(1,1),' C3(1,2)=' ,C3(1,2),' C3(1,3)=' ,C
&3(1,3)
WRITE(NW1,*)'C3(2,1)=' ,C3(2,1),' C3(2,2)=' ,C3(2,2),' C3(2,3)=' ,C
&3(2,3)
WRITE(NW1,*)' COMPRESSION STOP DATA IF IGAS.LT.21)'
WRITE(NW1,*)'      IGAS=' ,IGAS
WRITE(NW1,*)'      EPSE1=' ,EPSE1,'      EGE1=' ,EGE1
WRITE(NW1,*)'      EPSE2=' ,EPSE2,'      EGE2=' ,EGE2
WRITE(NW1,*)'      LOCATION OF STOP ELEMENT      XCR=' ,XCR
WRITE(NW1,*)'      WIDTH OF STOP ELEMENT      WCS=' ,WCS

```

```

1030 WRITE(NW1,*)'EFFECTIVE DEPTH OF STOP      HCS=',HCS
      WRITE(NW1,*)'PRESCRIBED PRESSURE,P1MAX  =',P1MAX,'(PSI)'
      WRITE(NW1,*)'PRESCRIBED PRESSURE,P2MAX  =',P2MAX,'(PSI)'
      WRITE(NW1,*)
      WRITE(NW1,*)'INITIAL GAP BETWEEN FLANGE 1 & 2,GAP10  =',GAP10,'(
&IN) '
      WRITE(NW1,*)'INITIAL GAP BETWEEN FLANGE 2 & 3,GAP20  =',GAP20,'(
&IN) '
      WRITE(NW1,*)
      IF(IG.EQ.0) GO TO 1040
      IF(IG.EQ.1) GO TO 1050
      WRITE(NW1,*)'IG=',IG,'      RING TYPE GASKET.'
      WRITE(NW1,*)'DISTANCE FROM BOLT LINE TO RING GASKET OUTER EDGE,GG
&  =',GG,'(IN) '
      WRITE(NW1,*)'WIDTH OF RING TYPE GASKET,WIDG          =',WIDG,'(I
&N) '
      WRITE(NW1,*)'RING TYPE GASKET REPRESENTED BY 2,3,4 SPRINGS.'
      GO TO 1060
1040 WRITE(NW1,*)'IG=',IG,'      FULL FACE GASKET.'
      GO TO 1060
1050 WRITE(NW1,*)'IG=',IG,'      FULL FACE GASKET INBOARD OF BOLT CIRCLE.'
1060 WRITE(NW1,*)'NUMBER OF GASKET SPRINGS,NG              =',NG
      WRITE(NW1,*)'NUMBER OF SPRINGS INBOARD BOLT CIRCLE,NING =',NING
      IF(KLEAK.EQ.0) GO TO 1061
      WRITE(NW1,*)'KLEAK=1,ASSUME LEAKAGE WHEN ALL SPRINGS INBOARD OF BO
&LT HOLES FAIL.'
      GO TO 1062
1061 WRITE(NW1,*)'KLEAK=0,ASSUME LEAKAGE WHEN ALL SPRINGS INBOARD OF BO
&LT CIRCLE FAIL.'
1062 WRITE(NW1,*)
      WRITE(NW1,*)'PRELOADING PRINTOUT STEP SIZE,SIZE1      =',SIZE1,'(
&PSI) '
      WRITE(NW1,*)'PRESSURIZING PRINTOUT STEP SIZE,SIZE2   =',SIZE2,'(
&PSI) '
      IF(N1.EQ.0) GO TO 1070
      IF(N1.EQ.1) GO TO 1080
      WRITE(NW1,*)'N1=',N1,'      INTERMEDIATE OUTPUT
&.'
      GO TO 1090
1070 WRITE(NW1,*)'N1=',N1,'      LIMITED OUTPUT.'
      GO TO 1090
1080 WRITE(NW1,*)'N1=',N1,'      FULL OUTPUT FOR FLANGE AND GASKET.'
1090 WRITE(NW1,*)
      WRITE(NW1,*)'BOLT PRESTRESS                          =',CCC
      WRITE(NW1,*)'BOLT ALLOWABLE STRESS FACTOR,SAFCB     =',SAFCB
      WRITE(NW1,*)
      WRITE(NW1,*)'PRELOADING INCREMENT SIZE,DDD          =',DDD,'(IN
&) '
      WRITE(NW1,*)'PRESSURIZING INCREMENT SIZE,PDD        =',PDD,'(PS
&I) '
1091 CONTINUE

```

C CALCULATION OF CONSTANTS

```

WL=A+B
BKO=3.14159265*EB*(DB*DB)/(4.0*BL)
D=2.*3.14159265*(RB-A)/FLOAT(NB)
BRKO=3.14159265*EB*(DB**4)/(64.0*BL)
PRESIG=CCC
ALSIGB=SAFCB*SIGMBY
FI1=3.14159265/6.0*RB*(HF1**3)/(FLOAT(NB)*(1.0-(POIS1**2)))
FI2=3.14159265/6.0*RB*(HF2**3)/(FLOAT(NB)*(1.0-(POIS2**2)))
FI3=3.14159265/6.0*RB*(HF3**3)/(FLOAT(NB)*(1.0-(POIS3**2)))
  IF(NTST.GE.1) GO TO 1101
  WRITE(NW1,*)
  WRITE(NW1,*)
  WRITE(NW1,*)'**** SOME CONSTANTS ****'
  WRITE(NW1,*)'WL=',WL
  WRITE(NW1,*)'BKO=',BKO,'; BRKO=',BRKO
  WRITE(NW1,*)'D=',D
  WRITE(NW1,*)'BOLT PRESTRESS, PRESIG=',PRESIG
  WRITE(NW1,*)'BOLT ALLOWABLE STRESS, ALSIGB=',ALSIGB
  WRITE(NW1,*)'FI1=',FI1,' FI2=',FI2,' FI3=',FI3
1101  CONTINUE
  IF(IG.NE.2) GO TO 1300
  XG(1)=- (A+WIDG+GG)/2.0
  AG(1)=3.14159265*((RB-WIDG-GG)**2-(RB-A)**2)/FLOAT(NB)
  DO 1200 I=2,4
    XG(I)=- (GG+(FLOAT(5)-FLOAT(I)-0.5)*WIDG/(FLOAT(5)-2.0))
    AG(I)=3.14159265*((RB+XG(I)+WIDG/6.0)**2-(RB+XG(I)-WIDG/6.0)**2
&      )/FLOAT(NB)
1200  CONTINUE
  XG(5)=-GG/2.0
  AG(5)=3.14159265*(RB**2-(RB-GG)**2)/FLOAT(NB)
  IF(IGAS.LT.20)XG(IGAS)=-XCR
  IF(IGAS.LT.20)AG(IGAS)=2*3.14160*(RB+XG(IGAS))*WCS/FLOAT(NB)
  GO TO 1500
1300  DO 1400 I=1,NING
    XG(I)=- (A*FLOAT(2*NING-(2*I-1))/FLOAT(2*NING))
    AG(I)=2.0*3.14159265*(RB+XG(I))*A/FLOAT(NING*NB)
1400  CONTINUE
1500  NINGP1=NING+1
  DO 1600 I=NINGP1,NG
    XG(I)=B*FLOAT(2*(I-NING)-1)/FLOAT(2*(NG-NING))
    AG(I)=2.0*3.14159265*(RB+XG(I))*B/FLOAT((NG-NING)*NB)
1600  CONTINUE
1700  WRITE(NW1,*)'XG(I):',(XG(I),I=1,NG)
  WRITE(NW1,*)'AG(I):',(AG(I),I=1,NG)
  EGE1=EGE1*HG1/HCS
  EGE2=EGE2*HG2/HCS
  AL=A/WL
  ELR=WL/RB
C INITIAL VALUES.
Z1=WL/RB**2
L2=3-NFL

```

```

L3=NFL-2
WRITE(NW1,*)' NFL=',NFL,' L2=',L2,' L3=',L3
NNN=1
ISTG=1
KP=1
BK=BK0
  BFO=0.
  BF1D=0.
  BF3D=0.
BRK=BRK0
NYIELD=0
NSTOP=0
MTM1=0
MTM2=0
DO 1900 I=1,NG
  W1(I)=0.0
  W2(I)=0.0
  W3(I)=0.0
  WA1=0.0
  WA2=0.0
  WA3=0.0
  ROTAA1=0.0
  ROTAA2=0.0
  ROTAA3=0.0
  LAMDA1(I)=0
  LAMDA2(I)=0
  SIGM1(I)=0.0
  SIGM2(I)=0.0
  SIGMF1(I)=0.
  SIGMF2(I)=0.
  LOAD1(I)=1
  LOAD2(I)=1
  MEPS1(I)=1
  MEPS2(I)=1
  EPS1(I)=0.
  EPS2(I)=0.
  FEPS1(I)=0.
  FEPS2(I)=0.
  LAST1(I)=1
  LAST2(I)=1
  FG1F(I)=0.0
  FG3F(I)=0.0
C TO COMPUTE INITIAL GASKET SPRING RATES.
  GK1(I)=AG(I)*EG1/HG1
  GK2(I)=AG(I)*EG2/HG2
  GK1GK2(I)=GK1(I)+GK2(I)
1900 CONTINUE
  BM=0.0
  GAP1=GAP10
  GAP2=GAP20
  P1=0.0
  P2=0.0

```

```

DO 1905 I=1,21
  BMTR1(I)=0.0
  BMTR3(I)=0.0
  BMTT1(I)=0.0
  BMTT3(I)=0.0
1905 CONTINUE
C PRELOADING INCREMENTS
  P1D=0.0
  P2D=0.0
  DDA=DDD
C GASKET SPRING RATE CORRECTION FOR RING TYPE GASKET.
  IF(IG.EQ.0) GO TO 1930
  IF(IG.EQ.1) GO TO 1910
  GK1(1)=0.0
  GK1(5)=0.0
  GK2(1)=0.0
  GK2(5)=0.0
  GK1GK2(1)=0.0
  GK1GK2(5)=0.0
1910 DO 1920 I=NINGP1,NG
  GK1(I)=0.0
  GK2(I)=0.0
  GK1GK2(I)=0.0
1920 CONTINUE
1930 CONTINUE
  WRITE(NW1,*)
  WRITE(NW1,*)
  WRITE(NW1,*)
  WRITE(NW1,*) '***** PRELOADING STAGE OUTPUT *****'
  WRITE(NW1,*) 'PRELOADING INCREMENTS:'
  WRITE(NW1,*) 'P1D=',P1D
  WRITE(NW1,*) 'P2D=',P2D
  WRITE(NW1,*) 'DDA=',DDD, ' LOAD STEP MODIFIER=',DSPEC
  DDA0=DDA
  WRITE(NW1,*) 'CURRENT GASKET SPRING RATES'
  WRITE(NW1,*) ' GK1=',(GK1(M),M=1,NG)
  WRITE(NW1,*) ' GK2=',(GK2(M),M=1,NG)
C TO COMPUTE STIFFNESS MATRIX COEFFICIENTS AND FORCE VECTOR.
2200 CONTINUE
  NIT=0
2201 CONTINUE
  CALL COEFI
  NEQ=5
  IF(NFL.EQ.2)NEQ=3
  CALL LEQT(AA,BB,NEQ)
  CALL ANALYS(NIT,NIT1,ICLK)
  IF(ICLK.GT.0) GO TO 2201
C IF ISTG=2, TURN INTO PRESSURIZING STAGE;
C OTHERWISE, REPEAT CALCULATION OF PRELOADING STAGE.
  IF(ISTG.EQ.2) GO TO 2300
  GO TO 2200

```

```

C CALCULATION OF PRESSURIZING STAGE.
2300 CONTINUE
WRITE(NW1,*)
WRITE(NW1,*)
WRITE(NW1,*)
WRITE(NW1,*)'***** PRESSURIZING STAGE OUTPUT *****'
NUNL=1
IF(IG.EQ.2.AND.IGAS.NE.1)NUNL=2
NSTRT=NUNL
P1D=PDD
P2D=P1D*P2MAX/P1MAX
DDA=0.0
NO21=0
NNN=1
C GASKET SPRINGS 1 OF THE TWO GASKETS ARE ASSUMED TO BE IN
C UNLOADING AT FIRST PRESSURIZING STEP; OTHERS ARE STILL IN LOADING.
DO 4301 I=NSTRT,NUNL
IF(LOAD1(I).LT.0)GO TO 4304
CK=SIGMF1(I)/(EPSF1(I)*DSDE01)-1.0
GK1(I)=SIGMF1(I)*(1.0+CN1*CK)/(EPSF1(I)*(1.0+CK))*AG(I)/HG1
4304 CONTINUE
IF(NFL.EQ.2)GO TO 4306
IF(LOAD2(I).LT.0) GO TO 4306
CK=SIGMF2(I)/(EPSF2(I)*DSDE02)-1.0
GK2(I)=SIGMF2(I)*(1.0+CN2*CK)/(EPSF2(I)*(1.0+CK))*AG(I)/HG2
4306 CONTINUE
LAST1(I)=-1
LAST2(I)=-1
4301 CONTINUE
WRITE(6,*)' PRESSURIZING BOTH SIDES OF UNIT TOGETHER'
WRITE(NW1,*)'P1 AND P2 PRESSURIZED SIMULTANEOUSLY.'
4400 CONTINUE
IF(NO21.LE.1)NO21=NO21+1
IF(NO21.EQ.1) GO TO 4500
P1D=PDD
P2D=P1D*P2MAX/P1MAX
GO TO 4600
4500 P1D=0.00001*PDD
P2D=P1D*P2MAX/P1MAX
WRITE(NW1,*)' GK1=',(GK1(M),M=1,NG)
WRITE(NW1,*)' GK2=',(GK2(M),M=1,NG)
4600 CONTINUE
4800 CONTINUE
NIT=0
4801 CONTINUE
CALL COEFI
CALL LEQT(AA,BB,NEQ)
CALL ANALYS(NIT,NIT1,ICLK)
IF(ICLK.GT.0)GO TO 4801
C TO CHECK PRESSURE.
IF(P1.LT.P1MAX) GO TO 4400
WRITE(6,*)'PRESSURIZING STAGE COMPLETED.'
```

```

WRITE(NW1,*)'PRESSURIZING STAGE COMPLETED.'
STOP
END

C
$CONTROL SEGMENT=SEGMAIN
C SUBROUTINE COEF1 COMPUTES ELEMENTS OF STIFFNESS MATRIX AND
C FORCE VECTOR
SUBROUTINE COEF1
  IMPLICIT DOUBLE PRECISION (A-H,O-Z)
  COMMON /AAA/AA(12,12),BB(12),BBF(12)
  COMMON /CC/A,B,RB,NB,NG,NING,GG,WIDG,WL
  COMMON /BBC/EF1,POIS1,HF1,SIGFY1,EF2,POIS2,HF2,SIGFY2,
&          EF3,POIS3,HF3,SIGFY3
  COMMON /FF/C1(2,3),C2(2,3),C3(2,3)
  COMMON /GG/BF1D,BF3D,P1MAX,P2MAX,BFO
  COMMON /II/IG,KLEAK,NPMODE,SIZE1,SIZE2,N1,CCC,SAFCB,MATRIX
  COMMON /QQ/GK1(12),GK2(12),GK1GK2(12)
  COMMON /KK/NNN,ISTG,KP,NW1
  COMMON /RR/BK0,BRK0,BK,BRK,D,PRESIG,ALSIGB
  COMMON /SS/FI1,FI2,FI3
  COMMON/RST/Z1,NFL,L2,L3
  COMMON /TT/P1,P2,P1D,P2D,DDA,DDAO,DSPEC
  BKK=A*A*BK
  CALL SUM(GK1,SK1,SXK1,SX2K1)
  AA(1,1)=BK-D*C1(1,1)+SK1
  AA(2,1)=D*(-C1(1,2))+SXK1+A*BK
  AA(3,1)=-SXK1-L2*A*BK
  AA(4,1)=-BK*L3
  AA(5,1)=-L3*A*BK
  AA(2,2)=-D*C1(2,2)+BKK
&      +SX2K1+BRK+EF1*FI1*WL/(RB*RB)
  AA(3,2)=-SX2K1-L2*(BRK+BKK)
  AA(4,2)=-L3*A*BK
  AA(5,2)=-BRK*L3-L3*BKK
  CALL SUM(GK1GK2,SKK,SXKK,SX2KK)
  CALL SUM(GK2,SK2,SXK2,SX2K2)
  AA(3,3)=SX2KK-D*C2(2,2)+L2*(BRK+BKK)+EF2*FI2*Z1
  AA(4,3)=-SXK2
  AA(5,3)=-SX2K2
  AA(4,4)=SK2-D*C3(1,1)+BK*L3
  AA(5,4)=SXK2-D*C3(1,2)+L3*A*BK
  AA(5,5)=SX2K2-D*C3(2,2)+L3*(BRK+BKK)+EF3*FI3*Z1
  DO 84 I=1,5
    AA(I,I)=AA(I,I)/EF1
  DO 85 J=1,5
    IF(J.GT.I) AA(J,I)=AA(J,I)/EF1
85  CONTINUE
84  CONTINUE
  DO 8000 I=1,5
  DO 8001 J=1,5
  AA(I,J)=AA(J,I)
8001 CONTINUE

```

```

8000 CONTINUE
      BK1=DDA*BK
      BB(1)=-P1D*(-D*C1(1,3))+BK*DDA
      BB(2)=-P1D*(-D*C1(2,3))+A*BK*DDA
      BB(3)=P2D*(-D*C2(2,3))
      &      -P1D*(-D*C2(2,3))-L2*DDA*BK*A
      BB(4)=P2D*(D*C3(1,3))-BK*DDA*L3
      BB(5)=P2D*(D*C3(2,3))-L3*A*BK*DDA
C TO KEEP FORCE VECTOR VALUES IN "BBF(12)" FOR PRINTOUT.
      DO 100 I=1,5
          BBF(I)=BB(I)
100 CONTINUE
      RETURN
      END

C
$CONTROL SEGMENT=SEGMAIN
C THIS SUBROUTINE SUM IS USED FOR COMPUTING SUMATIONS IN
C COEFFICIENT COMPUTATION
      SUBROUTINE SUM(GK,SK,SXK,SX2K)
          IMPLICIT DOUBLE PRECISION (A-H,O-Z)
          DIMENSION GK(12)
          COMMON /CC/A,B,RB,NB,NG,NING,GG,WIDG,WL
          COMMON /OO/XG(12),AG(12)
          SK=0.0
          SXK=0.0
          SX2K=0.0
          DO 5001 I=1,NG
              SK=SK+GK(I)
              SXK=SXK+(XG(I)+A)*GK(I)
              SX2K=SX2K+(XG(I)+A)*(XG(I)+A)*GK(I)
5001 CONTINUE
          RETURN
          END

$CONTROL SEGMENT=SEGMAIN
C SUBROUTINE LEQT IS A SIMULTANEOUS-EQUATION-SOLVER.
      SUBROUTINE LEQT(Q,F,N)
          IMPLICIT DOUBLE PRECISION (A-H,O-Z)
          DIMENSION A(12,13),Q(12,12),X(12),F(12)
          M=N+1
          L=N-1
          DO 1 I=1,N
              DO 1 J=1,N
1              A(I,J)=Q(I,J)
              DO 3 I=1,N
3              A(I,M)=F(I)
              DO 12 K=1,L
                  JJ=K
                  BIG=DABS(A(K,K))
                  KP1=K+1
                  DO 7 I=KP1,N
                      AB=DABS(A(I,K))
                      IF(BIG-AB) 6,7,7
6                  BIG=AB

```

```

JJ=I
7  CONTINUE
  IF(JJ-K) 8,10,8
8  DO 9 J=K,M
  TEMP=A(JJ,J)
  A(JJ,J)=A(K,J)
9  A(K,J)=TEMP
10 DO 11 I=KP1,N
  QUOT=A(I,K)/A(K,K)
  DO 11 J=KP1,M
11 A(I,J)=A(I,J)-QUOT*A(K,J)
  DO 12 I=KP1,N
12 A(I,K)=0.0
  X(N)=A(N,M)/A(N,N)
  DO 14 NN=1,L
  SUM=0.0
  I=N-NN
  IP1=I+1
  DO 13 J=IP1,N
  SUM=SUM+A(I,J)*X(J)
13 X(I)=(A(I,M)-SUM)/A(I,I)
14 DO 15 I=1,N
15 F(I)=X(I)
  RETURN
  END

```

C

\$CONTROL SEGMENT=SEG1

C SUBROUTINE "ANALYS" IS USED FOR ANALIZING RATE DEFCRATIONS AND
C COMPUTING NONLINEAR PROPERTIES, AND GETTING RESULTS.

```

  SUBROUTINE ANALYS(NIT,NIT1,ICLK)
    IMPLICIT DOUBLE PRECISION (A-H,O-Z)
    DIMENSION W1D(12),W2D(12),W3D(12),DEPS1(12),DEPS2(12)
    DIMENSION G1(21),G2(21),G3(21),MAST1(12),MAST2(12)
    DIMENSION FORCE1(12),FORCE2(12),FMG1D(12),FMG3D(12)
    DIMENSION XX(21),SFGX1(21),SFGX3(21),KO(21),G2XX(21),G3XX(21),
&      WXX1D(21),WXX3D(21),RXX1D(21),RXX3D(21),BMTR1D(21),
&      BMTR3D(21),BMTT1D(21),BMTT3D(21),SIGFR1(21),SIGFR3(21),
&      SIGFT1(21),SIGFT3(21)
    COMMON /AAA/AA(12,12),BB(12),BBF(12)
    COMMON /AAB/DB,BL,EB,SIGMBY
    COMMON /BBC/EF1,POIS1,HF1,SIGFY1,EF2,POIS2,HF2,SIGFY2,EF3,
&      POIS3,HF3,SIGFY3
    COMMON /CC/A,B,RB,NB,NG,NING,GG,WIDG,WL
    COMMON /DD/EG1,HG1,COEF1,EPS11,CN1,DSDE01
    COMMON /EE/EG2,HG2,COEF2,EPS12,CN2,DSDE02
    COMMON /FF/C1(2,3),C2(2,3),C3(2,3)
    COMMON /GG/BF1D,BF3D,P1MAX,P2MAX,BFO
    COMMON /HH/GAP1,GAP2,MTM1,MTM2,NYIELD,NSTOP
    COMMON /II/IG,KLEAK,NPMODE,SIZE1,SIZE2,N1,CCC,SAFCB,MATRIX
    COMMON /KK/NNN,ISTG,KP,NW1
    COMMON /LAM/LAMDA1(12),LAMDA2(12),LOAD1(12),LOAD2(12)

```

```

COMMON /MM/LAST1(12),LAST2(12),FEPS1(12),FEPS2(12)
COMMON /OO/XG(12),AG(12)
COMMON /EEP/MEPS1(12),MEPS2(12),EPS1(12),EPS2(12)
COMMON /SIGF/SIGMF1(12),SIGMF2(12),SIGM1(12),SIGM2(12)
COMMON/ESIG/ EPSF1(12),EPSF2(12)
COMMON /QQ/GK1(12),GK2(12),GK1GK2(12)
COMMON /RR/BK0,BRK0,BK,BRK,D,PRESIG,ALSIGB
COMMON /SS/FI1,F12,F13
COMMON/RST/Z1,NFL,L2,L3
COMMON /TT/P1,P2,P1D,P2D,DDA,DDAO,DSPEC
COMMON /VV/W1(12),W2(12),W3(12),WA1,WA2,WA3,ROTA1,ROTA2,ROTA3
COMMON /WW/BM,BF,BMTR1(21),BMTR3(21),BMTT1(21),BMTT3(21),
&      FG1F(12),FG3F(12)
COMMON/ZZZ/EPS21,EPS22,EPSL1,EPSL2
COMMON/XYZ/EGE1,EGE2,EPSE1,EPSE2,IGAS
C CURRENT VALUES OF RATE VARIABLES.
DO 38505 I=1,5
  BB(I)=BB(I)/EF1
38505  CONTINUE
      W01D=BB(1)
      THET1D=BB(2)
      W02D=0.
      THET2D=BB(3)
      W03D=BB(4)
      THET3D=BB(5)
      IF(NFL.EQ.2)W03D=0.
      IF(NFL.EQ.2)THET3D=0.
C CURRENT VALUES OF DEFORMATION RATES AND DEFORMATIONS OF SPRINGS.
  ICHK=0
  DO 100 I=1,NG
C TO COMPUTE DEFORMATION RATES OF FLANGES AT EACH GASKET
C SPRING POSITION.
  G1(I)=XG(I)+A
  W1D(I)=W01D+G1(I)*THET1D
  W2D(I)=W02D+G1(I)*THET2D
  W3D(I)=W03D+G1(I)*THET3D
C TO COMPUTE DEFORMATIONS OF FLANGES AT EACH GASKET SPRING POSITION
  DEPS1(I)=(W1D(I)-W2D(I))/HG1
  DEPS2(I)=(W2D(I)-W3D(I))/HG2
  MAST1(I)=LAST1(I)
  MAST2(I)=LAST2(I)
  IF(GK1(I).EQ.0.)GO TO 10
  IF(LAST1(I)*DEPS1(I).GE.0.) GO TO 10
  ICHK=ICHK+1
  IF(LOAD1(I).EQ.1)ICHK=ICHK-1
  IF(LOAD1(I).EQ.1) GO TO 10
  LAST1(I)=-LAST1(I)
  IF(I.EQ.IGAS) GO TO 10
  IF(LAST1(I).LT.0) GO TO 11
  IF(LOAD1(I).LT.0)GO TO 11
  IF(EPS1(I).LE.EPS11)EGINST=EG1
  EGINST=SIGM1(I)/EPS11

```

```

IF(EPS1(I).GT.EPSL1)EGINST=SIGM1(I)/EPS21
IF(EPS1(I).EQ.0.) EGINST=0.
GO TO 12
11 CONTINUE
CK=SIGMF1(I)/(EPSF1(I)*DSDE01)-1.
EGINST=(SIGMF1(I)/(EPSF1(I)*(1.+CK)))*
1(1.+CK*CN1*((EPS1(I)/EPSF1(I))**(CN1-1.)))
12 CONTINUE
GK1(I)=EGINST*AG(I)/HG1
10 CONTINUE
IF(NFL.EQ.2) GO TO 20
IF(GK2(I).EQ.0.)GO TO 20
IF(LAST2(I)*DEPS2(I).GE.0.) GO TO 20
ICLK=ICLK+1
LAST2(I)=-LAST2(I)
IF(LOAD2(I).EQ.1)ICLK=ICLK-1
IF(LOAD2(I).EQ.1) GO TO 20
IF(I.EQ.IGAS) GO TO 20
IF(LAST2(I).LT.0) GO TO 21
IF(LOAD2(I).LT.0)GO TO 21
IF(EPS2(I).LE.EPS12)EGINST=EG2
EGINST=SIGM2(I)/EPS12
IF(EPS2(I).GT.EPSL2)EGINST=SIGM2(I)/EPS22
IF(EPS2(I).EQ.0.) EGINST=0.
GO TO 22
21 CONTINUE
CK=SIGMF2(I)/(EPSF2(I)*DSDE02)-1.
EGINST=(SIGMF2(I)/(EPSF2(I)*(1.+CK)))*
1(1.+CK*CN2*((EPS2(I)/EPSF2(I))**(CN2-1.)))
22 CONTINUE
GK2(I)=EGINST*AG(I)/HG2
20 CONTINUE
100 CONTINUE
IF(ICLK.EQ.0.AND.NIT.GT.0) GO TO 10001
NIT=NIT+1
IF(NIT.GT.2**NIT1) NIT=-1004
IF(NIT1.LE.1) ICHK=0.
IF(NIT1.LE.1)GO TO 10001
IF(NIT.LT.0)WRITE(NW1,*) 'ITERATIONS EXCEEDED IN
1SIMULTANEOUS EQUATION SOLVER'
IF(NIT.LT.0)WRITE(NW1,*) P1,P2,ICLK,NIT
IF(NIT.LT.0)WRITE(NW1,*) 'LOAD1', (LOAD1(I),I=1,NG)
IF(NIT.LT.0)WRITE(NW1,*) 'MAST1', (MAST1(I),I=1,NG)
IF(NIT.LT.0)WRITE(NW1,*) 'LAST1', (LAST1(I),I=1,NG)
IF(NIT.LT.0)WRITE(NW1,*) (DEPS1(I),I=1,NG)
IF(NIT.LT.0)WRITE(NW1,*) 'LOAD2', (LOAD2(I),I=1,NG)
IF(NIT.LT.0)WRITE(NW1,*) 'MAST2', (MAST2(I),I=1,NG)
IF(NIT.LT.0)WRITE(NW1,*) 'LAST2', (LAST2(I),I=1,NG)
IF(NIT.LT.0)WRITE(NW1,*) (DEPS2(I),I=1,NG)
IF(NIT.EQ.-1000)STOP
IF(ICLK.EQ.0)GO TO 10001

```

```

        RETURN
10001 CONTINUE
C****ITERATIONS SUCCESSFUL--CALCULATE VALUES FOR THIS STEP
        RAT=1.0
        RAT1=RAT
        RAT2=RAT
        IF(IGAS.GT.20) GO TO 31
        DE1=EPSE1-EPS1(IGAS)
        DE2=EPSE2-EPS2(IGAS)
        IF(DE1.LT.0.0.AND.DE2.LT.0.0)GO TO 31
        IF(FEPS1(IGAS).GT.0.AND.DEPS1(IGAS).GT.DE1)RAT1=DE1/DEPS1(IGAS)
        IF(FEPS2(IGAS).GT.0.AND.DEPS2(IGAS).GT.DE2)RAT2=DE2/DEPS2(IGAS)
        RAT=DABS(RAT1)
        IF(DABS(RAT2).LT.RAT)RAT=DABS(RAT2)
        W01D=RAT*W01D
        THET1D=THET1D*RAT
        THET2D=THET2D*RAT
        W03D=W03D*RAT
        THET3D=THET3D*RAT
31 CONTINUE
        DO 30 I=1,NG
        DEPS1(I)=RAT*DEPS1(I)
        DEPS2(I)=RAT*DEPS2(I)
        W1D(I)=W1D(I)*RAT
        W2D(I)=W2D(I)*RAT
        W3D(I)=W3D(I)*RAT
        EPS1(I)=EPS1(I)+DEPS1(I)
        EPS2(I)=EPS2(I)+DEPS2(I)
        IF(FEPS1(I).GE.0.0.AND.DEPS1(I).LT.0)MEPS1(I)=2
        IF(FEPS1(I).LT.0.0.AND.DEPS1(I).GT.0)MEPS1(I)=3
        IF(FEPS2(I).GE.0.0.AND.DEPS2(I).LT.0)MEPS2(I)=2
        IF(FEPS2(I).LT.0.0.AND.DEPS2(I).GT.0)MEPS2(I)=3
        FEPS1(I)=DEPS1(I)
        FEPS2(I)=DEPS2(I)
        W1(I)=W1(I)+W1D(I)
        W2(I)=W2(I)+W2D(I)
        W3(I)=W3(I)+W3D(I)
30 CONTINUE
        WA1D=W01D
        WA2D=W02D
        WA3D=W03D
C ROTATION INCREMENT OF BOLT.
        ROTAD=THET1D-L2*THET2D-L3*THET3D
C BOLT BENDING AND EXTENSION CALCULATIONS
        BMD=BRK*ROTAD
        EV1D=C1(1,1)*WA1D+C1(1,2)*THET1D+C1(1,3)*P1D
        EM1D=C1(2,1)*WA1D+C1(2,2)*THET1D+C1(2,3)*P1D
        EV3D=C3(1,1)*WA3D+C3(1,2)*THET3D+C3(1,3)*P2D
        EM3D=C3(2,1)*WA3D+C3(2,2)*THET3D+C3(2,3)*P2D
        DWB=(L3*W03D+L2*W02D-W01D)+A*(L3*THET3D+L2*THET2D-THET1D)
        BEXT=DDA+DWB

```

```

      BFO=BFO+BEXT*BK
      TD=-BEXT*BK
      BM=BM+BMD
      IF(IG.EQ.0) GO TO 400
      IF(IG.EQ.1) GO TO 200
      IF(IGAS.NE.1) EPS1(1)=0.0
      IF(IGAS.NE.5) EPS1(5)=0.0
      IF(IGAS.NE.1) EPS2(1)=0.0
      IF(IGAS.NE.5) EPS2(5)=0.0
200   NINGP1=NING+1
      DO 300 I=NINGP1,NG
         IF(I.EQ.IGAS) GO TO 300
         EPS1(I)=0.0
         EPS2(I)=0.0
300   CONTINUE
C TO CHECK METAL-TO-METAL CONTACT.
400   CONTINUE
      IF(IG.EQ.0) GO TO 1000
C TO COMPUTE DEFLECTIONS OF OUTER EDGES OF FLANGES.
      WOUT1=W01D+THET1D*WL
      WOUT2=W02D+THET2D*WL
      WOUT3=W03D+THET3D*WL
      GAP1=GAP1-(WOUT1-WOUT2)
      IF(GAP1.GT.0.0) GO TO 700
      MTM1=1
      GO TO 800
700   MTM1=0
800   GAP2=GAP2-(WOUT2-WOUT3)
      IF(GAP2.GT.0.0) GO TO 900
      MTM2=1
      GO TO 1000
900   MTM2=0
1000  DO 1230 I=1,NG
C EPS IS CURRENT VALUE OF GASKET STRAIN;
      IF(DEPS1(I).GT.0.00)GO TO 1160
      LOAD1(I)=-1
      GO TO 1170
1160  LOAD1(I)=1
      IF(EPSF1(I).LE.EPS1(I))EPSF1(I)=EPS1(I)
1170  CONTINUE
      LAST1(I)=LOAD1(I)
1180  CONTINUE
      IF(DEPS2(I).GT.0.00) GO TO 1210
      LOAD2(I)=-1
      GO TO 1220
1210  LOAD2(I)=1
      IF(EPSF2(I).LE.EPS2(I))EPSF2(I)=EPS2(I)
1220  CONTINUE
      LAST2(I)=LOAD2(I)
      IF(NFL.EQ.2)EPSF2(I)=1.
1230  CONTINUE
C

```

```

C TO DETERMINE CURRENT VALUES OF PRESSURES P1,P2.
  P1=P1+P1D
  P2=P2+P2D
C TO CHECK WHETHER PRESCRIBED MAX.PRESSURE REACHED.
  IF(P1.GE.P1MAX) GO TO 1270
  GO TO 1300
C NSTOP=1 TO PRINT FINAL RESULTS AND TO TERMINATE THE PROGRAM.
1270 WRITE(6,*)'PRESSURE REACHES PRESCRIBED VALUE;ANALYSIS COMPLETED'
  WRITE(NW1,*)
  WRITE(NW1,*)'PRESSURE REACHES PRESCRIBED VALUE;ANALYSIS COMPLETED'
  WRITE(NW1,*)
  NSTOP=1
C TO COMPUTE GASKET SPRING RATES,STRESSES,AND FORCES.
1300 CONTINUE
C
1305 DO 1400 I=1,NG
C FOR GASKET 1.
  IF(I.NE.IGAS)GO TO 18000
  IF(EPS1(I).GT.0.95*EPSE1.AND.ISTG.EQ.1)DDA=DSPEC*DDAO
  IF(EPS1(I).LT.EPSE1)GO TO 1330
  SIGM1(I)=SIGM1(I)+GK1(I)*HG1/AG(I)*DEPS1(I)
  EGINST=EGE1
  IF(SIGM1(I).GT.SIGMF1(I))SIGMF1(I)=SIGM1(I)
  GO TO 1340
18000 CONTINUE
  IF(EPS1(I).EQ.0.)GO TO 1330
  IF(LOAD1(I).EQ.-1) GO TO 1320
  IF(MEPS1(I).EQ.3.AND.EPSF1(I).GT.EPS1(I)) GO TO 1320
  IF(EPS1(I).LE.EPS11) GO TO 1310
  SIGM1(I)=SIGM1(I)+GK1(I)*HG1/AG(I)*DEPS1(I)
  EGINST=SIGM1(I)/EPS11
  IF(EPS1(I).GT.EPS11)EGINST=SIGM1(I)/EPS21
  IF(SIGMF1(I).LT.SIGM1(I))SIGMF1(I)=SIGM1(I)
  GO TO 1340
1310 EGINST=EG1
  SIGM1(I)=EG1*EPS1(I)
  SIGMF1(I)=SIGM1(I)
  GO TO 1340
1320 CONTINUE
  CK=SIGMF1(I)/(EPSF1(I)*DSDE01)-1.0
  EGINST=(SIGMF1(I)/(EPSF1(I)*(1.0+CK)))
  & *(1.0+CK*CN1*((EPS1(I)/EPSF1(I))**(CN1-1.0)))
  SIGM1(I)=SIGM1(I)+
  & GK1(I)*HG1/AG(I)*DEPS1(I)
  GO TO 1340
1330 EGINST=0.0
  SIGM1(I)=0.0
1340 GK1(I)=EGINST*AG(I)/HG1
  FORCE1(I)=SIGM1(I)*AG(I)
C FOR GASKET 2.
  IF(NFL.EQ.2) GO TO 1380
  IF(I.NE.IGAS)GO TO 18001

```

```

      IF(EPS2(I).GT.0.95*EPSE2.AND.ISTG.EQ.1)DDA=DSPEC*DDAO
      IF(EPS2(I).LT.EPSE2)GO TO 1380
      SIGM2(I)=SIGM2(I)+GK2(I)*HG2/AG(I)*DEPS2(I)
      EGINST=EGE2
      IF(SIGM2(I).GT.SIGMF2(I))SIGMF2(I)=SIGM2(I)
      GO TO 1390
18001 CONTINUE
      IF(EPS2(I).EQ.0) GO TO 1380
      IF(LOAD2(I).EQ.-1) GO TO 1370
      IF(MEPS2(I).EQ.3.AND.EPSF2(I).GT.EPS2(I)) GO TO 1370
      IF(EPS2(I).LE.EPS12) GO TO 1360
      SIGM2(I)=SIGM2(I)+GK2(I)*HG2/AG(I)*DEPS2(I)
      SIGMF2(I)=SIGM2(I)
      EGINST=SIGM2(I)/EPS12
      IF(EPS2(I).GT.EPSL2)EGINST=SIGM2(I)/EPS22
      GO TO 1390
1360   EGINST=EG2
      SIGM2(I)=EG2*EPS2(I)
      IF(SIGMF2(I).LT.SIGM2(I))SIGMF2(I)=SIGM2(I)
      GO TO 1390
1370   CONTINUE
      CK=SIGMF2(I)/(EPSF2(I)*DSDE02)-1.0
      EGINST=(SIGMF2(I)/(EPSF2(I)*(1.0+CK)))
      &      *(1.0+CK*CN2*((EPS2(I)/EPSF2(I))**(CN2-1.0)))
      SIGM2(I)=SIGM2(I)+
      & GK2(I)*HG2/AG(I)*DEPS2(I)
      GO TO 1390
1380   EGINST=0.0
      SIGM2(I)=0.0
1390   GK2(I)=EGINST*AG(I)/HG2
      FORCE2(I)=SIGM2(I)*AG(I)
1400 CONTINUE
      IF(ISTG.EQ.2) GO TO 1410
      IF(IGAS.GT.20) GO TO 1410
      FG1=BFO
      FG2=BFO
      DO 1401 I=1,NG
      IF(I.EQ.IGAS) GO TO 1401
      FG1=FG1-FORCE1(I)
      FG2=FG2-FORCE2(I)
1401 CONTINUE
      IF(FG1.LE.0.) FG1=0.
      IF(FG2.LE.0.)FG2=0.
      IF(FORCE1(IGAS).GT.0.)R1=FG1/FORCE1(IGAS)
      IF(FORCE2(IGAS).GT.0.)R2=FG2/FORCE2(IGAS)
      IF(FG1.EQ.0.)R1=1.
      IF(FG2.EQ.0.)R2=1.
      SIGM1(IGAS)=R1*SIGM1(IGAS)
      FORCE1(IGAS)=R1*FORCE1(IGAS)
      SIGMF1(IGAS)=R1*SIGMF1(IGAS)
      SIGM2(IGAS)=R2*SIGM2(IGAS)

```

```

      FORCE2(IGAS)=R2*FORCE2(IGAS)
      SIGMF2(IGAS)=R2*SIGMF2(IGAS)
1410  CONTINUE
      IF(IG.EQ.0) GO TO 1430
      IF(IG.EQ.1) GO TO 1415
      IF(IGAS.NE.1)GK1(1)=0.0
      IF(IGAS.NE.5)GK1(5)=0.0
      IF(IGAS.NE.1)GK2(1)=0.0
      IF(IGAS.NE.5)GK2(5)=0.0
      IF(IGAS.NE.1)FORCE1(1)=0.0
      IF(IGAS.NE.5)FORCE1(5)=0.0
      IF(IGAS.NE.1)FORCE2(1)=0.0
      IF(IGAS.NE.5)FORCE2(5)=0.0
      IF(IGAS.NE.1)SIGM1(1)=0.0
      IF(IGAS.NE.5)SIGM1(5)=0.0
      IF(IGAS.NE.1)SIGM2(1)=0.0
      IF(IGAS.NE.5)SIGM2(5)=0.0
      IF(IGAS.NE.1)SIGMF1(1)=0.0
      IF(IGAS.NE.5)SIGMF1(5)=0.0
      IF(IGAS.NE.1)SIGMF2(1)=0.0
      IF(IGAS.NE.5)SIGMF2(5)=0.0
1415  DO 1420 I=NINGP1,NG
      IF(IGAS.NE.I)GK1(I)=0.0
      IF(IGAS.NE.I)GK2(I)=0.0
      IF(IGAS.NE.I)FORCE1(I)=0.0
      IF(IGAS.NE.I)FORCE2(I)=0.0
      IF(IGAS.NE.I)SIGM1(I)=0.0
      IF(IGAS.NE.I)SIGM2(I)=0.0
      IF(IGAS.NE.I)SIGMF1(I)=0.0
      IF(IGAS.NE.I)SIGMF2(I)=0.0
1420  CONTINUE
1430  IF(MTM1.EQ.0) GO TO 1440
      GK1(10)=1.0E+8
1440  IF(MTM2.EQ.0) GO TO 1450
      GK2(10)=1.0E+8
1450  CONTINUE
      DO 19742 J=1,NG
      GK1GK2(J)=GK1(J)+GK2(J)
19742  CONTINUE
      IF(ISTG.EQ.1)GO TO 1610
C TO CHECK GASKET LEAKAGE.
C COMPUTATION OF GASKET SPRING FAILURE INDEX:
C LAMDA=0,IF TIGHT; LAMDA=1,IF LEAK.
      P1C=P1*COEF1
      P2C=P2*COEF2
      DO 1530 I=1,NG
      IF(DABS(SIGM1(I)).LE.P1C) GO TO 1470
      LAMDA1(I)=0
      GO TO 1480
1470  LAMDA1(I)=1
1480  IF(DABS(SIGM2(I)).LT.P2C) GO TO 1490

```

```

        LAMDA2(I)=0
        GO TO 1500
1490    LAMDA2(I)=1
1500    CONTINUE
1530    CONTINUE
C LEAKAGE CRITERION:NLEAK,THE NUMBER OF GASKET SPRINGS INSIDE BOLT HOLES
    IF(IG.EQ.2) GO TO 1540
    NLEAK=IDINT((A-DB/2.0)/(A/FLOAT(NING)))
    IF(KLEAK.EQ.0) NLEAK=NING
    GO TO 1550
1540    NLEAK=4
        IF(IGAS.EQ.5.AND.KLEAK.EQ.0)NLEAK=5
C TO CHECK GASKET 1 LEAKAGE
1550    LEAK=0
        DO 1560 I=1,NLEAK
            LEAK=LEAK+LAMDA1(I)
1560    CONTINUE
    IF(LEAK.LT.NLEAK) GO TO 1580
    NSTOP=1
    WRITE(6,*)'GASKET 1 LEAKAGE OCCURS AT P1=',P1,', P2=',P2
    IF(KLEAK.EQ.0) GO TO 1570
    WRITE(6,*)'WHEN ALL GASKET SPRINGS INBOARD OF BOLT HOLE(N=',NLEAK,
&          ') FAIL SIMULTANEOUSLY.'
    GO TO 1571
1570    WRITE(6,*)'WHEN ALL GASKET SPRINGS INBOARD OF BOLT CIRCLE(N=',NLEA
&K,') FAIL SIMULTANEOUSLY.'
1571    WRITE(NW1,*)'GASKET 1 LEAKAGE OCCURS AT P1=',P1,', P2=',P2
    IF(KLEAK.EQ.0) GO TO 1572
    WRITE(NW1,*)'WHEN ALL GASKET SPRINGS INBOARD OF BOLT HOLE(N=',
&          NLEAK,') FAIL SIMULTANEOUSLY.'
    GO TO 1573
1572    WRITE(NW1,*)'WHEN ALL GASKET SPRINGS INBOARD OF BOLT CIRCLE(N=',NL
&EAK,') FAIL SIMULTANEOUSLY.'
C TO PRINTOUT THE FINAL RESULTS.
1573    WRITE(NW1,*)
        GO TO 1610
C TO CHECK GASKET 2 LEAKAGE
1580    LEAK=0
        IF(NFL.EQ.2) GO TO 1605
        DO 1590 I=1,NLEAK
            LEAK=LEAK+LAMDA2(I)
1590    CONTINUE
    IF(LEAK.LT.NLEAK) GO TO 1610
    NSTOP=1
    WRITE(6,*)'GASKET 2 LEAKAGE OCCURS AT P1=',P1,', P2=',P2
    IF(KLEAK.EQ.0) GO TO 1600
    WRITE(6,*)'WHEN ALL GASKET SPRINGS INBOARD OF BOLT HOLE(N=',NLEAK,
&          ') FAIL SIMULTANEOUSLY.'
    GO TO 1601
1600    WRITE(6,*)'WHEN ALL GASKET SPRINGS INBOARD OF BOLT CIRCLE(N=',NLEA
&K,') FAIL SIMULTANEOUSLY.'

```

```

1601 WRITE(NW1,*)'GASKET 2 LEAKAGE OCCURS AT P1=',P1,', P2=',P2
      IF(KLEAK.EQ.0) GO TO 1602
      WRITE(NW1,*)'WHEN ALL GASKET SPRINGS INBOARD OF BOLT HOLE(N=',
& NLEAK,') FAIL SIMULTANEOUSLY.'
      GO TO 1603
1602 WRITE(NW1,*)'WHEN ALL GASKET SPRINGS INBOARD OF BOLT CIRCLE(N=',NL
& EAK,') FAIL SIMULTANEOUSLY.'
C TO PRINTOUT THE FINAL RESULTS.
1603 WRITE(NW1,*)
1605 CONTINUE
C TO COMPUTE FLANGE STRESSES AND CHECK THEIR STRENGTH.
1610 DO 1620 I=1,10
      XX(I)=-A+(0.5+FLOAT(I-1))*A/10.0
1620 CONTINUE
      XX(11)=(B-A)/40.0
      DO 1630 I=12,21
      XX(I)=(0.5+FLOAT(I-12))*B/10.0
1630 CONTINUE
      S=3.14159265*2.0*(RB-A)/FLOAT(NB)
      S1=S*(1.-A/RB)
C FOR FLANGE 1
      DO 1640 I=1,NG
      FMG1D(I)=- (FORCE1(I)-FG1F(I))
      FMG3D(I)=FORCE2(I)-FG3F(I)
1640 CONTINUE
      DO 1700 I=1,21
      SFGX1(I)=0.0
      DO 1670 J=1,NG
      IF(XG(J).GT.XX(I)) GO TO 1650
      KX=1
      GO TO 1660
1650 KX=0
1660 SFGX1(I)=SFGX1(I)+FMG1D(J)*(XX(I)-XG(J))*FLOAT(KX)
1670 CONTINUE
      IF(XX(I).GT.0.0) GO TO 1680
      KO(I)=0
      GO TO 1690
1680 KO(I)=1
1690 G1(I)=(XX(I)+A)
      WXX1D(I)=W01D+THET1D*G1(I)
      RXX1D(I)=THET1D
      WXX3D(I)=W03D+THET3D*G1(I)
      RXX3D(I)=THET3D
1700 CONTINUE
C COMPUTATION OF INCREMENTS OF BENDING MOMENTS OF FLANGE 1.
      BMAXR1=0.0
      BMAXT1=0.0
      DO 1730 I=1,21
      BMTR1D(I)=(SFGX1(I)+BMD*FLOAT(KO(I))-TD*XX(I)*FLOAT(KO(I))
& +S1*EV1D*(A+XX(I))-S1*EM1D+S1*EF1*(HF1**3))*(WXX1D(I)

```

```

      & -WA1D)/(12.0*RB**2))/(S*(1.+XX(I)/RB))
      BMTT1D(I)=EF1*(HF1**3)*RXX1D(I)/(12.0*RB)+POIS1*BMTR1D(I)
C COMPUTATION OF BENDING MOMENTS OF FLANGE-1.
      BMTR1(I)=BMTR1(I)+BMTT1D(I)
      BMTT1(I)=BMTT1(I)+BMTT1D(I)
C TO DETERMINE MAXIMUM MOMENTS OF FLANGE 1.
      IF(DABS(BMTR1(I)).LT.BMAXR1) GO TO 1710
      BMAXR1=DABS(BMTR1(I))
      IIR1=I
1710  IF(DABS(BMTT1(I)).LT.BMAXT1) GO TO 1720
      BMAXT1=DABS(BMTT1(I))
      IIT1=I
C TO COMPUTE FLANGE STRESSES.
1720  SIGFR1(I)=6.0*BMTR1(I)/(HF1*HF1)
      SIGFT1(I)=6.0*BMTT1(I)/(HF1*HF1)
1730  CONTINUE
C FOR FLANGE 3.
      DO 1740 I=1,NG
      FG1F(I)=FORCE1(I)
      FG3F(I)=FORCE2(I)
1740  CONTINUE
      DO 1790 I=1,21
      SFGX3(I)=0.0
      DO 1770 J=1,NG
      IF(XG(J).GT.XX(I)) GO TO 1750
      KX=1
      GO TO 1760
1750  KX=0
1760  SFGX3(I)=SFGX3(I)+FMG3D(J)*(XX(I)-XG(J))*FLOAT(KX)
1770  CONTINUE
      IF(XX(I).GT.0.0) GO TO 1780
      KO(I)=0
      GO TO 1790
1780  KO(I)=1
1790  CONTINUE
      BMD=-BRK*ROTAD
      TD=BEXT*BK
      EV3D=C3(1,1)*WA3D+C3(1,2)*THET3D+C3(1,3)*P2D
      EM3D=C3(2,1)*WA3D+C3(2,2)*THET3D+C3(2,3)*P2D
      BMAXR3=0.0
      BMAXT3=0.0
      DO 1820 I=1,21
      BMTR3D(I)=(SFGX3(I)+BMD*FLOAT(KO(I))-TD*XX(I)*FLOAT(KO(I))
      & +S*EV3D*(A+XX(I))-S*EM3D+S*EF3*(HF3**3)*(WXX3D(I)
      & -WA3D)/(12.0*RB**2))/S
      BMTT3D(I)=EF3*(HF3**3)*RXX3D(I)/(12.0*RB)+POIS3*BMTR3D(I)
      BMTR3(I)=BMTR3(I)+BMTT3D(I)
      BMTT3(I)=BMTT3(I)+BMTT3D(I)
      IF(DABS(BMTR3(I)).LT.BMAXR3) GO TO 1800
      BMAXR3=DABS(BMTR3(I))
      IIR3=I
1800  IF(DABS(BMTT3(I)).LT.BMAXT3) GO TO 1810

```

```

        BMAXT3=DABS(BMTT3(I))
        I1T3=I
1810    SIGFR3(I)=6.0*BMTR3(I)/(HF3*HF3)
        SIGFT3(I)=6.0*BMTT3(I)/(HF3*HF3)
1820    CONTINUE
C TO COMPUTE FLANGE DISPLACEMENTS AND ROTATIONS AT INNER EDGE.
    WA1=WA1+WA1D
    WA2=WA2+WA2D
    WA3=WA3+WA3D
    ROTAA1=ROTA1+THET1D
    ROTAA2=ROTA2+THET2D
    ROTAA3=ROTA3+THET3D
    EQ1D=C1(1,1)*WA1+C1(1,2)*ROTA1+C1(1,3)*P1
    ER1D=C1(2,1)*WA1+C1(2,2)*ROTA1+C1(2,3)*P1
    EQ2D=C2(1,1)*WA2+C2(1,2)*ROTA2+C2(1,3)*(P1-P2)
    ER2D=C2(2,1)*WA2+C2(2,2)*ROTA2+C2(2,3)*(P1-P2)
    EQ3D=C3(1,1)*WA3+C3(1,2)*ROTA3+C3(1,3)*P2
    ER3D=C3(2,1)*WA3+C3(2,2)*ROTA3+C3(2,3)*P2
C TO COMPUTE BOLT STRESS
C BOLT TENSILE STRESS
    SIGB1=4.0*DABS(BFO)/(3.14159265*DB*DB)
    SIGB2=32.0*DABS(BM)/(3.14159265*(DB**3))
C MAXIMUM BOLT STRESS
    SIGMB=SIGB1+SIGB2
C TO CHECK WHETHER PRESCRIBED PRELOADING BOLT STRESS REACHED.
GO TO 1910
1830    CONTINUE
        WRITE(6,*) ' '
        WRITE(6,*) ' '
        WRITE(6,*) ' '
        WRITE(NW1,*)
        WRITE(NW1,*) 'PRELOADING STAGE COMPLETED AT BOLT TENSILE STRESS=',S
&IGB1
        WRITE(NW1,*) 'P1=',P1,'(PSI); P2=',P2,'(PSI)'
C OPTION: TO PRINTOUT STIFFNESS MATRIX AND FORCE VECTOR.
    IF(MATRIX.EQ.0) GO TO 2980
    IF(MATRIX.EQ.1) GO TO 12345
    WRITE(NW1,*) 'STIFFNESS MATRIX,((AA(I,J),I=1,5),J=1,5):'
    WRITE(NW1,55555)((AA(I,J),I=1,5),J=1,5)
55555    FORMAT(5(1X,1PD11.4))
        WRITE(NW1,*) 'FORCE VECTOR, (BBF(I),I=1,5):'
        WRITE(NW1,*) (BBF(I),I=1,5)
12345    WRITE(NW1,*) 'INCREMENTAL DEFORMATION PARAMETERS:'
        WRITE(NW1,*) 'W01D,THET1D,THET2D,W03D,THET3D'
        WRITE(NW1,*) (BB(I),I=1,5)
2980    WRITE(NW1,*) 'CURRENT BOLT INFORMATION'
        WRITE(NW1,*) ' BFO=',BFO,'NO. OF ITER.=' ,NIT
        WRITE(NW1,*) ' BOLT STRETCH RATE=',BEXT,' BK=',BK
        WRITE(NW1,*) ' BOLT ROTATION RATE=',ROTAD,' BRK=',BRK
        WRITE(6,*) 'BOLT TENSILE STRESS=',SIGB1
    8    FORMAT(4I13,5X,D10.3,3X,2(F10.5,3X,F10.3,3X))
        WRITE(NW1,*) 'BOLT YIELD FACTOR =',FACTOR

```

```

WRITE(NW1,*)'INBOARD EDGE DISPLACEMENTS & ROTATIONS'
  WRITE(NW1,*) ' WA1,WA2,WA3=',WA1,WA2,WA3
  WRITE(NW1,*) 'ROT1,ROT2,ROT3=',ROTA1,ROTA2,ROTA3
WRITE(NW1,*)'CURRENT GASKET SPRING RATES'
  WRITE(NW1,*)' GK1=',(GK1(M),M=1,NG)
  WRITE(NW1,*)' GK2=',(GK2(M),M=1,NG)
WRITE(NW1,*)'INBOARD EDGE FORCES AND MOMENTS'
  WRITE(NW1,*)' V1=',EQ1D,' M1=',ER1D
  WRITE(NW1,*)' V2=',EQ2D,' M2=',ER2D
  WRITE(NW1,*)' V3=',EQ3D,' M3=',ER3D
WRITE(NW1,*)'
      GASKET      INDEX MESP      LOAD(1)      LEAK(1)
& SPRING          GASKET          GASKET          UNLOADING          UNLOAD
&ING'
WRITE(NW1,*)'
      SPRING
& RATE          STRAIN          STRESS          OR          OR
&'              FROM          FROM          FROM          FROM
WRITE(NW1,*)'
      NUMBER          1,2,OR 3          UNLOADING          SEAL(0)
&'              STRAIN          STRAIN          STRES
&S'
WRITE(NW1,*)'FOR GASKET 1:'
DO 1870 I=1,NG
  WRITE(NW1,8)I, MEPS1(I),LOAD1(I),LAMDA1(I),GK1(I),EPS1(I),
&          SIGM1(I),EPSF1(I),SIGMF1(I)
1870 CONTINUE
  WRITE(NW1,*)
  IF(NFL.EQ.2)GO TO 1885
  WRITE(NW1,*)'FOR GASKET 2:'
DO 1880 I=1,NG
  WRITE(NW1,8)I,MEPS2(I),LOAD2(I),LAMDA2(I),GK2(I),EPS2(I),
&          SIGM2(I),EPSF2(I),SIGMF2(I)
1880 CONTINUE
1885 CONTINUE
  WRITE(NW1,*)'FLANGE 1-2 CONTACT:',MTM1,'; FLANGE 2-3 CONTACT:',MT
&M2
  WRITE(NW1,*)'MAXIMUM FLANGE 1 STRESS(R):',SIGFR1(IIR1),' AT X=',
&          XX(IIR1)
  WRITE(NW1,*)'MAXIMUM FLANGE 1 STRESS(T):',SIGFT1(IIT1),' AT X=',
&          XX(IIT1)
  IF(NFL.EQ.2) GO TO 1892
  WRITE(NW1,*)'MAXIMUM FLANGE 3 STRESS(R):',SIGFR3(IIR3),' AT X=',
&          XX(IIR3)
  WRITE(NW1,*)'MAXIMUM FLANGE 3 STRESS(T):',SIGFT3(IIT3),' AT X=',
&          XX(IIT3)
1892 CONTINUE
  WRITE(NW1,*)'BOLT STRESS (PSI):',SIGMB,'(',SIGB1,'+',SIGB2,')'.
  WRITE(NW1,*)'          AND IS',PCTB,'% ALLOWABLE STRESS.'
  IF(NYIELD.EQ.1) WRITE(NW1,*)'WARNING:BOLT YIELDS PARTIALLY.'
  IF(NYIELD.EQ.2)WRITE(NW1,*)'BOLT HAS YIELDED COMPLETELY'
C TO TERMINATE PRELOADING STAGE AND TURN INTO PRESSURIZING STAGE
  ISTG=2
  RETURN

```

```

C TO CHECK BOLT STRENGTH
1910  BFY=3.14159265*DB*DB*SIGMBY/4.0
      BMY=3.14159265*(DB**3)*SIGMBY/32.0
      ALPHAB=1.0-DABS(BFO)/BFY-DABS(BM)/BMY
      IF(ALPHAB.LT.0.)SIGMB=SIGMBY
      CRI=0.412*DABS(BM)/BMY
      IF(ALPHAB.GT.-CRI) GO TO 1940
      ALPHAB=-CRI

C
1940  FACTOR=1.0+ALPHAB/CRI
      IF(ALPHAB.GT.0.)FACTOR=1.0
      BK=BKO*FACTOR
      BRK=BRKO*FACTOR
      IF(FACTOR.LT.1.)NYIELD=1
      IF(FACTOR.EQ.0.) NYIELD=2
      PCTB=100.0*SIGMB/ALSIGB
      IF(FACTOR.LT.0.75.AND.ISTG.EQ.1)GO TO 1830
      IF(ISTG.EQ.1.AND.SIGB1.GE.PRESIG)GO TO 1830
C PRINTOUT OPTIONS.
      IF(NSTOP.EQ.1) GO TO 2150
      IF(ISTG.EQ.2) GO TO 1970
      PPP=FLOAT(NNN)*SIZE1
      IF(SIGMB.GE.PPP) GO TO 2100
      RETURN
1970  PPP=FLOAT(NNN)*SIZE2
      IF(P1.GE.PPP.OR.P2.GE.PPP) GO TO 2100
      RETURN
2100  NNN=NNN+1
C
2150  CONTINUE
      WRITE(6,*) ' '
      WRITE(6,*) ' '
      WRITE(6,*) ' '
      WRITE(6,*) 'P1=',P1,'(PSI);   P2=',P2,'(PSI)'
2200  WRITE(NW1,*) 'P1=',P1,'(PSI);   P2=',P2,'(PSI)'
C OPTION: TO PRINTOUT STIFFNESS MATRIX AND FORCE VECTOR.
      IF(MATRIX.EQ.0) GO TO 29801
      IF(MATRIX.EQ.1) GO TO 12346
      WRITE(NW1,*) 'STIFFNESS MATRIX,((AA(I,J),I=1,5),J=1,5):'
      WRITE(NW1,55555)((AA(I,J),I=1,5),J=1,5)
      WRITE(NW1,*) 'FORCE VECTOR,(BBF(I),I=1,5):'
      WRITE(NW1,*) (BBF(I),I=1,5)
12346  WRITE(NW1,*) 'INCREMENTAL DEFORMATION PARAMETERS:'
      WRITE(NW1,*) 'W01D,THET1D,THET2D,W03D,THET3D'
      WRITE(NW1,*) (BB(I),I=1,5)
29801  WRITE(NW1,*) 'CURRENT BOLT INFORMATION'
      WRITE(NW1,*) 'BFO=',BFO,'NO. OF ITER.=' ,NIT
      WRITE(NW1,*) ' BOLT STRETCH RATE=',BEXT,' BK=',BK
      WRITE(NW1,*) ' BOLT ROTATION RATE=',ROTAD,' BRK=',BRK
      WRITE(6,*) 'BOLT TENSILE STRESS=',SIGB1
      WRITE(NW1,*) 'BOLT YIELD FACTOR =',FACTOR

```

```

WRITE(NW1,*)'INBOARD EDGE DISPLACEMENTS & ROTATIONS'
  WRITE(NW1,*) ' WA1,WA2,WA3=',WA1,WA2,WA3
  WRITE(NW1,*) 'ROT1,ROT2,ROT3=',ROTA1,ROTA2,ROTA3
WRITE(NW1,*)'CURRENT GASKET SPRING RATES'
  WRITE(NW1,*)' GK1=',(GK1(M),M=1,NG)
  WRITE(NW1,*)' GK2=',(GK2(M),M=1,NG)
WRITE(NW1,*)'INBOARD EDGE FORCES AND MOMENTS'
  WRITE(NW1,*)' V1=',EQ1D,' M1=',ER1D
  WRITE(NW1,*)' V2=',EQ2D,' M2=',ER2D
  WRITE(NW1,*)' V3=',EQ3D,' M3=',ER3D
IF(N1.EQ.1) GO TO 2400
IF(N1.EQ.2) GO TO 3000
IF(N1.EQ.3) GO TO 3300
C PRINTOUT FORMAT 1: LIMITED PRINTOUT.
WRITE(NW1,*)'GASKET 1 LEAK INDEX,LAMDA1(I):',(LAMDA1(I),I=1,NING)
  IF(NFL.EQ.2) GO TO 36050
WRITE(NW1,*)'GASKET 2 LEAK INDEX,LAMDA2(I):',(LAMDA2(I),I=1,NING)
36050 CONTINUE
WRITE(NW1,*)'FLANGE 1-2 CONTACT:',MTM1,'; FLANGE 2-3 CONTACT:',MT
&M2
WRITE(NW1,*)'MAXIMUM FLANGE 1 STRESS(R):',SIGFR1(IIR1),' AT X=',
& XX(IIR1)
WRITE(NW1,*)'MAXIMUM FLANGE 1 STRESS(T):',SIGFT1(IIT1),' AT X=',
& XX(IIT1)
  IF(NFL.EQ.2) GO TO 36094
WRITE(NW1,*)'MAXIMUM FLANGE 3 STRESS(R):',SIGFR3(IIR3),' AT X=',
& XX(IIR3)
WRITE(NW1,*)'MAXIMUM FLANGE 3 STRESS(T):',SIGFT3(IIT3),' AT X=',
& XX(IIT3)
36094 CONTINUE
WRITE(NW1,*)'BOLT STRESS (PSI):',SIGMB,'(' ,SIGB1,'+',SIGB2,')'
WRITE(NW1,*) ' AND IS',PCTB,'% ALLOWABLE STRESS.'
IF(NYIELD.EQ.1) WRITE(NW1,*)'WARNING:BOLT YIELDS PARTIALLY.'
  IF(NYIELD.EQ.2)WRITE(NW1,*)'BOLT HAS YIELDED COMPLETELY'
WRITE(NW1,*)
IF(NSTOP.EQ.1) STOP
RETURN
C PRINTOUT FORMAT 2: FULL OUTPUT PRINTOUT.
2400 CONTINUE
WRITE(NW1,*)'
& STRAIN          GASKET          INDEX MESP          LOAD(1)          LEAK(1)
&ING'            GASKET          GASKET          UNLOADING        UNLOAD
WRITE(NW1,*)'
& RATE           STRAIN          STRESS          OR              OR
&'              STRAIN          STRESS          FROM            FROM
&
WRITE(NW1,*)'          NUMBER          1,2,OR 3        UNLOADING        SEAL(0)
&                STRAIN          STRESS          STRAIN          STRES
&S'
WRITE(NW1,*)'FOR GASKET 1:'
DO 2800 I=1,NG
  WRITE(NW1,8)I,MEPS1(I),LOAD1(I),LAMDA1(I),DEPS1(I),EPS1(I),
& SIGM1(I),EPSF1(I),SIGMF1(I)

```

```

2800 CONTINUE
      IF(NFL.EQ.2) GO TO 2905
      WRITE(NW1,*)
      WRITE(NW1,*)'FOR GASKET 2:'
      DO 2900 I=1,NG
        WRITE(NW1,8)I,MEPS2(I),LOAD2(I),LAMDA2(I),DEPS2(I),EPS2(I),
&          SIGM2(I),EPSF2(I),SIGMF2(I)
2900 CONTINUE
2905 CONTINUE
      WRITE(NW1,*)'FLANGE 1-2 CONTACT:',MTM1,'; FLANGE 2-3 CONTACT:',MT
&M2
      WRITE(NW1,*)'FLANGE STRESS (PSI):'
      WRITE(NW1,*)'  POSITION          SIGFR1          SIGFT1          SIG
&FR3          SIGFT3'
      DO 2950 I=1,21
        WRITE(NW1,*)XX(I),SIGFR1(I),SIGFT1(I),SIGFR3(I),SIGFT3(I)
2950 CONTINUE
      WRITE(NW1,*)'BOLT STRESS (PSI):',SIGMB,'(',SIGB1,'+',SIGB2,')'.
      WRITE(NW1,*)'          AND IS',PCTB,'% ALLOWABLE STRESS.'
      IF(NYIELD.EQ.1) WRITE(NW1,*)'WARNING:BOLT YIELDS PARTIALLY.'
      IF(NYIELD.EQ.2)WRITE(NW1,*)'BOLT HAS YIELDED COMPLETELY'
      IF(NSTOP.NE.1) RETURN
      STOP
C PRINTOUT FORMAT 3: FULL OUTPUT FOR FLANGES,BUT NOT FOR GASKETS.
3000 CONTINUE
      WRITE(NW1,*)'GASKET 1 LEAK INDEX,LAMDA1(I):',(LAMDA1(I),I=1,NING)
      IF(NFL.EQ.2) GO TO 37000
      WRITE(NW1,*)'GASKET 2 LEAK INDEX,LAMDA2(I):',(LAMDA2(I),I=1,NING)
37000 CONTINUE
      WRITE(NW1,*)'FLANGE 1-2 CONTACT:',MTM1,'; FLANGE 2-3 CONTACT:',MT
&M2
      WRITE(NW1,*)'FLANGE STRESS (PSI):'
      WRITE(NW1,*)'  POSITION          SIGFR1          SIGFT1
&SIGFR3          SIGFT3'
      DO 3250 I=1,21
        WRITE(NW1,*)XX(I),SIGFR1(I),SIGFT1(I),SIGFR3(I),SIGFT3(I)
3250 CONTINUE
      WRITE(NW1,*)'BOLT STRESS (PSI):',SIGMB,'(',SIGB1,'+',SIGB2,')'.
      WRITE(NW1,*)'          AND IS',PCTB,'% ALLOWABLE STRESS.'
      IF(NYIELD.EQ.1) WRITE(NW1,*)'WARNING:BOLT YIELDS PARTIALLY.'
      IF(NYIELD.EQ.2)WRITE(NW1,*)'BOLT HAS YIELDED COMPLETELY'
      WRITE(NW1,*)
      IF(NSTOP.EQ.1) STOP
      RETURN
C PRINTOUT FORMAT 4:FULL OUTPUT FOR GASKET,BUT NOT FOR FLANGE.
3300 CONTINUE
      WRITE(NW1,*)'          GASKET          INDEX MESP          LOAD(1)          LEAK(1)
& STRAIN          GASKET          GASKET          UNLOADING          UNLOAD
&ING'
      WRITE(NW1,*)'          STRAIN
& RATE          STRAIN          STRESS          OR          OR
&'          FROM          FROM

```

```

WRITE(NW1,*)'          NUMBER      1,2,OR 3      UNLOADING      SEAL(0)
&                               STRAIN          STRES
&S'
WRITE(NW1,*)'FOR GASKET 1:'
DO 3700 I=1,NG
  WRITE(NW1,8)I,MEPS1(I),LOAD1(I),LAMDA1(I),DEPS1(I),EPS1(I),
&          SIGM1(I),EPSF1(I),SIGMF1(I)
3700 CONTINUE
  IF(NFL.EQ.2) GO TO 3805
  WRITE(NW1,*)
  WRITE(NW1,*)'FOR GASKET 2:'
  DO 3800 I=1,NG
    WRITE(NW1,8)I,MEPS2(I),LOAD2(I),LAMDA2(I),DEPS2(I),EPS2(I),
&          SIGM2(I),EPSF2(I),SIGMF2(I)
3800 CONTINUE
3805 CONTINUE
  WRITE(NW1,*)'FLANGE 1-2 CONTACT:',MTM1,'; FLANGE 2-3 CONTACT:',MT
&M2
  WRITE(NW1,*)'MAXIMUM FLANGE 1 STRESS(R):',SIGFR1(IIR1),' AT X=',
&          XX(IIR1)
  WRITE(NW1,*)'MAXIMUM FLANGE 1 STRESS(T):',SIGFT1(IIT1),' AT X=',
&          XX(IIT1)
  IF(NFL.EQ.2) GO TO 3807
  WRITE(NW1,*)'MAXIMUM FLANGE 3 STRESS(R):',SIGFR3(IIR3),' AT X=',
&          XX(IIR3)
  WRITE(NW1,*)'MAXIMUM FLANGE 3 STRESS(T):',SIGFT3(IIT3),' AT X=',
&          XX(IIT3)
3807 CONTINUE
  WRITE(NW1,*)'BOLT STRESS (PSI):',SIGMB,'(',SIGB1,'+',SIGB2,')'
  WRITE(NW1,*)'          AND IS',PCTB,'% ALLOWABLE STRESS.'
  IF(NYIELD.EQ.1) WRITE(NW1,*)'WARNING:BOLT YIELDS PARTIALLY.'
  IF(NYIELD.EQ.2) WRITE(NW1,*)'BOLT HAS YIELDED COMPLETELY'
  WRITE(NW1,*)
  IF(NSTOP.EQ.1) STOP
  RETURN
  END

```

```

PROGRAM MAIN
IMPLICIT DOUBLE PRECISION(A-H,O-Z)
DOUBLE PRECISION K,L,LG
INTEGER BCN
INTEGER FLAG
DIMENSION Z(12,21),TUBE(8,21)
DIMENSION Y(12,21)
COMMON/MTINP/ A(12,12),B(12),INDIC
COMMON/PARAM/ XL,H,N,JNDIC,KNDIC,NR,NW
COMMON/COM2/ BCN(12,2),BNA(6),BNB(6)
COMMON/COM3/ XCHG(21),DINT(21),XY(21)
COMMON/COM4/OMEGA,DET,LNDIC
COMMON/STORE/UDUMMY(24)
COMMON/COM5/FLAG
COMMON/DIM1/E1,E2,ET,H1,H2,B1,B2,C11,C12,C13,C21,C22,C23,K,S,GS1
COMMON/DIM2/GS2,L,GM,LG
COMMON/TEST/NTST

C
C   SET FLAG FOR HELP
C   FLAG=0

C
C   ....SETUP INPUT PARAMETERS
C   WRITE(6,501)
501  FORMAT(17H BEGINNING DBLTS1)
C   READ(5,*) NR,NW,NTST
C   WRITE(NW,*) '   DOUBLE TUBESHEET ANALYSIS PROGRAM'
C   WRITE(NW,*) '   PREPARED BY A.I. SOLER SEPT. 1983'
C   WRITE(NW,*)
C   WRITE(NW,*) '   OUTPUT OF RAW INPUT DATA'
500  FORMAT(2I2)
C   ....
C   READ(NR,*) XL,H,N,JNDIC,KNDIC,INDIC,LNDIC
C   WRITE(NW,8001) XL,H,N,JNDIC,KNDIC,INDIC,LNDIC
C   GO TO (1,6,8,9),INDIC
1    DO 5 I=1,N
5    READ(NR,*) (A(I,J),J=1,N)
    READ(NR,*) (B(I),I=1,N)
    GO TO 9
6    DO 7 I=1,N
7    READ(NR,*) (A(I,J),J=1,N)
    GO TO 9
8    READ(NR,*) (B(I),I=1,N)
9    N1=N/2
    READ(NR,*) (BNA(I),I=1,N1)
    WRITE(NW,8002) (BNA(M),M=1,N1)
    READ(NR,*) (BNB(I),I=1,N1)
    WRITE(NW,8002) (BNB(M),M=1,N1)
    DO 10 J=1,2
10   READ(NR,*) (BCN(I,J),I=1,N)
    DO 11 I=1,N
12  FORMAT (I4,10X,I4)
11  WRITE(NW,12) (BCN(I,J),J=1,2)

```

```

      IF(JNDIC.GT.0) READ(NR,*)(XCHG(I),DINT(I),I=1,JNDIC)
      IF(KNDIC.GT.0) READ(NR,*)(XY(I),I=1,KNDIC)
      WRITE(NW,8002)(XY(I),I=1,KNDIC)
C     ....PRINT OUT INPUT PARAMETERS
C     ....
      WRITE(NW,7000)
      WRITE(NW,7001) XL,H,N,KNDIC,JNDIC
      WRITE(NW,7003)
      IF(LNDIC.EQ.1) GO TO 20
15     READ(NR,7002,END=60) OMEGA
      IF(NTST.EQ.1)WRITE(NW,*)'ENT COMP FROM MAIN'
20     CALL COMP(Y)
      IF(LNDIC.EQ.2) GO TO 55
C     DEFINE Z ARRAY
      DO100 I=1,KNDIC
        Z(1,I)=E1*H1*Y(1,I)
        Z(2,I)=E2*H2*Y(2,I)
        Z(3,I)=E1*H1*Y(3,I)
        Z(4,I)=E2*H2*Y(4,I)
        Z(5,I)=E1*H1*H1*Y(5,I)
        Z(6,I)=E2*H2*H2*Y(6,I)
        Z(7,I)=H1*Y(7,I)
        Z(8,I)=H2*Y(8,I)
        Z(9,I)=Y(9,I)
        Z(10,I)=Y(10,I)
        Z(11,I)=H1*Y(11,I)
        Z(12,I)=H2*Y(12,I)
100 CONTINUE
C     DEFINE TUBE ARRAY
      DO110 I=1,KNDIC
        TUBE(1,I)=6.*GM*Z(7,I)+3.*GM*(H1+L)*Z(9,I)-6.*GM*Z(8,I)+3.*GM*(H2+
11) *Z(10,I)+18.*L*GM*(Z(1,I)/(GS1*H1)+Z(2,I)/(GS2*H2))/5.
        TUBE(2,I)=3.*GM*L*Z(7,I)+GM*(1.5*L*H1+2.*L*L+6.*LG)*Z(9,I)-3.*GM*L
1 *Z(8,I)+GM*(1.5*L*H2+L*L-6.*LG)*Z(10,I)+12.*(1.+3.*LG/(L*L))*Z(1,I
2) *L*L*GM/(5.*GS1*H1)+6.*(1.-6.*LG/(L*L))*Z(2,I)*L*L*GM/(5.*GS2*H2)
        TUBE(3,I)=B1*(Z(12,I)-Z(11,I))
        TUBE(4,I)=-TUBE(1,I)
        TUBE(5,I)=3.*GM*L*Z(7,I)+GM*(1.5*L*H1+L*L-6.*LG)*Z(9,I)-3.*GM*L*Z(
18,I)+GM*(1.5*L*H2+2.*L*L+6.*LG)*Z(10,I)+6.*(1.-6.*LG/(L*L))*Z(1,I)
2 *L*L*GM/(5.*GS1*H1)+12.*(1.+3.*LG/(L*L))*Z(2,I)*L*L*GM/(5.*GS2*H2)
        TUBE(6,I)=-B2*Z(12,I)
        TUBE(7,I)=2.*ET*K/(S*S*S)*(C11*Z(8,I)+C12*S*Z(10,I)+C13*Z(2,I)*S/(
1GS2*H2))
        TUBE(8,I)=2.*ET*K/(S*S)*(C21*Z(8,I)+C22*S*Z(10,I)+C23*Z(2,I)*S/(GS
12*H2))
110 CONTINUE
      WRITE(NW,*)'      RESULTS FOR TUBESHEETS'
9002  FORMAT(13(1X,1PD9.2))
      WRITE(NW,*)'      R/RO          V1          V2          N1          N2          W1
1M1          M2          U1          U2          A1          A2
2          W2          '
      DO 90000 KK=1,KNDIC

```

```

        WRITE(NW,9002)XY(KK),(Z(I, KK),I=1,N)
90000 CONTINUE
        WRITE(NW,*)
        WRITE(NW,*)'          RESULTS FOR TUBE ARRAY'
        WRITE(NW,*)'  R/RO    H1TUBE    M1TUBE    F1TUBE    H2TUBE    M2
1TUBE    F2TUBE    H3TUBE    M3TUBE
        DO 91000 KK=1,KNDIC
        WRITE(NW,9002)XY(KK),(TUBE(I, KK),I=1,8)
91000 CONTINUE
        STOP
55    WRITE(NW,7004) OMEGA,DET
        GO TO 15
60    WRITE(NW,7005)
6000 FORMAT(9(A8))
7000 FORMAT(1H1,10X,'A GENERAL COMPUTER PROGRAM FOR THE SOLUTION OF A
1 TWO POINT BOUNDARY VALUE PROBLEM, WRITTEN BY G.J. HUTCHINS.'////)
7001  FORMAT(30X,'LENGTH OF FUN X =',F10.5, //30X,'STEP SIZE =',
1 6X,F10.5, //30X,'NUMBER OF EQS. =',I5, //30X,'NO. OUTPT PTS. =',I5,
2 //30X,'STEP SIZE CHGS. =',I5)
7003 FORMAT(1H0,////)
7002 FORMAT(F15.6)
7004 FORMAT(////////,1H,'OMEGA EQUAL TO',D14.6,'PRODUCES A DETERMINANT
1 EQUAL TO ',D14.6)
7005 FORMAT(////,1H,30X,'PROBLEM END')
7008 FORMAT(1H1,////)
8001 FORMAT(2F10.5,5I5)
8002 FORMAT(7F10.5)
8003  FORMAT(18I4)
9003 FORMAT(' ',A8,8(3X,D11.4))
        STOP
        END
SUBROUTINE COMP(Y)
IMPLICIT DOUBLE PRECISION(A-H,O-Z)
INTEGER BCN
        DIMENSION          Y(12,21),PYY(84,21)
COMMON/COM1/  YR(84),FR(84)
COMMON/COM2/  BCN(12,2),BNA(6),BNB(6)
COMMON/COM3/  XCHG(21),DINT(21),XY(21)
COMMON/COM4/  OMEGA,DET,LNDIC
COMMON/PARAM/  XL,H,N,JNDIC,KNDIC,NR,NW
COMMON/TEST/NTST
        N1=N/2
        N2=N1+1
        N4=N2*N
        I1=1
        ISUB=1
        K=1
C
C  INITIALIZE X
X=0.DO
I2=1

```

```

C ....ASSIGN INITIAL CONDITIONS
C ....
      DO 5 I=1,N
      DO 5 J=1,N2
5     Y(I,J)=0.DO
      DO 15 I=1,N
      IF(BCN(I,1).EQ.0) GO TO 10
      GO TO 15
10    Y(I,1)=BNA(K)
      K=K+1
15    CONTINUE
      DO 30 I3=1,N1
      DO 20 I=I1,N
      IF(BCN(I,1).EQ.1) GO TO 25
20    CONTINUE
25    Y(I,I3+1)=1.DO
      I1=I+1
30    CONTINUE
      DO 31 I=1,N
      DO 31 J=1,N2
      IJ=I+(J-1)*N
31    YR(IJ)=Y(I,J)
C ....CHANGE STEPSIZE
C ....
35    IF(JNDIC.EQ.0.OR.LNDIC.EQ.2) GO TO 40
      IF(X.LT.XCHG(I2)-H/2.0) GO TO 40
      H=H*DINT(I2)
      I2=I2+1
      IF(I2.GT.JNDIC) XCHG(I2)=XL+H
      WRITE(NW,4500) X,H
C ....ASSIGN VALUES OF YR TO TEMPORARY STORAGE FOR PRINT OUT
C ....
40    IF(KNDIC.EQ.0.OR.LNDIC.EQ.2) GO TO 50
      IF(X.LT.XY(ISUB)-H/2.0) GO TO 50
      DO 45 I=1,N4
45    PYY(I,ISUB)=YR(I)
      ISUB=ISUB+1
C ....IF X EXCEEDS XL TERMINATE INTEGRATION
C ....
50    IF(X.GT.XL-H/2.0) GO TO 60
C CALL RUNGE TO INTEGRATE ACROSS NEXT STEP
C
      IER=0
      IF(NTST.EQ.1)WRITE(NW,*)'ENT RUNG FROM COMP'
      CALL RUNGE(X,IER,N4)
      IF(IER.EQ.0) GO TO 35
      WRITE(NW,4400) X
      WRITE(NW,4350)(YR(I),I=1,N)
      GO TO 535
60    CONTINUE
C ....SOLVE FOR BOUNDARY CONDITIONS

```

```

C     ....
      IF(NTST.EQ.1)WRITE(NW,*)'ENT BCON FROM COMP'
      CALL BCON
      IF(LNDIC.EQ.2) RETURN
C     ....SOLVE FOR Y
C     ....
      DO 75 K=1,KNDIC
      DO 70 I=1,N
      Y(I,K)=0.0
      DO 70 J=1,N2
      IJ=I+(J-1)*N
      70  Y(I,K)=PYY(IJ,K)*YR(J)+Y(I,K)
      75  CONTINUE
      535 RETURN
      4350 FORMAT(3X,'THE VALUE OF YR BEFORE REGISTER IS LOWERED IS:')
      1  //(1H,6D14.6))
      4400 FORMAT(3X,'EXPONENT OVERFLOW X=',D14.6)
      4500 FORMAT(//3X,'AT X=',F12.4,3X,
      1  'THE STEPSIZE H WAS CHANGED TO',F12.4)
      END
C
C     *****
C     SUBROUTINE HELP (R,FLAG)
C     THIS SUBROUTINE LOADS EQUATIONS FOR SOLUTION OF DOUBLE TUBE SHEET
C
C     THIS IS SUBROUTINE HELP           NONDIMENSIONALIZED VERSION
C     FORMS MATRIX A + B
C
      IMPLICIT DOUBLE PRECISION(A-I,K-Z)
      INTEGER FLAG,NR,NW,N,JNDIC,KNDIC
      INTEGER TRASH,NTST
      COMMON/MTINP/A(12,12),B(12),TRASH
      COMMON/COM6/JSKIP
      COMMON/DIM1/E1,E2,ET,H1,H2,B1,B2,C11,C12,C13,C21,C22,C23,I,S,GS1
      COMMON/DIM2/GS2,L,GM,LG
      COMMON/STORE/T1,T2,ALF1,ALF2,NU1,NU2,ETA1,ETA2,TG11,
      1TG22,L2,P,T,D,ARADI,P1,P2,P3,FN,BEGIN,ALFAT,ALFAS,TTUBE,TSHELL
      COMMON/PARAM/ XL,H,N,JNDIC,KNDIC,NR,NW
      COMMON/TEST/ NTST
      IF(NTST.EQ.1)WRITE(NW,*) FLAG
C
C     SKIP READ DATA
C
      IF (FLAG.GT.0) GO TO 1000
C
C     DATA READ IN
      8  FORMAT(8D12.5)
C
      1  FORMAT(8F10.0)
      READ(NR,*)H1,T1,ALF1,E1,NU1,ETA1,TG11
      WRITE(NW,8)H1,T1,ALF1,E1,NU1,ETA1,TG11

```

```

READ(NR,*)H2,T2,ALF2,E2,NU2,ETA2,TG22
WRITE(NW,8)H2,T2,ALF2,E2,NU2,ETA2,TG22
2  FORMAT(6F10.3,F12.0)
READ(NR,*) L, L2, S, P, T, D, ET
WRITE(NW,2) L,L2,S,P,T,D,ET
3  FORMAT(F10.3,3F10.1,F6.3,F6.3)
READ(NR,*)ARADI,P1,P2,P3,FN
WRITE(NW,3)ARADI,P1,P2,P3,FN
READ(NR,*)ALFAT,ALFAS,TTUBE,TSHELL
WRITE(NW,8)ALFAT,ALFAS,TTUBE,TSHELL
6  FORMAT (I10 ,F10.5)
READ(NR,*) JSKIP ,BEGIN
WRITE(NW,6) JSKIP ,BEGIN
C   JSKIP   UPPER BOUND FOR NUMBER OF MATRIX PRINTED
C   BEGIN   VALUE WHERE MATRIX FOR LARGE R VALUES ARE BEGUN
C
C   READ OUT DATA
C
10  FORMAT(1H1)
WRITE(NW,10)
11  FORMAT(11X,'INPUT DATA')
WRITE(NW,11)
12  FORMAT('0','TUBE SHEET ONE:')
WRITE(NW,12)
13  FORMAT(' ',' E1=',F10.0,3X,'NU1=',F5.3,3X,'THICKNESS=',F4.1,3X,'T
1EMP.=',F5.1)
WRITE(NW,13)E1,NU1,H1,T1
14  FORMAT(' ',' ETA1(=ES1/E1)=',F7.4,3X,'THERMAL COEFF.='F11.8)
WRITE(NW,14)ETA1,ALF1
15  FORMAT('0','TUBE SHEET TWO:')
WRITE(NW,15)
16  FORMAT(' ',' E2=',F10.0,3X,'NU2=',F5.3,3X,'THICKNESS=',F4.1,3X,'T
1EMP.=',F5.1)
WRITE(NW,16)E2,NU2,H2,T2
17  FORMAT(' ',' ETA2(=ES2/E2)=',F7.4,3X,'THERMAL COEFF.='F11.8)
WRITE(NW,17)ETA2,ALF2
18  FORMAT('0','TUBES:')
WRITE(NW,18)
19  FORMAT(' ',' DISTANCE L1=',F5.1,3X,'DISTANCE L2=',F5.1,3X,'DISTAN
1CE S=',F5.1)
WRITE(NW,19)L,L2,S
20  FORMAT(' ',' PITCH=',F5.2,3X,'THICKNESS=',F5.3,3X,'DIAMETER=',F4.
11,3X,'ET=',F10.0)
WRITE(NW,20)P,T,D,ET
WRITE(NW,*)' AXIAL THERMAL DATA'
WRITE(NW,*)' ALFAT=',ALFAT,' ALFAS=',ALFAS,' TTUBE='
1,TTUBE,' TSHELL=',TSHELL
21  FORMAT('0','GENERAL:')
WRITE(NW,21)
22  FORMAT(' ',' SHELL RADIUS=',F6.2,3X,'P1=',F6.1,3X,'P2=',F6.1,3X,'
1P3=',F6.1)
WRITE(NW,22)ARADI,P1,P2,P3

```

```

23  FORMAT(' ',3X,'FN=',F6.3)
    WRITE(NW,23)FN
24  FORMAT('O','MATRIX TERMS SHIFT AT R EQUALS',F8.5)
    WRITE(NW,24)BEGIN
25  FORMAT('O')
    WRITE(NW,25)
1000 CONTINUE
C    ASSIGN VALUES TO CONSTANT TERMS FROM INPUT DATA
C
PIE= 3.141592654
NU=.30
I=(D**4-(D-2.0*T)**4)*PIE/64
G=ET/(2.0*(1.0+NU))
LG=8.0*ET/(G*(PIE*(D**2-(D-2.0*T)**2)))*I
LM1=1.0-PIE*((D-2.0*T)**2)/(((P**2)*DSQRT(12.DO)))
LM2=1.0-PIE*(D**2)/((P**2)*DSQRT(12.DO))
KS1=(E1*H1)/(1.-NU1*NU1)*ETA1
KS2=(E2*H2)/(1.-NU2*NU2)*ETA2
C11=9.*FN/2.-12.
C12=3.*(FN/2.-1.)+C11*H2/(2.*S)
C13=18./5.*(FN/2.-1.)
C21=3.*(FN/2.-1.)
C22=FN/2.+C21*H2/(2.*S)
C23=.6*FN
    ATUBE=PIE*(D-T)*T
    AAA=P*P*DSIN(PIE/3.DO)
    X1=ET*ATUBE/AAA
    XT=X1*ALFAT*TTUBE
    XS=X1*ALFAS*TSHELL
GM=2.0*ET*I/(L**3+12.0*L*LG)
GMA=GM
GS1=E1/(2.*(1.+NU1))
GS2=E2/(2.*(1.+NU2))
MS1=KS1*H1*TG11*(1.+NU1)*ALF1/12.
MS2=KS2*H2*TG22*(1.+NU2)*ALF2/12.
NS1=KS1*ALF1*T1*(1.+NU1)
NS2=KS2*ALF2*T2*(1.+NU2)
SQG=2./((DSQRT(3.DO))*P**2)
B1=PIE*T*(D-T)*ET/L
B2=PIE*T*(D-T)*ET/L2
PL1=P1*LM1
PU1=P2*LM2
PL2=P2*LM2
PU2=P3*LM2
F=GM*SQG
AR=ARAD1
C    SET FLAGS FOR LATER ROUTINES
    FLAG=2
C
C    REENTER AFTER SKIPPING READ & WRITE STATEMENTS
C    AND INITIALIZATION OF CONSTANT TERMS

```

```

C
C BOMB STOP 1
  IF (FLAG.EQ.0) GO TO 6000
  DO 50 J1=1,12
C   INITIALIZE ARRAY A & B
  B(J1) =0.0
  DO 50 J2=1,12
50 A(J1,J2)=0.0
C
C
C SKIP TERMS FOR R CLOSE TO ZERO
C
  IF (R.GE.BEGIN) GO TO 2000
C *****
C MATRIX VALUES FOR R CLOSE TO ZERO
C *****
  A(1,11)=-AR*SQG*B1/(2.*E1)
  A(1,12)=AR*SQG*B1*H2/(2.*H1*E1)
  A(2,11)=AR*SQG*B1*H1/(2.*H2*E2)
  A(2,12)=-AR*(B1+B2)/(2.*E2)*SQG
  A(3,7)=3.*AR*F/E1
  A(3,8)=-3.*AR*F*H2/(E1*H1)
  A(3,9)=1.5*AR*F*(H1+L)/(E1*H1)
  A(3,10)=1.5*AR*F*(H2+L)/(E1*H1)
  A(4,7)=-3.*AR*F*H1/(E2*H2)
  A(4,8)=1.5*SQG*AR/E2*2.*(ET*I*C11/(3.*S*S)+GM)
  A(4,9)=-1.5*AR*F*(H1+L)/(E2*H2)
  A(4,10)=1.5*AR*SQG/(E2*H2)*(2.*ET*I*C12/(3.*S*S)-GM*(H2+L))
  A(5,7)=1.5*AR*F/E1*(1.+L/H1)
  A(5,8)=-1.5*AR*F*H2/(E1*H1)*(1.+L/H1)
  A(5,9)=AR*F/(E1*H1)*(0.75*(H1+L)+(0.75*L*H1+L*L+3.*LG)/H1)
  A(5,10)=AR*F/(E1*H1)*(0.75*(H2+L)+(0.75*L*H2+L*L-3.*LG)/H1)
  A(6,7)=1.5*AR*F*H1/(E2*H2)*(1.+L/H2)
  A(6,8)=1.5*AR*SQG/E2*(ET*I*C11/(3.*S*S)+2.*ET*I*C21/(3.*H2*S*S)-
1 GM*(1.+L/H2))
  A(6,9)=AR*F/(E2*H2)*(0.75*(H1+L)+(0.75*L*H1+.5*L*L-3.*LG)/H2)
  A(6,10)=AR*SQG/(E2*H2)*(0.75*GM*(H2+L)+ET*I*(C12/(2.*S*S)+C22/(H2*
1 S))+GM/H2*(0.75*L*H2+L*L+3.*LG))
  A(7,3)=AR*(1.-NU1)/(ETA1*H1)
  A(8,4)=AR*(1.-NU2)/(ETA2*H2)
  A(9,5)=12.*AR*(1.-NU1)/(ETA1*H1)
  A(10,6)=12.*AR*(1.-NU2)/(ETA2*H2)
  A(11,9)=-AR/H1
  A(12,10)=-AR/H2
C *****
  B(1)=AR/(2.*H1*E1)*(PL1-PU1-XT)
  B(2)=AR/(2.*H2*E2)*(PL2-PU2+XS)
  B(7)=AR*NS1/(ETA1*H1*H1*E1)*(1.-NU1)
  B(8)=AR*NS2/(ETA2*H2*H2*E2)*(1.-NU2)
  B(9)=12.*AR*MS1*(1.-NU1)/(ETA1*H1*H1*H1*E1)
  B(10)=12.*AR*MS2*(1.-NU2)/(ETA2*H2*H2*H2*E2)

```

```

C
C   END MATRIX TERMS EXCLUSIVELY FOR R CLOSE TO ZERO
C
C   *****
C   MATRIX TERMS FOR ANY R
C   *****
2000 CONTINUE
   A(11,1)=-AR*E1*6./(5.*H1*GS1)
   A(11,9)=-AR/H1
   A(12,2)=-6.*AR*E2/(5.*H2*GS2)
   A(12,10)=-AR/H2
C
C   END OF COMMON TERMS
C
C   IF (R.LT.BEGIN) GO TO 3000
C   BOMB STOP 2
C   IF (R.EQ.0.D0) GO TO 6001
C   *****
C   MATRIX TERMS FOR R MUCH > ZERO
C   *****
   A(1,1)=-1./R
   A(1,11)=-AR*SQG*B1/E1
   A(1,12)=AR*H2*SQG*B1/(E1*H1)
   A(2,2)=-1./R
   A(2,11)=AR*H1*SQG*B1/(E2*H2)
   A(2,12)=-AR*SQG*(B1+B2)/E2
   A(3,1)=18.*F*L*AR/(5.*GS1*H1)
   A(3,2)=18.*F*L*AR*E2/(5.*GS2*H1*E1)
   A(3,3)=(NU1-1.)/R
   A(3,7)=ETA1*H1/(AR*R*R)+6.*AR*F/E1
   A(3,8)=-6.*AR*H2*F/(E1*H1)
   A(3,9)=3.*AR*F*(H1+L)/(E1*H1)
   A(3,10)=3.*AR*F*(H2+L)/(E1*H1)
   A(4,1)=-18.*AR*F*L*E1/(5.*GS1*H2*E2)
   A(4,2)=2.*ET*I*C13*AR*SQG/(GS2*H2*S*S)-18.*AR*F*L/(GS2*H2*5.)
   A(4,4)=(NU2-1.)/R
   A(4,7)=-6.*AR*F*H1/(E2*H2)
   A(4,8)=6.*SQG*AR*(ET*I*C11/(3.*S*S*S)+GM)/E2+ETA2*H2/(AR*R*R)
   A(4,9)=-3.*AR*F*(H1+L)/(E2*H2)
   A(4,10)=(2.*ET*I*C12/(3.*S*S)-GM*(H2+L))*3.*AR*SQG/(E2*H2)
   A(5,1)=-AR/H1+9.*AR*L*F/(5.*GS1*H1)+12.*AR*F*L*(1.+3.*LG/(L*L))/
1  (5.*H1*H1*GS1)
   A(5,2)=9.*AR*L*F*E2*H2/(5.*GS2*H2*H1*E2)+6.*E2*AR*F*L*(1.-6.*LG
1  / (L*L))/(E1*H1*H1*GS2*5.)
   A(5,5)=(NU1-1.)/R
   A(5,7)=3.*AR*F*(1.+L/H1)/E1
   A(5,8)=-3.*AR*F*H2*(1.+L/H1)/(E1*H1)
   A(5,9)=ETA1*H1/(12.*AR*R*R)+AR*F/(E1*H1)*(1.5*(H1+L)+(1.5*L*H1+2.
1  *L*L+6.*LG)/H1)
   A(5,10)=AR*F/(E1*H1)*(1.5*(H2+L)+(1.5*L*H2+L*L-6.*LG)/H1)
   A(6,1)=6.*AR*F*(1.-6.*LG/(L*L))*E1*L/(5.*E2*H2*H2*GS1)

```

```

A(6,2)=-AR/H2+ET*I/(GS2*H2*H2)*(2.*AR*SQGC23/S+SQGAR*H2*C13/(S*S
1 ))+12.*AR*F*L*L*(1.+3.*LG/(L*L))/(5.*GS2*H2*H2)
A(6,6)=A(4,4)
A(6,7)=3.*AR*F*H1*(1.+L/H2)/(E2*H2)
A(6,8)=1.5*AR*SQGE2*(2.*ET*I*C11/(3.*S*S*S)-2.*GM+2./H2*(ET*I*C21
1 *2./(3.*S*S)-GM*L))
A(6,9)=AR*F/(E2*H2)*(1.5*(H1+L)+(1.5*H1*L+L*L-6.*LG)/H2)
A(6,10)=AR*SQG*(1.5*GM*(H2+L)+ET*I*(2.*S/H2*C22+C12)/(S*S)+GM/H2*
1 (1.5*L*H2+2.*L*L+6.*LG))/(E2*H2)+ETA2*H2/(12.*AR*R*R)
A(7,3)=AR*(1.-NU1*NU1)/(ETA1*H1)
A(7,7)=-NU1/R
A(8,4)=AR*(1.-NU2*NU2)/(ETA2*H2)
A(8,8)=-NU2/R
A(9,5)=12.*AR*(1.-NU1*NU1)/(ETA1*H1)
A(9,9)=A(7,7)
A(10,6)=12.*AR*(1.-NU2*NU2)/(ETA2*H2)
A(10,10)=A(8,8)
C *****
B(1)=AR*(PL1-PU1)/(E1*H1)
B(2)=AR*(PL2-PU2)/(E2*H2)
B(3)=NS1*(NU1-1.)/(R*E1*H1)
B(4)=NS2*(NU2-1.)/(R*E2*H2)
B(5)=MS1*(NU1-1.)/(R*E1*H1*H1)
B(6)=MS2*(NU2-1.)/(R*E2*H2*H2)
B(7)=AR*NS1/(H1*KS1)
B(8)=AR*NS2/(H2*KS2)
B(9)=12.*AR*MS1*(1.-NU1*NU1)/(ETA1*H1*H1*H1*E1)
B(10)=12.*AR*MS2*(1.-NU2*NU2)/(ETA2*H2*H2*H2*E2)
C
3000 CONTINUE
RETURN
7000 FORMAT (1H0, ' BOMB STOP 1 ' )
6000 WRITE(NW,7000)
STOP
7001 FORMAT (1H0, ' BOMB STOP 2' )
6001 WRITE(NW,7001 )
STOP
END
SUBROUTINE RUNGE (X,IER,N)
C
IMPLICIT DOUBLE PRECISION(A-H,0-Z)
DIMENSION PHI(84),SAVEY(84)
COMMON/PARAM/ XL,H,NR,JNDIC,KNDIC,NRR,NW
COMMON/COM1/ Y (84),F (84)
COMMON/TEST/NTST
IER1 = 0
IF(NTST.EQ.1)WRITE(NW,*)'ENT FUN1 FROM RUNG'
CALL FUNCT(X,IER1,N)
IF(IER1.NE.0) GO TO 2500
DO 22 J=1,N
SAVEY(J) = Y(J)
PHI(J) = F(J)

```

```

22  Y(J) = SAVEY(J) + H*F(J)/2.DO
    X = X+H/2.DO
    IF(NTST.EQ.1)WRITE(NW,*)'ENT FUN2 FROM RUNG'
    CALL FUNCT(X,IER1,N)
    IF(IER1.NE.0) GO TO 2500
    DO 33 J=1,N
    PHI(J) = PHI(J) + 2.DO*F(J)
33  Y(J) = SAVEY(J) + H*F(J)/2.DO
    IER1 = 0
    IF(NTST.EQ.1)WRITE(NW,*)'ENT FUN3 FROM RUNG'
    CALL FUNCT(X,IER1,N)
    IF(IER1.NE.0) GO TO 2500
    DO 44 J=1,N
    PHI(J) = PHI(J) + 2.DO*F(J)
44  Y(J) = SAVEY(J) + H*F(J)
    X = X +H/2.DO
    IER1 = 0
    IF(NTST.EQ.1)WRITE(NW,*)'ENT FUN4 FROM RUNG'
    CALL FUNCT(X,IER1,N)
    IF(IER1.NE.0) GO TO 2500
    DO 55 J=1,N
55  Y(J)=SAVEY(J)+(PHI(J)+F(J))*H/6.DO
    RETURN
2500 WRITE(NW,9000) IER1
9000 FORMAT( ' ERROR IN RUNGE.  IER1 = ',I5)
    IER = 10
    RETURN
    END
    SUBROUTINE BCON
    IMPLICIT DOUBLE PRECISION(A-H,O-Z)
    INTEGER BCN
    DIMENSION T(30,30)
    COMMON/PARAM/ XL,H,N,JNDIC,KNDIC,NR,NW
    COMMON/COM1/  YR(84),FR(84)
    COMMON/COM2/  BCN(12,2),BNA(6),BNB(6)
    COMMON/COM4/OMEGA,DET,LNDIC
    COMMON/TEST/NTST
    N1=N/2
    N2=N1+1
    N3=N1**2
C   ...REARRANGE MATRIX
C   ....
    DO 30 I=1,N
    DO 30 J=1,N
30  T(I,J)=0.DO
    J1=1
    DO 55 I=1,N1
    IF(BCN(I,2).NE.0) GO TO 35
    T(I,I)=1.DO
    IF(I.EQ.N1) GO TO 35
    GO TO 55
35  DO 45 J=J1,N1

```

```

      IF(BCN(J+N1,2).NE.0) GO TO 40
      T(I,J+N1)=1.DO
      T(J+N1,I)=1.DO
      GO TO 50
40    T(J+N1,J+N1)=1.DO
45    CONTINUE
50    J1=J+1
55    CONTINUE
      DO 60 I=1,N
      DO 60 J=1,N2
      IJ=I+(J-1)*N
      FR(IJ)=0.0
      DO 60 K=1,N
      KJ=K+(J-1)*N
60    FR(IJ)=T(I,K)*YR(KJ)+FR(IJ)
C     ....PARTITION MATRIX
C     ....
      DO 65 I=1,N3,N1
      DO 65 J=1,N1
      IJ=I+J-1
      IJ1=IJ+I+N-1
65    YR(IJ)=FR(IJ1)
      DO 70 I=1,N1
70    FR(I)=BNB(I)-FR(I)
      IF(LNDIC.EQ.1) GO TO 80
      IF(NTST.EQ.1)WRITE(NW,*)'ENT MINV FROM BCON'
      CALL MINV(N1,N3,DET)
      RETURN
80    CONTINUE
      IF(NTST.EQ.1)WRITE(NW,*)'ENT SIMQ FROM BCON'
      CALL SIMQ(N1,KS)
      IF(KS.NE.0) GO TO 2600
      YR(1)=1.0
      DO 85 I=1,N1
85    YR(I+1)=FR(I)
      RETURN
2600 WRITE(NW,4200) KS
4200 FORMAT(3X,'CALCULATION TERMINATED.  KS=',I5)
      RETURN
      END
      SUBROUTINE SIMQ(N,KS)
      IMPLICIT DOUBLE PRECISION(A-H,O-Z)
      DOUBLE PRECISION BIGA,TOL,A,B
      COMMON/COM1/ A (84),B (84)
C
C     FORWARD SOLUTION
C
      TOL=0.DO
      KS=0
      JJ=-N
      DO 65 J=1,N
      JY=J+1

```

```

      JJ=JJ+N+1
      BIGA=0.DO
      IT=JJ-J
      DO 30 I=J,N
C
C      SEARCH FOR MAXIMUM COEFFICIENT IN COLUMN
C
      IJ=IT+I
      IF(DABS(BIGA)-DABS(A(IJ))) 20,30,30
20  BIGA=A(IJ)
      IMAX=I
30  CONTINUE
C
C      TEST FOR PIVOT LESS THAN TOLERANCE (SINGULAR MATRIX)
C      TEST FOR PIVOT LESS THAN TOLERANCE (SINGULAR MATRIX)
C
      IF(DABS(BIGA)-TOL) 35,35,40
35  KS=1
      RETURN
C
C      INTERCHANGE ROWS IF NECESSARY
C
40  I1=J+N*(J-2)
      IT=IMAX-J
      DO 50 K=J,N
          I1=I1+N
          I2=I1+IT
          SAVE=A(I1)
          A(I1)=A(I2)
          A(I2)=SAVE
C
C      DIVIDE EQUATION BY LEADING COEFFICIENT
C
50  A(I1)=A(I1)/BIGA
      SAVE=B(IMAX)
      B(IMAX)=B(J)
      B(J)=SAVE/BIGA
C      ELIMINATE NEXT VARIABLE
C
      IF(J-N) 55,70,55
55  IQS=N*(J-1)
      DO 65 IX=JY,N
          IXJ=IQS+IX
          IT=J-IX
          DO 60 JX=JY,N
              IXJX=N*(JX-1)+IX
              JJX=IXJX+IT
60  A(IXJX)=A(IXJX)-(A(IXJ)*A(JJX))
65  B(IX)=B(IX)-(B(J)*A(IXJ))
C
C      BACK SOLUTION

```

C

```

70 NY=N-1
   IF(NY.EQ.0) GO TO 81
   IT=N*N
   DO 80 J=1,NY
     IA=IT-J
     IB=N-J
     IC=N
     DO 80 K=1,J
       B(IB)=B(IB)-A(IA)*B(IC)
       IA=IA-N
80   IC=IC-1
81  CONTINUE
   RETURN
   END
   SUBROUTINE FUNCT(X,IER,N)
   IMPLICIT DOUBLE PRECISION(A-H,O-Z)
   COMMON/PARAM/ XL,H,NR,JNDIC,KNDIC,NRR,NW
   COMMON/MTINP/ A(12,12),B(12),INDIC
   COMMON/COM1/ Y (84),F (84)
   COMMON/COM4/OMEGA,DET,LNDIC
   COMMON/COM5/FLAG
   COMMON/COM6/JSKIP
   COMMON/TEST/NTST
   INTEGER FLAG
   DATA M/0/
   DATA XS/1234569.DO/
   M=M+1
   N2=NR/2+1
C ...GUARD AGAINST OVERFLOW
C ....
   IER=0
   DO 3I=1,N
     IF(DABS(Y(I)).GE.10.D70) GO TO 9050
3    CONTINUE
     GO TO (25,5,10,20),INDIC
5    CONTINUE
C ....INSERT EXPRESSIONS FOR VARIABLE ELEMENTS OF
C ....LOAD VECTOR B
     GO TO 25
10   CONTINUE
C ....INSERT EXPRESSIONS FOR VARIABLE ELEMENTS OF
C ...MATRIX A
     GO TO 25
20   CONTINUE
C ....INSERT EXPRESSIONS FOR VARIABLE ELEMENTS OF
C ...MATRIX A AND LOAD VECTOR B
C
     IF(NTST.EQ.1)WRITE(NW,*)'ENT HELP FROM FUNC'
     CALL HELP (X,FLAG)

```

```

C
25  IF(M.GT.JSKIP) GO TO 38
    IF(XS.EQ.X) GO TO 38
C....PRINT OUT A AND B MATRICES
C....
    GO TO (26,27),LNDIC
26  WRITE(NW,7000)  X
    WRITE(NW,7005)
    GO TO 28
27  WRITE(NW,7001)
28  K1=1
    K2=12
29  IF(K2.GE.NR) K2=NR
    DO 30 I=1,NR
30  WRITE(NW,7002)(A(I,J),J=K1,K2)
    IF(K2.EQ.NR) GO TO 35
    K1=K2+1
    K2=K2+12
    WRITE(NW,7003)
    GO TO 29
35  CONTINUE
    IF(LNDIC.EQ.2) GO TO 38
    WRITE(NW,7003)
    WRITE(NW,7004)(B(I),I=1,NR)
    WRITE(NW,7003)
38  CONTINUE
    XS=X
    DO 45 I=1,NR
    DO 40 J=1,N2
    IJ=I+(J-1)*NR
    F(IJ)=0.0
    DO 40 K=1,NR
    KJ=K+(J-1)*NR
40  F(IJ)=A(I,K)*Y(KJ)+F(IJ)
45  F(I)=F(I)+B(I)
    RETURN
9050  IER=1
    RETURN
7000  FORMAT(1H,////,30X,'STATIC SOLUTION',////,20X,'THE INPUT MATRICES
$  A AND B ARE FOR X EQUALS ',F10.5 )
7001  FORMAT(1H,////30X,'NATURAL FREQUENCY ANALYSIS',////,30X,'THE
1  INPUT MATRIX A IS:')
7002  FORMAT(1X,12D9.2)
7003  FORMAT(1H,////)
7004  FORMAT(30X,D12.6)
7005  FORMAT(1H0)
    END
    SUBROUTINE MINV(N,N1,D)
C
    IMPLICIT DOUBLE PRECISION(A-H,O-Z)
    DIMENSION L(30),M(30)
    COMMON/COM1/A(84),B(84)
    COMMON/PARAM/ XL,H,NR,JNDIC,KNDIC,NRR,NW

```

```

D=1.0
NK=-N
DO 80 K=1,N
NK=NK+N
L(K)=K
M(K)=K
KK=NK+K
BIGA=A(KK)
DO 20 J=K,N
IZ=N*(J-1)
DO 20 I=K,N
IJ=IZ+I
10 IF(DABS(BIGA)-DABS(A(IJ))) 15,20,20
15 BIGA=A(IJ)
L(K)=I
M(K)=J
20 CONTINUE
J=L(K)
IF(J-K) 35,35,25
25 KI=K-N
DO 30 I=1,N
KI=KI+N
HOLD=-A(KI)
JI=KI-K+J
A(KI)=A(JI)
30 A(JI)=HOLD
35 I=M(K)
IF(I-K) 45,45,38
38 JP=N*(I-1)
DO 40 J=1,N
JK=NK+J
JI=JP+J
HOLD=-A(JK)
A(JK)=A(JI)
40 A(JI)=HOLD
45 IF(BIGA) 48,46,48
46 D=0.0
WRITE(NW,5000) D
5000 FORMAT(///,'MATRIX IS SINGULAR D=',F14.6)
RETURN
48 DO 55 I=1,N
IF(I-K) 50,55,50
50 IK=NK+I
A(IK)=A(IK)/(-BIGA)
55 CONTINUE
DO 65 I=1,N
IK=NK+I
HOLD=A(IK)
IJ=I-N
DO 65 J=1,N
IJ=IJ+N
IF(I-K) 60,65,60

```

```

60 IF(J-K) 62,65,62
62 KJ=IJ-I+K
   A(IJ)=HOLD*A(KJ)+A(IJ)
65 CONTINUE
   KJ=K-N
   DO 75 J=1,N
   KJ=KJ+N
   IF(J-K) 70,75,70
70 A(KJ)=A(KJ)/BIGA
75 CONTINUE
   D=D*BIGA
   A(KK)=1.0/BIGA
80 CONTINUE
   K=N
100 K=(K-1)
   IF(K) 150,150,105
105 I=L(K)
   IF(I-K) 120,120,108
108 JQ=N*(K-1)
   JR=N*(I-1)
   DO 110 J=1,N
   JK=JQ+J
   HOLD=A(JK)
   JI=JR+J
   A(JK)=-A(JI)
110 A(JI) =HOLD
120 J=M(K)
   IF(J-K) 100,100,125
125 KI=K-N
   DO 130 I=1,N
   KI=KI+N
   HOLD=A(KI)
   JI=KI-K+J
   A(KI)=-A(JI)
130 A(JI) =HOLD
   GO TO 100
150 CONTINUE
   RETURN
   END

```

6. JOINTS FOR HIGH PRESSURE CLOSURES

6.1 INTRODUCTION AND STANDARD INDUSTRY DESIGNS

In the preceding three chapters we studied the characteristics of bolted joints where the axial separating force due to internal pressure is counteracted by preloading the bolts. The bolts must have sufficient “pull” to oppose the axial pressure load, and to provide sufficient residual pressure on the gasket to effect the seal. Such bolted joints find wide use in the pressure vessel industry from low pressure to medium pressure applications. Since the thickness of the flat cover increases directly in proportion to the product of the shell diameter and the square root of the pressure, bolted flange closures become quite heavy and unwieldy as the pressure and diameter of the vessel increase. The number and diameter of bolts required to provide the necessary preload (Section 3.7) may exceed what can be arranged on the minimum circumferential pitch (set to accommodate a box wrench) on the bolt circle. This may necessitate two bolt circles, increased moment arms, and therefore, even heavier designs. It may be advisable, therefore, to explore “boltless” flange designs whenever the pressure/diameter combination is such that the shell thickness exceeds 1.5”.

“Boltless” flanges* can be divided into two broad categories, namely (i) axially locked design; and (ii), pressure actuated design. A brief description of the two categories follows.

i. Axially Locked Design

In this design, the pressure load is resisted by a suitable means and the gasket is loaded by a set of bolts which do not participate in opposing the axial header load. Numerous means to contain the axial header load are reported in the literature [6.1.1]. We discuss in the following a few devices which have proven records of success.

Threaded Joint

In this construction, the cover (often referred to as the “plug” in high pressure sealing technology) has helical threads, usually of a buttress type, which engage matching female threads in the shell. Figure 6.1.1 shows a typical threaded joint of this type. This joint is occasionally referred to as

*This term will be employed to indicate the family of flange designs wherein the pressure load is not resisted by the bolts.

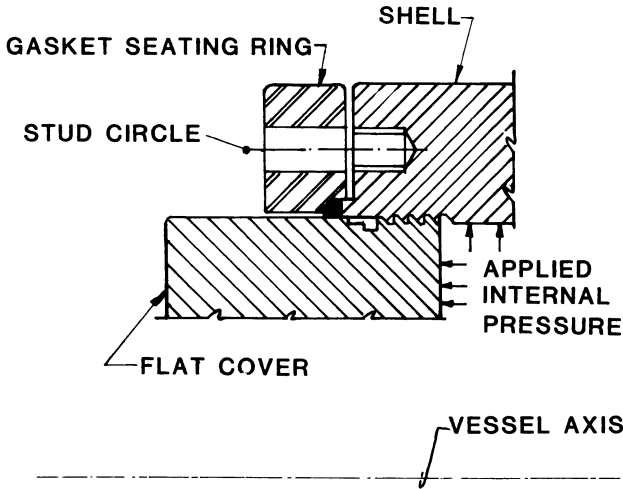


Fig. 6.1.1. Casale joint.

the Casale Joint. Figure 6.1.2 shows a Casale Joint used in connecting two courses of a shell. Figure 6.1.3 shows yet another arrangement where the threads are protected from direct contact with the contained fluid by utilizing an intermediate threaded barrel.

Figure 6.1.4 shows a double Casale joint wherein two bolt lines compress the gasket symmetrically. The chief demerit of the Casale Joint lies in the accuracy required in the machining operation to match the threads on the mating pieces. This deficiency is removed in the so-called Bredtschneider type closure, which employs shear blocks to carry the axial load.

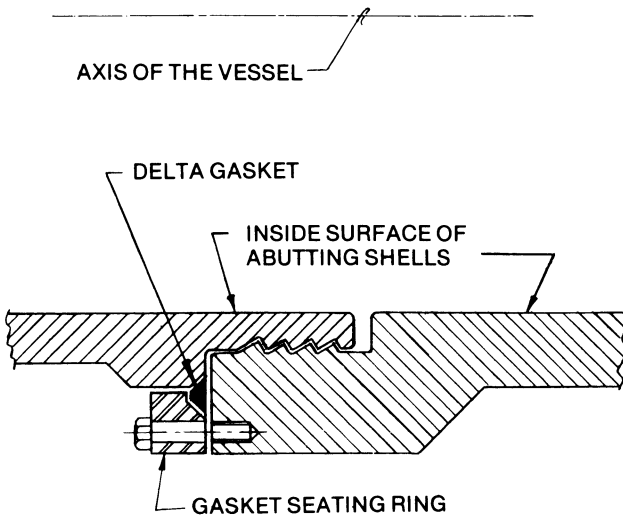


Fig. 6.1.2. Casale joint connecting two shell courses.

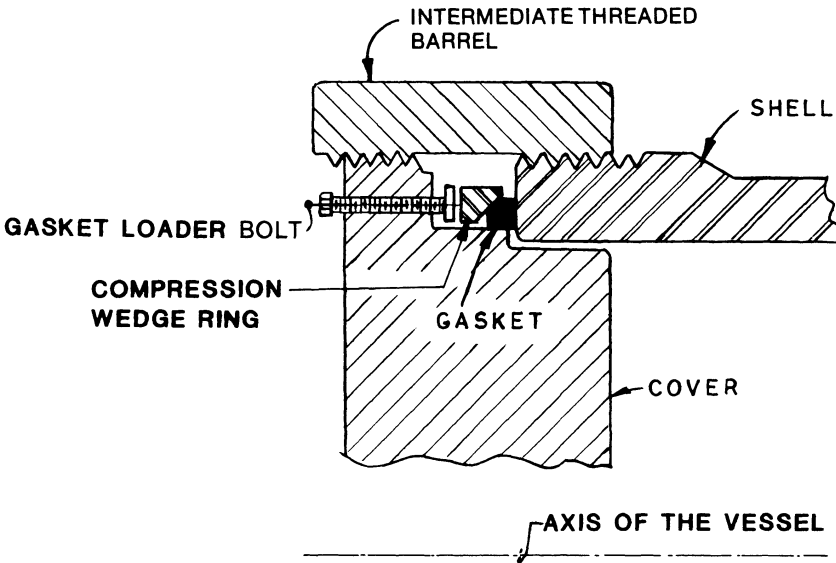


Fig. 6.1.3. Casale joint with intermediate barrel.

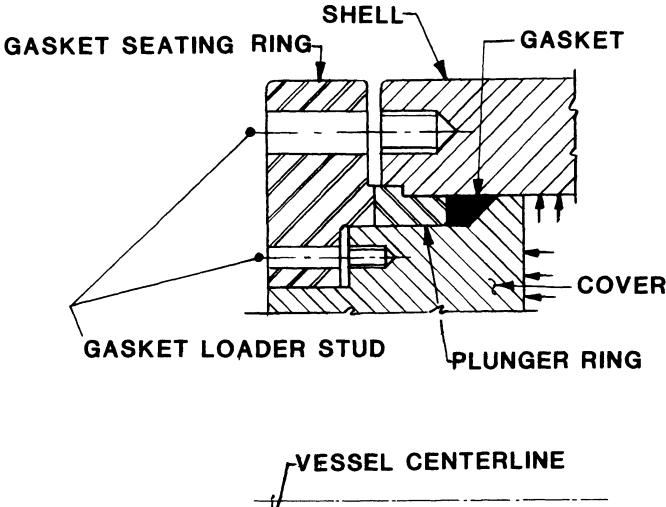


Fig. 6.1.4. Double Casale joint.

Bredtschneider Closure

This type of closure employs shear blocks to resist the header load. Figure 6.1.5 shows this closure with a delta sealing ring. The shear blocks are in the form of segmented rings which are held in place by the “backing” or “positioner” ring. Stevens-Guille, et al. [6.1.2] report successful ap-

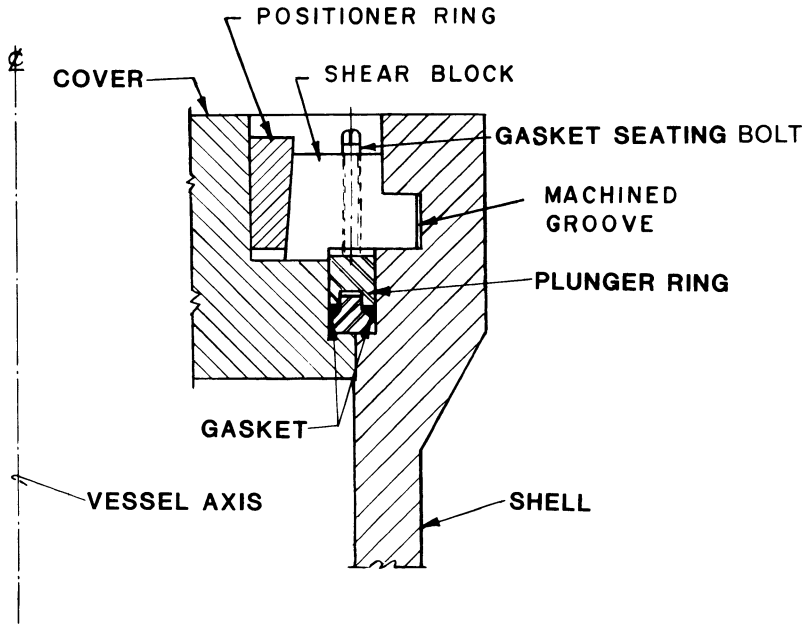


Fig. 6.1.5. Shear block.

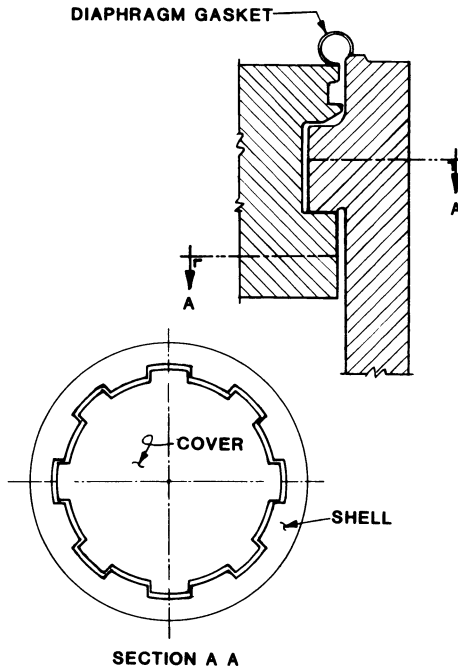
plication of this closure in high pressure ammonia heat exchangers (internal pressure = 5200 lb/sq. in.) using BS1503-161 Grade 28A (similar to ASTM-A181 Grade 1) fully annealed gasket material. A more expensive variation of the shear block concept is the so-called breech block design, shown in Fig. 6.1.6. The plug is inserted through the matching slots into the barrel ring, and then turned to lock it in place.

Shear Stud Closure

Figure 6.1.7 shows the cross section of a shear stud closure with an O-ring gasket. This design has the advantage of minimizing the end moment on the shell barrel. The number, length, and diameter of the studs can be selected to resist the header load without overstressing the studs. We note that if we imagine the number of studs to increase indefinitely until the threads of adjacent studs make contact, then the shear strength of this design will approach that of the threaded closure discussed before. Stud diameters in the range of 1 to 2 1/2" are usually used. The length-to-diameter ratio in the range of 4 to 5 presents no problem when tapping the holes.

Shear Pin Design

In this construction, blind circular holes, making an angle with the generatrix of the cylinder holes, are drilled through the barrel-cover assembly (Fig. 6.1.8). The holes may be oriented into the plane that is radial



SECTION A A
Fig. 6.1.6. Breech block.

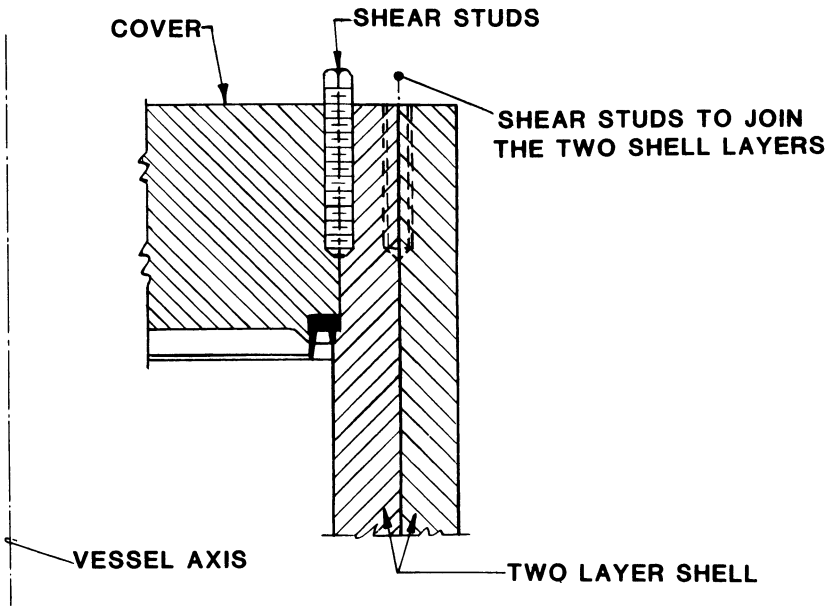


Fig. 6.1.7. Shear stud.

(Fig. 6.1.8a) or into the plane that is tangential (Fig. 6.1.8b) to the cylinder surface. Close fitting, but not precision fitting, shear pins are dropped into these holes. The obliqueness of the pin axis with respect to the shell axis imparts the required axial load bearing ability to the shear pins. As pointed out by Jorgensen [6.1.1], it is preferable to rotate the pins in the tangential plane, since orienting the pins into the radial plane reduces the available pin cross-sectional area in shear. It is recognized that orienting all pins identically would cause a net reactive moment on the plug and the shell. This can be avoided by arranging the pins in groups with the alternate groups in mirror image directions to each other. Figures 6.1.8c and 6.1.8d show the developed layout of two possible arrangements.

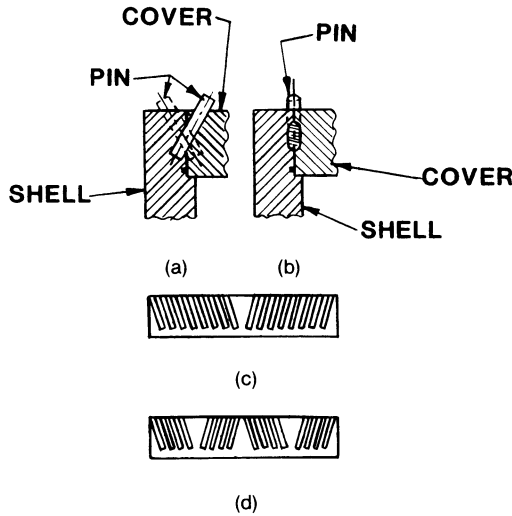


Fig. 6.1.8. Shear pin design.

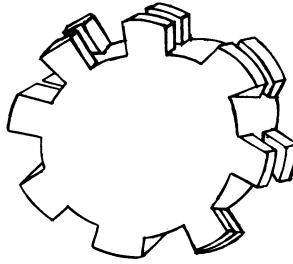
Shear Band Design

Sprockets cut out in the outer rim of the plug fit into corresponding slots in the shell barrel. The assembly is restrained from relative axial movement by rectangular cross section bars placed in circumferential grooves cut out on the barrel-plug assembly. Figure 6.1.9 shows the essential details of this construction.

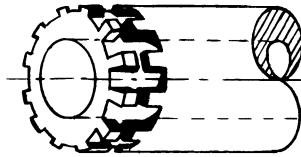
Yoke Ring

Figure 6.1.10 shows two pipe ends joined and sealed using two yoke rings. The ends of the pipe have machined hubs which are clamped together using the segmental “yoke” rings. This concept has been widely utilized in piping joints and in small diameter heat exchangers for high pressure service. References [6.1.3–4] give the details of one such patent employing this concept.

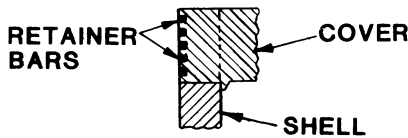




(a) COVER WITH SPROCKET



(b) CYLINDER WITH SPROCKET



(c) CROSS-SECTIONAL VIEW

Fig. 6.1.9. Shear band design.

The above description of restraining devices is by no means all inclusive. Numerous other designs evolved by skillful engineers and successfully put in practice have never been published in the open literature and therefore remain unrecorded. References (6.1.6-10) describe other closure devices which are not discussed here for lack of space. Undoubtedly, many more will be devised in the future.

ii. Pressure Actuated Closure

Pressure actuated joints are truly boltless joints. The underlying concept of this class of closures is often referred to as the “unsupported area

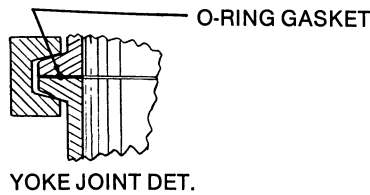
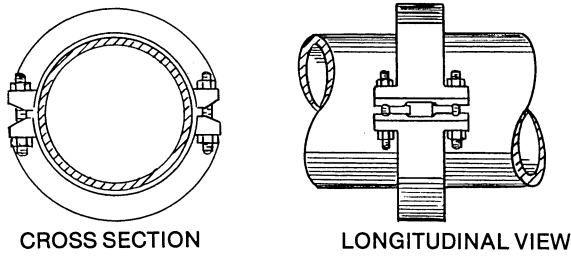


Fig. 6.1.10. Yoke type joint (U.S. Patent No. 3077360).

principle'' widely attributed to P. W. Bridgeman [6.1.4]. Figure 6.1.11 illustrates an application of this concept [6.1.5]. An endless elastic ring is forced into the circumferential groove. To accomplish this fit-up operation, the elastic ring is equipped with a diametral rod containing a turnbuckle. Using the turnbuckle the ring is deformed into an oval shape. The initial deformation is carefully controlled such that a permanent set in the ring

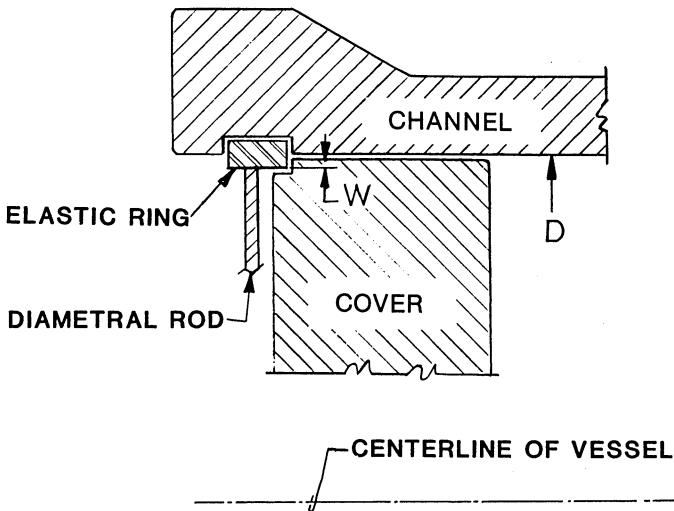


Fig. 6.1.11. Rectangular seal ring closure.

does not occur. The ring is inserted into the groove in the manner of Fig. 6.1.12. The seal ring is made of a machinable material which can withstand the axial thrust of pressure load without failing. Referring to Fig. 6.1.11, the compressive bearing stress, σ , on the seal ring is obtained from consideration of equilibrium.

$$\sigma = \frac{D^2 p}{4(D' - w)w}; \quad D' = \text{cover diameter} \tag{6.1.1}$$

The most desirable value of σ can be set by selecting the appropriate value of w . Anderson [6.1.5] reports excellent results with joints of this type. Another joint, based on the Bridgeman principle, utilizes a wedge-shaped seal ring. This joint is described in the next section, wherein mathematical formulas to size its components are also derived.

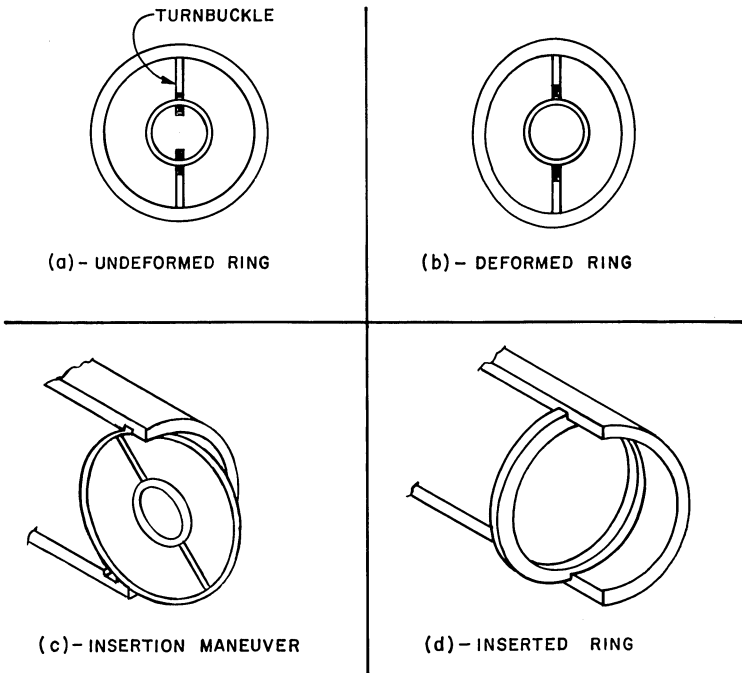


Fig. 6.1.12. Seal ring insertion procedure.

6.2 WEDGE SEAL RING CLOSURE

6.2.1 Joint Description

Figure 6.2.1 shows a schematic outline of this type of closure. The joint consists of five principal parts, namely: (i), the shell, which contains a circumferential slot machined near its end; (ii), the cover, which resists the

pressure loading in the manner of a laterally loaded flat circular plate; (iii), the retainer shoe, which is a segmented split ring made to fit in the circumferential slot in the shell; (iv), a solid follower ring; and (v), the five-sided seal ring. The element numbers shown on Fig. 6.2.1 refer to our analysis to be discussed shortly.

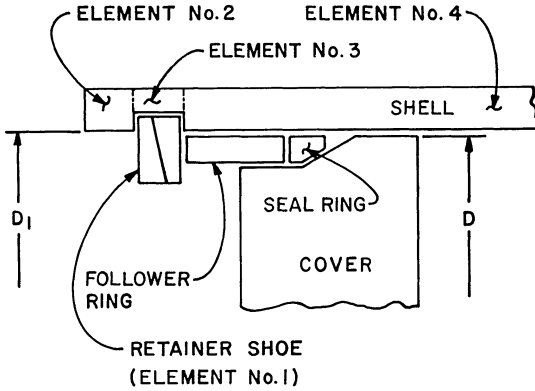


Fig. 6.2.1. Wedge seal ring closure.

It is clear that the retainer shoe can not be installed into the shell slot unless it is made into segments. The number of segments should be minimized so that the reduction in the strength of the ring is kept to the minimum. Figure 6.2.2 shows the segmenting pattern which produces three segments. These three segments, when assembled, add up to a complete circular ring. We note that the chord of largest segment, D^* , should be less than the shell barrel opening diameter, D_1 , to permit its installation in the

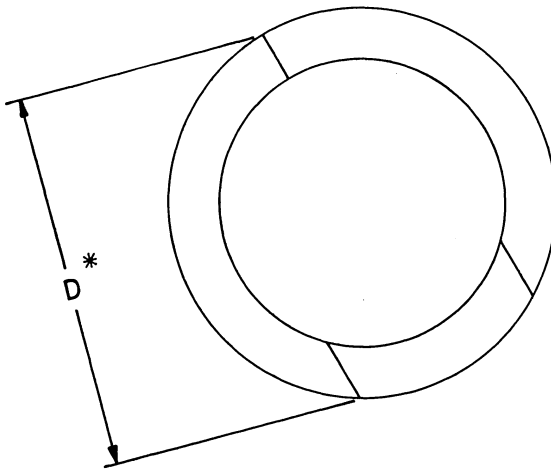


Fig. 6.2.2. Segmenting scheme.

slot. The retainer shoe should fit in the slot with minimal clearance in the longitudinal direction (less than 1/16"). It should project inwards sufficiently to provide adequate bearing surface for the follower ring.

The follower is a solid ring which slides into the inside diameter of the shell barrel with a small radial clearance (1/32"). The seal ring is of the general shape shown in Fig. 6.2.3. The two surfaces which produce the seal are shown as darkened lines in Fig. 6.2.3. The seal surfaces should be machined to a minimum of 32AA finish. The geometric dimensions d_1 , d_2 , θ , and radial clearance ϵ , are important design parameters which can be varied to obtain the most optimum ring cross section for a particular condition of service. The dimensions d_3 and d_4 are relatively unimportant. Typically, they are set in the range of 3/16" to 1/4".

The cover is machined such that the seal ring's inclined face can ride on its machined surface in conformal contact. Upon application of internal pressure, the cover experiences an axial force F_{ax} equal to:

$$F_{ax} = \frac{\pi}{4} D^2 p \tag{6.2.1}$$

This force tends to push the seal ring up the inclined machined surface on the cover. If F_{ax} is sufficiently large, then the seal ring expands to overcome the radial clearance ϵ , and develops a contact force R_2 with the channel inside surface. The seal ring dimensions should be selected in such a manner that the hoop stress in the ring does not exceed the yield point of the ring material under this forced expansion while the surface pressures on the two bearing surfaces reach values of 60 to 80% of the material yield point. The seal ring material should be softer than the shell and cover materials and should be metallurgically compatible with them. Materials which tend to bind or gall each other when subjected to normal pressure should not be used. Finally, the angle θ should be selected in such a manner that the seal ring develops an (axial) repulsive force with respect to the cover when the joint is depressurized. Indeed, ease of disassembly is a very important

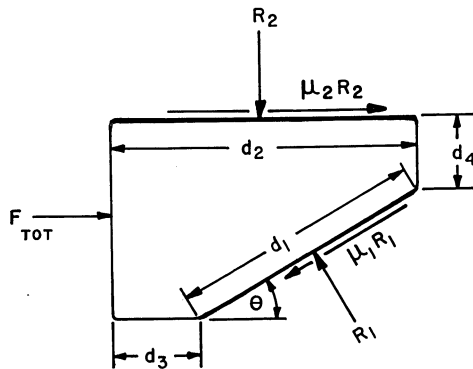


Fig. 6.2.3. Freebody of seal ring.

consideration in pressure actuated closures. The pressure vessel industry abounds in examples of joints that produce successful seal under pressure but are difficult to disassemble.

6.2.2 Analysis of Sealing Action

Although the actual stress field in the seal ring is quite complicated, the net reactions R_1 and R_2 (Fig. 6.2.3) can be computed using a strength-of-materials approach, as described below.

For purposes of analysis, the seal ring is modelled as a thin elastic ring subject to a net radially outward force due to its contact with the two rigid surfaces (the shell on the outside and the cover on the inside). Figure 6.2.3 shows the freebody diagram of the ring. Change of shape of the cross section is neglected in the analysis. $\mu_1 R_1$ is the friction force between the cover and the seal ring which opposes the axial movement of the cover. $\mu_2 R_2$ is the friction force between the shell and the seal ring which opposes the axial movement of the seal ring with respect to the channel.* It is noted that $\mu_2 R_2$ will be zero if the retainer shoe-follower ring assembly is assumed to be rigid (so that no movement of the seal ring relative to the channel can occur). It will be shown that setting $\mu_2 = 0$ leads to conservative results. Axial equilibrium of the cover itself yields:

$$F_{ax} = R_1 \sin\theta + \mu_1 R_1 \cos\theta$$

or

$$R_1 = \frac{F_{ax}}{\sin\theta + \mu_1 \cos\theta} \quad (6.2.2)$$

Axial force equilibrium of the seal ring (Fig. 6.2.3) yields:

$$F_{TOT} = R_1 \sin\theta + \mu_1 R_1 \cos\theta - \mu_2 R_2 \quad (6.2.3)$$

Substituting for R_1 from Eq. (6.2.2) we have:

$$F_{TOT} = F_{ax} - \mu_2 R_2 \quad (6.2.4)$$

Thus the axial force per unit circumference on the follower ring is $F = F_{TOT}/2\pi r$. F is maximum if $\mu_2 = 0$. The net radial force P per unit circumference (positive if radially outwards), acting on the seal ring is given by:

$$P = \frac{R_1 \cos\theta - \mu_1 R_1 \sin\theta - R_2}{2\pi r} \quad (6.2.5)$$

where r is the mean radius of the seal ring.

If ϵ is the initial diametral gap between the seal ring and the channel, then the radial force P is given in terms of ϵ by the thin ring relationship

$$\epsilon = \frac{2Pr^2}{AE} \quad (6.2.6)$$

*The term "channel" and "shell" are used interchangeably here to denote the cylindrical pressure vessel.

From Eqs. (6.2.5)–(6.2.6) we have:

$$R_2 = R_1 (\cos\theta - \mu_1 \sin\theta) - \frac{\pi A E \epsilon}{r} \quad (6.2.7)$$

Thus both R_1 and R_2 are determined in terms of the known quantities F_{ax} and ϵ .

The design objective is to ensure that the average surface pressures corresponding to the normal surface forces R_1 and R_2 are in the range of 60 to 80% of the yield strength of the seal ring material. It is recognized that two assumptions mentioned in the foregoing introduce compensating errors in the predicted values of R_1 and R_2 . Neglecting the elasticity of the cover and the shell will tend to overpredict these reactions. On the other hand, neglecting the axial expansion of the ring cross section due to its axial compression will tend to underpredict R_1 and R_2 . Despite its simplified approach, this analysis has been found to be adequate for practical design work.

6.2.3 Disassembly Analysis

As stated before, the ring dimensions, especially the angle θ , should be proportioned such that the ring is pushed along the cover when the joint is depressurized. This requires that the axial component of R_1 should exceed the axial component of the surface friction forces; i.e.

$$R_1 \sin\theta > \mu_1 R_1 \cos\theta \quad (6.2.8)$$

which gives:

$$\tan\theta > \mu_1 \quad (6.2.9)$$

6.2.4 Sizing the Retainer Shoe

An approximate solution for the stress levels in the retainer shoe (segmented ring) and in the shell is obtained by analyzing the load transfer using the classical strength-of-materials relations. For this purpose, the loaded region is sub-divided into four elements as shown in Fig. 6.2.4. The axial header force F , calculated from Eq. (6.2.4), is transmitted through the follower ring to the retainer shoe which causes the segmented ring to rotate and establish contact loads F_2 and F_1 with elements 2 and 4, respectively. We assume that sufficient radial clearance between the shoe and element 3 exists to preclude contact between them. Figure 6.2.4 shows the freebody diagram for the four elements. Moment M_{ij} and shear Q_{ij} denote the discontinuity resultants between elements i and j . Due to rotation of element 1, the line load of application of F will move outwards. However, for conservatism in the analysis, it is assumed to be applied at the mid-surface circle of the follower ring. Elements 1, 2 and 3 are modelled by ring theory equations (Ref. Section 3.9), and element 4 is modelled as an axisymmetrically end loaded thin circular shell. Let a_i , t_i and h_i denote the mean radius, thickness (axial dimension) and width of the ring element i , respectively. By inspection of the freebody diagrams of the three elements

we can write the expressions for the net moment M_i about the central plane and the net radial force Q_i for each element i in Fig. 6.2.4.

$$M_1 = F r_1 + F_2 r_2 - F_1 r_3$$

$$Q_1 = 0$$

$$M_2 = -M_{23} + Q_{23} \frac{t_2}{2} + F_2(r_4 + r_5)$$

$$Q_2 = -Q_{23} \tag{6.2.10}$$

$$M_3 = M_{23} - M_{34} + Q_{23} \frac{t_3}{2} + Q_{34} \frac{t_3}{2}$$

$$Q_3 = Q_{23} - Q_{34}$$

Similarly, the moment M_4 about the mid-surface of element 4 and the net radial shear per unit of circumference are given as

$$M_4 = M_{34} - F_2 r_7 - F_1 r_6; \quad Q_4 = Q_{34}$$

In the above equations, positive moments are those which turn the ring section clockwise in the plane of the paper, and positive radial force increases the ring diameter. In the above, we have assumed that all moment and force resultants are referenced to the appropriate ring radius a_i . That is, terms of order r/a are neglected in comparison with unity.

Referring to Section 3.9, rotation θ_i , of ring i , is given by:

$$\theta_i = \frac{\chi_i M_i a_i^2}{E I_i} = \alpha_i M_i \tag{6.2.11}$$

$$\alpha_i = \frac{\chi_i a_i^2}{E I_i} \tag{6.2.12}$$

where χ_i is a factor which accounts for the weakening effect of the segmenting ($\chi_i = 1$ for elements 2 and 3).

Similarly, the radial displacement δ_i of the centerline of ring i due to Q_i is given by:

$$\delta_i = \frac{Q_i a_i^2}{h_i t_i E} = \gamma_i Q_i \tag{6.2.13}$$

where:

$$\gamma_i = \frac{a_i^2}{h_i t_i E} \tag{6.2.14}$$

Finally, thin shell theory gives the rotation θ_4 and displacement δ_4 for the point B on element 4 (see Appendix A).

$$\theta_4 = \frac{1}{2 \beta^2 D} [2\beta M_4 + Q_4] \tag{a}$$

$$\delta_4 = \frac{1}{2 \beta^3 D} [\beta M_4 + Q_4] \tag{b}$$

(6.2.15)

where

$$\beta = \left[\frac{3(1-\nu^2)}{a_4^2 h_4^2} \right]^{1/4}; \quad D = \frac{E h_4^3}{12(1-\nu^2)} \quad (c)$$

Matching displacements and rotations at points *A* and *B* gives 4 linear algebraic equations. If we assume that the segmented ring has to rotate by θ_0 before establishing contact with elements 2 and 4, then rotational continuity requires:

$$\theta_2 = \theta_1 - \theta_0 \quad (6.2.16)$$

where θ_0 is dependent on the gap in the axial direction between the shoe and the groove; that is, θ_0 is calculated from the geometry of the joint.

A sixth equation follows from axial equilibrium of element 1:

$$(a_1 + r_2)F_2 - (a_1 + r_3)F_1 = (a_1 - r_1)F \quad (6.2.17)$$

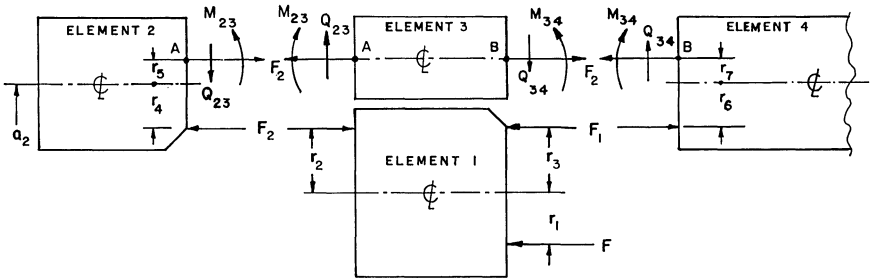


Fig. 6.2.4. Freebody diagram of shell shoe assembly.

Thus six simultaneous algebraic equations in six unknowns, M_{23} , Q_{23} , M_{34} , Q_{34} , F_1 , F_2 are set up which can be solved using a standard linear equation solver subroutine. The matrix equation is written in the standard form $[A]\{x\} = \{f\}$ with $\{x\}^T = [M_{23}, Q_{23}, M_{34}, Q_{34}, F_1, F_2]$. Coefficients of the non-zero terms of the $[A]$ matrix and $\{f\}$ vector are listed below for reference.

$$A(1,1) = \alpha_2;$$

$$A(1,2) = \frac{-t_2 \alpha_2}{2}$$

$$A(1,5) = -\alpha_1 r_3;$$

$$A(1,6) = -[\alpha_1 r_2 - \alpha_2 (r_4 + r_5)]$$

$$A(2,1) = (\alpha_2 + \alpha_3);$$

$$A(2,2) = \frac{\alpha_3 t_3 - \alpha_2 t_2}{2}$$

$$A(2,3) = -\alpha_3;$$

$$A(2,4) = \frac{\alpha_3 t_3}{2}$$

$$A(2,6) = -\alpha_2 (r_4 + r_5);$$

$$A(3,1) = \frac{\alpha_2 t_2 - \alpha_3 t_3}{2}$$

$$A(3,2) = -\gamma_2 - \gamma_3 - \frac{\alpha_2 t_2^2}{4} - \frac{\alpha_3 t_3^2}{4}; \quad A(3,3) = \frac{\alpha_3 t_3}{2}$$

$$A(3,4) = \gamma_3 - \frac{\alpha_3 t_3^2}{4}; \quad A(3,6) = \frac{-\alpha_2 t_2 (r_4 + r_5)}{2}$$

$$A(4,1) = \alpha_3; \quad A(4,2) = \frac{\alpha_3 t_3}{2}$$

$$A(4,3) = -\left(\alpha_3 + \frac{1}{\beta D}\right); \quad A(4,4) = \left[\frac{\alpha_3 t_3}{2} - \frac{1}{2\beta^2 D}\right]$$

$$A(4,5) = \frac{r_6}{\beta D}; \quad A(4,6) = \frac{r_7}{\beta D}$$

$$A(5,1) = \frac{-\alpha_3 t_3}{2}; \quad A(5,2) = \gamma_3 - \frac{\alpha_3 t_3^2}{4}$$

$$A(5,3) = \frac{\alpha_3 t_3}{2} - \frac{1}{2\beta^2 D}; \quad A(5,4) = -\left[\frac{\alpha_3 t_3^2}{4} + \gamma_3 + \frac{1}{2\beta^3 D}\right]$$

$$A(5,5) = \frac{r_6}{2\beta^2 D}; \quad A(5,6) = \frac{r_7}{2\beta^2 D}$$

$$A(6,5) = -(a_1 + r_3); \quad A(6,6) = (a_1 + r_2)$$

$$f(1) = -\alpha_1 r_1 F + \theta_0; \quad f(6) = (a_1 - r_1)F$$

Having determined the ring moments, the corresponding ring stresses are calculated using the formulas given in Section 3.9. Since this analysis is for a rather specialized closure, we leave it to the interested reader to computerize the calculation and design procedure.

NOMENCLATURE

- A = Cross-sectional area of the seal ring (Fig. 6.2.3)
- a_i = Mid-surface radius of element i (Fig. 6.2.4)
- D = Flexural rigidity of the channel barrel (Section 6.2.4)
- D' = Outer diameter of the cover in Fig. 6.1.11
- F = Axial force per unit circumference on the seal ring
- F_{ax} = Total axial force on the cover due to internal pressure
- F_{TOT} = Total axial force on the follower ring due to pressure
- F_1 = Contact force per unit circumference between elements 1 and 4 in Fig. 6.2.4
- F_2 = Contact force per unit circumference between elements 1 and 2 in Fig. 6.2.4

- M_i = Moments per unit circumference about mid-plane of ring element i
 M_{ij} = Interface discontinuity moment per unit circumference between element i and element j
 Q_i = Radial force per unit circumference in ring element i
 Q_{ij} = Radial discontinuity shear per unit circumference between elements i and j
 r = mean radius of the contact annulus between the follower ring and the seal ring
 r_1, r_2, \dots, r_7 = Radial dimensions (Fig. 6.2.4)
 R_1 = Total reaction force on the seal ring/cover interface (Fig. 6.2.3)
 R_2 = Total reaction force on the seal ring-shell interface (Fig. 6.2.3)
 α_i = Rotation coefficient for ring element i (Eq. 6.2.12)
 β = Attenuation coefficients of channel barrel
 ϵ = Initial diametral gap (Eq. 6.2.6)
 θ_i = Rotation of ring element i (Eq. 6.2.11)
 μ_i = Coefficient of static friction between seal ring and channel/cover (Fig. 6.2.3)
 ν = Poisson ratio of channel material

REFERENCES

- [6.1.1] Jorgensen, S. M., "Closures and Shell Joints for Large High Pressure Cylinders," ASME Paper No. 68-PVP-9.
 [6.1.2] Stevens-Guille, P. D., Newmarch, J. E., Thorpe, C. R., and Eccleston, R. J., "Sealing Forces for Leak-Tight Operation of a Self-Energized Pressure Vessel," ASME Paper No. 78-PVP-16.
 [6.1.3] Israel, P., "Closure Device and Fastening Means Therefor," U.S. Patent No. 3077360, February, 1963.
 [6.1.4] Butcher, H. H., "Industrial Sealing Technology," p. 66, John Wiley, New York, (1979).
 [6.1.5] Anderson, H. H., "Self-Seal Joint for Very High Pressures," ASME Paper No. 67-WA/PVP-5.
 [6.1.6] Ruiz, C., and El Magrissy, M. I. R., "Flangeless Closure Joints: Experimental Validation of an Unconventional Design," Second International Conference Pressure Vessel Technology, Part I, ASME, pp. 597-610 (1973).
 [6.1.7] Lankston, R. J., "Closure Arrangement for Pressure Device," U.S. Patent No. 4,288,001 (1981).
 [6.1.8] Platts, D. J., "Closure Member," U.S. Patent No. 4,102,474 (1978).
 [6.1.9] Luker, J. G., "Pressure Vessel and Closure Assembly Therefor," U.S. Patent No. 3,310,329 (1967).
 [6.1.10] Shaw, R. W., "Unitary Quick-Opening Closure Device," U.S. Patent No. 3,187,929 (1965).

7 TUBE-TO-TUBESHEET JOINTS

7.1 JOINT TYPES

A variety of methods are used for making the joint between the tubesheet and the tubes. The joining technique must lend itself to mass production and to uniformity of quality. The most common attachment techniques are:

- (i) Roller expansion
- (ii) Hydraulic expansion
- (iii) Impact welding
- (iv) Edge welding
- (v) Butt welding

Of the above, roller expanding is by far the most common. Frequently, one or more of the joining methods are used together to improve joint reliability. For example, edge welding (iv) is frequently used in conjunction with roller or hydraulic expansion.

The importance of a sound tube-to-tubesheet joint cannot be overemphasized. However, strength requirements of the joint depend on the operating condition and the exchanger style. It is obvious that tube joints in fixed tubesheet heat exchangers without expansion joints are subject to much greater axial load than those containing a shell expansion joint; therefore, with identical operating conditions, the axial pull in the tubes of a U-tube or floating head exchanger is likely to be much smaller than that in a fixed tubesheet construction. The leak-tightness requirements are also service dependent. Whereas a relatively large amount of leak would be tolerated in a recuperator or regenerative heat exchanger (identical fluid media inside and outside tubes), even minute leak rates may be unacceptable in heat exchangers where the two heat exchanging fluids form an explosive mixture. Joint leakage can have profound effects on the entire process system. For example, in-leakage of raw circulating water into the steam cycle at the condenser tube-to-tubesheet joint has been a vexing problem affecting operational reliability of power plants [7.1.1]. A brief description of the aforementioned joining techniques is presented, followed by a simplified procedure for estimating joint strength. A method for evaluating the joint temperature under operating conditions is also described.

7.2 EXPANDING METHODS

Commercial tubes have a certain, though small, diametral and ovality

tolerance. Drilled and reamed holes in the tubesheets also have a certain scatter in their finished diameter. According to TEMA [7.2.1], 96% of all tube holes for 1" diameter tubes can be in the 1.008" to 1.014" diameter range. The materials section of the ASME codes specifies that the outer diameter of one inch SA249-TP304 (welded stainless steel) tubing can be in the $1" \pm 0.006"$ range. This implies that if the smallest diameter tube were to be expanded into the largest size permissible hole, then the tubes must be expanded by 0.020" before the tubewall contacts the hole inside surface. Using Lame's formula for thin rings, the associated tube hoop stress is estimated by:

$$S = \frac{E_t \delta}{a} \quad (7.2.1)$$

where E_t , δ and a are the tube material Young's modulus, radial clearance and tube radius, respectively. Substituting 30×10^6 psi for E_t , 0.01" for δ , and 0.5" for a , gives $S = 0.6 \times 10^6$ psi.

Clearly, the circumferential strain in the tube is plastic. Upon withdrawal of internal pressure, the tube will contract by a small fraction of the initial expansion (elastic springback). If the expanding force were to be continued past the point where contact with the tubesheet hole occurs, then expansion of the tube hole commences. Initially, the tube hole deformation is elastic, until the circumferential strain in the tubesheet at the interface diameter reaches the material's yield point. With additional increase in the expansion load, the plastic zone propagates into the tubesheet ligament. The most desirable expansion is one which produces maximum interface pressure between the tube and tubesheet hole upon withdrawal of the expansion force. The optimal expansion is a function of a number of variables, such as yield stress and Young's moduli of tube and tubesheet materials, width of the ligament, and tube gage. The leak tightness of the joint also depends on other less quantifiable parameters such as tube hole and tube surface finish, hole and the tube ovality, surface hardness of tube and holes, expanding technique, etc. For this reason, prototype testing is the most reliable method to establish the correct amount of expansion.

7.3 ROLLER EXPANDING

Introduced during the mid-nineteenth century [7.3.1], this method of tube-to-tubesheet fastening continues to be the dominant technique to this day. The roller expander (Fig. 7.3.1) consists of a cylindrical cage which loosely holds a cluster (3 to 7) of hardened tapered steel rollers. A similarly tapered mandrel is inserted through the cage causing the rollers to make line contact with the tube surface on the outside and with the mandrel on the inside. A pneumatic or electrical drive turns the mandrel (usually in the range of 400 to 1000 rpm) which, in turn, causes the rollers to rotate. The axis of the rollers is set at a small angle with respect to the mandrel's axis of rotation. This causes the rotational motion of the mandrel to produce an

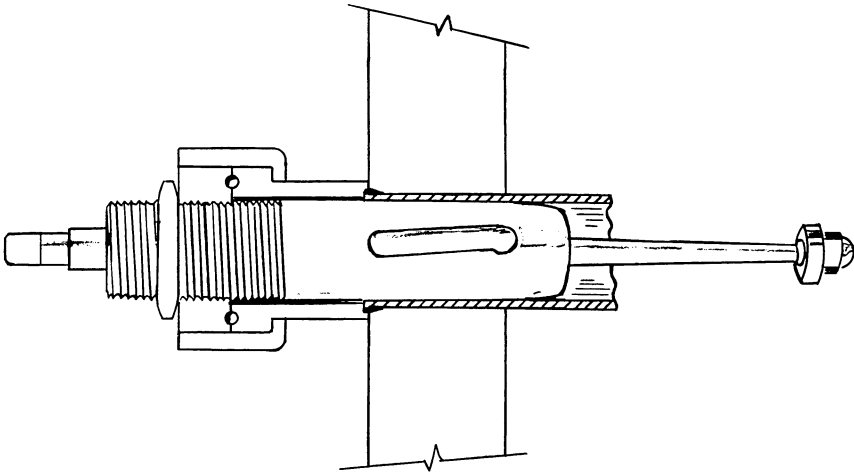


Fig. 7.3.1. Typical roller expander.

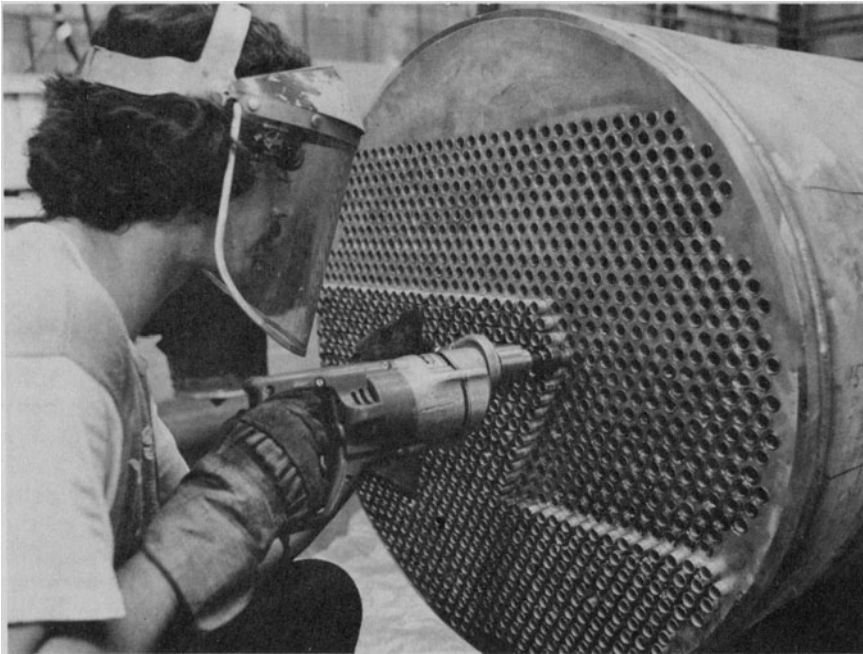
axial force in addition to a rotatory torque on the rollers. Since the rollers are kept from moving axially by the thrust collar, the reactive force makes the mandrel “force-feed.” In pneumatic drives, a pre-set limit torque switch controls the extent of rolling. The torque is set to correspond to a desirable “apparent tube thinning” (typically in a 5 to 20 lb-ft range). The device is hand held and therefore the operator, aided by the inertia of the hardware, must absorb the reactive torque (see Photograph 7a).

A set of rollers rotating at high speed produces a moving set of contact patches where the stresses reach very high values [7.3.2]. The material extrudes out in the axial direction and thus can produce a substantial compressive stress in the tube if the other end of the tube is held. This situation is particularly problematic in double tubesheet exchangers. A careful rolling sequence in double tubesheet exchangers is necessary to reduce this tube pre-load [7.3.3]. The quality of the bond produced by roller expansion depends primarily on the following parameters:

- (i) Number of rollers
- (ii) Mandrel speed
- (iii) Finish of tube outside surface and tubesheet hole inside surface.
- (iv) Tubesheet ligament size.
- (v) Stress-strain curves of tube and tubesheet material.

In practice, roller lubricant, tube and tubesheet surface cleanliness, condition of rollers, etc., also influence joint quality.

One important fact to bear in mind while roller expanding tubes is the danger of “over-rolling”. Rolling the tubes beyond the optimal value can unload adjacent joints and cause them to leak under hydrostatic test. Over-rolling often occurs when the operator tries to seal an obstinate leaking joint



Photograph 7.a. Roller expanding operation.

by increasing the roll torque. When repeated rolling of the same joint is performed it is advisable to provide support to tube holes in adjacent tubes with tapered pins. Over-rolling also carries the danger of cracking the tube, particularly in rapidly work-hardening materials, such as titanium.

The current practice in the U.S. is to limit the length of roll to 2" [7.2.1]. TEMA standards give detailed guidelines on rolling length for different classes of service.

7.4 HYDRAULIC EXPANSION

As the name implies, hydraulic expansion entails direct pressurization of the tube using a fluid (usually water) medium. The tube segment to be expanded is pressurized in the range of 30 to 50 ksi. The length of tube to be expanded can be set by adjusting the location of an O-ring seal on the interior of the tube. There is no limitation on the tube length that can be expanded at one time. This is a distinct advantage over roller expanding which must be restricted to a 2"–2.5" expansion length at one time due to limitations on the torque, friction between mandrel and rollers, etc. Another advantage of hydraulic expansion is its ability to handle non-circularity in tube and tube hole cross sections without any difficulty. Since the pressure is applied uniformly, there is no extrusion of the tube from the zone of expansion, and therefore, no noticeable wall reduction. However, since the tube diameter is increased in the expanded zone, the Poisson effect

causes the tubes to shorten by a small amount. This may put the tube in tension if the other end of the tube is previously secured. This may happen, for instance, in expanding the tubes in the second tubesheet in a fixed tubesheet heat exchanger. Podhorsky and Krips [7.4.1] discuss the concept of combining roller and hydraulic expansions to produce a desired amount of pre-strain in the tube. Since mechanical rolling elongates the tubes, and hydraulic expansion shortens them, Podhorsky and Krips suggest using them in combination. Singh and Soler [7.4.2] show how tube pre-stress in stationary tubesheet heat exchangers can be exploited to reduce stress levels.

7.5 IMPACT WELDING

The origin of this technology lies in explosion cladding of plates first attempted in the 1950's. The process may be defined as a controlled solid state welding operation in which coalescence is obtained by a high velocity impact between the surfaces to be joined. Controlled detonation of a suitably positioned explosive charge produces a collision front which traverses the surface areas being joined. Hardwick [7.5.1] states the velocity of this collision front should not exceed 120% of the sonic velocity of the materials. Figure 7.5.1 shows the schematic set-up for this operation. The tubesheet hole is prepared with conical countersink 1/2" to 5/8" long at an included angle in the range of 10° to 20°. The polymeric insert serves to locate the charge and to transmit the pressure front to the tube in a controlled manner. To ensure a uniform bonding in the conical region, the end effects are eliminated by setting the tube with a small protrusion beyond the

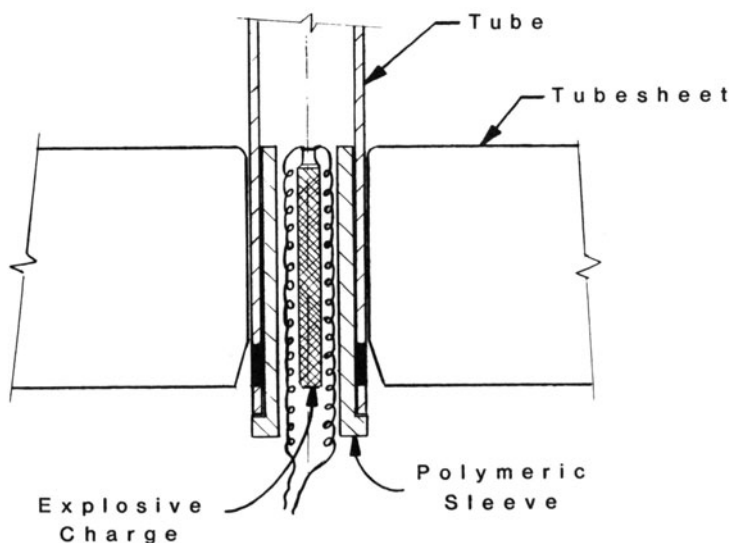


Fig. 7.5.1. Impact welding.

tubesheet face. This protrusion is severed from the tube, producing a uniformly welded joint in the countersink region.

Since its introduction a few years ago, this method has proved to be a reliable joining technique. However, it suffers from some limitations. The chief limitation is the minimum required ligament size. Table 7.5.1 gives the recommended minimum ligament width as a function of tube gage. The last column in Table 7.5.1 gives the minimum ligament width if the surrounding tube holes are temporarily plugged using a tapered plug to provide additional support to the ligaments subject to explosion impact.

Table 7.5.1. Minimum Tubesheet Ligament

Tube Gage (inch)	Ligament Width	
	Unsupported (inch)	Supported (inch)
0.028	5/16	1/4
0.036	5/16	1/4
0.048	3/8	5/16
0.064	7/16	3/8
0.080	1/2	7/16
0.104	5/8	9/16

High pressure applications require a heavy tube gage which forces the tubesheet ligament to be enlarged. This is a severe penalty, since increased ligament increases heat exchanger diameter, affects its thermal performance, and, in general, increases the hardware cost. The limitation of this technique can be overcome by boring out the tube ends and thus locally reducing the tube wall thickness.

Several factors outweigh the disadvantages of this method for some applications. For example, whereas welding requires material compatibility, this method can bond two otherwise unweldable materials. The tube hole diameter tolerance has little impact on the joint quality. Indeed, this method finds field repair application in leak-tightening previously rolled joints where repeated or overzealous rolling has caused substantial enlargement of the holes. It appears that explosion bonding will receive increased attention in the future in heat exchangers employing thick tubesheets, such as high pressure feedwater heaters.

It should be noted that the bell mouth shaped tube inlet produced by explosion bonding reduces turbulence and tube end erosion due to flow of incoming tubeside fluid. This is an incidental design improvement of some value where carbon steel tubesheets and tubes are used and where the incoming tubeside fluid is erosive in nature.

7.6 EDGE WELDING

Figure 7.6.1 shows a typical flush edge welding detail used in commercial heat exchanger fabrication. Flush welding (Photograph 7.b) is used in

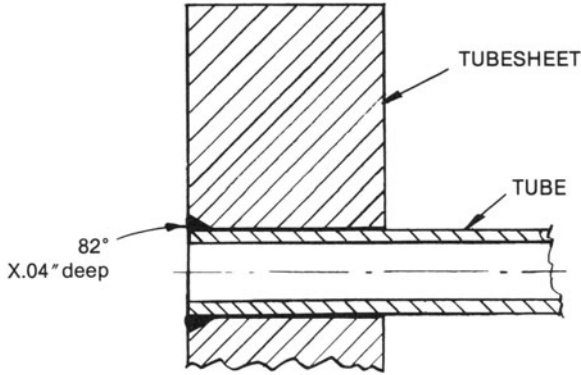
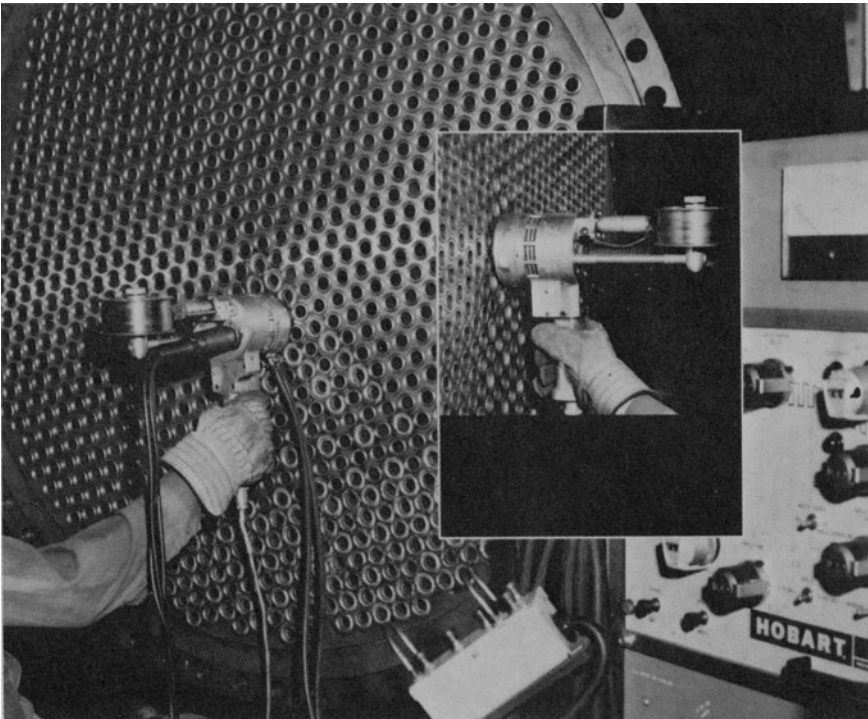


Fig. 7.6.1. Edge welding detail.



Photograph 7.b. Edge welding using a semiautomatic TIG welder. (Courtesy Southern Heat Exchanger Inc., Tuscaloosa, Ala.)

joining thin wall tubes on a tight layout pitch to the tubesheet. Where the pitch is not so tight, a tripanned tubesheet fillet weld (Fig. 7.6.2) may be used. Tripanning the tubesheet provides better heat capacitance balance between the tube and tubesheet. Direct fillet welds are also made where tube

gage permits such a weld (Fig. 7.6.3 and Photograph 7.c). Where an increased leak path or modification of welded zone chemistry is desired, an added fusion ring can also be employed (Fig. 7.6.4). The fusion ring tends to heat up and move during welding causing operational difficulties and quality hazards; mechanical means must be employed to prevent this problem. Welding for any of the above details can be performed autogenously. The edge welding is usually performed using a handheld tungsten inert gas welder. The welding device circuitry provides for the following sequential operation: pre-purging the weld area with shielding gas, arc initiation, torch travel around the tube periphery (through one revolution plus ≈ 20 degrees to fuse the startup area), controlled arc decay and finally, delayed purge to prevent weld oxidation. Where the tube and tubesheet materials are compatible, no filler material is used. Some alloys, such as wrought copper-nickels and nickel, produce gassing porosity when welded autogenously. Addition of a slurry type deoxidizer such as titanium hydride is known to help in such situations. The titanium deoxidizer is also reported to be useful in making crack-prone welds such as those involving aluminum bronze tubes or tubesheets. The ASME Code [7.6.1] gives some schematic details of tube-to-tubesheet weld joints. Formulas to compute allowable joint axial load are also given in this code. Experiments by Applebitt, et al. [7.6.2] indicate that fillet welded joints hold up well under thermal shock.

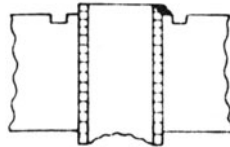


Fig. 7.6.2. Tripanned tubesheet fillet weld.

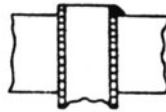


Fig. 7.6.3. Fillet weld.

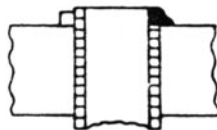
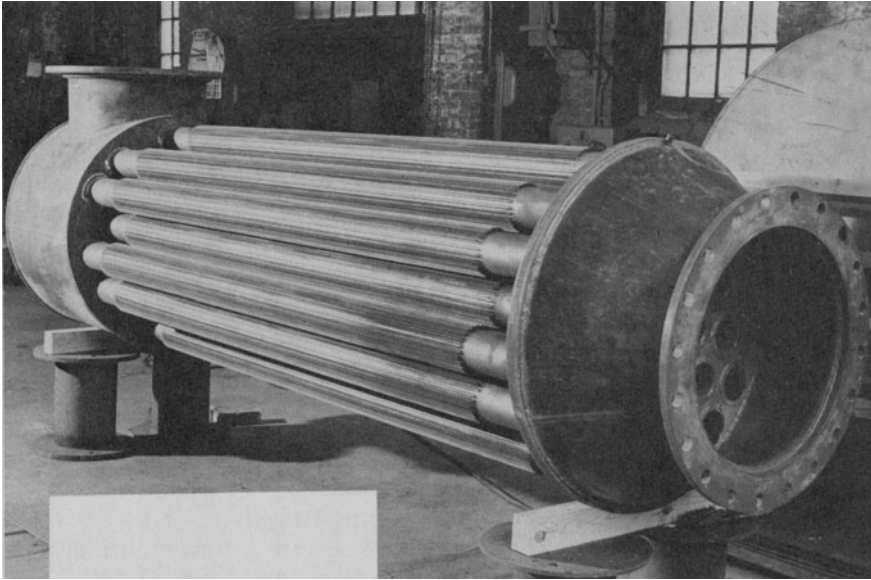


Fig. 7.6.4. Fillet weld with added fusion ring.



Photograph 7.c. Heat exchanger with longitudinally finned tubes; tubes fillet welded to the tubesheet. (Courtesy of Joseph Oat Corporation, Camden, N.J.)

7.7 BUTT WELDING

In relatively rare applications, the shellside face of the tubesheet is machined to make beveled nipples which are butt welded to the tube ends (Fig. 7.7.1). The height of the nipple is selected to produce a sound weld and to enable radiography or volumetric examination (as appropriate) of the weld. Butt welded joints are seldom used due to the expense associated with tubesheet milling to form the nipples.

Unlike other types of joints, this method leaves no crevice between the tubes and the tubesheet hole. Since tube ends are not mechanically worked, corrosion problems attributed to grain realignment due to severe tube straining in other methods are avoided.

7.8 TUBE-TO-TUBESHEET INTERFACE PRESSURE

Since the ultimate object in the tube-tubesheet joining process is to maximize the tube-to-tubesheet contact pressure, a method to evaluate this pressure is an essential element in selecting optimum parameters for expansion. Works by Dudley [7.3.1] and Brown [7.8.1] helped explain the roller expanding phenomena in physical terms. Analytical work by Goodier and Schoessow [7.8.2], and the companion experimental paper by Grimison and Lee [7.8.3] are important milestones in improving our understanding of the tube expansion process. Goodier and Schoessow developed expressions

for elastic-plastic loading and unloading of the joint assuming a condition of plane stress and the von Mises yielding criterion [7.8.4]. The effect of tube wall thickness, relative magnitudes of tube and tubesheet yield strengths, etc., was systematically investigated. Additional experimental work by Alexander and Ford [7.8.5], Beston [7.8.6], Culver and Ford [7.8.7] and Uragami, et al. [7.8.8] also provide added information on this subject. Wilson [7.8.9] presented a finite element analysis of the tube/tubesheet joint to investigate the residual stress distribution in the roll transition region.

In this section, a plane stress model of the tube to tubesheet joint is first considered. Plastic action is based on the Tresca yield condition in order to illustrate the loading and unloading paths by simple analysis. In an appendix to this chapter, a more complex plane stress model is examined, incorporating large deformations, and thermal as well as mechanical loading. A simple numerical model is used there to study the tube roll problem at room temperature and to study the effect on the joint of a subsequent thermal cycling. In the numerical study, the von Mises Yield criterion is used to establish the onset of plastic action.

For the initial analytical solution, we derive expressions to estimate the tube-tubesheet interface pressure, the final tube hole radius, and the stress field in the tube/ligament region, by using elementary two dimensional elasticity and plasticity equations. The following assumptions are made:

- i The tubesheet is modelled as an infinite circular plate with a central hole of radius r_2 . This assumption overestimates the strength of the tubesheet ligament.
- ii The tube and tubesheet materials are assumed to be elastic-perfectly plastic. Figure 7.8.1 shows the typical stress-strain curve of such a material.

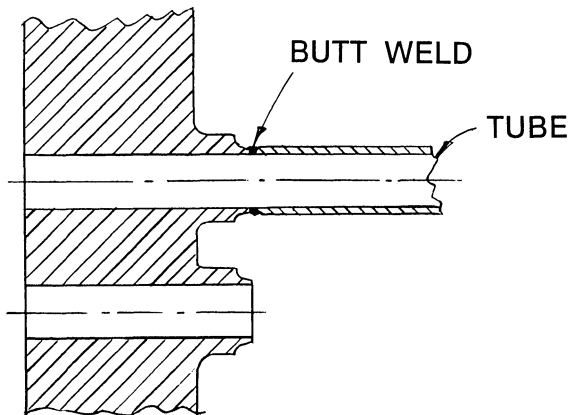


Fig. 7.7.1. Butt weld detail.

- iii The tube is modelled as a thin walled shell of mean radius r_t' and thickness t' . The portion of the tube inside the tubesheet is assumed to be disconnected from the remainder; i.e., the abutting tube segment is assumed to exert no restraint to the radial movement of the tube due to expander pressure.
- iv Both tube and tubesheet satisfy the Tresca yield criterion, which states that yield commences when the maximum stress intensity reaches twice the yield point shear stress of the material.
- v The tubesheet is assumed to be in a state of plane stress.
- vi Deformation theory [7.8.4] is used to evaluate displacements in the plastic range.
- vii The tube is assumed to yield prior to its contact with the tubesheet.
- viii The expansion of the tube and tubesheet is assumed to be radially symmetric. This condition is most closely realized in hydraulic expansion.

7.8.1 Initial Expansion of the Tube

Under internal pressure p_0' , the circumferential stress σ_θ and the average radial stress σ_r are given by classical thin shell equations:

$$\begin{aligned}\sigma_\theta &= \frac{p_0' r_t'}{t'} \\ \sigma_r &= \frac{-p_0'}{2}\end{aligned}\quad (7.8.1)$$

Since σ_θ and σ_r are of opposite signs, the maximum stress intensity (equal to twice the maximum shear stress) is $(\sigma_\theta - \sigma_r)$.

The plane stress assumption implies:

$$\epsilon_\theta = \frac{1}{E_t} [\sigma_\theta - \nu \sigma_r] = \frac{u}{r_t'} \quad (7.8.2)$$

where u is the radial deflection of the tube centerline.

Substituting σ_θ and σ_r from Eq. (7.8.1) into Eq. (7.8.2) yields

$$p_0' \left(\frac{r_t'}{t'} + \frac{\nu}{2} \right) = \frac{E_t u}{r_t'} \quad (7.8.3)$$

Using the Tresca yield criterion, the pressure to cause tube yielding is given by

$$\sigma_\theta - \sigma_r = \sigma_T = p_0' \left(\frac{r_t'}{t'} + \frac{1}{2} \right)$$

Therefore

$$p_0' = (\sigma_T t' / r_t') / (1 + t' / 2r_t') \quad (7.8.4)$$

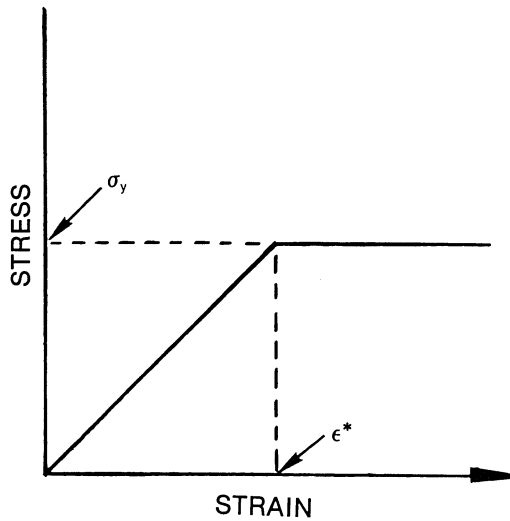


Fig. 7.8.1. Stress-strain curve for elastic-perfectly plastic material.

From Eqs. (7.8.3) and (7.8.4) we obtain

$$\frac{u}{r_i'} = \frac{\sigma_T \left(1 + \frac{v_T'}{2r_i'}\right)}{E_t \left(1 + \frac{t'}{2r_i'}\right)} \quad (7.8.5)$$

If the radial clearance c exceeds u , given by Eq. (7.8.5), then the tube will yield before contact with the tubesheet is made.

Upon initiation of yielding, the tube wall cannot support any further increase in internal pressure. In the plastic deformation stage, the tube radius increases, and the tube wall thickness decreases. Referring to Eq. (7.8.4), we note that the corresponding internal pressure will be smaller than p_0' . Let us denote the pressure supported by the tube when it contacts the tubesheet by p_0 and let the corresponding tube mean radius and thickness be given by r_t and t , respectively. If we assume that the change in thickness and the change in mean radius during the expansion to radius r_t are caused solely by plastic straining, then [7.8.4]

$$\Delta t'/t' = \phi \left(\sigma_r - \frac{\sigma_\theta}{2} \right)$$

$$\Delta r_t'/r_i' = \phi \left(\sigma_\theta - \frac{\sigma_r}{2} \right)$$

where ϕ is a proportionality parameter which relates the plastic strain increment to current stress.

If we neglect σ_r in comparison with σ_θ , we obtain:

$$\Delta t' / t' = -\frac{\Delta r'_i}{2r'_i}; \quad \Delta r'_i \cong c$$

With $t = t' + \Delta t'$, we obtain the new tube thickness and mean radius at contact as

$$\begin{aligned} t &= t'(1 - c/2r'_i) \\ r_i &= r'_i + c \end{aligned} \quad (7.8.6)$$

The tube stresses at the initiation of contact are

$$\sigma_\theta = \frac{p_0 r_i}{t}$$

$$\sigma_r = \frac{-p_0}{2}$$

Since

$$\sigma_T = \sigma_\theta - \sigma_r$$

we obtain:

$$p_0 = \frac{\sigma_T t / r_i}{1 + t/2r_i} \quad (7.8.7)$$

Increase in pressure over p_0 results in the development of an interface pressure at the tube/tubesheet surface, and an elastic stress field in the tubesheet. If the pressure is raised sufficiently, then the inner region of the tubesheet ligament also becomes plastic. The plastic zone expands as the pressure is increased. The necessary expressions to determine the extent of the plastic zone for a given internal pressure are now derived.

7.8.2 Loading of Tube and Tubesheet

Let p denote the applied pressure on the inside surface of the tube. Then

$$p = p_0 + p_i \quad (7.8.8)$$

where p_i is the increment of pressure applied subsequent to tube-tubesheet contact. Let the corresponding interface pressure between the tube and the tubesheet and between the elastic and plastic regions of the tubesheet be denoted by p_c and p_e , respectively.

i. Tube

The circumferential and radial stresses in the tube are given by:

$$\sigma_\theta = (p_0 + p_i - p_c) \frac{r_i}{t} + \sigma_r$$

$$\sigma_r = \frac{-1}{2} (p_0 + p_i + p_c)$$

$$\sigma_T = \sigma_\theta - \sigma_r = (p_0 + p_i - p_c) \frac{r_i}{t}$$

Note that since $p_0 + p_i - p_c$ may be small, we cannot neglect σ_r in comparison with σ_θ in the case where comparable pressures are being applied to both surfaces of the tube.

Substituting for σ_T from Eq. (7.8.7) we have

$$p_i = p_c + p_0 t / 2r_i \quad (7.8.9)$$

Utilizing the equations for p_c and p_0 from Eqs. (7.8.9) and (7.8.7), σ_r and σ_θ are conveniently expressed as

$$\sigma_\theta = -p_i + \sigma_T(1 + t^2/4r_i^2)/(1 + t/2r_i) \quad (7.8.10)$$

$$\sigma_r = -p_i - \sigma_T(t/2r_i)(1 - t/2r_i)/(1 + t/2r_i)$$

From the above equations we can show that the maximum increment of pressure p_i that the joint can withstand is given by setting $\sigma_\theta = 0$, which yields

$$p_{i(\max)} = \sigma_T(1 + t^2/4r_i^2)/(1 + t/2r_i) \quad (7.8.11)$$

Equations (7.8.9) and (7.8.11) give the corresponding value of p_c if the tube governs the maximum joint load

$$p_{c(\max)} = \sigma_T(1 - t/2r_i) \quad (7.8.12)$$

Figure 7.8.2 shows pictorially the variation of σ_θ , σ_r and stress intensity $S = \sigma_\theta - \sigma_r$ as a function of p_i . Note that if p_i is increased beyond $p_{i(\max)}$ then σ_θ becomes negative and the maximum stress intensity S becomes numerically equal to $|\sigma_r| > |\sigma_T|$. Since the maximum stress intensity in a Tresca material can not exceed σ_T , we conclude that $p_{i(\max)}$ is an upper limit on the incremental internal pressure if the tube material governs the joint load.

When $p_i = p_{i(\max)}$ the total pressure p is given by

$$p = p_0 + p_{i(\max)} = \sigma_T(1 + t/2r_i) \quad (7.8.13)$$

We can now examine the stress and strain field in the tubesheet ligament under the internal pressure p_c .

ii. Tubesheet

As stated before, the tubesheet ligament is modelled as an infinite plate with a circular hole subject to internal pressure. We assume that the radius r_e defines the boundary between the inner (plastic) and outer (elastic) zones. The stress intensity is constant, and is set equal to σ_s , up to radius r_e . σ_s is the yield stress of the tubesheet material.

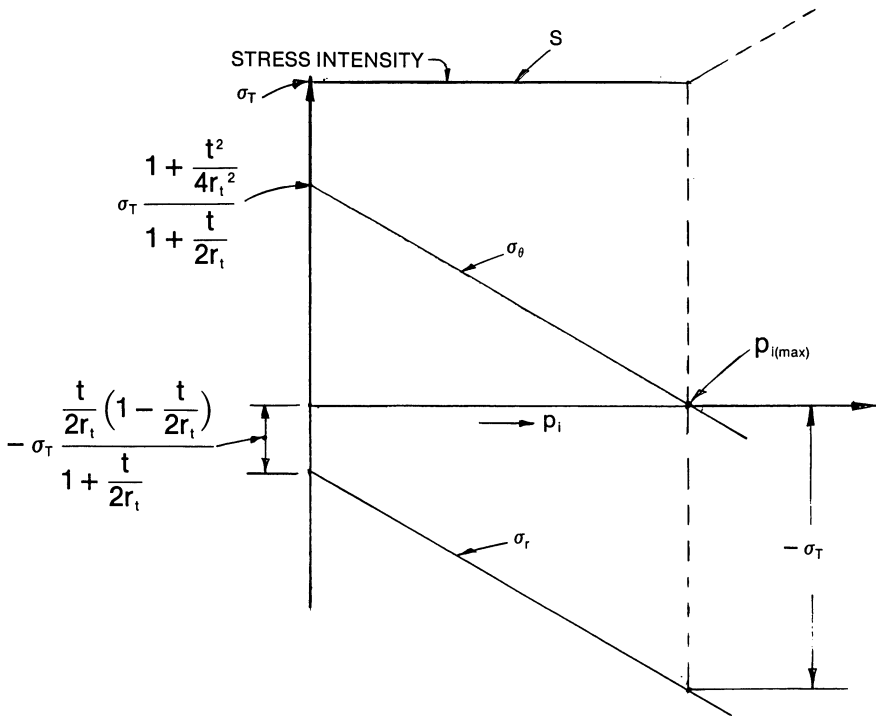


Fig. 7.8.2. Variation of σ_θ , σ_r and S with p_i .

Plastic Region; $r_2 \leq r \leq r_e$:

Equilibrium yields:

$$\frac{d\sigma_r}{dr} = \frac{\sigma_\theta - \sigma_r}{r} = \frac{\sigma_s}{r}$$

Therefore

$$\sigma_r = \sigma_s \ln r + C$$

Utilizing the boundary condition

$$\sigma_r = -p_c \text{ at } r=r_2$$

gives

$$\sigma_r = -p_c + \sigma_s \ln \frac{r}{r_2} \tag{7.8.14}$$

$$\sigma_\theta = -p_c + \sigma_s (1 + \ln r/r_2)$$

Elastic Region; $r > r_e$:

Equilibrium yields:

$$\frac{d\sigma_r}{dr} = \frac{\sigma_\theta - \sigma_r}{r}$$

The plane stress assumption, together with Hooke's Law, gives the final solution of the elastic problem in the form:

$$\begin{aligned}\sigma_r &= -p_e \frac{r_e^2}{r^2} \\ \sigma_\theta &= p_e \frac{r_e^2}{r^2} \\ u &= \frac{(1+\nu)p_e r_e^2}{Er}\end{aligned}\quad (7.8.15)$$

where $\sigma_r = -p_e$ at $r = r_e$.

Boundary Condition:

At $r = r_e$, $\sigma_\theta - \sigma_r = \sigma_s$

From Eq. (7.8.15), we obtain $p_e = 0.5 \sigma_s$ (7.8.16)

At $r = r_e$; σ_r must be continuous; i.e., using Eq. (7.8.14)

$$-p_c + \sigma_s \ln \frac{r_e}{r_2} = -p_e = -0.5 \sigma_s$$

or

$$p_c = 0.5 \sigma_s + \sigma_s \ln \frac{r_e}{r_2} \quad (7.8.17)$$

For a given p_c , r_e is determined by Eq. (7.8.17).

If the tubesheet material governs the joint load, the maximum value of pressure p_c that can be applied is given by setting $\sigma_\theta = 0$ at $r = r_2$. This gives:

$$p_{c(\max)} = \sigma_s \quad (7.8.18)$$

Corresponding to $p_{c(\max)}$, r_e is given by Eq. (7.8.17)

$$r_e = r_2 e^{0.5}$$

or

$$r_e = 1.6487 r_2$$

Thus, the maximum contact pressure p_c is given by the smaller of the two limits defined by Eqs. (7.8.12) and (7.8.18);

$$p_{c\max} = \min[\sigma_s, \sigma_T(1 - t/2r_t)] = \sigma^* \quad (7.8.19)$$

The maximum internal pressure is given for the general case as

$$p_{\text{MAX}} = \sigma^* + \sigma_T t / r_t \quad (7.8.20)$$

7.8.3 Displacement in the Tubesheet

The elastic region solution gives, at $r = r_e$

$$u = \frac{(1 + \nu)\sigma_s r_e}{2E} \quad (7.8.21)$$

In the plastic region, the following strain-stress relationships are assumed [7.8.4].

$$\begin{aligned} \epsilon_r &= \phi(\sigma_r - 0.5\sigma_\theta) = \frac{du}{dr} \\ \epsilon_\theta &= \phi(\sigma_\theta - 0.5\sigma_r) = \frac{u}{r} \end{aligned} \quad (7.8.22)$$

ϕ is determined from the compatibility equation

$$\frac{d\epsilon_\theta}{dr} = \frac{\epsilon_r - \epsilon_\theta}{r}$$

Substituting for ϵ_r and ϵ_θ from above, we have

$$\frac{d}{dr} \{(2\sigma_\theta - \sigma_r)\phi\} = \frac{3(\sigma_r - \sigma_\theta)\phi}{r}$$

Substituting for σ_θ from Eq. (7.8.14), for p_c from Eq. (7.8.17) and replacing $(\sigma_\theta - \sigma_r)$ by σ_s in the above equation yields

$$\frac{d\phi}{dr} + \frac{4\phi}{\left(\frac{3}{2} + \ln \frac{r}{r_e}\right)r} = 0$$

This is integrated to give

$$\phi = \frac{A}{\left(\frac{3}{2} + \ln \frac{r}{r_e}\right)^4} \quad (7.8.23)$$

where A is an integration constant. The radial deformation in the plastic region is given by the circumferential strain-displacement relationship of Eq. (7.8.22).

$$\epsilon_\theta = \frac{u}{r} = \phi(\sigma_\theta - 0.5\sigma_r)$$

Substituting for σ_θ and σ_r as before, we obtain

$$u(r) = \frac{\sigma_s r}{2} \frac{A}{\left(\frac{3}{2} + \ln \frac{r}{r_e}\right)^3} \quad (7.8.24)$$

Matching the radial displacement at the elastic-plastic interface gives the value of A via Eqs. (7.8.21) and (7.8.24)

$$A = \frac{27}{8} \frac{(1 + \nu)}{E}$$

Therefore

$$\frac{u(r)}{r} = \frac{27}{16} \frac{\sigma_s(1 + \nu)}{E \left(\frac{3}{2} + \ln \frac{r}{r_e} \right)^3}; \quad r_2 \leq r \leq r_e \quad (7.8.25)$$

The final hole radius after loading is

$$r_2^* = r_2 + u(r_2) = r_2 \left[1 + \frac{27}{16} \frac{\sigma_s(1 + \nu)}{E \left(\frac{3}{2} + \ln \frac{r_2}{r_e} \right)^3} \right] \quad (7.8.26)$$

The final tube thickness, after loading, is

$$t^* = t \left[1 - \frac{u(r_2)}{2r_2} \right] \quad (7.8.27)$$

and the tube final mean radius is

$$r_i^* = r_2^* - 0.5t^* \quad (7.8.28)$$

7.8.4 Unloading of the System

We now consider incremental unloading behavior of the system. Assuming elastic action during unloading, the relationship between the tube/tubesheet contact pressure increment p_c^* and the pressure increment p^* on the inside of the tube wall is derived as follows:

For a given set of increments, the radial displacement increment U at the outside surface of the tube is given, in terms of the average strain increments $\epsilon_r, \epsilon_\theta$, as:

$$\frac{U}{r_i^*} = \epsilon_\theta + \frac{t^*}{2r_i^*} \epsilon_r \quad (7.8.29)$$

Substituting for the elastic strain increments using the elastic strain/stress relations, and then eliminating the stress components yield the relation between U, p^*, p_c^* as:

$$\frac{U}{r_i^*} \cong \left(1 - \frac{t^*}{2r_i^*} \right) \frac{p^* r_i^*}{E_i t^*} - \left(1 + \frac{t^*}{2r_i^*} [1 - 2\nu] \right) \frac{p_c^* r_i^*}{E_i t^*} \quad (7.8.30)$$

It is important to keep terms of order t^*/r_t^* in the above expression since we will observe that the leading terms cancel leaving the terms of order t^*/r_t^* as the dominant contribution.

The elastic displacement increment at any r in the tubesheet during unloading is given as (see Eq. (7.8.15))

$$U = p_c^* (1 + \nu) r_2^{*2} / Er \quad (7.8.31)$$

We require displacement increment continuity at $r = r_2^*$; this yields the relation between p^* , p_c^* as

$$p_c^* = p^* (1 - t^*/2r_t^*) / (1 + \lambda t^*/r_t^*) \quad (7.8.32)$$

where

$$\lambda = \frac{E_t(1 + \nu)}{E} \frac{r_2^*}{r_t^*} + \frac{(1 - 2\nu)}{2}$$

The final contact pressure, assuming no yielding of either tube or tubesheet during unloading, is p_c' where

$$p_c' = p_{c(\max)} + p_c^* \quad (7.8.33)$$

and p^* in Eq. (7.8.32) is set equal to the negative of $p_{(\max)}$. For total unloading in the elastic range, Eqs. (7.8.19), (7.8.20) yield the result

$$p_c' \approx \frac{\sigma^* t^*/r_t^* (\lambda + 0.5) - \sigma_T \frac{t}{r_t} (1 - t^*/2r_t^*)}{(1 + \lambda t^*/r_t^*)} \quad (7.8.34)$$

Note that the result for p_c' is valid only for tube geometries where the thickness is much less than the mean diameter so that the membrane solution employed is reasonably descriptive of the actual state of stress. Note also that the above solution accounts for large deformation effects (thickness and radius changes) in a very approximate manner.

7.8.5 Tube Pull-Out Load

If we now consider that the residual contact pressure p_c' , predicted by Eq. (7.8.34), represents an average value through the tubesheet thickness then a tube pull-out load P^* can be defined from the equilibrium equation

$$P^* = \mu (2\pi r_2^* L p_c') \quad (7.8.35)$$

μ can be thought of as an effective coefficient of friction and L represents the roll depth of the tube into the tubesheet. Reference [7.8.2] presents one derivation of an effective μ ; herein is presented a related approach which makes use of an energy minimization principle. Figure 7.8.3 shows a section of an ungrooved tube that has been rolled into the tubesheet. For a thin tube, the equilibrium equations in terms of stress components are:

$$\frac{\partial \sigma_{rx}}{\partial \xi} + \frac{\sigma_{rx}}{r_t^*} + \frac{\partial \sigma_{xx}}{\partial x} = 0 \quad (7.8.36)$$

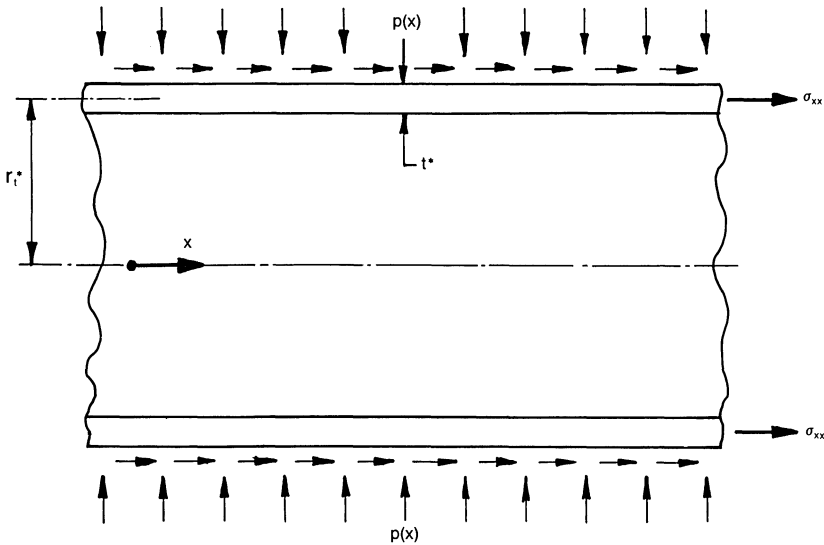


Fig. 7.8.3. Stresses on tube section during pull-out.

$$r_t^* \left[\frac{\partial \sigma_{rr}}{\partial \zeta} + \frac{\partial \sigma_{rx}}{\partial x} \right] + \sigma_{rr} = \sigma_{\theta\theta} \quad (7.8.37)$$

$\zeta = r - r_t^*$ is a coordinate defined from the middle surface of the tube wall so that $-t^*/2 \leq \zeta \leq t^*/2$. If f is the local coefficient of friction between the surfaces of the tube and tubesheet, and if we assume that the tube is thin, then we may approximate the stresses σ_{rr} , σ_{rx} , σ_{xx} as:

$$\sigma_{xx} = F(x); \quad \sigma_{rr} = -\frac{p(x)}{2} (1 + 2\zeta/t^*) \quad (7.8.38)$$

$$\sigma_{rx} = \frac{fp(x)}{2} (1 + 2\zeta/t^*)$$

For a thin tube ($t^*/2r_t^* \ll 1$), the equilibrium equation (7.8.36) requires that $F(x)$ and $p(x)$ satisfy

$$\frac{dF}{dx} + \frac{fp}{t^*} \approx 0 \quad (7.8.39)$$

Substituting Eq. (7.8.38) into Eq. (7.8.37) yields a solution for $\sigma_{\theta\theta}(x)$ as

$$\sigma_{\theta\theta} \approx -\frac{r_t^* p}{t^*} + fr_t^* p (1 + 2\zeta/t^*) \quad (7.8.40)$$

The complementary energy for the tube section of length L , rolled within the tubesheet, is:

$$\frac{U_c}{2\pi} = \int_0^L \int_{-\frac{t^*}{2}}^{\frac{t^*}{2}} \left[\frac{(\sigma_{rr}^2 + \sigma_{\theta\theta}^2 + \sigma_{xx}^2)}{2E_t} - \frac{\nu}{E_t} (\sigma_{rr}\sigma_{\theta\theta} + \sigma_{\theta\theta}\sigma_{xx} + \sigma_{xx}\sigma_{rr}) + \frac{\sigma_{xr}^2}{2G_t} \right] r_t^* d\zeta dx; \quad G_t = E_t/2(1+\nu) \quad (7.8.41)$$

Substituting the stress expressions given into Eq. (7.8.41), and integrating with respect to ζ , yield an expression for U_c in terms of $F(x)$, $p(x)$ and their derivatives with respect to x . If we assume that L is such that $t^*/L \ll 1$, and that $F(x)$, $p(x)$ are slowly varying along the tube, then an order of magnitude analysis simplifies U_c to the result:

$$\frac{U_c}{2\pi} = \frac{t^* r_t^*}{2E_t} \int_0^L \left\{ \frac{r_t^{*2}}{f^2} \left(\frac{dF}{dx} \right)^2 + F^2 \right\} dx \quad (7.8.42)$$

Requiring that $F(x)$ be such as to render U_c a minimum yields the differential equation for $F(x)$ in the region $0 \leq x \leq L$ as

$$\frac{d^2 F}{dx^2} - \frac{f^2}{r_t^{*2}} F = 0 \quad (7.8.43)$$

We solve Eq. (7.8.43) subject to the end conditions $F(0) = 0$, $2\pi r_t^* t^* F(L) = -P^*$, where P^* is the pull-out load. The solutions for $F(x)$, and for $p(x)$, takes the form

$$F(x) = -\frac{P^*}{2\pi r_t^* t^*} \frac{\sinh(fx/r_t^*)}{\sinh(fL/r_t^*)} \quad (7.8.44)$$

$$p(x) = \frac{P^*}{2\pi r_t^{*2}} \frac{\cosh(fx/r_t^*)}{\sinh(fL/r_t^*)}$$

$p(x)$ represents a contact pressure between tube and tubesheet that is somewhat reduced from the residual contact pressure p_c' . This contact pressure decrease is due to the Poisson effect induced by the application of the longitudinal stress σ_{xx} . To relate $p(x)$ and p_c' note that the change in contact pressure $p_c' - p(x)$ causes a decrease in tubesheet hole radius r_2^* , and a corresponding decrease in tube mean radius r_t^* . The application of σ_{xx} also induces a change in tube mean radius. These changes are assumed to be elastic and compatibility of the displacements, averaged over the length L , is assumed to be maintained. This gives the equation:

$$-\frac{1}{L} \int_0^L (p_c' - p) \frac{r_2^*}{E} (1+\nu) dx \approx \frac{1}{L} \int_0^L \frac{(p_c' - p) r_t^{*2} dx}{E_t t^*}$$

$$+ \frac{\nu}{L} \frac{r_t^*}{E_t} \int_0^L \sigma_{xx}(x) dx \quad (7.8.45)$$

Using the expressions for $p(x)$, $F(x)$ (and hence, σ_{xx}) yields a relation between P^* and p_c' , the residual contact pressure prior to application of P^* . We obtain

$$P^* = 2\pi f r_t^* L p_c' \left\{ \frac{1 + \alpha}{1 + \alpha + \nu \Psi} \right\} \quad (7.8.46)$$

where

$$\alpha = (1 + \nu) \frac{E_t}{E} \frac{t^* r_2^*}{r_t^{*2}}; \quad \Psi = \frac{\cosh(fL/r_t^*) - 1}{\sinh(fL/r_t^*)}$$

Comparison of Eq. (7.8.46) with Eq. (7.8.35) defines the effective coefficient of friction μ in terms of the local coefficient of friction f ($0.3 < f < 1.0$) and the joint geometry.

It is clear that the joint strength (maximum pull-out load) is directly related to the maximum residual contact pressure p_c' . The use of different tube and tubesheet materials has a pronounced effect on the value of p_c' .

7.8.6 Computation of Residual Pressure

Table 7.8.1 gives representative material properties for typical tube and tubesheet materials.

Table 7.8.1. Tube/Tubesheet Material Properties

Material	Alloy No.	$E \times 10^{-7}$ psi	$\sigma_y \times 10^{-4}$ psi
TUBES			
Admiralty	443	1.6	1.5
Stainless Steel		2.9	3.0
90:10 Cu. Ni.	706	1.8	1.5
70:30 Cu.Ni.	715	2.2	1.8
Aluminum Bronze	608	1.75	1.9
Aluminum Brass	687	1.6	1.8
Arsenical Copper	142	1.7	3.0
Titanium		1.49	4.0
TUBESHEETS			
Muntz	565	1.5	2.0
Steel		2.9	3.0
Aluminum Bronze D	614	1.7	3.0
Silicon Bronze	655	1.5	1.8
90:10 Cu. Ni.	706	1.8	1.5
70:30 Cu.Ni.	715	2.2	2.0

Appendix 7.B gives the FORTRAN coding to compute p_c' using the equations developed in Sub-Sections 7.8.1–7.8.4. Table 7.8.2 presents results using different tube-tubesheet combinations.

Table 7.8.2. p_c' For various Tube/Tubesheet Combinations Using Eq. (7.8.34)

Tube	Tubesheet	p_{\max}	$p_{c(\max)}$	p_c'
$t' = 0.049''$	O.D. = 0.75'' $c = 0.005''$	(psi)	(psi)	(psi)
Titanium	Muntz	25471	20000	563
Steel	Steel	32052	27948	4132
Admiralty	Steel	16026	13974	880
90:10 Cu.Ni.	Muntz	16026	13974	2590
Steel	90:10 Cu.Ni.	19104	15000	2185
70:30 Cu.Ni.	90:10 Cu.Ni.	17462	15000	2610
70:30 Cu.Ni.	Steel	19231	16769	1713
$t' = 0.028''$	O.D. = 0.75'' $c = 0.005''$			
Steel	Steel	31139	28861	2284
70:30 Cu.Ni.	Steel	18684	17316	943
Steel	70:30 Cu.Ni.	20279	18000	1187

7.8.7 Re-Analysis of the Tube Rolling Problem Using the von Mises Yield Criteria

The simple analysis presented in the previous section utilized a yield criteria suitable for analytical manipulations. In the true tube rolling problem, one should be concerned not only with the initial residual roll pressure at assembly, but also with the residual roll pressure during unit operation. Thus, the question of tube/tubesheet behavior under a temperature change becomes of interest during examination of the tube rolling process. Also of interest is the correct treatment of elastic plastic behavior during unloading and the true effect of large deformations (i.e., thickness changes). All of these questions are most easily addressed by approaching the tube-tubesheet rolled joint problem from a numerical viewpoint. Since the theory and analysis are somewhat beyond the level of sophistication intended for this text, this more advanced treatment of the problem is given in an Appendix. Appendix 7.C contains the theory and some analysis using the numerical code developed from the basic theory. A user manual and a listing of the code is provided in Appendix 7.D.

7.9 LIGAMENT TEMPERATURE

7.9.1 Introduction

Gardner [7.9.1] showed that the ligament material of the tubesheet is mainly at the tubeside fluid temperature except for a thin skin facing the shellside fluid where a steep temperature gradient exists. Therefore, the so-called "thermal skin effect" produces only localized stresses (known as "peak stresses" in the lexicon of the ASME Codes). The body of the tubesheet usually does not experience a "global" thermal stress.

Singh and Holtz [7.9.2] presented a generalized form of Gardner's solution which shows that under certain circumstances the thermal gradient may not be limited to the shellside skin. In fact, the thermal gradient may introduce significant rotation at the tubesheet rim resulting in leakage when the tubesheet is also used as a flange. Such a situation occurs whenever the shellside heat transfer coefficient is relatively high and the tube material possesses low thermal conductivity.

The knowledge of the tubesheet/tubewall temperature field is especially important in the case of "rolled only" joints. The interfacial pressure between the tubewall and tubesheet provides the protection against leakage between the two pressurized chambers. Under the operating condition, the development of a differential temperature in conjunction with different coefficients of thermal expansion between the tubesheet ligament and the tubewall may reduce the interface pressure below the threshold necessary to maintain a leak proof joint. Industrial design standards [7.9.3] provide empirical guidelines on the maximum allowable "joint temperature". A detailed knowledge of the temperature distribution in the tubewall and tubesheet ligament region is the first logical step towards the formulation of a mathematical criterion for determining the sealworthiness of "rolled only" joints.

A similar situation arises in the case of double tubesheet designs. The tubesheet in contact with the shellside fluid may be at a substantially different temperature than the tubeside tubesheet if the shellside heat transfer is much higher than the tubeside coefficient. In such an event, the tube segments spanning the two tubesheets may experience severe bending and shear stresses [7.9.4]. The subject of double tubesheets is treated in some detail in Chapter 10.

A simplified mathematical model to estimate the ligament temperature distribution based on the work in reference [7.9.2] is given in the next section. A step-by-step computation procedure is given in Sub-Section 7.9.3. The computer program LIGTEM, based on this analysis, is presented in Sub-Section 7.9.4. A numerical example utilizing this computer program is also discussed.

7.9.2 Analysis

The cross section of a typical ligament surrounding a tube is shown in Fig. 7.9.1. During steady state conditions, the temperature field in all ligaments will be identical; hence, attention is focused on a composite region consisting of one tube and its associated tubesheet ligament. It is also known that the variation of temperature is mainly in the direction of the tube axis. In other words, the temperature changes in the lateral (in-plane) direction are, relatively speaking, quite small. These considerations lead us to model the tube-ligament assemblage as two interfacing coaxial cylinders. The inner cylinder is the tube which contains a fluid at temperature T_f . The outer cylinder is the tubesheet ligament. The noncircular cross section of the

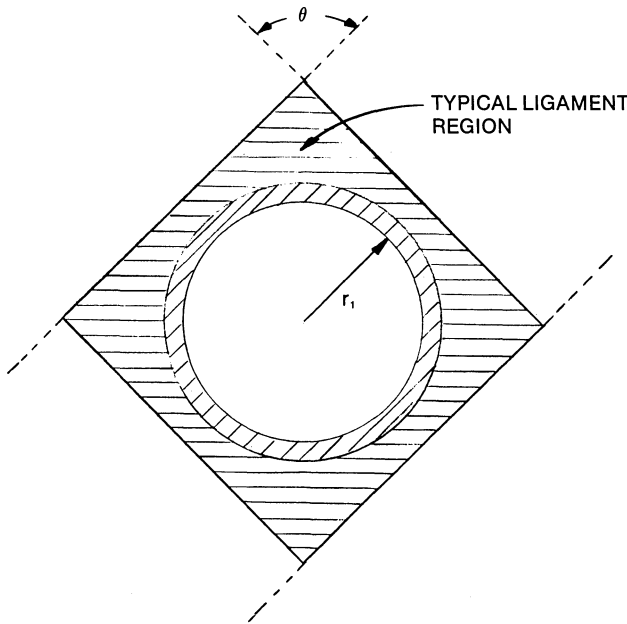


Fig.7.9.1. Ligament cross section.

ligament is replaced by an equivalent circular section of equal cross-sectional area. This approximation is tenable so long as the temperature gradient in the lateral direction is small. It can be shown that the outer radius of the equivalent cylinder is given by

$$r_3 = \bar{p} \left(\frac{\sin \theta}{\pi} \right) \tag{7.9.1}$$

where θ is the layout angle (Fig. 7.9.1) and \bar{p} is the layout pitch. Thus, the idealized problem under consideration is that of two coaxial cylinders subject to a heat source at temperature T_i on the inside cylindrical surface, T_s on the outside exposed surface of the inner cylinder and right lateral surface of outer cylinder, and T_l on the left lateral surface of both cylinders (Fig. 7.9.2). The inner cylinder is assumed to be infinitely long. For the purpose of analysis, the inner cylinder is subdivided into two regions, indicated by 1 and 1' in Fig. 7.9.2. Assuming regions 1 and 2 to be at temperature T_1 and T_2 (functions of x), respectively, the governing heat-conduction equations are:

$$k_1 \frac{d^2 T_1}{dx^2} + \frac{[h_i S_1 (T_i - T_1) - q_{12} S_2]}{a_1} = 0 \tag{7.9.2}$$

where

S_1 = circumference of inner tube surface

S_2 = circumference of tube outer surface
 q_{12} = heat flux from region 1 to region 2
 k_1 = conductivity of region 1 (tube) material
 a_1 = cross-sectional area of region 1

$$\text{Note: } S_1 = 2\pi r_1; \quad S_2 = 2\pi r_2 \quad (7.9.2a)$$

$$a_1 = \pi(r_2^2 - r_1^2) \quad (7.9.2b)$$

Similarly, the governing equation for region 2 is

$$k_2 \frac{d^2 T_2}{dx^2} + \frac{q_{12} S_2}{a_2} = 0 \quad (7.9.3)$$

where

$$a_2 = \pi(r_3^2 - r_2^2) \quad (7.9.4)$$

Let

$$q_{12} = h_{12}(T_1 - T_2) \quad (7.9.5)$$

where h_{12} is the equivalent inter-region heat-transfer coefficient. An approximate expression for h_{12} is derived later in this chapter. Substituting for q_{12} in Eqs. (7.9.2) and (7.9.3), and rearranging terms, yields

$$\left(k_1 \frac{d^2}{dx^2} - \frac{h_t S_1}{a_1} - \frac{h_{12} S_1}{a_1} \right) T_1 + \frac{h_{12} S_2}{a_1} T_2 + \frac{h_t S_1 T_t}{a_1} = 0 \quad (7.9.6)$$

$$\left(k_2 \frac{d^2}{dx^2} - \frac{h_{12} S_2}{a_2} \right) T_2 + \frac{h_{12} S_2}{a_2} T_1 = 0 \quad (7.9.7)$$

or

$$T_1 = \frac{a_2}{h_{12} S_2} \left(\frac{h_{12} S_2}{a_2} - k_2 \frac{d^2}{dx^2} \right) T_2 \quad (7.9.8)$$

Substituting for T_1 in Eq. (7.9.6) yields a fourth order ordinary differential equation for T_2

$$c_1 \frac{d^4 T_2}{dx^4} + c_2 \frac{d^2 T_2}{dx^2} + c_3 T_2 + c_4 = 0 \quad (7.9.9)$$

where

$$c_1 = \frac{-k_1 k_2 a_2}{h_{12} S_2} \quad (a)$$

$$c_2 = k_1 + \frac{k_2 a_2}{h_{12} S_2} \left(\frac{h_t S_1}{a_1} + \frac{h_{12} S_2}{a_1} \right) \quad (b)$$

$$c_3 = \frac{-h_t S_1}{a_1} \quad (c)$$

$$c_4 = \frac{h_t S_1 T_t}{a_1} \quad (d)$$

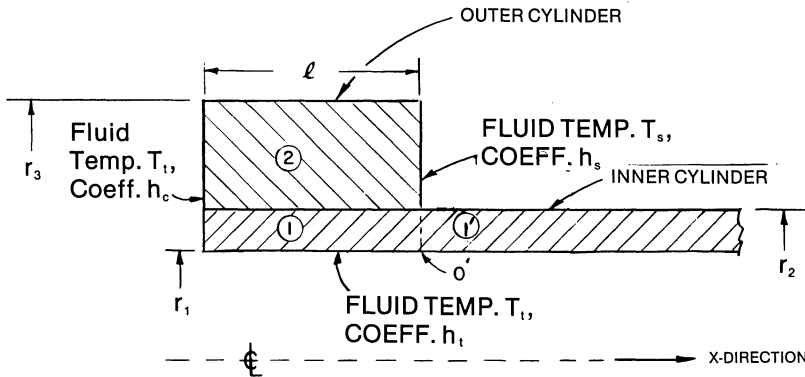


Fig. 7.9.2. Idealized heat transfer section.

The complete solution of Eq. (7.9.9) is given in terms of four undetermined constants of integration, b_i ($i = 1, 2, 3, 4$),

$$T_2 = b_1 e^{m_1 x} + b_2 e^{-m_1 x} + b_3 e^{m_2 x} + b_4 e^{-m_2 x} - \frac{c_4}{c_3} \quad (7.9.11)$$

where

$$m_i = \left\{ \frac{-c_2 + (-1)^{i+1} (c_2^2 - 4c_1 c_3)^{1/2}}{2c_1} \right\}^{1/2}; \quad i = 1, 2 \quad (7.9.12)$$

By virtue of Eq. (7.9.8) we have:

$$T_1 = d_1 e^{m_1 x} + d_2 e^{-m_1 x} + d_3 e^{m_2 x} + d_4 e^{-m_2 x} - \frac{c_4}{c_3} \quad (7.9.13)$$

where

$$d_1 = \omega_1 b_1, \quad d_2 = \omega_1 b_2, \quad d_3 = \omega_2 b_3, \quad d_4 = \omega_2 b_4 \quad (7.9.14)$$

and

$$\omega_i = \left[\frac{-k_2 a_2}{h_{12} S_2} m_i^2 + 1 \right]; \quad i = 1, 2 \quad (7.9.15)$$

The four constants of integration, b_i , are evaluated by utilizing the boundary conditions at $x = 0, l$. These are

region 2

$$\text{At } x=0; \quad k_2 \frac{dT_2}{dx} = -h_c (T_1 - T_2) \Big|_{x=0} \quad (a)$$

$$\text{At } x=l; \quad k_2 \frac{dT_2}{dx} = -h_s (T_2 - T_s) \Big|_{x=l} \quad (b)$$

region 1

$$(7.9.16)$$

$$\text{At } x=0; \quad k_1 \frac{dT_1}{dx} = -h_c(T_i - T_1) \quad (c)$$

$$\text{At } x=l; \quad \frac{dT_1}{dx} = \frac{dT_1'}{dx} \Big|_{x=0} \text{ in region } 1' \quad (d)$$

To determine the temperature gradient in region 1', we model the region as a very long tube attached to a source at temperature T^* subject to heat transfer from a fluid at temperature T_i on its inside surface (coefficient h_i) and from a fluid at temperature T_s on its outside surface (coefficient h_s'). The solution for the temperature field follows directly from the heat conduction equation

$$T_1' = c_1 e^{-\alpha x} + c_2 e^{\alpha x} + \frac{\beta^2}{\alpha^2} \quad (7.9.17)$$

where

$$\alpha^2 = \frac{h_s' S_2 + h_i S_1}{k_1 a_1} \quad (a)$$

$$\beta^2 = \frac{h_s' S_2 T_s + h_i S_1 T_i}{k_1 a_1} \quad (b)$$

and for region 1', $x=0$ occurs at point 0' in Fig. 7.9.2.

T_1' is required to be finite as x becomes large, which implies that $c_2 = 0$. Furthermore, at $x=0$, $T_1' = T^*$, which yields

$$c_1 = T^* - \frac{\beta^2}{\alpha^2}$$

Hence

$$T_1' = \left(T^* - \frac{\beta^2}{\alpha^2} \right) e^{-\alpha x} + \frac{\beta^2}{\alpha^2}$$

and

$$\frac{dT_1'}{dx} \Big|_{x=0} = -\alpha \left(T^* - \frac{\beta^2}{\alpha^2} \right) \quad (7.9.19)$$

Equation (7.9.16d) can be combined with Eq. (7.9.19) to furnish an independent algebraic equation in the undetermined constants, b_i . Equations (7.9.16a)-(7.9.16c) provide the other three algebraic equations. The resulting system of four linear algebraic equations can be represented in subscript notation as

$$A_{ij} b_j = f_i; \quad i=1,4 \quad (7.9.20)$$

Summation on the repeated subscript ($j=1, \dots, 4$) is implied in Eq. (7.9.20).

The coefficients of the $[A]$ matrix and the $\{f\}$ vector are given in Appendix 7.A.

Equation (7.9.20) is solved for the four b_i 's using a standard Gaussian

elimination subroutine. The expressions for T_2 and T_1 follow directly thereafter from Eqs. (7.9.11) and (7.9.13), respectively. In this manner, the temperature field is completely determined. At this point, the description for the entire solution scheme is complete, except for the intra-region coefficient h_{12} . A simple expression for h_{12} is now devised which is consistent with the level of accuracy of the total solution. To do this, we must introduce a radial variation to the temperature field.

It is well known [7.9.5] that the general solution for temperature distribution in an axisymmetric long cylinder is a logarithmic function in the radius, r . Hence, it is reasonable to assume the temperature field to be logarithmic in radius r for the inner and outer cylinders. The unknown constants are evaluated using boundary and interface conditions; thus, we assume, for the purpose of obtaining h_{12} ,

$$t_1(r) = g_1 \ln r + n_1; \quad r_1 \leq r \leq r_2 \quad (a)$$

$$t_2(r) = g_2 \ln r + n_2; \quad r_2 \leq r \leq r_3 \quad (b)$$

g_1, g_2, n_1 and n_2 are evaluated under the following conditions:

$$\text{At } r=r', \quad t=T_1$$

$$r=r''; \quad t=T_2$$

$$r=r_2, \quad t \text{ is continuous}$$

$$r=r_2, \quad k_1 \frac{dt}{dr} = k_2 \frac{dt}{dr}$$

r' and r'' are logarithmic mean radii in regions 1 and 2, respectively; i.e.,

$$r' = \frac{r_2 - r_1}{\ln \frac{r_2}{r_1}}; \quad r'' = \frac{r_3 - r_2}{\ln \frac{r_3}{r_2}} \quad (7.9.22)$$

The foregoing relationships determine the four undeterminant coefficients in Eq. (7.9.21).

Recalling that the heat flux at $r=r_2$ is $h_{12}(T_1 - T_2)$, we obtain the final expression for h_{12} as:

$$h_{12} = \frac{-k_1}{r_2 \ln \left[\left(\frac{r_2}{r''} \right)^{k_1/k_2} \left(\frac{r'}{r_2} \right) \right]} \quad (7.9.23)$$

7.9.3 Solution Procedure

A step-by-step description of the solution procedure is given in the following to facilitate direct use of the preceding analysis without the encumbrance of assimilating the details.

(i) Input Data:

(a) Geometry Data – tubesheet thickness, l ; tube inner and outer radii

(r_1 and r_2); tube layout pitch, \bar{p} ; layout angle, θ (Fig. 7.9.1).

(b) Thermal property data – tube material conductivity k_1 ; tubesheet material conductivity k_2 .

(c) Heat-transfer data* – channel side heat-transfer coefficient h_c ; in-tube heat transfer coefficient, h_i ; shell side heat-transfer coefficient h_s on tubesheet surface; h_s' on tube surface; tubeside fluid temperature T_i ; shell side fluid temperature T_s .

(ii) Compute r_3 from Eq. (7.9.1) and h_{12} from Eqs. (7.9.22)–(7.9.23).

(iii) Compute S_1 , S_2 (Eq. (7.9.2a)), a_1 and a_2 (Eqs. (7.9.2b) and (7.9.4)). Compute c_1 , c_2 , c_3 and c_4 from Eq. (7.9.10); and m_i from Eq. (7.9.12); ω_i from Eq. (7.9.15), α and β from Eq. (7.9.18).

(iv) Compute all 16 coefficients of A_{ij} and four terms of f_i (Appendix 7.A).

(v) Solve the 4×4 linear equation set (Eq. (7.9.20)) to obtain values of b_1 , b_2 , b_3 and b_4 .

(vi) The temperature in the ligament is obtained as a function of x from Eq. (7.9.11); determine d_i ($i=1, \dots, 4$) from Eqs. (7.9.14) and (7.9.15). The tubewall temperature as a function of x is obtained from Eq. (7.9.13).

7.9.4 Numerical Example – Computer Program LIGTEM

Computer program LIGTEM automates the analysis presented in the preceding sub-sections. The input data instruction for LIGTEM is presented in Table 7.9.1. A typical example problem considered in the following illustrates the application of the computer program.

A tubesheet in contact with tubeside fluid at 100°F , and shellside fluid at 300°F is analyzed. The basic data is given below:

- (i) Geometry data: $l = 0.975''$; $r_1 = 0.435''$; $r_2 = 0.5''$; $\theta = 60$ deg.
- (ii) Thermal property data: Tube material conductivity $k_1 = 9.3$ Btu/hr.-ft.- $^\circ\text{F}$; Tubesheet material conductivity, $k_2 = 30$ Btu/hr-ft.- $^\circ\text{F}$.
- (iii) Heat-transfer data: channel side coefficient, $h_c = 50$ Btu/sq.ft.- $^\circ\text{F}$ -hr. Shell side coefficients, $h_s = h_s' = 1000$ Btu/hr.-sq.ft.- $^\circ\text{F}$.
- (iv) All surface fouling factors are assumed to be zero.

The tubewall temperature is plotted in Fig. 7.9.3 as a function of x labelled as case A. Figure 7.9.3 also shows the tube wall temperature variation when all coefficients are set equal ($h_s = h_c = h_i = 50$ Btu/hr-sq.ft.- $^\circ\text{F}$) and the conductivities k_1 and k_2 are also set equal ($k_1 = k_2 = 9.3$ Btu/hr-sq.ft.- $^\circ\text{F}$). This latter case is labelled Case B. Note that a temperature gradient exists through the thickness of the tubesheet. Therefore, a global thermal stress in the tubesheet will be developed. Global thermal stresses produced are important in evaluating plastic breakdown of the structure

*If a fouling factor on any of these surfaces is specified, then the corresponding coefficients should be accordingly adjusted to account for fouling.

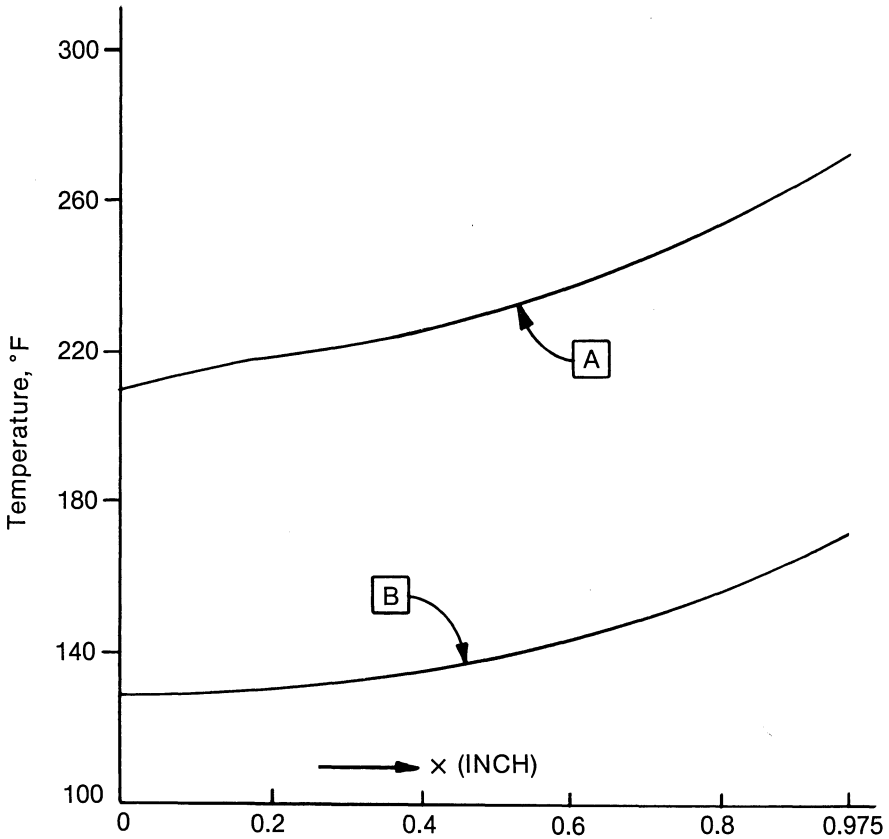


Fig. 7.9.3. Tubesheet through-thickness temperature distribution for the example problem.

under cyclic conditions. The thermal stresses so produced are “secondary stresses” rather than “peak stresses”. Secondary stresses warrant closer attention in tubesheet design, especially in units subject to large operating cycles. Furthermore, an axial thermal gradient may produce “bowing” of the tubesheet. In designs where the tubesheet also serves as a flange, such a bowing may cause joint leakage. Less perceptibly, bowing of the tubesheet may cause the pass partition plates to lose contact on the tubesheet surface thereby inducing an interpass leakage. Equally important, the tubesheet ligament temperature distribution under operating conditions has an impact on the sealworthiness of “rolled only” joint conditions. We will demonstrate this in our more sophisticated tube-tubesheet rolled joint analysis in Appendix 7.C.

Table 7.9.1 Input Data for LIGTEM (All input is free field)

Line 1; Geometry and Conductivity data:

Item	Fortran Symbol
Tube outside diameter, inch	THOLE
Tube wall thickness, inch	TWALL
Tubesheet thickness, inch	L
Conductivity of tube material (Btu/hr.-°F-ft.)	K1
Conductivity of tubesheet material (Btu/hr.-°F-ft.)	K2
Line 2; Film coefficient and fouling factor:	
Shell side film coefficient on tube surface (Btu/hr.-sq.ft.-°F)	HO
Tube inside film coefficient (Btu/hr.-sq.ft.-°F)	HI
Channel film coefficient on tubesheet surface (Btu/hr.-sq.ft.-°F)	HIC
Shell side film coefficient on tubesheet surface (Btu/hr.-sq.ft.-°F)	HIS
Shellside tube surface fouling factor (Hr.-sq.ft.-°F/Btu)	R0
Tube inside surface fouling factor (Hr.-sq.ft.-°F/Btu)	RI
Tubeside fouling factor on tubesheet surface (Hr.sq.ft.-°F/Btu)	RIC
Shellside fouling factor on tubesheet surface (Hr.sq.ft.-°F/Btu)	RIS
Line 3	
Tube layout pitch, inch	PITCH
Layout angle, degrees	LAYOUT
Tubeside fluid temperature	TT
Shellside fluid temperature	TS
Number of thickness increments in which the tubesheet temperature is to be printed out	NSTEP

PROGRAM LIGTEM

```
C TUBE SHEET LIGAMENT TEMPERATURE CALCULATING PROGRAM
```

```
C
```

```
C APRIL 5, 1978
```

```
C
```

```
REAL K1,K2,K12,M1,M2,L,M1L,M2L
DIMENSION ARC(4,4),A(16),B(4)
```

```
C
```

```
C TEMPERATURE DISTRIBUTION STATEMENT FUNCTIONS - TUBE WALL AND
C TUBESHEET LIGAMENT , RESPECTIVELY
```

```
C
```

```
T1(X)=W1*B(1)*EXP(M1*X) + W1*B(2)*EXP(-M1*X) + W2*B(3)*EXP(M2*X)
$ + W2*B(4)*EXP(-M2*X) - C4/C3
```

```

T2(X)=B(1)*EXP(M1*X) + B(2)*EXP(-M1*X) + B(3)*EXP(M2*X)
$ + B(4)*EXP(-M2*X) - C4/C3
C
  IPR=6
  ICR=5
  PI=3.14159
  WRITE(IPR,2000)
  READ(5,*,END=3000) THOLE,TWALL,L,K1,K2
  ACCEPT HO,HI,HIC,HIS,RO,RI,RIC,RIS
  ACCEPT PITCH,ANGLE,TT,TS,ASTEP
C
  NSTEP=ASTEP
  WRITE(IPR,2005)THOLE,TWALL,L,K1,K2,HO,HI,HIC,RO,RI,PITCH,ANGLE,TT,
  $TS,NSTEP
C
C CONVERT TO CONSISTENT SET OF DIMENSIONS
C
  THOLE=THOLE/12.
  TWALL=TWALL/12.
  L=L/12.
  ANGLE=ANGLE/180.*PI
C
C CALCULATE VARIOUS DIMENSIONS
C
  TID=THOLE-2.*TWALL
  S1=PI*TID
  S2=PI*THOLE
  IF(ABS(ANGLE-PI/2.).LT..0001) A3=PITCH*PITCH
  IF(ABS(ANGLE-PI/2.).GE..0001) A3=PITCH*PITCH*SIN(2.*ANGLE)
  R3=SQRT(A3/PI)/12.
  R2=THOLE/2.
  R1=TID/2.
C
C COMPUTE VARIOUS CROSSECTIONAL AREAS
C
  AT=PI*R3**2
  AT2=PI*THOLE**2/4.
  AT1=PI*TID**2/4.
  A2=AT-AT2
  A1=AT2-AT1
C
C COMPUTE HEAT TRANSFER COEFFICIENT H12
C
  R1P=(R2-R1)/ALOG(R2/R1)
  R2P=(R3-R2)/ALOG(R3/R2)
  K12=K1/K2
  H12=-K1/R2/ALOG((R2/R2P)**K12*R1P/R2)
C
C COMPUTE OVERALL TUBE AND SHELLSIDE FILM COEFFICIENTS
C
  HC=1./HIC + RIC

```

$HC=1./HC$
 $HT=1./HI + RI$
 $HT=1./HT$
 $HS=1./HO + RO$
 $HS=1./HS$
 $HIS=1./HIS + RIS$
 $HIS=1./HIS$

C
 C DETERMINE COEFFICIENTS OF INDICIAL EQUATIONS FOR THE GOVERNING
 C TEMPERATURE DISTRIBUTION DIFFERENTIAL EQUATION

$C1=-K1*K2*A2/H12/S2$
 $C2=K1+K2*A2/H12/S2*(HT*S1/A1 + H12*S2/A1)$
 $C3=-HT*S1/A1$
 $C4=HT*S1*TT/A1$

C
 C DETERMINE POWER COEFFICIENTS OF THE EXPONENTI+L SOLUTION TO THE
 C GOVERNING DIFFERENTIAL EQUATION

$YP=(-C2+SQRT(C2**2-4.*C1*C3))/2./C1$
 $YN=(-C2-SQRT(C2**2-4.*C1*C3))/2./C1$
 $M1=SQRT(YP)$
 $M2=SQRT(YN)$

C
 C DETERMINE AUXILIARY COEFFICIENTS OF THE DIFFERENTIAL EQUATION

$W1=1.-K2*A2*M1**2/H12/S2$
 $W2=1.-K2*A2*M2**2/H12/S2$

C
 C TO DETERMINE COEFFICIENTS B(I) BY SOLVING THE SET OF LINEAR
 C SIMULTANEOUS EQUATIONS --

C
 C DEFINE COEFFICIENTS OF THE SET OF LINEAR SIMULTANEOUS EQUATIONS
 C AND DEFINE THE FORCING VECTOR

$ARC(1,1)=K2*M1-HC$
 $ARC(1,2)=-K2*M1-HC$
 $ARC(1,3)=K2*M2-HC$
 $ARC(1,4)=-K2*M2-HC$
 $B(1)=-HC*(TT+C4/C3)$

C
 $M1L=M1*L$
 $M2L=M2*L$
 $ARC(2,1)=K2*M1*EXP(M1L) + HIS*EXP(M1L)$
 $ARC(2,2)=-K2*M1*EXP(-M1L) + HIS*EXP(-M1L)$
 $ARC(2,3)=K2*M2*EXP(M2L) + HIS*EXP(M2L)$
 $ARC(2,4)=-K2*M2*EXP(-M2L) + HIS*EXP(-M2L)$
 $B(2)=HIS*(C4/C3 + TS)$

C
 $ARC(3,1)=K1*W1*M1 - W1*HC$
 $ARC(3,2)=-K1*W1*M1 - W1*HC$

```

ARC(3,3)=K1*W2*M2 - W2*HC
RC(3,4)=-K1*W2*M2 - W2*HC
B(3)=-HC*(C4/C3 + TT)

```

C

```

ALPHA=(HS*S2 + HT*S1)/K1/A1
ALPHA=SQRT(ALPHA)
BETA=(HS*S2*TS + HT*S1*TT)/K1/A1
BETA=SQRT(BETA)
ARC(4,1)=W1*M1*EXP(M1L) + ALPHA*W1*EXP(M1L)
ARC(4,2)=-W1*M1*EXP(-M1L) + ALPHA*W1*EXP(-M1L)
ARC(4,3)=W2*M2*EXP(M2L)+ALPHA*W2*EXP(M2L)
ARC(4,4)=-W2*M2*EXP(-M2L) + ALPHA*W2*EXP(-M2L)
B(4)=ALPHA*C4/C3 + BETA**2/ALPHA

```

C

C REARRANGE COEFFICIENT ARRAY FOR IBM SOLVING ROUTINE FORMAT

C

```

DO 50 J=1,4
DO 50 I=1,4
    IC=I+(J-1)*4
    A(IC)=ARC(I,J)
50 CONTINUE
N=4
CALL SIMQ(A,B,N,KS)
IF(KS.EQ.1) GO TO 200

```

C

C CALCULATE AND PRINT THE TEMPERATURE DISTRIBUTIONS

C

```

WRITE(IPR,2001)
STEP=L/NSTEP
NS=NSTEP + 1
DO 100 I=1,NS
    X=0.+(I-1)*STEP
    XI=X*12.
    T1X=T1(X)
    T2X=T2(X)
    WRITE(IPR,2010)XI,T1X,T2X
100 CONTINUE
STOP
200 WRITE(IPR,2002)
3000 STOP
1000 FORMAT(5E16.8)
2000 FORMAT(1H1,2X,"---- CALCULATION OF AVERAGE TUBESHEET LIGAMENT TEM
$PERATURES")
2001 FORMAT(///,6X,"---- TEMPERATURE DISTRIBUTION IN TUBE WALL AND TUBE
$SHEET LIGAMENT"///T2,"LOCATION",T15,"TEMPERATURES,DEG F"/T5,"IN.",
$T12,"TUBE WALL",T24,"TUBESHEET LIG."/)
2002 FORMAT(1H0,"SINGULAR SET OF EQUATIONS EXIST")
2005 FORMAT(1H0," INPUT DATA"//
$2X,"TUBE HOLE DIAMETER,IN.",T41,F10.3/
$,2X,"TUBE WALL THICKNESS,IN.",T41,F10.3/
$2X,"TUBE SHEET THICKNESS,IN.",T41,F10.3/
$2X,"TUBE COND.,BTU/HR/DEG F/FT2",T41,F10.3/

```

```

$2X,"TS COND.,BTU/HR/DEG F/FT2",T41,F10.3//,
$2X,"SHELLFILM COEFF.,BTU/HR/DEG F/FT2",T41,F10.3/
$2X,"TUBE FILM COEFF.,BTU/HR/DEG F/FT2",T41,F10.3/
$2X,"CHANNEL FILM COEFF.,BTU/HR/DEG F/FT2",T41,F10.3/
$2X,"SHELL FOULING FACTOR,1/(BTU/HR/DEG F/FT2)",T45,F7.4/
$2X,"TUBE FOULING FACTOR,1/(BTU/HR/DEG F/FT2)",T45,F7.4//,
$2X,"TUBE PITCH",T41,F10.3/
$2X,"TUBE LAYOUT ANGLE",T41,F10.3/
$2X,"TUBE SIDE TEMPERATURE,DEG F",T41,F10.3/
$2X,"SHELL SIDE TEMPERATURE,DEG F",T41,F10.3/
$2X,"NUMBER OF LOCATION INCREMENTS",T43,I4//)
2010 FORMAT(1H0,1X,F5.2,T13,F7.2,T27,F7.2)
END

```

7.10 TUBE REMOVAL AND TUBE PLUGGING

Tube plugging is ordinarily the last resort to block off inter-mixing of shell and tubeside fluids. It is obviously preferable to remove and replace a leaky tube with a new tube. Removing a leaky tube is often not without hazards. The welded connection with the tubesheet must be broken using a suitable cutter. The portion of the tube inside the tubesheet may have to be machined out to free the tube. All of this metal removing operation in tight header space in an installed unit carries the danger of harming nearby "good" tubes. Engineers have attempted other, more benign, techniques of tube removal. The sand pushing method reported by Schroeder [7.10.1] is disarmingly simple; and reportedly highly effective. Schroeder's method is illustrated in Fig. 7.10.1. A soft plug of felt, rubber, or other pliable material with diameter which is snug with the tube I.D. is inserted to retain sand or grit. Sand or grit (80 mesh aluminum oxide was used in the reported successful cases), is then introduced to a depth equivalent to approximately five tube diameters. A push rod sized to fit the inside diameter of the tube is inserted and an axial load is applied. The grit mass is compacted and the friction between grit and tubewall transfers the push rod force to the tube wall. Tests indicate that the amount of force that can be applied is only limited by the strength of the push rod. It is desirable to push both ends of the tube simultaneously with equal force when removing U-tubes. Hydraulically operated tube removal tools have also been used recently with success.

Plugging the tube is not without complications. A tube plug is designed to block the flow through the tube which in turn alters the temperature field in the vicinity of the plugged hole. The added mass of the plug also alters the "thermal capacitance" of the tubesheet around the plugged hole. Therefore, the plugged portion of the tubesheet lags the rest of the metal in any temperature changes brought about by fluctuations in the tubeside

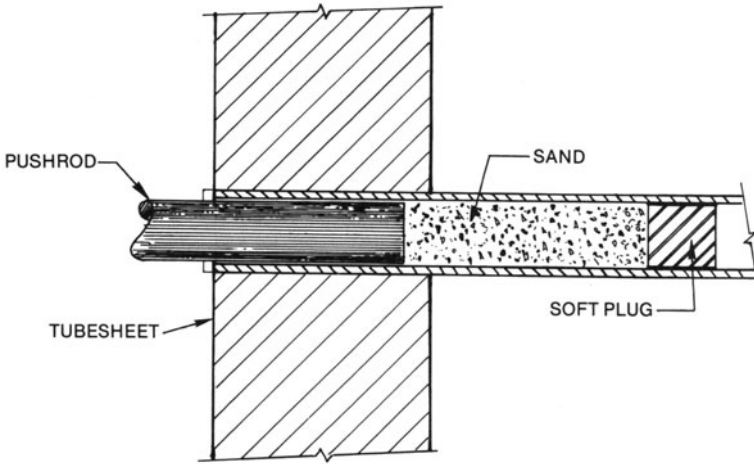


Fig. 7.10.1. Sand pushing method for tube removal (reprinted with the courtesy of the American Society for Metals, Metals Park, Ohio).

fluid. The resulting thermal fatigue stress is detrimental to the tubes in the vicinity of the plugged holes. This phenomenon is responsible for the “cluster” effect in tube failures: The tube failures tend to cluster around a “plugged” tube. Plant operators are known to attempt to overcome the problem by “insurance plugging” which means that a number of good tubes around a failed tube are plugged to buy insurance against in-use failures. In reality, this only exacerbates the problem. Tube plugging should be avoided wherever possible. Unfortunately, there is little alternative in those situations where the tube is trapped, such as the inner rows in a U-bundle. The engineer, however, can exercise good judgement in the selection of the most appropriate plug design from among the wide variety available.

The most common and inexpensive plug is the tapered plug shown in Fig. 7.10.2. Such a plug is usually hammered in place with predictably uncertain results. The blow of the hammer, if too great, may crack adjacent tube-tubesheet welds and precipitate additional leakage. A more sophisticated plug, the two piece tapered plug shown in Fig. 7.10.3, suffers from the same drawback. The outer sleeve in the two piece plug can be plain or serrated as shown in Fig. 7.10.4. The serrated outer sheath can cut through the scale and highs of pitted surfaces and therefore is more suitable for tubes with corroded interior.

The hydraulic or controlled detonation induced plug expansion is more desirable. Figure 7.10.5 shows a plug suitable for impact bonding. The hollow interior of the plug minimizes the increase of local tubesheet thermal inertia. The outer serrations effect the necessary seal.

Another practical concept, promoted as the “Pop”-a-plug system by its propounders [7.10.2], utilizes the two piece tapered plug mounted at the end

of a machined “breakable” location to install the plug at any location within the tube length. Figure 7.10.6 shows the concept in schematic form. The ability of this technique to install the plug at any location along the tube length is hailed as its major advantage by its inventors. Many other techniques of tube plugging are also reported in the commercial heat exchanger technology literature [7.10.3].

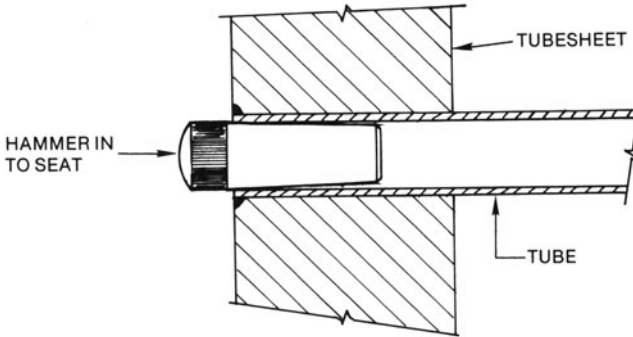


Fig. 7.10.2. Tapered plug used for tube plugging

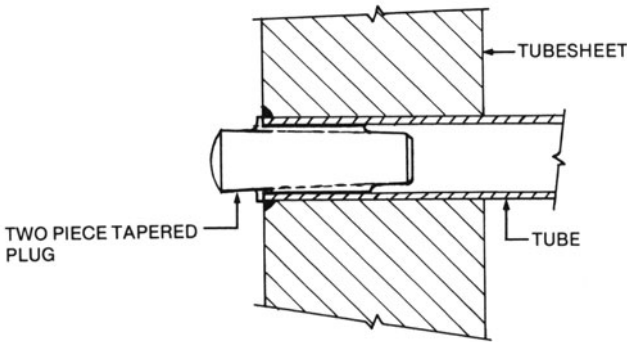


Fig. 7.10.3. Two piece tapered plug

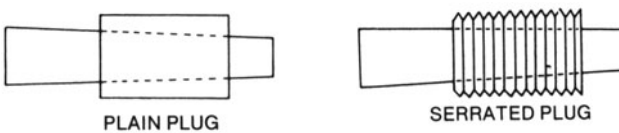


Fig. 7.10.4. Outer sleeve design in two piece tapered plug (Courtesy American Society for Metals)

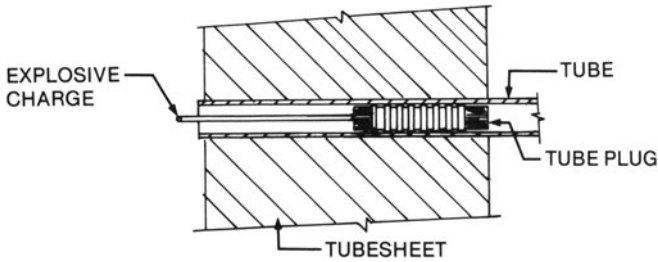


Fig. 7.10.5. Explosive plug design. (Courtesy ASM, Ohio)

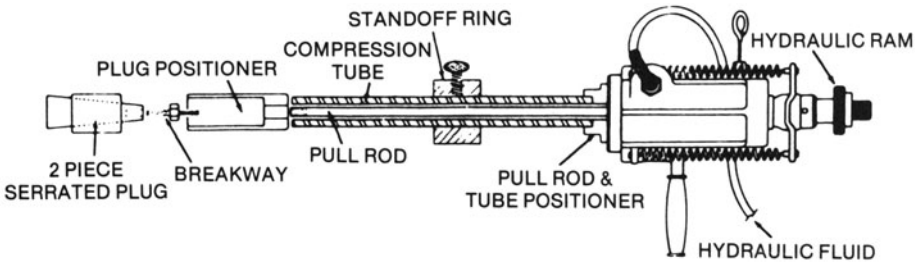


Fig. 7.10.6. Pop-a-plug concept (Courtesy ASM, Ohio)

NOMENCLATURE

- $[A]$ = Coefficient matrix (4×4) (Eq. (7.9.20))
- a_1 = Lateral cross-sectional area of region 1 (Fig. 7.9.2)
- a_2 = Lateral cross-sectional area of region 2 (Fig. 7.9.2)
- b_i = Constants of integration, $i = 1, 2, 3, 4$ (Eq. (7.9.11))
- c = Radial clearance between tube outside surface and tubesheet hole
- c_i = Derived coefficients, $i = 1, 2, 3, 4$ (Eq. (7.9.10))
- d_i = Constants of integration, $i = 1, 2, 3, 4$ (Eq. (7.9.13))
- E = Young's Modulus of tubesheet material
- E_t = Tube material Young's Modulus
- $\{f\}$ = Right-hand side vector (4 elements) (Eq. (7.9.20))
- f = Local coefficient of friction on tube/tubesheet surface (Section 7.8.5)
- h_{12} = Heat-transfer coefficient corresponding to a_{12} (Eq. (7.9.5))
- h_c = Heat-transfer coefficient on the tubesheet surface in the tubeside chamber
- h_t = In-tube heat-transfer coefficient
- h_s = Shell side heat-transfer coefficient on the tubesheet surface
- h'_s = Shellside heat transfer coefficient on the tube surface.
- k_1 = Thermal conductivity of tube material
- k_2 = Thermal conductivity of tube material
- l = Tubesheet thickness
- L = Roll depth of tube into tubesheet (Eq. (7.8.35))

- m_1, m_2 = Quantities defined in terms of c_i ($i = 1, 2, 3, 4$) (Eq. (7.9.12))
 \bar{p} = Layout pitch (Eq. (7.9.1))
 $p_{\max}, p_{c(\max)}$ = Maximum expansion pressure, and tube/tubesheet contact pressure during joint expansion; respectively
 $p(x)$ = Contact pressure distribution (Sub-section 7.8.5)
 p_c' = Final contact pressure after unloading.
 p_c = Contact pressure between tube wall and tubesheet during loading condition
 p_c^* = Contact pressure increment
 p_e = Interface pressure between elastic and plastic regions of tubesheet ligament
 p_i = Incremental pressure in the tube hole above p_0
 p_0 = Internal pressure in the tube at tube wall/tubesheet hole contact after yielding of the tube
 p^* = Increment of internal pressure
 P^* = Tube pull out load
 p_0' = Pressure to cause initial tube yielding
 q_{12} = Heat flux from region 1 to region 2
 r', r'' = Functions of r_1, r_2 and r_3 (Eq. (7.9.22))
 r_e = Interface radius between elastic and plastic zones in the tubesheet ligament
 r_t = Tube mean radius corresponding to tube wall thickness t .
 r_t' = Undeformed tube mean radius
 r_t^* = Final tube mean radius after loading
 r_1 = Tube hole radius
 r_2 = Tube outer radius
 r_2^* = Final hole radius after loading
 r_3 = Equivalent ligament radius (Fig. 7.9.2)
 S = Stress intensity in the tube material
 S_i = Circumference corresponding to radius r_i ($i = 1, 2, 3$)
 T_1 = Average cross-sectional temperature of tube wall
 T_2 = Average cross-sectional temperature of tube sheet ligament
 T_1' = Average tube wall cross-sectional temperature in region 1'
 T_t = Tubeside fluid temperature
 T_s = Shellside fluid temperature
 t = Tube wall thickness at the point of contact with the tubesheet hole.
 t' = Undeformed tube wall thickness
 t^* = Final tube thickness
 u = Radial deflection of tube mid-surface
 U = Radial displacement increment

- U_c = Complementary energy
 α, β = Parameters which define tube metal temperature in region 1' (Eq. (7.9.18))
 ϵ_r = Radial strain
 ϵ_z = Longitudinal strain
 ϵ_θ = Circumferential tube strain
 ν = Poisson's ratio of tube and tubesheet materials
 σ_θ = Circumferential stress in the tube
 σ_r = Radial stress in the tube
 σ_T = Yield stress of the tube material in simple tension
 σ_s = Yield stress of the tubesheet material in simple tension
 θ = Layout angle (Fig. 7.9.1)
 ω_1, ω_2 = Coefficients which relate d_i to b_i (Eq. (7.9.15))
 ϕ = Plasticity proportionality factor relating plastic strain increments to stress
 μ = Effective coefficient of friction.

ADDITIONAL OR CHANGED NOMENCLATURE FOR APPENDIX 7.C

- A_i, B_i, D_i^* = Coefficients of incremental equations
 C_i, D_i, R_i^*
 E_j, G_j = Layer material properties
 $\dot{\epsilon}_{\theta i}, \dot{\epsilon}_{r i}$ = Layer plastic strain rates
 h_i = Thickness of layer i
 k_i = Artificial parameter to indicate plasticity in layer i
 N = Number of layers (Fig. 7.C.1b)
 p_i = Interface pressure between layer i and $i+1$ (see Fig. 7.C.1)
 p_R, p_c = Limiting roll pressure, contact pressure (Eq. (7.C.26))
 r_i = Mean radius of layer i
 r_1^*, h_1^* = Tube mean radius, thickness at contact with tubesheet
 T = Temperature rate for heating/cooling cycle
 \dot{u}_i = Layer velocities
 $\dot{\epsilon}_{\theta i}, \dot{\epsilon}_{r i}$ = Layer total strain rates
 λ_i = Plasticity proportionality factor (see Eq. (7.C.7))
 σ_T, σ_{TS} = Uniaxial yield stress of tube, tubesheet material
 $\sigma_{y i}$ = Yield stress in i th layer

REFERENCES

- [7.1.1] Boyer, R. C., "Condenser Tube-to-Tubesheet Joint Leakage: An Overview," ASME Paper No. 81-JPGC-Pwr-6.
 [7.2.1] Standards of Tubular Exchanger Manufacturers Association, 6th edition, New York (1978).
 [7.3.1] Dudley, F. E., "Electronic Control Method for the Precision, Expanding of Tubes," ASME Winter Annual Meeting, Paper No. 53-A-133 (1953).

- [7.3.2] Singh, K. P., and Paul, B., "Stress Concentration in Crowned Rollers," *Journal of Engineering for Industry*, Trans. ASME, Vol. 97, Series B, No. 3, pp. 990-994 (1975).
- [7.3.3] Yokell, S., "Heat Exchanger Tube-to-Tubesheet Connections," *Chemical Engineering* (February 8, 1982).
- [7.4.1] Podhorsky, M., and Krips, H., "Hydraulic Expansion of Tubes," V.G.B. Krabtwerk-Stechnik, 1 pp. 81-87 (1979).
- [7.4.2] Singh, K. P., and Soler, A. I., "A Design Concept for Minimizing Stress Levels in Stationary Tubesheet Heat Exchangers," *International Journal of Pressure Vessel and Piping*, Applied Science Publishers, Vol. 13, pp. 19-32 (1983).
- [7.5.1] Hardwick, R., "Methods for Fabricating and Plugging of Tube-to-Tubesheet Joints by Explosion Welding," *Welding Journal* (April 1975).
- [7.6.1] ASME Boiler and Pressure Vessel Code, Section VIII, 1 Div. 1, Appendix A (1983).
- [7.6.2] Apblett, W. R., Montrone, E. D., Wolowdiuk, W., "Thermal Shock Testing of Fillet-Type Tube-to-Tubesheet Welds," ASME Paper No. 76-PVP-35, Trans. of the ASME, *Journal of Pressure Vessel Technology* (c.'77).
- [7.8.1] Brown, G. J., and Fisher, E. F., "Tube Expanding and Related Subjects," *Trans. of the ASME*, pp. 563-575 (May, 1954).
- [7.8.2] Goodier, J. N., and Schoessow, G. J., "The Holding Power and Hydraulic Tightness of Expanded Tube Joints: Analysis of Stress and Deformation," *Trans. ASME*, pp. 489-496 (July, 1941).
- [7.8.3] Grimison, E. D., and Lee, G. H., "Experimental Investigation of Tube Expanding," *Trans. ASME*, pp. 497-505 (July, 1943).
- [7.8.4] Mendelson, Alexander, "Plasticity: Theory & Application, MacMillan, New York (1968).
- [7.8.5] Alexander, J. M., and Ford, H., "Experimental Investigations of the Process of Expanding Boiler Tubes," *International Journal of Mechanical Engineers*, pp. 351-367 (January, 1956).
- [7.8.6] Beston, P. G., "Development of the Zircolloy Coolant Tube to End Fitting Joint for NPD II," Report to the Canadian General Electric Co., Ltd., Peterborough, Ontario, Canada (1959).
- [7.8.7] Culver, L. D., and Ford, H., "Experimental Study of Some Variables of the Tube Expanding Process," *Institute of Mechanical Engineers Proceedings*, Vol. 73, No. 4, pp. 399-413 (1959).
- [7.8.8] Uragami, K., Sugino, M., Urushibasta, S., Kodama, T., and Fujiwara, Y., "Experimental Residual Stress Analysis of Tube-to-Tubesheet Joints During Expansion," *The American Society of Mechanical Engineers*, ASME Paper No. 82-PVP-61 (July, 1982).
- [7.8.9] Wilson, R. M., "The Elastic-Plastic Behaviour of a Tube

- During Expansion,” The American Society of Mechanical Engineers, ASME Paper No. 78-PVP-112 (June, 1978).
- [7.9.1] Gardner, K. A., “Heat Exchanger Tubesheet Temperatures,” The Refiner and Natural Gasoline Manufacturer (March, 1942).
- [7.9.2] Singh, K. P., and Holtz, M., “An Approximate Method for Evaluating the Temperature Field in Tubesheet Ligaments of Tubular Heat Exchangers under Steady State Conditions,” *Journal of Engineering for Power*, Trans. ASME, Vol. 104, pp. 895-900 (October, 1982).
- [7.9.3] Standards for Power Plant Heat Exchangers, 1st edition, Heat Exchange Institute, p. 10 (1980).
- [7.9.4] Soler, A. I., “Tube Stresses due to In-Plane Thermal Expansion of Tubesheets in Closely Spaced Double Tubesheets,” *International Journal of Pressure Vessel & Piping*, Vol. 7, pp. 119-132 (1979).
- [7.9.5] Jakob, M., “Heat Transfer,” Vol. I, p. 133, Wiley (1967).
- [7.10.1] Schroeder, J. W., “Sand Pushing for Tube Removal,” Second Symposium on Shell and Tube Exchangers, W. R. Applett (ed.), American Society for Metals, Metals Park, Ohio (1981).
- [7.10.2] Martin, J. E., and Jorgensen, G., “Testing and Plugging Heat Exchanger Tubes to Withstand 5,000 psi by Removing One Head Only,” American Society for Metals, Metals Park, Ohio (1981).
- [7.10.3] Noe, R., and Sahansra, and Costic, M. W., Report on Explosion Plugs in Feedwater Heaters and Heat Exchangers, Feedwater Heater Workshop Proceedings, Electric Power Research Institute, Palo Alto, California WS-78-133 (1979).
- [7.B.1] Singh, K. P., and Soler, A. I., “HEXDES User Manual,” Arcturus Publishers, Cherry Hill, N.J. (1984).

APPENDIX 7.A

Coefficients of [A] Matrix and {f} Vector

$$\begin{aligned}
 A_{11} &= k_2 m_1 - h_c; & A_{21} &= (k_2 m_1 + h_s) e^{m_1 l} \\
 A_{12} &= -k_2 m_1 - h_c; & A_{22} &= (-k_2 m_1 + h_s) e^{-m_1 l} \\
 A_{13} &= k_2 m_2 - h_c; & A_{23} &= (k_2 m_2 + h_s) e^{m_2 l} \\
 A_{14} &= -k_2 m_2 - h_c; & A_{24} &= (-k_2 m_2 + h_s) e^{-m_2 l} \\
 f_1 &= -h_c \left(T_i + \frac{c_4}{c_3} \right); & f_2 &= h_s \left(\frac{c_4}{c_3} + T_s \right) \\
 A_{31} &= (k_1 m_1 - h_c) \omega_1; & A_{41} &= \omega_1 (m_1 + \alpha) e^{m_1 l} \\
 A_{32} &= -(k_1 m_1 + h_c) \omega_1; & A_{42} &= \omega_1 (-m_1 + \alpha) e^{-m_1 l}
 \end{aligned}$$

$$\begin{aligned}
 A_{33} &= (k_1 m_2 - h_c) \omega_2; & A_{43} &= \omega_2 (m_2 + \alpha) e^{m_2 l} \\
 A_{34} &= -(k_1 m_2 + h_c) \omega_2; & A_{44} &= \omega_2 (-m_2 + \alpha) e^{-m_2 l} \\
 f_3 &= -h_c \left(T_i + \frac{c_4}{c_3} \right); & f_4 &= \frac{\beta^2}{\alpha} + \frac{\alpha c_4}{c_3}
 \end{aligned}$$

APPENDIX 7.B

COMPUTER CODE FOR EVALUATION OF RESIDUAL ROLL PRESSURE USING TRESCA YIELD CONDITION

User Information

The code is written in Fortran 66 for execution on a TRS80-MODIII microcomputer. The code assumes input from the keyboard, and outputs prompts to the screen, and results to a printer. The listing of the source code is provided as well as the results leading to Table 7.8.2 in the text. Complete documentation on this code may be found in [7.B.1].

PROGRAM TBROLL

```

C**PROGRAM TO COMPUTE TUBE ROLL PRESSURE BASED ON
C**TRESCA YIELD CONDITION, MAXIMUM TUBE ROLL, AND TUBE
C**YIELD PRIOR TO CONTACT. TRS-80 MODIII FORTRAN
C****INPUT VARIABLE LIST
C**TOD=TUBE OUTER DIAMETER INPUT ZERO TO END JOB
C** TT=TUBE NOMINAL THICKNESS
C** C=NOMINAL RADIAL CLEARANCE
C** ET=YOUNG'S MODULUS OF TUBE MATERIAL
C** ES=YOUNG'S MODULUS OF TUBESHEET MATERIAL
C** YT=YIELD STRESS OF TUBE MATERIAL
C** YS=YIELD STRESS OF TUBESHEET MATERIAL
400 CONTINUE
WRITE(2,50)
50 FORMAT(1X,'*****')
WRITE(5,1)
1 FORMAT(' INPUT TOD,TT,C 3(1X,F6.3)')
READ(1,2) TOD,TT,C
IF(TOD.LE.0.) STOP
2 FORMAT(1X,3F6.3)
WRITE(5,3)
3 FORMAT(' INPUT ET,ES,YT,YS 4(1X,E10.3)')
READ(1,4) ET,ES,YT,YS
4 FORMAT(1X,4E10.3)
WRITE(2,12)
12 FORMAT('*****')
WRITE(2,5) TOD,TT,C

```

```

5   FORMAT(1H0,'TOD=',F6.3,' TT=',F6.3,' C=',F6.3)
   WRITE(2,6) ET,ES
6   FORMAT(' ET=',F10.0,' ES=',F10.0)
   WRITE(2,7) YT,YS
7   FORMAT(' YT=',F10.0,' YS=',F10.0)
C****CALCULATIONS
   RM=.5*(TOD-TT)
   T1=TT*(1.-.5*C/RM)
   R2=(TOD+2.*C)/2.
   R1=R2-.5*T1
   X1=YT*(1.+15*TT/RM)/(ET*(1.+5*TT/RM))
   X2=C/RM
   IF(X2.LT.X1) WRITE(5,8)
8   FORMAT(' TUBE DOES NOT YIELD PRIOR TO CONTACT')
   IF(X2.LT.X1) GO TO 400
   YT1=YT*(1.-T1/(2.*R1))
   PC=AMIN1(YT1,YS)
   PMAX=PC+YT*T1/R1
   X3=27.*1.3/16.*YS/ES
   R2S=R2*(1.+X3)
   U2=R2*X3
   T1S=T1*(1.-.5*X3)
   R1S=R2S-.5*T1S
   ELAM=ET/ES*1.3*R2S/R1S+.2
   Z1=(1.-.5*T1S/R1S)
   PCF=PC*T1S/R1S*(.5+ELAM)-YT*T1/R1*Z1
   PCF1=PCF
   PCF=PCF1/(1.+ELAM*T1S/R1S)
C*****OUTPUT
   WRITE(2,20) PMAX,PC,PCF,PCF1
   WRITE(2,21) R1,R1S,RM
21  FORMAT(1H0,' R1=',F6.3,' R1S=',F6.3,' RM=',F6.3)
   WRITE(2,22) T1,T1S,R2,R2S
22  FORMAT(' T1=',F6.3,' T1S=',F6.3,' R2=',F6.3,' R2S=',F6.3)
20  FORMAT(1H0,' PM=',F9.1,' PCM=',F9.1,' PCF=',F9.1,' PCF1=',F9.1)
   GO TO 400
   END

```

SAMPLE OUTPUT FROM TBROLL

```

TOD= .750 TT= .049 C= .005
ET= 14900000. ES= 15000000.
YT= 40000. YS= 20000.

```

```

PM= 25471.3 PCM= 20000.0 PCF= 463.1 PCF1= 562.6

```

R1= .356 R1S= .357 RM= .350
 T1= .049 T1S= .049 R2= .380 R2S= .381

TOD= .750 TT= .049 C= .005
 ET= 29000000. ES= 29000000.
 YT= 30000. YS= 30000.

PM= 32051.8 PCM= 27948.2 PCF= 3396.2 PCF1= 4131.5

R1= .356 R1S= .357 RM= .350
 T1= .049 T1S= .049 R2= .380 R2S= .381

TOD= .750 TT= .049 C= .005
 ET= 16000000. ES= 29000000.
 YT= 15000. YS= 30000.

PM= 16025.9 PCM= 13974.1 PCF= 777.9 PCF1= 880.3

R1= .356 R1S= .357 RM= .350
 T1= .049 T1S= .049 R2= .380 R2S= .381

TOD= .750 TT= .049 C= .005
 ET= 18000000. ES= 15000000.
 YT= 15000. YS= 20000.

PM= 16025.9 PCM= 13974.1 PCF= 2064.9 PCF1= 2589.6

R1= .356 R1S= .357 RM= .350
 T1= .049 T1S= .049 R2= .380 R2S= .381

TOD= .750 TT= .049 C= .005
 ET= 29000000. ES= 18000000.
 YT= 30000. YS= 15000.

PM= 19103.5 PCM= 15000.0 PCF= 1640.1 PCF1= 2185.3

R1= .356 R1S= .356 RM= .350
 T1= .049 T1S= .049 R2= .380 R2S= .381

TOD= .750 TT= .049 C= .005
 ET= 22000000. ES= 18000000.
 YT= 18000. YS= 15000.

PM= 17462.1 PCM= 15000.0 PCF= 2073.4 PCF1= 2610.0

R1= .356 R1S= .356 RM= .350
T1= .049 T1S= .049 R2= .380 R2S= .381

TOD= .750 TT= .049 C= .005
ET= 22000000. ES= 29000000.
YT= 18000. YS= 30000.

PM= 19231.1 PCM= 16768.9 PCF= 1463.0 PCF1= 1712.9

R1= .356 R1S= .357 RM= .350
T1= .049 T1S= .049 R2= .380 R2S= .381

TOD= .750 TT= .028 C= .005
ET= 29000000. ES= 29000000.
YT= 30000. YS= 30000.

PM= 31139.3 PCM= 28860.7 PCF= 2044.1 PCF1= 2283.8

R1= .366 R1S= .367 RM= .361
T1= .028 T1S= .028 R2= .380 R2S= .381

TOD= .750 TT= .028 C= .005
ET= 22000000. ES= 29000000.
YT= 18000. YS= 30000.

PM= 18683.6 PCM= 17316.4 PCF= 863.5 PCF1= 943.4

R1= .366 R1S= .367 RM= .361
T1= .028 T1S= .028 R2= .380 R2S= .381

TOD= .750 TT= .028 C= .005
ET= 29000000. ES= 22000000.
YT= 30000. YS= 18000.

PM= 20278.6 PCM= 18000.0 PCF= 1032.1 PCF1= 1186.8

R1= .366 R1S= .367 RM= .361
T1= .028 T1S= .028 R2= .380 R2S= .381

APPENDIX 7.C

TUBE-TUBESHEET JOINT LOADING INCLUDING THERMAL EFFECTS

It is the purpose of this appendix to establish a special purpose computer solution of the 2-D rolling problem which includes elastic-plastic behavior, large deformations, and establishes residual contact pressures both immediately after initial room temperature rolling, and also after a subsequent temperature cycle. The analysis places no restrictions on yielding of the tube or tubesheet during any phase of the simulation. The motivation herein is to present a modern analysis tool to predict the residual rolling pressure between tube and tubesheet.

Analysis

The roller or hydraulic expansion process is characterized initially by a tube loading stage. Subsequent to tube-to-tubesheet contact, as the internal pressure continuously increases, loading of the tubesheet begins. Tubesheet deformation is initially elastic until the state of stress in the tubesheet at the hole surface satisfies the yield criteria. With additional increase in rolling pressure, the plastic zone in the tubesheet increases until a maximum rolling pressure is reached. With subsequent decrease of the rolling pressure, both tube and tubesheet are unloaded, but a residual contact pressure will exist at the interface of the tube and tubesheet after all of the internal pressure is removed. Reversed yielding may occur during this unloading in either or both tube and tubesheet.

If the tube and tubesheet are made of different materials, any subsequent temperature change of the joint from the rolling temperature to the unit operating temperature changes the tube-to-tubesheet contact pressure. The residual contact pressure after a single temperature cycle depends on joint geometry, material properties of tube and tubesheet, temperature range, and maximum rolling pressure initially applied.

Figure 7.C.1a shows the configuration considered. The configuration is idealized by a set of concentric membrane elements in 2-D plane stress as shown in Fig. 7.C.1b. There are N membrane elements (layers) with the innermost element being the tube; the remaining membrane elements represent the tubesheet. The elements (layers) are numbered starting from the tube (element 1); the i th element (layer) has mean radius r_i and thickness h_i .

The following assumptions are made for the detailed analysis:

- a) The tube and tubesheet materials satisfy the von Mises Yield Criterion; strain hardening is neglected.
- b) No creep occurs in the temperature range considered.
- c) Temperature changes in tube and tubesheet are uniform and have the

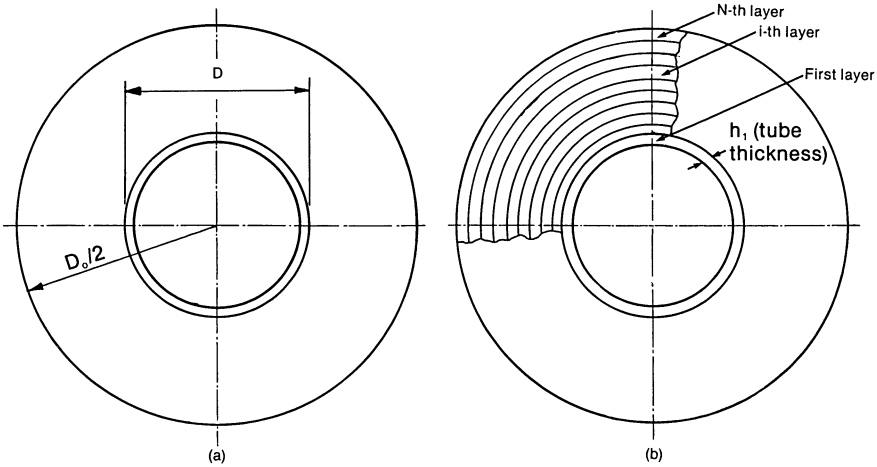


Fig. 7.C.1. Tube-to-Tubesheet Joint model.

same value at any stage in the simulation.

d) Material properties are temperature independent.

Figure 7.C.2 is a free-body diagram of the *i*th layer showing “internal” pressure p_{i-1} , and “external” pressure p_i . The average radial stress in the *i*th layer is

$$\sigma_{ri} = -\frac{1}{2}(p_{i-1} + p_i) \tag{7.C.1}$$

Equilibrium of the *i*th element requires that

$$\sigma_{\theta} = \frac{d}{dr}(r\sigma_r)$$

The average *i*th layer hoop stress is defined as

$$\sigma_{\theta i} = \frac{1}{h_i} \int_{r_i-h_i/2}^{r_i+h_i/2} \sigma_{\theta} dr = \frac{r_i}{h_i}(p_{i-1} - p_i) + \sigma_{ri} \tag{7.C.2}$$

The average stresses σ_{ri} , $\sigma_{\theta i}$ characterize the state of stress in the *i*th layer.

When rolling pressure p_0 is changed by an increment \dot{p}_0 and system temperature T is changed by an increment \dot{T} , the interface pressures p_i (between layer $i + 1$ and layer i) undergo incremental changes \dot{p}_i . The incremental changes in σ_{ri} , $\sigma_{\theta i}$ are

$$2\dot{\sigma}_{ri} = -(\dot{p}_{i-1} + \dot{p}_i) \tag{7.C.3}$$

$$\dot{\sigma}_{\theta i} = (\dot{p}_{i-1} - \dot{p}_i) \frac{r_i}{h_i} + (\sigma_{\theta i} - \sigma_{ri})(\dot{\epsilon}_{\theta i} - \dot{\epsilon}_{ri}) + \dot{\sigma}_{ri} \tag{7.C.4}$$

where incremental strain relations for each layer are:

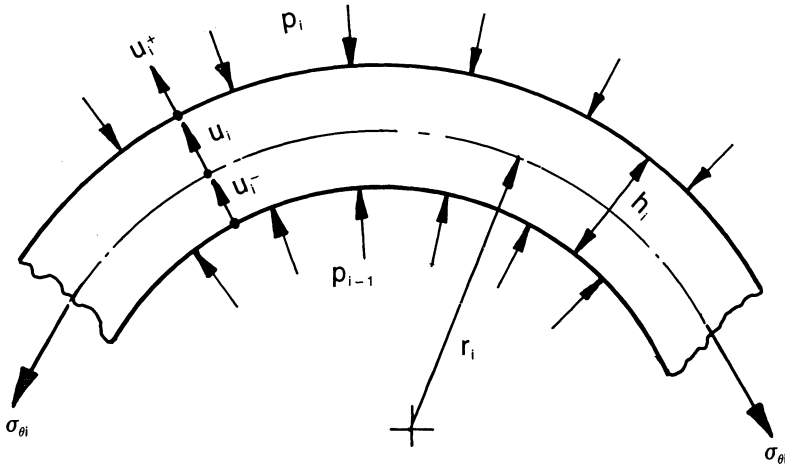


Fig. 7.C.2. Stress and displacement definitions for a typical element.

$$\frac{\dot{h}_i}{h_i} = \dot{\epsilon}_{ri} = \frac{1}{E_i} (\dot{\sigma}_{ri} - \nu \dot{\sigma}_{\theta i}) + \dot{\epsilon}_{ri} + \alpha_i \dot{T} \quad (7.C.5)$$

$$\frac{\dot{r}_i}{r_i} = \dot{\epsilon}_{\theta i} = \frac{1}{E_i} (\dot{\sigma}_{\theta i} - \nu \dot{\sigma}_{ri}) + \dot{\epsilon}_{\theta i} + \alpha_i \dot{T} \quad (7.C.6)$$

For ideal plasticity, subject to plane stress conditions, the plastic strain increments, $\dot{\epsilon}_{ri}$, $\dot{\epsilon}_{\theta i}$ can be written as

$$\dot{\epsilon}_{ri} = \frac{\lambda_i}{3} (2\sigma_{ri} - \sigma_{\theta i}); \dot{\epsilon}_{\theta i} = \frac{\lambda_i}{3} (2\sigma_{\theta i} - \sigma_{ri}) \quad (7.C.7)$$

Using Eqs. (7.C.5), (7.C.6) in Eq. (7.C.4) yields $\dot{\sigma}_{\theta j}$ as

$$\left(1 - \frac{\sigma_{\theta j} - \sigma_{rj}}{2G_j}\right) \dot{\sigma}_{\theta j} = \dot{p}_{j-1} \left[\frac{\sigma_{\theta j} - \sigma_{rj}}{4G_j} - \frac{1}{2} + \frac{r_j}{h_j} \right] + \dot{p}_j \\ \times \left[\frac{\sigma_{\theta j} - \sigma_{rj}}{4G_j} - \frac{1}{2} - \frac{r_j}{h_j} \right] + (\sigma_{\theta j} - \sigma_{rj}) \Delta \dot{\epsilon}_j \quad j=1,2, \dots, 10 \quad (7.C.8)$$

where $\Delta \dot{\epsilon}_j = \dot{\epsilon}_{\theta j} - \dot{\epsilon}_{rj}$. Note that in Eq. (7.C.8) the term $(\sigma_{\theta j} - \sigma_{rj})/G_j$ represents large deformation effects during elastic loading. Since this term is of order 10^{-3} for most metals, one concludes that large deformation effects may be significant only during plastic action.

The displacement increments at the inner and outer surfaces of the i th membrane layer are given in terms of strain increments as

$$\dot{u}_i^- = r_i \dot{\epsilon}_{\theta i} - \frac{h_i}{2} \dot{\epsilon}_{ri} \quad (7.C.9)$$

$$\dot{u}_i^+ = r_i \dot{\epsilon}_{\theta i} + \frac{h_i}{2} \dot{\epsilon}_{ri} \quad (7.C.10)$$

Compatibility equations for a unit idealized as N layers are the $N-1$ equations.

$$\dot{u}_{i-1}^- = \dot{u}_i^+ \quad i=1,2, \dots, N-1 \quad (7.C.11)$$

The strain increments are eliminated in terms of stress increments, and the stress increments are eliminated in favor of interface pressure increments. After some algebraic manipulation, $N-1$ compatibility equations are evolved from Eq. (7.C.11) in the form

$$A_i \dot{p}_{i-1} + B_i \dot{p}_i + C_i \dot{p}_{i+1} + D_i \lambda_i k_i + D_i^* \lambda_{i+1} k_{i+1} = R_i \dot{T} \quad (7.C.12)$$

where $i=1,2, \dots, (N-1)$; N being the number of layers including the tube as the first layer. The coefficients $A_i, B_i, C_i, D_i, D_i^*, R_i$ are given at the end of this Appendix. Note that no approximations save plane stress, and the membrane assumption have been employed to obtain Eq. (7.C.12).

The artificially inserted parameter $k_i, i=1,2 \dots, N$ satisfies the conditions:

$$\begin{aligned} k_i &= 0 && \text{if layer } i \text{ is elastic during the increment;} \\ k_i &= 1 && \text{if layer } i \text{ experiences plastic flow during the increment.} \end{aligned}$$

If all layers remain elastic, since $k_i=0, i=1,2 \dots, N$, the $N-1$ compatibility equations are solvable for the $N-1$ interface pressure increments. Once yielding has occurred in one or more layers, Eq. (7.C.12) are insufficient to determine interface pressure increments. Additional equations are obtained from the von Mises yield condition. If σ_{yi} is the uniaxial yield stress in the i th layer, then

$$\sigma_{\theta i}^2 - \sigma_{\theta i} \sigma_{r i} + \sigma_{r i}^2 \leq \sigma_{y i}^2 \quad i=1,2 \dots, N \quad (7.C.13)$$

with the equality sign applying when yielding occurs. In incremental form, for any yielded layer, we may write

$$(2\sigma_{\theta i} - \sigma_{r i}) \dot{\sigma}_{\theta i} + (2\sigma_{r i} - \sigma_{\theta i}) \dot{\sigma}_{r i} = 0 \quad i=1,2, \dots, M \quad (7.C.14)$$

where M is the number of yielded layers during the increment. Rewriting the above equation in terms of incremental pressures yields the N equations

$$k_i (F_i \dot{p}_{i-1} + M_i \dot{p}_i) + H_i \lambda_i = 0 \quad i=1,2, \dots, N \quad (7.C.15)$$

Equations (7.C.12), (7.C.15) are $2N-1$ equations for the incremental pressures $\dot{p}_i, i=1,2, \dots, N-1$ and the plasticity proportionality parameters $\lambda_i, i=1,2, \dots, N$ at each stage of the simulation. The boundary conditions are assumed as:

$$\begin{aligned} \dot{p}_0 &= \text{known loading increment;} \\ \dot{p}_N &= 0; \\ \dot{T} &= \text{known temperature increment.} \end{aligned} \quad (7.C.16)$$

The tube rolling process considered consists of tube loading by p_0 to initial contact with the tubesheet, a subsequent loading and unloading ($\dot{p}_0 \neq 0, \dot{T}=0$) to establish a room temperature residual contact pressure, and a subsequent temperature cycle ($\dot{p}_0=0$ and $\dot{T} \neq 0$) to examine thermal

effects in the absence of creep. In the developed computer code in Appendix 7.D, a total of ten layers are modelled. The first layer represents the tube and has an initial layer thickness equal to the nominal tube thickness. The remaining nine layers modelling the tubesheet each have thickness HS .

Since clearance c initially exists between tube and tubesheet, the tube state of stress when tube to tubesheet contact initially occurs must be established. At first yield, the stress increments are

$$\Delta\sigma_{ri} = -p_0/2; \quad \Delta\sigma_{\theta i} = p_0 r_1/h_1 - p_0/2 \quad (7.C.17)$$

and the yield condition gives

$$p_0 = \frac{\sigma_{y1} h_1 / r_1}{(1 - h_1/2r_1 + h_1^2/4r_1^2)^{1/2}} \quad (7.C.18)$$

Dimensional changes may be ignored in the elastic deformation phase and we find that tube yield occurs prior to tubesheet contact, if

$$c/r_1 > \sigma_{y1}/E_1 \quad (7.C.19)$$

If the clearance c is small and tube yield does not occur prior to contact with the tubesheet, then the roll pressure at contact and the tube stress state is found from the geometric relation

$$r_1^* = r_1 + \frac{h_1}{2} + c - \frac{h_1^*}{2} \quad (7.C.20)$$

where r_1^* , h_1^* , are the tube mean radius and thickness at contact. Equation (7.C.20) can be rewritten as

$$\Delta r_1 + \Delta h_1/2 = c \quad (7.C.21)$$

Since

$$\Delta r_1 = \frac{r_1}{E_1} (\Delta\sigma_{\theta 1} - \nu\Delta\sigma_{r 1}); \quad \Delta h_1 = \frac{h_1}{E_1} (\Delta\sigma_{r 1} - \nu\Delta\sigma_{\theta 1}) \quad (7.C.22)$$

the roll pressure p_0 at contact may be established.

If tube yield occurs prior to tubesheet contact, then the additional change in roll pressure, tube mean radius, and tube thickness occurring during the increment between first yield and contact with the tubesheet must be computed. For the increment between first yield and contact, Eq. (7.C.15) yields:

$$F_1 \dot{p}_0 + H_1 \lambda_1 = 0 \quad (7.C.23)$$

We can obtain a second equation involving \dot{p}_0 , λ_1 by computing the quantity $\Delta r_1 + \Delta h_1/2$ between first yield and contact. The result of this calculation must be equal to the clearance remaining between the tube at first yield, and the tube hole surface.

Thus, we can obtain solutions for \dot{p}_0 , λ_1 associated with the geometry changes between tube initial yield and first contact. Therefore, the tube stress state, the new tube geometry, and the rolling pressure are known at the onset of tubesheet loading.

Application

A computer program simulating the roller expansion process based on our theoretical incremental analysis has been developed and is listed in Appendix 7.D. The program includes determination of the tube state at initial contact with the tubesheet, simulation of a loading and unloading stage with $\dot{p}_0 \neq 0$, $\dot{T}=0$, and simulation of a temperature load and unload cycle with $\dot{p}_0=0$, $\dot{T} \neq 0$. During the increments, within each stage of loading or unloading, proper account is taken of geometry changes and plastic behavior.

The main purposes of this program are: (a) to determine the residual contact pressure after unloading or after temperature change for a given joint, so as to predict the joint holding power; and (b) to analyze the effect of various parameters and load cycles on the final residual contact pressure obtained. Table 7.C.1 shows the possible scenarios that evolve based on a considerable number of simulations using the computer code.

Table 7.C.1. Tube/Tubesheet Scenario*

<u>Initial Contact</u>	<u>Loading</u>	<u>Unloading</u>	<u>Temperature Change**</u>
Tube remains elastic	Specified value of maximum applied pressure is reached	Tube and tubesheet remain elastic	$[(\alpha_T - \alpha_{TS})\Delta T > 0]$ $[(\alpha_T - \alpha_{TS})\Delta T < 0]$ Tube is elastic or undergoes no stress change
	All layers yield before maximum roll pressure obtained	Tube and tubesheet both experience reversed yield	Tubesheet can be either elastic or plastic
Tube yields prior to contact	Tube yield strength controls max. roll pressure	Either tube or tubesheet experiences reversed yield	No change in stress state occurs as the temperature load is imposed or removed
	Tubesheet yield strength controls max. roll pressure	Tube/tubesheet contact is lost	Tube/tubesheet contact is lost

*Note that the result in any column may lead to any of the results in the succeeding columns.

**Scenarios apply to thermal loading or unloading.

$\sigma_r = -p_R$ and $-p_C$, where p_R , p_C are the roll and contact pressures, respectively. One finds that in order that σ_θ be real at the locations considered, p_R , p_C must be limited to the values

$$p_R \leq (4/3)^{1/2} \sigma_T; \quad p_C \leq (4/3)^{1/2} \sigma_{TS} \quad (7.C.26)$$

where σ_T , σ_{TS} refer to the uniaxial yield stress of the tube and tubesheet material, respectively. The limiting values are independent of the outer radius assumed to model the tubesheet. In fact, the previous conclusion is usually found associated with the solution of the infinite sheet having an internally pressurized hole [7.8.4], and leads to the results that there is a limiting radius beyond which plasticity cannot propagate. In this finite radius tubesheet model, the limits on p_R , p_C apply, but the extent of the plastic region depends on the particular geometry assumed. In fact, if the assumed outer limit of the tubesheet is taken too small, complete plastification, with subsequent unlimited deformation, can occur prior to achieving the roll or contact pressures limits. In the computer code developed, the above limits of p_R , p_C , and the requirement that the outermost membrane layer remain elastic are automatically imposed as absolute upper bounds on the pressure loading.

Table 7.C.2 shows the results of a verification study where tube and tubesheet are both of the same material, the clearance is zero, and a final roll pressure of 16,000 psi is imposed. All layers remain elastic and the results are compared with the Lamé solution for the thick cylinder. The percent errors are well within the limits for design purposes even with an increment size of 50 psi.

Table 7.C.2. Interface Pressures – Comparison with Exact Solution

Layer Thickness $HS = 0.55''$ Pressure Increment $\dot{p}_0 = 10$ psi			Layer thickness $HS = 0.85''$ Pressure Increment $\dot{p}_0 = 50$ psi		
Program	Lamé	Error(%)	Program	Lamé	Error(%)
16000	16000	0	16000	16000	0
11448.4	11453.5	.0445	11722	11744	.186
8078.0	8085.1	.0878	7294	7327	.449
5796	5796.2	.107	4786	4809	.496
4166	4170.3	.103	3223	3241	.554
2970	2974.1	.138	2183	2197	.570
2065	2068.5	.169	1457	1469	.795
1364	1366.5	.183	943	939	.799
810	811.3	.160	539	543	.785
364	364.6	.164	236	238.9	1.214
0	0	0	0	0	0

Table 7.C.3 presents geometry and loading conditions for a typical construction. Two simulations are performed with the tube material 70:30 Cu-Ni in both analyses. The thermal cycle is the same for both simulations, and the possibility of heat up and cool down is considered.

Table 7.C.3 Simulation with 70:30 Cu Ni Tubing

	<u>Tube</u>	<u>Tubesheet 1</u>	<u>Tubesheet 2</u>
Material	70:30 Cu-Ni	90:10 Cu-Ni	Steel
E(psi)	2.2×10^7	1.8×10^7	2.9×10^7
σ_y (psi)	1.8×10^4	1.5×10^4	3×10^4
α	9×10^{-6}	9.5×10^{-6}	6.5×10^{-6}
Tube O.D. (in.)		0.75	0.75
Tube thickness (in.)		0.049	0.028

$c = 0.005''$, layer thickness = $0.085''$, $T_{roll} = 70^\circ F$, $T_{operating} = \pm 300^\circ F$.

In both runs, the layer thickness is $0.085''$ so the ratio of outer radius/inner radius of the tubesheet model is 3.04. With this geometry, the upper limit of mechanical loading is governed by Eq. (7.C.26). Tables 7.C.4 and 7.C.5 show some computer output from the two simulations, assuming that the operating temperature is higher than the roll temperature. Note that with tubesheet #1, the limit on roll pressure is governed by the tubesheet yield strength. There is a significant plastic region in the tubesheet at the peak load. For the Cu-Ni/Cu-Ni combination, reversed yielding occurs in both tube and tubesheet, while for the Cu-Ni/steel combination, reversed

**Table 7.C.4. Cu-Ni/Cu-Ni Simulation
Tube yields prior to contact.**

(1) Loading Stage.											
Rolling Pressure (psi)	Contact Pressure (psi)	1	2	3	4	5	6	7	8	9	10
2541.9	.0	1*	0*	0	0	0	0	0	0	0	0
6000.0	3287	1	0	0	0	0	0	0	0	0	0
18000.0	15415.5	1	1	1	1	1	0	0	0	0	0
19660.0	17320.7	1	1	1	1	1	1	1	1	0	0
Contact Pressure Reaches Tubesheet Strength Control Value.											
(2) Unloading Stage.											
Rolling Pressure (psi)	Contact Pressure (psi)	1	2	3	4	5	6	7	8	9	10
18000.0	16129.4	0	0	0	0	0	0	0	0	0	0
10000.0	10418.	0	0	0	0	0	0	0	0	0	0
6000.0	7563.2	0	0	0	0	0	0	0	0	0	0
.0	2335.1	1	1	0	0	0	0	0	0	0	0
(3) Temperature Change Stage.											
Temperature (Degs.F.)	Contact Pressure (psi)	1	2	3	4	5	6	7	8	9	10
(A) Temperature Goes from Room Temp. to Operating Temp.											
70.0	2335.1	1	1	0	0	0	0	0	0	0	0
220.0	2235.	0	1	0	0	0	0	0	0	0	0
300.0	2181.2	0	1	0	0	0	0	0	0	0	0
(B) Temperature Goes from Operating Temp. to Room Temp.											
220.0	2238.6	0	0	0	0	0	0	0	0	0	0
70.0	2334.3	1	0	0	0	0	0	0	0	0	0

*"0" indicates elastic behavior, "1" indicates a yielded layer.

yield occurs only in the tube. For the Cu-Ni/Cu-Ni combination, there is a 6.5% reduction in tube-tubesheet contact pressure at the operating temperature of 300°F; the tubesheet layer remains in a yielded state. Upon removal of the temperature load, the full contact pressure is essentially recovered. In the Cu-Ni/steel combination, the limit on roll pressure is governed by the tube material and there is a relatively limited plastic zone in the tubesheet. During the thermal loading to 300°F, there is essentially no change in stress state during loading to operating temperature; removal of the thermal loading causes a significant reduction in final tube/tubesheet contact pressure. The rationale for this behavior will be discussed shortly, but we note here that the primary difference in behavior during thermal loading is caused by the difference in sign of quantity $(\alpha_T - \alpha_{TS})\Delta T$ in the two simulations. Table 7.C.6 presents the results of the Cu-Ni/Cu-Ni assemblage during thermal cycling to a lower temperature of -300°F. Notice that during cool-down the contact pressure remains essentially unchanged and there is a significant drop in contact pressure when ambient temperature is recovered. Only the temperature cycle is shown in Table 7.C.6; the roll process is the same as presented in Table 7.C.4.

Table 7.C.5. Cu-Ni/Steel Simulation
Tube yields prior to contact.

(1) Loading Stage.		Contact Pressure			Plastic Layers						
Rolling Pressure (psi)	Contact Pressure (psi)	1	2	3	4	5	6	7	8	9	10
1392.4	.0	1	0	0	0	0	0	0	0	0	0
4000.0	2527.	1	0	0	0	0	0	0	0	0	0
10000.0	8427.1	1	0	0	0	0	0	0	0	0	0
14000.0	12446.6	1	0	0	0	0	0	0	0	0	0
20780.0	19704.	1	1	0	0	0	0	0	0	0	0
Rolling Pressure Reaches Tube Strength Control Critical Value											
(2) Unloading Stage.		Contact Pressure			Plastic Layers						
Rolling Pressure (psi)	Contact Pressure (psi)	1	2	3	4	5	6	7	8	9	10
20000.0	19024.	0	0	0	0	0	0	0	0	0	0
14000.0	13823.	0	0	0	0	0	0	0	0	0	0
6000.0	6888.6	0	0	0	0	0	0	0	0	0	0
.0	1337.4	1	0	0	0	0	0	0	0	0	0
(3) Temperature Change Stage.		Contact Pressure			Plastic Layers						
Temperature (Degs.F.)	Contact Pressure (psi)	1	2	3	4	5	6	7	8	9	10
(A) Temperature Goes from Room Temp. to Operating Temp.											
70.0	1337.4	1	0	0	0	0	0	0	0	0	0
170.0	1337.9	1	0	0	0	0	0	0	0	0	0
300.0	1338.6	1	0	0	0	0	0	0	0	0	0
(B) Temperature Goes From Operating Temp. to Room Temp.											
270.0	1225.4	0	0	0	0	0	0	0	0	0	0
170.0	835.0	0	0	0	0	0	0	0	0	0	0
70.0	445.0	0	0	0	0	0	0	0	0	0	0

Table 7.C.6 Thermal Cycling of a Cu Ni/Cu Ni Assemblage to -300°F

(3) Temperature Change Stage.

Temperature (Degs.F.)	Contact Pressure (psi)	Plastic Layers									
		1	2	3	4	5	6	7	8	9	10
(A) Temperature Goes From Room Temp. to Operating Temp.											
70.0	2335.1	1	0	0	0	0	0	0	0	0	0
-80.0	2335.4	1	0	0	0	0	0	0	0	0	0
-230.0	2335.7	1	0	0	0	0	0	0	0	0	0
-300.0	2335.8	1	0	0	0	0	0	0	0	0	0
(B) Temperature Goes From Operating Temp. to Room Temp.											
-280.0	2314.5	0	1	0	0	0	0	0	0	0	0
-180.0	2202.4	0	1	0	0	0	0	0	0	0	0
-80.0	2090.3	0	1	0	0	0	0	0	0	0	0
70.0	1922.2	0	1	0	0	0	0	0	0	0	0

The final simulation demonstrating the application of the developed code, involves a Muntz tubesheet with either 70:30 Cu-Ni tubes (see Table 7.C.3) or Titanium tubing. The Muntz/Titanium combination is popular in the re-tubing of power plant condensers. Table 7.C.7 summarizes the tube/tubesheet properties and Tables 7.C.8 and 7.C.9 show the results of the simulation. The tube thickness is 0.028" in both cases.

Table 7.C.7. Titanium Tube/Muntz Tubesheet Properties

	Tube	Tubesheet
Material	Titanium	Muntz
E(psi)	1.49×10^7	1.5×10^7
σ_y (psi)	4.0×10^4	2.0×10^4
α_T	4.8×10^{-6}	11.6×10^{-6}
tube O.D. (in.)	0.75	
tube thickness (in.)	0.028	
$c = 0.005"$, layer thickness = 0.085", $T_{roll} = 70^\circ\text{F}$, $T_{operating} = 300^\circ\text{F}$		

We note the considerable reduction in residual contact pressure with the Titanium tubing. Because of the significant difference in thermal expansion coefficients between Titanium and Muntz, the increase in temperature to 187°F causes complete loss of tube to tubesheet contact pressure.

It remains for us to show why the contact pressure is essentially unchanged during thermal loading under certain conditions. Consider specifically the Cu-Ni/Cu-Ni assemblage reported in Tables 7.C.4-7.C.6. During any portion of the thermal cycle, the state of stress in the tube layer is

$$\sigma_\theta = -p_1 \frac{r_i}{h_i} + \sigma_r; \quad \sigma_r = -\frac{p_1}{2} \tag{7.C.27}$$

Hence

$$\sigma_{\theta} = \sigma_r \left(\frac{2r_i}{h_i} + 1 \right) \tag{7.C.28}$$

Figure 7.C.3 shows the $\sigma_r, \sigma_{\theta}$ plane for the entire load-unload-thermal cycle. Point 2 is the beginning of the mechanical rolling stage subsequent to tube/tubesheet contact. Point 3 is the end of the loading stage. Point 4 is the end of the unloading stage and shows that the tube undergoes reversed yield. Equation (7.C.28) is plotted on Fig. 7.C.3 through Point 4 and the origin. Regardless of the “direction” of thermal loading, the tube state must lie along this line (if one neglects small geometry changes). Point 5 is the end of the thermal load cycle reported in Table 7.C.4; the return to room temperature simply causes a return to Point 4 in Fig. 4. However, when the temperature is lowered in the run shown in Table 7.C.6, the tube cannot satisfy Eq. (7.C.28) and the yield condition unless there is no change in state of stress; that is, the tube state of stress would like to move to Point 6 but cannot go beyond the yield limit. An examination of expanded stress output for Table 7.C.7 (not shown here) indicates that the state of stress

**Table 7.C.8. 70:30 Cu-Ni/Muntz Simulation
Tube yields prior to contact.**

(1) Loading Stage.		Contact Pressure (psi)	Plastic Layers										
Rolling Pressure (psi)			1	2	3	4	5	6	7	8	9	10	
1392.4		.0	1	0	0	0	0	0	0	0	0	0	0
4000.0		2527.3	1	0	0	0	0	0	0	0	0	0	0
14000.0		12448.5	1	1	0	0	0	0	0	0	0	0	0
20000.0		18782.3	1	1	1	1	0	0	0	0	0	0	0
20780.0		19713.3	1	1	1	1	0	0	0	0	0	0	0
Rolling Pressure Reaches Tube Strength Control Value.													
(2) Unloading Stage.		Contact Pressure (psi)	Plastic Layers										
Rolling Pressure (psi)			1	2	3	4	5	6	7	8	9	10	
20780.0		19713.3	1	1	1	1	0	0	0	0	0	0	0
16000.0		15858.5	0	0	0	0	0	0	0	0	0	0	0
8000.0		8917.0	1	0	0	0	0	0	0	0	0	0	0
2000.0		3243.6	1	0	0	0	0	0	0	0	0	0	0
.0		1328.0	1	0	0	0	0	0	0	0	0	0	0
(3) Temperature Change Stage.		Contact Pressure (psi)	Plastic Layers										
Temperature (Degs.F.)			1	2	3	4	5	6	7	8	9	10	
(A) Temperature Goes From Room Temp. To Operating Temp.													
70.0		1328.0	1	0	0	0	0	0	0	0	0	0	0
220.0		770.9	0	0	0	0	0	0	0	0	0	0	0
300.0		472.	0	0	0	0	0	0	0	0	0	0	0
(B) Temperature Goes From Operating Temp. to Room Temp.													
270.0		584.1	0	0	0	0	0	0	0	0	0	0	0
170.0		957.8	0	0	0	0	0	0	0	0	0	0	0
70.0		1328.0	1	0	0	0	0	0	0	0	0	0	0

remains essentially unchanged throughout the entire unit while the temperature falls to -300°F . Subsequent heating of the unit, then causes the point in stress state to move toward the origin in an elastic manner.

**Table 7.C.9. Titanium/Muntz Simulation
Tube yields prior to contact.**

(1) Loading Stage.		Plastic Layers									
Rolling Pressure (psi)	Contact Pressure (psi)	1	2	3	4	5	6	7	8	9	10
3095.1	.0	1	0	0	0	0	0	0	0	0	0
8000.0	4752.6	1	0	0	0	0	0	0	0	0	0
16000.0	12579.4	1	1	0	0	0	0	0	0	0	0
20000.0	16534.2	1	1	1	0	0	0	0	0	0	0
26520.0	23093.5	1	1	1	1	1	1	1	1	0	0
Contact Pressure Reaches Tubesheet Strength Control Value.											
(2) Unloading Stage.		Plastic Layers									
Rolling Pressure (psi)	Contact Pressure (psi)	1	2	3	4	5	6	7	8	9	10
26000.0	22650.6	0	0	0	0	0	0	0	0	0	0
20000.0	17565.	0	0	0	0	0	0	0	0	0	0
12000.0	10787.2	0	0	0	0	0	0	0	0	0	0
6000.0	5705.2	0	0	0	0	0	0	0	0	0	0
2000.0	2397.2	0	1	0	0	0	0	0	0	0	0
.0	771.2	0	1	0	0	0	0	0	0	0	0
(3) Temperature Change Stage.		Plastic Layers									
Temperature (Degr.F.)	Contact Pressure (psi)	1	2	3	4	5	6	7	8	9	10
(A) Temperature Goes From Room Temp. to Operating Temp.											
70.0	771.2	0	1	0	0	0	0	0	0	0	0
170.0	109.7	0	1	0	0	0	0	0	0	0	0
187.0	-2.6	0	1	0	0	0	0	0	0	0	0

No Contact Analysis Between Tube and Tubesheet. Joint Fails.

Coefficients of Eq. (7.C.12)

To establish the coefficients define the quantities

$$\bar{s}_j = (\sigma_{\theta j} - \sigma_{rj})/4G_j; \quad \bar{u}_j = 1 - 2\bar{s}_j$$

$$A_{j1} = \frac{1}{\bar{u}_j} \left[\bar{s}_j - \frac{1}{2} + \frac{r_j}{h_j} \right] + \frac{\nu}{2}$$

$$A_{j2} = \frac{1}{\bar{u}_j} \left[\bar{s}_j - \frac{1}{2} - \frac{r_j}{h_j} \right] + \frac{\nu}{2}$$

$$A_{j3} = \frac{\sigma_{\theta j} - \sigma_{rj}}{\bar{u}_j} + E_j$$

$G_j, E_j =$ Shear modulus, Young's Modulus of layer j

$$A_{j4} = \frac{\nu}{\bar{u}_j} \left[\bar{s}_j - \frac{1}{2} + \frac{r_j}{h_j} \right] + \frac{1}{2}$$

$$A_{j5} = \frac{\nu}{\bar{u}_j} \left[\bar{s}_j - \frac{1}{2} - \frac{r_j}{h_j} \right] + \frac{1}{2}$$

$$A_{j6} = \frac{\nu(\sigma_{\theta j} - \sigma_{rj})}{\bar{u}_j} + E_j$$

$$A_j = -\frac{r_j}{E_j} [A_{j1} - h_j A_{j4} / 2r_j]; \quad A_j^* = \frac{r_j}{E_j} [A_{j2} - h_j A_{j5} / 2r_j]$$

$$B_j = \frac{r_{j+1}}{E_{j+1}} (A_{(j+1)1} + \frac{h_{j+1}}{2r_{j+1}} A_{(j+1)4}) - A_j^*$$

$$C_j = \frac{r_{j+1}}{E_{j+1}} [A_{(j+1)2} + h_{j+1} A_{(j+1)5} / 2r_{j+1}]$$

Next, if $\bar{A}_j, \bar{B}_j, \bar{C}_j, \bar{D}_j$ are defined as

$$\bar{A}_j = \frac{r_{j+1}}{E_{j+1}} \left[A_{(j+1)3} + \frac{\nu h_{j+1}}{2r_{j+1}} \frac{(\sigma_{\theta j+1} - \sigma_{rj+1})}{\bar{u}_{j+1}} \right]$$

$$j=0, 1, \dots, 9$$

$$\bar{B}_j = \frac{r_{j+1}}{E_{j+1}} \left[\frac{h_{j+1} A_{(j+1)6}}{2r_{j+1}} + \frac{(\sigma_{\theta j+1} - \sigma_{rj+1})}{\bar{u}_{j+1}} \right]$$

$$\bar{C}_j = \frac{r_j}{E_j} \left[A_{j3} - \frac{\nu h_j}{2r_j} \frac{(\sigma_{\theta j} - \sigma_{rj})}{\bar{u}_j} \right]$$

$$j=1, 2, \dots, 10$$

$$\bar{D}_j = \frac{r_j}{E_j} \left[\frac{h_j A_{j6}}{2r_j} - \frac{(\sigma_{\theta j} - \sigma_{rj})}{\bar{u}_j} \right]$$

then

$$D_j = \frac{1}{3} (\bar{C}_j - 2\bar{D}_j) \sigma_{rj} - \frac{1}{3} (2\bar{C}_j - \bar{D}_j) \sigma_{\theta j}$$

$$D_j^* = -\frac{1}{3} (\bar{A}_j + 2\bar{B}_j) \sigma_{rj+1} + \frac{1}{3} (2\bar{A}_j + \bar{B}_j) \sigma_{\theta j+1}$$

Finally, the right-hand side is

$$R_j = r_j(1 + h_j/2r_j)\alpha_j - r_{j+1}(1 - h_{j+1}/2r_{j+1})\alpha_{j+1}$$

where α_j = coefficient of thermal expansion of layer j .

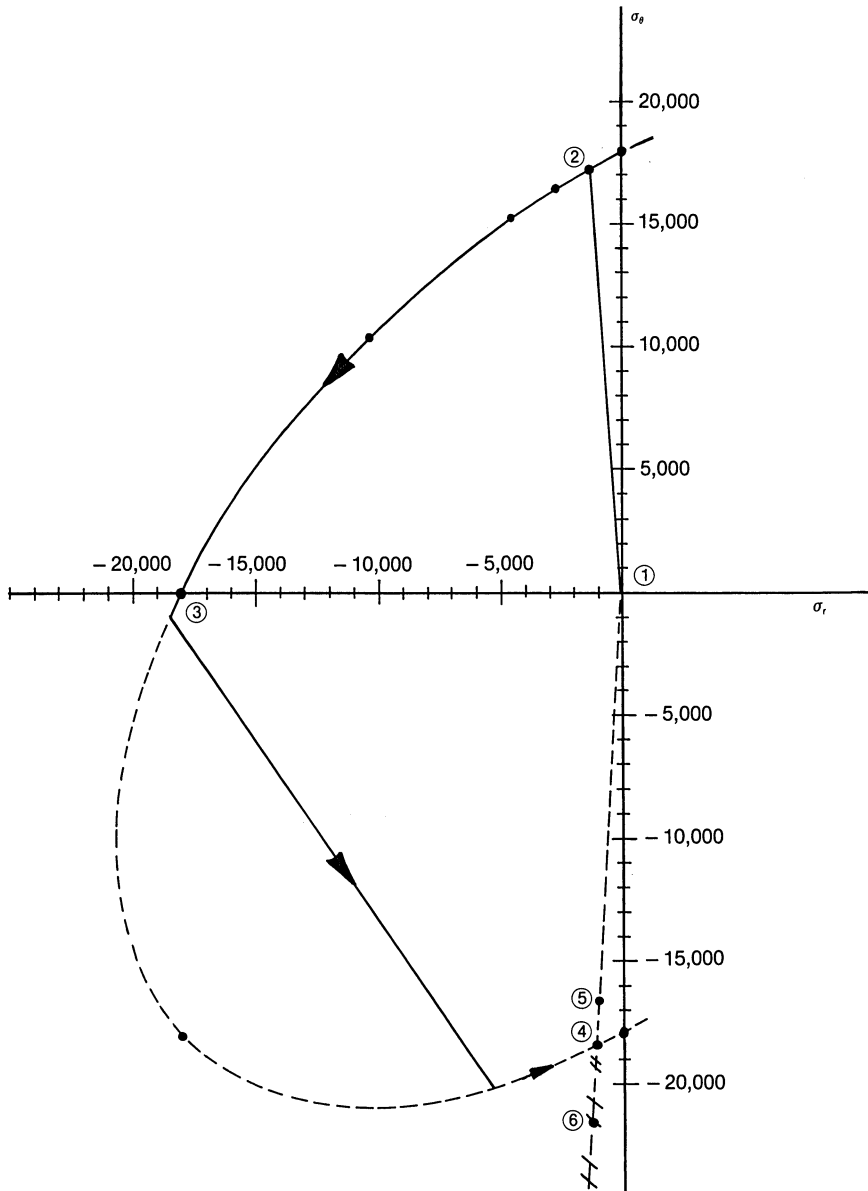


Fig. 7.C.3. σ_r vs σ_θ (Cu-Ni tube and tubesheet materials).

Coefficients of Eq. (7.C.15)

$$F_i = \frac{(2\sigma_{\theta j} - \sigma_{rj})}{\bar{u}_j} \left(\bar{s}_j - \frac{1}{2} + \frac{r_j}{h_j} \right) - \frac{1}{2} (2\sigma_{rj} - \sigma_{\theta j})$$

$$M_j = \frac{(2\sigma_{\theta j} - \sigma_{rj})}{\bar{u}_j} \left(\bar{s}_j - \frac{1}{2} - \frac{r_j}{h_j} \right) - \frac{1}{2} (2\sigma_{rj} - \sigma_{\theta j})$$

$$H_j = (2\sigma_{\theta j} - \sigma_{rj})(\sigma_{\theta j} - \sigma_{rj})^2 / \bar{u}_j$$

APPENDIX 7.D**USER MANUAL AND COMPUTER CODE FOR TUBE ROLLING PROGRAM GENROLL****1. Introduction**

This program is for an elastic-plastic analysis for tube rolling process, using the analysis of Appendix 7.C.

This process can be divided into three stages:

- 1) Loading stage: The internal pressure applied to the tube increases from zero to a max. value causing tube and tubesheet to produce elastic and plastic deformations.
- 2) Unloading stage: The internal pressure applied to the tube decreases from a max. value to zero, and a certain amount of residual contact pressure between tube and tubesheet remains at the end of the unloading stage.
- 3) Temperature change stage: The residual contact pressure changes due to different values of thermal expansion coefficients of tube and tubesheet materials during heating/cooling.

2. Input Data from Data File (Logical Unit Number [LUN]14)**LINE 1**

- DOUT – tube outside diameter (in.)
 T0 – tube wall thickness (in.)
 ANU – Poisson's ratio

LINE 2

- C – radial clearance (in.)
 P00 – assumed maximum rolling pressure (psi)
 TOP – unit operating temperature (°F)
 (the assembly temperature is taken at 70°F)

LINE 3

- DP00 – value of rolling pressure increment (< 10 psi)
 DT0 – value of temperature increment ($< 1^{\circ}\text{F}$)
 HS – tubesheet layer thickness (in.)

LINE 4

- PSTEP – printout step size during mechanical loading and unloading stage (psi)
 TSTEP – printout step size during thermal loading and unloading stage ($^{\circ}\text{F}$)
 NPR = 0 normal printout
 = 1 expanded printout including layer stresses and displacements
 NRETUN = 0 no return to assembly temperature after a thermal change
 > 0 incremental return to assembly temperature after a thermal loading

3. Input from Terminal (Logical Unit Number [LUN5])

- ET – Young's Modulus of Tube Material (psi)
 SYT – Yield stress of tube material (psi)
 ALPHAT – coefficient of thermal expansion of tube material (in./in. $^{\circ}\text{F}$)
 ES }
 SYS } Same as above for tubesheet material
 ALPHAS }

PROGRAM GENROLL

C TUBE ROLLING PROGRAM. OCT.1982, BY XU HONG AND A.I.SOLER
 C THIS PROGRAM IS A ELASTIC-PLASTIC ANALYSIS OF TUBE-TUBESHEET ROLLING
 C JOINT. THE RESIDUAL CONTACT PRESSURE BETWEEN TUBE AND TUBESHEET DEPENDS
 C UPON FOLLOWING FACTORS:
 C (1) STRUCTURAL GEOMETRY:RADIUS AND THICKNESS OF THE TUBE,CLEARANCE;
 C (2) MECHANICAL PROPERTIES OF TUBE AND TUBESHEET MATERIALS;
 C (3) THE MAXIMUM ROLLING PRESSURE;
 C (4) THE TEMPERATURE CHANGE FROM ASSEMBLING TEMP.TO OPERATING TEMP..
 C****USER SHOULD SET COMPUTER TO INITIALIZE ALL VARIABLES TO ZERO****
 C

```

DIMENSION P(10),DP(9),
&          ALAMD(10),DPJM1(10),DPJ(10),ETI(10),ERI(10),
&          ETJ(10),ERJ(10),SRT(10),STR(10),B1(10),B2(10),
&          DEPSR(10),DEPST(10),DUUP(10),DIS(10),DPIM1(10),DPI(10)
DIMENSION KJ1(10)
COMMON /TT/ET,ANU,ALPHAT,T,GT
COMMON /SS/ES,ALPHAS,HS,GS
COMMON /DD/DPO,DT
COMMON /AA/R(10),ST(10),SR(10),EQUI(10)

```

```

COMMON /CC/A(19,19),B(19)
COMMON /KK/K(10)
COMMON /LL/TTH(10)
C
C INPUT DATA FROM DATA FILE.
  READ(14,*)DOUT,TO,ANU
  READ(14,*)C,POO, TOP,TROLL
  READ(14,*)DPOO,DTO,HS
  READ(14,*)PSTEP,TSTEP,NPR,NRETUN
C NWR----PRINTOUT IN EACH STAGE WILL BE 'NWR' TIMES.
C NPR=0,NORMAL PRINTOUT;
C NPR=1,PRINTOUT INCLUDES STRESSES AND DISPLACEMENT OF EACH LAYER.
C INPUT DATA FROM TERMIMAL.
  WRITE(6,*)'PROGRAM IS RUNNING.....'
  WRITE(6,*)'INPUT ET,SYT,ALPHAT,ES,SYS,ALPHAS, IN FREE FORMAT.'
  READ(5,*)ET,SYT,ALPHAT,ES,SYS,ALPHAS
C
C PRINTOUT INPUT DATA.
  WRITE(6,*)'***** INPUT DATA *****'
  WRITE(6,*)'TUBE OUTSIDE DIAMETER,DOUT=',DOUT,'(IN)'
  WRITE(6,*)'TUBE WALLTHICKNESS,TO=',TO,'(IN)'
  WRITE(6,*)'POISSON RATIO,ANU=',ANU
  WRITE(6,*)'RADIUS CLEARANCE,C=',C,'(IN)'
  WRITE(6,*)'MAXIMUM ROLLING PRESSURE,POO=',POO,'(PSI)'
  WRITE(6,*)'ROLLING TEMPERATURE,TROLL=',TROLL,'(DEGS.F.)'
  WRITE(6,*)'OPERATING TEMPERATURE, TOP=',TOP,'(DEGS.F.)'
  WRITE(6,*)'STEP SIZE OF ROLLING PRESSURE INCREMENT,DPOO=',DPOO,'(P
&SI)'
  WRITE(6,*)'STEP SIZE OF TEMPERATURE INCREMENT,DTO=',DTO,'(DEGS.F.)
&'
  WRITE(6,*)'LAYER THICKNESS ASSUMED,HS=',HS,'(IN)'
  WRITE(6,*)'PRINTOUT STEP SIZE FOR ROLLING PRESSURE,PSTEP=',PSTEP
  WRITE(6,*)'PRINTOUT STEP SIZE FOR TEMPERATURE,TSTEP=',TSTEP
  WRITE(6,*)'PRINTOUT OPTIONS,NPR=',NPR
  WRITE(6,*)'TEMPERATURE RETURN OPTIONS,NRETUN=',NRETUN
  WRITE(6,*)
  WRITE(12,*)'***** INPUT DATA *****'
  WRITE(12,*)'TUBE OUTSIDE DIAMETER,DOUT=',DOUT,'(IN)'
  WRITE(12,*)'TUBE WALLTHICKNESS,TO=',TO,'(IN)'
  WRITE(12,*)'POISSON RATIO,ANU=',ANU
  WRITE(12,*)'RADIUS CLEARANCE,C=',C,'(IN)'
  WRITE(12,*)'MAXIMUM ROLLING PRESSURE,POO=',POO,'(PSI)'
  WRITE(12,*)'ROLLING TEMPERATURE,TROLL=',TROLL,'(DEGS.F.)'
  WRITE(12,*)'OPERATING TEMPERATURE, TOP=',TOP,'(DEGS.F.)'
  WRITE(12,*)'STEP SIZE OF ROLLING PRESSURE INCREMENT,DPOO=',DPOO,'(
&PSI)'
  WRITE(12,*)'STEP SIZE OF TEMPERATURE INCREMENT,DTO=',DTO,'(DEGS.F.
&)'
  WRITE(12,*)'LAYER THICKNESS ASSUMED,HS=',HS,'(IN)'
  WRITE(12,*)'PRINTOUT STEP SIZE FOR ROLLING PRESSURE,PSTEP=',PSTEP
  WRITE(12,*)'PRINTOUT STEP SIZE FOR TEMPERATURE,TSTEP=',TSTEP
  WRITE(12,*)'PRINTOUT OPTIONS,NPR=',NPR
  WRITE(12,*)'TEMPERATURE RETURN OPTIONS,NRETUN=',NRETUN

```



```

REDS=ANU*PP*PP/(TOR*TOR*GGG2*ET)+PP*(0.5+1.0/TOR)/3.0
REDC=- (2.0/TOR-0.5)/(TOR*TOR*GGG2*((2.0/TOR-0.5)*GGG1/GGG2
&      +0.5/TOR+0.25))
REDA=((GGG1*REDC+1.0/(TOR*TOR))/GGG2+0.5*ANU*REDC)*PP*PP/ET
&      +PP*(2.0/TOR-0.5)/3.0
OMEGA=(REDT*REDC*PP*PP-REDS)/REDA
RSTA=RO*(1.0+(1.0/TOR-0.5+0.5*ANU)*PP/ET)
TSTA=TO*(1.0+(0.5*ANU-0.5-ANU/TOR)*PP/ET)
RE=RSTA+0.5*TSTA
RHOLE=0.5*DOUT+C
DTP=OMEGA*TSTA/RSTA*(RHOLE-RE)/(1.+0.5*TSTA/RSTA*OMEGA)
T=TO+DTE+DTP
GO TO 200
100  WRITE(6,*)
      WRITE(6,*)'TUBE REMAINS ELASTIC WHEN CONTACT BEGINS.'
      WRITE(12,*)
      WRITE(12,*)'TUBE REMAINS ELASTIC WHEN CONTACT BEGINS.'
C INITIAL CONTACT STATE FOR ELASTIC TUBE CASE:
CCC=TO*(ANU/TOR+0.5-0.5*ANU)-2.0*RO*(1.0/TOR-0.5+0.5*ANU)
PO=-2.0*ET*C/CCC
T=TO*(1.0+2.0*C*(ANU/TOR+0.5-0.5*ANU)/CCC)
C
C SOME INITIAL VALUES AND CONSTANTS.
200  R(1)=0.5*DOUT+C-0.5*T
      TOR=T/R(1)
      SQT=SQRT(1.-.5*TOR+.25*TOR*TOR)
      IF(NPLAS.EQ.1)PO=TOR*SYT/SQT
      DO 300 I=1,9
          J=I+1
          R(J)=0.5*DOUT+C+(0.5+FLOAT(I-1))*HS
          P(I)=0.0
          DIS(I)=0.0
          ALAMD(I)=0.0
          TTH(I)=HS
          IF(I.EQ.1) TTH(1)=T
300  CONTINUE
      IF(NPLAS.EQ.1)ALAMD(1)=DTP/(OMEGA*TSTA*REDA)
      P(10)=0.0
      DIS(10)=0.0
      ALAMD(10)=0.0
      TTH(10)=HS
      TEMP=TROLL
      PCRIT=SYT*SQRT(4.0/3.0)
      PCRIS=SYS*SQRT(4.0/3.0)
      DO 350 I=1,10
          K(I)=0
350  CONTINUE
      IF(NPLAS.EQ.1) K(1)=1
C
      IF(NPLAS.EQ.1)KJ1(1)=1
C TO CHECK MAXIMUM ROLLING PRESSURE WHETHER TOO SMALL.
      IF(PO0.GT.PO) GO TO 500

```

```

WRITE(6,*)
WRITE(6,*)'P00=',P00,';    P0=',P0
WRITE(6,*)'MAXIMUM ROLLING PRESSURE TOO SMALL.INITIAL CONTACT CAN
&NOT OCCUR.'
WRITE(12,*)
WRITE(12,*)'P00=',P00,';    P0=',P0
WRITE(12,*)'MAXIMUM ROLLING PRESSURE TOO SMALL.INITIAL CONTACT CAN
& NOT OCCUR.'
WRITE(6,*)'INPUT NEW ROLLING PRESSURE: P00, IN FREE FORMAT.'
WRITE(6,*)'OR INPUT -1.0/ TO STOP.'
READ(5,*)P00
IF(P00.GT.-0.99) GO TO 50
STOP

```

C

C

500 NSTAGE=1

C NSTAGE=1 IS LOADING STAGE CONTROLLER

PPP=P0/PSTEP

KK=IFIX(PPP)+1

DPO=DPO0

DT=0.0

WRITE(6,*)

WRITE(6,*)

WRITE(6,*)' (1) LOADING STAGE.'

WRITE(6,*)'ROLLING PRESSURE CONTACT PRESSURE PLASTIC LAYERS

& PRESSURES BETWEEN LAYERS (PSI)

& TUBE'

WRITE(6,*)' (PSI) (PSI) 1 2 3 4 5 6 7 8 9 10

& 2-3 3-4 4-5 5-6 6-7 7-8 8-9 9-10

& THK.'

WRITE(6,*)

WRITE(12,*)

WRITE(12,*)

WRITE(12,*)' (1) LOADING STAGE.'

WRITE(12,*)'ROLLING PRESSURE CONTACT PRESSURE PLASTIC LAYERS

& PRESSURES BETWEEN LAYERS (PSI)

& TUBE'

WRITE(12,*)' (PSI) (PSI) 1 2 3 4 5 6 7 8 9 1

&0 2-3 3-4 4-5 5-6 6-7 7-8 8-9 9-10

& THK.'

WRITE(12,*)

550 FORMAT(3X,F8.1,10X,F9.1,4X,10(I2),3X,8(F6.0,2X),F7.6)

NN=1

C TO COMPUTE STRESSES FOR EACH LAYER.

SR(1)=-0.5*(P0+P(1))

ST(1)=(P0-P(1))*R(1)/TTH(1)+SR(1)

DO 700 I=2,10

SR(I)=-0.5*(P(I-1)+P(I))

ST(I)=(P(I-1)-P(I))*R(1)/TTH(I)+SR(I)

700 CONTINUE

600 CONTINUE

C

C TO COMPUTE INTERFACE DISPLACEMENTS AND LAYER THICKNESSES.

```

C (1) INITIAL VALUES OF INTERFACE DISPLACEMENTS.
      IF(NSTAGE.NE.1) GO TO 3500
      IF (NN.NE.1) GO TO 3500
      GO TO 10000
C (2) TO COMPUTE CURRENT VALUES OF DIS(I) AND TTT.
3500 DO 4200 I=1,10
      IF(ALAMD(I).EQ.0.)KJ1(I)=0
      IF(ALAMD(I).NE.0.)KJ1(I)=IFIX(ALAMD(I)/ABS(ALAMD(I)))
      IF(I.EQ.1) GO TO 4000
      E=ES
      GO TO 4100
4000 E=ET
4100 DPJM1(1)=- (0.5+ANU*R(I)/TTH(I)-0.5*ANU)/E
      DPJ(I)=(-0.5+ANU*R(I)/TTH(I)+0.5*ANU)/E
      DPIM1(I)=(R(I)/TTH(I)-0.5+0.5*ANU)/E
      DPI(I)=(-R(I)/TTH(I)-0.5+0.5*ANU)/E
      ERI(I)=(ST(I)-SR(I))/E
      ETI(I)=1.0-ERI(I)
      STR(I)=(2.0*ST(I)-SR(I))/3.0
      ETJ(I)=ANU*ERI(I)
      ERJ(I)=1.0-ETJ(I)
      SRT(I)=(2.0*SR(I)-ST(I))/3.0
4200 CONTINUE
      B1(1)=DPJM1(1)*DPO+DPJ(1)*DP(1)+SRT(1)*ALAMD(1)+ALPHAT*DT
      B2(1)=DPIM1(1)*DPO+DPI(1)*DP(1)+STR(1)*ALAMD(1)+ALPHAT*DT
      DO 4300 I=2,9
          B1(I)=DPJM1(I)*DP(I-1)+DPJ(I)*DP(I)+SRT(I)*ALAMD(I)+ALPHAS*DT
          B2(I)=DPIM1(I)*DP(I-1)+DPI(I)*DP(I)+STR(I)*ALAMD(I)+ALPHAS*DT
4300 CONTINUE
      B1(10)=DPJM1(10)*DP(9)+SRT(10)*ALAMD(10)+ALPHAS*DT
      B2(10)=DPIM1(10)*DP(9)+STR(10)*ALAMD(10)+ALPHAS*DT
      DO 5300 I=1,10
          DEPSR(I)=(ETI(I)*B1(I)-ETJ(I)*B2(I))/(ERJ(I)*ETI(I)
          &          -ETJ(I)*ERI(I))
          DEPST(I)=(B2(I)-ERI(I)*DEPSR(I))/ETI(I)
          DUUP(I)=R(I)*DEPST(I)+0.5*TTH(I)*DEPSR(I)
C DIS(I) IS INTERFACE DISPLACEMENT BETWEEN I AND I+1 LAYERS.
      DIS(I)=DIS(I)+DUUP(I)
C TTH(I) IS THE CURRENT VALUE OF I-TH LAYER THICKNESS.
      TTH(I)=TTH(I)*(1.0+DEPSR(I))
      R(I)=R(I)*(1.0+DEPST(I))
5300 CONTINUE
      SR(1)=-.5*(PG+P(1))
      ST(1)=(PO-P(1))*R(1)/TTH(1)+SR(1)
      DO 70000 I=2,10
          SR(I)=-.5*(P(I-1)+P(I))
          ST(I)=(P(I-1)-P(I))*R(I)/TTH(1)+SR(I)
70000 CONTINUE
C
C TO CHECK WHETHER EACH LAYER YIELDS OR NOT.
C (IF YIELD,K=1;IF NOT YIELD,K=0)
      IF(NSTAGE.EQ.4) GO TO 30000

```

```

        IF(NSTAGE.EQ.3) GO TO 30000
        IF(NSTAGE.EQ.2) GO TO 20000
C TO DETERMINE K(I) FOR LOADING STAGE.
10000 DO 11000 I=1,10
        IF(K(I).EQ.0) GO TO 10050
C DURING LOADING STAGE, ONCE A LAYER YIELDS, IT REMAINS YIELD.
        K(I)=1
        IF(I.EQ.1) GO TO 10020
        EQUI(I)=SYS
        GO TO 11000
10020  EQUI(1)=SYT
        GO TO 11000
10050  EQUI(I)=SQRT(ST(I)*ST(I)-ST(I)*SR(I)+SR(I)*SR(I))
        IF(I.EQ.1) GO TO 10200
        IF(EQUI(I).LT.SYS) GO TO 10100
        EQUI(I)=SYS
        K(I)=1
        GO TO 11000
10100  K(I)=0
        GO TO 11000
10200  IF(EQUI(1).LT.SYT) GO TO 10300
        EQUI(1)=SYT
        K(1)=1
        GO TO 11000
10300  K(I)=0
11000 CONTINUE
        GO TO 8000
C TO DETERMINE K(I) FOR UNLOADING STAGE.
C DURING UNLOADING K(I)=0, UNLESS REVERSED YIELD TAKES PLACE.
C (REVERSED YIELD CONDITION: ST(I)<SR(I) AND EQUI(I)>SYT (OR SYS))
20000 DO 22000 I=1,10
        EQUI(I)=SQRT(ST(I)*ST(I)-ST(I)*SR(I)+SR(I)*SR(I))
        IF(ST(I).LT.SR(I)) GO TO 20100
        K(I)=0
        IF(I.EQ.1) GO TO 20050
        IF(EQUI(I).GT.SYS) EQUI(I)=SYS
        GO TO 22000
20050  IF(EQUI(1).GT.SYT) EQUI(1)=SYT
        GO TO 22000
20100  IF(I.EQ.1) GO TO 20300
        IF(EQUI(I).LT.SYS) GO TO 20200
        K(I)=1
        EQUI(I)=SYS
        GO TO 22000
20200  K(I)=0
        GO TO 22000
20300  IF(EQUI(I).LT.SYT) GO TO 20400
        K(1)=1
        EQUI(1)=SYT
        GO TO 22000
20400  K(1)=0
22000 CONTINUE

```

```

GO TO 8000
C TO DETERMINE K(I) FOR TEMPERATURE CHANGE STAGE.
30000 DO 33000 I=1,10
    EQUI(I)=SQRT(ST(I)*ST(I)-ST(I)*SR(I)+SR(I)*SR(I))
    IF(((ALPHAT-ALPHAS)*DT).GE.0.0) GO TO 32000
C FOR CONTRACTION CASE:
    IF(I.EQ.1) GO TO 31200
    IF(EQUI(I).GT.SYS) EQUI(I)=SYS
    K(I)=0
    IF(EQUI(I).EQ.SYS) K(I)=1
    IF(EQUI(I).EQ.SYS.AND.ALAMD(I).LT.0.0) K(I)=0
    GO TO 33000
31200 IF(EQUI(1).GT.SYT) EQUI(1)=SYT
    K(1)=0
    GO TO 33000
C FOR EXPANSION CASE:
32000 IF(I.EQ.1) GO TO 32300
    IF(EQUI(I).LT.SYS) GO TO 32100
    EQUI(I)=SYS
    K(I)=1
    IF(EQUI(I).EQ.SYS.AND.ALAMD(I).LT.0.) K(I)=0
    GO TO 33000
32100 K(I)=0
    GO TO 33000
32300 IF(EQUI(1).LT.SYT) GO TO 32400
    EQUI(1)=SYT
    K(1)=1
    GO TO 33000
32400 K(I)=0
33000 CONTINUE
C
C PRINTOUT INITIAL VALUES FOR EACH STAGE OF THE THREE.
8000 IF(NN.NE.1) GO TO 750
    IF(NSTAGE.EQ.4) GO TO 720
    IF(NSTAGE.EQ.3) GO TO 720
    WRITE(6,550)PO,P(1),(KJ1(I),I=1,10),(P(I),I=2,9),TTH(1)
    WRITE(12,550)PO,P(1),(KJ1(I),I=1,10),(P(I),I=2,9),TTH(1)
    IF(NPR.EQ.0) GO TO 740
    WRITE(6,705)(DIS(I),I=1,9)
    WRITE(6,706)(TTH(I),I=2,10)
    WRITE(6,710)(ST(I),I=1,10)
    WRITE(6,715)(SR(I),I=1,10)
    WRITE(6,718)(EQUI(I),I=1,10)
    WRITE(12,705)(DIS(I),I=1,9)
    WRITE(12,706)(TTH(I),I=2,10)
    WRITE(12,710)(ST(I),I=1,10)
    WRITE(12,715)(SR(I),I=1,10)
    WRITE(12,718)(EQUI(I),I=1,10)
    WRITE(6,*)
    WRITE(12,*)
705 FORMAT(1X,28HINTERFACE DISPLACEMENTS(IN):,9(2X,F9.7))
706 FORMAT(1X,28H LAYER THICKNESSES (IN.):,9(2X,F9.7))

```

```

710  FORMAT(1X,6HST(I):,2X,10(3X,F8.1))
715  FORMAT(1X,6HSR(I):,2X,10(3X,F8.1))
718  FORMAT(1X,8HEQUI(I):,10(3X,F8.1))
      GO TO 740
720  WRITE(6,1380)TEMP,P(1),(KJ1(I),I=1,10),(P(I),I=2,9),TTH(1)
      WRITE(12,1380)TEMP,P(1),(KJ1(I),I=1,10),(P(I),I=2,9),TTH(1)
      IF(NPR.EQ.0) GO TO 740
      WRITE(6,705)(DIS(I),I=1,9)
      WRITE(6,706)(TTH(I),I=2,10)
      WRITE(6,710)(ST(I),I=1,10)
      WRITE(6,715)(SR(I),I=1,10)
      WRITE(6,718)(EQUI(I),I=1,10)
      WRITE(12,705)(DIS(I),I=1,9)
      WRITE(12,706)(TTH(I),I=2,10)
      WRITE(12,710)(ST(I),I=1,10)
      WRITE(12,715)(SR(I),I=1,10)
      WRITE(12,718)(EQUI(I),I=1,10)
      WRITE(6,*)
      WRITE(12,*)
740  IF(NSTAGE.EQ.1) GO TO 750
      NN=2
C
C TO CHECK INCREMENTS OF ROLLING PRESSURE AND TEMP.FOR PRINTOUT.
750  IF(NSTAGE.EQ.3) GO TO 1400
      IF(NSTAGE.EQ.2) GO TO 900
      IF(NSTAGE.EQ.4) GO TO 1570
C
C PRINTOUT FOR LOADING STAGE.
      IF(PO.LT.(FLOAT(KK)*PSTEP)) GO TO 800
      WRITE(6,550)PO,P(1),(KJ1(I),I=1,10),(P(I),I=2,9),TTH(1)
      WRITE(12,550)PO,P(1),(KJ1(I),I=1,10),(P(I),I=2,9),TTH(1)
      IF(NPR.EQ.0) GO TO 760
      WRITE(6,705)(DIS(I),I=1,9)
      WRITE(6,706)(TTH(I),I=2,10)
      WRITE(6,710)(ST(I),I=1,10)
      WRITE(6,715)(SR(I),I=1,10)
      WRITE(6,718)(EQUI(I),I=1,10)
      WRITE(12,705)(DIS(I),I=1,9)
      WRITE(12,706)(TTH(I),I=2,10)
      WRITE(12,710)(ST(I),I=1,10)
      WRITE(12,715)(SR(I),I=1,10)
      WRITE(12,718)(EQUI(I),I=1,10)
      WRITE(6,*)
      WRITE(12,*)
760  KK=KK+1
C
C CHECK FOR LOADING STAGE---FOR MAXIMUM ROLLING PRESSURE.
800  IF((PCRIT-PO).LE.DP00) GO TO 810
      IF((PCRIS-P(1)).LE.DP00) GO TO 820
      IF(K(9).EQ.1) GO TO 830
      IF(PO.LT.P00) GO TO 1600
      WRITE(6,550)PO,P(1),(KJ1(I),I=1,10),(P(I),I=2,9),TTH(1)
      WRITE(6,*)'ROLLING PRESSURE REACHES PRE-SPECIFIED VALUE.'

```

```

WRITE(12,550)PO,P(1),(KJ1(I),I=1,10),(P(I),I=2,9),TTH(1)
WRITE(12,*)'ROLLING PRESSURE REACHES PRE-SPECIFIED VALUE.'
GO TO 840
810 WRITE(6,550)PO,P(1),(KJ1(I),I=1,10),(P(I),I=2,9),TTH(1)
WRITE(6,*)'ROLLING PRESSURE REACHES TUBE STRENGTH CONTROL CRITICAL
& VALUE.'
WRITE(12,550)PO,P(1),(KJ1(I),I=1,10),(P(I),I=2,9),TTH(1)
WRITE(12,*)'ROLLING PRESSURE REACHES TUBE STRENGTH CONTROL CRITICA
&L VALUE.'
GO TO 840
820 WRITE(6,550)PO,P(1),(KJ1(I),I=1,10),(P(I),I=2,9),TTH(1)
WRITE(6,*)'CONTACT PRESSURE REACHES TUBESHEET STRENGTH CONTROL CRI
&TICAL VALUE.'
WRITE(12,550)PO,P(1),(KJ1(I),I=1,10),(P(I),I=2,9),TTH(1)
WRITE(12,*)'CONTACT PRESSURE REACHES TUBESHEET STRENGTH CONTROL CR
&ITICAL VALUE.'
GO TO 840
830 WRITE(6,550)PO,P(1),(KJ1(I),I=1,10),(P(I),I=2,9),TTH(1)
WRITE(6,*)'ALL LAYERS EXCEPT THE OUTERMOST LAYER YIELD.'
WRITE(12,550)PO,P(1),(KJ1(I),I=1,10),(P(I),I=2,9),TTH(1)
WRITE(12,*)'ALL LAYERS EXCEPT THE OUTERMOST LAYER YIELD.'
POMAX=PO
840 NSTAGE=2
PFINAL=PO
PFF=PSTEP*FLOAT(IFIX(PFINAL/PSTEP))
C NSTAGE=2 IS UNLOADING STAGE CONTROLER.
KK=1
DPO=-DPOO
DT=0.0
WRITE(6,*)
WRITE(6,*)
WRITE(6,*)'(2) UNLOADING STAGE.'
WRITE(6,*)'ROLLING PRESSURE CONTACT PRESSURE PLASTIC LAYERS
& PRESSURES BETWEEN LAYERS (PSI)
& TUBE'
WRITE(6,*)'(PSI) (PSI) 1 2 3 4 5 6 7 8 9 10
& 2-3 3-4 4-5 5-6 6-7 7-8 8-9 9-10
& THK.'
WRITE(6,*)
WRITE(12,*)
WRITE(12,*)
WRITE(12,*)'(2) UNLOADING STAGE.'
WRITE(12,*)'ROLLING PRESSURE CONTACT PRESSURE PLASTIC LAYERS
& PRESSURES BETWEEN LAYERS (PSI)
& TUBE'
WRITE(12,*)'(PSI) (PSI) 1 2 3 4 5 6 7 8 9 1
&O 2-3 3-4 4-5 5-6 6-7 7-8 8-9 9-10
& THK.'
WRITE(12,*)
NN=1
GO TO 8000

```

C

C PRINTOUT FOR UNLOADING STAGE.

```

900  IF(KK.NE.1) GO TO 905
      IF(PO.GT.PFF) GO TO 950
      GO TO 910
905  IF(PO.GT.(PFF-PSTEP*FLOAT(KK-1))) GO TO 950
910  WRITE(6,550)PO,P(1),(KJ1(I),I=1,10),(P(I),I=2,9),TTH(1)
      WRITE(12,550)PO,P(1),(KJ1(I),I=1,10),(P(I),I=2,9),TTH(1)
      IF(NPR.EQ.0) GO TO 920
      WRITE(6,705)(DIS(I),I=1,9)
      WRITE(6,706)(TTH(I),I=2,10)
      WRITE(6,710)(ST(I),I=1,10)
      WRITE(6,715)(SR(I),I=1,10)
      WRITE(6,718)(EQUI(I),I=1,10)
      WRITE(12,705)(DIS(I),I=1,9)
      WRITE(12,706)(TTH(I),I=2,10)
      WRITE(12,710)(ST(I),I=1,10)
      WRITE(12,715)(SR(I),I=1,10)
      WRITE(12,718)(EQUI(I),I=1,10)
      WRITE(6,*)
      WRITE(12,*)
920  KK=KK+1

```

C

C CHECK FOR UNLOADING STAGE.

C CHECK FOR CONTACT.

```

950  IF(P(1).GT.0.0) GO TO 1000
      WRITE(6,550)PO,P(1),(KJ1(I),I=1,10),(P(I),I=2,9),TTH(1)
      WRITE(12,550)PO,P(1),(KJ1(I),I=1,10),(P(I),I=2,9),TTH(1)
      WRITE(6,*)'NO CONTACT BETWEEN TUBE AND TUBESHEET.'
      WRITE(12,*)'NO CONTACT BETWEEN TUBE AND TUBESHEET.'
      GO TO 1590

```

C CHECK FOR ROLLING PRESSURE.

```

1000 IF(PO.GT.DPO0) GO TO 1600
      IF(PO.LE.0.0001) GO TO 1100
      DPO=-PO+0.0001
      GO TO 1600
1100 WRITE(6,550)PO,P(1),(KJ1(I),I=1,10),(P(I),I=2,9),TTH(1)
      WRITE(12,550)PO,P(1),(KJ1(I),I=1,10),(P(I),I=2,9),TTH(1)
      P1RMT=P(1)
      NSTAGE=3

```

C NSTAGE=3 IS TEMPERATURE CHANGE STAGE CONTROLLER.

```

      KK=1
      NN=1
      DPO=0.0
      IF(DTO.EQ.0.0) GO TO 1590
      IF(TOP.EQ.TROLL) GO TO 1590
      IF(TOP.LT.TROLL) GO TO 1200
      DT=DTC
      GO TO 1300
1200 DT=-DTC
1300 WRITE(6,*)
      WRITE(6,*)
      WRITE(6,*)'(3) TEMPERATURE CHANGE STAGE.'

```

```

WRITE(6,*)' TEMPERATURE CONTACT PRESSURE PLASTIC LAYERS
&          PRESSURES BETWEEN LAYERS (PSI)
& TUBE'
WRITE(6,*)' (DEGS.F.) (PSI) 1 2 3 4 5 6 7 8 9 10
& 2-3 3-4 4-5 5-6 6-7 7-8 8-9 9-10
& THK.'
WRITE(6,*)
WRITE(6,*)'(A) TEMPERATURE GOES FROM ROOM TEMP TO OPERATING TEMP'
WRITE(6,*)
WRITE(12,*)
WRITE(12,*)
WRITE(12,*)' (3) TEMPERATURE CHANGE STAGE.
WRITE(12,*)' TEMPERATURE CONTACT PRESSURE PLASTIC LAYERS
&          PRESSURES BETWEEN LAYERS (PSI)
& TUBE'
WRITE(12,*)' (DEGS.F.) (PSI) 1 2 3 4 5 6 7 8 9 1
&O 2-3 3-4 4-5 5-6 6-7 7-8 8-9 9-10
& THK.'
WRITE(12,*)
WRITE(12,*)'(A) TEMPERATURE GOES FROM ROOM TEMP TO OPERATING TEMP'
WRITE(12,*)
NN=1
1380 FORMAT(4X,F7.1,10X,F9.1,4X,10(I2),3X,8(F6.0,2X),F7.6)
GO TO 8000

C
C PRINTOUT FOR TEMPERATURE CHANGE STAGE.
1400 IF(TOP.LT.TROLL) GO TO 1410
IF(TEMP.LT.(TROLL+FLOAT(KK)*TSTEP)) GO TO 1480
GO TO 1430
1410 IF(TEMP.GT.(TROLL-FLOAT(KK)*TSTEP)) GO TO 1480
1430 WRITE(6,1380)TEMP,P(1),(KJ1(I),I=1,10),(P(I),I=2,9),TTH(1)
WRITE(12,1380)TEMP,P(1),(KJ1(I),I=1,10),(P(I),I=2,9),TTH(1)
IF(NPR.EQ.0) GO TO 1450
WRITE(6,705)(DIS(I),I=1,9)
WRITE(6,706)(TTH(I),I=2,10)
WRITE(6,710)(ST(I),I=1,10)
WRITE(6,715)(SR(I),I=1,10)
WRITE(6,718)(EQUI(I),I=1,10)
WRITE(12,705)(DIS(I),I=1,9)
WRITE(12,706)(TTH(I),I=2,10)
WRITE(12,710)(ST(I),I=1,10)
WRITE(12,715)(SR(I),I=1,10)
WRITE(12,718)(EQUI(I),I=1,10)
WRITE(6,*)
WRITE(12,*)
1450 KK=KK+1
C
C CHECK FOR TEMP. CHANGE STAGE.
C CHECK FOR CONTACT.
1480 IF(P(1).GT.0.0) GO TO 1500
WRITE(6,1380)TEMP,P(1),(KJ1(I),I=1,10),(P(I),I=2,9),TTH(1)
WRITE(6,*)'NO CONTACT BETWEEN TUBE AND TUBESHEET.JOINT FAILS.'
```

```

WRITE(12,1380)TEMP,P(1),(KJ1(I),I=1,10),(P(I),I=2,9),TTH(1)
WRITE(12,*)'NO CONTACT BETWEEN TUBE AND TUBESHEET.JOINT FAILS.'
GO TO 1590
C CHECK FOR TEMPERATURE LIMIT.
1500 IF(TOP.LT.TROLL) GO TO 1550
    IF(TEMP.LT.TOP) GO TO 1600
    GO TO 1560
1550 IF(TEMP.GT.TOP) GO TO 1600
1560 WRITE(6,1380)TEMP,P(1),(KJ1(I),I=1,10),(P(I),I=2,9),TTH(1)
    WRITE(12,1380)TEMP,P(1),(KJ1(I),I=1,10),(P(I),I=2,9),TTH(1)
    IF(NRETUN.EQ.0) GO TO 1590
C LET TEMPERATURE RETURN TO ROOM TEMPERATURE.
    NSTAGE=4
    DPO=0.0
    IF(TOP.LT.TROLL) GO TO 1564
    DT=-DT0
    GO TO 1566
1564 DT=DT0
    NN=1
1566 WRITE(6,*)
    WRITE(6,*)
    WRITE(6,*)'(B) TEMPERATURE GOES FROM OPERATING TEMP TO ROOM TEMP'
    WRITE(6,*)
    WRITE(12,*)
    WRITE(12,*)
    WRITE(12,*)'(B) TEMPERATURE GOES FROM OPERATING TEMP TO ROOM TEMP'
    WRITE(12,*)
    GO TO 8000
C
C PRINTOUT FOR TEMPERATURE RETURN TO ROOM TEMP. CASE.
1570 IF(TOP.LT.TROLL) GO TO 1575
    IF(TEMP.GT.(TROLL+TSTEP*FLOAT(KK))) GO TO 1585
    GO TO 1580
1575 IF(TEMP.LT.(TROLL-TSTEP*FLOAT(KK))) GO TO 1585
1580 WRITE(6,1380)TEMP,P(1),(KJ1(I),I=1,10),(P(I),I=2,9),TTH(1)
    WRITE(12,1380)TEMP,P(1),(KJ1(I),I=1,10),(P(I),I=2,9),TTH(1)
    IF(NPR.EQ.0) GO TO 1582
    WRITE(6,705)(DIS(I),I=1,9)
    WRITE(6,706)(TTH(I),I=2,10)
    WRITE(6,710)(ST(I),I=1,10)
    WRITE(6,715)(SR(I),I=1,10)
    WRITE(6,718)(EQUI(I),I=1,10)
    WRITE(12,705)(DIS(I),I=1,9)
    WRITE(12,706)(TTH(I),I=2,10)
    WRITE(12,710)(ST(I),I=1,10)
    WRITE(12,715)(SR(I),I=1,10)
    WRITE(12,718)(EQUI(I),I=1,10)
    WRITE(6,*)
    WRITE(12,*)
1582 KK=KK-1
C
C CHECK FOR TEMPERATURE RETURN CASE.
C CHECK FOR CONTACT.

```

```

1585 IF(P(1).GT.0.0) GO TO 1586
WRITE(6,1380)TEMP,P(1),(KJ1(I),I=1,10),(P(I),I=2,9),TTH(1)
WRITE(6,*)'NO CONTACT BETWEEN TUBE AND TUBESHEET.JOINT FAILS.'
WRITE(12,1380)TEMP,P(1),(KJ1(I),I=1,10),(P(I),I=2,9),TTH(1)
WRITE(12,*)'NO CONTACT BETWEEN TUBE AND TUBESHEET.JOINT FAILS.'
GO TO 1590
C CHECK FOR TEMPERATURE LIMIT.
1586 IF(TOP.LT.TROLL) GO TO 1587
IF(TEMP.GT.TROLL) GO TO 1600
GO TO 1588
1587 IF(TEMP.LT.TROLL) GO TO 1600
1588 WRITE(6,1380)TEMP,P(1),(KJ1(I),I=1,10),(P(I),I=2,9),TTH(1)
WRITE(12,1380)TEMP,P(1),(KJ1(I),I=1,10),(P(I),I=2,9),TTH(1)
C
C TO END A SESSION AND TO ASK FOR ANOTHER.
1590 WRITE(6,*)'ANALYSIS COMPLETED.'
WRITE(12,*)'ANALYSIS COMPLETED.'
WRITE(12,*)
WRITE(6,*)'INPUT NEW ET,SYT,ALPHAT,ES,SYS,ALPHAS ,IN FREE FORMAT.'
WRITE(6,*)'OR INPUT -1.0/ TO STOP.'
READ(5,*)ET,SYT,ALPHAT,ES,SYS,ALPHAS
IF(ET.GT.-0.99) GO TO 50
STOP
C
C TO COMPUTE COEFFICIENTS OF SIMULTANEOUS EQUATIONS.
1600 IF(NSTAGE.NE.1) GO TO 1650
IF(NN.NE.1) GO TO 1650
POA=PO
PO=DPO*FLOAT(IFIX(PO/DPO)+1)
DPO=PO-POA
NN=2
PO=POA
1650 CALL COEFFI
C TO SOLVE SIMULTANEOUS EQUATIONS FOR PRESSURE INCREMENTS.
CALL LEQT(A,B,19)
C TO COMPUTE PRESSURES BETWEEN LAYERS.
DO 1700 I=1,9
J=2*I-1
DP(I)=B(J)
P(I)=P(I)+DP(I)
II=2*I
ALAMD(I)=B(II)
1700 CONTINUE
ALAMD(10)=B(19)
C TO GIVE INCREMENTS TO ROLLING PRESSURE AND TEMPERATURE.
PO=PO+DPO
TEMP=TEMP+DT
IF(NSTAGE.EQ.1) DPO=DPO0
GO TO 600
END

```

C
C

C
C
C

```

C SUBROUTINE 'COEFFI' COMPUTES COEFFICIENTS OF SIMULTANEOUS EQUATIONS.
  SUBROUTINE COEFFI
    DIMENSION SOG(10),OMSOG(10),TERM1(10),TERM2(10),TERM3(10),
    &          TERM4(10),TERM5(10),TERM6(10),AA(9),BB(9),C(9),D(9),
    &          FF(9),CPJM1(9),RTJ(9),CPJP1(9),CPJ(9),CLJP1(9),CLJ(9),
    &          RTJP1(9),CKPJ(10),CKPJM1(10),CKLJ(10),
    &          STMSR(10)
    COMMON /TT/ET,ANU,ALPHAT,T,GT
    COMMON /SS/ES,ALPHAS,HS,GS
    COMMON /DD/DPO,DT
    COMMON /AA/R(10),ST(10),SR(10),EQUI(10)
    COMMON /CC/A(19,19),B(19)
    COMMON /KK/K(10)
    COMMON /LL/TTH(10)
    DO 700 I=1,10
      IF(I.EQ.1) GO TO 500
      E=ES
      G=GS
      GO TO 600
500    E=ET
      G=GT
600    STMSR(I)=ST(I)-SR(I)
      SOG(I)=STMSR(I)/G
      OMSOG(I)=1.0-0.5*SOG(I)
      TERM1(I)=(0.25*SOG(I)-0.5+R(I)/TTH(I))/OMSOG(I)+0.5*ANU
      TERM2(I)=(0.25*SOG(I)-0.5-R(I)/TTH(I))/OMSOG(I)+0.5*ANU
      TERM3(I)=STMSR(I)/OMSOG(I)+E
      TERM4(I)=0.5+ANU*(0.25*SOG(I)-0.5+R(I)/TTH(I))/OMSOG(I)
      TERM5(I)=0.5+ANU*(0.25*SOG(I)-0.5-R(I)/TTH(I))/OMSOG(I)
      TERM6(I)=E+ANU*STMSR(I)/OMSOG(I)
700    CONTINUE
      DO 800 I=1,9
        AA(I)=(R(I+1)*TERM3(I+1)+0.5*TTH(I+1)*ANU*STMSR(I+1)/
    &OMSOG(I+1))/ES
        BB(I)=(0.5*TTH(I+1)*TERM6(I+1)+R(I+1)*STMSR(I+1)/OMSOG(I+1))/ES
800    CONTINUE
      DO 1100 I=1,9
        IF(I.EQ.1) GO TO 900
        E=ES
        ALPHA=ALPHAS
        GO TO 1000
900    E=ET
        ALPHA=ALPHAT
1000   C(I)=(R(I)*TERM3(I)-0.5*TTH(I)*ANU*STMSR(I)/OMSOG(I))/E
        D(I)=(0.5*TTH(I)*TERM6(I)-R(I)*STMSR(I)/OMSOG(I))/E
        FF(I)=(R(I)*TERM2(I)-0.5*TTH(I)*TERM5(I))/E
        CPJM1(I)=-(R(I)*TERM1(I)-0.5*TTH(I)*TERM4(I))/E
        RTJ(I)=(R(I)+0.5*TTH(I))*ALPHA
1100  CONTINUE

```

```

DO 1200 I=1,9
  CPJP1(I)=(R(I+1)*TERM2(I+1)+0.5*TTH(I+1)*TERM5(I+1))/ES
  CPJ(I)=(R(I+1)*TERM1(I+1)+0.5*TTH(I+1)*TERM4(I+1))/ES-FF(I)
  CLJP1(I)=-((AA(I)+2.0*BB(I))*SR(I+1)-(2.0*AA(I)+BB(I))*ST(I+1))
&
  /3.0
  CLJ(I)=-((2.0*C(I)-D(I))*ST(I)-(C(I)-2.0*D(I))*SR(I))/3.0
  RTJP1(I)=- (R(I+1)-0.5*TTH(I+1))*ALPHAS
1200 CONTINUE
DO 1500 I=1,10
  CKPJ(I)=(2.0*ST(I)-SR(I))*(0.25*SOG(I)-0.5-R(I)/TTH(I))
&
  /OMSOG(I)-0.5*(2.0*SR(I)-ST(I))
  CKPJM1(I)=(2.0*ST(I)-SR(I))*(0.25*SOG(I)-0.5+R(I)/TTH(I))
&
  /OMSOG(I)-0.5*(2.0*SR(I)-ST(I))
  CKLJ(I)=(2.0*ST(I)-SR(I))*((ST(I)-SR(I))**2)/OMSOG(I)
  IF(CKLJ(I).EQ.0.)CKLJ(I)=1.
1500 CONTINUE
DO 1700 J=1,19
  DO 1600 I=1,19
    A(I,J)=0.0
1600 CONTINUE
1700 CONTINUE
A(1,1)=CPJ(1)
A(1,2)=FLOAT(K(1))*CLJ(1)
A(1,3)=CPJP1(1)
A(1,4)=FLOAT(K(2))*CLJP1(1)
A(2,1)=CPJM1(2)
A(2,3)=CPJ(2)
A(2,4)=FLOAT(K(2))*CLJ(2)
A(2,5)=CPJP1(2)
A(2,6)=FLOAT(K(3))*CLJP1(2)
A(3,3)=CPJM1(3)
A(3,5)=CPJ(3)
A(3,6)=FLOAT(K(3))*CLJ(3)
A(3,7)=CPJP1(3)
A(3,8)=FLOAT(K(4))*CLJP1(3)
A(4,5)=CPJM1(4)
A(4,7)=CPJ(4)
A(4,8)=FLOAT(K(4))*CLJ(4)
A(4,9)=CPJP1(4)
A(4,10)=FLOAT(K(5))*CLJP1(4)
A(5,7)=CPJM1(5)
A(5,9)=CPJ(5)
A(5,10)=FLOAT(K(5))*CLJ(5)
A(5,11)=CPJP1(5)
A(5,12)=FLOAT(K(6))*CLJP1(5)
A(6,9)=CPJM1(6)
A(6,11)=CPJ(6)
A(6,12)=FLOAT(K(6))*CLJ(6)
A(6,13)=CPJP1(6)
A(6,14)=FLOAT(K(7))*CLJP1(6)
A(7,11)=CPJM1(7)
A(7,13)=CPJ(7)

```

```

A(7,14)=FLOAT(K(7))*CLJ(7)
A(7,15)=CPJP1(7)
A(7,16)=FLOAT(K(8))*CLJP1(7)
A(8,13)=CPJM1(8)
A(8,15)=CPJ(8)
A(8,16)=FLOAT(K(8))*CLJ(8)
A(8,17)=CPJP1(8)
A(8,18)=FLOAT(K(9))*CLJP1(8)
A(9,15)=CPJM1(9)
A(9,17)=CPJ(9)
A(9,18)=FLOAT(K(9))*CLJ(9)
A(9,19)=FLOAT(K(10))*CLJP1(9)
A(10,1)=CKPJ(1)*FLOAT(K(1))
A(10,2)=CKLJ(1)
A(11,1)=CKPJM1(2)*FLOAT(K(2))
A(11,3)=CKPJ(2)*FLOAT(K(2))
A(11,4)=CKLJ(2)
A(12,3)=CKPJM1(3)*FLOAT(K(3))
A(12,5)=CKPJ(3)*FLOAT(K(3))
A(12,6)=CKLJ(3)
A(13,5)=CKPJM1(4)*FLOAT(K(4))
A(13,7)=CKPJ(4)*FLOAT(K(4))
A(13,8)=CKLJ(4)
A(14,7)=CKPJM1(5)*FLOAT(K(5))
A(14,9)=CKPJ(5)*FLOAT(K(5))
A(14,10)=CKLJ(5)
A(15,9)=CKPJM1(6)*FLOAT(K(6))
A(15,11)=CKPJ(6)*FLOAT(K(6))
A(15,12)=CKLJ(6)
A(16,11)=CKPJM1(7)*FLOAT(K(7))
A(16,13)=CKPJ(7)*FLOAT(K(7))
A(16,14)=CKLJ(7)
A(17,13)=CKPJM1(8)*FLOAT(K(8))
A(17,15)=CKPJ(8)*FLOAT(K(8))
A(17,16)=CKLJ(8)
A(18,15)=CKPJM1(9)*FLOAT(K(9))
A(18,17)=CKPJ(9)*FLOAT(K(9))
A(18,18)=CKLJ(9)
A(19,17)=CKPJM1(10)*FLOAT(K(10))
A(19,19)=CKLJ(10)
DO 1800 I=1,19
    B(I)=0.0
1800 CONTINUE
    B(1)=-CPJM1(1)*DPO+(RTJ(1)+RTJP1(1))*DT
    DO 1900 I=2,9
        B(I)=(RTJ(I)+RTJP1(I))*DT
1900 CONTINUE
    B(10)=-CKPJM1(1)*DPO*FLOAT(K(1))
    RETURN
    END

```

C
C

```

C
C
C
C SUBROUTINE 'LEQT' IS A SIMULTANEOUS EQUATION SOLVER.
  SUBROUTINE LEQT(Q,F,N)
    DIMENSION A(19,20),Q(19,19),X(19),F(19)
    M=N+1
    L=N-1
    DO 1 I=1,N
    DO 1 J=1,N
1    A(I,J)=Q(I,J)
    DO 3 I=1,N
3    A(I,M)=F(I)
    DO 12 K=1,L
    JJ=K
    BIG=ABS(A(K,K))
    KP1=K+1
    DO 7 I=KP1,N
    AB=ABS(A(I,K))
    IF(BIG-AB) 6,7,7
6    BIG=AB
    JJ=I
7    CONTINUE
    IF(JJ-K) 8,10,8
8    DO 9 J=K,M
    TEMP=A(JJ,J)
    A(JJ,J)=A(K,J)
9    A(K,J)=TEMP
10   DO 11 I=KP1,N
    QUOT=A(I,K)/A(K,K)
    DO 11 J=KP1,M
11   A(I,J)=A(I,J)-QUOT*A(K,J)
    DO 12 I=KP1,N
12   A(I,K)=0.0
    X(N)=A(N,M)/A(N,N)
    DO 14 NN=1,L
    SUM=0.0
    I=N-NN
    IP1=I+1
    DO 13 J=IP1,N
13   SUM=SUM+A(I,J)*X(J)
14   X(I)=(A(I,M)-SUM)/A(I,I)
    DO 15 I=1,N
15   F(I)=X(I)
    RETURN
  END

```

8. TUBESHEETS FOR U-TUBE HEAT EXCHANGERS

8.1 INTRODUCTION

The tubesheet constitutes a structurally important and economically significant element in a tubular heat exchanger. The thickness of the tubesheet affects the hardware cost in a number of ways. The time spent to drill and to ream the tube holes is directly related to the tubesheet thickness. The portion of the tube length lying within the tubesheet is effectively lost for heat transfer and must be replaced by increasing the tube (and hence the unit) overall length. The depth of the tube roll is also dependent on the tubesheet thickness; typically, the depth of the roll is specified as the tubesheet thickness less 1/8 in. Although some industry standards provide for limiting the maximum roll depth to 2 in., many process conditions warrant complete elimination of the stagnant annulus between the tube and the tubesheet on the shellside which necessitates a full depth roll. All of these factors pertaining to the tubesheet have a bearing on equipment cost.

The design attention commanded by the tubesheet does not stem from considerations of economy alone. The tubesheet is also the principal barrier between the shellside and the tubeside chambers. It experiences the operating transients of both heat exchanging streams. The tubesheet's own uneven thermal capacitance (low capacitance of the perforated interior and high capacitance of the solid outer rim) contributes to the development of thermal stresses. These considerations have sustained an ongoing interest in both experimental and analytical investigations into the structural behavior of tubesheets.

A thorough analysis of the stresses in the tubesheet is a daunting task since significant residual stresses are locked into the tubesheet during fabrication operations. The drilling operation often imports a bow to the tubesheet discernible to the naked eye. Welding of the tube ends to the tubesheet (see Chapter 7) also produces plastic strains which warp the tubesheet. Weld overlays, when performed, have a similar effect. In nearly all cases, the tubesheet is not stress relieved after weld overlaying, drilling, and tube welding. Therefore, plastic residual stresses are permanently locked into the tubesheet. Precise mathematical means to quantify these residual stresses do not yet exist.

The study of the tubesheet behavior under operating conditions (pressure and thermal loading) is fairly well established, however. The standard analysis techniques are typified by the works of Gardner [8.1.1-8.1.3] and

Miller [8.1.4]. Since their pioneering efforts, there have been many similar papers published dealing with the analysis of heat exchanger tubesheets. All of these works advocate the use of classical plate theory together with a reduced elastic modulus to simulate the weakening effect of the perforations. In the case of fixed or floating head construction, an elastic foundation simulating deflection restraint provided by the tubes is also included. The elastic foundation effect complicates the analysis significantly; hence, Chapter 9 is devoted in its entirety to integral and floating head tubesheet analysis.

In U-tube exchangers, the tubes are normally considered to have little effect on the restraint of tubesheet movement. However, the tubes do provide some rotational resistance to tubesheet bending since the presence of support baffles prevents free tube movement as the tubesheet flexes under pressure loading. This effect has been investigated in [8.1.3, 8.1.5]. It is concluded in these references that, for U-tube units designed for relatively low pressure service, carrying out the design computations including tube rotational resistance, can lead to a more efficient utilization of material. However, in most practical situations the geometry and operating conditions are such that inclusion of the effect of tube rotational resistance on tubesheet bending is not warranted considering the complexity of the analysis that ensues.

This chapter focuses on the analysis of a U-tube heat exchanger tubesheet having a perforated region modelled as an axisymmetrically loaded thin circular plate, and an unperforated rim modelled as a ring. It is attached to the heat exchanger body by one of three attachment configurations: 1) integral attachment to both shell and channel; 2) integral attachment to either shell or channel with gasketed construction on the non-integral side; 3) two sided gasketed attachment. The reader is encouraged to compare the relative simplicity of the analysis presented herein for the complete integral construction with the analysis presented in [8.1.6] for the same construction, but, including tube rotational resistance and treatment of the unperforated rim as an annular plate rather than as a ring.

Despite all of the effort directed toward rigorous analysis and design of U-tube tubesheets using plate theory, effective moduli, correct account of interaction with shell and channel, etc., perhaps the most used formula for establishing the thickness of a tubesheet in a U-tube exchanger is the empirical formula set forth by the Tubular Exchanger Manufacturers Association [TEMA] in their Standards [8.1.7].

$$h = GC_T \left(\frac{|p|}{S_A} \right)^{1/2} \quad (8.1.1)$$

where $0.5 \leq C_T \leq 0.625$ is a parameter that indicates the degree of edge rotational resistance (pinned or clamped), h is the tubesheet thickness, G is the diameter of the tubesheet region exposed to pressure, p is the design pressure, and S_A is the allowable stress for the tubesheet material at the

design temperature. Despite the fact that the typical U-tube exchanger design involves a large number of geometric and material parameters, the simple formula, given by Eq. (8.1.1), has served the industry well in the design of standard units. It is the intent herein, to illustrate in the simplest manner possible, those parameters which must influence the design of the tubesheet even though they do not appear in Eq. (8.1.1). Simple design formulas will be developed which enable the user to accurately account for perforated region, unperforated rim, and edge attachment conditions in the design of this class of heat exchangers. Prior to beginning the analytical treatment of U-tube exchanger tubesheets, some remarks should be made on the modelling of the effects of the perforations. Consider that the tubesheet is modelled as a composite structure consisting of a perforated inner region and a solid outer region. The radius a , marking the interface between the perforated and unperforated region, is defined in the ASME Pressure Vessel Code by the formula:

$$a = r_o + \frac{d^*}{4} \quad (8.1.2)$$

r_o is the outermost tube hole center radius, and d^* is the tube hole diameter. Although other definitions of the perforated radius may be found, even within the ASME Code, Eq. (8.1.2.) will be adopted for the work in this chapter. The ligament width H , the tube pitch P and the ligament efficiency η are related by the following equations:

$$\eta = H/P; \quad H = P - d^* \quad (8.1.3)$$

Following standard practice, the perforated region of the tubesheet is replaced by an equivalent solid elastic plate with effective elastic constants; the ligament efficiency η is the prime parameter influencing the value of these effective constants. The ASME Code contains curves giving values for the effective elastic constants of the equivalent solid plate as a function of the ligament efficiency and of the actual elastic constants of the plate material. Figure 8.1.1 shows typical curves (adapted from Ref. [8.6.1]) for tubesheets having a diagonal tube array; Fig. 8.1.2 gives data for square arrays. Considerable effort has been directed toward development of expressions for the effective elastic constants of perforated plates; cited as an example is one of the many works of O'Donnell, et al. on the subject [8.1.9]. Reference [8.1.10] contains a comprehensive summary of some work pertaining to effective elastic constants and suggests a correlation for the work of several investigators in the form of a simple analytical expression. For our purposes, we adopt the graphical expressions for the effective constants given by Figs. 8.1.1 and 8.1.2 and commence the analysis of U-tube exchanger tubesheets by a consideration of the perforated region extending to radius a .

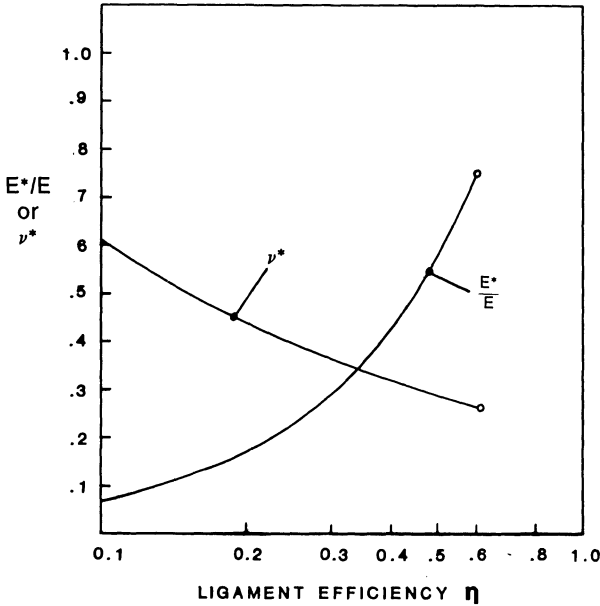
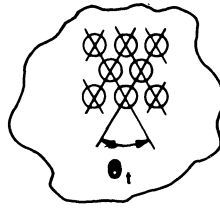


Fig. 8.1.1. Effective elastic constants – triangular pattern.

8.2 ANALYSIS OF PERFORATED REGION

We consider a homogeneous circular plate of outer radius a . Equation (8.1.2) suggests a suitable choice for the radius a . The pressure difference across the tubesheet thickness is p , where:

$$p = p_T - p_s \tag{8.2.1}$$

p_T, p_s represent tubeside and shellside pressures, respectively. We assume that the effect of the perforations on the deflection analysis of the tubesheet is accounted for by the introduction of effective elastic constants E^*, ν^* . Figure 8.2.1 shows the sign convention for moments and shears in the perforated region. This is identical to the sign convention used in Chapter 4. In Chapter 4, major emphasis was placed on the development of a computer code to determine the interaction between flanges, gaskets, and tubesheet (including the rim), in a three element joint gasketed on both shell side and

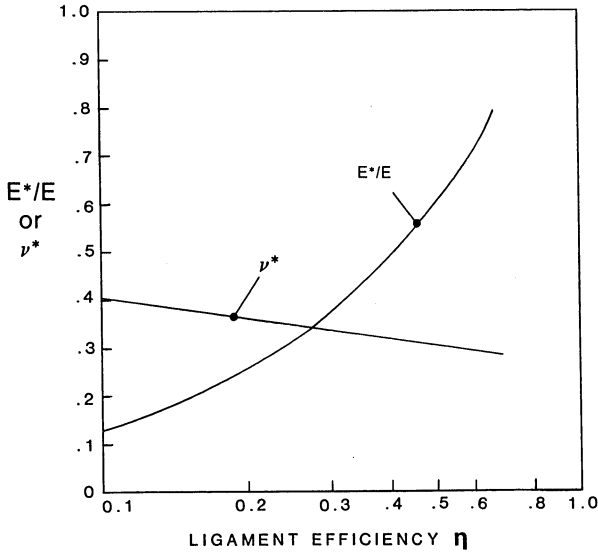
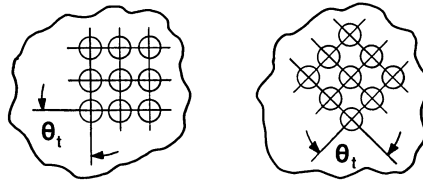


Fig. 8.1.2. Effective elastic constants-square pattern.

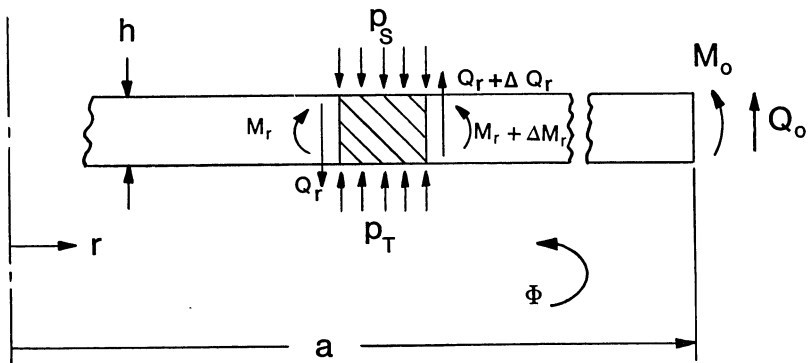


Fig. 8.2.1. Forces and moments in perforated region of U-tube heat exchanger tubesheet.

tube side. Consideration of flange-tubesheet contact outside of the gasket radii was also included. This chapter concentrates on the effect of different constructions, outboard of radius a , on stress analysis of the tubesheet. We begin by extracting some results from Chapter 4; in particular, differentiation of Eq. (4.3.17), with respect to r , gives the slope $\Phi(r)$ as:

$$\Phi(r) = 2\gamma_2 r + \frac{p r^3}{16 D^*} \quad (8.2.2)$$

Equation (4.3.19) gives the radial bending moment $M_r(r)$ as:

$$M_r(r) = 2\gamma_2 D^*(1 + \nu^*) + (3 + \nu^*) \frac{p r^2}{16} \quad (8.2.3)$$

Herein, the notation D^* is used to define the effective plate flexural rigidity in the perforated region

$$D^* = E^* h^3 / [12(1 - \nu^{*2})] \quad (8.2.4)$$

To determine the integration constant γ_2 , we impose the condition that $M_r(a) = M_0$. Solving for γ_2 and eliminating γ_2 from Eq. (8.2.2) and Eq. (8.2.3) leads to the following results for the tubesheet slope at $r=a$, and the radial bending moment:

$$\Phi(a) = \frac{1}{D^*(1 + \nu^*)} \left[aM_0 - \frac{p a^3}{8} \right] \quad (8.2.5)$$

$$M_r(r) = M_0 - \frac{(3 + \nu^*)}{16} p a^2 (1 - r^2/a^2) \quad (8.2.6)$$

The circumferential bending moment $M_\theta(r)$, defined by the relation

$$M_\theta(r) = D^*(1 - \nu^{*2})\Phi/r + \nu M_r$$

takes the form:

$$M_\theta(r) = M_0 - (3 + \nu^*) \frac{p a^2}{16} + \frac{(1 + 3\nu^*)}{16} p r^2 \quad (8.2.7)$$

Parameters, K_a , M^* are now introduced to express the linear relationship between M_0 and $\Phi(a)$ so that

$$a M_0 \equiv -K_a \Phi(a) + a M^* \quad (8.2.8)$$

Eliminating Φ/a and using Eq. (8.2.5) yields:

$$a M_0 = \frac{a M^* + \mu p a^3 / 8}{1 + \mu} \quad (8.2.9)$$

The edge stiffness parameter μ is defined by the relation

$$\mu = K_a / [D^*(1 + \nu^*)] \quad (8.2.10)$$

Since our purpose is to evaluate maximum tubesheet stress, we must determine the maximum bending moment in the tubesheet. The maximum bending moment occurs either at $r=0$ or at $r=a$. Summarizing the results, we have:

$$M_r(a) = \frac{M^*}{1+\mu} + \frac{\mu}{1+\mu} \frac{p a^2}{8}$$

$$M_\theta(a) = \frac{M^*}{1+\mu} - \frac{p a^2}{8} \left(1 - \nu^* - \frac{\mu}{1+\mu}\right) \quad (8.2.11)$$

$$M_r(0) = M_\theta(0) = \frac{M^*}{1+\mu} - \frac{p a^2}{16} \left(3 + \nu^* - \frac{2\mu}{1+\mu}\right)$$

For a plate simply supported at $r=a$, $\mu=0$; for a plate clamped at $r=a$, $\mu \rightarrow \infty$. Examination of the general solutions given in Eq. (8.2.11) shows that the maximum plate bending moment is influenced by p , M^* , and μ . To determine M^* and μ for any configuration requires detailed analysis of the shell-channel-tubesheet construction outboard of radius a . In this chapter, the three constructions shown in Fig. 8.2.2 are examined.

Figure 8.2.2a shows a representative case of two side integral construction where both shell and channel are welded to the tubesheet. We assume, in this analysis, that the middle surface of the shell and channel are both at $r=b$ (this need not be the case in an actual unit). Figure 8.2.2b shows a case of bolted construction on the channel side and integral construction on the shell side. The effects of bolt loading on the tubesheet stress must be included in the analysis of this construction. Finally, Fig. 8.2.2c shows the case of a unit gasketed on both channel and shell side. In the next sections, each of these constructions shall be analyzed in turn; the intent being solely to define M^* and μ for use in Eq. (8.2.11).

8.3 ANALYSIS OF TWO SIDE INTEGRAL CONSTRUCTION

Figure 8.3.1 shows a free body of the component parts with force and moment resultants. It is assumed that the unperforated rim behaves like a ring and satisfies the relation (see Section 3.9):

$$\theta_R = \frac{a^* M_R}{D_R \ln b/a} \quad (8.3.1)$$

where $D_R = Eh^3/[12(1-\nu^2)]$, $a^* = (a+b)/2$ and M_R is the net moment per unit of circumferential length, acting at the ring centroid P^* in the direction of the ring rotation θ_R . We recognize that for larger b/a ratios, it might be more appropriate to consider the unperforated rim as an annular plate; however, to maintain relative simplicity in the analysis, we restrict consideration to the ring theory. It is shown in Ref. [8.3.1] that the predictions from ring theory and annular plate theory are within 6% if $b/a \leq 1.35$. In

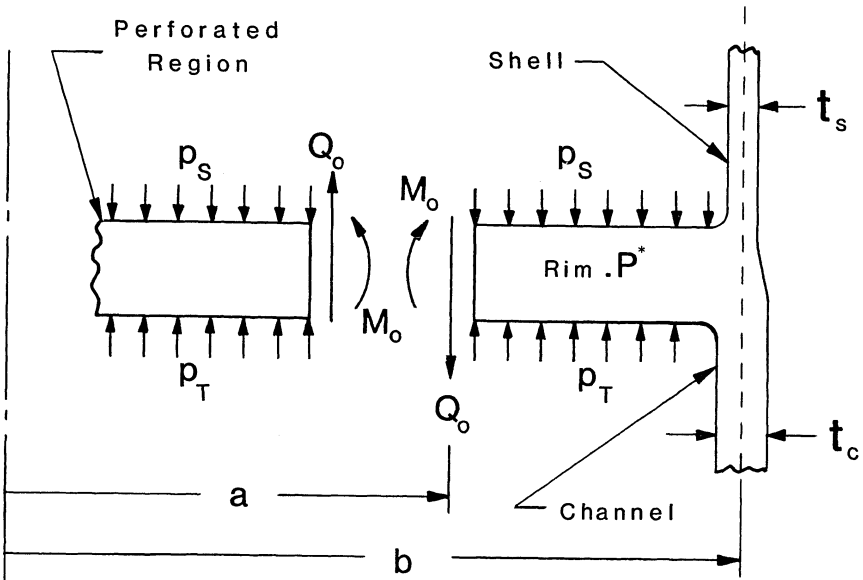


Fig. 8.2.2a. Two side integral construction.

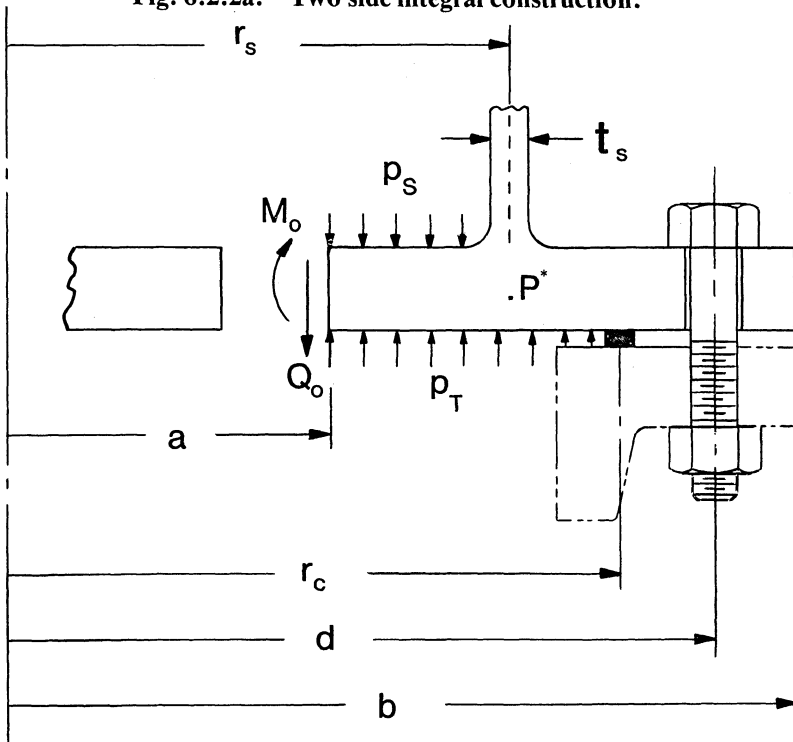


Fig. 8.2.2b One side integral construction.

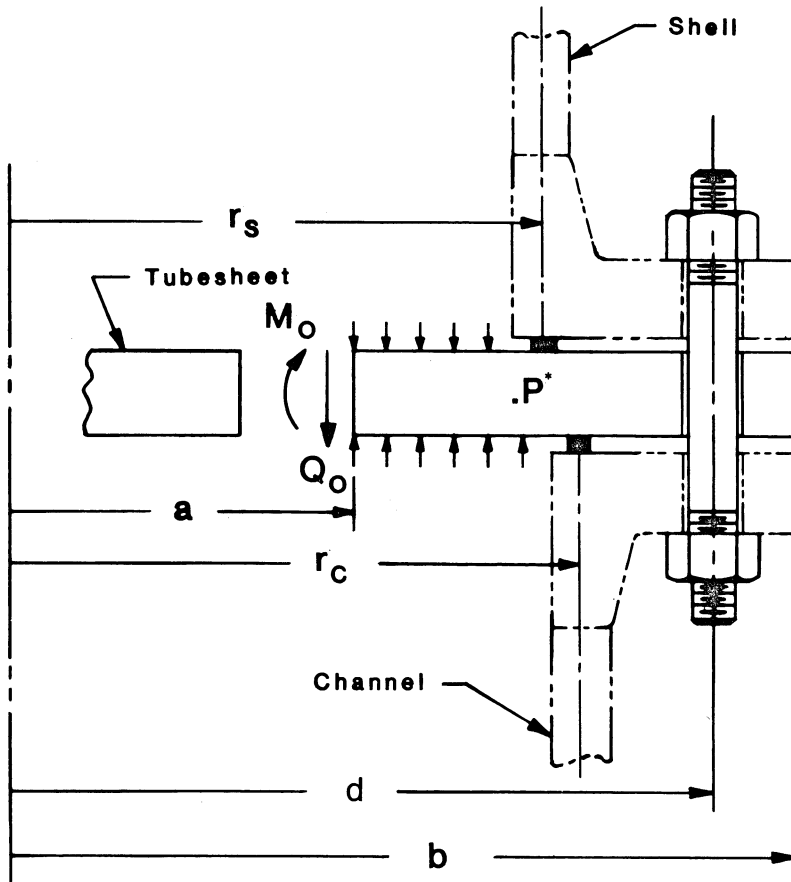


Fig. 8.2.2c. Two side gasket construction.

view of the major assumption we have made in the entire tubesheet analysis that classical plate theory is valid for perforated tubesheet analysis, the use of a ring theory to describe the unperforated tubesheet rim is acceptable for design purposes even for b/a somewhat larger than 1.35. In the next chapter, an analysis is carried out using annular plate theory to describe the behavior of the unperforated rim. The reader will see quite clearly the additional complexity of the plate solution.

The shell and channel are treated as thin cylindrical shells for the purpose of relating edge shears and moments to edge displacements and rotations. For the moment, we retain the displacement due to local pressure acting on the cylindrical wall. For either the shell or channel, we can therefore write:

$$\delta = \frac{\alpha_{11} V b^3}{D} - \frac{\alpha_{12} M b^2}{D} - \delta^*$$

In Eq. (8.3.3) it is assumed the Poisson's ratio is 0.3 for either the shell or the channel. In what follows, we append the subscript "c" for channel side or "s" for shell side to Eq. (8.3.2) as needed. If radial growth of the tubesheet is neglected, then the following compatibility equations may be written:

$$\delta_c = \frac{h}{2} \theta_R = \frac{h}{2} \theta_c \quad (8.3.4)$$

$$\delta_s = -\frac{h}{2} \theta_R = \frac{h}{2} \theta_s$$

Employing the appropriate form of Eq. (8.3.2) in Eq. (8.3.4) yields the following relationship (for both the channel and the shell):

$$V = \frac{M}{b} K_0 + \frac{\delta^* D}{b^3 J}; \quad K_0 = \frac{\alpha_{12} + \alpha_{22} h/2b}{\alpha_{11} + \alpha_{12} h/2b}; \quad J = \alpha_{11} + \alpha_{12} h/2b \quad (8.3.5)$$

Using Eq. (8.3.5), written explicitly for either the shell or channel, in the second of Eq. (8.3.2), and employing the relationship $\theta_R = \theta_c = -\theta_s$, yields the final relationships between the edge bending moment in either the channel or shell, and the rotation of the annular rim. These relationships are given as:

$$bM_c = \frac{D_c}{K_c^*} \theta_R + 0.2572 p_T t_c b^2 \quad (8.3.6)$$

$$bM_s = -\frac{D_s}{K_s^*} \theta_R + 0.2572 p_s t_s b^2$$

Equations (8.3.6) determine the local edge bending moment in terms of the edge rotation and the local pressure acting on the cylindrical wall. In these equations, Poisson's ratio is set to 0.3, and K^* for either shell or channel is:

$$K^* = \frac{\alpha_{11} \alpha_{22} - \alpha_{12}^2}{\alpha_{11} + \alpha_{12} \frac{h}{2b}} \quad (8.3.7)$$

In the manipulations to this point, we have retained the effect of local pressure acting on the cylindrical walls of the shell and channel. Thus, our final expressions for shell and channel edge moment are completely consistent with the theory of shells employed. In our subsequent calculations using Eqs. (8.3.5) and (8.3.6), we choose to neglect these local pressure terms. Our justification is that retention of these terms beyond this point makes little difference on the final magnitude of the bending moments of Eq. (8.2.11); the final plate bending moments of Eq. (8.2.11) are most strongly dominated by the pressure difference across the plate surface.

If we now use Eq. (8.3.6) in Eq. (8.3.5) (after dropping the local pressure effects in both sets of equations), we can also relate the shear force resultants V_c , V_s to the ring rotation:

$$V_c = \frac{K_{0c}}{K_c^*} \frac{D_c}{b^2} \theta_R; \quad V_s = -\frac{K_{0s}}{K_s^*} \frac{D_s}{b^2} \theta_R \quad (8.3.8)$$

From Fig. 8.3.1, the net moment M_R acting on the ring cross section is given by the equation

$$\begin{aligned} a^* M_R = a M_0 - a Q_0 \frac{(b-a)}{2} + b \left[M_s - M_c + \frac{h}{2} (V_s - V_c) \right] \\ + \frac{p b^2}{4} (b-a) \end{aligned} \quad (8.3.9)$$

Using Eqs. (8.3.6), (8.3.8) to eliminate the grouping $M_s - M_c + h/2 (V_s - V_c)$, and noting that:

$$a Q_0 = -p a^2 / 2 \quad (8.3.10)$$

enables us to construct a final relationship between θ_R , M_0 and p in the form:

$$D_R \ln(b/a) \theta_R \left(1 + \frac{\lambda_2}{\ln(b/a)} \right) = a M_0 + \frac{p(b^2 + a^2)(b-a)}{4} \quad (8.3.11)$$

where the parameter λ_2 is given as:

$$\lambda_2 = \frac{D_s}{D_R K_s^*} \left(1 + \frac{h K_{0s}}{2b} \right) + \frac{D_c}{D_R K_c^*} \left(1 + \frac{h K_{0c}}{2b} \right) \quad (8.3.12)$$

Note that in Eq. (8.3.12), D_s , D_c , D_R are computed for the shell, channel, and rim, respectively. From Figs. 8.2.1, 8.3.1, we see that $\Phi(a) = -\theta_R$; therefore, comparing Eq. (8.2.8) with Eq. (8.3.11) enables us to identify K_a , M^* for the two sided integral construction as:

$$K_a = D_R (\ln(b/a) + \lambda_2) \quad (8.3.13)$$

$$M^* = -\frac{p a^2}{4} \left(\frac{b^2}{a^2} + 1 \right) \left(\frac{b}{a} - 1 \right) \quad (8.3.14)$$

Using Eqs. (8.3.3), (8.3.5), and (8.3.7) enables us to write

$$\begin{aligned} \frac{1}{K^*} &= 2.568 \left(\frac{b}{t} \right)^{1/2} + 1.651 \left(\frac{h}{t} \right) \\ \frac{K}{K^*} &= 3.301 \frac{b}{t} \left[1 + 1.285 \frac{bh}{t^2} \right] \end{aligned} \quad (8.3.15)$$

where $t = t_c$ or t_s .

If the flexural efficiency for the perforated region of the tubesheet is defined as e , where:

$$e = D^*/D_R = \frac{E^*(1-\nu^2)}{E(1-\nu^{*2})} \quad (8.3.16)$$

then the edge stiffness parameter μ given in Eq. (8.2.10) becomes:

$$\mu = \frac{\ln b/a + \lambda_2}{e(1+\nu^*)} \quad (8.3.17)$$

For the two side integral construction, Eqs. (8.3.14) and (8.3.17) are sufficient to completely evaluate the maximum bending moment in the tubesheet for any shell, channel, rim configuration within the limits of these approximations.

8.4 ANALYSIS OF ONE SIDE INTEGRAL, ONE SIDE GASKETED CONSTRUCTION

Consider the construction shown in Fig. 8.2.2b, the corresponding free body diagram is given in Fig. 8.4.1. We assume that the bolt loading B (per unit of circumferential length) is specified by the designer as one of the known input quantities. It has been shown in Chapter 3 that the bolt loading changes from preload to operating condition and, under certain circumstances, the change may be a substantial fraction of the pressure load. Chapter 3 also shows that the bolt load change is dependent on the flange parameters, on the bolt spring constant, and on the gasket spring rates. We assume in this chapter that the designer has made any computations deemed necessary to establish B for the preload and for the operating conditions. We recall that the focus here is to examine the effects of the unit construction outboard of the tubesheet perforated region on the stress distribution inside the perforated region.

An analysis of the adjacent channel flange, under the assumption that there is a hydrostatic end load on the channel, yields the following relation between peripheral loadings B , G_c as:

$$r_c G_c = B d - \frac{p_T r_c^2}{2} \quad (8.4.1)$$

We use the same ring assumption stated by Eq. (8.3.1) and construct the net moment a^*M_R on the ring. After elimination of the effect of the gasket loading G_c using Eq. (8.4.1), the effect of Q_0 by using Eq. (8.3.10), and subsequent manipulation of all of the terms involving p_T , p_s , we obtain:

$$a^*M_R = aM_0 + \frac{N_B L_B d}{2\pi} \left(1 - \frac{r_c}{d}\right) + r_s \left[M_s + \frac{h}{2} V_s\right] + \gamma_T \frac{p_T a^3}{4} - \gamma_s \frac{p_s a^3}{4} \quad (8.4.2)$$

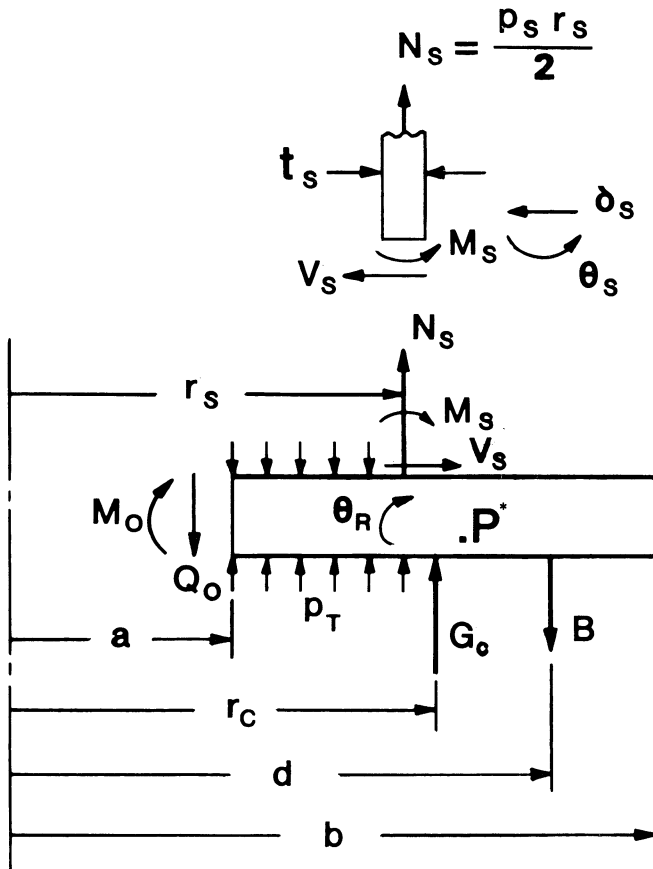


Fig. 8.4.1. Free body analysis of one side integral construction.

where L_B is defined as the total bolt load, by the relation

$$2\pi B d = N_B L_B; \quad N_B = \text{number of bolts in the unit} \quad (8.4.3)$$

The parameters γ_T, γ_s are defined as

$$\gamma_T = \left(\frac{r_c}{a} - 1\right) \left(\frac{r_c^2}{a^2} + 1\right) \quad (8.4.4)$$

$$\gamma_s = \left(\frac{r_s}{a} - 1\right) \left(\frac{r_s^2}{a^2} + 1\right)$$

The analysis of Section 8.3 suffices to determine $M_s + h/2 V_s$ in terms of the ring rotation θ_R , and hence, we can easily construct the final relationship between θ_R, M_0 and p_T, p_s in the form:

$$D_R \ln(b/a) \theta_R \left(1 + \frac{\lambda_1}{\ln b/a}\right) = a M_0 + \frac{N_B L_B d}{2\pi} \left(1 - \frac{r_c}{d}\right) + \frac{a^3}{4} (\gamma_T p_T - \gamma_s p_s) \quad (8.4.5)$$

where:

$$\lambda_1 = \frac{D_s}{D_R K_s^*} \left(1 + \frac{h}{2r_s} K_{0s}\right) \quad (8.4.6)$$

K_{0s} , K_s^* are given by Eq. (8.3.15) with $t = t_s$ and b replaced by r_s . Hence, for the one side integral–one side gasketed construction we obtain M^* , μ as:

$$M^* = -\frac{N_B L_B}{2\pi} \frac{d}{a} \left(1 - \frac{r_c}{d}\right) - \frac{a^2}{4} (\gamma_T p_T - \gamma_s p_s) \quad (8.4.7)$$

$$\mu = \frac{\ln(b/a) + \lambda_1}{e(1 + \nu^*)} \quad (8.4.8)$$

With M^* , μ determined for this outboard construction, we can examine the stress distribution in the perforated region of the tubesheet. If the channel side is integral, with the shell side gasketed, then λ_1 should be replaced by the appropriate channel constants and r_c in the bolt loading term should be replaced by r_s .

8.5 ANALYSIS OF TWO-SIDE GASKETED CONSTRUCTION

Figure 8.5.1 shows the free body diagram of the unit described in Fig. 8.2.2c. If we assume that specified bolt peripheral loading B and hydrostatic end loads are applied to both shell and channel, then the gasket loads G_s and G_c are simply related to the bolt loading B and to the respective hydrostatic loadings. We obtain, from a free body analysis of the adjacent shell and channel, the results:

$$r_s G_s = B d - \frac{p_s r_s^2}{2} \quad (8.5.1)$$

$$r_c G_c = B d - \frac{p_T r_c^2}{2}$$

Following the method previously described in Sections 8.3 and 8.4, we obtain the expression for the net moment on the ring as:

$$a^* M_R = a M_0 + B d (r_s - r_c) + \frac{a^3}{4} (\gamma_T p_T - \gamma_s p_s) \quad (8.5.2)$$

where the parameters γ_T , γ_s are defined by Eq. (8.4.4). Introducing the total bolt load L_B defined in Eq. (8.4.3), we obtain the parameters M^* , μ for the two sided gasket construction as:

$$M^* = \frac{N_B L_B}{2\pi} \frac{(r_s - r_c)}{a} - \frac{a^2}{4} (\gamma_T p_T - \gamma_s p_s) \quad (8.5.3)$$

$$\mu = \frac{\ln(b/a)}{e(1 + \nu^*)} \quad (8.5.4)$$

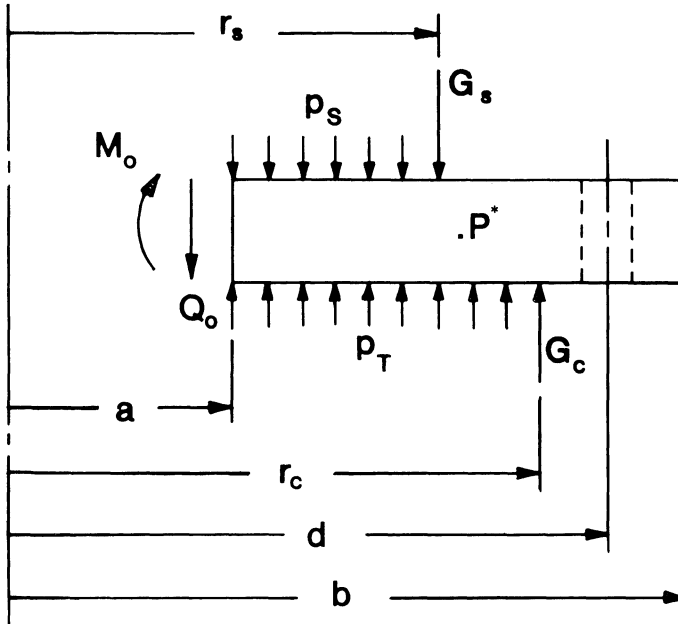


Fig. 8.5.1. Free body analysis of two side gasketed construction.

8.6 TUBESHEET STRESS ANALYSIS

The analyses in Sections 8.2–8.5 lead to the evaluation of the maximum bending moment in the perforated region of the tubesheet based on the assumption that the region $r < a$ is fully perforated. With the maximum bending moment determined, the maximum bending stress at the extreme fiber of the tubesheet is

$$\sigma = \frac{6 M_{\max}}{\eta_s h^2} \quad (8.6.1)$$

where M_{\max} is the maximum bending moment for the construction considered and $\eta_s < 1$ is a stress efficiency generally assumed to be equal to the ligament efficiency defined in Eq. (8.3.1). The purpose of the stress efficiency factor is to reflect the expected stress amplification caused by the

perforations. Here we can see an immediate analysis difficulty since the derivation of M_{max} hinges upon consideration of the tubesheet as fully perforated. If the analytical results predict maximum moments to be in the center of the unit, it is clear that Eq. (8.6.1) overestimates the stress in the central portion of a U-tube tubesheet. The central region must be undrilled by the very nature of the construction; to account for this solid central portion requires analysis of a non-symmetric construction. This difficulty is surmounted by replacing the actual unit, containing an undrilled central region, with an idealized fully perforated unit, for the purpose of a design analysis. The replacement of the actual unit with an idealized unit involves the introduction of an effective tube pitch greater than the actual tube pitch; in this way, we can define an effective ligament and/or stress efficiency that is greater than the efficiency predicted by the actual tube pitch. Using a pseudo stress efficiency in Eq. (8.6.1) and a pseudo ligament efficiency to determine E^* , ν^* appears to yield results that reflect the satisfactory performance experienced by many in-service units. The development of the concept of an idealized, fully perforated unit, for analysis purposes, is outlined in the following, and is implemented in all of the numerical results presented in this chapter.

Consider Fig. 8.6.1, which shows a plan form view of a typical U-tube exchanger tubesheet. Assume that N_T , the number of tube holes in the unit, P , the actual pitch, and θ_t , the perforation angle are known. Then, the actual tubed area A_T is given as:

$$A_T \approx N_T P^2 \sin\theta_t \tag{8.6.2}$$

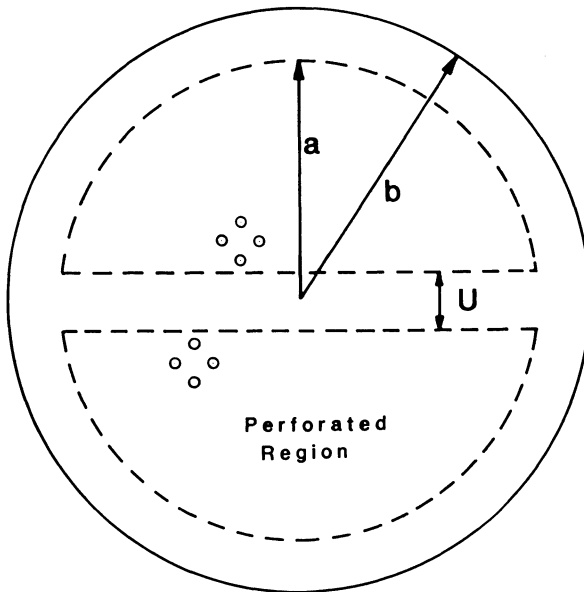


Fig. 8.6.1. Plan view of tubesheet.

The untubed region, within the radius a , is approximately expressed as (assume U known as shown in Fig. 8.6.1)

$$A_{UT} \approx 2Ua \quad (8.6.3)$$

We define an effective tube pitch P' by the equation

$$\pi a^2 = N_T P'^2 \sin \theta_t = A_T + A_{UT} \quad (8.6.4)$$

Equation (8.6.2)–(8.6.4) leads to a result for P' as

$$P' = P \left\{ 1 + \frac{A_{UT}}{\pi a^2 - A_{UT}} \right\}^{1/2} \quad (8.6.5)$$

We suggest the use P' instead of P in Eq. (8.1.3) to determine η and η_s . Note that the ASME Code also suggests a similar replacement in its modification to the simple design formula in Eqs. (8.1.1) [8.6.1]. Both the replacement suggested here and in the cited reference are designed to force a lower calculated stress in the central region of the actual unit.

Appendix 8.A contains the listing of a short computer code, written in BASIC, suitable for the design of U-tube heat exchanger tubesheets. The program is written assuming that the CRT screen as well as hard copy output is desired. The input required is self-explanatory and is listed in Appendix 8.A. The program utilizes the concept of effective tube hole diameter, based on roll depth, introduced in Ref. [8.6.1]; namely in the computation of ligament efficiency, an effective tube hole diameter d_1 , is employed, defined by:

$$d_1 = d^* - 2 t^* \left[\frac{E_T}{E_{TS}} \cdot \frac{S_T}{S_A} \right] \cdot \frac{RD}{100} \quad (8.6.6)$$

where t^* is the tube thickness, E_T , E_{TS} are the Young's Moduli of the tube and tubesheet material, and S_T , S_A are the ASME Code allowable stresses for the tube and tubesheet material. RD is the depth of roll expressed as a percentage of tubesheet thickness (i.e., a roll to 50% of tubesheet thickness implies $RD = 50.0$). Regardless of the predicted value of d_1 from Eq. (8.6.6), a lower limit on d is imposed by the additional condition

$$d_1 \geq d^* - 2t^* \quad (8.6.7)$$

In the analyses to follow, we consider the design as meeting structural requirements in the perforated region of the tubesheet if the maximum bending stress remains below $1.5 S_A$ where S_A is the allowable stress given in the ASME Code [8.6.1] for the corresponding design temperature.

To illustrate the application of the method presented here, consider the three U-tube heat exchanger sample problems given by TEMA in Ref. [8.6.2]. For the purposes of this discussion, some information needed for the solution is listed in Table 8.6.1.

Table 8.6.1 Data for U-Tube Sample Problems

Item	Ex. 1	Ex. 2	Ex. 3
TEMA Prob. Number	8	9	10
Construction	Chan. Int., shell gask.	2 side gask.	Int. both sides
Design Pressures (psi)	$p_T = 1000$ $p_s = 0$	$p_T = -15$ $p_s = 450$	$p_T = 2850$ $p_s = 0$
Tube O.D. (")	0.75	0.75	0.75
Tube Thickness (")	0.083	0.083	0.083
a (")	8.875	8.875	8.875
b (")	13.375	11.25	10.875
Tube Pitch (")	0.9375	0.9375	0.9375
TEMA Calculated Thickness from Eq. (8.1.1) for uncorroded condition	2.6857	2.19	3.758"

Values used for b in examples 1 and 2 assume that the tubesheet is extended beyond the gasket circle. The value for b in example 3 is the mean channel radius. Additional input information is given in Tables 8.6.2-4. Where necessary, our best estimates for dimensions are used when not specifically given in Ref. [8.6.2]. Ligament efficiencies are obtained from Fig. 8.1.1 using Eq. (8.1.3) with P' from Eq. (8.6.5) replacing P and d_l from Eq. (8.6.6) replacing d^* .

All materials are steel with $E = 29 \times 10^6$ psi; $S_A = 17,500$ psi. The tube layout pattern is assumed similar to that given with TEMA problem 10 [8.6.2]; "a" is estimated and an untubed central area = 36 in.² is computed from the information given in Ref. [8.6.2]. Tables 8.6.2, 8.6.3, and 8.6.4 show the printed computer output for the three sample problems. Note that for example 1, with one side integral construction, a tubesheet thickness of 2.375" is acceptable if we seek only to limit tubesheet stress. For example 2, with two sided gasketed construction, the method given herein suggests that the thickness must be larger than that given by the TEMA approach. Finally, for the integral construction, we obtain essentially the same thickness as predicted by the TEMA simplified approach.

The reader should be cautioned not to draw general conclusions from the numerical simulations. One can say, however, that the TEMA Eq. (8.1.1), despite its simplicity, does appear to yield reliably accurate results for tubesheets in U-tube exchangers. Where the TEMA result underestimates tubesheet thickness, that doesn't necessarily infer an unsafe design; all we can say is that a TEMA tubesheet would then encroach somewhat on the safety factor as mandated by the ASME for pressure vessels. The utility of the more complete procedure suggested in this chapter is that the results are capable of predicting tubesheet behavior for a wide class of geometries and material combinations; through use of the computer code, solutions are obtained with minimal effort on the user's part.

As a final numerical illustration of the analysis method for U-tube exchangers, Table 8.6.5 presents results for a configuration involving dif-

ferent gasket radii and edge bolting. The numerical data used is for illustrative purposes only and is not necessarily representative of an actual construction. The two sets of results show the stress state under bolt load alone, and under bolt load plus pressure.

Note that in all of the computer simulations, results are given for the shell and channel stresses. These results are given so that the user may check that the shell and channel thicknesses are adequate to support the membrane hoop stresses, and the membrane plus bending axial stresses.

Using Eq. (8.3.6), it is clear that the extreme fiber stress in the shell and channel, in an integral construction, is given as

$$\sigma_c = \frac{p_T b}{2t} \pm \frac{6M_c}{t_c^2} = \frac{p_T b}{2t_c} \pm \left[\frac{6D_c}{bK_c^*} \frac{\theta_R}{t_c^2} + 1.5432 \frac{p_T b}{t_c} \right] \quad (8.6.8)$$

$$\sigma_s = \frac{p_s b}{2t_s} \pm \frac{6M_s}{t_s^2} = \frac{p_s b}{2t_s} \pm \left[-\frac{6D_s}{bK_s^*} \frac{\theta_R}{t_s^2} + 1.5432 \frac{p_s b}{t_s} \right]$$

We note that $\theta_R = -\Phi(a)$, and that Eq. (8.2.5) gives a relation between $\Phi(a)$, M_0 , and the pressure difference across the tubesheet. Using the relation for $M_r(a)$ given by the first of Eq. (8.2.11) and solving for $aM_0 - pa^3/8$ yields

$$aM_0 - pa^3/8 = -\frac{a}{\mu} [M_r(a) - M^*] \quad (8.6.9)$$

Therefore, substitution of Eq. (8.6.9) in Eq. (8.2.5) yields

$$\theta_R = \frac{a}{D^*(1+\nu^*)\mu} [M_r(a) - M^*] \quad (8.6.10)$$

Table 8.6.2

```

*****
ONE SIDE INTEGRAL ONE SIDE GASKETED CONSTRUCTION
A= 8.875          B= 13.375
E*/E= .445       NUSTAR= .31
E (SHEET)= 2.9E+07      E (SHELL) 0
E (CHANNEL)= 2.9E+07
TS= .375         TC= .875
RS= 9.8125       RC= 10.9375
ROLL DEPTH/THICKNESS= .95
TUBE OD= .75     TUBE THICKNESS= .083
TUBE MODULUS= 2.9E+07      TUBE ALLOWABLE STRESS= 17500
MODIFIED PITCH P'= 1.01421      EFFECTIVE HOLE DIAM. D1= .5923
UNTUBED AREA= 36           TUBE PITCH= .9375
ACTUAL LIGAMENT EFFICIENCY= .368213
EFFECTIVE LIGAMENT EFFICIENCY= .416002
TUBESIDE PRESSURE= 1000      SHELLSIDE PRESSURE= 0
DIFFERENTIAL PRESSURE= 1000
BOLT LOAD= 0
NUMBER OF BOLTS= 0          BOLT RADIUS= 12.5
*****
RESULTS FOR TUBESHEET THICKNESS= 2.6857
SA= 17500          TUBESHEET DESIGN STRESS= 26250
CLAMPING PARAMETER MU= 16.5482
MOMENT PARAMETER MSTAR=-11526.4
SHELL HOOP MEMBRANE STRESS= 0

```

CHANNEL HOOP MEMBRANE STRESS= 12500
 ALLOWABLE MEMBRANE STRESS SHELL= 17500
 ALLOWABLE MEMBRANE STRESS CHANNEL= 17500
 SHELL TOTAL AXIAL STRESS= 0
 CHANNEL TOTAL AXIAL STRESS= 30819.4
 ALLOWABLE SHELL STRESS= 26250
 ALLOWABLE CHANNEL STRESS= 26250
 MOMR(A)= 8627.79 MOMH(A)= 1834.26 MOMR(O)=-7666.84

DESIGN BENDING MOMENT= 8627.79
 FOR H= 2.6857 THE CALCULATED STRESS IS 17252.1

 RESULTS FOR TUBESHEET THICKNESS= 2.375
 SA= 17500 TUBESHEET DESIGN STRESS= 26250
 CLAMPING PARAMETER MU= 18.8787
 MOMENT PARAMETER MSTAR=-11526.4
 SHELL HOOP MEMBRANE STRESS= 0
 CHANNEL HOOP MEMBRANE STRESS= 12500
 ALLOWABLE MEMBRANE STRESS SHELL= 17500
 ALLOWABLE MEMBRANE STRESS CHANNEL= 17500
 SHELL TOTAL AXIAL STRESS= 0
 CHANNEL TOTAL AXIAL STRESS= 31999.9
 ALLOWABLE SHELL STRESS= 26250
 ALLOWABLE CHANNEL STRESS= 26250
 MOMR(A)= 8770.57 MOMH(A)= 1977.04 MOMR(O)=-7524.07

DESIGN BENDING MOMENT= 8770.57
 FOR H= 2.375 THE CALCULATED STRESS IS 22426.3

Table 8.6.3

 TWO SIDE GASKETED CONSTRUCTION
 A= 8.875 B= 11.25
 E*/E= .445 NUSTAR= .31
 E (SHEET)= 2.9E+07 E (SHELL) O
 E (CHANNEL)= 0
 TS= .375 TC= .375
 RS= 10.75 RC= 10.75
 ROLL DEPTH/THICKNESS= .95
 TUBE OD= .75 TUBE THICKNESS= .083
 TUBE MODULUS= 2.9E+07 TUBE ALLOWABLE STRESS= 17500
 MODIFIED PITCH P'= 1.01421 EFFECTIVE HOLE DIAM. D1= .5923
 UNTUBED AREA= 36 TUBE PITCH= .9375
 ACTUAL LIGAMENT EFFICIENCY= .368213
 EFFECTIVE LIGAMENT EFFICIENCY= .416002
 TUBESIDE PRESSURE= 0 SHELLSIDE PRESSURE= 450
 DIFFERENTIAL PRESSURE=-450
 BOLT LOAD= 0
 NUMBER OF BOLTS= 0 BOLT RADIUS= 11

 RESULTS FOR TUBESHEET THICKNESS= 2.19
 SA= 17500 TUBESHEET DESIGN STRESS= 26250
 CLAMPING PARAMETER MU= .404049
 MOMENT PARAMETER MSTAR= 4618.71
 SHELL HOOP MEMBRANE STRESS= 12900
 CHANNEL HOOP MEMBRANE STRESS= 0
 ALLOWABLE MEMBRANE STRESS SHELL= 17500
 ALLOWABLE MEMBRANE STRESS CHANNEL= 17500
 SHELL TOTAL AXIAL STRESS= 6450
 CHANNEL TOTAL AXIAL STRESS= 0
 ALLOWABLE SHELL STRESS= 26250
 ALLOWABLE CHANNEL STRESS= 26250
 MOMR(A)= 2014.57 MOMH(A)= 5071.66 MOMR(O)= 9347.15

DESIGN BENDING MOMENT= 9347.15
 FOR H= 2.19 THE CALCULATED STRESS IS 28109.1

Table 8.6.4

```

*****
INTEGRAL CONSTRUCTION
A= 8.875          B= 10.875
E*/E= .445       NUSTAR= .31
E (SHEET)= 2.9E+07      E (SHELL) 2.9E+07
E (CHANNEL)= 2.9E+07
TS= .375         TC= 3.25
RS= 10.875       RC= 10.875
ROLL DEPTH/THICKNESS= .95
TUBE OD= .75     TUBE THICKNESS= .083
TUBE MODULUS= 2.9E+07      TUBE ALLOWABLE STRESS= 17500
MODIFIED PITCH P'= 1.01421      EFFECTIVE HOLE DIAM. D1= .5923
UNTUBED AREA= 36           TUBE PITCH= .9375
ACTUAL LIGAMENT EFFICIENCY= .368213
EFFECTIVE LIGAMENT EFFICIENCY= .416002
TUBESIDE PRESSURE= 2850      SHELLSIDE PRESSURE= 0
DIFFERENTIAL PRESSURE= 2850
BOLT LOAD= 0
NUMBER OF BOLTS= 0          BOLT RADIUS= 0
*****
RESULTS FOR TUBESHEET THICKNESS= 3.758
SA= 17500          TUBESHEET DESIGN STRESS= 26250
CLAMPING PARAMETER MU= 30.7258
MOMENT PARAMETER MSTAR=-31636
SHELL HOOP MEMBRANE STRESS= 0
CHANNEL HOOP MEMBRANE STRESS= 9536.54
ALLOWABLE MEMBRANE STRESS SHELL= 17500
ALLOWABLE MEMBRANE STRESS CHANNEL= 17500
SHELL TOTAL AXIAL STRESS= 3369.3
CHANNEL TOTAL AXIAL STRESS= 25836.3
ALLOWABLE SHELL STRESS= 26250
ALLOWABLE CHANNEL STRESS= 26250
MOMR(A)= 26178.6          MOMH(A)= 6817.05          MOMR(O)=-20261.1
DESIGN BENDING MOMENT= 26178.6
FOR H= 3.758          THE CALCULATED STRESS IS 26735.6

```

Table 8.6.5

```

*****
TWO SIDE GASKETED CONSTRUCTION
A= 8.15          B= 12.5
E*/E= .435       NUSTAR= .31
E (SHEET)= 2.8E+07      E (SHELL) 0
E (CHANNEL)= 0
TS= .5           TC= .5
RS= 9.5          RC= 9
ROLL DEPTH/THICKNESS= .95
TUBE OD= 1       TUBE THICKNESS= .065
TUBE MODULUS= 2.8E+07      TUBE ALLOWABLE STRESS= 18700
MODIFIED PITCH P'= 1.48106      EFFECTIVE HOLE DIAM. D1= .8765
UNTUBED AREA= 60           TUBE PITCH= 1.25
ACTUAL LIGAMENT EFFICIENCY= .2988
EFFECTIVE LIGAMENT EFFICIENCY= .408193
TUBESIDE PRESSURE= 0        SHELLSIDE PRESSURE= 0
DIFFERENTIAL PRESSURE= 0
BOLT LOAD= 12500
NUMBER OF BOLTS= 16        BOLT RADIUS= 10.5
*****
RESULTS FOR TUBESHEET THICKNESS= 2
SA= 18700          TUBESHEET DESIGN STRESS= 28050
CLAMPING PARAMETER MU= .745536
MOMENT PARAMETER MSTAR=-1953.81
SHELL HOOP MEMBRANE STRESS= 0
CHANNEL HOOP MEMBRANE STRESS= 0
ALLOWABLE MEMBRANE STRESS SHELL= 18700
ALLOWABLE MEMBRANE STRESS CHANNEL= 18700
SHELL TOTAL AXIAL STRESS= 0
CHANNEL TOTAL AXIAL STRESS= 0
ALLOWABLE SHELL STRESS= 0
ALLOWABLE CHANNEL STRESS= 0
MOMR(A)=-1119.32          MOMH(A)=-1119.32          MOMR(O)=-1119.32
DESIGN BENDING MOMENT= 1119.32
FOR H= 2          THE CALCULATED STRESS IS 4113.2

```

```

A= 8.15          B= 12.5
E*/E= .435      NUSTAR= .31
E (SHEET)= 2.8E+07      E (SHELL) 0
E (CHANNEL)= 0
TS= .5          TC= .5
RS= 9.5         RC= 9
ROLL DEPTH/THICKNESS= .95
TUBE OD= 1      TUBE THICKNESS= .065
TUBE MODULUS= 2.8E+07      TUBE ALLOWABLE STRESS= 18700
MODIFIED PITCH P'= 1.48106      EFFECTIVE HOLE DIAM. D1= .8765
UNTUBED AREA= 60          TUBE PITCH= 1.25
ACTUAL LIGAMENT EFFICIENCY= .2988
EFFECTIVE LIGAMENT EFFICIENCY= .408193
TUBESIDE PRESSURE= 500      SHELLSIDE PRESSURE= 0
DIFFERENTIAL PRESSURE= 500
BOLT LOAD= 12500
NUMBER OF BOLTS= 16          BOLT RADIUS= 10.5

*****
RESULTS FOR TUBESHEET THICKNESS= 2
SA= 18700      TUBESHEET DESIGN STRESS= 28050
CLAMPING PARAMETER MU= .745536
MOMENT PARAMETER MSTAR=-3875.73
SHELL HOOP MEMBRANE STRESS= 0
CHANNEL HOOP MEMBRANE STRESS= 9000
ALLOWABLE MEMBRANE STRESS SHELL= 18700
ALLOWABLE MEMBRANE STRESS CHANNEL= 18700
SHELL TOTAL AXIAL STRESS= 0
CHANNEL TOTAL AXIAL STRESS= 18388.8
ALLOWABLE SHELL STRESS= 0
ALLOWABLE CHANNEL STRESS= 0
KOMR(A)=-447.26          MOHH(A)=-3311.73          MOMR(O)=-7317.84

DESIGN BENDING MOMENT= 7317.84
FOR H= 2          THE CALCULATED STRESS IS 26891.1
    
```

With θ_R computed, σ_c , σ_s can be determined. The ASME Code suggests that the maximum value of the extreme fiber stress at the joint should not exceed 1.5 times the allowable stress of the shell or channel material. In a given configuration, should this stress be exceeded, the geometry should be changed either by increasing the tubesheet thickness or by increasing the appropriate cylindrical wall thickness near the joint. The tubesheet thickness need not exceed the thickness calculated if one assumed a one side gasketed joint in making the computations. Returning to the sample analyses illustrated here, we see that for the one side integral construction, the axial membrane plus bending stress exceeds the allowable value for a mechanically loaded joint. Strict adherence to ASME Code design rules at this point would dictate investigation of a local increase in channel thickness near the joint, or alternatively, an increase in tubesheet thickness above the TEMA prediction of 2.6857". It is quite possible that a designer could eliminate the problem in this specific case by simply requesting actual property test data on the material batch so as to possibly permit a slight increase in the material allowable stress in the channel.

NOMENCLATURE

- a = Radius of perforated region
- a^* = Mean radius of unperforated rim
- A_{UT} = Untubed region within perforated area
- b = Outer radius of unperforated region of tubesheet



- B, N_B = Bolt load; number of bolts
 C_T = TEMA coefficient
 D = Generic term for flexural rigidity of a plate or shell type structure.
 d = Bolt circle radius
 d_1 = Effective tube hole diameter defined by Eq. (8.6.6)
 D^* = Effective flexural rigidity of the perforated region.
 d^*, t^* = Tube hole diameter; tube thickness
 e = Flexural efficiency defined by Eq. (8.3.16)
 E^*, ν^* = Effective elastic constants of tubesheet perforated region
 E_T, E = Young's Moduli of tube, tubesheet
 G = Effective diameter of gasket
 G_s, G_c = Gasket forces defined by Eq. (8.5.1)
 h = Tubesheet thickness
 H = Ligament width
 K_a = Rotational spring rate of the outer edge of the perforated region.
 M^* = Edge loading parameter (Eq. (8.2.8))
 M_0 = Radial bending moment at $r = a$ (per unit circumference)
 M_r, M_θ = Radial, circumferential bending moments in perforated region of tubesheet
 M_R = Effective ring moment
 M_T, M_S = Channel, shell edge bending moments
 N_T = Number of tubes in tubesheet
 p = Differential pressure across tubesheet
 p_T, p_s = Tubeside, shellside pressure, respectively
 P, P' = Tube layout pitch; effective tube pitch
 Q_0 = Shear per unit circumference at the edge of the perforated region
 r = Radial coordinate of tubesheet
 r_c, r_s = Mean radius of channel, shell; mean radius of channel, shell gasket
 RD = Roll depth (percentage of tubesheet thickness)
 S_A = Allowable stress from ASME code
 t_c, t_s = Channel, shell thickness
 U = Defined in Fig. 8.6.1
 V_T, V_S = Channel, shell edge shear forces
 δ^* = Increase in shell/channel radius due to membrane effect of pressure
 δ, θ = Edge deflection, rotation of shell, channel
 θ_i = Perforation angle (Fig. 8.1.1)
 η = Ligament efficiency
 γ_T, γ_S = Coefficients defined by Eq. (8.4.4)
 μ = Edge stiffness parameter defined in Eq. (8.2.10)
 $\Phi(a)$ = Tubesheet rotation at $r = a$

Subscripts

- s = pertains to the shell
 c = pertains to the channel (tubeside)
 R = pertains to the tubesheet rim

REFERENCES

- [8.1.1] Gardner, K. A., "Heat Exchanger Tube Sheet Design," *Journal of Applied Mechanics*, Vol. 70, 15, p. 377 (1948).
- [8.1.2] Gardner, K. A., "Heat Exchanger Tube Sheet Design—2 Fixed Tube Sheets," *Journal of Applied Mechanics*, Vol. 74, p. 159 (June 1952).
- [8.1.3] Gardner, K. A., "Heat Exchanger Tube Sheet Design, Part 3: U-Tube and Bayonet-Tube Sheets," *Journal of Applied Mechanics*, Vol. 82, p. 25 (March 1960).
- [8.1.4] Miller, K. A. G., "The Design of Tubeplates in Heat Exchangers," Proceedings of the Institution of Mechanical Engineers, London, Vol. 1B, p. 215 (1952–53).
- [8.1.5] Soler, A. I., "Tubesheet Design in U-Tube Exchangers Including the Effect of Tube Rotational Restraint," *Journal of Engineering for Industry*, Trans. ASME, Vol. 98, No. 4, pp. 1157–1160 (1976).
- [8.1.6] Soler, A. I., and Soehrens, J. E., "Design Curves for Stress Analysis of U-Tube Heat Exchanger Tubesheet with Integral Channel and Head," *Journal of Pressure Vessel Technology*, Vol. 100, p. 221 (May 1978).
- [8.1.7] "Standards of the Tubular Exchanger Manufacturers Association," Sixth Edition, N.Y. (1978).
- [8.1.8] "ASME Pressure Vessel Code," Section VIII, Div. 2, N.Y. 1980, Article 4.9, p. 461.
- [8.1.9] O'Donnell, W. J., "Effective Elastic Constants for the Bending of Thin Perforated Plates with Triangular and Square Penetration Patterns," *Journal of Engineering for Power*, Trans. ASME, B, Vol. 95, p. 121 (February 1973).
- [8.1.10] Soler, A. I., and Hill, W. S., "Effective Bending Properties for Stress Analysis of Rectangular Tubesheets," *Journal of Engineering for Power*, Vol. 99, No. 3, p. 365 (July 1977).
- [8.3.1] Burgreen, D., "Pressure Vessel Analysis," C. P. Press, pp. 195–200 (1979).
- [8.6.1] "ASME Pressure Vessel Code," Section VIII, Div. 1, Non Mandatory Appendix U, N.Y. (1980).
- [8.6.2] "Standards of the Tubular Exchanger Manufacturers Association – Sample Problem Book," TEMA, Tarrytown, N.Y. (1980).

APPENDIX 8.A

COMPUTER CODE "UTUBE"

This code is written in TRS80 Model III BASIC language. The user is prompted on the screen for certain input. The input quantities required (in consistent units) are:

- NT = Construction type = 2 (both sides integral)
 1 (one side integral, one side gasketed)
 0 (two sides gasketed)
- A,B = Outer radius of perforated region, outer radius of unperforated rim
- ET,ES,EC = Young's Modulus of tubesheet, shell, channel, respectively (input 0 for ES, EC if shell, channel gasketed)
- TS,TC = Shell, channel wall thicknesses
- RS,RC = Shell, channel mean radii (see Fig. 8.2.2)
- SA = Tubesheet code allowable stress at temperature
- OM = A stress amplifier which should be input as 1.0
- VS,VC = Code allowable stress for shell and channel at temperature
- RD = Roll depth (% of thickness)
- TD,TT,FT,ST = Tube O.D., thickness, Young's Modulus, allowable stress from code
- TP = Tube pitch from drawings
- UA = Untubed area within radius A
- ER,NU = Effective property inputs E^*/E , ν^* which are determined from Figs. 8.1.1, 8.1.2 using a program computed effective ligament efficiency
- LB,NB,D = Load on a single bolt, number of bolts, bolt circle radius
- PT,PS = Tubeside, shellside pressures
- Note: Subsequent analysis is carried out for $P = PT - PS$

LISTING OF UTUBE/BAS

```

10 CLS
20 LPRINT:LPRINT:LPRINT"*****"
30 REM U-TUBE HEX CALCULATIONS WRITTEN BY DR.A.I.SOLER JAN.1983
40 PRINT"UNIT TYPE=2 INTEGRAL CONSTRUCTION"
50 PRINT"      =1 ONE SIDE INTEGRAL, ONE SIDE GASKETED"
60 PRINT"      =0 TWO SIDE GASKETED CONSTRUCTION"
70 INPUT"INPUT UNIT TYPE 2,1,OR 0";NT
80 IF NT=2 THEN LPRINT"INTEGRAL CONSTRUCTION" ELSE GOTO 100
90 GOTO130
100 IF NT=1 THEN LPRINT" ONE SIDE INTEGRAL ONE SIDE GASKETED CONSTRUCTION" ELSE
LPRINT "TWO SIDE GASKETED CONSTRUCTION"
110 PRINT" A=OUTER RADIUS OF PERFORATED REGION"
120 PRINT" B=OUTER RADIUS OF UNPERFORATED RIM"
130 INPUT"INPUT A,B";A,B:PRINT"FOR TYPE 1 OR 0 SHELL AND/OR CHANNEL MODULUS ARE
ZERO"
140 INPUT"ETUBESHEET,ESHELL,ECHANNEL";ET,ES,EC
150 INPUT"INPUT SHELL,CHANNEL THICKNESSES";TS,TC:INPUT"SHELL,CHANNEL RADII";RS,RC

```

```

C:INPUT"INPUT TUBESHEET ALLOWABLE STRESS,OMEGA";SA,OM
160 INPUT"INPUT ALLOWABLE STRESS FOR SHELL, FOR CHANNEL";VS,VC
170 INPUT"INPUT % ROLL DEPTH ASSUMED";RD:RD=RD/100:INPUT"INPUT TUBE OD, THICKNESS
,MODULUS, ALLOWABLE STRESS";TD, TT, FT, ST
180 INPUT"INPUT TUBE PITCH";TP
190 INPUT"INPUT UNTUBED AREA IN PROPER UNITS";UA
200 X1=1+UA/(3.14*A*A*U):P1=TP*SQR(X1)
210 D1=TD-2*TT*RD*FT/ET*ST/SA:IFD1<(TD-2*TT) THEN D1=TD-2*TT
220 LE=(P1-D1)/P1:LI=(TP-D1)/TP:PRINT"ACTUAL LIGAMENT EFF.=";LI,"EFFECTIVE L.E. =
";LE:PRINT" E, NU = EFFECTIVE PROPERTIES FROM CHARTS GIVEN AS A FUNCTION
O F LIGAMENT EFFICIENCY"
230 INPUT"ENTER E*/E, NU*";ER, NU:EP=ER*(1-NU*NU)
240 PRINT" FOR A TYPE 1 UNIT A NON-ZERO BOLT CIRCLE RADIUS"
250 PRINT" MUST BE INPUT TO PREVENT PROGRAM ERROR"
255 PRINT" IF BOLT LOAD=0 ANY BOLT RADIUS MAY BE INPUT"
260 INPUT"INPUT BOLT LOAD, NUMBER OF BOLTS, BOLT RADIUS";LB, NB, D
270 INPUT"INPUT TUBESIDE, SHELLSIDE PRESSURES";PT, PS
280 P=PT-PS:K=B/A:LPRINT"A=";A,"B=";B:LPRINT"E*/E=";ER,"MUSTAR=";NU:LPRINT"E (SH
EET)=";ET,"E (SHELL)";ES:LPRINT"E (CHANNEL)=";EC
290 IF NT=2 THEN B=RC
300 IF NT=2 THEN RS=RC
310 LPRINT"TS=";TS,"TC=";TC:LPRINT"RS=";RS,"RC=";RC
320 LPRINT"ROLL DEPTH/THICKNESS=";RD:LPRINT"TUBE OD=";TD,"TUBE THICKNESS=";TT:LPR
INT"TUBE MODULUS=";FT,"TUBE ALLOWABLE STRESS=";ST
330 LPRINT"MODIFIED PITCH P'=";P1," EFFECTIVE HOLE DIAM. D1=";D1
340 LPRINT"UNTUBED AREA=";UA,"TUBE PITCH=";TP
350 LPRINT"ACTUAL LIGAMENT EFFICIENCY=";LI
360 LPRINT"EFFECTIVE LIGAMENT EFFICIENCY=";LE
370 LPRINT"TUBESIDE PRESSURE=";PT,"SHELLSIDE PRESSURE=";PS
380 LPRINT"DIFFERENTIAL PRESSURE=";P
390 LPRINT"BOLT LOAD=";LB:LPRINT"NUMBER OF BOLTS=";NB,"BOLT RADIUS=";D
400 PRINT"CHOOSE H=0 TO END JOB, -1 TO GO TO LINE 190, -2 TO GO TO LINE 250, -3 TO
GO TO LINE 260, OR SIMPLY INPUT A VALUE OF H TO PROCEED WITH COMPUTATIONS"
410 INPUT"INPUT ESTIMATE OF TUBESHEET THICKNESS";H: M1=H
420 IF M1>0 THEN GOTO 430 ELSE M1=-M1:ON M1 GOTO 190 ,260 ,270
430 IFH=0 END
440 LPRINT"*****"
450 LPRINT" RESULTS FOR TUBESHEET THICKNESS=";H
460 SD=1.5*OM*SA:LPRINT"SA=";SA,"TUBESHEET DESIGN STRESS=";SD
470 CS=2.568*SQR(RS/TS)+1.651*H/TS:CC=2.568*SQR(RC/TC)+1.651*H/TC
480 BS=3.301*RS/TS*(1+1.285*RS*H/(TS*TS)):BC=3.301*RC/TC*(1+1.285*RC*H/(TC*TC))
490 LA=ES*TS*(ET*H*(3)*(CS+.5*H*BS/RS)):LA=LA+EC*TC*(3/(ET*H*(3)*(CC+.5*H*BC/RC))
500 MU=(LA+LOG(K))/(EP*(1-NU)):LPRINT"CLAMPING PARAMETER MU=";MU
510 GT=(RC/A-1)*((RC/A)*(2+1)):GS=(RS/A-1)*((RS/A)*(2+1))
520 IF NT=2 THEN EM=-.25*P*A*A*(K+1)*(K-1) ELSE EM=-.25*A*A*(GT*PT-GS*PS)
530 IF NT=1 THEN EM=EM-NB*LB/6.28*D/A*(1-RC/D)
540 IF NT=0 THEN EM=EM-NB*LB/6.28*(RS-RC)/A
550 LPRINT"MOMENT PARAMETER MSTAR=";EM
560 SP=PS*RS/TS:CP=PT*RC/TC
570 LPRINT"SHELL HOOP MEMBRANE STRESS=";SP
580 LPRINT"CHANNEL HOOP MEMBRANE STRESS=";CP
590 LPRINT"ALLOWABLE MEMBRANE STRESS SHELL=";VS;WS=1.5*VS;WC=1.5*VC
600 LPRINT"ALLOWABLE MEMBRANE STRESS CHANNEL=";VC
610 MA=EM+.125*MU*P*A*A:MA=MA/(1+MU)
620 DM=(MA-EM)/D2:DM/(K+H*(3*(1+NU)*MU*EP)*6/ET
630 SX=TC*D2+CC*EC+1.5432*CP:SY=-TS*D2+CS*ES+1.5432*SP
640 S1=.5*CP+SX:S2=.5*CP-SX
650 S3=.5*SP+SY:S4=.5*SP-SY
660 IF ABS(S3)>ABS(S4) THEN SS=S3 ELSE SS=S4
670 IF ABS(S1)>ABS(S2) THEN SC=S1 ELSE SC=S2
675 IF EC=0 THEN SC=CP/2.
676 IF ES=0 THEN SS=SP/2.
680 LPRINT"SHELL TOTAL AXIAL STRESS=";SS:LPRINT"CHANNEL TOTAL AXIAL STRESS=";SC:
LPRINT"ALLOWABLE SHELL STRESS=";WS:LPRINT"ALLOWABLE CHANNEL STRESS=";WC
690 MO=-.125*P*A*A*(1-NU-MU/(1+MU))+EM/(1+MU)
700 MO=EM/(1+MU)-P*A*A/16*(3+NU-2*MU/(1+MU))
710 LPRINT"MO(M)=";MA,"MOM(A)=";MO,"MOM(O)=";MO
720 MT=ABS(MA):IF MT<ABS(MO) THEN MT=ABS(MO)
730 IF MT<ABS(MO) THEN MT=ABS(MO)
740 LPRINT"DESIGN BENDING MOMENT=";MT
750 PRINT"THE DESIGN STRESS FOR THE TUBESHEET IS ";SD
760 PRINT"THE SHELL TOTAL AXIAL STRESS IS";SS;" THE CHANNEL TOTAL AXIAL STRESS I
S";SC
770 PRINT"THE STRESS ALLOWABLES FOR SHELL AND CHANNEL ARE";WS,WC
780 PRINT"THE SHELL HOOP MEMBRANE STRESS="SP:PRINT"THE CHANNEL HOOP MEMBRANE S
TRESS=";CP
790 PRINT"THE SHELL, CHANNEL MEMBRANE ALLOWABLES=";VS,VC
800 SB=6*MT/(LE*H*H):LPRINT"FOR H=";H,"THE CALCULATED STRESS IS ";SB:PRINT"FOR
H=";H;" THE CALCULATED STRESS IS=";SB:LPRINT:LPRINT:GOTO400

```

9. TUBESHEETS IN FIXED AND FLOATING HEAD HEAT EXCHANGERS

9.1 SCOPE OF ANALYSIS

Fixed and floating head heat exchanger constructions find widespread application in the power and process industries. Fig. 9.1.1 shows a typical vertically mounted unit. We have included on that figure the nomenclature to be used in subsequent derivations. The response of the two tubesheets to external mechanical and/or thermal loading is not independent; the tube bundle provides a load transfer mechanism between the two tubesheets. A rigorous analysis of the unit, to determine tubesheet thicknesses, must consider the effects of coupling between the tubesheets when determining the stress and deformation in the tubesheets, tubes, shell, and channels. Unfortunately, the analysis becomes significantly more difficult to carry out compared to the analysis for U-tube heat exchanger tubesheets discussed previously.

The inherent complexity in the design of the tubesheets for a fixed tubesheet exchanger is apparent from the TEMA standards [9.1.1] which gives non-iterative design formulas for all exchanger geometries save the fixed tubesheet type. TEMA design rules take credit for the supportive action of the tubes in reducing the tubesheet bending stress. This, however, implies that the mechanical design of the tubesheet must be carried out with an eye on the tube axial stress and on the tube/tubesheet joint load. Unacceptably high tube-to-tubesheet joint loads are clearly a matter of grave design concern. Designers alleviate these loads by inserting an expansion joint in the shell. Addition of the expansion joint, however, relieves tube axial load at the expense of increasing the tubesheet bending stress. Optimal design calls for a judicious balance between the expansion joint axial stiffness and the tubesheet thickness. Such opportunities for economies in design and enhancement of operational reliability have spawned considerable research interest in the stress analysis of fixed tubesheet exchangers [9.1.2–10]. In floating tubesheet design, the axial deformation of the shell is decoupled from tube and tubesheet deformations. However, coupling between the tube axial load and tubesheet flexure remains. Therefore, opportunities for design optimization similar to the fixed tubesheet problem still exist. Such a design study is best conducted on a digital computer. Therefore, our goal in this chapter is to provide a logical development of fixed and floating tubesheet exchanger stress analysis, beginning with a generalized computer oriented treatment, and

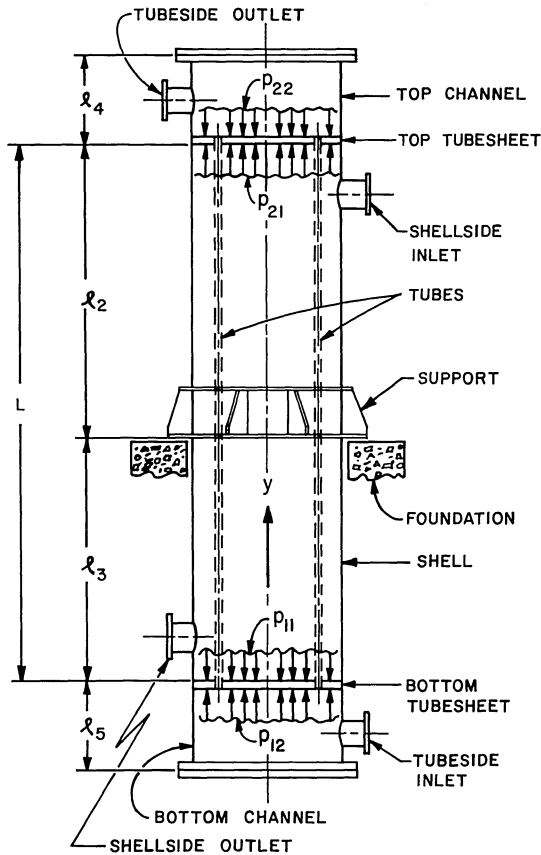


Fig. 9.1.1. Vertically mounted integral tubesheet heat exchanger.

simplifying down to practical graphical methods.

The sections devoted to analysis will discuss three main topics. Initially, we deal with analysis of a vertically mounted heat exchanger having two dissimilar fixed tubesheets. In general, each tubesheet may have a different thickness and a different method of attachment to the heat exchanger barrel. The interaction between the two tubesheets is retained in the formulation. During the development, the modifications required to permit the analysis of a unit having one fixed tubesheet and one floating tubesheet are indicated. Based on the theoretical analysis, we can develop a computer solution, and we illustrate its application by using a typical heat exchanger specification.

Because of the complexity of the initial simulation, we omit many details of the algebraic manipulations and emphasize only key results. Therefore,

the second topic discussed in this chapter considers an analysis of a symmetrical unit containing identical tubesheets, and constant shell and channel side pressures. This assumed symmetry permits us to analyze only one half of the unit. This simplification permits an exposition in more detail of the manipulations required to develop the final formulation. Despite the considerable simplifications, we still find that numerical results are best obtained using a computer solution. To this end, a second computer code is included, based on the simpler analysis, and its application illustrated.

The final item of attention in this chapter focuses on even further simplification of the analytical formulation. We show how the complex computer-dependent formulations can be drastically simplified to provide acceptable results for design purposes using graphical data. In the course of this simplification, we show how the formulas for tubesheet design found in the TEMA Standards [9.1.1] are developed from the more rigorous theoretical analysis. In summary, this chapter presents the complete gamut of tubesheet analysis ranging from a generalized complex model to the simplified design formulas of TEMA.

The stress analysis of a general fixed tubesheet heat exchanger presented in the subsequent sections proceeds in the following manner:

- (i) Write the expression for the change in length of the tube in terms of its net surface pressure, the tube temperature rise, gravity effects (vertical units), and end loads. Of these only the end loads are unknown. A similar relationship for the shell is written.
- (ii) Model the tubesheet as an annular rim bounding an "equivalent inner plate"; the latter simulates the rigidity of the perforated region. The net pressure on the annular plate (tubesheet rim) is simply the algebraic difference of the shell and tubeside pressures. The pressure on the equivalent inner plate is obtained by "smearing" the tube end loads and shellside and tubeside pressures acting on the respective ligaments*, over the tubed region surface.
- (iii) Classical plate bending theory furnishes the necessary relations between the lateral deflection of the tubesheets and its surface loads, which include the smeared out tube end loads.
- (iv) The change in the axial length of the tubes at any radius r within the tubed region must be algebraically equal to the sum of the change in the length of the shell and the deflection of the tubesheets. This compatibility condition, along with the classical requirements of deflection, slope, moment, and shear continuity at the tubesheet-shell-channel junctions and at the interface of the tubed and annular regions, furnish the necessary information to completely define the deformation and stresses in the shell, in the tubes, and in the tubesheets. Formal details are presented below.

*The ligament area for the shellside pressure is the outside of the tubes, the ligament area on the tubeside is greater by the amount of the tube metal cross sectional area.

9.2 EFFECTIVE PRESSURE ON TUBESHEET DUE TO THE TUBE BUNDLE

In the previous chapter, concerned with the stress analysis of tubesheets in U-tube type exchangers, the tubing plays a limited role. The only effect of the tubing considered there is the possible modification to the tubesheet ligament efficiency if we take credit for the tube wall thickness. In fixed or floating head construction, however, the tubes play a significant role in supporting the applied loading. Therefore, we must pay considerable attention to incorporating the tube effect into any mathematical model of the unit.

In this section, we consider a single tube as an elastic tension-compression member and show that its effect on the tubesheet is to apply a surface pressure proportional to the tubesheet deformation. Our sole aim in this section is to formulate an expression for the effective surface pressure on the tubesheet due to the tubes acting as stays.

Let us consider a single tube located at radial distance r from the center of the tubesheet and introduce the following notations:

$E_T; \nu_T; \alpha_T$	= Young's modulus; Poisson's ratio; coefficient of thermal expansion of the tube material
$A_T; L; d; t$	= Tube metal cross section area; effective length; outer diameter; wall thickness
$p_s^*; p_t^*$	= Shellside; tubeside pressures averaged over the tube length
$\Delta_{TG}, \Delta_{T\theta}, \Delta_{TPR}$	= Change in tube free length due to gravitational effects; due to thermal growth; and due to Poisson ratio effects
δ	= Total change in length of the tube
μ_T	= Weight/unit volume of tube metal

Figure 9.2.1 shows a free body of a single vertical tube with end forces F_1, F_2 . We now relate these end forces F_1, F_2 to the tube growth δ by applying force equilibrium and Hooke's Law. At any section x , the axial force $F(x)$ is:

$$F(x) = \mu_T A_T x + F_1 \quad (9.2.1)$$

where $\mu_T A_T$ = weight of tube per unit length. Equation (9.2.1) is simply a statement of force equilibrium in the direction parallel to the axis of the tube. The simple one-dimensional Hooke's Law relating the axial extension of the tube to the axial force, yields an expression for the total growth of the tube due to axial force, due to gravity, due to thermal expansion, and due to Poisson's ratio effects:

$$\delta = \frac{F_1 L}{E_T A_T} + \Delta_{TG} + \Delta_{T\theta} + \Delta_{TPR} \quad (9.2.2)$$

where

$$\begin{aligned} \Delta_{TG} &= \mu_T L^2 / (2E_T) \\ \Delta_{TPR} &= \nu(p_s^* d - p_i^* [d - 2t])L / (2E_T t) \end{aligned} \tag{9.2.3}$$

The first term in Eq. (9.2.2) is the tube growth due to an end force F_1 ; the remaining terms are the growth due to dead weight, the growth due to free thermal expansion, and the growth due to Poisson ratio effects when the tube is under internal and external pressure. Evaluating Eq. (9.2.1) at $x = L$, and using Eq. (9.2.2) yields expressions for F_1 and F_2 in the form

$$\begin{aligned} F_1 &= \frac{E_T A_T}{L} (\delta - \Delta_{TG} - \Delta_{T\theta} - \Delta_{TPR}) \\ F_2 &= \frac{E_T A_T}{L} (\delta + \Delta_{TG} - \Delta_{T\theta} - \Delta_{TPR}) \end{aligned} \tag{9.2.4}$$

If ‘‘a’’ is the effective outer radius of the tubesheet perforated region and n is the number of tubes in the unit, then effective pressures q_{T1} , q_{T2} acting on the tubesheets, due to the presence of the tubes, are:

$$\begin{aligned} q_{T1} &= n F_1 / \pi a^2 = \xi (\delta - \Delta_{TG} - \Delta_{T\theta} - \Delta_{TPR}) \\ q_{T2} &= n F_2 / \pi a^2 = \xi (\delta + \Delta_{TG} - \Delta_{T\theta} - \Delta_{TPR}) \end{aligned} \tag{9.2.5}$$

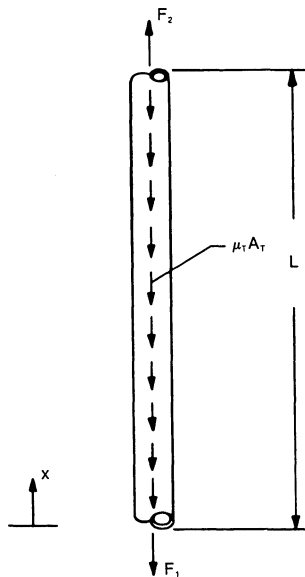


Fig. 9.2.1. Freebody of a single tube.

where

$$\xi = n E_T A_T / \pi a^2 L \quad (9.2.6)$$

Thus, we have shown that the effect of the tube array on the tubesheets is an effective pressure, proportional to the change in tube length. The key point to be made here is that since the tubes are held between two deforming tubesheets, they can stretch or compress and therefore support load. No such action occurs in a U-tube unit.

9.3 ANALYSIS OF A PERFORATED CIRCULAR TUBESHEET

We now formulate the solutions valid in the perforated region of the tubesheet. The tubesheets are considered as thin plates (Kirchoff's plate theory) and are analyzed under the effects of the known applied loads (pressure and thermal) as well as under the effects of the effective pressures due to the tubing. We will see that the effect of the tubes, in coupling together the equations for the two tubesheets, increases the complexity of the solution.

Figure 9.3.1 shows the perforated region of the two interconnected tubesheets in their deflected positions. Positive directions of tubesheet moments, shears, rotations, and deflections are shown on the figure. The analysis considers each tubesheet as governed by the assumptions of classical plate theory subject to the following requirements (see Ref. [9.3.1], or Appendix A at the end of the text):

- (i) Shear deformation and the effect of transverse normal strains due to surface pressures are neglected.
- (ii) Both tubesheets are perforated in a regular pattern giving rise to the same effective radius a .
- (iii) Applied loading and boundary conditions are independent of circumferential location.
- (iv) The effect of individual tubes in the tube bundle is replaced by the effective pressures q_{T1} and q_{T2} .
- (v) Temperature gradients through the tubesheet thickness are neglected.

In Figs. 9.1.1, 9.3.1, we define the various applied pressures p_{ij} by the relations:

$$\begin{aligned} p_{11} &= p_s + \mu_1^* L - \Delta p_s \\ p_{12} &= p_c + \mu_2^* (L + l_4) + \Delta p_t \end{aligned} \quad (9.3.1)$$

$$p_{21} = p_s$$

$$p_{22} = p_c + \mu_2^* l_4$$

The quantity p_s is the shellside static pressure at the top level of the shellside chamber, p_c is the channel static pressure at the top channel cover level, μ_i^* ($i=1,2$) are the weight densities of shell and tube side fluids, respectively, and Δp_s , Δp_t are the total pressure drops in the shell and tube side streams, respectively. Note that the hydrostatic heads can also be used to simulate seismic effects parallel to the exchanger barrel by introducing a seismic acceleration factor.

We model each tubesheet in the analysis as having a perforated inner region and a solid outer annular region. The radius “ a ”, marking the interface between perforated and unperforated region, has been previously discussed in Chapter 8, and is assumed to be given by the formula [9.3.2]

$$a = r_c + \frac{P - h_L}{4} \tag{9.3.2}$$

Here, we use the notation that the radius r_c is taken to the outermost tube hole center, P is the nominal tube pitch, and h_L is the nominal tube ligament width. A ligament efficiency η is then defined, as in Chapter 8, by the relation:

$$\eta = 1 - d^*/P \tag{9.3.3}$$

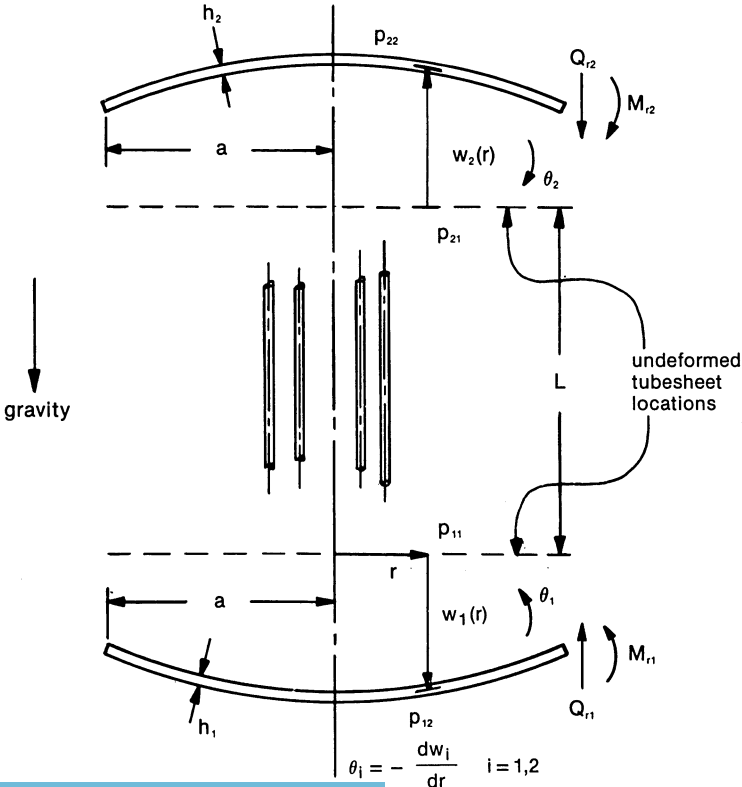


Fig. 9.3.1. Deformation and stress variables for tubesheets.

where d^* is an effective tube hole diameter which may include part or all of the tube wall (see Chapter 8 for details).

In this analysis for fixed and floating head units, we will assume that the tubesheet interior is fully perforated; hence, we need not incorporate any interior solid regions into a modified definition of ligament efficiency. As noted in Chapter 8, for analysis purposes, the perforated region of the tubesheet is replaced by an equivalent solid region having effective elastic constants; the ligament efficiency η is the significant parameter influencing the values of these effective constants. References [9.3.3, 9.3.4] contain discussions on the subject of elastic constants for tubesheets, and a correlation of the work of several investigators into a usable analytical expression for one of the effective constants. In our analyses here, we denote the effective constants for a particular perforated region as E^* , ν^* and we assume that these effective values are available.

We will show, in what follows, that with minor changes in definition, and in boundary conditions, the same basic model can be employed to analyze units where both tubesheets are fixed to the shell (integral construction), or where one tubesheet (say the upper tubesheet) is permitted to float, (floating head construction). The details of the analysis are carried through first for integral construction; subsequently, the changes required to adapt the equations to model floating head construction are discussed.

In order to obtain the solutions valid in the interior region of the tubesheets, we define $w_i(r)$, ($i=1,2$) to be the elastic deformation (normal to the tubesheet plane) of the i th tubesheet *relative to the shell*; then referring to Fig. 9.1.1, we can write down the expression for the total change in tube length as

$$\delta(r) = w_1(r) + w_2(r) + \Delta_S + \Delta_{S\theta} + \mu_S(l_3^2 - l_2^2)/2E_S \quad (9.3.4)$$

Here, Δ_S represents the elastic stretch of the shell due to axial forces, and due to internal pressure (Poisson ratio effects). $\Delta_{S\theta}$ represents the stretch of the shell due to the shell average temperature change above the assembly condition, and μ_S is the shell metal weight density. We can now use Eqs. (9.2.5), (9.3.1), and (9.3.4) to obtain expressions for the net surface pressure on each tubesheet in terms of w_1 , w_2 , and the applied loadings. Defining the positive pressure directions in the positive direction of w_1, w_2 , the net effective pressure on the bottom tubesheet is

$$q_1 = \frac{p_{11}A_0^*}{A_1^*} - q_{r1} - \frac{p_{12}A_l^*}{A_1^*}$$

Similarly, the net effective pressure on the top tubesheet is

$$q_2 = \frac{p_{21}A_0^*}{A_1^*} - q_{r2} - \frac{p_{22}A_l^*}{A_1^*}$$

Substituting for q_{T1} and q_{T2} from Eq. (9.2.5), and replacing δ by the r.h.s. of Eq. (9.3.4) gives the effective pressures as

$$q_1(r) = Q_1 - \xi(w_1 + w_2); \quad q_2(r) = Q_2 - \xi(w_1 + w_2) \quad (9.3.5)$$

Q_i are defined as

$$Q_1 = \frac{1}{A_1^*} (p_{11}A_0^* - p_{12}A_1^*) + \xi(\Delta_{T\theta} - \Delta_{S\theta} - \Delta_S + \Delta_{TPR}) \\ + \Delta_{TG} - \mu_S(l_3^2 - l_2^2)/2E_S \quad (9.3.6)$$

$$Q_2 = \frac{1}{A_1^*} (p_{21}A_0^* - p_{22}A_1^*) + \xi(\Delta_{T\theta} - \Delta_{S\theta} - \Delta_S - \Delta_{TG} + \Delta_{TPR}) \\ - \mu_S(l_3^2 - l_2^2)/2E_S$$

In the above, A_1^* , A_i^* , A_0^* are defined as $A_1^* = \pi a^2$, A_i^* = total tubesheet plan form area within radius a after drilling (including tube walls), and $A_0^* = A_i^* - nA_T$. Note that if gravitational pressure loss and pressure gradient effects are neglected, then the above expressions simplify considerably, since

$$\mu_S = \mu_T = 0; \quad p_{22} = p_{12}; \quad p_{21} = p_{11}; \quad Q_1 = Q_2$$

We note that all quantities in Eq. (9.3.6) are known at this point except Δ_S , w_1 and w_2 . With tubesheet pressures q_1, q_2 , now defined, the governing equations for the deformation of the tubesheets in the perforated region $r \leq a$ can be written down immediately by referring to the general plate equation in Appendix A at the end of the text. The final equations for deflection w_i are:

$$D_i \nabla^4 w_i = Q_i - \xi(w_1 + w_2); \quad i = 1, 2 \quad (9.3.7)$$

The tubesheet stiffness coefficients D_1^* , D_2^* are given in terms of the effective elastic constants E_i^* , ν_i^* and the thicknesses h_i as

$$D_i^* = \frac{E_i^* h_i^3}{12(1 - \nu_i^{*2})}; \quad i = 1, 2 \quad (9.3.8)$$

Solutions to the coupled system of equations are most directly obtained by solving initially for the combination $w_1 + w_2$ and $w_1 - w_2$. For the interested reader, the details of the solution are given in Appendix 9.A. The final expressions for displacement, rotation, bending moments and peripheral shear force can be written, in the region $0 \leq r \leq a$, in the form ($i = 1, 2$):

$$w_i(r) = \frac{\lambda_i}{2} \left[A_0 + A_3 r^2 + \frac{C_4 r^4}{64} \right] + \frac{C_3}{2\beta^4} + \mu_i [A_1 \phi_1(\beta r) + A_2 \phi_2(\beta r)] \quad (9.3.9)$$

$$\frac{dw_i}{dr} = \frac{\lambda_i}{2} \left[2A_3 r + \frac{C_4 r^3}{16} \right] + \mu_i \beta [A_1 \phi_1'(\beta r) + A_2 \phi_2'(\beta r)] \quad (9.3.10)$$

$$\frac{M_{ri}}{D_i^*} = -\frac{\lambda_i}{2} \left[2A_3 (1 + \nu_i^*) + \frac{C_4 r^2}{16} (3 + \nu_i^*) \right] - \mu_i \beta^2 [A_2 \psi_{2i} - A_1 \psi_{1i}] \quad (9.3.11)$$

$$\frac{Q_{ri}}{D_i^*} = \frac{\lambda_i}{4} C_4 r + \mu_i \beta^3 [A_2 \phi_1' - A_1 \phi_2'] \quad (9.3.12)$$

$$M_{\theta i} = \nu^* M_{ri} - D_i^* (1 - \nu_i^{*2}) \frac{1}{r} \frac{dw_i}{dr} \quad (9.3.13)$$

In Eqs. (9.3.9)–(9.3.12) the following parameters have been introduced:

$$\lambda_i = (-1)^{i+1}; \quad \beta_i^4 = \xi / D_i^*; \quad \mu_i = \beta_i^4 / \beta^4; \quad i = 1, 2 \quad (9.3.14)$$

where $\beta^4 = \beta_1^4 + \beta_2^4$ and ξ is given by Eq. (9.2.6). The parameters C_3, C_4 , defined in terms of the known Q_i , are

$$C_3 = \frac{Q_1}{D_1^*} + \frac{Q_2}{D_2^*}; \quad C_4 = 2 \left(\mu_2 \frac{Q_1}{D_1^*} - \mu_1 \frac{Q_2}{D_2^*} \right) \quad (9.3.15)$$

The functions $\phi_i(\beta r)$, $i = 1, 2$, introduced above, are the Ber and Bei Kelvin functions. ϕ_i' indicates differentiation with respect to the argument βr , and functions $\psi_{1i}(\beta r)$, $\psi_{2i}(\beta r)$ are defined as:

$$\begin{aligned} \psi_{1i}(\beta r) &= \phi_2(\beta r) + \frac{(1 - \nu_i^*)}{\beta r} \phi_1'(\beta r) \\ \psi_{2i}(\beta r) &= \phi_1(\beta r) - \frac{(1 - \nu_i^*)}{\beta r} \phi_2'(\beta r) \end{aligned} \quad (9.3.16)$$

The solutions in the perforated regions given by Eqs. (9.3.9–12) contain four integration constants A_0, A_1, A_2, A_3 . These integration constants will shortly be determined in order to satisfy appropriate boundary or continuity conditions.

9.4 ANALYSIS OF AN UNPERFORATED TUBESHEET RIM

We now turn to an analysis of the unperforated rim which connects the tubesheet perforated region to the shell and channel. Figure 9.4.1 shows a free body of the lower tubesheet and adjacent shell and channel. Shell and channel stress resultants are shown on this figure for subsequent use in the

solution formulation. The outer radius b is defined to be the average of the shell and channel mean radii a_s, a_c , respectively. The region $a \leq r \leq b$ (the rim of the tubesheet) is treated in the subsequent analysis as an annular plate since it is conceivable to have a unit with significant untubed rim region. The expression for deflection $w_i(r)$ in this annular region can be obtained from simple plate theory as ($i=1,2$):

$$w_i(r) = B_{0i} + B_{1i}r^2 + B_{2i} \ln r + B_{3i}r^2 \ln r + \frac{\Delta p_i r^4}{64D_i} \tag{9.4.1}$$

$B_{0i} - B_{3i}$ are additional constants of integration, $D_i = E_i h_i^3 / [12(1 - \nu_i^2)]$, and we introduce new pressure terms $\Delta p_1, \Delta p_2$ with the relations

$$\Delta p_1 = p_{11} - p_{12}; \quad \Delta p_2 = p_{21} - p_{22} \tag{9.4.2}$$

Appropriate differentiation of the displacement function yields expressions for the rotations, bending moments, and shear force, for $i = 1, 2$

$$\frac{dw_i}{dr} = 2B_{1i}r + \frac{B_{2i}}{r} + B_{3i}(r + 2r \ln r) + \frac{\Delta p_i r^3}{16 D_i} \tag{9.4.3}$$

$$M_{ri} = -D_i \left[2B_{1i}(1 + \nu) - \frac{B_{2i}}{r^2}(1 - \nu) + B_{3i}(3 + \nu) + 2B_{3i}(1 + \nu) \ln r + \frac{(3 + \nu)}{16D_i} \Delta p_i r^2 \right] \tag{9.4.4}$$

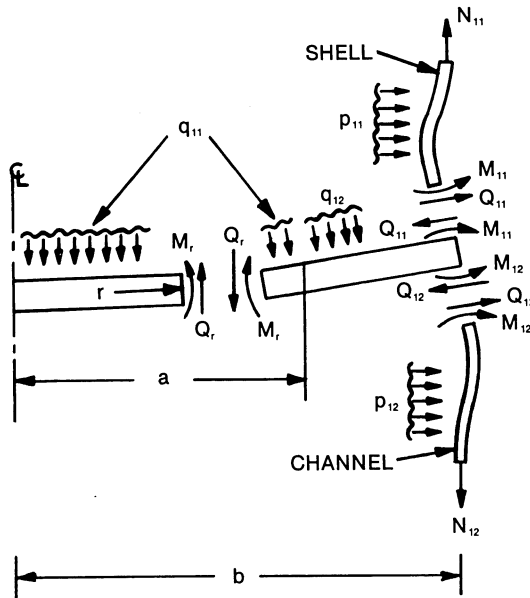


Fig. 9.4.1. Freebody of lower tubesheet, shell and channel (members shown in deformed condition).

$$Q_{ri} = D_i \left[\frac{4B_{3i}}{r} + \frac{\Delta p_i r}{2D_i} \right] \quad (9.4.5)$$

$$M_{\theta i} = \nu M_{ri} - D_i (1 - \nu^2) \frac{1}{r} \frac{dw_i}{dr} \quad (9.4.6)$$

The solutions so far determined are expressed in terms of twelve unknown integration constants, namely $A_0, A_1, A_2, A_3, B_{0i}, B_{2i}, B_{3i}$, ($i=1,2$). From Fig. 9.4.1, we see that there are five additional unknown reactions at the lower tubesheet-shell-channel junction, namely $M_{11}, Q_{11}, N_{11}, M_{12}$, and Q_{12} . Similarly, there may be five additional unknown reactions at the upper tubesheet-shell-channel junction for the integral tubesheet heat exchanger unit being modelled. Therefore, in order to solve for the twenty-two unknown quantities, we must impose a like number of equilibrium and/or continuity conditions between the tubesheet perforated region and the annular rim, between the rim and the shell, and between the rim and the channel. These continuity conditions, imposed on both tubesheets, provide twenty-two linear equations to enable the unknown constants to be determined. We now discuss the specification of these twenty-two conditions which permit us to determine the integration constants. Referring to Fig. 9.4.1, we see first that the header force resultant in the lower channel barrel is completely defined by force equilibrium requirements on the lower channel; a force balance in the direction of N_{12} yields

$$N_{12} = \frac{p_{12} a_c}{2} + \frac{W_1}{2\pi a_c} \quad (9.4.7)$$

W_1 is the total weight of the lower channel including all of the contained fluid supported by the lower channel. If the analysis being undertaken is of a horizontal vessel than $W_1 = 0$ in Eq. (9.4.7). Figure 9.4.2 shows free body diagrams of the upper tubesheet unperforated rim, the upper channel barrel, and the upper part of the heat exchanger shell; five more unknown force and moment resultants are introduced, namely $M_{21}, Q_{21}, N_{21}, M_{22}$ and Q_{22} . We see here that the upper channel barrel force resultant N_{22} is also obtained directly from force equilibrium requirements on the upper channel

$$N_{22} = \frac{p_{22} a_c}{2} - \frac{W_{c2}}{2\pi a_c} \quad (9.4.8)$$

W_{c2} is the weight of the upper barrel. The twenty-two unknown constants can be represented by the vector $\{x\}$, where

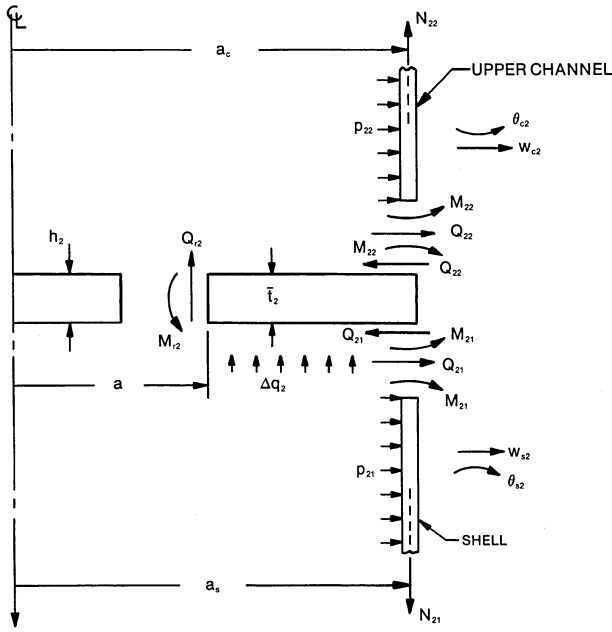


Fig. 9.4.2. Freebody of upper tubesheet, shell, and channel (members shown in undeformed condition).

$$\{x\}^T = \begin{bmatrix} A_0, A_1, A_2, A_3, B_{01}, B_{11}, B_{21}, B_{31}, \\ B_{02}, B_{12}, B_{22}, B_{32}, N_{11}, M_{11}, Q_{11}, \\ N_{21}, M_{21}, Q_{21}, M_{12}, Q_{12}, M_{22}, Q_{22} \end{bmatrix} \quad (9.4.9)$$

We now set down the twenty-two algebraic equations that determine the elements of $\{x\}$. We will first state the conditions and then give a brief discussion of each set of conditions. Eight of these twenty-two equations come from enforcing compatibility of displacement, rotation, moment and shear at $r = a$ of each tubesheet. That is, there can be no sudden jump in the value of these quantities as we cross from the perforated region into the unperforated rim. Force and moment relations, involving tubesheet, shell and channel unknowns at $r = b$ of each tubesheet, yield four additional conditions; two more relations arise from the condition that the tubesheet displacement must be zero at $r = b$ since the displacement was defined relative to the shell. The remaining eight equations are obtained by requiring continuity of displacement and rotation between the shell, channel and tubesheet at $r = b$. Appendix 9.B presents the computer code FIXSHEET and user guide to analyze the configuration considered; the computer code accepts necessary geometry, material, and loading data,

solves the above-mentioned twenty-two equations, and calculates and outputs all relevant information necessary to qualify the unit for service under specified stress and deformation limits. Since computer implementation is emphasized, there is no compelling reason here to involve the reader with extensive algebraic manipulation in search of elusive simplifications; it is sufficient to present the relevant equations in sufficient clarity for the potential user to move from text to computer implementation with confidence.

As noted previously, continuity requirements at $r = a$ of each tubesheet require that the following eight conditions be satisfied (i taking on the values 1,2)

$$w_i(a) \text{ (Eq. (9.3.9))} = w_i(a) \text{ (Eq. (9.4.1))} \quad (9.4.10)$$

$$\left. \frac{dw_i}{dr} \right)_{r=a} \text{ (Eq. (9.3.10))} = \left. \frac{dw_i}{dr} \right)_{r=a} \text{ (Eq. (9.4.3))} \quad (9.4.11)$$

$$M_{ri})_{r=a} \text{ (Eq. (9.3.11))} = M_{ri})_{r=a} \text{ (Eq. (9.4.4.))} \quad (9.4.12)$$

$$Q_{ri})_{r=a} \text{ (Eq. (9.3.12))} = Q_{ri})_{r=a} \text{ (Eq. (9.4.5))} \quad (9.4.13)$$

From Fig. 9.4.1, we note that the net shear and moment, referred to the tubesheet midsurface at $r=b$, can be written in terms of the shell and channel resultants, as (\bar{t}_1 is the thickness of the annular rim)

$$Q_{r1}(b) = N_{11} - N_{12}; \quad M_{r1}(b) = -M_{11} + M_{12} - \frac{\bar{t}_1}{2} (Q_{12} - Q_{11}) \quad (9.4.14)$$

From Fig. 9.4.2, we can construct a similar set of relations at the upper tubesheet connection:

$$Q_{r2}(b) = N_{21} - N_{22}; \quad M_{r2}(b) = -M_{21} + M_{22} - \frac{\bar{t}_2}{2} (Q_{22} - Q_{21}) \quad (9.4.15)$$

We can use the above equations to evolve four relations involving the unknown elements of $\{x\}$ by using Eq. (9.4.4) and (9.4.5) (for $i = 1,2$) in Eqs. (9.4.14) and (9.4.15).

Since $w_i(r)$ has been defined as the elastic lateral displacement of the i th tubesheet relative to the shell (recall Eq. (9.3.4)), two additional relations are obtained by using Eq. (9.4.1) for $i = 1,2$ and requiring that

$$w_i(b) = 0, \quad i = 1,2 \quad (9.4.16)$$

The remaining eight compatibility equations are easily visualized from Figs. 9.4.1 and 9.4.2 and enforce displacement and rotational compatibility at $r = b$. These equations are simply the geometric conditions

$$w_{s1} = \left. \frac{\bar{t}_1}{2} \frac{dw_1}{dr} \right)_{r=b} = -\frac{\bar{t}_1}{2} \theta_{s1} \quad (9.4.17)$$

$$w_{c1} = -\frac{\bar{t}_1}{2} \left. \frac{dw_1}{dr} \right)_{r=b} = -\frac{\bar{t}_1}{2} \theta_{c1} \quad (9.4.18)$$

$$w_{s2} = \frac{\bar{t}_2}{2} \left. \frac{dw_2}{dr} \right)_{r=b} = -\frac{\bar{t}_2}{2} \theta_{s2} \quad (9.4.19)$$

$$w_{c2} = -\frac{\bar{t}_2}{2} \left. \frac{dw_2}{dr} \right)_{r=b} = -\frac{\bar{t}_2}{2} \theta_{c2} \quad (9.4.20)$$

In the above eight equations, Eq. (9.4.3) (for $i = 1,2$) provides the expression for dw_i/dr ; the expressions for w_{si} , w_{ci} , θ_{si} , θ_{ci} follow from the equations of classical thin cylinder theory. Referring to Appendix A on the general plate and shell equations, we can easily show that w_{sj} , θ_{sj} , ($j = 1,2$) are given as

$$w_{sj} = \frac{p_{j1} a_s^2}{E_s h_s} - \frac{\nu_s N_{j1} a_s}{E_s h_s} + \frac{1}{2\beta_s^3 D_s} (\beta_s M_{j1} + Q_{j1}) \quad (9.4.21)$$

$$\theta_{sj} = \frac{1}{2\beta_s^2 D_s} (2\beta_s M_{j1} + Q_{j1}) \quad (9.4.22)$$

The shell flexural rigidity D_s and attenuation coefficient β_s are defined by the relations

$$D_s = \frac{E_s h_s^3}{12(1-\nu_s^2)}; \quad \beta_s^4 = \frac{3(1-\nu_s^2)}{a_s^2 h_s^2} \quad (9.4.23)$$

Similarly for the channel barrels, for $j = 1,2$, we can write

$$w_{cj} = \frac{p_{j2} a_c^2}{E_c h_c} - \frac{\nu_c N_{j2} a_c}{E_c h_c} + \frac{1}{2\beta_c^3 D_c} (\beta_c M_{j2} + Q_{j2}) \quad (9.4.24)$$

$$\theta_{cj} = \frac{1}{2\beta_c^2 D_c} (2\beta_c M_{j2} + Q_{j2}) \quad (9.4.25)$$

Note that in Eqs. (9.4.21), (9.4.22), (9.4.24), and (9.4.25), the positive directions for moments and shears are opposite to the directions used in Appendix A. The channel barrel flexural rigidity and attenuation coefficient are defined as:

$$D_c = \frac{E_c h_c^3}{12(1-\nu_c^2)}; \quad \beta_c^4 = \frac{3(1-\nu_c^2)}{a_c^2 h_c^2} \quad (9.4.26)$$

To complete the set of conditions, we note that the elastic stretch of the shell, introduced in Eq. (9.3.4) and later submerged into the parameters Q_i

by Eqs. (9.3.5), (9.3.6), is given in terms of the unknown shell resultants N_{11} , N_{21} and the shellside pressures p_{11} , p_{21} as

$$\Delta_s = \frac{1}{E_s h_s} \left\{ N_{11} l_3 + N_{21} l_2 - \nu_s a_s \frac{(l_2 + l_3)}{2} (p_{11} + p_{21}) \right\} \quad (9.4.27)$$

Equation (9.4.27) could be used to completely eliminate Δ_s from the formulation; however, it is convenient to treat Δ_s as an assumed parameter and permit the computer to iterate on the solution until Eq. (9.4.27) is satisfied to the desired degree of accuracy. Note that a shell side expansion joint may be simply accommodated by introducing the term N_{21}/K_{EJ} or N_{11}/K_{EJ} , where K_{EJ} is the spring constant per unit circumferential shell length of the expansion joint, on the right side of Eq. (9.4.27).

9.5 METHOD OF SOLUTION AND COMPUTER IMPLEMENTATION

The previous sections have set down a brief description of the relevant equations governing the behavior of a fixed tubesheet heat exchanger under applied mechanical and thermal load. As noted, we made no attempt to write these equations out in full; rather our aim has been solely to indicate that all equilibrium and compatibility requirements are satisfied. In this section, we discuss the solution procedure for the previous equations that is utilized in the computer code of Appendix 9.B.

Rather than eliminate Δ_s from the twenty-two governing equations, we use the following iteration scheme for computer implementation.

- i Assume a value for Δ_s , the elastic expansion of the shell between the two tubesheets.
- ii Use the assumed value in Eqs. (9.3.6) to compute Q_1 and Q_2 for given loading conditions.
- iii Set up and solve the twenty-two equations for the unknown elements of the vector $\{x\}$ defined by Eq. (9.4.9).
- iv Use Eq. (9.4.27) to compute a corrected value of Δ_s once N_{11} , N_{12} are obtained from step 3.
- v If the value of Δ_s calculated in step 4 is equal to the assumed value in step 1 (within a specified tolerance), then coverage is achieved and the solution established. If convergence is not achieved, then assume a new Δ_s as the average of the assumed Δ_s and the corrected Δ_s from the previous step and return to step 2.

The aforementioned procedure is implemented into the computer code presented in Appendix 9.B. A variety of simulations indicate that satisfactory convergence is achieved with two or three iterations. Once the vector $\{x\}$ is determined, all stress and displacement variables of interest may be computed at any point in the unit. For example, tube stress at the lower tubesheet is given as

$$\sigma_{T1} = \frac{E_T}{L} [w_1 + w_2 + \Delta_S + \Delta_{S\theta} - \Delta_{T\theta} + \mu_S (l_3^2 - l_2^2)/2E_S - \mu_T L^2/2E_T - \Delta_{TPR}] \quad (9.5.1)$$

The corresponding tube stress at the upper tubesheet is given as

$$\sigma_{T2} = \sigma_{T1} + \mu_T L \quad (9.5.2)$$

The longitudinal membrane stress in the shell, σ_s , is given by

$$\sigma_s = \frac{N_{11}}{h_s} + \mu_s y ; (0 < y < l_3) \quad (9.5.3)$$

$$\sigma_s = \frac{N_{21}}{h_s} - \mu_s (L - y) ; y > l_3$$

where y is measured along the tubes starting at the lower tubesheet. Bending stress at the surface of the shell or channel at the tubesheet junction is computed as

$$\sigma_B = \frac{6M_{ij}}{\bar{h}^2} \quad \text{where } \bar{h} = h_s \text{ or } h_c \text{ and } i, j \text{ have appropriate values} \quad (9.5.4)$$

Finally, tubesheet bending stresses σ_r, σ_θ may be computed in either tubesheet, at any r , by using calculated values of M_r, M_θ . For structural integrity checks of the tubesheet, it is oftentimes convenient to define the stress intensity in the tubesheet by the relation

$$\sigma = \frac{6K^* M_i}{\eta h_i^2} \quad i = 1, 2 \quad (9.5.5)$$

where η is the ligament efficiency, and M_i is the largest in absolute value of M_r and M_θ in the i th tubesheet. The stress multiplier K^* in Eq. (9.5.5) is defined in [9.3.1]. Appendix 9.B contains the user manual, and listing for computer code FIXSHEET.

Prior to illustrating our analysis with a numerical example, we must discuss the computation of the differential thermal expansion term $\Delta_{T\theta} - \Delta_{S\theta}$ appearing in Eq. (9.3.6). We will show how this quantity can be derived in terms of the coefficients of thermal expansion of the tube and shell materials, and in terms of the inlet and outlet temperatures of the tubeside and shellside streams.

9.5.1 Differential Thermal Expansion Between the Shell and the Tubes

We will construct an expression for the differential thermal expansion $\Delta_{T\theta} - \Delta_{S\theta}$, defined as the net longitudinal expansion of the tubes *over* the

shell. The tube side and shell side fluids are assumed to exchange sensible heat as shown in Fig. 9.5.1. All of the assumptions invoked in the derivation of the well known ‘‘Log-Mean Temperature Difference’’ [9.5.1] are presumed to hold. Referring to Fig. 9.5.1, the *LMTD*, θ_m , is defined as

$$\theta_m = \frac{1}{L} \int \bar{\theta} dy$$

which can be solved to give

$$\theta_m = \frac{\theta_{\max} - \theta_{\min}}{\ln \frac{\theta_{\max}}{\theta_{\min}}} \quad (9.5.6)$$

where

$$\theta_{\max} = \text{Larger of (numerical magnitudes) } \{ (t_i - T_o), (t_o - T_i) \}$$

$$\theta_{\min} = \text{Smaller of (numerical magnitudes) } \{ (t_i - T_o), (t_o - T_i) \}$$

The algebraic signs of θ_{\max} and θ_{\min} in Eq. (9.5.6) are assumed to be retained. We note that the metal temperature of the tubes at a generic point A is given by

$$t_m = \alpha'_1 T + (1 - \alpha'_1) t \quad (9.5.7)$$

where

$$\alpha'_1 = \frac{0.5 R_m + R_{ft} + R_t}{R_s + R_{fs} + R_m + R_{ft} + R_t} \quad (9.5.8)$$

In Eq. (9.5.8), R_m = the tube metal resistance referred to the outer tube surface, R_{fs} , R_{ft} = the shell side and tube side fouling resistance, referred to the tube outer surface, and R_s , R_t are the film resistances for the shell side and tube side, referred to the tube outer surface. If we let $\delta^* = \Delta_{T\theta} - \Delta_{S\theta}$

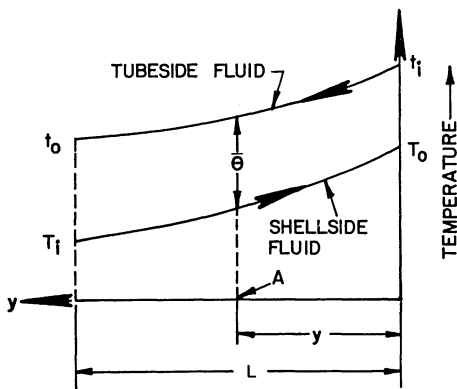


Fig. 9.5.1. Fluid temperature profiles.

$$\frac{d\delta^*}{dy} = \alpha_t (t_m - t_a) - \alpha_s (T - t_a) \quad (9.5.9)$$

Substituting for t_m from Eq. (9.5.7) yields

$$\frac{d\delta^*}{dy} = a_1 T + a_2 t + a_3 \quad (9.5.10)$$

where

$$\begin{aligned} a_1 &= \alpha'_1 \alpha_t - \alpha_s \\ a_2 &= (1 - \alpha'_1) \alpha_t \\ a_3 &= (\alpha_s - \alpha_t) t_a \end{aligned} \quad (9.5.11)$$

From Eq. (9.5.10) we obtain by differentiation:

$$\frac{d^2 \delta^*}{dy^2} = a_1 \frac{dT}{dy} + a_2 \frac{dt}{dy} \quad (9.5.12)$$

The requirement of continuity of heat flux across a differential surface of length dy yields: (C_{vs} , C_{vt} are specific heats of the respective fluids)

$$dQ = Uc\bar{\theta}dy = -W_s C_{vs} dT = -W_t C_{vt} dt \quad (a)$$

or

$$\frac{dT}{dy} = \frac{-Uc}{W_s C_{vs}} \bar{\theta} = \frac{-(T_o - T_i)}{L\theta_m} \bar{\theta} \quad (b) \quad (9.5.13)$$

$$\frac{dt}{dy} = \frac{-Uc}{W_t C_{vt}} \bar{\theta} = \frac{-(t_i - t_o)}{L\theta_m} \bar{\theta} \quad (c)$$

where $\bar{\theta} = t - T$, U is the overall heat transfer coefficient, c is the tube circumference, and W_t, W_s are the appropriate flow rates. From Eqs. (9.5.12)–(9.5.13), we obtain

$$\frac{d^2 \delta^*}{dy^2} = -\rho_1 \bar{\theta} \quad (9.5.14)$$

where

$$\rho_1 = \frac{a_1(T_o - T_i) + a_2(t_i - t_o)}{L\theta_m} \quad (9.5.15)$$

Performing double integration in Eq. (9.5.14) we have

$$\delta^* = -\rho_1 \int_0^L dy_1 \int_0^{y_1} \bar{\theta} dy + L \frac{d\delta^*}{dy} \Big|_{y=0}$$

Appealing to the multiple integration formula and Eq. (9.5.10), we have

$$\delta^* = -\rho_1 \int_0^L (L-y) \bar{\theta} dy + L(a_1 T_o + a_2 t_i + a_3) \quad (9.5.15a)$$

We now require a simple expression for the integral

$$I = \int y \bar{\theta} dy \quad (9.5.16)$$

From Eq. (9.5.13a), we note

$$\int y \bar{\theta} dy = \frac{-W_s C_{vs}}{Uc} \int y dT$$

$$\int y \bar{\theta} dy = \frac{-W_t C_{vt}}{Uc} \int y dt$$

Hence

$$\left(\frac{Uc}{W_t C_{vt}} - \frac{Uc}{W_s C_{vs}} \right) \int y \bar{\theta} dy = - \int y d\bar{\theta}$$

or

$$\int y \bar{\theta} dy = \frac{-1}{\rho_2} \int y d\bar{\theta} \quad (9.5.17)$$

where

$$\rho_2 = \frac{Uc}{W_t C_{vt}} - \frac{Uc}{W_s C_{vs}}$$

which is further simplified, via Eq. (9.5.13b,c), to

$$\rho_2 = \frac{(t_i - t_o) - (T_o - T_i)}{L\theta_m} \quad (9.5.18)$$

Using Eq. (9.5.17), performing the necessary integrations in Eq. (9.5.15a), and simplifying, yields

$$\delta^* = L[(a_1 T_o + a_2 t_i + a_3) - \Lambda(t_i - T_o - \theta_m)] \quad (9.5.19)$$

where

$$\Lambda = \frac{a_1 (T_o - T_i) + a_2 (t_i - t_o)}{(t_i - t_o) - (T_o - T_i)} \quad (9.5.20)$$

Equation (9.5.19) defines δ^* , where the term θ_m is defined by Eq. (9.5.6). The constants a_1 , a_2 , and a_3 are defined in Eq. (9.5.11). A less accurate expression for δ^* , currently used in the industry, is given by

$$\delta^* = L[\alpha_i(t'_m - t_a) - 0.5\alpha_s(T_i + T_o - 2t_a)] \quad (9.5.21)$$

where

$$t'_m = \frac{1}{2} [\alpha'_i(T_i + T_o) + (1 - \alpha'_i)(t_i + t_o)] \quad (9.5.22)$$

9.5.2 Sample Application of Analysis

To illustrate the solution procedure we consider a typical vertically mounted integral tubesheet heat exchanger with specified shell side and tube side design pressures equal to 300 psi and 100 psi, respectively. Other pertinent data is given below. $a_s = a_c = b = 18.19"$, $a = 16.5"$, $L = 432"$, $l_2 = 228"$, $l_3 = 204"$, $W_1 = 2760 \#$, $W_{c2} = 1270 \#$, $\Delta p_t = \Delta p_s = 0$. Shell and channel; SA240-304 material, $h_s = 0.375"$, $E_s = E_c = 29 \times 10^6$ psi, $\nu_s = \nu_c = 0.3$, $\mu_s = \mu_c = 0.289 \#/\text{in.}^3$, $h_c = 0.3125"$. Tubes; 70:30 Cu-Ni material, 1348 tubes, $5/8"$ O.D. $\times 0.049"$ wall, roller expanded into $0.635"$ diameter nominal holes in the tubesheet at $0.8125"$ triangular pitch, $E_T = 22 \times 10^6$ psi, and $\mu_T = 0.322 \#/\text{in.}^3$. Taking credit for 95% of the tube wall in the ligament, we have $h_L = 0.2706"$ which yields, via Eq. (9.3.3), $\eta = 0.333$. Using the curves given in the ASME Codes, the effective elastic constants of the equivalent solid plate for the perforated region are estimated as $E_1^* = 9.19 \times 10^6$ psi, $\nu_1^* = 0.35$, where $E_1 = 31.7 \times 10^6$ psi and $\nu_1 = 0.3$ for the tubesheet material (monel). Both tubesheets are of equal thickness.

The following additional data is required to evaluate the differential thermal expansion δ^* .

$t_i = 78^\circ\text{F}$, $t_o = 131.8^\circ\text{F}$, $T_i = 201.5^\circ\text{F}$, $T_o = 106^\circ\text{F}$, $t_a = 70^\circ\text{F}$, $\alpha_i = 8.2 \times 10^{-6} \text{ }^\circ\text{F}^{-1}$, $R_m = 0.000136$, $R_{jt} = 0$, $R_{js} = 0.0005$, $R_s = 0.0005714$, $R_t = 0.000677$. All thermal resistances are in $\text{ft}^2 \text{ }^\circ\text{F} \text{ - Hr/Btu}$. $\alpha_s = 9.5 \times 10^{-6} \text{ }^\circ\text{F}^{-1}$.

Equations (9.5.8) and (9.5.6), respectively, yield $\alpha'_i = 0.3956$, and $\theta_m = -45.7^\circ\text{F}$. Performing the required arithmetic in Eqs. (9.5.11), (9.5.19), and (9.5.20), we obtain $\delta^* = -0.1373"$. The less accurate formula, Eq. (9.5.21), yields $-0.1551"$ a nearly 13% overestimate over the accurate value. This difference may be more pronounced in other cases.

Using the TEMA [9.1.1] design method, the tubesheet thickness is calculated to be $1.14"$ corresponding to $\delta^* = -0.1551"$, and tubesheet allowable stress equal to 23250 psi.

The maximum tube and shell stresses are predicted to be 1800 psi and 3320 psi, respectively. Figure 9.5.2 shows the tubesheet radial bending moment, M_r , (in the equivalent solid plate) due to the individual action of pressure and δ^* , and also their combined effect. Both tubesheets develop identical reactions in this case. The peak value of M_r , 2410 $\#/\text{in.}$, occurs at $r = 13.1"$. This corresponds to approximately 33800 psi maximum tubesheet bending stress (stress multiplier $K^* = 1.01$). Thus the calculated bending stress in the tubesheet is nearly 46% over the nominal stress used in

the TEMA calculations. Recalling that the ASME Code permits the primary bending stresses to exceed the nominal allowable stress by 50%, the TEMA designed tubesheet shows a remarkably close agreement with the results of this analysis.

The tube longitudinal stress is tabulated for selected values of r in Table 9.5.1. We note that the maximum tube tensile stress occurs at $r = a$. We also observe in Table 9.5.1 that the maximum tube compressive stress occurs at a small value of r , and it will be maximized when shell side pressure is not present. The shell longitudinal stress is computed to be -430 psi.

Table 9.5.1. Tube Longitudinal Stress, σ_t , psi, as a Function of Radius, Nominal Design Pressures, and Differential Thermal Expansion

Loading Case	Radius r					
	0	3.3"	6.6"	9.9"	13.2"	16.5"
d. Tubeside pressure only	-613.	-618.	-596	-439	-11.	677
c. Shellside pressure only	1374	1378	1322	1011	216	-996
b. Differential expansion only	-532	-553	-486	67	1621	4188
a. Combination of above loads	229	207	240	639	1826	2869

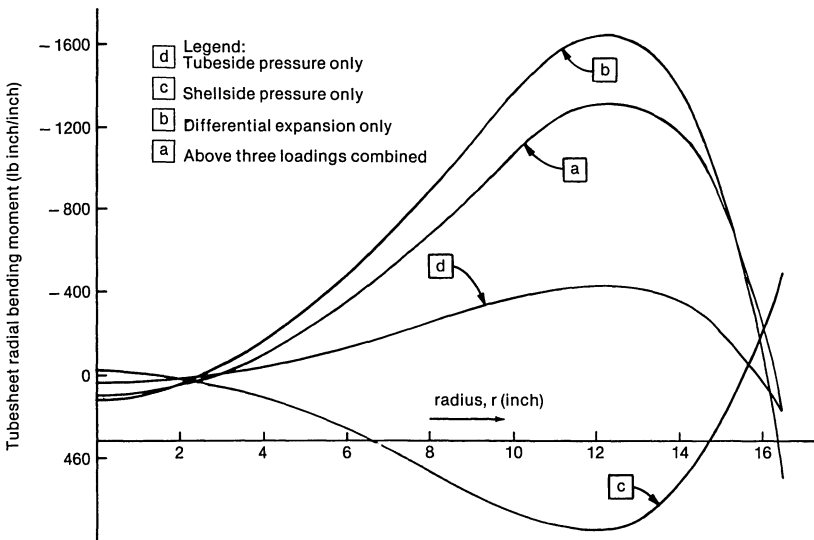


Fig. 9.5.2. Bending moment in the tubesheet as a function of radius.

We next compute the stresses in the tubesheet, tubes and the shell taking into account the weight of metal, contained fluids (water), and assuming that the exchanger is subject to a vertical seismic acceleration of 3g. $\mu_1^* = 62.4$ lb./cubic ft. Multiplying the weights and densities by 4 (to account for the vertical seismic acceleration factor of 3), and performing the necessary arithmetic in Eq. (9.3.1) yields, $p_{11} = 362.4$ psi, $p_{12} = 167.3$ psi, $p_{21} = 300$ psi and $p_{22} = 104.9$ psi.

Similarly, Eqs. (9.4.7)-(9.4.8) yield, $N_{12} = 1618.2$ lb./in. and $N_{22} = 909.6$ lb./in. Table 9.5.2 shows the radial bending moment in the bottom and top tubesheets for selected values of the radius r . The contribution of each loading component is separately shown. The maximum value of M_r due to the combined action of all loads in the lower tubesheets occurs at $r = 13.2$ in. (-2532 lb.-in./in.). In the upper tubesheet, it occurs at $r = 11.55$ " (-2741 lb.-in./in.). This corresponds to a maximum bending stress of 35100 psi and 38000 psi, respectively. The maximum tensile tube longitudinal stress (Fig. 9.5.3) is 7104 psi at $r = a$ (at top tubesheet level), and the maximum compressive stress is -224 psi at $r = 4.95$ " (Bottom tubesheet level).

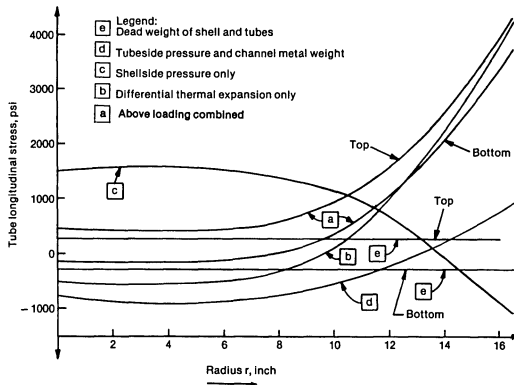


Fig. 9.5.3. Tube longitudinal stress as a function of radius.

Finally, Fig. 9.5.3 and Table 9.5.2 illustrate a typical structural response of integral tubesheet heat exchangers. Table 9.5.2 shows that the radial moment distributions in the two tubesheets are markedly different. Moreover, the stress resultants due to each load type (dead weight, differential expansion, etc.) are also quite different. Thus, in general it is difficult to identify a priori the load combinations that will produce the maximum stress in (either of the two) tubesheets. Figure 9.5.3 shows that the tube side pressure develops compressive stresses in the inner tube rows, and tensile stresses in the outer tube rows. Negative values of δ^* also produce compression in the inner tube rows, although the stresses in the outer tube rows are tensile and more severe. These observations underscore some of the less ostensible structural characteristics of fixed tubesheet exchangers.

Table 9.5.2. Tubesheet Radial Bending Moment, M_r , lb-in./in., as a Function of Radius

Loading Case	Radius (in.)											
	0	3.3	6.6	9.9	13.2	16.5	0					
	LOWER TUBESHEET			UPPER TUBESHEET								
(e) Deadweight only	1349	1261	997	556	-65	-878	-1351	-1261	-991	-542	83	16.5
(d) Tubeside pressure and channel weights, only	-668	-685	-738	-772	-512	712	733	623	290	-211	-604	-220
(c) Shellside pressure only	512	572	750	945	724	-924	-576	-442	-45	517	809	-178
(b) Differential expansion only	104	-69	-593	-1338	-1582	497	104	-69	-593	-1338	-1582	497
(a) Combination of above loads	1297	1080	416	-609	-1436	-593	-1090	-1149	-1339	-1573	-1294	971

We have, in the above, shown the application of the fixed tubesheet computer code, FIXSHEET described in Appendix 9.B. In the next section, we include some remarks concerning the modification of the program so it can be used for the analysis of floating head units.

9.6 MODIFICATIONS FOR FLOATING HEAD EXCHANGERS

It is a straightforward exercise to modify the above formulation and solution procedure to accommodate most floating head units. In what follows, we assume the upper tubesheet as the floating tubesheet, and the lower tubesheet as the stationary tubesheet. For a unit with a floating head, the total tube growth* does not depend on the shell growth. Hence, the initial modification to the equations governing fixed tubesheet exchangers, to make them apply to a unit having a floating head, is to redefine the growth δ as

$$\delta = w_1 + w_2 \quad (9.6.1)$$

where $w_i(r)$ $i = 1, 2$, are absolute tubesheet lateral deformations. Equation (9.6.1) replaces Eq. (9.3.4) and we clearly see that Eqs. (9.3.4), (9.3.6) are simplified by omitting all reference to $\Delta_{S\theta}$, Δ_S , μ_S $(l_3^2 - l_2^2)/2E_S$. We note that shell growth in a floating head unit imposes a rigid body movement on both tubesheets but has no effect on the state of stress.

For typical floating head constructions, examination of Fig. 9.4.2 indicates that the first of Eqs. (9.4.15) should be replaced by the condition

$$Q_{r_2}(b) = Q^* \quad (9.6.2)$$

where Q^* is a specified edge shear. Since the shell force resultant N_{21} in the region $l_2 \leq y \leq L$ is now a known quantity, dependent only on the particular floating head construction being modelled, and since Q_{21} , M_{21} no longer have any significance to the tubesheet solution, we must remove three conditions from the set of twenty-two conditions discussed in Section 9.4. Equation (9.4.16) for $i=2$ is deleted since $w_2(b)$ is not required to match any shell movements; the two additional deleted conditions are those expressed by Eq. (9.4.19). If we choose to ignore any compatibility requirements between the floating tubesheet and its floating channel cover, then we may also ignore the requirements of Eq. (9.4.20) and neglect Q_{21} , M_{21} . In such a case, the second of Eqs. (9.4.15) may be replaced by the requirement that $M_{r_2}(b)$ be given a known edge value, M^* . Note that since Δ_S no longer enters the formulation through the parameters Q_1 , Q_2 , analysis of a floating head unit requires no iteration. N_{12} is determined from the first of Eq. (9.4.14). Δ_S is still given by Eq. (9.4.27) but need be evaluated only to establish the constant term in the displacement $w_1(r)$; the effect of Δ_S does not enter the tubesheet stress state since it has the

*The terms "growth" is used loosely here to indicate "change in length".

character of a rigid body movement. It would be a relatively straightforward process to modify the general computer code to enable treatment of floating head construction. Particular values used for Q^* and M^* and for N_{21} would depend on the particular floating head construction being simulated. For example, referring to Chapter 1 Appendix 1.A, (Fig. 1.A.4) we see that the shell force N_{21} may be obtained from the equation

$$N_{21} = \frac{a_c}{a_s} N_{22} + \frac{(p_{21} - p_{22})}{2a_s} (a_s^2 - a_c^2) - \mu_s h_s (L - y) \quad (9.6.3)$$

for the case of a TEMA Class S or T construction. N_{22} , the channel force resultant, is also determined from an analysis of the particular construction. For a TEMA Class W construction, Eq. (9.4.8) could be used to evaluate N_{22} . For an outside packed floating head (TEMA Class P), the appropriate expression for N_{21} is

$$N_{21} \cong 0 \quad (9.6.4)$$

if we neglect friction at the packing-tubesheet skirt interface, and gravity effects.

The specified edge loadings Q^* and M^* have appropriate forms depending upon unit construction. For example, TEMA class W construction dictates that

$$Q^* = M^* = 0 \quad (9.6.5)$$

while TEMA Class P construction may be simulated by the expression

$$Q^* = \frac{p_{22} b}{2} \quad (9.6.6)$$

TEMA Class S construction may be approximated by $M^* = 0$ and by an appropriate value for Q^* , while TEMA class T construction would be simulated by a Q^* and M^* appropriate to the bolting condition. Strictly speaking, for some head simulations, the value of b used for the floating tubesheet will be different from the value of b used for the stationary tubesheet and hence the b/a ratio for *each* tubesheet needs to be input into any computer coding. In the code presented in Appendix 9.B, these changes are not incorporated. The user is cautioned, therefore, to apply the code in its present version only to fixed tubesheet exchangers with integral channels.

9.7 SIMPLIFIED ANALYSIS OF STATIONARY TUBESHEET IN AN INTEGRAL OR FLOATING HEAD HEAT EXCHANGER

We have just presented the development of the governing equations for a fixed tubesheet heat exchanger based on modelling each of the two tubesheets as thin plates resting on an elastic foundation. The foundation represents the effect of the tube assembly and has the effect of coupling the behavior of the two tubesheets under mechanical and/or thermal load. The

resulting equation set is not amenable to any simplified hand calculations; the user must rely on a computer to effect a solution. At the other end of the spectrum of tubesheet design methods for fixed tubesheet heat exchangers is the simplified calculation provided in Ref. [9.1.1]. This simplified approach to choosing a tubesheet thickness requires some iteration but the entire calculation procedure can be carried out manually.

In this and the following sections, we devote considerable attention to showing how the complex, and rather rigorous, developments of Sections 9.2–9.6 can be reduced, in a systematic manner, to evolve the simplified design formula found in the TEMA Standards [9.1.1]. We will clearly demonstrate all of the assumptions that must be made to evolve the simplified approach so that the user will have a clear understanding of any hidden restrictions on the applicability of the TEMA method set forth in [9.1.1]. In the course of our development, we also take the opportunity to develop some simpler computer codes based on the equations we develop.

We now introduce certain additional assumptions which lead to considerable simplification of the field equations. Because of the simplifications, we can proceed much further with manipulation of the equations and illustrate, in detail, the evaluation of the boundary conditions. The computer is still found to be a necessity even with the simplifications; however, here we employ the computer code only for numerical calculations, not as an equation solver. In the course of the analysis of this section, we find it convenient to use the notation employed in Refs. [8.1.1, 8.1.2, and 8.1.3]. We introduce these notation changes since these cited works are well known in the heat exchanger stress analysis community; and some notations therein have acquired synonymity with the quantities they represent.

The following additional considerations are employed in conjunction with the previous general analysis:

- i. The deformation and geometry of both tubesheets in the unit are assumed identical.
- ii. The unperforated rims are assumed to be identical and are modelled as rings rather than as annular plates.
- iii. Gravitational, fluid flow pressure loss, and pressure gradient effects are ignored.

Of all the above assumptions, the first one requires some discussion. In a unit with both tubesheets of integral construction, the assumption may be very nearly true. However, in floating head construction, even if the tubesheet geometry is the same, the boundary conditions at the edge of the unit are certainly different; thus, assumption 1 in floating head construction is usually far from being satisfied. Assumptions 1 and 3 do, however, permit us to assume symmetry of the unit about the midpoint of the shell, and focus attention only on one half of the system and hence on a single tubesheet-shell-tube interaction problem. Therefore, in the interest of searching for a simpler representation as well as giving more insight into the

various equilibrium and compatibility conditions that arise, we choose to invoke these assumptions in this section.

If complete symmetry about the midpoint of the heat exchanger is assumed, then $w_1(r) = w_2(r)$ and $dw_1/dr = dw_2/dr$. By virtue of our assumption of symmetry and the neglect of gravity and pressure gradients, we see from Eqs. (9.3.6) and (9.3.15) that $C_4 = 0$. If we now form the expression $w_1(r) - w_2(r) = 0$ by using Eq. (9.3.9) for $i = 1, 2$, and take note of the values for λ_i, μ_i given by Eq. (9.3.14), we obtain $A_0 + A_3 r^2 = 0$. Similarly, using Eq. (9.3.10) and forming $dw_1/dr - dw_2/dr = 0$ yields $A_3 r = 0$. We therefore conclude that our additional assumptions introduced in this section immediately result in the determination that $A_0 = A_3 = 0$ in the expressions for tubesheet behavior in the perforated region. To bring the form of the resulting simplified solutions into coincidence with the works of Refs. [8.1.1, 8.1.2, and 8.1.3], we introduce the new variables $v(r)$ and $\theta(r)$ into Eqs. (9.3.9)–(9.3.12). These new variables are related to our variables used in Section 9.6 as follows:

$$v = -w; \quad \theta = \frac{dv}{dr} \quad (9.7.1)$$

From Eq. (9.3.14), we note that $\beta_1 = \beta_2$ for our symmetric case so that $\beta^4 = 2\xi/D^*$ with ξ defined in Eq. (9.2.6) and D^* defined in Eq. (9.3.8). We also find it useful to introduce a dimensionless parameter x_a defined by

$$x_a = \beta a; \quad x = x_a r / a \quad (9.7.2a)$$

Making the indicated substitutions, the following expression for x_a is obtained:

$$x_a = a \left[\frac{24n E_T A_T (1 - \nu^{*2})}{\pi a^2 L E^* h^3} \right]^{1/4} \quad (9.7.2b)$$

We will encounter x_a repeatedly in subsequent analyses.

It is seen that x_a turns out to essentially relate the stiffnesses of the tubesheet and the tubes. Generally speaking, smaller values of x_a usually result when thick tubesheets are involved in the design so that the tubesheet stiffness effect predominates. Large values of x_a usually imply a unit with a stiff tube bundle and a thinner tubesheet.

The general solutions given in Eqs. (9.3.9)–(9.3.13) can now be rewritten as (drop the subscript notation and use the upper tubesheet sign convention for moments and shears—see Fig. 9.3.1)

$$vD^*/a^4 = -Q/x_a^4 + (C/x_a^4)[\phi_1 + H\phi_2] \quad (9.7.3)$$

$$\theta D^*/a^3 = (C/x_a^3)[\phi_1' + H\phi_2'] \quad (9.7.4)$$

$$M_r x_a^2 / a^2 = C[H\psi_2 - \psi_1] \quad (9.7.5)$$

$$Q_r / a = (C/x_a)[\phi_2' - H\phi_1'] \quad (9.7.6)$$

$$M_\theta = \nu^* M_r + \frac{D^*}{a} (1 - \nu^{*2}) \left(\frac{x_a}{x} \right) \theta \quad (9.7.7)$$

Note that the integration constants A_1, A_2 have been replaced by related constants C, H , and that ϕ_i, ψ_i are functions of x (Eq. (9.7.2)).

Our analysis in this section will consist of the following parts:

i. We consider first the perforated region of the tubesheet and assume that it is subjected to a moment M_a and a shear V_a at the edge of the region (radius a). Applying these edge conditions enables us to determine the integration constants C and H , and hence, to completely determine the solution in the perforated region in terms of M_a, V_a , and the load parameter Q (which involves N_s and the various pressure terms).

ii. We next turn our attention to the annular ring, the shell, and the channel. Using classical thin shell theory, we can determine the loading, acting on the ring, due to the presence of the shell and the channel. We subsequently form an expression for the rotation of the ring, in terms of the applied pressures, the bolt load (if any), and the edge loads M_a, V_a .

iii. We will find that the problem is completely solvable once we determine M_a, V_a , and N_s (in the case of a fixed tubesheet exchanger). We will show that three equations to determine the above quantities are evolved from a force equilibrium equation, together with two compatibility equations which enforce rotation compatibility between the ring and the perforated region, and which enforce displacement compatibility between the tubesheet and the shell.

The net pressure acting on the tubesheet is given by Eq. (9.3.5) and can be rewritten in terms of our new notation, as

$$q = Q + 2\xi v = C(\phi_1 + H\phi_2) \quad (9.7.8)$$

The loading term $Q = Q_1 = Q_2$ in the previous equations is given by Eq. (9.3.6). We also choose to include here a shell expansion joint. As noted in Section 9.4, a shell expansion joint is easily introduced into the expression for Δ_s ; we define S_j , the spring rate of the joint (total axial force divided by elongation) so that Eq. (9.4.27) becomes, for the symmetric unit being discussed here,

$$\Delta_s = \frac{N_s L}{E_s h_s} + \frac{N_s}{(S_j/2\pi b)} - \frac{\nu b L p_s}{E_s h_s} = \frac{N_s L}{E_s h_s} \left[1 + \frac{2\pi b E_s h_s}{L S_j} \right] - \frac{\nu b L p_s}{E_s h_s} \quad (9.7.9)$$

For later use, we introduce a parameter J defined as

$$1/J = 1 + \frac{2\pi b E_s h_s}{S_j L} \quad (9.7.10)$$

In Eq. (9.7.9) and (9.7.10), we have used b as the mean radius of the shell. If we now substitute the complete expression for Δ_s into Eq. (9.3.6), we find that the loading parameter Q , for this symmetric unit, is given in terms of the thermal loading, the pressure loading, and the shell side meridional tension by the equation

$$Q/2\xi = L/2 \left[\alpha_T \Delta T_T - \alpha_s \Delta T_s + \frac{\lambda_s p_s}{E_s} - \frac{\lambda_T p_t}{E_T} \right] - \frac{N_s L}{2E_s h_s J} \quad (9.7.11)$$

where we have used the expression $L(\alpha_T \Delta T_T - \alpha_s \Delta T_s) = \Delta_{T\theta} - \Delta_{S\theta}$.

Here $N_s = N_{11} = N_{21}$ is the axial force per unit circumferential length in the shell, and λ_s, λ_T are defined by the relations

$$\begin{aligned} \lambda_s &= \frac{E_s}{\xi L} \left(\frac{A_0^*}{A_1^*} \right) + \frac{\nu b}{h_s} + \frac{\nu d}{2t} \frac{E_s}{E_T} \\ \lambda_T &= \frac{E_T}{\xi L} \left(\frac{A_1^*}{A_1^*} \right) + \frac{\nu(d-2t)}{2t} \end{aligned} \quad (9.7.12)$$

A_0^*, A_1^*, A_1^* are the tubesheet areas defined just after Eq. (9.3.6). p_s, p_t are the shellside and tubeside pressures.

9.7.1 Evaluation of Integration Constants

In this sub-section, we express the constants C and H in terms of shear V_a and M_a at the edge of the perforated region. Subsequently, the lateral deflection v and rotation θ are also written in terms of M_a and V_a .

We can determine the integration constants C and H to satisfy the boundary conditions

$$M_r(x_a) = M_a; \quad Q_r(x_a) = V_a \quad (9.7.13)$$

M_a, V_a are the edge moment and force resultants at the edge of the perforated region. Figure 9.7.1 shows these resultants acting on the untubed rim. Using Eqs. (9.7.5)–(9.7.6), evaluated at $x=x_a$, leads to two equations for determination of C and H ; in terms of M_a, V_a , the radial bending moment is

$$M_r(x) = M_a Q_M(x) + a V_a Q_V(x) \quad (9.7.14)$$

where the moment distribution functions $Q_M(x), Q_V(x)$ are given as

$$Q_M(x) = [\psi_2(x) \phi_2'(x_a) - \psi_1(x) \phi_1'(x_a)] / Z_a$$

$$Q_V(x) = [\psi_2(x) \psi_1(x_a) - \psi_1(x) \psi_2(x_a)] / x_a Z_a$$

$$Z_a = \phi_2'(x_a) \psi_2(x_a) - \phi_1'(x_a) \psi_1(x_a)$$

The tubesheet cross section rotation angle θ is given in terms of M_a and V_a by

$$\frac{\theta(x)D^*}{a} = M_a Z_M(x) + aV_a Z_V(x) \tag{9.7.15}$$

where

$$Z_M(x) = [\phi_1'(x)\phi_1'(x_a) + \phi_2'(x)\phi_2'(x_a)]/(x_a Z_a)$$

$$Z_V(x) = [\phi_1'(x)\psi_2(x_a) + \phi_2'(x)\psi_1(x_a)]/(x_a^2 Z_a)$$

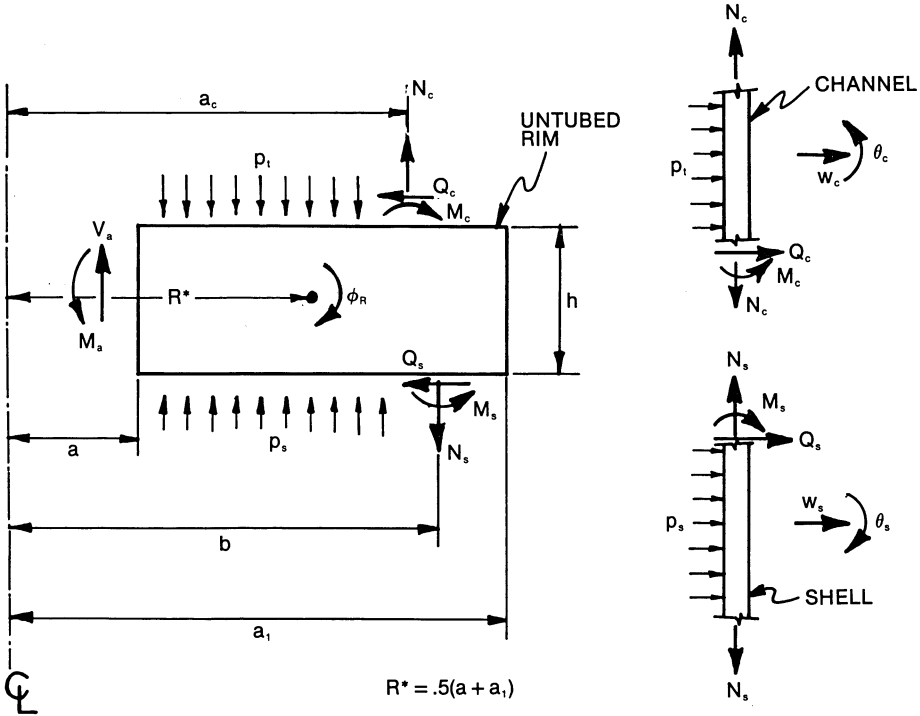


Fig. 9.7.1. Two side integral construction.

Similarly, after eliminating C and H , we find that the tubesheet lateral displacement is

$$\frac{v(x)D^*}{a^2} = -\frac{Qa^2}{x_a^4} + M_a Z_V(x) + aV_a Z_D(x) \tag{9.7.16}$$

where

$$Z_D(x) = [\phi_1(x)\psi_2(x_a) + \phi_2(x)\psi_1(x_a)]/(x_a^3 Z_a)$$

Finally, the effective tube pressure is given in terms of M_a , V_a by

$$q(x) = \frac{M_a x_a^4}{a^2} Z_V(x) + \frac{V_a x_a^4}{a} Z_D(x) \tag{9.7.17}$$

We see that the tubesheet behavior in the perforated region is determined as soon as M_a , V_a are obtained for any conditions of edge support. In Chapter 8, we showed how tubesheet design equations for tubesheets in U-tube exchangers could be developed for a variety of support conditions. In particular, we considered two side integral, one side integral—one side gasketed, and two side gasketed. Now that we have made the assumption here that the untubed annular region follows the tenets of ring theory, we can pursue the same line of analysis and examine the effect of the three classes of edge support on the final design equations for the tubesheets in fixed and floating head units. Figures 9.7.1, 9.7.2, and 9.7.3 show the free body diagrams for the untubed rim for the three classes of edge support being considered.

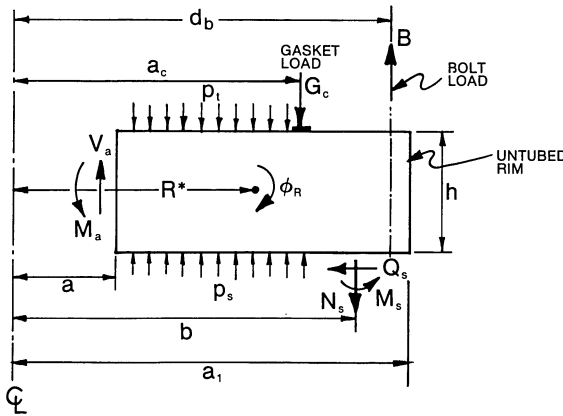


Fig. 9.7.2. Channel side gasketed, shell side integral construction.

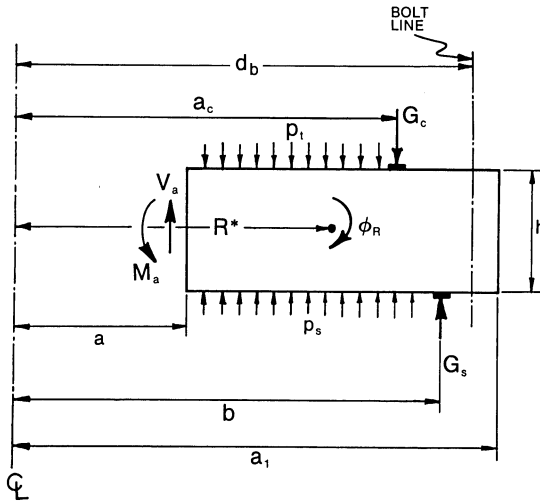


Fig. 9.7.3. Two side gasketed construction.

9.7.2 Development of Expressions for Ring Rotation

Two Side Integral Support

Referring to Fig. 9.7.1, we see that force equilibrium along the heat exchanger axis yields the result

$$N_s b = a V_a + p_t b^2 / 2 + \Delta p (b^2 - a^2) / 2 \quad (9.7.18)$$

where we have used the result that $N_c = p_t a_c / 2$, and we have set $\Delta p = p_s - p_t$. The net ring moment M_R , acting at radius R^* on the ring in the direction of the ring rotation ϕ_R shown in Fig. 9.7.1, is given as

$$\begin{aligned} R^* M_R = & -a M_a + a V_a (R^* - a) + N_s b (b - R^*) - N_c a_c (a_c - R^*) \\ & - \frac{p_t}{2} (a_c^2 - a^2) \left(R^* - \frac{[a_c + a]}{2} \right) + \frac{p_s}{2} (b^2 - a^2) \left(R^* - \frac{[a + b]}{2} \right) \\ & + a_c \left(M_c - \frac{h}{2} Q_c \right) - b \left(M_s - \frac{h}{2} Q_s \right) \end{aligned} \quad (9.7.19)$$

We now consider the shell Eqs. (9.4.21)–(9.4.25). In the interest of simplicity, we neglect the Poisson effect in these equations so that the axial shell or channel membrane force does not contribute to the lateral deflection. Specializing the shell equations to the notation of Fig. 9.7.1 yields

$$w_s = \frac{(\beta_s M_s + Q_s)}{2\beta_s^3 D_s} + \frac{p_s b^2}{E_s h_s}; \quad \theta_s = \frac{(2\beta_s M_s + Q_s)}{2\beta_s^2 D_s} \quad (9.7.20)$$

$$w_c = \frac{(\beta_c M_c + Q_c)}{2\beta_c^3 D_c} + \frac{p_t a_c^2}{E_c h_c}; \quad \theta_c = \frac{(2\beta_c M_c + Q_c)}{2\beta_c^2 D_c}$$

We now assume that radial movement at the tubesheet midsurface can be ignored. Therefore, requiring compatible displacement between ring and channel, and between ring and shell yields

$$w_c = -\frac{h}{2} \theta_c; \quad w_s = -\frac{h}{2} \theta_s \quad (9.7.21)$$

Using Eq. (9.7.20) in Eq. (9.7.21) enables us to determine Q_c and Q_s as:

$$\begin{aligned} Q_c = & -\bar{\gamma}_c \beta_c M_c - \frac{2\beta_c^3 D_c}{1 + \beta_c h/2} \left(\frac{p_t a_c^2}{E_c h_c} \right) \\ Q_s = & -\bar{\gamma}_s \beta_s M_s - \frac{2\beta_s^3 D_s}{1 + \beta_s h/2} \left(\frac{p_s b^2}{E_s h_s} \right) \end{aligned} \quad (9.7.22)$$

where

$$\bar{\gamma}_c = (1 + \beta_c h)/(1 + \beta_c h/2); \quad \bar{\gamma}_s = (1 + \beta_s h)/(1 + \beta_s h/2)$$

Q_s and Q_c are now eliminated from the expressions for θ_s and θ_c , and the requirements on cross section rotation imposed:

$$\theta_s = -\theta_c = \phi_R \quad (9.7.23)$$

These conditions allow us to obtain expressions for M_s , M_c in terms of the ring rotation ϕ_R as

$$M_c = -2(1 + \beta_c h/2)\beta_c D_c \phi_R + 2\beta_c^2 D_c \left(\frac{p_t a_c^2}{E_c h_c} \right) \quad (9.7.24)$$

$$M_s = 2(1 + \beta_s h/2)\beta_s D_s \phi_R + 2\beta_s^2 D_s \left(\frac{p_s b^2}{E_s h_s} \right)$$

Eliminating M_c , M_s from Eq. (9.7.22) allows us to write Q_c , Q_s in terms of ϕ_R . Therefore, we can now return to Eq. (9.7.19) and eliminate M_c , M_s , Q_c , Q_s from the expression in favor of terms involving ϕ_R . We note also that the equation relating ϕ_R and the net ring moment M_R is the familiar ring equation (see Section 3.9)

$$\phi_R = \frac{12R^* M_R}{Eh^3 \ln \bar{K}}; \quad \bar{K} = a_1/a \quad (9.7.25)$$

Finally, N_s can be eliminated from the expression for M_R by using Eq. (9.7.18). After all of the indicated substitutions are in place, Eq. (9.7.19) and Eq. (9.7.25) yield the relation between ϕ_R , V_a , M_a , p_s , p_t as

$$\frac{Eh^3}{12} (\ln \bar{K} + \mu) \phi_R = a^2 V_a (K - 1) - a M_a + p_s a^3 \gamma_s + p_t a^3 \gamma_t \quad (9.7.26)$$

In Eq. (9.7.26). we have introduced the rotational resistance parameter μ and the coefficients γ_s , γ_t defined by the relations

$$\frac{Eh^3 \mu}{24} = \beta_s b D_s (1 + \beta_s h + \beta_s^2 h^2/2) + \beta_c a_c D_c (1 + \beta_c h + \beta_c^2 h^2/2)$$

$$\gamma_s = [(K^2 - 1)(K - 1)/4] - [2\beta_s^2 D_s (1 + \beta_s h) K^3 / E_s h_s] \quad (9.7.27)$$

$$\gamma_t = [(K_c^2 - 1)(K_c + 1)/4] - (K_c^3 - K)/2 + [2\beta_c^2 D_c (1 + \beta_c h) K_c^3 / E_c h_c]$$

where we recall that $K = b/a$ and we have defined

$$K_c = a_c/a \quad (9.7.28)$$

Note that μ is completely defined in terms of the geometric data and elastic constants of the rim, the shell and the channel. Therefore Eq. (9.7.26) defines the rotation of the rim ϕ_R in terms of edge shear V_a and edge moment M_a . The corresponding expression for rotation of the perforated region was developed in sub-section 9.7.1 (Eq. 9.7.15).

One Side Integral – One Side Gasketed Support

We now consider Fig. 9.7.2 and develop the expression for ϕ_R similar to Eq. (9.7.26) for this class of support. On the channel side (gasketed), the line load B , giving the effect of the bolt preload, is related to the gasket load G_c by the condition

$$G_c a_c = B d_b - p_c a_c^2 / 2 \quad (9.7.29)$$

Forming the net ring moment M_R yields the expression

$$\begin{aligned} R^* M_R = & -a M_a + a V_a (R^* - a) - \frac{p_t}{2} (a_c^2 - a^2) \left(R^* - \frac{(a_c + a)}{2} \right) \\ & + \frac{p_s}{2} (b^2 - a^2) \left(R^* - \frac{(b + a)}{2} \right) + G_c a_c (a_c - R^*) - B d_b (d_b - R^*) \\ & + N_s b (b - R^*) - b \left(M_s - \frac{h}{2} Q_s \right) \end{aligned} \quad (9.7.30)$$

Eliminating G_c by using Eq. (9.7.29), N_s by using Eq. (9.7.18), M_s , Q_s by using Eqs. (9.7.22) and (9.7.24), and employing the ring relation (9.7.25) yields the final result:

$$\frac{E h^3}{12} (\ln \bar{K}) \phi_R = a^2 V_a (K - 1) - a M_a + a^3 (p_s \gamma_s + p_t \gamma_t) + B d_b a \gamma_b \quad (9.7.31)$$

where, for this case,

$$\begin{aligned} \frac{E h^3}{24} \mu &= \beta_s b D_s (1 + \beta_s h + \beta_s^2 h^2 / 2) \\ \gamma_t &= [(K_c^2 - 1)(K_c + 1)/4] - (K_c^2 - K)/2 \\ \gamma_b &= K_c - d_b / a \end{aligned} \quad (9.7.32)$$

and γ_s is the same as given by Eq. (9.7.27).

Two Side Gasketed Support

Here, we employ Fig. 9.7.3 to obtain an appropriate expression for $R^* M_R$ and note the additional gasket relation

$$G_s b = B d_b - N_s b \quad (9.7.33)$$

The equation for the net ring moment M_R for this case is

$$\begin{aligned} R^* M_R = & -a M_a + a V_a (R^* - a) - \frac{p_t}{2} (a_c^2 - a^2) \left(R^* - \frac{[a_c + a]}{2} \right) \\ & + \frac{p_s}{2} (b^2 - a^2) \left(R^* - \frac{[b + a]}{2} \right) + G_c a_c (a_c - R^*) - G_s b (b - R^*) \end{aligned} \quad (9.7.34)$$

Proceeding as before, and eliminating G_c , G_s , N_s , yields

$$\frac{Eh^3}{12} (\ln \bar{K}) \phi_R = a^2 V_a (K-1) - a M_a + a^3 (p_s \gamma_s + p_t \gamma_t) + B d_b a \gamma_b \quad (9.7.35)$$

where

$$\begin{aligned} \gamma_s &= (K^2 - 1)(K-1)/4 \\ \gamma_b &= K_c - K \end{aligned} \quad (9.7.36)$$

and γ_c is as given in Eq. (9.7.32).

9.7.3 Determination of Perforated Region Edge Force, Edge Moment, and Shell Axial Force

We can summarize the analysis to this point by noting that it remains for us to determine V_a , M_a and, for the case of a fixed tubesheet exchanger, the shell force N_s . We see that one equation relating V_a and N_s is the ring force equilibrium Eq. (9.7.18); a second equation relating V_a and M_a is the rotation compatibility requirement that at $x = x_a$, the tubesheet rotation at the edge of the perforated interior be equal to the untubed rim rotation.

$$\theta(x_a) = \phi_R \quad (9.7.37)$$

We write Eqs. (9.7.26), (9.7.31), and (9.7.35), in the general symbolic form

$$\frac{Eh^3}{12} (\ln \bar{K} + \mu) \phi_R = -a M_a + a^2 V_a (K-1) + a^3 (p_t \gamma_t + p_s \gamma_s) + B d_b a \gamma_b \quad (9.7.38)$$

(note that for certain constructions, μ , γ_b , γ_t , γ_s may be zero) and use Eq. (9.7.15) for $\theta(x_a)$; then Eq. (9.7.37) yields an expression relating V_a and M_a in the form

$$M_a = \bar{Q} a V_a + M_a^* \quad (9.7.39)$$

where

$$\bar{Q} = \frac{K-1 - \frac{(1-\nu^2)}{e} (\ln \bar{K} + \mu) Z_V(x_a)}{1 + \frac{(1-\nu^2)}{e} (\ln \bar{K} + \mu) Z_M(x_a)} \quad (9.7.40)$$

$$M_a^* = \frac{p_t a^2 \gamma_t + p_s a^2 \gamma_s + B d_b \gamma_b}{1 + \frac{(1-\nu^2)}{e} (\ln \bar{K} + \mu) Z_M(x_a)} \quad (9.7.41)$$

and

$$D^* = eD; \quad D = Eh^3/12(1-\nu^2) \quad (9.7.42)$$

The parameter “ e ” serves to define the flexural efficiency for the perforated region.

For the case of a floating head exchanger, we point out that equilibrium

Eq. (9.7.18) can be solved directly for aV_a since N_s is a known quantity. For example, for the class of constructions where it is permissible to assume $N_s = p_s b/2$, if we assume $a_c = b$ for simplicity, then Eq. (9.7.18) yields

$$aV_a = \Delta p a^2 / 2 \quad (9.7.43)$$

so that Eq. (9.7.39) solves directly for M_a to yield

$$M_a = \frac{\Delta p a^2}{2} \bar{Q} + \frac{a^2(p_t \gamma_t + p_s \gamma_s) + B d_b \gamma_b}{1 + \frac{(1 - \nu^2)}{e} (\ln \bar{K} + \mu) Z_M(x_a)} \quad (9.7.44)$$

With M_a given by Eq. (9.7.44), we can find the state of stress in the tubesheet by substitution into Eq. (9.7.14) to determine the radial bending moment distribution, and by substitution into Eq. (9.7.17) to determine the tube loading. As noted earlier in Section 9.6, no iterative solution is required in floating head construction since shell length change is decoupled from the lateral deflection of the tubesheet.

For the case of integral tubesheet construction, however, N_s cannot be determined from statics alone, so that we must determine V_a , M_a and N_s together. The ring equilibrium equation, Eq. (9.7.18), remains valid as does the relation between M_a and V_a deduced in Eq. (9.7.39). A third equation is provided by noting that for integral tubesheet construction, the tubesheet deformation is defined relative to the shell (recall the discussion leading to Eq. (9.3.4)); therefore, we use Eq. (9.7.15) and Eq. (9.7.16) in the relation

$$v(x_a) + a\theta(x_a)(K - 1) = 0 \quad (9.7.45)$$

which assures that the tubesheet displacement at $r = b$ is equal to zero. The resulting equation is an additional condition relating N_s , V_a , M_a .

$$\begin{aligned} \frac{Q_a^4}{D^* x_a^4} &= \frac{a^2 M_a}{D^*} [Z_V(x_a) + (K - 1) Z_M(x_a)] \\ &+ \frac{a^3 V_a}{D^*} [Z_D(x_a) + (K - 1) Z_V(x_a)] \end{aligned} \quad (9.7.46)$$

where $Q_a^4 / D^* x_a^4 = Q / 2\xi$ involves N_s as well as the pressure and temperature loads. Equations (9.7.18), (9.7.39), and (9.7.46) suffice to determine V_a , M_a , N_s for specified pressure and temperature conditions. With M_a , V_a , and N_s determined, the radial bending moment distribution in the perforated region and the tube loading are obtained from Eqs. (9.7.14)–(9.7.17). The details of the solution are briefly outlined in the following.

Let Q_e , $\rho_1(x_a)$, $\rho_2(x_a)$, ξ^* be defined by the relations:

$$Q_e = \alpha_T \Delta T_T - \alpha_S \Delta T_S + \frac{\lambda_S p_s}{E_S} - \frac{p_t}{E_T} \left(\lambda_T + \frac{E_T}{2E_S} \frac{b}{h_s} \frac{1}{J} \right)$$

$$\rho_1(x_a) = Z_V(x_a) + (K-1)Z_M(x_a) \quad (9.7.47)$$

$$\rho_2(x_a) = Z_D(x_a) + (K-1)Z_V(x_a); \quad \xi^* = 2\pi b E_s h_s / n E_T A_T$$

Q_e is a measure of the unit loading, with λ_s , λ_T given by Eq. (9.7.12) and J defined in Eq. (9.7.10). The functions Z_V , Z_M , Z_D are defined in Eqs. (9.7.15) and (9.7.16). ξ^* is simply the ratio of shell axial stiffness to total tube bundle axial stiffness. In terms of these new quantities, Eq. (9.7.46) now becomes

$$\frac{L}{2} \left(Q_e + \frac{p_t b}{2E_s J h_s} \right) - \frac{N_s L}{2E_s J h_s} = \frac{a^2 M_a}{D^*} \rho_1 + \frac{a^2 V_a}{D^*} \rho_2 \quad (9.7.48)$$

If we eliminate M_a by using Eq. (9.7.39), and eliminate N_s by using Eq. (9.7.18), we can obtain an expression for aV_a which, after some manipulation, can be written in the form

$$aV_a = \frac{a^2 P_e}{2} = \frac{aKE_s h_s J Q_e - 0.5[J\xi^* x_a^4 \rho_1(x_a) M_a^* + \Delta p a^2 (K^2 - 1)]}{1 + J\xi^* Q_z x_a^4 / 2} \quad (9.7.49)$$

P_e can be thought of as an equivalent uniform pressure, applied to the surface of the perforated region, which represents the effect of all mechanical and thermal loads applied to the particular construction on the tubesheet perforated surface.

The function $Q_z(x_a, K)$ in Eq. (9.7.49) is defined as

$$Q_z(x_a, K) = \rho_2(x_a, K) + \bar{Q} \rho_1(x_a, K) \quad (9.7.50)$$

and we have made use of the following relationship between x_a and h

$$E_s h_s / EL = \frac{x_a^4 e}{48(1-\nu^2)} \left(\frac{h}{a} \right)^3 \frac{\xi^*}{K} \quad (9.7.51)$$

Equation (9.7.51) can be developed by using Eq. (9.7.2) together with Eqs. (9.2.6) and (9.3.8).

We note that Eq. (9.7.49) serves to define the effective pressure, due to mechanical and thermal load, acting on the fixed tubesheet. The introduction of the effective pressure simply brings the form of Eq. (9.7.49) into correspondence with the similar result for a floating head unit given in Eq. (9.7.43). We will see later that a further reduced form of Eq. (9.7.49) plays a key role in the simplified TEMA method in [9.1.1]. For a given unit geometry and loading, aV_a is completely specified so that Eq. (9.7.39) provides a final solution for M_a . The radial bending moment distribution can be written in terms of aV_a as:

$$M_r(x) = aV_a [Q_V(x) + \bar{Q} Q_M(x)] + Q_M(x) M_a^* \quad (9.7.52)$$

Similar expressions, in terms of aV_a , can be easily derived for $M_\theta(x)$, and for the tube loading function.

Despite the simplifications that have been made in this section, the presence of Bessel Functions still demands computer implementation to effect numerical results. We have provided, in Appendix 9.C, a user's guide and Fortran source code to generate results based on the analysis outlined in this section. In what follows, specific design examples are presented to illustrate the application of this computer code. Some of the design results obtained here will be referred to again in subsequent sections as we continue our simplification of the tubesheet equations down to the TEMA hand calculation form.

9.7.4 Computer Analysis Using Program FIXFLOAT of Appendix 9.C:

A parametric analysis of a fixed tubesheet heat exchanger using the foregoing analysis is presented in the following. The example configuration analyzed is one which amplifies the discrepancy between the FIXFLOAT solution and the TEMA design formulas. The TEMA fixed tubesheet design method, introduced in the fifth edition of the standards wrought a breakthrough in the state-of-the-art design practice. However, the simplifications used to produce a manual design procedure exact the inevitable toll in accuracy in a certain range of parameters. We attempt to delineate the range of doubtful accuracy by examining a suitably chosen problem.

Table 9.7.1 shows the complete input and output for a typical analysis of a tubesheet with integral support in a fixed tubesheet heat exchanger. The initial part of the table is an echo of the problem input as accepted by the computer code. The expansion joint spring constant has been set to a value sufficiently large so that the system response ignores any expansion joint effect. The code is designed to be executed by a user at an interactive terminal; the programming is such that transfer of the source code to any machine should proceed with little difficulty.

The computer code in this sample application requests user input for tubesheet, shell, and channel thickness, a value for the local shell thickness amplification factor FRA, a stiffness value for the expansion joint spring rate, a support parameter, and a printout control. FRA provides for a local thickness change of the effective shell and channel wall, in the vicinity of the tubesheet-shell-channel joint, to simulate an increased rotational resistance at the connection, say, due to a hubbed flange. The local bending stress in the wall, at the joint, is also reduced if $FRA > 1$. Considering the shell, for example, the computer code replaces the shell thickness TS with the effective shell thickness ($TS \cdot FRA$) in all computations dealing with rotation of the shell wall in the vicinity of the tubesheet joint. Axial growth of the shell, however, is based solely on TS. The support parameter takes the values 0, 1, or 2. The value "2" corresponds to a tubesheet integral with both channel and shell; the value "1" implies that the tubesheet is integral with the shell side only; and, the value "0" implies both sides gasketed.

Continuing with the description of the workings of the computer code, after all input data is reprinted in report format, the code computes and

prints out the tubesheet ligament efficiency (see Chapter 8) and requests input of E^*/E and ν^* from appropriate curves (see Figs. 8.1.1 and 8.1.2 for example). In this particular example, for an assumed tubesheet thickness of 4.375", output is requested for shellside pressure, for thermal loading, and for a combination of pressure plus thermal loading. We particularly point out that, for the configuration being examined, the computed value of the parameter x_a (see Eq. (9.7.2) or (Eq. 9.7.51)) is 1.52. We will recall this piece of information in subsequent discussion of the results. Table 9.7.1 also contains a summary of the output for the three loading cases. It is clear

Table 9.7.1. Analysis of Fixed Tubesheet Construction Using Program FIXFLOAT

```

***** INPUT DATA *****
SAMPLE PROBLEM A
STEP SIZE FOR MOMENT PRINTOUT,NP=    20
XA:  4.37500
SUPPORT TYPE--2=I/I; 1=G/I; 0=G/C NST=    2
MEAN RADIUS OF CHANNEL, AC=  12.0000
MEAN RADIUS OF SHELL, B=  12.0000
MEAN RADIUS OF DRILLED PORTION OF TUBESHEET,A=  10.0000
SHELLWALL THICKNESS,TS=  .500000
CHANNEL THICKNESS, TC=  .500000
OUTER RING RADIUS, A1=  12.0000
BOLT CIRCLE RADIUS, D=  12.0000
BOLT PRELOAD, BLD=  .000000E+00
NUMBER OF BOLTS, NB=    40
OUTER DIAMETER OF TUBE,D=  .750000
TUBEWALL THICKNESS,T=  .490000E-01
NUMBER OF TUBES,NT=    382
TUBE LENGTH,RLENTH=  192.000
TUBE PITCH,PITCH=  .937500
TUBE PATTERN DRILLING ANGLE,THETA=  60.0000
ELASTIC MODULUS OF TUBE MATERIAL,ET=  .240000E+08
ELASTIC MODULUS OF TUBESHEET MATERIAL,E=  .280000E+08
ELASTIC MODULUS OF SHELL MATERIAL,ES=  .290000E+08
ALLOWABLE STRESS OF TUBESHEET MATERIAL,SALL=  17500.0
SHELL EXPANSION JOINT STIFFNESS,SJ=  .290000E+12
EXPANSION JOINT BELLOWS INSIDE DIAMETER,DJ=  24.0000
EXPANSION COEFFICIENT OF TUBE,ALPHAT=  .900000E-05
EXPANSION COEFFICIENT OF SHELL,ALPHAS=  .700000E-05
TUBESHEET DESIGN STRESS FACTOR,OMEGA=  2.00000
TUBESIDE PRESSURE,PTO=  .000000E+00
SHELLSIDE PRESSURE,PSO=  200.000
OPERATING TEMPERATURE OF TUBE,TEMPTO=  350.000
OPERATING TEMPERATURE OF SHELL,TEMPSO=  200.000
ASSEMBLY TEMPERATURE OF THE UNIT,TEMPA=  70.0000
CALCULATION OPTIONS (NTYPE=0,CALCULATION FOR FLOATING HEAD UNIT;NTYPE=1,FOR FIXED TUBESHEET),NTYPE=    1
RATIO OF ROLL DEPTH TO TUBESHEET THICKNESS=  1.00000
PRINTOUT OPTIONS (NW=0,DO NOT PRINT OUT QV,QM VS X;NW=1,PRINT OUT QV,QM VS X),NW=    0
POISSON RATIO,BNU=  .300000
LIGAMENT EFFICIENCY,EFS=  .289600
VALUE OF E*/E READ IN =  .270000
EFFECTIVE POISSON RATIO,ANUSTA=  .370000
EFFECTIVE MODULUS OF TUBESHEET,ESTAR=  .756000E+07
FLEXURAL RIGIDITY RATIO,EFRR=  .284671

```

```

***** OUTPUT DATA *****
SAMPLE PROBLEM A
FOLLOWING RESULTS ARE FOR FIXED TUBESHEET:

B/A = 1.20000      AC/A= 1.20000      A1/A= 1.20000
DELTA= .131213
U= .382986
1 . XA= 1.52204

```

```

*****
*****
*****
(1) SHELLSIDE PRESSURE LOAD ONLY:

```

```

SAMPLE PROBLEM A
-----INTERMEDIATE COEFFICIENTS-----
AMU= .254056

```

*Refer to Appendix 9.C for aid in the definition of terms.

LIMIT VALUES OF TEMA PARAMETERS

LAMDA= .450661E-01 FM=MA)MAX/(P*A*A)= .141962
 FQ=QZ*XA**4/2.= 1.21714

-----RESULTS FOR TUBESHEET THICKNESS H= 4.37500 ,SHELL THICKNESS TS= .500000 CHANNEL THICKNESS TC= .500000
 LOCAL SHELL/CHANNEL THICKNESS AT JOINT= .500000
 .500000
 1.5*SA= 26250.0 ; 1.5*OMEGA*SA= 52500.0
 EDGE SUPPORT PARAMETER NST= 2
 AVA= 5257.14 ; MA= -613.441
 MAXIMUM RADIAL BENDING MOMENT,AMRMAX= 1492.62 ,AT X= .000000E+00 ; R/A= .000000E+00
 RADIAL BENDING MOMENT DISTRIBUTION:
 1492.62 1413.85 1174.45 765.721 174.684 -613.441
 MAXIMUM RADIAL BENDING STRESS,SRTS= 1615.65
 MAXIMUM CIRCUMFERENTIAL BENDING MOMENT,AMTMAX= 1492.62 AT X= .000000E+00 ; R/A= .000000E+00
 CIRCUMFERENTIAL BENDING MOMENT DISTRIBUTION:
 1492.62 1443.32 1293.80 1039.39 673.095 186.746
 MAXIMUM CIRCUMFERENTIAL BENDING STRESS,STTS= 1615.65
 MAX.TUBESHEET STRESS,STRESS= 1615.65
 OUTERMOST TUBE TENSILE LOAD,STRESS= 39.5824 366.806
 LONGITUDINAL SHELL STRESS,SS= 1609.52
 EDGE BENDING STRESS IN SHELL,SBS= 10133.0
 EDGE BENDING STRESS IN CHANNEL,SBC= 1409.74
 TOTAL LONGITUDINAL SHELL STRESS,STOT= 11742.5
 SHEAR STRESS AT EDGE,SSHR= 414.928
 TUBESHEET RING ROTATION,PHYR= .449318E-02 (DEGREE.)

(3) SHELLSIDE PRESSURE + THERMAL LOAD:

SAMPLE PROBLEM A

-----INTERMEDIATE COEFFICIENTS-----

AMU= .254056

LIMIT VALUES OF TEMA PARAMETERS

LAMDA= .450661E-01 FM=MA)MAX/(P*A*A)= .183658
 FQ=QZ*XA**4/2.= 1.21714

-----RESULTS FOR TUBESHEET THICKNESS H= 4.37500 ,SHELL THICKNESS TS= .500000 CHANNEL THICKNESS TC= .500000
 LOCAL SHELL/CHANNEL THICKNESS AT JOINT= .500000
 .500000
 1.5*SA= 26250.0 ; 1.5*OMEGA*SA= 52500.0
 EDGE SUPPORT PARAMETER NST= 2
 AVA= 124717. ; MA= -3114.92
 MAXIMUM RADIAL BENDING MOMENT,AMRMAX= 45810.6 ,AT X= .000000E+00 ; R/A= .000000E+00
 RADIAL BENDING MOMENT DISTRIBUTION:
 45810.6 44027.8 38584.7 29208.1 15478.3 -3114.92
 MAXIMUM RADIAL BENDING STRESS,SRTS= 49586.4
 MAXIMUM CIRCUMFERENTIAL BENDING MOMENT,AMTMAX= 45810.6 AT X= .000000E+00 ; R/A= .000000E+00
 CIRCUMFERENTIAL BENDING MOMENT DISTRIBUTION:
 45810.6 44695.1 41298.4 35474.6 26998.4 15591.7
 MAXIMUM CIRCUMFERENTIAL BENDING STRESS,STTS= 49586.4
 MAX.TUBESHEET STRESS,STRESS= 49586.4
 OUTERMOST TUBE TENSILE LOAD,STRESS= -2019.28 -18712.5
 LONGITUDINAL SHELL STRESS,SS= 21519.6
 EDGE BENDING STRESS IN SHELL,SBS= 65778.8
 EDGE BENDING STRESS IN CHANNEL,SBC= 57055.6
 TOTAL LONGITUDINAL SHELL STRESS,STOT= 87298.4
 SHEAR STRESS AT EDGE,SSHR= 9843.51
 TUBESHEET RING ROTATION,PHYR= .181850 (DEGREE.)

-----TEMA RESULT FOR TUBESHEET THICKNESS-----

TEMA RESULT:BENDING CONTROL THICKNESS,HHB= 2.14447

that in this application, the thermal loading dominates the response. Output of the bending moment distribution is given from the center of the tubesheet to the outer edge of the perforated region at user specified increments. For the purposes of the ensuing discussion of particular design results, the following criteria are suggested for design limits. If S_A is the specified allowable stress under membrane type mechanical loading, then stress limits for primary membrane stress or for primary bending stress plus membrane stress are S_A and $1.5S_A$, respectively (see Chapter 2). When thermal loading alone, or in combination with mechanical loading, is present, membrane stress is presumed limited to $1.5S_A$, and membrane plus bending stress at a given location is limited to $3S_A$.*

Examining the final combined output in Table 9.7.1 shows that, for the assumed tubesheet thickness of 4.375", the tubesheet stress just meets the secondary stress limits of $3S_A = 52500$ psi for combined thermal and mechanical load. The longitudinal shell membrane stress exceeds $S_A = 17,500$ psi, but since this stress is also dominated by thermal loading, it may be considered as a secondary stress. Because of severe local bending at the shell-head-tubesheet joint, the total shell stress at the joint exceeds $3S_A$. The values given for the parameters λ , FM , and FQ will be discussed further in a later section. The small value of 0.254 for the rotational resistance parameter μ (AMU in the output) indicates that the tubesheet receives little rotational support from the barrel of the exchanger.

The final option in the computer code permits an iterative calculation of the tubesheet thickness per the TEMA formulas in Ref. [9.1.1]. We see that the TEMA formula predicts a significantly thinner tubesheet thickness (2.14") with tubesheet bending being the controlling factor. Note that this final TEMA calculation option is only valid for fixed tubesheet exchangers and assumes that $b = a = a_c = 12$ ". In subsequent discussions in this chapter comments will be made on the significant discrepancy between the results just quoted and the results predicted by the well established but approximate TEMA formulation.

Table 9.7.2 summarizes a series of simulation cases using the computer code. The five studies done all involve the fixed tubesheet exchanger whose configuration and loading is set down in Table 9.7.1.

Table 9.7.2. Summary of Sample Applications

Case	Remark
1	Base configuration (see Table 9.7.1)
2	Increase shell and channel thickness from 0.5" to 0.75"
3	Base case except effective shell/channel thickness increased to 1.125" near tubesheet, shell and channel junction by changing FRA
4	Base case except $a = b$ so untubed rim is eliminated.
5	Base case except channel side rotational resistance neglected

*If the unit is subjected to loadings causing stress reversals, then the limit on secondary stress combinations should be applied to the stress *range*.

Table 9.7.3, below, summarizes the important results of the above case studies. Case 2 shows the results obtained when the shell and channel thicknesses are increased to 0.75" everywhere in the unit. As expected, the rotational resistance parameter AMU (μ as defined by Eq. (9.7.27)) is increased, although its value is such as to still imply minimal rotational restraint of the tubesheet. The increase in shell wall thickness has a negligible effect on tubesheet stress; the tubesheet stress level increases slightly because the thermal load is now acting on a stiffer system. As expected, the mean shell stress decreases significantly; the local shell stress, primarily due to bending at the joint, also decreases but still exceeds $3S_A$. Therefore, the design is still marginal if the previously stated design limits are assumed to govern.

Table 9.7.3 Summary of Results from Sample Calculations Using Program "FIXFLOAT" for Fixed Tubesheet Heat Exchanger

Case	Tubesheet Max. Stress (psi)	Shell/Channel Max. Stress (psi)	Shell Tensile Stress (psi)	x_a	μ
1	49586	87298	21520	1.52	.254
2	50899	78965	16995	1.52	.547
3	43315	56553	17482	1.52	1.20
4	41993	78995	21883	1.67	.254
5	53366	95607	21216	1.52	.127

Case 3 examines the effect of locally increasing the shell thickness to $HLOC = TS \cdot FRA$ where $FRA = 1.5$ with all other geometry the same as that given in Table 9.7.1. The results of the thermal plus mechanical load combination show that increasing the shell bending resistance near the tubesheet joint reduces both the tubesheet stress level and the local membrane plus bending stress in the shell.

It is important to note that the TEMA tubesheet design formula [9.1.1] makes no computation of local membrane plus bending stress in the shell and in the channel wall. However, even if this stress level is not considered in the more detailed computation, there still exists a significant discrepancy between our prediction of minimum tubesheet thickness and that of TEMA using the simple formulas of the TEMA standards. It is emphasized again that the computed value of x_a for this configuration, based solely on a tubesheet stress level that does not exceed $3S_A$, is significantly under 3.0. The significance of this point will be clarified later in this chapter when we discuss, in detail, the simplifications required to evolve the TEMA design method.

In case 4, we examine the effect of the unperforated rim on the response of a fixed tubesheet exchanger under mechanical and thermal loads. The case 1 configuration in Table 9.7.1 is recomputed with the only modification being that the perforated radius a is increased to equal $b =$

12" so that the effect of any unperforated rim is eliminated. Results for a tubesheet thickness of 4.375" are presented. A direct comparison with the results given in Table 9.7.1 shows that for the loading and geometry considered, it is *non-conservative to neglect the effect of an unperforated rim*. Whether this non-conservatism extends through the entire gamut of loadings and geometries can only be ascertained by parametric analysis; one can only be cautioned that unit design based on assuming $b/a = 1$ for the sake of simplicity may lead to underprediction of tubesheet maximum stress.

Finally, in case 5, we present results for the unit with the channel side rotational resistance neglected. Some stress increase is observed in the unit. We note that in none of the simulations carried out was the rotation resistance parameter very large. Therefore, the tubesheet behaved essentially as a simply supported unit. The significant rotations at the outer radius leads to the high shell and channel local bending stresses. In a real situation, local yielding will occur in the shell and channel wall near the joint at some load level; subsequent to that point, the tubesheet will truly behave like a simply supported unit until the maximum load state is reached.

The foregoing discussion highlights the potential limitation of the TEMA solution method. The example problem chosen is somewhat contrived to magnify the difference since TEMA methods give remarkably accurate solutions for the great majority of practical cases. A detailed comparison of analysis-based methods and TEMA formulas may be found in [9.7.1]. A study, similar to the above, for a floating tubesheet construction is next presented.

Table 9.7.4. Analysis of Stationary Tubesheet in a Floating Head Construction Using Program FIXFLOAT

```

***** INPUT DATA*****
SAMPLE PROB. B FLOATING HEAD
STEP SIZE FOR MOMENT PRINTOUT,NP= 20
XA: 5.50000
SUPPORT TYPE--2=1/1; 1=6/1; 0=G/G NST= 2
MEAN RADIUS OF CHANNEL, AC= 16.5000
MEAN RADIUS OF SHELL, B= 16.5000
MEAN RADIUS OF DRILLED PORTION OF TUBESHEET,A= 13.5200
SHELLWALL THICKNESS,TS= 2.25000
CHANNEL THICKNESS, TC= 2.25000
OUTER RING RADIUS, A1= 16.5000
BOLT CIRCLE RADIUS, D= 16.5000
BOLT PRELOAD, BLD=-.000000E+00
NUMBER OF BOLTS, NB= 40
OUTER DIAMETER OF TUBE,D= 1.00000
TUBEWALL THICKNESS,T= .650000E-01
NUMBER OF TUBES,NT= 341
TUBE LENGTH,RLNTH= 168.000
TUBE PITCH,PITCH= 1.25000
TUBE PATTERN DRILLING ANGLE,THETA= 90.0000
ELASTIC MODULUS OF TUBE MATERIAL,ET= .287000E+08
ELASTIC MODULUS OF TUBESHEET MATERIAL,E= .276000E+08
ELASTIC MODULUS OF SHELL MATERIAL,ES= .276000E+08
ALLOWABLE STRESS OF TUBESHEET MATERIAL,SALL= 15000.0
SHELL EXPANSION JOINT STIFFNESS,SJ= .276000E+12
EXPANSION JOINT BELLOWS INSIDE DIAMETER,DJ= 33.0000
TUBESHEET DESIGN STRESS FACTOR,OMEGA= 2.00000
TUBESIDE PRESSURE,PTO= 2015.00
SHELLSIDE PRESSURE,PSO= .000000E+00
CALCULATION OPTIONS (NTYPE=0,CALCULATION FOR FLOATING HEAD UNIT;NTYPE=1,FOR FIXED TUBESHEET),NTYPE= 0
RATIO OF ROLL DEPTH TO TUBESHEET THICKNESS= 1.00000
PRINTOUT OPTIONS (NW=0,DO NOT PRINT OUT QV,QM VS X;NW=1,PRINT OUT QV,QM VS X), NW= 0
POISSON RATIO,BNU= .300000
LIGAMENT EFFICIENCY,EFS= .304000
VALUE OF E*/E READ IN = .380000
EFFECTIVE POISSON RATIO,ANUSTA= .335000
EFFECTIVE MODULUS OF TUBESHEET,ESTAR= .104880E+08
FLEXURAL RIGIDITY RATIO,EFRR= .389513

***** OUTPUT DATA *****
SAMPLE PROB. B FLOATING HEAD
FOLLOWING RESULTS ARE FOR THE FIXED TUBESHEET OF A FLOATING HEAD UNIT:

B/A = 1.22041 AC/A= 1.22041 A1/A= 1.22041
DELTA= .113377
U= .405137
1 . XA= 1.67662
(2) TUBESIDE PRESSURE LOAD ONLY:
SAMPLE PROB. B FLOATING HEAD
-----INTERMEDIATE COEFFICIENTS-----
AMU= 2.97087
LIMIT VALUES OF TEMA PARAMETERS
LAMDA= .403933 FM=(MA)MAX/(P*A*A)= .106855
FQ=QZ*XA**4/2.= .000000E+00

-----RESULTS FOR TUBESHEET THICKNESS H= 5.50000 ,SHELL THICKNESS TS= 2.25000 CHANNEL THICKNESS TC= 2.25000
LOCAL SHELL/CHANNEL THICKNESS AT JOINT= 2.25000 2.25000
1.5*SA= 22500.0 ; 1.5*OMEGA*SA= 45000.0
EDGE SUPPORT PARAMETER NST= 2
AVA= -184161. ; MA= 39357.0
MAXIMUM RADIAL BENDING MOMENT,AMRMAX= 39357.0 ,AT X= 1.67662 ; R/A= 1.00000
RADIAL BENDING MOMENT DISTRIBUTION:
-34322.8 -31550.0 -23127.2 -8765.61 11934.4 39357.0
MAXIMUM RADIAL BENDING STRESS,SRTS= 25678.8
MAXIMUM CIRCUMFERENTIAL BENDING MOMENT,AMTMAX= 34322.8 AT X= .000000E+00 ; R/A= .000000E+00
CIRCUMFERENTIAL BENDING MOMENT DISTRIBUTION:
-34322.8 -32656.7 -27605.8 -19023.7 -6703.56 9564.62
MAXIMUM CIRCUMFERENTIAL BENDING STRESS,STTS= 22394.2
MAX. TUBESHEET STRESS, STRESS= 25678.8 7773.26
OUTERMOST TUBE TENSILE LOAD, STRESS= 1484.15
LONGITUDINAL SHELL STRESS,SS= .000000E+00
EDGE BENDING STRESS IN SHELL, SBS= 20289.0
EDGE BENDING STRESS IN CHANNEL, SBC= 47143.3
TOTAL LONGITUDINAL SHELL STRESS,STOT= 20289.0
SHEAR STRESS AT EDGE, Sshr= -8146.78
TUBESHEET RING ROTATION,PHYR= -.510539E-01 (DEGREE.)

```

*Refer to Appendix 9.C for aid in the definition of terms.

Table 9.7.4 presents complete results obtained for the stationary tubesheet of a typical floating head exchanger. Analysis is performed for a shell thickness of 2.25" and for a tubesheet thickness of 5.5". Note that the calculated value of μ , the rotational restraint parameter, is approximately 3.0 indicating that the shell restraint on tubesheet bending is probably not equivalent to a fully clamped support. It is of interest to note that the TEMA method, which considers shell rotational restraint to be simply a function of shell thickness to diameter ratio, would consider this unit as being clamped. The results obtained using the complete analysis of this section indicate that with a tubesheet thickness of 5.5", the maximum tubesheet bending stress, occurring at the center of the tubesheet, is somewhat in excess of the allowable value under solely mechanical loading of $1.5S_A = 22500$ psi. Table 9.7.5 shows the results of certain simulation studies carried out on this floating head configuration. Case 6, of course, is the base case presented in Table 9.7.4 for an assumed tubesheet thickness of 5.5".

Table 9.7.5. Summary of Results from Sample Calculations for Floating Head Exchanger

Case	Tubesheet Max. Stress (psi)	Barrel Max. Stress (psi)	x_a	μ
6	25679	54531	1.68	2.97
7	23560	---	---	---
8	29443	---	1.65	10^{10}
9	41444	55234	1.85	2.97
10	26073	52936	1.55	1.81

In case 7, we simply increase the thickness of the tubesheet to 6.25" in an attempt to achieve a stress level below 22500 psi. Using a thickness of 6.25" reduces the tubesheet stress to 23560 psi. Using the method in [9.1.1], for a clamped unit, and assuming a tubesheet fully perforated with pressurized diameter 33", predicts that a 4.84" tubesheet yields a satisfactory design. Case 8 results indicate what happens to the configuration if we assume an artificially large FRA value in order to obtain a very large value for μ . In this case (compare with case 6) the maximum tubesheet stress shifts to the outer edge of the perforated region but still exceeds the permitted value of $1.5S_A$. Thus, the results of the computer calculation indicate that a thickness in excess of 6.25" is required for adequate design following the spirit of the ASME Code.

Cases 9 and 10 are the same as cases 6 and 7 except that the unperforated rim has been removed. It is seen that for this geometry and load value, the presence of an unperforated rim has a *beneficial* effect on tubesheet stress; that is, a thicker tubesheet is required to keep the tubesheet stress on the order of $1.5S_A$ if no unperforated rim is present for the same tubesheet outer diameter.

Other than to note that the computed x_a value for the unit considered in Tables 9.7.5 is below 2.0, no attempt is made here to explain the discrepancy between our results and the predictions obtained from use of the TEMA formula [9.1.1] for thickness of a stationary tubesheet in a floating head exchanger. We note, however, that when the analysis is applied to a situation where a thinner tubesheet results, yielding an x_a value much in excess of 3.0, the agreement between TEMA and our more rigorous computer analysis is better. We will demonstrate this fact shortly.

The next sections examine further simplifications to our tubesheet analysis and consider the derivation of the TEMA design formula. We will show that this potential limitation of the TEMA fixed tubesheet design formula can be correlated with the value of x_a appropriate to the configuration.

9.8 REDUCTION OF ANALYSIS TO SIMPLIFIED FORM

We have demonstrated that rigorous analysis of a fixed or floating head exchanger tubesheet leads to equations of sufficient complexity to require the use of special purpose computer codes to effect usable design results. In this section, we focus our attention on reducing our complex formulation to simplified forms which are amenable to hand computation, if desired. We will show that if we can present some of the key expressions involving Kelvin functions in either graphical form, or in their simplified asymptotic representation, then we will be able to reduce our computerized formulation to a procedure amenable to manual computations. The endpoint of our discussions here in this section will be the well established TEMA design formula [9.1.1] for fixed tubesheets; we will demonstrate how the TEMA design equations can be developed, in a logical manner, from the rigorous analyses presented here to this point. As a by-product of our reductions, we will also develop a design procedure that involves the use of graphical data in conjunction with manual (or computerized) computations. *This intermediate design procedure can be classified as a method that is less restrictive than the TEMA procedure, yet involves sufficient simplification to permit a manual computation of tubesheet thickness.*

We begin our simplifications by defining the parameter Φ , where

$$\Phi = (1 - \nu^2)(\ln \bar{K} + \mu) / e \quad (9.8.1)$$

In Eq. (9.8.1), \bar{K} is the unperforated ring outer to inner radius ratio (see Fig. 9.7.1), μ is the ring rotational stiffness parameter, and e is the flexural efficiency of the perforated region. We note that for a given unit configuration, any assumed tubesheet thickness will provide a numerical value for Φ . In terms of the parameter Φ , the function $\bar{Q}(x_a, K, \Phi)$, given by Eq. (9.7.40), can be written as

$$\bar{Q} = \frac{K - 1 - \Phi Z_V(x_a)}{1 + \Phi Z_M(x_a)} \quad (9.8.2)$$

Computation of \bar{Q} for any assumed geometry and material specifications can be made once the value of x_a is established and Z_V , Z_M calculated. Equation (9.7.51) is a convenient equation to evaluate x_a for any assumed tubesheet thickness. A manual computation of \bar{Q} is easily performed by using Fig. 9.8.1a,b which provide data for Z_V , Z_M as functions of x_a . We note that the range of \bar{Q} , for values of $\bar{K} \leq 1.5$, $0 \leq \Phi \leq \infty$, is roughly given by the expression below

$$-0.25 \leq \bar{Q} \leq 0.5 \quad (9.8.3)$$

In constructing results for Z_V , Z_M , we have arbitrarily assumed $\nu^* = 0.40$. We now recall the equation for aV_a (Eq. (9.7.49)). For ease in following our developments, we repeat some relevant expressions here

$$aV_a = \frac{a^2 P_e}{2} = \frac{aKE_s h_s J Q_e - 0.5 J \xi^* x_a^4 \rho_1(x_a) M_a^* - \Delta p a^2 (K^2 - 1)/2}{1 + J \xi^* Q_z x_a^4 / 2} \quad (9.7.49)$$

$$Q_z = \rho_2(x_a, K) + \bar{Q} \rho_1(x_a, K) \quad (9.7.50)$$

where

$$\rho_1(x_a, K) = Z_V(x_a) + (K - 1)Z_M(x_a) \quad (9.7.47)$$

$$\rho_2(x_a, K) = Z_D(x_a) + (K - 1)Z_V(x_a)$$

From these expressions, we see that defining $F_q = Q_z x_a^4 / 2$ yields an expression for F_q in the symbolic form:

$$F_q = q_{z1}(x_a, \bar{Q}) + (K - 1)q_{z2}(x_a, \bar{Q}) \quad (9.8.4)$$

where

$$q_{z1}(x_a, \bar{Q}) = [Z_D(x_a) + \bar{Q}Z_V(x_a)]x_a^4/2 \quad (9.8.5)$$

$$q_{z2}(x_a, \bar{Q}) = [Z_V(x_a) + \bar{Q}Z_M(x_a)]x_a^4/2$$

If we restrict ν^* to be 0.40 wherever it appears in Z_D, Z_V, Z_M , then Figs. 9.8.2 and 9.8.3 provide graphical results for q_{z1} , q_{z2} as a function of x_a with \bar{Q} as a parameter. Thus, with the aid of this data, the parameter F_q is easily computed from Eq. (9.8.4). We note also that $\rho_1(x_a, K)$ is also easily computed using the data provided by Fig. 9.8.1a,b. We now see that a manual computation of aV_a in the case of a fixed tubesheet exchanger is

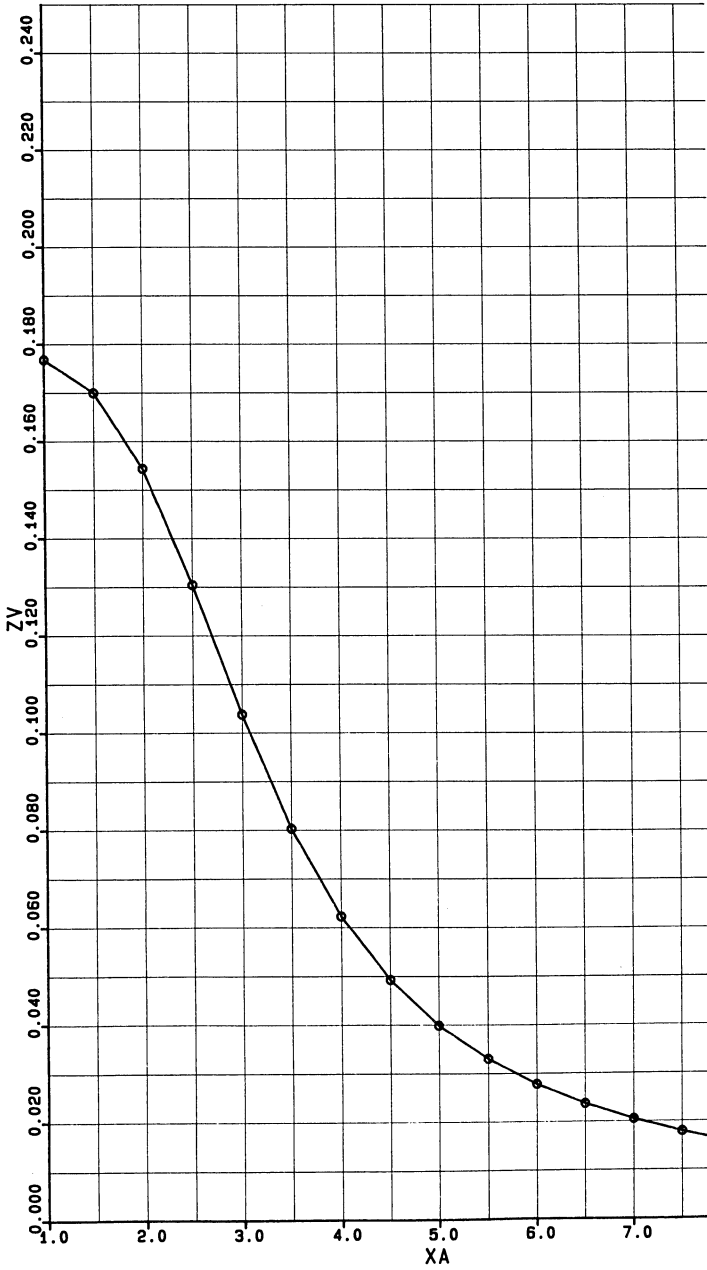


Fig. 9.8.1a. Z_V vs. x_a .

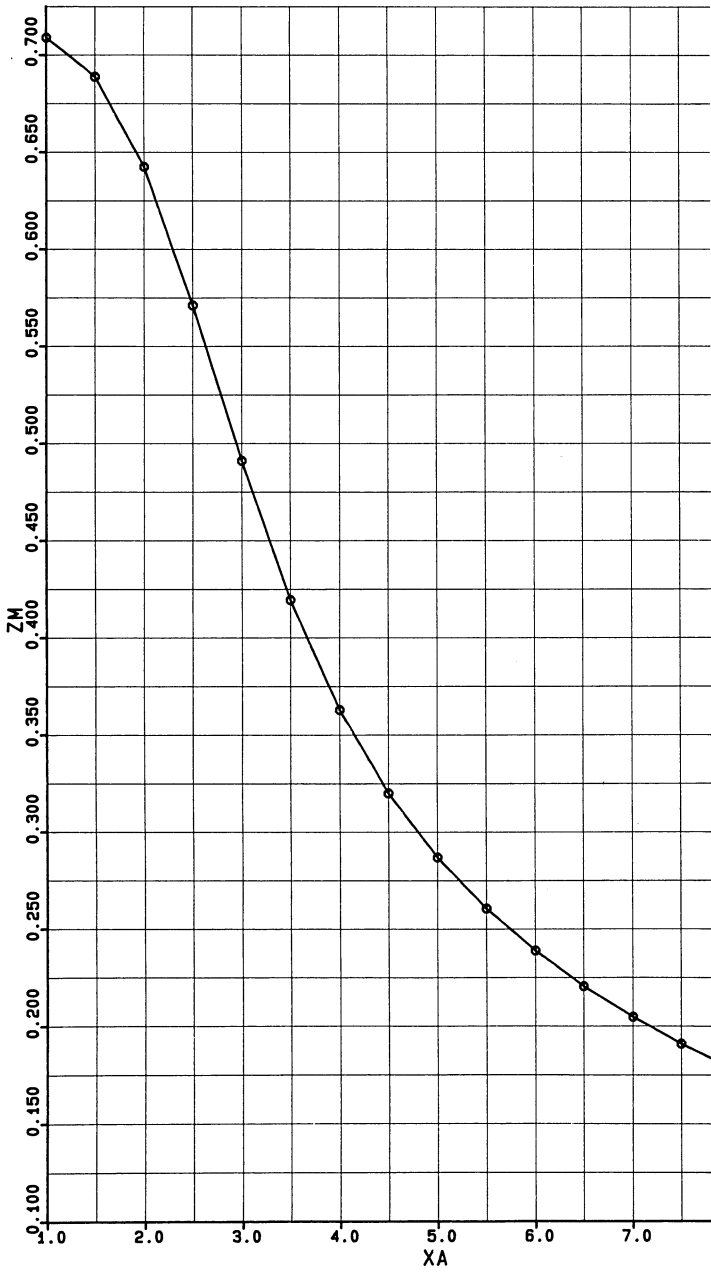


Fig. 9.8.1b. Z_M vs. x_A .

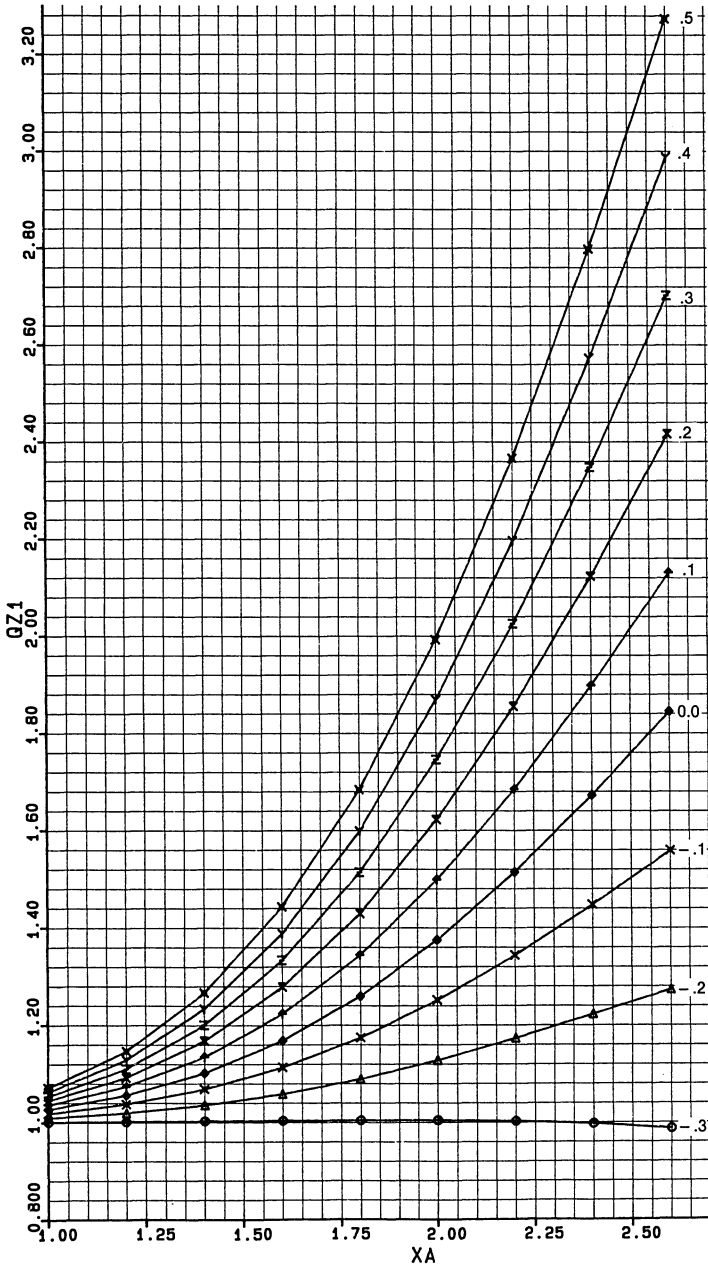


Fig. 9.8.2a. Q_{z1} vs. X_A .

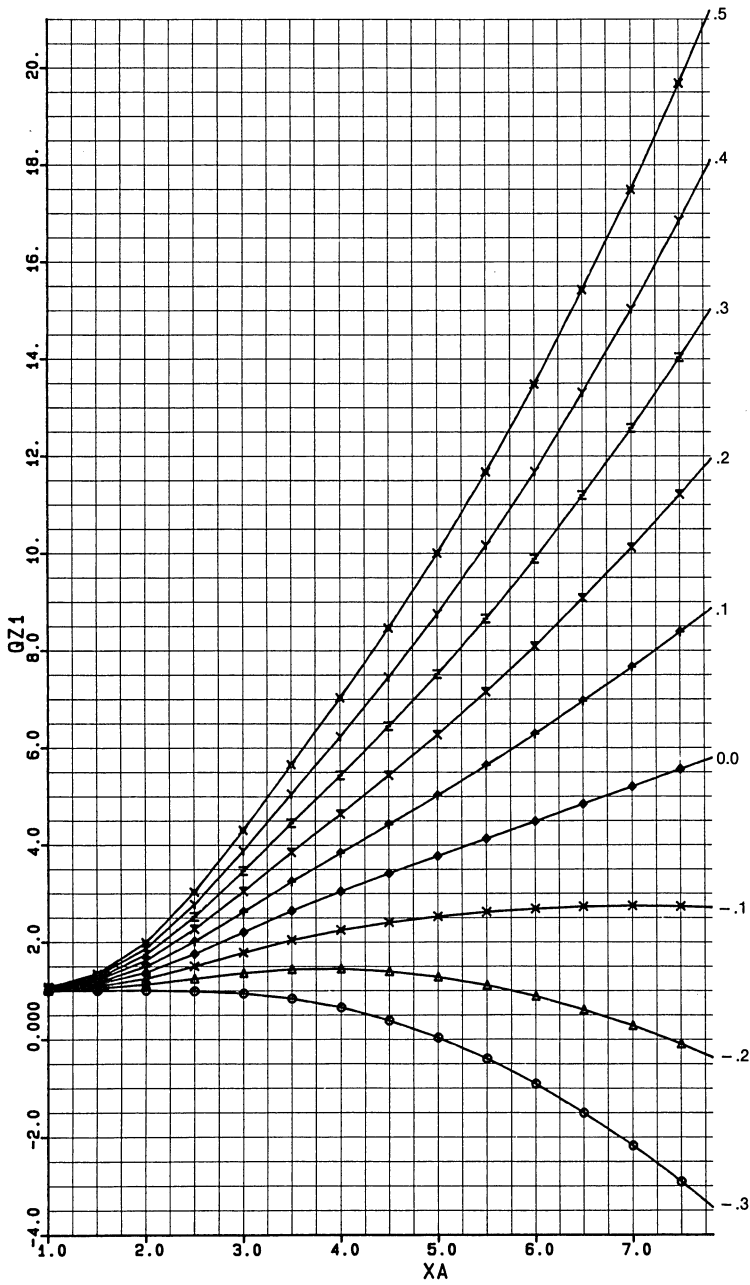


Fig. 9.8.2b. q_{z1} vs. x_a .

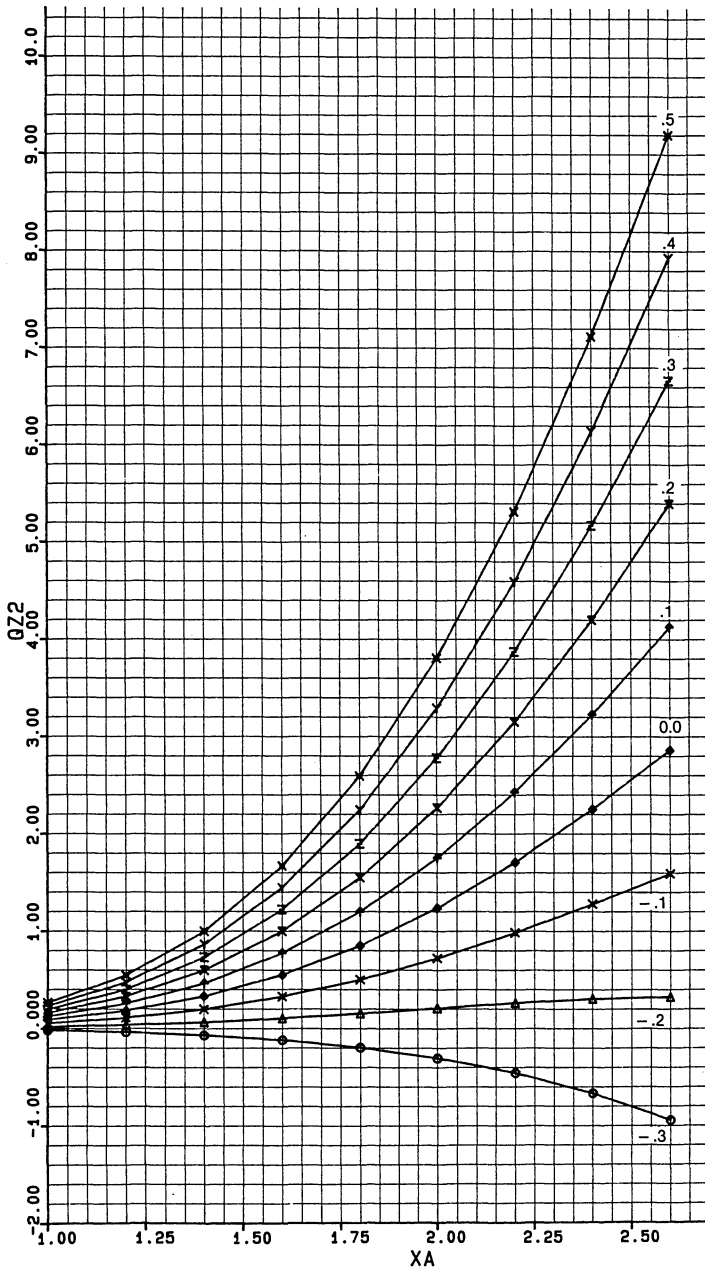


Fig. 9.8.3a. q_{z2} vs. X_a .

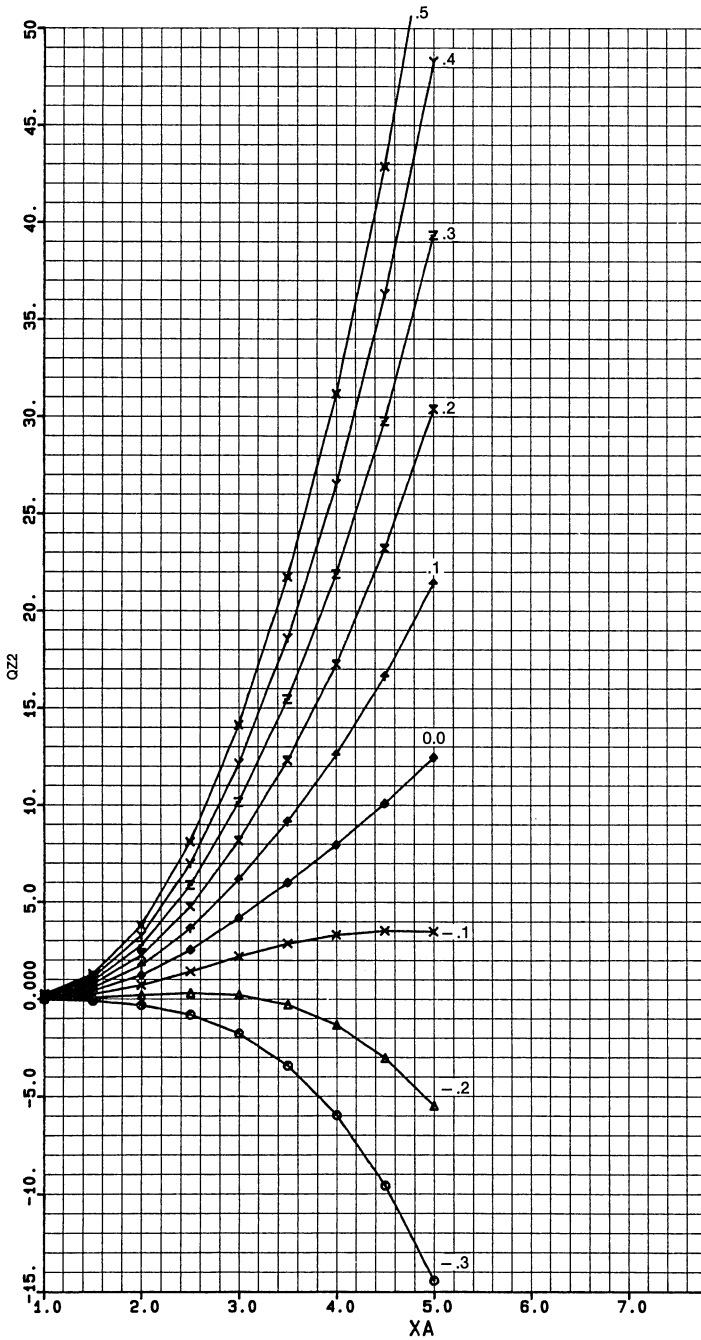


Fig. 9.8.3b. q_{z2} vs. X_A .

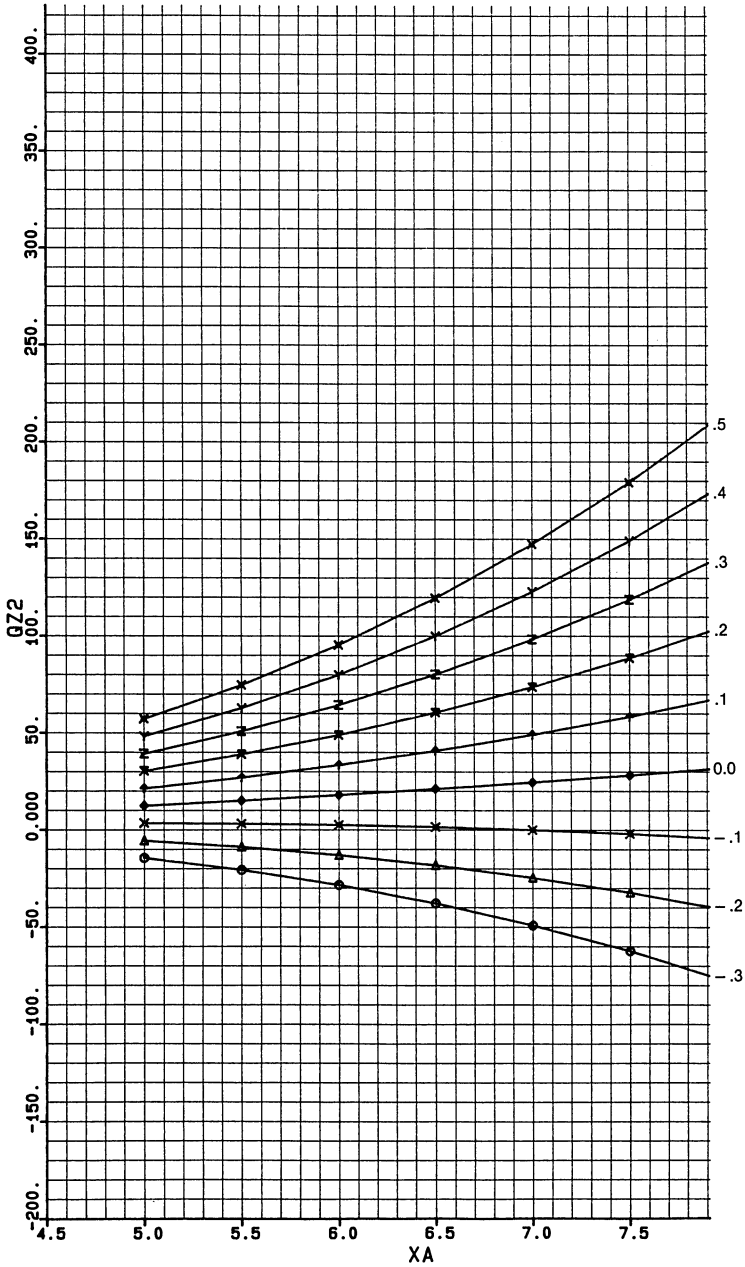


Fig. 9.8.3c. q_{z2} vs. x_a .

feasible using Eq. (9.7.49) and (9.7.51) and the graphical data provided. We recall that our only approximation to this point has been a setting of ν^* to be 0.40 wherever it appears in Z_D, Z_V, Z_M (see the definitions of these functions given earlier in this chapter). It would be a simple matter to provide additional curves for other values of ν^* ; we choose here, however, to use our results for *all* ligament efficiencies.

Summarizing our efforts to this point, we have assumed that the unit geometry, material, and loading have been specified, including an assumption on the necessary tubesheet thickness. We have been able to compute x_a , the parameters \bar{Q} and \bar{Q}^* , and can determine $aV_a = a^2 P_e / 2$. The calculations can all be carried out manually since we have reduced the complicating effect of the Kelvin functions to graphical form. At this point, we can also compute M_a / aV_a using the equation

$$\frac{M_a}{aV_a} = \bar{Q} + \frac{M_a^*}{aV_a} = \bar{Q}^* \quad (9.8.6)$$

If we recall Eqs. (9.7.39) and (9.7.41), we see that the neglect of M_a^* in Eq. (9.8.6) is akin to saying that we will neglect the effects of pressure loading acting on the shell and channel walls, and on the unperforated rim, and consider only the contribution of effective pressure P_e . Note that for some floating head units, $P_e = \Delta p = p_s - p$, (see Eqs. (9.7.18) and (9.7.43)).

With \bar{Q}^* determined for the configuration, we can now evaluate the effective tube pressure $q(x)$, and the tubesheet rotation $\theta(x)$. For our design purposes here, it is sufficient to compute the tube pressure and the tubesheet rotation only at $x = x_a$ since the values are critical for design at this location. From Eqs. (9.7.15) and (9.7.17), we find that $q(x_a)$, $\theta(x_a)$ can be written in the form

$$\frac{q(x_a) a^2}{2aV_a} = [Z_D(x_a) + \bar{Q}^* Z_V(x_a)] x_a^4 / 2 \quad (9.8.7)$$

$$\frac{\theta(x_a) D^* x_a^4}{2a^2 V_a} = [Z_V(x_a) + \bar{Q}^* Z_M(x_a)] x_a^4 / 2$$

We see that $q(x_a)$, $\theta(x_a)$ can be obtained using Figs. 9.8.2 and 9.8.3 by simply interpreting the parameter as \bar{Q}^* in those figures. We do note however that we cannot easily establish what the bounds on \bar{Q}^* are for the wide range of configurations that we might encounter in practice; thus for use in design codes, we may need to expand the parameter range in Figs. 9.8.2 and 9.8.3. In any case, having results for $q(x_a)$ enables a hand calculation of the tube load at the outer limit of the perforated region. Similarly, having results for $\theta(x_a)$ (equal to the rotation of the unperforated rim) enables us to compute the edge bending moment M_c , M_s in the shell and channel using Eqs. (9.7.24).

To establish the validity of our assumed tubesheet thickness, we must also

calculate the maximum stress in the perforated region of the tubesheet. We assume here that the radial bending moment always governs the design. From Eq. (9.7.14), we find that

$$\frac{M_r(x)}{aV_a} = Q_V(x) + \bar{Q}^* Q_M(x)$$

which can be rewritten as

$$\frac{M_r(x)}{a^2 P_e} = \frac{1}{2} (Q_V(x) + \bar{Q}^* Q_M(x))$$

For design purposes, we need the maximum value for $M_r(x)$; we write this in the form

$$M_{r\max} = a^2 P_e F_M(x_a, \bar{Q}^*)$$

where

(9.8.8)

$$2F_M(x_a, \bar{Q}^*) = |\max[Q_V(x) + \bar{Q}^* Q_M(x)]|$$

Figure 9.8.4 presents results for F_M as a function of x_a and the parameter \bar{Q}^* . Again, in a practical case, these curves may need to be extended since \bar{Q}^* may not fall in the range plotted. Note that the neglect of M_a^* in the computation of M_a (see Eq. (9.8.6)) insures that $\bar{Q}^* = \bar{Q}$. It is of interest to note that for certain negative values of \bar{Q}^* , $2F_M \rightarrow \bar{Q}^*$ for either the entire x_a range, or for the higher values of x_a . It can be shown that this occurs when the maximum moment occurs at x_a ; i.e., we can easily show analytically that $Q_V(x_a) + \bar{Q}^* Q_M(x_a) = \bar{Q}^*$.

A solution procedure can now be developed based on the graphical data. If all geometry, material, and loading parameters are specified, then an assumed tubesheet thickness h establishes x_a , $\Phi(x_a)$ and \bar{Q} . Using appropriate graphical data, \bar{Q}^* and F_M can be ascertained, and therefore P_e and $M_{r\max}$ can be established. The maximum radial bending stress is then given as:

$$\sigma_B = \frac{6M_{r\max}}{\eta_s h^2} = \left(\frac{2a}{h}\right)^2 \left(\frac{1.5 F_M P_e}{\eta_s}\right) \quad (9.8.9)$$

The stress efficiency η_s is usually set equal to the ligament efficiency η . If S_A is the allowable material stress under membrane behavior, then an ASME design criteria for tubesheet bending may be interpreted as a limit on the radial bending stress σ_B

$$\sigma_B \leq 1.5\Omega S_A \quad (9.8.9a)$$

where $\Omega = 1.0$ if P_e involves only pressure loading, and $\Omega = 2.0$ if P_e involves only thermal loading or both mechanical and thermal loading. We can think of the design procedure as being continuing assumptions for the

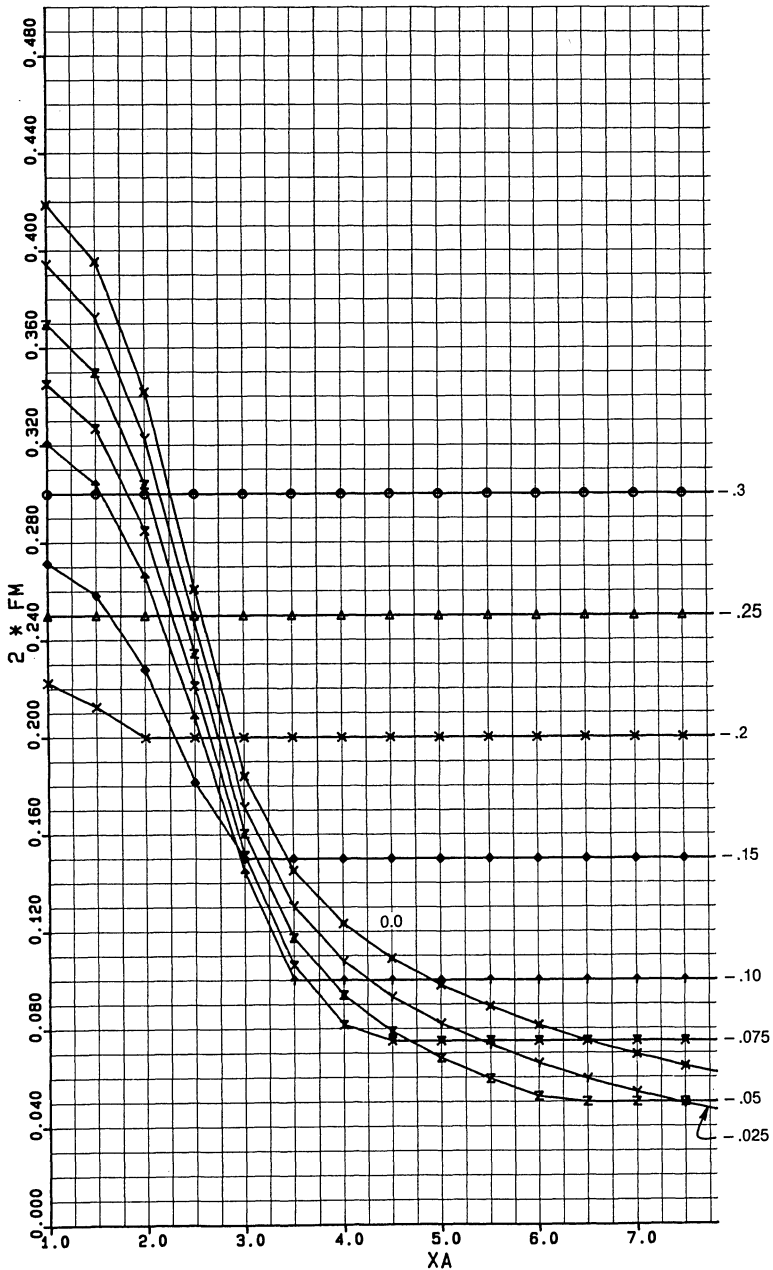


Fig. 9.8.4a. $2 F_M$ vs X_A .

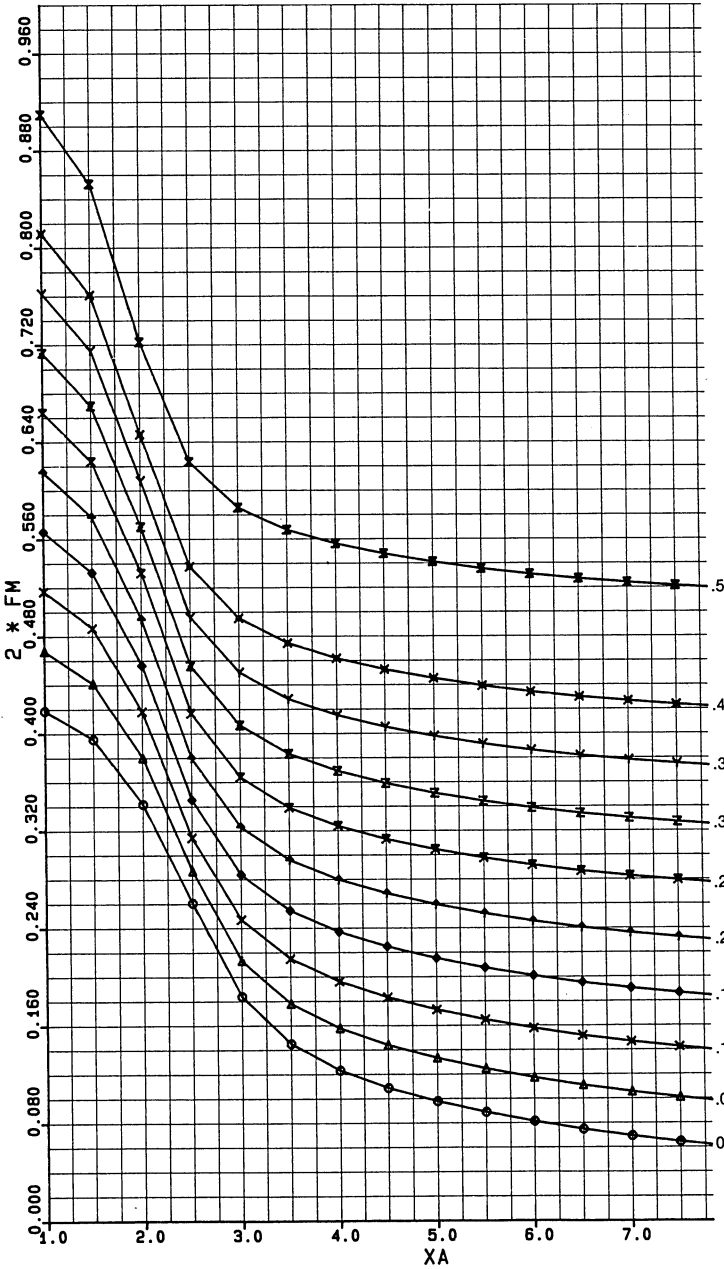


Fig. 9.8.4b. $2 F_M$ vs. x_a .

tubesheet thickness h until an acceptable value of σ_B , satisfying Eq. (9.8.9a), is obtained.

The use of Figs. 9.8.1–9.8.4 enables a manual determination of h to be carried out with relatively small effort for the entire range of x_a values, edge restraint conditions, and geometries. Alternatively, a programmable calculator or a microcomputer can be efficiently utilized to perform all of the required calculations based on data read in from the appropriate figures by the designer. Appendix 9.D presents an interactive BASIC code, developed for a TRS-80 Model III, that uses the information from Figs. 9.8.1–9.8.4, and generates values for tubesheet stress, tube effective pressure and ring rotation. Table 9.8.1 shows typical hardcopy results obtained using the simplified method based on the same input data used for the fixed tubesheet exchanger example presented in the previous section. The program requires that a printer be available.

Summarizing our efforts to this point, we note that we have gone through two levels of simplification of the most general tubesheet equations and have developed design approaches of varied sophistication. It is now of interest to consider even further reductions of the simplified method presented in this section. Specifically, our intent now is to show how the simple TEMA design formulation [9.1.1], for a tubesheet in a fixed tubesheet heat exchanger, is evolved from the work given here.

To this end, we invoke the following additional assumptions:

- (i) We assume that there is no unperforated rim, and that $b = a = a_c = a_s$.
- (ii) We neglect M_a^* completely in this analysis.*
- (iii) We restrict consideration to units configured so that $x_a \gg 3$.

All of the above assumptions are necessary to evolve the TEMA design formula. We note that with the above considerations $\bar{Q}^* = \bar{Q}$, and the effective pressure can be written as (recall Eqs. (9.7.49) and (9.7.50))

$$aV_a = a^2 P_e / 2 = \frac{aE_s h_s J Q_e}{1 + J\xi^* F_q(x_a)} \quad (9.8.10)$$

$$F_q = Q_z x_a^4 / 2$$

Since tubesheet thickness h is proportional to $1/x_a^{1.333}$ (see Eq. (9.7.2b)), a limitation to $x_a > 3$ restricts a TEMA designed tubesheet to an upper limit on thickness in order to obtain valid results. As we have already seen in some of the numerical studies in the previous section, there are certainly some units which may not meet this limitation. The current TEMA design standards [9.1.1] do not explicitly point out this potential limitation.

For the moment, we restrict the boundary rotational restraint parameter

*That is, we consider the only loadings of importance to be the pressure difference in the perforated region, and the thermal loading caused by differential changes in length in the tubes and in the shell due to temperature (see the analysis leading to Eqs. (9.7.39–41)).

Table 9.8.1

ASME FIXED TUBESHEET

SUPPORT PARAMETER= 2

ES= 2.9E+07 E= 2.8E+07 ET= 2.4E+07 EC= 2.9E+07
 HS= .5 L= 192 SA= 17500 HC= .5
 NT= 382 TOD= .75
 HT= .049
 AS= 7E-06 AT= 9E-06
 TEMPS= 130 TEMPT= 280
 PSHELL= 200 PTUBE= 0

B= 12 A= 10 SE= .2896 FE= .2847
 RC= 12 R1= 12
 BL= 0 D= 0
 K= 1.2 KC= 1.2 KBAR= 1.2

VALUE OF MU= .253939

AVA= 125787

MA=-2798.74

FQ= 1.205 FM= .187

DESIGN STRESS = 52500

FOR XA= 1.522 AND PHI= 1.39444

ZV= .169 ZN= .6875

QZ1= 1.125 QZ2= .4

EFFECTIVE PRESSURE= 2515.73

ASSUMED THICKNESS= 4.375

THE FINAL TUBESHEET STRESS= 50921.7

THE VALUE FOR Q(XA), THE TUBE EFF. PRESSURE= 2817.62

THE VALUE FOR THETA(XA), THE RING ROTATION= 2.91428E-03

BENDING STRESS IN CHANNEL=-52388.9

BENDING STRESS IN SHELL= 61056.2

LONGITUDINAL DIRECT SHELL STRESS= 21697.8

LONGITUDINAL DIRECT CHANNEL STRESS= 0

to be either simply supported ($\Phi=0$) or to be completely restrained ($\Phi\rightarrow\infty$).
 The condition $K=1$ reduces the term Q_z of Eq. (9.7.50) to the result

$$Q_z = Z_D(x_a) + \bar{Q}Z_V(x_a) \quad (9.8.11)$$

where, using Eq. (9.8.2), we see that

$$\bar{Q} = 0 \text{ (simply supported tubesheet, } \Phi \rightarrow 0)$$

$$\bar{Q} \cong -\frac{Z_V(x_a)}{Z_M(x_a)} \text{ (clamped tubesheet } \Phi \rightarrow \infty)$$

It is important to emphasize that the use of the condition $K=1$ and the restriction to the limiting cases of either pinned or clamped tubesheet edge conditions eliminates the flexural efficiency e as a parameter in the determination of αV_a . Using the expressions for $Z_V(x_a)$ and $Z_M(x_a)$ (see Eq. (9.7.15)), \bar{Q} becomes

$$\bar{Q} = -\bar{\lambda} \left\{ \frac{\phi_1(x_a)\phi_1'(x_a) + \phi_2(x_a)\phi_2'(x_a)}{x_a[\phi_1'^2(x_a) + \phi_2'^2(x_a)]} \right\} \quad (9.8.12)$$

where we introduce the parameter $\bar{\lambda}$. $\bar{\lambda} = 0$ for the pinned tubesheet and $\bar{\lambda} = 1$ for the clamped tubesheet. We continue the derivation of the TEMA tubesheet formula by reduction of the more general analysis, by using the following Bessel Function expansions for large values of x_a [9.8.1].

$$\begin{aligned} \phi_1^2(x_a) + \phi_2^2(x_a) &\approx \frac{e^{\sqrt{2}x_a}}{2\pi x_a} \left(1 + \frac{1}{4\sqrt{2}x_a} + \dots \right) \\ \phi_1(x_a)\phi_2'(x_a) = \phi_1'(x_a)\phi_2(x_a) &\approx \frac{e^{\sqrt{2}x_a}}{2\pi x_a\sqrt{2}} \left(1 + \frac{\sqrt{2}}{8x_a} + \dots \right) \\ \phi_1(x_a)\phi_1'(x_a) + \phi_2(x_a)\phi_2'(x_a) &\approx \frac{e^{\sqrt{2}x_a}}{2\pi x_a\sqrt{2}} \left(1 - \frac{3\sqrt{2}}{8x_a} + \dots \right) \\ \phi_1'^2(x_a) + \phi_2'^2(x_a) &\approx \frac{e^{\sqrt{2}x_a}}{2\pi x_a} \left(1 - \frac{3}{4\sqrt{2}x_a} + \dots \right) \end{aligned} \quad (9.8.13)$$

Using Eq. (9.8.13) in Eq. (9.8.12) gives an asymptotic expression for \bar{Q} , valid for large x_a , as

$$\bar{Q} \rightarrow -\frac{\bar{\lambda}}{\sqrt{2}x_a}; \quad \begin{array}{l} \bar{\lambda} = 0 \text{ (simply supported)} \\ \bar{\lambda} = 1 \text{ (clamped)} \end{array} \quad (9.8.14)$$

We note in passing that the parameter $\bar{\lambda}$ is also calculated and is part of the output in the computer code of Section 9.7 (Appendix 9.C). F_q , given by Eq. (9.8.10), as well as F_M , defined in Eq. (9.8.8), are also calculated and printed out in the computer code of Appendix 9.C.

If we use Eq. (9.8.13), the expressions for $Z_D(x_a)$, $Z_V(x_a)$, given in Eqs. (9.7.15) and (9.7.16), give the following asymptotic results:

$$\begin{aligned} Z_D(x_a) &\rightarrow \frac{\sqrt{2}}{x_a^3} \left[1 + \frac{(1-\nu^*)\sqrt{2}}{2x_a} \right] \\ Z_V(x_a) &\rightarrow \frac{1}{x_a^2} \left[1 - \frac{\sqrt{2}}{2x_a} + \frac{\sqrt{2}(1-\nu^*)}{x_a} \right] \end{aligned} \quad (9.8.15)$$

The asymptotic expression for the quantity $F_q = Q_z x_a^4 / 2$, in the expression for aV_a given by Eq. (9.8.10), can be written in the form:

$$\frac{Q_z x_a^4}{2} \rightarrow \frac{(1-\nu^*)}{2} - \frac{\bar{\lambda}}{4} (1-2\nu^*) + \frac{\sqrt{2}}{2} x_a \left(1 - \frac{\bar{\lambda}}{2} \right) \quad (9.8.16)$$

For $\bar{\lambda} = 1$ (clamped),

$$F_q = \frac{Q_z x_a^4}{2} \rightarrow \frac{1}{4} (1 + \sqrt{2} x_a) \quad (9.8.17)$$

while for $\bar{\lambda} = 0$ (simply supported), and $\nu^* = 0.5$ we have

$$F_q = \frac{Q_z x_a^4}{2} \rightarrow \frac{1}{4} (1 + 2\sqrt{2} x_a) \quad (9.8.18)$$

It is clear from our previous analyses that the rotational resistance provided by the shell-channel assemblage is, in fact, a function of the tubesheet thickness. Nevertheless, the TEMA design approach is to introduce a factor F , dependent solely on the barrel thickness to diameter ratio, which is used to specify the degree of edge rotational restraint provided to the tubesheet. For the fixed tubesheet heat exchanger the TEMA factor F is in the range $0.8 < F < 1.0$. $F = 0.8$ represents a clamped tubesheet while $F = 1.0$ is appropriate for a simply supported tubesheet. There is no basis in fact for the TEMA F factor, yet it appears to have served quite well in practical usage for units within the range of validity of the TEMA approximations.

Using the F factor, Malek [9.8.2] shows that Eqs. (9.8.17) and (9.8.18) are fit by the empirical relation

$$F_q = \frac{Q_z x_a^4}{2} = 0.25 + 1.766(F - 0.6)x_a \quad (9.8.19)$$

with $F = 0.8$ matching Eq. (9.8.17) and $F = 1.0$ matching Eq. (9.8.18). The factor F_q in the form represented by Eq. (9.8.19), is defined by TEMA in [9.1.1], once the replacement of x_a is made using Eq. (9.7.51). Introducing the pressurized diameter $G = 2a$ yields

$$F_q = 0.25 + (F - 0.6) \left[\frac{6(1 - \nu^2)(1.766)^4}{e} \frac{E_s h_s}{E L \xi^*} \left(\frac{G}{h} \right)^3 \right]^{0.25} \quad (9.8.20)$$

To obtain the result quoted in the TEMA Standards, e is set equal to 0.177 (corresponding to a tube pitch to diameter ratio = 1.25). Since F_q involves the tubesheet thickness h , the TEMA calculation procedure for tubesheet thickness in a fixed tubesheet exchanger still requires iteration. A value for tubesheet thickness h must be assumed in order to compute F_q and hence the effective pressure P_e (see Eq. (9.8.10)). Using Q_e , given by Eq. (9.7.47) for either thermal loading, for tubeside pressure, or for shellside pressure, brings Eq. (9.8.10) into the proper TEMA form; to obtain an exact correspondence requires that, within the limits of the classical thin plate and shell theory employed here, terms involving the ratio of shell thickness to shell diameter in Ref. [9.1.1] should be neglected in comparison to unity.

Once the effective pressure P_e is calculated, the maximum radial bending moment follows from Eq. (9.8.8). Gardner [8.1.1, 8.1.2] shows that for

large x_a and for $b/a=1$, $F_M(x_a)$ can be approximated for either simply supported or for clamped units by

$$|F_M| \approx e^{-\pi/4} / 2x_a \quad (\text{simply supported}) \quad (9.8.21)$$

$$|F_M| \approx \sqrt{2} / 4x_a \quad (\text{clamped})$$

Equation (9.8.9) can now be formally solved for h to yield

$$\frac{h}{2a} = \left(\frac{F_M}{\eta_s} \right)^{1/2} \left(\frac{P_e}{\Omega S_A} \right)^{1/2} \quad (9.8.22)$$

Note that since $F_M = F_M(x_a)$, and since $P_e = P_e(h)$ for a fixed tubesheet heat exchanger, Eq. (9.8.22) does not provide a direct solution for tubesheet thickness. For a stationary tubesheet in a floating head heat exchanger, P_e is known in terms of the pressure differential; however, F_M is still a function of x_a . In an attempt at some simplification, TEMA replaces the factor $(F_M(x_a)/\eta_s)^{1/2}$ by $F/2$ (where $0.8 < F < 1.0$ is the TEMA rotational resistance parameter), and therefore evolves a final approximate equation for tubesheet thickness as

$$\left(\frac{h}{2a} \right)_{\text{TEMA}} = \frac{F}{2} \left(\frac{P_e}{\Omega S_A} \right)^{1/2} \quad (9.8.23)$$

For a fixed tubesheet exchanger, Eq. (9.8.23) still requires iteration; P_e can only be determined after a tubesheet thickness is assumed. For the stationary tubesheet of a floating heat exchanger, Eq. (9.8.23) does provide a direct solution for h since P_e does not involve the tubesheet thickness h .

It is of interest to calculate the ratio

$$h^* = \frac{(F/2)_{\text{TEMA}}}{(|F_M|/\eta_s)^{1/2}} = \frac{(h)_{\text{TEMA}}}{(h)_{\text{Eq. (9.8.22)}}} \quad (9.8.24)$$

which, for the same given value of effective pressure P_e , gives a comparison of the TEMA formula for tubesheet thickness with a formula following the "design by analysis" approach for large x_a . For this illustration, we use the ligament efficiency $\eta_s = 0.2$ or 0.3 (which are reasonable for many practical units). The table below shows the value of h^* for different x_a . Equation (9.8.21) is used in obtaining tabulated results.

Table 9.8.2. h^* vs. x_a for Simply Supported and Clamped Tubesheets

x_a	$b/a=1, x_a > 3$			
	Simply Supported, η_s		Clamped, η_s	
	0.2	0.3	0.2	0.3
3	0.811	0.993	0.52	0.638
5	1.047	1.282	0.673	0.824
7	1.239	1.52	0.795	0.975
10	1.481	1.81	0.95	1.17

It is obvious that if we consider Eq. (9.8.22) as the “exact” solution in the range $x_a > 3$, then for the conditions considered, the TEMA tubesheet thickness formula is conservative if the tubesheet support permits rotation, but possibly yields a non-conservative thickness value if the tubesheet-shell joint inhibits rotation. Nevertheless, despite its potential non-conservative thickness prediction, the TEMA formulation has been utilized with a high degree of success for a considerable time period in the heat exchanger industry. It is clear that in the range $x_a > 3$ the essential difference between the TEMA calculation of thickness by Eq. (9.8.23) and the “exact” calculation of thickness by Eq. (9.8.9) (or (9.8.22)) is the neglect of the stress efficiency factor η_s and the elimination of the variation of $|F_M|$ with x_a . The intent of TEMA is clearly one of simplicity; that is, to provide a simple formula for thickness requiring minimal iterations. It is useful to compare the TEMA analysis with our final simplified method espoused herein using graphical data. We will take care in these comparisons to choose a configuration where $x_a > 3$ (i.e., within the range of the approximations leading to the TEMA design formula).

The vehicle for comparison is Sample Problem 4 in the TEMA Sample Problem Book [9.8.3]. We consider the following fixed tubesheet exchanger with tubesheets not extended as flanges:

Shell Side

20" O.D.; 0.25" wall-thickness; mean shell metal temperature 250°F; no shell expansion joint; SA-312-304 material.

Tubesheets

Material SA-240-304 at 300°F

Tubing

300-3/4" O.D. \times 16BWG (0.065") \times 20 ft long; SA-249-304; 15/16" triangular pitch; mean tube wall metal temperature = 180°F; $\alpha_t = 9.28 \times 10^{-6}$ in./in. °F

Shellside = 180 psig; Tubeside = full vacuum and 180 psig

The TEMA iterative solution assumes a tubesheet thickness of 1.25", and bases the solution on the length between tubesheet faces of 237.5", a mean assembly temperature of 70°F, and an allowable stress $S_A = 16,600$ psi. Following TEMA, the critical pressure for design is based on an effective pressure involving tubeside pressure plus thermal loading. The F factor in the TEMA solution is 1.0 based on a shell wall thickness of 0.25" and an inner diameter of 19.5". The final calculated tubesheet thickness is 1.24" using the TEMA method and is deemed to be in good agreement with the initial assumed value of 1.25".

The microcomputer code given in Appendix 9.D, which utilizes graphical input, is used to reexamine the above problem, first under the assumption that the effective roll depth is zero (see Chapter 8) so that the ligament and

flexural efficiencies are based on the tube O.D.; and second, under the assumption of a 100% effective roll so that the ligament and flexural efficiencies are based on the tube I.D. The computer code examines only the critical combination of tubeside pressure and thermal loading. The criteria for allowable stress (Eq. (9.8.9a)) is used as the design requirement. The stress efficiency SE , (η_s), is taken as the ligament efficiency in either case, and the flexural efficiency e (determined from Eq. (9.7.42)), is denoted as FE in the code. Table 9.8.3 shows the output obtained on the printer when running the code. From the results given in Table 9.8.3, we see clearly the effect of stress efficiency on the computed thickness. For the case where the tube wall is neglected in the computation of ligament efficiency, the predicted thickness is greater than 1.25". When the tube wall is included in the ligament efficiency calculations, the predicted tubesheet thickness is approximately 1.0". The TEMA calculated thickness is bounded by these two values and the computed x_a value using either approach is in the range of $3.20 > x_a > 4.10$. The results obtained herein again demonstrate that under certain conditions, the margin of safety defined by the ASME Code may be encroached upon by a fixed tubesheet designed strictly by the TEMA formulas given in [9.1.1]. The concept of ligament efficiency and stress efficiency appears to be an effect that should be incorporated into any tubesheet design methodology. Note that the value for x_a obtained for the final configuration is greater than 3.0; it is seen that in this example, there is essentially no great difference in the tubesheet thicknesses predicted by the TEMA formula and by the computer methods developed here. However, we must point out that shell and channel bending stress levels are still very high and indicate that a considerable amount of plastic action has occurred at the joints. The next section presents some additional solutions which elaborate on the critical role played by the parameter x_a .

Table 9.8.3. Solution of TEMA Sample Problem 4 (Ref. 9.8.3) Using the Computer Code "MICROFIXFLOAT" in Appendix 9.D

```

ASME FIXED TUBESHEET
SUPPORT PARAMETER= 2
ES= 2.8E+07      E= 2.8E+07      ET= 2.8E+07      EC= 2.8E+07
HS= .25         L= 237.5        SA= 16600        HC= .25
NT= 300        TOD= .75
HT= .065
AS= 9.4E-06     AT= 9.28E-06
TEMPS= 180     TEMPT= 110
PSHELL= 0      PTUBE= 180

B= 9.75        A= 9.75        SE= .2          FE= .261
RC= 9.75      R1= 9.75
BL= 0         D= 0
K= 1         KC= 1         KBAR= 1
VALUE OF MU= .489898

```

AVA=-32562.2
 MA= 2882.71
 FQ= 2.1 FM= .055
 DESIGN STRESS = 49800
 FOR XA= 3.39314 AND PHI= 1.70807
 ZV= .085 ZM= .435
 QZ1= 2.1 QZ2= 3.5
 EFFECTIVE PRESSURE=-685.07
 ASSUMED THICKNESS= 1.5
 THE FINAL TUBESHEET STRESS=-47757.9
 THE VALUE FOR Q(XA), THE TUBE EFF. PRESSURE=-1438.65
 THE VALUE FOR THETA(XA), THE RING ROTATION=-7.42262E-03
 BENDING STRESS IN CHANNEL= 88864.3
 BENDING STRESS IN SHELL=-76036.8
 LONGITUDINAL DIRECT SHELL STRESS=-9848.86
 LONGITUDINAL DIRECT CHANNEL STRESS= 3510
 B= 9.75 A= 9.75 SE= .339 FE= .417
 RC= 9.75 R1= 9.75
 BL= 0 D= 0
 K= 1 KC= 1 KBAR= 1
 VALUE OF MU= 1.19266
 AVA=-30095.3
 MA= 2568.68
 FQ= 2.5 FM= .0425
 DESIGN STRESS = 49800
 FOR XA= 4.09069 AND PHI= 2.60268
 ZV= .06 ZM= .355
 QZ1= 2.5 QZ2= 4.5
 EFFECTIVE PRESSURE=-633.168
 ASSUMED THICKNESS= 1
 THE FINAL TUBESHEET STRESS=-45276
 THE VALUE FOR Q(XA), THE TUBE EFF. PRESSURE=-1646.24
 THE VALUE FOR THETA(XA), THE RING ROTATION=-7.84031E-03
 BENDING STRESS IN CHANNEL= 82917.2
 BENDING STRESS IN SHELL=-70095.2
 LONGITUDINAL DIRECT SHELL STRESS=-8836.77
 LONGITUDINAL DIRECT CHANNEL STRESS= 3510

9.9 RANGE OF APPLICATION OF THE TEMA BENDING EQUATIONS GIVEN IN REF. [9.1.1]

In previous sections of this chapter, we have shown that the well established TEMA tubesheet equations may give results not in agreement with results predicted by the design by analysis methods developed in this chapter. We have pointed out earlier, without elaboration, that in cases where discrepancies between the results arise, the value of the parameter x_a , predicted by the rigorous formulations, is significantly less than 3.0. Now that we have examined the approximations inherent in the TEMA design formulas, and have shown that the TEMA equations are based on asymptotic approximations of certain Bessel Functions which limit their range of validity to $x_a > 3.0$, such discrepancies are not totally unexpected. In addition, a further approximation introduced into the TEMA equations essentially neglects an important functional variation of x_a and replaces this

functional variation of x_a with a constant depending only on a presumed degree of edge restraint. These approximations, taken in toto, can lead to some discrepancy in results when the calculated unit thickness turns out to imply x_a to be on the order of 3.0 or less.

We now re-examine some of our earlier examples in order to clearly demonstrate the effect of the final x_a value obtained. We give some results of simulations which show that when the unit geometry, material parameters, and loading are such as to predict a parameter value for $x_a > 3$, then results obtained from the comprehensive analysis of Section 9.7 and from the TEMA design formula, are in reasonable agreement.

We first consider a re-analysis of the unit configuration described by Table 9.7.1. The loading on this fixed tubesheet heat exchanger is decreased so that the final tubesheet thickness will be relatively thin (leading to a larger x_a value). Specifically, in this re-analysis, the tube and shell metal temperature are reduced to 98°F, 83°F, respectively. We also consider a reanalysis of the stationary tubesheet in the floating head exchanger previously described by Table 9.7.4. For this unit, we reduce the pressure loading to 300 psi in order to reduce the final tubesheet thickness. Table 9.9.1 shows the results obtained for these units with lower loadings, and the corresponding predictions using the TEMA design formulas for the same units.

Table 9.9.1. Comparison of Computer Solutions (FIXFLOAT) of Section 9.7 with TEMA for Units with $x_a > 3$

Case	b/a	Tubesheet Max. Stress (psi)	Shell Max. Stress (psi)	FIXFLOAT thickness (in.)	x_a	μ	TEMA thickness (in.)
11	1	48823	16340	.675	6.77	16.53	.61
12	1.2	33013	28612	.675	6.18	16.53	—
13	1.2	53600	26089	.438	8.56	53.8	—
14	1.0	22592	35484	2.25	3.62	2.12	2.33
15	1.0	24924	35612	2.125	3.78	2.42	—
16	1.2	12137	38411	2.125	3.42	2.42	—

Case 11 reconsiders the fixed tubesheet heat exchanger of Section 9.7 (case 1 of Tables 9.7.2 and 9.7.3). Recall that the critical load case is pressure plus thermal loading so that the tubesheet stress can be set as high as $3S_A = 52500$ psi (see Table 9.7.1). We see from Table 9.9.1 that neglecting the unperforated rim gives a tubesheet thickness below 0.675" for a satisfactory design as predicted by FIXFLOAT. While this tubesheet thickness would not be used in a practical application with 3/4" O.D. tubes, the purpose here is served since the computed x_a value is 6.77. The TEMA thickness calculated for this unit is 0.61". Cases 12 and 13 in Table 9.9.1 examine the effect of including the unperforated rim in the analysis as carried out by FIXFLOAT on this unit with a relatively thin tubesheet. By comparison of the stress results for cases 12, 13, we see that the inclusion of

the unperforated rim reduces the tubesheet thickness required to a value slightly in excess of 0.4375". We recall that in Section 9.7, a similar study on the effect of unperforated rim led to the conclusion that including the rim caused higher unit stresses. Here, we find that the critical stresses are lowered! The difference in our conclusion now is simply caused by the fact that the higher loaded unit of Section 9.7 gives maximum tubesheet stress at the center; here, the unit with lower thermal loading has the critical stress for tubesheet design at the outer limit of the perforated zone. Thus, we conclude that the effect of unperforated rim and the location of maximum tubesheet stress level are inexorably connected insofar as drawing any conclusion as to the conservatism of the final result for a fixed tubesheet heat exchanger.

Case 14 of Table 9.9.1 re-examines the design of the stationary tubesheet in the floating head unit previously analyzed in Section 9.7 (see Table 9.7.4 for results). Here, we lower the tubeside pressure to 300 psi so as to predict a thickness leading to a larger x_a value (recall that $x_a < 2.0$ in the initial solution). In the revised problem, x_a increases to 3.62 and the computer simulation predicts an acceptable tubesheet thickness of 2.25" using a shell wall thickness of 0.75" and neglecting the unperforated rim. The corresponding solution using the TEMA equation in Ref. [9.1.1] predicts that a tubesheet thickness of 2.33" is required and that the unit should be considered as simply supported.

The final cases considered in Table 9.9.1 show the effect of unperforated rim on this low load (thinner tubesheet) floating head exchanger configuration. We see that for the same assumed tubesheet thickness (2.125"), the inclusion of unperforated rim again lowers the stress level in the stationary tubesheet of a floating head heat exchanger.

Based on the analysis and discussions presented in this chapter, we suggest that the tubesheet analyst carefully examine any suggested simple design formulas for the range of validity of their predictions. The microcomputer code presented in Appendix 9.D provides a viable technique for preliminary design analysis when coupled with accurate graphical data.

To satisfy the requirements of design by analysis specifications, the more elaborate and sophisticated computer codes of Appendices 9.B and 9.C should be considered for specific applications. On the basis of the analyses presented here, the TEMA design formulas of the sixth edition (and earlier editions) should be applied with caution when the predicted value of x_a is near or below 3.0.

9.10 CLOSURE

A comprehensive method for stress analysis of fixed and floating head type heat exchangers has been presented. The reduction of governing equations written for a generalized case to the specific case of symmetrical geometry (identical pair of tubesheets, and spatially invariant pressure in each chamber) is carried out systematically to elucidate the assumptions

made in the industry design standards. Enroute the process of simplification, the heretofore unstated limitations of the TEMA formulas for fixed tubesheet exchangers are uncovered. The significance of these limitations in practical design work is illustrated by numerical examples. The chapter contains three computer programs, with varying levels of rigor and scope, which can be used for design/analysis work. The need for computer codes for routine design application is of unarguable importance in fixed tubesheet exchanger design work, owing to the “structural quirks” of this type of construction. For example, increasing the tubesheet thickness can *increase* the tubesheet stress [9.1.9]; and as shown in this chapter, increasing the rim width can increase the tubesheet stress!! The limiting loading condition may consist of any combination of shellside pressure, tubeside pressure, and differential thermal expansion between the shell and the tubes. The last loading may itself consist of several cases (depending on the number of operating conditions). The search for the most limiting loading group is best carried out using a computer program. The computer code can be utilized to arrive at the optimal design by adjusting the tubesheet thickness, shell expansion joint stiffness, and shell and channel thicknesses at their junctions with the tubesheet. The optimal design is one which minimizes the tubesheet thickness and tube to tubesheet joint load, and provides ample margin against tube buckling.

The analysis presented in this chapter is limited to axially symmetric loadings. The cases of multi-pass units and large untubed regions, encountered in units with impingement plates, and no-tubes-in-window designs, are not covered. Such non-axisymmetric problems are best tackled by a suitable finite element program. The analysis is based on thin plate and shell equations, and therefore is limited to the designs where these theories hold.

NOMENCLATURE

- a = Radius of perforated region
 a_1 = Outer radius of ring (Fig. 9.7.1)
 A_1^*, A_7^*, A_0^* = Area measures defined after Eq. (9.3.6)
 a_s = Shell mean radius (Sections 9.2–9.6)
 b = Shell mean radius (Section 9.7)
 a_c = Channel mean radius (Sections 9.2–9.7)
 A_0, A_1, A_2, A_3 = Integration constants (Eqs. (9.3.9)–(9.3.12))
 A_T = Tube metal cross section area
 B_{ji} ($j=0,1,2,3$
 $i=1,2$) = Integration constants appearing in deflection Eq. (9.4.1) for unperforated rim
 B = Bolt line load (defined by Eq. (8.4.3)) shown in Fig. 9.7.2
 C_{vs}, C_{vt} = Specific heats of the shellside, tubeside streams, respectively
 C_3, C_4 = Load parameters defined in Eq. (9.3.15)
 $D_i = E_i h_i^3 / [12(1 - \nu_i^2)]$

- D_s = Shell flexural rigidity = $E_s h_s^3 / [12(1 - \nu_s^2)]$
 d = Tube outer diameter
 D_c = Channel flexural rigidity
 D^* = Effective flexural rigidity of tubesheet (Eq. (9.3.8))
 E = Young's Modulus of unperforated ring (used in Section 9.7, first defined in Eq. (9.7.25))
 E_s = Young's modulus of shell metal
 E_T = Young's modulus for tube material
 E_i^*, ν_i^* = Effective elastic constants for tubesheet i ($i=1$ lower, $i=2$, upper)
 e = Flexural efficiency of the perforated interior of the tubesheet—Eq. (9.7.42)
 E_i, ν_i = Unmodified Young's modulus and Poisson ratio of tubesheet i , respectively
 F = TEMA tubesheet edge support factor
 F_M, F_q = Tubesheet functions defined in Section 9.8
 F_1, F_2 = End forces in a single tube (Eq. (9.2.5))
 G_c, G_s = Gasket loads (Eqs. (9.7.29), (9.7.33))
 h_L = Tubesheet nominal ligament width
 h_1, h_2 = Tubesheet thicknesses—Section 9.3
 h_c, h_s = Channel, shell thickness, respectively
 h = Tubesheet thickness (Section 9.7-8)
 J = Expansion joint parameter (Eq. (9.7.10))
 K_c = a_c/a (Eq. (9.7.28))
 K_{EJ} = Expansion joint spring rate
 \bar{K} = a_1/a (Eq. (9.7.25))
 K = b/a
 K^* = Defined in Eq. (9.5.5)
 l_i ($i=2, \dots$) = Lengths defined in Fig. 9.1.1
 L = Tube effective length between tubesheets
 $M_{ri}, M_{\theta i}$ = Tubesheet bending moments
 M_a^* = Tubesheet moment parameter defined in Eq. (9.7.41)
 M_r = Tubesheet bending moment (Eq. (9.7.5))
 M_R = Net moment on unperforated rim—Eq. (9.7.19)
 M_a, V_a = Tubesheet moment and shear at the edge of the perforated region
 M^*, Q^* = Specified edge loads in a floating head unit
 M_c, M_s = Edge moments in channel, shell (Eq. (9.7.24))
 N_s = Shell axial force in fixed tubesheet exchanger
 N_{ij} = Membrane forces in shell or channel (Eqs. (9.4.7), (9.4.8))
 n = Number of tubes in unit
 P = Tube pitch
 p_{ij} = Tubesheet pressures (Eq. (9.3.1))
 p_s = Shellside static pressure at top of chamber (Eq. (9.3.1)) or design shellside pressure

- p_t = Design tubeside pressure
 p_c = Channel static pressure at the top channel cover level (Eq. (9.3.1))
 $\rho_1(x_a), \rho_2(x_a)$ = Functions of x_a defined by Eq. (9.7.47)
 P_e = Effective tubesheet pressure on a tubesheet in a fixed tubesheet exchanger (Eq. (9.7.49))
 p_s^*, p_t^* = Shellside and tubeside pressures averaged over the tube length
 q_{z1}, q_{z2} = Functions of x_a defined by Eq. (9.8.5)
 q_{T1}, q_{T2} = Effective pressures on tubesheets due to tube loading
 Q_i = Parameters defined by Eq. (9.3.6)
 Q_{ri} = Tubesheet shear forces
 Q_e = Load parameter defined by Eq. (9.7.42)
 Q_c, Q_s = Edge shears in channel, shell (Eq. (9.7.22))
 Q = Parameter relating M_a, V_a (Eq. (9.7.40))
 R_m = Tube metal resistance
 R_{fs} = Shellside fouling resistance
 R_{ft} = Tubeside fouling resistance
 R_s = Shellside film resistance
 R_t = Tubeside film resistance
 R^* = Centroidal radius of unperforated ring (Fig. 9.7.1)
 $Q_M(x), Q_V(x)$ = Moment distribution functions defined in Eq. (9.7.14)
 Q_r = Tubesheet shear force (Eq. (9.7.6))
 r_c = Radius to outermost tube hole center (Eq. (9.3.2))
 Q_z = Defined by Eq. (9.7.50)
 S_j = Spring rate of expansion joint (Eq. (9.7.9))
 t = Tube wall thickness
 T, t = Generic temperatures (Eq. (9.5.7)) used only in subsection 9.5.1
 \bar{t}_i = Thickness of unperforated rim (Fig. 9.4.2)
 t_i, T_o, t_o, T_i = Temperatures defined in Fig. 9.5.1 and used in subsection 9.5.1
 U = Overall heat transfer coefficient
 v = Displacement of tubesheet in perforated region (Section 9.7—Eq. (9.7.3))
 W_s, W_t = Flow rates of shellside, tubeside streams
 $w_i(r)$ = Tubesheet displacement (Eq. (9.3.4))
 w_c, w_s = Channel and shell radial displacement
 x_a = Dimensionless tubesheet design parameter – defined in Eq. (9.7.2)
 x = Dimensionless radial coordinate = βr describing radial location in perforated tubesheet
 y = Coordinate measured along the tube starting at the lower tubesheet (Eq. (9.5.3))
 Z_a, Z_M, Z_V, Z_D = Functions of x, x_a —Eqs. (9.7.15), (9.7.16)
 α_t = Coefficient of thermal expansion for tube metal

- α_s = Coefficient of thermal expansion of shell metal
 β = Defined by $\beta^4 = 2\xi / D^*$ in Section 9.7
 β_s = Shell attenuation coefficient (Eq. (9.4.23))
 β_c = Channel attenuation coefficient
 $\gamma_s, \gamma_c, \gamma_B$ = Coefficients defined in Section 9.7
 δ = Total extension of tube in a fixed or floating head heat exchanger
 δ^* = Defined in Eq. (9.5.9) as $\Delta_{T\theta} - \Delta_{S\theta}$
 Δ_{TG} = Change in tube free length due to gravity
 $\Delta_{T\theta}$ = Change in tube free length due to temperature
 Δ_{TPR} = Change in tube free length due to Poisson ratio effects
 ΔT_T = Effective temperature change, above assembly temperature, of the tube wall
 ΔT_s = Effective change in temperature, above assembly temperature, of the shell wall.
 Δ_s = Elastic stretch of shell (Eq. (9.4.27))
 $\Delta_{S\theta}$ = Change in shell free length due to temperature change
 Δp_i = Pressure differences defined in Eq. (9.4.2)
 ϕ_i, ψ_i = Bessel Functions (Eq. (9.3.16))
 Φ = Rotational stiffness parameter (Eq. (9.8.1))
 η_s = Stress efficiency factor
 $\lambda_i, \beta_i, \mu_i$ = Parameters defined in Eq. (9.3.14)
 $\bar{\lambda}$ = Fixity parameter introduced in Eq. (9.8.12)
 λ_s, λ_T = Parameters defined in Eq. (9.7.12)
 η = Ligament efficiency
 ξ = Tube spring rate (Eq. (9.2.6))
 μ_T = Weight/unit volume of tube metal
 μ_s = Weight/unit volume of shell metal
 μ_1^* = Weight density of shellside fluid (Eq. (9.3.1))
 μ_2^* = Weight density of tubeside fluid (Eq. (9.3.1))
 ρ_i = Parameters used in subsection 9.5.1 and defined by Eqs. (9.5.15), (9.5.18)
 Λ = Parameter defined by Eq. (9.5.20)
 θ_c, θ_s = Channel and shell edge rotations
 θ = Rotation of tubesheet in perforated region (Eq. (9.7.4))
 μ = Rotational stiffness parameter (Eq. (9.7.27))
 θ_m = Log-mean temperature difference (Eq. (9.5.6))
 σ_T = Tube stress (Eq. (9.5.2))
 θ = Temperature difference defined by Eq. (9.5.13)
 σ_B = Radial bending stress in tubesheet
 ν_T = Poisson's ratio for tube material
 Ω = Allowable stress amplification factor

REFERENCES

- [9.1.1] *Standards of Tubular Exchanger Manufacturers Association*, TEMA, Inc., Tarrytown, NY, 6th Edition (1978).
- [9.1.2] Gardner, K. A., "Heat Exchanger Tubesheet Design—2 Fixed Tubesheets," *Journal of Applied Mechanics*, Trans. ASME, Vol. 74, pp. 159–166 (1952).
- [9.1.3] Miller, K. A. G., "The Design of Tube Plates of Heat Exchangers," *Proc. Ins. Mech. Eng., Series B*, Vol. 1, pp. 215–231 (1951).
- [9.1.4] Yu, Y. Y., "Rational Analysis of Heat Exchanger Tubesheet Stresses," *Journal of Applied Mechanics*, Trans. ASME, Vol. 78, pp. 468–473 (1956).
- [9.1.5] Boon, G. B., and Walsh, R. A., "Fixed Tubesheet Heat Exchangers," *Journal of Applied Mechanics*, Trans. ASME, Vol. 86, pp. 175–180 (1964).
- [9.1.6] Chiang, C. C., "Structural Design Optimization of Once-through Type Heat Exchangers," ASME paper no. 77-JPGC-NE-3 (1977).
- [9.1.7] Gardner, K. A., "Tubesheet Design: A Basis for Standardization," *Proceedings of the First International Conference on Pressure Vessel Technology: Part I, Design and Analysis*, pp. 621–648, ASME, New York (1969).
- [9.1.8] Hayashi, K., "An Analysis Procedure for Fixed Tubesheet Heat Exchangers," *Proc. of the Third International Conference on Pressure Vessel Technology: Part I, Analysis, Design and Inspection*, 363–373, ASME, New York (1977).
- [9.1.9] Singh, K. P., "Analysis of Vertically Mounted Through-tube Heat Exchangers," *Journal of Engineering for Power*, Trans. ASME, Vol. 100, No. 2, pp. 380–390 (1978).
- [9.1.10] Singh, K. P., and Soler, A. I., "A Design Concept for Maximizing Stress Levels in Stationary Tubesheet Heat Exchangers," *Int. J. Pres. Ves. and Piping* 13, pp. 19–32 (1983).
- [9.3.1] Timoshenko, S. P., and Woinowski-Krieger, S., *Theory of Plates and Shells*, 2nd Edition, McGraw-Hill, N.Y., pp. 51–78 (1959).
- [9.3.2] *ASME Boiler and Pressure Vessel Code, Section III*, Division I, Subsection NA, ASME, New York (1974).
- [9.3.3] *Pressure Vessel and Piping: Design and Analysis*, Vol. 2, Chapter 4, ASME (1972).
- [9.3.4] Soler, A. I., and Hill, W. S., "Effective Bending Properties for Stress Analysis of Rectangular Tubesheets," *Trans ASME, Journal of Engineering for Power*, Vol. 99, No. 3, pp. 365–370 (July 1977).
- [9.5.1] Rohsenow, W. M., and Hartnett, J. P., eds., *Handbook of Heat Transfer*, Section 18, "Heat Exchangers," by A. C. Mueller, McGraw-Hill, New York (1973).

- [9.7.1] Singh, K. P., and Soler, A. I., "HEXDES User Manual," Arc-turus Publishers Inc., Cherry Hill, N.J. (1984).
- [9.8.1] Abramowitz, M., and Stegun, I. A., *Handbook of Mathematical Functions*, Dover Publications, New York, p. 383 (1965).
- [9.8.2] Malek, R. G., "A New Approach to Exchanger Tubesheet Design," *Hydrocarbon Processing*, Gulf Publishing, Houston (Jan. 1977).
- [9.8.3] *Standards of Tubular Exchanger Manufacturers Association, Sample Problem Book for 6th Edition*, TEMA, (1980).

APPENDIX 9.A

SOLUTION OF COUPLED PLATE EQUATIONS

Let us consider the equations (Eq. 9.3.7);

$$D_1 \nabla^4 w_1 = Q_1 - \xi(w_1 + w_2)$$

$$D_2 \nabla^4 w_2 = Q_2 - \xi(w_1 + w_2)$$

where $\nabla^4()$ is the biharmonic operator and is solely a function of r in this application. Let

$$z_1 = w_1 + w_2; \quad z_2 = w_1 - w_2$$

Then z_1 satisfies the equation

$$\nabla^4 z_1 + \beta^4 z_1 = \bar{C}_3$$

where

$$\beta^4 = \beta_1^4 + \beta_2^4 = \xi/D_1 + \xi/D_2$$

and

$$\bar{C}_3 = Q_1/D_1 + Q_2/D_2 = \text{constant}$$

A solution for z_1 which remains finite at $r = 0$ is given as

$$z_1 = \bar{C}_3/\beta^4 + A_1 \phi_1(\beta r) + A_2 \phi_2(\beta r)$$

where ϕ_1, ϕ_2 , are the Ber and Bei functions, respectively. A corresponding equation for the function z_2 is

$$\nabla^4 z_2 = \frac{2}{\beta^4} (\beta_2^4 Q_1 - \beta_1^4 Q_2) + (\beta_2^4 - \beta_1^4) \left(z_1 - \frac{\bar{C}_3}{\beta^4} \right)$$

and a solution for $z_2(r)$ which remains finite at $r = 0$ is given by

$$z_2(r) = A_0 + A_3 r^2 + \frac{(\beta_1^4 - \beta_2^4)}{\beta^4} [A_1 \phi_1(\beta r) + A_2 \phi_2(\beta r)] + \bar{C}_4 r^4 / 64$$

where

$$\bar{C}_4 = \frac{2}{\beta^4} (\beta_2^4 Q_1 - \beta_1^4 Q_2) = \text{constant}$$

Solutions for $w_1(r)$, $w_2(r)$ in terms of the four integration constants $A_0 - A_4$ are easily obtained from the equations

$$w_1 = \frac{z_1 + z_2}{2}; \quad w_2 = \frac{z_1 - z_2}{2}$$

APPENDIX 9.B

COMPUTER PROGRAM FIXSHEET

9.B.1 Scope

Computer program FIXSHEET performs a complete stress analysis of integral tubesheet heat exchangers (integral both shell and tubeside) in the manner of the analysis presented in Sections 9.2–9.5. The scope of the current version of the code, produced in this appendix, is delineated below.

- (i) Geometry: The program assumes that the two tubesheets are identical, and are integrally connected (welded) to their respective shell and channel ends.
- (ii) Orientation: Both vertical and horizontal orientations are permitted. The program allows input of different shell and channel pressures at the two tubesheet locations which means that the effect of elevation in vertically mounted units, pressure loss due to fluid flow, and seismic acceleration effects in all orientations can be incorporated. This feature is of particular importance in relatively long heat exchangers. Equation 9.3.1 gives the necessary formulas to compute the various static pressures.
- (iii) Channel header loads: The longitudinal force per unit circumference in both channel headers are known from direct equilibrium and are therefore input quantities in the program. Formal expressions for these header loads are given by Eqs. 9.4.7–8. In addition, header loads arising from other sources (not included in Eqs. 9.4.7–8), such as the axial thrust from a connected piping, may be incorporated.
- (iv) Unequal shell course thicknesses: In long heat exchangers, designers often increase shell thickness in the courses containing nozzle penetrations to make the shell “self-reinforcing”. The shell thickness adjacent to the tubesheets (assumed to be equal near the two tubesheets) should be input. The designer may adjust the shell Young’s Modulus that the modified Young’s modulus times the input shell thickness is equal to the unmodified Young’s modulus times the average shell thickness. This is an approximate way to incorporate the effect of unequal shell course thicknesses.

- (v) Expansion Joint: In vertically mounted units, the expansion joint may be located above or below the main support (Fig. 9.1.1). The case of no expansion joint is simulated by setting the expansion joint stiffness an order of magnitude larger than the shell axial stiffness.

The present version of the code does not treat non-integral channel, or floating head designs. The ability to treat such cases can be readily incorporated as discussed in Section 9.6.

9.B.2 Input Data For: FIXSHEET

All Input is in Free Field Format

Line 1: Index = 0, means another set of data follows this set.
= 1, means terminate the program after running this problem set

Line 2: Heading cards, any alphanumeric string 72 characters long

Line 3: Tubesheet and tube data

<u>Item</u>	<u>Fortran Symbol</u>
Ligament area in the perforated region	AL
Area outside the tubes in the tubed region on the tubesheet surface in the shellside	AO
Mean tube radius	TUBRAD
Poisson's ratio of tube material	PRT
Tubewall thickness	TUBWAL

Line 4: Pressure data (Fig. 9.1.1)

Shellside pressure at the bottom tubesheet level, p_{11}	P11
Shellside pressure at the top tubesheet level, p_{21}	P21
Channelside pressure at the bottom tubesheet level, p_{12}	P12
Channelside pressure at the top tubesheet level, p_{22}	P22
Bottom channel longitudinal force per unit circumference	AN12
Top channel longitudinal force per unit circumference	AN22

Line 5: Other data

Free differential expansion of tubes over the shell	DELTA
---	-------

<u>Item</u>	<u>Fortran Symbol</u>
Young's modulus of tube material	ET
Outer radius of tubesheet	BR
<i>Line 6: Tubesheet data</i>	
Tubesheet Thickness	T
Equivalent Poisson's ratio of the perforated region	PR1
Poisson's ratio of tubesheet material	PR2
Equivalent Young's modulus of the perforated interior	E1
Young's modulus of tubesheet material	E2
Interface radius of perforated region and annular rim	A
<i>Line 7: Channel and shell data</i>	
Channel material Poisson's ratio	PRC
Channel material Young's modulus	EC
Channel wall thickness	HC
Shell material Poisson's ratio	PRS
Shell material Young's modulus	ES
Shell wall thickness	HS
<i>Line 8: Miscellaneous data</i>	
Weight density of tube material	AMUT
Weight density of shell material	AMUS
Length of shell above the support line, l_2	EL2
Length of shell below the support line, l_3	EL3
Expansion joint locator index = 0, expansion joint is between the lower tubesheet and support; = 1, expansion joint is between the top tubesheet and the support)	IEXP
Expansion joint axial stiffness, (force per unit circumference for unit axial separation of the joint)	AKEXP
Return to line 1 if INDEX = 0 in the preceding card set.	

PROGRAM FIXSHEET

```

C  DEFINITION:
C  INDEX = 0: REPEAT WITH A NEW SET OF DATA
C  INDEX = 1: TERMINATE THE PROGRAM
DIMENSION B(22,22) , G(500), F(22),W(3),RM(3),Q(3),DWDR(3),TM(3)
DIMENSION HEAD(18)
CHARACTER TODAY*27
CALL DATE(TODAY)
1 READ(5,559) (HEAD(I),I=1,18)
ACCEPT INDEX
ACCEPT AL,AO,TUBRAD,PRT,TUBWAL
ACCEPT P11,P21,P12,P22,AN12,AN22
ACCEPT DELTA,ET,BR
ACCEPT T,PR1,PR2,E1,E2,A
ACCEPT PRC,EC,HC,PRS,ES,HS
ACCEPT AMUT,AMUS,EL2,EL3,IEXP,AKEXP
TOL=.0001
EL = EL2 +EL3
A1=3.1415*A*A
AT = AL-AO
AI = A1-AL
ASTAR=3.1415*BR*BR
TBWEIT=(EL2+EL3)*AMUT*(AL-AO)
PTWEIT=TBWEIT/A1

C
DISPLAY TODAY
WRITE(6,711) (HEAD(I),I=1,18)
WRITE(6,700) AI,AL,AO,A1,ASTAR,AT,P11,P21,P12,P22, DELTA,EL,ET,BR
WRITE(6,701) T,PR1,PR2,E1,E2,A, PRC,EC,HC,PRS,ES,HS
DISPLAY "TUBE WEIGHT PRESSURE=",PTWEIT
DISPLAY "AN12,AN22=" ,AN12,AN22
DELWT=.5*((AMUT*EL*EL/ET)-(AMUS*(EL3*EL3-EL2*EL2)/ES))
1 -PRT*.5*(P12+P22-P11-P21)*TUBRAD*EL/(TUBWAL*ET)
D1=E1*T**3/ (12.*(1.0-PR1*PR1))
D2=E2*T**3/ (12.*(1.0-PR2*PR2))
DS=ES*HS**3/ (12.*(1.0-PRS*PRS))
DC=EC*HC**3/ (12.*(1.0-PRC*PRC))
BETAS=SQRT(SQRT(3.*(1.0-PRS*PRS)))/ (BR*HS))
BETAC=SQRT(SQRT(3.*(1.0-PRC*PRC)))/ (BR*HC))
S=D1/D2
P1=P11-P12
P2=P21-P22
Z=ET*AT/(A1*EL)
Z1=2.*Z/D1
WRITE(6,706) S,P1,P2,Z1
WRITE(6,703) D1,D2,DS,DC,BETAC,BETAS
FK=Z1**.25
X=FK*A
CALL BESSEL(X,BERO,BER1,BER2,BER3,BE10,BE11,BE12,BE13)
FLOG=ALOG(A)
FLOGB=ALOG(BR)
DELS=0.
DO 500 N=1,200
C2=(P21*AO - P22*AL) /A1 + Z*(DELTA-DELS+DELWT)-PTWEIT
C1=(P11*AO - P12*AL) /A1 + Z*(DELTA-DELS+DELWT)

```

```

C3=(C1+C2)/D1
C4=(C1-C2)/D1
C   DEVELOP MATRIX
      100 I=1,22
      F(I) = 0.
      DO 200 J=1,22
200  B(I,J) =0.0
      100 CONTINUE
C
      B(1,1) =BERO*.5
      B(1,2) =2.*BEI0/(FK*FK)
      B(1,3) =.5
      B(1,4) =.5*A*A
      B(1,5)=-1.0
      B(1,6)=-A*A
      B(1,7)=-FLOG
      B(1,8) =-A*A*FLOG
      F(1)=P1*(A**4) / (64.*D2) - .5*(C3/Z1*(1.0-BERO) + C4*(A**4)/64.)
      B(2,1) = FK*BER1*.5
      B(2,2) = 2.*BEI1/FK
      B(2,4) =A
      B(2,6) =-2.*A
      B(2,7) =-1.0/A
      B(2,8)=- ( A +2.*A*FLOG)
      F(2)=(P1*A**3/(16.*D2))- .5*(-C3*FK/Z1*BER1+C4*A**3/16.)
C
      B(3,1)= .5*S*(FK*FK*BER2 + PR1*FK/A*BER1)
      B(3,2) = 2.*S*(BEI2+PR1*BEI1/(FK*A))
      B(3,4) = S*( 1.0+PR1)
      B(3,6) = -2.*(1.0+PR2)
      B(3,7) =(1.0-PR2)/(A*A)
      B(3,8) =-(3.+PR2 + 2.*(1.0+PR2)*FLOG)
      F(3) = P1*A*A*(3.+PR2)/( 16.*D2) + C3*.5*S*(FK*FK/Z1*BER2 + PR1
1 *FK*BER1/(Z1*A)) - S*C4*A*A/32.*(3.0+PR1)
C
      B(4,1)=-.5*S*FK**3*BEI1
      B(4,2) = 2.*S*FK*BER1
C
      B(4,8)=-4./A
      F(4) = (P1*A/(2.*D2))- (C3*.5*S*FK**3*BEI1/Z1)-.25*C4*S*A
      B(5,1) =B(1,1)
      B(5,2) = B(1,2)
      B(5,3)=-B(1,3)
      B(5,4)=-B(1,4)
      B(5,9)= B(1,5)
      B(5,10)= B(1,6)
      B(5,11)= B(1,7)
      B(5,12)= B(1,8)
      F(5)=P2*(A**4) / (64.*D2) - .5*(C3*(1.0-BERO)/Z1- C4*(A**4)/64.)
C
      B(6,1) = B(2,1)
      B(6,2) = B(2,2)
      B(6,4) = -B(2,4)
      B(6,10) = B(2,6)
      B(6,11) = B(2,7)
      B(6,12) = B(2,8)

```

$$F(6) = P2*(A**3) / (16.*D2) + .5*(FK/Z1*C3*BER1 + C4*(A**3)/16.)$$

C

$$B(7,1) = B(3,1)$$

$$B(7,2) = B(3,2)$$

$$B(7,4) = -B(3,4)$$

$$B(7,10) = B(3,6)$$

$$B(7,11) = B(3,7)$$

$$B(7,12) = B(3,8)$$

$$F(7) = P2*A*A*(3.+PR2)/(16.*D2)+ S*C3*.5*(FK*FK*BER2/Z1 + PR1$$

$$1 *FK*BER1/(Z1*A))+C4*S*A*A*(3.+PR1)/32.$$

C

$$B(8,1) = B(4,1)$$

$$B(8,2) = B(4,2)$$

$$B(8,11) = B(4,7)$$

$$B(8,12) = B(4,8)$$

$$F(8) = (P2*A/(2.*D2))-(C3*.5*S*FK**3*BE11/Z1)+.25*C4*S*A$$

C

$$B(9,5) = 1.0$$

$$B(9,6) = BR*BR$$

$$B(9,7) = FLOGB$$

$$B(9,8) = BR*BR*FLOGB$$

$$F(9) = -P1*(BR**4)/(64.*D2)$$

C

$$B(10,9) = B(9,5)$$

$$B(10,10) = B(9,6)$$

$$B(10,11) = B(9,7)$$

$$B(10,12) = B(9,8)$$

$$F(10) = -P2*(BR**4)/(64.*D2)$$

C

$$B(11,6) = 2.* (1.0+PR2)$$

$$B(11,7) = -(1.0-PR2)/(BR*BR)$$

$$B(11,8) = ((3.+PR2) + 2.*(1.0+PR2))*FLOGB$$

$$B(11,19) = 1.0/D2$$

$$B(11,14) = -1.0 /D2$$

$$B(11,15) = .5*T/D2$$

$$B(11,20) = -B(11,15)$$

$$F(11) = -P1*BR*BR*(3.+PR2)/(16.*D2)$$

C

$$B(12,10) = B(11,6)$$

$$B(12,11) = B(11,7)$$

$$B(12,12) = B(11,8)$$

$$B(12,21) = 1.0/D2$$

$$B(12,17) = -1.0/D2$$

$$B(12,18) = B(11,15)$$

$$B(12,22) = B(11,20)$$

$$F(12) = -P2*BR*BR*(3.+PR2)/(16.*D2)$$

C

$$B(13,8) = 4./BR$$

$$B(13,13) = -1.0/D2$$

$$F(13) = -(AN12+P1*BR*.5)/D2$$

C

$$B(14,12) = B(13,8)$$

$$B(14,16) = B(13,13)$$

$$F(14) = -(AN22+P2*BR*.5)/D2$$

C

$$B(15,6) = BR*T$$

$$\begin{aligned}
 B(15,7) &= T/(2*BR) \\
 B(15,8) &= 0.5*T*BR*(1.+2*FLOGB) \\
 B(15,13) &= PRS*BR/(ES*HS) \\
 B(15,14) &= -1.0/(2.*BETAS*BETAS*DS) \\
 B(15,15) &= B(15,14) /BETAS \\
 F(15) &= P11*BR*BR/(ES*HS) -P1*T*BR**3/(32.*D2) \\
 B(16,10) &= B(15,6) \\
 B(16,11) &= B(15,7) \\
 B(16,12) &= B(15,8) \\
 B(16,16) &= B(15,13) \\
 B(16,17) &= B(15,14) \\
 B(16,18) &= B(15,15) \\
 F(16) &= P21*BR*BR/(ES*HS)-P2*T*BR**3/(32.*D2) \\
 B(17,6) &= - BR*T \\
 B(17,7) &= -T/(2.*BR) \\
 B(17,8) &= -T*BR*.5*(1+2*FLOGB) \\
 B(17,19) &= -1.0/(2.*BETAC*BETAC*DC) \\
 B(17,20) &= B(17,19)/BETAC \\
 F(17) &= P12*BR*BR/(EC*HC) - PRC*AN12*BR/(EC*HC) +P1*T*BR**3/ \\
 &1 (32.*D2)
 \end{aligned}$$

C

$$\begin{aligned}
 B(18,10) &= B(17,6) \\
 B(18,11) &= B(17,7) \\
 B(18,12) &= B(17,8) \\
 B(18,21) &= B(17,19) \\
 B(18,22) &= B(17,20) \\
 F(18) &= P22*BR*BR/(EC*HC) - PRC*AN22*BR/(EC*HC)+P2*T*BR**3/(32*D2)
 \end{aligned}$$

C

$$\begin{aligned}
 B(19,14) &= 2./(BETAS*DS) \\
 B(19,15) &= 1.0/(BETAS*BETAS*DS) \\
 B(19,19) &= 2./(BETAC*DC) \\
 B(19,20) &= 1./(BETAC*BETAC*DC) \\
 F(19) &= 0.0
 \end{aligned}$$

C

$$\begin{aligned}
 B(20,17) &= B(19,14) \\
 B(20,18) &= B(19,15) \\
 B(20,21) &= B(19,19) \\
 B(20,22) &= B(19,20) \\
 F(20) &= 0.0
 \end{aligned}$$

C

$$\begin{aligned}
 B(21,6) &= 2.*BR \\
 B(21,7) &= 1.0/BR \\
 B(21,8) &= BR + 2.*BR*FLOGB \\
 B(21,14) &= 1.0/(BETAS*DS) \\
 B(21,15) &= 1.0/(2.*BETAS*BETAS*DS) \\
 F(21) &= -P1*(BR**3) / (16.*D2)
 \end{aligned}$$

C

$$\begin{aligned}
 B(22,10) &= B(21,6) \\
 B(22,11) &= B(21,7) \\
 B(22,12) &= B(21,8) \\
 B(22,17) &= B(21,14) \\
 B(22,18) &= B(21,15) \\
 F(22) &= -P2*BR**3/(16.*D2)
 \end{aligned}$$

C

C

DO 300 I=1,22

```

DO 400 J= 1,22
400 G((I-1)*22 + J) = B(J,I)
300 CONTINUE
    CALL SIMQ(G,F,22,KS)
    IF(KS.EQ.0) GO TO 450
    WRITE(6,702)
    STOP
450 CONTINUE
C
    DELT = (F(13)*EL3+F(16)*EL2 - .5*EL*PRS*BR*(P11+P21))/(ES*HS)
    1 + (F(10+3*IEXP)/(AKEXP))
    IF( ABS(DELT-DELS) .LT. ABS(.001*DELS)) GO TO 350
    DISPLAY DELS,DELT
500 DELS=.5*(DELS+DELT)
    WRITE(6,707)
    STOP
350 CONTINUE
    WRITE(6,704) (F(I), I=1,22) ,DELS
    WRITE(6,709)
    DO 520 I=1,21
    R= A*(I-1)*.05
    RR=R*R
    X= FK*R
    CALL BESSEL(X,BERO,BER1,BER2,BER3,BEIO,BE11,BE12,BE13)
    DO 530 J=1,2
    N= (-1)**(J+1)
    W(J) = .5*((C3/Z1 + (F(1)-C3/Z1) * BERO + 4.*F(2)*BEIO/(FK*FK)) +
    1 N*(F(3)+F(4)*RR + C4*R**4/64.))
    IF(I .EQ. 1)GO TO 529
    RM(J) = -.5*D1*(F(1)*(FK*FK*BER2 + FK*PR1*BER1/R) +
    1 F(2)*(4.*BEI2+4.*BEI1*PR1/(FK*R))-C3*(FK*FK*BER2/Z1 + FK*PR1*BER1
    2 /(Z1*R)) + N*(2.*F(4)*R + C4*RR*(3.+PR1)/16.))
    TM(J)=-.5*D1*(F(1)*(PR1*FK*FK*BER2+FK*BER1/R) + 4.*F(2)*(BEI2
    1 *PR1+BEI1/(FK*R))-C3*((FK*BER1/(Z1*R))+ (PR1*FK*FK*BER2/Z1))
    2 +N*(2*F(4)*(1.+PR1) + C4*R*R*(1.+3.*PR1)/16.))
    Q(J) = .5*D1*(F(1)*(FK**3*BER3 + FK*FK*BER2/R - FK*BER1/RR)
    1 + F(2)*4.*(FK*BEI3 + BEI2/R - BEI1/(FK*RR)) - C3*(FK**3*BER3
    2 /Z1 + FK*FK*BER2/(Z1*R) - FK*BER1/(Z1*RR)) + N*C4*R*.5)
    GO TO 530
529 Q(J)=0.
    RM(J)= -D1*(1+PR1)*(F(2) + N*F(4))
    TM(J) = RM(J)
530 DWDR(J) = .5*((FK*(F(1) - C3/Z1)*BER1 + 4.*F(2)/FK *BEI1) + N*
    1 (2.*F(4)*R + C4*R**3/16.))
    STUBE=- (DELTA+DELWT-DELS-W(1)-W(2))*ET/EL
    STTOP = STUBE +AMUT*EL
    WRITE(6,708) R,(W(J),TM(J),RM(J),Q(J),J=1,2),STUBE,STTOP
520 CONTINUE
    WRITE(6,710)
    DO 540 I=1,5
    R= A+(I-1)*(BR-A)*.25
    RR=R*R
    RLOG= ALOG(R)
    X=FK*R
    CALL BESSEL(X,BERO,BER1,BER2,BER3,BEIO,BE11,BE12,BE13)
    DO 550 J=1,2

```

```

M=(J-1)*4
P=P1+(P2-P1)*(J-1)
W(J) = F(5+M) + F(6+M)*RR + F(7+M)*RLOG + F(8+M)*RR*RLOG + P*R**4
1 / (64.*D2)
RM(J) = -D2*(2.*F(6+M)*(1.+PR2) - F(7+M)*(1.-PR2)/RR + F(8+M)*((3.
3 +PR2) + 2.*RLOG*(1.+PR2)) + P*RR*(3.+PR2)/(16.*D2))
Q(J) = D2*(4.*F(8+M)/R + P*R/(2.*D2))
550 DWDR(J) = 2.*F(6+M)*R + F(7+M)/R + F(8+M)*(R+2.*R*RLOG)
1 + P*R**3/(16.*D2)
WRITE(6,708) R,(W(J), DWDR(J), RM(J), Q(J), J=1,2)
540 CONTINUE
559 FORMAT(18A4)
700 FORMAT(///,5X, "D A T A",/,5X, 30("--"),//,
15X,"TUBE HOLE AREA (AI) =", F10.1, /, 5X,"LIGAMENT AREA (AL) =",
2 F10.1,/, 5X, "AREA OUTSIDE OF TUBES(AO) =", F10.1,/,
35X,"TOTAL PERFORATED PLATE AREA(A1) =", F10.1,/,
4 5X, "CHANNEL BARREL AREA (ASTAR) =",F10.1,/,
5 5X,"TUBE METAL CROSS SECTION (AT) =",F10.3,//,
6 30X,"BOTTOM",4X,"TOP" ,/, 5X,"SHELL PRESSURE (P11,P21)",F7.0,
7 2X,F6.0,/,5X,"TUBE PRESSURE (P12,P22)", F7.0,2X,F6.0,//,
8 5X,"DIFFERENTIAL THERMAL EXPANSION OF TUBES OVER SHELL (DELTA) ="
9 ,E15.4,/,5X,"SHELL LENGTH (EL)=", F9.3,/,
1 5X,"YOUNGS MODULUS OF TUBE (ET) =",E15.4,/,
2 5X,"SHELL AND CHANNEL MEAN RADIUS (BR) =",F12.4)
701 FORMAT(/, 5X, "TUBESHEET THICKNESS (T) =",F8.4,/,
1 5X, "POISSON RATIO OF TUBESHEET AND RIM (PR1,PR2) =",2(3X,F8.4),/
2 ,5X,"YOUNGS MODULUS OF TUBESHEET AND RIM (E1,E2) ",2(3X,E10.2),/,
3 5X, "INTERFACE RADIUS (A) =",F10.4,//,
4 14X,"POISSON RATIO",3X,"YOUNGS MOD",3X,"THK",/,
5 5X,"CHANNEL",5X,F4.2,10X,E8.2,3X, F6.4, /,
6 6X,"SHELL" ,6X,F4.2,10X, E8.2,3X,F6.4,/,5X,30("--"),///)
702 FORMAT(5X," SINGULAR SET OF EQUATIONS, NO SOLUTION")
703 FORMAT(5X, "D1,D2=", 2E14.4,3X, "DS,DC=",2E14.4,3X, "BETAC,BETAS="
1 , 2E14.4)
704 FORMAT(1H0,/,10X,"ROOTS",/,5X, "RHO 0",7X, "RHO 2",7X, "RHO 1",7
1X, "RHO 3",7X, "ALFA1",7X, "BETA1",7X, "GAM 1",7X, "DEL 1",7X,
2 "ALFA",7X,"BETA2",7X,"GAMA2",/, 11(2X,E10.3)//
3 5X,"DELTA2",9X,"N11",9X,"M11",9X,"Q11",9X,"N21",9X,"M21 ",9X,
4 "Q21 ",7X,"M12 ",7X, "Q12 ",7X,"M22 ",7X, "Q22 ",
5 /,11(2X,E10.3),///, 5X, "DELTA S =",E12.4)
705 FORMAT(///," DELTA S =",E12.3)
706 FORMAT(/,5X,"RIGIDITY RATIO (S) =",F6.3, ",",6X,"P1=",F6.0, ",",6X,
1"P2=",F6.0, ",",6X,"Z1=",E12.3)
707 FORMAT(5X,"NO CONVEGENCE IN DELTA S")
708 FORMAT(F8.3,10E12.4)
709 FORMAT(1H1,17X,"BBB 000 TTT TTT 000 MMM",12X,14("-"),
1" TTT 000 PPP ",15("-"),7X,"TUBESTRESS",/,10X,6("-"),
2" BBB 000 TTT TTT 000 MMM ",8("-"),18X,"TTT 000 PPP",
3//,4X,"R",2(11X,"W",10X,"TM",11X,"MR",10X,"Q"),8X,"BOTTOM",8X,
4"TOP",//)
710 FORMAT(/)
711 FORMAT(///,5X,18A4)
IF(INDEX.EQ.0) GO TO 1
STOP
END
SUBROUTINE BESSEL (XP, BERO, BER1, BER2, BER3, BE10, BE11, BE12, BE13)

```

```

    DIMENSION G(4),A(4),B(4),C(4)
    EXTERNAL CALC
    X=XP*.5
    X4=X**4
    F=1.0
    DO 100 J=1,4
100  G(J)=0.0
    DO 200 I=1,51,2
    K=I-1
    CALL CALC(K,A,F)
    F=F*(2*K+1)*(2*I)
    CALL CALC(I,B,F)
    DO 300 J=1,4
    C(J)=(X4**K)*(A(J)-X4* B(J))
300  G(J)=G(J)+C(J)
    DO 301 J=1,4
301  C(J)=ABS(C(J)/G(J))
    IF(AMAX1(C(1),C(2),C(3),C(4)) .LT. .00001) GOTO 400
    00 F=F*(2*I+1)*(2*I+2)
400  BERO=G(1)
    BER1=-G(2)*(X**3)
    BEI0=G(3)*X*X
    IF(XP.LT. 1.0E-6) GOTO 500
    BEI1=G(4)*X
    BER2=-BEI0-BER1/XP
    BEI2= BERO-BEI1/XP
    BER3=-BEI1 + BER1/(XP*XP) - BER2/XP
    BEI3= BER1 + BEI1/(XP*XP) - BEI2/XP
    GOTO 600
500  BER2=0.
    BEI2=.5
    BER3=0.
    BEI3=0.
600  CONTINUE
    I=(I+1) /2
    RETURN
    END
    SUBROUTINE CALC(K,A,F)
    DIMENSION A(4)
    A(1)=1.0/(F**F)
    A(2) = 2.*(K+1)/ ((F*(2*K+1)*(2*K+2))**2 )
    A(3)=1.0/ ((F*(2*K+1))**2)
    A(4) =(2.* K+1)*A(3)
    RETURN
    END
    SUBROUTINE SIMQ(A,B,N,KS)
    DIMENSION A(400),B(20)
    TOL=0.0
    KS=0
    JJ=-N
    DO 65 J=1,N
    JY=J+1
    JJ=JJ+N+1
    BIGA=0.
    IT=JJ-J
    DO 30 I=J,N

```

```

    IJ=IT+I
    IF (ABS(BIGA)-ABS(A(IJ))) 20,30,30
20  BIGA=A(IJ)
    IMAX=I
30  CONTINUE
    IF (ABS(BIGA)-TOL) 35,35,40
35  KS=1
    RETURN
40  I1=J+N*(J-2)
    IT=IMAX-J
    DO 50 K=J,N
        I1=I1+N
        I2=I1+IT
        SAVE=A(I1)
        A(I1)=A(I2)
        A(I2)=SAVE
50  A(I1)=A(I1)/BIGA
    SAVE=B(IMAX)
    B(IMAX)=B(J)
    B(J)=SAVE/BIGA
    IF(J-N) 55,70,55
    IQS=N*(J-1)
    DO 65 IX=JY,N
        IXJ=IQS+IX
        IT=J-IX
        DO 60 JX=JY,N
            IXJX=N*(JX-1)+IX
            JJX=IXJX+IT
60  A(IXJX)=A(IXJX)-(A(IXJ)*A(JJX))
65  B(IX)=B(IX)-(B(J)*A(IXJ))
70  NY=N-1
    IT=N*N
    DO 80 J=1,NY
        IA=IT-J
        IB=N-J
        IC=N
        DO 80 K=1,J
            B(IB)=B(IB)-A(IA)*B(IC)
        IA=IA-N
80  IC=IC-1
    RETURN
    END

```

APPENDIX 9.C

USER MANUAL FOR TUBESHEET ANALYSIS PROGRAM “FIX-FLOAT” AND SOURCE LISTING

I. Introduction

This program can be used for the following kinds of tubesheet.

- (i) tubesheets of fixed tubesheet heat exchanger,
- (ii) fixed tubesheet of floating head heat exchanger.

This program can be used in two ways:

(a) to compute tubesheet thickness and stresses for given range of values of x_a :

$$x_a = \left(\frac{2aU}{h} \right)^{3/4}; \quad U^3 = \frac{3(1-\nu^2)\delta E_T a}{ELe}; \quad \delta = \frac{Nt(d-t)}{a^2}$$

h, a = tubesheet thickness and perforated region radius; d, t = tube O.D., thickness. This option is useful for parametric studies. Option (b), described below, is more attuned to the designer's needs.

(b) to compute stresses for a given tubesheet thickness and compute a thickness for comparison using the formulas outlined in the TEMA Standards.

For a fixed tubesheet heat exchanger, the program computes stresses for the following six load combinations so that the maximum stresses can be found.

- (1) shellside pressure load only;
- (2) thermal load only;
- (3) shellside pressure and thermal load;
- (4) tubeside pressure and thermal load;
- (5) shellside and tubeside pressure loads;
- (6) tubeside pressure load only.

For the fixed tubesheet of a floating head construction the program computes stresses for the following load cases:

- (1) shellside pressure alone
- (2) tubeside pressure alone

II. Input Data

A. Input data from terminal (follows line 2 of the data file, described on the next page)

When $NXA = 0$, $XA(1) = 0$, the program will compute stresses for a given tubesheet thickness, and will compute a thickness using the TEMA method. The computer will request the following input data from the keyboard.

(i) Input support type:

NST = 2 both shell and channel joints integral

NST = 1 channel side gasketed

- (ii) NST = 0 both sides of unit gasketed
 H thickness of tubesheet given for computing stress
 TS shell thickness
 TC channel thickness
 FRA local amplification factor for shell thickness
 SJ The stiffness of shell expansion joint (for no joint, reading in 0.0 gives a value of SJ = 10^4 times the shell Young's Modulus)
 NQ Input data report printout option (0,1,2) 0 = full, 1 = medium, 2 = limited
- (iii) Code will ask for E^*/E , ν^* after giving a printout of ligament efficiency. Data should be obtained from available published charts in this text or elsewhere.
- (iv) Code will also ask for JSTART, JSTOP (the beginning and ending parameters of a do loop). The parameters 1-6 refer to the load cases given above. The user can select all or any group in ascending order. In putting 0 for JSTART ends the loading cases.

Code will return to input line (ii) of terminal input or go on to compute an estimate of a TEMA thickness, depending on the answers given to the terminal queries.

B. Input data from data file (logical unit number 14)

- Line (1) NXA – Number of values of x_a , $0 \leq NXA \leq 10$
 JHP – Printout step size for details. If JHP = 0, program sets JHP = 5 automatically. (used with NW option, line 7).
 NS – Low limit for moment printout. If NS = 0, program sets NS = 1 automatically.
 NF – High limit for moment printout. If NF = 0, program sets NF = 101 automatically.
 NP – Step size for moment printout. If NP = 0, program sets NP = 5 automatically.
 L – Logical unit number for output

- Line (2) XA(I), I = 1, NXA – input values of x_a . If NXA, XA(1) are not equal to zero, this program computes tubesheet thickness and stresses for every given XA. If NXA = 0, XA(1) = 0, this program computes stresses for given tubesheet thickness, and computes TEMA thickness for comparison).

- Line (3)
- B – Mean radius of shell
 - A – Mean radius of tubesheet drilled portion
 - AC – Mean radius of channel
 - AI – Outer radius of tubesheet untubed rim
 - DI – Radius of bolt circle
 - SALL – Allowable stress of tubesheet material
 - DJ – Expansion joint bellows I.D.
- Line (4)
- D – Outer diameter of tube
 - T – Tube wall thickness
 - NT – Number of tubes
 - RLENGTH – Effective tube length between tubesheets
 - PITCH – Tube pitch
 - THETA – Tube pattern drilling angle (degrees)
- Line (5)
- ET – Young's Modulus of tube material
 - ES – Young's Modulus of shell material
 - ALPHAT – Thermal expansion coefficient of tube material
 - ALPHAS – Thermal expansion coefficient of shell material
 - OMEGA – Tubesheet design stress factor = 2.0
 - AREA* – Total area enclosed by perimeter of perforated region
 - PERIM* – Tube layout perimeter
- Line (6)
- E – Young's Modulus of tubesheet
 - EC – Young's Modulus of channel
 - PTO – Tubeside pressure
 - PSO – Shellside Pressure
 - TEMPTO – Operating temperature of tube (and tubesheet)
 - TEMPSO – Operating temperature of shell
 - TEMPA – Assembly temperature of the unit (°F)
 - BLT – Bolt load for seating of one bolt
 - NB – Number of bolts
- Line (7)
- NTYPE – Calculation option: NTYPE = 0, calculation for the fixed tubesheet of floating head unit. NTYPE = 1 for fixed tubesheet unit.
 - RTUBE – Ratio of roll depth to assumed tubesheet thickness

* πA^2 and $2\pi A$ are defaults. These quantities are only used for a TEMA calculation.

NW – Printout option

NW = 0, do not printout QV, QM vs. X

NW = 1, printout QV, QM vs. X

Line (8) (Only if NXA not equal to zero, i.e., user is inputting XA values rather than thickness of the tubesheet)

TS	} see part A user input
TC	
FRA	
SJ	
NQ	
NST	

PROGRAM FIXFLOAT

```

PROGRAM MAIN
C TUBESHEET ANALYSIS PROGRAM. VERSION 11/83 A.SOLER
  DIMENSION XA(10),QM(101,10),QV(101,10),AMR(101,10),AMRMAX(10),
&           QMT(101,10),QVT(101,10),AMT(101,10),AMTMAX(10),XT(10)
&           ,XR(10)
  CHARACTER*4 TITLE(20)
  READ(14,*) NXA,JHP,NS,NF,NP,L
  IF(JHP.EQ.0) JHP=5
  IF(NS.EQ.0) NS=1
  IF(NF.EQ.0) NF=101
  IF(NP.EQ.0) NP=5
  READ(14,*) XA
C IF NXA,XA(1) ARE NOT EQUAL TO 0,THIS PROGRAM COMPUTES TUBESHEET
C THICKNESS AND STRESS FOR GIVEN XA;
C IF NXA=0,XA(1)=0,THIS PROGRAM COMPUTES STRESSES FOR GIVEN
C TUBESHEET THICKNESS,AND COMPUTES TEMA THICKNESS FOR COMPARISON.
  WRITE(6,*)' TUBESHEET PROGRAM VERSION 4 APRIL 1983'
  IF(XA(1).EQ.0.0) WRITE(6,*)'PROGRAM IS RUNNING... '
  IF(XA(1).EQ.0.)WRITE(6,*)' INPUT TUBESHEET EDGE SUPPORT TYPE'
  IF(XA(1).EQ.0.) READ(5,*) NST
  IF(XA(1).EQ.0.0) WRITE(6,*)' INPUT VALUES FOR H,TS,TC,FRA,SJ,NQ:'
  IF(XA(1).EQ.0.0) READ(5,*) XA(1),TS,TC,FRA,SJ,NQ
  WRITE(6,*)' INPUT A RUN TITLE FOR I.D. PURPOSES'
  READ(5,30000)(TITLE(J),J=1,20)
30000  FORMAT(20A4)
  READ(14,*) B,A,AC,A1,D1, SALL,DJ
  READ(14,*) D,T,NT,RLENTN,PITCH,THETA
  READ(14,*) ET,ES,ALPHAT,ALPHAS,OMEGA,AREA,PERIMT
  READ(14,*) E,EC,PTO,PSO,TEMPTO,TEMPSO,TEMPTA,BLT,NB
  READ(14,*) NTYPE,RTUBE,NW
  IF(NXA.NE.0) READ(14,*)TS,TC,FRA,SJ,NQ,NST
C PRINTOUT OF INPUT DATA.
  IF(SJ.EQ.0.0) SJ=10000.0*ES
  IF(DJ.EQ.0.0) DJ=2.0*B
  IF(AREA.EQ.0.0) AREA=3.14159265*A*A

```

```

IF(PERIMT.EQ.0.0) PERIMT=2.0*3.14159265*A
IF(FRA.EQ.0.0) FRA=1.0
SPRIM=1.5*SALL
SSEC=1.5*OMEGA*SALL
  BNU=0.3
WRITE(L,*)'***** INPUT DATA *****'
  WRITE(L,30000)(TITLE(J),J=1,20)
IF(NQ.EQ.2) GO TO 36310
WRITE(L,*)'STEP SIZE FOR MOMENT PRINTOUT,NP=',NP
WRITE(L,*)'XA:',(XA(I),I=1,NXA)
WRITE(L,*)' SUPPORT TYPE--2=I/I; 1=G/I; 0=G/G NST=',NST
WRITE(L,*)' MEAN RADIUS OF CHANNEL, AC=',AC
WRITE(L,*)' MEAN RADIUS OF SHELL, B=',B
WRITE(L,*)' MEAN RADIUS OF DRILLED PORTION OF TUBESHEET,A=',A
WRITE(L,*)' SHELLWALL THICKNESS,TS=',TS
WRITE(L,*)' CHANNEL THICKNESS, TC=',TC
WRITE(L,*)' OUTER RING RADIUS, A1=',A1
WRITE(L,*)' BOLT CIRCLE RADIUS, D=',D1
WRITE(L,*)' BOLT PRELOAD, BLD=',BLT
WRITE(L,*)' NUMBER OF BOLTS, NB=',NB
WRITE(L,*)' OUTER DIAMETER OF TUBE,D=',D
WRITE(L,*)' TUBEWALL THICKNESS,T=',T
WRITE(L,*)' NUMBER OF TUBES,NT=',NT
WRITE(L,*)' TUBE LENGTH,RLENTH=',RLENTH
WRITE(L,*)' TUBE PITCH,PITCH=',PITCH
WRITE(L,*)' TUBE PATTERN DRILLING ANGLE,THETA=',THETA
WRITE(L,*)' ELASTIC MODULUS OF TUBE MATERIAL,ET=',ET
WRITE(L,*)' ELASTIC MODULUS OF TUBESHEET MATERIAL,E=',E
WRITE(L,*)' ELASTIC MODULUS OF SHELL MATERIAL,ES=',ES
WRITE(L,*)' ALLOWABLE STRESS OF TUBESHEET MATERIAL,SALL=',SALL
WRITE(L,*)' SHELL EXPANSION JOINT STIFFNESS,SJ=',SJ
WRITE(L,*)' EXPANSION JOINT BELLOWS INSIDE DIAMETER,DJ=',DJ
IF(NTYPE.EQ.0) GO TO 36311
WRITE(L,*)' EXPANSION COEFFICIENT OF TUBE,ALPHAT=',ALPHAT
WRITE(L,*)' EXPANSION COEFFICIENT OF SHELL,ALPHAS=',ALPHAS
36311 CONTINUE
WRITE(L,*)' TUBESHEET DESIGN STRESS FACTOR,OMEGA=',OMEGA
WRITE(L,*)' TUBESIDE PRESSURE,PTO=',PTO
WRITE(L,*)' SHELLSIDE PRESSURE,PSO=',PSO
IF(NTYPE.EQ.0) GO TO 36312
WRITE(L,*)' OPERATING TEMPERATURE OF TUBE,TEMPTO=',TEMPTO
WRITE(L,*)' OPERATING TEMPERATURE OF SHELL,TEMPSO=',TEMPSO
36312 CONTINUE
IF(NQ.EQ.1) GO TO 36310
WRITE(L,*)' CALCULATION OPTIONS (NTYPE=0,CALCULATION FOR FLOATING
& HEAD UNIT;NTYPE=1,FOR FIXED TUBESHEET),NTYPE=',NTYPE
WRITE(L,*)' RATIO OF ROLL DEPTH TO TUBESHEET THICKNESS=',RTUBE
WRITE(L,*)' PRINTOUT OPTIONS (NW=0,DO NOT PRINT OUT QV,QM VS X;NW=1
&,PRINT OUT QV,QM VS X), NW=',NW
WRITE(L,*)' POISSON RATIO,BNU=',BNU
36310 CONTINUE
  BD=NB*BLT/6.28
  EFS=(PITCH-D+RTUBE*2.0*T*ET/E)/PITCH
  EFS1=(PITCH-D+2*T)/PITCH
  IF(EFS.GT.EFS1)EFS=EFS1

```

```

WRITE(L,*)'LIGAMENT EFFICIENCY,EFS=',EFS
IF(L.NE.6)WRITE(6,*)'LIGAMENT EFFICIENCY=',EFS
WRITE(6,*)'INPUT E*/E,NUSTAR FROM CHARTS'
WRITE(6,*)' IF E*/E READ IN AS NEG. NUMBER, THEN INPUT'
WRITE(6,*)' VALUE INTERPRETED AS -(FLEX.EFF.)/E'
READ(5,*) ESTAR,ANUSTA
WRITE(L,*)' VALUE OF E*/E READ IN =',ESTAR
ESTAR=ESTAR*E
WRITE(L,*)'EFFECTIVE POISSON RATIO,ANUSTA=',ANUSTA
WRITE(L,*)'EFFECTIVE MODULUS OF TUBESHEET,ESTAR=',ESTAR
EFRR=(ESTAR*0.91)/(E*(1.0-(ANUSTA**2)))
IF(ESTAR.LT.0.0) GO TO 10
GO TO 20
10  EFRR=-ESTAR
20  CONTINUE
WRITE(L,*)'FLEXURAL RIGIDITY RATIO,EFRR=',EFRR
WRITE(L,*)
WRITE(L,*)'***** OUTPUT DATA *****'
WRITE(L,30000)(TITLE(JK),JK=1,20)
IF(NTYPE.EQ.1) GO TO 50
WRITE(L,*)'FOLLOWING RESULTS ARE FOR THE FIXED TUBESHEET OF A FLOA
&TING HEAD UNIT:'
GO TO 80
50  WRITE(L,*)'FOLLOWING RESULTS ARE FOR FIXED TUBESHEET:'
80  THETA=THETA*3.14159265/180.0
.S=1.0-3.14159265*D*D/(4.0*PITCH*PITCH*SIN(THETA))
FT=1.0-3.14159265*((D-2.0*T)**2)/(4.0*PITCH*PITCH*SIN(THETA))
AT=3.14159265*(D*D-((D-2.0*T)**2))/4.0
10000 CONTINUE
IF(SJ.EQ.0.0) SJ=10000.0*ES
IF(FRA.EQ.0.0) FRA=1.0
ALJ=2*ES*B*TS*3.14159265/(SJ*RLNTH)
PSYS=FS*PITCH*PITCH*SIN(THETA)/AT+1.0*BNU*B*ET/(TS*ES)+0.5*BNU
PSYT=FT*PITCH*PITCH*SIN(THETA)/AT+BNU*(0.5*D/T-1.0)
& +0.5*B*ET/(TS*ES)*(1+ALJ)
RK=B/A
RKC=AC/A
RKB=A1/A
BATAC=(3.*(1.-BNU*BNU))**.25/SQRT(AC*FRA*TC)
DS=ES*(FRA*TS)**3/10.91
DC=EC*(FRA*TC)**3/10.91
BATAS=(3.0*(1.0-BNU*BNU))**.25/SQRT(B*TS*FRA)
DALTA=FLOAT(NT)*T*(D-T)/(A*A)
U=(3.0*(1.0-0.3*0.3)*DALTA*ET*A/(E*RLNTH*EFRR))**(1.0/3.0)
WRITE(L,*)
WRITE(L,*)'B/A =',RK,' AC/A=',RKC,' A1/A=',RKB
WRITE(L,*)'DELTA=',DALTA
WRITE(L,*)'U=',U
NTST=0
IF(NXA.EQ.0) NTST=1
IF(NXA.EQ.0) XA(1)=(2.0*A*U/XA(1))**(3.0/4.0)
IF(NXA.EQ.0) NXA=1
DO 1000 I=1,NXA
CALL BESSEL(XA(I),BER0,BER1,BER2,BE10,BE11,BE12)
Z1XA=BER0
Z2XA=BE10

```

```

Z3XA=BER1
Z4XA=BEI1
Z5XA=(1.0-ANUSTA)*BEI2+ANUSTA*BERO
Z6XA=-(1.0-ANUSTA)*BER2+ANUSTA*BEI0
Z7XA=Z1XA*Z3XA+Z2XA*Z4XA
Z9XA=Z3XA**2+Z4XA**2
Z10XA=Z4XA*Z5XA-Z3XA*Z6XA
WRITE(L,*)I,'. XA=',XA(I)
IF(NW.EQ.0) GO TO 90
WRITE(L,*)' R/A X QV QM
& QVT QMT'
JPRNT=JHP
90 DO 100 J=1,101
X=XA(I)*FLOAT(J-1)/FLOAT(100)
CALL BESSEL(X,BERO,BE1,BE2,BE10,BE11,BE12)
Z5X=(1.0-ANUSTA)*BEI2+ANUSTA*BERO
Z6X=-(1.0-ANUSTA)*BER2+ANUSTA*BEI0
QM(J,I)=(Z5X*Z4XA-Z6X*Z3XA)/Z10XA
QV(J,I)=(Z5X*Z6XA-Z6X*Z5XA)/(XA(I)*Z10XA)
QMT(J,I)=(BER1*Z3XA+BE11*Z4XA)/(XA(I)*Z10XA)
QVT(J,I)=(BER1*Z5XA+BE11*Z6XA)/(XA(I)*XA(I)*Z10XA)
HO10=FLOAT(J-1)/FLOAT(100)
IF(NW.EQ.0) GO TO 100
IF(J.LT.JPRNT) GO TO 100
JPRNT=JPRNT+JHP
100 WRITE(L,*)HO10,X,QV(J,I),QM(J,I),QVT(J,I),QMT(J,I)
CONTINUE
U1=Z9XA/(XA(I)*Z10XA)
U2=Z7XA/(XA(I)*XA(I)*Z10XA)
U3=(Z1XA*Z5XA+Z2XA*Z6XA)/(Z10XA*(XA(I)**3))
HH=2.0*A*U/(XA(I)**(4.0/3.0))
GAMS=.25*(RK*RK-1)*(RK-1)
IF(NST.GT.0)GAMS=GAMS-BATAS**2*(FRA*TS)**2*RK**3
1*(1.+BATAS*HH)/(6.*(1.-BNU*BNU))
GAMC=.25*(RKC**2-1.)*(RKC+1.)-.5*(RKC**3-RK)
IF(NST.GT.1)GAMC=GAMC+BATAC**2*(FRA*TC)**2*RKC**3
1*(1.+BATAC*HH)/(6.*(1.-BNU*BNU))
GAMB=0.
IF(NST.EQ.0)GAMB=RKC-RK
IF(NST.EQ.1)GAMB=RKC-D1/A
AMU=0.
IF(NST.GE.1)AMU=BATAS*B*DS*(1.+BATAS*HH+(BATAS*HH)**2/2.)
IF(NST.EQ.2)AMU=AMU+BATAC*AC*DC*(1.+BATAC*HH+(BATAC*HH)**2/2.)
AMU=24.*AMU/(E*HH**3)
C FOR KNOWN RK,EFRR,AMU,XA(I),COMPUTE FOLLOWING VARIABLES:
AMUNU=(ALOG(RKB)+AMU)*(1.-BNU*BNU)/EFRR
QD=1.+AMUNU*U1
Q2=((RK-1.0)/1.0-AMUNU*U2)/QD
IF(NTYPE.EQ.1) GO TO 300
C FOR FLOATING HEAD UNIT, THE FIXED TUBESHEET BENDING MOMENT:
WRITE(6,*)' INPUT KSTART,KSTOP (0-2)'
READ(5,*) KK1,KK2
IF(KK1.EQ.0) GO TO 1000
DO 8000 KKK=KK1,KK2
IF(KKK.EQ.2) GO TO 110
WRITE(L,*)' (1) SHELLSIDE PRESSURE LOAD ONLY:'

```

```

PT=0.0
PS=PSO
GO TO 115
110 WRITE(L,*)' (2) TUBESIDE PRESSURE LOAD ONLY:'
PT=PTO
PS=0.0
115 AVA=0.5*(PS-PT)*A*A
Q1=(PT*A**2*GAMC+PS*A*A*GAMS+BD*GAMB)/QD
AMA=Q2*(PS-PT)*A*A/2.+Q1
AMRMAX(I)=0.0
AMTMAX(I)=0.0
DO 200 J=1,101
AMR(J,I)=AMA*QM(J,I)+AVA*QV(J,I)
IF(J.EQ.1) GO TO 556
X=XA(I)*FLOAT(J-1)/FLOAT(100)
AMT(J,I)=ANUSTA*AMR(J,I)+(1.0-ANUSTA**2)*XA(I)/X
& *(AMA*QMT(J,I)+AVA*QVT(J,I))
556 IF(J.EQ.1) AMT(J,I)=AMR(J,I)
IF(ABS(AMR(J,I)).GE.AMRMAX(I)) GO TO 150
GO TO 160
150 AMRMAX(I)=ABS(AMR(J,I))
XR(I)=XA(I)*FLOAT(J-1)/FLOAT(100)
JR=J
160 IF(ABS(AMT(J,I)).GE.AMTMAX(I)) GO TO 170
GO TO 200
170 AMTMAX(I)=ABS(AMT(J,I))
XT(I)=XA(I)*FLOAT(J-1)/FLOAT(100)
JT=J
200 CONTINUE
GO TO 600
C FOR FIXED TUBESHEET UNIT, TUBESHEET BENDING MOMENT:
300 CONTINUE
WRITE(6,*)' INPUT JSTART,JSTOP (0-6)'
READ(5,*) JJJ1,JJJ2
IF(JJJ1.EQ.0) GO TO 1000
DO 8000 JJJ=JJJ1,JJJ2
WRITE(L,*)'*****'
WRITE(L,*)'*****'
WRITE(L,*)'*****'
GO TO (301,302,303,304,305,306),JJJ
301 WRITE(L,*)' (1) SHELLSIDE PRESSURE LOAD ONLY:'
PT=0.0
PS=PSO
TEMPS=TEMPA
TEMPT=TEMPA
GO TO 350
302 WRITE(L,*)' (2) THERMAL LOAD ONLY:'
PS=0.0
PT=0.0
TEMPT=TEMPTO
TEMPS=TEMPSO
GO TO 350
303 WRITE(L,*)' (3) SHELLSIDE PRESSURE + THERMAL LOAD:'
PT=0.0
PS=PSO
TEMPT=TEMPTO

```

```

TEMPS=TEMPSO
GO TO 350
304 CONTINUE
WRITE(L,*)' (4) SHELLSIDE AND TUBESIDE PRESSURE + THERMAL LOAD:
PS=PSO
PT=PTO
TEMPT=TEMPTO
TEMPS=TEMPSO
GO TO 350
310 WRITE(L,*)' (4) TUBESIDE PRESSURE + THERMAL LOAD:
PS=0.0
PT=PTO
TEMPT=TEMPTO
TEMPS=TEMPSO
GO TO 350
305 CONTINUE
WRITE(L,*)' (5) SHELLSIDE AND TUBESIDE PRESSURE LOADS:
TEMPS=TEMPA
TEMPT=TEMPA
PT=PTO
PS=PSO
GO TO 350
306 WRITE(L,*)' (6) TUBESIDE PRESSURE LOAD ONLY:
PS=0.0
PT=PTO
TEMPS=TEMPA
TEMPT=TEMPA
350 CONTINUE
EMASTR=(PT*A*A*GAMC+PS*A*A*GAMS+BD*GAMB)/QD
Z1=U2+(RK-1)*U1
Z2=U3+(RK-1)*U2
QZ=Z2+Q2*Z1
ALJ=2.0*ES*3.14159265*B*TS/(SJ*RLNTH)
AJ=1./(1.+ALJ)
P7=ALPHAT*(TEMPT-TEMPA)-ALPHAS*(TEMPS-TEMPA)+(PSYS*PS-PSYT*PT)/ET
XIS=6.28319*B*ES*TS/(NT*ET*AT)
X1=.5*AJ*XIS*XA(I)**4*Z1*EMASTR+.5*(PS-PT)*A*A*(RK*RK-1)
X2=QZ*XA(I)**4/2.
AVA=(A*RK*ES*TS*AJ*P7-X1)/(1.+AJ*XIS*X2)
AMA=Q2*AVA+EMASTR
AMRMAX(I)=0.0
AMTMAX(I)=0.0
DO 500 J=1,101
AMR(J,I)=AVA*QV(J,I)+AMA*QM(J,I)
IF(J.EQ.1) GO TO 555
X=XA(I)*FLOAT(J-1)/FLOAT(100)
AMT(J,I)=ANUSTA*AMR(J,I)+(1.0-ANUSTA**2)*XA(I)/X
& * (AMA*QMT(J,I)+AVA*QVT(J,I))
555 IF(J.EQ.1) AMT(J,I)=AMR(J,I)
IF(ABS(AMR(J,I)).GE.AMRMAX(I)) GO TO 400
GO TO 450
400 AMRMAX(I)=ABS(AMR(J,I))
XR(I)=XA(I)*FLOAT(J-1)/FLOAT(100)
JR=J
450 IF(ABS(AMT(J,I)).GE.AMTMAX(I)) GO TO 460
GO TO 500

```

```

460  AMTMAX(I)=ABS(AMT(J,I))
      XT(I)=XA(I)*FLOAT(J-1)/FLOAT(100)
      JT=J
500  CONTINUE
C THE OUTERMOST TUBE LOAD:
600  RROA=FLOAT(JR-1)/FLOAT(100)
      RTOA=FLOAT(JT-1)/FLOAT(100)
      WT=-PITCH*PITCH*SIN(THETA)*(PT*FT-PS*FS
& +AVA*((XA(I)**4)/(A*A))*(Q2*U2+U3)+EMASTR*U2)
      STUBE=WT/(0.7854*(D**2-(D-2.0*T)**2))
C TUBESHEET EDGE SHEAR STRESS:
      SSHR=AVA/(EFS*HH*A)
C THE MAXIMUM RADIAL BENDING STRESS OF TUBESHEET:
      SRTS=6.0*AMRMAX(I)/(EFS*HH*HH)
C THE MAXIMUM CIRCUMFERENTIAL BENDING STRESS OF TUBESHEET:
      STTS=6.0*AMTMAX(I)/(EFS*HH*HH)
C THE LONGITUDINAL SHELL STRESS:
      SS=(2.0*AVA/A+PS*A*((RK**2)-1.0)+A*PT)/(2.0*TS*RK)
      SCS=PT*AC/(2.*TC)
C THE BENDING MOMENT IN THE SHELL (OR CHANNEL):
      PHYR=12.0*A/((ALOG(RKB)+AMU)*E*(HH**3))
& *((RK-1.0)*AVA-AMA+EMASTR*QD)
      AMBS+=2.0*BATAS*(ES*(TS*FRA)**3/10.91)*(1.0+BATAS*HH*0.5)*PHYR
      AMBS=AMBS+2*BATAS**2*PS*B**2*(FRA*TS)**2/10.91
      IF(NST.EQ.0) AMBS=0.
      AMBC=-2*BATAC*DC*(1.+5*BATAC*HH)*PHYR
      AMBC=AMBC+2*BATAC**2*PT*AC**2*(FRA*TC)**2/10.91
      IF(NST.LT.2)AMBC=0.
      SBS=6.0*ABS(AMBS)/(TS*TS*FRA*FRA)
      SBC=6*ABS(AMBC)/(TC*TC*FRA*FRA)
      STOT=ABS(SS/FRA)+SBS
      STOTC=ABS(SCS/FRA)+SBC
      STRESS=STTS
      IF(SRTS.GE.STRESS) STRESS=SRTS
      PHYDG=PHYR*180.0/3.14159265
      HLOCS=TS*FRA
      HLOCC=TC*FRA
OUTPUT PRINTOUT
      WRITE(L,3000Q)(TITLE(K1),K1=1,20)
      WRITE(L,*)'-----INTERMEDIATE COEFFICIENTS-----'
      WRITE(L,*)'AMU=',AMU
      ELAMI=-1.414*XA(I)*Q2
      EFM1=AMRMAX(I)/(2.*ABS(AVA))
      WRITE(L,*)' LIMIT VALUES OF TEMA PARAMETERS'
      WRITE(L,*)' LAMDA=',ELAMI,' FM=(MA)MAX/(P*A*A)=' ,EFM1
      WRITE(L,*)' FQ=QZ*XA**4/2.=' ,X2
      WRITE(L,*)' '
      IF(NW.EQ.0) GO TO 800
      WRITE(L,*)'U1=',U1,' U2=',U2,' U3=',U3
      IF(NTYPE.EQ.1) GO TO 700
      WRITE(L,*)'QD=',QD,' Q2=',Q2
      GO TO 800
700  WRITE(L,*)'QD=',QD,' Q2=',Q2
      WRITE(L,*)'Z1=',Z1,' Z2=',Z2,' QZ=',QZ
      WRITE(L,*)'P7=',P7
800  WRITE(L,*)'-----RESULTS FOR TUBESHEET THICKNESS H=',HH,' ,SHELL THI

```

```

&CKNESS TS=' ,TS,' CHANNEL THICKNESS TC=' ,TC
WRITE(L,*)' LOCAL SHELL/CHANNEL THICKNESS AT JOINT=' , HLOCS,HLOCC
WRITE(L,*)' 1.5*SA=' ,SPRIM,' ; 1.5*OMEGA*SA=' ,SSEC
WRITE(L,*)' EDGE SUPPORT PARAMETER NST=' ,NST
WRITE(L,*)' AVA=' ,AVA,' ; MA=' ,AMA
WRITE(L,*)' MAXIMUM RADIAL BENDING MOMENT,AMRMAX=' ,AMRMAX(I),' ,AT X
&=' ,XR(I),' ; R/A=' ,RROA
WRITE(L,*)' RADIAL BENDING MOMENT DISTRIBUTION:'
WRITE(L,*) (AMR(J,I),J=NS,NF,NP)
WRITE(L,*)' MAXIMUM RADIAL BENDING STRESS,SRTS=' ,SRTS
WRITE(L,*)' MAXIMUM CIRCUMFERENTIAL BENDING MOMENT,AMTMAX=' ,AMTMAX(
&I),' ,AT X=' ,XT(I),' ; R/A=' ,RTOA
WRITE(L,*)' CIRCUMFERENTIAL BENDING MOMENT DISTRIBUTION:'
WRITE(L,*) (AMT(J,I),J=NS,NF,NP)
WRITE(L,*)' MAXIMUM CIRCUMFERENTIAL BENDING STRESS,STTS=' ,STTS
WRITE(L,*)' MAX.TUBESHEET STRESS,STRESS=' ,STRESS
WRITE(L,*)' OUTERMOST TUBE TENSILE LOAD,STRESS=' ,WT,STUBE
WRITE(L,*)' LONGITUDINAL SHELL STRESS,SS=' ,SS
WRITE(L,*)' EDGE BENDING STRESS IN SHELL,SBS=' ,SBS
WRITE(L,*)' EDGE BENDING STRESS IN CHANNEL,SBC='
1,SBC
WRITE(L,*)' TOTAL LONGITUDINAL SHELL STRESS,STOT=' ,
&STOT
WRITE(L,*)' TOTAL LONGITUDINAL HEAD STRESS=' ,STOTC
WRITE(L,*)' SHEAR STRESS AT EDGE,SSHR=' ,SSHR
WRITE(L,*)' TUBESHEET RING ROTATION,PHYR=' ,PHYDG,' (DEGREE.)'
WRITE(L,*)
8000 CONTINUE
1000 CONTINUE
IF(NTST.NE.1) GO TO 4000
WRITE(6,*)' INPUT NEW HH,TS,TC,FRA,SJ;OR INPUT -1/ '
C FOLLOWING VALUE OF XA(1) IS REALLY A NEW SHEET THICKNESS.
READ(5,*)XA(1),TS,TC,FRA,SJ
IF(XA(1).EQ.-1.0) GO TO 4000
NXA=0
DO 20000 I=1,5
WRITE(L,*)
20000 CONTINUE
GO TO 10000
4000 WRITE(L,*)
WRITE(6,*)' IF NEED AN "TEMA" TUBESHEET THICKNESS,INPUT "1";'
WRITE(6,*)' IF NOT,INPUT "0".'
READ(5,*) NEED
IF(NEED.EQ.0) GO TO 9000
WRITE(6,*)' INPUT ASSUMED TUBESHEET THICKNESS,HHA,TO START TRIAL:'
READ(5,*) HHA
C COMPUTE TUBESHEET THICKNESS USING TEMA METHOD FOR COMPARISON.
C (1) EQUIVALENT DIFFERENTIAL EXPANSION PRESSURE:PD
WRITE(L,*)'-----TEMA RESULT FOR TUBESHEET THICKNESS-----'
NSTEP=1
DO=2.0*B+2.0*TS
IF(SJ.GT.9900.0*ES) GO TO 1010
IF(SJ.LT.(DO-TS)*TS*ES/(10.0*RLENTH)) GO TO 1020
AJ=1.0/(1.0+(3.14159265*TS*ES*(DO-TS))/(SJ*RLENTH))
GO TO 1030
1010 AJ=1.0

```

```

GO TO 1030
1020 AJ=0.0
1030 RATSID=TS/(2.0*B)
C FOR FLOATING HEAD AND FIXED TUBESHEET EXCHANGER
IF(RATSID.LT.0.02) GO TO 1040
IF(RATSID.LT.0.05) GO TO 1050
F=0.8
GO TO 1200
1040 F=1.0
GO TO 1200
1050 F=1.0-(RATSID-0.02)*0.2/0.03
GO TO 1200
1200 AK=ES*TS*(DO-TS)/(ET*T*NT*(D-T))
G=2.0*B
2000 FQ=0.25+(F-0.6)*((300.0*TS*ES*((G/HHA)**3)/(AK*RLNTH*E))**0.25)
IF(FQ.LT.1.0) FQ=1.0
PD=4.0*AJ*ES*TS*(ALPHAS*(TEMPSO-TEMPA)-ALPHAT*(TEMPTO-TEMPA))/
& ((DO-3.0*TS)*(1.0+AJ*AK*FQ))
PBT=0.
PBS=0.
C (3) EFFECTIVE SHELLSIDE DESIGN PRESSURE:PEFCS
FS=1.0-FLOAT(NT)*((D/G)**2)
PSE=PSO*(0.4*AJ*(1.5+AK*(1.5+FS))-(((1.0-AJ)/2.0)*((DJ*DJ)/(G*G))
& -1.0))/((1.0+AJ*AK*FQ))
P1=ABS((PSE-PD)/2.0)
P2=ABS(PSE)
P3=ABS(PBS)
P4=ABS((PSE-PD-PBS)/2.0)
P5=ABS((PBS+PD)/2.0)
P6=ABS(PSE-PBS)
PEFCS=AMAX1(P1,P2,P3,P4,P5,P6)
C (4) EFFECTIVE TUBESIDE DESIGN PRESSURE:PEFCT
FT=1.0-FLOAT(NT)*(((D-2.0*T)/G)**2)
IF(HHA.EQ.-1.0) WRITE(L,*)'HHB=',HHB,' PCT=',PCT,'%.'
IF(HHA.EQ.-1.0) GO TO 1500
PTE=PTO*(1.0+0.4*AJ*AK*(1.5+FT))/((1.0+AJ*AK*FQ))
IF(PSE.LT.0.0) GO TO 1300
P1=ABS((PTE+PBT+PD)/2.0)
P2=ABS(PTE+PBT)
PEFCT=AMAX1(P1,P2)
GO TO 1400
1300 P1=ABS((PTE-PSE+PBT+PD)/2.0)
P2=ABS(PTE-PSE+PBT)
PEFCT=AMAX1(P1,P2)
C (5) EFFECTIVE DIFFERENTIAL DESIGN PRESSURE:PEDF
1400 P1=ABS(PTE-PSE+PBT)
P2=ABS((PTE-PSE+PBT+PD)/2.0)
P3=ABS(PBS)
P4=ABS((PBS+PD)/2.0)
P5=ABS(PTE-PSE)
P6=ABS((PTE-PSE+PD)/2.0)
P7=ABS(PBT)
PEDF=AMAX1(P1,P2,P3,P4,P5,P6,P7)
C DESIGN PRESSURE
PPP=AMAX1(PEFCS,PEFCT,PEDF)
IF(NTYPE.EQ.0)PPP=ABS(PT-PS)

```

```

WRITE(6,*)'PS,PT,PDIF,PDESIGN=',PEFCS,PEFCT,PEDF,PPP
IF(NSTEP.EQ.1) GO TO 1450
GO TO 1550
C (6) TUBESHEET THICKNESS----BENDING FORMULA
1450 HHB=0.5*F*G*(SQRT(PPP/SALL))
      IF(NTYPE.EQ.0) GO TO 1500
      PCT=(HHB-HHA)*100.0/HHA
      IF(ABS(PCT).LT.1.5)WRITE(6,*)'HBEND=',HHB
      IF(ABS(PCT).LT.1.5)WRITE(L,*)'HBEND=',HHB
      IF(ABS(PCT).LT.1.5) GO TO 1500
      WRITE(6,*)'BENDING PCT,',PCT,'% IS LARGER THAN THE ALLOWABLE 1.5
& %.'
      WRITE(6,*)'TRY A NEW THICKNESS,HHA,AGAIN.'
      WRITE(6,*)'INPUT A NEW HHA,OR INPUT -1/ TO STOP TRIAL.'
      READ(5,*) HHA
      IF(HHA.EQ.-1.0) WRITE(6,*)'HHB=',HHB,' PCT=',PCT,'%.'
      IF(HHA.EQ.-1.0) GO TO 9000
      GO TO 2000
C (7) TUBESHEET THICKNESS----SHEAR FORMULA
1500 CON=1.6*(1.0-D/PITCH)**2
      IF(PPP/SALL.LT.CON) GO TO 1600
      DL=4.0*AREA/PERIMT
1550 HHS=0.31*DL*(PPP/SALL)/(1.0-D/PITCH)
      IF(NTYPE.EQ.0) GO TO 1560
      PCT=(HHS-HHA)*100.0/HHA
      IF(ABS(PCT).LT.1.5)WRITE(6,*)'HSHR=',HHS
      IF(ABS(PCT).LT.1.5)WRITE(L,*)'HSHR=',HHS
      IF(ABS(PCT).LT.1.5) GO TO 1560
      WRITE(6,*)'SHEAR PCT,',PCT,'% IS LARGER THAN THE ALLOWABLE 1.5
& %.'
      WRITE(6,*)'TRY A NEW THICKNESS,HHA,AGAIN.'
      WRITE(6,*)'INPUT A NEW HHA,OR INPUT -1/ TO STOP TRIAL.'
      READ(5,*) HHA
      IF(HHA.EQ.-1.0) WRITE(6,*)'HHS=',HHS,' PCT=',PCT,'%.'
      IF(HHA.EQ.-1.0) GO TO 9000
      NSTEP=2
      GO TO 2000
1560 CONTINUE
      IF(HHS.LT.HHB) GO TO 1600
      WRITE(6,*)'TEMA RESULT:SHEAR CONTROL THICKNESS,HHS=',HHS
      WRITE(L,*)'TEMA RESULT:SHEAR CONTROL THICKNESS,HHS=',HHS
      GO TO 9000
1600 WRITE(6,*)'TEMA RESULT:BENDING CONTROL THICKNESS,HHB=',HHB
      WRITE(L,*)'TEMA RESULT:BENDING CONTROL THICKNESS,HHB=',HHB
9000 STOP
      END
      SUBROUTINE BESSEL(XP,BERO,BER1,BER2,BE10,BE11,BE12)
      DIMENSION G(4),A(4),B(4),C(4)
      X=XP/2.0
      X4=X**4
      F=1.0
      DO 100 J=1,4
100 G(J)=0.0
      DG 200 I=1,51,2
      K=I-1
      CALL CALC(K,A,F)

```

```

F=F*(2.0*FLOAT(K)+1.0)*(2.0*FLOAT(I))
CALL CALC(I,B,F)
DO 300 J=1,4
X55=1.0
IF(K.GT.0) X55=X4**K
C(J)=X55*(A(J)-X4*B(J))
300 G(J)=C(J)+G(J)
DO 301 J=1,4
301 C(J)=ABS(C(J))/G(J)
IF(AMAX1(C(1),C(2),C(3),C(4)).LT.0.00001) GO TO 400
200 F=F*(2.0*FLOAT(I)+1.0)*(2.0*FLOAT(I)+2.0)
400 BERO=G(1)
BER1=-G(2)*(X**3)
BEI0=G(3)*X*X
BEI1=X*G(4)
IF(XP.LT.1.0E-6) GO TO 500
BER2=-BEI0-BER1/XP
BEI2=BER0-BEI1/XP
GO TO 600
500 BER2=0.0
BEI2=0.5
600 CONTINUE
RETURN
END

C
C
C
C
C

SUBROUTINE CALC(K,A,F)
DIMENSION A(4)
A(1)=1.0/(F**F)
A(2)=2.0*(FLOAT(K)+1.0)/((F*(2.0*FLOAT(K)+1.0)
& *(2.0*FLOAT(K)+2.0))**2)
A(3)=1.0/((F*(2.0*FLOAT(K)+1.0))**2)
A(4)=(2.0*FLOAT(K)+1.0)*A(3)
RETURN
END

```

APPENDIX 9.D

BASIC COMPUTER CODE MICRO-FIXFLOAT FOR SIMPLIFIED CALCULATION OF TUBESHEET THICKNESS

User Information:

User inputs FT or FH depending on unit type (fixed or floating head).

User inputs tubesheet support parameter 0,1,2

User also decides whether to include effect of M_a^*

ES,E,ET,EC = Young's modulus of shell, tubesheet, tubes, channel, respectively

HS, HC = shell and channel thickness

L	= tube length between tubesheets
NT	= number of tubes
TOD,HT	= tube O.D., thickness
J	= expansion joint coefficient as defined by TEMA (Read in 1 or 0. Read in 1 if floating head unit)
SA	= ASME code allowable stress for tubesheet material
AS,AT	= coefficient of thermal expansion for shell, tube material, respectively
TS,TT	= temperature rise above ambient for shell, tube metal, respectively
PS,PT	= shellside, tubeside pressures
B,A,RC,R1	= radii b, a, a_c, a_1 , from Figs. 9.7.1–9.7.3
SE	= stress efficiency (set this value equal to ligament efficiency calculated on basis of % roll, materials, etc.)
FE	= flexural efficiency e calculated from Figs. 8.1.1, 8.1.2
BL,D	= Bolt line load, bolt circle radius

- ** If $B < 0$, program ends
 If $B = 0$, program returns to first line of input data requested.

Use of this code requires input of graphical data from Figs. 9.8.1–9.8.4 when prompted.

LISTING OF "MICRO-FIXFLOAT"

```

10 CLS:LPRINT:LPRINT
20 PRINT"DIRECT SOLUTION OF TUBESHEET EQUATIONS":INPUT READ IN TYPE 'FT'(FIXED
TUBESHEET UNIT) OR 'FH'(STATIONARY TUBESHEET OF A FLOATING HEAD UNIT);F#
30 IF F#="FT" THEN PRINT"ASME FIXED TUBESHEET" ELSE PRINT"ASME STATIONARY TUBESH
EET IN FLOATING HEAD EXCHANGER"
40 IF F#="FH" THEN LPRINT"ASME FIXED TUBESHEET" ELSE LPRINT"ASME STATIONARY TUBE
SHEET IN FLOATING HEAD EXCHANGER"
50 PRINT"INPUT SUPPORT TYPE 0,1,2"
60 PRINT"TYPE=0 G/G"
70 PRINT"    #1 G/I"
80 PRINT"    #2 I/I"
90 INPUT "SUPPORT PARAMETER=";ZS
100 LPRINT" SUPPORT PARAMETER=";ZS
110 INPUT "IF MA(STAR) IS TO BE ZERO INPUT 0, ELSE INPUT 1";I
120 INPUT "READ IN ES,EC,E,ET";ES,EC,E,ET
130 INPUT"READ IN HS,HC,L,NT";HS,HC,L,NT
140 INPUT"READ IN TOD,HT,J,SA";TD,HT,J,SA
150 IF F#="FH" THEN GOTO 170
160 INPUT"READ IN AS,AT,TS,TT";AS,AT,TS,TT
170 INPUT"READ IN PS,PT";PS,PT:DP=- (PT-PS)
180 LPRINT"ES=";ES," E=";E," ET=";ET," EC=";EC
190 LPRINT"HS=";HS," L=";L," SA=";SA," HC=";HC
200 LPRINT"NT=";NT," TOD=";TD:LPRINT"HT=";HT
210 IF F#="FH" THEN GOTO 230
220 LPRINT"AS=";AS," AT=";AT:LPRINT"TENPS=";TS," TENPT=";TT
230 LPRINT"PSHELL=";PS," PTUBE=";PT
240 INPUT READ IN B,A,SE,FE";B,A,SE,FE
250 IF B<0 THEN END ELSE IF B=0 GOTO 120
260 INPUT"READ IN RC,R1";RC,R1
270 INPUT "READ IN BL,D";BL,D
280 LPRINT:LPRINT:LPRINT

```

```

290 IS=1:IC=1
300 IF ZS<2 THEN IC=0
310 IF ZS=0 THEN IS=0
320 U=1
330 LPRINT"B=";B,"A=";A,"SE=";SE,"FE=";FE
340 LPRINT"RC=";RC,"R1=";R1:LPRINT"BL=";BL,"D=";D
350 PI=3.14159:AA=PI*(TD-HT)*HT:C1=2*PI*B*ES*HS/(NT*ET*AA)
360 INPUT" READ IN TRIAL VALUE FOR H ";H
370 X4=48*.91*ES*HS/(C1*FE*E*L)*(A/H){3*B/A
380 XA=X4{.25
390 BS=(2.73){.25/(B*HS){.5
400 BC=(2.73){.25/(RC*HC){.5
410 DS=IS*ES*HS{3/10.92:DC=IC*EC*HC{3/10.91
420 MU=BS*B*DS*(1+BS*H+(BS*H){2/2.}
430 IF ZS=2 THEN MU=MU+BC*RC*DC*(1+BC*H+(BC*H){2/2)
440 IF ZS=0 THEN MU=0
450 KB=R1/A*KC=RC/A;K=B/A;MU=MU*24/(E*H*H*H)
460 LPRINT"K=";K,"KC=";KC,"KBAR=";KB:LPRINT"VALUE OF MU=";MU
470 PH=.91/FE*(MU+LOG(KB))
480 PRINT" XA=";XA,"PHI=";PH
490 INPUT" INPUT ZV FROM GRAPH";ZV:INPUT" INPUT ZM FROM GRAPH";ZM
500 QB=(K-1-PH*ZV)/(1+PH*ZM):PRINT"QBAR=";QB
510 REM CALCULATE MA(STAR) HERE *****
520 GS=(K*K-1)*(K-1)/4:IF ZS>0 THEN GS=GS-2*BS*BS*DS*(1+BS*H)*K*K/(ES*HS)
530 GC=(KC*KC-1)*(KC+1)/4-.5*(KC*KC*KC-K)
540 IF ZS=2 THEN GC=GC+2*BC*BC*DC*(1+BC*H)*KC*KC*KC/(EC*HC)
550 GB=0:IF ZS=1 THEN GB=KC-D/A
560 IF ZS=0 THEN GB=KC-K
570 MS=A{2*(PT*GC+PS*GS)+BL*D*GB:MS=MS/I/(1+PH*ZM)
580 REM CALCULATE PE *****
590 Z1=0:Z2=0:FQ=0:IF F#="FH" THEN GOTO700
600 INPUT"READ IN QZ1 FROM GRAPH";Z1:INPUT"READ IN QZ2 FROM GRAPH";Z2
610 QZ=Z1+(K-1)*Z2:FQ=QZ:Z3=1+J*C1:FQ:RH=ZV+(K-1)*ZM
620 QE=J*(AT*TT-AS*TS):IF QE=0 THEN U=1 ELSE U=2
630 A1=PI*A*A:AL=A1-(NT*PI*(TD-2*HT){2}/4.
640 AO=AL-NT*AA
650 LT=AL/(NT*AA)+.15*(TD-2*HT)/HT
660 LS=ES/ET*A1/(NT*AA)*AO/A1+.3*B/HS+.15*TD/HT*ES/ET
670 QE=QE+J*LS*PS/ES-PT/ET*(J*LT+ET*B/(2*ES*HS))
680 PE=B*ES*HS*QE-(PS-PT)*.5*A*A*(K*K-1)*I
690 PE=PE-.5*J*C1*X4*RH*MS:PE=PE/Z3*2/(A*A)
700 IF F#="FH" THEN PE=DP
710 VA=PE*A*A/2:QS=QB*MS/VA:PRINT"QBAR(STAR)=";QS
720 INPUT"READ IN VALUE FOR 2*FM FROM GRAPH";FX:FM=.5*FX
730 LPRINT" AVA=";VA:MA=VA*QB*MS:LPRINT" MA=";MA
740 LPRINT" FQ=";FQ," FM=";FM
750 SB=1.5*U*SA:SC=6*FM*PE*A*A/(SE*H*H)
760 PRINT" ALLOWABLE DESIGN STRESS=";SB
770 PRINT" CALCULATED TUBESHEET STRESS=";SC
780 INPUT" DO YOU WANT ANOTHER TRIAL? (Y/N)";Y#
790 IF Y#="N" THEN GOTO 800 ELSE GOTO 360
800 LPRINT" DESIGN STRESS =";SB
810 LPRINT" FOR XA=";XA," AND PHI=";PH
820 LPRINT" ZV=";ZV," ZM=";ZM
830 LPRINT" QZ1=";Z1," QZ2=";Z2
840 LPRINT" EFFECTIVE PRESSURE=";PE
850 LPRINT" ASSUMED THICKNESS=";H
860 LPRINT" THE FINAL TUBESHEET STRESS=";SC
870 PRINT"QBAR(STAR)=";QS:INPUT"USING NEW QBAR(STAR) INPUT NEW QZ1";Z1
880 INPUT"USING NEW QBAR(STAR) INPUT NEW QZ2";Z2
890 YQ=Z1*2*VA/(A*A):YR=2.*Z2*A*VA/(FE*E*H*H*H/10.92*X4{4
900 LPRINT"THE VALUE FOR Q(XA), THE TUBE EFF. PRESSURE=";YQ
910 LPRINT"THE VALUE FOR THETA(XA), THE RING ROTATION=";YR
920 MB=2*(1+BS*H/2)*BS*DS*YR+2*BS*BS*DS*(PS*B*B/(ES*HS))
930 IF ZS=0 THEN MB=0
940 MC=-2*(1+BC*H/2)*BC*DC*YR+2*BC*BC*DC*PT*RC*RC/(EC*HC)
950 IF ZS<2 THEN MC=0
960 SC=6*MC/(HC*HC):SS=6*MB/(HS*HS)
970 LPRINT"BENDING STRESS IN CHANNEL=";SC
980 LPRINT"BENDING STRESS IN SHELL=";SS
990 SL=(2*VA/A+PS*A*(K*K-1)+A*PT)/(2*HC*K)
1000 CL=PT*RC/(2*HC)
1010 LPRINT"LONGITUDINAL DIRECT SHELL STRESS=";SL
1020 LPRINT"LONGITUDINAL DIRECT CHANNEL STRESS=";CL
1030 FOR JJ=1T06:LPRINT:NEXT JJ:GOTO 240

```

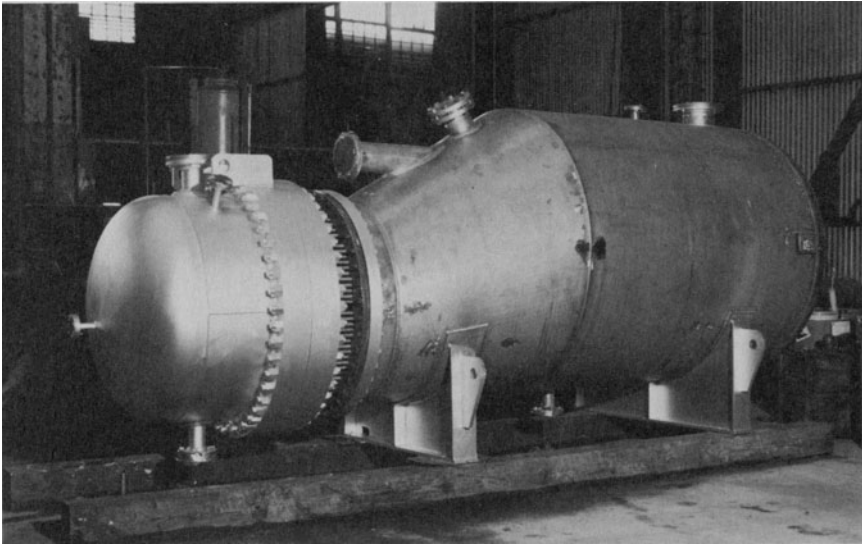
10. SPECIAL TUBESHEET CONSTRUCTION – DOUBLE TUBESHEET

10.1 INTRODUCTION

In many heat exchange applications, intermingling of shellside and tubeside fluids may cause undesirable results, not the least of which may be safety related. Therefore, prevention of any fluid leakage between shell side and tube side of shell and tube heat exchangers becomes a prime design consideration. One method to inhibit mixing of component fluids is to employ double tubesheet construction. Double tubesheet construction has been used in submarine systems primarily for safety reasons. In commercial applications, double tubesheet designs in standard heat exchangers have been used for a variety of reasons, such as the case where mixing of shell and tube side streams could lead to an explosive mixture. In recent years, double tubesheet construction has also been found in large power plant condensers. In the condenser application to large rectangular tubesheets, the primary concern has been prevention of contamination of treated and demineralized water due to the leakage of circulating water (raw water) into the condenser steam space.

The double tubesheet configuration consists basically of two tubesheets, which may be closely spaced, at either or both ends of the exchanger, connected to each other by the tubing. The two tubesheets can have different edge conditions, and may be close enough to act together as a single “sandwich” plate under mechanical and thermal loading. This configuration may be employed in U-tube exchangers, floating head units, or in fixed tube construction. Photograph 10.a shows a double tubesheet in a kettle reboiler. In certain applications, the gap between the two closely spaced tubesheets may be enclosed and filled with a non-reacting fluid at a slightly higher pressure than either the shell side or tube side streams. In this case, tube joint leakage in either tubesheet causes leakage of nonreacting fluid *into* either the shell side or tube side.

Previous chapters of this text have been concerned with analysis of single tubesheets in fixed, U-tube, and floating head types of heat exchanger construction. Tubesheet design for stress in single tubesheet construction is governed either by mechanical loading alone, or by a combination of mechanical and thermal loading. The thermal loading considered heretofore occurs in fixed tubesheet heat exchangers and induces bending in the tubesheet due to differential thermal growth between the tubes and the shell wall along the length of the unit; the critical design stress in the



Photograph 10.a. Double tubesheet construction in a kettle reboiler. (Courtesy Joseph Oat Corporation, Camden, N.J.)

tubesheet is caused by tubesheet bending alone. In a double tubesheet construction, in addition to the usual thermal loading, a new thermal condition arises due to in-plane differential thermal loading of the two tubesheets. This differential radial expansion of the adjacent tubesheets can be caused by the two tubesheets having different coefficients of thermal expansion and/or different mean metal temperatures. Depending on the restraint provided against radial growth at the outer edge, membrane stresses as well as bending stresses can arise in the tubesheets. The tube bundle, between the two tubesheets, induces coupling between out-of-plane bending and direct radial expansion of the two tubesheets. Therefore, in contrast to the single tubesheet analyses examined previously, any double tubesheet analysis must encompass both tubesheet bending and tubesheet radial growth. The key design quantities of interest are not only tubesheet stress and axial stress in the tubing, but additionally, tube bending and shear stress in the portion of the tube bundle between the two closely spaced tubesheets. These last items are generally most affected by the gap between the two tubesheets.

Because of the presence of two tubesheets, and the consequential coupling between bending and radial expansion, this configuration is amenable to solution only by computer analysis.

This chapter presents a complete formulation of the governing equations for two closely spaced fully perforated double tubesheets. A computer code is developed based on a direct integration of the governing equations. Typical numerical results are presented to show the influence of various

loadings on the system behavior. Because of the character of the solution technique used, the method fails when the gap/tubesheet diameter ratio becomes very small. To overcome this problem, the second part of this chapter focuses on a special purpose finite element computer code complete with pre and post-processors to study the double tubesheet problem when the gap between tubesheets is small enough to consider only shear and extension in the tubes. As a by-product of the finite element code, the effect of shear deformation on a single thick tubesheet can also be studied quite efficiently. Therefore, this chapter will also present some results for single tubesheets which clarify the accuracy of the thin plate theories (used in Chapters 8 and 9) when applied to configurations where shear deformation and non-classical stress distributions through the tubesheet thickness may be of some importance.

10.2 FORMULATION OF THE DOUBLE TUBESHEET EQUATIONS

Figure 10.2.1 shows the double tubesheet configuration to be modelled. We assume that only one half of the heat exchanger need be modelled, and hence, only one pair of tubesheets requires a detailed analysis.

Prior to beginning the detailed analysis with all couplings included, it is appropriate to briefly note a simplified approach to the development of a method to choose the spacing L between tubesheets. As mentioned above, the gap spacing L strongly influences the tube bending and shear stress induced by differential radial growth of the two tubesheets. For the moment, if we assume that the tubesheets do not bend, but simply grow radially by different amounts due to thermal action, then a simple relation between the stress, the thermal loading, and the gap length L can be

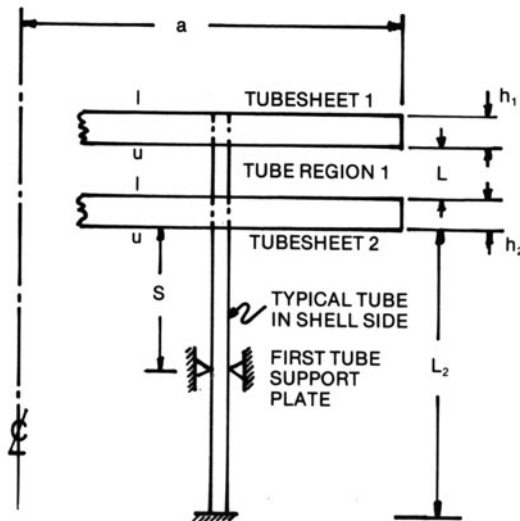


Fig. 10.2.1. Double tubesheet configuration.

developed by focusing attention on a single tube, treated as a guided cantilever beam, undergoing a differential end displacement Δ . For a thin walled tube, treated as a beam of length L , subject to zero end rotations, and to displacement Δ at one end, we can derive the following relationship [10.2.1].

$$L = \left[\frac{3E_T d \Delta}{\sigma_A} \right]^{1/2} \quad (10.2.1)$$

In Eq. (10.2.1), E_T = tube Young's Modulus, d = tube outer diameter, σ_A = allowable stress of tube material in tension, and $\Delta = |\alpha_1 T_1 - \alpha_2 T_2| l$. In the foregoing, Δ represents the unrestrained differential in-plane thermal movement between the tubesheets that induces lateral tube flexure, α_i ($i = 1, 2$) are thermal expansion coefficients of the two tubesheet materials, and T_i are the respective temperature changes above the unit assembly temperature. The length l is the characteristic length over which unrestrained radial thermal expansion of the tubesheet occurs; in the case shown in Fig. 10.2.1, $l = a$. Application of the above equation is reasonable when the resulting L is such that $d/L \ll 0.1$. Choice of the gap length L , while fixing the tube bending moment, does not yield any information about stress in the tubesheet and therefore cannot be touted as a complete design method. In addition, the application of the above equation to large units generally results in gap spacings in excess of 10 inches. This large gap can lead to alignment problems during assembly, and unit costs may be increased because of excess tubing which does not contribute to heat transfer capacity. The cost penalty is significant when expensive, corrosive resisting tube materials are used.

It has been suggested [10.2.1] that the above problems may be reduced or eliminated by decreasing the gap L between tubesheets. Reducing the gap, however, requires appropriate design procedures which accurately account for tubesheet interaction, for effects of tube and tubesheet shear as well as bending, and for all mechanical and thermal loadings. Formulations of the double tubesheet problem, which include interaction between adjacent tubesheets, have been presented in the literature; representative of these are References [10.2.2, 10.2.3]. However, the formulation in [10.2.2] becomes suspect for smaller gap length L since tube shear deformation has been neglected. The following sections focus on the development of the complete field equations for closely spaced double tubesheets which, in theory, can treat problems involving both large and small gap spacings. The work to be discussed closely follows an ASME paper. [10.2.4].

10.3 THEORETICAL ANALYSIS OF DOUBLE TUBESHEET CONSTRUCTION USING PLATE THEORY

In this section, we outline the development of the field equations governing the double tubesheet behavior. We begin with the equations of classical plate theory as presented in Appendix A at the end of the text, and

extend the analysis to two coupled tubesheets. Axisymmetric loading and geometry is assumed herein in keeping with accepted tubesheet design practice. The local effects of the perforation array are replaced by effective stress and flexural efficiency factors as has been done in previous chapters. We also assume that both tubesheets are fully perforated. Figure 10.3.1 shows an element of one of the tubesheets with all force and moment resultants acting. N_r , M_r , V , N_θ , M_θ are the stress resultants used in a classical plate analysis, while τ , q , m are surface loadings defined with appropriate subscripts to reflect their surface of application.* These surface loadings on either tubesheet reflect the effect of applied external loading and the effect of the tube bundle. Note that in contrast to previous analyses in this text, the effect of tube shear and tube rotation on tubesheet response is included in the analysis. In previous chapters, only the elastic foundation effect of the tubes acting in tension and compression was accounted for in the analysis. This led to q being the only surface loading acting on the tubesheet. Here, we include the effect of tube end moments (which leads to a surface moment m on the tubesheets), and the effect of tube end shear force (which leads to a surface shear τ loading on the tubesheet).

Our procedure in this chapter will be to write equilibrium and constitutive equations for each of the tubesheets being modelled. We will then consider equilibrium equations for the tube regions and we will show how the tube bundle couples the behavior of the two tubesheets through the requirement for compatibility at the tube-tubesheet joint. It will also become clear as to why we need to consider in-plane expansion of the tubesheets as well as the familiar bending components. The result of all of our development will be a set of equations governing the spatial distribution of twelve variables characterizing the behavior of the configuration.

We first write down the classical equilibrium equations for a plate element. The force and moment equilibrium equations for either of the two tubesheets described by Fig. 10.3.1 are written as ($i = 1, 2$):†

$$\frac{dV_i}{dr} + \frac{V_i}{r} = q_{ui} + q_{li} \quad (10.3.1a)$$

$$\frac{dN_{ri}}{dr} + \frac{N_{ri} - N_{\theta i}}{r} + \tau_{li} - \tau_{ui} = 0 \quad (10.3.1b)$$

$$\frac{dM_{ri}}{dr} + \frac{M_{ri} - M_{\theta i}}{r} + V_i - \left\{ m_{ui} + m_{li} + \frac{h_i}{2} [\tau_{ui} + \tau_{li}] \right\} = 0 \quad (10.3.1c)$$

A detailed development of these equations may be found in Appendix A and in [10.3.1, 10.3.2]. The usual displacement assumptions for thin plate theory, including shear effects, are employed herein. The radial

* l and u surfaces are indicated in Fig. 10.2.1

† Subscript “ i ” is appended to the field quantities to indicate that they pertain to tubesheet i ($i = 1, 2$) in Fig. 10.2.1

displacement U_{ri} and the lateral displacement U_{zi} for each tubesheet are taken as ($i = 1, 2$):

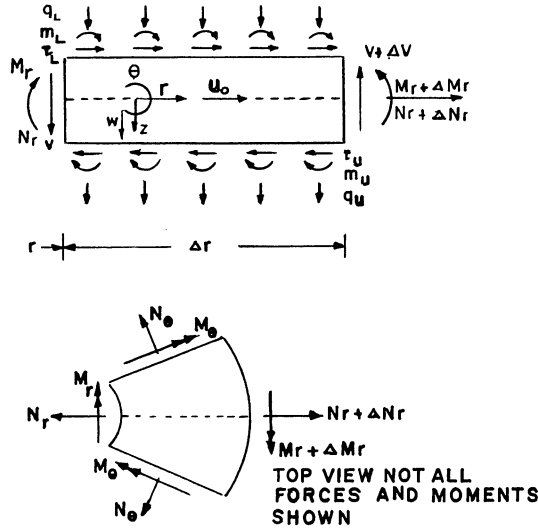


Fig. 10.3.1. Tubesheet free body diagram.

$$\begin{aligned}
 U_{ri}(r, z) &= U_{oi}(r) + z\theta_i(r) \\
 U_{zi}(r, z) &= W_i(r)
 \end{aligned}
 \tag{10.3.2}$$

If we start from Hooke’s law relating radial and circumferential stresses to radial and circumferential total and thermal strains, we can average the equations through the thickness of the plate, and evolve a set of constitutive equations relating forces and moments $N_r, M_r, N_\theta, M_\theta$ to deformation variables U_o, θ, W . Appendix A* illustrates this averaging procedure for a typical plate element. For the circular plate element of interest here, we obtain

$$\begin{aligned}
 \frac{dU_{oi}}{dr} &= -\nu_i \frac{U_{oi}}{r} + \frac{N_{ri} + N_i^*}{K_i} \\
 \frac{d\theta_i}{dr} &= -\nu_i \frac{\theta_i}{r} + \frac{M_{ri} + M_i^*}{D_i}
 \end{aligned}
 \tag{10.3.3}$$

$$\begin{aligned}
 N_{\theta i} &= E_i h_i \frac{U_{oi}}{r} + \nu_i N_{ri} - N_i^*(1 - \nu_i) \\
 M_{\theta i} &= \frac{E_i h_i^2}{12} \frac{\theta_i}{r} + \nu_i M_{ri} - M_i^*(1 - \nu_i)
 \end{aligned}$$

*Appendix A follows Chapter 22 in this book.

In Eq. (10.3.3), the following quantities have been defined following Appendix A:

$$\begin{aligned}
 N_i^* &= \frac{E_i \alpha_i}{1 - \nu_i} \int_{-0.5h_i}^{0.5h_i} T_i(r, z) dz; & M_i^* &= \frac{E_i \alpha_i}{1 - \nu_i} \int_{-0.5h_i}^{0.5h_i} z T_i(r, z) dz \\
 K_i &= \frac{E_i h_i}{1 - \nu_i^2}; & D_i &= \frac{K_i h_i^2}{12}
 \end{aligned}
 \tag{10.3.4}$$

E_i, ν_i, α_i are the effective Young’s Modulus, Poisson’s Ratio, and coefficient of thermal expansion for the tubesheet, and $T_i(r, z)$ is the temperature distribution in the tubesheet.

The familiar equation relating plate shear force and averaged shear strain for a plate is used here to provide the relations between the lateral deformation and the plate rotation. For $i = 1, 2$, we have

$$\frac{dW_i}{dr} = -\theta_i - \frac{6}{5} \frac{V_i}{G_i h_i}
 \tag{10.3.5}$$

where G_i is the shear modulus of the i th tubesheet.

Equation (10.3.5) involves an arbitrary introduction of the factor $6/5$ to reflect shear deformation effects in plates. The neglect of shear deformation in the tubesheets can be accommodated by simply setting the shear modulus $G_i = \infty$ in Eq. (10.3.5). Note that inclusion of the shear deformation effect means that the cross section rotation θ is different from the centerline slope dW/dr .

The surface loadings τ, q, m involve the applied pressures in the three regions of interest shown in Fig. 10.2.1, and also provide the mechanism for coupling the response of the two tubesheets. Figure 10.3.2 shows a typical deformed tube with force, moment, and kinematic variables defined. Reference [10.3.3] presents a stiffness matrix for a beam (tube) which includes the effect of shear deformation. It is shown there that the relation between end force resultants and kinematical quantities arising due to beam (tube) bending can be written in the matrix form:

$$\begin{bmatrix} H_{1T} \\ M_{1T} \\ H_{2T} \\ M_{2T} \end{bmatrix} = \gamma [K_T] \begin{bmatrix} \bar{V}_1 \\ \psi_{11} \\ \bar{V}_2 \\ \psi_{12} \end{bmatrix}
 \tag{10.3.6}$$

where

$$\gamma = \frac{2E_T I_T / L^3}{1 + 12g / L^2}; \quad g = 2E_T I_T / G_T A_T
 \tag{10.3.7}$$

and the stiffness matrix $[K_T]$ has the form:

$$[K_T] = \begin{bmatrix} 6 & 3L & -6 & 3L \\ 3L & 2L^2(1+3g/L^2) & -3L_T & L^2(1-6g/L^2) \\ -6 & -3L & 6 & -3L \\ 3L & L^2(1-6g/L^2) & -3L & 2L^2(1+3g/L^2) \end{bmatrix}$$

(10.3.8)

E_T , G_T , I_T , A_T , are the tube Young's modulus, shear modulus, metal moment of inertia, and metal area, respectively. Considering the tube as a beam described by the above matrix relation, we can represent the effect of the tubing between the two tubesheets in Fig. 10.2.1 by relating resultants H_{iT} , M_{iT} , to τ , m , q , and by relating \bar{V} , ψ to tubesheet deformation variables.

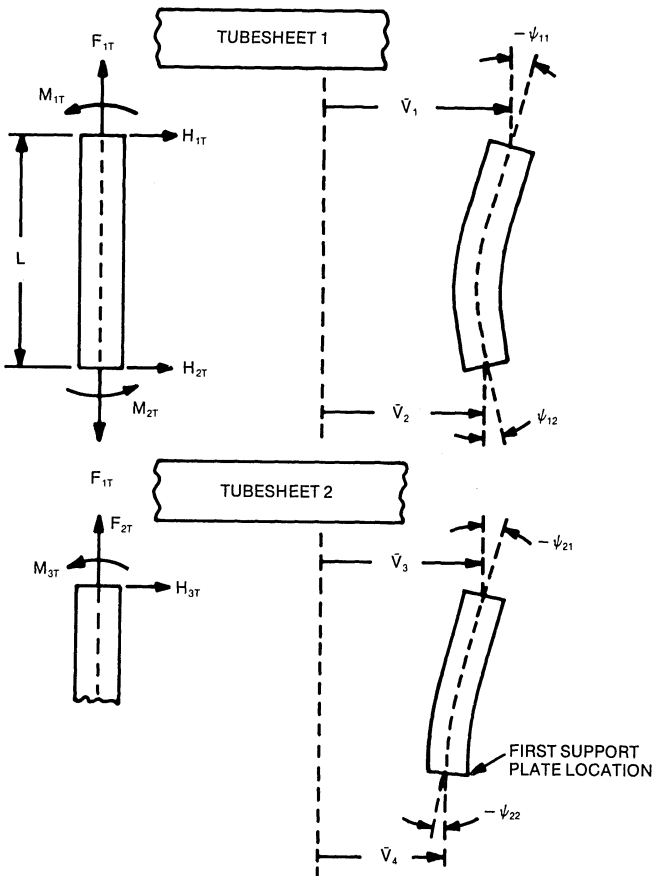


Fig. 10.3.2. Tube free body diagram.

The effect of the tubing on the shell side of the assemblage is represented by shear force and bending moment H_{3T} , M_{3T} , Eqs. (10.3.6)–(10.3.8) hold also for the shell side tubing (with appropriate notation changes), although we may neglect the tube shear deformation in that area. We let the length of shell side tubing considered for bending effects, be S , the span to the first support plate; if we assume that $\bar{V}_4 = 0$ (see Fig. 10.3.2), the following relations are obtained by manipulating Eqs. (10.3.6)–(10.3.8) applied to the shell side tubing.

$$H_{3T} = \frac{2E_T I_T}{S^3} (6\bar{V}_3 + 3S[\psi_{21} + \psi_{22}]) \quad (10.3.9)$$

$$M_{3T} = \frac{2E_T I_T}{S^3} (3S\bar{V}_3 + S^2[2\psi_{21} + \psi_{22}]) \quad (10.3.10)$$

We now assume that $\psi_{22} = a\bar{V}_3 + b\psi_{21}$ where a , b are constants chosen to reflect the presence of the remaining cross baffles not modelled in Fig. 10.2.1. Reference [10.3.4] shows that if we now consider a hypothetical configuration where $\bar{V}_3 = 0$, then a separate theoretical development leads to

$$M_{3T} = \frac{F_n E_T I_T}{S} \psi_{22}; \quad (3 \leq F_n \leq 4) \quad (10.3.11)$$

where F_n is a function of the number of baffles and of the baffle spacing. Comparing Eq. (10.3.10) (with $\bar{V}_3 = 0$ and $\psi_{22} = \psi_{22}(\bar{V}_3, \psi_{21})$) with Eq. (10.3.11) leads to the result

$$b = (F_n/2) - 2$$

Since the matrix $[K^*]$ defined by the equations

$$\begin{Bmatrix} H_{3T} \\ M_{3T} \end{Bmatrix} = [K^*] \begin{Bmatrix} \bar{V}_3 \\ \psi_{21} \end{Bmatrix} \quad (10.3.12)$$

and implied by Eqs. (10.3.9)–(10.3.10), must be symmetric, then the remaining parameter a is given as

$$a = 3b/S$$

and the matrix $[K^*]$ is given as:

$$[K^*] = \frac{2E_T I_T}{S^3} \begin{bmatrix} \frac{9}{2}F_n - 12 & 3S\left(\frac{F_n}{2} - 1\right) \\ 3S\left(\frac{F_n}{2} - 1\right) & \frac{F_n}{2} S^2 \end{bmatrix} \quad (10.3.13)$$

Examination of Figs. 10.3.1, 10.3.2 shows that the tube deformation variables are related to the kinematic variables describing tubesheet deformation by the following expressions:

$$\begin{aligned}\bar{V}_1 &= U_{01} + (h_1/2)\theta_1; & \bar{V}_2 &= U_{02} - (h_2/2)\theta_2 \\ \bar{V}_3 &= U_{02} + (h_2/2)\theta_2; & \psi_{11} &= -\frac{dW_1}{dr} \\ \psi_{12} &= \psi_{21} = -\frac{dW_2}{dr}\end{aligned}\quad (10.3.14)$$

It is clear from the above relations that we have assumed that the tube and the tubesheets have equal displacement values at the respective tubesheet surfaces. Also, we have assumed that a tube cross section remains perpendicular to the tubesheet mid-surface. Finally, note that we make no attempt to model the effects of the tube within the tubesheet.

The previous analysis of the tubing serves to describe the effect of tube shear and bending in the two tubed regions of interest. The effect of tube stretching, giving rise to tube axial forces F_{1T} , F_{2T} , leads to the following ‘‘elastic foundation’’ relations which neglect Poisson effects of internal pressure in the tubing:

$$\begin{aligned}F_{1T} &= \frac{E_T A_T}{L} (W_2 - W_1) - \alpha_T E_T A_T \Delta \bar{T}_1 \\ F_{2T} &= -\frac{E_T A_T}{L_2} W_2 - \alpha_T E_T A_T \Delta \bar{T}_2\end{aligned}\quad (10.3.15)$$

$\Delta \bar{T}_1$, $\Delta \bar{T}_2$ represent tube metal mean temperature changes above the initial assembly temperature. In the following analyses, we choose to neglect $\Delta \bar{T}_1$, $\Delta \bar{T}_2$ since we are interested primarily in the effects of *radial* thermal growth on the configuration. The effects of $\Delta \bar{T}_1$, $\Delta \bar{T}_2$ are easily included in the subsequent solution method and computer code.

Figure 10.3.3 shows the familiar tube pattern in the drilled portion of a tubesheet. We consider the mechanical loading on the double tubesheet configuration to be a tubeside pressure p_1 , a shell side pressure p_3 , and possibly a pressure p_2 in the gap between the two closely spaced tubesheets. The tubesheet solidity factor λ_i ($i = 1, 2$) is defined by the relations (See Fig. 10.3.3).

$$\lambda_i = 1 - A_{\text{HOLE}}^{(i)} / A \quad (10.3.16)$$

$A_{\text{HOLE}} = \pi d_h^2 / 4$; $A = P^2 \sin 2\phi$; d_h is the effective hole diameter. λ_1 for the tube side pressure is based on the tube inside diameter, while λ_2 for the shell side and for the gap region is based on the outer diameter of the tubing. In terms of quantities previously defined, the effective pressures on each face of the double tubesheet configuration are given as (see Figs. 10.3.1–10.3.2).

Tubesheet #1

$$q_{n1} = \lambda_1 p_1; \quad m_{n1} = \tau_{n1} = 0$$

$$q_{u1} = -\lambda_2 p_2 + F_{1T}/A; \quad m_{u1} = M_{1T}/A; \quad \tau_{u1} = H_{1T}/A \quad (10.3.17)$$

Tubesheet #2

$$q_{n2} = \lambda_2 p_2 - F_{1T}/A; \quad m_{n2} = \frac{M_{2T}}{A}; \quad \tau_{n2} = -H_{2T}/A$$

$$q_{u2} = -\lambda_2 p_3 + F_{2T}/A; \quad m_{u2} = M_{3T}/A; \quad \tau_{u2} = H_{3T}/A \quad (10.3.18)$$

We see that tubesheet coupling is induced through the appearance of tube force and moment resultants in the effective pressures q_{u1} , q_{n2} that act on the surfaces of the tubesheets.

With the addition of appropriate boundary conditions at $r=0$ and $r=a$ for each tubesheet, the formulation of the field equations is complete. In the next section we give the outlines of a complete solution of the field equations. A source code using the solution procedure is given in Appendix 10.A. A typical set of results from a simulation is also presented. In closing, we note that it should be clear, that the above field equations do not lend themselves to any simple reduction to code-type design rules.

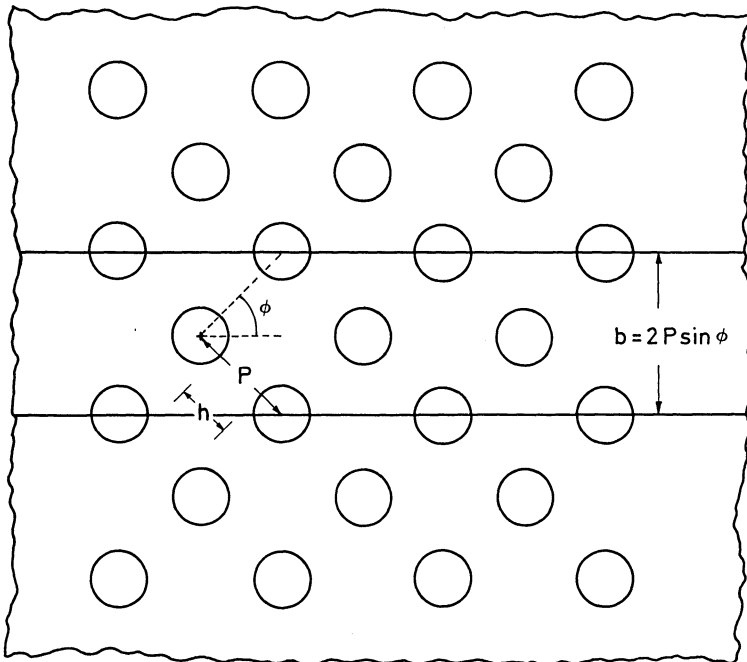


Fig. 10.3.3. Triangular (or staggered) tube layout.

10.4 SOLUTION OF THE DOUBLE TUBESHEET EQUATIONS BY DIRECT INTEGRATION AND APPLICATION TO A SELECTED UNIT

Using the final two equations in the set (10.3.3) permits elimination of $N_{\theta i}$, $M_{\theta i}$ ($i=1,2$) from the remaining equilibrium and constitutive equations. The complete set of field equations governing the behavior of double tubesheets can then be cast as a system of twelve coupled first order ordinary differential equations involving six force and moment resultants, and six deformation variables. In matrix form, the field equations evolve into the final set of twelve equations given below:

$$\frac{d}{dr} \{z\} = [A] \{z\} + \{B(p)\} + \{C(T)\} \quad (10.4.1)$$

It is not important, for our purposes herein, to explicitly set down the specific quantities appearing in $[A]$, $\{B\}$, and $\{C\}$.

The dependent variable $\{z\}$ vector is concisely written as

$$\{z\}^T = \{V_1, V_2, N_{r1}, N_{r2}, M_{r1}, M_{r2}, U_{01}, U_{02}, \theta_1, \theta_2, W_1, W_2\}^T \quad (10.4.2)$$

where $\{z\}^T$ is the transposed matrix.

- $V_1; V_2$ = Shear force per unit circumference in tubesheets 1 and 2, respectively (Fig. 10.3.1).
- $N_{r1}; N_{r2}$ = Radial in-plane force per unit circumference in tubesheets 1, 2, respectively (Fig. 10.3.1).
- $M_{r1}; M_{r2}$ = Radial bending moments per unit circumference in tubesheets 1, 2, respectively (Fig. 10.3.1).
- $U_{01}; U_{02}$ = In-plane radial displacement of tubesheets 1, 2, respectively (Fig. 10.3.1).
- $\theta_1; \theta_2$ = Mid-surface rotations of tubesheets 1, 2, respectively (Fig. 10.3.1).
- $W_1; W_2$ = Lateral deflection of mid-surface of tubesheets 1, 2, respectively.

The 12×12 matrix $[A]$, and the column matrices $\{B\}$, $\{C\}$ involve the independent variable r , various geometric and material properties of the system, and the contribution of the mechanical and thermal loadings. Associated with Eq. (10.4.1) are six boundary conditions at the center of the tubesheet $r=0$, as well as six boundary conditions which must be specified at $r=a$. Symmetry, and the requirements of finiteness of the solution at $r=0$, implies that we must impose the following conditions at $r=0$:

$$V_1 = V_2 = U_{01} = U_{02} = \theta_1 = \theta_2 = 0 \quad (10.4.3)$$

The six conditions imposed at $r=a$ depend on the type of construction utilized to support the outer circumference of the two tubesheets.

The set of equations (10.4.1), with properly assigned boundary conditions, form a well posed boundary value problem which is most efficiently

solved by changing the problem into a series of initial value problems and then utilizing direct numerical integration along the radial coordinate. The technique is well documented in Ref. [10.4.1]. In Appendix 10.A, we present a computer code for analysis of double tubesheets using the theory set forth above. The particular solution algorithm used in the code is described in Reference [10.4.2].

It is not our intent to dwell on the details of the computer implementation of the double tubesheet field equations; rather, we content ourselves with an illustration of the application of the computer code and with elucidation of the problems that must be considered in a double tubesheet design. Therefore, we consider a specific configuration and investigate the effect of gap spacing L , and the effect of boundary conditions at $r=a$, on critical stresses in the various configuration components. The double tubesheet problem defined by the data in Table 10.4.1 is used for the numerical illustration with appropriate account taken of the weakening effect of the perforations in the tubesheets.

Table 10.4.1. Double Tubesheet Specifications

Tubesheet 1

$$E_1 = 30 \times 10^6 \text{ psi}$$

$$\eta_1 = E_1^*/E_1 = 0.3; \quad \nu_1 = 0.28; \quad h_1 = 1''$$

$$\alpha_1 = 9.3 \times 10^{-6} \text{ (in./in. } ^\circ\text{F)}; \text{ Shell radius } a = 20''$$

Tubesheet 2

$$E_2 = 30 \times 10^6 \text{ psi}; \quad \eta_2 = E_2^*/E_2 = 0.3;$$

$$\nu_2 = 0.28; \quad h_2 = 1''; \quad \alpha_2 = 6.3 \times 10^{-6} \text{ (in./in. } ^\circ\text{F)}$$

Tubes

$$\text{Pitch} = 1.25''; \text{ tube wall thickness} = 0.049''$$

$$\text{Tube O.D.} = 1''; \quad S = 40''$$

$$E_T = 30 \times 10^6 \text{ psi}; \quad L_2 = 200''$$

Loading

$$p_1 = 100 \text{ psi}; \quad p_2 = p_3 = 0$$

$$T_1 = T_2 = 100^\circ\text{F}$$

We initially consider the case of mechanical loading only. As boundary conditions for the outer rim of the tubesheets, we assume, at $r = a$,

$$N_{r1} = N_{r2} = \theta_1 = \theta_2 = W_1 = W_2 = 0, \quad (10.4.4)$$

so that the outer rim of both tubesheets is restrained against lateral out of plane deformation and cross-section rotation, but is free to expand radially.

Numerical solution of the foregoing configuration has been obtained for

various gap spacings L between the two tubesheets using the computer code DOUBLESHEET in Appendix 10.A. The range of L is given below:

$$10'' \geq L \geq 0.5'' \quad (10.4.5)$$

Results of the study are shown in Fig. 10.4.1, where various force and moment resultants at $r=a$ are plotted against the dimensionless gap variable

$$x = L/L_0; \quad L_0 = 10'' \quad (10.4.6)$$

In order to plot all of the results on the same scale, the vertical axis of Fig. 10.4.1 represents the absolute value of any of the dimensionless quantities M_i/M_0 ; V_i/V_0 ; H_{iT}/H_{T_0} ; M_{iT}/M_0 . M_i , V_i , H_{iT} , M_{iT} are defined in Fig. 10.3.1 for the i th tubesheet, and in Fig. 10.3.2 for the tubes. The reference values, M_0 , V_0 , H_{T_0} , for plotting purposes, are taken as

$$\begin{aligned} M_0 &= 100 \text{ lb. in./in.} \\ V_0 &= H_{T_0} = 100 \text{ lb. in./in.} \end{aligned} \quad (10.4.7)$$

The ordinate of the figure is labelled with a generic F/F_0 .

Figure 10.4.1 shows, for the mechanical loading $p_1 = 100$ psi, the critical stress resultants at $r=a$ as a function of the gap between the tubesheets. The curve for tube moment M_{iT} has been extended, without calculations, to zero gap spacing since it is clear that the tube bending moment must approach zero as the gap is eliminated. The tube shear force, H_{iT} , must also approach a finite value for zero gap, but the numerical simulation was not carried to a small enough gap so that this limit could be ascertained. From a practical point of view, it appears that the lower limit of gap spacing investigated is sufficient for most practical designs. Once tube forces and moments are determined, stress levels in the various components are easily identified. For example, from the results shown in Fig. 10.4.1, the maximum shear stress in the tubes (due to H_{iT}) and the axial stress in the tubes (due to M_{iT}) is obtained, for a gap of 0.5'', as

$$\begin{aligned} \bar{\tau} &= 2 \frac{H_{iT}}{A_T} = 6776.4 \text{ psi} \\ \sigma_a &= \frac{M_{iT}d}{2I_T} = 3924 \text{ psi} \end{aligned} \quad (10.4.8)$$

For design checks, the bending stress at the rim of tubesheet 1 may be found from the relation

$$\sigma_B = 6M_1/h_1^2\eta_s = 1848/\eta_s \text{ psi} \quad (10.4.9)$$

Note that the gross bending stress must be scaled up by the stress efficiency η_s for each tubesheet.

Although not shown in Fig. 10.4.1, shear transfer between the tubesheets, for the case of small separation, allows the double tubesheet assemblage to resist gross lateral movement by developing direct compressive forces in

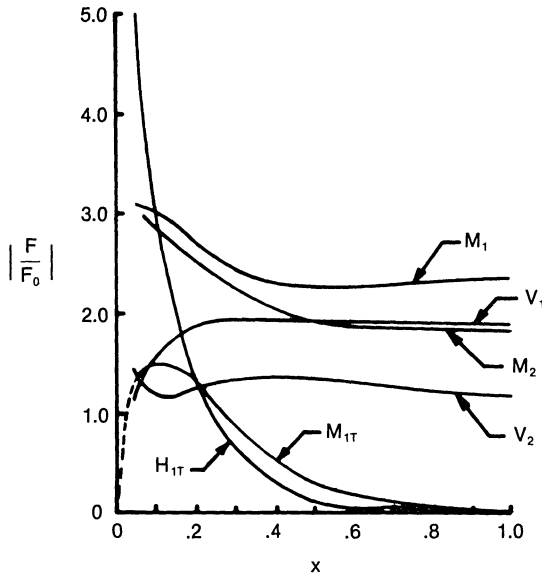


Fig. 10.4.1. Force and moment resultants versus separation for mechanical loading.

tubesheet 1, and direct tensile forces in tubesheet 2. These direct radial forces are negligible near $r=a$ because of the specified boundary conditions on radial deformation; i.e., the tubesheets are allowed to freely expand radially in this example, and reach their maximum value at the center of the tubesheets.

For mechanical loading only, significant stress reduction in the tubesheets is obtainable using the double tubesheet configuration since direct tension and compression loads in the two tubesheets act to develop a major portion of the internal bending moment that arises to resist bending of the assemblage.

A more interesting set of results is obtained for the case of purely thermal loading of the tubesheet configuration. We develop a thermal driving force here by specifying different thermal expansion coefficients, but the same temperature rise for both tubesheets. It is clear from the original equations that the numerical results shown in Fig. 10.4.2 are valid for any thermal driving force as long as the combinations, $(\alpha_1 T_1)$, $(\alpha_2 T_2)$, remain unchanged.

Figure 10.4.2 shows the variation of relevant force and moment resultants that appear critical for design purposes, as a function of tubesheet gap. Reference values for M_0 , V_0 , H_{T_0} are again given by Eq. (10.4.7) for ease in plotting. Initially, results are obtained for the same boundary conditions used for the case of mechanical loading. The results obtained for thermal loading indicate that changes in values of the forces

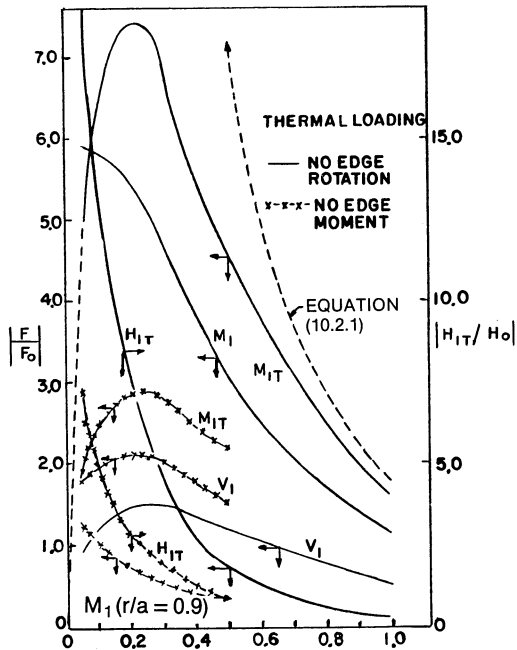


Fig. 10.4.2 Force and moment resultants versus separation for thermal loading.

and moment resultants, as tubesheet separation decreases, are considerably more severe than in the case of mechanical loading alone. It is clear, however, that the design of a double tubesheet configuration with a small separation between tubesheets is possible; from the results shown in Fig. 10.4.2, the direct shear stress in the tubes, due to the force H_{1T} , will probably govern the design. As noted in the beginning of this chapter, the new loading configuration requires checking not only the tubesheets, but also the tube stresses in the region between the tubesheets.

For the configuration studied, we have also plotted results for the tube bending moment that are implied by using Eq. (10.2.1) but instead solving for the stress induced for a given separation, L . The results show the expected conservative nature of Eq. (10.2.1) when the tubesheet separation is large, and also indicate the departure from reality that results if Eq. (10.2.1) is applied to a configuration where significant tubesheet interaction occurs (i.e., for small gaps).

To assess the possible effect of different boundary conditions at $r=a$ on the design, we now reconsider the double tubesheet configuration under thermal load, and replace the boundary conditions given in Eq. (10.4.4) by a new set of boundary conditions at $r=a$:

$$N_{r1} = N_{r2} = M_{r1} = M_{r2} = W_1 = W_2 = 0 \quad (10.4.10)$$

That is, we presumably make the system somewhat more flexible by allowing cross-section rotation to occur at the outer edge of both tubesheets. Figure 10.4.2 also shows some results of interest which occur for this set of edge conditions. Of significance to contemplated designs is the fact that tube shear forces and bending moments decrease dramatically; it is clear that this might have been expected since, in a thermal loading situation, one can generally surmise that an increase in system flexibility will decrease the thermal stresses. As noted previously, all of the results illustrated have been obtained using the computer code in Appendix 10.A. The input data file and the final results for one set of values used in producing Fig. 10.2.1 is included in Appendix 10.B.

Our prime motivation to this point has been to show that double tubesheet designs having gap spacing on the order of one or two tube diameters are certainly feasible, but require a more refined analysis to ensure structural integrity in service under mechanical and thermal loading. The results obtained for the single configuration studied seem to imply that stress caused by in plane thermal loadings are more sensitive to the tubesheet separation. In any specific design study, the computer solution should be used to obtain maximum force and moment resultants in all critical areas. If desired, extensive parametric studies can be carried out to ascertain the effect on the design of varying one or more of the geometric or material parameters. Of course, in the case of a fixed tubesheet exchanger, the effect of differential axial growth between tubes and tubesheet needs to be considered. As noted, the code given in Appendix 10.A must be modified to include this effect. Such an effect can be added quite simply if the elastic stretch of the shell is neglected. As noted previously, the effect of tube mean temperature change appears in the expressions for tube axial force given by Eq. (10.3.15). From Eq. (10.3.18), we note that the effect of F_{2T} appears in the effective pressure acting on the tubesheet exposed to the shellside stream. Referring back to Chapter 9 dealing with fixed tubesheets, it can be seen by referring to Eq. (9.3.6) or (9.7.11) for the effective pressure as defined there, that the effect of the thermal differential between shell and tube may be simply incorporated by replacing $\alpha_T \Delta \bar{T}_2$ in Eq. (10.3.15) by the quantity $(\alpha_T \Delta \bar{T}_2 - \alpha_s \Delta \bar{T}_s)$ with α_s , $\Delta \bar{T}_s$ representing the coefficient of thermal expansion and the temperature change of the shell above the initial assembly temperature. This simple modification does assume that the stretch of the shell due to axial force is neglected; however, because of this any stress results obtained due to the driving force $\alpha_T \Delta \bar{T}_2 - \alpha_s \Delta \bar{T}_s$ will be conservative. The effect of including this driving force will simply modify one of the terms in the matrix C in Eq. (10.4.1). If axial growth is included, then W_2 should be zero at the outer edge when setting the boundary conditions in the computer simulation.

Because of the numerical solution method used in this chapter, which requires that a boundary value problem be changed to a series of initial value problems, the procedure becomes extremely sensitive to the ratio, L/a . For L/a too small, the solution procedure may yield inaccurate results.

During the course of the solution, subtraction of nearly equal large numbers occurs and all control of error is lost. The occurrence of this difficulty has long been recognized by the users of this solution procedure [10.4.1], [10.4.2], and extensions of the technique to overcome this problem are well established. We note that the present computer simulation of the double tubesheet problem may also experience this effect to some extent and therefore is unsuitable for analysis of very small gaps in very large units. Any user of the code DOUBLESHEET should remain alert to this difficulty. We discuss, in the next sections of this chapter, the application of the finite element method to double tubesheet design. We also use the finite element method to re-consider a selected single tubesheet unit; the specific intent of the re-consideration being the examination of the effect of tubesheet thickness to radius ratio on the validity of our previous "design by analysis" solutions based on thin plate theory (covered in Chapters 8 and 9).

10.5 THE FINITE ELEMENT METHOD IN TUBESHEET ANALYSIS

With the advent of large mainframe computers and, more recently, super mini-computers, the application of finite element analysis to routine day to day structural design problems becomes feasible and cost effective. The finite element method is an established procedure for idealizing a body for structural, dynamic, or thermal analysis, by discrete beam, shell, or solid elements, etc. It is not the purpose of this section to expound on the underlying theory of the finite element method; rather, we intend to show by example how the method can be applied to tubesheet analysis. For the reader desiring some background on the theory and application of the finite element method, we suggest Refs. [10.5.1], [10.5.2], although there are many other similar texts which may be used.

In order to provide a convenient starting point for our discussion, we will briefly describe the fundamentals of the finite element method so that the reader has some feel for the analyses to follow. As a vehicle for our description, we consider the two dimensional structure shown in Fig. 10.5.1.

We idealize the body by a series of triangular elements using a fine enough mesh to adequately follow the structure boundaries, and to adequately model any displacement or stress gradients expected. A typical element having nodes I, J, K is shown in the enlarged view with its nodal displacements. The essence of the finite element method is a description of the displacement distribution $u(x,y), v(x,y)$, within each element, in terms of the displacements at the corner nodes of each element. The local spatial variations within the element are the defined "shape functions" $P(x,y)$ for the element; therefore, a displacement distribution can be written, for example, as

$$u(x,y) = U_I P_I(x,y) + U_J P_J(x,y) + U_K P_K(x,y) \quad (10.5.1)$$

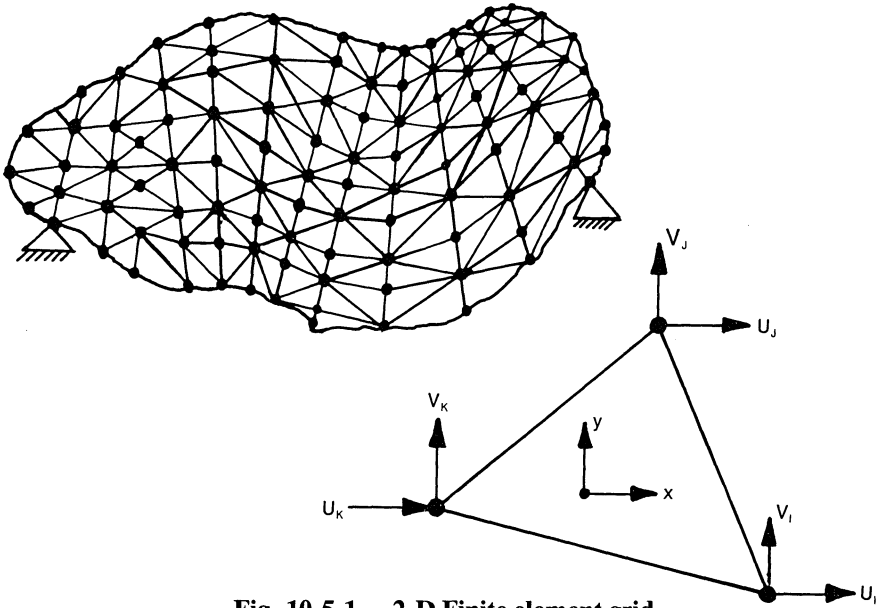


Fig. 10.5.1. 2-D Finite element grid.

where U_I , U_J , U_K are nodal displacements in the global x direction of the complete structure. The shape functions, within each element, must satisfy certain criteria in order to ensure that the results of the analysis will converge to the exact solution in the limit as the number of elements used increases and the element mesh becomes finer. For our purposes here, we need not discuss these criteria for convergence any further. The usual finite element formulation employs an energy principle to evolve the element stiffness matrix associated with the particular choice of displacement assumptions. Using well documented and verified techniques, the individual element stiffnesses can be assembled into a global stiffness matrix for the entire structure. The final equations that are solved, in the case of a linearly elastic structure, are a set of linear algebraic equations for the unknown nodal displacements at each unconstrained nodal point. In the case shown in Fig. 10.5.1, if there are N unconstrained nodes in the model, the unknowns are the N nodal displacement U , and the N nodal displacements V . In the course of developing these final equations, appropriate account is taken of the contribution of the given applied loads, and any coordinate transformations between local element coordinate systems and the primary global coordinate system.

It is clear that N is usually a very large number for most practical structures; hence, solution of the resulting equations for the $2N$ displacement unknowns, while conceptually simple, requires the aid of efficient computer coding and the availability of either special purpose or general purpose computer codes pertinent to the problem under con-

sideration. The bare essence of any finite element computer code contains a “user friendly” routine to input a model description (materials, node points, loading, boundary conditions), a routine or set of routines to calculate element stiffness matrices and to assemble the global stiffness matrix, an efficient equation solver, and a routine or set of routines to calculate and to output results at the element level. If the code is to be used by different personnel of varying experience levels, pre-and post-processing routines are usually made available for ease in input and interpretation of results.

For our purposes, we focus on the use of the finite element method for the analysis of double tubesheets, and for the analysis of a single thick tubesheet. Specifically, for the latter example, we use a finite element code to study the effect of thickness to radius ratio of a typical tubesheet on the state of stress. In the previous chapters, the tubesheet has always been modelled, for analysis purposes, by classical thin plate theory. This leads to bending stress distributions which are linear through the tubesheet thickness. For small thickness to radius ratios, the classical plate assumptions turn out to be adequate. However, for units with larger thickness to radius ratios, the question must arise as to how valid the results are in view of the fact that the underlying plate theory becomes suspect at large thickness to radius ratios.

10.6 SAMPLE RESULTS USING THE FINITE ELEMENT METHOD

We consider as an initial example the following double tubesheet configuration:

Tubesheet O.D. = 40"; perforated diameter = 38"; gap between tubesheets = 0.25"

Tubesheet 1 – geometry and material

$h_1 = 1.0"$, $E_1 = 15 \times 10^6$ psi; $E_1^*/E_1 = 0.22$; $\nu_1^* = 0.4$
 $\alpha_1 = 11.6 \times 10^{-6}$ in./in.°F; ligament/stress efficiency = 0.25

Tubesheet 2 – geometry and material

$h_2 = 2.0"$; $E_2 = 30 \times 10^6$ psi; $E_2^*/E_2 = 0.22$; $\nu_2^* = 0.4$
 $\alpha_2 = 6.5 \times 10^{-6}$ in./in.°F; ligament/stress efficiency = 0.25

Boundary Conditions at Outer Edge

Tubesheet 1 – clamped; tubesheet 2 – simply supported

Tubes

Tube O.D. = 1.0"; wall thickness = 0.049"
 $E_T = 30 \times 10^6$ psi; $\alpha_T = 6.5 \times 10^{-6}$ in./in.°F
 Half length of unit = 100"

Loading

$p_1 = p_2 = p_3 = 0$; reference temperature = 70°
 operating temperature of tubesheet 1 = 90°
 operating temperature of tubesheet 2 = 120°

A finite element model has been constructed using 310 node points and 270 elements. The finite element code used is a 2-D plane and axisymmetric code with three and four node elements. For a double tubesheet analysis, each tubesheet is modelled by three layers of elements; the tube array between the tubesheets is modelled by a single layer of elements. Element properties for the tube layer are modified, where appropriate, to account for the tube pattern, and to give the correct shear and tensile resistance to the adjacent tubesheet. The tube foundation effect on the shellside of the assemblage is also modelled by plane elements with tensile properties chosen to reflect the correct foundation resistance. We have also used a pre-processor for ease in data input, and a post-processor to aid in summarizing the results. Because of their length, we have not included these three codes in the text; the codes are, however, available separately on tape with all of the other computer codes used in this text. It suffices to state that to develop the input file for this double tubesheet example problem requires only nine lines of data input. Figure 10.6.1 shows the distribution of radial stress at the center of the tubesheets and at the edge of the perforated region. We take note of the large bending moment at the edge of tubesheet 1 due to the clamped boundary condition. We notice also the beginnings of a non-linear stress distribution through the thickness. By employing the finite element method for double tubesheet constructions, we will have no problem examining very small gaps. Therefore, the finite element approach here complements our earlier special purpose code double tubesheet analysis which may be "gap limited" in certain circumstances.

As a second example of the potential of the finite element method in tubesheet analysis, we consider a thick circular steel plate of outer radius =

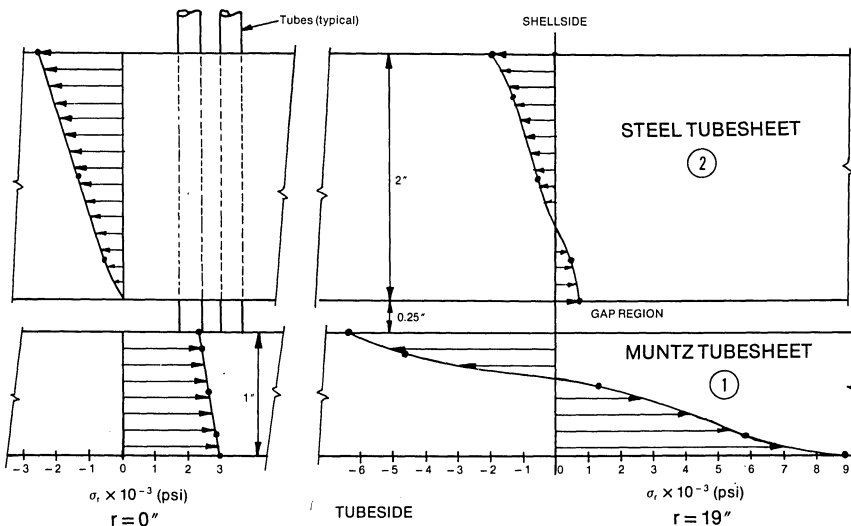


Fig. 10.6.1. Double tubesheet finite element analysis – results for σ_r .

20", thickness = 8", and Young's Modulus $E = 30 \times 10^6$ psi. We subject this plate to a surface pressure $p = 1000$ psi and assume clamped boundary conditions at the outer edge. Our purpose here is simply to compare the predictions of a finite element solution with results obtained using classical thin plate theory. The finite element results are obtained using the same pre-processor, finite element code, and post-processor used above in the first example.

The model of a single tubesheet contains the same 310 node points and 270 elements; here the single tubesheet is modelled by seven layers of elements. Figure 10.6.2 shows the radial stress distribution at the center and at the clamped outer edge of the tubesheet. For this second example, we have assumed a ligament efficiency equal to unity, and input values for tube moduli so small that the tube elastic foundation effect becomes insignificant. Thus, our finite element special purpose tubesheet code simply models a clamped circular plate under a uniform surface pressure. Figure 10.6.2 clearly shows the effect of large thickness to radius ratio. For the geometry and material assumed for this example, classical thin plate theory gives a linear stress distribution through the thickness with maximum extreme fiber stresses

$$|\sigma_r(0)| = 3 \frac{(1 + \nu)}{8} p \frac{R^2}{h^2}; \quad |\sigma_r(R)| = \frac{3}{4} p \frac{R^2}{h^2} \tag{10.6.1}$$

For the geometry and loading given here, Eq. (10.6.1) gives radial stress extreme fiber values of $|\sigma_r(0)| = 3047$ psi, $|\sigma_r(R)| = 4688$ psi, respectively. Figure 10.6.2 shows the stress distribution predicted by the thin plate theory at the two locations in question.

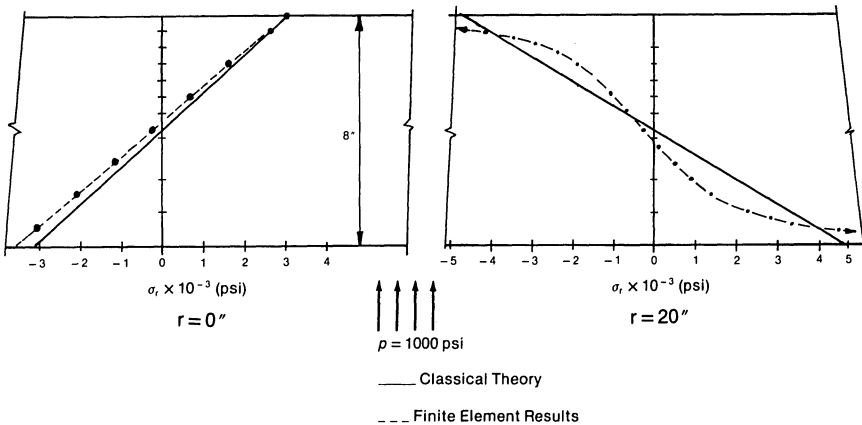


Fig. 10.6.2. σ_r in thick circular plate – $H/R = 0.4$.

The results of the finite element solution (which can be thought of as the exact solution) are also plotted in Fig. 10.6.2. We can see the effects of the thin plate approximation especially at the outer edge. Classical plate theory will significantly underestimate the maximum extreme fiber stress near the clamped edge. However, since this stress can be considered as a peak stress, its value mostly influences the fatigue life at the clamped edge. Nevertheless, the results obtained here do point out that simply calculating a stress using one of our tubesheet design methods based on classical theory does not guarantee that the stress level actually exists in the unit. If the tubesheet geometry does not fall within the bounds of a thin plate theory, it is highly likely that there will be some tubesheet locations where the stress is highly non-linear through the thickness.

If we calculate the central plate deflection using thin plate theory, we obtain

$$\delta = \frac{pR^4}{64D} = 0.001776'' \quad (D = Eh^3/12(1-\nu^2)) \quad (10.6.2)$$

The finite element displacement at the center of the tubesheet is 0.00297'' which is significantly larger. This discrepancy is simply the effect of shear deformation. In classical plate theory, deformation due to shear is neglected in order to evolve simple theories. For the thick plate analyzed here, shear deformation (and other 2-D effects) increases the central deflection by 50%.

NOMENCLATURE

- a = Radius of perforated region in Table 10.4.1
- d = Tube diameter (Eq. (10.2.1))
- d_h = Effective hole diameter (Eq. (10.3.16))
- D_i = Out-of-plane rigidity of tubesheet (Eq. (10.3.4))
- E_T = Young's Modulus of tube
- E_i = Tubesheet Young's Modulus ($i = 1,2$ for two tubesheets)
- E_i^* = Effective Young's Modulus for perforated region
- F_T, H_T, M_T = Tube force resultants
- h = Thickness of single tubesheet used in finite element model (Section 10.6)
- h_i = Tubesheet thickness in i th tubesheet
- I_T, A_T = Tube geometric properties
- K_i = In-plane rigidity of tubesheet (Eq. (10.3.4))
- l = Characteristic length for unrestrained expansion
- L = Length of tube between double tubesheets
- L_2 = Half length of tubes (Fig. 10.2.1)
- $M_{ri}, M_{\theta i}$ = Tubesheet bending moments
- $N_{ri}, N_{\theta i}$ = Tubesheet membrane force resultants
- N_i^*, M_i^* = Thermal forces and moments
- p_1, p_2, p_3 = Pressures in fluid region defined in Fig. 10.2.1
- r = Radial coordinate

- R = Radius of tubesheet (Eq. (10.6.1)) used in finite element model
 S = Span of tubing from shellside face of the tubesheet to first baffle
 T_i = Mean temperature rise above assembly temperature of tubesheets
 U_I, U_J, U_K = Finite element nodal displacements (Eq. (10.6.1))
 U_{0i}, θ_i, W_i = Tubesheet deformation variables (Eq. (10.3.2))
 V_i = Tubesheet shear resultant
 \bar{V}_i = Tube end displacements (Fig. 10.3.2)
 α_i = Tubesheet coefficients of thermal expansion
 α_T = Coefficient of thermal expansion of tube material
 Δ = Differential displacement of tube ends
 $\Delta \bar{T}_i$ = Mean temperature rise above assembly temperature of tubes (Eq. (10.3.15))
 η_i = Deflection efficiency = E_i^*/E_i
 η_s = Tubesheet stress efficiency (Eq. (10.4.9))
 γ, g = Coefficients defined in (Eq. (10.3.7))
 λ_1, λ_2 = Solidity factors (Eq. (10.3.16))
 ν_i = Poisson's ratio (effective) for i th tubesheet
 σ_A = Allowable stress of tube
 τ, m, q = Surface loadings on tubesheets
 $\bar{\tau}, \sigma_a$ = Tube stress (Eq. (10.4.8))

REFERENCES

- [10.2.1] Yokell, S., "Double Tubesheet Heat Exchanger Design Stops Shell-Tube Leakage," *Chemical Engineering*, p. 133-136 (May 1973).
 [10.2.2] Zudans, Z., Yen, T. C., and Steigelmann, W. H., "Thermal Stress Techniques in the Nuclear Industry," Chapter 5, American Elsevier Company, New York (1965).
 [10.2.3] Cook, R. D., "A Mechanical Analysis of Coupled Tube Sheets," *University Microfilm, Inc.*, Ann Arbor, Michigan, (1963).
 [10.2.4] Soler, A. I., "Analysis of Closely Spaced Double Tubesheets Under Mechanical and Thermal Loadings," ASME Paper 77-JPGC-NE-21 (September 1977).
 [10.3.1] Vinson, J. R., "Structural Mechanics: The Behavior of Plates and Shells," J. Wiley, New York, Chapters 3, 4 (1974).
 [10.3.2] Boley, B. A., and Weiner, J. H., "Theory of Thermal Stresses," John Wiley, New York, Chapter 12 (1960).
 [10.3.3] Severn, R. T., "Inclusion of Shear Deformation in the Stiffness Matrix for a Beam Element," *Journal of Strain Analysis*, Vol. 5, No. 4, pp. 239-241 (1970).
 [10.3.4] Gardner, K. A., "Heat Exchanger Tubesheet Design," *Journal of Applied Mechanics*, Trans. ASME, Vol. 70, p. A-377 (1948).

- [10.4.1] Kraus, H., "Thin Elastic Shells," J. Wiley, pp. 419-430 (1967).
 [10.4.2] Hutchins, G. J., and Soler, A. I., "New Results on Application of Multi-Segment Stepwise Integration of First Order Equations," *Journal of Computer Methods in Applied Mechanics and Engineering*, pp. 307-316 (1972).
 [10.5.1] Desai, C. S., and Abel, J. F., "Introduction to the Finite Element Method - A Numerical Method for Engineering Analysis," Van Nostrand, N.Y. (1972).
 [10.5.2] Becker, E., Carey, G., and Oden, J., "Finite Elements - An Introduction - Vol. 1, Prentice-Hall, N.J. (1981).

APPENDIX 10.A

USER'S MANUAL FOR DOUBLE TUBESHEET ANALYSIS— COMPUTER CODE "DOUBLESHEET"

The computer code gives a step by step solution of the matrix equations

$$\{Y'\} = [A]\{Y\} + \{B\}$$

starting from the center of the tubesheet pair out to the edge of the perforated region. No untubed rim is considered in the analysis. The vector Y contains the dimensionless variables for shear forces, membrane forces, bending moments, radial displacements, cross section rotations, and transverse displacements, for tubesheets 1 and 2, respectively. Denoting the dimensionless variables by overbars, the final dimensioned variables are given by the vector

$$\{Z\}^T = [V_1, V_2, N_1, N_2, M_1, M_2, U_1, U_2, \theta_1, \theta_2, W_1, W_2]$$

where

$$\begin{aligned} V_i &= E_i h_i \bar{V}_i; & N_i &= \bar{N}_i E_i h_i \\ M_i &= \bar{M}_i E_i h_i^2; & U_i &= \bar{U}_i / h_i; & \theta_i &= \bar{\theta}_i \\ W_i &= \bar{W}_i / h_i \end{aligned}$$

Upon execution, the code requests keyboard input for NR, NW, NTST, which are the logical unit numbers for subsequent read in data (NR) and for subsequent output (NW). NTST should be set equal to zero. Subsequent input requirements, from file NR, are given below and should be input in free format.

LINE 1

- XL 1.0 (length of integration region (dimensionless))
 H initial integration step size
 N 12 (number of equations)
 JNDIC number of stepsize changes in the integration length 0-1

KNDIC number of output points along tubesheet radius
 LNDIC 4
 INDIC 1

LINE 2

(BNA(I), I = 1, N/2) The values of the N/2 prescribed variables (6 total) at the center of the tubesheets.

LINE 3

(BNB(I), I = 1, N/2) The values of the N/2 prescribed variables (6 total) at the outer radius of the tubesheets.

LINE 4

(BCN(I,1), I = 1, 12) If the Ith variable is specified at $r = 0$, $BCN(I,1) = 0$; if the variable is to be determined, $BCN(I,1) = 1$

LINE 5

(BCN(I,2), I = 1, 12) Same as line 4 except for outer radius of tubesheet.

LINE 6 (Insert only if JNDIC > 0)

(XCHG(I), DINT(I), I = 1, JNDIC)

Locations where step size H will be changed in the dimensionless integration region (0-1.) to increase stepsize DINT should be greater than unity. To decrease stepsize DINT should be less than unity. That is, $DINT(1) = 2$ will double the stepsize at XCHG(1), while $DINT(2) = 0.5$ will return the stepsize to its initial value at XCHG(2). Up to 21 changes are permitted.

LINE 7

(insert only if KNDIC > 0) (XY(I), I = 1, KNDIC).

Locations (in the region 0-1.) where printout of the fundamental variables may be obtained. Up to 21 locations, including 0.0, and 1.0 may be input.

LINE 8 – tubesheet 1 properties

H1 = thickness
 T1 = mean metal temperature above assembly
 ALF1 = coefficient of thermal expansion
 E1 = Young's Modulus
 NU1 = effective Poisson's ratio (modified by perforations)

ETA1 = $E^*/E1$ for tubesheet 1 perforation effect

TG11 = temperature difference across surfaces (based on linear gradient)

LINE 9 – tubesheet 2 properties

H2

T2

ALF2

E2

NU2

ETA2

TG22

LINE 10

L = tubesheet gap

L2 = halflength of tubes

S = spacing to first baffle

P = tube pitch

T = tube nominal thickness

D = tube diameter

ET = tube Young's Modulus

LINE 11

ARADI = tubesheet outer radius

P1 = pressure p_1

P2 = pressure p_2

P3 = pressure p_3

FN = coefficient F_n (Eq. (10.3.11))

LINE 13

JSKIP = upper bound for number of matrix printouts (used only for debugging). Set to 0 for production runs.

BEGIN = Value for dimensionless independent variable where shift from A matrix valid for small radius to A matrix valid for larger radius occurs. Set equal to 0.01.

LINE 14

ALFAT = coefficient of thermal expansion for tube axial growth.

ALFAS = coefficient of thermal expansion for shell axial growth.

TTUBE = temperature rise of tube above assembly temperature.

TSHELL = temperature rise of shell above assembly temperature

PROGRAM DOUBLESHEET

```

$CONTROL USLINIT,INIT,LOCATION,FILE=21-23,FILE=30-31,FILE=59-64,FILE=5-6
$CONTROL MAP,SEGMENT=SEGMAIN
PROGRAM MAIN
IMPLICIT DOUBLE PRECISION(A-H,O-Z)
DOUBLE PRECISION K,L,LG
INTEGER BCN
INTEGER FLAG
DIMENSION Z(12,21),TUBE(8,21)
DIMENSION Y(12,21)
COMMON/MTINP/ A(12,12),B(12),INDIC
COMMON/PARAM/ XL,H,N,JNDIC,KNDIC,NR,NW
COMMON/COM2/ BCN(12,2),BNA(6),BNB(6)
COMMON/COM3/ XCHG(21),DINT(21),XY(21)
COMMON/COM4/OMEGA,DET,LNDIC
COMMON/STORE/UDUMMY(24)
COMMON/COM5/FLAG
COMMON/DIM1/E1,E2,ET,H1,H2,B1,B2,C11,C12,C13,C21,C22,C23,K,S,GS1
COMMON/DIM2/GS2,L,GM,LG
COMMON/TEST/NTST

C
C   SET FLAG FOR HELP
C   FLAG=0

C
C   ....SETUP INPUT PARAMETERS
501  WRITE(6,501)
      FORMAT(17H BEGINNING DBLTS1)
      READ(5,*) NR,NW,NTST
      WRITE(NW,*) ' DOUBLE TUBESHEET ANALYSIS PROGRAM'
      WRITE(NW,*) ' PREPARED BY A.I. SOLER SEPT. 1983'
      WRITE(NW,*)
      WRITE(NW,*) ' OUTPUT OF RAW INPUT DATA'
500  FORMAT(2I2)
C   ....
      READ(NR,*) XL,H,N,JNDIC,KNDIC,INDIC,LNDIC
      WRITE(NW,8001) XL,H,N,JNDIC,KNDIC,INDIC,LNDIC
      GO TO (1,6,8,9),INDIC
1    DO 5 I=1,N
5    READ(NR,*)(A(I,J),J=1,N)
      READ(NR,*)(B(I),I=1,N)
      GO TO 9
6    DO 7 I=1,N
7    READ(NR,*)(A(I,J),J=1,N)
      GO TO 9
8    READ(NR,*)(B(I),I=1,N)
9    N1=N/2
      READ(NR,*)(BNA(I),I=1,N1)
      WRITE(NW,8002)(BNA(M),M=1,N1)
      READ(NR,*)(BNB(I),I=1,N1)
      WRITE(NW,8002)(BNB(M),M=1,N1)

```

```

DO 10 J=1,2
10 READ(NR,*)(BCN(I,J),I=1,N)
DO 11 I=1,N
12 FORMAT (I4,10X,I4)
11 WRITE(NW,12)(BCN(I,J),J=1,2)
IF(JNDIC.GT.0) READ(NR,*)(XCHG(I),DINT(I),I=1,JNDIC)
IF(KNDIC.GT.0) READ(NR,*)(XY(I),I=1,KNDIC)
WRITE(NW,8002)(XY(I),I=1,KNDIC)
C ....PRINT OUT INPUT PARAMETERS
C ....

WRITE(NW,7000)
WRITE(NW,7001) XL,H,N,KNDIC,JNDIC
WRITE(NW,7003)
IF(LNDIC.EQ.1) GO TO 20
15 READ(NR,7002,END=60) OMEGA
IF(NTST.EQ.1)WRITE(NW,*)'ENT COMP FROM MAIN'
20 CALL COMP(Y)
IF(LNDIC.EQ.2) GO TO 55
C DEFINE Z ARRAY
DO100 I=1,KNDIC
Z(1,I)=E1*H1*Y(1,I)
Z(2,I)=E2*H2*Y(2,I)
Z(3,I)=E1*H1*Y(3,I)
Z(4,I)=E2*H2*Y(4,I)
Z(5,I)=E1*H1*H1*Y(5,I)
Z(6,I)=E2*H2*H2*Y(6,I)
Z(7,I)=H1*Y(7,I)
Z(8,I)=H2*Y(8,I)
Z(9,I)=Y(9,I)
Z(10,I)=Y(10,I)
Z(11,I)=H1*Y(11,I)
Z(12,I)=H2*Y(12,I)
100 CONTINUE
C DEFINE TUBE ARRAY
DO110 I=1,KNDIC
TUBE(1,I)=6.*GM*Z(7,I)+3.*GM*(H1+L)*Z(9,I)-6.*GM*Z(8,I)+3.*GM*(H2+
1L)*Z(10,I)+18.*L*GM*(Z(1,I)/(GS1*H1)+Z(2,I)/(GS2*H2))/5.
TUBE(2,I)=3.*GM*L*Z(7,I)+GM*(1.5*L*H1+2.*L*L+6.*LG)*Z(9,I)-3.*GM*L
1*Z(8,I)+GM*(1.5*L*H2+L*L-6.*LG)*Z(10,I)+12.*(1.+3.*LG/(L*L))*Z(1,I)
2)*L*L*GM/(5.*GS1*H1)+6.*(1.-6.*LG/(L*L))*Z(2,I)*L*L*GM/(5.*GS2*H2)
TUBE(3,I)=B1*(Z(12,I)-Z(11,I))
TUBE(4,I)=-TUBE(1,I)
TUBE(5,I)=3.*GM*L*Z(7,I)+GM*(1.5*L*H1+L*L-6.*LG)*Z(9,I)-3.*GM*L*Z(
18,I)+GM*(1.5*L*H2+2.*L*L+6.*LG)*Z(10,I)+6.*(1.-6.*LG/(L*L))*Z(1,I)
2)*L*L*GM/(5.*GS1*H1)+12.*(1.+3.*LG/(L*L))*Z(2,I)*L*L*GM/(5.*GS2*H2)
TUBE(6,I)=-B2*Z(12,I)
TUBE(7,I)=2.*ET*K/(S*S*S)*(C11*Z(8,I)+C12*S*Z(10,I)+C13*Z(2,I)*S/(
1GS2*H2))
TUBE(8,I)=2.*ET*K/(S*S)*(C21*Z(8,I)+C22*S*Z(10,I)+C23*Z(2,I)*S/(GS
12*H2))
110 CONTINUE
WRITE(NW,*) ' RESULTS FOR TUBESHEETS'

```

```

9002  FORMAT(13(1X,1PD9.2))
      WRITE(NW,*)' R/RO      V1      V2      N1      N2
1M1      M2      U1      U2      A1      A2      W1
2      W2
      DO 90000 KK=1,KNDIC
      WRITE(NW,9002)XY(KK),(Z(I,KK),I=1,N)
90000 CONTINUE
      WRITE(NW,*)
      WRITE(NW,*)'      RESULTS FOR TUBE ARRAY'
      WRITE(NW,*)' R/RO      H1TUBE  M1TUBE  F1TUBE  H2TUBE  M2
1TUBE  F2TUBE  H3TUBE  M3TUBE  '
      DO 91000 KK=1,KNDIC
      WRITE(NW,9002)XY(KK),(TUBE(I,KK),I=1,8)
91000 CONTINUE
      STOP
55  WRITE(NW,7004) OMEGA,DET
      GO TO 15
60  WRITE(NW,7005)
6000 FORMAT(9(A8))
7000 FORMAT(1H1,10X,'A GENERAL COMPUTER PROGRAM FOR THE SOLUTION OF A
1 TWO POINT BOUNDARY VALUE PROBLEM.////)
7001  FORMAT(30X,'LENGTH OF FUN X =',F10.5, '//30X,'STEPSIZE =',
1 6X,F10.5, '//30X,'NUMBER OF EQS. =',15, '//30X,'NO. OUTPT PTS. =',15,
2 //30X,'STEPSIZE CHGS. =',15)
7003  FORMAT(1H0,////)
7002  FORMAT(F15.6)
7004  FORMAT(//////,1H,'OMEGA EQUAL TO',D14.6,'PRODUCES A DETERMINANT
1 EQUAL TO ',D14.6)
7005  FORMAT(////,1H,30X,'PROBLEM END')
7008  FORMAT(1H1,///)
8001  FORMAT(2F10.5,5I5)
8002  FORMAT(7F10.5)
8003  FORMAT(18I4)
9003  FORMAT(' ',A8,8(3X,D11.4))
      STOP
      END

```

```

SUBROUTINE COMP(Y)
IMPLICIT DOUBLE PRECISION(A-H,O-Z)
INTEGER BCN
DIMENSION      Y(12,21),PYY(84,21)
COMMON/COM1/  YR(84),FR(84)
COMMON/COM2/  BCN(12,2),BNA(6),BNB(6)
COMMON/COM3/  XCHG(21),DINT(21),XY(21)
COMMON/COM4/  OMEGA,DET,LNDIC
COMMON/PARAM/ XL,H,N,JNDIC,KNDIC,NR,NW
COMMON/TEST/NTST
N1=N/2
N2=N1+1
N4=N2*N
I1=1
ISUB=1

```

```

      K=1
C
C   INITIALIZE X
      X=0.DO
      I2=1
C   ....ASSIGN INITIAL CONDITIONS
C   ....
      DO 5 I=1,N
      DO 5 J=1,N2
5     Y(I,J)=0.DO
      DO 15 I=1,N
      IF(BCN(I,1).EQ.0) GO TO 10
      GO TO 15
10    Y(I,1)=BNA(K)
      K=K+1
15    CONTINUE
      DO 30 I3=1,N1
      DO 20 I=I1,N
      IF(BCN(I,1).EQ.1) GO TO 25
20    CONTINUE
25    Y(I,I3+1)=1.DO
      I1=I+1
30    CONTINUE
      DO 31 I=1,N
      DO 31 J=1,N2

      IJ=I+(J-1)*N
31    YR(IJ)=Y(I,J)
C   ....CHANGE STEPSIZE
C   ....
35    IF(JNDIC.EQ.0.OR.LNDIC.EQ.2) GO TO 40
      IF(X.LT.XCHG(I2)-H/2.0) GO TO 40
      H=H*DINT(I2)
      I2=I2+1
      IF(I2.GT.JNDIC) XCHG(I2)=XL+H
      WRITE(NW,4500) X,H
C   ....ASSIGN VALUES OF YR TO TEMPORARY STORAGE FOR PRINT OUT
C   ....
40    IF(KNDIC.EQ.0.OR.LNDIC.EQ.2) GO TO 50
      IF(X.LT.XY(ISUB)-H/2.0) GO TO 50
      DO 45 I=1,N4
45    PYY(I,ISUB)=YR(I)
      ISUB=ISUB+1
C   ....IF X EXCEEDS XL TERMINATE INTEGRATION
C   ....
50    IF(X.GT.XL-H/2.0) GO TO 60
C   CALL RUNGE TO INTEGRATE ACROSS NEXT STEP
C
      IER=0
      IF(NTST.EQ.1)WRITE(NW,*)'ENT RUNG FROM COMP'
      CALL RUNGE(X,IER,N4)
      IF(IER.EQ.0) GO TO 35
      WRITE(NW,4400) X

```

```

        WRITE(NW,4350)(YR(I),I=1,N)
        GO TO 535
60     CONTINUE
C     ....SOLVE FOR BOUNDARY CONDITIONS
C     ....
        IF(NTST.EQ.1)WRITE(NW,*)'ENT BCON FROM COMP'
        CALL BCON
        IF(LNDIC.EQ.2) RETURN
C     ....SOLVE FOR Y
C     ....
        DO 75 K=1,KNDIC
        DO 70 I=1,N
        Y(I,K)=0.0
        DO 70 J=1,N2
        IJ=I+(J-1)*N
        70  Y(I,K)=PYY(IJ,K)*YR(J)+Y(I,K)
        75  CONTINUE
535    RETURN
4350  FORMAT(3X,'THE VALUE OF YR BEFORE REGISTER IS LOWERED IS:'
1      //(1H,6D14.6))
4400  FORMAT(3X,'EXPONENT OVERFLOW X=',D14.6)
4500  FORMAT(///3X,'AT X=',F12.4,3X,
1      'THE STEPSIZE H WAS CHANGED TO',F12.4)
        END
C
C     *****
C     SUBROUTINE HELP (R,FLAG)
C     THIS SUBROUTINE LOADS EQUATIONS FOR SOLUTION OF DOUBLE TUBE SHEET
C
C     THIS IS SUBROUTINE HELP           NONDIMENSIONALIZED VERSION
C     FORMS MATRIX A + B
C
        IMPLICIT DOUBLE PRECISION(A-I,K-Z)
        INTEGER FLAG,NR,NW,N,JNDIC,KNDIC
        INTEGER TRASH,NTST
        COMMON/MTINP/A(12,12),B(12),TRASH
        COMMON/COM6/JSKIP
        COMMON/DIM1/E1,E2,ET,H1,H2,B1,B2,C11,C12,C13,C21,C22,C23,I,S,GS1
        COMMON/DIM2/GS2,L,GM,LG
        COMMON/STORE/T1,T2,ALF1,ALF2,NU1,NU2,ETA1,ETA2,TG11,
1TG22,L2,P,T,D,ARAD1,P1,P2,P3,FN,BEGIN,ALFAT,ALFAS,TTUBE,TSHELL
        COMMON/PARAM/ XL,H,N,JNDIC,KNDIC,NR,NW
        COMMON/TEST/ NTST
        IF(NTST.EQ.1)WRITE(NW,*) FLAG
C
C     SKIP READ DATA
C
        IF (FLAG.GT.0) GO TO 1000
C
C     DATA READ IN
C     8     FORMAT(8D12.5)
C

```

```

1  FORMAT(8F10.0)
   READ(NR,*)H1,T1,ALF1,E1,NU1,ETA1,TG11
   WRITE(NW,8)H1,T1,ALF1,E1,NU1,ETA1,TG11
   READ(NR,*)H2,T2,ALF2,E2,NU2,ETA2,TG22
   WRITE(NW,8)H2,T2,ALF2,E2,NU2,ETA2,TG22
2  FORMAT(6F10.3,F12.0)
   READ(NR,*) L, L2, S, P, T, D, ET
   WRITE(NW,2) L,L2,S,P,T,D,ET
3  FORMAT(F10.3,3F10.1,F6.3,F6.3)
   READ(NR,*)ARADI,P1,P2,P3,FN
   WRITE(NW,3)ARADI,P1,P2,P3,FN
   READ(NR,*)ALFAT,ALFAS,TTUBE,TSHELL
   WRITE(NW,8)ALFAT,ALFAS,TTUBE,TSHELL
6  FORMAT (I10 ,F10.5)
   READ(NR,*) JSKIP ,BEGIN
   WRITE(NW,6) JSKIP ,BEGIN
C   JSKIP      UPPER BOUND FOR NUMBER OF MATRIX PRINTED
C   BEGIN      VALUE WHERE MATRIX FOR LARGE R VALUES ARE BEGUN
C
C   READ OUT DATA
C
10 FORMAT(1H1)
   WRITE(NW,10)
11 FORMAT(11X,'INPUT DATA')
   WRITE(NW,11)
12 FORMAT('0',' TUBE SHEET ONE:')
   WRITE(NW,12)
13 FORMAT(' ',' E1=',F10.0,3X,'NU1=',F5.3,3X,'THICKNESS=',F4.1,3X,'T
1EMP.=',F5.1)
   WRITE(NW,13)E1,NU1,H1,T1
14 FORMAT(' ',' ETA1(=ES1/E1)=',F7.4,3X,'THERMAL COEFF.='F11.8)
   WRITE(NW,14)ETA1,ALF1
15 FORMAT('0',' TUBE SHEET TWO:')
   WRITE(NW,15)
16 FORMAT(' ',' E2=',F10.0,3X,'NU2=',F5.3,3X,'THICKNESS=',F4.1,3X,'T
1EMP.=',F5.1)
   WRITE(NW,16)E2,NU2,H2,T2
17 FORMAT(' ',' ETA2(=ES2/E2)=',F7.4,3X,'THERMAL COEFF.='F11.8)
   WRITE(NW,17)ETA2,ALF2
18 FORMAT('0',' TUBES:')
   WRITE(NW,18)
19 FORMAT(' ',' DISTANCE L1=',F5.1,3X,'DISTANCE L2=',F5.1,3X,'DISTAN
1CE S=',F5.1)
   WRITE(NW,19)L,L2,S
20 FORMAT(' ',' PITCH=',F5.2,3X,'THICKNESS=',F5.3,3X,'DIAMETER=',F4.
11,3X,'ET=',F10.0)
   WRITE(NW,20)P,T,D,ET
   WRITE(NW,*)' AXIAL THERMAL DATA'
   WRITE(NW,*)' ALFAT=',ALFAT,' ALFAS=',ALFAS,' TTUBE='
1,TTUBE,' TSHELL=',TSHELL
21 FORMAT('0','GENERAL:')
   WRITE(NW,21)

```

```

22  FORMAT(' ', ' SHELL RADIUS=' ,F6.2,3X, 'P1=' ,F6.1,3X, 'P2=' ,F6.1,3X, '
1P3=' ,F6.1)
    WRITE(NW,22)ARADI,P1,P2,P3
23  FORMAT(' ', '3X, 'FN=' ,F6.3)
    WRITE(NW,23)FN
24  FORMAT('0', 'MATRIX TERMS SHIFT AT R EQUALS',F8.5)
    WRITE(NW,24)BEGIN
25  FORMAT('0')
    WRITE(NW,25)
1000 CONTINUE
C    ASSIGN VALUES TO CONSTANT TERMS FROM INPUT DATA
C
    PIE= 3.141592654
    NU=.30
    I=(D**4-(D-2.0*T)**4)*PIE/64
    G=ET/(2.0*(1.0+NU))
    LG=8.0*ET/(G*(PIE*(D**2-(D-2.0*T)**2)))*I
    LM1=1.0-PIE*((D-2.0*T)**2)/(((P**2)*DSQRT(12.DO)))
    LM2=1.0-PIE*(D**2)/((P**2)*DSQRT(12.DO))
    KS1=(E1*H1)/(1.-NU1*NU1)*ETA1
    KS2=(E2*H2)/(1.-NU2*NU2)*ETA2
    C11=9.*FN/2.-12.
    C12=3.*(FN/2.-1.)+C11*H2/(2.*S)
    C13=18./5.*(FN/2.-1.)
    C21=3.*(FN/2.-1.)
    C22=FN/2.+C21*H2/(2.*S)
    C23=.6*FN
    ATUBE=PIE*(D-T)*T
    AAA=P*P*DSIN(PIE/3.DO)
    X1=ET*ATUBE/AAA
    XT=X1*ALFAT*TTUBE
    XS=X1*ALFAS*TSHELL
    GM=2.0*ET*I/(L**3+12.0*L*LG)
    GMA=GM
    GS1=E1/(2.*(1.+NU1))
    GS2=E2/(2.*(1.+NU2))
    MS1=KS1*H1*TG11*(1.+NU1)*ALF1/12.
    MS2=KS2*H2*TG22*(1.+NU2)*ALF2/12.
    NS1=KS1*ALF1*T1*(1.+NU1)
    NS2=KS2*ALF2*T2*(1.+NU2)
    SQG=2./((DSQRT(3.DO))*P**2)
    B1=PIE*T*(D-T)*ET/L
    B2=PIE*T*(D-T)*ET/L2
    PL1=P1*LM1
    PU1=P2*LM2
    PL2=P2*LM2
    PU2=P3*LM2
    F=GM*SQG
    AR=ARADI
C    SET FLAGS FOR LATER ROUTINES
    FLAG=2

```

C

```

C REENTER AFTER SKIPPING READ & WRITE STATEMENTS
C AND INITIALIZATION OF CONSTANT TERMS
C
C BOMB STOP 1
  IF (FLAG.EQ.0) GO TO 6000
  DO 50 J1=1,12
C INITIALIZE ARRAY A & B
  B(J1) =0.0
  DO 50 J2=1,12
50 A(J1,J2)=0.0

C
C
C SKIP TERMS FOR R CLOSE TO ZERO
C
  IF (R.GE.BEGIN) GO TO 2000
C *****
C MATRIX VALUES FOR R CLOSE TO ZERO
C *****
  A(1,11)=-AR*SQG*B1/(2.*E1)
  A(1,12)=AR*SQG*B1*H2/(2.*H1*E1)
  A(2,11)=AR*SQG*B1*H1/(2.*H2*E2)
  A(2,12)=-AR*(B1+B2)/(2.*E2)*SQG
  A(3,7)=3.*AR*F/E1
  A(3,8)=-3.*AR*F*H2/(E1*H1)
  A(3,9)=1.5*AR*F*(H1+L)/(E1*H1)
  A(3,10)=1.5*AR*F*(H2+L)/(E1*H1)
  A(4,7)=-3.*AR*F*H1/(E2*H2)
  A(4,8)=1.5*SQG*AR/E2*2.*(ET*I*C11/(3.*S*S)+GM)
  A(4,9)=-1.5*AR*F*(H1+L)/(E2*H2)
  A(4,10)=1.5*AR*SQG/(E2*H2)*(2.*ET*I*C12/(3.*S*S)-GM*(H2+L))
  A(5,7)=1.5*AR*F/E1*(1.+L/H1)
  A(5,8)=-1.5*AR*F*H2/(E1*H1)*(1.+L/H1)
  A(5,9)=AR*F/(E1*H1)*( .75*(H1+L)+( .75*L*H1+L*L+3.*LG)/H1)
  A(5,10)=AR*F/(E1*H1)*( .75*(H2+L)+( .75*L*H2+L*L-3.*LG)/H1)
  A(6,7)=1.5*AR*F*H1/(E2*H2)*(1.+L/H2)
  A(6,8)=1.5*AR*SQG/E2*(ET*I*C11/(3.*S*S)+2.*ET*I*C21/(3.*H2*S*S)-
1 GM*(1.+L/H2))
  A(6,9)=AR*F/(E2*H2)*( .75*(H1+L)+( .75*L*H1+.5*L*L-3.*LG)/H2)
  A(6,10)=AR*SQG/(E2*H2)*( .75*GM*(H2+L)+ET*I*(C12/(2.*S*S)+C22/(H2*
1 S))+GM/H2*( .75*L*H2+L*L+3.*LG))
  A(7,3)=AR*(1.-NU1)/(ETA1*H1)
  A(8,4)=AR*(1.-NU2)/(ETA2*H2)
  A(9,5)=12.*AR*(1.-NU1)/(ETA1*H1)
  A(10,6)=12.*AR*(1.-NU2)/(ETA2*H2)
  A(11,9)=-AR/H1
  A(12,10)=-AR/H2
C *****
  B(1)=AR/(2.*H1*E1)*(PL1-PU1-XT)
  B(2)=AR/(2.*H2*E2)*(PL2-PU2+XS)
  B(7)=AR*NS1/(ETA1*H1*H1*E1)*(1.-NU1)
  B(8)=AR*NS2/(ETA2*H2*H2*E2)*(1.-NU2)

```

```

B(9)=12.*AR*MS1*(1.-NU1)/(ETA1*H1*H1*H1*E1)
B(10)=12.*AR*MS2*(1.-NU2)/(ETA2*H2*H2*H2*E2)

C
C   END MATRIX TERMS EXCLUSIVELY FOR R CLOSE TO ZERO
C
C   *****
C MATRIX TERMS FOR ANY R
C   *****
2000 CONTINUE
A(11,1)=-AR*E1*6./(5.*H1*GS1)
A(11,9)=-AR/H1
A(12,2)=-6.*AR*E2/(5.*H2*GS2)
A(12,10)=-AR/H2

C
C   END OF COMMON TERMS
C
C   IF (R.LT.BEGIN) GO TO 3000
C   BOMB STOP 2
C   IF (R.EQ.0.DO) GO TO 6001
C   *****
C MATRIX TERMS FOR R MUCH > ZERO
C   *****
A(1,1)=-1./R
A(1,11)=-AR*SQG*B1/E1
A(1,12)=AR*H2*SQG*B1/(E1*H1)
A(2,2)=-1./R
A(2,11)=AR*H1*SQG*B1/(E2*H2)
A(2,12)=-AR*SQG*(B1+B2)/E2
A(3,1)=18.*F*L*AR/(5.*GS1*H1)
A(3,2)=18.*F*L*AR*E2/(5.*GS2*H1*E1)
A(3,3)=(NU1-1.)/R
A(3,7)=ETA1*H1/(AR*R*R)+6.*AR*F/E1
A(3,8)=-6.*AR*H2*F/(E1*H1)
A(3,9)=3.*AR*F*(H1+L)/(E1*H1)
A(3,10)=3.*AR*F*(H2+L)/(E1*H1)
A(4,1)=-18.*AR*F*L*E1/(5.*GS1*H2*E2)
A(4,2)=2.*ET*I*C13*AR*SQG/(GS2*H2*S*S)-18.*AR*F*L/(GS2*H2*5.)
A(4,4)=(NU2-1.)/R
A(4,7)=-6.*AR*F*H1/(E2*H2)
A(4,8)=6.*SQG*AR*(ET*I*C11/(3.*S*S*S)+GM)/E2+ETA2*H2/(AR*R*R)
A(4,9)=-3.*AR*F*(H1+L)/(E2*H2)
A(4,10)=(2.*ET*I*C12/(3.*S*S*S)-GM*(H2+L))*3.*AR*SQG/(E2*H2)
A(5,1)=-AR/H1+9.*AR*L*F/(5.*GS1*H1)+12.*AR*F*L*L*(1.+3.*LG/(L*L))/
1(5.*H1*H1*GS1)
A(5,2)=9.*AR*L*F*E2*H2/(5.*GS2*H2*H1*E2)+6.*E2*AR*F*L*L*(1.-6.*LG
1/(L*L))/(E1*H1*H1*GS2*5.)
A(5,5)=(NU1-1.)/R
A(5,7)=3.*AR*F*(1.+L/H1)/E1
A(5,8)=-3.*AR*F*H2*(1.+L/H1)/(E1*H1)
A(5,9)=ETA1*H1/(12.*AR*R*R)+AR*F/(E1*H1)*(1.5*(H1+L)+(1.5*L*H1+2.
1*L*L+6.*LG)/H1)
A(5,10)=AR*F/(E1*H1)*(1.5*(H2+L)+(1.5*L*H2+L*L-6.*LG)/H1)

```

```

A(6,1)=6.*AR*F*(1.-6.*LG/(L*L))*E1*L*L/(5.*E2*H2*H2*GS1)
A(6,2)=-AR/H2+ET*I/(GS2*H2*H2)*(2.*AR*SQG*C23/S+SQG*AR*H2*C13/(S*S
1))+12.*AR*F*L*L*(1.+3.*LG/(L*L))/(5.*GS2*H2*H2)
A(6,6)=A(4,4)
A(6,7)=3.*AR*F*H1*(1.+L/H2)/(E2*H2)
A(6,8)=1.5*AR*SQG/E2*(2.*ET*I*C11/(3.*S*S*S)-2.*GM+2./H2*(ET*I*C21
1)*2./(3.*S*S)-GM*L))
A(6,9)=AR*F/(E2*H2)*(1.5*(H1+L)+(1.5*H1*L+L*L-6.*LG)/H2)
A(6,10)=AR*SQG*(1.5*GM*(H2+L)+ET*I*(2.*S/H2*C22+C12)/(S*S)+GM/H2*
1(1.5*L*H2+2.*L*L+6.*LG))/(E2*H2)+ETA2*H2/(12.*AR*R*R)
A(7,3)=AR*(1.-NU1*NU1)/(ETA1*H1)
A(7,7)=-NU1/R
A(8,4)=AR*(1.-NU2*NU2)/(ETA2*H2)
A(8,8)=-NU2/R
A(9,5)=12.*AR*(1.-NU1*NU1)/(ETA1*H1)
A(9,9)=A(7,7)
A(10,6)=12.*AR*(1.-NU2*NU2)/(ETA2*H2)
A(10,10)=A(8,8)
C *****
B(1)=AR*(PL1-PU1)/(E1*H1)
B(2)=AR*(PL2-PU2)/(E2*H2)
B(3)=NS1*(NU1-1.)/(R*E1*H1)
B(4)=NS2*(NU2-1.)/(R*E2*H2)
B(5)=MS1*(NU1-1.)/(R*E1*H1*H1)
B(6)=MS2*(NU2-1.)/(R*E2*H2*H2)
B(7)=AR*NS1/(H1*KS1)
B(8)=AR*NS2/(H2*KS2)
B(9)=12.*AR*MS1*(1.-NU1*NU1)/(ETA1*H1*H1*H1*E1)
B(10)=12.*AR*MS2*(1.-NU2*NU2)/(ETA2*H2*H2*H2*E2)
C
3000 CONTINUE
      RETURN
7000 FORMAT (1H0, ' BOMB STOP 1  ' )
6000 WRITE(NW,7000)
      STOP
7001 FORMAT (1H0, ' BOMB STOP 2' )
6001 WRITE(NW,7001 )
      STOP
      END
      SUBROUTINE RUNGE (X,IER,N)
C
      IMPLICIT DOUBLE PRECISION(A-H,O-Z)
      DIMENSION PHI(84),SAVEY(84)
      COMMON/PARAM/ XL,H,NR,JNDIC,KNDIC,NRR,NW
      COMMON/COM1/ Y (84),F (84)
      COMMON/TEST/NTST
      IER1 = 0
      IF(NTST.EQ.1)WRITE(NW,*)'ENT FUN1 FROM RUNG'
      CALL FUNCT(X,IER1,N)
      IF(IER1.NE.0) GO TO 2500
      DO 22 J=1,N
      SAVEY(J) = Y(J)

```

```

      PHI(J) = F(J)
22  Y(J) = SAVEY(J) + H*F(J)/2.DO
      X = X+H/2.DO
      IF(NTST.EQ.1)WRITE(NW,*)'ENT FUN2 FROM RUNG'
      CALL FUNCT(X,IER1,N)
      IF(IER1.NE.0) GO TO 2500
      DO 33 J=1,N
      PHI(J) = PHI(J) + 2.DO*F(J)
33  Y(J) = SAVEY(J) + H*F(J)/2.DO
      IER1 = 0
      IF(NTST.EQ.1)WRITE(NW,*)'ENT FUN3 FROM RUNG'
      CALL FUNCT(X,IER1,N)
      IF(IER1.NE.0) GO TO 2500
      DO 44 J=1,N
      PHI(J) = PHI(J) + 2.DO*F(J)
44  Y(J) = SAVEY(J) + H*F(J)

      X = X +H/2.DO
      IER1 = 0
      IF(NTST.EQ.1)WRITE(NW,*)'ENT FUN4 FROM RUNG'
      CALL FUNCT(X,IER1,N)
      IF(IER1.NE.0) GO TO 2500
      DO 55 J=1,N
55  Y(J)=SAVEY(J)+(PHI(J)+F(J))*H/6.DO
      RETURN
2500 WRITE(NW,9000) IER1
9000 FORMAT( ' ERROR IN RUNGE.  IER1 = ',I5)
      IER = 10
      RETURN
      END
      SUBROUTINE BCON
      IMPLICIT DOUBLE PRECISION(A-H,O-Z)
      INTEGER BCN
      DIMENSION T(30,30)
      COMMON/PARAM/ XL,H,N,JNDIC,KNDIC,NR,NW
      COMMON/COM1/ YR(84),FR(84)
      COMMON/COM2/ BCN(12,2),BNA(6),BNB(6)
      COMMON/COM4/OMEGA,DET,LNDIC
      COMMON/TEST/NTST
      N1=N/2
      N2=N1+1
      N3=N1**2

C ....REARRANGE MATRIX
C ....
      DO 30 I=1,N
      DO 30 J=1,N
30  T(I,J)=0.DO
      J1=1
      DO 55 I=1,N1
      IF(BCN(I,2).NE.0) GO TO 35
      T(I,I)=1.DO
      IF(I.EQ.N1) GO TO 35

```

```

      GO TO 55
35   DO 45 J=J1,N1
      IF(BCN(J+N1,2).NE.0) GO TO 40
      T(I,J+N1)=1.DO
      T(J+N1,I)=1.DO
      GO TO 50
40   T(J+N1,J+N1)=1.DO
45   CONTINUE
50   J1=J+1
55   CONTINUE
      DO 60 I=1,N
      DO 60 J=1,N2
      IJ=I+(J-1)*N
      FR(IJ)=0.0
      DO 60 K=1,N
      KJ=K+(J-1)*N
60   FR(IJ)=T(I,K)*YR(KJ)+FR(IJ)
C    ....PARTITION MATRIX
C    ....
      DO 65 I=1,N3,N1
      DO 65 J=1,N1
      IJ=I+J-1
      IJ1=IJ+I+N-1
65   YR(IJ)=FR(IJ1)

      DO 70 I=1,N1
70   FR(I)=BNB(I)-FR(I)
      IF(LNDIC.EQ.1) GO TO 80
      IF(NTST.EQ.1) WRITE(NW,*) 'ENT MINV FROM BCON'
      CALL MINV(N1,N3,DET)
      RETURN
80   CONTINUE
      IF(NTST.EQ.1) WRITE(NW,*) 'ENT SIMQ FROM BCON'
      CALL SIMQ(N1,KS)
      IF(KS.NE.0) GO TO 2600
      YR(1)=1.0
      DO 85 I=1,N1
85   YR(I+1)=FR(I)
      RETURN
2600 WRITE(NW,4200) KS
4200 FORMAT(3X,'CALCULATION TERMINATED. KS=',15)
      RETURN
      END
      SUBROUTINE SIMQ(N,KS)
      IMPLICIT DOUBLE PRECISION(A-H,O-Z)
      DOUBLE PRECISION BIGA,TOL,A,B
      COMMON/COM1/ A (84),B (84)

```

```

C
C    FORWARD SOLUTION
C

```

```

TOL=0.DO
KS=0

```

```

JJ=-N
DO 65 J=1,N
JY=J+1
JJ=JJ+N+1
BIGA=0.DO
IT=JJ-J
DO 30 I=J,N

C
C      SEARCH FOR MAXIMUM COEFFICIENT IN COLUMN
C
      IJ=IT+I
      IF(DABS(BIGA)-DABS(A(IJ))) 20,30,30
20  BIGA=A(IJ)
      IMAX=I
30  CONTINUE

C
C      TEST FOR PIVOT LESS THAN TOLERANCE (SINGULAR MATRIX)
C      TEST FOR PIVOT LESS THAN TOLERANCE (SINGULAR MATRIX)
C
      IF(DABS(BIGA)-TOL) 35,35,40
35  KS=1
      RETURN

C
C      INTERCHANGE ROWS IF NECESSARY
C
40  I1=J+N*(J-2)
      IT=IMAX-J
      DO 50 K=J,N
      I1=I1+N
      I2=I1+IT
      SAVE=A(I1)
      A(I1)=A(I2)
      A(I2)=SAVE

C
C      DIVIDE EQUATION BY LEADING COEFFICIENT
C
50  A(I1)=A(I1)/BIGA
      SAVE=B(IMAX)
      B(IMAX)=B(J)
      B(J)=SAVE/BIGA

C
C      ELIMINATE NEXT VARIABLE

      IF(J-N) 55,70,55
55  IQS=N*(J-1)
      DO 65 IX=JY,N
      IXJ=IQS+IX
      IT=J-IX
      DO 60 JX=JY,N
      IXJX=N*(JX-1)+IX
      JJX=IXJX+IT
60  A(IXJX)=A(IXJX)-(A(IXJ)*A(JJX))

```

```

65 B(IX)=B(IX)-(B(J)*A(IXJ))
C
C     BACK SOLUTION
C
70 NY=N-1
   IF(NY.EQ.0) GO TO 81
   IT=N*N
   DO 80 J=1,NY
   IA=IT-J
   IB=N-J
   IC=N
   DO 80 K=1,J
   B(IB)=B(IB)-A(IA)*B(IC)
   IA=IA-N
80 IC=IC-1
81 CONTINUE
   RETURN
   END
   SUBROUTINE FUNCT(X,IER,N)
   IMPLICIT DOUBLE PRECISION(A-H,O-Z)
   COMMON/PARAM/ XL,H,NR,JNDIC,KNDIC,NRR,NW
   COMMON/MTINP/ A(12,12),B(12),INDIC
   COMMON/COM1/ Y (84),F (84)
   COMMON/COM4/OMEGA,DET,LNDIC
   COMMON/COM5/FLAG
   COMMON/COM6/JSKIP
   COMMON/TEST/NTST
   INTEGER FLAG
   DATA M/O/
   DATA XS/1234569.DO/
   M=M+1
   N2=NR/2+1
C   ....GUARD AGAINST OVERFLOW
C   ....
   IER=0
   DO 3I=1,N
   IF(DABS(Y(I)).GE.10.D70) GO TO 9050
3   CONTINUE
   GO TO (25,5,10,20),INDIC
5   CONTINUE

   ..INSERT EXPRESSIONS FOR VARIABLE ELEMENTS OF
C   ....LOAD VECTOR B
   GO TO 25
10  CONTINUE
C   ....INSERT EXPRESSIONS FOR VARIABLE ELEMENTS OF
C   ....MATRIX A
   GO TO 25
20  CONTINUE
C   ....INSERT EXPRESSIONS FOR VARIABLE ELEMENTS OF
C   ....MATRIX A AND LOAD VECTOR B
C
   IF(NTST.EQ.1)WRITE(NW,*)'ENT HELP FROM FUNC'
```

```

      CALL HELP (X,FLAG)
C
25   IF(M.GT.JSKIP) GO TO 38
      IF(XS.EQ.X) GO TO 38
C....PRINT OUT A AND B MATRICES
C....
      GO TO (26,27),LNDIC
26   WRITE(NW,7000) X
      WRITE(NW,7005)
      GO TO 28
27   WRITE(NW,7001)
28   K1=1
      K2=12
29   IF(K2.GE.NR) K2=NR
      DO 30 I=1, NR
30   WRITE(NW,7002)(A(I,J),J=K1,K2)
      IF(K2.EQ.NR) GO TO 35
      K1=K2+1
      K2=K2+12
      WRITE(NW,7003)
      GO TO 29
35   CONTINUE
      IF(LNDIC.EQ.2) GO TO 38
      WRITE(NW,7003)
      WRITE(NW,7004)(B(I),I=1, NR)
      WRITE(NW,7003)
38   CONTINUE
      XS=X
      DO 45 I=1, NR
      DO 40 J=1, N2
      IJ=I+(J-1)*NR
      F(IJ)=0.0
      DO 40 K=1, NR
      KJ=K+(J-1)*NR
40   F(IJ)=A(I,K)*Y(KJ)+F(IJ)
45   F(I)=F(I)+B(I)
      RETURN
9050  IER=1
      RETURN
7000  FORMAT(1H,////,30X,'STATIC SOLUTION',////,20X,'THE INPUT MATRICES
$  A AND B ARE FOR X EQUALS ',F10.5 )
7001  FORMAT(1H,///30X,'NATURAL FREQUENCY ANALYSIS',////,30X,'THE
1  INPUT MATRIX A IS:')
7002  FORMAT(1X,12D9.2)
7003  FORMAT(1H,////)
7004  FORMAT(30X,D12.6)
7005  FORMAT(1HO)

      END
      SUBROUTINE MINV(N,N1,D)
C
      IMPLICIT DOUBLE PRECISION(A-H,O-Z)
      DIMENSION L(30),M(30)

```

```

COMMON/COM1/A(84),B(84)
COMMON/PARAM/ XL,H,NR,JNDIC,KNDIC,NRR,NW
D=1.0
NK=-N
DO 80 K=1,N
NK=NK+N
L(K)=K
M(K)=K
KK=NK+K
BIGA=A(KK)
DO 20 J=K,N
IZ=N*(J-1)
DO 20 I=K,N
IJ=IZ+I
10 IF(DABS(BIGA)-DABS(A(IJ))) 15,20,20
15 BIGA=A(IJ)
L(K)=I
M(K)=J
20 CONTINUE
J=L(K)
IF(J-K) 35,35,25
25 KI=K-N
DO 30 I=1,N
KI=KI+N
HOLD=-A(KI)
JI=KI-K+J
A(KI)=A(JI)
30 A(JI) =HOLD
35 I=M(K)
IF(I-K) 45,45,38
38 JP=N*(I-1)
DO 40 J=1,N
JK=NK+J
JI=JP+J
HOLD=-A(JK)
A(JK)=A(JI)
40 A(JI) =HOLD
45 IF(BIGA) 48,46,48
46 D=0.0
WRITE(NW,5000) D
5000 FORMAT(///,'MATRIX IS SINGULAR D=',F14.6)
RETURN
48 DO 55 I=1,N
IF(I-K) 50,55,50
50 IK=NK+I
A(IK)=A(IK)/(-BIGA)
55 CONTINUE
DO 65 I=1,N
IK=NK+I
HOLD=A(IK)
IJ=I-N
DO 65 J=1,N

```

```

      IJ=IJ+N
      IF(I-K) 60,65,60
60    IF(J-K) 62,65,62
62    KJ=IJ-I+K
      A(IJ)=HOLD*A(KJ)+A(IJ)
65    CONTINUE
      KJ=K-N
      DO 75 J=1,N
      KJ=KJ+N
      IF(J-K) 70,75,70
70    A(KJ)=A(KJ)/BIGA
75    CONTINUE
      D=D*BIGA
      A(KK)=1.0/BIGA
80    CONTINUE
      K=N
100   K=(K-1)
      IF(K) 150,150,105
105   I=L(K)
      IF(I-K) 120,120,108
108   JQ=N*(K-1)
      JR=N*(I-1)
      DO 110 J=1,N
      JK=JQ+J
      HOLD=A(JK)
      JI=JR+J
      A(JK)=-A(JI)
110   A(JI) =HOLD
120   J=M(K)
      IF(J-K) 100,100,125
125   KI=K-N
      DO 130 I=1,N
      KI=KI+N
      HOLD=A(KI)
      JI=KI-K+J
      A(KI)=-A(JI)
130   A(JI) =HOLD
      GO TO 100
150   CONTINUE
      RETURN
      END

```

APPENDIX 10.B

SAMPLE INPUT AND OUTPUT FILES
FOR EXAMPLE PROBLEM OF SECTION 10.4

*** INPUT DATA FILE ***

```

1.,.004,12,2,8,4,1
0.,0.,0.,0.,0.,0.
0.,0.,0.,0.,0.,0.
0,0,1,1,1,1,0,0,0,0,1,1
1,1,0,0,1,1,1,1,0,0,0,0
.005,2.,.9,.5
0.,.3,.6,.9,.925,.95,.975,1.
1.,100.,.0000093,30000000.,.28,.3,0.
1.,100.,.0000063,30000000.,.28,.3,0.
.5,200.,40.,1.25,.049,1.,30000000.
20.,0.,0.,0.,3.46
0.,0.,0.,0.
0.,.01
    
```

*** OUTPUT OF RESULTS***

DOUBLE TUBESHEET ANALYSIS PROGRAM
PREPARED BY A.I. SOLER SEPT. 1983

OUTPUT OF RAW INPUT DATA

1.00000	.00400	12	2	8	4	1		
.00000	.00000	.00000	.00000	.00000	.00000	.00000	.00000	
.00000	.00000	.00000	.00000	.00000	.00000	.00000	.00000	
0	1							
0	1							
1	0							
1	0							
1	1							
1	1							
0	1							
0	1							
0	0							
0	0							
1	0							
1	0							
.00000	.30000	.60000	.90000	.92500	.95000	.97500		
1.00000								

1 A GENERAL COMPUTER PROGRAM FOR THE SOLUTION OF A TWO POINT BOUNDAR

LENGTH OF FUN X = 1.00000
 STEPSIZE = .00400
 NUMBER OF EQS. = 12
 NO. OUTPT PTS. = 8
 STEPSIZE CHGS. = 2

```
.10000D+01 .10000D+03 .93000D-05 .30000D+08 .28000D+00 .30000D+00 .0000
.10000D+01 .10000D+03 .63000D-05 .30000D+08 .28000D+00 .30000D+00 .0000
.500 200.000 40.000 1.250 .049 1.000 30000000.
20.000 .0 .0 .0 3.460
.00000D+00 .00000D+00 .00000D+00 .00000D+00
0 .01000
```

1

INPUT DATA

OTUBE SHEET ONE:

E1= 30000000. NU1= .280 THICKNESS= 1.0 TEMP.=100.0
 ETA1(=E1/E1)= .3000 THERMAL COEFF.= .00000930

OTUBE SHEET TWO:

E2= 30000000. NU2= .280 THICKNESS= 1.0 TEMP.=100.0
 ETA2(=E2/E2)= .3000 THERMAL COEFF.= .00000630

OTUBES:

DISTANCE L1= .5 DISTANCE L2=200.0 DISTANCE S= 40.0
 PITCH= 1.25 THICKNESS= .049 DIAMETER= 1.0 ET= 30000000.

AXIAL THERMAL DATA

ALFAT= .0000000000000000E+00 ALFAS= .0000000000000000E+00 TTUBE= .000000

OGENERAL:

SHELL RADIUS= 20.00 P1= .0 P2= .0 P3= .0
 FN= 3.460

OMATRIX TERMS SHIFT AT R EQUALS .01000

0

AT X= .0040 THE STEPSIZE H WAS CHANGED TO .0080

AT X= .9000 THE STEPSIZE H WAS CHANGED TO .0040

RESULTS FOR TUBESHEETS

R/RO	V1	V2	N1	N2	M1	M2	U1
0.00D+00	0.00D+00	0.00D+00	-1.96D+03	1.95D+03	1.15D+01	1.14D+01	0.00D+0
3.00D-01	2.90D+01	3.44D+01	-1.88D+03	1.87D+03	3.35D+00	3.26D+00	4.66D-0
6.00D-01	6.79D+01	7.46D+01	-1.60D+03	1.60D+03	-2.61D+01	-2.61D+01	9.35D-0
9.00D-01	9.69D+01	9.77D+01	-1.04D+03	1.04D+03	-3.91D+01	-3.91D+01	1.44D-0
9.25D-01	9.59D+01	9.72D+01	-9.43D+02	9.43D+02	-2.12D+00	-2.35D+00	1.48D-0
9.50D-01	9.37D+01	9.63D+01	-7.92D+02	7.92D+02	7.42D+01	7.33D+01	1.52D-0
9.75D-01	9.10D+01	9.48D+01	-4.86D+02	4.86D+02	2.62D+02	2.62D+02	1.57D-0
1.00D+00	9.12D+01	9.12D+01	-2.23D-01	3.89D-01	5.92D+02	5.95D+02	1.62D-0

RESULTS FOR TUBE ARRAY							
R/RO	H1TUBE	M1TUBE	F1TUBE	H2TUBE	M2TUBE	F2TUBE	H3TUBE
0.00D+00	0.00D+00	0.00D+00	1.19D+01	0.00D+00	0.00D+00	2.65D+01	0.00D+0
3.00D-01	4.59D+01	1.15D+01	1.42D+01	-4.59D+01	1.14D+01	3.05D+01	3.33D-0
6.00D-01	1.07D+02	2.67D+01	1.73D+01	-1.07D+02	2.67D+01	3.48D+01	4.89D-0
9.00D-01	2.67D+02	6.61D+01	5.89D+00	-2.67D+02	6.74D+01	1.26D+01	2.69D-0
9.25D-01	3.73D+02	9.25D+01	2.88D+00	-3.73D+02	9.38D+01	8.80D+00	2.73D-0
9.50D-01	5.75D+02	1.43D+02	2.62D-01	-5.75D+02	1.44D+02	5.03D+00	3.20D-0
9.75D-01	1.06D+03	2.64D+02	0.00D+00	-1.06D+03	2.65D+02	1.35D+00	4.92D-0
1.00D+00	1.90D+03	4.75D+02	0.00D+00	-1.90D+03	4.75D+02	0.00D+00	8.47D-0

11. RECTANGULAR TUBESHEETS— APPLICATION TO POWER PLANT CONDENSERS

11.1 INTRODUCTION

In previous chapters dealing with tubesheet stress analysis, we have focused exclusively on circular units and we have assumed that tubesheet geometry, loading, and edge conditions did not vary around the periphery. These restrictions permitted us to develop considerably detailed analytical models, leading either to numerical solution procedures, or to simplified, almost closed form, analytical solutions. Since the large majority of tubesheets are of circular shape, these analyses and solution methods have wide applicability. Tubesheets of non-circular shapes, however, are also used, particularly in low pressure, large volume flow rate conditions. Specifically, in this chapter, we will focus on the class of rectangular tubesheets used in large power plant condensers. We will provide a detailed discussion of the loading conditions and the geometry to highlight the complexities that obstruct the effort to obtain a satisfactory simplified solution. In the next section, we will first fully describe the power condenser tubesheet environment and provide an overview of the tubesheet design problem. Following this introductory material, we will present a very approximate design method, based on the theory of a beam strip on an elastic foundation. This approximate analysis, although replete with assumptions, both substantiated and unsubstantiated, at least permits investigation of the effect of various tubesheet parameters. We will fully develop the approximate method and show an application of it to the condenser tubesheet design problem.

11.2 THE CONDENSER TUBESHEET DESIGN PROBLEM

Figure 11.2.1 shows a side view of the basic power plant condenser. The dimensions of a typical tubesheet in a single pass of tubes may be of the order of $12' \times 10'$, encompassing 16,000 tubes. Steam from the low pressure turbine is condensed inside of the condenser shell and gives up its latent heat to cooling water flowing through the tubes. The cooling water enters an inlet waterbox, passes through the tubes, and leaves the condenser through the outlet waterbox. Figure 11.2.1 shows a single pass unit for simplicity, although multiple pass units are used in many installations. Prior to the early '60's, most condenser installations were at minimum height above the cooling water source and often used a siphon circuit to minimize

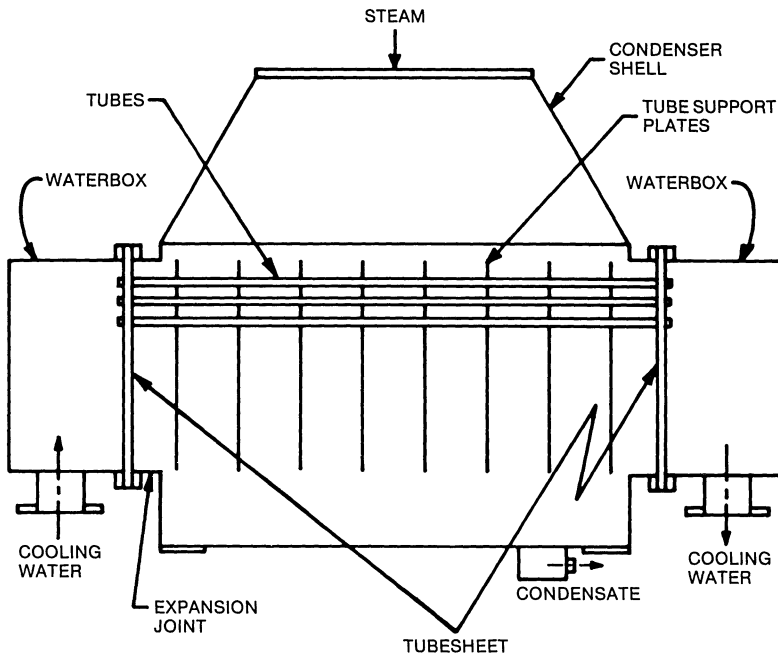


Fig. 11.2.1. Sectional view of condenser.

pumping requirements. Under these siphon circuit conditions, the circulating water system pressure (in the waterboxes and tubes) seldom exceeded 20–30 psi. Since under normal operating conditions, the condenser shell operates under a partial vacuum, the condenser tubesheet seldom experienced a pressure differential higher than 45 psi. Because of these relatively low operating pressures, design of condenser tubesheets was usually based on manufacturer's standards developed over years of service. Generally speaking, very little stress analysis of the condenser tubesheet appears to have been done on siphon circuit units; most tubesheets are on the order of 1" to 1.25" thick regardless of the particular operating pressure and the unit size. It appears that the choice of tubesheet thickness was made not from any consideration of bending stress in the tubesheet, but rather from the dictum that a certain minimum tubesheet thickness was required in order to provide sufficient surface for a satisfactory rolled tube-to-tubesheet joint. Typically, a one-inch minimum tubesheet thickness was needed to provide adequate resistance against tube pullout under load.

In recent years, as environmental concerns have played a larger role in plant design, the condenser tubesheet operating conditions have changed. Since the warm circulating water discharged from the condenser outlet can cause thermal pollution of the heat sink, many of the new units designed

since the 1960's require use of closed loop cooling systems. Where suitable holding techniques cannot limit thermal discharges to acceptable temperature levels, cooling towers are employed in the circulating water system to dissipate the heat from the condensing steam. Because of long piping runs and added static heads involved in cooling tower circuits, circulating water system pressures in the condenser waterboxes have increased considerably. It is now not uncommon to have 100 psi specified as unit design pressure with 150 psi mandated for the hydrostatic test condition. This large pressure increase, coupled with the popularity of substantial increases in plant sizes in the late 1960's through the middle 1970's (leading to condensers with larger tubesheets), has prompted a detailed stress analysis of condenser tubesheets to ensure that the tubesheet thickness is sufficient to keep stress levels within margins specified by safety codes.

Prior to outlining the stress analysis procedure, it is necessary to delineate the various loadings involved, the structural geometries for typical installations, and the influence that these factors have on formulation of simplified design methods. Although variations in condenser geometries abound, Fig. 11.2.1 shows the basic configuration of condenser shell, tube bundle, tube support plates, tubesheets, and waterboxes. The unbalanced hydrostatic pressure on the waterbox is generally resisted solely by the tubes since an expansion joint is normally placed at one end of the shell. This expansion joint is almost always present in large units to minimize thermal stresses arising from differential expansion between tubes and shell (along the tube axis). The presence of the expansion joint means that for tubesheet stress analysis purposes, we can consider a floating head heat exchanger, carrying only mechanical loading, albeit of rectangular shape. If we neglect the small axial loading transmitted by the shell expansion joint, we see that the major loads acting on the tubesheet are the hydrostatic load from the waterbox and the local tubesheet surface pressure. These loadings are shown graphically in Fig. 11.2.2 and are resisted by loading of the individual tubes. Generally, the hydrostatic pull from the waterbox will vary around the periphery of the tubesheet. This is due to the fact that not only must the tubesheet resist the direct load (the product of waterbox pressure and the full projected cross-section area of the waterbox), but must also resist bending moments caused by eccentric placement of large circulating water inlet and outlet nozzles. Thus, we can clearly see that the design problem for the condenser tubesheet involves consideration of a non-uniform loading state acting around the periphery. At this point, we note that the *distribution* of this peripheral loading is unknown.

In addition to the complications of non-uniform loading of the tubesheet from the waterbox, the condenser tubesheet requires two coordinates to describe a point. The problem is further complicated by a non-uniform tube layout pattern. Figure 11.2.3 shows an idealized layout of a typical unit, we note that the tube bundle is certainly not a uniformly spaced assemblage of tubes. The perforated portion of the tubesheet will generally have an irregular boundary with unperforated lanes. It is also quite common, as illustrated in Fig. 11.2.2, to have a narrower width of tube bundle at the top

of the unit. This non-uniform geometry helps to improve steam distribution inside the condenser, but complicates the development of any straight-forward analytical stress analysis method immeasurably.

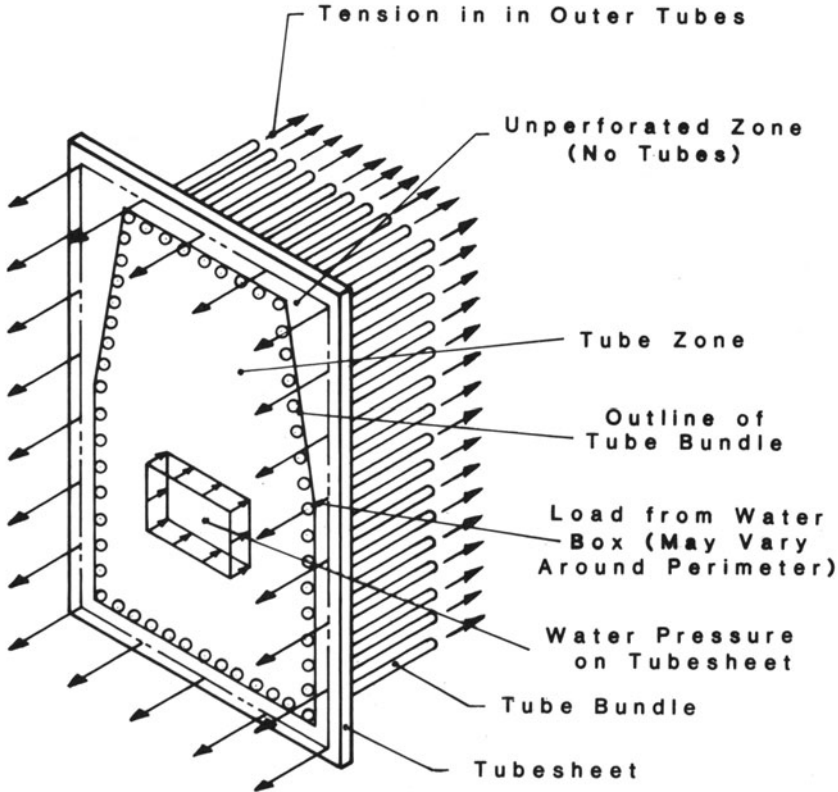


Fig. 11.2.2. Idealized representation of tubesheet loading.

In Chapter 10, we gave an example of the application of the finite element method to the analysis of tubesheets. Although the particular application there involved a symmetric geometry and a circular tubesheet, thus permitting use of a two-dimensional finite element code, the method may be applied to any three-dimensional structure. Therefore, if the designer has access to a general purpose finite element code, has the funds and time available to execute the job, and has the proper background and training to evaluate and interpret the results, the exact solution to the waterbox-tubesheet-tube interaction problem in the specific application being discussed is within reach. In fact, given the various waterbox custom designs with nozzles, stiffeners, etc., at various orientations, the finite element method offers the only approach to a reliable solution for the stress and deformation pattern in the unit. Unfortunately, routine application of

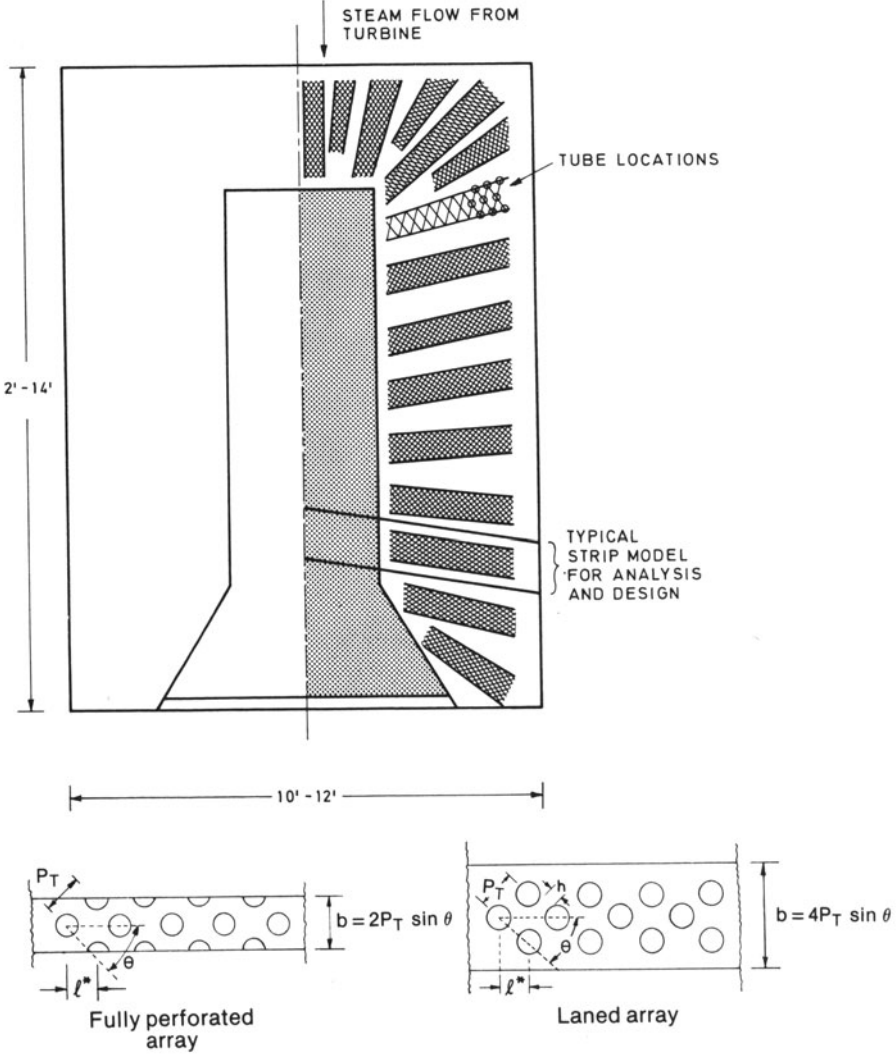


Fig. 11.2.3. Tubesheet layout showing beam strips.

the finite element method to the condenser tubesheet waterbox-tube interaction problem does not appear to be a standard tool of design as yet. We suppose that the main reason for this lack of application may be that responses to client plant specifications must be completed in a relatively short time and the finite element method requires input of a large amount of data to develop an accurate model. The aforementioned problem can be overcome by writing special purpose pre- and post-processors that envelope

the application of the general purpose finite element code. To our knowledge, such special purpose pre-processors do not exist for the rectangular condenser waterbox-tubesheet-tube configuration.

In the middle 1970's, when large nuclear plants were being ordered in the United States and tubesheet stress analysis was recognized to be of considerable import in the evaluation of a particular condenser design, the Heat Exchange Institute (HEI) (an association of heat transfer equipment manufacturers) published a discussion of the condenser tubesheet design problem, and a description of a possible approximate analysis that could serve as a means of choosing a tubesheet thickness under a given set of loads [11.2.1]. In subsequent technical papers [11.2.2, 11.2.3], the rectangular condenser tubesheet design problem was discussed further, and some approximate methodology presented. In Refs. [11.2.4, 11.2.5], an attempt was made to correlate a particular application of the previously proposed approximate method to a solution obtained using the finite element method. Because of its simplicity and popular appeal, it is appropriate to present here a complete discussion of the "approximate method" for application to the design of rectangular tubesheets.

11.3 INTRODUCTORY REMARKS ON ANALYSIS OF A RECTANGULAR TUBESHEET USING BEAM STRIPS

In this section, we begin the presentation of the beam strip method espoused as an approximate analysis procedure for condenser tubesheets. During the course of the development, we employ certain sweeping assumptions dealing with the behavior of the waterbox-tubesheet-tube configuration. We note at the outset that some of these assumptions can be substantiated by experience while others are employed, without substantiation, solely to permit the development a simplified, usable solution. We begin with a few comments, concerning the beam strip method as set forth in Refs. [11.1.1, 11.1.2]. The beam strip method discussed in those works begins with the designer disregarding the detailed interaction between the waterbox and the tubesheet. Rather, the effect of the waterbox is represented solely by the overall force and moment that is transmitted to the tube array by the peripheral loading distribution around the tubesheet. The tubesheet itself is not treated as a rectangular plate on an elastic foundation, but rather is analyzed by considering a few selected beam strips resting on an elastic foundation. The design models representative tubesheet strips as beams on an elastic foundation with strip geometry, elastic properties, and foundation parameters chosen to reflect local geometry of the tubesheet and the tube pattern. The modelling of tubesheet, elastic foundation properties, strip loading, and strip boundary conditions permits complete solution of the problem to determine the stresses for a given element (tubesheet) thickness. It is apparent that successful employment of the beam strip method depends on correct choice of beam strip location, correct assessment of the edge loading acting on the chosen strip, and correct assessment of the degree of fixity against edge rotation available at the strip

edge due to the adjacent waterbox structure. Figures 11.3.1, 11.3.2, 11.3.3, serve to illustrate the modeling of a beam strip. It is clear from the final

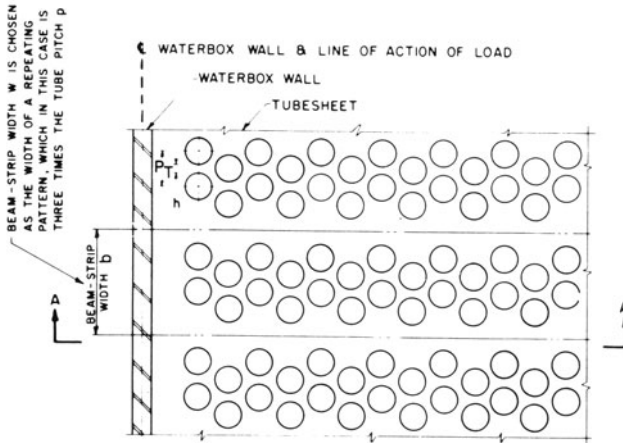


Fig. 11.3.1. Choice of beam-strip for a laned tube pattern of triangular pitch.

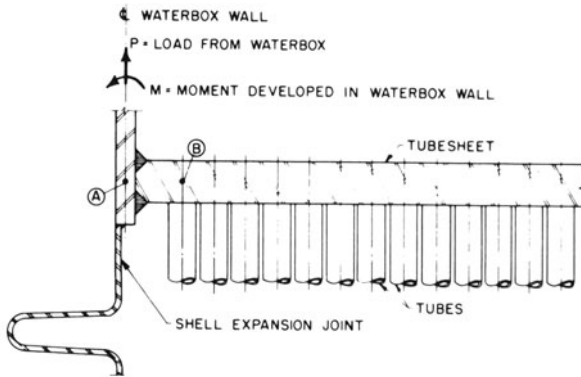


Fig. 11.3.2. Section A-A through beam strip of Fig. 11.3.1, showing loading from the waterbox acting on the end of the beam-strip.

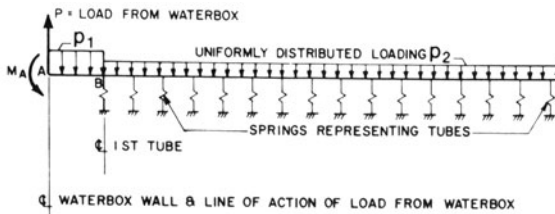


Fig. 11.3.3. Structural model for beam-strip of Fig. 11.3.1 with tubes represented by a spring foundation.

model shown in Fig. 11.3.3 that for properly chosen values for P , p_1 , p_2 , and M_A , the strip deformation and stress pattern can easily be established using beam analysis. Ref. [11.1.2] especially points out the difficulties in choosing P and M_A . It is pointed out there that we have no direct knowledge of how the hydrostatic pull of the waterbox is distributed around the edge of the tubesheet; therefore, the designer working with an isolated beam strip must essentially make an educated guess as to the distribution of peripheral load around the tubesheet boundary that will be equivalent to the known applied force and moment resultant. Another uncertainty in the strip analysis model is the specification of end restraint on the chosen strip. The restraint against the tubesheet rotation not only can vary with type of waterbox, but also can vary around the tubesheet periphery. These variations have a strong influence on the tubesheet design since maximum tube load and tubesheet bending stresses are a strong function of end rotational restraint.

We now discuss a modification to the beam strip method that uses multiple beam strips to support the applied load and moment. We will show that the employment of multiple beam strips will automatically choose the proper peripheral load distribution consistent with the assumptions employed in the overall analysis. The discussion herein is based on work reported in [11.2.3].

Figure 11.3.4 shows a free body diagram of the condenser waterbox. We make the assumption that the waterbox is sufficiently rigid to force the *edge*

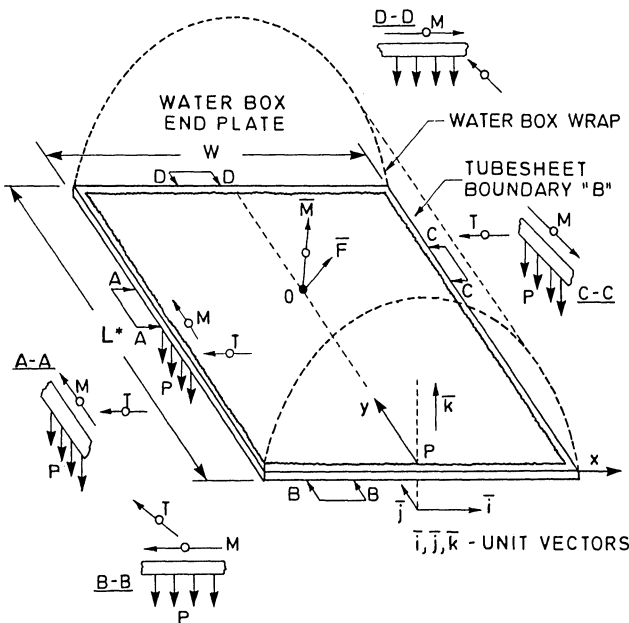


Fig. 11.3.4. Waterbox free body.

of the tubesheet to undergo only a rigid body deformation. Because of this restriction placed on the tubesheet edge motion, we need not consider the load and deformation pattern in the waterbox in any great detail; it suffices to consider only the resultant force vector \bar{F} and the resultant moment vector \bar{M} representing the total effect of internal waterbox pressure, nozzle loadings, dead weight, etc. The only portion of \bar{F} and \bar{M} which are resisted by the tubes and therefore induce tubesheet bending deformation are the force components $F_z \bar{k}$ and the moment components $M_x \bar{i} + M_y \bar{j}$. As shown in the figure, overall equilibrium is maintained by the presence of the tubesheet edge shear force $P(x,y)$, the tubesheet edge bending moment $M(x,y)$, and the tubesheet edge twisting moment $T(x,y)$. These edge reactions are given per unit of tubesheet periphery and are distributed around the four edges of the tubesheet. If we can solve for these edge reactions in terms of the components of the applied loading F_z , M_x , and M_y , and further, if we can establish the tubesheet stress and deformation pattern in terms of these edge reactions, then our design problem is solvable. Our task here is to introduce enough assumptions to successfully accomplish the above tasks and to yield a meaningful approximate analysis.

Using the notation of Fig. 11.3.4, the stated rigidity of the waterbox permits us to assume that the edge of the tubesheet undergoes a rigid body deformation $w_B \bar{k}$, where

$$w_B(x_B, y_B) = \delta_0 + y_B \theta_x + x_B \theta_y \quad (11.3.1)$$

The notation x_B , y_B denotes a specific location on the tubesheet edge "B" (see Fig. 11.3.4). The essence of the multiple beam strip design method presented here is to determine δ_0 , θ_x , θ_y in order to ensure satisfaction of the overall equilibrium equations implied by Fig. 11.3.4. Once these parameters are established, then the distribution of loading around the tubesheet periphery will be automatically determined; there will be no need for the designer to make an arbitrary decision for this distribution as he is forced to do if he considers only a single strip at some guessed at critical location.

Our task now is to establish relationships between the boundary displacement $w_B(x_B, y_B)$ and the edge reactions P , M , T . If we were able to solve the exact plate equations analytically, we would find that P , M , T at one point of the edge involve the edge displacements at all other points around the edge. Since our goal here is simplicity, we invoke the beam strip assumption that edge reactions at a particular point are related only to the edge displacements at that same point. That is, we will employ *multiple* beam strips around the periphery of the tubesheet to establish the relationship between P , M , T , at a given location, and w_B at the same location. Figure 11.2.3 shows conceptually the breakup of a tubesheet into beam strips for analysis purposes. Typical strip patterns are also shown in Fig. 11.2.3. The number and orientation of these beam strips is left to the designer, but are presumably chosen to best reflect the variations in tube patterns around the periphery.

From Fig. 11.3.4, we now write down the equilibrium equations for the structure. We need only satisfy force equilibrium in the z direction, and moment equilibrium about the x and y axes through any point, say point P , on the tubesheet surface. We obtain the following three equations:

$$F_z = \oint P(x_B, y_B) ds \quad (11.3.2)$$

$$M_x + F_z y_L = \oint y_B P(x_B, y_B) ds + \sum_{j=1}^2 \oint_j M(x_B, y_B) ds + \sum_{j=3}^4 \oint_j T(x_B, y_B) ds \quad (11.3.3)$$

$$-M_y + F_z x_L = \oint x_B P(x_B, y_B) ds + \sum_{j=3}^4 \oint_j M(x_B, y_B) ds + \sum_{j=1}^2 \oint_j T(x_B, y_B) ds \quad (11.3.4)$$

In Eqs. (11.3.2)–(11.3.4), the following notation has been introduced for convenience:

$\overline{PO} = y_L \bar{j} + x_L \bar{i}$, locates the point of application of the resultants \bar{F} and \bar{M} .

$\oint () ds$ = the line integral around the entire periphery “B”

$\oint_j () ds$ = the line integral along the boundary segment B_j . $j=1$ is the segment $y=0$, $j=2$ is the segment $y=L^*$, $j=3$ represents the segment $x=W/2$, and $j=4$ represents the segment $x=-W/2$. The integration element ds is $\pm dy$, $\pm dx$, depending on the segment involved.

Equations (11.3.2)–(11.3.4) provide three scalar equations to determine δ_0 , θ_x , θ_y , once we have determined relationships between $P(x_B, y_B)$, $M(x_B, y_B)$, and $T(x_B, y_B)$ in terms of δ_0 , θ_x , and θ_y .

As noted above, the multiple strip method relies upon making the beam strip approximation all around the tubesheet edge in order to evolve analytical expressions for P , M and T in terms of the local tubesheet edge displacement. We can presume that the use of multiple strip theory will provide conservative results for the tubesheet analysis if we make the correct choice of edge rotational restraint conditions. We make this last statement on the basis that the use of beam strips for analysis purposes simply replaces the actual plate-like tubesheet by a weaker series of independently deflecting strips with no cross-connection.

11.4 ANALYSIS OF A SINGLE BEAM STRIP

In this section, we present a detailed exposition of the beam strip analysis and we show how the local tubesheet edge displacement w_B can be related to P , M , T , the strip edge reactions. We will show that the simplification of the tubesheet model to a series of elastic strips leads to the derivation of a series of local spring constants such that the relationships given below apply at each boundary point $x_B = x_{Bi}$, $y_B = y_{Bi}$.

$$\begin{aligned} P(x_{Bi}, y_{Bi}) &= K_i w_{Bi} + K_{pi} p \\ M(x_{Bi}, y_{Bi}) &= C_{Mi} w_{Bi} - C_{pi} p \\ T(x_{Bi}, y_{Bi}) &= C_{Ti} \theta \end{aligned} \quad (11.4.1)$$

In the above equations, the local spring rates K_i , K_{pi} , C_{Mi} , C_{pi} , C_{Ti} are functions of particular location around the tubesheet periphery. The rotation angle $\theta = \theta_x$ along the edges $x_B = \pm W/2$, $\theta = \theta_y$ along the edges $y_B = 0, L^*$, and the direction of T is such as to always resist twisting of the strip. It is essential to realize that the feature of the beam strip assumption is that it permits the statement to be made that edge reactions P , M , T on a strip are affected only by local pressure, geometry, and edge displacements of the *same* strip.

In the following pages, we present a fairly complete development of the relevant spring rates. It is necessary to study the following analysis in detail to obtain an in-depth understanding of the formulation. However, for those interested primarily in application rather than analysis, a cursory reading up to the beginning of Section 11.5 will be sufficient.

We begin the detailed analysis by considering Fig. 11.4.1, which shows a free body of the unperforated region of length L of a typical beam strip, and a free body of the adjacent perforated region. The width of the beam strip to be analyzed is b , and is chosen on the basis of the local tube pattern. Particular choices for b have already been shown in Fig. 11.2.3. Force and moment equilibrium requirements yield the following equations relating edge reactions P_1 , M_1 to interior reactions P_2 , M_2 :

$$P_2 = P_1 - pbL; \quad M_2 = M_1 - P_1 L + \frac{pbL^2}{2} \quad (11.4.2)$$

If D_1 denotes the bending modulus EI of the beam strip of width b , thickness t , and length L , then simple beam theory can be used to relate the deflections and rotations at each end of the unperforated strip. If we examine the untubed strip in Fig. 11.4.1, we see that the deflections and rotations at $\xi = 0, L$ are related by the expressions

$$\begin{aligned} w_1(L) &= w_1(0) - L\theta_1(0) - \Delta w_c \\ \theta_1(L) &= \theta_1(0) + \Delta\theta_c \end{aligned} \quad (11.4.3)$$

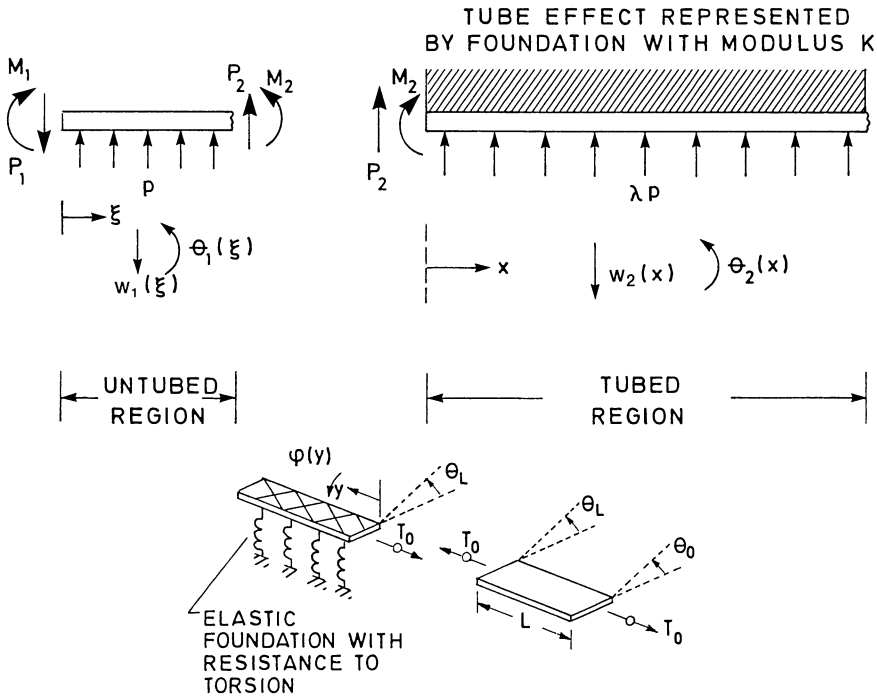


Fig. 11.4.1. Free body of strip for bending and twisting analysis.

where Δw_c , $\Delta \theta_c$ are the elastic deformation and rotation of a beam strip clamped at $\xi = 0$ and subjected to pressure load along the strip, and end loads P_2 , M_2 , respectively, at $\xi = L$. From any strength-of-materials text, results for Δw_c and $\Delta \theta_c$ are given as

$$\Delta w_c = \frac{P_2 L^3}{3D_1} + \frac{M_2 L^2}{2D_1} + \frac{p b L^4}{8D_1} \tag{11.4.4}$$

$$\Delta \theta_c = \frac{P_2 L^2}{2D_1} + \frac{M_2 L}{D_1} + \frac{p b L^3}{6D_1}$$

If we substitute Eq. (11.4.4) into Eq. (11.4.3) and then use Eq. (11.4.2), to put the results in terms of P_1 , M_1 , we obtain the following set of equations for the untubed strip region:

$$w_1(L) = w_1(0) - \theta_1(0)L + \frac{P_1 L^3}{6D_1} - \frac{M_1 L^2}{2D_1} - \frac{p b L^4}{24D_1} \tag{11.4.5}$$

$$\theta_1(L) = \theta_1(0) - \frac{P_1 L^2}{2D_1} + \frac{M_1 L}{D_1} + \frac{p b L^3}{6D_1} \tag{11.4.6}$$

As stated previously, our goal in this section is to obtain relations between P_1 , M_1 and $w_1(0)$ (which is the edge displacement denoted as w_B earlier). These final relations will evolve from Eqs. (11.4.5), (11.4.6) after we eliminate $\theta_1(L)$, $w_1(L)$. We must now analyze the interior perforated region in order to determine $w_1(L)$ in terms of the characteristics of the interior region of the tubesheet.

To begin an analysis of the perforated beam strip, we consider the interior strip to be subjected to edge loads P_2 , M_2 , and to a surface pressure $\lambda p = f^* p b$. The factor f^* reflects the fact that the strip is perforated. We have previously encountered this pressure reduction factor in our work on circular tubesheets. The beam strip in the perforated region feels the effect of the condenser tubing as an elastic foundation; as pointed out in previous chapters, each tube resists longitudinal force by stretching and therefore behaves as a simple spring. We take the spring constant of a single tube in tension or compression as $E_T A_T / L_T$ where E_T , A_T , L_T are the Young's Modulus, the metal area of the tube, and the half length of the condenser between tubesheets, respectively. In addition, as shown in Chapter 10, since each tube is supported at discrete points along the length of the condenser by full width baffle plates, some resistance against bending of the tubesheet is also provided by the tube array. As noted in Chapter 10, a single tube, pinned at both ends and subjected to an end moment M_n , has the following relation between M_n and the magnitude of the end rotation $|\theta_n|$.

$$M_n / |\theta_n| = \frac{F_n E_T I_T}{S}; \quad (3 \leq F_n \leq 4) \quad (11.4.7)$$

F_n is a function of the number of baffles and the baffle spacing, I_T is the tube metal moment of inertia, and S is the span from the tubesheet to the first baffle support plate.

If we wish to account for both the extensional resistance of the tubing as well as for the rotational resistance, we can develop the governing equations for the beam deflection by a proper reduction of the field equations for double tubesheets presented in Chapter 10. Accounting for the fact that we are dealing with a beam strip rather than a portion of a circular plate (let $dr \rightarrow dx$ and $r \rightarrow \infty$ in the relevant equations of Chapter 10), we can write the necessary field equations for bending (say for tubesheet 1) as

$$\frac{dV}{dx} = q_u + q_L \quad (11.4.8)$$

$$\frac{dM}{dx} + V - m = 0 \quad (11.4.9)$$

$$M = D \frac{d\theta_2}{dx}; \quad \theta_2 = - \frac{dw_2}{dx} \quad (11.4.10)$$

$$q_u + q_L = -f^*pb - K_\delta w_2 \quad (11.4.11)$$

$$-m = K^* \frac{dw_2}{dx} \quad (11.4.12)$$

We have temporarily employed the sign convention used in Chapter 10 and we have used D to represent the EI of the beam strip (appropriately modified to reflect the perforation effect). D is the bending modulus of the interior of the strip with appropriate reduction for the effect of perforations (i.e., including an effective Young's Modulus), w_2 is the deflection of the strip in the perforated region, θ_2 is the cross section rotation, and K_δ , K^* are the spring constants reflecting tube resistance to deflection and to rotation of the tubesheet. If l^* is the length, along the beam strip, of a repeated tube pattern (see Fig. 11.2.3), and n is the number of tubes in the strip area bl^* , then

$$K_\delta = n E_T A_T / L_T l^*; \quad K^* = n F_n E_T I_T / l^* S \quad (11.4.13)$$

If we combine Eqs. (11.4.8)–(11.4.13) into a single equation for the deflection $w_2(x)$, and if we define the parameter $\beta^4 = K_\delta / 4D$, then we can obtain the equation

$$\frac{d^4 w_2}{dx^4} - 4 \beta^4 \rho^2 \frac{d^2 w_2}{dx^2} + 4 \beta^4 w_2 = -\frac{f^*pb}{D} \quad (11.4.14)$$

where

$$\rho^2 = \frac{F_n}{8} \frac{L_T}{S} d_o^2 \left(1 - \frac{2t_T}{d_o} + \frac{2t_T^2}{d_o^2} \right) \quad (11.4.15)$$

Equation (11.4.15), involving the tube outer diameter d_o and wall thickness t_T , evolves by noting that the ratio I_T / A_T of the tube cross section is $0.125 d_o^2 (1 - 2t_T / d_o + 2t_T^2 / d_o^2)$.

If we neglect the effect of tube resistance to tubesheet rotation, then the second term in Eq. (11.4.14) disappears and the ordinary beam on elastic foundation equation results.

The solution to Eq. (11.4.14), valid in the semi-infinite region $x > 0$, can be written in the form

$$w_2(x) = e^{-\beta(1-\rho^2\beta^2)^{1/2}x} [A \sin \beta(1+\rho^2\beta^2)^{1/2}x + B \cos \beta(1+\rho^2\beta^2)^{1/2}x] \quad (11.4.16)$$

assuming that the tube rotational resistance effect is small enough so that $\rho^2\beta^2 < 1$. A and B represent constants of integration which can be evaluated in terms of M_2 and P_2 at $x = 0$. Noting the directions for positive moments and shears used in Chapter 10 and comparing with Fig. 11.4.1, we have

$$\frac{M(0)}{D} = \frac{M_2}{D} = - \frac{d^2 w_2}{dx^2} \Big|_0 \quad (11.4.17)$$

$$\frac{V(0)}{D} = - \frac{P_2}{D} = \frac{d^3 w_2}{dx^3} \Big|_0 - \frac{K^*}{D} \frac{dw_2}{dx} \Big|_0; \quad \frac{K^*}{D} = 4\beta^4 \rho^2 \quad (11.4.18)$$

After differentiation with respect to x of Eq. (11.4.16), evaluation of the results at $x = 0$, and substitution into Eqs. (11.4.17), (11.4.18), we can solve for A and B in terms of P_2 and M_2 . If we then use Eq. (11.4.16) and its first derivative to evaluate $w_2(0)$ and $\theta_2(0) = -dw_2/dx|_0$, we obtain the expressions

$$w_2(0) = \frac{d_{11}}{2\beta^3 D} P_2 - \frac{d_{12}}{2\beta^2 D} M_2 - \frac{f^* pb}{K_6} \quad (11.4.19)$$

$$-\theta_2(0) = - \frac{d_{12}}{2\beta^2 D} P_2 + \frac{d_{22}}{\beta D} M_2 \quad (11.4.20)$$

where

$$d_{11} = d_{22} = \frac{(1 - \beta^2 \rho^2)^{1/2}}{(1 + 2\beta^2 \rho^2)}; \quad d_{12} = \frac{1}{1 + 2\beta^2 \rho^2} \quad (11.4.21)$$

Having the results for the perforated strip represented by Eqs. (11.4.19)–(11.4.21), the results for the unperforated region represented by Eq. (11.4.5), (11.4.6), the equation of equilibrium, (11.4.2), and the compatibility conditions

$$w_1(L) = w_2(0); \quad \theta_1(L) = \theta_2(0) \quad (11.4.22)$$

we can combine the results into the final symbolic form

$$2\beta^3 D(w_1(0) - \theta_1(0)L) = P_1 B_{11} - \beta M_1 B_{12} - pbLB_{13} \quad (11.4.23)$$

$$2\beta^2 D\theta_1(0) = P_1 B_{21} - \beta M_1 B_{22} - pbLB_{23} \quad (11.4.24)$$

where

$$B_{11} = d_{11} + \beta L d_{12} - \beta^3 L^3 / 3D_1$$

$$B_{12} = d_{12} + 2\beta L d_{22} - \beta^2 L^2 D / D_1$$

$$B_{13} = d_{11} + d_{12} \beta L / 2 + f^* / 2\beta L - \beta^3 L^3 D / 12D_1 \quad (11.4.25)$$

$$B_{21} = d_{12} + \beta^2 L^2 D / D_1$$

$$B_{22} = 2d_{22} + 2\beta L D / D_1$$

$$B_{23} = d_{12} + \beta L d_{22} + \beta^2 L^2 D / 3D_1$$

Equations (11.4.23), (11.4.24) are almost in the final form desired in that they relate the beam strip edge reactions P_1 , M_1 to the beam strip local edge displacement $w_1(0) = w_b$. However, the relations still involve $\theta_1(0)$ which reflects a measure of the resistance to strip rotation provided by the heretofore neglected waterbox structure adjacent to the particular beam strip being considered. Without a detailed waterbox analysis, a proper relation for $\theta_1(0)$ is difficult to establish. For the moment, we simply state that if a detailed analysis of the local waterbox structure could be made, we would find that $\theta_1(0)$ is proportional to M_1 , and to the local pressure p acting on the waterbox. Without any analysis, we simply write this relation in the form:

$$\theta_1(0) = \frac{\epsilon_1}{1 - \epsilon_1} \frac{B_{22}}{2\beta D} M_1 - \frac{\epsilon_2 B_{23}}{2\beta^2 D} p b L \quad (11.4.26)$$

ϵ_1 , ϵ_2 are convenient parameters that reflect the character of the restraint provided by the waterbox. The first term in Eq. (11.4.26) is simply the rotational stiffness of the waterbox structure attached to the tubesheet strip; the second term gives the influence of local waterbox pressure on the edge rotation. Using Eq. (11.4.26) in Eq. (11.4.24) and solving for M_1 yields the result

$$M_1 = (1 - \epsilon_1) \left[\frac{B_{21}}{\beta B_{22}} P_1 - (1 - \epsilon_2) \frac{B_{23}}{\beta B_{22}} p b L \right] \quad (11.4.27)$$

We can see that a particular waterbox structure having a parameter value $\epsilon = 1$ corresponds to a simply supported edge for the tubesheet strip. Similarly, a clamped edge ($\theta_1(0) = 0$) is provided by the adjacent waterbox structure if the parameter values ϵ_1 , ϵ_2 are both set equal to zero.

The spring rate functions for strip bending, defined in Eq. (11.4.1) at the beginning of this section, are now directly obtainable by combining Eqs. (11.4.23), (11.4.24), (11.4.26), and (11.4.27) to obtain forces and moments per unit of tubesheet periphery as

$$\begin{aligned} P &= P_1 / b = K w_1(0) + K_p p \\ M &= M_1 / b = C_M w_1(0) - C_p p \end{aligned} \quad (11.4.28)$$

where

$$K = \frac{2\beta^3 D / b}{B_{11} + \beta L B_{21} - \frac{(1 - \epsilon_1)}{B_{22}} [B_{12} + \beta L B_{22}] B_{21}} \quad (11.4.29)$$

$$\frac{K_p}{L} = \frac{B_{13} + \beta L B_{23} - \beta(1 - \epsilon_1)(1 - \epsilon_2) \frac{B_{23}}{\beta B_{22}} (B_{12} + \beta L B_{22})}{B_{11} + \beta L B_{21} - (1 - \epsilon_1) \frac{B_{21}}{B_{22}} [B_{12} + \beta L B_{22}]} \quad (11.4.30)$$

$$C_M = (1 - \epsilon_1) \frac{B_{21}}{\beta B_{22}} K \quad (11.4.31)$$

$$\frac{C_p}{L} = (1 - \epsilon_1) \left[(1 - \epsilon_2) \frac{B_{23}}{\beta B_{22}} - \left(\frac{K_p}{L} \right) \frac{B_{21}}{\beta B_{22}} \right] \quad (11.4.32)$$

It is clear that K , K_p , C_M , C_p , being functions of local strip geometry, will in general, vary around the tubesheet periphery.

A similar, but much simpler analysis, using the free body for torsion in Fig. 11.4.1, yields the twisting spring rate function C_T in Eq. (11.4.1), consistent with the beam strip idealization, as

$$C_T = \frac{GJ}{bL} \frac{\mu}{1 + \mu} \quad (11.4.33)$$

where

$$\mu = \frac{G^*J}{GJ} \sigma L; \quad \sigma^2 = \frac{\rho^2 K_\delta}{(G^*J)} \quad (11.4.34)$$

GJ , G^*J are the torsional rigidities of the beam strip rectangular cross section in the unperforated and perforated regions, respectively. C_T will also vary around the tubesheet periphery. We suggest here that a reasonable approximation for J for a strip of width b and thickness t is

$$J \approx 0.3 \frac{b^4 t^4}{(bt^3 + tb^3)} \quad (11.4.35)$$

Having established appropriate values for the spring rates in Eq. (11.4.1), as promised, we now return to the mainstream of our development and employ Eq. (11.4.1) in the satisfaction of the overall equilibrium equations and in the eventual determination of the edge displacement parameters δ_0 , θ_x , θ_y first introduced in Eq. (11.3.1).

11.5 DEVELOPMENT OF FINAL EQUATIONS FOR EDGE DISPLACEMENTS

In the previous section, we presented a derivation of the relevant parameters reflecting the modelling of a tubesheet region by a beam strip. The spring rates obtained are functions of local strip geometry, of material properties, and of foundation moduli; they include the effect of interaction between the particular beam strip and the adjacent waterbox structure. In the development of the strip spring rates, we require the effective moduli E^* (and G^*) which reflect the perforation effect. The same procedures suggested in previous chapters for circular tubesheets can be applied here to obtain the reduced moduli required for each strip around the tubesheet periphery.

We are now in a position to complete the formulation of the equilibrium

equations, which to this point are represented by Eqs. (11.3.2)–(11.3.4). If we use Eqs. (11.4.1) and replace w_{Bi} by the edge displacement of Eq. (11.3.1), then the following three equations can be obtained to solve for δ_0 , θ_x , θ_y :

$$\begin{aligned} A_{11}\delta_0 + A_{12}\theta_x + A_{13}\theta_y &= F_z - B_1p \\ A_{21}\delta_0 + A_{22}\theta_x + A_{23}\theta_y &= F_z y_L + M_x - B_2p \\ A_{31}\delta_0 + A_{32}\theta_x + A_{33}\theta_y &= F_z x_L - M_y - B_3p \end{aligned} \quad (11.5.1)$$

Appendix 11.A contains a summary of the expressions for A_{ij} and B_i in terms of line integrals of the various spring rates. The Appendix also gives some details on the computation of the coefficients. We note that in a large majority of configurations, the y - z plane in Fig. 11.3.4 is a symmetry plane. In such a case, $x_L = M_y = B_3 = A_{13} = A_{31} = A_{23} = A_{32} = \theta_y = 0$, and Eqs. (11.5.1) reduce to two equations to solve for δ and θ_x . The solutions are easily obtained once the A_{ij} , B_i , which reflect the variation of tubesheet flexibility around the periphery, are computed. Finally, we recall that F_z , M_x , M_y , are all expressible in terms of the waterbox hydrostatic pressure, plus any additional known mechanical loads.

Some comments on the computation of the parameters ϵ_1 , ϵ_2 as defined in Eq. (11.4.26) are now warranted. As noted in Refs. [11.2.1, 11.2.2], these values must be estimated by the tubesheet designer and reflect interaction between the tubesheet strip and the adjacent waterbox structure. In essence, the choice, or rational derivation of appropriate values for ϵ_1 , ϵ_2 , reflects an attempt to incorporate the stiffening effect of the waterbox on the tubesheet while still essentially neglecting consideration of the complex stress and deformation patterns that certainly arise in a loaded waterbox. Results of a finite element study of an idealized waterbox tubesheet unit [11.2.5] verify that the complex waterbox geometry causes the edge fixity parameters ϵ_1 , ϵ_2 to vary considerably around the tubesheet periphery.

We will show later that the values set for ϵ_i can strongly influence the results obtained for a particular tubesheet geometry. Therefore, in lieu of an arbitrary choice of the ϵ_i parameters based on experience (or guesswork), we suggest that a strip model be employed for the adjacent waterbox structure solely to provide some rational for the choice of ϵ_1 , ϵ_2 . Figure 11.5.1 shows some representative geometries for waterbox strips which can be used to obtain ϵ_1 , ϵ_2 . For example, considering Fig. 11.5.1b with $L_1 = 0$ for simplicity, we can write expressions for δ_1 , θ_1 as follows:

$$\begin{aligned} \delta_1 &= \frac{H_1 L_3^3}{3EI} - \frac{M_1 L_3^2}{2EI} - \frac{p L_3^4 b}{8EI} \\ \theta_1 &= -\frac{H_1 L_3^2}{2EI} + \frac{M_1 L_3}{EI} + \frac{p L_3^3 b}{6EI} \end{aligned} \quad (11.5.2)$$

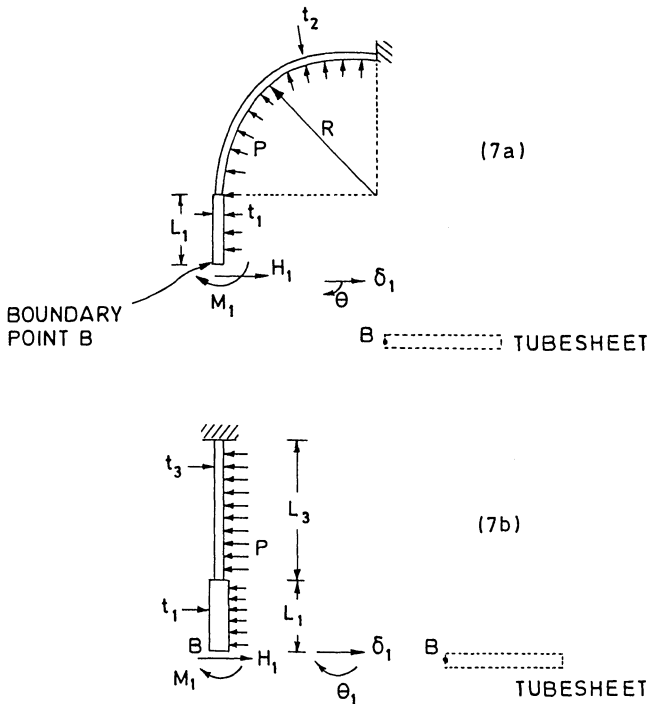


Fig. 11.5.1. Waterbox strip geometry.

Requiring that $\delta_1 = 0$ yields a solution for H_1 as

$$H_1 = \frac{3}{2} \frac{M_1}{L_3} + \frac{3}{8} pL_3 b \tag{11.5.3}$$

so that the rotation θ_1 at the junction with the tubesheet has the form:

$$\theta_1 = \frac{M_1 L_3}{4EI} - \frac{pbL_3^3}{48EI} \tag{11.5.4}$$

Comparing Eq. (11.5.4) with Eq. (11.4.26) yields equations to determine ϵ_1 , ϵ_2 in terms of the waterbox-tubesheet material parameters and geometry as

$$\frac{\epsilon_1}{1 - \epsilon_1} = \left(\frac{2\beta D}{B_{22}} \right) \frac{L_3}{4EI}; \quad \epsilon_2 = \frac{2\beta^2 D}{B_{23} L} \left(\frac{L_3^2}{48EI} \right) \tag{11.5.5}$$

Similar estimates for ϵ_1 , ϵ_2 can be obtained for other waterbox strips around the tubesheet periphery. We can easily demonstrate the importance of a realistic choice for the value of the edge fixity parameters. Consider, for example, a beam strip with no unperforated region, zero surface pressure, but subjected to an edge load P_1 . Also, assume that the rotational

resistance of the tubes can be neglected so that $1 \pm \beta^2 \rho^2 \approx 1$. For this case, with $L = 0$, and no surface pressure, the edge moment M_1 becomes

$$M_1 = (1 - \epsilon_1) \frac{P_1}{2\beta} \quad (11.5.6)$$

We can also show that the solution for the interior bending moment distribution $M(x)$ in this case, can be obtained from the general solution (given as Eq. (11.4.16)) in the form

$$M(x) = \left\{ M_1 (\cos\beta x + \sin\beta x) - \frac{P_1}{\beta} \sin\beta x \right\} e^{-\beta x} \quad (11.5.7)$$

We can plot $M(x)\beta/P_1$ versus x for various values of ϵ_1 in order to examine the effect of ϵ_1 . Figure 11.5.2 shows the results of such a calculation. It is clear that for this idealized problem, the most efficient use of material is associated with an edge fixity factor $\epsilon_1 = 0.6$. In the context of this exercise, we note that values of $\epsilon_1 < 0$ are of mathematical interest only.

Assuming that we can establish a reasonable estimate of the fixity parameters for each tubesheet strip used in modelling a particular unit, then Eqs. (11.5.1) solve for δ_0 , θ_x , θ_y , appropriate to the unit geometry and loading, and establish the edge boundary displacement $w_B(x_B, y_B)$ (see Eq. (11.3.1)) around the periphery. Substitution back into Eqs. (11.4.1) then yields numerical values for the edge loading on each beam strip around the tubesheet. We have thus established the peripheral load distribution acting on the tubesheet consistent with the assumed edge displacement pattern. Tubesheet design can proceed by examining the strip having the most severe edge loading to establish stress levels and tube loading. Usually, critical stresses are at the edge and at the beginning of the perforated regions. To find the bending moment in the interior of the perforated region, the designer must calculate $M(x) = -Dd^2 w_2/dx^2$ with $w_2(x)$ given by Eq. (11.4.16). Note that calculated bending stresses in the perforated region should be amplified by the appropriate stress efficiency factor to account for the effect of the perforations.

The approximate method presented here can easily be coded into a user oriented design package. The method is, of course, of interest only if it can be established that it yields useful results. Experience with the concepts and design methods of this chapter indicates that the approximate method appears to yield useful results when considered as an application aid in the preliminary design stage. The method has been applied to evaluate certain units which have experienced field failures. Usually, these failures manifest themselves by tube pull out around the unit periphery (due to excessive tube loading) or to severe tubesheet bending. In most cases, the failure is not due to unit underdesign, but rather to an unanticipated overload above design pressures. In most cases, these reported tubesheet problems surfaced on units designed prior to industry awareness of the need for strength design due to higher waterbox pressures. The multiple beam strip method has been applied to certain of these reported failures, and, when good engineering

practice has been employed in developing the model, is found to predict either an overstress condition or high tube loads under the conditions actually present in the field when a particular failure occurred. Although the beam strip method can be useful in simplifying a very complex problem to a relatively simple analysis, the potential user is cautioned that the method is best employed in a preliminary design analysis and then only in conjunction with conservative design margins on tubesheet stress levels and on allowable tube loading.

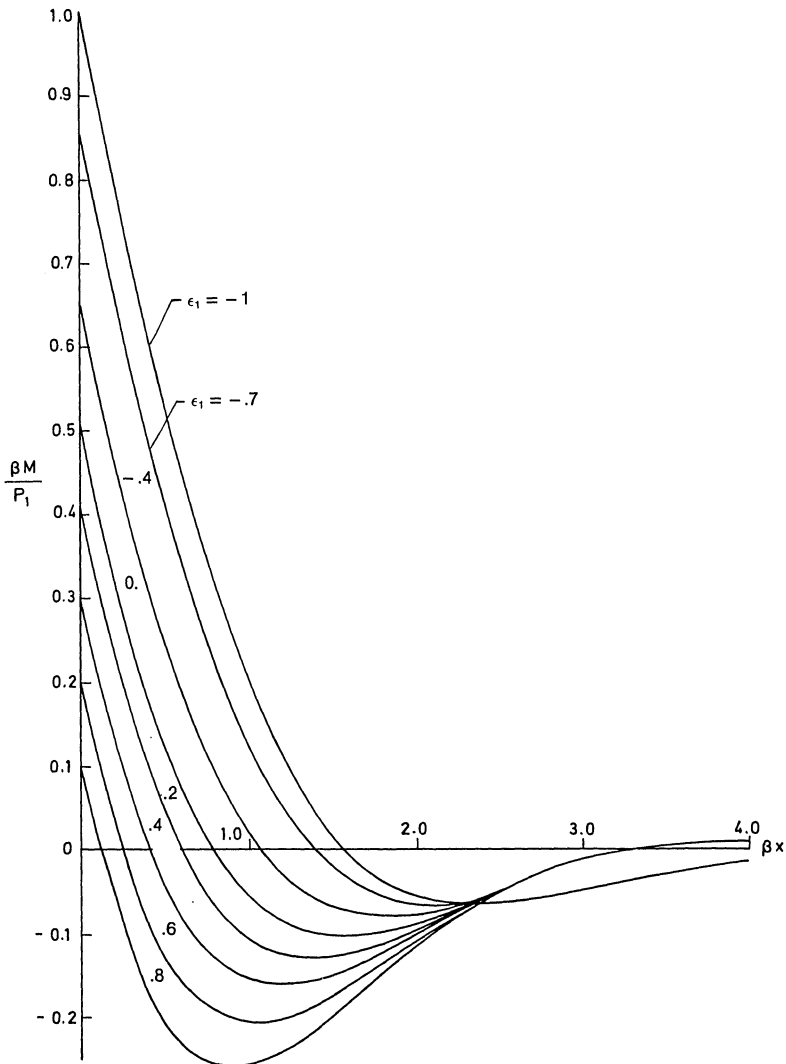


Fig. 11.5.2. Bending moment distribution in tubed region.

11.6 A SPECIFIC APPLICATION OF THE MULTIPLE BEAM STRIP METHOD TO INVESTIGATE THE EFFECTS OF TUBESHEET GEOMETRIC AND MATERIAL PARAMETERS

In this section, we show a typical application of the multiple beam strip method. Usually, a user will write a special purpose computer code incorporating the strip equations with a pre- and post-processor for data input and results interpretation.

The designer must input geometry and material properties required to compute F_z , M_x , M_y , to compute strip spring rates, and to compute edge fixity parameters. The user must also input the number and type of strips (tube patterns) to be modelled around the periphery. Experience indicates that 10–15 strips along the long edges is sufficient to define a typical tubesheet. For an assumed tubesheet thickness, the computer code can calculate the coefficients A_i , B_i necessary to assemble and solve the equilibrium Eqs. (11.5.1). Thus, the boundary displacement around the periphery, per unit applied hydrostatic pressure, can be computed. With this deformation determined, stresses and tube loads per unit pressure can be calculated for each strip location. Based on allowable design stress and tube load, a maximum hydrostatic pressure for the assumed tubesheet thickness can be ascertained. Generally, only tubesheet thickness would be varied until a unit which meets design specifications is achieved. The reduced area in the perforated region available for load carrying should be correctly accounted for using a stress efficiency factor in the computation of strip stresses in the perforated region. Depending on geometry and edge fixity, the maximum strip stress at a given peripheral location will be either at the edge of the strip, at the interface between the unperforated and perforated region, or in the interior of the perforated region.

Since the condenser waterbox-tubesheet unit is generally a custom design requiring special purpose computer coding, we do not present any source code for the method given in this chapter; however, we will present results of a typical application study using the multiple beam strip method. To illustrate the design method, we consider the following hypothetical construction which has been used in Ref. [11.2.3], and repeat the sample calculations presented there.

Tubesheet: $L^* = 120$ in.; $W = 72$ in.
 $E = 29 \times 10^6$ psi

Tubes: Outer diameter = 1 in.; length = 360 in.; thickness = 0.049 in.; ligament width = 0.25 in.; $E_T = 16 \times 10^6$ psi. Tube pattern is 60° diagonal* along the lower edge of width W , and 60° laned† along sides of length L^* and along the top edge. (See Fig. 11.3.4).

*The term “diagonal” refers to a fully perforated region, and 60° refers to angle θ (see Fig. 11.2.3).

†The term “laned” refers to a region having an interrupted tube layout (see Fig. 11.2.3).

Waterbox: $E = 29 \times 10^6$ psi; 180° wrap (Fig. 11.5.1a) along the sides, with $R = 36$ in.; $t_2 = 0.5$ in., $L_1 = 3$ in., $t_1 = 1.25$ in. Along the top and bottom edges, the waterbox is represented as flat plate (Fig. 11.5.1b) with $L_1 + L_3 = 18$ in., $t_1 = t_3 = 1.25$ in.

Loading: The effects of waterbox pressurization are assumed as an external moment M_x having magnitude 1.83×10^6 in.lb. at a hydrostatic pressure of 50 psi, and an external force $F_z = 432,000$ lbs. at the same hydrostatic pressure. The waterbox metal weight and weight of internal water yields a constant positive external moment $M_x = 0.163 \times 10^6$ in.lbs.

The property values and design stress levels employed are typical of a steel waterbox and tubesheet with aluminum brass tubes. The bending stress at hydrotest pressure is assumed to be limited to 1.25 times the material yield stress for the purposes of establishing maximum allowable pressures for a given tubesheet thickness.

The computer simulation of the unit described above is executed for an initial tubesheet thickness of 1 inch and increased in increments of 0.25 inch. The result of each simulation is the allowable hydrotest pressure consistent with the permitted maximum stress level. The design method should also check maximum tube loading around the periphery and terminate the simulation at a lower pressure if the designated maximum tube load is exceeded anywhere around the periphery. For the sample calculations here, the maximum allowable tube load is set high enough so that the limiting hydrostatic test pressure is always governed by maximum bending stress conditions in the tubesheet. In actual design situations, the limiting criteria may well be maximum tube loading, rather than the tubesheet stress level emphasized in the simulation reported here. When high tube loads govern a design, the tube loading may be reduced by reducing the external loads on the tubesheet, or by increasing the number of peripheral tubes which can carry the loading.

Results of a number of simulations are summarized in Fig. 11.6.1 with the results presented in S.I. units. The permitted unit test pressure p is presented as a function of tubesheet thickness. Also presented are results for maximum tube load/unit pressure as a function of tubesheet thickness. The following unit simulations are used to illustrate effects of certain geometry and material variations on maximum pressure and on maximum tube load.

Case 1—The unit as previously described.

Case 2—Same configuration as case 1, with tube material changed to steel.

Case 3—Same configuration as case 1, with tubesheet material changed to Muntz metal ($E = 15 \times 10^6$ psi).

Case 4—Same configuration as case 3, with waterbox plate assumed sufficiently ribbed to maintain the tubesheet periphery fully fixed against rotation.

The material yield stresses governing the permissible unit bending stress levels are:

Muntz—20,000 psi; Steel—30,000 psi

The four cases (5–8) also shown in Fig. 11.6.1 are similar to cases 1–4 above except that the tube pattern around the periphery is changed. We replace the 60° laned strips along the unit side with 30° diagonal strips. Along the top edge, we replace the laned configuration with 60° fully diagonal strips. Thus, cases 5–8 compare with cases 1–4, respectively, and illustrate the effect of tube layout.

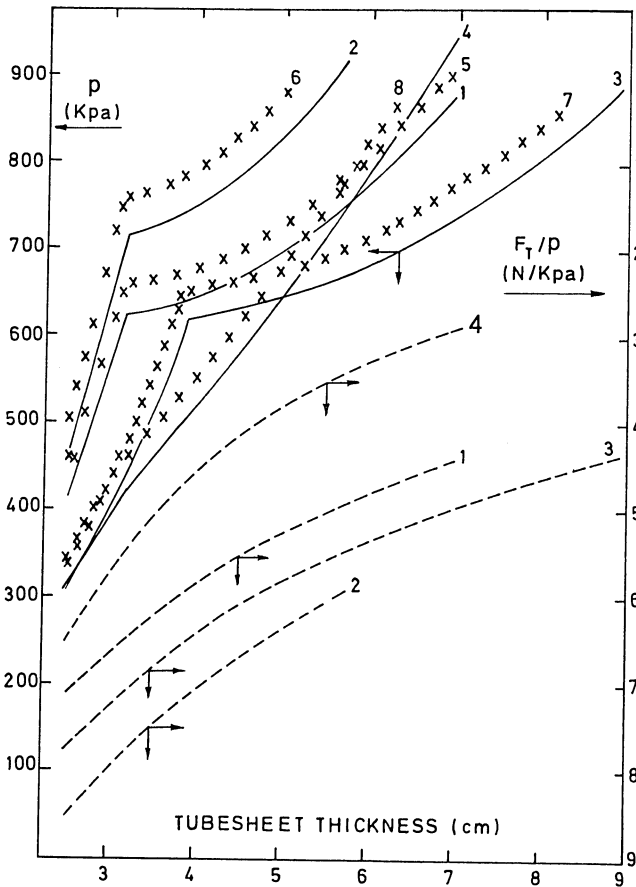


Fig. 11.6.1. Results of typical simulation.

Figure 11.6.1 shows the expected general results that increasing tubesheet thickness permits the unit to sustain a higher test pressure with lower maximum tube load/unit pressure. The decrease in tube loading/unit pressure is a direct effect of thicker tubesheets spreading the total load over more tubes. Examination of the results for cases 1 and 2 on Fig. 11.6.1 shows that increased tube Young's Modulus and yield stress results in a decrease in permitted pressure for a given thickness. Finally, comparison of case 3 and case 4 illustrates the effect of waterbox stiffening on unit allowable pressures. The cause of the abrupt change in local slope of the pressure curves for cases 1-3 is easily explained by the location of the maximum stress that limits the pressure. For cases 1-3, the limiting bending moment occurs at the joint between the tubesheet strip and the adjacent waterbox plate. For smaller tubesheet thickness, the limiting stress is in the tubesheet. As the tubesheet thickness increases the limiting stress occurs in the waterbox wall adjacent to the tubesheet. We note that in this study the waterbox plate thickness does not change as the tubesheet thickness is increased. As the tubesheet thickness increases, the allowable unit pressure continues to increase, albeit at a much slower rate. The increase reflects the effect of edge fixity condition ϵ_1 which tends to increase as the tubesheet thickness increases. For the case 4 simulation, the waterbox plate never governs the limiting stress state; the limiting stress condition always occurs in the tubesheet. For the particular configuration studied, the 1 inch tubesheet thickness has its limiting stress condition at the edge; for increased thickness, the limiting state occurs at the beginning of the perforated region.

It is of interest to note the change in edge fixity parameter as the tubesheet thickness increases with the waterbox plate geometry constant. We find for case 3, for example, that for the 60° diagonal strips along the lower edge, the interaction with the flat plate waterbox yields the range of values $0.9 > (1 - \epsilon_1) > 0.41$ for tubesheet thickness 1.0-3.5 inch, respectively. The lamed strips on the side of the unit in case 3 have edge fixity variations $0.76 > (1 - \epsilon_1) > 0.17$ for the tubesheet thickness range given above. These lower values reflect the increased flexibility of the cylindrical wrap.

The effect of a change in tube pattern on test pressure is shown by the second set of pressure-thickness results in Fig. 11.6.1 (cases 5-8). The trends are similar to cases 1-4, but the pressure permitted for a given thickness is increased.

11.7 CONCLUDING REMARKS

In closing this chapter, we emphasize again that the complex nature of the condenser waterbox-tubesheet-tube configuration makes it very difficult to evolve any simplified, accurate analysis technique. We have presented the outline of a very approximate method which has the virtue of relative simplicity and appears useful if applied with caution and good engineering judgment. The method is based on simulating the tubesheet by a series of

well chosen beam strips reflecting the tubesheet geometric characteristics, and simulating the waterbox by parameters that hopefully reflect the character of the edge restraint provided by the waterbox. We close this chapter with the caution to a potential user that if the preliminary design appears marginal, good engineering practice dictates that a more elaborate finite element analysis of the complete unit, with all components included, be considered in order to accurately establish the merits of the probable configuration.

NOMENCLATURE

- A_{ij}, B_i = Parameters defined by (Eq. (11.5.1)) and in Appendix 11.A
 b = Width of beam strip (Fig. 11.2.3)
 B_{ij} = Coefficients defined by (Eq. (11.4.25))
 C_M, C_p, C_T = Local spring rates for edge moments (Eq. (11.4.1))
 D_1, D = Bending modulus of beam strip in unperforated and perforated region, respectively
 d_{ij} = Coefficients defined by (Eq. (11.4.21))
 d_o = Tube outer diameter
 E = Young's Modulus
 f^* = Amplitude modifier for pressure in perforated region (Eq. (11.4.11))
 F_z = Waterbox direct load
 J = Approximate torsional parameter defined by (Eq. (11.4.35))
 K, K_p = Local spring rates for edge displacement (Eq. (11.4.1))
 K_δ = Tube spring rate for deflection (Eq. (11.4.13))
 K^* = Tube spring rate for rotation (Eq. (11.4.13))
 L = Length of unperforated region (Section 11.4) of a beam strip
 L^* = Height of waterbox (Fig. 11.3.4)
 L_T = Half length of condenser shell
 M_A = Edge moment
 M, T = Edge moments on tubesheet (Fig. 11.3.4)
 M_1, M_2 = Beam strip moments (Eq. (11.4.2), Fig. 11.4.1)
 $M(x)$ = Tubesheet strip moment defined by (Eq. (11.5.7))
 M_x, M_y = Waterbox external moments (Fig. 11.3.4)
 p = Tubesheet pressure (Eq. (11.4.2))
 P = Edge load on tubesheet (Fig. 11.3.4)
 P_1, P_2 = Beam shear loads (Eq. (11.4.2), Fig. 11.4.1)
 t_T = Tube wall thickness
 t = Tubesheet thickness
 w_2 = Tubesheet displacement in perforated region
 w_B = Edge deformation of tubesheet (Eq. (11.3.1))
 W = Width of waterbox

- x_L = x coordinate of point of application of external resultants
 y_L = y coordinate of point of application of external resultants
 β = Foundation decay parameter (Eq. (11.4.14))
 $\delta_o, \theta_x, \theta_y$ = Tubesheet deformation parameters (Eq. (11.3.1))
 ϵ_1, ϵ_2 = Edge fixity parameters defined in (Eq. (11.4.26))
 $\Delta\theta_c$ = Elastic rotation of clamped beam strip (Eq. (11.4.4))
 Δw_c = Elastic deformation of clamped beam strip (Eq. (11.4.4))
 ρ = Parameter defined by (Eq. (11.4.15))

REFERENCES

- [11.2.1] "Heat Exchange Institute Standards for Steam Surface Condensers," HEI, 7th Edition, Cleveland, Ohio, pp. 37-43 (1978).
 [11.2.2] Bernstein, M. D., and Soler, A. I., "The Tubesheet Analysis Method in the New HEI Condenser Standards," *ASME Journal of Engineering for Power*, Vol. 100, pp. 363-368 (April 1978).
 [11.2.3] Soler, A. I., "Stress Analysis of Rectangular Tubesheets for Condensers," ASME Paper 80-C2/NE-14, presented at the ASME Nuclear Engineering Conference (August 1980).
 [11.2.4] Soler, A. I., "Structural Design Concepts for Increased Reliability and Safety in Power Plant Condensing Systems," EPRI Report FP-507, Vol. 2, Project 372-1 (September 1978).
 [11.2.5] Soler, A. I., "A Preliminary Assessment of the HEI Tubesheet Design Method - Comparison With a Finite Element Solution," *ASME, Volume H00119, Advances in Reliability and Stress Analysis*, pp. 127-146 (1979).

APPENDIX 11.A

COEFFICIENTS OF A-MATRIX AND B-VECTOR

Using already defined notation and the usual meaning for line integration, we obtain the following results for the coefficients A_{ij} , B_i ; $i, j = 1, 2, 3$

$$A_{11} = \oint K_i ds; \quad A_{12} = \oint y_B K_i ds; \quad A_{13} = \oint x_B K_i ds$$

$$B_1 = \oint K_{p_i} ds$$

$$A_{21} = A_{12} + \sum_{j=1}^2 \oint_j C_{M_j} ds_j$$

$$A_{22} = \oint y_B^2 K_i ds + \sum_{j=1}^2 \oint_j y_{Bj} C_{Mj} ds_j + \sum_{j=3}^4 \oint_j C_{Tj} ds_j$$

$$A_{23} = \oint y_B x_B K_i ds + \sum_{j=1}^2 \oint_j x_{Bj} C_{Mj} ds_j$$

$$B_2 = \oint y_B K_i ds - \sum_{j=1}^2 \oint_j C_{pj} ds_j$$

$$A_{31} = A_{13} + \sum_{j=3}^4 \oint_j C_{Mj} ds_j$$

$$A_{32} = A_{23} + \sum_{j=3}^4 \oint_j y_{Bj} C_{Mj} ds_j$$

$$A_{33} = \oint x_B^2 K_i ds + \sum_{j=3}^4 \oint_j x_{Bj} C_{Mj} ds_j + \sum_{j=1}^2 \oint_j C_{Tj} ds_j$$

$$B_3 = \oint x_B K_{pi} ds - \sum_{j=3}^4 \oint_j C_{pj} ds_j$$

We note that the calculation of A_{ij} , B_i is actually carried out by replacing the integration process by a finite summation process. For example, let us refer to Fig. 11.3.4 and calculate the coefficient A_{11} . We assume that the tubesheet has been replaced by a series of NX strips along the x -half axis and NY strips along the y -axis. We also assume that the unit in question has the \bar{j} , \bar{k} plane as a plane of symmetry and that the spring rates K_i have been computed from Eq. (11.4.29) for each strip around the periphery. Suppose we now let dx_i , dy_j represent the assumed finite width of each strip along the x , y axes, respectively. That is, suppose we have:

$$2 \sum_{i=1}^{NX} dx_i = W; \quad \sum_{j=1}^{NY} dy_j = L^*$$

Then, the coefficient A_{11} can be calculated from the summations shown below:

$$\frac{A_{11}}{2} = \sum_{i=1}^{NX} (K_i dx_i)_B + \sum_{j=1}^{NY} K_j dy_j + \sum_{i=1}^{NX} (K_i dx_i)_T$$

12. FLAT COVER

12.1 INTRODUCTION

A removable flat cover is frequently utilized as the main closure for the tubeside chamber in tubular heat exchangers. In fact, of the five front end styles shown in the TEMA Standards (ref. Table 1.3.1), three contain removable bolted flat covers. Removing a bolted cover does not involve disconnecting channel connections, and the required removal space can be quite small. The cover can be hung from a “davit” or a “hinge” (Photograph 12.a) attached to the mating flange, which can facilitate cover removal. Figure 12.1.1 shows a bolted flat cover in a multiple tube pass unit. Figure 12.1.2 shows a typical davit arrangement. Instead of a davit, a hydraulic or air operated hinge and door set up may be used. These attributes make removal of the cover perhaps the most expeditious way to gain access to the tube-to-tubesheet joint for tube cleaning or for tube plugging operations. In applications involving expensive alloys for the tubeside material, a carbon steel flat cover is easily faced with a liner of the required alloy material thus yielding savings in the hardware cost. Finally, the circular shape makes the flat cover one of the simplest pressure vessel shapes to analyze for pressure loadings. Rules for flat cover design have appeared since early editions of the ASME Boiler and Pressure Vessel Codes. The ASME Code rules are intended only to limit the maximum stress level in the cover. Heat exchanger designers have long recognized, however, that in addition to serving the pressure retaining function, the flat cover also plays an implicit role in the thermal-hydraulic performance of multiple tube pass heat exchangers. The operating pressure causes the cover to flex resulting in increased separation between the edge of the pass partition plates and the cover surface. The gasket “ribs” spring-back as the cover withdraws, under pressure, from the partition plate edge. However, the resilience of the “ribs” may not equal the amount of separation, and a crevice between the cover and the pass partition plates can be formed. This phenomenon is identical to the one discussed in Chapter 4 in reference to the removable tube sheets in U-tube heat exchangers. The differential pressure between the adjoining pass partition chambers determines the rate of bypass of the tubeside fluid. In Chapter 1, some remarks on pass partition arrangement were presented to aid in reducing the overall effect of the bypass on the total heat duty of the heat exchanger. However, it is recognized that the bypass cannot be completely eliminated in most multi-pass designs without limiting the maximum cover deflection. For this reason, the heat exchanger design standards [12.1.1-2] provide deflection



Photograph 12.a. Fixed tubesheet heat exchanger with hinge mounted flat cover (courtesy Joseph Oat Corporation).

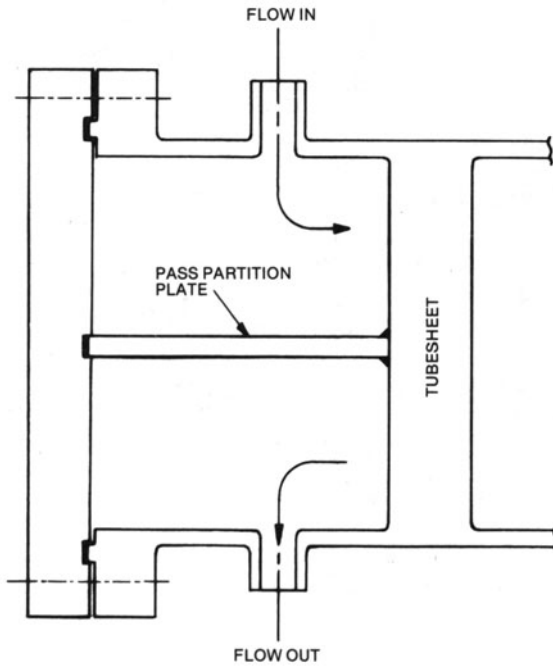


Fig. 12.1.1. Bolted cover with a diametral groove for seating the pass partition plate.

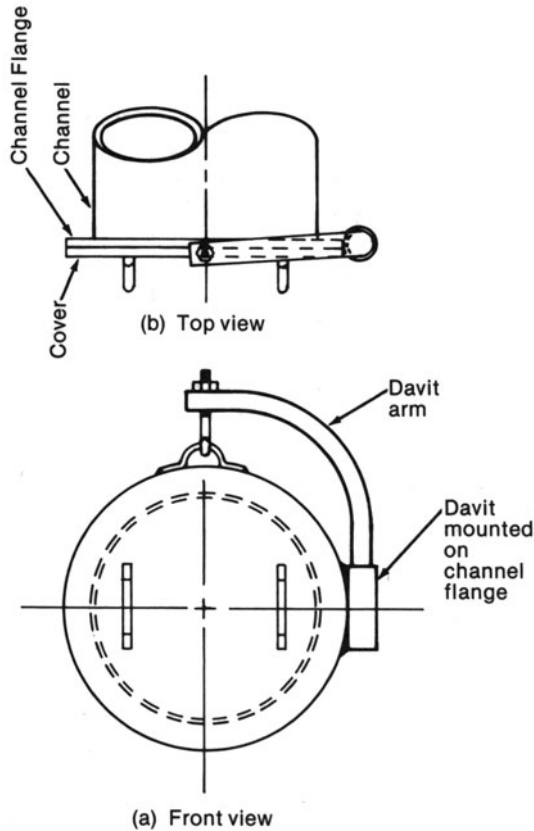


Fig. 12.1.2. Flat cover equipped with a davit arm.

limiting formulas for cover thickness calculation. The derivation of the cover formulas presented in the TEMA [12.1.1] and HEI [12.1.2] Standards is presented here based on our conjecture as to their bases and assumptions. The basis for the ASME Code [12.1.3] cover formula is also given for completeness.

In Chapter 4, controlled metal-to-metal contact was discussed as a means to reduce tubesheet deflection and inter-tube-pass leakage. The viability of this concept in flat cover design is also examined in this chapter. Interaction equations for a lap joint flange bolted to a flat cover are derived in Section 12.3. The computer program LAPCOV, based on this derivation, is utilized to study cover deflection as a function of joint geometry. The relationships to correlate interpass leakage to derating of the heat duty are given in Section 12.5. Explicit formulas for a two tube pass heat exchanger are derived in Section 12.6. Analysis of a welding neck or ring type flange bolted to a cover is illustrated in Section 12.8 through the use of computer program TRIEL (which was described in Chapter 4).

12.2 CONVENTIONAL DESIGN FORMULAS*

12.2.1 ASME Code [Ref. 12.1.3]

The cover is idealized as a circular plate of diameter d and corroded thickness t simply supported at its outer edges. d represents the effective diameter of the gasket as defined in the Code. The portion of the cover outside the effective gasket circle is neglected. The radial bending moment due to the non-concentricity of the bolt load line with the gasket reaction load line is considered to be applied around the edge of the idealized circular plate in a symmetrical manner. If the total bolt load (assumed to be equal to the bolt pre-stress times the total bolt root area) is W and the radial offset between the gasket reaction circle and bolt load circle is h_G , then the moment per unit circumference is:

$$M = \frac{Wh_G}{\pi d}$$

The stress field in the cover due to M is uniform over the surface of the cover and the maximum radial and tangential bending stress at any point is given by [12.2.1]:

$$\sigma_r^{[M]} = \sigma_t^{[M]} = \frac{6M}{t^2} = \frac{6}{\pi} \frac{Wh_G}{dt^2}$$

or

$$\sigma_r^{[M]} = \sigma_t^{[M]} = 1.9 \frac{Wh_G}{dt^2} \quad (12.2.1)$$

Similarly, the maximum stress in a simply supported circular plate of outer diameter d subject to a lateral pressure p is given by [ref. Section 2.4]:

$$\sigma_r^{[p]} = \sigma_t^{[p]} = \frac{3(3 + \nu)}{32} \frac{pd^2}{t^2}$$

where ν is the Poisson ratio of the cover material (almost universally assumed to be 0.3 for ductile metals). Therefore:

$$\sigma_r^{[p]} = \sigma_t^{[p]} = \frac{Cpd^2}{t^2} \quad (12.2.2)$$

where:

$$C = \frac{3(3 + \nu)}{32} \approx 0.3$$

The ASME Code assumes that the bolt load W does not change when the flanged joint is pressurized. We also note that the stresses due to M and P

*Where not specifically defined, the notations used in deriving the formulas in each subsection in this section correspond to those used in the pertinent standard. Each term is defined where it first appears in the text. The definition of many terms in this section does not appear in the nomenclature.

are additive. Setting the combined stress equal to the allowable stress for the cover material SE (E is the joint efficiency, as defined by the ASME Code, of the welded butt joints, if any, in the cover) leads to the well-known code formula for cover thickness:

$$t = d \left[\frac{Cp}{SE} + \frac{1.9 Wh_G}{SEd^3} \right]^{1/2} \quad (12.2.3)$$

12.2.2 TEMA Standards [Ref. 12.1.1]

TEMA Standards have a deflection based formula which seeks to limit the maximum deflection of the flat cover of a multi-tube pass unit to 0.030". The structural model is similar to that of the ASME Code. The cover is simulated as a circular flat plate of diameter G , corroded thickness T subject to lateral pressure p , and to a symmetrically distributed edge moment M . The diameter G is the mean gasket diameter, not the effective gasket diameter as defined in the ASME Code [12.1.3]. The edge moment M is computed by assuming that all the bolts (total cross sectional area A_B) are stressed to a value $45000/d_B^{1/2}$, where d_B is the nominal bolt diameter. If h_G represents the radial offset between the mean gasket circle and bolt circle, then M is given by:

$$M = \frac{h_G A_B (45000/d_B^{1/2})}{\pi G}$$

The formula for the maximum deflection, δ , due to pressure p and edge moment M , is readily obtained from Roark [12.2.1] as

$$\delta = \frac{3F(1-\nu)(5+\nu)G^2}{64\pi ET^3} + \frac{6(1-\nu)MG^2}{4ET^3}$$

where ν is Poisson's ratio, T is the cover thickness, and $F = \pi G^2 p/4$. Setting $\nu = 0.3$, $\delta = 0.03$ ", and rearranging terms gives the TEMA cover plate thickness formula:

$$T \approx \left[\frac{1.425 G^4 p}{E} + \frac{0.5 h_G A_B G \times 10^6}{E d_B^{1/2}} \right]^{1/3}$$

12.2.3 Heat Exchange Institute [Ref. 12.1.2]

The formula for cover thickness given in Ref. [12.1.2] is derived in the same manner as the TEMA formula, except for two simplifications which are not made: the maximum cover deflection δ is left to the discretion of the designer, and the total bolt load W appears explicitly in the formula; i.e., the bolt stress level is not specified.

All three design formulae discussed in the foregoing neglect the effect of the outer portion (beyond a hypothetical mean gasket circle) of the cover and the variation in the bolt load as the joint is pressurized. Reduction in

cover deflection due to special design features, such as controlled metal-to-metal contact outside the bolt circle, soft gaskets, or stiff bolts (over bolting), cannot be accounted for using these formulas. The analysis presented in the following section removes these limitations.

12.3 FLANGE-COVER INTERACTION

In Chapter 4, the interaction of two welding neck flanges and a sandwiched tubesheet, the so-called “three element joint,” was studied. In this section, we will derive the interaction relationship for a flat circular cover bolted to a lap joint flange. This formulation will enable us to study the variation of the residual gasket compression load and the bolt pull due to change in pressure, cover and flange ring thickness, etc. Having established the deflection profile of the cover, the leakage area under the pass partition lanes can be calculated and the corresponding inter-pass leakage rates can be evaluated. The analysis procedure also permits incorporation of the metal-to-metal contact concepts described in Section 3.14. The analysis presented in this section is computerized by the code LAPCOV described and listed in Section 12.7.

12.3.1 Cover

Figure 12.3.1 shows the joint to be analyzed. The flat cover is modeled as a thin circular plate of outer radius r_b integrally connected to an annular ring of inner and outer radii r_b and b , respectively (Fig. 12.3.2). The cover is subject to a ring load H_G at radius r_0 (gasket compression load) under the seating condition. In the pressurized condition, a uniform pressure load H_p acts over the circular region bounded by radius r_0 , and a changed gasket ring load ($H_G - \Delta H_G$) acts at radius r_0 . We can also assume that a contact load F_e may be acting on the outer ring at a radial distance ($e - e_1$) from the bolt circle. Figure 12.3.2 shows the freebody of the cover where H_1 , H_2 and H_3 represent the gasket ring load, pressure load, and contact load, respectively. The values of H_1 , H_2 and H_3 will change depending on the loading condition and the joint geometry. For example, under the seating condition, $H_2 = 0$ (zero pressure); for raised face designs, $H_3 = 0$ (no metal-to-metal contact). We will write the expression for the cover deflection in terms of H_1 , H_2 and H_3 . Results for specific loading conditions can then be obtained by using appropriate values for those loads. The thickness of the cover in the inner ($r < r_b$) and outer regions ($r > r_b$) is assumed to be t_1 and t_2 , respectively. The following main assumptions are made in constructing this model:

- (i) The weakening effect of pass partition grooves in the cover is neglected. However, different thicknesses of the cover inboard and outboard of the bolt circle is allowed.
- (ii) The gasket load is assumed to be a lineal ring load acting at the effective gasket radius r_0 as defined in Section 3.5.

- (iv) The weakening effect of the bolt holes in the cover is neglected.
- (v) The annular portion of the cover beyond the bolt circle is modeled as a narrow ring (Section 3.9). Similarly, the flange ring of the lap joint flange is also modeled as a narrow ring.

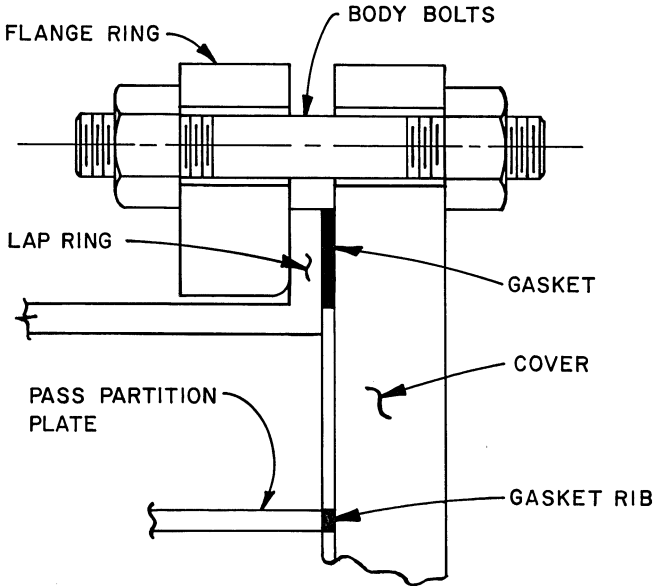


Fig. 12.3.1. Lap joint flange bolted to a flat cover.

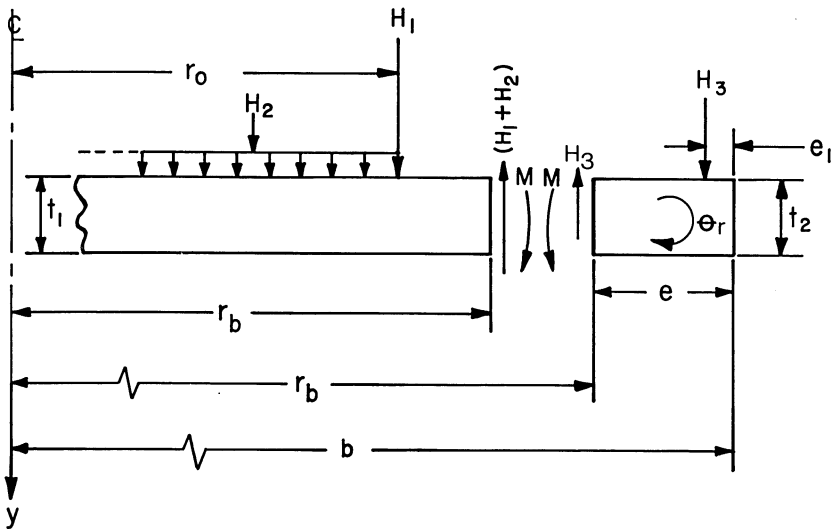


Fig. 12.3.2. Freebody of flat cover.

The expression for the discontinuity moment M at the bolt circle, in terms of H_1 , H_2 , and H_3 , is derived as follows:

The lateral deflections of the inner plate with respect to its boundary ($r=r_b$) due to axisymmetric loads H_1 and H_2 are given by classical plate theory solutions [12.2.1].

The deflection y_1 due to H_1 is given by:

$$y_1(r) = \frac{\alpha_0 H_1 \phi(r)}{t_1^3} \quad (12.3.1)$$

where $\phi(r)$ is given by:

$$\begin{aligned} \phi(r) = & \alpha_1 (r_b^2 - r^2) - (r^2 + r_0^2) \ln \frac{r_b}{r} \\ & - \frac{\alpha_2 r_0^2 (r_b^2 - r^2)}{r_b^2}; \quad r \geq r_0 \end{aligned} \quad (a)$$

$$\phi(r) = \alpha_1 (r_b^2 - r^2) - (r^2 + r_0^2) \ln \frac{r_b}{r_0} \quad (12.3.2)$$

$$+ (r^2 - r_0^2) - \frac{\alpha_2 r_0^2 (r_b^2 - r^2)}{r_b^2}; \quad r \leq r_0 \quad (b)$$

and:

$$\alpha_0 = \frac{3(1-\nu^2)}{2\pi E_1} \quad (a)$$

$$\alpha_1 = \frac{(3+\nu)}{2(1-\nu)} \quad (b) \quad (12.3.3)$$

$$\alpha_2 = \frac{(1-\nu)}{2(1+\nu)} \quad (c)$$

Similarly, the deflection $y_2(r)$ due to the distributed load H_2 is given by [12.2.1]:

$$y_2(r) = \frac{\alpha_0 H_2 \psi(r)}{t_1^3} \quad (12.3.4)$$

where $\psi(r)$ is given by:

$$\begin{aligned} \psi(r) = & \frac{1}{8} \left[\alpha_3 (r_b^2 - r^2) - 4\alpha_2 \frac{r_0^2 (r_b^2 - r^2)}{r_b^2} \right. \\ & \left. - (8r^2 + 4r_0^2) \ln \frac{r_b}{r} \right]; \quad r \geq r_0 \end{aligned} \quad (a)$$

$$\psi(r) = \frac{1}{8} \left[4r_b^2 - 5r_0^2 + \frac{r^4}{r_0^2} - (8r^2 + 4r_0^2) \ln \frac{r_b}{r_0} \right]$$

(12.3.5)

$$- \frac{4\alpha_2 r_0^2 (r_b^2 - r^2)}{r_b^2} + 8\alpha_4 (r_b^2 - r^2)]; \quad r \leq r_0 \quad (b)$$

and:

$$\alpha_3 = \frac{12 + 4\nu}{1 + \nu} \quad (a)$$

(12.3.6)

$$\alpha_4 = \frac{1}{(1 + \nu)} \quad (b)$$

Finally, the deflection y_3 due to the edge moment M is given by:

$$y_3 = - \frac{6(1 - \nu)M(r_b^2 - r^2)}{E_1 t_1^3} = \frac{-\Omega(r)M}{t_1^3} \quad (12.3.7)$$

Therefore, the net slope of the inner plate, θ_c , at radius $r = r_b$ (its outer edge) is given by:

$$\theta_c = \left. \frac{dy_1}{dr} \right|_{r=r_b} + \left. \frac{dy_2}{dr} \right|_{r=r_b} + \left. \frac{dy_3}{dr} \right|_{r=r_b} \quad (12.3.8)$$

Referring to Fig. 12.3.2, the slope is positive if the section rotates clockwise in the plane of the paper.

Differentiating Eqs. (12.3.2a), (12.3.5a) and (12.3.7) with respect to r and substituting $r = r_b$, we find that Eq. (12.3.8) becomes:

$$\theta_c = \frac{\alpha_0 \gamma_1 H_1}{t_1^3} + \frac{\alpha_0 \gamma_2 H_2}{t_1^3} + \frac{\alpha_5 M}{t_1^3} \quad (12.3.9)$$

where:

$$\alpha_5 = \frac{12(1 - \nu)r_b}{E_1} \quad (a)$$

$$\gamma_1 = (1 - 2\alpha_1)r_b + \frac{r_0^2}{r_b} (1 + 2\alpha_2) < 0 \quad (b)$$

(12.3.10)

$$\gamma_2 = \frac{1}{2} \left[\frac{r_b^3}{r_0^2} - 4r_b \ln \frac{r_b}{r_0} + \frac{2\alpha_2 r_0^2}{r_b} - 4r_b \alpha_4 \right] < 0 \quad (c)$$

The expression for rotation of the annular ring (positive if clockwise in Fig.

12.3.2) is found by first writing the expression for the moment about its mean circumference.

The moment per unit circumference is given by:

$$m_r = -\frac{Mr_b}{r_{av}} + \frac{H_3(e-e_1)}{2\pi r_{av}} \quad (12.3.11)$$

where:

$$e = (b - r_b) \quad (a)$$

$$r_{av} = \frac{1}{2}(b + r_b) \quad (b) \quad (12.3.12)$$

The equation for rotation of the annular ring, θ_r , follows from Eq. (3.9. 4).

$$\theta_r = -\frac{1}{t_2^3} [\gamma_3 M - \gamma_4 H_3] \quad (12.3.13)$$

where:

$$\gamma_3 = \frac{12r_{av}r_b}{E_1 e} \quad (a)$$

$$\gamma_4 = \frac{6r_{av}(e-e_1)}{E_1 e \pi} \quad (b) \quad (12.3.14)$$

Equating the rotation of the ring (Eq. (12.3.13)) to that of the edge of the inner plate (Eq. (12.3.9)), yields an expression for M as

$$M = \beta_1 H_1 + \beta_2 H_2 + \beta_3 H_3 \quad (12.3.15)$$

where

$$\beta_1 = \frac{-\alpha_0 \gamma_1}{\gamma_3 t'^3 + \alpha_5} \quad (a)$$

$$\beta_2 = \frac{-\alpha_0 \gamma_2}{\gamma_3 t'^3 + \alpha_5} \quad (b)$$

$$\beta_3 = \frac{\gamma_4 t'^3}{\gamma_3 t'^3 + \alpha_5} \quad (c) \quad (12.3.16)$$

$$\beta_3 = \frac{\gamma_4 t'^3}{\gamma_3 t'^3 + \alpha_5} \quad (c)$$

$$t' = t_1/t_2 \quad (d)$$

The total deflection of the cover, $y_c(r)$, at any radius r , with respect to the bolt circle ($r=r_b$), can now be expressed in terms of H_1 , H_2 and H_3 . Since

$$y_c(r) = y_1 + y_2 + y_3$$

then, from Eqs. (12.3.1), (12.3.4) and (12.3.7):

$$y_c(r) = \frac{1}{t_1^3} [\alpha_0 H_1 \phi(r) + \alpha_0 H_2 \psi(r) - \Omega(r) M]$$

Substituting for M from Eq. (12.3.15), we have:

$$y_c(r) = \frac{1}{t_1^3} [\{\alpha_0 \phi(r) - \beta_1 \Omega(r)\} H_1 + \{\alpha_0 \psi(r) - \beta_2 \Omega(r)\} H_2 - \beta_3 \Omega(r) H_3] \quad (12.3.17)$$

Thus, the deflection of the cover, y_c , with respect to the bolt circle, is expressed in terms of three loads, namely, the ring load H_1 acting at radius r_0 , the pressure load H_2 acting over the circular surface of radius r_0 , and the ring load H_3 acting on the circle of radius $(b - e_1)$. In order to determine deflection of the cover under the "seating" and the pressurized conditions, it is necessary to evaluate these loads under these conditions. This is accomplished by developing the cover-flange interaction relations.

12.3.2 Flange Ring

The ASME Code [12.1.3] specifies lever arms for the gasket load and header load due to pressure. Let h_G and h_p denote the radial distances of the effective gasket load circle and total header load circle from the bolt circle, respectively. If H_1 , H_2 and H_3 represent the gasket load, total header load, and metal-to-metal contact load, respectively, then the net moment per unit circumference at radius r_m is (ref. Fig. 12.3.3):

$$m_r = \frac{(H_1 h_G + H_2 h_p) - H_3 (b - e_1 - r_b)}{2\pi r_m}$$

where r_m denotes the mean radius of the flange ring. It should be noted that h_G may not be equal to $(r_b - r_0)$ in all cases. In particular, the gasket load is assumed to bear on the flange ring at the mid-circle of the annular contact patch between the lap ring and the backing ring in Fig. 12.3.1. This mid-circle may or may not coincide with the effective gasket load circle.

The flange ring rotation θ_f , corresponding to m_r , (positive if clockwise in Fig. 12.3.3), is given by

$$\theta_f = \frac{\rho_1' H_1}{t_f^3} + \frac{\rho_2' H_2}{t_f^3} - \frac{\rho_3' H_3}{t_f^3} \quad (12.3.18)$$

where:

$$\rho_1' = \frac{6r_m h_G}{\pi w E_f} \quad (a)$$

$$\rho_2' = \frac{6r_m h_p}{\pi w E_f} \quad (b) \quad (12.3.19)$$

$$\rho_3' = \frac{6(b - e_1 - r_b) r_m}{\pi w E_f} \quad (c)$$

Therefore, the lateral deflection of the flange ring at $r = r_0$ (gasket circle), with respect to the bolt circle, is

$$y_f = \theta_f (r_b - r_0)$$

or:

$$y_f = \frac{\rho_1}{t_f^3} H_1 + \frac{\rho_2}{t_f^3} H_2 - \frac{\rho_3}{t_f^3} H_3 \quad (12.3.20)$$

$$\rho_1 = \frac{6r_m h_G}{\pi w E_f} (r_b - r_0) \quad (a)$$

$$\rho_2 = \frac{6r_m h_p}{\pi w E_f} (r_b - r_0) \quad (b) \quad (12.3.21)$$

$$\rho_3 = \frac{6r_m (b - e_1 - r_b) (r_b - r_0)}{\pi w E_f} \quad (c)$$

12.3.3 Interaction Relations

i. Raised Face Designs

Let us first consider the case where there is no metal-to-metal contact under either the seating or the pressurized condition, i.e., $H_3 = F_e = 0$.

Under the seating condition, let H_G represent the total gasket compression load. H_G also equals the bolt load. When the joint is pressurized, let the new gasket load corresponding to header load H_p be given by $H_G - \Delta H_G$. Therefore, the total bolt load during the pressurized condition is $(H_G - \Delta H_G + H_p)$. Hence, the increase in the bolt load as the joint is pressurized is given by $(H_p - \Delta H_G)$. If K_b represents the axial stiffness of the body bolts (Section 3.10), then the elongation of the bolt line due to pressurization of the joint (equal to the separation of the flange and the cover at the bolt circle) is given by:

$$\delta_b = \frac{H_p - \Delta H_G}{K_b} \quad (12.3.22)$$

Relaxation of the gasket, δ_G , from the seating condition to the pressurized condition is given by:

$$\delta_G = \frac{\Delta H_G}{K_G} \quad (12.3.23)$$

where K_G is the gasket spring rate during unloading. Since $y_c(r_0)$, $y_f(r_0)$ are both positive if they tend to separate the elements (see Fig. 12.3.4)

$$\delta_G - \delta_b = [y_c(r_0) + y_f(r_0)]_{\text{Pressurized condition}} - [y_c(r_0) + y_f(r_0)]_{\text{Seating condition}}$$

We have, utilizing Eqs. (12.3.17) and (12.3.20),

$$\frac{\Delta H_G}{K_G} - \frac{H_p - \Delta H_G}{K_b} = \frac{1}{t_f^3} [-\{\alpha_0 \phi(r_0) - \beta_1 \Omega(r_0)\} \Delta H_G$$

$$+ \{\alpha_0 \psi(r_0) - \beta_2 \Omega(r_0)\} H_p] + \frac{\rho_2}{t_f^3} H_p - \frac{\rho_1}{t_f^3} \Delta H_G$$

Therefore:

$$\Delta H_G = \omega H_p \quad (12.3.24)$$

where:

$$\omega = \frac{\frac{1}{K_b} + \frac{1}{t_1^3} (\alpha_0 \psi_0 - \Omega_0 \beta_2) + \frac{\rho_2}{t_f^3}}{\frac{1}{K_G} + \frac{1}{K_b} + \frac{1}{t_1^3} (\alpha_0 \phi_0 - \Omega_0 \beta_1) + \frac{\rho_1}{t_f^3}} \quad (12.3.25)$$

where abbreviations ϕ_0 , ψ_0 , Ω_0 are used to indicate that these functions are evaluated at $r=r_0$.

Equations (12.3.24–25) give the variation in the gasket load for a given pressure load. Thus, if the gasket seating load H_G is defined, then the loads on the cover under a given pressure become known.

ii. Controlled Metal-to-Metal Contact

Now let us consider the case where the flange and cover faces are machined in such a manner that under the seating condition a gap ϵ_0 is developed between the two surfaces at the “contact circle,” located at a radial offset e_1 from the outer edge (Fig. 12.3.3). When the joint is pressurized, the flange ring and the cover rotate and further reduce the gap ϵ_0 . As the pressure is increased, eventually the gap closes and a contact force F_e is developed. Formulas to compute the residual gasket pressure, bolt load, contact load F_e , or gap ϵ (as the case may be) as a function of the pressure load H_p are derived in the following:

We recall that the rotation of the flange ring θ_f can be expressed as a function of the three loads H_1 , H_2 and H_3 , i.e.,

$$\theta_f(H_1, H_2, H_3) = \frac{\rho_1'}{t_f^3} H_1 + \frac{\rho_2'}{t_f^3} H_2 - \frac{\rho_3'}{t_f^3} H_3 \quad (12.3.26)$$

where ρ_1' , ρ_2' and ρ_3' are functions of flange ring geometric dimensions. Similarly, the rotation of the cover ring θ_r can be expressed as a function of H_1 , H_2 and H_3 by using Eqs. (12.3.13) and (12.3.15). Thus:

$$\theta_r(H_1, H_2, H_3) = -\frac{1}{t_2^3} [\gamma_3 \beta_1 H_1 + \gamma_3 \beta_2 H_2 + (\gamma_3 \beta_3 - \gamma_4) H_3] \quad (12.3.27)$$

Assuming that contact at the “contact circle” is not yet established, the gap at the contact circle, ϵ , under a header load H_p is given by:

$$\epsilon = \epsilon_0 + \delta_b - (b - e_1 - r_b) [\theta_f(H_G - \Delta H_G, H_p, 0) - \theta_f(H_G, 0, 0)] + (b - e_1 - r_b) [\theta_r(H_G - \Delta H_G, H_p, 0) - \theta_r(H_G, 0, 0)] \quad (12.3.28)$$

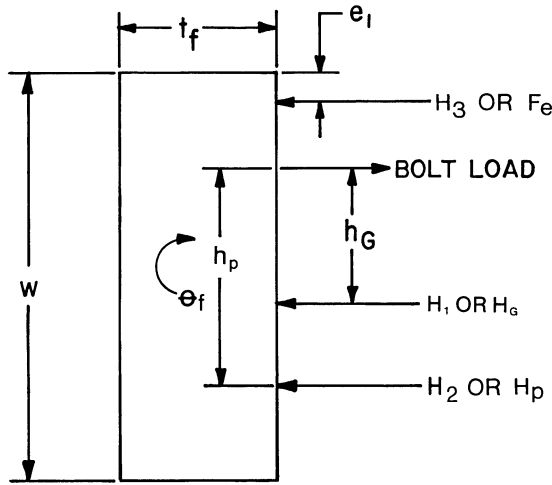


Fig. 12.3.3. Freebody of flange ring (cross section).

The negative sign in front of the term multiplying θ_f becomes clear by referring to Fig. 12.3.4 wherein the sign convention for θ_f and θ_r (cover ring rotation) is shown. Note that positive θ_f tends to close the gap at the “contact circle,” whereas positive θ_r tends to open the gap. δ_b is the additional stretch of the bolts due to the change in the bolt load.

$$\delta_b = \frac{H_p - \Delta H_G}{K_b}$$

Substituting for θ_f , θ_r , etc., we have

$$\begin{aligned} \epsilon = \epsilon_0 + \frac{H_p - \Delta H_G}{K_b} - \frac{b - e_1 - r_b}{t_f^3} [\rho_2' H_p - \rho_1' \Delta H_G] \\ - \frac{(b - e_1 - r_b)}{t_2^3} [\gamma_3 \beta_2 H_p - \gamma_3 \beta_1 \Delta H_G] \end{aligned}$$

Since $\Delta H_G = \omega H_p$ (Eq. (12.3.24)), we have:

$$\epsilon = \epsilon_0 + \kappa H_p \quad (12.3.29)$$

$$\text{where } \kappa = \left[\frac{1 - \omega}{K_b} - \frac{(b - e_1 - r_b)}{t_f^3} (\rho_2' - \rho_1' \omega) \right.$$

$$\left. - \frac{(b - e_1 - r_b)}{t_2^3} \{ \gamma_3 \beta_2 - \omega \gamma_3 \beta_1 \} \right] \quad (12.3.30)$$

If $\epsilon < 0$, as calculated from Eq. (12.3.29), then a contact force F_e must be developed to satisfy the impenetrability requirement of the two surfaces at the radius $r = (b - e_1)$. Thus, in lieu of Eq. (12.3.29), we obtain an equation for F_e by setting $\epsilon = 0$.

We have:

$$\epsilon = 0 = \epsilon_0 + \delta_b - (b - e_1 - r_b) [\theta_f (H_G - \Delta H_G, H_p, F_e) - \theta_f (H_G, 0, 0)] \\ + (b - e_1 - r_b) [\theta_r (H_G - \Delta H_G, H_p, F_e) - \theta_c (H_G, 0, 0)]$$

where:

$$\delta_b = \frac{H_p + F_e - \Delta H_G}{K_b}$$

Proceeding as before, we have:

$$0 = \epsilon_0 + \frac{F_e}{K_b} + (b - e_1 - r_b) F_e \left[\frac{\rho_3'}{t_f^3} - \frac{(\gamma_3 \beta_3 - \gamma_4)}{t_2^3} \right] \\ + \Delta H_G \left[-\frac{1}{K_b} + \frac{(b - e_1 - r_b) \rho_1'}{t_f^3} + \frac{(b - e_1 - r_b) \gamma_3 \beta_1}{t_2^3} \right] \\ + H_p \left[\frac{1}{K_b} - \frac{(b - e_1 - r_b) \rho_2'}{t_f^3} - \frac{(b - e_1 - r_b) \gamma_3 \beta_2}{t_2^3} \right]$$

or:

$$F_e = a_1 + a_2 H_p + a_3 \Delta H_G \quad (12.3.31)$$

where:

$$a_1 = -\epsilon_0 / \left[\frac{1}{K_b} + (b - e_1 - r_b) \left\{ \frac{\rho_3'}{t_f^3} - \frac{(\gamma_3 \beta_3 - \gamma_4)}{t_2^3} \right\} \right] \quad (a)$$

$$a_2 = \frac{- \left[\frac{1}{K_b} - \frac{(b - e_1 - r_b) \rho_2'}{t_f^3} - \frac{(b - e_1 - r_b) \gamma_3 \beta_2}{t_2^3} \right]}{\left[\frac{1}{K_b} + (b - e_1 - r_b) \left\{ \frac{\rho_3'}{t_f^3} - \frac{(\gamma_3 \beta_3 - \gamma_4)}{t_2^3} \right\} \right]} \quad (b) \quad (12.3.32)$$

$$a_3 = \frac{- \left[-\frac{1}{K_b} + \frac{(b - e_1 - r_b) \rho_1'}{t_f^3} + \frac{(b - e_1 - r_b) \gamma_3 \beta_1}{t_2^3} \right]}{\left[\frac{1}{K_b} + (b - e_1 - r_b) \left\{ \frac{\rho_3'}{t_f^3} - \frac{(\gamma_3 \beta_3 - \gamma_4)}{t_2^3} \right\} \right]} \quad (c)$$

Finally, displacement compatibility at the gasket location ($r=r_0$) requires that the total relaxation of the gasket equal the sum of the bolt stretch and the total separation (relative to the bolt circle) between cover and flange ring at $r=r_0$ as the loadings (H_1, H_2, H_3) change from $(H_G, 0, 0)$ to $(H_G - \Delta H_G, H_p, F_e)$.

Proceeding in the manner of the preceding sub-section, we have, after some algebra:

$$\Delta H_G = a_4 H_p + a_5 F_e \quad (12.3.33)$$

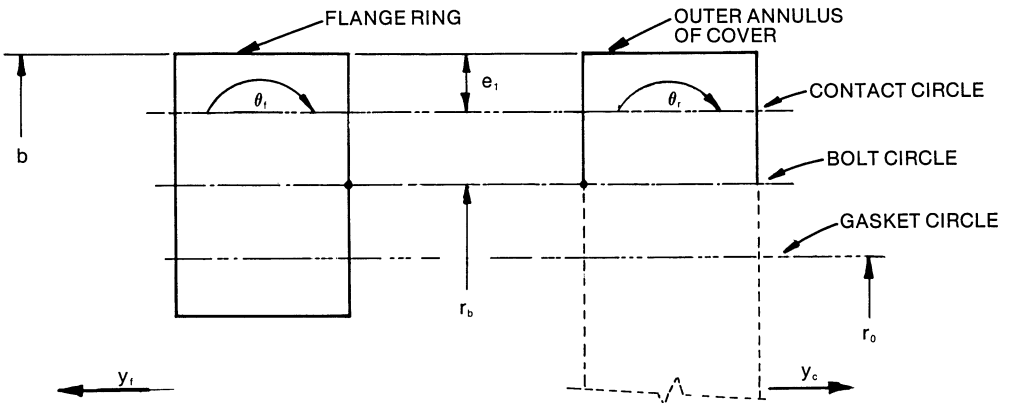


Fig. 12.3.4. Assumed rotation directions for cover outer annulus and flange ring.

where:

$$a_4 = \frac{\frac{1}{K_b} - \frac{\rho_2}{t_f^3} + \frac{\alpha_0 \psi_0 - \beta_2 \Omega_0}{t_1^3}}{\frac{1}{K_b} + \frac{1}{K_G} + \frac{\rho_1}{t_f^3} + \frac{\alpha_0 \phi_0 - \beta_1 \Omega_0}{t_1^3}} \quad (a)$$

$$a_5 = \frac{\frac{1}{K_b} - \frac{\rho_3}{t_f^3} - \frac{\beta_3 \Omega_0}{t_1^3}}{\frac{1}{K_G} + \frac{1}{K_b} + \frac{\rho_1}{t_f^3} + \frac{\alpha_0 \phi_0 - \beta_1 \Omega_0}{t_1^3}} \quad (b) \quad (12.3.34)$$

From Eqs. (12.3.31) and (12.3.33), we have:

$$F_e = \frac{a_1}{1 - a_3 a_5} + \frac{a_2 + a_3 a_4}{1 - a_3 a_5} H_p \quad (12.3.35)$$

$$\Delta H_G = \left[\frac{a_4 + a_2 a_5}{1 - a_3 a_5} \right] H_p + \frac{a_1 a_5}{1 - a_3 a_5} \quad (12.3.36)$$

Thus F_e and ΔH_G are determined in terms of H_p .

12.4 COVER AND FLANGE RING STRESSES

The analyses in the preceding section treated three loads on the inner disc of the cover (Fig. 12.3.2); namely, a ring load H_1 at radius r_0 , a pressure

load H_2 over a circle of radius r_0 , and a radially symmetric edge moment M acting on the outer edge (radius = r_b). Formulas for defining these loadings under the pressurized condition were developed in terms of their values for the seating condition. In practical designs the maximum stresses and deflection in the cover occur at the center ($r=0$). The maximum cover bending stress σ_c , at the center in terms of the loads shown in Fig. 12.3.2 is given by [12.2.1]:

$$\sigma_b = C_1 H_1 + C_2 H_2 + C_3 M \quad (12.4.1)$$

where:

$$C_1 = \frac{3}{2\pi t_1^2} \left[\frac{1-\nu}{2} + (1+\nu) \ln \frac{r_b}{r_0} - (1-\nu) \frac{r_0^2}{2r_b^2} \right] \quad (a)$$

$$C_2 = \frac{3}{2\pi t_1^2} \left[1 + (1+\nu) \ln \frac{r_b}{r_0} - (1-\nu) \frac{r_0^2}{4r_b^2} \right] \quad (b)$$

$$C_3 = \frac{-6}{t_1^2} \quad (c) \quad (12.4.2)$$

We recall Eq. (12.3.15) which gives M in terms of H_1 , H_2 and H_3 . Thus, we have:

$$\sigma_c = (C_1 + C_3 \beta_1) H_1 + (C_2 + C_3 \beta_2) H_2 + C_3 \beta_3 H_3 \quad (12.4.3)$$

The radial and tangential bending stresses are equal at the center due to the symmetry of the loadings.

Finally, the maximum stress in the flange ring S_{\max} is given as a function of the ring rotation by Eq. (3.9.5).

$$S_{\max} = \frac{E_f t_f \theta_f}{2r_m} \quad (12.4.4)$$

where θ_f is defined by Eq. (12.3.18) in terms of H_1 , H_2 and H_3 .

12.5 LOSS IN HEAT DUTY DUE TO FLOW BYPASS

The expressions derived in the preceding sections give the cover deflection for a cover-lap joint flange construction under seating and pressurized conditions. We will assume that the pass partition ribs are compressed under the seating condition (a desirable and realistic situation). It is difficult to ascertain the amount of rib spring-back as the cover undergoes additional deflection due to pressure. For purposes of obtaining a conservative estimate of the bypass area, any rib spring-back will be neglected. Let Δy represent the added cover deflection from seating to pressurized condition, i.e.,

$$\Delta y = y_c |_{\text{Pressurized}} - y_c |_{\text{Seating}}$$

Then the leakage area under a pass partition plate is given by:

$$A_L = \int \Delta y ds$$

where the integration is to be carried out over the extent of the pass partition plate line. Having determined A_L , the inter-pass leakage ΔW_i is computed using the method described in Chapter 4.

It is shown in Ref. [12.5.1] that for a two pass heat exchanger the reduction in the heat duty can be expressed directly in terms of the basic thermal performance variables of the heat exchanger. This derivation is presented in the next section due to its relevance to the mechanical design of bolted covers even though the subject matter primarily belongs in the realm of thermal design of heat exchangers.

12.6 THERMAL PERFORMANCE OF TWO TUBE PASS HEAT EXCHANGERS

Let us assume that out of a total tubeside flow rate of W_i , ΔW_i bypasses the heat transfer process on the tube surface by flowing through the “crevice” formed by the deflection of the cover. We will relate the bypass stream ΔW_i to the reduction in overall exchanger heat duty of a two tube pass heat exchanger. Without any loss of generality, we assume that the coolant is on the tubeside. Then, the thermal performance of a heat exchanger expressed in terms of its heat duty, Q , is defined as:

$$Q = W_i C_i (S_2 - S_1) \quad (12.6.1)$$

or:
$$Q = W_i C_i P (T_1 - S_1) \quad (12.6.2)$$

S_1 , S_2 are the tubeside fluid inlet and outlet temperature, T_1 is the inlet temperature of the shellside fluid, and P is the “temperature effectiveness”, defined as:

$$P = \frac{S_2 - S_1}{T_1 - S_1} \quad (12.6.3)$$

P is defined as the ratio of the temperature change of the tubeside to the difference between the two inlet temperatures.

If the tubeside flow rate is reduced by ΔW_i , the corresponding heat duty $Q - \Delta Q$ is given by:

$$Q - \Delta Q = (W_i - \Delta W_i) C_i (P - \Delta P) (T_1 - S_1) \quad (12.6.4)$$

From Eqs. (12.6.2) and (12.6.4) we have, neglecting terms of higher order:

$$\Delta Q = (\Delta W_i C_i P + \Delta P W_i C_i) (T_1 - S_1)$$

Hence:

$$\frac{\Delta Q}{Q} = \frac{\Delta W_i}{W_i} + \frac{\Delta P}{P} \quad (12.6.5)$$

The NTU (number of transfer units) of the heat exchanger is defined as:

$$\eta = \frac{UA}{W_i C_i}$$

$$\eta - \Delta\eta = \frac{UA}{(W_t - \Delta W_t)C_t}$$

or:

$$\Delta\eta = \frac{-UA}{C_t} \left[\frac{1}{(W_t - \Delta W_t)} - \frac{1}{W_t} \right]$$

In the above derivation, we have tacitly assumed that the overall heat transfer coefficient, U , remains unchanged as the effective tubeside flow rate is perturbed. This assumption is supportable as long as the by-pass stream is a small fraction of the total flow rate, i.e., as long as

$$\frac{\Delta W_t}{W_t} \ll 1.$$

Simplifying further, and neglecting terms of higher order, we have

$$\frac{\Delta\eta}{\eta} = \frac{-\Delta W_t}{W_t} \quad (12.6.6)$$

Substituting in Eq. (12.6.5), we have:

$$\frac{\Delta Q}{Q} = \frac{-\Delta\eta}{\eta} + \frac{\Delta P}{P} \quad (12.6.7)$$

Or, in differential form:

$$\frac{dQ}{Q} = -\frac{d\eta}{\eta} + \frac{dP}{P}$$

As shown in Ref. [12.6.1]:

$$dP = \frac{\partial P}{\partial \eta} d\eta + \frac{\partial P}{\partial R} dR$$

where R is the thermal flow rate ratio (also called “capacity flow rate ratio”):

Hence:

$$\frac{dQ}{Q} = \frac{-d\eta}{\eta} + \frac{1}{P} \left[\frac{\partial P}{\partial \eta} d\eta + \frac{\partial P}{\partial R} dR \right] \quad (12.6.8)$$

The derivatives $\partial P/\partial \eta$ and $\partial P/\partial R$ follow directly from the characteristic equation for the heat exchanger [12.6.1].

Finally, the change dR , in the heat capacity rate ratio R due to a reduction ΔW_t in tubeside flow rate, is given by:

$$dR = \frac{W_t C_t}{W_s C_s} - \frac{(W_t - dW_t) C_t}{W_s C_s}$$

or

$$dR = \frac{dW_t C_t}{W_s C_s} = R \frac{dW_t}{W_t}$$

This, along with Eq. (12.6.6) yields:

$$\frac{dW_t}{W_t} = \frac{dR}{R} = \frac{-d\eta}{\eta} \quad (12.6.9)$$

Substituting for $d\eta$ and dR in Eq. (12.6.8) we have:

$$\frac{dQ}{Q} = \frac{dW_t}{W_t} + \frac{1}{P} \left[-\frac{\partial P}{\partial \eta} \eta + \frac{\partial P}{\partial R} R \right] \frac{dW_t}{W_t}$$

or:

$$\frac{dQ}{Q} = f \frac{dW_t}{W_t} \quad (12.6.10)$$

where:

$$f = \frac{1}{P} \left[-\eta \frac{\partial P}{\partial \eta} + R \frac{\partial P}{\partial R} \right] + 1 \quad (12.6.11)$$

Thus, for a given heat exchanger geometry and operating data, the fractional reduction in Q due to flow bypass dW_t is readily determined.

12.7 COMPUTER PROGRAM LAPCOV

12.7.1 Program Description

Computer program LAPCOV is based on the lap joint-flat cover interaction analysis presented in Section 12.3. The program listing given in the following pages has the definition of all input and output data. The workings of the program and its input data are further explained with reference to the example problem below.

12.7.2 Example

The case of a 30" nominal diameter (O.D.) channel equipped with a lap joint flange bolted to a flat cover is examined.

The cover is 33.875" O.D. \times 1.75" thick. The flange ring is 30" I.D. \times 33.875" O.D. \times 2.5" thick. Twenty-eight 3/4" diameter \times 5" long effective length bolts are used to assemble the joint. The internal pressure is 150 psi. The gasket is 1/16" thick compressed asbestos; 31.25" O.D. \times 30" I.D. Its minimum seating stresses and gasket factor are cited to be 3700 psi and 2.75, respectively. The annulus of contact between the flange and lap

rings is 30.25" I.D. \times 31.25" O.D. We define effective gasket diameter, $2r_0$, as the mean diameter of the annulus, in the manner of the ASME Code [12.1.3, Appendix II]. Therefore, the total header load is given by:

$$H_p = \pi r_0^2 p = 111,396 \text{ lb.}$$

Using the formulas given in the ASME Code [12.1.3], the flange design bolt load [W In Ref. 12.1.3] is computed to be 176,311 lb.

The ASME Code divides the header load into two components; the load acting over a circle of radius $(b-w)$, and the remainder acting on the annulus of outer radius r_0 and inner radius $(b-w)$. Using the lever arms (denoted by h_D and h_G in the Code) for these loads given by the ASME Code, the effective offset of the header load circle h_p is given by:

$$h_p = \frac{(b-w)^2}{r_0^2} h_D + \frac{r_0^2 - (b-w)^2}{r_0^2} h_G = 1.05''$$

Strictly speaking, the foregoing definitions of lever arms do not have a rigorous basis. The definitions are maintained to be consistent with the ASME code in view of its widespread use and acceptance. The gasket unloading modulus K_G is estimated to be 17.63×10^6 lb/in.; and the bolt stiffness is computed using Eq. (3.10.4b).

Table 12.7.1 gives the input data listing for this problem. Two cases are studied:

- (i) Raised face design where no edge load at the contact circle is developed. This is accomplished by setting ϵ_0 equal to a large number (10" in the sample problem).
- (ii) Controlled contact design. It is assumed that the gap ϵ_0 at the contact circle is 0.0 under the seating condition.

The outputs for these two cases may be found following the program listing. Comparing the two outputs, it is observed that the controlled metal-to-metal contact has little effect on reducing the cover deflection, although it has a pronounced effect in reducing flange ring stress and rotation. The cover deflection in the output is given with respect to the location of the cover bolt circle ($r=r_b$) under the seating condition.

In case (i) (no metal-to-metal contact) the cover deflection at the center increases by $0.0477'' - 0.0086'' = 0.0391''$ as the joint is pressurized. Since the spring-back of most gaskets is less than 0.015", this joint can be predicted to develop a crevice between the cover and the pass partition rib. In such a case, the designer should provide a groove in the cover, (see Fig. 12.1.1) to seat the gasket so as to protect it from being washed out by the inter-pass leakage stream.

Table 12.7.1. Input Data for LAPCOV

Line 1: Problem identification (alphanumeric)

Line 2:* Cover dimensions

Variable	Symbol (Sec. 12.3)	Fortran Symbol	Value for the example problem
Cover thickness inboard of bolt circle	t_1	T11	1.75"
Cover thickness outboard of bolt circle	t_2	T12	1.75"
Effective gasket radius†	r_0	RO	15.375"
Bolt circle radius	r_b	RB	16.125"
Outer cover radius	b	B	16.938"
Location for contact circle	e_1	E1	0
Gasket circle offset	h_G	HG	0.75"
Header load circle offset†	h_p	HP	1.05"

Line 3: Flange data

Variable	Symbol (Sec. 12.3)	Fortran Symbol	Value for the example problem
Flange ring thickness	t_f	TF	2.5"
Flange ring width	w	W	1.938"
Initial gap at contact circle (under seating condition)†	ϵ_0	ESPO	10",0"

Line 4: Miscellaneous data:

Variable	Symbol (Sec. 12.3)	Fortran Symbol	Value for the example problem
Gasket unloading stiffness†	K_G	KG	17.63×10^6 lb/in.
Bolt stiffness†	K_b	KG	50.74×10^6
Young's modulus of cover material	E_1	YM1	30×10^6 psi
Young's modulus of flange material	E_f	YM2	30×10^6 psi
Total header load due to pressure	H_p	PL	111396 lb
Total gasket load under seating condition	H_G	GL	176311 lb

12.8 FLAT COVER BOLTED TO A WELDING NECK FLANGE

Computer program TRIEL described in Section 4.8 can be used to analyze such a joint. Since TRIEL is written for a three element joint consisting of two flanges and a tubesheet, it is necessary to prepare the input data in a certain manner to simulate a flange-cover joint. The following comments help explain the necessary provisions.

Notes: *Input format is freefield

†These input quantities are further explained in Subsection 12.7.2.

- (i) The flat cover can be simulated using the tubesheet input data by setting the Young's Modulus and Poisson ratio of the perforated interior equal to that of the rim.
- (ii) The bonnet flange input data simulates the joint flange.
- (iii) Fictitious dimensions can be input for the shell flange. Its Young's Modulus should be set an order of magnitude greater than the bonnet flange so as to make this flange much stiffer in rotation than the bonnet flange. The shellside gasket effective radius should be set equal to the bolt circle radius, and the shellside pressure should be set equal to zero. The shellside gasket stiffness should be set an order of magnitude greater than the joint gasket stiffness.
- (iv) The bonnet gasket data should correspond to the joint gasket data.
- (v) The bolt length is computed in TRIEL by summing the thicknesses of the two flanges, gaskets and the tubesheet. The bolt axial stiffness is inversely proportional to the bolt length and directly proportional to its Young's Modulus. The effect of the added bolt length, implied by the addition of the shell flange and shellside gasket, can be offset by increasing the bolt material Young's Modulus in the same proportion in which the bolt length is increased.

PROGRAM LAPCOV

```

C -----
C  COMPUTER PROGRAM LAPCOV,REV.0
C  BY K.P.SINGH AND LEE NG, NOV. 1982
C  COMPUTES THE RESPONSE OF A BOLTED COVER-LAP JOINT
C  FLANGE UNDER SEATING AND PRESSURIZED CONDITIONS
C  UTILIZING THE ANALYSIS PRESENTED IN SECTION 12.3
C -----
C  FORTRAN VARIABLES:
C  ***INPUT LIST : INPUT ALL DATA IN CONSISTENT UNITS***
C  TITLE   : TITLE FOR RUN; ANY ALPHANUMERIC-80 CHARACTERS LONG
C  T11    : THICKNESS OF THE COVER(R>RB)
C  T12    :      "      "      "      "      (R<RB)
C  RO     : EFFECTIVE GASKET RADIUS
C  RB     : BOLT CIRCLE RADIUS
C  B      : OUTER RADIUS OF COVER AND FLANGE
C  E1     : LOCATION OF THE METAL-TO-METAL CONTACT CIRCLE FROM
C           THE OUTER EDGE OF FLANGE AND COVER
C  HG     : RADIAL DISTANCE OF THE EFFECTIVE GASKET LOAD CIRCLE
C           ON THE LAP JOINT FLANGE RING FROM THE BOLT CIRCLE
C  HP     : RADIAL DISTANCE OF THE HEADER LOAD CIRCLE ON THE
C           FLANGE RING FROM THE BOLT CIRCLE
C  TF     : FLANGE RING THICKNESS
C  W      : RADIAL WIDTH OF FLANGE RING
C  EPSO   : INITIAL GAP BETWEEN THE FLANGE AND COVER AT
C           CONTROLLED METAL-TO-METAL CONTACT RADIUS

```

```

C          SET EPSO EQUAL LARGE(E.G. 10) FOR RAISED FACE DESIGNS
C   KG      : GASKET STIFFNESS
C   KB      : BOLT STIFFNESS
C   YM1     : YOUNG'S MODULUS OF COVER MATERIAL
C   YM2     : YOUNG'S MODULUS OF FLANGE MATERIAL
C   PL      : PRESSURE LOADING
C   GL      : GASKET LOADING.
C *****
C ***OTHER INPORTANT VARIABLES***
C   PR      : POISSON'S RATIO
C   PRSQ    : POISSON' RATIO SQUARED
C   FE      : CONTACT LOAD
C   RM      : MEAN FLANGE RING RADIUS
C   RAV     : AVERAGE OF RB AND B
C   E       : RADIAL DISTANCE BETWEEN BOLT CIRCLE AND OUTER EDGE
C            OF FLANGE
C   DELGL   : DROP IN GASKET LOAD.
C   BL      : BOLT LOAD
C   BSTRCH  : BOLT STRETCH
C   COVSTRS : MAX. COVER BENDING STRESS.
C   FLROT   : FLANGE ROTATION,DEG.
C   SMAX    : MAX. RING STRESS.
C   RAD     : RADIUS
C   DEFST   : COVER DEFLECTION WITH RESPECT TO COVER LOCATION
C            AT R=RB UNDER SEATING CONDITION
C   DEFP    : COVER DEFLECTION WITH RESPECT TO COVER LOCATION
C            AT R=RB UNDER PRESSURIZED CONDITION
C
C   ALFA'S,BETA'S,GAMA'S,RHO'S,OMEGA,KAPPA CORRESPOND
C   TO THE GREEK SYMBOLS USED FOR DEFINITIONS IN THE ANALYSIS.
C   A1,A2,A3,A4,A5,C1,C2,C3 CORRESPOND TO THE COEFFICIENTS
C   (SUBSCRIBED LOWER CASE ALPHABETS) USED IN THE ANALYSIS.
C
C   DEN     : COMMON DENOMINATOR FOR COMPUTING A1,A2,A3
C   DENN    :      "      "      "      "      A4,A5
C
C   ***RESULTS HAVE UNITS CONSISTENT WITH THOSE OF INPUT DATA***
C   *****
C   DIMENSION TITLE(20)
C   REAL KB,KG,KAPPA
C *****
C STATEMENT FUNCTIONS:
C   PHI(R)=ALFA1*(RB*RB-R*R)-(R*R+R0*R0)*ALOG(RB/RO)
C   +      +(R*R-R0*R0)-ALFA2*R0*R0*(RB*RB-R*R)/(RB*RB)
C   PSI(R)=(4.*RB*RB-5.*R0*R0+(R**4/(R0*R0))
C   +      -(8.*R*R+4.*R0*R0)*ALOG(RB/RO)
C   +      -4.*ALFA2*R0*R0*(RB*RB-R*R)/(RB*RB)
C   +      +8.*ALFA4*(RB*RB-R*R))/8.
C   OM(R) =6.*(1-PR)*(RB*RB-R*R)/YM1
C   SIGMAC(H1,H2,H3)=(C1+C3*BETA1)*H1+(C2+C3*BETA2)*H2+C3*BETA3*H3
C   THETAF(H1,H2,H3)=(RHO1P*H1+RHO2P*H2-RHO3P*H3)/(TF**3)
C   YC(R,H1,H2,H3)=((ALFA0*PHI(R)-BETA1*OM(R))*H1

```

```

+          + (ALFA0*PSI(R)-BETA2*OM(R))*H2
+          -BETA3*OM(R)*H3)/(T11**3)
C
C *****INPUT DATA*****
  READ(5,5) (TITLE(I),I=1,20)
  5  FORMAT(20A4)
  WRITE(6,6) (TITLE(I),I=1,20)
  6  FORMAT(6X,20A4)
C COVER DIMENSIONS
  READ(5,*) T11,T12,RO,RB,B,E1,HG,HP
C FLANGE DATA
  READ(5,*) TF,W,EPSO
C STIFFNESS DATA,YOUNG'S MODULI,LOADS
  READ(5,*) KG,KB,YM1,YM2,PL,GL
  WRITE(6,20) T11,T12,RO,RB,B,E1,HG,HP
  20  FORMAT(16X,"*****INPUT DATA*****"/
+6X,"THICKNESS OF THE COVER(R>RB) ..... =",F10.4/
+6X,"THICKNESS OF THE COVER(R<RB) ..... =",F10.4/
+6X,"EFFECTIVE GASKET RADIUS ..... =",F10.4/
+6X,"BOLT CIRCLE RADIUS ..... =",F10.4/
+6X,"OUTER RADIUS OF COVER AND FLANGE ..... =",F10.4/
+6X,"LOCATION OF THE METAL-TO-METAL CONTACT CIRCLE FROM"/
+6X,"THE OUTER EDGE OF FLANGE AND COVER ..... =",F10.4/
+6X,"RADIAL DISTANCE OF THE EFFECTIVE GASKET LOAD"/
+6X,"CIRCLE ON THE LAP JOINT FLANGE RING FROM"/
+6X,"THE BOLT CIRCLE ..... =",F10.4/
+6X,"RADIAL DISTANCE OF THE HEADER LOAD CIRCLE ON THE"/
+6X,"FLANGE RING FROM THE BOLT CIRCLE ..... =",F10.4)
  WRITE(6,21) TF,W,EPSO,KG,KB,YM1,YM2,PL,GL
  21  FORMAT(16X,"-----"/
+6X,"FLANGE RING THICKNESS ..... =",F10.4/
+6X,"RADIAL WIDTH OF FLANGE RING ..... =",F10.4/
+6X,"INITIAL GAP BETWEEN THE FLANGE AND COVER AT CONTROLLED"/
+6X,"METAL-TO-METAL CONTACT RADIUS ..... =",F10.4/
+16X,"-----"/
+6X,"GASKET STIFFNESS ..... =",E10.4/
+6X,"BOLT STIFFNESS ..... =",E10.4/
+6X,"YOUNG'S MODULUS OF COVER MATERIAL..... =",E10.4/
+6X,"YOUNG'S MODULUS OF FLANGE MATERIAL ..... =",E10.4/
+6X,"PRESSURE LOADING ..... =",F10.1/
+6X,"GASKET LOADING ..... =",F10.1/
+6X,"*****"/)
C *****
C COMPUTE CONSTANTS
  PI=3.14159
  PR=0.3
  PRSQ=0.09
  FE=0.0
  RM=B-0.5*W
  ALFA0=3.*(1.-PRSQ)/(2.*PI*YM1)
  ALFA1=(3.+PR)/(2.*(1.+PR))
  ALFA2=(1.-PR)/(2.*(1.+PR))

```



```

ALFA3=(12.+4.*PR)/(1.+PR)
ALFA4=1./(1.+PR)
ALFA5=12.*(1.-PR)*RB/YM1
GAMA1=(1.-2.*ALFA1)*RB+RO*RO*(1.+2.*ALFA2)/RB
GAMA2=0.5*((RB**3/RC**2)-(4.*RB*ALOG(RB/RO))
+ (2.*ALFA2*RO*RO/RB)-(4.*RB*ALFA4))
RAV=0.5*(B+RB)
E=B-RB
TPRM=T11/T12
GAMA3=12.*RAV*RB/(YM1*E)
GAMA4=6.*RAV*(B-RB-E1)/(YM1*(B-RB)*PI)
DENOM=GAMA3*TPRM**3+ALFA5
BETA1--(ALFAO*GAMA1)/DENOM
BETA2--(ALFAO*GAMA2)/DENOM
BETA3=GAMA4*TPRM**3/DENOM
RHO1P=6.*RM*HG/(PI*W*YM2)
RHO2P=6.*RM*HP/(PI*W*YM2)
RHO3P=6.*(B-E1-RB)*RM/(PI*W*YM2)
RHO1=RHO1P*(RB-RO)
RHO2=RHO2P*(RB-RO)
RHO3=RHO3P*(RB-RO)
OMX=(1./KB)+(RHO2/TF**3)+(ALFAO*PSI(RO)-OM(RO)*BETA2)/(T11**3)
OMY=(1./KB)+(1./KG)+(ALFAO*PHI(RO)-OM(RO)*BETA1)/(T11**3)
+ (RHO1/TF**3)
OMEGA=OMX/OMY
KAPPA=((1.-OMEGA)/KB)-((B-E1-RB)*(RHO2P-RHO1P*OMEGA)/(TF**3))
+ -(B-E1-RB)*(GAMA3*BETA2-OMEGA*(GAMA3*BETA1))/(T12**3)

```

C *****

C COMPUTE THE SEPARATION UNDER PRESSURE LOAD PL

```

WRITE(6,45)
45 FORMAT(16X,"*****RESULTS*****")
EPS=EPSO+KAPPA*PL
IF(EPS.GT.0.) GO TO 100
WRITE(6,50)
50 FORMAT(6X,"***METAL-TO-METAL CONTACT CONDITION***")
DEN=(1./KB)+(B-E1-RB)*((RHO3P/TF**3)-(GAMA3*BETA3-GAMA4)/(T12**3))
A1=-EPSO/DEN
A2--((1./KB)-((B-E1-RB)*RHO2P/TF**3)
+ -(B-E1-RB)*((GAMA3*BETA2)/T12**3))/DEN
A3--((-1./KB)+((B-E1-RB)*RHO1P/TF**3)
+ ((B-E1-RB)*(GAMA3*BETA1)/T12**3))/DEN
DENN=(1./KG)+(1./KB)+(RHO1/TF**3)
+ ((ALFAO*PHI(RO)-BETA1*OM(RO))/T11**3)
A4=((1./KB)+(RHO2/TF**3)
+ (ALFAO*PSI(RO)-BETA2*OM(RO))/T11**3)/DENN
A5=((1./KB)-(RHO3/TF**3)-BETA3*OM(RO)/T11**3)/DENN
FE=(A1/(1.-A3*A5))+((A2+A3*A4)/(1.-A3*A5))*PL
DELGL=A4*PL+A5*FE
WRITE(6,60) DELGL
GO TO 120

```

```

100 DELGL=OMEGA*PL
    WRITE(6,60) DELGL
60  FORMAT(6X,"DROP IN GASKET LOAD ..... =",F10.1)
120 CONTINUE
    BL=PL+FE+GL-DELGL
    BSTRCH=(BL-GL)/KB
    WRITE(6,70) FE,BL,BSTRCH
70  FORMAT(6X,"CONTACT LOAD ..... =",F10.1/
+6X,"BOLT LOAD(PRESSURIZED CONDITION) ..... =",F10.1/
+6X,"BOLT STRETCH ..... =",F10.4)

C *****
C COMPUTE COVER AND FLANGE RING STRESS
    C1=(1.5/(PI*T11**2))*((1-PR)*0.5+(1.+PR)*ALOG(RB/RO)
+    - (1.-PR)*RO*RO/(2.*RB*RB))
    C2=(1.5/(PI*T11**2))*(1.+(1.+PR)*ALOG(RB/RO)
+    - (1.-PR)*0.25*RO*RO/(RB*RB))
    C3=-6./(T11*T11)

C
    WRITE(6,75)
75  FORMAT(6X,"_____"/
+21X,"MAXIMUM",8X,"FLANGE",5X,"MAXIMUM COVER"/
+19X,"RING STRESS",5X,"ROTATION",4X,"BENDING STRESS")
C SEATING CONDITION
    COVSTRS=SIGMAC(GL,0.,0.)
    FLROT=THETAF(GL,0.,0.)*180./PI
    SMAX=YM2*TF*FLROT/(2.*RM)*PI/180.
    WRITE(6,80) SMAX,FLROT,COVSTRS
80  FORMAT(7X,"SEATING"/6X,"CONDITION",3X,F10.1,7X,F5.3,7X,F10.1)
C
C PRESSURIZED CONDITION
    GLP=GL-DELGL
    COVSTRS=SIGMAC(GLP,PL,FE)
    FLROT=THETAF(GLP,PL,FE)*180./PI
    SMAX=YM2*TF*FLROT/(2.*RM)*PI/180.
    WRITE(6,85) SMAX,FLROT,COVSTRS
85  FORMAT(6X,"PRESSURIZED"/6X,"CONDITION",3X,F10.1,7X,F5.3,7X,F10.1/
+6X,"_____"/)

C *****
C PRINT COVER DEFLECTION WITH RESPECT TO COVER LOCATION AT R=RB
C UNDER SEATING AND PRESSURIZED CONDITIONS
    WRITE(6,87)
87  FORMAT(30X,"DEFLECTION OF COVER"/30X,"-----"/
+10X,"RADIUS",10X,"SEATING",10X,"PRESSURIZED"/25X,
+"CONDITION",10X,"CONDITION")
    DO 200 I=1,11
    RAD=(I-1)*RB*0.1
    DEFST=YC(RAD,GL,0.,0.)
    DEFP =YC(RAD,GLP,PL,FE)+BSTRCH
    IF(DEFST.LT.0.0001) DEFST=0.0
    IF(DEFP.LT.0.0001) DEFP=0.0
    WRITE(6,90) RAD,DEFST,DEFP

```

```

90 FORMAT(8X,F8.3,10X,F5.4,15X,F5.4)
200 CONTINUE
WRITE(6,95)
95 FORMAT(6X," _____")
    
```

```

.....SAMPLE PROBLEM CASE #1: NO CONTACT LOAD.....
*****INPUT DATA*****
THICKNESS OF THE COVER(R>RB) ..... = 1.7500
THICKNESS OF THE COVER(R<RB) ..... = 1.7500
EFFECTIVE GASKET RADIUS ..... = 15.3750
BOLT CIRCLE RADIUS ..... = 16.1250
OUTER RADIUS OF COVER AND FLANGE ..... = 16.9375
LOCATION OF THE METAL-TO-METAL CONTACT CIRCLE FROM
THE OUTER EDGE OF FLANGE AND COVER ..... = .0000
RADIAL DISTANCE OF THE EFFECTIVE GASKET LOAD
CIRCLE ON THE LAP JOINT FLANGE RING FROM
THE BOLT CIRCLE ..... = .7500
RADIAL DISTANCE OF THE HEADER LOAD CIRCLE ON THE
FLANGE RING FROM THE BOLT CIRCLE ..... = 1.0500
-----
FLANGE RING THICKNESS ..... = 2.5000
RADIAL WIDTH OF FLANGE RING ..... = 1.9375
INITIAL GAP BETWEEN THE FLANGE AND COVER AT CONTROLLED
METAL-TO-METAL CONTACT RADIUS ..... = 10.0000
-----
GASKET STIFFNESS ..... = .1763E+08
BOLT STIFFNESS ..... = .5074E+08
YOUNG'S MODULUS OF COVER MATERIAL..... = .3000E+08
YOUNG'S MODULUS OF FLANGE MATERIAL ..... = .3000E+08
PRESSURE LOADING ..... = 111396.0
GASKET LOADING ..... = 176311.0
*****
    
```

```

*****RESULTS*****
DROP IN GASKET LOAD ..... = 81368.1
CONTACT LOAD ..... = .0
BOLT LOAD(PRESSURIZED CONDITION) ..... = 206338.9
BOLT STRETCH ..... = .0006
    
```

	MAXIMUM RING STRESS	FLANGE ROTATION	MAXIMUM COVER BENDING STRESS
SEATING CONDITION	10427.8	.254	2493.0
PRESSURIZED CONDITION	14839.1	.362	16707.1

DEFLECTION OF COVER

RADIUS	SEATING CONDITION	PRESSURIZED CONDITION
.000	.0086	.0477
1.612	.0085	.0472
3.225	.0083	.0454
4.837	.0079	.0426
6.450	.0073	.0388
8.063	.0065	.0339
9.675	.0055	.0283
11.288	.0044	.0219
12.900	.0031	.0151
14.512	.0016	.0079
16.125	.0000	.0006

.....SAMPLE PROBLEM CASE #2: EDGE LOAD, EPSO=0.....
 *****INPUT DATA*****

THICKNESS OF THE COVER(R>RB) = 1.7500
 THICKNESS OF THE COVER(R<RB) = 1.7500
 EFFECTIVE GASKET RADIUS = 15.3750
 BOLT CIRCLE RADIUS = 16.1250
 OUTER RADIUS OF COVER AND FLANGE = 16.9375
 LOCATION OF THE METAL-TO-METAL CONTACT CIRCLE FROM
 THE OUTER EDGE OF FLANGE AND COVER = .0000
 RADIAL DISTANCE OF THE EFFECTIVE GASKET LOAD
 CIRCLE ON THE LAP JOINT FLANGE RING FROM
 THE BOLT CIRCLE = .7500
 RADIAL DISTANCE OF THE HEADER LOAD CIRCLE ON THE
 FLANGE RING FROM THE BOLT CIRCLE = 1.0500

FLANGE RING THICKNESS = 2.5000
 RADIAL WIDTH OF FLANGE RING = 1.9375
 INITIAL GAP BETWEEN THE FLANGE AND COVER AT CONTROLLED
 METAL-TO-METAL CONTACT RADIUS = .0000

GASKET STIFFNESS = .1763E+08
 BOLT STIFFNESS = .5074E+08
 YOUNG'S MODULUS OF COVER MATERIAL..... = .3000E+08
 YOUNG'S MODULUS OF FLANGE MATERIAL = .3000E+08
 PRESSURE LOADING = 111396.0
 GASKET LOADING = 176311.0

*****RESULTS*****

METAL-TO-METAL CONTACT CONDITION

DROP IN GASKET LOAD	=	76931.4
CONTACT LOAD	=	79872.2
BOLT LOAD(PRESSURIZED CONDITION)	=	290647.8
BOLT STRETCH	=	.0023

	MAXIMUM RING STRESS	FLANGE ROTATION	MAXIMUM COVER BENDING STRESS
SEATING CONDITION	10427.8	.254	2493.0
PRESSURIZED CONDITION	9983.9	.244	15556.6

DEFLECTION OF COVER

RADIUS	SEATING CONDITION	PRESSURIZED CONDITION
.000	.0086	.0454
1.612	.0085	.0449
3.225	.0083	.0433
4.837	.0079	.0407
6.450	.0073	.0371
8.063	.0065	.0326
9.675	.0055	.0274
11.288	.0044	.0216
12.900	.0031	.0153
14.512	.0016	.0088
16.125	.0000	.0022

NOMENCLATURE

- $a_1, a_2 \dots a_5$ = Flange/cover interaction parameters (Eqs. (12.3.32), (12.3.34))
- A_L = Leakage gap area due to cover deflection (Section 12.5)
- A_b = Total root area of all the body bolts
- A = Total heat transfer surface area on heat exchanger tubes
- b = Outer radius of cover and flange
- C_s = Specific heat of shellside fluid
- C_t = Specific heat of tubeside fluid
- E_1 = Young's modulus of cover material
- E_f = Young's modulus of flange ring material
- e = Radial distance between the bolt circle and outer edge of flange ($e = b - r_b$)
- e_1 = Location of the metal-to-metal contact load from the

- outer edge of flange and cover (Fig. 12.3.3)
- F_e = Contact load under the pressurized condition
- H_1 = Generic term to indicate gasket surface ring load
- H_2 = Generic term to indicate pressure load on the cover over a circle of radius r_0
- H_3 = Generic term to indicate “metal-to-metal” contact load
- H_G = Seating condition gasket load
- H_p = Total header pressure load on the circle defined by radius r_0
- h_p = Radial distance of the header load circle from the flange ring bolt circle
- h_G = Radial distance of the effective gasket load circle on the lap joint flange ring from the bolt circle
- K_b = Bolt stiffness
- K_G = Gasket stiffness (Eq. (12.3.23))
- M = Discontinuity moment per unit circumference (Fig. 12.3.2)
- p = Pressure
- P = Temperature effectiveness (Section 12.6)
- Q = Heat duty (Section 12.6)
- ΔQ = Incremental change in heat duty due to inter-tube-pass leakage
- r_{av} = Mean radius of the cover outer annulus (Eq. (12.3.12))
- r = Radius
- R = Thermal flow rate ratio
- ΔR = Incremental change in R due to inter-pass leakage
- r_b = Bolt circle radius
- r_m = Mean flange ring radius
- r_0 = Effective gasket radius
- S_1, S_2 = Inlet and outlet temperatures of tubeside fluid, respectively
- t_1 = Thickness of the cover ($r < r_b$)
- t_2 = Thickness of the cover ($r > r_b$)
- t' = Ratio of t_1 to t_2 (Eq. (12.3.16))
- T_1, T_2 = Shellside fluid inlet and outlet temperature, respectively
- t_f = Flange ring thickness
- U = Overall heat transfer coefficient
- W_s = Shellside stream flow rate
- W_t = Tubeside flow rate
- w = Radial width of flange ring
- $y_c(r)$ = Total deflection of the cover at radius r with respect to $r = r_b$
- $y_f(r)$ = Total deflection of the flange ring at radius r with respect to $r = r_b$
- $\alpha_0, \alpha_1, \alpha_2$ = Functions of E_1 and ν (Eq. (12.3.3))
- $\beta_1, \beta_2, \beta_3$ = Rotation coefficients (Eq. (12.3.16))

- ΔW_l = Leakage rate from tube pass 1 to pass 2 due to bowing of channel cover
 δ_b = Bolt stretch as the joint loading is changed from the seating to the pressurized condition
 ΔH_G = Drop in gasket load as the joint is pressurized
 ϵ_0 = Total gap between the flange ring and the cover at the "contact circle" (radius $r = b - e_1$)
 η = NTU of the heat exchanger (number of transfer units)
 $\gamma_1, \gamma_2, \gamma_3, \gamma_4$ = Cover parameters (Eq. (12.3.10), Eq. (12.3.14))
 ν = Poisson's ratio of cover and flange materials
 $\rho_1', \rho_2', \rho_3'$ = Flange ring parameters (Eq. (12.3.19))
 ρ_1, ρ_2, ρ_3 = Flange ring parameters (Eq. (12.3.21))
 θ_c = Slope of the cover at the bolt circle radius ($r = r_b$)

REFERENCES

- [12.1.1] "Standards of Tubular Exchanger Manufacturers Association," Sixth edition, New York (1978).
 [12.1.2] "Standards for Power Plant Heat Exchangers," First edition, Heat Exchange Institute, Cleveland (1980).
 [12.1.3] "ASME Boiler and Pressure Vessel Code, Section VIII, Div. I," The American Society of Mechanical Engineers, UG-34, New York (1983).
 [12.2.1] Roark, R. J., "Formulas for Stress and Strain," Fourth edition, pp. 216-219, McGraw-Hill (1965).
 [12.2.2] "1982 Addenda to Standards of Tubular Exchanger Manufacturing Association," Sixth edition, TEMA (1982).
 [12.5.1] Singh, K. P., "A Method to Quantify Heat Duty Derating Due to Inter-Pass Leakage in Bolted Cover Heat Exchangers," *Heat Transfer Engineering*, Vol. 4, No. 3/4 (1983).
 [12.6.1] Singh, K. P., "Some Fundamental Relationships for Tubular Heat Exchanger Thermal Performance," Trans. of the ASME, *Journal of Heat Transfer*, Vol. 103, pp. 573-578 (August, 1981).

13. PRESSURE VESSEL HEADS

13.1 INTRODUCTION

Closures for heat exchangers and pressure vessels are either in the form of flat covers (Chapter 12) or formed heads. The latter is the subject of this chapter. TEMA [13.1.1] designations “B” and “M”, respectively, refer to formed head front and rear closures (Table 1.3.1). Figure 4.1.1 shows a TEMA “BEU” heat exchanger where the shell closure is in the shape of a formed head. In contrast to a flat cover which resists pressure only by bending, a formed head resists pressure primarily by developing membrane (in-plane) stresses. Therefore, the thickness of a formed head can be considerably less than that of a flat cover. From the heat transfer perspective, a welded head design is superior to the bolted flat cover variety because any concern of interpass leakage between tubeside passes, through the closure-pass partition interface, is eliminated in the former construction. On the other hand, welding pass partition plates to the inside contour of the head can be a laborious operation, specially in small size units. Where quantities so warrant, heads can be cast with integral pass partition plates, thus eliminating the need for onerous welding.

The pressure vessel designer has considerable latitude in selecting head geometry. The most common variety is the so-called “torispherical” head which is characterized by four geometric quantities: head inside diameter D_i ; crown radius L ; knuckle radius r ; and head thickness t_h . Figure 13.1.1 shows the details of the torispherical head geometry.

Figure 13.1.1 also introduces the terms “inside depth of dish IDD ”, and “straight flange” used in the pressure vessel trade. IDD is a geometric function of L and r , and straight flange, SF , denotes the cylindrical extension of the head integrally formed with it. By varying the ratios L/D_i and L/r , heads for different shapes can be produced. Heads wherein $L \approx D_i$ and $r \approx 0.06D_i$ are referred to as “ASME Flanged and Dished Heads” in the commercial pressure vessel industry. Other popular variations are the so-called 80 : 10 head where $L \approx 0.8D_i$, and $r \approx 0.1L$, and ellipsoidal head, generated by rotating a two-by-one ellipse (ratio of major to minor diameter equal to two) about the minor axis. As a rule of thumb, the deeper the head the smaller is the required thickness to resist a given pressure. The designer, therefore, selects head shape by minimizing the sum of the plate material cost and the cost of forming. Sometimes, other factors such as total volume capacity of the pressure vessel for a specified vessel length and diameter may also play a role. In general, computation of the head thickness for a particular set of design conditions is a well prescribed procedure. One finds

all necessary formulas in the usual design codes [13.1.2]. However, design codes are not meant to foster an understanding of the mechanics of the pressure vessel behavior; such illumination efforts are left to the many books on “shell theory”. Unfortunately, the books on “theory of shells” oftentimes dwell more on the pedagogical aspects of the problem; the needs of the pressure vessel designer are more utilitarian in nature. He seeks a grasp of the subject matter in such a form that, when faced with design conditions not covered in the code, he can devise reliable designs “in-the-spirit-of-the-code”. This chapter is aimed at providing the necessary insight to enable the designer to produce such solutions.

Strictly speaking, a pressure vessel head does not possess a constant thickness. The process of forming “thins out” areas of sharp curvature, and “thickens” adjacent regions of more moderate curvature. Such variations in head thickness can be specially pronounced when forming is performed in the “hot” condition. Cold forming produces only minor thickness variations. Our focus in this chapter lies in providing the reader with the necessary background and tools such that he can make a quantitative evaluation of the effects of thickness variation, nozzle penetrations, etc.. The material provided herein also helps the reader relate to the background of the ASME Code formulas.

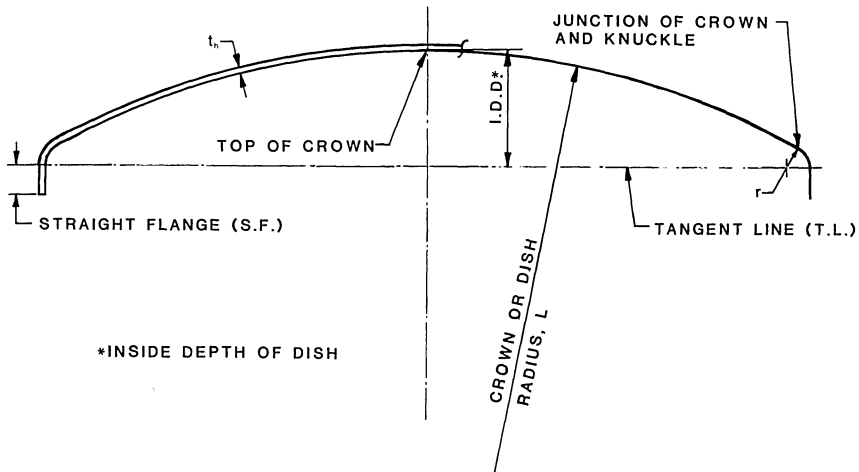


Fig. 13.1.1. Torispherical head.

13.2 GEOMETRY OF SHELLS OF REVOLUTION

The middle surface of a pressure vessel head is a surface of revolution. It is defined by rotating a plane curve about an axis lying in the plane of the curve. The generator curve is referred to as the “meridian”. Every point on the meridian sweeps a circle of radius equal to its distance from the axis of rotation. These circles are parallel to each other, and are simply referred to

as “parallels”. Figure 13.2.1 shows a typical meridian and a typical parallel. The surface of revolution thus formed has certain properties which facilitate stress analysis of membranes having that surface shape. We state those properties below without proof; readers interested in their

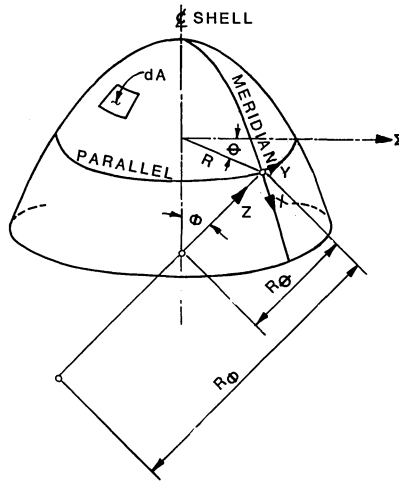


Fig. 13.2.1 Geometry of a surface of revolution.

mathematical proofs should refer to any text on differential geometry [13.2.1]. Some texts on shell theory also contain adequate treatment of the properties of shell surfaces [13.2.2-3].

- (i) Meridians and parallels form an orthogonal net of curves (Fig. 13.2.2). In other words, vectors tangent to the meridional curve and parallel circles at any point are perpendicular to each other.
- (ii) Meridians and parallels are also directions in which the curvatures of the surface reach maximum and minimum values. Therefore, the normal radii of curvature associated with the parallels and meridians are the principal radii of curvature. Consequently, a membrane shell loaded symmetrically (e.g., by internal pressure) will develop principal stresses along its meridians and parallels.
- (iii) The meridional radius of curvature at any point, R_ϕ , is defined by the radius of curvature of the meridian at that point. The normal to the surface coincides with the normal to the meridian. The expressions for R_ϕ follows from elementary calculus.

$$R_\phi = \left| \frac{(1 + y'^2)^{3/2}}{y''} \right| \tag{13.2.1}$$

where $y=y(x)$ defines the meridional curve, and prime denotes

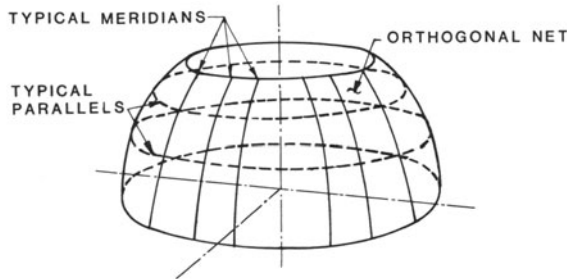


Fig. 13.2.2. Surface of revolution showing orthogonal net of meridians and parallels.

derivative with respect to x (Fig. 13.2.3). The radius of curvature corresponding to the “parallel” is given by

$$R_\theta = \frac{R}{\sin \phi} \quad (13.2.2)$$

where ϕ is the angle between the normal to the meridian and the axis of revolution (Fig. 13.2.1) and R is the distance of the point from the axis of revolution. Equation (13.2.2) indicates that R_θ at a point is given by the length of the normal to the meridian between that point and the axis of revolution. This result simplifies membrane stress analysis of pressure vessel heads considerably, and also permits a simple graphical interpretation of circumferential stresses (stresses directed along the parallel), as we will show later.

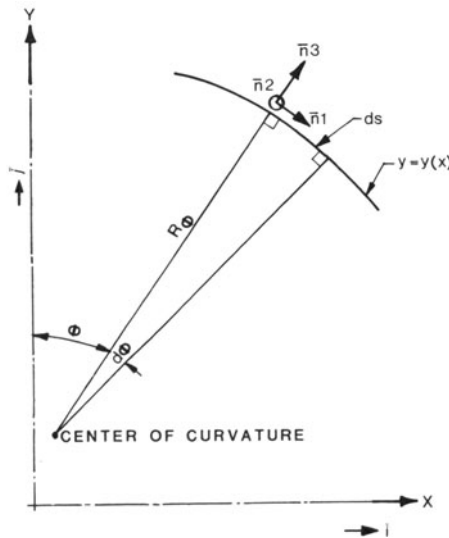
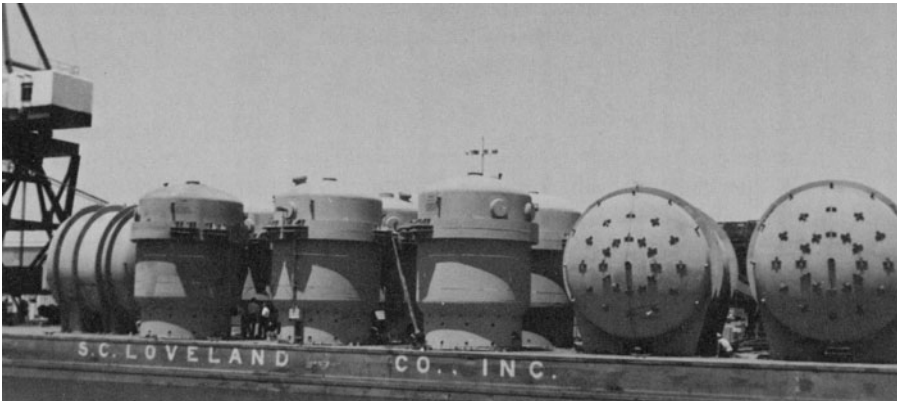


Fig. 13.2.3. Differential meridional element.

- (iv) At every point on the meridional curve (Fig. 13.2.3), we may construct the orthogonal triad of unit vectors \bar{n}_1 , \bar{n}_2 , \bar{n}_3 . \bar{n}_1 is the tangent unit vector to the meridian, \bar{n}_2 is the tangent unit vector to the parallel at the point, and \bar{n}_3 is the normal unit vector, perpendicular to both \bar{n}_1 and \bar{n}_2 . By convention, the parametric curves at each point are assumed to be arranged so that the direction of \bar{n}_3 is from the concave side to the convex side of the surface. It can be shown that under the above stated conditions

$$\frac{\partial \bar{n}_1}{\partial \phi} = -\bar{n}_3; \quad \frac{\partial \bar{n}_2}{\partial \theta} = -\bar{i} = -\cos\phi \bar{n}_1 - \sin\phi \bar{n}_3 \quad (13.2.4)$$



Pressure vessels loaded on a barge for shipment. (Courtesy Joseph Oat Corporation, Camden, NJ.)

13.3 MEMBRANE THEORY FOR SHELLS OF REVOLUTION

First proposed by Lamé and Clapeyron in the early nineteenth century, membrane theory assumes that a shell resists external loading through membrane action alone. That is, only a stress state uniform through the thickness develops in response to external loading. It is an excellent assumption for shells of revolution formed by meridians with gently varying curvature. Membrane theory for shells is analogous to the common assumption of pinned joints in truss structures. In reality, a truss is a highly indeterminate structure. But the assumption of “momentless truss joints” makes the solution procedure statically determinate while retaining the essential attributes of the “more rigorous” solution. Likewise, membrane theory of shells renders the stress analysis of shells statically determinate. Internal stress resultants are computed directly in terms of applied loadings. The computation of deformations is not necessary, and the stresses do not depend on the elastic properties of the shell material. We review the equilibrium equations for membrane shell theory below which will furnish

the necessary background to perform the analysis of common pressure vessel heads.

Equilibrium Equations

Figure 13.3.1 shows a differential element of a shell of revolution formed by the intersection of two parallels and two meridians. Angle θ locates the element in the circumferential direction in relation to an assumed reference meridional plane. ϕ is the angle between the axis of revolution and the normal to the differential element. It is assumed that the unit normal \bar{n}_3 always points from the concave to the convex side of the surface. R_ϕ and R_θ are the principal radii of curvature. If the loading on the shell is axisymmetric, then symmetry considerations require that the shear stresses on the principal planes of the surface (meridional and parallel) vanish. We let N_ϕ and N_θ denote membrane stress resultants in the meridional and circumferential directions, respectively; i.e.

$$\begin{aligned} N_\phi &= \sigma_\phi t \\ N_\theta &= \sigma_\theta t \end{aligned} \quad (13.3.1)$$

σ_θ and σ_ϕ are circumferential and meridional membrane stresses acting on the element, and t is the thickness of the shell. Symmetry dictates that N_θ be equal on both meridional edges of the element. Figure 13.3.2 shows the vector forces acting on the isolated element. The resultants \bar{T}_1 , \bar{T}_2 are defined in terms of their components along the \bar{n}_i directions as

$$\bar{T}_1 = N_\phi \bar{n}_1; \quad \bar{T}_2 = N_\theta \bar{n}_2 \quad (13.3.2)$$

while the area of the differential element is

$$dA = RR_\phi d\phi d\theta \quad (13.3.3)$$

Referring to Fig. 13.3.2, the vector force equilibrium equation for the element (vector sum of all forces must equal zero) gives

$$\begin{aligned} -\bar{T}_1 R d\theta + \bar{T}_1 R d\theta + \frac{\partial}{\partial \phi} (\bar{T}_1 R d\theta) d\phi \\ -\bar{T}_2 R_\phi d\phi + \bar{T}_2 R_\phi d_\phi + \frac{\partial}{\partial \theta} (\bar{T}_2 R_\phi d\phi) d\theta + (p_x \bar{n}_1 + p_z \bar{n}_3) dA = 0 \end{aligned}$$

which simplifies to the result

$$\frac{\partial}{\partial \phi} (\bar{T}_1 R) + \frac{\partial}{\partial \theta} (\bar{T}_2 R_\phi) + p_x R R_\phi \bar{n}_1 + p_z R R_\phi \bar{n}_3 = 0 \quad (13.3.4)$$

after using Eq. (13.3.3) and dividing through by $d\theta d\phi$.

We now use Eq. (13.3.2) to eliminate \bar{T}_1 and \bar{T}_2 and formally carry out the indicated differentiations to obtain

$$\frac{\partial}{\partial \phi} (N_\phi R) \bar{n}_1 + N_\phi R \frac{\partial \bar{n}_1}{\partial \phi} + N_\theta R_\phi \frac{\partial \bar{n}_2}{\partial \theta} + R R_\phi (p_x \bar{n}_1 + p_z \bar{n}_3) = 0 \quad (13.3.5)$$

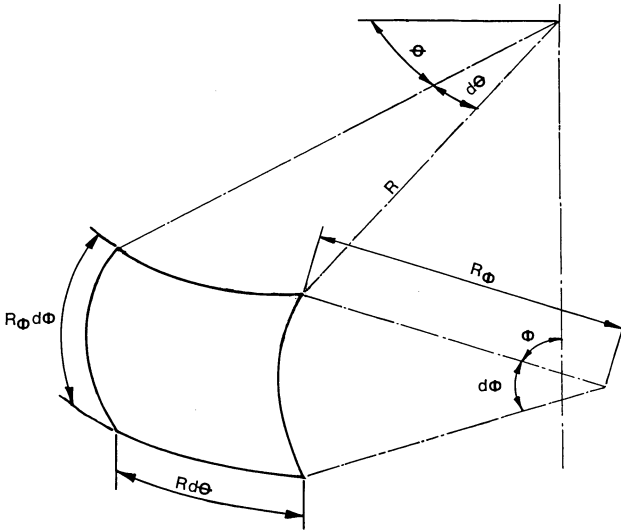


Fig. 13.3.1. Differential element.

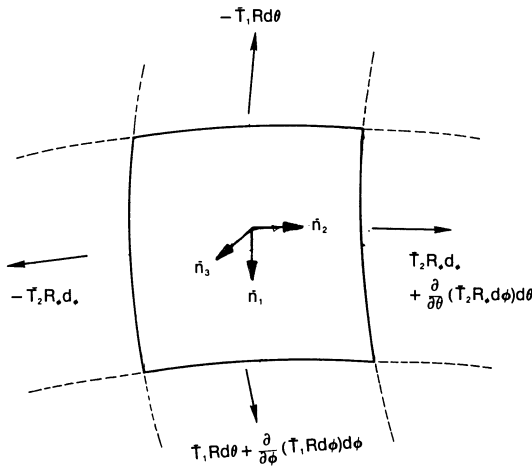


Fig. 13.3.2. Stress resultants for axisymmetric loading.

Note that in obtaining Eq. (13.3.5), we have used the fact that $N_\theta R_\phi$ is not a function of θ . Equations (13.2.4) can now be used to eliminate $\partial \bar{n}_1 / \partial \phi$, $\partial \bar{n}_2 / \partial \theta$; after grouping terms, Eq. (13.3.5) becomes

$$\left[\frac{\partial}{\partial \phi} (N_\phi R) - N_\theta R_\phi \cos \phi + p_x R R_\phi \right] \bar{n}_1 + [-N_\phi R - N_\theta R_\phi \sin \phi + p_z R R_\phi] \bar{n}_3 = 0 \tag{13.3.6}$$

The vector equilibrium equation (13.3.6) immediately yields the two relevant scalar force equilibrium equations

$$\frac{N_\phi}{R_\phi} + \frac{N_\theta \sin \phi}{R} = p_z \quad (13.3.7)$$

$$\frac{\partial}{\partial \phi} (N_\phi R) - N_\theta R_\phi \cos \phi + p_x R R_\phi = 0 \quad (13.3.8)$$

The above equations represent force equilibrium requirements in the local directions \bar{n}_3 , \bar{n}_1 , respectively. We note that for given $p_x(\phi)$, $p_z(\phi)$, the problem is statically determinate in that N_ϕ , N_θ can be completely determined from the equilibrium equations. We also note that the quantity $R/\sin \phi$ can be replaced by R_θ in Eq. (13.3.7) by virtue of Eq. (13.2.2). We now manipulate the above equations to evolve a formal solution for N_ϕ . Multiplying Eq. (13.3.8) through by $\sin \phi$, and using the identity

$$\frac{\partial}{\partial \phi} (N_\phi R_\theta \sin^2 \phi) = \sin \phi \frac{\partial}{\partial \phi} (N_\phi R_\theta \sin \phi) + N_\phi R_\theta \sin \phi \cos \phi$$

permits us to rewrite Eq. (13.3.8) in the form

$$\begin{aligned} \frac{\partial}{\partial \phi} (N_\phi R_\theta \sin^2 \phi) - N_\phi R_\theta \sin \phi \cos \phi \\ - N_\theta R_\phi \sin \phi \cos \phi + p_x R_\phi R_\theta \sin^2 \phi = 0 \end{aligned}$$

We now employ the relationship

$N_\theta R_\phi + N_\phi R_\theta = p_z R_\theta R_\phi$ from Eq. (13.3.7), to obtain

$$\frac{\partial}{\partial \phi} (N_\phi R_\theta \sin^2 \phi) - p_z R_\theta R_\phi \sin \phi \cos \phi + p_x R_\theta R_\phi \sin^2 \phi = 0$$

The above equation yields a formal solution for N_ϕ , in terms of the geometry and the applied loading, as

$$N_\phi = \frac{1}{R_\theta \sin^2 \phi} \int_\phi R_\theta R_\phi \sin \phi (p_z \cos \phi - p_x \sin \phi) d\phi + C_1 / R_\theta \sin^2 \phi \quad (13.3.9)$$

Equations (13.3.7), (13.3.9) give the desired solutions for N_θ , N_ϕ in terms of externally applied loading only. If the extent of the shell surface involves values of $\phi = 0, \pi, 2\pi$, then $C_1 = 0$. Otherwise, C_1 can be shown to be related to the total force applied to a reference parallel. A simple relationship involving the meridional internal force N_ϕ can be found by considering the freebody of the shell below a parallel (Fig. 13.3.3). If W

represents the resultant of all (axisymmetric) external loads (in the direction of the axis of revolution) acting on a *closed* shell of revolution which gives a single-connected curve contour upon projection on a parallel, then

$$\begin{aligned} W &= N_\phi 2\pi R \sin\phi \\ &= N_\phi 2\pi R_\theta \sin^2\phi \end{aligned}$$

or

$$N_\phi = \frac{W}{2\pi R_\theta \sin^2\phi} \quad (13.3.10)$$

A comparison of Eqs. (13.3.9), (13.3.10) yields a physical interpretation of the integral on the right side of Eq. (13.3.9) for the class of shells considered. If internal pressure p_z is the only external loading, then $W = \pi R^2 p_z = \pi R_\theta^2 \sin^2\phi p_z$.

Substituting for W above yields

$$N_\phi = \frac{\pi R_\theta^2 \sin^2\phi p_z}{2\pi R_\theta \sin^2\phi}$$

or

$$N_\phi = \frac{p_z R_\theta}{2} \quad (13.3.11)$$

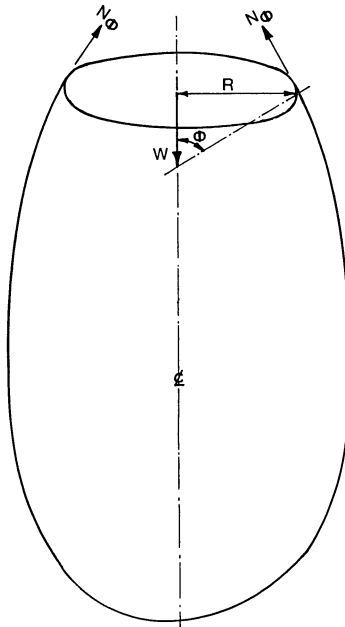


Fig. 13.3.3. Freebody of a shell of revolution cut by a parallel plane.

Since $W = \pi R^2 p_z$ is valid only for a closed shell of revolution which gives a single-connected curve contour upon projection on a parallel, Eq. (13.3.11) is not applicable to shells that have multiply-connected parallel cross sections, e.g., toroidal shells. Simply stated, Eq. (13.3.11) is valid only if R_θ remains finite. For shells which have multiply connected cross sections on a parallel plane, R_θ does not remain finite for all values of ϕ . We will discuss the implications of this further in Section 13.4.

For the class of shells where Eq. (13.3.11) does apply (Fig. 13.3.3), if we substitute for N_ϕ in Eq. (13.3.7) and rearrange terms, we obtain a solution for N_θ as

$$N_\theta = \frac{p_z R_\theta}{2} \left(2 - \frac{R_\theta}{R_\phi} \right) \quad (13.3.12)$$

We note that if $R_\theta/R_\phi > 2$, then N_θ becomes negative which indicates a compressive circumferential stress. This fact accounts for “wrinkling” of the circumference of thin ellipsoidal heads and torispherical heads under certain combinations of load and geometry.

Equation (13.3.12) can be shown to have an interesting pictorial interpretation which turns out to be quite valuable in practical design work. We will discuss this in Section 13.5.

13.4 STRESS ANALYSIS OF MEMBRANE SHELLS UNDER INTERNAL PRESSURE

Equations (13.3.11–12) can be utilized to determine the membrane stress field in common pressure vessel shapes subjected only to internal pressure. This analysis yields stresses which are quite accurate except near regions of discontinuity in curvature and near shell supports. Since such regions almost always exist in practical situations, a complete characterization of the shell stress field using membrane theory alone is not possible. Nevertheless, excellent approximations of the uniform through-thickness stress field in the regions of discontinuity are made by using membrane solutions. Before undertaking the stress solutions near discontinuities or supports in Section 13.8, we illustrate the application of membrane theory results to some typical pressure vessel shapes.

An inspection of Eqs. (13.3.11) and (13.3.12) indicates that the membrane stresses at a point are readily determined if the principal radii of curvature of the surface are known. In some simple cases, these radii are self-evident; in others they require some algebra. We consider here the cylindrical shell, the conical shell, the ellipsoidal shell, and finally, the toroidal shell.

(i) Cylindrical Shell

Let us consider a closed ended cylindrical shell of radius R under pressure p .

The meridian is a straight line, therefore, $R_\phi = \infty$. As stated in Section 13.2, R_θ is the distance of the material point on the surface from the axis of revolution along the normal to the surface. In this case $R_\theta = R$, the shell radius.

Equation (13.3.11) yields ($p_z = p$)

$$N_\phi = \frac{pR}{2}$$

Using Eq. (13.3.1) to obtain the meridional stress, yields

$$\sigma_\phi = \frac{pR}{2t} \quad (13.4.1)$$

while Eq. (13.3.12) yields:

$$N_\theta = pR$$

or

$$\sigma_\theta = \frac{pR}{t} \quad (13.4.2)$$

These are the well known Lamé's equations for thin cylinders under internal pressure p .

(ii) Conical Shell

The case of a conical shell with semi-vertex angle α , under internal pressure, can be treated in a similar manner. Since the generatrix is again a straight line, $R_\phi = \infty$. Referring to Fig. 13.4.1, in terms of the semi-vertex angle

$$R_\theta = R/\cos\alpha, \text{ and } p_z = p$$

From Eqs. (13.3.11)–(12), stresses at point 0 in Fig. 13.4.1 are:

$$N_\phi = \frac{pR}{2\cos\alpha} \rightarrow \sigma_\phi = \frac{pR}{2t\cos\alpha} \quad (13.4.3)$$

$$N_\theta = \frac{pR}{\cos\alpha} \rightarrow \sigma_\theta = \frac{pR}{t\cos\alpha} \quad (13.4.4)$$

(iii) Ellipsoidal Shell

The meridian of an ellipsoidal head is defined by the equation (Fig. 13.4.2):

$$\frac{x^2}{a^2} + \frac{y^2}{b^2} = 1$$

or

$$y = b \left(1 - \frac{x^2}{a^2} \right)^{1/2} \quad (13.4.5)$$

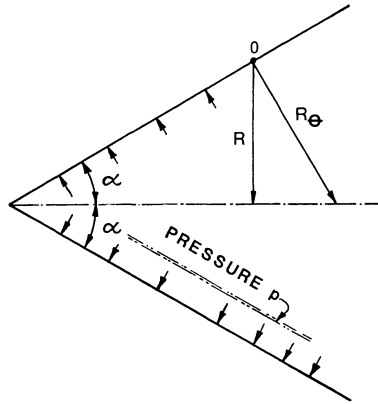


Fig. 13.4.1. Conical shell under internal pressure.

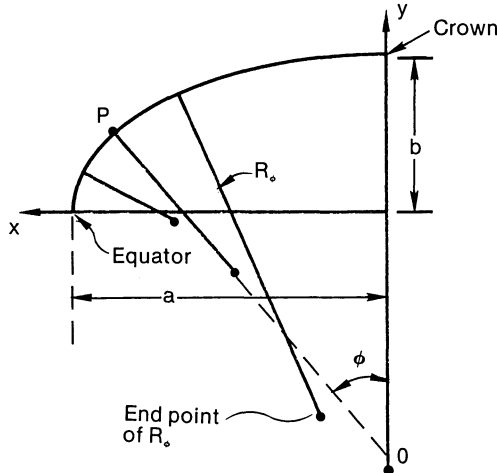


Fig. 13.4.2. Meridional radius of 2:1 ellipsoidal head at typical locations (to scale).

The meridional radius of curvature R_ϕ has been defined by Eq. (13.2.1) as

$$R_\phi = \left| \frac{(1 + y'^2)^{3/2}}{y''} \right| \tag{13.2.1}$$

where prime indicates derivative with respect to x . Differentiating Eq. (13.4.5) we have

$$\frac{dy}{dx} = -\frac{bx}{a^2} \left(1 - \frac{x^2}{a^2}\right)^{-1/2} = \frac{-b^2x}{a^2y} \tag{13.4.6}$$

$$\frac{d^2y}{dx^2} = \frac{-b^2}{a^2y} + \frac{b^2x}{a^2y^2} \frac{dy}{dx}$$

Substituting for dy/dx , using the fact that $x^2 = a^2(1 - y^2/b^2)$, and rearranging terms, yields

$$\frac{d^2y}{dx^2} = \frac{-b^4}{a^2y^3} \quad (13.4.7)$$

Using y' and y'' from Eqs. (13.4.6), (13.4.7), in Eq. (13.2.1) and simplifying, yields

$$R_\phi = \frac{(a^4y^2 + b^4x^2)^{3/2}}{a^4b^4} \quad (13.4.8)$$

Figure 13.4.2 shows the meridional radius R_ϕ drawn to scale for a few points. We note that R_ϕ is the largest at the crown and gets smaller as the equator is approached.

The circumferential radius of curvature at the point P is given by the length of the line OP in Fig. 13.4.2; that is,

$$\begin{aligned} R_\theta &= x/\sin\phi = x \sec\phi/\tan\phi \\ &= x(1 + \tan^2\phi)^{1/2}/\tan\phi \end{aligned}$$

$$\text{Since } \tan\phi = -\frac{dy}{dx} = b^2x/a^2y;$$

$$R_\theta = \frac{(a^4y^2 + b^4x^2)^{1/2}}{b^2} \quad (13.4.9)$$

Therefore, comparing Eqs. (13.4.8), (13.4.9), yields

$$R_\phi = \frac{b^2R_\theta^3}{a^4} \quad (13.4.10)$$

The principal membrane stresses readily follow from Eqs. (13.3.11-12) and (13.3.1).

$$\sigma_\phi = \frac{pR_\theta}{2t} = \frac{p(a^4y^2 + b^4x^2)^{1/2}}{2b^2t} \quad (13.4.11)$$

$$\sigma_\theta = \frac{pR_\theta}{2t} \left[2 - \frac{R_\theta}{R_\phi} \right]$$

Since

$$\frac{R_\theta}{R_\phi} = \frac{a^4}{b^2R_\theta^2} \text{ (from Eq. 13.4.10),}$$

$$\sigma_\theta = \frac{pR_\theta}{2t} \left(2 - \frac{a^4}{b^2R_\theta^2} \right)$$

Substituting for R_θ from Eq. (13.4.9) gives

$$\sigma_\theta = \frac{pR_\theta}{2t} \left[2 - \frac{a^4 b^2}{(a^4 y^2 + b^4 x^2)} \right]$$

or

$$\sigma_\theta = \frac{pR_\theta}{2t} \left[\frac{2(a^4 y^2 + b^4 x^2) - a^4 b^2}{(a^4 y^2 + b^4 x^2)} \right] \quad (13.4.12)$$

At the equator, $x = a, y = 0$, which gives

$$R_\theta = a, \quad R_\phi = b^2/a \quad (13.4.13)$$

Therefore, at the equator:

$$\sigma_\theta = \frac{pa}{2t} [2 - a^2/b^2]$$

$$\sigma_\phi = \frac{pa}{2t}$$

Note that σ_θ becomes compressive if

$$2 - a^2/b^2 < 0$$

or $a/b > \sqrt{2}$

Therefore, the hoop stress at the equator of an ellipsoidal head of a/b ratio 1.414 equals zero. Similarly, at the top of the crown,

$$x=0, \quad y=b, \quad R_\theta = R_\phi = a^2/b$$

Hence

$$\sigma_\phi = \frac{pa^2}{2bt} = \sigma_\theta$$

Figure 13.4.3 shows plots of σ_θ and σ_ϕ , normalized by pa/t , as a function of x/a for two values of aspect ratio a/b . Note for 2:1 ellipsoidal heads, σ_θ at the equator and at the top of the crown have equal and opposite values; $+pa/t$ at the top, and $-pa/t$ at the equator. The meridional stress is always tensile and reaches the maximum value at the top of the crown. Figure 13.4.3 indicates that the maximum stress intensity* will very likely occur at the equator in ellipsoidal heads if σ_θ becomes negative there ($a/b > 1.414$). The negative σ_θ is seen to increase rapidly with increased a/b ratio. For this reason, ellipsoidal heads are seldom made with a/b ratio in excess of 2.

(iv) Toroidal Shell Under Internal Pressure

A toroidal shell is produced by rotating a meridian in the shape of a circle about a coplanar axis as shown in Fig. 13.4.4. The radius of the generator

*Refer to Section 2.6 (Chapter 2) for definition.

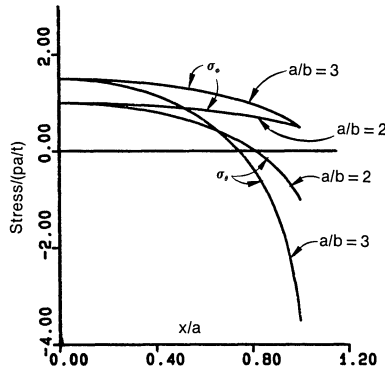


Fig. 13.4.3. Membrane stresses in ellipsoidal heads.

circle r_0 , and the distance of its center from the axis of rotation, R_0 , characterize the shape of the torus. The toroidal or doughnut shaped shell has its most famous application in the Tokamak fusion reactor vessel. The toroidal shell also has wide industrial application; U-bends of heat exchangers are the most familiar example in the tubular exchanger industry. The radii of principal curvature of the toroidal shell are quite straightforward to ascertain. The meridional radius of curvature R_ϕ is obviously r_0 at all points on the surface of the shell. The circumferential radius of curvature R_θ at a point A is given by Fig. 13.4.4, as ($0 < \phi < 2\pi$)

$$R_\theta = r_0 + R_0/\sin\phi \tag{13.4.14}$$

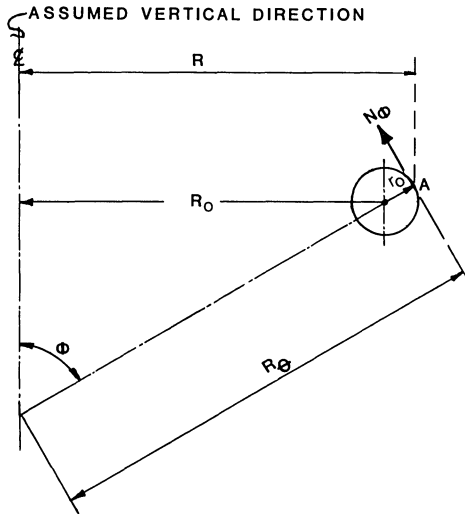


Fig. 13.4.4. Meridian for generating a toroidal shell.

The internal force that resists this load is N_ϕ acting on the edge AA'; its component in the vertical direction is given by

$$Rd\theta N_\phi \sin\phi$$

where, from Fig. 13.4.4,

$$R = R_0 + r_0 \sin\phi$$

Equating internal and external forces yields

$$\frac{p}{2} (2R_0 + r_0 \sin\phi) r_0 \sin\phi d\theta = N_\phi (R_0 + r_0 \sin\phi) \sin\phi d\theta$$

or

$$N_\phi = \frac{pr_0}{2} \frac{(2R_0 + r_0 \sin\phi)}{(R_0 + r_0 \sin\phi)} \quad (13.4.16)$$

We note that Eq. (13.4.16) can also be derived directly from Eq. (13.3.9) using the appropriate expressions for R_θ , R_ϕ and performing the integrations. To determine N_θ , we observe that Eq. (13.3.7) is still applicable since it was derived without any restrictions pertinent to the multiply-connected nature of the meridian curve.

From Eq. (13.3.7), solving for N_θ yields

$$\frac{N_\theta}{R_\theta} = p - \frac{N_\phi}{R_\phi}$$

or

$$\frac{N_\theta}{R_\theta} = p - \frac{pr_0}{2r_0} \frac{(2R_0 + r_0 \sin\phi)}{(R_0 + r_0 \sin\phi)} = \frac{pr_0 \sin\phi}{2(R_0 + r_0 \sin\phi)}$$

Therefore, we finally obtain

$$N_\theta = \frac{pr_0}{2} \quad (13.4.17)$$

where the expression for R_θ from Eq. (13.4.14) has been utilized.

N_θ is found to be constant over the entire surface of the toroid. The corresponding stress σ_θ (from Eq. (13.3.1)) is often referred to as the "longitudinal stress" following the notation for straight cylindrical shells. Similarly, the meridional stress σ_ϕ corresponding to N_ϕ is known as the "hoop stress". σ_ϕ is a function of ϕ ; its value at any point can be found by using Eq. (13.4.16) in Eq. (13.3.1).

For example, the value of σ_ϕ at the two ends of the equator are given by $\phi = \pi/2, 3\pi/2$. At the inside edge (crotch end):

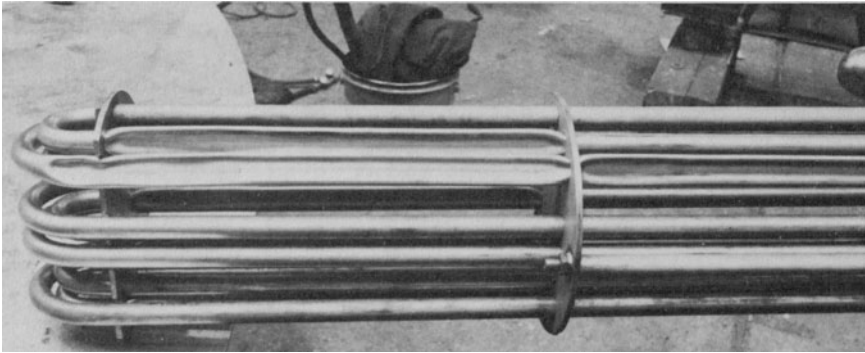
$$\phi = 3\pi/2; \quad \sigma_\phi = \frac{pr_0}{2t} \frac{2R_0 - r_0}{R_0 - r_0} \quad (13.4.18)$$

At the outside edge of the equator

$$\phi = \pi/2; \quad \sigma_\phi = \frac{pr_0}{2t} \frac{2R_0 + r_0}{R_0 + r_0} \quad (13.4.19)$$

Similarly, at the top of the shell edge BB' in Fig. 13.4.5; $\phi=0$, $\sigma_\phi = pr_0/t$.

We see that in a toroidal membrane shell under internal pressure, both principal stresses are tensile and the maximum principal stress occurs at the crotch. Fortunately, the process of forming toroidal shells (e.g., U-tubes) tends to thin out the outer edge and thicken the crotch region. Harvey [13.4.1] reports that in destructive internal pressure tests the U-bend sections of the U-tube never failed. Photograph 13.a shows a portion of a buckled U-tube subjected to external pressure. We note that the straight tube segment next to the toroidal shape failed first. These experiments attest to the superb pressure bearing capability of the toroidal shape.



Photograph 13.a. Failed U-tube under external pressure.

13.5 PHYSICAL INTERPRETATION OF N_θ

We restrict consideration to shells having singly connected surfaces. Let us consider the area A of the region formed by the normal lines to the end of a meridional segment $d\phi$. Figure 13.5.1 shows the case wherein $R_\phi > R_\theta$.

The length of the intercept on the axis, q , is given by the expression

$$q = (R_\phi - R_\theta) d\phi$$

Therefore,

$$A = \frac{1}{2} (q + R_\theta d\phi) R_\theta$$

or

$$A = \frac{R_\theta R_\phi d\phi}{2} \left(2 - \frac{R_\theta}{R_\phi} \right) \quad (13.5.1)$$

From Eq. (13.3.12) we have

$$\frac{R_\theta}{2} \left(2 - \frac{R_\theta}{R_\phi} \right) = \frac{N_\theta}{p_z}$$

Therefore

$$A = (R_\phi d\phi) \frac{N_\theta}{p_z} \quad (13.5.2)$$

or

$$N_\theta = \frac{p_z A}{ds} \quad (13.5.3)$$

where $ds = R_\phi d\phi$ is the length of meridional arc.

Equation (13.5.3) states that the circumferential stress resultant is given by the *product of pressure and the area of the cross hatched region of Fig. 13.5.1 divided by the meridional arc length*. We note that this result is valid only for shells of revolution whose projection on a plane of parallels is a simply connected curve.

Next, let us consider the case where $R_\phi < R_\theta$; i.e., when the intersection of the normal vectors from the ends of the meridional arc occurs between the arc and the axis of revolution (Fig. 13.5.2). The area of the region to the right of the intersection point O is

$$A_p = R_\phi^2 \frac{d\phi}{2}$$

Similarly, the area to the left of point O (hatched in Fig. 13.5.2) is

$$A_n = \frac{(R_\theta - R_\phi)^2 d\phi}{2}$$

Hence

$$A_p - A_n = A = \frac{R_\theta R_\phi d\phi}{2} \left(2 - \frac{R_\theta}{R_\phi} \right)$$

which once again leads to Eq. (13.5.3).

Therefore

$$N_\theta = \frac{p_z A}{ds}$$

where A is the area defined by the segment of the meridional arc, the axis of revolution and the normal rays to the tangents from the extremities of the arc. If the two rays cross before reaching the axis of revolution then the triangular area between the diverging rays and the axis of revolution is to be considered negative. The portion between the intersection and the arc is positive. These areas will be referred to as “pressure areas”.

This theorem can be used to *approximately* evaluate local hoop stresses in

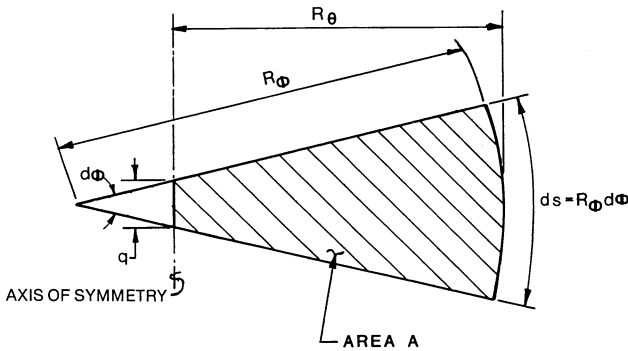


Fig. 13.5.1. Area A shown by hatched region.

 NEGATIVE AREA

 POSITIVE AREA

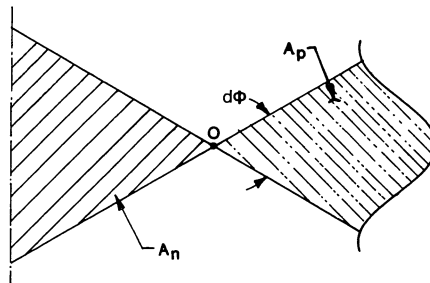


Fig. 13.5.2. Positive area A_p , negative area A_n together define the net pressure area.

shells in regions of sharp geometric discontinuity. Indeed, this concept forms the basis of the “area replacement method for reinforcements” of the ASME Boiler and Pressure Vessel Codes. Zick, et al. [13.5.1] show various applications of this concept. We will refer to this method as the “unsupported area principle” after Zick, et al. [13.5.1]. A few illustrative cases are considered below.

Figure 13.5.3 shows a typical pressure vessel consisting of a cylindrical shell, a top head of spherical profile, and a conical bottom head. Both top and bottom heads have symmetrically located cylindrical nozzles. The two variations of this pressure vessel shown differ only with respect to the junctions between the different parts. In version (b), knuckles provide smooth transitions in the regions of change of surface curvature. Version (a), on the other hand, has sharp discontinuities. Pressure areas for the main geometric shapes are shown in the diagram for version (a). The

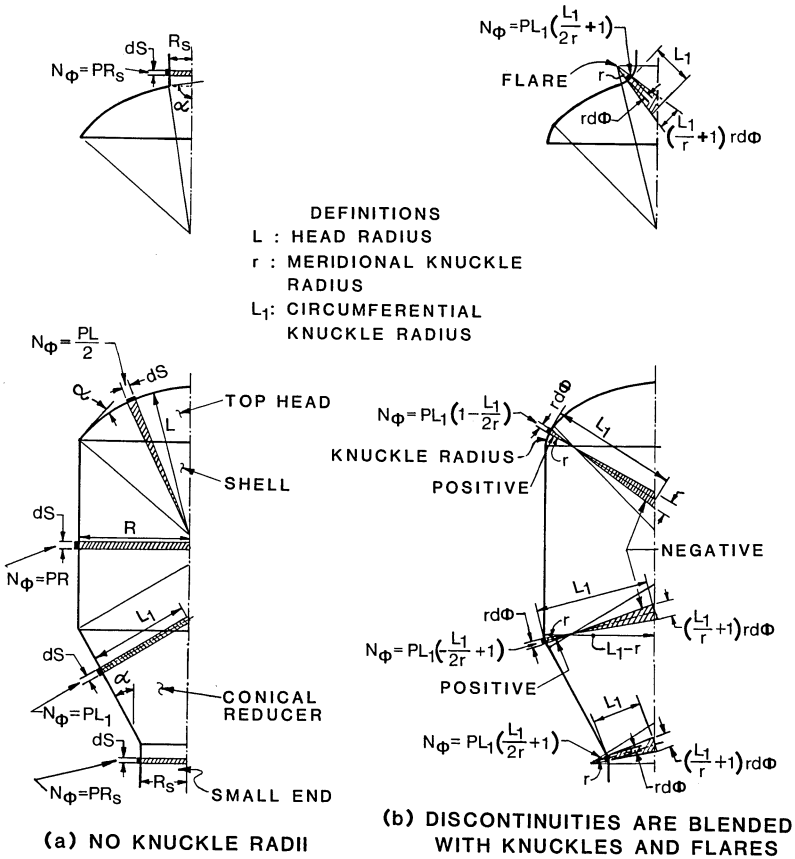


Fig. 13.5.3. Illustration of unsupported area principle.

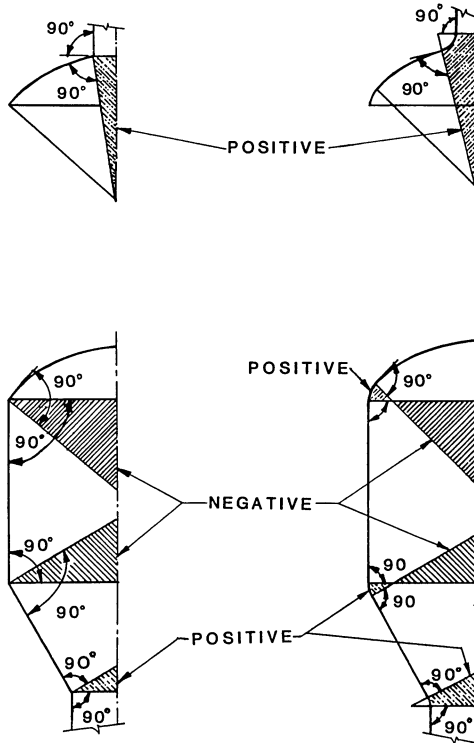
pressure areas for the knuckle and flare regions of version (b) are also shown. These pressure areas clearly show that the circumferential membrane stresses in the “flares” are also tensile, whereas those in the knuckle zone can be compressive (negative total pressure area). Note that the portion of a toroidal shell considered here satisfies Eq. (13.3.10) so all of our area formulas hold.

Figure 13.5.4 shows the pressure areas at the discontinuities for two versions. The following observations can be made:

- (i) Sharp discontinuities produce finite pressure areas (negative at head to shell, and shell to cone large ends; positive at shell to cone small ends). These finite areas correspond to infinitesimally small shell arc length. Therefore, N_ϕ can reach high (in the limit, infinite) values.
- (ii) Transitions have the effect of adding positive pressure areas. Where the transitions are knuckles the reduction in the total pressure area is

obvious. Flares augment the total positive pressure area. However, the circumferential stress resultant N_θ is still reduced because of increased arc length ds when a flare is present.

It is clear from the foregoing that the computed value of N_ϕ in the region of discontinuity will depend on the size of the arc ds used in constructing pressure areas. Zick, et al. [13.5.1] suggest using the arc of the shell $k\sqrt{Lt_h}$ on both sides of the point of discontinuity; L is the larger of the circumferential radii of curvature of the adjoining shapes,* t_h is the local thickness of the pressure part, and k is a constant which depends on the type of discontinuity. The use of this technique is illustrated in the next section by considering the junction of a conical head and a cylinder.



(a) SHARP DISCONTINUITY (b) SMOOTH TRANSITION

Fig. 13.5.4. Pressure areas at discontinuity.

*Recall circumferential radius of curvature at a point is equal to the distance of the point from the axis of rotation along the normal to the meridian.

13.6 DERIVATION OF ASME CODE FORMULA FOR THE LARGE END OF A REDUCER

Figure 13.6.1 shows the junction of a conical shell of semi-angle α with a cylindrical shell of radius R_L . The ASME Boiler and Pressure Vessel Code, Section VIII, Division 1, Appendix I [13.1.2], gives the following formula for the required metal reinforcement area A_r at the junction.

$$A_r = \frac{pR_L^2}{2SE'} \left(1 - \frac{\Delta}{\alpha}\right) \tan \alpha \tag{13.6.1}$$

where Δ , given in tabular form, can be approximated as

$$\Delta \approx 320(p/SE')^{1/2} \tag{13.6.2}$$

In the above equation p is internal pressure, SE' denotes allowable stress corrected for weld joint efficiency E' , and α is in degrees. We will now derive an expression for A_r analogous to Eq. (13.6.1) using the unsupported area principle described in the preceding section.

The required thickness of the shell, t_s , which will develop a hoop stress equal to SE' is given by Lamé's formula.

$$t_s = \frac{pR_L}{SE'} \tag{13.6.3}$$

Similarly, the thickness of the conical portion, t_c , is given by Eq. (13.4.4),

$$t_c = \frac{pR_L}{SE' \cos \alpha} = t_s / \cos \alpha \tag{13.6.4}$$

Substituting for p/SE' from Eq. (13.6.3) into Eqs. (13.6.1-2), and substituting for Δ using Eq. (13.6.2) yields

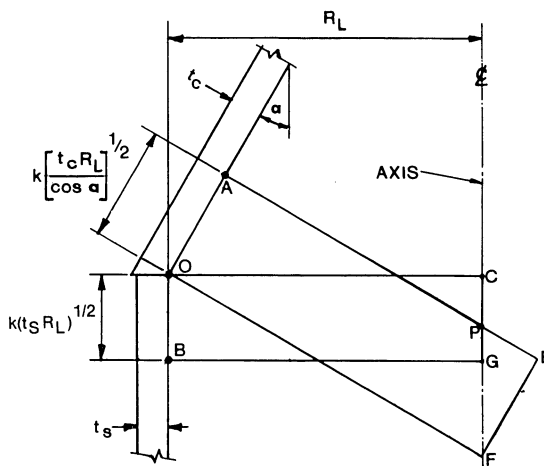


Fig. 13.6.1. Unsupported areas for cone to shell junction.

$$A_r = \frac{t_s R_L}{2} \left[\tan \alpha - \frac{320 \tan \alpha}{\alpha} (t_s / R_L)^{1/2} \right] \quad (13.6.5)$$

The average hoop stress is computed over a total arc length which extends $k(R_\theta t)^{1/2}$ in both directions from the discontinuity. Note in this case, $R_\theta = R_L / \cos \alpha$, $t = t_c = t_s / \cos \alpha$ in the cone, and $R_\theta = R_L$, $t = t_s$ in the shell. k is a constant which depends on the nature of the discontinuity. For the present case, good agreement with the code rules is obtained for $k = 0.7$.

The total pressure area from Fig. 13.6.1 is given by the sum of the areas defined by the vertex points labeled in the figure.

$$A = \text{OAEF} - \text{PEF} + \text{OCGB} - \text{OCF} \quad (13.6.6)$$

Substituting for the different areas, we have

$$A = \frac{k R_L (t_s R_L)^{1/2}}{\cos^2 \alpha} - \frac{k^2 t_s R_L \tan \alpha}{2 \cos^2 \alpha} + k R_L (t_s R_L)^{1/2} - \frac{R_L^2 \tan \alpha}{2} \quad (13.6.7)$$

The required metal area to be added, A_m , should be such that the compressive hoop stress equals SE' ; i.e.

$$SE' \left[A_m + k t_s (t_s R_L)^{1/2} + \frac{k t_s}{\cos^2 \alpha} (t_s R_L)^{1/2} \right] = -pA \quad (13.6.8)$$

Substituting for A from Eq. (13.6.7), using the relation $p/SE' = t_s/R_L$ (from Eq. (13.6.3)), simplifying, and solving for A_m , yields

$$A_m = \frac{t_s R_L}{2} [\tan \alpha - C (t_s / R_L)^{1/2}] \quad (13.6.9)$$

where

$$C = 4k \left[1 + \frac{1 - \tan \alpha \frac{k}{4} (t_s / R_L)^{1/2}}{\cos^2 \alpha} \right] \quad (13.6.10)$$

The expression for A_m derived above using the unsupported area principle has an uncanny similarity to its counterpart A_r (Eq. (13.6.5)) given by the Code. Table 13.6.1 shows a comparison between the value of C (Eq. (13.6.10)) and the equivalent term in the Code formula.

Table 13.6.1. Comparison of the Values of C Between ASME Code and Unsupported Area Principle

Semi-Cone Angle, Degrees	ASME Code	Unsupported Area Method	
		$t_s / R_L = 0.1$	$t_s / R_L = 0.01$
10	5.65	5.66	5.68
20	5.82	5.94	5.95
30	6.12	6.41	6.50

13.7 MEMBRANE DISPLACEMENT

Membrane theory for shells of revolution yields a statically determinate problem which enables us to calculate the internal stresses in terms of the externally applied loadings from equilibrium considerations alone. Therefore, computation of the shell displacements is completely bypassed. However, as stated before, membrane theory cannot reliably predict the stress field in the region of sharp changes in shell curvature or stiffness (thickness). Unfortunately, such rapid changes in curvature and stiffness, known as “gross structural discontinuities” (Chapter 2), are quite commonplace in pressure vessels. The junction between the knuckle and the crown and the junction between the knuckle and the shell skirt in a torispherical head are classical examples of such discontinuities. Indeed, geometric discontinuities are the rule rather than the exception in pressure vessel construction. The effect of a sharp discontinuity can be explained as follows:

The presence of a geometric discontinuity implies a sharp change in the meridional radii of curvature across the discontinuity. Equations for the membrane stresses derived in Section 13.3 indicate that the membrane stresses are directly dependent on the radii of curvature. Therefore, the membrane stresses in the two abutting portions of the shell will be unequal. Unequal membrane stresses must imply unequal deformations because of the stress-strain relations. Therefore, additional reactions at the junction must be developed to keep the two portions of the shell together. These reactions are known as “discontinuity stress resultants”; they modify the stress field in both shells in the immediate vicinity of the junction. The effect of these discontinuity resultants dies out rapidly as we move away from the discontinuity along either side of the junction. This, essentially localized, effect of discontinuity reactions is often termed the “boundary layer” effect in an obvious analogy with fluid flows. A rough estimate of the discontinuity effects can be made using the unsupported area method as described in the preceding section. A more precise evaluation requires calculation of membrane displacements and enforcement of displacement compatibility. In this section, necessary relationships to evaluate the membrane displacements are developed.

Hooke’s law for a two-dimensional stress field gives the following relationship between strains and stresses in the absence of any thermal strains:

$$\begin{aligned}\epsilon_{\phi} &= \frac{1}{E} [\sigma_{\phi} - \nu\sigma_{\theta}] \\ \epsilon_{\theta} &= \frac{1}{E} [\sigma_{\theta} - \nu\sigma_{\phi}]\end{aligned}\quad (13.7.1)$$

where ϵ and σ denote strain and stress, respectively. Subscripts ϕ and θ indicate meridional and circumferential directions, respectively. E is the

Young's modulus of the shell material, and ν is its Poisson's ratio. Strains can also be written in terms of stress resultants N_ϕ and N_θ using Eq. (13.3.1):

$$\epsilon_\phi = \frac{1}{Et} [N_\phi - \nu N_\theta]$$

$$\epsilon_\theta = \frac{1}{Et} [N_\theta - \nu N_\phi] \quad (13.7.2)$$

We recall that N_θ and N_ϕ are known from equilibrium (viz., Eqs. (13.3.7), (13.3.8), or (13.3.11-12)); therefore, the strains ϵ_ϕ and ϵ_θ are known. In order to determine displacements, we need to examine the strain displacement relationships for the membrane shell. These relations follow from the kinematics of a shell element as shown below.

Figure 13.7.1 shows a differential element of the meridian before (solid line) and after deformation (dotted lines). End A of the element displaces to point A' by an amount w in the radial direction (normal to the middle surface), and u in the meridional direction (positive in the direction of increasing ϕ). The corresponding displacements of end point B to end point B' are:

$$w + \frac{\partial w}{\partial \phi} d\phi \text{ in the normal direction,}$$

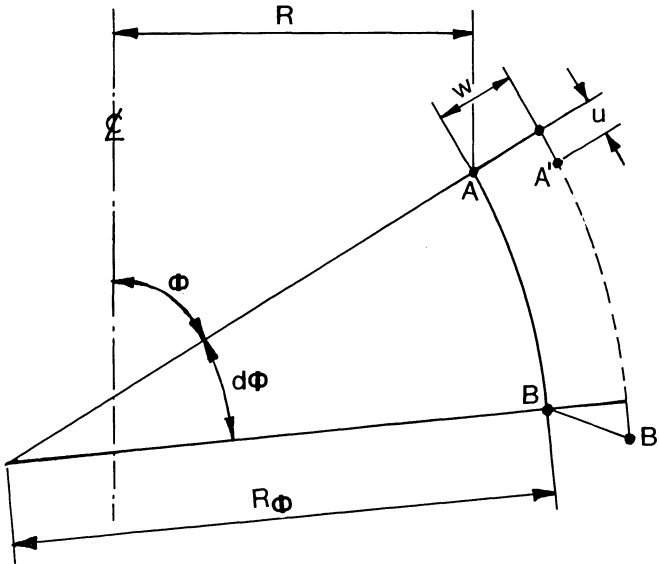


Fig. 13.7.1. Displacement of a differential element.

and

$$u + \frac{\partial u}{\partial \phi} d\phi \text{ in the tangential direction.}$$

From trigonometry, we see that the increase in the radius R of the parallel at point A due to this set of displacements is given by:

$$\delta R = w \sin \phi + u \cos \phi \quad (13.7.3)$$

Therefore, the circumferential strain is

$$\epsilon_{\theta} = \frac{\delta R}{R} = \frac{w \sin \phi + u \cos \phi}{R} \quad (13.7.4)$$

From (Eq. 13.2.2), $R = R_{\theta} \sin \phi$; hence

$$\epsilon_{\theta} = \frac{w}{R_{\theta}} + \frac{u}{R_{\theta}} \cot \phi$$

or

$$w = R_{\theta} \epsilon_{\theta} - u \cot \phi \quad (13.7.5)$$

The elongation of the element AB has two components; (i), the difference in tangential displacement of B over A

$$\frac{\partial u}{\partial \phi} d\phi$$

and (ii), the increase in the meridional radius to $R_{\phi} + w$ (neglecting terms of higher order), which causes the increase $[(R_{\phi} + w) d\phi - R_{\phi} d\phi]$ in the element length. Therefore, the total increase in the length of element AB is

$$\frac{\partial u}{\partial \phi} d\phi + w d\phi$$

Hence, the meridional strain ϵ_{ϕ} is

$$\epsilon_{\phi} = \frac{\frac{\partial u}{\partial \phi} d\phi + w d\phi}{R_{\phi} d\phi}$$

or

$$\epsilon_{\phi} = \frac{1}{R_{\phi}} \frac{\partial u}{\partial \phi} + \frac{w}{R_{\phi}} \quad (13.7.6)$$

Substituting for w from Eq. (13.7.5), we have

$$\frac{\partial u}{\partial \phi} - u \cot \phi = R_{\phi} \epsilon_{\phi} - R_{\theta} \epsilon_{\theta} \quad (13.7.7)$$

Since the right-hand side is a known function of ϕ , say $f(\phi)$, Eq. (13.7.7) can be integrated to obtain u .

Let

$$f(\phi) = R_\phi \epsilon_\phi - R_\theta \epsilon_\theta \quad (13.7.8)$$

Then

$$\frac{\partial u}{\partial \phi} - u \cot \phi = f(\phi)$$

or after multiplying through by $\operatorname{cosec} \phi$

$$\operatorname{cosec} \phi \frac{\partial u}{\partial \phi} - u \cot \phi \operatorname{cosec} \phi = f(\phi) \operatorname{cosec} \phi$$

Therefore

$$\frac{\partial}{\partial \phi} (u \operatorname{cosec} \phi) = f(\phi) \operatorname{cosec} \phi$$

which integrates to

$$u \operatorname{cosec} \phi = \int \frac{f(\phi)}{\sin \phi} d\phi + c$$

or, finally

$$u = \sin \phi \left[\int \frac{f(\phi)}{\sin \phi} d\phi + c \right] \quad (13.7.9)$$

The function $f(\phi)$ can be expressed in terms of principal radii of curvature and stress resultants by using Eqs. (13.7.2) and (13.3.11–12).

$$\begin{aligned} f(\phi) &= R_\phi \epsilon_\phi - R_\theta \epsilon_\theta \\ &= \frac{1}{Et} [R_\phi (N_\phi - \nu N_\theta) - R_\theta (N_\theta - \nu N_\phi)] \end{aligned}$$

or, for the class of shells where Eqs. (13.3.11–12) apply, (i.e., closed shells having R_θ finite everywhere)

$$\begin{aligned} f(\phi) &= \frac{pR_\theta}{2Et} \left[R_\phi \left(1 - 2\nu + \nu \frac{R_\theta}{R_\phi} \right) \right. \\ &\quad \left. - R_\theta \left(2 - \nu - \frac{R_\theta}{R_\phi} \right) \right] \end{aligned} \quad (13.7.10)$$

Equations (13.7.5), (13.7.9), (13.7.10) give complete expressions for meridional and normal displacement. It is, however, frequently convenient to deal in terms of horizontal and vertical displacements and rotation ω (Fig. 13.7.2). These are given in terms of u and w by the simple relations given below:

$$\delta R = w \sin \phi + u \cos \phi = R \epsilon_\theta$$

$$h = w \cos \phi - u \sin \phi$$

$$\omega = -\frac{1}{R_\phi} \frac{\partial w}{\partial \phi} \quad (13.7.11)$$

In general, the computation of u and w requires evaluation of the integral in Eq. (13.7.9). On the other hand, δR can be computed directly from the stresses via Eq. (13.7.4);

$$\delta R = R\epsilon_\theta = \frac{R}{E} (\sigma_\theta - \nu\sigma_\phi)$$

or

$$\delta R = \frac{pR_\theta^2 \sin \phi}{2Et} \left(2 - \nu - \frac{R_\theta}{R_\phi} \right) \quad (13.7.12)$$

We also note that when $\phi = \pi/2$, as is the case at the equator of heads, $w = \delta R$. Recall that Eq. (13.7.12) is derived for a specific class of shells of revolution where Eqs. (13.3.11–12) can be used for N_θ, N_ϕ .

Explicit solutions for some common shell configurations are given below:

(i) *Cylindrical shell (closed ends)*

$$\phi = \text{constant} = \pi/2; \quad R_\theta = R$$

From Eq. (13.7.5)

$$\delta R = w = R_\theta \epsilon_\theta = \frac{R}{E} (\sigma_\theta - \nu\sigma_\phi)$$

Substituting for σ_θ and σ_ϕ from Eqs. (13.4.1–2);

$$\delta R = w = \frac{pR^2}{Et} (1 - 0.5\nu) \quad (13.7.13)$$

(ii) *Spherical Shell*

Reference [13.7.1] gives the solution for the pressurized edge supported spherical shell shown in Fig. 13.7.3. Since the segment shown is not closed, Eq. (13.7.12) does not apply; Ref. [13.7.1] provides the correct expression.

$$\delta R = \frac{pR^2}{Et} \sin \phi \left[1 - \frac{1 + \nu}{2} \left(1 - \frac{\sin^2 \phi_2}{\sin^2 \phi} \right) \right] \quad (13.7.14)$$

$$\omega = 0$$

For a hemispherical head, $\phi_1 = \pi/2$, $\phi_2 = 0$, and either Eq. (13.7.12) or Eq. (13.7.14) give, at $\phi = \phi_1$, the result

$$\delta R = \frac{pR^2}{2Et} (1 - \nu) \quad (13.7.15)$$

(iii) *Ellipsoidal Shell*

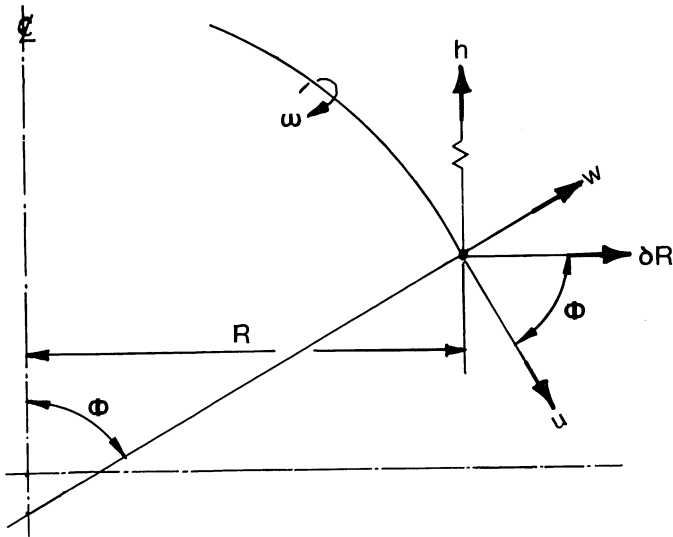


Fig. 13.7.2. Relationship between displacements.

Reference [13.7.1], with the aspect ratio $a/b = \eta$, gives

$$h = \frac{pa^2}{4Et} \left[(3\eta^2 + 1 - 2\nu) \frac{\cos\phi}{1 + \rho^2 \sin^2\phi} - 2\eta^2 \cos^2\phi + \frac{\rho}{\eta} \left(\eta^2 - \frac{1}{2} + \nu \right) \ln \left(\frac{\eta + \rho \cos\phi}{\eta - \rho \cos\phi} \right) \right] \quad (13.7.16)$$

$$\omega = \frac{pR_\theta}{2Et \tan\phi} \left(\frac{R_\theta}{R_\phi} - 1 \right) \left(\frac{R_\theta}{R_\phi} + 3 \right) \quad (13.7.17)$$

where

$$\rho = (\eta^2 - 1)^{1/2}$$

δR is obtained directly from Eq. (13.7.12).

At the equator, $\phi = \pi/2$ and Eq. (13.4.13) gives $R_\theta = a$; $R_\phi = b^2/a$. Therefore

$$\omega|_{\phi=\pi/2} = 0$$

$$\delta R|_{\phi=\pi/2} = \frac{pa^2}{2Et} \left(2 - \nu - \frac{a^2}{b^2} \right) \quad (13.7.18)$$

δR will be negative if $a/b > (2 - \nu)^{1/2}$

(iv) Conical Head (Fig. 13.7.4)

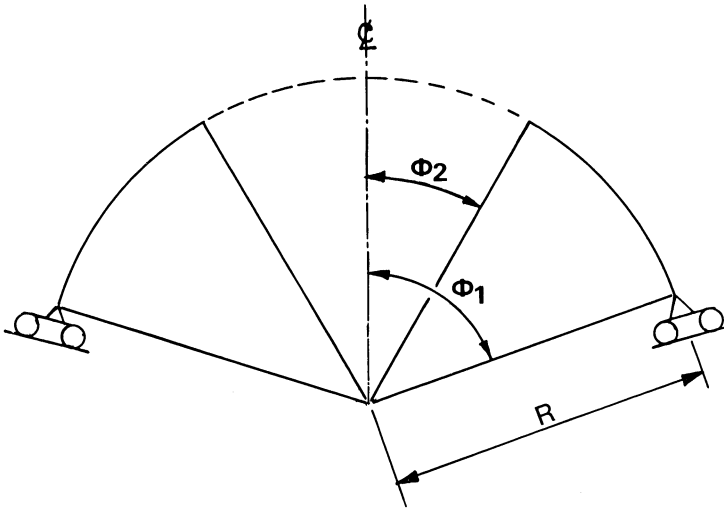


Fig. 13.7.3. Segment of spherical shell.

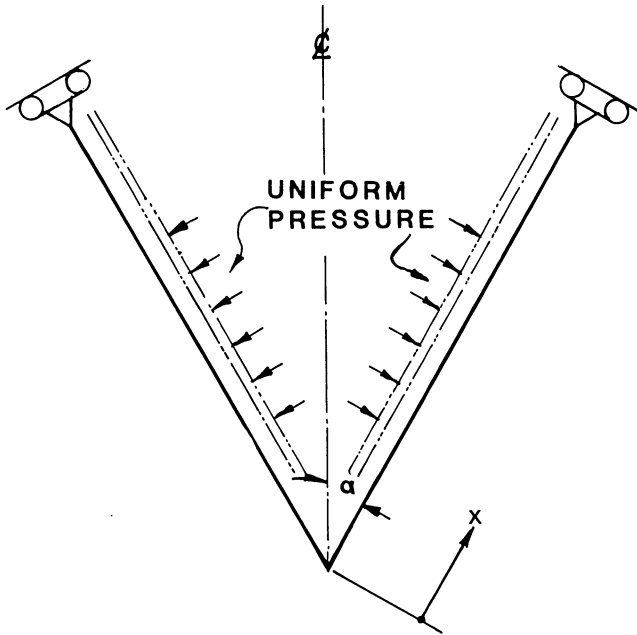


Fig. 13.7.4. Uniformly loaded conical shell.

At a distance x along the generator, Ref. [13.7.1] gives

$$\delta R = \frac{px^2}{Et} \sin \alpha \tan \alpha (1 - 0.5\nu) \quad (13.7.19)$$

$$\omega = \frac{3}{2} \frac{px}{Et} \tan^2 \alpha \quad (13.7.20)$$

The above formulas are convenient for local discontinuity analysis. In general, the expressions for displacements for shells generated by an irregular shape meridian requires numerical integration of the integral in Eq. (13.7.9).

13.8 EVALUATION OF DISCONTINUITY EFFECTS

Abrupt changes in the meridional curvature produce a mismatch in the displacement of the shell on the two sides of the discontinuity. In order that the junction may remain unbreached, additional interface moments and shear must be developed. Equal and opposite amounts of discontinuity reactions act on the two edges such that the total displacement and rotation are equal. This effect can be examined by reviewing the membrane displacements at the junction of a cylindrical shell and a hemispherical head. From Eq. (13.7.13), the radial membrane displacement $\delta R = \Delta_s$ of the shell is

$$\Delta_s = \frac{pR^2}{Et_s} (1 - 0.5\nu) \quad (13.8.1)$$

From Eq. (13.7.15), the radial displacement of the hemispherical head $\delta R = \Delta_h$ is

$$\Delta_h = \frac{pR^2}{2Et_h} (1 - \nu) \quad (13.8.2)$$

where t_s and t_h denote shell and head thicknesses, respectively. If the two thicknesses are the same, and Poisson's ratio $\nu = 0.3$, then

$$\frac{\Delta_s}{\Delta_h} = \frac{2(1 - 0.5\nu)}{1 - \nu} = 2.43$$

In other words, a cylindrical shell of identical thickness expands 2.43 times more than the expansion of a spherical head as computed from membrane theory. Figure 13.8.1 shows that interface reactions are needed to establish displacement and slope compatibility. The effect of rotationally symmetric edge shear and moment on a cylinder is studied in Appendix A. Similar expressions for shells of other configurations are quite involved. In most cases, however, it is not necessary to contend with such involved analyses. If the thickness of the shell is small in comparison with the equatorial radius such that $R/t > 50$, then the bending behavior of the shell and head can be approximated by that of a cylinder of equal radius. This approximation is

frequently referred to as Geckler's assumptions. As shown in Appendix A, the edge displacement Δr and rotation $\Delta\theta$ of a shell loaded by an edge moment M_0 are given by

$$\Delta r = \frac{M_0}{2\beta_s^2 D_s} = a_2 M_0$$

$$\Delta\theta = \frac{M_0}{\beta_s D_s} = a_1 M_0 \tag{13.8.3}$$

where β_s and D_s are the attenuation coefficient and the flexural rigidity of the shell, respectively

$$\beta_s = \left[\frac{3(1-\nu^2)}{R^2 t_s^2} \right]^{1/4} \tag{13.8.4}$$

$$D_s = \frac{Et_s^3}{12(1-\nu^2)} = \frac{Et_s}{4R^2 \beta_s^4} \tag{13.8.5}$$

Similarly, the displacement Δr and rotation $\Delta\theta$ of the edge due to an edge shear Q_0 are given by

$$\Delta r = Q_0 / 2\beta_s^3 D_s = a_3 Q_0 \tag{13.8.6}$$

$$\Delta\theta = Q_0 / 2\beta_s^2 D_s = a_2 Q_0 \tag{13.8.7}$$

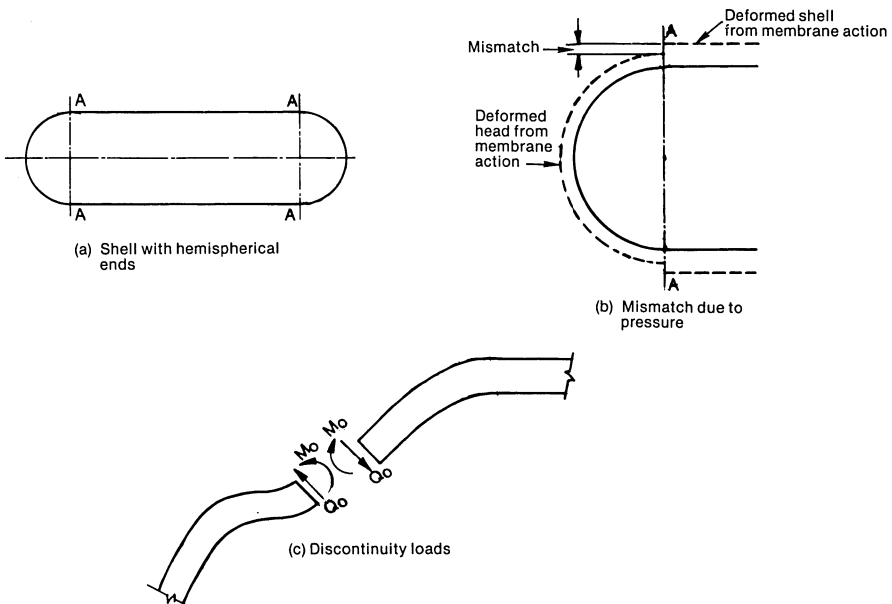


Fig. 13.8.1. Discontinuity effects in a pressure vessel with hemispherical ends.

In the foregoing, a_1 , a_2 and a_3 are defined strictly for convenience of notation as

$$a_1 = \frac{1}{\beta_s D_s}; \quad a_2 = \frac{1}{2\beta_s^2 D_s}; \quad a_3 = \frac{1}{2\beta_s^3 D_s} \quad (13.8.8)$$

Using the above results, general expressions for discontinuity reactions can be derived for the junction of a shell and head, where the shell generator is tangential to the head meridian at the junction. This case occurs in a great majority of pressure vessels (a notable exception being the case where a conical shell is welded to a cylindrical shell without an intermediate knuckle). In such cases, the edges do not rotate due to membrane effects. The only discontinuity is due to a radial displacement differential between the two components, say δ' . To fix our ideas, let us append a second subscript to the constant a 's defined above. The value 1 for the second subscript pertains to the shell; the value 2 corresponds to the head. Finally, δ' is the membrane radial displacement of shell minus that of the head at the joint. Continuity requires that the displacement of the head due to pressure (membrane solution) plus the displacements due to discontinuity moment and shear must equal the total displacement of the shell due to the same set of effects. This implies the equation

$$\delta_s(M_0, Q_0) + \Delta_s = \delta_h(M_0, Q_0) + \Delta_h$$

In terms of our expressions here, $\delta' = \Delta_s - \Delta_h$

or

$$\delta' = (a_{22}M_0 + a_{32}Q_0) - (a_{21}M_0 - a_{31}Q_0)$$

or

$$\delta' = (a_{22} - a_{21})M_0 + (a_{32} + a_{31})Q_0 \quad (13.8.9)$$

Similarly, the edge rotations in the two components must match. In this particular case, the only rotational contributions are from the effects of M_0 and Q_0 . Hence, we have

$$a_{12}M_0 + a_{22}Q_0 = a_{21}Q_0 - a_{11}M_0 \quad (13.8.10)$$

which relates M_0 , Q_0 by the expression

$$M_0 = \frac{a_{21} - a_{22}}{a_{11} + a_{12}} Q_0$$

We write the result in the form

$$M_0 = \zeta Q_0 \quad (13.8.11)$$

where

$$\zeta = \frac{a_{21} - a_{22}}{a_{11} + a_{12}} \quad (13.8.12)$$

We note that if the head and shell have equal rigidity and attenuation

coefficients (which in practice means equal Young's moduli and thicknesses), then $\zeta = 0$. Thus the discontinuity moment is not needed to satisfy compatibility at a junction when the two parts have equal E and t .

Finally, from Eq. (13.8.9)

$$Q_0 = \frac{\delta'}{(a_{22} - a_{21})\zeta + (a_{32} + a_{31})} \quad (13.8.13)$$

Equation (13.8.13) gives the discontinuity shear. The stresses and displacements due to these discontinuity reactions can be computed using the formulas given in Appendix A, which are

$$\delta_s = \frac{1}{2\beta^3 D} [\beta M_0 \phi(\beta x) + Q_0 \lambda(\beta x)] \quad (13.8.14)$$

$$M_x = D \frac{\partial^2 \delta_s}{\partial x^2} \quad (13.8.15)$$

$$M_\theta = \nu M_x \quad (13.8.16)$$

where

$$\phi(\beta x) = e^{-\beta x} (\cos \beta x - \sin \beta x)$$

$$\lambda(\beta x) = e^{-\beta x} \cos \beta x$$

Example

Let us consider a cylindrical vessel with hemispherical head with all parts having equal thickness t , subjected to an internal pressure p :

The radial mismatch δ' is given from Eqs. (13.8.1-2)

$$\delta' = \Delta_s - \Delta_h = \frac{pR^2}{2Et} \quad (13.8.17)$$

Since $t_s = t_h = t$, $\zeta = 0$, $\rightarrow M_0 = 0$; and, from Eq. (13.8.8), $a_{31} = a_{32} = 1/2\beta^3 D$

Substituting for D from Eq. (13.8.5) we have

$$a_{31} = a_{32} = \frac{2R^2 \beta}{Et}$$

Therefore,

$$Q_0 = \frac{\delta'}{(a_{31} + a_{32})} = \frac{pR^2}{2Et} \frac{Et}{4R^2 \beta}$$

or

$$Q_0 = \frac{p}{8\beta} \quad (13.8.18)$$

The discontinuity moment, as a function of x , is given by Eqs. (13.8.14-15):

$$\begin{aligned}
 M_x &= \frac{DQ_0}{2\beta^3 D} (2\beta^2 e^{-\beta x} \sin\beta x) = \frac{Q_0}{\beta} e^{-\beta x} \sin\beta x \\
 &= \frac{pRt}{8[3(1-\nu^2)]^{1/2}} e^{-\beta x} \sin\beta x
 \end{aligned}$$

This moment attains its maximum value at $x = \pi/4\beta$.

Combining the maximum bending stress due to the discontinuity moment with the membrane stress, the maximum longitudinal stress in the cylindrical shell is:

$$\begin{aligned}
 \sigma_{\max} &= \frac{pR}{2t} + \frac{3}{4} \frac{pR}{t[3(1-\nu^2)]^{1/2}} e^{-\frac{\pi}{4}} \sin \frac{\pi}{4} \\
 &= 1.293 \frac{pR}{2t}
 \end{aligned}$$

The stress in the circumferential direction consists of three components:

- (i) hoop stress due to membrane effects;
- (ii) hoop stress caused by the deflection δ_s due to discontinuity edge load; and,
- (iii) bending stress produced by M_θ .

Thus, the maximum circumferential stress at the outside surface of the cylindrical shell is:

$$\sigma_t = \frac{pR}{t} + \frac{E\delta_s}{a} + \frac{6M_\theta}{t^2}$$

or

$$\sigma_t = \frac{pR}{t} \left[1 - \frac{1}{4} e^{-\beta x} \cos\beta x + \frac{3\nu e^{-\beta x} \sin\beta x}{4[3(1-\nu^2)]^{1/2}} \right]$$

For $\nu = 0.3$, this stress attains its maximum value at $\beta x = 1.85$ and has the value

$$\sigma_{t\max} = 1.032 \frac{pR}{t}$$

Since the membrane stresses in the head are half of the cylinder hoop stress, the maximum stress will turn out to occur in the cylindrical shell (for the case of equal thickness of cylindrical and spherical shells).

Analyses for shell-head junctions where the head is ellipsoidal, torispherical or toriconical, can be carried out in a similar manner. The procedure described in Section 13.7 gives the membrane radial displacement. The corresponding discontinuity moment and shear follow from Eqs. (13.8.13) and (13.8.11), respectively. The discontinuity moments and displacement are defined by Eqs. (13.8.14)–(13.8.16). This method of discontinuity analysis is sufficiently accurate for routine stress analysis of

pressure vessels. Additional examples of discontinuity analyses and subsequent stress evaluation near the joint can be found in Refs. [13.2.2, 13.2.3, 13.7.1].

NOMENCLATURE

- A_m = Required metal area to be added
 a, b = Major and minor semi-diameters of elliptical meridian curve
 A_p, A_n = Positive and negative areas of intercept (Fig. 13.5.2)
 A = Algebraic sum of A_p and A_n
 a_1, a_2 , etc. = Deformation coefficient (Eq. (13.8.8))
 a_{1i}, a_{2i} = Deformation coefficient for shell number i
 c = Integration constant (Eq. (13.7.9))
 D_i = Head inside diameter
 dA = Area of differential element (Fig. 13.3.2)
 D = Flexural rigidity of shell of thickness t
 E' = Weld joint efficiency
 E = Young's modulus
 h = Displacement component parallel to axis of revolution (Fig. 13.7.2)
 k = Discontinuity constant (Section 13.6)
 L = Crown radius (Fig. 13.1.1); also meridional radius of curvature of head (Fig. 13.5.3)
 M_0 = Discontinuity edge moment
 N_ϕ = Meridional stress resultant per unit length
 N_θ = Circumferential stress resultant per unit length
 $\bar{n}_1, \bar{n}_2, \bar{n}_3$ = Unit vectors (Fig. 13.2.3)
 p = Internal pressure (if without a subscript)
 p_x, p_y, p_z = Surface load per unit area in local x, y or z direction, respectively (Fig. 13.3.2)
 Q_0 = Discontinuity edge shear
 r = Knuckle or flare radius
 R = Radius of "parallel" circle (Fig. 13.2.1)
 R_0 = Distance of center of meridian circle from the axis of rotation (toroidal shell)
 r_0 = Radius of generatrix circle for producing toroidal shell
 R_ϕ = Meridional (principal) radius of curvature
 R_θ = Circumferential (principal) radius of curvature
 R_L = Radius of large end of cone
 SE' = Net allowable stress, equal to Code allowable stress times weld joint efficiency, E' (Eq. (13.6.1))
 t_c = Cone thickness
 t = Generic thickness term for shell of revolution
 u = Meridional direction displacement
 w = Displacement normal to the mid-surface of the shell
 α = Semi-angle of conical head

- β = Attenuation coefficient
 δR = Increase in the radial distance of the meridian due to membrane displacement from the axis of revolution
 δ' = Δ_s less Δ_h
 Δ_s = Radial displacement of cylindrical shell under pressure due to membrane effects (= δR) (Eq. (13.8.1))
 Δ_h = Radial displacement of head at the equator (= δR) due to membrane effects (Eq. (13.8.2))
 Δr = Radial edge displacement of shell of revolution due to edge loading
 $\Delta\theta$ = Edge rotation of shell of revolution due to edge loading
 $\epsilon_\phi, \epsilon_\theta$ = Meridional and circumferential strains, respectively
 ν = Poisson's ratio
 ϕ = Angle between normal to the meridian and the axis of the shell of revolution
 σ_θ = Circumferential membrane stress
 σ_ϕ = Longitudinal membrane stress
 η = Ratio of major and minor diameters of the generator ellipse
 ω = Rotation of the meridional arc due to membrane effects (Fig. 13.7.2)

Subscripts

- s = Means that the quantity pertains to the shell
 h = Means that the quantity pertains to the head
 ϕ = Meridional direction
 θ = Circumferential direction

REFERENCES

- [13.1.1] "Standards of Tubular Exchanger Manufacturers Association," TEMA Inc., 25 N. Broadway, Tarrytown, NY, 6th edition (1978).
 [13.1.2] ASME Boiler and Pressure Vessel Code, Section VIII, Div. 1, The American Society of Mechanical Engineers, New York (1983).
 [13.2.1] Struik, D. J., "Differential Geometry," Addison-Wesley, Reading, PA (1950).
 [13.2.2] Kraus, Harry, "Thin Elastic Shells," Wiley, New York (1967).
 [13.2.3] Novozhilov, V. V., "The Theory of Thin Shells," Noordhoff, Groningen, The Netherlands (1959).
 [13.4.1] Harvey, J. F., "Pressure Component Construction," pp. 51-52, Von Nostrand, New York (1980).
 [13.5.1] Zick, L. P., and St. Germain, A. R., "Circumferential Stresses in Pressure Vessel Shells of Revolution," *Journal of Engineering for Industry*, Trans. ASME, pp. 201-218 (May 1963).
 [13.7.1] Baker, E. H., Kovalevsky, L., and Rish, F. L., "Structural Analysis of Shells," McGraw-Hill (1972).
 [13.7.2] Timoshenko, S., and Woinowski, Krieger, S., "Theory of Plates and Shells," McGraw-Hill, New York (1959).

14. THERMAL STRESSES IN U-BENDS

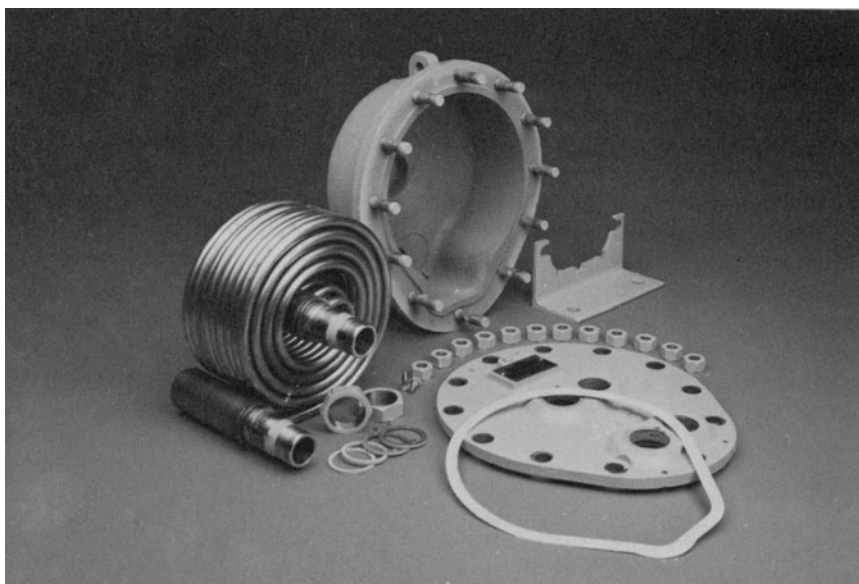
14.1 INTRODUCTION

The tubular heat exchanger, being a device to transfer heat between two fluids at different temperatures, is a natural candidate for thermal expansion related problems. Indeed thermal stresses merit careful analysis in the design of all kinds of heat transfer apparatus. In shell-and-tube exchangers, the thermal stress problem usually stems from the differential expansion between the shell and the tubes. The tubes are in (turbulent) contact with both fluids undergoing the heat transfer process, whereas the shell is in contact with the shell-side fluid only. The resultant differential expansion between the shell and the tubes, sometimes abetted by the difference in the thermal expansion coefficients of the tube and the shell materials, is a major source of structural problems in fixed tubesheet heat exchangers. Chapter 9 deals with the methods to predict the stress field in fixed tubesheet exchangers. As stated in Chapter 1, this drawback of the fixed tubesheet design is eliminated by resorting to U-tube construction, wherein the longitudinal expansion of the shell is physically isolated from that of the tubes. This inherent feature of U-tube design has fostered the mistaken belief that U-tube designs are immune from axial thermal expansion problems. While the relative differential expansion between the shell and the tube bundle is certainly eliminated as a potential design problem in the U-tube construction, the thermal stress problem now manifests itself in the tube bundle. The straight tube segments in different tube passes are, in general, subject to different flow patterns and to different fluid temperatures. As a consequence, the two constituent legs of a U-tube expand or contract by unequal amounts. Since the U-tubes are clamped (“built-in”) at the tubesheet for all intents and purposes, the semicircular bends at the rear end of the bundle must absorb most of the differential expansion between the adjoining legs. Often, the attendant stresses are quite high.

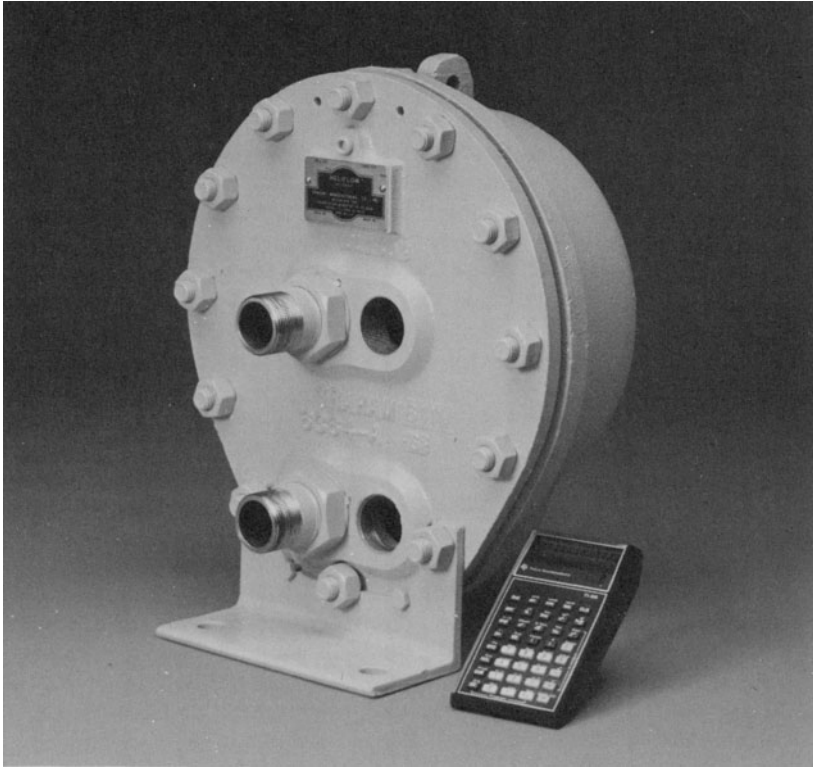
Consideration of high U-bend stresses in shell-and-tube heat exchangers have prompted the development of other design concepts such as helical and serpentine shapes. The “Heliflow”[®] exchanger, produced by Graham Manufacturing Company of Batavia, New York, utilizes a helical tube bundle as shown in Photographs 14.a-b. The “heliflow” bundle is slightly compressed between the casing and the baseplate during assembly of the unit. Thus any out-of-plane vibration of the windings is suppressed while maintaining the thermal expansion absorption capability. The helical gap

between the winding rows provides the flow path for the shellside fluid. Thus, the countercurrency of the shell and tubeside fluids is ensured. The compactness of the “heliflow” unit lends itself to application in high pressure, high temperature drop, small heat transfer surface (two sq. ft. to four hundred sq. ft.) designs.

In general, for most practical applications, the U-tube design possesses sufficient flexibility such that the inter-leg temperature difference is not a cause for serious concern as long as temperature changes are not severe. The potential inadequacy of the U-tube develops only when the temperature changes across the exchanger are relatively large. We emphasize here that this situation is becoming more and more commonplace as system designers seek to extract more performance out of heat exchangers. The problem is especially severe in equipment used in “regeneration” type of applications. The steam generator blow-down heat exchanger often used in Pressurized Water Reactor Power Plant designs is a typical example of this situation. The main function of this heat exchanger is to recapture most of the enthalpy of the blow-down stream. The blow-down stream must be cooled to low enough temperatures to make it compatible with down-stream equipment (e.g., demineralizers). On the other hand, it is desirable to heat the coolant stream to as high a temperature as feasible to make the unit thermodynamically attractive. Thus, both shell and tube-side fluids in a blow-down exchanger are subject to large temperature changes. All prerequisites for possible overstress in the U-bends are present.



Photograph 14.a. Parts of heliflow heat exchanger (Courtesy Graham Manufacturing Co., Batavia, N.Y.)



Photograph 14.b. Heliflow heat exchanger in assembled form; the adjacent calculator gives an estimate of its size (Courtesy Graham Manufacturing Co.).



Photograph 14.c. Typical U-tube bundle.

In addition to the potential of U-bend overstress due to differential expansion effects, there can be a series of additional side effects. Large U-bend stresses are accompanied by appreciable contact forces between the tube wall and the support baffle, especially at baffles located adjacent to the U-bends. In unit operations subject to a large number of thermal cycles these contact forces pose a real threat of wear and fretting damage to the tube surfaces. In addition, axial force in the tube, developed due to the thermal expansion loads, may be dangerous to the integrity of rolled-only tube-to-tubesheet joints (ref. Chapter 7). Furthermore, axial stress in the tubes alters their natural frequency of vibration. The influence of tube natural frequency on the stability of the tube against flow induced vibration is well known to heat exchanger engineers and is discussed in some depth later (Chapter 16).

In this chapter, a workable set of equations is developed to enable direct computation of the U-bend stresses so as to enable the designer to ascertain the potential for overstress. The solution is devised within the framework of linear elasticity theory by employing Castigliano's First Theorem. The computer program UBAX, devised to perform the numerical work, is also presented. A practical example is used to illustrate the solution procedure. A simple formula based on an idealized linear model is also derived for application in those routine cases which do not warrant computerized analysis. Photograph 14.c shows a typical U-tube bundle.

The first step in the analysis is to determine the metal temperature of the legs and, of course, the U-bends. We will assume here that the tube metal temperatures (hence, the differential thermal expansion between the legs, δ , and change in radius of the U-bend, Δ) are known. The object is to evaluate the stresses and displacement fields in the U-tube. The mathematical model and solution procedure are described in the following section. Practical design remedies to alleviate U-bend stresses are also pointed out and discussed in some detail. The listing of the computer program "UBAX" based on the analysis of this chapter is given in Section 14.7 along with instructions for its use.

14.2 ANALYSIS

Figure 14.2.1 shows the center line of a U-tube of straight length l_s and bend radius r laterally supported at a number of locations by cross baffles. The two legs of the "U" overhang by specified amounts S_1 and S_2 , respectively, beyond the last support baffles labeled as tangent line baffles (TL) in Fig. 14.2.1. We assume that the U-tube is subject to a temperature field such that, under free expansion, leg 1 expands by an amount δ over leg 2, and the radius of the bend increases by an amount Δ . It is intuitively apparent that the bend region would be subject to the most severe stresses. Therefore, it is reasonable to expect that the characteristics of the support provided by the TL baffles would be especially important. Since the baffle holes are drilled with a certain clearance (usually in the range of 0.015 in. to

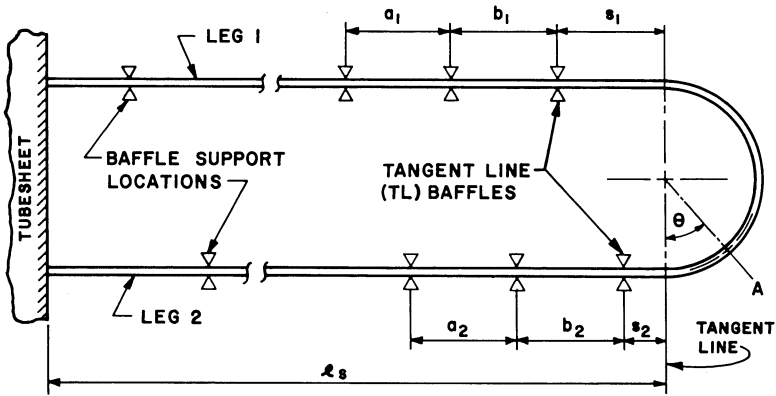


Fig. 14.2.1 U-tube geometry.

0.03 in.) [14.2.1], it is necessary to model these support locations with a specified clearance. We define this available clearance in each leg i as ξ_i . We now proceed to derive the necessary equations to solve the strength-of-materials problem.

The solution procedure is best described by considering a freebody of the U-bend segments including the overhang spans (Fig. 14.2.2). P is the unknown axial force developed in the legs. R represents the lateral shear. M_1 and M_2 denote the bending moments produced at the TL baffle locations O_1 and O_2 , respectively. Let:

$$\begin{aligned} M_1 &= K_1 \alpha_1 \\ M_2 &= K_2 \alpha_2 \end{aligned} \tag{14.2.1}$$

where α_1 and α_2 denote in-plane rotations of legs 1 and 2 at points O_1 and O_2 respectively. K_1 and K_2 are the corresponding spring constants. These spring constants represent the influence of adjacent tube spans and baffle support conditions. For a baffle support modeled with a small clearance, K_i will be a highly nonlinear function of α_i . More on this point will follow later in this section. At this stage in the analysis, it is assumed that K_1 and K_2 are known quantities.

Referring to Fig. 14.2.2, moment equilibrium yields: $M_1 + R(S_1 - S_2) - 2Pr - M_2 = 0$. Since $M_i = K_i \alpha_i$, we have:

$$\alpha_1 = \frac{1}{K_1} [K_2 \alpha_2 + 2Pr - R(S_1 - S_2)] \tag{14.2.2}$$

To evaluate the four principal unknowns in this formulation, namely α_1 , α_2 , P and R , three additional equations are required. These equations are derived by using a generalized form of the theorem of Castigliano [14.2.2].

We note that the total strain energy U in the U-bend segment (Fig. 14.2.2) is given by:

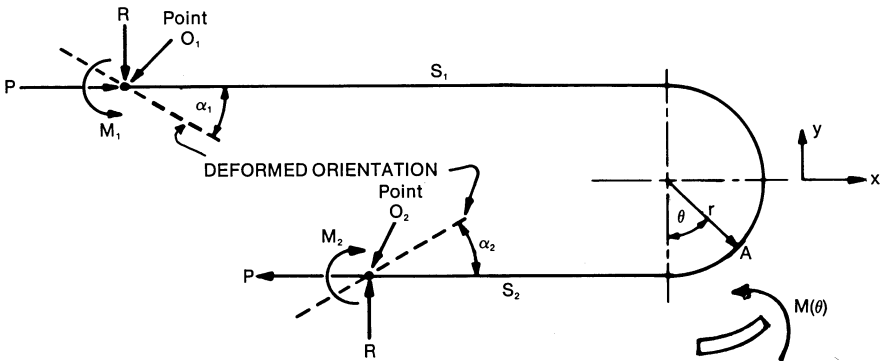


Fig. 14.2.2. Freebody of U-bend segment.

$$U = \int \frac{N^2}{2EA} ds + \int \frac{\Phi V^2}{2GA} ds + \int_{(S_1, S_2)} \frac{M^2}{2EI} ds + \lambda \int_0^\pi \frac{M^2 d\theta}{2EAy_0} + \int_0^\pi \frac{MN}{EA} d\theta \quad (14.2.3)$$

The first two terms in the integral are contributions to the strain energy due to the axial force and lateral shear, respectively. The integral extends over the entire length of the element. The third and fourth terms are flexural strain energy in the straight and curved segments, respectively. Finally, the last term represents the contribution to the strain energy due to non-coincidence of neutral and centroidal axes in curved members. The symbols N , V and M , respectively, denote axial tension, lateral shear, and bending moment (positive if it increases the curvature of the semi-circular bend) at a generic point. The functional forms for N , V , M are obtained by examining appropriate free bodies and writing the equilibrium equations involving N , V , M at a typical point and P , R , and M_2 . For example, referring to Fig. 14.2.2, the moment M at angular position $0 < \theta < \pi$ is given as

$$M(\theta) = M_2 + R(S_2 + r \sin\theta) + Pr(1 - \cos\theta) \quad (14.2.4)$$

Similarly, the direct tensile force, parallel to the tube middle surface, at A is

$$N = P \cos\theta - R \sin\theta \quad (14.2.5)$$

The quantity y_0 is the distance of the centroidal axis from the neutral axis when the curved segment is subject to pure flexure. For an annular cross section of outer radius c_o and inner radius c_i , y_0 is defined as [14.2.3]:

$$y_0 = \frac{zr}{z+1} \quad (14.2.6)$$

where:

$$z = -1 + \frac{2r}{c_0^2 - c_i^2} [(r^2 - c_i^2)^{1/2} - (r^2 - c_0^2)^{1/2}] \quad (14.2.7)$$

Φ (in Eq. (14.2.3)) is the shear stress distribution factor. For thin annular cross sections, Φ is equal to 2.0. λ is the flexibility factor attributable to the elastic ovaling of thin walled circular cross sections of curved elements during bending. A generally accepted semi-empirical expression for λ is due to Rodabaugh and George [14.2.4]:

$$\lambda = \frac{f}{1 + \frac{6pc_m}{Et} \left(\frac{c_m}{t}\right)^{4/3} \cdot \left(\frac{r}{c_m}\right)^{1/3}} \geq 1 \quad (14.2.8)$$

where

$$f = \frac{1.65c_m^2}{tr} \quad (14.2.9)$$

c_m is the mean radius of the tube, t is the wall thickness of the tubing, and p is the internal pressure.

The theorem of Castigliano states that the generalized elastic displacement q , at the point of application of a corresponding externally applied generalized force Q , with respect to an immovable reference point, is given by

$$q = \frac{\partial U}{\partial Q}$$

Referring to Fig. 14.2.2, if point O_1 is chosen as the reference point, then the partial derivative of U with respect to P , R and M_2 must respectively equal the elastic $-x$ and y direction displacement, and the rotation of point O_2 . Table 14.2.1, below, gives the total displacements of point O_2 relative to point O_1 , and the rigid body movement which is required to be subtracted from the total movement to give the elastic component. The notation used in Table 14.2.1 is described in Fig. 14.2.3.

As an example of the construction of Table 14.2.1, we consider the y direction movement in the direction of R at point O_2 . To bring point O_2 from the undeformed position to the deformed position shown in Fig. 14.2.3, we note that relative to point O_1 , the point O_2 , in the absence of R , would move a distance -2Δ due to free thermal expansion. The application of R induces a deflection $2\Delta - \epsilon_2$. Due to the movement of point O_1 , we also have a rigid body displacement of amount $\epsilon_1 - (S_1 - S_2)\alpha_1$ occurring to O_2 . We have tacitly assumed that ϵ_i are less than or equal to the available clearances ξ_i .

Therefore, Castigliano's Theorem requires (referring to Fig. 14.2.3):

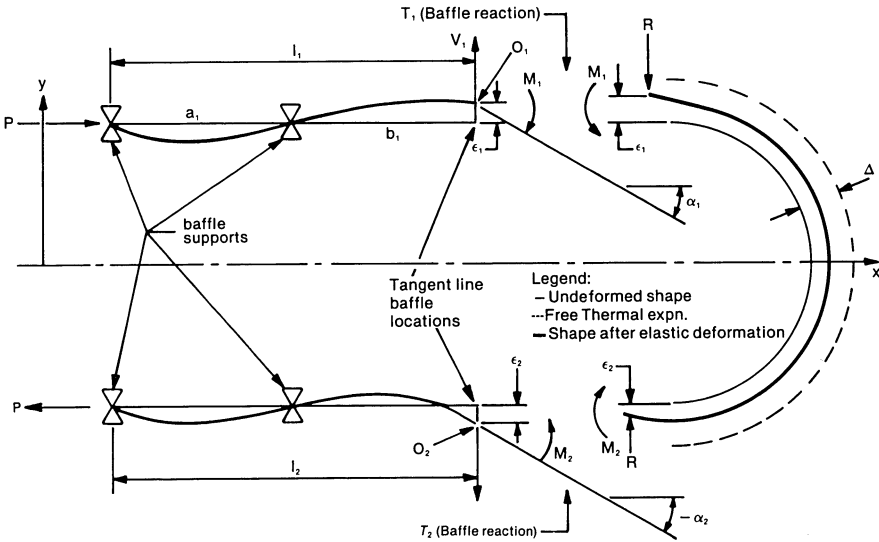


Fig. 14.2.3. Two span model and U-bend deformation sequence.

Table 14.2.1 Total and Rigid Body Movements of Point O₂

Component	Total Movement	Rigid Body Movement
- x-direction (movement in the direction of P)	$\delta - \frac{P(2l_s - S_1 - S_2)}{EA}$	$2r\alpha_1$
y-direction (movement in the direction of R)	$(2\Delta - \epsilon_2)$	$\epsilon_1 - (S_1 - S_2)\alpha_1$
Rotation in the direction of M ₂	$-\alpha_2$	α_1

$$\frac{\partial U}{\partial P} = \delta - 2r\alpha_1 - \frac{P(2l_s - S_1 - S_2)}{AE} \quad (14.2.10)$$

$$\frac{\partial U}{\partial R} = -(\epsilon_1 + \epsilon_2 - 2\Delta) + (S_1 - S_2)\alpha_1 \quad (14.2.11)$$

$$\frac{\partial U}{\partial M_2} = -(\alpha_1 + \alpha_2) \quad (14.2.12)$$

Using Eqs. (14.2.3) and (14.2.10–12), after performing necessary integrations and algebraic manipulations (omitted here for brevity), three additional linear equations in α_1 , α_2 , R and P are obtained. α_1 is eliminated from these equations using Eq. (14.2.2). The resulting set of three linear equations may be written in subscript notation as:

$$\sum_{j=1}^3 B_{ij}x_j = f_i; \quad i = 1, 2, 3 \quad (14.2.13)$$

with the implied identities

$$\{x\}^T = [\alpha_2, R, P] \quad \text{and} \quad \{f\}^T = [\delta, 2\Delta - \epsilon_1 - \epsilon_2, 0]$$

ϵ_1 and ϵ_2 denote outward displacements of points O_1 and O_2 (Fig. 14.2.3).

The elements of the $[B]$ matrix are given in Appendix 14.A for reference. Solving Eq. (14.2.11) yields explicit expressions for R , P and α_2 as follows:

$$R = \frac{1}{D} \left[\left(B_{23} - \frac{B_{21}B_{33}}{B_{31}} \right) \delta - \left(B_{13} - \frac{B_{11}B_{33}}{B_{31}} \right) (2\Delta - \epsilon_1 - \epsilon_2) \right] \quad (14.2.14)$$

$$P = \frac{1}{D} \left[\left(B_{12} - \frac{B_{11}B_{32}}{B_{31}} \right) (2\Delta - \epsilon_1 - \epsilon_2) - \left(B_{22} - \frac{B_{21}B_{32}}{B_{31}} \right) \delta \right] \quad (14.2.15)$$

$$\alpha_2 = -\frac{1}{B_{31}} (B_{32}R + B_{33}P) \quad (14.2.16)$$

where:

$$D = \left(B_{12} - \frac{B_{11}B_{32}}{B_{31}} \right) \left(B_{23} - \frac{B_{21}B_{33}}{B_{31}} \right) - \left(B_{22} - \frac{B_{21}B_{32}}{B_{31}} \right) \left(B_{13} - \frac{B_{11}B_{33}}{B_{31}} \right) \quad (14.2.17)$$

All unknowns in the problem can now be computed provided the rotational stiffnesses K_1 and K_2 are known. We recognize that the stiffnesses strongly depend on the adjacent spans; however, the influence of remote spans on K_i is minimal. Hence to develop a simple expression for K_i , we consider the two-span model shown in Fig. 14.2.3. Referring to Fig. 14.2.3, the following relationships follow from the classical beam flexure theory.

$$EI\epsilon_i = \frac{V_i l_i b_i^2}{3} - \frac{M_i b_i (2l_i + b_i)}{6} \quad (14.2.18)$$

$$EI\alpha_i = \frac{M_i (2b_i + l_i)}{3} - \frac{V_i b_i (3l_i - a_i)}{6} \quad (14.2.19)$$

where $i=1,2$ for the two legs, respectively. Eliminating V_i between Eqs. (14.2.18) and (14.2.19), and solving for M_i , yields the equations

$$\alpha_i = \rho_i M_i - \eta_i \quad (14.2.20)$$

where

$$\rho_i = \frac{1}{EI} \left[\frac{2b_i + l_i}{3} - \frac{(3l_i - a_i)(2l_i + b_i)}{12l_i} \right] \quad (14.2.21)$$

$$\eta_i = \frac{(3l_i - a_i)\epsilon_i}{2l_i b_i} \quad (14.2.22)$$

Thus, Eqs. (14.2.1) and (14.2.20) yield the required expression for K_i ; we have:

$$K_i = \frac{1}{\rho_i} + \frac{\eta_i}{\rho_i \alpha_i} \quad (14.2.23)$$

Note that η_i vanishes when ϵ_i is zero and K_i becomes independent of α_i . However, if a small lateral displacement at the Tangent Line (TL) baffle location is allowed, then K_i becomes dependent on α_i .

Finally, the reaction at the TL baffle location are given by:

$$T_i = R - V_i; \quad i=1,2 \quad (14.2.24)$$

where V_i follows from Eq. (14.2.18):

$$V_i = \frac{3}{l_i b_i^2} \left[EI\epsilon_i + \frac{M_i b_i}{6} (2l_i + b_i) \right] \quad (14.2.25)$$

The solution procedure to solve a specific problem can now be described.

14.3 METHOD OF SOLUTION

The solution is fairly straightforward for the case where the TL baffles are assumed to have zero clearance. Incidentally this is also a conservative approximation since it will result in an overestimate of the computed U-bend stresses. The rotational stiffnesses, K_i , follow from Eq. (14.2.23). Equations (14.2.14-17) yield the magnitudes of R , P and α_2 , respectively. α_1 is computed from Eq. (14.2.2).

The computation is a bit more involved if small clearances at the TL baffle locations are stipulated. Let ξ_1 , ξ_2 denote the available clearances at leg 1 (in the positive y -direction), and at leg 2 (in the negative y -direction). To determine if the tube will move and take up the clearances, we proceed as follows:

Step (1): Assume $\epsilon_1 = \xi_1$, and $\epsilon_2 = \xi_2$, compute K_i from Eq. (14.2.23) assuming $\eta_i = 0$.

Step (2): Solve for R , P and α_2 using equations (14.2.14-17), and compute α_1 using Eq. (14.2.2).

Step (3): Having evaluated α_i , M_i ($i=1,2$) are computed from Eq. (14.2.20). The corrected values of K_i are then given by $K_i' = M_i/\alpha_i$.

Step (4): If K_i' is equal to the initially assumed K_i within a specified tolerance (say 0.1 percent absolute error), then the solution is said to have converged. The values of R , P , and α_i computed in Step 2 are the solution values. However, if K_i' is different from K_i , then we assume new K_i equal to the average of the previous K_i and the K_i' computed in the preceding step.

Step (5): Return to Step (2).

This procedure is repeated until the solution converges. It is found that convergence require as many as eight to ten iterations.

The crucial check on whether the tube will indeed contact the baffle by undergoing the assumed lateral displacements can now be made. A physically meaningful solution requires that for non-zero ϵ_i , the baffle reactions T_i must satisfy the condition

$$\frac{T_i}{\epsilon_i} > 0; \quad i=1,2 \quad (14.3.1)$$

where T_i ($i=1,2$) are defined by Eq. (14.2.24).

If Eq. (14.3.1) is not satisfied, then the assumed displacements ϵ_1 and ϵ_2 may be excessive, or be in the wrong direction. If the search process for compatible ϵ_i shows that the tube does not contact the baffle hole in either positive or negative direction, then the natural inference for an intermediate displacement would require that the corresponding T_i be zero. Following the foregoing logical steps, an appropriate solution algorithm can be derived to determine the correct lateral displacements.

It is of some interest to observe that the solution is greatly complicated by the incorporation of clearances at TL baffle supports. The complication will proportionately increase if clearances at other baffle locations are also introduced. These, however, will have a much weaker influence on the U-bend stress field.

We note that the rotational stiffnesses developed in the preceding section are based on a two-span beam model. Additional beam spans can be accounted for by modifying Eqs. (14.2.18) and (14.2.19). However, such refinements do not add much to the accuracy of the results.

Having determined the principal unknowns in the problem, the stress field in the U-tube is found from static equilibrium. As noted previously, the moment M and direct force N at a point A (Figs. 14.2.1-2) are given by:

$$M = M_2 + R(S_2 + r \sin\theta) + Pr(1 - \cos\theta) \quad (14.3.2a)$$

$$N = P \cos\theta - R \sin\theta \quad (14.3.2b)$$

The maximum bending stress due to M is given by:

$$\sigma_b = \frac{\psi M c_0}{I} \quad (14.3.3)$$

where ψ is the meridional stress concentration factor associated with ovaling of thin walled cross sections. A widely accepted expression for ψ , due to Rodabaugh, et al. [14.2.4], is given below:

$$\psi = \frac{\psi_0}{1 + \frac{13 p c_m}{4 E t} \left(\frac{c_m}{t}\right)^{3/2} \left(\frac{r}{c_m}\right)^{2/3}} \geq 1 \quad (14.3.4)$$

with ψ_0 defined as

$$\psi_0 = \frac{0.9}{\left(\frac{tr}{c_m^2}\right)^{2/3}} \quad (14.3.5)$$

We must point out here that the foregoing expression for ψ yields values which are almost one half of the theoretical value derived by Clark and Reissner [14.3.1], and later refined by Cheng and Thailer [14.3.2]. The maximum stress σ_b (Eq. (14.3.3)) is a circumferential bending stress which occurs at the tube cross-section centroidal axis transverse to the plane of bending. Thus, the longitudinal stress intensification factor is not required to compute the peak stress intensity. To perform a complete stress analysis, however, expressions for the stress intensification factors as a function of the meridional angle (as derived in Ref. [14.3.2]) may be used. As mentioned before, these theoretical expressions for ψ are nearly twice as large as that given by the widely used formula of Rodabaugh, et al.

14.4 AN EXAMPLE

To illustrate the solution technique and to study the effect of major design parameters, we consider a typical U-tube having 0.75 in. O.D., 16 B.W.G. (0.065 in.) wall, 1.25 in. bend radius, 100 in. long straight legs, and subject to an inter-leg differential expansion δ equal to 0.05 in. The radial expansion of the U-bend is taken as 0.002 in., and the Young's Modulus of the tube material is assumed to be 30×10^6 psi.

As a basic configuration, we assume that $a_i = b_i = 10$ in., $\xi_i = 0$, and $S_i = 1$ in. ($i = 1, 2$). The effect of variation of a_i , b_i , S_i , tube radius r , tube wall, and baffle location clearances ξ_i on the stress field in the tube will be studied. The object here is to identify those parameters which are most effective in reducing tube bending stress. The program "UBAX", described later, is used to generate these results.

The bending stress in the U-bend as a function of angular orientation θ is shown in Fig. 14.4.1 (Case A). Curves B and C correspond to overhang dimensions $S_i = 0$ and 2 in., respectively. Note that the bending stress is a rather strong function of S_i . Providing a 2 inch overhang on both legs of the U reduces the maximum bending stress by over 40 percent in comparison to zero overhang. The location of the maximum bending stress also shifts as S_i is changed. By considering equilibrium of the curved segment, it can be shown that σ_{\max} will occur at either $\theta = 0, \pi$ or $\theta > \pi/2$. Referring to Fig. 14.2.2, we again write down the moment M at an angular location θ .

$$M = M_2 + R(S_2 + r \sin\theta) + Pr(1 - \cos\theta) \tag{14.4.1}$$

For an extremum, we require that

$$\frac{\partial M}{\partial \theta} = 0 \rightarrow Rr \cos\theta^* + Pr \sin\theta^* = 0$$

$$\text{or } \theta^* = \tan^{-1}\left(\frac{-R}{P}\right) \tag{14.4.2}$$

where θ^* defines the candidate location for maximum bending stress.

Furthermore, for a maximum

$$\frac{\partial^2 M}{\partial \theta^2} < 0$$

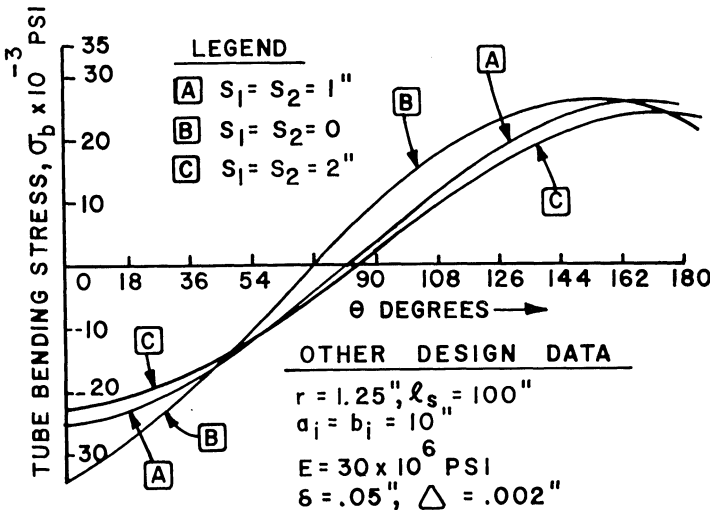


Fig. 14.4.1. Variation of circumferential bending stress with angular orientation.

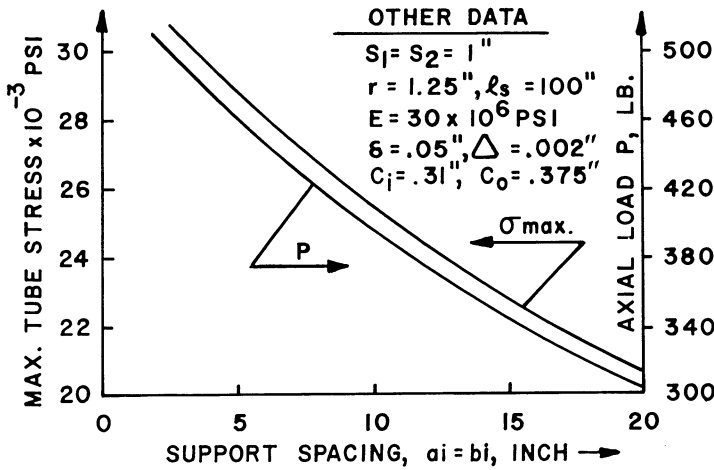


Fig. 14.4.2. Maximum tube stress σ_{max} and axial load P vs. support spacing.

which implies

$$P \cos\theta - R \sin\theta < 0 \tag{14.4.3}$$

In the above equation, θ is measured from the tangent line of the leg in tension, i.e., P is assumed always to be positive. Two conditions may exist:

a. Positive R : This means (Eq. (14.4.2)) that θ^* will lie in the second quadrant, i.e., $\pi/2 < \theta < \pi$.

Inequality (14.4.3) yields:

$$\tan\theta < \frac{P}{R} \text{ at } \theta = \theta^*$$

Substituting for $\tan\theta^*$, gives the requirement for a maximum to be $P^2 > -R^2$.

This requirement is obviously satisfied for all R and P . Therefore, θ^* defines the location of maximum bending stress.

b. Negative R : Eq. (14.4.2) requires that the maximum lie in the first quadrant, i.e., $\theta < \pi/2$. Inequality (14.4.3) yields:

$$\tan\theta > \frac{P}{R} \text{ at } \theta = \theta^*$$

which implies that $P^2 < -R^2$.

This condition obviously cannot be satisfied. Hence negative R implies that the maximum tube bending stress must occur at the boundary; i.e., at $\theta = 0$ or $\theta = \pi$.

Finally, it is apparent that stresses in the U-bend can be optimized by adjusting S_1 and S_2 to make the stress variation as closely symmetrical with respect to $\theta = \pi/2$ as possible.

Table 14.4.1 shows principal quantities of interest for some selected values of ξ_1 and ξ_2 . The remainder of the design data corresponds to the basic configuration. The maximum tube stress σ_{max} and tube axial load P

are seen to be rather weakly dependent on ϵ_i . This indicates that the baffle clearance at the tangent line baffle has a limited influence in mitigating tube bend stresses in typical geometries.

Table 14.4.1. Maximum Tube Stress, Axial Load, Support Reactions Versus Clearance at the Tangent Line Baffle

ξ_1 in.	ξ_2 in.	P lb.	T_1 lb.	T_2 lb.	Max. Tube Stress, σ_{\max} psi
0	0	391.4	14.7	137.1	25600
-.004	.008	376.8	-67.9	45.3	24916
-.008	.012	367	-64.9	42.3	24280
-.022	.025	334	-32.9	53.9	22016

Figure 14.4.2 shows the variation of σ_{\max} and P with a_i and b_i (assumed equal). Both curves are convex to the origin indicating that σ_{\max} and P increase rapidly at small support spacings. It is clear that baffle spacings have a marked effect on σ_{\max} and P . Increasing a_i and b_i from 10 in. to 20 in. decreases σ_{\max} by over 23 percent. However, there are practical limitations on the baffle spacings due to consideration of heat transfer, flow induced vibration, etc. Noting that the axial load produces tensile stresses in one leg and compressive stresses in another, the baffle spacings in the tension leg can be made larger than the compression leg while maintaining the same factor of safety against flow induced vibration. In general, adjusting a_i and b_i provides an effective tool to generate a favorable stress field in the U-tube.

Another design parameter with a profound influence in the U-bend stress field is the bend radius r . Generally r can be increased without such limitations as accompany the baffle spacings. The only drawback in increasing r is the reduction in the number of tubes that can be assembled in a given tubesheet size. Figure 14.4.3 shows σ_{\max} and P as a function of r . Both curves are convex to the origin indicating that the tube stresses rise rapidly with a decrease in the bend radius.

Table 14.4.2 contains some representative results for 3/4 in. and 5/8 in. tubing for three different tube gages. It is to be noted that the maximum tube bending stresses increase with reduction in tube wall for 3/4 in. tubing. This is contrary to the general experience with thermal induced stresses. However, this paradox is explained by noting that the tube stress intensification factor ψ is increased with reduction in the tube wall. Thus, as the tube wall is decreased, the bending stresses are boosted by virtue of the increase in ψ and reduced by the increase in the flexibility of the system. This suggests the possibility of an optimum thickness. Observing the results for 5/8 in. tubing, we note that an optimum does indeed exist for this tube size in the reported range of tube gages in Table 14.4.2. The stresses corresponding to 18 BWG are the lowest. In general, the tube bending

stresses will increase with reduction in the tube wall in the most common working range of tube wall thickness. It should be emphasized, however, that using a smaller diameter tubing will always reduce the maximum stress as demonstrated by the numerical results in Table 14.4.2.

Table 14.4.2. Maximum Tube Stress σ_{\max} , Support Reactions T_i , and Axial Load P , Versus Tube O.D. and Gage

		Tube Dimensions		T_1 lb	T_2 lb	P lb	σ_{\max} psi
Size	Outer Rad. in.	Inner Rad. in.					
3/4 in.	16 BWG	.375	.31	14.74	137.1	391.4	25550
	18 BWG	.375	.326	8.9	98.	285.2	29305
	20 BWG	.375	.34	5.9	64.8	188.6	33515
5/8 in.	16 BWG	.3125	.2475	9.2	93.3	269.	23700
	18 BWG	.3125	.2635	4.3	67.	200.6	23310
	20 BWG	.3125	.2775	2	44.5	136.	27180

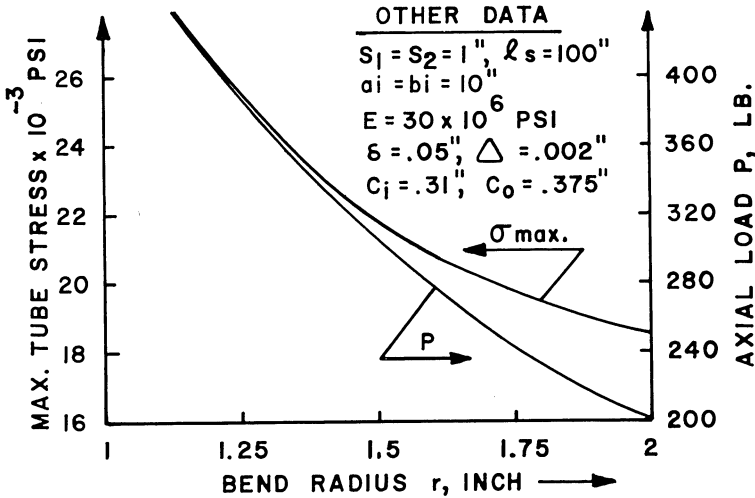


Fig. 14.4.3. Maximum tube stress σ_{\max} and axial load P vs. bend radius.

14.5 DISCUSSION

We have shown, via a numerical example, that the U-bend stresses can reach high magnitudes in commonplace designs. Some design strategies to alleviate the U-bend stress have been examined in depth. The effect of overhang span S_i on the tube stress is found to be considerable. On the other hand, baffle clearances ξ_i at the TL baffle do not appreciably reduce the stress level in the tube in our example problem. Among other design parameters having a pronounced effect on the bend stress, tube O.D. and bend radius deserve special attention. Both parameters are found to have an important influence on the peak bending stress.

The example problem indicates that the maximum tube bending stress can increase with increased tube gage for 3/4 in. tubing (Table 14.4.2). This conclusion is at variance with the characteristics responses of structures to thermal loadings. Increased structural flexibility is generally expected to reduce the maximum stress in the system. This discrepant behavior of the U-tube is explained by noting that the stress intensification factor ψ rapidly increases with reduction in the tube wall. Thus even though the net internal moment is reduced by increased tube flexibility, the bending stress may sustain a net increase due to the effect of the stress intensification factor. For some geometries, an optimum gage may exist which minimizes the bending stress.

In addition to these geometric parameters, other design alternatives to reduce the U-bend stress should be explored. For example, arranging more passes in the tubeside will decrease the net temperature change in any pair of passes, thus reducing δ . U-tubes in various passes can also be made of different length to reduce δ in the most critical pair of tube passes connected by U-tubes. Shell-side flow arrangement also has a bearing on the U-bend differential expansion problem. It can be shown that subjecting both legs of a U-tube to the same shell stream will result in a smaller δ than the configuration where the two legs are in contact with two different shell streams. Thus the U-tube differential expansion in a one shell pass-two tube pass exchanger will be less than that in a two-tube-two shell pass exchanger, for an otherwise identical geometry. Heat transfer aspects must be studied in conjunction with the structural problem to devise the most suitable design in a given situation.

14.6 A PRACTICAL DESIGN FORMULA

Our study of the numerical example problem in the preceding section indicates that the baffle hole clearance has little effect on the maximum tube bending stress. Therefore, assuming zero clearance $\xi_1 = \xi_2 = \epsilon_1 = \epsilon_2 = \Delta = 0$ should have a negligible impact on the solution. We will also assume that the baffle spacing is uniform throughout, i.e., $a_1 = a_2 = b_1 = b_2 = d$. Finally, the less important components of the strain energy; namely, those due to direct and shear stresses are neglected. These assumptions simplify the algebra considerably. With these simplifications, the task of evaluating the axial force P and lateral shear R for a specified inter-leg differential expansion δ is reduced to the following simple steps.

- (i) Compute the ratio of effective inertias of the bend and the straight regions.

$$\rho = \frac{I'}{I} = \frac{2y_0 r}{c_m^2 \lambda}$$

- (ii) Evaluate the following quantities:

$$B_{11} = \frac{24}{7d} \left(\frac{\pi r^2}{\rho} + 2rS_1 + \frac{7dr}{12} \right)$$

$$B_{12} = \frac{1}{EI} \left[\frac{r^2}{\rho} (\pi S_2 + 2r) - S_1 r (S_1 - 2S_2) - \frac{7rd}{12} (S_1 - S_2) \right]$$

$$B_{13} = \frac{r^2}{EI} \left[\frac{3\pi r}{2\rho} + 4S_1 + \frac{7d}{6} \right] + \frac{2l_s}{EA}$$

$$B_{21} = \frac{24}{7d} \left[\frac{(\pi S_2 + 2r)r}{\rho} - \frac{(S_1 - S_2)^2 - 2S_2^2}{2} - \frac{7(S_1 - S_2)d}{24} \right]$$

$$B_{22} = \frac{r}{\rho EI} \left\{ S_2 (\pi S_2 + 2r) + r \left(\frac{\pi r}{2} + 2S_2 \right) \right\} \\ + \frac{1}{3EI} \left\{ (S_1 - S_2)^3 + 2S_2^3 \right\} + \frac{7(S_1 - S_2)^2 d}{24EI}$$

$$B_{23} = \frac{r^2}{\rho EI} (\pi S_2 + 2r) - \frac{rS_1}{EI} (S_1 - 2S_2) - \frac{7dr(S_1 - S_2)}{12EI}$$

$$B_{31} = 2 + \frac{24(S_1 + S_2)}{7d} + \frac{24\pi r}{7d\rho}$$

$$B_{32} = \frac{1}{2EI} \{ 2S_2^2 - (S_1 - S_2)^2 \} + \frac{r}{\rho EI} (\pi S_2 + 2r) - \frac{7d(S_1 - S_2)}{24EI}$$

$$B_{33} = \frac{\pi r^2}{\rho EI} + \frac{7dr}{12EI} + \frac{2rS_1}{EI}$$

(iii) The following quantities are defined in terms of the previously computed B_{ij} .

$$x = B_{23}B_{31} - B_{21}B_{33}$$

$$y = B_{22}B_{31} - B_{21}B_{32}$$

$$z = B_{13}B_{31} - B_{11}B_{33}$$

$$w = B_{12}B_{31} - B_{11}B_{32}$$

(iv) The axial force P and lateral shear R are then given by

$$P = \frac{-B_{31}y\delta}{wx - yz}$$

$$R = \frac{B_{31}x\delta}{wx - yz}$$

(v) Evaluate K_2 from Eq. (14.2.23); and ψ from Eq. (14.3.4).

(vi) Having evaluated P and R , the bending moment at any angular

location θ (Point A in Fig. 14.2.1) is given by Eq. (14.3.2a); and the associated bending stress is given by Eq. (14.3.3).

The above steps provide a computation procedure which can be easily carried out on a manual or programmable calculator.

14.7 COMPUTER PROGRAM UBAX

Computer program UBAX computes the bending and direct stresses in the tube overhang and U-bend regions due to a specified inter-leg differential thermal expansion δ . The leg in compression is labelled as leg 1. The U-bend radius is also assumed to have increased by Δ due to temperature rise. The input data is explained in Table 14.7.1. The program permits the specification of radial clearances EPS1 and EPS2 at “tangent line” baffle locations. A positive value of EPS1 means that the clearance is available in leg 1 in the positive y -direction (Fig. 14.2.3). A positive value of EPS2 means that the clearance is available in leg 2 in the negative y -direction. The program assumes that the tube has moved to take up the available clearances. The net baffle reactions T_i at the “tangent line” baffles are printed-out. If the ratio of the baffle reaction to the specified clearances is not positive or zero, then the solution is not admissible. In such a case, the values of EPS1 and EPS2 should be revised and the program rerun. Such iteration steps are not required if both EPS1 and EPS2 are set equal to zero (linear problem).

Table 14.7.1. Input Data for Program UBAX: All Input is in Free Field Format

Line 1: Heading Card			
Line 2:	Quantity	Mathematical Symbol	Fortran Symbol
	Overhang of leg one (Fig. 14.2.2)	S_1	S1
	Overhang of leg two (Fig. 14.2.2)	S_2	S2
	Straight length of tube leg (Fig. 14.2.1)	l_s	ELL
	Second Baffle Spacing of leg 1 (Fig. 14.2.3)	a_1	A1
	Second Baffle spacing of leg 2 (Fig. 14.2.3)	a_2	A2
	Last baffle spacing in leg 1 from U-bend end support (Fig. 14.2.1)	b_1	B1
	Last baffle spacing in leg two for U-bend end support	b_2	B2
	U-bend mean radius	r	R
	Young's Modulus of tube material	E	E
	Inside radius of tube cross section annulus	c_i	AR
	Outside radius of tube cross section annulus	c_o	BR
Line 3	Quantity	Mathematical Symbol	Fortran Symbol
	Free thermal expansion of leg 1 over leg 2	δ	DELTA
	Available radial clearance at tangent line baffle in leg 1 in positive y -direction	ξ_1	EPS1
	Available radial clearance at tangent line baffle in leg 2 in negative y -direction	ξ_2	EPS2
	Increase in U-bend mean radius due to its temperature rise	Δ	DEL

PROGRAM UBAX

```

C -----
C COMPUTER PROGRAM UBAX, REV 0
C BY K.P. SINGH, JAN 1983
C COMPUTES TUBE STRESSES IN U-BENDS DUE TO THERMAL EXPANSION
C -----
C FORTRAN VARIABLES:
C ***INPUT LIST : INPUT ALL DATA IN CONSISTENT UNITS***
C TITLE : TITLE FOR RUN, ANY ALPHANUMERIC 80 CHARACTERS LONG
C S1 : OVERHANG OF LEG ONE
C S2 : OVERHANG OF LEG TWO
C ELL : STRAIGHT LENGTH OF TUBE LEG
C A1 : BAFFLE SPACING OF LEG ONE
C A2 : BAFFLE SPACING OF LEG TWO
C B1 : SECOND BAFFLE SPACING IN LEG ONE FROM U-BEND END
C B2 : SECOND BAFFLE SPACING IN LEG TWO FROM U-BEND END
C R : U-BEND MEAN RADIUS
C E : YOUNG'S MODULUS OF TUBE MATERIAL
C AR : INSIDE RADIUS OF TUBE CROSS-SECTION ANNULUS
C BR : OUTSIDE RADIUS OF TUBE CROSS-SECTION ANNULUS
C DELTA: FREE THERMAL EXPANSION OF LEG ONE OVER LEG TWO
C EPS1 : AVAILABLE RADIAL CLEARANCE AT TANGENT LINE
C BAFFLE IN LEG ONE
C EPS2 : AVAILABLE RADIAL CLEARANCE AT TANGENT LINE
C BAFFLE IN LEG TWO
C DEL : INCREASE IN U-BEND MEAN RADIUS DUE TO ITS
C TEMPERATURE RISE
C *****
DIMENSION TITLE(20)
COMMON/ONE/E,AMOM
COMMON/TWO/BR,AR,Z,R
READ(5,5) (TITLE(I),I=1,20)
5 FORMAT(20A4)
WRITE(6,6) (TITLE(I),I=1,20)
6 FORMAT(6X,20A4)
READ(5,*) S1,S2,ELL,B1,B2,A1,A2,R,E,AR,BR
TOL= .001
RM=.5*(AR+BR)
WRITE(6,705)
WRITE(6,701)
READ(5,*) DELTA,EPS1,EPS2,DEL
WRITE(6,700) S1,S2,ELL,ELL,B1,B2,A1,A2,DELTA,EPS1,EPS2,
1 R,E,AR,BR,DEL
EL1 = A1+B1
EL2 = A2+B2
PI = 3.14159
AREA=PI*(BR*BR-AR*AR)
AMOM=.25*PI*(BR**4-AR**4)
AK1=E*AMOM/((2*B1+EL1)/3.-(3*EL1-A1)*(2*EL1+B1)/(12*EL1))

```

```

AK2=E*AMOM/((2*B2+EL2)/3.-(3*EL2-A2)*(2*EL2+B2)/(12*EL2))
Z = -1.+(2.*R*(SQRT(R*R-AR*AR) -SQRT(R*R-BR*BR))/(BR*BR-AR*AR))
YO = Z*R/(Z+1.)
AMOMP = AREA*YO*R*R*(BR-AR)/(1.65*RM*RM)
DO 100 I=1,20
A11 = AK2*((PI*R*R/(E*AMOMP)) + (2.*R*S1/(E*AMOMP))
++(2.*R/AK1))
A12 = (R*R*(PI*S2 +2.*R) / (E*AMOMP)) - (R*S1*(S1-2.*S2)
+ / (E*AMOMP)) - (2*R*(S1-S2)/AK1) - (2*R/(E*AREA))
A13 = R*R*((3.*PI*R/(2.*E*AMOMP)) + (4.*S1/(E*AMOMP))
++(4. /AK1)) + (2.*ELL-.5*PI*R+2.6*PI*R) / (E*AREA)
A21 = AK2*(R*(PI*S2 +2.*R) / (E*AMOMP) -.5*((S1-S2)**2 -
+2*S2*S2)/(E*AMOM) - (S1-S2)/AK1) - (2*AK2/(E*AREA))
A22 = R*(S2*(PI*S2+2*R) + R*(.5*PI*R +2.*S2))/(E*AMOMP)
++((S1-S2)**3 + 2.*S2**3) / (3.*E*AMOM) + (S1-S2)*(S1-S2)/AK1
- (PI*R*.5 +4.*S2-2.6*PI*R - (S1+S2)*5.2)/(E*AREA)
A23 = R*R*(PI*S2+2.*R) / (E*AMOMP) - R*S1*(S1-2.*S2) / (E*AMOM)
+ -2.*R*(S1-S2)/AK1 - (2.*R/(E*AREA))
A31 = 1.+(AK2/AK1) + (AK2*(S1+S2)/(E*AMOM)) + (AK2*PI*R
+/(E*AMOMP))
A32 = (.5*(2.*S2*S2 - (S1-S2)*(S1-S2)) / (E*AMOM))
++ (R*(PI*S2+2.*R)/(E*AMOMP)) - ((S1-S2)/AK1) - (2./ (E*AREA))
A33 = (PI*R*R/(E*AMOMP)) + (2.*R/AK1) + (2.*R*S1/(E*AMOM))
B12 = A13-A11*A33/A31
B11 = A12-A11*A32/A31
B21 = A22-A21*A32/A31
B22 = A23-A21*A33/A31
D = B11* B22-B12*B21
RF = (DELTA*B22-B12*(2.*DEL-EPS1-EPS2))/D
P = (B11*(2.*DEL-EPS1-EPS2) -B21*DELTA)/D
ALF2=- (A32*RF+A33*P)/A31
ALF1 = (AK2*ALF2 +2.*P*R-RF*(S1-S2))/AK1
CALL STRAIT(EPS1,A1,B1,ALF1,AK1,AKC1,V1)
CALL STRAIT(EPS2,A2,B2,ALF2,AK2,AKC2,V2)
ER1 = ABS((AK1-AKC1)/AK1)
ER2 = ABS((AK2-AKC2)/AK2)
IF(ER1.LT. TOL .AND. ER2 .LT. TOL) GOTO 200
AK1=.5*(AK1+AKC1)
100 AK2=.5*(AK2+AKC2)
WRITE(6,706)
STOP
200 T1=RF-V1
T2 = (RF-V2)
IF(EPS1 .EQ. 0. .AND. EPS2 .EQ. 0.)GO TO 300
RATIO1=T1/EPS1
RATIO2=T2/EPS2
IF(RATIO1.LT.0 .OR. RATIO2.LT.0)GO TO 400
300 AM1=ALF1*AK1
I=1
WRITE(6,708)I
CALL STRESS(A1,B1,S1,AM1,V1,-P,RF,1)

```

```

AM2=ALF2*AK2
I=2
WRITE(6,708)I
CALL STRESS(A2,B2,S2,AM2,V2,P,RF,2)
1000 STOP
400 WRITE(6,709) RATIO1,RATIO2
STCP
700 FORMAT(4X,"TANGENT LINE TO LAST BAFFLE = S",2(3X,F7.4),/,4X,
+ "STRAIGHT TUBE LENGTH = LS",6X,2(5X,F5.1),/,4X,
+ "LAST BAFFLE SPACE = B",10X,2(5X,F5.2),/,4X,
+ "NEXT TO LAST BAFFLE SPACE = A ",2(5X,F5.2),/,4X,
+ "DIFFERENTIAL THERMAL EXPANSION",8X,3X,F7.5,/,4X,
+ "MAX. ALLOWABLE OUTWARD DISPLACEMENT"/4X,
+ "AT TANGENT LINE = EPS",14X,F7.5,3X,F7.5//4X
+ "U-BEND RADIUS = ",T32,F7.3,/,4X,"YOUNG'S MODULUS = ",
+ T31,E12.3,/,4X,"TUBE INNER RADIUS = ",T34,F5.3,/,4X,
+ "TUBE OUTER RADIUS = ",T34,F5.3/4X,"RADIAL EXPANSION OF UBEND="
+ ,T34,F7.5)
701 FORMAT(/,T41,"LEG 1",T51,"LEG 2",/)
705 FORMAT(1H0,5X,"***TUBE STRESSES DUE TO THERMAL GROWTH***")
706 FORMAT(1H0,"***NO CONVERGENCE***")
708 FORMAT(/,7X,"S T R E S S E S   I N   L E G ",I1,/,
1 4X," X      BENDING    TENSILE    TOTAL",/)
709 FORMAT(1H0,5X,"T1/EPS1 =",F12.3,5X,"T2/EPS2 =",F12.3/
+6X,"INCOMPATIBLE CLEARANCES!;CALCULATION STOPPED!")
END
SUBROUTINE STRAIT(EPS,A,B,ALFA,AK,AKC,V)
COMMON/ONE/E,AMOM
EI = E*AMOM
EL = A+B
RO1 = (((2.*B+EL)/3.)-((3.*EL-A)*(2.*EL+B)/(12.*EL)))/EI
RO2 = (3.*EL-A)/(2.*EL*B)*EPS
AKC = (1./RO1) + (RO2/(ALFA*RO1))
V=(3.*(EI*EPS+AK*ALFA*B*(2.*EL+B)/6.)/(EL*B*B))
RETURN
END
SUBROUTINE STRESS(A,B,S,AM,V,P,RF,ICASE)
COMMON/ONE/E,AMGM
COMMON/TWO/BR,AR,Z,R
PI=3.14159
ZSI=BR/AMOM
RM=.5*(AR+BR)
AREA=PI*(BR*BR-AR*AR)
T2=- (AM/A)+(V*(A+B)/A)
T3=V-T2
SIGD=P/AREA
DO 10 I=1,6
X=(I-1)*.2*A
AMX=T3*X
SIGB=AMX*ZSI
SIGT=ABS(SIGB)+ABS(SIGD)
WRITE(6,800) X,SIGB,SIGD,SIGT

```

```

10 CONTINUE
  DO 20 I=7,11
    X=A+.2*(I-6)*B
    AMX=T3*X+T2*(X-A)
    SIGB=AMX*ZSI
    SIGT=ABS(SIGB)+ABS(SIGD)
    WRITE(6,800)X,SIGB,SIGD,SIGT
  20 CONTINUE
    DO 30 I=12,16
      X=A+B+(I-11)*.2*S
      AMX=AM+RF*(X-A-B)
      SIGB=AMX*ZSI
      SIGT=ABS(SIGB)+ABS(SIGD)
      WRITE(6,800)X,SIGB,SIGD,SIGT
    30 CONTINUE
      IF(ICASE.EQ.1)GO TO 100
      H=(BR-AR)*R/RM**2
      PSI=.9/H** .6666667
      IF(PSI .LT. 1.)PSI=1.
      WRITE(6,820)
      DO 40 I=16,26
        THETA=(I-16)*PI*.1
        DEG=THETA*180./PI
        AMX=AM+RF*(S+R*SIN(THETA))+P*R*(1-COS(THETA))
        AN=P*COS(THETA)-RF*SIN(THETA)
        SIGB=AMX*PSI*ZSI
        SIGD=AN/AREA
        SIGT=ABS(SIGB)+ABS(SIGD)
        WRITE(6,810)DEG,SIGB,SIGD,SIGT
      40 CONTINUE
      800 FORMAT(4X,F7.3,3(3X,F7.0))
      810 FORMAT(4X,F6.0,3(3X,F7.0))
      820 FORMAT(///,10X,"STRESSES IN U-BEND REGION",//,
        1 4X," DEG      BENDING      TENSILE      TOTAL",/)
100 RETURN
  END

```

NOMENCLATURE

- a_i, b_i , etc. = Baffle spacings (Fig. 14.2.1)
 A = Cross-sectional area of tube metal
 c_i, c_o = Inner and Outer radius of the tube, respectively
 c_m = Mean radius of tube
 d = Uniform spacing between support locations (Section 14.6)
 E = Young's modulus of tube material
 G = Shear modulus of tube material
 I = Plane moment of inertia of tube cross section
 K_i = Rotational spring constant ($i = 1, 2$)
 l_i = Sum of a_i and b_i (Fig. 14.2.3)
 l_s = Straight length of tube leg (Fig. 14.2.1)
 M = Bending moment at a generic point in the U-tube

- N = Axial tension at a generic point in the U-tube
 P = Axial force
 p = Internal pressure
 R = Lateral shear at overhang baffle support locations
 r = Mean bend radius
 S_i = Overhang of leg i ($i = 1, 2$ – Fig. 14.2.1)
 T_1, T_2 = Support point reactions at TL Baffle location (Fig. 14.2.3)
 t = Tube wall thickness
 U = Gross strain energy in the freebody (Fig. 14.2.2)
 V = Lateral shear at a generic point in the U-tube
 y_0 = Distance between the neutral and centroidal axes in the U-bend region (Eq. (14.2.6))
 α_1, α_2 = Rotation of tube legs at points O_1 and O_2 , respectively (Fig. 14.2.2)
 δ = Free thermal expansion of leg 1 over leg 2 (Fig. 14.2.1)
 Δ = Increase in radius r of the bend due to its temperature rise
 θ = Angular orientation of Point A in the curved region (Fig. 14.2.2)
 θ^* = Location of maximum bending stress
 λ = Flexibility factor
 ϵ_i = Outward displacement of leg i at TL baffle location (Fig. 14.2.3)
 ψ = Stress intensification factor for the U-bend
 ξ_1, ξ_2 = Available clearance at TL baffle in leg in positive and negative y -directions, respectively
 σ_{\max} = Maximum tube stress in the bend region

REFERENCES

- [14.2.1] “Standards of Tubular Exchanger Manufacturers Association,” Sixth edition, p. 27, TEMA, Inc., Tarrytown, New York (1978).
 [14.2.2] Sokolnikoff, I. S., “Mathematical Theory of Elasticity,” Second Edition, McGraw-Hill, New York, p. 394, (1956).
 [14.2.3] Seely, F. B., and Smith, J. O., “Advanced Mechanics of Materials,” Second Edition, Wiley, New York, p. 665 (1965).
 [14.2.4] Rodabaugh, E. C., and George, H. H., “Effect of Internal Pressure on Flexibility and Stress-Intensification Factors of Curved Pipe or Welding Elbows,” Pressure Vessel and Piping Design, Collected Papers 1927–1959, ASME, pp. 467–476, (1960).
 [14.3.1] Clark, R. A., and Reissner, E., “Bending of Curved Tubes,” Advances in Applied Mechanics, Vol. 2, Academy Press, New York, pp. 93–122 (1951).
 [14.3.2] Cheng, D. H., and Thailer, H. J., “On Bending of Curved Tubes,” Pressure Vessels and Piping: Design and Analysis, Vol. 2, ASME, New York, pp. 1175–1179, (1972).

APPENDIX 14.A

ELEMENTS OF (B) MATRIX

$$B_{11} = \left(\frac{\pi r^2}{EI'} + \frac{2rS_1}{EI} + \frac{2r}{K_1} \right) K_2$$

$$B_{12} = \frac{r^2}{EI'} (\pi S_2 + 2r) - \frac{rS_1}{EI} (S_1 - 2S_2) - \frac{2r}{K_1} (S_1 - S_2) - \frac{2r}{EA}$$

$$B_{13} = r^2 \left\{ \frac{3\pi r}{2EI'} + \frac{4S_1}{EI} + \frac{4}{K_1} \right\} + \frac{1}{EA} \left(2l_s - \frac{\pi r}{2} \right) + \frac{\Phi \pi r}{2GA}$$

$$B_{21} = \left[\frac{(\pi S_2 + 2r)r}{EI'} - \frac{1}{2EI} \{ (S_1 - S_2)^2 - 2S_2^2 \} - \frac{2}{EA} - \frac{(S_2 - S_2)}{K_1} \right] K_2$$

$$B_{22} = \frac{r}{EI'} \left\{ S_2 (\pi S_2 + 2r) + r \left(\frac{\pi r}{2} + 2S_2 \right) \right\} \\ + \frac{1}{3EI} \{ (S_1 - S_2)^3 + 2S_2^3 \} \\ + \frac{(S_1 - S_2)^2}{K_1} - \frac{\pi r}{2EA} - \frac{4S_2}{EA} + \frac{\Phi \pi r}{2AG} + \frac{\Phi (S_1 + S_2)}{GA}$$

$$B_{23} = \frac{r^2}{EI'} (\pi S_2 + 2r) - \frac{rS_1}{EI} (S_1 - 2S_2) - \frac{2r(S_1 - S_2)}{K_1} - \frac{2r}{EA}$$

$$B_{31} = 1 + \frac{K_2}{K_1} + \frac{K_2(S_1 + S_2)}{EI} + \frac{K_2 \pi r}{EI'}$$

$$B_{32} = \frac{1}{2EI} \{ 2S_2^2 - (S_1 - S_2)^2 \} + \frac{r}{EI'} (\pi S_2 + 2r) - \frac{(S_1 - S_2)}{K_1} - \frac{2}{EA}$$

$$B_{33} = \frac{\pi r^2}{EI'} + \frac{2r}{K_1} + \frac{2rS_1}{EI}$$

$$I' = Ay_0 r / \lambda$$

15. EXPANSION JOINTS

15.1 INTRODUCTION

Differential longitudinal expansion between the shell and the tube bundle is a well known problem in fixed tubesheet heat exchanger design. The differential expansion occurs from two sources: (a) temperature; and (b) pressure. Temperature induced differential growth warrants no further explanation. Its presence is directly related to the *raison d' être* of the exchanger. The effect of pressure induced differential growth, often overlooked in practical design work in fixed tubesheet exchangers, has been analyzed in Chapter 9. In physical terms, the mismatch in the axial deformation of the shell and tube bundle is caused by the difference in the state of their pressure loadings. The shell is under an internal pressure p_s , whereas the tubes are subject to a net external pressure of $(p_s - p_t)$. In simple terms, if $p_s > p_t$, then the Poisson effect will cause the shell to shrink, and the tubes to expand, resulting in a net differential expansion. A more complete accounting of the pressure induced differential expansion requires consideration of axial forces in the tubes and in the shell, consideration of the deflection profile of the tubesheet, etc. Such a complete analysis has been presented in Chapter 9, where a method for incorporating the presence of an expansion joint is also described. In the scheme of the overall stress analysis, the only quantity required to characterize the behavior of the expansion joint is its "spring rate," defined as the axial pull per unit circumference of the shell divided by the axial spread of the joint and has the units of force per square linear dimension (e.g., pounds per square inch). The mechanical design of the heat exchanger should, however, not be confined to the evaluation of spring rate alone. The expansion joint forms the pressure boundary, sometimes the most vulnerable one, in a heat exchanger. Its fragility arises from the fact that it must be made "flexible" to alleviate differential expansion induced stresses. It is difficult to build-in flexibility and ruggedness in the same component. Indeed, the first question in the selection of the expansion joint centers around the question of the optimum blend of flexibility, ruggedness, and economy required in the actual application. At present, the governing safety codes provide little guidance in the matter. The ASME Code tackles the issue in Code Case 1177-7 which states that the requirements of U-2 (g) of Section VIII of the Boiler and Pressure Vessel Code be satisfied. In this manner the Code recognizes the use of any rational stress analysis of expansion joints. The above referenced Code case also recognizes that expansion joints cannot normally be designed such that the combination of direct, local membrane

and secondary bending stresses is below the Code tabulated allowable stress. An ASME working group [15.1.1] is presently developing a set of design rules for expansion joints.

Over the years, many practical forms of heat exchanger expansion joints have been developed. A brief description of the available types is presented in the next section. Methods to compute the spring rate and the stress field in the expansion joint, with appropriate reference to prior work and current design practice, are given in subsequent sections. An overview of some practical methods for evaluating the cycle life of expansion joints is also presented.

Although the foregoing introduction is entirely focused on fixed tubesheet exchangers, this is not to imply that expansion joints are exclusively used in fixed tubesheet designs. In single pass floating heat exchangers, the expansion joint is located in the pipe between the floating head cover and the shell cover to enable differential thermal expansion between the tube bundle and the shell. Expansion joints are also widely utilized in piping runs to alleviate thermal expansion stresses.

15.2 TYPES OF EXPANSION JOINTS

Expansion joints may be broadly classified in two categories; (i) formed head; and (ii) formed membrane. A brief description of each style follows.

(i) *Formed head:* This type is made by welding together two specially formed heads. Figure 15.2.1 shows two “flanged and flued heads” welded together. A “flanged and flued head” consists of: (a) an outer shell; (b) two outer tori (flange); (c) two annular plates; (d) two inner tori (flue); and (e) two inner shells with butt weld to the two portions of the heat exchanger shell. The inner and outer tori serve to mitigate the severity of geometric discontinuities between plate and shell type members. The annular plate contributes significantly to lowering the spring rate. The radii of the tori are seldom made less than three times the expansion joint thickness. The thickness of the expansion joint is governed by the pressure and temperature loadings. Since the ASME Codes do not give formulas for sizing expansion joint thickness, empirical design practice in the industry commonly sets the flanged and flued expansion joint thickness equal to (or one “gage” less than) the shell thickness. Thus, this type of expansion joint is quite rugged and not very flexible. The joint is also quite economical to fabricate. Where the flexibility requirement is rather feeble, further economy can be realized by eliminating the annular plate (and the outer cylindrical shell resulting in the semi-torus construction (Fig. 15.2.2). Another variation is the so-called “flanged only” joint produced by eliminating the inner torus. Figure 15.2.3 shows three variations. In type (a), the corner weld between the expansion joint and the inner shell can be radiographed with some difficulty. The weld in the second style wherein the annular plate shell is extended cannot be radiographed or volumetrically examined at all. The same holds true for type c. The shell extension also

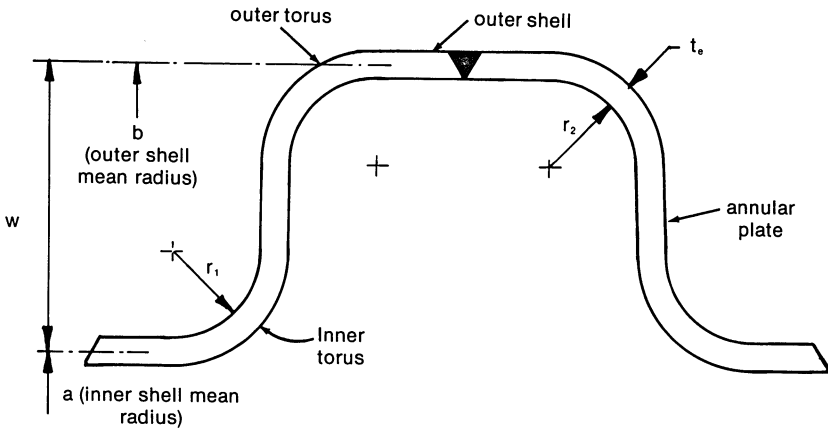


Fig. 15.2.1 Flanged and flued head expansion joint.

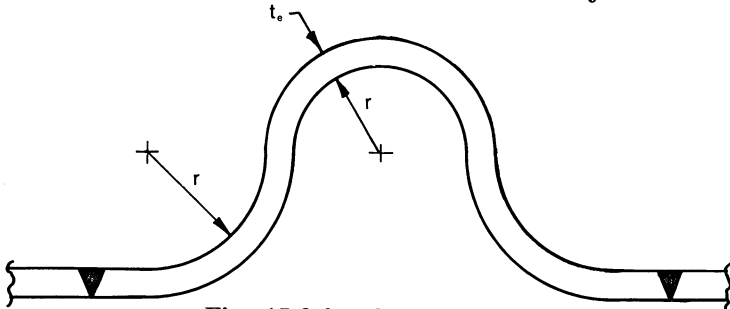


Fig. 15.2.2. Semi-torus.

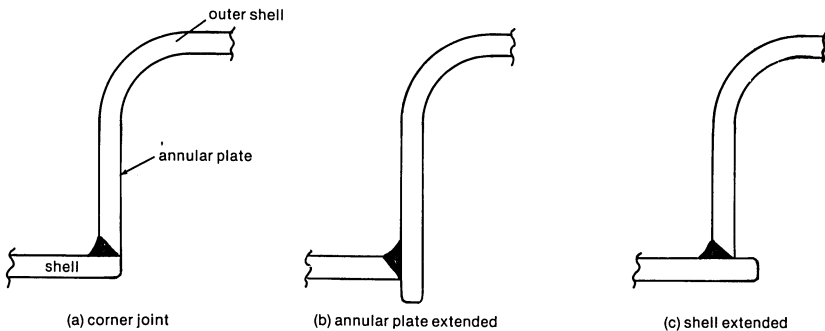


Fig. 15.2.3. Flanged-only expansion joint.

increases the axial rigidity of the joint. Nevertheless, this style is frequently employed where economy in hardware cost is the paramount consideration.

The expansion joint provides an otherwise wasted annular space around the bundle. Some designers take advantage of this space as a location to introduce the shellside fluid and to distribute it around the tube bundle. In such designs, the outer shell must be extended (by adding a shell course

between the two tori) to accommodate the shell inlet nozzle and its reinforcement (if required) (see Fig. 1.7.2). In such a construction, the inner shell extension serves as an “impingement plate” (see Section 1.7).

The corner welds in flanged-only expansion joints are regions of high stress concentration. They should be ground to a generous radius to minimize the stress concentration factor.

(ii) *Formed membrane*: Commonly known as “bellows” type, this class of expansion joints is made by forming convolutions from a thin (a few thousands of an inch) shell of a corrosion resistant material, such as austenitic stainless steel or a nickel base alloy. Figure 15.2.4 shows three variations of this type. Unreinforced bellows are used in low pressure applications. Reinforcing rings are added where instability of the bellows or “squirm”, is a concern. Bellows type construction represents an extreme in structural flexibility. However, it is rather fragile. External covers for bellows are often provided to protect personnel against the hazards of bellows blow-out. Use of multiple plies where each ply is individually capable of resisting pressure is another protective measure. In multiple ply designs, it is advisable to monitor the inter-ply pressure as an early detector of failure of the inner ply.

Another variation in the bellows design is the externally pressurized configuration shown in Fig. 15.2.5. This construction is obtained by manufacturing the bellows to a larger inside diameter than the outside diameter of the exchanger shell. The bellows are encased within the pressure retaining outer shell. The shellside pressure is baffled to be external to the bellows. Broyles [15.2.1] cites the many advantages of this construction. Transferring the pressure from the inside to the outside alleviates concern of bellows squirm, and eliminates any pockets which may become depositories of corrodents and sediments. Even a catastrophic failure of the bellows would simply direct the escaping shellside fluid through the open end of the bellows along the shell, thus mitigating the danger to nearby personnel. Moreover, a failed bellows unit can be replaced without taking the exchanger apart—this may be an attractive feature in many applications. Figure 15.2.6 shows an externally pressurized bellows expansion joint installed in a fixed tubesheet heat exchanger.

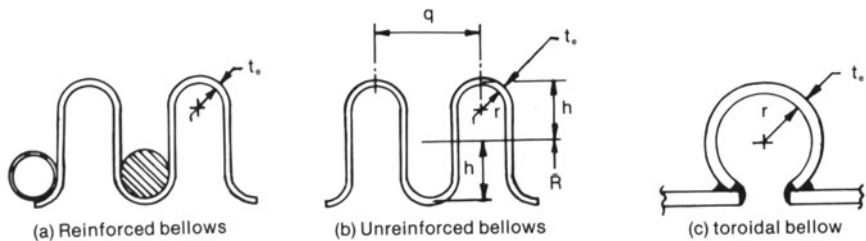


Fig. 15.2.4. Bellows shapes.

The number of convolutions in the bellows is a design variable. Similarly, the “formed head” type expansion joints may utilize more than one set of “flanged and flued” heads. Multiple expansion joints may be also necessary in the rare situations where the exchanger is mounted on three or more supports.

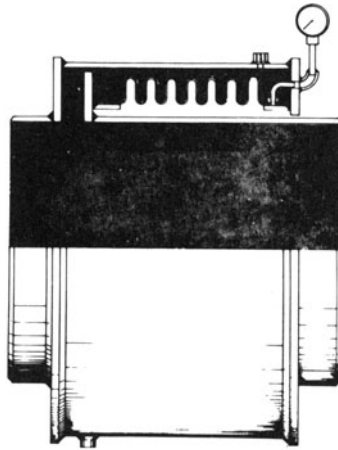


Fig. 15.2.5. Externally pressurized bellows expansion joint. (Reproduced from [15.2.1] by the courtesy of the American Society for Metals).

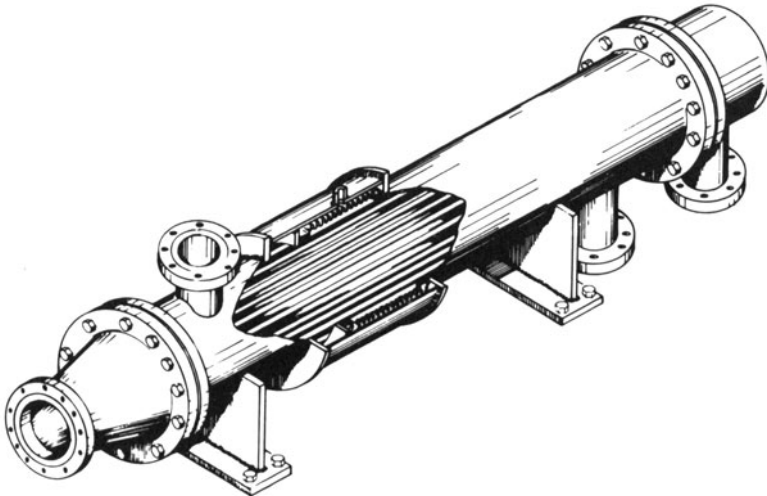


Fig. 15.2.6. Externally pressurized bellows expansion joint in fixed tubesheet heat exchanger. (Reproduced from [15.2.1] by the courtesy of the American Society for Metals).

15.3 STIFFNESS OF “FORMED HEAD” TYPE JOINTS

Kopp and Sayre [15.3.1] are generally credited with the first comprehensive effort to determine the axial stiffness of “flanged only” joints analytically. They also conducted some experimental tests to verify their mathematical model. Their model is based on the following simplifying assumptions.

a. The outer torus is replaced by an equivalent corner end. One half of the meridian of the outer torus (total length $\pi r_2/2$) is assigned to the outer plate and the other half is assigned to the outer shell. Figure 15.3.1 shows the idealized model.

b. The annular plate is modelled by a unit width beam strip. Similarly, the structural characteristics of the outer shell are not modelled using classical thin shell equations. Instead an approximate relationship is used. However, the inner shell (heat exchanger main shell) is modelled using thin shell bending equations.

Despite the unevenness of their analytical premise, Kopp and Sayre obtained good agreement with their experimental data. The simplicity of their approach apparently sits well with the design community; their method is still specified as the standard design approach in numerous design specifications.

Another notable attempt to treat “flanged and flued expansion joint” is due to Wolf and Mains [15.3.2]. Wolf and Mains advocated a finite element solution of the axisymmetrically loaded expansion joint problem. Their method did not attract wide usage, although it is generally believed that the ascendance of purely numerical methods in design work is only a matter of time.

In this section, we present a modified solution of the Kopp and Sayre model (Fig. 15.3.1) wherein all of the shell and plate elements are modelled using classical plate and shell theory methods. The resulting expressions are simple enough to be handled by a programmable calculator or a microcomputer. In a subsequent section, a finite element approach to this problem is also presented.

Analysis for Axial Load and Internal Pressure

Figure 15.3.1(b) shows the mathematical idealization of the expansion joint. The expressions for the bending of shelllike toroidal shapes are quite involved. Since the chief contribution of the tori lies in reducing the local bending stresses which are secondary stresses, and since secondary stresses (see Chapter 2) are of lesser importance, the elimination of the tori and replacement by sharp corners does not detract from the essence of our goal of developing a simple, practical solution. As the comparison with the finite element analysis presented in Section 15.5 shows, the elimination of the tori has a minor effect on the joint stiffness.

The expansion joint thus idealized has three element types, as shown in

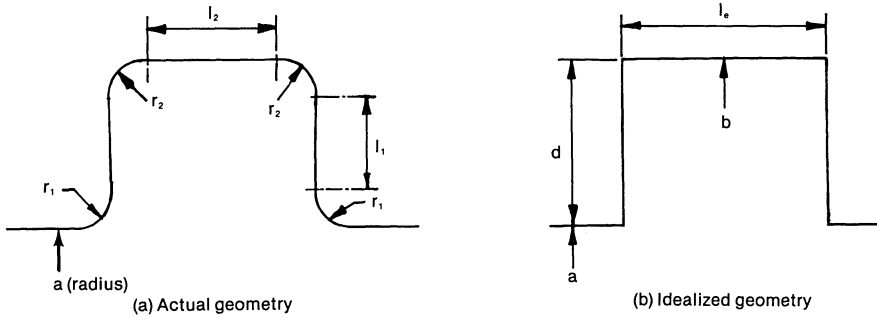


Fig. 15.3.1. Kopp and Sayre's model.

Fig. 15.3.2. Notice that the loading and internal stress resultants are symmetric with respect to the median transverse plane. Let F_{ax} represent the applied axial load per unit circumference on the exchanger shell and p denote the internal pressure acting on the joint. The discontinuity moments at junction A (inner shell/annular plate interface) and junction B (annular plate/outer shell interface) are labelled as M_1 and M_2 , respectively. Similarly, the shell edge shears are labelled as Q_1 and Q_2 . A standard discontinuity analysis at junctions A and B yields the necessary relationships to determine M_1 , M_2 , Q_1 and Q_2 . The necessary stress/deformation relationships for each element in the joint can be found in any standard text [15.3.3-4]. The basis for their derivations may also be found in Appendix A.

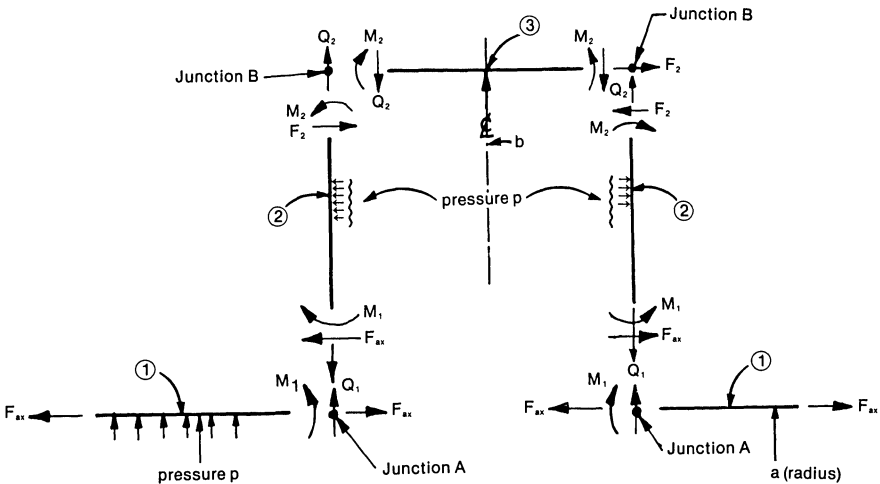


Fig. 15.3.2. Freebodies of the three constituent elements.

We begin by noting that equilibrium of one half of the joint, in the axial direction, gives F_2 in terms of F_{ax} .

$$2F_2 \pi b = 2\pi F_{ax} a + \pi(b^2 - a^2)p$$

or

$$F_2 = F_{ax} \frac{a}{b} + \frac{b^2 - a^2}{2b} p \quad (15.3.1)$$

To simplify the subsequent analysis, we will also assume that the radial movement of junctions A and B is zero. We now set down the necessary edge load – deflection/rotation relationship for each element.

(i) *Element 1 – Main Heat Exchanger Shell:* The radial deflection w_A and the rotation θ_A of the shell edge A are expressed in terms of edge moment M_1 and shear Q_1 , internal pressure p , and axial force F_{ax} , by the relations (Appendix A):

$$w_A = \frac{1}{2\beta_s^3 D_s} (\beta_s M_1 + Q_1) + \delta_s \quad (15.3.2)$$

where

$$\delta_s = \frac{pa^2}{Et_s} - \nu \frac{F_{ax} a}{Et_s} \quad (15.3.3)$$

$$\theta_A = \frac{1}{2\beta_s^2 D_s} (2\beta_s M_1 + Q_1) \quad (15.3.4)$$

The notation scheme used assumes radially outward deflection and counterclockwise rotation of edge A of the left shell to be positive.

The attenuation coefficient β_s and the flexural rigidity D_s of the shell are defined by

$$\beta_s = \left[\frac{3(1 - \nu^2)}{a^2 t_s^2} \right]^{0.25} \quad (15.3.5)$$

$$D_s = \frac{Et_s^3}{12(1 - \nu^2)} \quad (15.3.6)$$

Since the junction A is assumed to undergo zero radial displacement, Eq. (15.3.2) yields

$$Q_1 = -\beta_s M_1 - 2\beta_s^3 D_s \delta_s \quad (15.3.7)$$

Substituting for Q_1 in Eq. (15.3.4) gives M_1 as a function of θ_A .

$$\theta_A = y_1 M_1 - \beta_s \delta_s \quad (15.3.8)$$

where

$$y_1 = \frac{1}{2\beta_s D_s} \quad (15.3.9)$$

(ii) *Element 2 – Annular Plate:* The lateral loads acting on the annular plate can be broken up into two components; referring to Fig. 15.3.2, we consider the following groupings:

(a) Edge shear F_{ax} and moment M_1 at the inner edge ($r=a$); and an equilibrating edge shear at the outer edge along with edge moment M_2 .

(b) Pressure p acting on the lateral surface equilibrated by edge shear at the outer edge.

The total lateral deflection w of the plate with respect to its outer edge can be expressed as the sum of w_e due to edge load (component (a) above), and w_p due to lateral pressure (component (b) above).

$$w = w_e + w_p \quad (15.3.10)$$

Expressions for w_e and w_p are found in Ref. [15.3.3]. We will use the sign convention that the deflection is positive on element 2, if it is directed away from the transverse plane of symmetry of the joint (i.e., in the direction of F_{ax}).

From Ref. [15.3.3], we find that w_e can be written as:

$$w_e = M_1 g_1(r) + M_2 g_2(r) + F_{ax} f_1(r) \quad (15.3.11)$$

where

$$g_1(r) = \frac{1}{2} \frac{r^2 - b^2}{a^2 - b^2} \frac{a^2}{(1 + \nu)D_e} + \frac{a^2 b^2}{(a^2 - b^2)(1 - \nu)D_e} \ln \frac{r}{b} \quad (15.3.12)$$

$$g_2(r) = -\frac{1}{2} \frac{r^2 - b^2}{a^2 - b^2} \frac{b^2}{(1 + \nu)D_e} - \frac{a^2 b^2}{(a^2 - b^2)(1 - \nu)D_e} \ln \frac{r}{b} \quad (15.3.13)$$

$$f_1(r) = \frac{b^2 a}{4D_e} \left\{ \left(1 - \frac{r^2}{b^2}\right) \left[\frac{3 + \nu}{2(1 + \nu)} + \frac{a^2}{a^2 - b^2} \ln \frac{a}{b} \right] + \frac{r^2}{b^2} \ln \frac{r}{b} - \frac{2a^2}{a^2 - b^2} \frac{1 + \nu}{1 - \nu} \ln \frac{a}{b} \ln \frac{r}{b} \right\} \quad (15.3.14)$$

where r is the radial coordinate, and D_e represents the plate flexural rigidity.

$$D_e = \frac{Et_e^3}{12(1 - \nu^2)} \quad (15.3.15)$$

Differentiating:

$$\frac{dg_1}{dr} = \frac{ra^2}{(a^2 - b^2)(1 + \nu)D_e} + \frac{a^2 b^2}{(a^2 - b^2)(1 - \nu)D_e} \frac{1}{r} \quad (15.3.16)$$

$$\frac{dg_2}{dr} = -\frac{rb^2}{(a^2 - b^2)(1 + \nu)D_e} - \frac{a^2 b^2}{(a^2 - b^2)(1 - \nu)D_e} \frac{1}{r} \quad (15.3.17)$$

$$\frac{df_1}{dr} = \frac{b^2 a}{4D_e} \left\{ \frac{-2r}{b^2} \left[\frac{3 + \nu}{2(1 + \nu)} + \frac{a^2}{a^2 - b^2} \ln \frac{a}{b} \right] + \frac{2r}{b^2} \ln \frac{r}{b} + \frac{r}{b^2} - \frac{1}{r} \frac{2a^2}{a^2 - b^2} \frac{1 + \nu}{1 - \nu} \ln \frac{a}{b} \right\} \quad (15.3.18)$$

Similarly, we can write the following expression for w_p .

$$w_p = \frac{pb^4}{8D_e} \left\{ m_1 - m_2 \frac{r^2}{b^2} - m_3 \ln \frac{r}{b} + \frac{1}{8} \left(\frac{r}{b} \right)^4 - \frac{r^2 a^2}{b^4} \ln \frac{r}{b} \right\} \quad (15.3.19)$$

where

$$m_1 = \frac{5 + \nu}{8(1 + \nu)} - \frac{a^2(3 + \nu)}{4b^2(1 + \nu)} + \frac{(a/b)^4}{1 - (a/b)^2} \ln \frac{a}{b} \quad (a)$$

$$m_2 = \frac{3 + \nu}{4(1 + \nu)} \left(1 - \frac{a^2}{b^2} \right) + \frac{(a/b)^4}{1 - (a/b)^2} \ln \frac{a}{b} \quad (b) \quad (15.3.20)$$

$$m_3 = \frac{3 + \nu}{2(1 - \nu)} (a/b)^2 + \frac{2(1 + \nu)}{1 - \nu} \frac{(a/b)^4}{1 - (a/b)^2} \ln \frac{a}{b} \quad (c)$$

By differentiation of Eq. (15.3.19), we obtain the rotation variable $\theta_p(r)$ as:

$$\frac{dw_p}{dr} = \theta_p(r) = \frac{pb^4}{8D_e} \left[\frac{-2m_2 r}{b^2} - \frac{m_3}{r} + \frac{r^3}{2b^4} - \frac{2ra^2}{b^4} \ln \frac{r}{b} - \frac{ra^2}{b^4} \right] \quad (15.3.21)$$

(iii) *Element 3 – Outer Shell:* The outer shell is assumed to have thickness t_e , mean radius b , and length $l_e = l_2 + \pi r_2/2$. The shell is loaded by equal moments M_2 and shears Q_2 at its two edges. It is also subject to the axial load F_2 per unit circumference and to internal pressure p . At junction B , the radial deflection w_B (positive if directed away from the shell axis) and the rotation θ (positive if the left edge rotates clockwise in the plane of the paper) can be obtained from [15.3.4] and written in the form:

$$w_B = - \frac{2Q_2 \beta_e b^2}{Et_e} \chi_1(\alpha) + \frac{2M_2 \beta_e^2 b^2}{Et_e} \chi_2(\alpha) + \delta_e \quad (15.3.22)$$

$$\theta_B = \frac{-2Q_2 \beta_e^2 b^2}{Et_e} \chi_2(\alpha) + \frac{4M_2 \beta_e^3 b^2}{Et_e} \chi_3(\alpha) \quad (15.3.23)$$

where

$$\delta_e = \frac{pb^2}{Et_e} - \nu \frac{F_2 b}{Et_e} \quad (a)$$

$$\beta_e = \left[\frac{3(1 - \nu)^2}{b^2 t_e^2} \right]^{0.25} \quad (b)$$

$$\alpha = \beta_e \frac{l_e}{2} \quad (c)$$

$$\chi_1 = \frac{\cosh 2\alpha + \cos 2\alpha}{\sinh 2\alpha + \sin 2\alpha} \quad (d) \quad (15.3.24)$$

$$\chi_2 = \frac{\sinh 2\alpha - \sin 2\alpha}{\sinh 2\alpha + \sin 2\alpha} \quad (e)$$

$$\chi_3 = \frac{\cosh 2\alpha - \cos 2\alpha}{\sinh 2\alpha + \sin 2\alpha} \quad (f)$$

Since $w_B = 0$, we have from Eq. (15.3.22)

$$Q_2 = (M_2 \beta_e \chi_2 / \chi_1) + \frac{Et_e \delta_e}{2\beta b^2 \chi_1} \quad (15.3.25)$$

Substituting for Q_2 in Eq. (15.3.23) yields

$$\theta_B = y_2 M_2 - \frac{\beta_e \chi_2}{\chi_1} \delta_e \quad (15.3.26)$$

where

$$y_2 = \frac{4\beta_e^3 b^2}{Et_e} \chi_3 - \frac{2\beta_e^3 b^2 \chi_2^2}{Et_e \chi_1} \quad (15.3.27)$$

We can now enforce slope compatibility at junctions A and B in order to determine M_1 and M_2 . Compatibility of slope between the inner shell and the annular plate at junction A requires

$$\theta_A = \left. \frac{dw}{dr} \right|_{r=a} = \left. \frac{dw_e}{dr} \right|_{r=a} + \left. \frac{dw_p}{dr} \right|_{r=a}$$

Similarly, bearing in mind that the clockwise direction is positive for θ_B , compatibility of rotation between the outer shell and the annular plate at junction B requires that

$$\theta_B = - \left. \frac{dw}{dr} \right|_{r=b} = - \left. \frac{dw_e}{dr} \right|_{r=b} - \left. \frac{dw_p}{dr} \right|_{r=b}$$

Explicit expressions for all these quantities have been provided in the foregoing.

For convenience, let us denote the values of derivatives in Eqs. (15.3.16–18) at $r = a, b$ by the following simple notations;

$$x_1 = \left. \frac{dg_1}{dr} \right|_{r=a}; \quad x_2 = \left. \frac{dg_2}{dr} \right|_{r=a}; \quad x_3 = \left. \frac{df_1}{dr} \right|_{r=a}$$

$$x_4 = \left. \frac{dg_1}{dr} \right|_{r=b}; \quad x_5 = \left. \frac{dg_2}{dr} \right|_{r=b}; \quad x_6 = \left. \frac{df_1}{dr} \right|_{r=b}$$

Then, slope continuities at joints A and B produce the following simple algebraic equations for M_1 and M_2

$$(x_1 - y_1)M_1 + x_2M_2 = -x_3F_{ax} - \left. \frac{dw_p}{dr} \right|_{r=a} - \beta_s \delta_s \quad (15.3.28)$$

$$x_4M_1 + (x_5 + y_2)M_2 = -x_6F_{ax} - \left. \frac{dw_p}{dr} \right|_{r=b} + \frac{\beta_e \chi_2}{\chi_1} \delta_e$$

M_1 and M_2 readily follow from the above in terms of F_{ax} and p as

$$M_1 = \frac{1}{\Delta} \left[(x_5 + y_2) \left(-F_{ax}x_3 - \theta_p(a) - \beta_s \delta_s \right) - x_2 \left(-F_{ax}x_6 - \theta_p(b) + \frac{\beta_e \chi_2}{\chi_1} \right) \right] \quad (15.3.29)$$

$$M_2 = \frac{1}{\Delta} \left[(x_1 - y_1) \left(-F_{ax}x_6 - \theta_p(b) + \frac{\beta_e \chi_2}{\chi_1} \delta_e \right) - x_4 \left(-F_{ax}x_3 - \theta_p(a) - \beta_s \delta_s \right) \right] \quad (15.3.30)$$

where

$$\Delta = (x_1 - y_1)(x_5 + y_2) - x_2x_4 \quad (15.3.31)$$

Having determined M_1 and M_2 , the axial spread of the joint, δ , is given by

$$\delta = 2(w_e + w_p)|_{r=a} \quad (15.3.32)$$

where w_e and w_p are defined by Eqs. (15.3.11) and (15.3.19), respectively.

If the internal pressure p is zero, then the axial stiffness of the expansion joint is given by

$$K = \frac{F_{ax}}{\delta} \quad (15.3.33)$$

Computer program EXJOINT, presented in Appendix 15.A, performs the numerical computations for the analysis given in this section.

15.4 STRESSES IN THE EXPANSION JOINT

In the preceding section, we have presented the method to compute the internal stress resultants (M_1 , Q_1 , etc., in Fig. 15.3.2) in a joint subject to axial force F_{ax} and internal pressure p . The equations to determine stress distributions in the inner shell, annular plate and outer shell are presented in this section.

(i) *Inner Shell (element 1 in Fig. 15.3.2)*: Figure 15.4.1 shows a

freebody of the inner shell. The expression for the displacement w at a distance x from junction A is given by (Appendix A):

$$w = \delta_s + \frac{e^{-\beta_s x}}{2\beta_s^3 D_s} [\beta_s M_1 (\cos\beta_s x - \sin\beta_s x) + Q_1 \cos\beta_s x] \quad (15.4.1)$$

where

$$\delta_s = \frac{pa^2}{Et_s} - \nu \frac{F_{ax} a}{Et_s}$$

Therefore, the membrane stresses in the shell, due to discontinuity effects and applied loading, are:

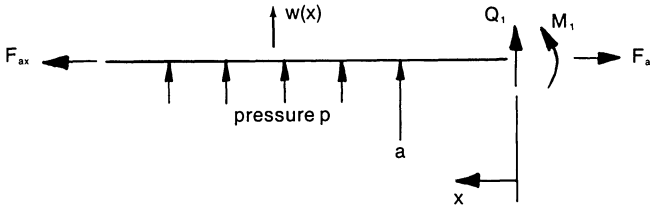


Fig. 15.4.1. Freebody of inner shell.

$$\text{Circumferential stress, } \sigma_{\theta m} = \frac{Ew}{a} \quad (a) \quad (15.4.2)$$

$$\text{Longitudinal stress, } \sigma_{lm} = \frac{F_{ax}}{a} \quad (b)$$

From Appendix A, we find that the longitudinal bending stress, σ_{lb} , and the circumferential bending stress, $\sigma_{\theta b}$ are given by:

$$\sigma_{lb} = \mp \frac{6D_s}{t_s^2} \frac{d^2 w}{dx^2}$$

$$\sigma_{\theta b} = \nu \sigma_{lb}$$

where positive σ_{lb} , $\sigma_{\theta b}$ imply compression of the outer fiber. Calculating the derivatives of w from Eq. (15.4.1), we have

$$\sigma_{lb} = \mp \frac{6}{\beta_s t_s^2} [\beta_s M_1 \phi(\beta_s x) + Q_1 \zeta(\beta_s x)] \quad (a)$$

$$\sigma_{\theta b} = \nu \sigma_{lb} \quad (b) \quad (15.4.3)$$

where

$$\phi(\beta_s x) = e^{-\beta_s x} (\cos\beta_s x + \sin\beta_s x) \quad (a) \quad (15.4.4)$$

$$\zeta(\beta_s x) = e^{-\beta_s x} \sin\beta_s x \quad (b)$$

These bending stresses involve only M_1 , Q_1 , and belong to the secondary category, since they attenuate rapidly with x . Reader should refer to Appendix A at the end of this text for a detailed characterization of these stresses.

(ii) *Annular Plate (element 2 in Fig. 15.3.2)*: The radial bending stress is the dominant stress in the annular plate. Referring to Appendix A, the radial bending stress, σ_r and the circumferential bending stress σ_θ in the annular plate are given by

$$\sigma_r = \frac{6M_r}{t_e^2}$$

$$\sigma_\theta = \frac{6M_\theta}{t_e^2}$$

where

$$M_r = D_e \left[\frac{d^2 w}{dr^2} + \frac{\nu}{r} \frac{dw}{dr} \right]$$

$$M_\theta = D_e \left[\frac{1}{r} \frac{dw}{dr} + \nu \frac{d^2 w}{dr^2} \right]$$

and w for the plate annulus is given by Eqs. (15.3.11), (15.3.19).

In addition to the bending stresses, the annular plate is also subject to in-plane radial loads Q_1 and Q_2 at its inner and outer boundaries, respectively. The in-plane radial and circumferential stresses due to Q_1 and Q_2 can be computed using the well-known Lamé cylinder formulas [15.4.1]. The radial membrane stress, σ_{rm} , is given in terms of Q_1, Q_2 as

$$\sigma_{rm} = \frac{1}{t_e(b^2 - a^2)} \left[\frac{a^2 b^2}{r^2} (Q_1 - Q_2) + Q_2 b^2 - Q_1 a^2 \right] \quad (15.4.5)$$

and the circumferential membrane stress, $\sigma_{\theta m}$, is given by

$$\sigma_{\theta m} = \frac{1}{t_e(b^2 - a^2)} \left[\frac{a^2 b^2}{r^2} (Q_2 - Q_1) + Q_2 b^2 - Q_1 a^2 \right] \quad (15.4.6)$$

(iii) *Outer Shell (element 3 in Fig. 15.3.3)*: The freebody of the outer shell is shown in Fig. 15.4.2. As shown in Appendix A, the solution for the axisymmetric bending displacement of a shell is

$$w = \delta_e + C_1 \sin\beta_e x \sinh\beta_e x + C_2 \sin\beta_e x \cos\beta_e x + C_3 \cos\beta_e x \sinh\beta_e x + C_4 \cos\beta_e x \cosh\beta_e x \quad (15.4.7)$$

Setting the origin at the mid-plane of the shell requires that w be an even function of x , i.e., $C_2 = C_3 = 0$.

The constants C_1 and C_4 are selected such that the following boundary conditions are satisfied;

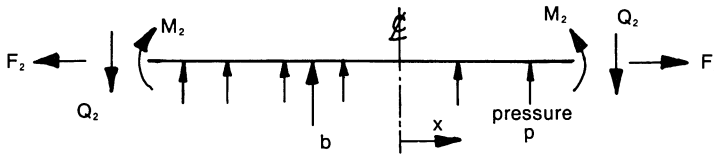


Fig. 15.4.2. Freebody of outer shell.

$$@x = l_e/2; D_e \frac{d^2 w}{dx^2} = M_2 \quad (15.4.8)$$

$$@x = l_e/2; w = 0$$

Performing the algebra, we have

$$C_1 = \frac{1}{Z} \left[\frac{j_2 M_2}{2\beta_e^2 D_e} - j_1 \delta_e \right] \quad (15.4.9)$$

$$C_4 = \frac{-1}{Z} \left[\frac{j_1 M_2}{2\beta_e^2 D_e} + j_2 \delta_e \right] \quad (15.4.10)$$

where

$$Z = j_1^2 + j_2^2 \quad (15.4.11)$$

$$j_1 = \sin \frac{\beta_e l_e}{2} \sinh \frac{\beta_e l_e}{2} \quad (15.4.12)$$

$$j_2 = \cos \frac{\beta_e l_e}{2} \cosh \frac{\beta_e l_e}{2} \quad (15.4.13)$$

Finally, the stresses in the outer shell are:

$$\text{Membrane hoop stress, } \sigma_{\theta m} = \frac{Ew}{b} \quad (a) \quad (15.4.14)$$

$$\text{Longitudinal hoop stress, } \sigma_{lw} = \frac{F_2}{t_e} \quad (b)$$

Longitudinal bending stress,

$$\sigma_{lb} = \frac{6M_x}{t_e^2} = \frac{6D_e}{t_e^2} \frac{d^2 w}{dx^2} = \frac{12D_e \beta_e}{t_e^2} [C_1 \cos \beta x \cosh \beta x - C_4 \sin \beta_e x \sinh \beta_e x] \quad (15.4.15)$$

$$\text{Circumferential bending stress, } \sigma_{\theta b} = \nu \sigma_{lb} \quad (15.4.16)$$

These equations are also coded in the computer program EXJOINT, described in Appendix 15.A.

An Example

Let us consider a flanged and flued head expansion joint defined by the following dimensions (Fig. 15.3.1).

$$a = 20''; t_s = t_e = 0.25''$$

$$r_1 = r_2 = 3t_e, l_1 = 2.25'', l_2 = 2.5''$$

Two loading cases are considered:

(i) An axial pull per unit circumference

$$F_{ax} = 1 \text{ lb/in.}$$

(ii) Lateral pressure $p = 1$ psi; no header (axial) load.

Referring to Fig. 15.3.1(b), the mathematical idealization of this joint yields the following data (see Appendix 15.A):

$$b = a + l_1 + \frac{\pi r_1}{4} + \frac{\pi r_2}{4} = 23.43''$$

$$l = l_2 + \frac{\pi r_2}{2} = 3.68''$$

The deformation of the joint under axial load and under internal pressure loads is illustrated in Figs. 15.4.3 and 15.4.4, respectively. The maximum longitudinal stress in the main and outer shells, and the maximum radial stress distribution in the annular plate, is shown in Figs. 15.4.5-7.

We note that the points of discontinuities (A and B in Fig. 15.3.2) are also the locations of highest stress. A more refined stress distribution in these regions can be obtained using the finite element method, as described in the next section.

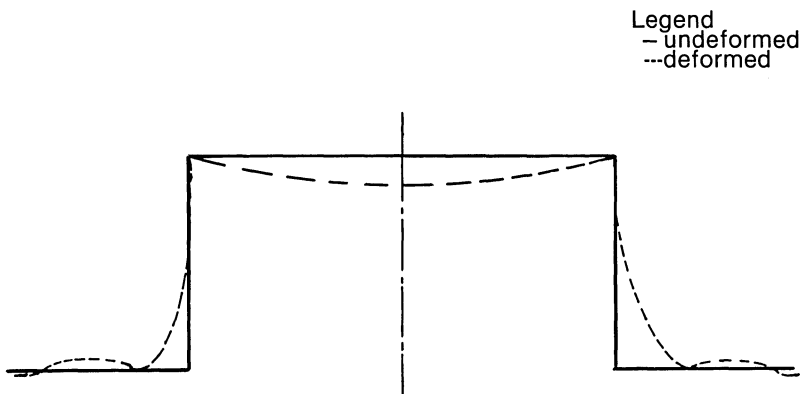


Fig. 15.4.3. Deformation of the expansion joint under axial load only (schematic drawing).

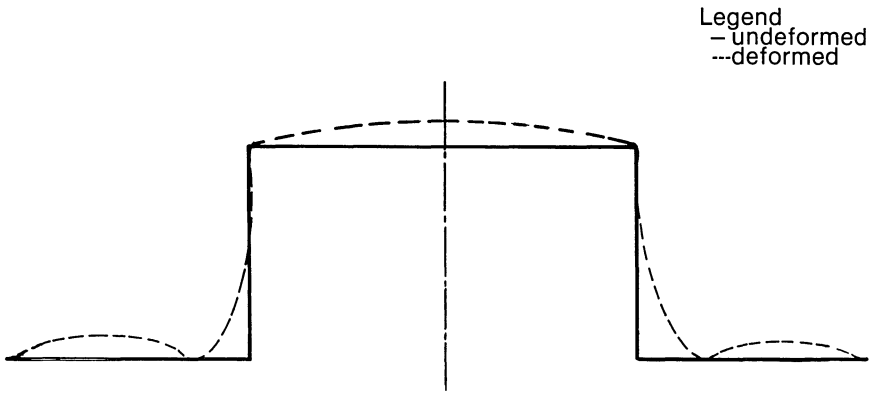


Fig. 15.4.4. Deformation of expansion joint under pressure loading only (schematic drawing).

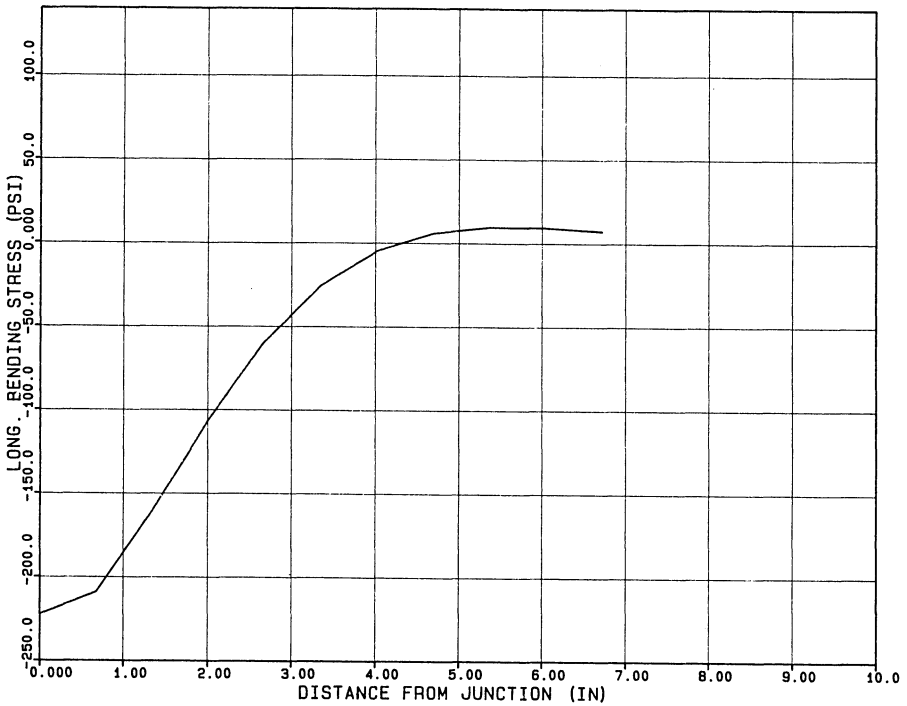


Fig. 15.4.5. Longitudinal bending stress in the main shell (example problem, unit internal pressure).

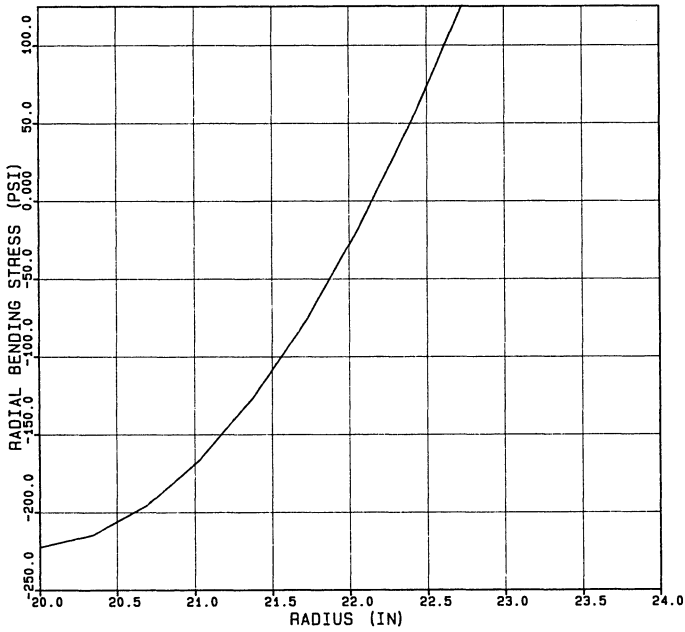


Fig. 15.4.6. Radial bending stress in the annular plate (example problem, unit internal pressure).

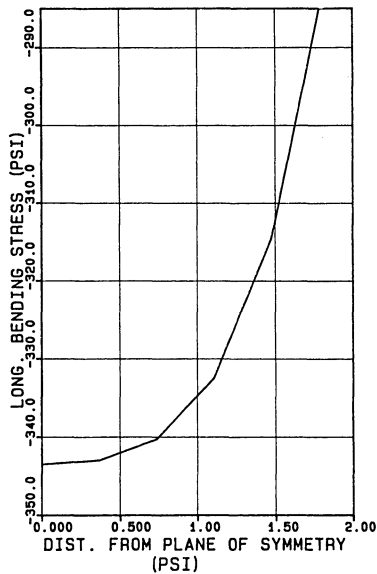


Fig. 15.4.7. Longitudinal bending stress in the outer shell (example problem unit internal pressure).

15.5 FINITE ELEMENT SOLUTION – COMPUTER PROGRAM FLANFLUE

The stress analysis method described in the preceding sections treats the problem of flanged and flued expansion joints in an approximate manner. The knuckle and flare radii are replaced by sharp discontinuities, and a classical discontinuity analysis is performed to obtain the stiffness of the joint and to determine the stress field. The analytical solution constructed in this manner gives reasonably good results for the joint flexibility. However, the predicted state of stresses at the junctions of the annular plate with inner and outer shells may be grossly overestimated. While this approach may be quite adequate for routine design work it is unable to provide a quantitative measure of the ameliorative effect of the flanged (inner torus) and flued (outer torus) shapes. Unfortunately, analytical modeling of the tori presents a formidable problem; specially since the ratio of the meridional radius to wall thickness of the tori seldom exceeds six to one. The analytical works of Clark [15.5.1], Gelletly [15.5.2–3], Turner [15.5.4], Laupa and Weil [15.5.5], among others, cannot be used due to the range of geometries involved. Wolf and Mains [15.3.2] overcame this problem by modeling the tori by a series of narrow rings. An alternative procedure is to equip a finite element program, capable of handling symmetrically loaded axisymmetric structures, with a pre-processor to simplify the tedium of data input. Such a program – “FLANFLUE” – has been developed for treating flanged and flued expansion joints. Figure 15.5.1 shows the standard element gridwork, node, and element numbering system.

The program requires the following input data: inner radius R_i , thickness of shell, thickness of joint, flare radius r_1 , knuckle radius r_2 , annular plate width l_1 , Young's modulus and the applied loads (viz., pressure and/or axial force on the joint). The Poisson's ratio is assumed to be equal to 0.3. The element gridwork is internally generated by the pre-processor, and the total “spread” of the joint and stress distribution in each element, are printed out. The deflection of every node is also printed out, providing a graphic view of the joint deformation.

Figures 15.5.2–3 show the plot of longitudinal and circumferential stress in the joint for the example problem (case i) of the preceding section. The stresses are plotted versus the section location. Referring to Fig. 15.5.1, Section 1, consists of elements 1, 2, 3 and Section 34 consists of elements 100, 101, 102. The extreme fiber stresses are plotted at the location corresponding to a “through thickness cut” along the three element centroids comprising each of the 34 sections making up the joint model. Figure 15.5.2 shows the variation of longitudinal stress on the outside and inside surfaces as a function of location, while Fig. 15.5.3 shows the circumferential surface stresses. The results shown are for the case of axial load alone. As expected, the maximum stress occurs on the outside surface of the inner toroidal section.

An unabridged documentation of FLANFLUE and its source coding are

available in [15.5.6]. Pre- and post-processors for finite element analysis have also been used in Chapter 10 for the analysis of tubesheets. The axisymmetric finite element code used there has also been employed here to obtain Figs. 15.5.2 and 15.5.3.

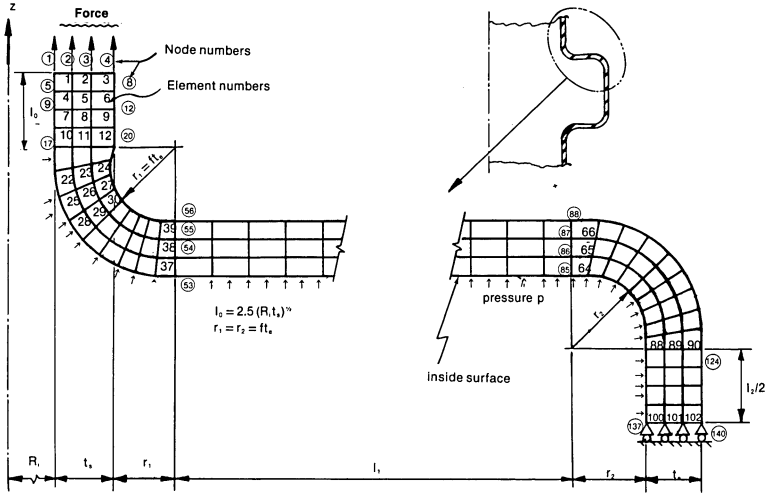


Fig. 15.5.1. Finite Element model for program FLANFLUE.

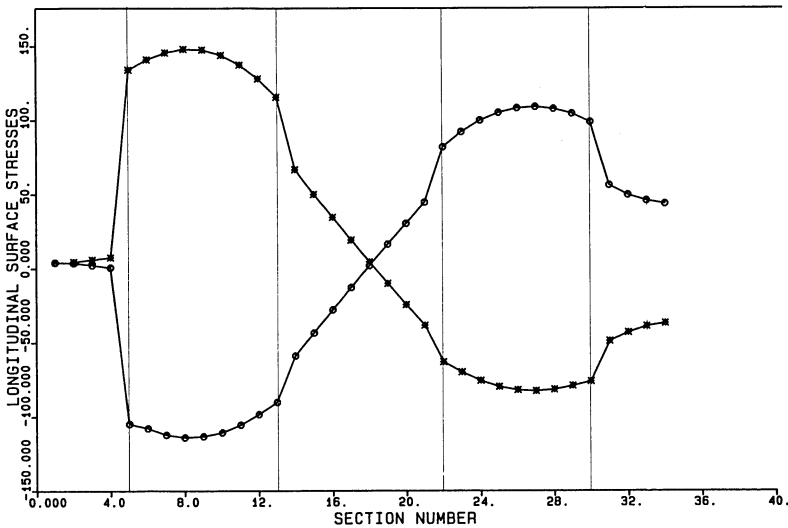


Fig. 15.5.2. Maximum longitudinal bending stress distribution for the example problem.

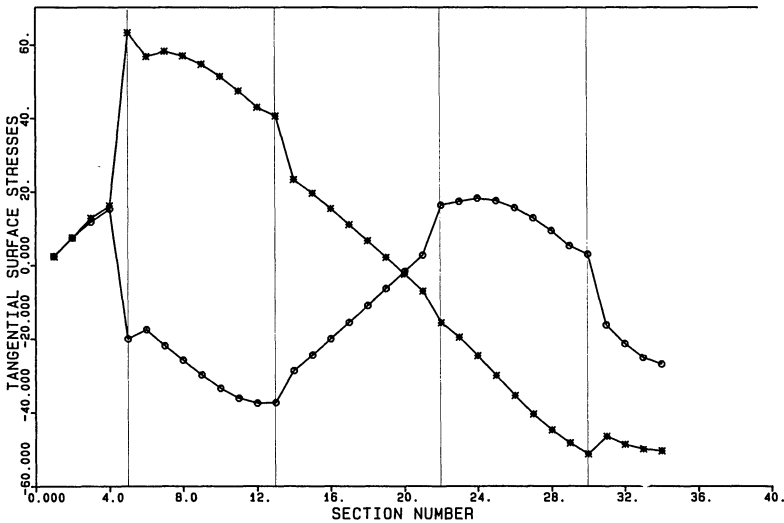


Fig. 15.5.3. Maximum circumferential stress distribution for the example problem.

15.6 BELLOWS EXPANSION JOINT FOR CYLINDRICAL VESSELS

Convolute bellows with (Fig. 15.2.4a) and without (Fig. 15.2.4b) root reinforcing rings are primarily used in piping systems to relieve thermal stresses. They also find occasional application in heat exchangers and in pressure vessels. The toroidal bellows (Fig. 15.2.4c) is less frequently used. Widespread industrial application of bellows have prompted a great deal of analytical and experimental research into their structural behavior. The primary focus in bellows design is directed towards their stability and their fatigue life. The possibility of instability of the bellows due to internal pressure is greatly increased if the stress levels at the inner crest of the bellows reach or exceed the material yield strength. Such a bellows instability is commonly known as “squirm”. For this reason, unreinforced convolute bellows are seldom used in the presence of internal pressures exceeding 30 psig. Root reinforcing rings abate bellows squirm and extend their pressure range; such reinforced bellows are frequently used in pressures as high as 300 psig.

The first comprehensive attempt to develop design guidelines for bellows design is due to Anderson [15.6.1]. Anderson’s work has been integrated into the standards of the Expansion Joint Manufacturers Association (EJMA), a trade group publication [15.6.2]. Anderson showed that the maximum stress in the bellows can be expressed in terms of the stresses in “an equivalent beam strip” modified by suitable coefficients. These coefficients are found to depend on two principal parameters; namely $r/\bar{R}t_e)^{1/2}$ and r/h (Fig. 15.2.4b).

The mathematical premise of EJMA's formulas are fully documented in [15.6.1], and are therefore not presented here. That document also contains a detailed set of specification guidelines for bellows procurement.

15.7 BELLOWS EXPANSION JOINTS FOR RECTANGULAR VESSELS

Rectangular cross section expansion joints are used in large ducts, in surface condensers, and in other rectangular vessels requiring thermal expansion relief. The Standards of the Expansion Joint Manufacturers Association (EJMA) provide suitable guidelines for their design, fabrication, quality assurance, testing, shipping, and installation. Figures 15.7.1-3, printed with the permission of EJMA, show the general arrangement, typical convolution profiles, and typical corner configurations of rectangular expansion joints.

The design formulas given in the EJMA standards are based on simple beam type models. The derivation of the joint "spring rate" f_i given below for a single convolution illustrates the general framework of these formulas. The spring rate is defined as the force required to elongate one convolution of the joint by unit distance. Figure 15.7.2 shows typical convolution shapes. An expansion joint containing n convolutions will have a net spring rate of f_i/n .

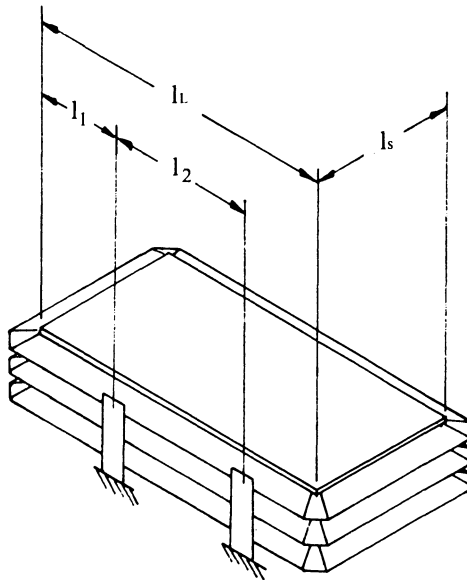


Fig. 15.7.1. General arrangement of rectangular expansion joints with supported sides (reprinted with the courtesy of EJMA, Inc.).

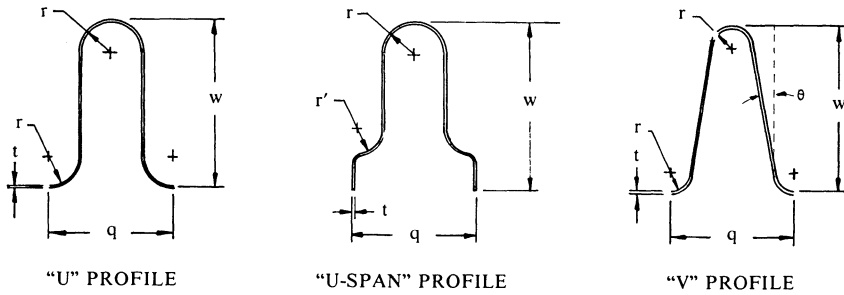


Fig. 15.7.2. Typical convolution profiles (reprinted with the courtesy of EJMA, Inc.).

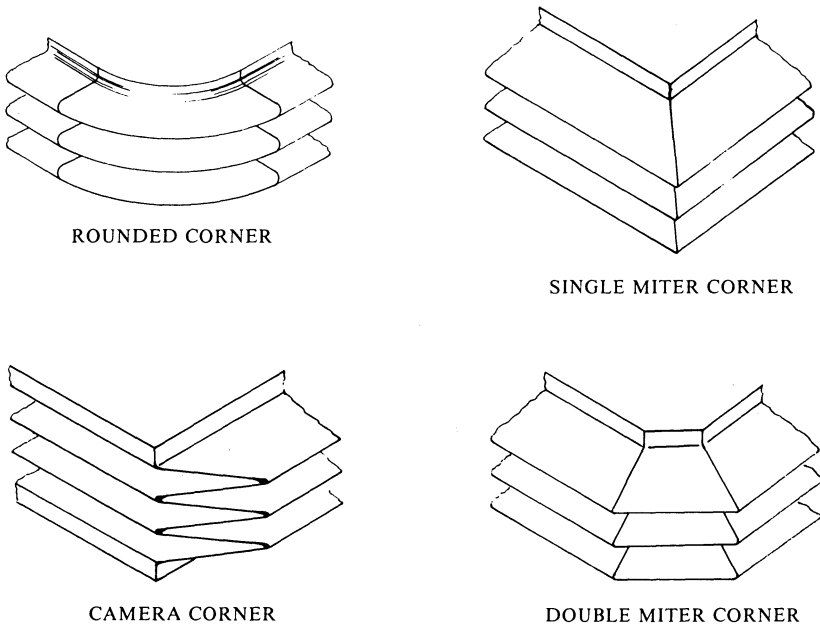


Fig. 15.7.3. Typical corner configurations (reprinted with the courtesy of EJMA, Inc.).

The expression for the spring rate is derived by considering a unit width slice of the U-profile convolution subject to two equal and opposite forces P trying to pry it apart. Assuming zero slope at the ends, and symmetry, the freebody of one quarter of the convolution has the form of Fig. 15.7.4. The bending moment at a point located at coordinate x from the end point A is:

$$M = Px \tag{15.7.1}$$

Similarly, the moment at the point C on the curved segment is:

$$M = P \left(\frac{w}{2} - r + r \sin \theta \right) \quad (15.7.2)$$

To determine the horizontal movement of point A with respect to point O , we use Castigliano's principle which states that the partial derivative of the strain energy with respect to the applied force P gives the displacement of the force P with respect to the fixed point. The strain energy U^* is given by strength-of-materials theory as

$$U^* = \int \frac{M^2}{2EI} dx \quad (15.7.3)$$

where E and I are the Young's modulus of the expansion joint material, and the moment of inertia of the section ($I = t^3/12$), respectively. The integration extends over the length of the freebody in Fig. 15.7.4. Hence, the displacement of point A is

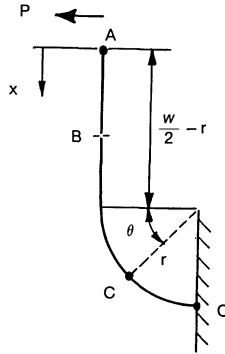


Fig. 15.7.4. Freebody of one quarter of a convolution.

$$\delta = \frac{\partial U^*}{\partial P} = \frac{1}{EI} \int M \frac{\partial M}{\partial P} dx$$

or

$$EI\delta = \int_0^{w/2 - r} Px^2 dx + P \int_0^{\pi/2} \left(\frac{w}{2} - r + r \sin \theta \right)^2 r d\theta \quad (15.7.4)$$

The first integral extends over the straight portion, and the second integral extends over the curved portion of the convolution segment. Integrating and rearranging terms, yields

$$\frac{EI\delta}{P} = \frac{\left(\frac{w}{2} - r\right)^3}{3} + \frac{\pi}{2} r \left(\frac{w}{2} - r\right)^2 + 2\left(\frac{w}{2} - r\right)r^2 + \pi r^3 \quad (15.7.5)$$

The separation of the two ends of the convolution, Δ , will be four times the separation between points O and A , i.e., $\Delta = 4\delta$. Hence,

$$\frac{EI\Delta}{P} = \frac{w^3}{6} + 0.57w^2r - 0.28wr^2 + 0.09r^3$$

or

$$EI\Delta \approx \frac{Pw^3}{6} \left(1 + 3.4 \frac{r}{w}\right) \quad (15.7.6)$$

where higher order terms in r/w have been neglected.

Referring to Fig. 15.7.1, the perimeter of the joint is $2(l_s + l_L)$; therefore, the total force F required to produce the separation Δ in the joint is

$$2(l_s + l_L) P.$$

Therefore, a relation between F and Δ is

$$EI\Delta = \frac{F}{(l_L + l_s)} \frac{w^3}{12} \left(1 + \frac{3.4r}{w}\right) \quad (15.7.7)$$

Solving for the ratio F/Δ yields

$$\frac{F}{\Delta} = \frac{12EI(l_L + l_s)}{w^3 \left(1 + \frac{3.4r}{w}\right)} \quad (15.7.8)$$

or

$$f_i = \frac{Et^3(l_L + l_s)}{w^3 \left(1 + \frac{3.4r}{w}\right)} \quad (15.7.9)$$

This is formula (3.62) of Ref. [15.6.2].

Other formulas can be derived in a similar manner. The entire EJMA procedure for stress evaluation in rectangular bellows has been programmed in the code "EJMAREC". This code is presented in Appendix 15.B.

15.8 FATIGUE LIFE

Since much of the stress in the expansion joint is of the secondary and peak type, calculated values in operating units exceeding the material yield

strength are not uncommon. Therefore, the joint design involves restricting the primary and the local membrane stresses to code specified limits, and computing the “cumulative damage factor” for the total stress range.* The concept of “cumulative damage factor” is a simple, yet reliable, method to determine the factor of safety against fatigue failure. It is assumed that the experimental data to correlate the stress intensity range to the cycle life of the expansion joint material is available. Let N_i denote the allowable number of cycles corresponding to the stress range S_i . Then the “usage factor” U_i of the joint, at the material point under consideration, due to n_i cycles of stress range S_i , is simply

$$U_i = \frac{n_i}{N_i} \quad (15.8.1)$$

If the material point is subjected to m different cycles of frequency n_i and corresponding stress range S_i ($i = 1, 2, \dots, m$), then the cumulative damage factor U is

$$U = \sum_{i=1}^m U_i = \sum_{i=1}^m \frac{n_i}{N_i} \quad (15.8.2)$$

Safety from fatigue failure requires that

$$U \leq 1 \quad (15.8.3)$$

M. W. Kellogg Company [15.8.1] presented the following formula relating N_i to S_i for stainless steel bellows which gave good agreement with the then published data (viz. Ref. [15.8.2], among others).

$$N_i = \left[\frac{1,600,000}{S_i} \right]^{3.5}$$

Using a factor of safety of 2 on the stress range, Ref. [15.8.1] recommends that designers use

$$N_i = \left(\frac{800,000}{S_i} \right)^{3.5} \quad (15.8.4)$$

Tavernelli and Coffin [15.8.3] found that the following formula gives good experimental agreement for steel, copper, aluminum, nickel, stainless steel and titanium

$$S_i = \frac{EC}{N_i^{1/2}} + 2\sigma_e \quad (15.8.5)$$

*Range of stress intensity is synonymous with the maximum principal stress range if all principal stresses at a point are of the same sign. In the case of expansion joints such is nearly always the case.

where

E = Young's modulus of the expansion joint material at the operating temperature

σ_e = Endurance limit for the expansion joint material

$$C = 1/2 \ln \left[\frac{100}{100 - \%R.A.} \right] \quad (15.8.6)$$

R.A. is the reduction in area in a tensile test of the material.

Using the above correlation, Langer [15.8.4] proposed the following expression for the acceptable number of cycles N_i at stress range S_i .

$$N_i = \frac{\left[\frac{E}{4} \ln \left(\frac{100}{100 - \%R.A.} \right) \right]^2}{(SF) \left(\frac{K_e S_i}{2} - S_e \right)^2} \quad (15.8.7)$$

where SF is the required factor of safety, and K_e denotes the stress/strain concentration factor at the material point under consideration. The ASME Code [15.8.5] requires that if a stress range S_i exceeds three times the allowable stress or twice the yield strength of the material, then S_i should be increased by a factor K_e prior to predicting cyclic life. K_e can be thought of as plasticity correction factor. The ASME Code [15.8.5] gives plots of $N_i - S_i$ for several common materials of construction.

Anderson [15.6.1] analyzed available data from fatigue tests on convoluted unreinforced bellows and determined that pressure stresses have a definite effect on fatigue life. He found the following equation to correlate a pseudo-stress S (psi) to cycle life N .

$$\text{Log}_{10} S = 6.24 - 0.236 \text{Log}_{10} N \quad (15.8.8)$$

The pseudo-stress S is equal to the sum of the maximum stress in the bellows due to bellows deflection and twice the maximum bellows stress due to pressure. It should be noted that the location of peak bending stresses due to pressure will, in general, not coincide with the location of peak deflection stress. Nevertheless, summing them for purposes of a fatigue life evaluation appears to be satisfactory for design purposes.

A similar correlation using available data from 43 tests on ring reinforced bellows gave:

$$\text{Log}_{10} S = 6.26 - 0.249 \text{Log}_{10} N$$

where the multiplier on pressure stress in stress S is 0.5 rather than 2. Anderson also found that the pressure stress multiplier has to be varied widely, from 0.2 to 1.0, for bellows operating at relatively high pressures (over 200 psi).

NOMENCLATURE

- a = Mean radius of inner (main heat exchanger) shell
 b = Mean radius of outer shell (element 3 in Fig. 15.3.2)
 D_s, D_e = Flexural rigidity of shell and expansion joint, respectively
 d = Effective offset of the expansion joint (Fig. 15.3.1)
 F_{ax} = Applied axial force per unit circumference of shell
 F_2 = Reaction force per unit circumference in the outer shell
 K = Joint stiffness (Eq. (15.3.33))
 K_e = Stress range amplification factor
 l_e = Effective length of outer shell (Fig. 15.3.1)
 l_1 = Width of the annular plate (Fig. 15.3.1)
 l_2 = Straight length of outer shell (Fig. 15.3.1)
 M_1, M_2 = Discontinuity moments at inner shell/annular plate, and annular plate/outer shell interface, respectively
 N_i = Cycle life at stress range S_i
 p = Generic term to denote internal pressure
 p_s, p_t = Shellside and tubeside pressures, respectively
 Q_1 = Discontinuity shear in the inner shell at its interface with the annular plate
 Q_2 = Discontinuity shear in the outer shell at its interface with the annular plate
 r = Radial coordinate
 r_1 = Inner torus radius (Fig. 15.3.1)
 r_2 = Knuckle (outer torus) radius (Fig. 15.3.2)
 S_i = Stress range
 t_e = Thickness of expansion joint
 t_s = Thickness of shell
 U = Damage factor (Eq. (15.8.2))
 w = Radial deflection of shell, lateral deflection of annular plate
 w_A = Radial displacement of junction A (Fig. 15.3.2)
 β_e, β_s = Attenuation coefficient of expansion joint and shell, respectively
 θ_A = Rotation of shell at junction A
 $\sigma_{\theta m}, \sigma_{\theta b}$ = Circumferential membrane and bending stress, respectively
 $\sigma_{l m}, \sigma_{l b}$ = Longitudinal membrane and bending stress, respectively
 $\sigma_{r m}$ = Radial membrane stress in annular plate
 $\sigma_{\theta m}$ = Circumferential membrane stress in annular plate
 δ_s = Radial expansion of inner shell due to internal pressure and axial load
 ν = Poisson's ratio

REFERENCES

- [15.1.1] Karcher, G. G., "Design Considerations for Heat Exchanger Expansion Joints," Presentation at the ASME Winter Annual

- Meeting (unpublished manuscript), Panel Session 6B, Atlanta, GA (1977).
- [15.2.1] Broyles, R. K., "Advantages of Externally Pressurized Expansion Joints in Fixed Tubesheet Heat Exchanger Applications," Second Symposium on Shell and Tube Heat Exchangers, pp. 233–238, The American Society for Metals, Metals Park, Ohio (1982).
- [15.3.1] Kopp, S., and Sayre, M. F., "Expansion Joints for Heat Exchangers," ASME Winter Annual Meeting, New York (1952).
- [15.3.2] Wolf, L. J., and Mains, R. M., "The Stress Analysis of Heat Exchanger Expansion Joints in the Elastic Range," *Journal of Engineering for Industry*, Trans. ASME, pp. 145–150 (Feb. 1973).
- [15.3.3] Way, S., "Plates" in "Handbook of Engineering Mechanics," W. Flugge (ed.), p. 39–28, McGraw-Hill (1962).
- [15.3.4] Timoshenko, S. P., and Winowsky-Krieger, S., "Theory of Plates and Shells," McGraw-Hill (1959).
- [15.4.1] Timoshenko, S. P., "Strength of Materials, Part II," pp. 205–214, Third Edition, Van Nostrand, New York (1958).
- [15.5.1] Clark, R. A., "On the Theory of Thin Elastic Toroidal Shells," *Journal of Math. and Phys.*, pp. 146–178 (Nov. 1950).
- [15.5.2] Gelletly, G. D., "Edge Influence Coefficients for Toroidal Shells of Positive Gaussian Curvature," *Journal of Engineering for Industry*, Trans. ASME, Series B, Vol. 82, No. 1, pp. 60–68. (Feb. 1960)
- [15.5.3] Gelletly, G. D., "Edge Influence Coefficients for Toroidal Shells of Negative Gaussian Curvature," *Journal of Engineering for Industry*, Trans. ASME, Series B, Vol. 82, No. 1, pp. 69–75 (Feb. 1960).
- [15.5.4] Turner, C. E., "Stress and Deflection Studies of Flat Plate and Toroidal Expansion Bellows, Subjected to Axial, Eccentric or Internal Pressure Loading," *Journal of Mechanical Engineering Science*, Vol. 1, No. 2 (1959).
- [15.5.5] Laupa, A., and Weil, N. A., "Analysis of U-Shaped Expansion Joints," *Journal of Applied Mechanics*, Trans. of the ASME, pp. 115–123 (Mar. 1962)
- [15.5.6] Singh, K. P., and Soler, A. I., "HEXDES User Manual," Arcurus Publishers, Cherry Hill N.J. (1984).
- [15.6.1] Anderson, W. F., "Analysis of Stresses in Bellows," U.S. Atomic Energy Commission, Report No. NAA-SR-4527 (1964).
- [15.6.2] Standards of The Expansion Joint Manufacturers Association, Inc.; Fifth edition Tarrytown, New York (1980).
- [15.8.1] Kellog, M. W., "Design of Piping Systems," Wiley (1956).
- [15.8.2] Feely, F. J., "Stress Studies on Piping Expansion Bellows," *Journal of Applied Mechanics*, Trans. ASME, pp. 135–141. (June, 1950).

- [15.8.3] Tavernelli, J. F., and Coffin, L. F., "Experimental Support for Generalized Equation Predicting Low Cycle Fatigue," Instron Engineering Corporation, Application Series M-3 (1959).
- [15.8.4] Langer, B. F., "Design of Pressure Vessels for Low-Cycle Fatigue," *J. Basic Engineering*, Vol. 84, No. 3 (Sept. 1962).
- [15.8.5] "Boiler and Pressure Vessel Code", Section III, Div I, Sub-section NB, The American Society of Mechanical Engineers (1983).

APPENDIX 15.A

COMPUTER PROGRAM EXJOINT

EXJOINT automates the analysis presented in Sections 15.3 and 15.4. The flanged and flued joint geometry is idealized in the manner of Fig. 15.3.1. Let R_i , r_1 and r_2 denote the inside radius, inner torus mean radius, and outer torus mean radius, respectively. Furthermore, let l_1 and l_2 denote the widths of the annular plate section and the outer shell, respectively. Finally, let t_s and t_e , respectively, denote the main shell and the expansion joint thicknesses. In terms of these data, the idealized dimensions are:

$$\begin{aligned}
 a &= R_i + 0.5t_s \\
 b &= a + l_1 + \frac{\pi r_1}{4} + \frac{\pi r_2}{4} \\
 l &= l_2 + \frac{\pi r_2}{2}
 \end{aligned}
 \tag{15.A.1}$$

In addition to the above data, the computer program requires input of the material Young's modulus, and the external loadings (axial pull per unit of main shell circumference, F_{ax} ; and internal pressure, p).

The output from the program lists the input data, and gives the deflection, direct and bending stresses in each of the three elements of the expansion joint. The output for the example problem of Section 15.4, corresponding to $F_{ax} = 1$ lb/in., is presented in the pages following the program listing. This output can be compared with the results utilizing the finite element code FLANFLUE presented in Figs. 15.5.2-3. We note that, the largest stress component, the maximum longitudinal stress predicted by EXJOINT is somewhat higher than the finite element solution, as would be expected. The joint stiffness predicted by EXJOINT is 3663.4 psi as compared to 3664.4 psi computed by FLANFLUE. This comparison demonstrates the remarkable accuracy of EXJOINT in predicting the spring rate.

PROGRAM EXJOINT

```

C -----
C COMPUTER PROGRAM EXJOINT, REV 0
C BY K.P. SINGH AND T.L. NG, DEC. 1983
C COMPUTES AXIAL STIFFNESS OF FLANGED AND FLUED EXPN JOINTS
C ALSO COMPUTES STRESSES IN THE JOINT FOR A GIVEN AXIAL
C LOAD AND/OR INTERNAL PRESSURE
C -----
C FORTRAN VARIABLES:
C ***INPUT LIST : INPUT ALL DATA IN CONSISTENT UNITS***
C
C TITLE: TITLE FOR PROBLEM; ANY ALPHANUMERIC-80 CHARACTERS LONG
C
C TS: SHELL THICKNESS
C TE: EXPANSION JOINT THICKNESS
C YM: YOUNGS MODULUS
C EL: EFFECTIVE LENGTH OF OUTER SHELL
C A: MEAN RADIUS OF SHELL
C B: MEAN RADIUS OF OUTER SHELL
C P: PRESSURE
C FAX: AXIAL LOAD PER UNIT CIRCUMFERENCE
C -----
C ***RESULTS HAVE UNITS CONSISTENT WITH INPUT DATA***
C
C *****
C
C DIMENSION TITLE(20)
C D(T) =YM*T**3/(12.*(1.-PR)**2)
C BETA(T,Z) = ((3.*(1.-PR*PR))/(Z*Z*T*T))**.25
C WP(R) =P*B**4*(XM1-XM2*R*R/(B*B)-XM3*ALOG(R/B)+.125*
1 (R/B)**4-R*R*A*A*ALOG(R/B)/(B**4))/(8.*D(TE))
C THP(R) = ((-2*XM2*R/(B*B))-(XM3/R)+(5*R**3/(B**4))-2*R*A*A
1 *ALOG(R/B)/(B**4)-(R*A*A/(B**4)))/(8.*D(TE))*P*B**4
C PHI(X) =EXPS*(COS(BETAS*X)+SIN(BETAS*X))
C ZETA(X) =EXPS*SIN(BETAS*X)
C W(X) =DELTA+(EXPS/(2.*BETAS**3*DS))*(BETAS*AM1*(COS(BETAS*X)
1 -SIN(BETAS*X))+AQ1*COS(BETAS*X))
C G1(R) = ((.5*(R*R-B*B)*AA/(1+PR))+(AA*B*B*ALOG(R/B)/(1.-PR)))/D(TE)
C G2(R) = ((-.5*BB*(R*R-B*B)/(1+PR))-(BB*A*A/(1-PR)*ALOG(R/B)))/D(TE)
C F1(R) = (B*B*A/(4.*D(TE)))*((1-(R/B)**2)*(PRR+AA*ALOG(A/B))
1 +((R/B)**2*ALOG(R/B))-(2.*AA*PRS*ALOG(A/B)*ALOG(R/B)))
C DG1(R) = ((R*AA/(1+PR))+(AA*B*B/((1-PR)*R)))/D(TE)
C DG2(R) = ((-R*BB/(1+PR))-(AA*B*B/((1-PR)*R)))/D(TE)
C DF1(R) = (B*B*A/(4.*D(TE)))*((-2.*R/(B*B))* (PRR+AA*ALOG(
1 A/B)+(2.*R*ALOG(R/B)/(B*B))+R/(B*B))
2 -(2.*AA*(1+PR)*ALOG(A/B)/(R*(1-PR))))
C DDG1(R) = (AA/((1+PR)*DE))-(AA*B*B/((1-PR)*DE*R*R))

```

```

DDG2(R)=(-BB/((1+PR)*DE))+(AA*B*B/((1-PR)*DE*R))
DDF1(R)=(B*B*A/(4.*DE))*((-2./B**2)*(PRR+AA*ALOG(AB))+
1      (2./B**2)*ALOG(R/B)+(3./(B**2)))+(2.*AA*PRS*ALOG(AB)
2      /(R*R))
DDWP(R)=(P*B**4/(8.*DE))*((-2*XM2/B**2)+(XM3/R**2)
1      +(1.5*R**2/B**4)-(2.*AB**2*ALOG(R/B)/B**2)-(3.*AB**2/B**2))
C
WE(R)=AM1*G1(R)+AM2*G2(R)+FAX*F1(R)
THE(R)=AM1*DG1(R)+AM2*DG2(R)+FAX*DF1(R)
TH(R)=THP(R)+THE(R)
DDWE(R)=AM1*DDG1(R)+AM2*DDG2(R)+FAX*DDF1(R)
DDW(R)=DDWE(R)+DDWP(R)
C
C ***READ AND PRINT TITLE OF PROBLEM***
READ(5,5) (TITLE(I),I=1,20)
WRITE(6,6) (TITLE(I),I=1,20)
5  FORMAT(20A4)
6  FORMAT(6X,20A4)
C
C ***INPUT DATA***
READ(5,*) TS,TE,YM,EL,A,B,P,FAX
C
C ***PRINT INPUT DATA***
WRITE(6,15) TS,TE,YM,EL,A,B,P,FAX
15  FORMAT(1H0/16X,"*****INPUT DATA*****"//
+6X,"SHELL THICKNESS ..... =",F10.3/
+6X,"EXPANSION JOINT THICKNESS ..... =",F10.3/
+6X,"YOUNGS MODULUS ..... =",E10.3/
+6X,"EFFECTIVE LENGTH OF OUTER SHELL ..... =",F10.3/
+6X,"MEAN RADIUS OF SHELL ..... =",F10.3/
+6X,"MEAN RADIUS OF OUTER SHELL ..... =",F10.3/
+6X,"PRESSURE ..... =",F10.3/
+6X,"AXIAL LOAD PER UNIT MAIN SHELL CIRCUMFERENCE .... =",F10.3/)
C
TQL=1.0E-06
PR=.3
FXX=(FAX*A+.5*P*(B*B-A*A))/B
DELTAS=(P*A*A/(YM*TS))-(A*PR*FAX/(YM*TS))
DELTAE=(P*B*B/(YM*TE))-(B*PR*FXX/(YM*TE))
AB=A/B
PRR=(3+PR)/(2.*(1+PR))
PRS=(1+PR)/(1-PR)
AA=A*A/(A*A-B*B)
BB=B*B/(A*A-B*B)
XM1=((5+PR)/(8.*(1+PR)))-(A*A*(3+PR)/(4.*B*B*(1+PR)))
1  +ALOG(AB)*AB**4/(1-AB**2)
XM2=((1-AB*AB)*(3+PR)*.25/(1+PR))+(ALOG(AB)*AB**4/(1-AB*AB))
XM3=(AB*AB*(3+PR)/(2*(1-PR)))+(2*ALOG(AB)*(1+PR)*AB**4/
1  ((1-PR)*(1-AB*AB)))
Y1=1./(2.*BETA(TS,A)*D(TS))
X1=DG1(A)

```

```

X2=DG2(A)
X3=DF1(A)
X4=DG1(B)
X5=DG2(B)
X6=DF1(B)
BE=BETA(TE,B)
BETAS =BETA(TS,A)
DS =D(TS)
DE= D(TE)
AL=BE*EL
DENOM=SINH(AL)+SIN(AL)
CHAI1=(COSH(AL)+COS(AL))/DENOM
CHAI2=(SINH(AL)-SIN(AL))/DENOM
CHAI3=(COSH(AL)-COS(AL))/DENOM
Y2=(4.*BE**3*B*B*CHAI3/(YM*TE))-(2.*BE**3*B*B*CHAI2
1  **2/(YM*TE*CHAI1))
DEL=(X1-Y1)*(X5+Y2)-X2*X4
AM1=((X5+Y2)*(-FAX*X3-THP(A)-BETA(TS,A)*DELTAS)-X2*(-FAX
  *X6-THP(B)+(BETA(TE,B)*DELTAE*CHAI2/CHAI1)))/DEL
AM2=((X1-Y1)*(-FAX*X6-THP(B)+(BETA(TE,B)*CHAI2*DELTAE/CHAI1
1  ))-X4*(-FAX*X3-THP(A)-BETA(TS,A)*DELTAS) )/DEL
SPREAD=2.*(AM1*G1(A)+AM2*G2(A)+FAX*F1(A)+WP(A))
C
WRITE(6,25) SPREAD
25 FORMAT(1H0,15X,"*****RESULTS*****"//
+6X,"JOINT SPREAD ..... =",E10.3/)
IF(ABS(FAX).LT.TOL) GO TO 100
AK=FAX/SPREAD
WRITE(6,26) AK
26 FORMAT(6X,"JOINT STIFFNESS ..... =",
+F10.3/)
C
100 AQ1=-BETAS*AM1-2.*BETAS**3*DS*DELTAS
AQ2=(AM2*BE*CHAI2/CHAI1)+(YM*TE*DELTAE/(2.*BE*B*B*CHAI1))
C CHECK SATISFACTION OF BOUNDARY CONDITIONS
THAS=AM1/(BETAS*DS)+AQ1*Y1/BETAS
THAP=TH(A)
THBP=TH(B)
THBS=(-2*AQ2*BE**2*B**2*CHAI2+4*AM2*BE**3*B**2*CHAI3)/(YM*TE)
C END CHECK
C
C ****STRESSES IN THE MAIN SHELL****
WRITE(6,35)
X 35 FORMAT(1H0/15X,"-----MAIN SHELL RESULTS-----"//
+10X,"X",7X,"RADIAL",5X,"LONGITUDINAL STRESS",3X,"CIRCUMFERENTIAL
+STRESS"/16X,"DEFLECTION",4X,"MEMBRANE",2X,"BENDING",6X,
+"MEMBRANE",3X,"BENDING"/)
SIGLM=FAX/TS
RANGE=3.*(A*TS)**.5
DO 10 I=1,11
X=(I-1)*RANGE*.1
EXPS=EXP(-BETAS*X)

```

```

WX=W(X)
SIGTHM=YM*WX/A
SIGLB=(6/(BETAS*TS*TS))*(BETAS*AM1*PHI(X)+AQ1*ZETA(X))
SIGTHB=PR*SIGLB
WRITE(6,45) X,WX,SIGLM,SIGLB,SIGTHM,SIGTHB
45  FORMAT(1H0,5X,F7.4,5E12.4)
10  CONTINUE

C
C *****COMPUTE ANNULAR PLATE STRESSES*****
WRITE(6,55)
55  FORMAT(1H0/15X,"-----ANNULAR PLATE RESULTS-----"//
+6X,"RADIUS",7X,"PLATE",3X,"CIRCUMFERENTIAL STRESS",7X,
+"RADIAL STRESS"/16X,"DEFLECTION",3X,"MEMBRANE BENDING",5X,
+"MEMBRANE BENDING"/)
DO 20 I=1,11
R=A+(I-1)*(B-A)*.1
WPLT=WE(R) +WP(R)
AMTHETA=DE*(TH(R)/R)+PR*DDW(R))
AMR=DE*(DDW(R)+(PR*TH(R)/R))
SIGTHETA=6.*AMTHETA/TE**2
SIGR=6.*AMR/TE**2
SRM=(AQ2-AQ1)*AA*(B/R)**2-AQ2*BB+AQ1*AA
STHM=(AQ1-AQ2)*AA*(B/R)**2-AQ2*BB+AQ1*AA
WRITE(6,65) R,WPLT,STHM,SIGTHETA,SRM,SIGR
65  FORMAT(1H0,5X,F7.4,5E12.4)
20  CONTINUE

C
C *****OUTER SHELL STRESSES*****
WRITE(6,75)
75  FORMAT(1H0/15X,"-----OUTER SHELL RESULTS-----"//
+10X,"X",7X,"RADIAL",5X,"LONGITUDINAL STRESS",3X,"CIRCUMFERENTIAL
+STRESS"/15X,"DEFLECTION",4X,"MEMBRANE BENDING",6X,
+"MEMBRANE BENDING"/)
AJ1=SIN(BE*EL*.5)*SINH(BE*EL*.5)
AJ2=COS(BE*EL*.5)*COSH(BE*EL*.5)
ZZ=AJ1**2 +AJ2**2
BEDE=.5/(BE**2*DE)
CONS1=(AJ2*AM2*BEDE-AJ1*DELTAE)/ZZ
CONS2=-(AJ1*AM2*BEDE+AJ2*DELTAE)/ZZ
SIGLM=FXX/TE
DO 30 I=1,6
X=(I-1)*.1*EL
CCX=CONS2*(COS(BE*X)*COSH(BE*X))
SSX=CONS1*(SIN(BE*X)*SINH(BE*X))
DEFLEC=DELTAE+CCX+SSX
SIGLB=(12.*DE*BE**2/(TE*TE))*(CCX-SSX)
SIGTHB=PR*SIGLB
SIGTHM=YM*DEFLEC/B
WRITE(6,95) X,DEFLEC,SIGLM,SIGLB,SIGTHM,SIGTHB
95  FORMAT(1H0,5X,F7.4,5E12.4)
30  CONTINUE

```

STOP
END

*** TEST PROBLEM UNIT PRESSURE ***

*****INPUT DATA*****

SHELL THICKNESS = .250
 EXPANSION JOINT THICKNESS = .250
 YOUNGS MODULUS = .300E+08
 EFFECTIVE LENGTH OF OUTER SHELL = 3.680
 MEAN RADIUS OF SHELL = 20.000
 MEAN RADIUS OF OUTER SHELL = 23.430
 PRESSURE = 1.000
 AXIAL LOAD PER UNIT MAIN SHELL CIRCUMFERENCE = .000

*****RESULTS*****

JOINT SPREAD = .565E-03

-----MAIN SHELL RESULTS-----

X	RADIAL DEFLECTION	LONGITUDINAL STRESS		CIRCUMFERENTIAL STRESS	
		MEMBRANE	BENDING	MEMBRANE	BENDING
.0000	.0000E+00	.0000E+00	-.2225E+03	.0000E+00	-.6676E+02
.6708	.3098E-04	.0000E+00	-.2092E+03	.4647E+02	-.6276E+02
1.3416	.4983E-04	.0000E+00	-.1607E+03	.7474E+02	-.4822E+02
2.0125	.5925E-04	.0000E+00	-.1058E+03	.8888E+02	-.3174E+02
2.6833	.6242E-04	.0000E+00	-.5901E+02	.9362E+02	-.1770E+02
3.3541	.6204E-04	.0000E+00	-.2543E+02	.9306E+02	-.7630E+01
4.0249	.6011E-04	.0000E+00	-.4761E+01	.9016E+02	-.1428E+01
4.6957	.5784E-04	.0000E+00	.5761E+01	.8676E+02	.1728E+01
5.3666	.5588E-04	.0000E+00	.9462E+01	.8382E+02	.2839E+01
6.0374	.5446E-04	.0000E+00	.9260E+01	.8169E+02	.2778E+01
6.7082	.5358E-04	.0000E+00	.7293E+01	.8036E+02	.2188E+01

-----ANNULAR PLATE RESULTS-----

RADIUS	PLATE DEFLECTION	CIRCUMFERENTIAL MEMBRANE	STRESS BENDING	RADIAL MEMBRANE	STRESS BENDING
20.0000	.2825E-03	.2090E+02	-.8624E+02	-.2828E+00	-.2225E+03
20.3430	.2616E-03	.2055E+02	-.8681E+02	.7140E-01	-.2147E+03
20.6860	.2375E-03	.2021E+02	-.8381E+02	.4082E+00	-.1959E+03
21.0290	.2107E-03	.1989E+02	-.7719E+02	.7286E+00	-.1666E+03
21.3720	.1814E-03	.1959E+02	-.6688E+02	.1034E+01	-.1270E+03
21.7150	.1503E-03	.1930E+02	-.5287E+02	.1324E+01	-.7730E+02
22.0580	.1182E-03	.1902E+02	-.3510E+02	.1602E+01	-.1780E+02
22.4010	.8599E-04	.1876E+02	-.1356E+02	.1866E+01	.5130E+02
22.7440	.5464E-04	.1850E+02	.1179E+02	.2119E+01	.1298E+03
23.0870	.2550E-04	.1826E+02	.4095E+02	.2361E+01	.2175E+03
23.4300	.0000E+00	.1803E+02	.7395E+02	.2592E+01	.3142E+03

-----OUTER SHELL RESULTS-----

X	RADIAL DEFLECTION	LONGITUDINAL MEMBRANE	STRESS BENDING	CIRCUMFERENTIAL MEMBRANE	STRESS BENDING
.0000	-.9347E-05	.1272E+02	-.3435E+03	-.1197E+02	-.1031E+03
.3680	-.9438E-05	.1272E+02	-.3430E+03	-.1208E+02	-.1029E+03
.7360	-.9477E-05	.1272E+02	-.3403E+03	-.1213E+02	-.1021E+03
1.1040	-.8768E-05	.1272E+02	-.3325E+03	-.1123E+02	-.9975E+02
1.4720	-.6150E-05	.1272E+02	-.3146E+03	-.7874E+01	-.9438E+02
1.8400	-.5912E-11	.1272E+02	-.2797E+03	-.7569E-05	-.8390E+02

*** TEST PROBLEM UNIT AXIAL LOAD ***

*****INPUT DATA*****

SHELL THICKNESS = .250
 EXPANSION JOINT THICKNESS = .250
 YOUNGS MODULUS = 3.00E+08
 EFFECTIVE LENGTH OF OUTER SHELL = 3.680
 MEAN RADIUS OF SHELL = 20.000
 MEAN RADIUS OF OUTER SHELL = 23.430
 PRESSURE = .000
 AXIAL LOAD PER UNIT MAIN SHELL CIRCUMFERENCE = 1.000

*****RESULTS*****

JOINT SPREAD = .273E-03
 JOINT STIFFNESS = 3663.448

-----MAIN SHELL RESULTS-----

X	RADIAL DEFLECTION		LONGITUDINAL STRESS		CIRCUMFERENTIAL STRESS	
			MEMBRANE	BENDING	MEMBRANE	BENDING
.0000	-.2728E-11	.4000E+01	-.1942E+03	-.4093E-05	-.5827E+02	
.6708	.9526E-05	.4000E+01	-.1213E+03	.1429E+02	-.3640E+02	
1.3416	.1184E-04	.4000E+01	-.6310E+02	.1776E+02	-.1893E+02	
2.0125	.1036E-04	.4000E+01	-.2340E+02	.1554E+02	-.7021E+01	
2.6833	.7413E-05	.4000E+01	-.3107E+00	.1112E+02	-.9320E-01	
3.3541	.4391E-05	.4000E+01	.1043E+02	.6586E+01	.3129E+01	
4.0249	.1943E-05	.4000E+01	.1329E+02	.2915E+01	.3986E+01	
4.6957	.2565E-06	.4000E+01	.1192E+02	.3848E+00	.3576E+01	
5.3666	-.7372E-06	.4000E+01	.8879E+01	-.1106E+01	.2664E+01	
6.0374	-.1209E-05	.4000E+01	.5676E+01	-.1814E+01	.1703E+01	
6.7082	-.1345E-05	.4000E+01	.3046E+01	-.2017E+01	.9139E+00	

-----ANNULAR PLATE RESULTS-----

RADIUS	PLATE DEFLECTION		CIRCUMFERENTIAL STRESS		RADIAL STRESS	
			MEMBRANE	BENDING	MEMBRANE	BENDING
20.0000	.1365E-03	-.4086E+01	-.6580E+02	.1187E+01	-.1942E+03	
20.3430	.1277E-03	-.3997E+01	-.5796E+02	.1099E+01	-.1596E+03	
20.6860	.1165E-03	-.3914E+01	-.4981E+02	.1015E+01	-.1260E+03	
21.0290	.1034E-03	-.3834E+01	-.4139E+02	.9356E+00	-.9341E+02	
21.3720	.8895E-04	-.3758E+01	-.3273E+02	.8596E+00	-.6169E+02	
21.7150	.7365E-04	-.3686E+01	-.2384E+02	.7873E+00	-.3083E+02	
22.0580	.5792E-04	-.3617E+01	-.1476E+02	.7183E+00	-.8003E+00	
22.4010	.4224E-04	-.3551E+01	-.5501E+01	.6524E+00	.2846E+02	
22.7440	.2710E-04	-.3488E+01	.3914E+01	.5895E+00	.5697E+02	
23.0870	.1287E-04	-.3428E+01	.1347E+02	.5294E+00	.8478E+02	
23.4300	.0000E+00	-.3370E+01	.2314E+02	.4719E+00	.1119E+03	

-----OUTER SHELL RESULTS-----

X	RADIAL DEFLECTION		LONGITUDINAL STRESS		CIRCUMFERENTIAL STRESS	
			MEMBRANE	BENDING	MEMBRANE	BENDING
.0000	-.1557E-04	.3414E+01	-.6376E+02	-.1993E+02	-.1913E+02	
.3680	-.1503E-04	.3414E+01	-.6607E+02	-.1924E+02	-.1982E+02	
.7360	-.1336E-04	.3414E+01	-.7281E+02	-.1710E+02	-.2184E+02	
1.1040	-.1044E-04	.3414E+01	-.8340E+02	-.1336E+02	-.2502E+02	
1.4720	-.6068E-05	.3414E+01	-.9684E+02	-.7769E+01	-.2905E+02	
1.8400	.1819E-11	.3414E+01	-.1116E+03	.2329E-05	-.3349E+02	

APPENDIX 15.B

COMPUTER PROGRAM EJMAREC

The source code calculates all quantities necessary for an EJMA stress analysis of a rectangular joint. As a criteria for an acceptable joint, the source code assumes that, given an allowable stress, S_A , the expansion joint is acceptable if

- | | |
|---|----------------|
| a. The maximum membrane stress due to pressure | $< S_A$ |
| b. The maximum membrane stress plus the maximum bending stress | $\leq 1.5 S_A$ |
| c. The maximum total stress due to pressure and due to movement | $\leq 3.0 S_A$ |

The source code also computes the spring rate, the joint deflection, and the overall forces and moments. The equations programmed are those of Section C-8.7 of the EJMA Standards for "U" profiles. A call to a subroutine for fatigue calculation is included, but the user must add his/her own fatigue requirements. The code listed here uses the following logical unit numbers.

- NR – input from a stored data file
- NW – output to a stored data file
- 5 – input from keyboard
- 6 – output to screen or typewriter terminal

The following data must be input from either file NR or from the keyboard (NR = 5). The units should be inches, pounds, etc.

LINE #1

W, R, EPS, ELL, ELS, THETA, IOPT

- W = depth of convolution
- R = meridional radius
- EPS = straight segment of convolution
- ELL = long span of joint
- ELS = short span of joint
- THETA = 0.
- IOPT = 0 if EN, T are given and only a single run is desired.
- = 1 if EN, T are to be chosen within range $1 < EN < 5$ and T between 12 and 19 gage. EN and T are defined in Line # 4.

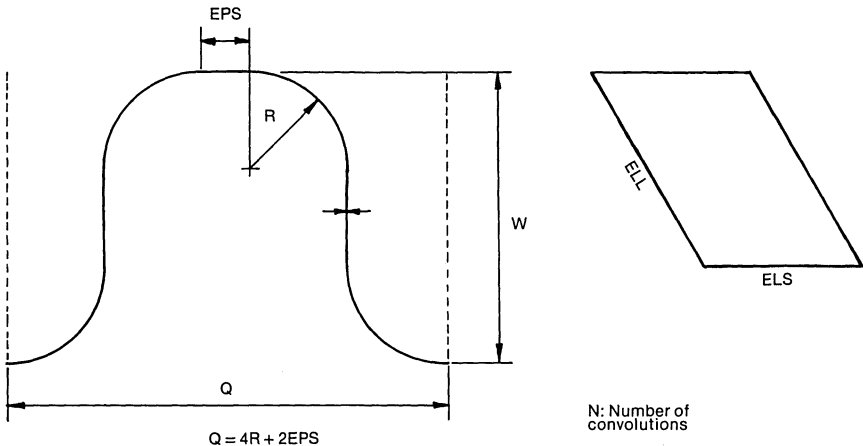


Fig. 15.B.1. Convolution geometry (code EJMAREC).

LINE #2

SLIMIT, YOUNG, SCF

- SLIMIT = allowable membrane stress
- YOUNG = E for material
- SCF = fatigue stress concentration factor (default = 1.0)

LINE #3

AXIAL, THL, THS, YL, YS, P

- AXIAL = increase in length due to axial movement
 - THL = θ_L
 - THS = θ_S
 - YL = shear movement in long direction
 - YS = shear movement in short direction
 - P = pressure (internal) to joint
- } See EJMA Standards for description

LINE #4 (Include only if IOPT = 0 on line 1)

T, EN

- T = thickness of bellows
- EN = number of convolutions (READ IN AS REAL NUMBER WITH DECIMAL POINT.)

LINE #5 (Same as line 1)

TO END JOB, READ IN W = 0 AS ONLY DATA ON THIS CARD.

SAMPLE DATA FILE

1. 2.75, 0.5625, 0.125, 107.25, 57.25, 0., 1
2. 60000., 27700000.
3. 0.3, 0.0056, 0.0056, 0.005, 0.01, 15.3
4. 0.,

Note that for this run, the code is being asked to choose the number of convolutions required and the thickness of the bellows metal. The code loops over the number of convolutions starting from 1, and then loops over the permitted gages (12 gage to 19 gage) until it finds a configuration that meets the stress requirements.

The output obtained from this sample run is presented here.

The quantities printed out during each iteration are given in the EJMA standards. Of importance for design are:

- AMOM = moment of inertia of convoluted section (EJMA Eq. C-52)
- SMEM = Eq. C-56 of EJMA (calculated for each direction and the maximum value printed)
- SP + SB = The maximum of [$|Eq. C-56| + |Eq. C-57|$] (for each direction), or Eq. C-58]. That is, SP + DB in the membrane plus bending component in the longitudinal direction, or is meridional bending stress
- SMP = Eq. C-58 (meridional bending stress due to pressure)
- SMP + SMD = maximum meridional bending stress due to pressure plus deflection (EJMA Eq. C-58 and Eq. C-59)
- EE = maximum combined extensional movement per convolution
- EC = maximum combined contractional movement per convolution
- SC = bellows spring constant (EJMA Eq. C-62)
- Y = bellows pressure deflection (EJMA Eq. C-60)
- SCF = stress concentration factor (input)
- SIGMA(ALT) = alternating stress range

When the final design configuration is achieved, the program also prints out the forces, F, V, M as defined in Table III of EJMA for the movement parallel to the long and short sides, respectively.

PROGRAM EJMAREC

```

PROGRAM MAIN
C*****PROGRAM EJMAREC 1983
C   INPUT DATA
C   R=MERIDIONAL RADIUS
C   W=CONVOLUTION DEPTHS
C   THETA=SEMI-V ANGLE (ZERO FOR U-SHAPE)
C   N=NUMBER OF CONVOLUTIONS
C   IOPT=RUN OPTION
C       =0 GIVEN # OF CONVOLUTIONS AND GAGE, COMPUTE STRESSES
C       =1 COMPUTE THE REQUIRED # OF CONVOLUTIONS AND GAGE,
C           GIVEN BELLOWS W AND R
C   ELL=LONG SPAN OF BELLOWS CROSS SECTION
C   ELS=SHORT SPAN OF BELLOWS CROSS SECTION
C   SLIMIT=ALLOWABLE STRESS (SECTION EIGHT )
C           FOR BELLOWS MATERIAL
C   T=BELLOWS THICKNESS
C   N=NO OF CONVOLUTIONS
C   AXIAL=AXIAL INCREASE IN BELLOWS LENGHT
C           DUE TO END FORCES
C   THL=ANGULAR ROTATION (RADIAN) PARALLEL TO LONG SIDE
C   THS=ANGULAR ROTATION (RADIAN) PARALLEL TO SHORT SIDE
C   YL=APPLIED LATERAL MOVEMENT OF ONE END WITH RESPECT
C       TO ANOTHER PARALLEL TO THE LONG SIDE
C   YS=APPLIED LATERAL MOVEMENT PARALLEL TO SHORT SIDE
C   P=INTERNAL PRESURE (EXTERNAL NEGATIVE)
C   YOUNG=YOUNG'S MODULUS OF BELLOWS MATERIAL
C   ELST=STEM BRACE UNSUPPORTED LENGTH
C   EPS=BELLOWS STRAGHT LENGTH INCREMENT
C
C   INTERNALLY COMPUTED DATA:
C
C   Q=BELLOWS PITCH
C   EL=TOTAL BELLOWS EFFECTIVE LENGTH
C   AMOM=MOMENT OF INERTIA OF BELLOWS CROSS SECTION
C   BETA=RATIO OF BELLOWS PERIMETER TO PITCH
C   EXXX=MAXIMUM MOMENT PER CONVELUTION DUE TO
C       MOVEMENT XXX
C   EE=MAXIMUM COMBINED EXTENTIONAL MOVEMENT PER
C       CONVOLUTION
C   EC=MAXIMUM COMBINED CONTRACTIGNAL MOVEMENT PER
C       CONVOLUTION
C*****
C   COMPUTER PROGRAM "REJMA"
C   COMMON/ONE/AMOM,X,BETA,Q,EPS
C   COMMON/TWO/ELL,ELS,T,W,YOUNG,R,N
C   COMMON/THREE/EC,EE,SC

```

```

COMMON/FOUR/DEFLEC,SPL,SPS,SLPL,SLPS,SMP,SMDE,SMDC
COMMON/FIVE/ SMEM,SMBENL,SMBENS,SMBEN,STHERM
COMMON/SIX/EXE,ETHL,ETHS,EYL,EYS
DIMENSION GAGE(8)
DATA GAGE/.1094,.0937,.0781,.0703,.0625,.0562,.050,.0437/
C DATA BLOCK FOR GAGE ARRAY GOES
C FROM 12 GAGE TO 19 GAGE,
C I.E. : GAGE (1)=12 GAGE
C READ GEOMETRY DATA AND INPUT OPTIONS
WRITE(6,6050)
6050 FORMAT(2X,'READ IN NR,NW, THE UNIT NUMBERS FOR IN AND OUT ')
READ(5,*)NR,NW
700 READ(NR,*)W,R,EPS,ELL,ELS,THETA,IOPT
IF(W.EQ.0.)STOP
READ(NR,*)SLIMIT,YOUNG,SCF
IF(SCF.EQ.0.)SCF=1.
C READ IN MOVEMENTS AND LOADS
READ(NR,*)AXIAL,THL,THS,YL,YS,P
IF(IOPT.EQ.0)READ(NR,*)T,EN
IF(IOPT.EQ.0)N=FIX(EN)
ELMAX=AMAX1(ELL,ELS)
C COMPUTE GEOMETRY DEPENDENT DATA
NI=5
NJ=8
IF(IOPT.EQ.0)NI=1
IF(IOPT.EQ.0)NJ=1
DO 100 I=1,NI
DO 100 J=1,NJ
IF(IOPT.EQ.0)GO TO 40
T=GAGE(J)
N=I
40 CONTINUE
CALL GEOM(THETA,W,R,ELMAX,T,N)
WRITE(NW,85)
85 FCRMAT(1X,' *****')
WRITE(NW,50)AMOM,Q
50 FORMAT(1X,'AMOM=',E15.5,3X,'Q=',F15.5)
EL=Q*N
CALL MOVE(AXIAL,THL,THS,YL,YS,EL)
CALL STRESS(P)
CALL CRITER(SLIMIT,IOUT,SRANGE,P)
IF(IOUT)110,110,90
90 WRITE(NW,95)T,N,IOUT
95 FORMAT(1X,'T=',F10.5,2X,'N=',I10,2X,'IOUT=',I10)
WRITE(NW,600)SMEM,SMBEN,SMP,STHERM
600 FORMAT(1X,'SMEM,SP+SB,SMP,SMP+SMD',4(1X,1PE11.4))
WRITE(NW,601)EC,EE,SC,DEFLEC
CALL FATIG(SRANGE,SCF)
WRITE(NW,802)SCF,SRANGE
802 FORMAT(1X,'SCF=',F6.3,' SIGMA(ALT)=',F15.0)
601 FORMAT(1X,'EC,EE,FI,Y=',4(1PE11.4,1X))
100 CONTINUE

```

```

110  CONTINUE
      WRITE(NW,85)
      WRITE(NW,240)
240  FORMAT(5X,19H***FINAL RESULTS***)
      WRITE(NW,120)T,N,EL
      WRITE(NW,600)SMEM,SMBEN,SMP,STHERM
      WRITE(NW,601)EC,EE,SC,DEFLEC
      CALL FORCE(EL,P,NW)
120  FORMAT(1X,'T=',F10.5,2X,'N=',I6,2X,'EL=',F15.5)
      GO TO 700
      END
C*****
      SUBROUTINE GEOM(THETA,W,R,ELMAX,T,N)
      COMMON/ONE/AMOM,X,BETA,Q,EPS
      PI=3.14189
      TOL=.001
      Q=4*R*COS(THETA)+TAN(THETA)*(2*W-4*R*(1-SIN(THETA)))
      I+2*EPS
      AMOM=N*((T*(2*W-Q)**3/48.0)+(0.4*Q*T*(W-0.2*Q)**2))
      BETA=((W/R)+1.15)*2*R/Q
      IF(THETA.GT.TOL)BETA=(2*PI*R+2*SQRT(Q*Q*0.25+W*W-R*(2*Q+4*W)))/Q
      X=1.0+AMOM*12*(N*Q/T)**3*(BETA/ELMAX**4)
      RETURN
      END
C
C*****
      SUBROUTINE MOVE(AXIAL,THL,THS,YL,YS,EL)
C  COMPUTES COMBINED COMPRESSIVE AND EXTENSIONAL
C  MOVEMENTS PER CONVOLUTION.
      COMMON/SIX/EXE,ETHL,ETHS,EYL,EYS
      COMMON/THREE/EC,EE,SC
      COMMON/TWO/ELL,ELS,T,W,YOUNG,R,N
      EXE=AXIAL/FLGAT(N)
      AXC=AXIAL
      ETHL=THL*ELL/(2.0*N)
      ETHS=THS*ELS/(2.0*N)
      EYL=3.0*ELL*YL/(N*(EL+AXC))
      EYS=3.0*ELS*YS/(N*(EL+AXC))
      EC=EYL+EYS+ETHL+ETHS-EXE
      EE=EYL+EYS+ETHL+ETHS+EXE
      RETURN
      END
C
C*****
      SUBROUTINE STRESS(P)
      COMMON/ONE/AMOM,X,BETA,Q,EPS
      COMMON/TWO/ELL,ELS,T,W,YOUNG,R,N
      COMMON/THREE/EC,EE,SC
      COMMON/FOUR/DEFLEC,SPL,SPS,SLPL,SLPS,SMP,SMDE,SMDC
C  COMPUTES MAXIMUM MERIDIONAL AND LONGITUDENAL STRESSES
      SLPLS(Y)=P*Y*Y*N*Q*0.5*W*(1.0-(1.0/X))/(12.0*AMOM)
      SMDC(Y)=5.0*YOUNG*T*Y/(3.0*W*W*((3.*R/W)+1.0))

```

```

      AB=T*(BETA*Q )
      SPS=P*ELS*Q/(2.0*AB)
      SPL=P*ELL*Q/(2.*AB)
      SLPL=SLPLS(ELL)
      SLPS=SLPLS(ELS)
      SMP=0.5*(W/T)**2.0*(1.0-1.3*R/W)*P
      SMDE=ABS(SMDEC(EE))+SMP
      SMDC=ABS(SMDEC(EC))+SMP
      DEFLEC=P*(N*Q)**4*BETA/(32.*YOUNG*T**3*X)
      SC=YOUNG*T**3*(ELL+ELS)/(W**3*(3.4*R/W+1.))
      RETURN
      END
C
C*****
SUBROUTINE CRITER(SLIMIT,IOUT,SRANGE,P)
C   COMPARES THE COMPUTED STRESSES WITH THE ALLOWABLES
      COMMON/FIVE/ SMEM,SMBENL,SMBENS,SMBEN,STHERM
      COMMON/FOUR/DEFLEC,SPL,SPS,SLPL,SLPS,SMP,SMDE,SMDC
      IOUT=0
      SMEM=AMAX1(SPL,SPS)
      SMBENL=SPL+SLPL
      SMBENS=SPS+SLPS
      SMBEN=AMAX1(SMBENL,SMBENS,SMP)
      STHERM=AMAX1(ABS(SMDE),ABS(SMDC))
      IF(SMEM.GT.SLIMIT)IOUT=10
      IF(SMBEN.GT.1.5*SLIMIT)IOUT=IOUT+100
      IF(STHERM.GT.3*SLIMIT)IOUT=IOUT+1000
      S1=AMAX1(SMBENL,SMBENS)
      S2=STHERM
      S3=-ABS(P/2.)
      S12=ABS(S1-S2)
      S23=ABS(S2-S3)
      S31=ABS(S3-S1)
      SRANGE=.5*AMAX1(S12,S23,S31)
      RETURN
      END
C*****
SUBROUTINE FORCE(EL,P,NW)
      COMMON/THREE/EC,EE,SC
      COMMON/SIX/EXE,ETHL,ETHS,EYL,EYS
      COMMON/TWO/ELL,ELS,T,W,YOUNG,R,N
      TL=ELL/3*((3*ELS+ELL)/(ELL+ELS))
      TS=ELS/3*((3*ELL+ELS)/(ELL+ELS))
      FA=SC*EXE
      EML=SC*TL*(ETHL+EYL)/4
      EMS=SC*TS*(ETHS+EYS)/4
      VL=SC*TL*EYL/EL
      VS=SC*TS*EYS/EL
      WRITE(NW,100)
100  FORMAT(1X,'FORCES AND MOMENTS')
      WRITE(NW,101)FA,VL,VS

```

```

101 FORMAT(1X, 'FA,VL,VS=',3(1PE11.4,1X), 'LBS. ')
      WRITE(NW,102)EML,EMS
102 FORMAT(1X, 'EML,EMS=',2(1PE11.4,1X), 'IN.LBS. ')
      RETURN

```

```

END

```

```

C*****

```

```

      SUBROUTINE FATIG(SRANGE,SCF)

```

```

      SRANGE=SCF*SRANGE

```

```

      RETURN

```

```

      END

```

```

*****

```

```

AMOM=      .61538E+00      Q=      2.50000
T=      .10940      N=      1      IOUT=      1000
SMEM,SP+SB,SMP,SMP+SMD 2.7598E+03 3.5485E+03 3.5485E+03 8.1001E+05
EC,EE,FI,Y= 1.3485E+00 1.9485E+00 1.6921E+05 1.3969E-03
SCF= 1.000      SIGMA(ALT)=      405011.

```

```

*****

```

```

AMOM=      .52706E+00      Q=      2.50000
T=      .09370      N=      1      IGUT=      1000
SMEM,SP+SB,SMP,SMP+SMD 3.2222E+03 4.8372E+03 4.8372E+03 6.9557E+05
EC,EE,FI,Y= 1.3485E+00 1.9485E+00 1.0631E+05 2.2218E-03
SCF= 1.000      SIGMA(ALT)=      347787.

```

```

*****

```

```

AMOM=      .43931E+00      Q=      2.50000
T=      .07810      N=      1      IOUT=      1000
SMEM,SP+SB,SMP,SMP+SMD 3.8658E+03 6.9627E+03 6.9627E+03 5.8269E+05
EC,EE,FI,Y= 1.3485E+00 1.9485E+00 6.1562E+04 3.8326E-03
SCF= 1.000      SIGMA(ALT)=      291350.

```

```

*****

```

```

AMOM=      .39544E+00      Q=      2.50000
T=      .07030      N=      1      IOUT=      1000
SMEM,SP+SB,SMP,SMP+SMD 4.2947E+03 8.5934E+03 8.5934E+03 5.2682E+05
EC,EE,FI,Y= 1.3485E+00 1.9485E+00 4.4898E+04 5.2508E-03
SCF= 1.000      SIGMA(ALT)=      263416.

```

```

*****

```

```

AMOM=      .35156E+00      Q=      2.50000
T=      .06250      N=      1      IOUT=      1000
SMEM,SP+SB,SMP,SMP+SMD 4.8307E+03 1.0872E+04 1.0872E+04 4.7160E+05
EC,EE,FI,Y= 1.3485E+00 1.9485E+00 3.1550E+04 7.4636E-03
SCF= 1.000      SIGMA(ALT)=      235806.

```

```

*****

```

```

AMOM=      .31612E+00      Q=      2.50000
T=      .05620      N=      1      IOUT=      1000
SMEM,SP+SB,SMP,SMP+SMD 5.3722E+03 1.3446E+04 1.3446E+04 4.2774E+05
EC,EE,FI,Y= 1.3485E+00 1.9485E+00 2.2939E+04 1.0252E-02
SCF= 1.000      SIGMA(ALT)=      213872.

```

```

*****

```

```

AMOM=      .28125E+00      Q=      2.50000
T=      .05000      N=      1      IOUT=      1000
SMEM,SP+SB,SMP,SMP+SMD 6.0384E+03 1.6988E+04 1.6988E+04 3.8557E+05
EC,EE,FI,Y= 1.3485E+00 1.9485E+00 1.6154E+04 1.4532E-02
SCF= 1.000      SIGMA(ALT)=      192790.

```

```

*****
AMOM= .24581E+00 Q= 2.50000
T= .04370 N= 1 IOUT= 1000
SMEM,SP+SB,SMP,SMP+SMD 6.9089E+03 2.2239E+04 2.2239E+04 3.4438E+05
EC,EE,FI,Y= 1.3485E+00 1.9485E+00 1.0785E+04 2.1709E-02
SCF= 1.000 SIGMA(ALT)= 172195.
*****
AMOM= .12308E+01 Q= 2.50000
T= .10940 N= 2 IOUT= 1000
SMEM,SP+SB,SMP,SMP+SMD 2.7598E+03 5.0654E+03 3.5485E+03 2.9082E+05
EC,EE,FI,Y= 3.9410E-01 6.9410E-01 1.6921E+05 2.1760E-02
SCF= 1.000 SIGMA(ALT)= 145415.
*****
AMOM= .10541E+01 Q= 2.50000
T= .09370 N= 2 IOUT= 1000
SMEM,SP+SB,SMP,SMP+SMD 3.2222E+03 6.8548E+03 4.8372E+03 2.5088E+05
EC,EE,FI,Y= 3.9410E-01 6.9410E-01 1.0631E+05 3.4283E-02
SCF= 1.000 SIGMA(ALT)= 125446.
*****
AMOM= .87862E+00 Q= 2.50000
T= .07810 N= 2 IOUT= 1000
SMEM,SP+SB,SMP,SMP+SMD 3.8658E+03 1.0036E+04 6.9627E+03 2.1205E+05
EC,EE,FI,Y= 3.9410E-01 6.9410E-01 6.1562E+04 5.8231E-02
SCF= 1.000 SIGMA(ALT)= 106026.
*****
AMOM= .79087E+00 Q= 2.50000
T= .07030 N= 2 IOUT= 1000
SMEM,SP+SB,SMP,SMP+SMD 4.2947E+03 1.2650E+04 8.5934E+03 1.9319E+05
EC,EE,FI,Y= 3.9410E-01 6.9410E-01 4.4898E+04 7.8851E-02
SCF= 1.000 SIGMA(ALT)= 96601.
*****
AMOM= .70313E+00 Q= 2.50000
*****
***FINAL RESULTS***
T= .06250 N= 2 EL= 5.00000
SMEM,SP+SB,SMP,SMP+SMD 4.8307E+03 1.6517E+04 1.0872E+04 1.7499E+05
EC,EE,FI,Y= 3.9410E-01 6.9410E-01 3.1550E+04 1.1029E-01
FORCES AND MOMENTS
FA,VL,VS= 4.7325E+03 5.8067E+04 4.4952E+04 LBS.
EML,EMS= 1.4439E+05 8.3985E+04 IN.LBS.

```

16. FLOW INDUCED VIBRATION

16.1 INTRODUCTION

A central goal in the thermal design of tubular heat exchangers is to utilize the available shellside pressure loss to maximize the shellside film coefficient. The most effective means of accomplishing this objective is to arrange the shellside fluid to flow across the tube bank. Single segmental baffles (Fig. 1.4.5) provide the nearest practical alternative to a pure cross flow arrangement. Due to its ability to actuate maximum heat transfer rate for available pressure loss in a *minimum* amount of space, the single segmental baffle design has become a standard construction detail. Early texts on heat exchanger rating methods [16.1.1–2] acknowledged the dominance of the single segmental baffle design. It was not until the '60's, when widespread failure of tubes began to occur [16.1.3], that another consequence of shellside cross flow – flow induced vibration – came to the fore. In retrospect, relatively high fouling factors used in the petrochemical, chemical, and process industries had indirectly prevented uncovering of the vibration problem. High fouling factors specified by the user blunted the heat exchanger designer's motivation to maximize the shellside coefficient by maximizing cross flow velocities. Lower fouling factors, coupled with greater flow rates used in the power industry, removed this disincentive. Moreover, the specified pressure loss in power plant heat exchangers also tended to be greater. Conventional wisdom held, correctly so, that higher cross flow velocity (in the absence of erosion related problems) produce better operating heat exchangers by reducing the deposition rate of crud and debris on tube surfaces. Designers have since learned that ignoring the effect of increased cross flow velocity on tube vibration failure can be an expensive mistake. It is indeed true that sporadic failure of tubes in operating heat exchangers occurred even before the '60's. However, the significance of flow induced vibration on heat exchanger reliability did not attract sufficient attention until tube failures became commonplace, particularly in the power industry. Finally, it should be added that parallel flow has also been reported to be responsible for some tube failures. However, even in ostensibly parallel flow induced failures, cross flow components of the turbulent stream have been held responsible by some investigators [16.1.4]. From a practical designer's point of view, the design focus should rightfully rest on the cross flow component of the flow velocity.

The last decade has witnessed vigorous research activity in the field of flow induced vibration in tube bundles. Numerous researchers have made

valuable contributions to our understanding of this phenomenon. Within the space limitations of this text, it is impossible to do justice to this subject matter in its entirety. Therefore, our goal herein is quite modest and focused. We attempt solely to foster a physical insight into the vibration problem, and to summarize the predictive methods proposed in the literature in a way suitable for use by the designer. Although prediction methods are presented in this chapter to aid in the heat exchanger design process, the designer should never lose sight of the elusive nature of the tube vibration problem. Unlike other subjects treated in this book, prediction methods for vibration remain essentially semi-empirical. Simple formulas cannot describe complex phenomena involving turbulent fluid flows. Although they are structured to bound the solution, imputing faultless performance to these correlations in all conditions of design would be unwise.

In the next two sections, a brief discussion of failure types and vulnerable regions in the heat exchanger is given. The following section on vibration mechanisms is essentially introductory. A summary of some published prediction methods, which are believed to be most reliable, is next presented. The chapter also contains a brief essay on the methods employed to avoid the vibration problem. Finally, a step-by-step computation procedure to predict the incidence of flow induced vibration is laid out in Section 16.13. The necessary material on topics relevant to the subject matter, e.g., hydrodynamic mass, damping, etc. is also provided. A self-contained section on tube natural frequency including U-tubes is provided to complete the development and to furnish the data needed to carry out the flow induced vibration analysis.

The reader is referred to the TEMA Standards [16.1.5] or Shah [16.1.6] for a practical treatment of this subject.

16.2 VIBRATION DAMAGE PATTERNS

Mechanical failure of a tube occurs in many different ways. The most commonly reported damages can be classified as follows:

i. Collision damage: The amplitude of tube vibration is sufficiently large so that tubes impact against each other. Tubes located in the bundle periphery may impact the vessel wall. The tube wall is worn thin and eventually splits open.

ii. Baffle damage: Baffle holes are drilled such that a diametral clearance of 1/64" (in tight fit designs) to 1/32" between tube and baffle hole exists.* Thus, the tubes are free to laterally displace inside the baffle holes. If the drag forces are sufficiently large, repetitive impact between the tube wall and the baffle inside surface is produced. Since the baffles are of

*TEMA Standards [16.1.5] give empirical rules on baffle hole clearance stated as a function of tube O.D. and unsupported span.

finite thickness, the pressure distribution on the tube wall surface along the axial direction is nearly uniform over the extent of the baffle thickness except at the edges where sharp pressure peaks are produced. This situation is analogous to the stress distribution on the rollers in a roller bearing. The high edge contact forces can initiate local damage which can sever the tubes in a short time.

iii. Tubesheet clamping effect: Tubes are rolled into the tubesheet to eliminate the crevice between the tube wall and the tubesheet hole. This joint thus simulates a built-in condition. The natural frequency of the tube span adjacent to the tubesheet is increased by this clamping effect. However, the stresses due to any lateral deflection of the tube are also maximum at the location where the tube emerges from the tubesheet, making it a prime candidate region for failure. Noting that one or both shell side nozzles are also located near the tubesheet in many designs, ordinarily high nozzle region velocities further contribute to tube failures in this region.

iv. Material defect propagation: Tubes vibrate with very small amplitudes even in "safe" designs. This is due to baffle hole tube wall clearances, and to flexibility of the tube span. To a perfectly homogeneous material such low level stress fluctuations are harmless. However, if the material contains macroscopic flaws strategically oriented with respect to the stress field, then such cracks can readily propagate and actuate tube failure. Corrosion and erosion can add to such failure mechanisms.

v. Metallurgical failure: Oxidation of the tube material and subsequent breaking up of the oxide layer can occur due to alternating stress in the tube produced by the fluid forces on the tube. As the oxidized layer breaks away, pits on the tube surface are formed. The pits on the tube surface act as stress raisers which drastically reduce tube life under alternating stress.

16.3 REGIONS OF TUBE FAILURE

Although tube failures have been reported in nearly all locations in heat exchangers, principal regions of concern are those regions where the tube span is relatively flexible, and/or the cross flow velocities are high. Thus the most important regions are:

i. U-bends: Outer rows of U-bundles have a relatively low frequency of vibration, and hence are more susceptible to flow induced vibration.

ii. Nozzle entrance and exit regions: Small flow area and impingement plates usually boost the local flow velocities.

iii. Tubesheet region: Tube spans adjacent to the tubesheet are generally larger than center region spans in order to accommodate nozzles, flanges, etc. Increased span often results in the flexibility of the end spans being higher than in the central spans. Lower flexibility means greater propensity for vibration.

iv. Baffled region: Tubes located in the baffle window have spans equal to twice the baffle spacings in single segmental and double segmental

designs. In triple and quadruple segmental designs (see Chapter 1), the spans are even larger multiples of the baffle spacings. Long spans result in reduced frequency of vibration, and hence a greater tendency for vibration damages.

v. Tubes under compressive stress: Compressive stresses reduce the natural frequency of vibration. In fixed tubesheet heat exchangers, compressive stresses can reach high magnitudes. Even U-tube straight segments can develop high axial stresses due to differential thermal expansion (see Chapter 14). Tubes under significant compressive loadings during the operating condition should be carefully examined for flow induced vibration.

16.4 VIBRATION MECHANISMS

16.4.1 Vortex Shedding

Consider a cylindrical body subject to a uniform cross flow. Figure 16.4.1 shows the variation of fluid pressure around the cylinder. The pressure at the leading edge is the highest and is known as the “stagnation pressure”. At low Reynolds number ($Re < 5$), the flow is essentially unseparated. As the flow velocity is increased, the pressure gradient around the cylinder tends to push the fluid boundary layer around both sides of the cylinder. Since the inside skin of the boundary layer moves more slowly than the outside, the sliding of the boundary layer is also accompanied by a “curling up”. Eventually, the curled up boundary layer (vortex) separates from the cylinder surface, creating a localized sharp drop in pressure. The shedding of the vortex takes place from the two sides of the cylinder alternately at uniform intervals. The proportionality parameter which relates the frequency of vortex shedding to the free stream flow velocity, u , and to the cylinder characteristic dimension, d_0 , is known as the “Strouhal Number”, S .

$$S = \frac{f_s d_0}{u} \quad (16.4.1)$$

The Strouhal number is plotted as a function of the Reynolds number in Fig. 16.4.2. It is seen that S is essentially constant (approximately 0.2) in the range of Reynolds number encountered in tubular heat exchangers [$5 \times 10^3 < Re < 10^5$]. In general, if the flow is not normal to the cylinder, u , in the above equation, is to be interpreted as the normal component (cross flow) of the free stream velocity.

Periodic breaking away of vortices from the sides of the cylinder produces a dynamic (time varying) force in the lift direction (direction perpendicular to fluid flow). It is well known that the amplitude of vibration of a single degree-of-freedom body, subject to a harmonic forcing function, grows rapidly with time if the forcing frequency coincides with the natural frequency of the system. This phenomenon is known as the con-

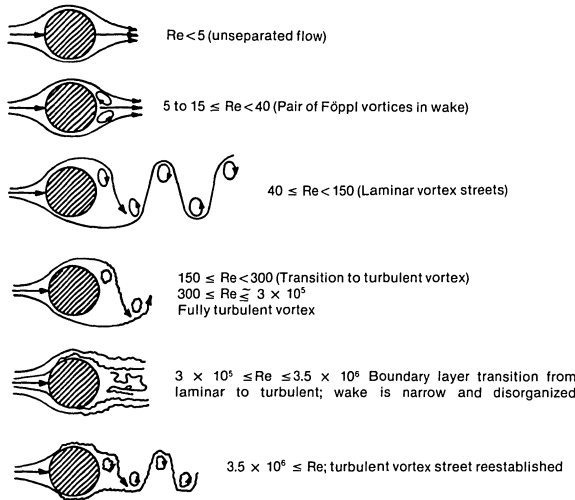


Fig. 16.4.1. Flow regimes across isolated circular cylinders [Ref. 16.4.1].

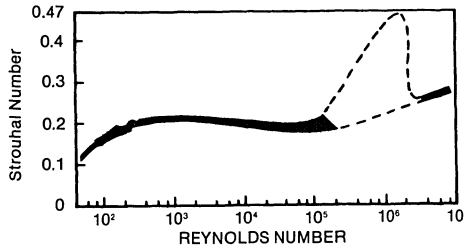


Fig. 16.4.2. Relationship between Strouhal and Reynolds numbers for isolated circular cylinders (Ref. 16.4.1).

dition of resonance. A tube is a continuous system, and therefore possesses an infinite number of natural frequencies. The lowest of this frequency set, the fundamental frequency, is the most important in flow induced vibration analysis, since this is the first frequency at which resonance would occur if the shedding frequency were gradually increased by increasing the cross flow velocity.

Experimental evidence indicates that once the shedding and natural frequencies are synchronized, vibration of the cylinder has a strong organizing effect on the shedding mechanism. The vortices are shed in an organized manner along the entire cylinder length. Moreover, the shedding frequency latches onto the tube natural frequency, even as the cross flow velocity is increased within a considerable range. This phenomenon is known as “lock-in”. A detailed exposition of this subject may be found in the book “Flow Induced Vibration” by R. D. Blevins [16.4.2].

Dynamic time varying lift forces due to vortex shedding require rhythmic separation of vortices from the cylinder surface. Such an organized phenomenon is too delicate to exist in a closely packed tube array. Observation of von Kármán streets in tube bundles of low solidity (large pitch to diameter ratios) led some investigators to propose vortex shedding as the actuating mechanisms behind tube vibration failures [16.4.3]. By now, however, there is general agreement that, except in rare cases, vortex shedding is not a credible mechanism for large amplitude tube vibration in commercial heat exchangers. It may, however, be responsible for acoustic resonance (Section 16.7.3).

16.4.2 Fluid-Elastic Excitation

Fluid-elastic excitation is most commonly associated with aircraft wing flutter and with galloping of ice-laden transmission lines. It is readily explained by considering the flow of fluid past a vibrating bluff body whose cross section is not symmetrical with respect to the direction of fluid flow. As shown in Fig. 16.4.3, the direction of the relative velocity of the fluid flow relative to the x -axis, α' , defines the line of action of the drag force, F_D ; the angle α' is defined by the velocity diagram where \dot{x} and \dot{y} denote the velocity of the body in the x and y directions, respectively. The angle α' is known as the "angle of attack". The force normal to the direction of F_D is known as the lift force, F_L . As the x and y components of the velocity of the vibrating body (\dot{x} and \dot{y} in Fig. 16.4.3) vary, the magnitudes of u_{rel} and of the angle of attack α' change. In a non-symmetric body the magnitude and direction of F_L vary rapidly with changes in \dot{x} and \dot{y} . Thus the motion of the body modifies the fluid force acting on it. This type of coupling of fluid forces and body motion is commonly referred to as fluid-elastic feedback. In a symmetric body, $F_L = 0$ and it can be shown that the mutual reinforcing of fluid forces and body motion is not possible. Therefore, an isolated tube cannot be excited due to cross flow by the fluid-elastic mechanism. The situation is somewhat different in a closely packed array of tubes. The movement of any one tube in the cluster modifies the flow field around the tubes in its vicinity. The non-symmetric alteration in the flow field is ac-

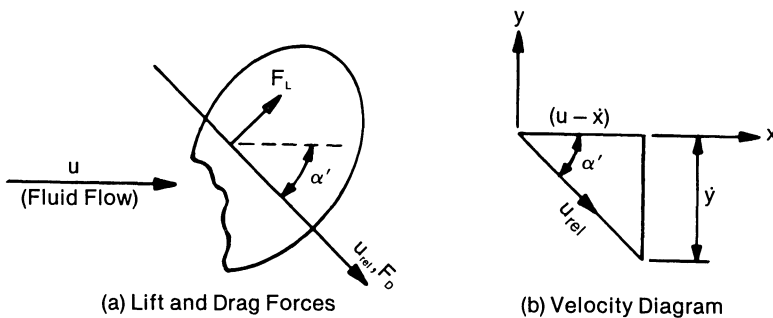


Fig. 16.4.3. Fluid flow past a bluff body.

accompanied by a change in the fluid forces. The changing fluid forces actuate movement of the affected tubes, which in turn further alters the fluid forces acting on the tubes. Thus, the displacement of a tube (due to its elastic compliance) exerts fluid forces on the neighboring tubes, causing the latter to also undergo elastic displacements. This mutual interplay of fluid forces and elastic displacements is known as fluid-elastic excitation. The central feature of this excitation is that the forcing function for the vibration of the tube is due primarily to relative displacement of neighboring tubes with respect to the subject tube rather than the geometry or movement of the tube itself. Another type of fluid-elastic excitation occurs due to “jet switching” which depends on the motion of the tube itself. Jet switching is discussed separately in the next sub-section.

Displacement actuated fluid-elastic feedback, henceforth referred to as “fluid-elastic excitation”, requires a certain arrangement of vibration pattern within the tube array. It has been experimentally observed and theoretically proved that a large number of fluid-elastic “modes” are possible. In all such “modes”, the maximum tube displacement remains nearly unchanged as the fluid velocity is increased until the “critical velocity” is reached. Increasing the fluid velocity past the critical velocity causes exponential growth in the tube displacement. Figure 16.4.4 shows a typical plot of maximum tube deflection versus flow velocity. Fortunately, the critical fluid velocity for a given tube array seems to be largely independent of the displacement modes excited [16.4.4]. Therefore, it is possible to define, through experiments and analysis, a critical velocity for a tube bundle. Numerous such tests have been conducted in the past 15 years. Connors’ experimental work and analytical correlation [16.4.5] is one of the earliest of published efforts to explain and quantify fluid-elastic excitation in closely packed tube arrays. Some of Connors’ experiments reported in Ref. [16.4.5] are quite instructive in explaining the nature of fluid-elastic excitation even though later research shows his model to account for only, a small fraction of the failure mechanisms. Nonetheless, the resumé of Connors’ experiment and model given below is helpful in evolving a physical insight into the tube instability phenomenon.

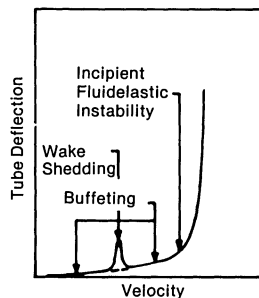


Fig. 16.4.4. General nature of tube maximum deflection as a function of crossflow velocity.

Connors' Experiment and Model

In Connors' experiment, a single tube row array consisting of five whole tubes and two end half tubes, approximately 8" long, is mounted in a wind tunnel (Fig. 16.4.5). The pitch to diameter ratio of the array is 1.41. The central tube is held fixed (immovable) and its ends are properly instrumented to measure lift and drag forces. Tubes on either side of the central tube, denoted as wing tubes in Fig. 16.4.5, are set up such that they can be rotated in prescribed elliptical orbits in symmetric patterns. The motions of the two wing tubes are synchronized so that they are always in the same vertical plane (Fig. 16.4.6). This arrangement simulates stream-wise sinusoidal relative motion of amplitude x_0 of the central tube with respect to transverse sinusoidal motions of amplitude y_0 of the wing tubes. Connors reported [16.4.5] that this mode of relative motion has been observed by other investigators, and therefore represented a credible mode for experimental simulation. Although the central tube in the experiment is actually fixed, it is convenient to talk in terms of its relative streamwise displacement with respect to the wing tubes. Figure 16.4.7 shows the measured drag force on the central tube, also referred to as the "measuring tube". The points $a, b \dots h$ on the drag force plots correspond to the same points shown in the orbital path of the wing tubes in Fig. 16.4.6. Figure 16.4.7 shows that the drag force is higher when the measuring tube is moving downstream with respect to the wing tubes. Since the drag force is

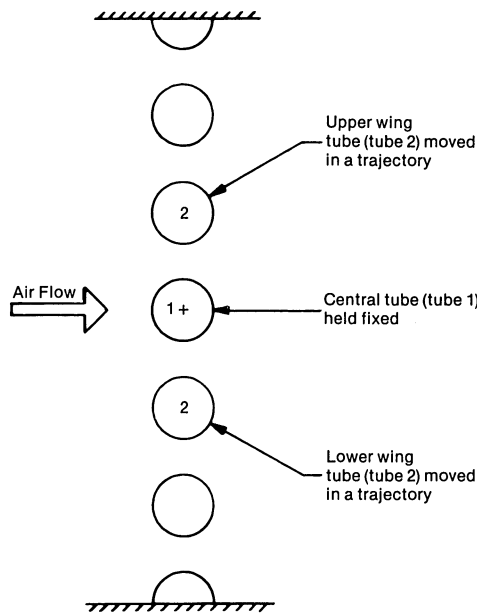


Fig. 16.4.5. Connors' tube row in wind tunnel.

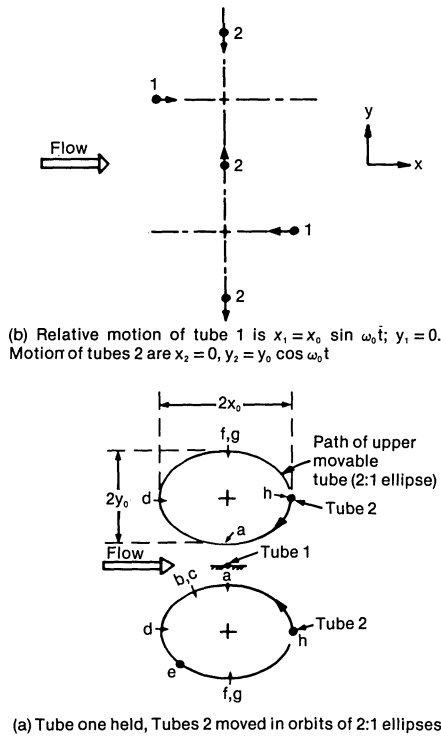


Fig. 16.4.6. Connors' experiment on fluid-elastic excitation.

codirectional with the tube velocity in this portion of the cycle, a positive energy is input into the tube in this segment of the cycle (from *h* to *d* in Fig. 16.4.7). The drag force opposes the tube motion in the remaining half of the cycle; however, its magnitude is smaller. Hence the area enclosed by the force displacement loop represents a net work input to the central tube during each cycle of motion. Figure 16.4.8 shows the force-displacement loop when the central tube is moved in the streamwise direction while holding the wing tubes at a fixed spacing. In both plots, the discontinuities in the drag force (viz. jump down from *b* to *c*; jump up from *f* to *g* in Fig. 16.4.7) are due to the “jet switching” effect which is further explained later. If the trapezoidal area due to “jet switching” is subtracted from the two force displacement loops, it is found that the fixed wing tube condition (Fig. 16.4.8) shows no net energy input into the tube. However, deleting the portion of the force-displacement loop due to “jet switching” in Fig. 16.4.7 (the vibrating wing tube condition) still shows a net energy input. Figure 16.4.9 is adapted from Fig. 16.4.7 by deleting the “jet switching” work area, and also by subtracting the mean drag from the ordinate in Fig. 16.4.7. The variable component of drag plotted in Fig. 16.4.9 clearly shows it to be largely in phase with the central tube velocity.

Further experiments show that the magnitude of the drag force on the measuring tube is directly dependent on the *transverse* amplitude of the wing tubes and is independent of the *streamwise* amplitude of the measuring tube. Recognizing that the variable component of the drag force is substantially in phase with the tube velocity, it can be idealized as a sinusoidal external force in phase with the tube velocity.

The work done by a sinusoidally varying force of amplitude, F_x , which is in phase with a sinusoidally oscillating body of amplitude x_0 is given by

$$\Delta W = \pi x_0 F_x$$

or

$$F_x = \Delta W_x / \pi x_0 \quad (16.4.2)$$

ΔW_x is the total area under the force-displacement loop (Fig. 16.4.9) and x_0 is the amplitude of the motion. It is found that a compatible drag coefficient C_x , defined as:

$$C_x = \frac{F_x}{\frac{1}{2} \rho v^2 d_0 l} \quad (16.4.3)$$

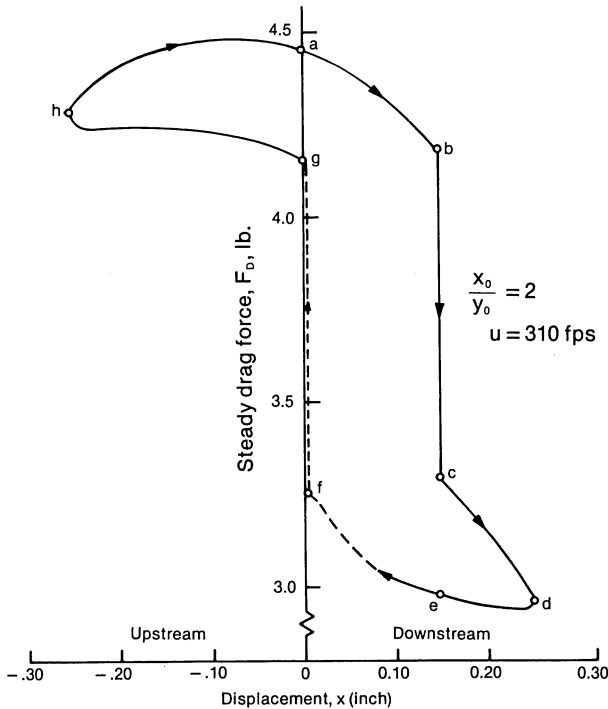


Fig. 16.4.7. Drag force-displacement plot of center tube. Center tube moves in streamwise direction, wing tubes move in transverse direction.

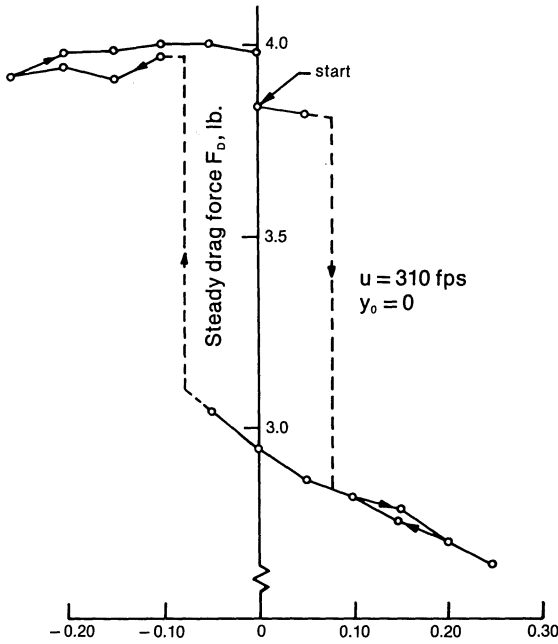


Fig. 16.4.8. Force-displacement loop when center tube moves in streamwise direction, wing tube spacing held fixed.

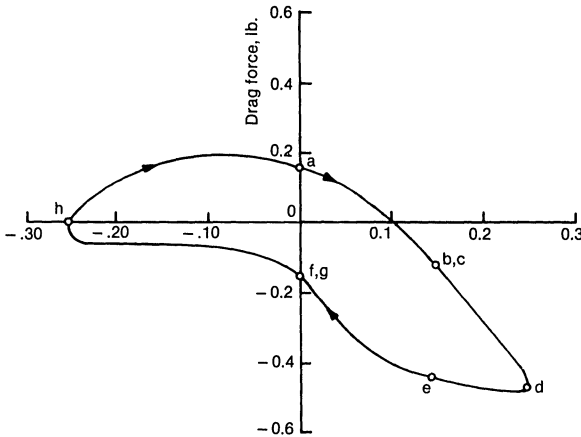


Fig. 16.4.9. Portion of drag force-displacement loop attributed to “displacement mechanism” (arrow indicates relative streamwise velocity direction of center tube).

correlates linearly with the amplitude of transverse motion of wing tubes; i.e.,

$$C_x = K_1 \frac{y_0}{d_0} \quad (16.4.4)$$

In the above equations, ρ and v represent the mass density and velocity (through the nominal gap between the tubes), respectively. d_0 denotes the tube O.D., and l is the tube length exposed to air flow. Thus:

$$\Delta W_x = K_1 \frac{1}{2} \pi \rho v^2 l x_0 y_0 \quad (16.4.5)$$

Connors conducted another experiment which simulated sinusoidal motion of the measuring tube in the transverse direction while the wing tubes moved in the streamwise direction 180° out of phase. Results similar to the symmetric tube experiment were found. The “jet switching mechanism” was again observed. If the area corresponding to the “jet switch” is again deleted from the lift force-displacement loop, then the lift force on the measuring tube is found to be in phase with the tube velocity for nearly the entire course of the displacement cycle. Proceeding as before, a sinusoidal lift force of amplitude F_y , in phase with the tube velocity, can be defined on the basis that it input the amount of work into the tube equal to the area within the lift force-displacement loop.

$$F_y = \frac{\Delta W_y}{\pi y_0} \quad (16.4.6)$$

where ΔW_y is the area of the lift force-displacement loop. We define a pseudo-lift coefficient C_y corresponding to F_y , in the usual manner.

$$C_y = \frac{F_y}{\frac{1}{2} \rho d_0 v^2 l} = \frac{\Delta W_y}{\pi y_0 \frac{1}{2} \rho v^2 d_0 l} \quad (16.4.7)$$

Connors found that C_y was independent of the measuring tube's amplitude, y_0 , in the lift direction, and that C_y correlated linearly with the amplitude of the wing tubes; i.e.,

$$C_y = K_2 \frac{x_0}{d_0} \quad (16.4.8)$$

Thus,

$$\Delta W_y = K_2 \pi \frac{1}{2} \rho v^2 l x_0 y_0 \quad (16.4.9)$$

Connors reasoned that for displacement actuated fluid-elastic excitation to ensue, the net energy input into the tube during a cycle must exceed the

energy dissipated by damping. For a single degree of freedom system executing simple harmonic motion of amplitude a , the energy dissipated by damping is given by (Section 16.9).

$$\Delta W_d = 4\pi^2 f^2 a^2 M_0 \delta \quad (16.4.10)$$

where M_0 , f , and δ are the mass, natural frequency and logarithmic decrement of the system, respectively. Using Eqs. (16.4.5), (16.4.9), (16.4.10), and substituting appropriate values of a , we have the stability threshold defined by:

$$K_1 \pi \frac{1}{2} \rho v^2 l x_0 y_0 = 4\pi^2 f^2 x_0^2 M_0 \delta \quad (a) \quad (16.4.11)$$

$$K_2 \pi \frac{1}{2} \rho v^2 l x_0 y_0 = 4\pi^2 f^2 y_0^2 M_0 \delta \quad (b)$$

These two equations must be satisfied simultaneously. The compatibility condition for the assumed mode of vibration is obtained by dividing the like sides of the two equations into each other:

$$\frac{K_1}{K_2} = \frac{x_0^2}{y_0^2}$$

or

$$\frac{x_0}{y_0} = \left(\frac{K_1}{K_2} \right)^{1/2} \quad (16.4.12)$$

Equation (16.4.12) defines the “mode shape” for fluid-elastic instability. Substituting for y_0 in the L.H.S. of Eq. (16.4.11a) gives:

$$\frac{v}{fd_0} = \alpha \left(\frac{m_0 \delta}{\rho d_0^2} \right)^{1/2} \quad (16.4.13)$$

where $m_0 = M_0/l$, and the instability constant α is given by:

$$\alpha = \frac{(8\pi)^{1/2}}{(K_1 K_2)^{1/4}} \quad (16.4.14)$$

Connors' value of α was 9.9. Later experiments, performed in water, have pushed the consensus value of α downwards. We will discuss the appropriate value for α , in the context of predictive methods, in a later section. It suffices here to state that the basic form of the stability relation involves two dimensionless parameters: dimensionless velocity $v/f_0 d_0$ and fluid-elastic parameter $m_0 \delta / \rho d_0^2$. As we will see, most fluid-elastic correlations are variations of the form of Eq. (16.4.13).

16.4.3 Jet Switching

In Connors' experiment described in the foregoing, the discontinuities in the drag force were attributed to a mechanism known as “jet switching”.

This phenomenon can be observed if fluid is made to flow past a row ($p/d_0 < 1.5$) of tubes. The fluid forms discrete jets as it issues from the space between the cylinders. These jets pair up in the wake of the tube array. Roberts [16.4.6] observed that the jet pairing can be switched back and forth if the tubes in a single row array are displaced alternately one upstream and one downstream by a sufficient amount. The drag force on a tube jumps up when two jets pair behind it, and drops equally abruptly where the jets separate (diverging wake). Figure 16.4.10 shows a rendering of the switching mechanism. Jet switching is seldom responsible for detrimental tube vibrations since it requires a rather specialized set of conditions for its occurrence. In particular, Roberts reports that jet switching cannot occur if the dimensionless velocity $v/fd_0 < 75$.

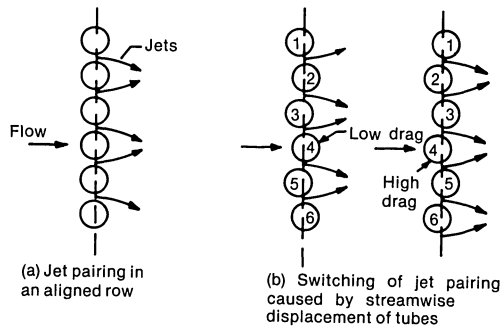


Fig. 16.4.10. Jet pairing in the wake of a tube row.

16.4.4 Acoustic Resonance

Acoustic vibration has been recognized as a serious problem in heat exchange equipment [16.4.7–10]. This problem is associated with high velocity flow of low density fluid in relatively large exchangers. This phenomenon depends on the generation of standing sound waves when the acoustic natural frequency coincides with the frequency of flow periodicity. Since in liquids the speed of sound is high and the equipment dimensions are compact, the acoustic frequencies tend to be quite high in exchangers with liquids in the shell-side. On the other hand, equipment handling gases and steam at low pressure tend to be less compact in size, implying low acoustic frequency. Due consideration of acoustic vibration is warranted in design of the latter class of equipment. Vortex shedding [16.4.11] and turbulent buffeting [16.4.12] have been advanced as the mechanisms responsible for producing the periodicity in energy input into the standing wave column. However, coupling of the input function frequency, and the resonant frequency of the gas does not always produce loud noise. The innate damping of the tube array plays a major role. Therefore, prediction of

acoustic resonance requires, among other things, a detailed knowledge of the frequency spectrum of the energy input into the standing wave stream, and its damping characteristics. Such data is hard to obtain in laboratory conditions, let alone in industrial equipment. Therefore, the predictive techniques rely on an admixture of empirical formulas and practical experience.

Acoustic resonance seldom locks in with tube vibration itself, and therefore poses little risk to the tube bundle. It can, however, produce significant dynamic loads on the walls of the equipment which must be borne by the equipment supports and attached piping. Formulation of the standing wave requires parallel reflecting walls, a clear lane perpendicular to the fluid flow direction and the tube bundle axis. These attributes of acoustic resonance make it relatively easy to diagnose, as discussed in Section 16.12. A summary of the prediction techniques is given in Section 16.7.4.

16.5 FLUID INERTIA MODEL FOR FLUID-ELASTIC INSTABILITY

As stated in Section 16.4.2, Connors' explanation of fluid-elastic instability requires a certain set of trajectories and phase differences in the motion of adjacent tubes. While many tube instabilities observed in laboratory tests exhibit the kind of organized motion suggested by Connors, many others do not. Experiments by Weaver and Grover [16.5.1], and by Weaver and Koroyonnakis [16.5.2], show that a flexible tube located amidst a group of fixed tubes also becomes unstable at approximately the same cross flow velocity as an array wherein all tubes are flexibly mounted. These observations indicate that a specialized set of motion of neighboring tubes is not essential to initiate tube instability. Prompted by these considerations, Lever and Weaver [16.4.4] proposed a theoretical model which explains fluid elastic instability in terms of the inertia of the flow stream. A simplified form of this model, based on their work, is presented in the following.

16.5.1 Fluid Inertia

In order to recognize the underlying mechanisms in this model it is important to gain an insight into the concept called "fluid inertia". A simple transient experiment of one dimensional channel flow illustrates the concept. Figure 16.5.1 shows a thin plate lying along the centerline of a parallel wall channel. The uniform inlet flow (velocity u_0), assumed to be incompressible and inviscid, divides smoothly around the plate such that the mass flow and velocity on either side of the plate are equal. At time $t=0$, the plate is moved laterally by $y=y_0$; where $y_0 \ll A_0$. The movement of the plate increases the area of the lower streamtube, and decreases the area of the upper streamtube by an equal amount. The mass flows through the

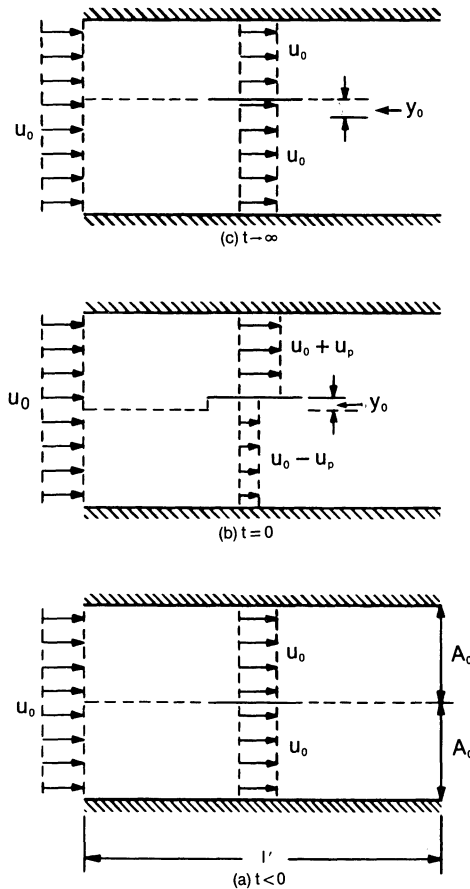


Fig. 16.5.1. Plate in parallel channel – dashed line shows position of dividing streamline.

two streamtubes do not readjust instantly. At $t=0$, the mass flows through the two streamtubes are still equal, causing the velocities to be unequal. Continuity gives the velocity perturbation at $t=0$ (neglecting higher order terms) as u_p , where

$$u_p = \frac{y_0}{A_0} u_0 \quad (16.5.1)$$

Eventually, velocity dependent losses will force the fluid to redistribute itself. The rate of readjustment of the flow is found to depend on the ratio l'/u_0 ; where l' is the length of the flow channel.

The flow through a tube bundle, however, is considerably more complicated. Figure 16.5.2 shows a pictorial idealization of the flow through a triangular tube array.

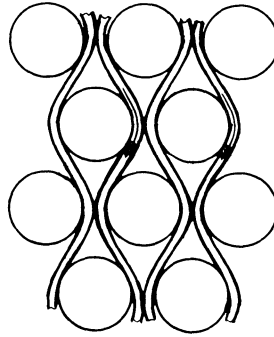


Fig. 16.5.2. Flow idealization in a tight packed triangular array.

Since motion of neighboring tubes does not appear to be essential to the onset of instability, the effect of fluid inertia can be assessed by considering the motion of one movable tube surrounded by fixed tubes. The boundaries around the flow channel straddle the inter-tube column space in such a way that the flow around each tube is identical. A unit depth of streamtubes around the movable tube is shown in Fig. 16.5.3. All characteristics of flow in a streamtube area, velocity and pressure are assumed to be functions of length s , along the streamtube, and of time t only; i.e., the flow is assumed to be one dimensional. This assumption is justifiable only for a close packed array. The movable tube is assumed to execute transverse vibrations

$$y(t) = y_0 \sin \omega t \tag{16.5.2}$$

At $t=0$, the two streamtubes that constitute the flow channel around the movable tube are identical in shape.

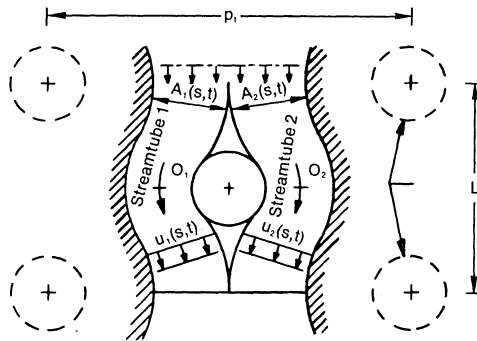


Fig. 16.5.3. Unit cell for fluid-elastic model.

As a first approximation we assume that, under steady state conditions, the flow area of the streamtubes is constant, and equal to A_0 , for all s . The area of streamtube 1 can be written as:

$$A_1(s,t) = A_0 + a(s) \sin[\omega t + \psi(s)]$$

The shape of the second streamtube lags the first by a half cycle of tube vibration, therefore:

$$A_2(s,t) = A_0 + a(s) \sin[\omega t - \pi + \psi(s)]$$

or

$$A_i(s,t) = A_0 + (-1)^{i+1} a(s) \sin[\omega t + \psi(s)] \quad (16.5.3)$$

The coordinate s is located at points O_1 and O_2 for streamtubes 1 and 2, respectively (Fig. 16.5.3).

Similarly, the flow velocity and pressure perturbation functions can be written as:

$$u_i(s,t) = u_0 + (-1)^{i+1} u_p(s) \sin[\omega t + \phi(s)]; \quad i=1,2 \quad (16.5.4)$$

$$P_i(s,t) = P_0 + (-1)^{i+1} P(s) \sin[\omega t + \theta(s)]; \quad i=1,2 \quad (16.5.5)$$

The steady state velocity u_0 and pressure P_0 are constant for all s by virtue of the constant streamtube area assumption made in the foregoing.

The velocity perturbation function $u_p(s)$, and the phase shift $\phi(s)$ can be determined from continuity if the area perturbation function $a(s)$, and its phase shift $\psi(s)$ are specified. The latter depends on fluid inertia. As a first approximation, Lever and Weaver propose that the phase lag between the tube vibration and the resulting flow area change (determined by the motion of the dividing streamline) be given by

$$\psi(s) = \omega \left(\frac{l'}{u_0} \right) \frac{s}{s_0}$$

where l' is the length of the streamline $= 2s_0$. Hence

$$\psi(s) = \frac{2\omega s}{u_0}; \quad -s_0 \leq s < 0 \quad (16.5.6)$$

Notice that the phase lag is zero at $s=0$ since the streamline must follow the tube movement. Further, since s is negative in the direction of the inlet, the harmonic variation in the streamtube area upstream of the tube lags the tube vibration, as expected. Finally, the magnitude of the streamtube area change function $a(s)$ is set equal to the amplitude of tube motion, y_0 .

$$a(s) = y_0 \quad (16.5.7)$$

The physical behavior of the flow field can now be explained in terms of harmonically varying streamtube areas. Motion of the tube alternately accelerates and decelerates the fluid adjacent to it. Mass redistribution of the flow lags the cylinder motion due to fluid inertia. The magnitude of the phase lag of the streamtube areas has been postulated a priori. The streamtube cross sectional area at all locations goes through a harmonic variation. The amplitude of variation is y_0 and the frequency is ω . Only the phase shift of the area variation is a function of s . The one dimensional mass continuity equation can now be used to quantify the nature of the velocity perturbation.

The one dimensional unsteady continuity equation for an incompressible fluid may be written as [16.5.3].

$$\frac{\partial A_i(s,t)}{\partial t} + \frac{\partial}{\partial s} [A_i(s,t)u_i(s,t)] = 0 \quad (16.5.8)$$

where

$$A_i = A_0 + (-1)^{i+1} y_0 \sin \left[\omega t + \frac{2\omega s}{u_0} \right] \quad (16.5.9)$$

$$u_i = u_0 + (-1)^{i+1} u_p(s) \sin [\omega t + \phi(s)] \quad (16.5.10)$$

Therefore,

$$\frac{\partial A_i}{\partial t} = (-1)^{i+1} y_0 \omega \cos \left[\omega t + \frac{2\omega s}{u_0} \right]$$

Substituting for $\partial A_i / \partial t$ in Eq. (16.5.8) and integrating along s starting from the inlet gives:

$$(-1)^{i+1} y_0 \omega \int_{-s_0}^s \cos \left(\omega t + \frac{2\omega s}{u_0} \right) ds + A_i(s,t) u_i(s,t) \Big|_{-s_0}^s = 0 \quad (16.5.11)$$

Substituting for A_i and u_i from above, noting that $u_i(-s_0, t) \equiv u_0$ (no velocity perturbation at inlet), and neglecting terms of higher order (containing the product $y_0 \cdot u_p(s)$) yield:

$$3 \frac{u_0 y_0}{2} \left[\sin \left(\omega t + \frac{2\omega s}{u_0} \right) - \sin \left(\omega t - \frac{2\omega s_0}{u_0} \right) \right] + A_0 u_p(s) \sin [\omega t + \phi(s)] = 0$$

or

$$\frac{3u_0 y_0}{A_0} \cos \left[\omega t + \frac{\omega(s-s_0)}{u_0} \right] \sin \frac{\omega(s+s_0)}{u_0} = u_p(s) \cos \left[\omega t + \phi(s) + \frac{\pi}{2} \right]$$

In order that this equation may hold for all values of s and t , it is required that

$$u_p(s) = \frac{3u_0 y_0}{A_0} \sin \frac{\omega(s+s_0)}{u_0} \quad (16.5.12)$$

$$\phi(s) = -\frac{\pi}{2} + \frac{\omega(s-s_0)}{u_0} \quad (16.5.13)$$

Equations (16.5.12-13) completely determine the velocity distribution function $u_i(s,t)$. The pressure distribution function can be similarly determined using the one dimensional momentum equation [16.5.3].

$$\frac{1}{\rho} \frac{\partial P_i(s,t)}{\partial s} + u_i(s,t) \frac{\partial u_i(s,t)}{\partial s} + \frac{\partial u_i(s,t)}{\partial t} = 0 \quad (16.5.14)$$

Substituting for $u_i(s,t)$, $P_i(s,t)$ from the foregoing, integrating over s and proceeding as before, the equation for the pressure perturbation function $P(s)$ is obtained in terms of known quantities:

$$\begin{aligned} P(s)\sin[\omega t + \theta(s)] = & \frac{3}{2} \rho u_0^2 \frac{y_0}{A_0} \left\{ \sin\omega t \left[\cos \frac{2\omega s}{u_0} - \cos \frac{2\omega s_0}{u_0} \right] \right. \\ & + \cos\omega t \left[\sin \frac{2\omega s}{u_0} + \sin \frac{2\omega s_0}{u_0} \right] \left. \right\} + \frac{3}{4} \rho u_0^2 \frac{y_0}{A_0} \left\{ \sin\omega t \left[\cos \frac{2\omega s}{u_0} \right. \right. \\ & - \cos \frac{2\omega s_0}{u_0} - \frac{2\omega(s+s_0)}{u_0} \sin \frac{2\omega s_0}{u_0} \left. \right] + \cos\omega t \left[\sin \frac{2\omega s}{u_0} \right. \\ & \left. \left. + \sin \frac{2\omega s_0}{u_0} - \frac{2\omega(s+s_0)}{u_0} \cos \frac{2\omega s_0}{u_0} \right] \right\} \end{aligned} \quad (16.5.15)$$

The pressure force leading to the transverse instability of the vibrating tube can be calculated from the pressure distribution along the two streamtubes if the position of flow attachment and separation on the tube surface are known.

$$F_p(t) = l' \int_{s_1}^{s_2} [P_1(s,t) - P_2(s,t)] \cos\beta ds \quad (16.5.16)$$

s_1 and s_2 represent the positions of flow attachment and separating, respectively, and l' is the tube length. Rather than calculate $F_p(t)$ from Eq. (16.5.16), $F_p(t)$ may be approximated by multiplying the pressure difference at the centerline of the tube, $P_1(0,t) - P_2(0,t)$, by an equivalent diameter, D_e . Weaver and Lever state that using $D_e = 0.5d_0$ gives excellent agreement with more detailed analyses. Performing the necessary algebra, the expression for the transverse force on the tube due to fluid inertia is given by:

$$F_p(t) = F_1 \sin\omega t + F_2 \cos\omega t \quad (16.5.17)$$

where

$$\begin{aligned} F_1 = & \frac{3}{2} \rho u_0^2 d_0 l' \frac{y_0}{A_0} \left[1 - \cos \frac{2\omega s_0}{u_0} \right] + \frac{3}{4} \rho u_0^2 d_0 l' \\ & \frac{y_0}{A_0} \left[1 - \cos \frac{2\omega s_0}{u_0} - \frac{2\omega s_0}{u_0} \sin \frac{2\omega s_0}{u_0} \right] \end{aligned} \quad (a) \quad (16.5.18)$$

$$\begin{aligned} F_2 = & \frac{3}{2} \rho u_0^2 d_0 l' \frac{y_0}{A_0} \sin \frac{2\omega s_0}{u_0} + \frac{3}{4} \rho u_0^2 d_0 l' \\ & \frac{y_0}{A_0} \left[\sin \frac{2\omega s_0}{u_0} - \frac{2\omega s_0}{u_0} \cos \frac{2\omega s_0}{u_0} \right] \end{aligned} \quad (b)$$

16.5.2 Stability Criterion

The equation of motion of the vibrating tube is given by

$$m\ddot{y} + C'\dot{y} + Ky = F_p(t) = F_1 \sin \omega t + F_2 \cos \omega t \quad (16.5.19)$$

where m is the total mass of the tube and K is its corresponding structural stiffness. The net system damping coefficient C' may be expressed as:

$$C' = \frac{m\omega\delta}{\pi} \quad (16.5.20)$$

where δ is the logarithmic decrement of damping. Noting Eq. (16.5.2), we see that

$$F_1 \sin \omega t + F_2 \cos \omega t = \frac{F_1}{y_0} y(t) + \frac{F_2}{y_0 \omega} \dot{y}(t).$$

Therefore, Eq. (16.5.19) can be written as:

$$m\ddot{y} + \left(C' - \frac{F_2}{\omega y_0}\right)\dot{y} + \left(K - \frac{F_1}{y_0}\right)y = 0$$

The criterion for instability is

$$C' - \frac{F_2}{\omega y_0} < 0 \quad (16.5.21)$$

since this has the effect of providing negative damping.

Substituting for F_2 and C' from Eqs. (16.5.18) and (16.5.20), respectively, the criterion for stability threshold is obtained in the form

$$\frac{m_0 \delta}{\rho d_0^2} - 3\pi \left(\frac{s_0}{d_0}\right)^2 \left(\frac{d_0}{A_0}\right) u_r^2 \left\{3 \sin \frac{1}{u_r} - \frac{1}{u_r} \cos \frac{1}{u_r}\right\} = 0 \quad (16.5.22)$$

where m_0 is tube mass per unit length and we have defined u_r as

$$u_r = \frac{u_0}{2\omega s_0} \quad (16.5.23)$$

The parameters A_0 and s_0 in the above equation can be defined in terms of the geometry of standard tube layouts. Referring to Fig. 16.5.3, if $\bar{\alpha}$ is the layout angle, then

$$A_0 = \frac{p_t - d_0}{4}; \quad \bar{\alpha} < 90^\circ \quad (16.5.24)$$

and

$$s_0 = \int_0^{L/2} \left[1 + \left(\frac{d\eta}{dx}\right)^2\right]^{1/2} dx; \quad \bar{\alpha} < 90^\circ \quad (16.5.25)$$

$\eta(x)$ describes the shape of the stream tube centerline as a function of x

measured along the longitudinal axis passing through the tube centerline. As a first approximation $\eta(x)$ can be assumed to be a sinusoidal function

$$\eta(x) = \frac{d_0}{4} \cos \frac{2\pi x}{L}; \quad \bar{\alpha} < 90^\circ \quad (16.5.26)$$

For $\bar{\alpha} = 90^\circ$ (square layout);

$$A_0 = \frac{p_t - d_0}{2}; \quad s_0 = p \quad (16.5.27)$$

Stability charts for the meaningful range of parameters can be generated from Eq. (16.5.22). Lever, et al., [16.4.4] show that inclusion of pressure drop due to flow around the tube, and due to fluid damping has little effect on the stability boundary. They also recommend adjusting D_e to account for the curvature of the streamtube which depends on the solidity of the array. Readers interested in further material on this model should consult Ref. [16.4.4].

16.6 NATURAL FREQUENCY

16.6.1 Basic Concepts

Calculation of the natural frequency of the heat exchanger tube is an essential step in estimating its potential for flow induced vibration failure. In the parlance of mechanical vibration theory, a tube is considered as a “distributed mass” or “continuous system”. Linear vibration of continuous systems possesses many attributes, some of which are of interest to us in this chapter. We state them with reference to the heat exchanger-tube without proof in the following. Readers who wish to explore this subject in depth can refer to any one of the many excellent texts [e.g., Refs. [16.6.1–5] on this subject.

(i) The free vibration of a tube is harmonic in nature; the solution for the motion has the general form

$$y(x,t) = \psi(x)\sin(\omega t + \theta) \quad (16.6.1)$$

where ω is the frequency of vibration, and $\psi(x)$ is called the “mode shape.”

(ii). The tube has an infinite number of mode shapes corresponding to an infinite number of natural frequencies. The foregoing equation can therefore be rewritten as:

$$y(x,t) = \psi_n(x)\sin(\omega_n t + \theta_n); \quad n = 1, 2, \dots \infty \quad (16.6.2)$$

where ψ_n , ω_n and θ_n are respectively the mode shape, the natural frequency, and the phase angle for the n th free vibration mode.

The smallest value of ω_n is referred to as the “fundamental frequency” and the corresponding vibration shape is known as the “fundamental mode shape”. A tube supported at its two ends and subjected to external fluid cross flow is, in general, excited in its fundamental mode. Indeed, all

predictive correlations to be given in Section 16.7 utilize the fundamental frequency of the tube. The meaning of the term “fundamental” requires careful consideration when multi-span tubes are involved. We will return to this matter later in this section.

A typical heat exchanger tube has two basic shapes, and two types of supports: The basic shapes are (a) straight span; and (b), U-bend. The common support conditions are: (a) fixed at the tubesheet; and (b), propped at the baffle supports. In reality, the baffle supports have clearances which render them non-linear when considered as props. The tubesheet is not rigid and therefore the “built-in” assumption is only approximately true. These approximations, however, are known to have little effect on the computed natural frequencies. In the next section, we consider free vibration of a single span tube; the results of our study will aid us in devising simplified formulas for computing meaningful frequencies for multi-span tubes.

16.6.2 Single Span Tube

The classical governing equation for vibration of a long slender tube of length l , mass m_0 per unit length, and sectional moment of inertia I , is given by (Fig. 16.6.1):

$$-EI \frac{\partial^4 y}{\partial x^4} = m_0 \frac{\partial^2 y}{\partial t^2} \quad 0 \leq x \leq l \quad (16.6.3)$$

where E is the Young's modulus of the tube material.

Assuming a solution of the form of Eq. (16.6.2), substituting in the above equation, and dividing throughout by $\sin(\omega_n t + \theta_n)$, yields

$$\frac{d^4 \psi_n}{dx^4} = \kappa^4 \psi_n \quad (16.6.4)$$

where

$$\kappa^4 = \frac{\omega_n^2 m_0}{EI} \quad (16.6.5)$$

ψ_n is any function of x whose fourth derivative is equal to the function itself multiplied by the constant, κ^4 . A convenient form of the solution is given by

$$\psi_n(x) = A_n(\cos \kappa x + \cosh \kappa x) + B_n(\cos \kappa x - \cosh \kappa x) + C_n(\sin \kappa x + \sinh \kappa x) + D_n(\sin \kappa x - \sinh \kappa x) \quad (16.6.6)$$

A_n , B_n , C_n and D_n are chosen to satisfy the tube end conditions. In applying the end conditions, the following expressions for derivatives of ψ_n will be useful.



Fig. 16.6.1. Vibrating tube.

$$\frac{d\psi_n}{dx} = \kappa [A_n(-\sin\kappa x + \sinh\kappa x) + B_n(-\sin\kappa x - \sinh\kappa x) + C_n(\cos\kappa x + \cosh\kappa x) + D_n(\cos\kappa x - \cosh\kappa x)] \quad (16.6.7)$$

$$\frac{d^2\psi_n}{dx^2} = \kappa^2 [A_n(-\cos\kappa x + \cosh\kappa x) + B_n(-\cos\kappa x - \cosh\kappa x) + C_n(-\sin\kappa x + \sinh\kappa x) + D_n(-\sin\kappa x - \sinh\kappa x)] \quad (16.6.8)$$

$$\frac{d^3\psi_n}{dx^3} = \kappa^3 [A_n(\sin\kappa x + \sinh\kappa x) + B_n(\sin\kappa x - \sinh\kappa x) + C_n(-\cos\kappa x + \cosh\kappa x) + D_n(-\cos\kappa x - \cosh\kappa x)] \quad (16.6.9)$$

We now consider various tube end conditions:

i. Both ends simply supported

The boundary conditions for a tube of length l are:

$$x = 0, l; y = 0 \text{ (zero deflection)}$$

$$x = 0, l; \frac{\partial^2 y}{\partial x^2} = 0 \text{ (zero end moments)}$$

These conditions imply (using Eq. (16.6.2))

$$\psi_n(0) = \psi_n(l) = 0$$

$$\psi_n''(0) = \psi_n''(l) = 0$$

where primes indicate differentiation with respect to x .

Using Eqs. (16.6.6–9), the conditions $\psi_n(0) = \psi_n''(0)$ yield

$$A_n = B_n = 0$$

The conditions $\psi_n(l) = \psi_n''(l)$ give the result

$$C_n(\sin\kappa l + \sinh\kappa l) + D_n(\sin\kappa l - \sinh\kappa l) = 0$$

$$C_n(-\sin\kappa l + \sinh\kappa l) + D_n(-\sin\kappa l - \sinh\kappa l) = 0$$

Therefore:

$$\frac{C_n}{D_n} = -\frac{\sin\kappa l - \sinh\kappa l}{\sin\kappa l + \sinh\kappa l} = \frac{\sin\kappa l + \sinh\kappa l}{-\sin\kappa l + \sinh\kappa l} \quad (16.6.10)$$

This yields the result

$$\sin\kappa l = 0 \quad (16.6.11)$$

or

$$\kappa l = n\pi$$

$$\kappa = \frac{n\pi}{l}; \quad n = 1, 2, \dots \infty \quad (16.6.12)$$

Having determined κ , the expression for the frequency ω_n follows from Eq. (16.6.5)

$$\frac{n^4 \pi^4}{l^4} = \frac{\omega_n^2 m_0}{EI}$$

or

$$\omega_n = \frac{n^2 \pi^2}{l^2} \left(\frac{EI}{m_0} \right)^{1/2} \text{ rad/sec} \quad (16.6.13)$$

The fundamental frequency corresponds to $n=1$ (first mode). Substituting Eq. (16.6.11) in Eq. (16.6.10) gives $C_n = D_n$. Referring to Eq. (16.6.7) the mode shapes are given to within an arbitrary constant, by

$$\sin \frac{n\pi x}{l} = 0; \quad n = 1, 2, \dots, \infty \quad (16.6.14)$$

ii. *One end fixed, the other end simply supported*

The boundary conditions are

$$\text{At } x=0, y=0; \quad \frac{\partial y}{\partial x} = 0 \text{ (zero slope condition)}$$

$$\text{At } x=l, y=0; \quad \frac{\partial^2 y}{\partial x^2} = 0 \text{ (zero moment condition)}$$

which imply:

$$\text{@ } x=0, \quad \psi_n = 0, \quad \psi_n' = 0$$

$$\text{@ } x=l, \quad \psi_n = 0, \quad \psi_n'' = 0$$

Utilizing Eqs. (16.6.6-8) we obtain the results

$$A_n = C_n = 0$$

$$\frac{B_n}{D_n} = - \frac{\sin \kappa l - \sinh \kappa l}{\cos \kappa l - \cosh \kappa l} = \frac{\sin \kappa l + \sinh \kappa l}{-\cos \kappa l - \cosh \kappa l} \quad (16.6.15)$$

Equation (16.6.15) can be simplified to give the characteristic equation

$$\tan \kappa l = \tanh \kappa l$$

The first few roots of this equation are found by numerical analysis to be

$$\kappa l = 3.927, 7.069, 10.210, \dots$$

Thus the natural frequency is given by Eq. (16.6.5) as

$$\omega_n = \frac{\lambda_n^2}{l^2} \left(\frac{EI}{m_0} \right)^{1/2}; \quad n = 1, 2, \dots \quad (16.6.16)$$

where

$$\lambda_n = 3.927, 7.069, 10.210, \dots$$

The single span tube frequency equation for the usual classical boundary conditions always has the general form of Eq. (16.6.16). The frequency constant λ_n depends on the nature of the boundary conditions. We have illustrated two cases here. Some other typical cases are summarized in Table 16.6.1.

Table 16.6.1. Natural Frequency and Mode Shapes for Uniform Beams

(i) Supports	(ii) Mode	(iii) Frequency Equation	(iv) Constants Eq. 16.6.6	(v) λ_n	(vi) Ratio of non-zero constants; R Column (iv)
Hinged- hinged	1	$\sin\lambda_n = 0$	$A_n = B_n = 0$ $\frac{C_n}{D_n} = 1$	π	1.0
	2			2π	1.0
	3			3π	1.0
	4			4π	1.0
	\vdots				
	n			$n\pi$	1.0
Clamped- clamped	1	$\cos\lambda_n \cosh\lambda_n = 1$	$A_n = C_n = 0$ $\frac{D_n}{B_n} = R$	4.73	-0.9825
	2			7.853	-1.0008
	3			10.996	-1.0000 -
	4			14.137	-1.0000 +
	\vdots				
	n			$\approx \frac{(2n+1)\pi}{2}$	-1.0000 -
Clamped- hinged	1	$\tan\lambda_n = \tanh\lambda_n$	$A_n = 0$	3.927	-1.0008
	2		$C_n = 0$	7.069	-1.0000 +
	3		$\frac{D_n}{B_n} = R$	10.210	-1.0000
	4			13.352	-1.0000
	\vdots				
	n			$\approx \frac{(4n+1)\pi}{4}$	-1.0000
Clamped- free	1	$\cos\lambda_n \cosh\lambda_n = -1$	$A_n = 0$	1.875	-0.7341
	2		$C_n = 0$	4.694	-1.0185
	3		$\frac{D_n}{B_n} = R$	7.855	-0.9992
	4			10.996	-1.0000 +
	\vdots				
	n			$\approx \frac{(2n-1)\pi}{2}$	-1.0000 -

16.6.3 Multiple Span Tube

Most heat exchangers have multiple baffle supports. The length of the individual spans and the shellside cross flow velocities may vary widely. However, state-of-the-art flow induced vibration prediction correlations (Section 16.7) are not sophisticated enough to treat the multi-span tube vibration problem by a single comprehensive analysis. Instead, the susceptibility to vibration of each tube span is examined individually. The value of the natural frequency, used in evaluating the vibration potential of a particular span, is taken as the value corresponding to the tube mode shape which shows the most appreciable relative deflection in that same span. In most cases, a close lower bound on the pertinent natural frequency of an interior span (baffle supports on both ends) is obtained by treating it as a pinned-pinned beam ($\lambda_n = n\pi$). Similarly, the pertinent frequency of an end span (tubesheet at one end, baffle support at the other), is obtained by simulating it as a fixed-pinned beam ($\lambda_1 = 3.927$). However, if the complete solution for the frequency equation is required, such a solution can be developed by considering each span as a separate beam with its origin at the left support. Equation (16.6.6) then applies to each span. Since the deflection can be set to zero at the origin of each section, $A_n = 0$, and the equation reduces to:

$$\psi_n = B_n(\cos \kappa x - \cosh \kappa x) + C_n(\sin \kappa x + \sinh \kappa x) + D_n(\sin \kappa x - \sinh \kappa x)$$

The solution procedure is illustrated by considering the N -span tube shown in Fig. 16.6.2. The subscript n can be dropped from ψ and from the constants of integration (B_n , C_n , etc.) in the following as long as we remember that there is an infinite set of solutions (normal modes) for the problem.

Let ψ_i denote the solution for span i ;

$$\psi_i = B_i(\cos \kappa x_i - \cosh \kappa x_i) + C_i(\sin \kappa x_i + \sinh \kappa x_i) + D_i(\sin \kappa x_i - \sinh \kappa x_i) \quad (16.6.17)$$

where B_i , C_i , and D_i are undetermined constants for span i .

The following boundary conditions are available:

$$(i). \quad \text{Left span; } @x_1 = 0, \psi' = 0 \quad (16.6.18)$$

$$(ii). \quad \text{Intermediate support between spans } i \text{ and } (i + 1);$$

Let x_i denote the length coordinate in this span, then

$$@x_i = l_i; \quad \psi_i = 0 \quad (16.6.19)$$

$$\left. \frac{d^2 \psi_i}{dx_i^2} \right|_{x_i=l_i} = \left. \frac{d^2 \psi_{i+1}}{dx_{i+1}^2} \right|_{x_{i+1}=0} \quad (\text{Moment continuity}) \quad (16.6.20)$$

$$\left. \frac{d\psi_i}{dx_i} \right|_{x_i=l_i} = \left. \frac{d\psi_{i+1}}{dx_{i+1}} \right|_{x_{i+1}=0} \quad (\text{Slope continuity}) \quad (16.6.21)$$

(iii). *Rightmost support (span N):*

$$@x_N = l_N, \psi_N = \psi_N' = 0 \text{ (two equations)} \quad (16.6.22)$$

Thus three equations at each one of the $(N-1)$ intermediate supports, and a total of three equations from the two end spans furnish $3N$ linear algebraic equations in the $3N$ unknowns (B_i , C_i , and D_i ; $i = 1, 2, \dots, N$).

The requirement for a non-trivial solution is that the coefficient determinant must vanish identically. Discrete values of κ which make the determinant zero define the normal modes.

This technique to obtain the natural frequencies for the multi-span tube is implemented in the computer program MULTSPAN, described in Appendix 16.A, wherein a numerical example is also given.

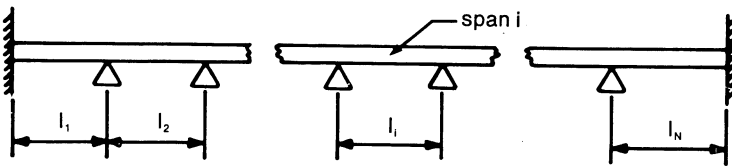


Fig. 16.6.2. Multi-span uniform beam with fixed ends.

16.6.4 Tube Under Axial Load

The very nature of the function of a heat exchanger subjects the tubes to a certain level of axial load. In fixed tubesheet heat exchangers without expansion joints, such loads can reach high values (see Chapter 9). Even U-tube exchangers develop some axial load in the legs of the U (ref. Chapter 14). As noted previously, compressive axial loads depress the natural frequency, tensile loads elevate it. The effect of a compressive axial load on the natural frequency is relatively minor so long as the load is a small fraction of the critical buckling load, F_{cr} . As a rough rule of thumb, a compressive load F reduces the natural frequency by a fraction ϵ , where $\epsilon = F/2F_{cr}$, as long as $F \ll F_{cr}$. At this point, all we can say is that the reduction in the frequency can certainly be significant as F approaches F_{cr} , but will not be expressible by the simple parameter ϵ .

Equations to determine the actual reduction in the natural frequency in the presence of an axial load are derived in the following. Specific formulas are presented for pinned-pinned, and for fixed-pinned configurations.

General Equations for a Single Span Beam

In the presence of an axial force F (positive if tensile) the equation of free vibration of the beam (Eq. (16.6.3)) is modified as follows:

$$-EI \frac{\partial^4 y}{\partial x^4} + F \frac{\partial^2 y}{\partial x^2} = m_0 \frac{\partial^2 y}{\partial t^2} \quad (16.6.23)$$

Assuming a solution of the form of Eq. (16.6.2), and proceeding as before, the deflection equation for ψ_n now takes the form:

$$\frac{d^4 \psi_n}{dx^4} - \frac{F}{EI} \frac{d^2 \psi_n}{dx^2} - \frac{m_0 \omega_n^2}{EI} \psi_n = 0 \quad (16.6.24)$$

We let

$$a_c = F/EI \quad (16.6.25)$$

and note that Eq. (16.6.5) defines the quantity $m_0 \omega_n^2 / EI$.

The solution of Eq. (16.6.24) is again given in terms of four constants of integration (A_n , B_n , C_n , and D_n) as:

$$\psi_n(x) = A_n \sinh m_1 x + B_n \cosh m_1 x + C_n \sin m_2 x + D_n \cos m_2 x \quad (16.6.26)$$

where the parameters m_1 , m_2 are defined below:

$$m_1 = \left[\frac{a_c + (a_c^2 + 4k^4)^{1/2}}{2} \right]^{1/2}$$

$$m_2 = \left[\frac{-a_c + (a_c^2 + 4k^4)^{1/2}}{2} \right]^{1/2} \quad (16.6.27)$$

A_n , B_n , etc. must be determined by the particular set of boundary conditions that are applicable for the tube.

Single Span Beam (Length = l); Simply Supported Ends

Following the procedure of Section 16.6.2 will lead to the following characteristic equation

$$\sin m_2 l = 0 \quad (16.6.28)$$

This gives, in conjunction with Eqs. (16.6.27) and (16.6.25), the frequency equation

$$\omega_n = \frac{n^2 \pi^2}{l^2} \left(\frac{EI}{m_0} \right)^{1/2} \left[1 + \frac{Fl^2}{EI \pi^2 n^2} \right]^{1/2} \quad (16.6.29)$$

Referring to Eq. (16.6.16), we note that due to F the natural frequency coefficient λ_n is modified by a factor Λ , where

$$\Lambda = \left(1 + \frac{Fl^2}{EI \pi^2 n^2} \right)^{1/4} \quad (16.6.30)$$

Noting that the critical Euler load for a pinned-pinned beam is

$$F_{cr} = \frac{\pi^2 EI}{l^2} \quad (16.6.31)$$

We have,

$$\Lambda = (1 + F/n^2 F_{cr})^{1/4} \quad (16.6.32)$$

Finally, the integration constants are defined by the following relationships:

$$B_n = D_n = 0$$

$$\frac{A_n}{C_n} = -\sin m_2 l / \sinh m_1 l \quad (16.6.33)$$

Substituting these expressions into Eq. (16.6.26) gives the mode shape. We note that for $F/n^2 F_{cr}$ small, $\Lambda^2 \approx 1 + F/2n^2 F_{cr}$ which proves our “rule of thumb”, mentioned previously, for $n = 1$.

Beam of Span l , One End Fixed, the Other Pinned

Applying the appropriate boundary conditions (given before in Section 16.6.2), and performing the necessary algebra, the following characteristic equation is obtained.

$$m_1 \tan m_2 l = m_2 \tanh m_1 l \quad (16.6.34)$$

Equation (16.6.34) can be solved for different values of F . The expression for fundamental natural frequency can be written in the familiar form

$$\omega = \frac{\lambda_1^2 \Lambda^2}{l^2} \left(\frac{EI}{m_0} \right)^{1/2}$$

where λ_1 is 3.927 for a fixed-pinned beam (Table 16.6.1). Λ is plotted in Fig. 16.6.3.

The integration constants are given by the following equations:

$$B_n = -D_n = -A_n \frac{\sinh m_1 l - \frac{m_1}{m_2} \cosh m_1 l}{\sin m_2 l - \cos m_2 l}$$

$$C_n = -A_n m_1 / m_2 \quad (16.6.35)$$

Substituting for these constants in Eq. (16.6.26) gives the mode shape.

16.6.5 U-Bend Region

The mathematical model for determining the natural frequency of the U-bend region is shown in Fig. 16.6.4. The extent of the tube modeled consists of the 180° bend region and the straight extensions up to the bend-end tube supports. Bending and rotational springs, located at the supports, model the structural contribution of the adjacent tube spans. One intermediate spring prop at angle θ_1 simulates the presence of intermediate tube supports.

Various cases of out-of-plane vibration of circular rings and U-tubes have been presented in Refs. [16. 6.6–8]. The work by Lee [16.6.8] is considered the most general case.

In the following the solution procedure for estimating the pertinent natural frequency of the U-bend region is presented. We follow the approach used in [16.6.8] in our development here.

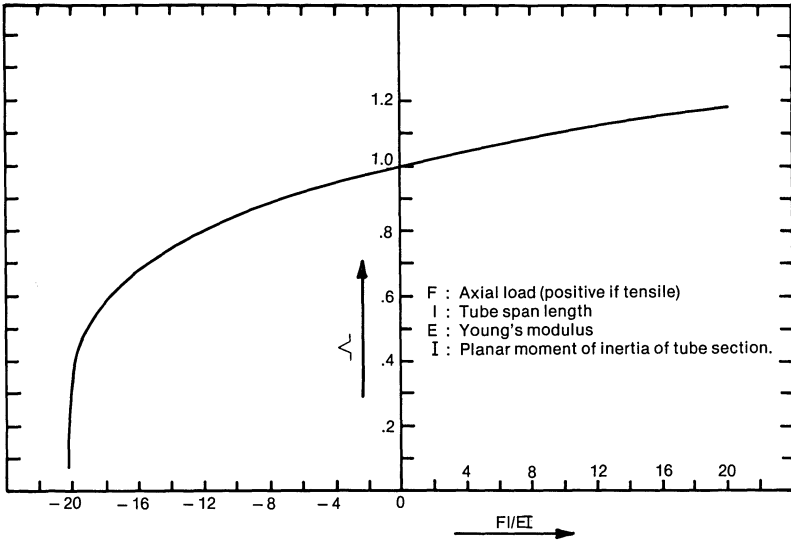


Fig. 16.6.3. λ as a function of dimensionless axial load.

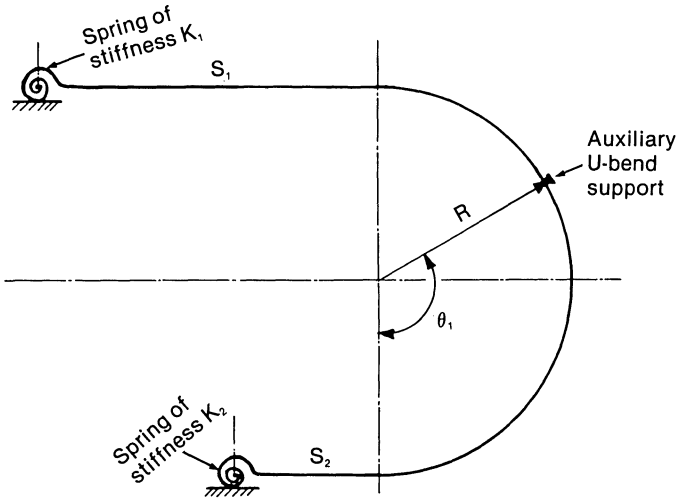


Fig. 16.6.4. U-bend geometry for computer program UVIB (Appendix 16.B).

16.6.5.1 Equations of Motion and Solution for a Circular Ring Segment

The out-of-plane vibration of a circular ring is characterized by two quantities: the out-of-plane displacement v_i and the twist β . The equations of motion are given by



$$\frac{\partial^4 v_t}{\partial \theta^4} - R \frac{\partial^2 \beta}{\partial \theta^2} - k \left(\frac{\partial^2 v_t}{\partial \theta^2} + R \frac{\partial^2 \beta}{\partial \theta^2} \right) = \frac{-m_0 R^4}{EI} \frac{\partial^2 v_t}{\partial t^2} \quad (16.6.36)$$

$$\frac{\partial^2 v_t}{\partial \theta^2} = \frac{1}{(1+k)} \left(R\beta - kR \frac{\partial^2 \beta}{\partial \theta^2} \right) \quad (16.6.37)$$

where m_0 is the mass per unit length and

$$k = 1/(1 + \nu) \quad (16.6.38)$$

We assume solutions of the form:

$$v_t(\theta, t) = V(\theta) \cos(\omega t + \phi) \quad (a)$$

$$R\beta(\theta, t) = W(\theta) \cos(\omega t + \phi) \quad (b)$$

Substituting for v_t , β , and their derivatives in Eqs. (16.6.36–37) and dividing throughout by $\cos(\omega t + \phi)$ yields:

$$V'''' - W'' - k(V'' + W'') = \frac{m_0 R^4}{EI} V \omega^2 \quad (a)$$

$$V'' = \frac{1}{1+k} (W - kW'') \quad (b)$$

where a prime indicates differentiation with respect to θ . Let

$$\frac{m_0 R^4}{EI k} \omega^2 = q \quad (16.6.41)$$

Equations (16.6.40) can be recast in the following form:

$$V = - \frac{1}{(1+k)q} [W'''' + 2W'' + W] \quad (16.6.42)$$

$$W'''' + 2W'''' + W''(1 - qk) + qW = 0 \quad (16.6.43)$$

Equation (16.6.43) is a sixth order ordinary differential equation. Therefore, its solution involves six constants of integration (say G_i ; $i = 1, 2, \dots, 6$). Assuming a solution of the form $e^{\lambda\theta}$; the characteristic equation for λ is given by

$$\lambda^6 + 2\lambda^4 + \lambda^2(1 - qk) + q = 0 \quad (16.6.44)$$

Equation (16.6.44) furnishes six roots say λ_i ; $i = 1, 2, \dots, 6$. Thus the solution for $W(\theta)$ may be formally written as:

$$W(\theta) = \sum_{i=1}^6 G_i e^{\lambda_i \theta} \quad (16.6.45)$$

The expression for V can also be written in terms of G_i ($i = 1 \dots 6$) using Eq. (16.6.42).

The six integration constants can be determined by using the end

boundary conditions. For example, the boundary conditions for a semi-circular tube fixed at its two ends are

$$@\theta=0,\pi; v_t = \beta = \frac{\partial V}{\partial \theta} = 0$$

16.6.5.2 Solution for the U-Tube Problem

The problem shown in Fig. 16.6.4 consists of two circular segment spans and two straight spans. We have just shown that the solution for a circular segment involves 6 constants of integration. It was also shown earlier in this section that the solution for a straight span contains four unknown constants of integration. Thus a total of 20 (2 times 6 plus 2 times 4) integration constants must be determined using the boundary and inter-span conditions. Discrete values of q (Eq. (16.6.41)) make the coefficient determinant zero. These values of q define the corresponding natural frequency, ω , by the relation (Eq. (16.6.41))

$$\omega = \frac{q^{1/2}}{R^2} \left[\frac{EI}{(1+\nu)m_0} \right]^{1/2} \text{ rad/sec} \quad (16.6.46)$$

A description of a suitable solution procedure, implemented in computer program "UVIB", is presented in Appendix 16.B. The general solution for the problem described by Fig. 16.6.4 is presented there; the source code is available separately [16.6.9]

16.6.5.3 Approximate Solutions

Approximate solutions for the fundamental frequency ω for some common design situations are given below:

i. No intermediate U-bend support, and U-bends supported symmetrically as shown in Fig. 16.6.5: l_s denotes the straight tube segment length between the baffle centerline and the U-bend tangent. l_b is the spacing between the baffle supports. A good approximation for the value of ω can be obtained by considering the natural frequency of a spring mounted cantilever of length $l_e = 1.35R + l_s$, where the support spring constant is taken as $\tau = 3EI/l_b$ (Fig. 16.6.6).

Following the method described in earlier parts of this section, the natural frequency is given by

$$\omega = \frac{\lambda^2}{l_e^2} \left(\frac{EI}{m_0} \right)^{1/2} \quad (16.6.47)$$

where λ is obtained by solving the transcendental equation

$$1 + \cos \lambda \cosh \lambda + 2\lambda \bar{\gamma} (\cos \lambda \sinh \lambda - \sin \lambda \cosh \lambda) = 0 \quad (16.6.48)$$

where

$$\bar{\gamma} = \frac{EI}{\pi l_e} = \frac{l_b}{3l_e} \tag{16.6.49}$$

The values of λ as a function of $\bar{\gamma}$ are given in Table 16.6.2.

Table 16.6.2. Values of λ (Eq. (16.6.47))

$\bar{\gamma}$	0	0.1	0.2	0.3	0.4	0.5	0.6	0.7	0.8	0.9	1.0
λ	1.85	1.62	1.47	1.38	1.31	1.25	1.20	1.16	1.13	1.10	1.08
$\bar{\gamma}$	1.1	1.2	1.3	1.4	1.5	1.6	1.7	1.8	1.9	2.0	
λ	1.05	1.03	1.01	1.0	.98	.97	.95	.94	.93	.92	

ii. Midspan supported, symmetrically held U-tube: Values for $q^{1/2}$ in Eq. (16.6.46) are plotted as a function of l_b/r in Fig. 16.6.7. The lowest out-of-plane natural frequency is defined by Eq. (16.6.46).

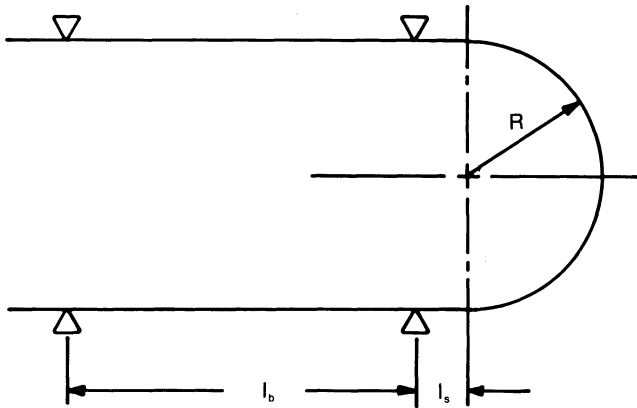


Fig. 16.6.5. Geometry for Eq. (16.6.47).

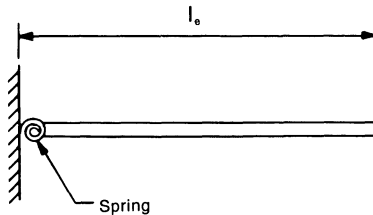


Fig. 16.6.6. Equivalent cantilever.

16.7 CORRELATIONS FOR VIBRATION PREDICTION

16.7.1 Fluid-Elastic Correlations

Fluid-elastic feedback based correlations give the maximum value of cross flow velocity as a function of tube diameter d_0 , natural frequency f , total tube mass per unit length m_0 , and total logarithmic decrement, δ ,

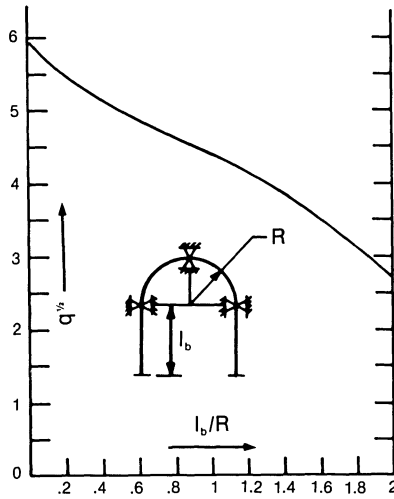


Fig. 16.6.7. Plot of $q^{1/2}$ for mid-span supported U-tube.

associated with the vibrating tube. All of the correlations have the general form:

$$\frac{v}{fd_0} = \alpha \left(\frac{m_0}{\rho d_0^2} \right)^a \delta^b \tag{16.7.1}$$

where

v = Mean gap cross flow velocity through the tube array:

$$v = \frac{P}{p - d_0} u \quad (p = \text{tube layout pitch})$$

α = Threshold instability constant (or Fluid-elastic parameter)
 ρ = Shellside medium fluid density

a and b are empirical constants. Most investigators use $a = b$. We will refer to the quantity $m_0 \delta / \rho d_0^2$ as the “damping parameter”, χ

$$\chi = \frac{m_0 \delta}{\rho d_0^2} \tag{16.7.2}$$

Similarly, the dimensionless velocity, v/fd_0 will be denoted as v^* .

There is a great deal of uncertainty in the precise definition of δ and m_0 . Sections 16.8–9 will address this matter in some detail. The quantity f refers to the natural frequency of the tube span, which is the frequency at which the span under consideration has, relatively speaking, its maximum vibration amplitudes.

Empirical correlations by numerous investigators are summarized below. This summary is essentially a compendium of published design guidelines. Our preferred calculation method out of this information base is presented in Section 16.13.

i. *Connors, Blevins, Savkar, Weaver and Grover, Pettigrew, et al.:*

$$v^* = \alpha \chi^{0.5} \quad (16.7.3)$$

Connors [16.4.5] uses the data of Moretti and Lowery [16.8.5] for the definition of hydrodynamic mass. Pettigrew et al., [16.7.1] consider the virtual mass coefficient (see Eq. (16.8.3)) $C_m = 1$.

α is the "threshold instability constant" which depends on the pitch to diameter ratio and on the tube layout. Connors gives the following formulas for α , for a square layout.

$$\alpha = 0.37 + 1.76 \frac{p_t}{d_0}; 1.41 \leq \frac{p_t}{d_0} \leq 2.12 \quad (16.7.3)$$

where p_t is the transverse pitch.

For 30° triangular array, Connors gives $\alpha = 10(p/d_0 - 1)$; $1.25 \leq p/d_0 \leq 1.41$, where p is the layout pitch. Pettigrew, et al., [16.7.2] recommend $\alpha = 3.3$ for design purposes. Gorman [16.7.3–4] and Halle, et al., [16.7.5–6] endorse Pettigrew's recommendation after examining the response of multiple span arrays under multipass flow conditions.

Savkar [16.7.7] proposes:

$$\alpha = 4.95 \left(\frac{p_t}{d_0} \right)^2 \quad (16.7.4)$$

for 30° triangular arrays.

Weaver and Grover [16.7.8] give the relation $v^* = 7.1\chi^{0.21}$ for $p/d_0 = 1.375$ in a 45° array.

Soper [16.7.9] conducted extensive wind-tunnel experiments to study the effect of tube layout on fluid-elastic stability of tube arrays. He found that:

- A 60° layout geometry is most prone to fluid-elastic instability, having a value of α approximately 2.2 for p/d_0 in the range of 1.27 to 1.78.
- A 30° geometry becomes less prone to fluid-elastic instability as the bundle solidity is reduced. α increases from 2.5 to 6.4 as p/d_0 is increased from 1.25 to 1.78.
- For the square geometry, the lowest critical velocity corresponds to $p/d_0 = 1.52$; both closer and wider spacings being more resistant to instability.
- A 45° layout exhibits the greatest resistance to fluid-elastic whirling; however, it is more prone to acoustic resonance.

ii. *Gilbert et al.:*

Gilbert, Sagner and Doyen [16.7.10] conducted extensive tests on tube arrays of different geometries and solidities in water and air. Their experiments indicate that:

$$\begin{aligned} v^* &\propto \chi^{0.5} & \chi > 20 \\ v^* &\propto \chi^{0.3} & 20 > \chi > 7 \end{aligned} \quad (16.7.5)$$

where v^* and χ are the reduced velocity and fluid-elastic parameter, respectively.

The correlation over the entire data set is given by the equation:

$$v^* = 2.7\chi^{0.34} \quad (16.7.6)$$

iii. *Chen and Jendrzejczyk:*

Using water flow based experimental data [16.7.11] gathered on twelve different arrays of different tube solidities and damping, Chen and Jendrzejczyk find the following correlation for design purposes.

$$v^* = 2.49\chi^{0.52} \quad (16.7.7)$$

iv. *Weaver and El-Kashlan:*

Weaver et al., [16.7.12] conducted experiments wherein δ was kept constant while $m_0/\rho d_0^2$ was varied, and vice versa. Their correlation has the form:

$$v^* \propto \left(\frac{m_0}{\rho d_0^2} \right)^{0.29} \delta^{0.2} \quad (16.7.8)$$

v. *Rémy and Bai:*

Rémy and Bai (16.7.13–15) evaluated a large number of experimental data on real life hardware. Recognizing the difficulties in ascertaining δ , they propose a design criterion of the form:

$$v^* = \alpha' \left(\frac{m_0}{\rho d_0^2} \right)^{1/2} \quad (16.7.9)$$

where $\alpha' = \alpha\delta^{1/2}$

vi. *Y. N. Chen:*

Y. N. Chen [16.4.11] proposed the following relationship for critical gap velocity, v_g , for fluid-elastic instability:

$$\frac{v_g}{fd_0} = \frac{\beta x \chi}{R_e^{0.25}} \quad (16.7.10)$$

where the correlating parameter β varies from 19 to 36. x is the smaller of (p_1/d_0) and $(2p_1/d_0)$. v_g is the velocity in the narrowest gap of the tube bank.

This correlation includes a weak dependence of the critical velocity on the Reynolds number. The critical velocity v_g is seen to vary linearly with the pitch to diameter ratio.

vii. *Paidoussis, et al.:*

Paidoussis [16.7.16] proposed the following design guideline by fitting a large bank of experimental data from various researchers:

$$\frac{v}{fd_0} = C \left(\frac{m_0}{\rho d_0^2} \right)^{0.4} \delta^{0.4} \left(\frac{p}{d_0} - 1 \right)^{0.5} \quad (16.7.11)$$

where $C = 5.8$ if one neglects a small number of experiments; $C = 2.3$ incorporates all data available at that time. p is the layout pitch.

More recently, Price and Paidoussis [16.7.17] have proposed the criterion

$$v^* = 16.9 \left[\frac{(p_t^2 + p_l^2)^{1/2}}{d_o} - 1 \right]^{1.7} [1 + \{1 + 0.365\chi\}^{1/2}] \quad (16.7.12)$$

viii. *S. S. Chen:*

S. S. Chen in [16.7.18] has developed a set of stability bounds for different standard tube layouts by plotting data from a large number of investigators [16.7.19–31]. Chen's plots may be found in Figs. 16.7.1 to 16.7.5. The same bounds are given in equation form by Table 16.7.1.

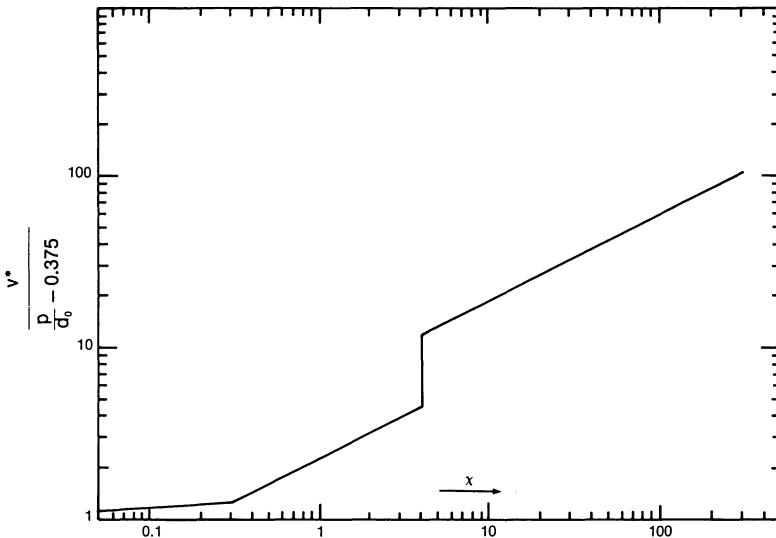


Fig. 16.7.1. Chen's stability diagram for single tube row transverse to flow.

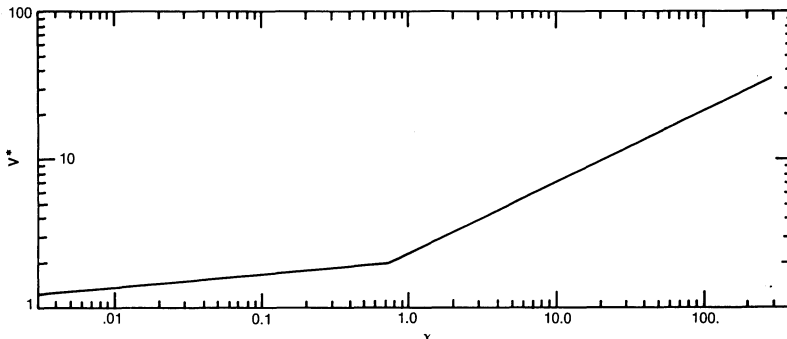


Fig. 16.7.2. Chen's stability diagram for square arrays.



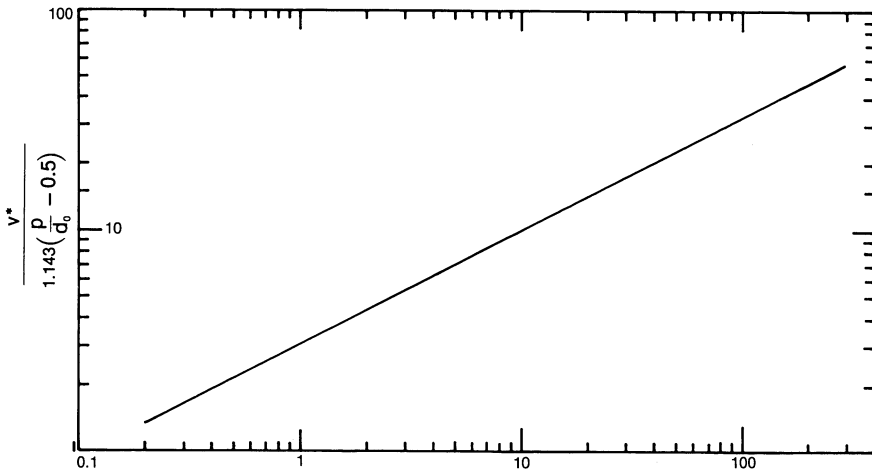


Fig. 16.7.3. Chen's stability diagram for rotated square arrays (45° layout).

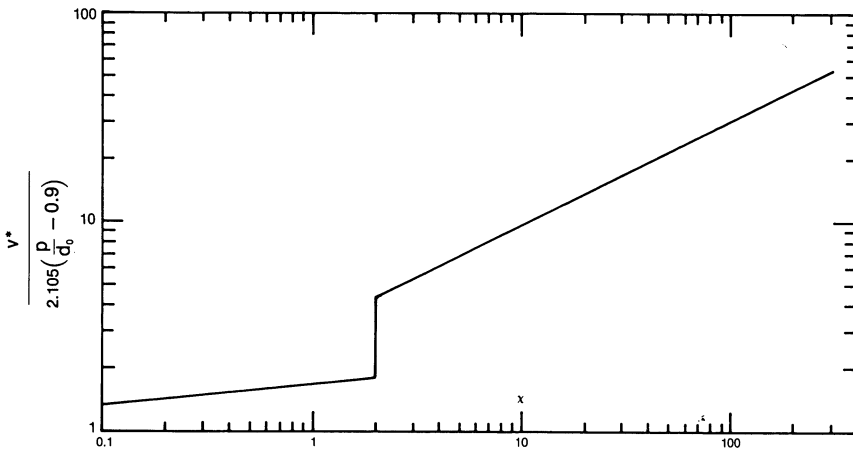


Fig. 16.7.4. Chen's stability diagram for triangular arrays (30° layout).

16.7.2 Turbulent Buffeting Correlations

The presence of turbulent flow is nearly universal in heat exchanger bundles. A turbulent flow field is characterized by a mean flow velocity on which a band of velocities associated with eddies and vortices are superposed. A tube in the path of such a flow experiences a steady drag force,

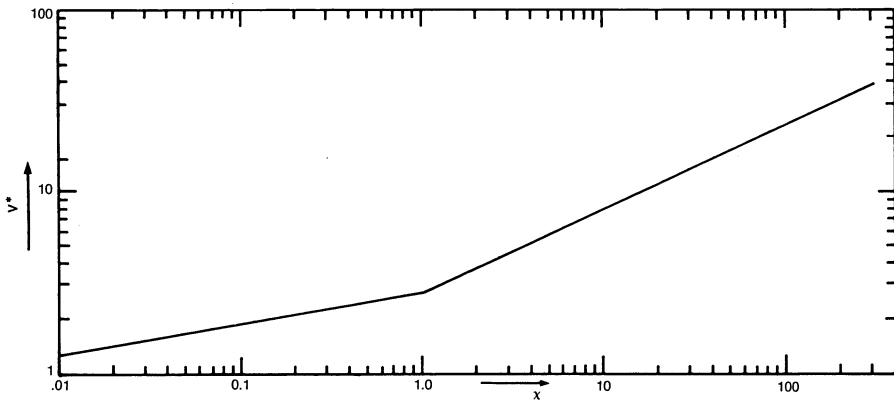


Fig. 16.7.5. Chen's stability diagram for rotated triangular arrays (60° layout).

Table 16.7.1. Lower Bound on Critical Flow Velocity from Ref. [16.7.18]

Array	Parameter Range for χ	$\frac{v}{fd_0}$
One Tube Row transverse to flow	$0.05 < \chi < 0.3$	$1.35(p/d_0 - 0.375)\chi^{0.06}$
	$0.3 < \chi < 4.0$	$2.30(p/d_0 - 0.375)\chi^{0.5}$
	$4.0 < \chi < 300$	$6.00(p/d_0 - 0.375)\chi^{0.5}$
Square (90°)	$0.03 < \chi < 0.7$	$2.10\chi^{0.15}$
	$0.7 < \chi < 300$	$2.35\chi^{0.5}$
Rotated Square (45°)	$0.1 < \chi < 300$	$3.54(p/d_0 - 0.5)\chi^{0.5}$
Triangular (30°)	$0.1 < \chi < 2$	$3.58(p/d_0 - 0.9)\chi^{0.1}$
	$2 < \chi < 300$	$6.53(p/d_0 - 0.9)\chi^{0.5}$
Rotated Triangular (60°)	$0.01 < \chi < 1$	$2.8\chi^{0.17}$
	$1 < \chi < 300$	$2.8\chi^{0.5}$

and a series of periodic forces associated with the eddies. Thus, the fluid force acting on the tube may be described as an aggregate of a band of pulsating forces. If the natural frequencies of the tube are far removed from the frequency range of the turbulent forces, then the energy imparted to the tube is small. The tube dissipates this energy through the damping mechanisms described in Section 16.9, and therefore the tube vibration amplitude remains small. However, if any of the tube natural frequencies

lies within the frequency spectrum of the turbulent forcing function, then a condition of resonance can be realized. From a designer's perspective, two questions are important.

- What is the range of frequencies associated with a turbulent flow in a tube bank?
- If the tube natural frequency lies within the range of forcing function frequencies, is the magnitude of the associated forces enough to actuate a large amplitude tube vibration?

Observations indicate that it is possible to define a "peak" turbulent buffeting frequency, f_{ib} , around which the hub of the turbulent flow energy is clustered. The answer to the second question requires precise knowledge about the randomness of the forcing function which is difficult to quantify even in laboratory tests. However, researchers have been able to bound the problem by developing relations for "some average of tube deflection amplitude" assuming an idealized level of coherence in the forcing functions. The details of the mathematical derivation are omitted here; however, the final working equations, excerpted from certain sources, are given in the following to facilitate design work.

i. Pettigrew and Gorman [16.7.1-3]:

In their generalized model, Pettigrew et al., recognize a finite correlation length for the flow excitation field, different boundary conditions for the tube, and a tube response in all of its normal modes. The practical formulas are finally derived, however, by assuming the excitation field to be fully correlated spanwise, the tube to be simply supported, and the vibration of the tube to be in the first mode. With these simplifications, the mid-span root-mean-square (rms) amplitude of the tube, y_{rms} , is given by:

$$y_{rms} = \frac{S_p^{1/2}}{(4\pi^5 f^3 m_0^2 \zeta)^{1/2}} \quad (16.7.13)$$

where S_p is the power-spectral-density of the excitation force per unit tube length. f and ζ denote the fundamental tube frequency and the corresponding fractional damping, respectively. S_p in Eq. (16.7.13) is defined in terms of the "effective random excitation coefficient" C_R^* which is plotted in Fig. 16.7.6 based on the data collected by Pettigrew and Gorman:

$$S_p^{1/2} = \frac{1}{2} \rho v^2 d_0 C_R^* \quad (16.7.14)$$

These values of C_R^* were determined by experiments in water. It is noted from Fig. 16.7.6 that the response of the tubes facing the shell inlet nozzle is predicted to be stronger than the tubes in the interior of the bundle.

ii. Blevins [16.7.26]:

Paidoussis [16.1.4] quotes the following expression for mid-span rms deflection of the tube due to Blevins:

$$y_{\text{rms}} = \frac{S_F^{1/2} J \psi(l/2)}{(64\pi^3 f^3 m_0^2 \zeta)^{1/2}} \quad (16.7.15)$$

where $\psi(l/2)$ is the mode shape deflection at mid-span, and J is the joint acceptance (which is unity for a perfectly correlated field). The power spectral density function S_F can be evaluated from Fig. 16.7.7 which is based on wind tunnel test data of Blevins, Gilbert and Villard [16.7.26].

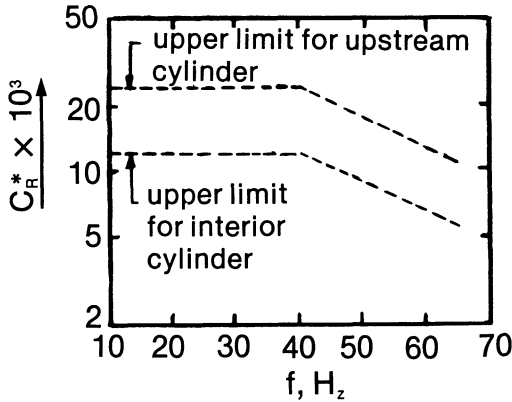


Fig. 16.7.6. Random excitation coefficient C_R^* for calculating buffeting response of a cylinder array in crossflow (Pettigrew, et al.).

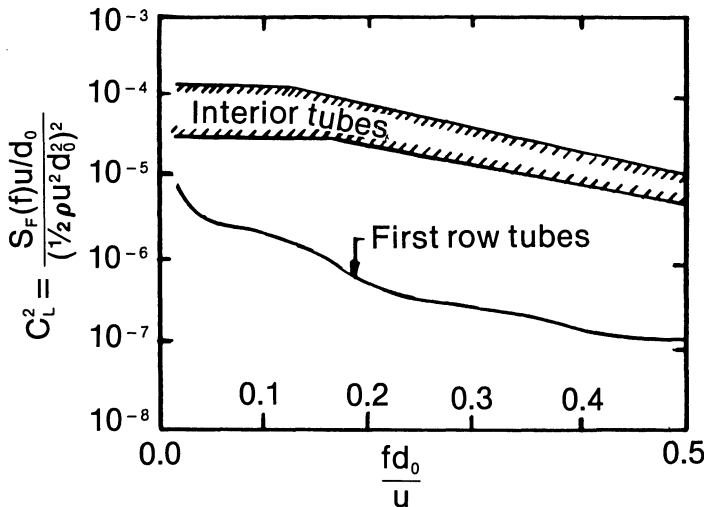


Fig. 16.7.7. Lift coefficient C_L for buffeting response of a cylinder in crossflow. (Blevins, et al.).

In contrast to the Pettigrew and Gorman data, the Blevins correlation seems to indicate that the interior tubes will experience greater deflection

than the upstream tubes. This is possibly due to differences in the upstream turbulence between the two sets of data.

iii. Owen [16.7.32]:

In a frequently quoted paper [16.7.32], Owen contested the thesis that rhythmic shedding of vortices was responsible for large amplitude tube vibration. Noting that any turbulent flow contains a fluctuating pressure field, Owen reasoned that the tubes extract energy from the turbulent energy spectrum selectively in the manner of a narrow band filter. Largely through heuristic reasoning, buttressed with experimental data, he proposed the following expression for the turbulent buffeting frequency, f_{ib} .

$$f_{ib} = \frac{v}{d_0 x_t x_i} \left[3.05 \left(1 - \frac{1}{x_t} \right)^2 + 0.28 \right] \quad (16.7.16)$$

where $x_t = p_t/d_0$ and $x_i = p_i/d_0$.

Tube amplitude will grow rapidly if the tube natural frequency coincides with f_{ib} . This formula is not recommended when $x_t \rightarrow 1$. Weaver and Grover [16.5.1] compared Owen's predicted frequency with their experimental data, and concluded that f_{ib} given by the above equation is quite reliable, even as $x_t \rightarrow 1$, so long as one uses the minimum gap velocity v_g instead of the mean gap velocity v in that equation.

16.7.3 Periodic Wake Shedding

As stated before, organized shedding of vortices observed in fluid flows past isolating cylinders is difficult to visualize in a densely packed tube array. Although what happens is not quite understood, certain experiments [16.7.2,33] indicate the existence of a well defined lateral displacement peak at a specific crossflow velocity for a tube bundle. Pettigrew and Gorman [16.7.31] observed that the peak response corresponds to the pseudo-Strouhal Number S between 0.34 to 0.67, where

$$S = \frac{f d_0}{v}$$

This phenomenon has been called "periodic wake shedding". Assuming a wake shedding force in the lift direction to be "fully correlated"* to the tube vibration, Pettigrew, et al., derived the expression for maximum rms deflection of the tube using standard techniques. The lift force due to periodic wake shedding may be defined in terms of a dynamic lift coefficient C_L as:

$$F_L = C_L \frac{\rho}{2} d_0 v^2 \text{ (per unit tube length)} \quad (16.7.17)$$

*A fully correlated forcing function is one whose time periodicity is identical to the vibrating body over the entire span of the body.

The tube response in the fundamental mode for a fully correlated forcing function can be shown to be

$$y(x) = \frac{m_0 \psi}{\omega C} \int_0^l F_L(x') \psi(x') dx' \quad (16.7.18)$$

where $\psi(x')$ is the mode shape, normalized such that

$$\int_0^l m_0 \psi^2 dx' = 1 \quad (16.7.19)$$

and C is the damping coefficient per unit length of tube. Assuming the velocity to be uniform over the tube span, the expression for $y(x)$ becomes:

$$y(x) = \frac{m_0 \psi F_L}{\omega C} \int_0^l \psi(x') dx' \quad (16.7.20)$$

As noted in Section 16.6, for practical design purposes, it is sufficiently accurate to treat a tube span situated between two baffles as having simply supported ends. For this case the normalized mode shape is

$$\psi(x) = \left(\frac{2}{m_0 l} \right)^{1/2} \sin \frac{\pi x}{l} \quad (16.7.21)$$

Substituting for ψ in the above integral and integrating we have

$$y(l/2) = F_L / (\pi^2 \delta m_0 f^2) \quad (16.7.22)$$

where $y(l/2)$ is the peak amplitude at mid-span.

Pettigrew et al., find that $C_L = 0.07$ gives an upper estimate of the rms midspan response due to periodic wake shedding resonance. They recommend keeping the maximum response to less than 2% of the tube diameter.

16.7.4 Acoustic Resonance Correlation

Prediction of acoustic resonance requires knowledge of: (i), the resonant acoustic frequency of the shellside chamber; (ii), the frequency of the exciting force; and (iii), the damping in the system.

i. Acoustic frequency:

The frequency of a sonic wave, f_a is related to the velocity of sound c and to the wave length of the sound wave λ by the simple relationship

$$c = f_a \lambda \quad (16.7.23)$$

In order that the walls of the heat exchanger act as "reflectors" of the sonic wave, λ must be an integral submultiple of the distance between the walls, w .

$$w = \frac{n\lambda}{2} \quad (a)$$

or

$$(16.7.24)$$

$$f_a = \frac{cn}{2w} \quad (b)$$

Figure 16.7.8 shows typical wave forms for $n = 1$ and 4. n may be thought of as the mode count for the gas oscillations. Finally, one dimensional wave theory gives the velocity of sound c in a gas medium as

$$c = \left[\frac{z\gamma g_c R^* T}{M} \right]^{1/2} \quad (16.7.25)$$

where

z = Compressibility factor for the gaseous medium at the coincident pressure and temperature.

γ = Ratio of specific heat at constant pressure to specific heat at constant volume of the medium

R^* = Universal gas constant

g_c = Gravitational constant

T = Absolute temperature of the gas

M = Molecular weight of the gas

The preceding three equations can be combined to yield the resonant acoustic frequency:

$$f_a = \frac{n}{2w} \left[\frac{z\gamma g_c R^* T}{M} \right]^{1/2}; \quad n = 1, 2, \dots \quad (16.7.26)$$

ii. Exciting frequency:

The exciting frequency can be calculated using the turbulent buffeting formula of Owen (Eq. (16.7.16)) or the vortex shedding formula (Eq. (16.4.1)) where the Strouhal number S is plotted as a function of x_i and x_i for various tube array geometries. Chen's charts, shown in Figs. 16.7.9 and 16.7.10, have been widely used by designers. Given the complexity of the subject, experimentalists [16.4.12] find either method satisfactory for correlation purposes.

iii. Damping:

Even in laboratory tests, the exciting frequency often coincides with the acoustic frequency and yet no standing wave develops. The reason lies in the energy dissipation inherent in the tube array. Based on their experimental data, Grotz and Arnold [16.7.34] proposed a damping parameter Φ based on the slenderness of the chamber, and on the wave length λ of the standing wave.

$$\Phi = \frac{\lambda}{2p_i'} \quad (16.7.27)$$

The parameter p_i' is the transverse passage width in the bundle. The criterion for ensuring absence of sonic resonance is

$$\Phi > 80 \quad (16.7.28)$$

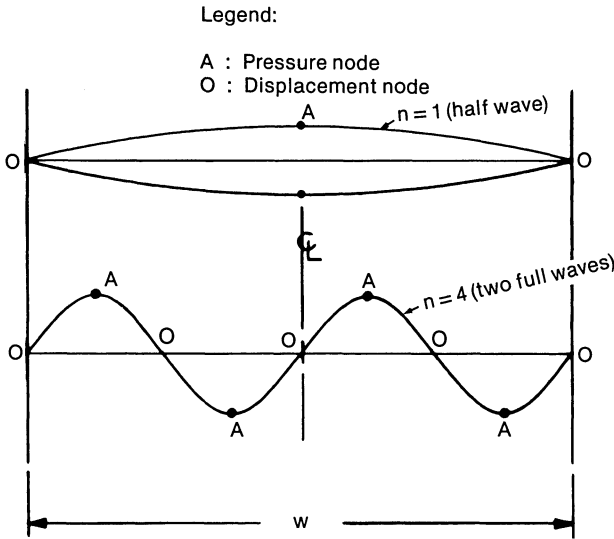


Fig. 16.7.8. Typical standing wave forms.

Several empirical criteria have been proposed to assess the possibility of acoustic resonance. Some of the frequently quoted ones are summarized below.

i. *Y. N. Chen:*

Chen [16.4.3, 16.7.35] has proposed empirical formulas for in-line arrays. According to Chen:

- a. Resonance may occur if the cross flow velocity v_c through the bundle exceeds the vortex shedding threshold:

$$v_c > \frac{fd_0}{S} \quad (16.7.29)$$

where S is obtained from Figs. 16.7.9–10.

- b. Probability of resonance is high if, in addition to satisfaction of (a) above, ψ^* exceeds 2000, where

$$\psi^* = \frac{\text{Re}}{Sx_l} \left(1 - \frac{1}{4x_l^2}\right) \quad (16.7.30)$$

ii. *Bryce, Wharmby and Fitzpatrick:*

Bryce, et al., [16.7.36] proposed that sonic resonance will only occur if:

$$\frac{v_c}{f_a d_0} > 2(x_l - 0.5) \quad (16.7.31)$$

iii. *Barrington:*

Barrington [16.4.10] defined the critical range of resonance as:

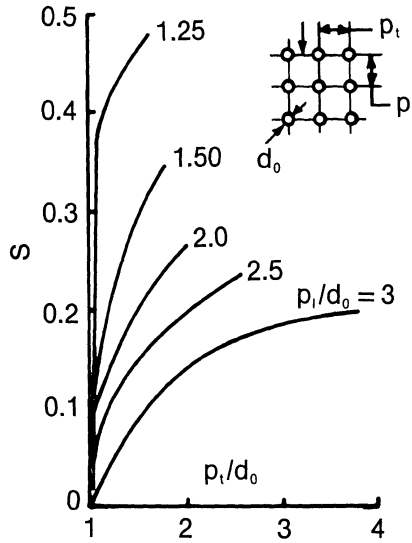


Fig. 16.7.9. Strouhal number for in-line banks of plain tubes.

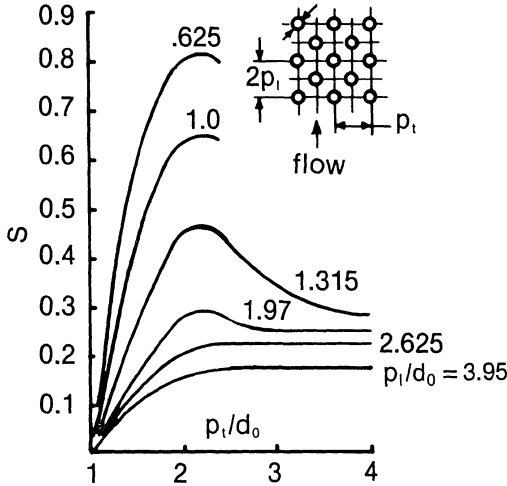


Fig. 16.7.10. Strouhal number for staggered bank (45° layout) of plain tubes.

$$0.8f_e < f_a < 1.2f_e \tag{16.7.32}$$

where f_e is the exciting frequency.

The acoustic frequency is given by Eq. (16.7.26), wherein w is the distance between the reflecting surfaces. Barrington presented two possible fundamental mode wave forms: the diametral wave form (Fig. 16.7.11);

and, inscribed square forms (Fig. 16.7.12). It is seen that the value of w is D and $0.707 D$, respectively. Other forms may also exist. However, a standing wave will form in a path which requires the least amount of exciting energy.

Clearly, these prediction methods are quite simplistic in the face of the highly complex nature of the acoustic vibration phenomenon.

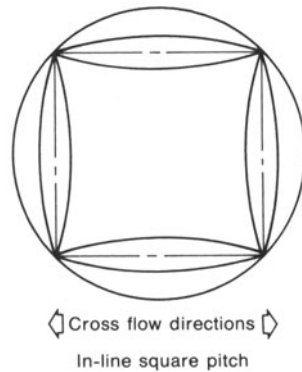
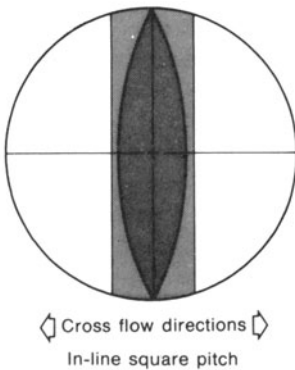
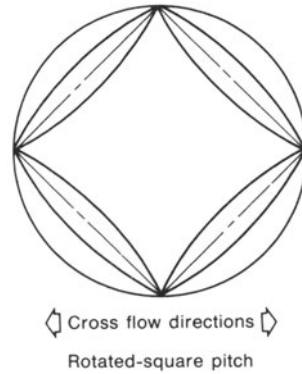
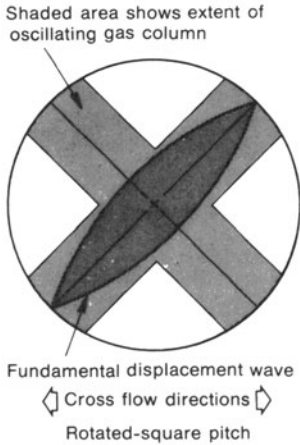


Fig. 16.7.11. Position of diametral standing wave.

Fig. 16.7.12. Position of inscribed square standing wave.

16.8 EFFECTIVE TUBE MASS

As seen in the preceding section, the effective mass of the tube plays an important role in all tube vibration prediction methods. The tube mass directly affects its natural frequency (Section 16.6) and therefore must be calculated with care. In what follows, the term “effective tube mass” refers to the total tube mass per unit tube length. This term has three contributory

components: (i), the metal mass of the tube per unit tube length; (ii), the contained fluid mass per unit length; and (iii), the hydrodynamic mass due to the presence of shellside fluid and the proximity of other tubes or the shell wall. The first two terms are readily calculated from basic data. Computation of the third term, the hydrodynamic mass, is more involved. Designers of ocean going vessels have long recognized the importance of hydrodynamic mass in the dynamic behavior of the body. Its consideration in heat exchanger tube vibration is equally important.

When the tubes vibrate inside the shell, the shellside fluid must be displaced to accommodate motion of the tube. This results in varying fluid pressures on the tube surface. The integrated effect of these pressures is the hydrodynamic force which acts on the tube in the manner of an inertia force. It is customary to include the effect of the hydrodynamic force by augmenting the mass of the vibrating body by the hydrodynamic (or virtual) mass.

An isolated cylinder, moving at a constant velocity in an ideal (inviscid) fluid, experiences no hydrodynamic force. This phenomenon is known as D'Alembert's paradox. In contrast, a body moving at a variable velocity experiences a resistance, and the body behaves as though an added mass has been firmly attached to it. The total force required to accelerate the body is given by:

$$F = (m + m_a) \ddot{x} + C_v \dot{x} \quad (16.8.1)$$

where m is the body mass, m_a is the hydrodynamic mass, x indicates the displacement coordinate, and C_v is the viscous damping coefficient. As in other sections of this text, the number of dots on a quantity indicates the order of its derivative with respect to time. The linear term $C_v \dot{x}$ approximates the effect of fluid viscosity. If the fluid is inviscid, then $C_v = 0$. Similarly, the forces acting on two proximate bodies of mass m_1 and m_2 , vibrating in an inviscid fluid medium, have the form [16.8.1].

$$F_1 = (m_1 + M_{11}) \ddot{x}_1 + M_{12} \ddot{x}_2 \quad (16.8.2)$$

$$F_2 = M_{21} \ddot{x}_1 + (m_2 + M_{22}) \ddot{x}_2$$

where F_1 and F_2 are forces acting on bodies m_1 , and m_2 , respectively. M_{11} , M_{12} , and M_{22} are terms in the 2×2 virtual mass matrix. This matrix is symmetric; $M_{12} = M_{21}$. The terms of this matrix depend on the inter-body gap, on the fluid density, etc. The previous statements are valid only for small amplitude vibrations; the equations for the forces F_1 and F_2 include non-linear terms in velocity and acceleration if the motions are not infinitesimal [16.8.2]. However, in calculations involving stability thresholds, one does not have to contend with large amplitude motion.

In general, the hydrodynamic mass matrix for a body having n degrees of freedom has $n(n+1)/2$ distinct terms. Similarly, k bodies, each with n degrees of freedom, require a matrix of order $(nk \times nk)$ for characterization of the virtual mass effect.

Since the virtual mass matrix is symmetric, one can find its eigenvalues. These eigenvalues are called effective virtual masses; and play the same role as the hydrodynamic mass of a single body [16.8.1]. Expression for virtual mass for many cases of practical interest are reported in Refs. [16.8.3–4]. The cases of interest for the tube vibration problem are summarized below. The virtual mass m_a is expressed in terms of the virtual mass coefficient, C_m , defined as

$$C_m = \frac{m_a}{\rho V'} \quad (16.8.3)$$

where V' is the fluid volume displaced by the body, and ρ is the fluid density.

i. A single cylinder in an infinite, viscous fluid:

This case is not of importance in heat exchanger tube bundles. However, it serves as an instructive benchmark. The values of C_m and C_v for a long cylinder vibrating perpendicular to its axis in an infinite viscous medium of kinematic viscosity ν' , is given by

$$C_m = \text{Re}(H) \quad (16.8.4)$$

$$C_v = -\rho\pi r^2\omega \text{Im}(H) \quad (16.8.5)$$

where H is defined by the equations

$$H = 1 + \frac{4K_1(\alpha)}{\alpha K_0(\alpha)} \quad (a)$$

$$\alpha = (i\Gamma)^{1/2} \quad (b) \quad (16.8.6)$$

$$\Gamma = \frac{\omega r^2}{\nu'} \quad (c)$$

K_1 and K_0 are modified Bessel functions of the second kind. When Γ is very large, we can obtain the following limiting forms:

$$C_m = 1 + 2(2/\Gamma)^{1/2}$$

$$\text{Im}(H) = -2(2/\Gamma)^{1/2} - (2/\Gamma)$$

Finally, if $\nu' = 0$ (inviscid fluid), then $H = 1$ which yields

$$C_m = 1; \quad C_v = 0$$

This is the familiar case in which the hydrodynamic mass is equal to the displaced fluid mass.

Values of H are given in Fig. 16.8.1 as a function of Γ .

ii. A circular cylinder near a wall:

The hydrodynamic mass of a circular cylinder near a parallel wall is independent of the motion in an ideal fluid; C_m is given in [16.8.3] by the expression

$$C_m = 1 + 4\sinh^2 \alpha^* \sum_{m=1}^{\infty} m \frac{e^{-3m\alpha^*}}{\sinh(m\alpha^*)}$$

where

$$\alpha^* = \ln \left[\frac{r + g + \{(r + g)^2 - r^2\}^{1/2}}{r} \right]$$

C_m is presented as a function of g/r in Fig. 16.8.2. r is the radius of the cylinder and g is the nominal gap. We note that C_m goes to 1 as $g/r \rightarrow \infty$ (the case of isolated body).

iii. A group of cylinders:

A group of k parallel tubes, arranged in a hexagonal array (Fig. 16.8.3), submerged in an infinite ideal fluid, and vibrating in the two orthogonal planes normal to the tube axes, requires a matrix of order $2k$ for

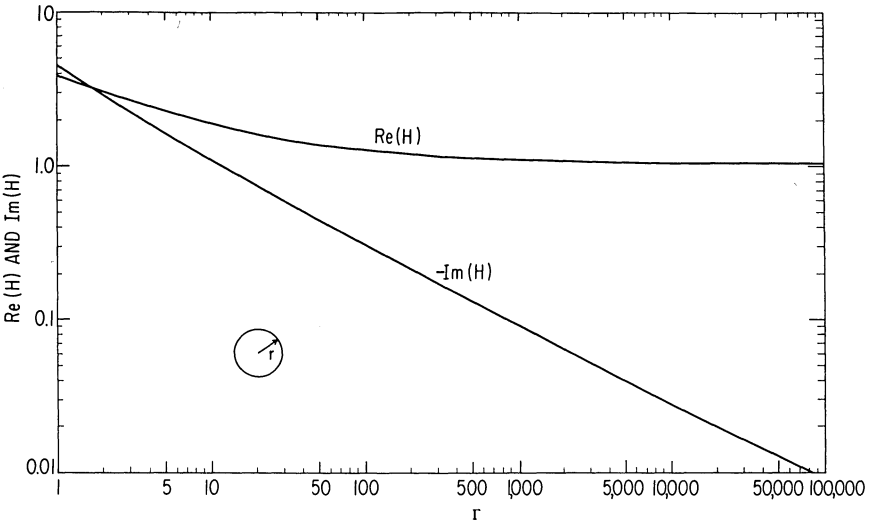


Fig. 16.8.1. $Re(H)$ and $Im(H)$ for a single cylinder in an infinite viscous fluid.

representation of its hydrodynamic mass matrix. As stated before, the eigenvalues of this mass matrix (actually, the maximum eigenvalue) are of interest in vibration prediction methods. Figure 16.8.4 shows the upper and lower bounds of the eigenvalue for different array sizes. We see that the eigenvalue bounds for 19 and 37 cylinder arrays are almost identical. Therefore, 19 or 37 cylinder array bounds may be used in practical design work for arrays of any size. TEMA Standards [16.1.5] recommends the upper bound corresponding to 19 cylinders for estimating C_m in practical designs.

Figure 16.8.4 highlights the significance of ligament efficiency in tube vibration analysis. Tighter arrays (small p/d) have a higher hydrodynamic

mass factor, C_m , and therefore cause a greater depression in the tube natural frequency.

The plot of C_m , due to Moretti and Lowery [16.8.5], is also presented in Fig. 16.8.5, since some correlations reported in Section 16.7.1 are based on their definition of C_m .

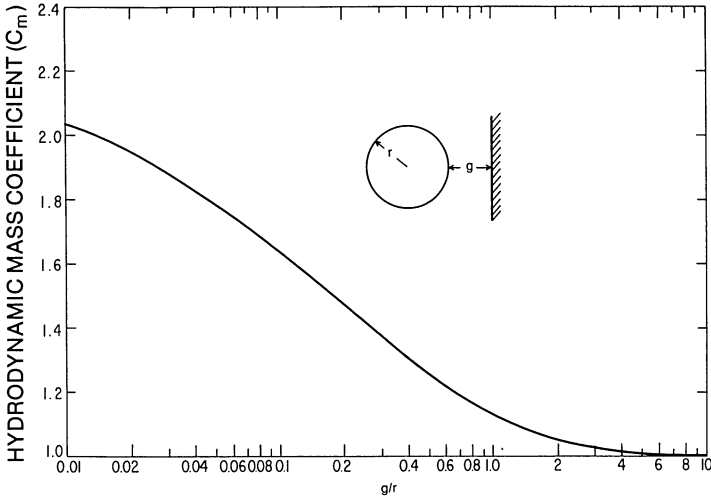


Fig. 16.8.2. Hydrodynamic mass coefficient for a cylinder vibrating near a wall.

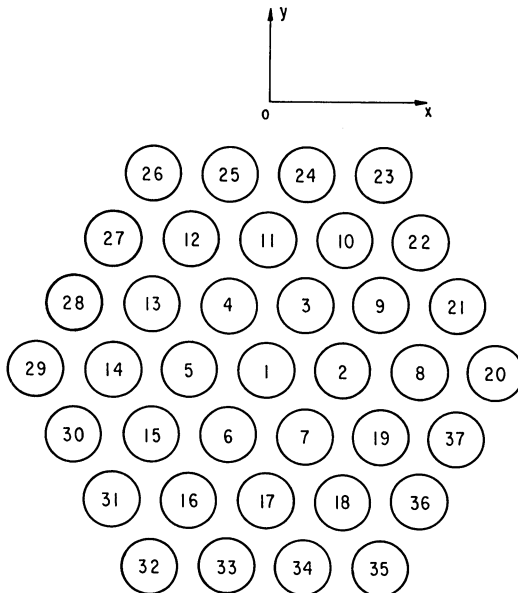


Fig. 16.8.3. Schematic of a tube bank arranged in a hexagonal pattern.

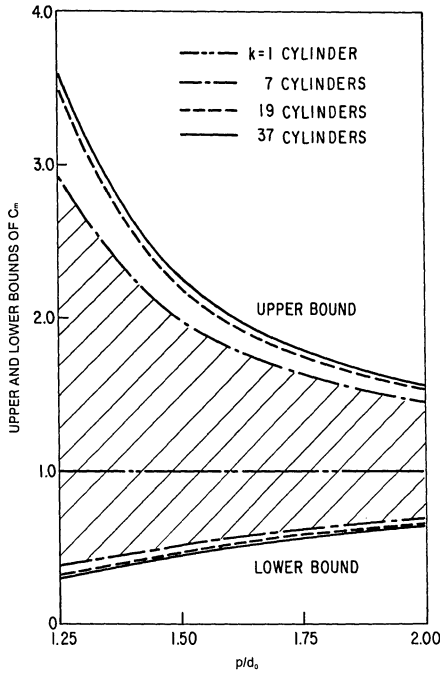


Fig. 16.8.4. Upper and lower bounds of the effective hydrodynamic mass coefficients as functions of the pitch-to-diameter ratio. (S.S. Chen)

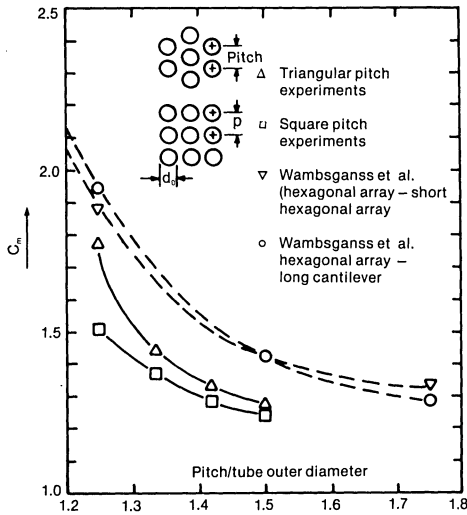


Fig. 16.8.5. Hydrodynamic mass coefficient, C_m by Moretti et al. [16.8.5].

16.9 DAMPING

16.9.1 Classification

A vibrating tube in a heat exchanger bundle dissipates energy through a variety of means. Scraping in the baffle holes is the most obvious. The non-conservative nature of the stress-strain diagram of the tube material (hysteresis) and the drag effects of the shellside fluid also contribute to energy removal from the tube. "Damping" is the general term used to define the ability of a structure to dissipate vibratory energy. Damping can be classified into three broad categories:

- (i) Structural Damping
- (ii) Internal Damping (material effects)
- (iii) Fluid Damping

As one would expect, structural damping is a strong function of the number and thickness of tube supports, the size of the baffle hole clearance, the surface adhesion effects between tube and baffle materials, etc. Internal damping due to hysteresis in the stress-strain curve, is usually not significant at small vibration amplitudes. However, Lowery and Moretti report [16.9.1] that the location of the longitudinal weld seam with respect to the plane of tube vibration has an effect on the measured damping; this is presumably due to altered material properties in the heat affected zone. Fluid damping is the most elusive component. It varies with the flow velocity of the shellside fluid, the solidity of the tube array, the density and viscosity of the shellside medium, etc. Theoretically, the total damping goes to zero when the critical velocity for fluid-elastic instability is reached (Section 16.5). When specifying damping, it is important to indicate whether "in-vacuo" or "in still fluid" condition exist.

Nearly all damping mechanisms are inherently non-linear in nature. However, the equivalent linear damping coefficient is normally used in predictive correlations. "Percentage of critical damping" and "logarithmic decrement" are common means of specifying linear damping. In the next sub-section, a brief exposition of linear damping concepts is given. The reader is referred to standard vibration texts for a more detailed treatment of the subject.

16.9.2 Damping Coefficient

Let us consider the vibration of a mass m_0 attached to a rigid frame through a spring of stiffness K and a linear damper of coefficient C (Fig. 16.9.1). The damper exerts a restoring force $C \cdot dx/dt$ on the mass when the latter has velocity dx/dt . The equation of motion for free vibration of mass m_0 (no externally applied forces) is given by

$$m_0 \frac{d^2 x}{dt^2} + C \frac{dx}{dt} + Kx = 0 \quad (16.9.1)$$

where t indicates the time coordinate. If the initial conditions are specified as $x = x_0$, and $dx/dt = v_0$ at $t = 0$, then the solution of Eq. (16.9.1) can be obtained using classical techniques [16.6.1]:

$$x = e^{-\eta t} \left[x_0 \cos \omega_d t + \frac{v_0 + \eta x_0}{\omega_d} \sin \omega_d t \right] \quad (16.9.2)$$

In Eq. (16.9.2), we have used the following familiar terms

$$\begin{aligned} \eta &= C/2m_0 & (a) \\ \omega_d &= \omega(1 - \eta^2/\omega^2)^{1/2} & (b) \\ \omega &= (K/m_0)^{1/2} & (c) \end{aligned} \quad (16.9.3)$$

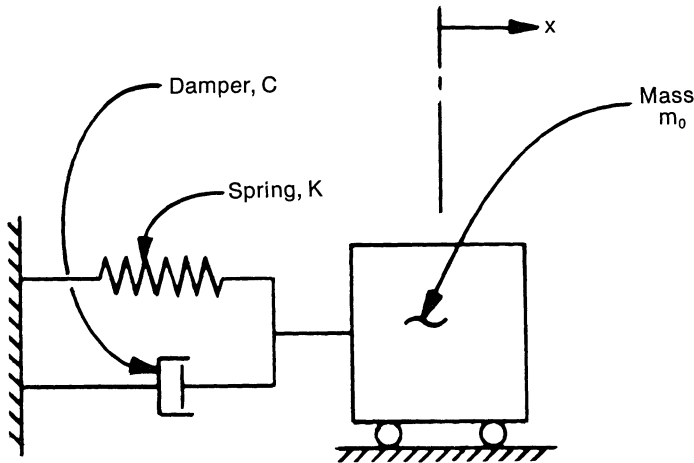


Fig. 16.9.1. Spring-mass-damper system.

With no loss in generality, we can apply the above result to the motion of a tube, approximated as a one degree of freedom system, by interpreting m_0 , C , K as mass, damping, and stiffness per unit length of tube. We note that when $\eta = \omega$, $\omega_d = 0$, and the motion is no longer periodic. The minimum amount of damping which renders the free vibration aperiodic is known as “critical damping”. The corresponding damping coefficient, C^* , is given by

$$\begin{aligned} \omega_d = 0 &\rightarrow \frac{C^*}{2m_0} = (K/m_0)^{1/2} & (16.9.4) \\ \text{or } C^* &= 2(Km_0)^{1/2} \end{aligned}$$

Figure 16.9.2 shows a typical plot of the vibration of mass m_0 subsequent to

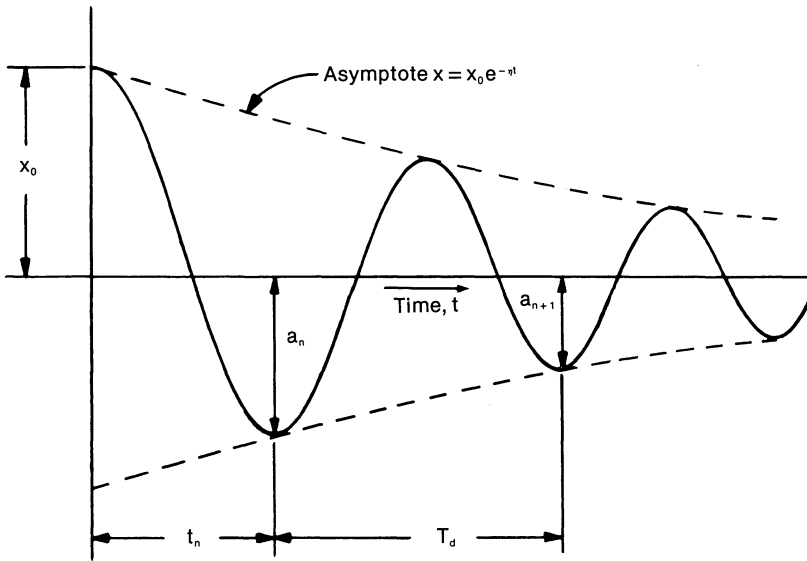


Fig. 16.9.2. Decay of free vibration amplitude.

its initial displacement x_0 at $t=0$. From Eq. (16.9.2), the ratio of two successive amplitudes is given by

$$\frac{a_n}{a_{n+1}} = \frac{e^{-\eta\tau}}{e^{-\eta(\tau+T_d)}} = e^{\eta T_d} \quad (16.9.5)$$

where T_d is the period of damped vibrations:

$$T_d = \frac{2\pi}{\omega_d} \quad (16.9.6)$$

Therefore, the logarithm of the ratio of consecutive amplitudes is given by

$$\delta = \text{Log}(a_n/a_{n+1}) = \eta T_d = \frac{2\pi\eta}{\omega_d}$$

for $\eta \ll \omega$ (small damping); $\omega_d \approx \omega$; hence

$$\delta = \frac{2\pi\eta}{\omega}$$

δ is called the logarithmic decrement.

Substituting for η and ω from Eq. (16.9.3) we have

$$\begin{aligned} \delta &= 2\pi \frac{(C/2m_0)}{(K/m_0)^{1/2}} = 2\pi \frac{C}{2(Km_0)^{1/2}} \\ &= 2\pi \frac{C}{C^*} \end{aligned}$$

Let ζ represent the ratio of actual to critical damping;

$$\zeta = C/C^* \quad (16.9.7)$$

then, δ is related to ζ by the equation

$$\delta = 2\pi\zeta \quad (16.9.8)$$

Thus the logarithmic decrement δ is 2π times the fractional damping available in the vibrating system. We now derive an expression for the energy removed by linear damping in the course of one cycle of motion.

The work done by the damper in one cycle on the mass, executing a harmonic motion at frequency ω_0 , is given by

$$\begin{aligned} E_d &= \int C \frac{dx}{dt} dx \\ &= C \int_{\tau}^{\tau + (2\pi/\omega_0)} \left(\frac{dx}{dt} \right)^2 dt \end{aligned}$$

Since $x = x_0 \sin \omega_0 t$

$$\frac{dx}{dt} = x_0 \omega_0 \cos \omega_0 t$$

Substituting for dx/dt in the above integral and integrating, we have

$$E_d = \pi C \omega_0 x_0^2 \quad (16.9.9)$$

The maximum kinetic energy of the vibrating mass, K_{\max} is

$$\begin{aligned} K_{\max} &= \frac{1}{2} m_0 \left(\frac{dx}{dt} \right)_{\max}^2 \\ &= \frac{1}{2} m_0 \omega_0^2 x_0^2 \end{aligned}$$

Therefore, the ratio of energy dissipated by the damper to the maximum kinetic energy of the system is

$$e^* = \frac{E_d}{K_{\max}} = \frac{\pi C \omega_0 x_0^2}{\frac{1}{2} m_0 \omega_0^2 x_0^2} = \frac{2\pi\zeta C^*}{m_0 \omega_0}$$

Substituting for C^* from Eq. (16.9.4), we have

$$e^* = \frac{4\pi\zeta\omega}{\omega_0} \quad (16.9.10)$$

If the mass vibrates at its own natural frequency, i.e., $\omega = \omega_0$ then

$$\frac{E_d}{K_{\max}} = e^* = 4\pi\zeta = 2\delta \quad (16.9.11)$$

Thus, for a lightly damped mass vibrating at its natural frequency, the logarithmic decrement δ , is proportional to the ratio of energy expended in viscous damping per cycle to the total kinetic energy of the system. Equations (16.9.10) or (16.9.11) enables defining an equivalent damping factor in those cases where the energy dissipation mechanism does not follow the linear viscous model, e.g., the form drag due to vibration of tubes in water.

The above expression is readily extended to multiple degree of freedom system by considering the equivalent linear damping in each mode of vibration.

16.9.3 Fluid Damping

We consider a vibrating cylindrical body of unit length and of diameter D subject to a uniform fluid flow of velocity u perpendicular to its axis. U_x and U_y represent the absolute velocities of the body in the x and y directions, respectively (Fig. 16.9.3). The relative velocity U_{rel} is given by

$$U_{rel}^2 = (U_x - u)^2 + U_y^2 \quad (16.9.12)$$

The drag force F_D on the cylinder acts at an angle γ with respect to the x -direction;

$$\gamma = \tan^{-1} \frac{U_y}{U_x - u} \quad (16.9.13)$$

and is given by the formula

$$\begin{aligned} F_D &= \frac{1}{2} \rho C_D U_{rel}^2 D \\ &= \frac{1}{2} \rho C_D D [(U_x - u)^2 + U_y^2] \end{aligned} \quad (16.9.14)$$

In Eq. (16.9.14), C_D is the drag coefficient, and ρ is the density of the fluid medium. Equations (16.9.13–14) indicate that the direction (angle γ) and the magnitude of the drag force will change as the vibratory velocities U_x and U_y vary with time. Changes in the fluid velocity u will also change the magnitude and direction of the fluid drag vector. Thus the energy dissipation produced by fluid damping *depends* on the fluid velocity and on the tube vibration amplitude (which is directly proportional to velocities U_x and U_y). Therefore, there is no unique value of fluid damping that can be ascribed to a particular tube bundle. Many researchers recommend using the value corresponding to “still fluid” conditions in predictive formulas to avoid confusion. Typical reported values of damping are summarized in the following sub-section.

16.9.4 Damping Data

Pettigrew and his co-workers provide some useful design data on the total

damping factor ζ . According to Pettigrew, et al., [16.9.2] the fluid damping component ζ_f , decreases with an increase in the natural frequency. Since the structural damping component ζ_s , is practically independent of frequency, the total damping decreases with increasing tube natural frequency. Damping data, reported in Table 16.9.1, below, substantiates the above statement. Table 16.9.1 also shows the value of normalized damping coefficient c_n where

$$c_n = \frac{C}{d_0} \tag{16.9.15}$$

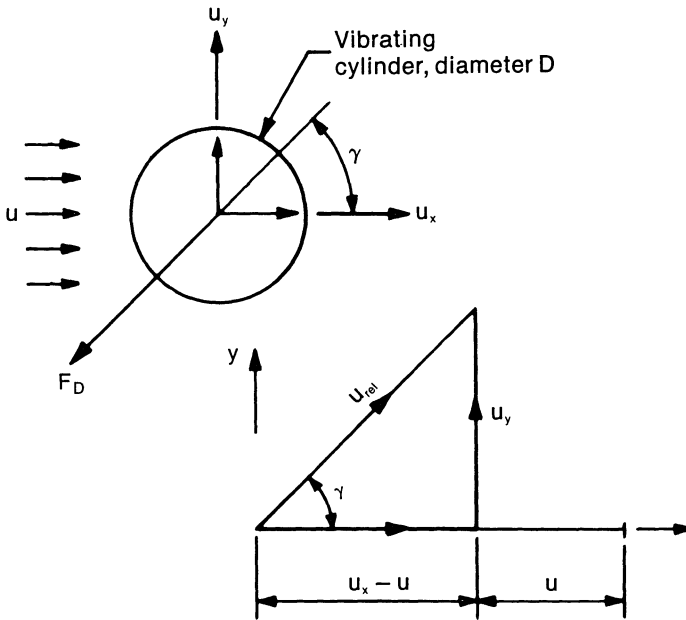


Fig. 16.9.3. Fluid flow past a cylinder.

Table 16.9.1. Damping Data from Pettigrew, et al. [16.9.2]

Component Description	Environment	Diam. (mm)	Material	f (Hz)	m_0 (kg/m)	ζ	c_n (kg/sec-m ²)
Process heat exchanger	water	19.0	stainless steel	44.4	1.04	0.0160	504
			steel	33.7		0.0246	574
Steam generator model	water	13.0	stainless steel	39.8	0.525	0.0216	438
			steel	63.5		0.0115	372
Moderator heat exchanger	water	13.0	Incoloy-800 T	140	0.462	0.0073	459
				227		0.0066	672
Fuel element	air-water	19.0	Zircaloy-2	45.0	1.79	0.060	3181
Steam generator model	steam-water	13.0	stainless steel	38.0	0.472	0.081	1407

Based on the data in Table 16.9.1, Pettigrew, et al., recommend

$$c_n = C/d_0 = \frac{2m_0 \omega \zeta}{d_0} = 400 \text{ Kg/sec-sq. meter for water (0.00147 lb-sec/in.}^3) \quad (16.9.16)$$

$$= 1400 \text{ Kg/sec-sq. meter for two phase mixtures (air-water, water-steam) (0.00515 lb-sec/in.}^3)$$

where m_0 (mass/unit length) is the sum of the tube mass, the contained fluid mass, and the displaced shellside fluid mass.

Viscous damping due to the vibration of an isolated tube, perpendicular to its axis, in a quiescent fluid, is given by the classical relationship due to Stokes [16.9.3]. For the component of the damping factor ζ due to the fluid:

$$\zeta_f = \frac{\pi d_0^2 \rho}{2m_0} \left\{ \left[\frac{2\nu'}{\omega d_0^2} \right]^{\frac{1}{2}} + \frac{2\nu'}{\omega d_0^2} \right\} \quad (16.9.17)$$

Since $2\nu'/\omega d_0^2 \ll 1$, the first term in braces is much larger than the second; Stokes's relationship can therefore be approximated as

$$\zeta_f = \frac{\pi d_0^2 \rho}{2m_0} \left(\frac{2\nu'}{\omega d_0^2} \right)^{\frac{1}{2}} \quad (16.9.18)$$

Connors, et al., [16.9.4] found that the fluid damping in a square array with pitch-to-diameter ratio equal to 1.33 is approximately 1.9 times the value of ζ_f given by Eq. (16.9.18). Connors, et al., give the following semi-empirical formulas for the fluid damping parameter, ζ_f , as a function of axial flow velocity u_{ax} .

$$\zeta_f = \frac{10.73}{2\pi} \left(\frac{\rho d_0^2}{m_0} \right) \left(\frac{\nu'}{f d_0^2} \right)^{\frac{1}{2}} e^{-0.00018 u_{ax} d_0 / \nu'} + \frac{0.327}{2\pi} \left(\frac{\rho d_0^2}{m_0} \right) \left(\frac{u_{ax}}{f d_0} \right) \left(\frac{\nu'}{d_0 u_{ax}} \right)^{0.22}$$

The above correlation was developed on the basis of data obtained in a rectangular array of $p/d_0 = 1.33$.

Chen and Wambsganss [16.9.5] obtained fluid damping data for a single 0.50" diameter rod vibrating within a 2" diameter annulus full of water. Their empirical formula for the fluid damping component is given as

$$\zeta_f = 0.003 + 2.44 \times 10^{-4} u_{ax} + 3.44 \times 10^{-6} u_{ax}^2 \quad (16.9.19)$$

where u_{ax} is axial flow velocity in ft/sec.

Despite the differences in the experiments, the magnitudes of ζ_f given by the two expressions above are quite close in the practical range ($u_{ax} < 30$ ft/sec).

Chen and Jendrzejczyk [16.9.6, 16.7.11] studied the variation of fluid damping with flow velocity in crossflow. Their findings indicate that fluid

damping in the drag direction increases with crossflow velocity. The damping in the lift direction can increase or decrease with flow velocity as shown in Fig. 16.9.4.

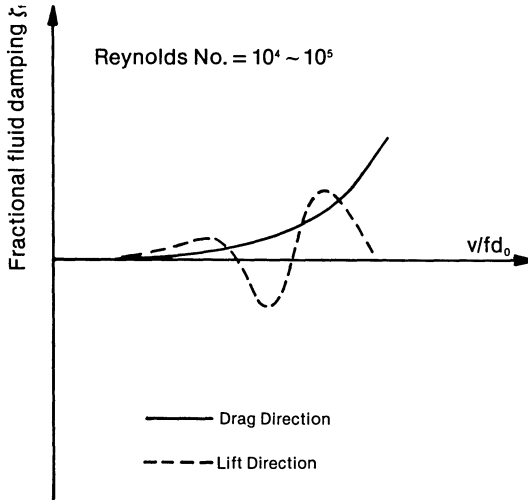


Fig. 16.9.4. General trend of fluid damping dependence on flow velocity for tube arrays.

16.10 CROSS FLOW VELOCITY

16.10.1 Computer Models

The flow of shellside fluid in a baffled heat exchanger is highly complex. Researchers seeking to predict shellside heat transfer with tolerable precision, recognized the need to better understand shellside velocity distribution [16.10.1]. Overall heat transfer rate is an integrated effect, and therefore even large errors in estimated velocity distribution “smear out” in the integrated heat transfer coefficient calculation. The success of vibration analysis, on the other hand, is directly predicated on the accuracy with which velocity distribution on the *subject tube* can be predicted. Indeed, the lack of information for defining the flow field in industrial heat exchangers has been a principal impediment in correlating laboratory data with industrial experience. However, three-dimensional fluid flow solution methods [16.10.2] are beginning to emerge. General purpose fluid flow computer programs [16.10.3] have been utilized to map out the velocity field in laboratory units with remarkable success. These codes possess the added capability of refining the prediction of shellside film coefficient. Such computerized methods are certain to supplant present day empirical velocity computation methods in the near future. In the interim, however, semi-empirical methods and sound engineering sense is the best that a

designer can be expected to muster. The so-called “Stream Analysis Method” developed by the Heat Transfer Research Institute [16.10.4] is perhaps the most respected of the semi-empirical techniques. The computer program “ST4”, a proprietary code of HTRI member companies, has been extensively used as a tool for predicting heat transfer, pressure loss and flow induced vibration potential. Its premise, the “Stream Analysis Method”, is outlined in Sub-Section 16.10.3. Solution procedures for specialized baffle configurations, such as “Triple Segmental Baffles” have also been proposed [Ref. 16.10.5]. Because of the comparatively high rate of failure in the U-bend region, a specialized solution for the U-bend region is presented in sub-section 16.10.4.

Since the flow velocity over a tube span is rarely uniform, it is necessary to define an equivalent uniform velocity for use in prediction techniques (Section 16.7). Such an expression is derived in the following.

16.10.2 Effective Velocity

The cross flow velocity on a typical tube span is not uniform. All of the vibration prediction methods pre-suppose a uniform velocity field across the tube bank. Connors [16.10.6] has proposed the following formulas for calculating the “effective velocity” v_e to be used in place of v in the formulas in Section 16.7:

$$v_e^2 = \frac{\int_0^l v^2 \psi^2 dx}{\int_0^l \psi^2 dx} \quad (16.10.1)$$

In the above equation v is the velocity distribution function, and ψ is the significant mode shape for the tube span under consideration. Expressions for ψ for some typical single span tube models can be found from the data in Table 16.6.1.

Equation (16.10.1) can be derived by making the following simplifying assumptions:

i. The tube span under consideration is vibrating in the significant mode for that span; i.e., the deflection of the span is

$$y(x,t) = K_1 \psi(x) \sin \omega t \quad (16.10.2)$$

where ω is the tube frequency corresponding to the mode shape $\psi(x)$, and K_1 is a proportionality constant.

ii. The fluid force per unit length $G(x,t)$ is in phase with the tube velocity and has the form

$$G(x,t) = K_2 \rho v^2 y \left(x, t + \frac{\pi}{2\omega} \right) \quad (16.10.3)$$

where $v = v(x)$.

iii. The energy removed by damping is uniformly distributed over the

tube length and the damping is a linear function of the assumed tube velocity.

The energy imparted to the tube by the fluid force in one vibration cycle is given by

$$E_1 = \iint G(x,t) dy dx$$

or

$$E_1 = \int_0^l dx \int_0^{2\pi} K_1^2 K_2 \omega \rho v^2(x) \psi^2(x) \cos^2 \omega t dt$$

or

$$E_1 = \pi \rho K_1^2 K_2 \int_0^l v^2(x) \psi^2(x) dx \quad (16.10.4)$$

The energy dissipated by viscous damping is:

$$\begin{aligned} E_2 &= \iint C \dot{y}^2 dy dx \\ &= CK_1^2 \omega^2 \int_0^l \int_0^{2\pi} \psi^2 \cos^2 \omega t dt dx \\ &= \pi CK_1^2 \omega \int_0^l \psi^2(x) dx \end{aligned} \quad (16.10.5)$$

Since, for a stability threshold $E_1 = E_2$, Eqs. (16.10.4) and (16.10.5) yield:

$$\rho K_2 v_e^2 = C \omega = 2C \pi f \quad (16.10.6)$$

where v_e^2 is defined by Eq. (16.10.1). Since by Eqs. (16.9.3)–(16.9.8), $C = \delta m_0 f / 2\pi^2$, we have:

$$\rho K_2 v_e^2 = \frac{2\delta m_0 f^2}{2\pi} \quad (16.10.7)$$

or

$$\begin{aligned} \frac{v_e^2}{f^2} &= \frac{1}{\pi K_2} \frac{m_0 \delta}{\rho} \\ \text{or} \quad \frac{v_e}{fd_0} &= \frac{1}{(\pi K_2)^{1/2}} \left(\frac{m_0 \delta}{\rho d_0^2} \right)^{1/2} \end{aligned} \quad (16.10.8)$$

The constant $(\pi K_2)^{-1/2}$ is the equivalent of the threshold stability constant in Connors' formulation (Eq. (16.7.3)).

Example: Let us consider a central tube span of length l . The significant mode shape for this span is (ref. Section 16.6.2):

$$\psi(x) = \sin \frac{\pi x}{l} \quad (16.10.9)$$

Let us compute the effective velocity for the case where the velocity is uniform only over the left quarter of the tube span, i.e.,

$$v(x) = v_0; 0 \leq x \leq l/4$$

$$= 0; l/4 < x \leq l$$

Substituting in Eq. (16.10.1) yields:

$$v_e = \frac{v_0^2 \int_0^{l/4} \sin^2 \frac{\pi x}{l} dx}{\int_0^l \sin^2 \frac{\pi x}{l} dx} \quad (16.10.10)$$

or

$$v_e = 0.3014v_0$$

16.10.3 Stream Analysis Method

The essence of the “Stream Analysis Method” lies in defining certain discrete flow paths for the flow of shellside fluid from one baffle space to the next. These flow passages are idealized as ducts with simulated friction factors. Classical piping network technique are used to determine the flow fraction in each flow passage.

The HTRI model of flow “streams” is shown in Fig. 16.10.1. The shellside flow is assumed to split into five parallel streams, defined as follows:

A-Stream: The stream which crosses the baffle through the annular clearances between the tubes and the baffle holes. This stream is essentially in parallel flow with respect to the axis of the tube bundle.

B-Stream: This is the crossflow stream which flows in the plane perpendicular to the baffle cuts. The velocity of the fluid in this stream is of importance in vibration analysis.

C-Stream: This stream occupies the two helical paths defined by the annular space between consecutive baffle cuts (Fig. 16.10.1). The flow area for this stream can be quite large in removable bundle heat exchangers, particularly in floating head types (ref. Chapter 1). Flow velocities in this stream are usually larger than the cross flow velocity. Tubes located on the outer periphery of the bundle, which are swept by this stream, are particularly susceptible to its effect. Designers should watch out for solitary tubes located in the path of C-Stream, since such tubes would most assuredly experience higher flow velocity than the tubes located in the bundle interior.

E-Stream: This stream flows parallel to the shell through the gap between the baffle outer circumference and inner wall of the shell. Although ineffective in heat transfer, this stream is completely benign for tube vibration.

F-Stream: This stream lies in the plane parallel to the B-Stream. However, it flows in the open passages formed by the pass partition lanes. Designers make some attempt to throttle this stream by placing “dummy

tubes'' in the pass partition lanes. Unfortunately, in some occasions, the dummy tubes vibrate violently and damage adjacent tubes by repeated impact! Tubes on the edges of the pass partition lanes swept by the F-Stream should be carefully examined for the effects of the F-Stream. The most desirable design provision is to rotate the baffles such that no pass partition lanes are perpendicular to baffle cuts.

Like dummy tubes in pass partition space, ''seal strips'' are sometimes utilized to choke off the C-Stream. Kissel (16.10.7) found that seal strips hasten the incidence of flow induced vibration due to increased local velocity. Figure 16.10.2 shows how sealing strips jeopardize the safety of the adjacent tubes.

The above discretization of flow passages has to be modified in the inlet and outlet zones where rapid flow expansions/contractions occur. HTRI's chief contribution to shellside flow visualization lay in defining the resistance of the flow passages by correlating the theory with the extensive data collected by the so-called Delaware project and other sources. Because of their proprietary nature, the friction factors cannot be presented here. However, the gist of the solution procedure can be summarized.

Figure 16.10.3 shows the equivalent pipe network model [16.10.4] for flow of the shellside fluid in the baffled region containing single segmental baffles. Nodes 1 through 6 are located at points of flow confluence and splits. In Fig. 16.10.3, nodes 3 and 4, called diametral nodes, are located at the center of the baffle windows. Node 1 is the mirror image of node 3, and node 6 is the mirror image of node 4. The pressure drop across a window is labelled ΔP_w ; and the pressure drop due to cross flow across the bundle of tubes is labelled ΔP_x . Nodes 2 and 5 are located midway between the diametral nodes. Let p_{ij} denote the pressure difference between nodes i and j ; then according to our nomenclature

$$p_{13} = p_{46} = \Delta P_x$$

$$p_{34} = \Delta P_w$$

$$p_{25} = \Delta P_x + \Delta P_w$$

Streams B, C, and F split at node 1 and rejoin at node 3, undergoing the pressure drop $p_{13} = \Delta P_x$. Streams A and E issue at node 2 and merge at node 5 undergoing the pressure drop $\Delta P_{25} = (\Delta P_x + \Delta P_w)$ in the process.

Each stream is assigned a flow passage area. The resistance to the flow of a particular stream in its passage is a function of the shape of the passage and the Reynolds number. For example, the pressure drop in stream B due to flow Q_B from node 1 to node 3 can be written as

$$p_{13} = \Delta P_x = G_B R_B Q_B^2$$

where R_B is the resistance factor which depends on Q_B , the B-stream flow rate. G_B is the constant term which lumps the flow-independent terms such as the reference flow cross sectional area, and fluid density.

The total flow Q must equal the sum of the contributory streams (mass continuity), i.e.,

$$Q = Q_A + Q_B + Q_C + Q_E + Q_F$$

The solution for the correct values of Q_B , Q_C , etc. can be obtained iteratively in one of several ways. For example, initial guesses on Q_A , Q_B , etc., consistent with the mass continuity requirement, can be made. The Reynolds number in each stream and the corresponding friction factors can then be calculated. Having computed the friction factors, the pressure drops in each stream between the node points are readily known. Pressure drop in any stream between two nodes must equal that in a parallel stream originating and merging at the same two nodes. These requirements can be phrased in terms of a relaxation scheme which modifies the stream flow rates (Q_B , Q_C . . . etc.) until the inter-nodal pressure drops in all streams are consistent with each other. Computer code ST4 developed by HTRI utilizes this stream analysis principle.

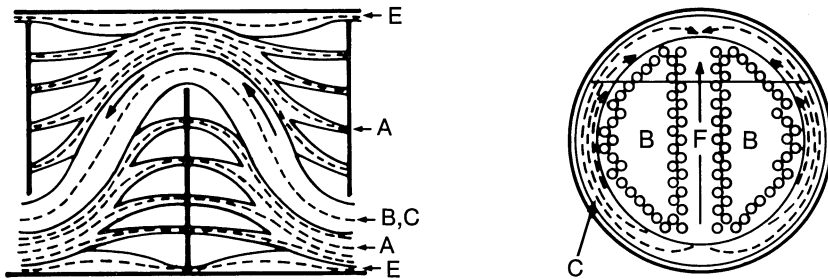


Fig. 16.10.1. "Stream Analysis" model of Tinker and HTRI.

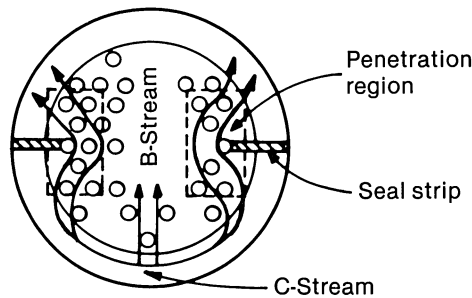


Fig. 16.10.2. Flow distortion due to seal strip.

16.10.4 Flow Distribution in the U-Bend Region

The flow field in the U-bends of a tube bundle containing double-segmental baffles is presented in Ref. [16.10.9]. A summary of that analysis is given in the following and forms the basis of the computer program "UFLOW" described in Appendix 16.C.

Bundle Configuration Analyzed

The baffle layout considered in this analysis is shown in Fig. 16.10.4. The inlet nozzle is located beyond the bundle to avoid direct impingement related tube erosion problems. The tubes are arranged in a staggered pattern (usually triangular) on a desired pitch determined by available pressure loss, and bundle diameter limitations. The tube pitch to diameter ratio varies in the range of 1.2–1.4. Double segmental baffles, shown in Fig. 16.10.4, consist of two basic baffle geometries which are identified as the “slotted baffle” and the “solid baffle”, respectively. The overlap (in the Z-

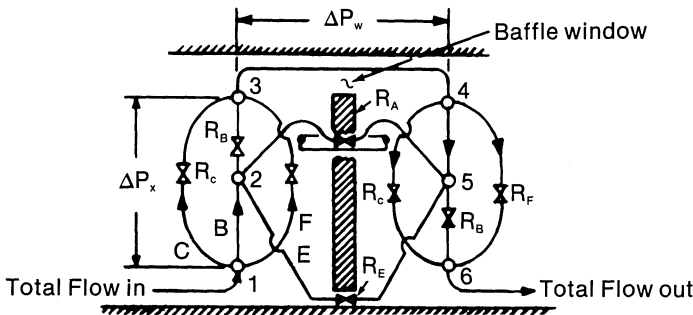


Fig. 16.10.3. Flow resistance model.

direction) between the two baffles, arranged alternately as shown in Fig. 16.10.5, determines the extent of cross flow of the shellside stream. The last baffle is of the slotted type such that the large diameter U-bends are supported at their points of tangency.* The small diameter U's, not supported by the last slotted baffle, are shortened to reduce their overhang (see Fig. 16.10.5 and Photograph 16.a). These shortened tubes thus escape the full thrust of the flow, and can usually be shown to not require any mid-span support. However, the tubes supported by the last slotted baffle “see” the complete shell stream, and hence must be carefully studied and protected from vibration. We describe the mathematical model which predicts the flow distribution and thus enables us, using the predication techniques of Section 16.7, to evaluate the vibration potential.

Planar Flow Model

A physically admissible flow model in the U-bend region can be constructed by recognizing that the shape of the opening at the baffle and the symmetry of the bundle about the $Y-Z$ plane encourages the flow streams to be parallel to the plane of the U-tubes ($Y-Z$ plane). The curvature of the shell surface, and the orientation of the inlet nozzle may introduce some velocity components perpendicular to the $Y-Z$ plane, but in general such deviations will be small due to the preponderant geometric symmetry of the

*In actual practice, a small projection of the straight segment beyond the last baffle is provided to facilitate assembly.

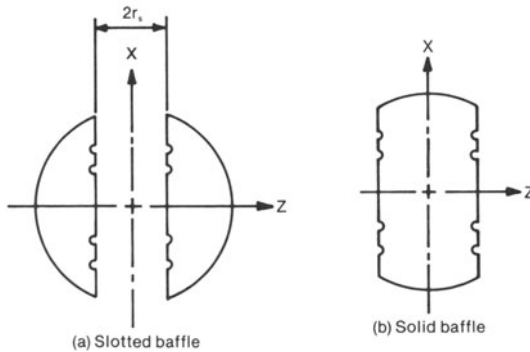


Fig. 16.10.4. Double segmental baffle shapes.

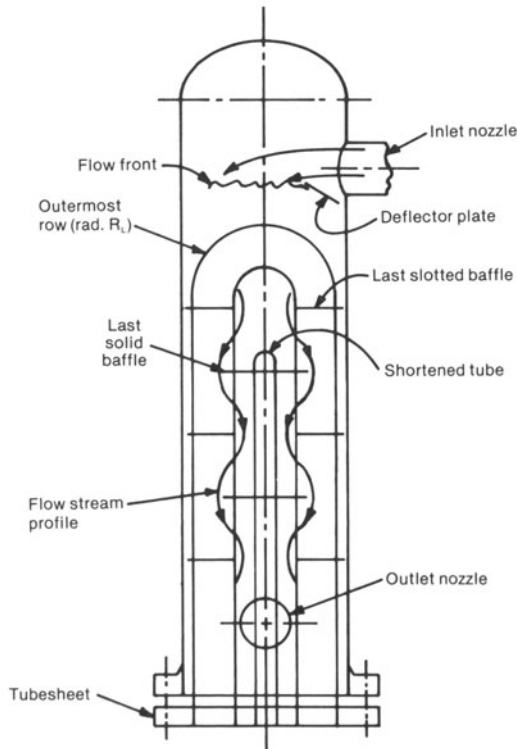
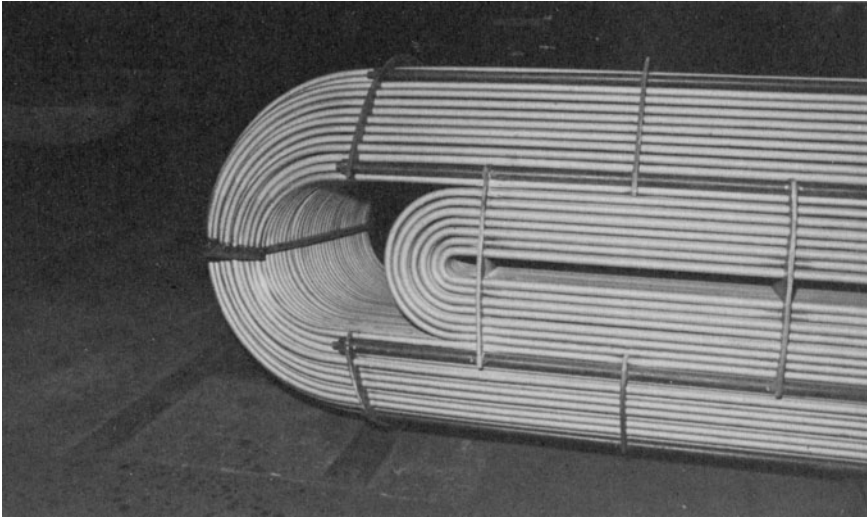


Fig. 16.10.5. Bundle geometry.

bundle. Hence, the flow can be assumed to be essentially stratified parallel to the plane of the U 's, and flowing radially inwards towards the baffle slit. To the approaching stream, the U-bundle appears to be a section of a perforated hemisphere (see Fig. 16.10.6). At height x (above the Y - Z plane),



Photograph 16-a. U-bend with inner rows shortened (Courtesy Joseph Oat Corporation, Camden, N.J.)

the tube stratum has a maximum radius y . The flow through a tube stratum of unit width (Fig. 16.10.7) is related to the pressure drop ΔP by:

$$\Delta P = \frac{\rho}{2} \left[\psi_1^* V_1^2 + \psi_2^* \sum_{i=1}^n V_i^2 \right] \quad (16.10.11)$$

where ρ is the fluid density at its bulk temperature and ψ_i^* are loss coefficients. The stratum at height x is assumed to have n tube rows. Let r_i denote the bend radius of the i th tube row where the innermost row (radius $r_s = r_1$ equal to one half of the baffle slot width) is designated as row 1. V_i denotes the flow velocity at row i . Thus, the radius of the n th row is $r_n = y$, and the associated flow velocity is V_n .

In Eq. (16.10.11), the first term in the right-hand side represents the pressure loss in contraction and expansion through the baffle window of radius $r_s (= r_1)$ and ψ_1^* is the corresponding coefficient. The second term represents the pressure drop as the stream traverses the radial path of length $(y - r_s)$ containing n tube rows. ψ_2^* is the corresponding coefficient which lumps the pressure drop due to momentum change, due to fluid skin friction, and due to turbulence loss in one term. The correlations for ψ_1^* and ψ_2^* will be further discussed later in this section.

If q^* denotes the flow rate at this stratum, then mass continuity yields:

$$q^* = \pi r_i V_i; \quad i = 1, 2, \dots, n. \quad (16.10.12)$$

where $r_1 = r_s$.

Substituting for V_1 and V_i from Eq. (16.10.12) into Eq. (16.10.11), we have

$$\frac{2\pi^2}{\rho} \frac{\Delta P}{\psi_1^*} = q^{*2} \left[\frac{1}{r_s^2} + \omega^* \sum_{i=1}^n \frac{1}{r_i^2} \right] \quad (16.10.13)$$

where

$$\omega^* = \frac{\psi_2^*}{\psi_1^*} \quad (16.10.14)$$

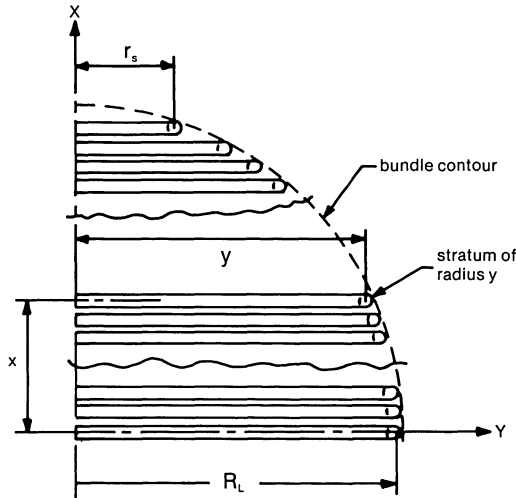


Fig. 16.10.6. One half of the U-bundle.

The numerical sum in Eq. (16.10.13) can be replaced by an integral if we note that the trapezoidal rule for numerical quadrature implies that

$$\frac{1}{h} \int_{a_1}^{a_2} f(x) dx = \sum_{i=1}^n f_i - 0.5(f_1 + f_n) \quad (16.10.15)$$

where f_i is the value of function $f(x)$ evaluated at the i th node; and h is the nodal spacing; i.e., $h = (a_2 - a_1)/(n - 1)$. Using Eq. (16.10.15) in Eq. (16.10.13) yields:

$$q^{*2} \left[\frac{1}{r_s^2} + \frac{\omega^*}{p_l} \int_{r_s}^y \frac{dr}{r^2} + \frac{\omega^*}{2} \left(\frac{1}{r_s^2} + \frac{1}{y^2} \right) \right] = C_p^2 \quad (16.10.16)$$

where

$$C_p^2 = \frac{2\pi^2}{\rho} \frac{\Delta P}{\psi_1^*} \quad (16.10.17)$$

and p_l is the longitudinal pitch, defined as the distance between the tube rows. Thus, for the stratum containing n tube rows

$$p_l = \frac{r_n - r_1}{n - 1} = \frac{y - r_s}{n - 1} \tag{16.10.18}$$

p_l is assumed to be a constant for the bundle.

Performing the necessary integration in Eq. (16.10.16) we have

$$q^* = \frac{C_p}{\left[\frac{1}{r_s^2} + \frac{\omega^*}{p_l} \left(\frac{1}{r_s} - \frac{1}{y} \right) + \frac{\omega^*}{2} \left(\frac{1}{r_s^2} + \frac{1}{y^2} \right) \right]^{1/2}} \tag{16.10.19}$$

C_p is an undetermined constant.

We next note that the flow through the entire bundle surface (segment of a hemisphere) and the open baffle window area is given by Q , where

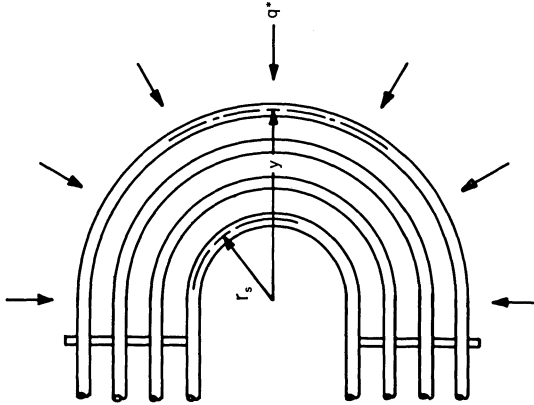


Fig. 16.10.7. Radial planar flow at stratum of radius y at height x .

$$Q = A_w V_w + 2\eta' \int_0^{x'} q^* dx \tag{16.10.20}$$

and

$$x' = (R_L^2 - r_s^2)^{1/2}$$

R_L is the outer bundle radius, and η' is the perforation coefficient of the bundle surface, defined as

$$\eta' = \frac{p_l - d_0}{p_l} \tag{16.10.21}$$

In Eq. (16.10.21), p_l and d_0 are the transverse tube pitch and tube O.D., respectively. A_w is the surface area of a semi-circular cylinder of radius r_s and length $2(R_L - x')$, where R_L denotes the inside radius of the shell. Substituting for q^* from Eq. (16.10.19) into Eq. (16.10.20), and integrating, we have

$$Q = A_w V_w + 2\eta' C_p R_L^2 I^* \quad (16.10.22)$$

where V_w is the window velocity evaluated at the surface of the semi-circular cylinder of radius r_s . The integral I^* is

$$I^* = \int_0^{\rho'} \left[X^2 + \frac{\omega^* R_L}{p_l} \{ X - (1 - z^2)^{-1/2} \} + \frac{\omega^*}{2} \{ X^2 + (1 - z^2)^{-1} \} \right]^{-1/2} dz \quad (16.10.23)$$

where

$$z = \frac{x}{R_L} \quad (16.10.24)$$

$$X = \frac{R_L}{r_s} \quad (16.10.25)$$

and

$$\rho' = (1 - X^{-2})^{1/2} \quad (16.10.26)$$

If N denotes the number of tube rows at the mid-plane of symmetry ($x = 0$), then the expression for I^* can be recast as follows:

$$I^* = \int_0^{\rho'} \left[X^2 + \frac{\omega^* X(N-1)}{X-1} \{ X - (1 - z^2)^{-1/2} \} + \frac{\omega^*}{2} \{ X^2 + (1 - z^2)^{-1} \} \right]^{-1/2} dz \quad (16.10.27)$$

I^* can be computed for a given ω^* , X and N by a suitable numerical quadrature scheme, such as Simpson's rule.

Notice from Eq. (16.10.19) that at $y = r_s$, (a single row stratum) $q^* = q_w$ is given by

$$q_w = \frac{C_p r_s}{(1 + \omega^*)^{1/2}} \quad (16.10.28)$$

Hence

$$V_w = \frac{C_p}{\pi(1 + \omega^*)^{1/2}} \quad (16.10.29)$$

Noting that

$$A_w = 2\pi r_s [R_s^2 - (R_L^2 - r_s^2)^{1/2}] \quad (16.10.30)$$

We have, by combining Eqs. (16.10.22), (16.10.29) and (16.10.30)

$$Q = 2C_p R_L^2 \left[\frac{\{ \xi - (1 - X^{-2})^{1/2} \}}{X(1 + \omega^*)^{1/2}} + \eta' I^* \right] \quad (16.10.31)$$

where

$$\xi = \frac{R_s}{R_L} \quad (16.10.32)$$

ξ is close to 1 for most practical designs. Equation (16.10.31) determines C_p . The velocity profile follows from Eqs. (16.10.12) and (16.10.19). Equation (16.10.19) is cast in a more convenient form below:

$$q^* = \frac{C_p}{\left[\frac{1}{r_s^2} + \frac{\omega^* X(N-1)}{(X-1)R_L} \left(\frac{1}{r_s} - \frac{1}{y} \right) + \frac{\omega^*}{2} \left(\frac{1}{r_s^2} + \frac{1}{y^2} \right) \right]^{1/2}} \quad (16.10.33)$$

where q^* is the volumetric flow rate through a stratum of unit width, and outer radius y . Hence, the velocity $V(y,r)$ at bend radius r in the stratum of outer radius y is given by

$$V(y,r) = \frac{C_p}{\pi r \left[\frac{1}{r_s^2} + \frac{\omega^* X(N-1)}{(X-1)R_L} \left(\frac{1}{r_s} - \frac{1}{y} \right) + \frac{\omega^*}{2} \left(\frac{1}{r_s^2} + \frac{1}{y^2} \right) \right]^{1/2}} \quad (16.10.34)$$

Finally, an expression for ω^* has to be devised. The contraction and expansion coefficient ψ_1^* depends on the shape of the orifice, its edge condition, and the ratio of contraction and expansion areas. According to Kays [16.10.10], the contraction coefficient C_c and expansion coefficient C_e are given, in the turbulent range,* by

$$C_c = 0.41(1 - \Lambda_1) \quad (16.10.35)$$

$$C_e = (1 - \Lambda_2)^2 \quad (16.10.36)$$

where Λ_1 is the ratio of the area of the contracted stream to the area of the uncontracted stream. Similarly, Λ_2 is the ratio of the unexpanded stream to the expanded stream cross sectional areas.

Lower bounds on C_c and C_e can be obtained by assuming the uncontracted (and expanded) areas to correspond to the surface of the smallest bend. Thus

$$\Lambda_1 = \Lambda_2 = \frac{2}{\pi} \quad (16.10.37)$$

Furthermore, we note that ψ_1^* is referred to the velocity at the semi-cylindrical surface in Eq. (16.10.11); hence

$$\psi_1^* = \frac{\pi^2}{4} (C_c + C_e) \quad (16.10.38)$$

*Contraction and expansion coefficients when multiplied by the velocity head, referred to the constricted channel cross section, give the corresponding pressure drops.

Equation (16.10.38) will in general give a lower bound for ψ_1^* , since the expressions for Λ_1 and Λ_2 are obviously overestimates. An upper bound on ψ_1^* can be found by setting Λ_1 and Λ_2 equal to the ratio of the baffle cut area A_c to the net longitudinal flow area in the shell A_s . Note that

$$A_c = 4R_s r_s \quad (16.10.39a)$$

and that

$$A_s = \frac{\pi}{4} (4R_s^2 - N' d_0^2) \quad (16.10.39b)$$

where N' is the total number of tubes in the shell adjacent to the baffle. Using the upper bound on the pressure loss coefficient ψ_1^* in Eq. (16.10.11) will overpredict the flow velocities through the bundle. This is discussed further in the following.

Experimentally measured values of the crossflow pressure drop coefficient ψ_2^* have been reported by several investigators, notably Bell [16.10.8]. ψ_2^* strongly depends on the transverse pitch p_t , on the layout arrangement, and to some extent, on the longitudinal pitch. The value of ψ_2^* can be found in the literature for the specified bundle geometry as a function of the crossflow Reynolds number, Re . Re should be based on the nominal flow velocity V' through the baffle, i.e.,

$$V' = \frac{Q}{A_c} \quad (16.10.40)$$

Unfortunately, accurate values of ψ_1^* and ψ_2^* are not known at present. Parametric experimental studies on prototypes are required to develop precise correlations for ψ_1^* and ψ_2^* . We recommend using the upper bound on ψ_1^* as developed in the foregoing. Furthermore, since ψ_2^* is based on a higher Reynolds number than is actually present in most of the bundle, the value of ψ_2^* calculated will be a lower bound. Hence, the dimensionless ratio ω^* will also be a lower bound. In physical terms, this implies that the flow path resistance of the bundle is underestimated and that of the frontal window region A_w is overestimated. Consequently, the flow velocities through the bundle will be overpredicted. From the viewpoint of predicting flow induced vibration, the direction of error in the velocity magnitudes is favorable. However, the error in calculating the shellside film coefficient will be on the unsafe side. Numerical studies indicate that the maximum increase in the flow velocity in typical tube bundles is less than 10% when ω^* is decreased by a factor of 4. This implies that a precise knowledge of ω^* does not appear to be crucial to the accuracy in prediction of the velocity field.

Finally, for the sake of comparison, we will compute the nominal flow velocity V^* penetrating the bundle surface, assuming that the flow is uniform over the surface and that the frontal window area is A_w . It follows that

$$Q = 2\pi\eta' V^* \int_0^{x'} y dx + A_w V^* \tag{16.10.41}$$

or

$$Q = V^* [2\pi\eta' (0.5R^2) \{ \alpha' + 0.5\sin 2\alpha' \} + 2\pi r_s \{ R_s - (R_L^2 - r_s^2)^{1/2} \}] \tag{16.10.42}$$

where

$$\alpha' = \sin^{-1} \rho' \tag{16.10.43}$$

Therefore,

$$Q = 2\pi R_L^2 V^* \left[0.5\eta' \{ \alpha' + 0.5\sin 2\alpha' \} + \frac{1}{X} \{ \xi - (1 - X^{-2}) \} \right]^{1/2} \tag{16.10.44}$$

Equation (16.10.44) determines V^* .

Example

To illustrate the method, the results for a two tube pass, U-tube heat exchanger of 24.75 in. I.D. are given. The maximum bend radius R_L is 11.8 in., and the baffle slit radius r_s is 3.69 in. The perforation efficiency η' is 0.2 (0.75 in. O.D. tubes laid out on 0.9375 in. pitch). There are a total of 11 tube rows in the midplane of the bundle ($x=0$). The volumetric flow rate Q is 21732 in.³/sec. The computer program UFLOW described in Appendix 16.C is used to solve the problem.

The velocity distributions corresponding to $\omega^* = 1$ for $y^* = y/R_L = 0.381, 0.588, 0.794, \text{ and } 1$ are plotted in Fig. 16.10.8 as a function of tube radius

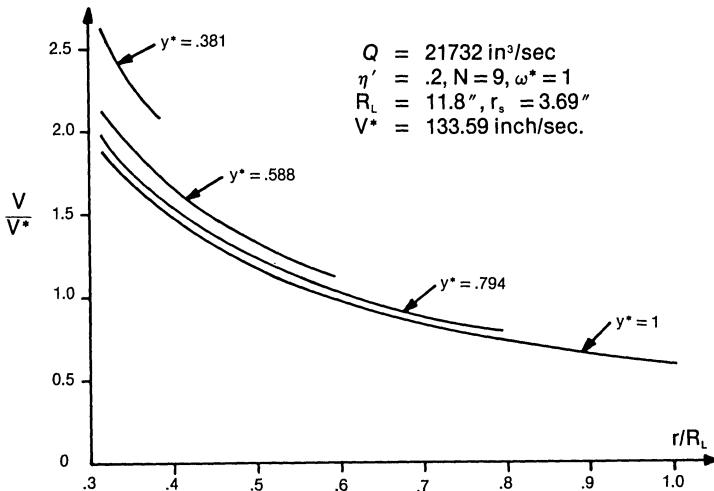


Fig. 16.10.8. Velocity profile for typical tube layers (example problem).

$r^* = r/R_L$. Some important general inferences may be drawn from Fig. 16.10.8. The velocity decreases monotonically with increasing y for a given tube radius. The velocity at the maximum bend radius ($x = 0$) may be a small fraction of the velocity in the baffle window, V_w . In the example problem, the ratio of the velocity at the maximum bend radius to the maximum window velocity V_w is found to be 0.204. Thus, for U-bundles with wide pass partition gaps near the largest bend radii, the window effect may produce localized high velocities. In such instances, the openings should be either closed using dummy tubes, and/or the midspans of such tubes should be adequately supported.

16.11 Vibration Due to Parallel Flow

Tube failures due to parallel flow are rather infrequent. However, the effect of parallel flow should be considered in exchangers where wide baffle spacings are common, such as in kettle reboilers and in condensers. There are several analytical tools for predicting vibration amplitudes of cylinders in parallel flow [16.11.1]–[16.11.6]. Strictly speaking, they apply to solitary cylinders rather than arrays. Unfortunately, the agreement between analytical solutions and experimental data has been disappointing, mainly due to the lack of accurate data on pressure field fluctuations. Until such time when the forcing function is reliably characterized, the heat exchanger designer's sole recourse is to use semi-empirical prognostications [16.11.1–8]. Some of the commonly quoted ones are summarized below.

i. Reavis:

Reavis's correlation for the rms deflection is primarily intended for nuclear reactor fuel assemblies. However, it may serve as a useful guide for heat exchanger tube arrays as well. The root-mean-square of the tube vibration amplitude is given by [16.11.1].

$$y_{\text{rms}} = C_R \eta_d \eta_D \eta_L \left[\frac{\rho d_0 v'^{0.5} N^{0.5}}{w f^{1.5} \zeta^{0.5}} \right] u_{ax} \quad (16.11.1)$$

where the result y_{rms} is given in inches, and

- w = Weight of the tube per unit length, lb/in.
- ρ = Fluid density, lb-sec²/in.⁴
- v' = Fluid kinematic viscosity, in.²/sec
- u_{ax} = Axial flow velocity (in./sec.)
- d_0 = Tube diameter, in.
- f = First mode natural frequency of tube, cycles/sec
- ζ = Fractional damping
- N = Number of tubes in the bundle

The dimensionless scaling factors η_d , η_D , and η_L , plotted in Fig. 16.11.1 are functions of pseudo-Strouhal numbers which depend on the tube length l and the hydraulic diameter of the flow channel D_h .

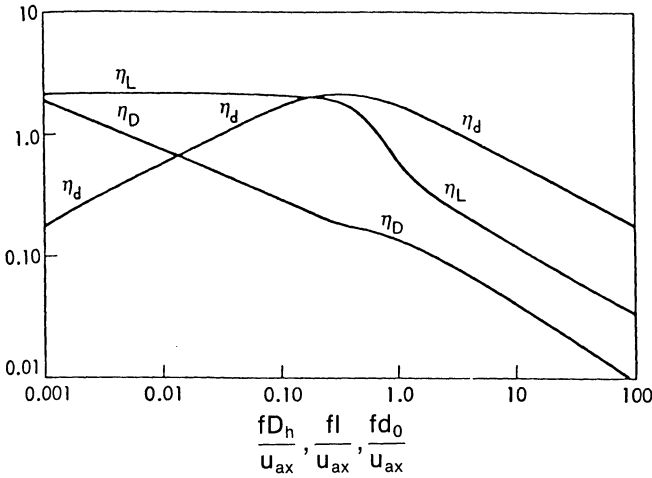


Fig. 16.11.1. Dimensionless scale factors, η .

$$\eta_d = F\left(\frac{fd_0}{u_{ax}}\right)$$

$$\eta_D = F\left(\frac{fD_h}{u_{ax}}\right)$$

$$\eta_L = F\left(\frac{fl}{u_{ax}}\right)$$

$F(\)$ in the above indicates “function of”.

C_R is the “disparity ratio” plotted in Fig. 16.11.2 as a function of D_h/l .

ii. *Paidoussis:*

The vibration amplitude y is given by [16.11.7] as:

$$\frac{y}{d_0} = 5 \times 10^{-4} K^* \lambda^{-4} \left\{ \frac{\bar{u}^{1.6} (l/d_0)^{1.8} \text{Re}^{0.25}}{(1 + \bar{u}^2)} \right\} \left\{ \frac{D_h}{d_0} \right\}^{0.4} \left\{ \frac{\beta^{2/3}}{(1 + 4\beta)} \right\} \quad (16.11.2)$$

where λ is the dimensionless first mode eigenvalue (Table 16.6.1) and \bar{u} is the dimensionless flow velocity

$$\bar{u} = \left(\frac{m' l^2}{EI} \right)^{1/2} u_{ax} \quad (16.11.3)$$

m' is the mass of fluid displaced by the cylinder (equal to the outer volume times the fluid density), l is the tube length, and EI is the flexural rigidity of the tube. Re is the Reynolds number, D_h is the hydraulic diameter, and β is the mass ratio:

$$\beta = \frac{m'}{m + m'} \tag{16.11.4}$$

m is taken as the tube mass including any contained fluid mass.

In Eq. (16.11.2), K^* is a parameter which is equal to 1 for very “quiet” circulating systems (e.g., low turbulence wind or water tunnels) and equal to 5 for industrial environments.

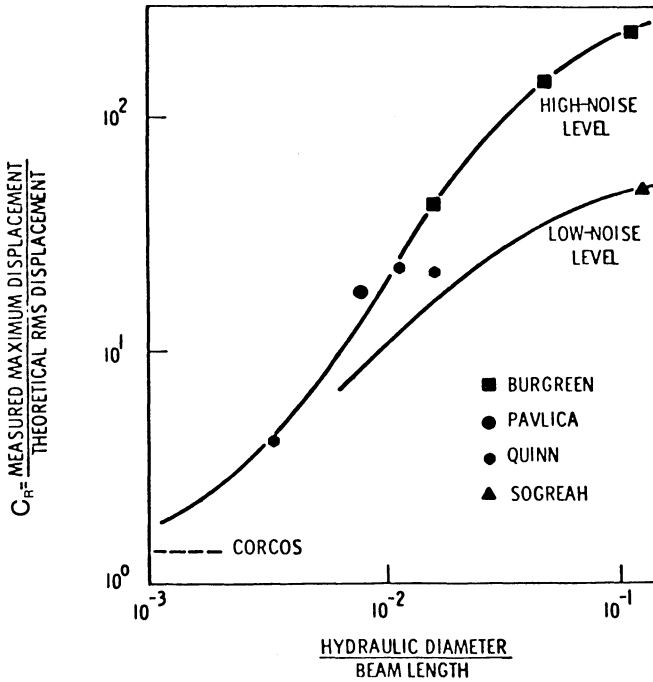


Fig. 16.11.2*. Average disparity between theoretical and experimental displacement.

iii. Y. N. Chen:

Chen [16.11.8] presents the following expression for tube vibration amplitude considering vibration to be a parametric resonance condition:

$$\frac{y}{D_h} = \left[1 - \left(\frac{u_{ax}}{U_c} \right)^2 \right]^{-1} \left[\frac{\beta^* u_{ax}}{U_c} \right]^2 \tag{16.11.5}$$

where

$$U_c = \left[\frac{\pi^2 EI}{l^2} \right] / \left[\frac{1}{4} C_L^* \rho d_0 L + \rho A \right]^{1/2} \tag{16.11.6}$$

In the above expression $A = \pi/4 d_0^2$ and C_L^* is the skin friction coefficient

*The literature sources for the data points of various researchers in this plot may be found in [16.11.1].

for axial fluid flow on the tube surface. $\beta^* = 1/2, 1$ and 2 corresponds to “quiet”, “average”, and “noisy” flow conditions, respectively.

iv. Chen and Weber:

This method, reported in [16.11.9], is based on predicting a turbulent eddy frequency which can produce resonant vibration of the tube if it coincides with the natural frequency of the tube.

The critical parallel flow velocity is given by

$$u_{\text{crit}} = fl \left[\beta \left(\frac{0.002l}{d_0} + 1 \right) \right]^{-1/2} \quad (16.11.7)$$

where β is defined by Eq. (16.11.4).

The dimensionless midspan amplitude is given by

$$y = 2D_h \frac{(u_{ax}/u_{\text{crit}})^2}{1 - \left(\frac{u_{ax}}{u_{\text{crit}}} \right)^2} \quad (16.11.8)$$

16.12 IDEAS FOR PREVENTING FLOW INDUCED VIBRATION PROBLEMS

16.12.1 Fluid-Elastic Instabilities

All fluid-elastic prediction correlations presented in Section 16.7.1 have the general form

$$\frac{v}{fd_0} \leq \alpha \left(\frac{m_0}{\rho d_0^2} \right)^a \delta^b \quad (16.12.1)$$

where α , a and b are constants and $0 < a, b < 1$. This relationship suggests that the stability threshold for the cross flow velocity v is increased if the pertinent natural frequency of the tube span is raised. An inspection of Eq. (16.6.16) indicates that the natural frequency is

- (i) inversely proportional to the square of the tube span.
- (ii) directly proportional to the square root of the Young's modulus of the tube.
- (iii) directly proportional to the square root of the ratio (I/m_0) .

Reducing the tube span causes a proportional increase in the cross flow velocity which in turn increases the shellside pressure loss. To minimize the pressure loss increase, the shell diameter is increased which raises the cost of the equipment. We will comment further on tube span reduction later in this section.

Supporting U-bends at mid-span has been extensively used to mitigate the consequences of out-of-plane vibration of U-tubes. Figure 16.12.1 shows the split baffle plate assembly concept. Photographs 16.a, b, and c show the

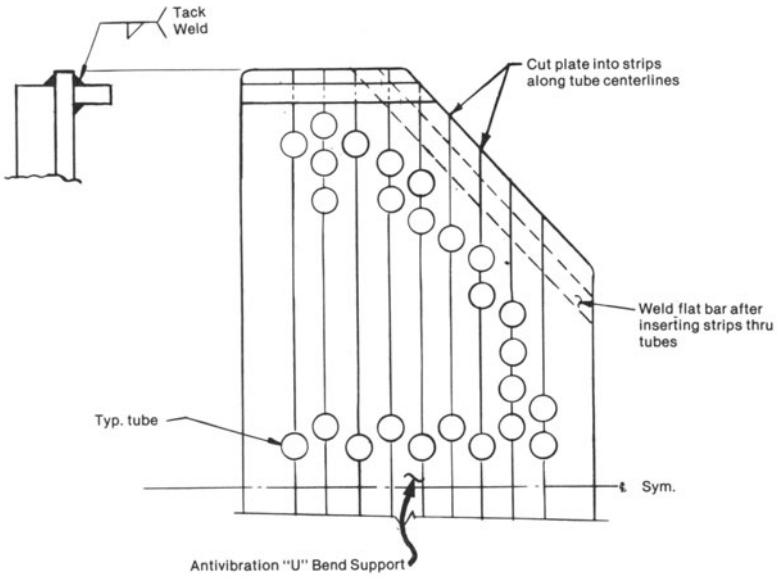
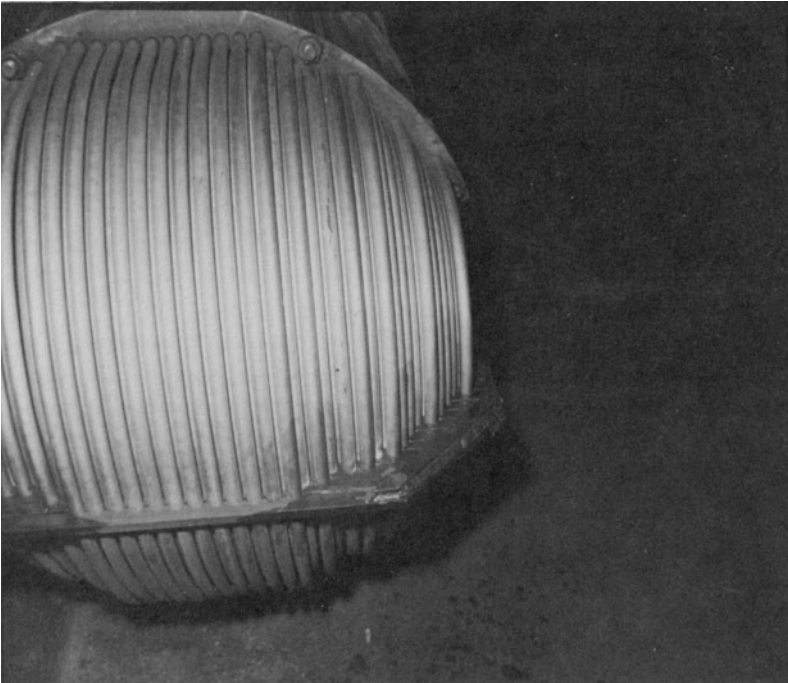
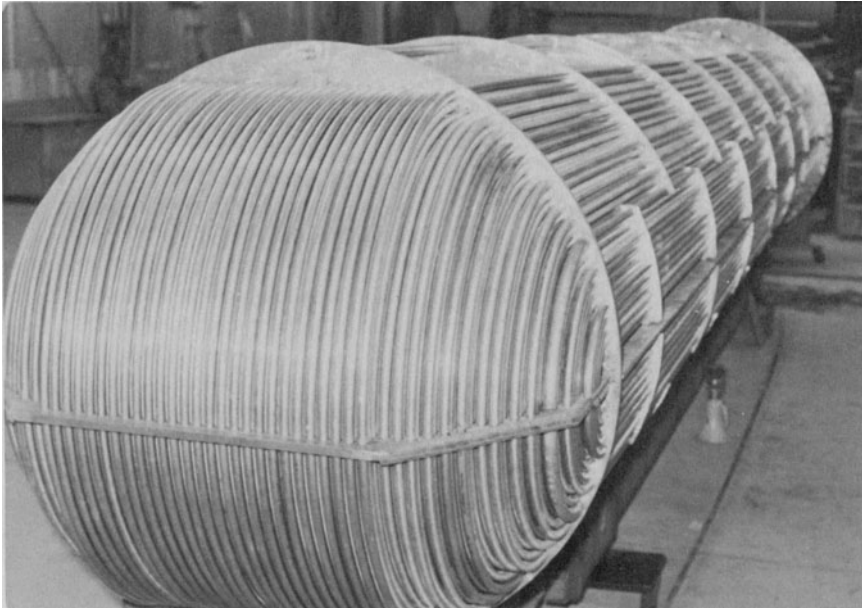


Fig. 16.12.1. Section through “U” bend of tubes.



Photograph 16-b. (Courtesy, Joseph Oat Corporation, Camden, NJ)



Photograph 16-c. (Courtesy Engineers and Fabricators Co., Houston, Texas)

application of this concept in practical hardware. In large diameter bends, sometimes two U-bend supports are applied.

In a similar vein, designers often provide auxiliary lateral supports in tube spans subjected to particularly high velocities; end spans of tube rows facing the inlet or outlet shellside nozzles (see Fig. 16.10.5) are likely candidates for auxiliary supports. Photograph 16.d shows a typical installation of auxiliary lateral supports in the inlet zone. A higher Young's modulus of tubes is desirable; however, other considerations generally determine tube material. Usually, the designer must make do with the Young's modulus available. In retubing operations, however, one should bear the effect of Young's modulus in mind. For example, replacing tubes made from austenitic stainless steel with 70:30 Cu-Ni material reduces the frequency of tube spans by the factor $(28/18.9)^{1/2} = 1.22$ due to Young's modulus effect. The values of Young's moduli used here are taken from Ref. [16.1.5], page 209, at 70°F.

The ratio of I/m_0 warrants further inquiry. For a thin walled tube I can be written as $\pi r^3 t$, where r and t are the nominal radius and thickness of the tube, respectively. The reference tube mass m_0 per unit length is given by

$$m_0 = m_i + m_t + m_a \quad (16.12.2)$$

where

$$m_i = \text{Mass of fluid contained inside the tube, per unit length} \doteq \pi d_i^2 \rho_i / 4 \\ \doteq \pi r^2 \rho_i$$

m_i = Mass of tube metal per unit length = $\pi d_0 t \rho_m \doteq 2\pi r t \rho_m$

m_a = Hydrodynamic mass = $C_m d_0^2 \rho \pi / 4 \doteq C_m \pi r^2 \rho$

Therefore

$$\frac{I}{m_0} = \frac{\pi r^3 t}{\pi r^2 \rho_i + C_m \pi r^2 \rho + 2\pi r t \rho_m} \quad (16.12.2)$$

We note that, for an empty-tube vibrating in vacuum $I/m_0 = r^2/2\rho_m$. Hence, the natural frequency is *independent* of tube wall thickness. In realistic operating conditions, the presence of m_i and m_a make the ratio I/m_0 weakly dependent on t . In any event, tube wall thickness should not be increased in hope of increasing the natural frequency. Increased tube gage, however, does increase tube life by providing greater protection from through-wall wear. The previous reasoning also explains the failure of reported attempts to shore up tube frequency and overcome vibration failures in the field by inserting solid rods into vibrating tubes.

From the foregoing, it follows that the ratio I/m_0 is a “better-than-linear” function of r . Therefore, larger tube diameter offers better protection against tube vibration. However, in reality, heat transfer and pressure loss considerations pre-empt tube vibration in selecting the tube diameter.



Photograph 16-d. Field fix of tube span in front of shell inlet.

Experience indicates that vibration failure in the baffled region often occurs in the tubes located in the window zone just beyond the edge of the baffle cut. An effective strategy to reduce the incidence of vibration in these tubes is to increase the longitudinal pitch near the baffle cuts. Figure 16.12.2 illustrates this concept. Increased longitudinal pitch has the added benefit of permitting straight baffle cut edges rather than the usual half-moon holes.

Finally, the effect of axial tube load on tube natural frequency (Section 16.6.4) should not be overlooked. Designers can sometimes arrange tube pass partitions in such a way that the tubes, belonging to the pass subject to the highest compressive load, are located in the baffle overlap region. Figure 16.12.3 shows 2 four tube pass arrangements. Assuming that the first pass tubes experience maximum compressive load in the operating condition, option (a) shows the first pass tubes located in the overlap zone, while in option (b) some of the tubes are located in the window zone. Since the tubes in the window zone have twice the span of the tubes in the overlap zone in a single segmental baffle layout, the fundamental frequency of the window tubes in the first pass span would be approximately one fourth the frequency of the overlap zone counterparts. Thus, the reduction in the frequency due to high axial compression in pass one tubes is (more than) counter-balanced by the reduced tube span for the overlap zone tubes. Therefore, option (a), which locates all highly compressed tubes in the overlap span, is more desirable from the vibration standpoint. Other pass arrangements incorporating the design goal of option (a) can be devised.

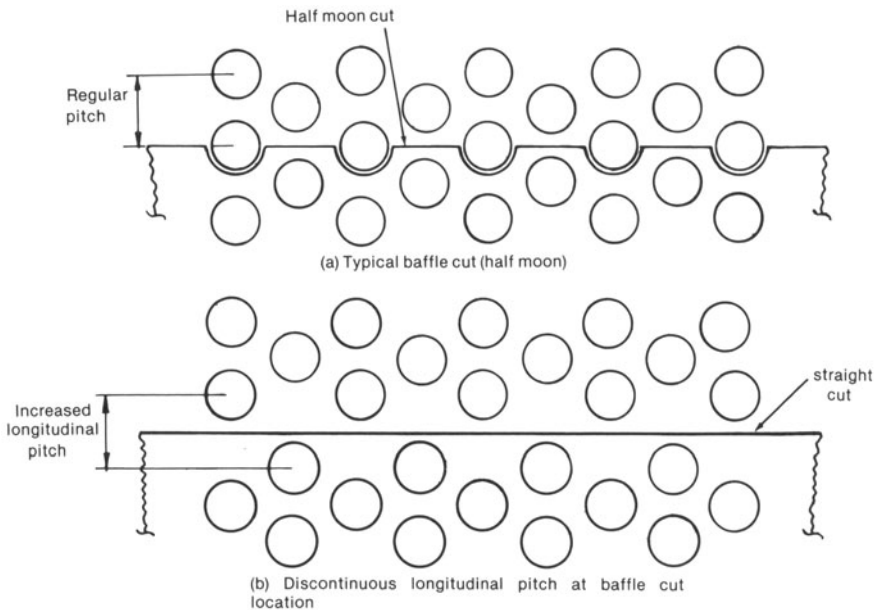


Fig. 16.12.2. Baffle cut schemes.

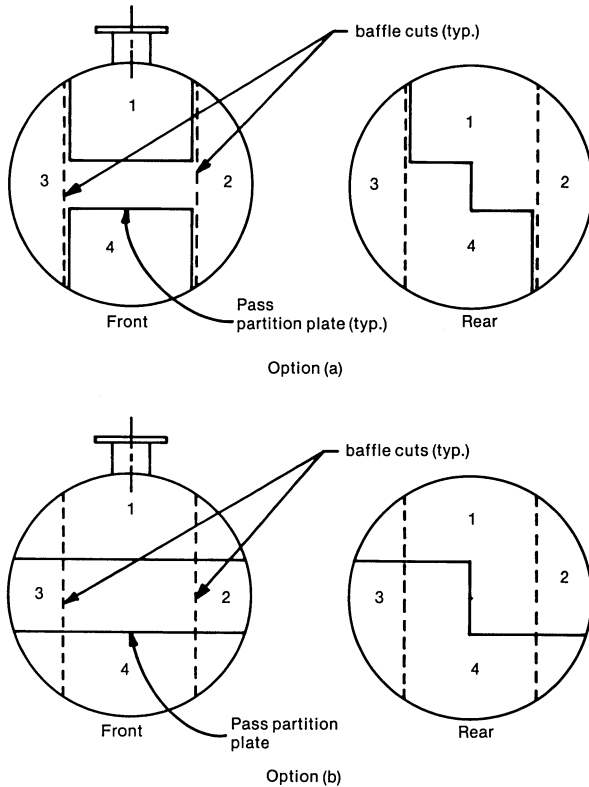


Fig. 16.12.3. Two options for 4-pass straight tube heat exchanger.

As mentioned in Chapter 7, some tube-to-tubesheet fastening techniques produce axial load in the tube. The sequence of fastening sometimes can be arranged to counteract the temperature induced axial load. For example, roller expanding first pass tube legs to the tubesheet, followed by the second pass in a two pass U-tube heat exchanger, puts the first pass tube legs in tension and the second pass in equal compression. This sequence of rolling helps preload the tubes correctly if the cold fluid is located in the tubeside of the heat exchanger.

Increasing tube support plate thickness has the salutary effect of increasing the total damping (δ in Eq. (16.12.1)). Moretti and his co-workers report measuring an almost 100% increase in structural damping as baffle thickness was increased [16.9.1].

An alternative approach to avert flow induced vibration failure lies in reducing the magnitude of the cross flow velocity itself. Increasing the layout pitch is the most obvious means towards this end. It is also the most effective. Increasing tube pitch from 0.9375" to 1" for 0.75" tubing has the effect of increasing the crossflow area by a factor of $(1.0-0.75)/(0.9375-0.75) = 1.33$. On the debit side of the ledger, increasing the tube

pitch increases shell size, and reduces shellside heat transfer coefficient with concomitant reduction in shellside pressure loss.

In addition to lowering the cross flow velocity, increased tube pitch to diameter ratio has a strong effect on increasing the “threshold instability constant α (Eq. (16.7.1)); the net effect of this is to increase the allowable cross flow velocity threshold.

Another way to reduce the cross flow component of the shellside flow is to employ multiple segmental baffles. Double segmental baffles, discussed in Chapter 1, produce a nearly 50% reduction in the cross flow velocity compared to single segmental baffles for equal baffle spacings. Even more drastic reductions can be realized if triple segmental baffles are used. The shellside film coefficient is, however, reduced. Nevertheless, viewed as an energy conversion apparatus, a multiple segmental baffled heat exchanger is more efficient than one equipped with single segmental baffles since the amount of heat transferred for a given amount of pressure loss (mechanical energy) is greater in the former than the latter.

The “No-tubes-in-window concept” illustrated in Fig. 16.12.4 is another strategy to avoid flow induced vibration, particularly in the central regions. Field experience indicates that tubes at the threshold of the baffle cut in the window region are most prone to vibrate. In the no-tubes-in-window construction, the tubes in the window are completely eliminated. However, the resulting increase in the shell diameter makes this concept prohibitively expensive in units operating at high shellside pressures. A design concept which does not suffer from this drawback utilizes narrow baffle strips (Fig. 16.12.5) which increase the natural frequency of the most susceptible row of tubes. This concept was used in many field modifications with success. HTRI’s experimental data also confirms its effectiveness. In Fig. 16.12.5, the “strips” divide the unsupported tube span equally, which maximizes the individual span frequency. Detailed consideration of the flow may suggest a different strip location scheme in specific applications.

Where large unsupported tube span is identified to be the source of

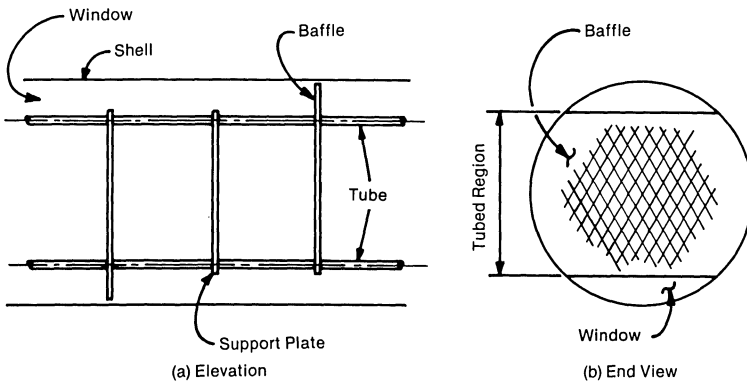


Fig. 16.12.4. No-tubes-in window construction.

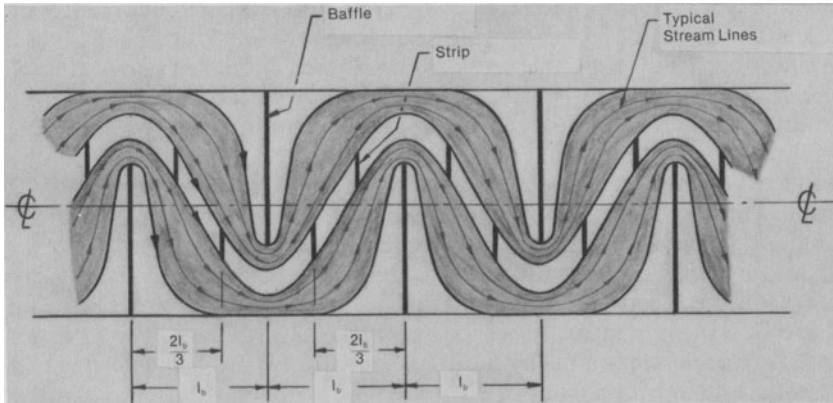


Fig. 16.12.5. Strip baffles to protect vulnerable window region tubes.

vibration problems, additional support to the span has been successfully provided by inserting strips of suitable thickness along clear lanes. Photograph 16.d shows the staking of the tube span adjacent to the tubesheet using such a method. These tubes required additional support to withstand high velocities caused by the presence of the shell inlet nozzle.

A proven technique to reduce unsupported tube span in operating heat exchangers has been reported by Eisinger [16.12.1–2]. Eisinger devised helical rods (Fig. 16.12.6–7) which can be installed in a bundle of regular geometry using a twisting motion while inserting. As shown in Fig. 16.12.6, these helical support bars can be inserted in any direction. An array of rods simulates a complete tube support. Figure 16.12.8 shows a successful solution of a flow induced vibration problem by placement of helical spacer grids in the desuperheating zone of a feedwater heater.

Since the insertion of helical bars requires a regular array, it cannot be used in designs which utilize the previously mentioned concept of discontinuous longitudinal pitch.

Finally, the use of a softer material for the tube supports helps to improve tube longevity. Tight tube to baffle clearances are also helpful.

16.12.2 Acoustic Resonance

Several techniques for abating sonic vibration have been suggested. Of these, addition of baffle plates is the most common. Baffles are installed parallel to the tubes and the flow direction (transverse to the axis of the sonic wave). Interposition of the baffle plate decreases the characteristic dimension of the chamber. Thus, the acoustic frequency (Eq. 16.7.26) is increased. Figure 16.12.9 shows a transverse baffle installed at the location of maximum particle movement in the first mode of a diametral wave form. This baffle would not affect the second mode wave form at all. The solid baffle placed at a point of maximum displacement in the second mode

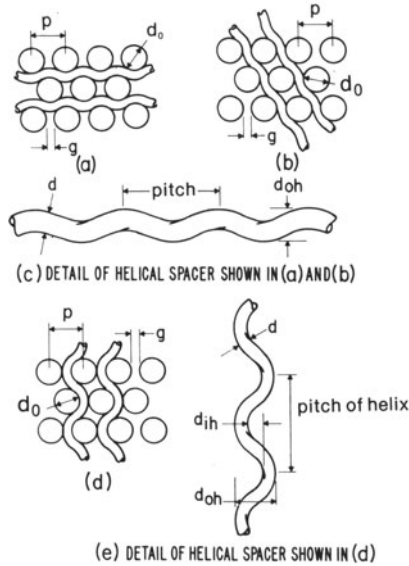


Fig. 16.12.6. Helical spacer positioned in a triangular pitch tube array in three possible directions.

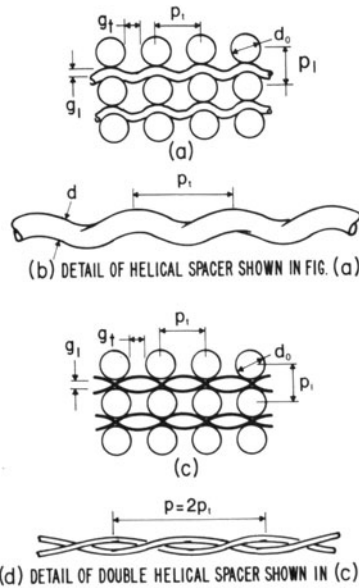


Fig. 16.12.7. Helical spacer (single and double helix) positioned in an in-line tube array.

would disrupt the second mode, but increase the fundamental mode frequency by only a modest amount, since the distance between the reflecting walls is reduced by only one fourth. The dotted line in Fig. 16.12.9 shows the modified first mode when the first baffle is installed (solid line). The second baffle (dotted line in Fig. 16.12.9) increases the first mode frequency even further.

Since the formation of a standing wave requires parallel reflecting walls, arranging the added baffle surface oblique to the wave front is highly effective in disrupting the fundamental and higher modes alike. Figure 16.12.10 shows an obliquely placed baffle used to disperse two sets of diametral wave forms. Interference of inscribed square wave form is also shown in Fig. 16.12.8.

A major demerit of baffle plates is that they produce stagnant heat transfer regions. However, the baffle plate need not be wide if the precise location of the wave channel can be ascertained; unfortunately, this is often easier said than done. The baffle plate must be made from an erosion resistant material since it lies directly in the path of the fluid flow (which may be high velocity gas with entrained liquid droplets).

Walker and Reislung [16.12.4] describe experiments in selective tube removal. Tubes are taken out at the pressure nodes of the standing wave. The method is found to be quite successful.

Zdravkovich and Nuttal [16.12.5] found that instead of removing tubes at the pressure nodes, simply displacing them either transversely or longitudinally achieves the same objective. They also recommend unequal longitudinal pitch in successive rows to be an effective antidote against sonic vibration.

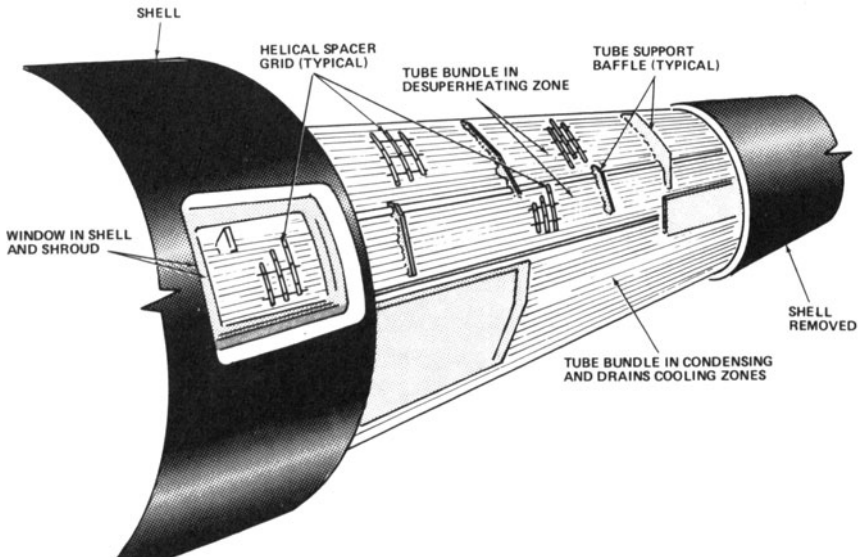


Fig. 16.12.8. Helical spacer grids in feedwater heater (Courtesy American Society for Metals, Metals Park, Ohio).

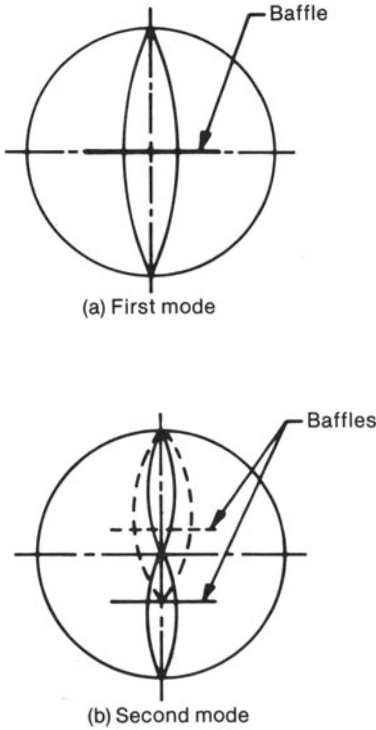


Fig. 16.12.9. Baffle placement for in-line square pitch.

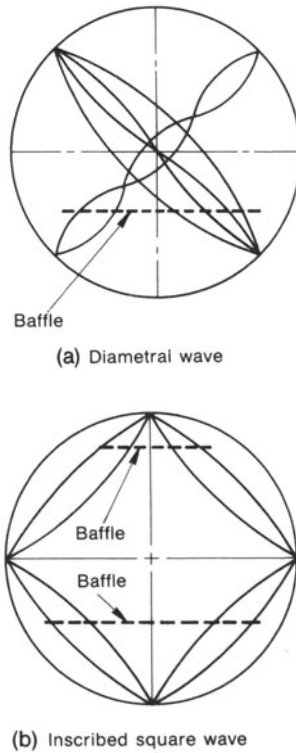


Fig. 16.12.10. Baffle placements for rotated square pitch.

16.13 FLOW INDUCED VIBRATION EVALUATION PROCEDURE

Practical computational procedures to evaluate the potential of flow induced vibration are presented in this section. Unlike most of the analyses described in this book, the degree of uncertainty in vibration calculations cannot be quantified. As such, these procedures can be used to give a high level of statistical confidence against flow induced vibration damage, but by no means are they guaranteed immunity from error. Furthermore, tube vibrations resulting from causes other than fluid flow have not been considered here. There are several reported instances of tube vibration caused by mechanical vibration of the heat exchanger from adjacent rotating equipment. Detrimental tube vibrations due to nucleate boiling (vigorous bubble formation), vapor flashing, etc. are also known to occur. Periodicity in the flow stream related to the blade speed and number of blades in the pump or blower in some cases are also known to have coincided with a tube

natural frequency causing resonant vibrations. The correlations recommended in the following do not account for such effects. As such, the conclusions derived from carrying out the vibration analysis are best described as “studied conjectures”.

We recommend that the designer separately consider each tube span of the tube bundle where either the cross flow velocity, the tube span length or span type (U-bend or straight) is different.

For each case, the calculation may proceed in the following steps:

- (i) Assemble all input data: The following input data is required.
 - (a) Tube outer diameter d_o ; inner diameter d_i ; tube metal density ρ_m ; tube span l or bend radius R ; Young’s modulus of tube material. Nominal wall thickness of the tube may be used in establishing the inside diameter. Tube section moment of inertia I is given as,

$$I = \frac{\pi}{64} (d_o^4 - d_i^4)$$
 - (b) Shellside fluid density ρ ; tubeside fluid density ρ_i ; kinematic viscosity of the shellside fluid ν' at the tube outside surface boundary layer temperature.
 - (c) The cross flow velocity, or velocity as a function of the span coordinate is assumed to be known. Section 16.10 gives some guidance in this matter.
 - (d) Tube axial load, if any, during operating conditions.
 - (e) Tube layout pitch p ; layout angle.
 - (f) For acoustic resonance calculations only, the values of molecular weight, specific heat ratio, and compressibility factor are also required.

(ii) Compute the total reference mass per unit length, m_0 : m_0 consists of three components; namely the tube metal mass, the mass of fluid inside the tube, and the hydrodynamic mass, m_a ; all expressed as mass per unit tube length, i.e.,

$$m_0 = m_t + m_i + m_a \quad (16.12.2)$$

where

$$m_t = \frac{\pi}{4} (d_o^2 - d_i^2) \rho_m \quad (a)$$

$$m_i = \frac{\pi}{4} d_i^2 \rho_i \quad (b) \quad (16.13.1)$$

$$m_a = C_m \frac{\pi}{4} d_o^2 \rho \quad (c)$$

The virtual mass coefficient C_m can be estimated from Fig. 16.8.5 (Moretti et al. data).

(iii) Establish the natural frequency and mode shape:

A tube span located between two baffle supports may be treated as single span beam with simply supported ends. A tube located between a tubesheet and a baffle can be modelled as a single span beam with fixed-pinned boundary conditions. The natural frequency and mode shape of a U-bend span are most conveniently found using computer program UVIB. For example, the natural frequency (fundamental) of a tube span between two baffles is estimated by Eq. (16.6.13) using $n = 1$:

$$\omega = \frac{\pi^2}{l^2} \left(\frac{EI}{m_0} \right)^{1/2} \text{ rads/sec} \quad (16.6.13)$$

The corresponding mode shape is

$$\psi(x) = \sin \frac{\pi x}{l} \quad (16.6.14)$$

The mode shape for the U-bend region would not be an elementary expression like the foregoing. However, it is merely necessary to have numerical values of ψ at discrete points on the span. This is an output from UVIB (Appendix 16.B).

The formulas given in Section 16.6 should be used to reduce the natural frequency if significant axial compression in the tube exists.

(iv) Effective velocity: If the cross flow velocity on the tube span under consideration is specified to be uniform then this step is omitted. On the other hand if the velocity is non-uniform, then Eq. (16.10.1) is used to compute the effective velocity v_e . An example in sub-section 16.10.2 illustrates the procedure.

(v) Logarithmic decrement δ ; Pettigrew's experiment-based prescription can be used to obtain an estimate of ζ (Section 16.9). According to Pettigrew

$$\zeta = \frac{c_n d_0}{2m_0' \omega} \quad (16.13.2)$$

where m_0' is the reference mass per unit length calculated using $C_m = 1$. $c_n = 0.00147 \text{ lb-sec/in.}^3$ for liquids, $c_n = 0.00515 \text{ lb-sec/in.}^3$ for vapors and two phase mixtures.

(vi) Fluid-elastic stability check: Evaluate the parameter

$$\chi = \frac{m_0 \delta}{\rho d_0^2} \quad (16.7.2)$$

Evaluate the quantity v/fd_0 in Table 16.7.1 for the appropriate layout arrangement and range of χ .

$$v^* = \frac{v}{fd_0}$$

or
$$v = fd_0 v^* \quad (16.13.3)$$

This calculated value of v is the maximum permissible cross flow velocity for this tube span.

(vii) Wake shedding check (not required for two phase mixtures or vapors): Corresponding to the actual gap velocity (or the effective velocity, if the flow is non-uniform over the span), denoted by v_{act} here, compute

$$S_{act} = \frac{fd_0}{v_{act}} \quad (16.13.4)$$

If $S_{act} < 1$, then compute the rms wake shedding response using Eq. (16.7.18) with an appropriate mode shape. Let y_{max} denote the maximum computed value of the rms deflection. Compute the pseudo-stress, σ^* in the tube assuming it to be uniformly loaded in such a manner that the maximum lateral deflection equals y_{max} . The suggested criterion of acceptability is:

$\sigma^* < \text{endurance stress of tube material}$

$$y_{max} < 0.2(p - d_0)$$

(viii) Acoustic vibration check (required only for vapors, gases, and two phase mixtures): Select the plausible reflecting surfaces for standing wave formation. Let the distance between them be given by w . Use Eq. (16.7.26) to compute the first mode acoustic frequency ($n=1$). Examine the inequalities of Y. N. Chen, Bryce et al., and Barrington. Violation of any of these indicates a potential vibration problem.

In addition to the above, the designer can compute the rms response due to random excitation (sub-section 16.7.2), and use the previously stated stress and displacement limits given in the context of wake shedding. In units with long unsupported spans and significant parallel flows, the checks given in Section 16.11 should be made.

Two examples presented below demonstrate use of the procedures described above.

Example 1: Water-to-Water heat exchanger: We will use this example to illustrate fluid-elastic and wake shedding calculation

(i) Input data:

Tube O.D. $d_0 = 0.75''$

Tube I.D. $d_i = 0.652''$

Tube metal density, $\rho_m = 7.468 \times 10^{-4} \text{ lb-sec}^2/\text{in.}^4$

Tube section moment of inertia,

$$I = \frac{\pi}{64} (0.75^4 - 0.652^4) = 66.6 \times 10^{-4} \text{ in.}^4$$

Shellside fluid density,

$$\rho = 0.929 \times 10^{-4} \text{ lb-sec}^2/\text{in.}^4$$

Tubeside fluid density, $\rho_i = \rho$

Kinematic viscosity of shellside fluid, $\nu' = 1.06 \times 10^{-3} \text{ in.}^2/\text{sec}$

The tube span, located between two baffles, is 30". The cross flow velocity is uniform and equal to 72 in./sec. The axial compressive force is zero. The tubes are laid out on 1" triangular (30°) pitch.

(ii) Compute total reference mass m_0

$$m_i = \frac{\pi}{4} (0.75^2 - 0.652^2)(7.468 \times 10^{-4})$$

or

$$m_i = 0.81 \times 10^{-4} \text{ lb-sec}^2/\text{in.}^2$$

$$m_i = \frac{\pi}{4} (0.6520)^2 (0.929 \times 10^{-4})$$

or

$$m_i = 0.31 \times 10^{-4} \text{ lb-sec}^2/\text{in.}^2$$

C_m is estimated to be 1.38 for $p/d_0 = 1.33$ from Moretti et al., data (Fig. 16.8.5). Therefore, the hydrodynamic mass per unit length is

$$m_a = C_m \frac{\pi}{4} (0.75)^2 (0.929 \times 10^{-4})$$

or

$$m_a = 0.57 \times 10^{-4} \text{ lb-sec}^2/\text{in.}^2$$

Therefore

$$m_0 = (0.81 + 0.31 + 0.57) \times 10^{-4} = 1.69 \times 10^{-4} \text{ lb-sec}^2/\text{in.}^2$$

Similarly, m_0' (same as m_0 except C_m is set equal to one) is, $m_0' = 1.53 \times 10^{-4} \text{ lb-sec}^2/\text{in.}^2$.

(iii) Natural frequency and mode shape: For pinned ends, and a single span beam:

$$\begin{aligned} \omega &= \frac{\pi^2}{l^2} \left(\frac{EI}{m_0} \right)^{1/2} \\ &= \frac{\pi^2}{30^2} \left[\frac{30 \times 10^6 \times 66.6 \times 10^{-4}}{1.69 \times 10^{-4}} \right]^{1/2} \end{aligned}$$

or

$$\omega = 377.1 \text{ rad/sec}$$

Cyclic frequency,

$$f = \frac{\omega}{2\pi} = 60.1 \text{ cps.}$$

The mode shape, as stated before, is

$$\psi(x) = \sin \frac{\pi x}{l}$$

(iv) Effective velocity: Since the flow velocity is uniform, the effective velocity is equal to the cross flow velocity.

$$v_{act} = 72 \text{ in./sec.}$$

(v) Fractional damping and logarithmic decrement: Pettigrew's formula yields

$$\zeta = \frac{(0.00147)(0.75)}{(2)(1.53 \times 10^{-4})(377.1)} = 9.55 \times 10^{-3}$$

$$\delta = 2\pi\zeta = 0.06$$

(vi) Fluid-elastic stability check:

$$\chi = \frac{(1.69 \times 10^{-4})(0.06)}{(0.929 \times 10^{-4})(0.75)^2} = 0.194$$

From Table 16.7.1, the expression for the dimensionless critical velocity in the range of $0.1 < \chi < 2$ for 30° layout is

$$v^* = 3.58 \left(\frac{p}{d_0} - 0.9 \right) \chi^{0.1}$$

or

$$v^* = 1.316$$

Therefore

$$v = f d_0 v^* = (60.1)(0.75)(1.316)$$

Hence the critical value v_{cr} is

$$v_{cr} = 59.3 \text{ in./sec}$$

Since $v_{ac} = 72 \text{ in./sec}$, this indicates a possibility of flow induced vibration.

(vi) Wake shedding:

$$S_{act} = \frac{f d_0}{v_{act}} = \frac{(60.1)(0.75)}{72}$$

or $S_{act} = 0.626$.

Therefore, the wake shedding calculation should be made. The expression for peak deflection for this case has been derived in final form in Eq. (16.7.22):

$$y_{\max} = F_L / (\pi^2 \delta m_0 f^2)$$

The lift force is given by Eq. (16.7.17)

$$F_L = C_L \frac{\rho}{2} d_0 v_{act}^2$$

Therefore,

$$F_L = \frac{(0.07)(0.929 \times 10^{-4})(0.75)(72)^2}{2}$$

or

$$F_L = 1.26 \times 10^{-2} \text{ lb/in.}$$

Hence,

$$\begin{aligned} y_{\max} &= \frac{1.26 \times 10^{-2}}{(\pi^2)(0.06)(1.69 \times 10^{-4})(60.1)^2} \\ &= 0.0348 \text{ in.} \end{aligned}$$

This is less than the limit of 0.2 ($p - d_0$) = 0.05".

The pseudo-stress corresponding to y_{\max} is computed by noting that the relationship between the midspan flexural stress and maximum static deflection in a uniformly loaded beam is:

$$\sigma^* = \frac{24}{5} \frac{E d_0 y_{\max}}{l^2}$$

Hence,

$$\begin{aligned} \sigma^* &= \frac{(24)(30 \times 10^6)(0.75)(0.035)}{(5)(30)^2} \\ \sigma^* &= 4200 \text{ psi} \end{aligned}$$

This is less than the endurance limit of the material. Therefore, wake shedding is not a cause for concern in this span.

Summarizing, we find that the velocity of 72" per second may be too high to meet fluid elastic stability bounds.

Example 2: Vapor in the shell side chamber. We will use this example to illustrate the application of acoustic resonance check. Let us consider a condenser of 80" inside shell diameter, containing 0.75" O.D. \times 0.049" wall tubes at 1" rotated square (45°) pitch. The tube span of 30" located between two baffles is to be evaluated for acoustic resonance. The calculated cross flow velocity is 50 ft/sec (= 600 in./sec). The molecular weight of the vapor is 18; its specific heat ratio γ and compressibility factor z are 1.3 and 1, respectively.

An inspection of the shell chamber (not shown here) indicates that the only open lane possibly available for a standing wave is the diametral lane

formed by the U-bends. The vapor density ρ is 0.338×10^{-6} lb-sec²/in.⁴, and the vapor bulk temperature is 800° Rankine.

For pitch to diameter ratio of $1/0.75 = 1.33$, the Strouhal number S is 0.66 (from Fig. 16.7.10).

For a diametral wave form, the distance between the reflecting surfaces, w , is 80".

The acoustic velocity c , is given by Eq. (16.7.25) as

$$c = \left[\frac{(1)(1.3)(386.4)(1544)(12)(800)}{18} \right]^{1/2}$$

or $c = 20338$ in./sec = 1695 ft/sec. (The universal gas constant R^* is taken as 1544 ft/°R).

Therefore, the acoustic frequency is (Eq. 16.7.24b).

$$f_a = \frac{(20338)(n)}{(2)(80)} = 127n \text{ cps}$$

The exciting frequency f_e is

$$f_e = \frac{SV}{d_0} = \frac{(0.66)(600)}{0.75} = 528 \text{ cps}$$

Therefore, f_a corresponding to $n=4$ (4th mode) is close enough to the exciting frequency to precipitate the formation of a standing wave (in the 4th mode).

Calculation for Chen's criteria (Eqs. (16.7.29–30)), and that of Bryce et al., (not presented here), also predict the onset of acoustic resonance.

The designer would be well advised to place dummy tubes in the open pass partition lane to eliminate the obvious path of standing wave formation.

NOMENCLATURE

- A_0 = Cross-sectional area of a streamtube before perturbation
- A_i = Cross flow area of stream tube i ($i=1,2$) as a function of location and time
- A_n, B_n, C_n, D_n = Constants of integration (Eq. (16.6.6))
- a = Amplitude of area fluctuation (Eq. (16.5.3))
- c = Damping coefficient
- C_c = Contraction coefficient
- C_e = Expansion coefficient
- C_L = Lift coefficient (Fig. 16.7.7)
- C_m = Virtual mass coefficient
- C_R = Disparity ratio (Fig. 16.11.2)
- C_R^* = Effective random excitation coefficient (Fig 16.7.7)
- c = Velocity of sound
- D_e = Equivalent area for lateral force due to pressure
- D_h = Hydraulic diameter

- d_0 = Tube outside diameter
 E = Young's modulus of tube material
 F = Axial load (Section 16.6)
 F_{cr} = Critical buckling load
 F_L = Lift force
 F_D = Drag force
 f = Tube natural frequency, Hz
 f_a = Sonic resonance frequency, Hz
 f_s = Vortex shedding frequency, Hz
 f_{tb} = Turbulent buffeting frequency
 F_p = Unsteady fluid pressure force
 g = Gap (Fig. 16.8.2)
 g_c = Gravitational constant
 I = Planar moment of inertia of tube section (Eq. (16.6.3))
 k = Function of Poisson ratio (Eq. (16.6.38))
 l = Tube length
 l' = Length of the flow channel (or stream line)
 l_b = Distance between baffle supports (Fig. 16.6.5)
 l_e = Equivalent U-bend length
 l_i = Length of span i (Fig. 16.6.2)
 M = Molecular weight of the gas
 M_0 = Total mass of the vibrating tube
 m_a = Hydrodynamic (virtual) mass (per unit length)
 m_1, m_2 = Parameters (Eq. (16.6.27))
 m_0 = Effective tube mass per unit length
 n = Mode shape number ($n = 1$; first mode)
 N = Number of spans
 P_0 = Steady state pressure in the stream tube (Section 16.5)
 P_i = Pressure in stream tube i (Section 16.5)
 $P(s)$ = Amplitude of pressure fluctuation
 p_t = Transverse pitch
 p_l = Longitudinal pitch
 p = Layout pitch
 q = Out-of-plane frequency coefficient (Eq. (16.6.41))
 R = U-bend radius
 Re = Reynolds number
 R^* = Universal gas constant
 r = Cylinder radius
 r_i = U-bend radius of i th row (Section 16.10)
 r_s = Smallest bend radius ($r_s = r_1$) (Section 16.10)
 R_L = Outermost tube bend radius
 R_s = Inside radius of the shell
 s_0 = Distance along stream tube to inlet
 s_1, s_2 = Position of flow attachment and separation points, respectively (Section 16.5)
 S = Strouhal number (Eq. (16.4.1))

- s = Length coordinate (Section 16.5)
 S_p, S_F = Power spectral density of the excitation force
 T = Absolute temperature of the gas
 T_d = Period of damped vibration
 t = Tube wall thickness
 u_0 = Uniform free stream flow velocity (Section 16.5)
 u_p = Perturbation in flow velocity (Section 16.5)
 u_i = Flow velocity in stream tube i (Section 16.5)
 u = Free Stream Flow Velocity (generic notation)
 u_r = Dimensionless flow velocity (Eq. (16.5.23))
 u_{rel} = Relative velocity (Fig. 16.4.3)
 u_{ax} = Parallel flow velocity
 v = Reference gap cross flow velocity
 v_g = Maximum gap velocity
 V' = Fluid volume displaced by the body
 v_e = Effective velocity (Eq. (16.10.1))
 v^* = Dimensionless fluid cross flow velocity ($v^* = v/fd_0$)
 v_t = Transverse displacement of the U-bend during out-of-plane vibration
 x_t = Ratio of transverse pitch to tube O.D.
 x_l = Ratio of longitudinal pitch to tube O.D.
 x_0, y_0 = Semi-major and minor diameters of the elliptic orbit in Connors' experiments (Fig. 16.4.6)
 \dot{x}, \dot{y} = Velocity of the vibrating body in x and y directions
 y_{rms} = Mid-span root-mean-square amplitude of tube deflection
 $y(t), \dot{y}, \ddot{y}$ = Displacement, velocity and acceleration of tube
 y_0 = Amplitude of tube vibration
 z = Compressibility factor for the gaseous medium
 α = "Fluid-elastic parameter" or "threshold instability constant"
 α' = Angle of attack (Fig. 16.4.3)
 β = Angle between surface normal and transverse axis of tube
 η_d, η_D, η_L = Dimensionless scale factors (Fig. 16.11.1)
 ρ_m = Density of tube metal
 ψ_1^*, ψ_2^* = Pressure loss coefficients (Section 16.10)
 $\eta(x)$ = Stream tube shape function
 $\theta(s)$ = Perturbation pressure phase function
 θ_n = Phase shift of n th mode (Section 16.6)
 λ = Wave length of Sonic Wave
 χ = Damping parameter (Eq. (16.7.2))
 δ = Logarithmic decrement corresponding with vibration in the fundamental mode
 ρ = Shellside fluid density
 ω = Circular frequency of tube vibration

- ω_n = nth mode natural frequency
 ω_d = Damped natural frequency (Eq. (16.9.3))
 $\phi(s)$ = Perturbation velocity phase shift function (Section 16.5)
 $\psi(s)$ = Perturbation area phase shift function
 $\psi_n(x)$ = Mode shape for the n th mode (Section 16.6)
 ν' = Fluid viscosity
 η = Damping factor (Eq. (16.9.3))
 κ = Frequency coefficient (Eq. (16.6.5))
 λ_n = Frequency constant (Eq. (16.6.16))
 ν = Poisson's ratio of tube material
 $\bar{\gamma}$ = Length ratio (Eq. (16.6.49))
 Λ = Frequency reduction factor
 ζ = Ratio of actual to critical damping (Eq. (16.9.7))

REFERENCES

- [16.1.1] Fraas, A. P., and Ozisik, M. N., "Heat Exchanger Design," Wiley (1965).
- [16.1.2] Kern, D. Q., "Process Heat Transfer," McGraw-Hill, New York, (1950).
- [16.1.3] Nelms, H. A., and Segaser, C. L., "Survey of Nuclear Reactor System Primary Circuit Heat Exchangers," ORNL-4399, Oak Ridge National Laboratory, Oak Ridge, Tenn. (1969).
- [16.1.4] Paidoussis, M. P., "Flow Induced Vibration of Cylindrical Structures: A Review of the State of the Art," McGill University, MERL Report No. 82-1, (Aug. 1982).
- [16.1.5] Standards of Tubular Exchanger Manufacturers Association, 6th edition, Section RCB-4 (1978).
- [16.1.6] Shah, R. K., "Flow Induced Vibration and Noise in Heat Exchangers," Proc. of the Seventh Heat and Mass Transfer Conference, Kharagpur, India (1983).
- [16.4.1] Lienhard, J. H., "Synopsis of Lift, Drag and Vortex Frequency Data for Rigid Circular Cylinders," Washington State University, College of Engineering, Research Division Bulletin 300 (1966).
- [16.4.2] Blevins, R. D., "Flow Induced Vibration," Van Nostrand, New York (1977).
- [16.4.3] Chen, Y. N., "Flow-Induced Vibration and Noise in Tube Bank Heat Exchangers due to von Kármán Streets," ASME *Journal of Engineering for Industry*, Vol. 90, pp. 134-146 (1968).
- [16.4.4] Lever, J. H., and Weaver, D. S., "A Theoretical Model for the Fluid elastic Instability in Heat Exchanger Tube Bundles," *Journal of Pressure Vessel Technology*, Trans. ASME, Vol. 104, pp. 147-158, (Aug. 1982).
- [16.4.5] Connors, H. J., "Fluidelastic Vibration of Tube Arrays Excited

- by Cross Flow,” *Flow Induced Vibration in Heat Exchangers*, The American Society of Mechanical Engineers, New York (1970).
- [16.4.6] Roberts, B. W., “Low Frequency, Aeroelastic Vibrations in a Cascade of Circular Cylinders,” *Mechanical Engineering Science Monograph*, No. 4, (September, 1966).
- [16.4.7] Paidoussis, M. P., “Flow-induced Vibration in Nuclear Reactors and Heat Exchangers: Practical Experiences and State of Knowledge,” in *Practical Experiences with Flow Induced Vibrations*, eds. E. Naudascher, and D. Rockwell, Springer-Verlag, pp. 1–81 (1979).
- [16.4.8] Rogers, J. D., and Pentersen, C. A., “Predicting Sonic Vibration in Cross Flow Heat Exchangers—Experience and Model Testing,” ASME Paper No. 77-WA/DE-28.
- [16.4.9] Barrington, E. A., “Experience with Acoustic Vibrations in Tubular Exchangers,” *Chemical Engineering Progress*, Vol. 69, No. 7, pp. 62–68 (1973).
- [16.4.10] Barrington, E. A., “Cure Exchanger Acoustic Vibration,” *Hydrocarbon Processing*, pp. 193–198, July (1978).
- [16.4.11] Chen, Y. N., “The Sensitive Tube Spacing Region of Tube Bank Heat Exchangers for Fluid-elastic Coupling in Cross Flow,” *Fluid Structure Interaction Phenomena in Pressure Vessel and Piping Systems*, ASME, ed. M. K. Au-Yang and J. Brown, Jr., pp. 1–18 (1977).
- [16.4.12] Fitzpatrick, J. A., and Donaldson, I. S., “A Preliminary Study of Flow and Acoustic Phenomena in Tube Banks,” ASME Paper No. 77-FE-7 (1977).
- [16.5.1] Weaver, D. S., and Grover, L. K., “Cross Flow Induced Vibrations in a Tube Bank—Turbulent Buffeting and Fluid Elastic Instability,” *Journal of Sound and Vibration*, Vol. 59, pp. 277–294 (1978).
- [16.5.2] Weaver, D. S., and Koroyannakis, D., “A Comparison of Cross Flow Induced Vibration of a Tube Bundle in Air and Water,” PVP Conference of ASME, Orlando, Florida (1982).
- [16.5.3] White, F. M., “Fluid Mechanics,” pp. 274–276, McGraw-Hill, New York (1979).
- [16.6.1] Timoshenko, S. P., Young, D. H., and Weaver, W., “Vibration Problems in Engineering,” fourth edition, Wiley, N.Y. (1974).
- [16.6.2] Harris, C. M., and Crede, C. E. (eds), “Shock and Vibration Handbook,” second edition, McGraw-Hill, N.Y. (1976).
- [16.6.3] Gorman, D. J., “Free Vibration Analysis of Beams and Shafts,” Wiley (1975).
- [16.6.4] Meirovitch, L., “Elements of Vibration Analysis,” McGraw-Hill (1975).
- [16.6.5] Thomson, W. T., “Vibration Theory and Applications,” Prentice Hall (1965).

- [16.6.6] Ojalvo, I. V., "Coupled Twist-Bending Vibrations of Incomplete Elastic Rings," *International Journal of Mechanical Science*, 4, pp. 53-72 (1962).
- [16.6.7] Archer, R. R., "Small Vibrations of Thin Incomplete Circular Rings," *International Journal of Mechanical Science*, 1, p. 45 (1960).
- [16.6.8] Lee, L. S. S., "Vibration of U-Bend Segments of Heat Exchanger Tubes," Atomic Energy of Canada, Report No. AECL-3735 (1971).
- [16.6.9] Singh, K. P., and Soler, A. I., "HEXDES User Manual," Arcturus Publishers, Cherry Hill, N.J. (1984).
- [16.7.1] Pettigrew, M. J., Sylvestre, Y., and Campagna, A. O., "Vibration Analysis of Heat Exchanger and Steam Generator Designs," *Nuclear Engineering and Design*, Vol. 48, pp. 97-115, (1978).
- [16.7.2] Pettigrew, M. J., and Gorman, D. J., "Vibration of Heat Exchanger Tube Bundles in Liquid and Two-Phase Cross Flow," in *Flow Induced Vibration Design Guidelines*, P. Y. Chen, (ed.), ASME, PVP, Vol. 52, pp. 89-110, (1981).
- [16.7.3] Gorman, D. J., "Experimental Study of the Flow Induced Vibration of Multi-Span Heat Exchanger Tube Bundles in Liquid Cross Flow," Paper B6/6, Trans. 6th International Conference on Structural Mechanisms in Reactor Technology, Paris (1981).
- [16.7.4] Gorman, D. J., "Further Experimental Studies of the Vibration of Multi-Span Heat Exchanger Tubes Subjected to Liquid Cross Flow," Paper 1.6, Proceedings of Third International Conference on Vibration in Nuclear Plant, Keswick, U.K. (1982).
- [16.7.5] Halle, H., Chenoweth, J. M., and Wambsganss, M. W., "Flow-Induced Tube Vibration Tests of Typical Industrial Heat Exchanger Configurations," presented at the ASME Design Engineering Conference, Hartford, Conn. ASME Paper 81-DET-37 (Sept. 1981).
- [16.7.6] Wambsganss, M. W., Halle, H., and Lawrence, W. P., "Tube Vibration in Industrial Size Test Heat Exchanger (30° Triangular Layout-Six Crosspass Configuration)," Argonne National Laboratories Tech. Memo. ANL-CT-81-42, (Oct. 1981).
- [16.7.7] Savkar, S. D., "A Brief Review of Flow Induced Vibrations of Tube Arrays in Cross Flow," *Journal of Fluids Engineering*, Trans. ASME, pp. 517-519, (September, 1977).
- [16.7.8] Weaver, D. S., and Grover, L. K. "Cross Flow Induced Vibrations in a Tube Bank - Turbulent Buffeting and Fluid elastic Instability," *Journal of Sound and Vibration*, 59 (2), pp. 277-294 (1978).

- [16.7.9] Soper, B. M., "The Effect of Tube Layout on the Fluid-elastic Instability of Tube Bundles in Cross Flow," *Flow Induced Heat Exchanger Tube Vibration – 1980*, ASME, HTD-Vol. 9, ed. J. M. Chenoweth and J. R. Stenner, pp. 1–9 (1980).
- [16.7.10] Gilbert, R. J., Sagner, M., and Doyen, R., "Vibration of Tube Arrays in Transversal Flow," Proc. UKAEA/BNES Third International Conference on Vibration in Nuclear Plant, Keswick, U.K. (1982).
- [16.7.11] Chen, S. S., and Jendrzeczyk, J. A., "Experiments on Fluidelastic Instability in Tube Banks Subjected to Liquid Cross Flow," *Journal of Sound and Vibration*, 78 (2), pp. 355–381 (1981).
- [16.7.12] Weaver, D. S., and El-Kashlan, M., "The Effect of Damping and Mass Ratio on the Stability of a Tube Bank," *Journal of Sound and Vibration*, Vol. 76, pp. 283–294 (1981).
- [16.7.13] Rémy, F. N., "Flow Induced Vibration of Tube Bundles in Two Phase Cross Flow," Proc. Conference on Vibration in Nuclear Plant, Keswick, U.K. (1982).
- [16.7.14] Bai, D., "Flow-Induced Vibrations of Multi-Span Tube Bundles of Large Condensers: Experimental Studies on Full Scale Models in Steam Cross-Flow," Proc. Conference on Vibration in Nuclear Plant, Keswick, U.K. (1982).
- [16.7.15] Rémy, F. N., and Bai, D., "Comparative Analysis of Cross-Flow Induced Vibrations of Tube Bundles," BHRA Int'l Conf. on Flow-Induced Vibrations in Fluid Engineering, Reading, U.K. (Sept. 1982).
- [16.7.16] Paidoussis, M. P., "Fluidelastic Vibration of Cylindrical Arrays in Axial and Crossflow: State of the Art," *Journal of Sound and Vibration*, 76(3), pp. 329–360 (1981).
- [16.7.17] Price, S. J., and Paidoussis, M. P., "Fluidelastic Instability of an Infinite Double Row of Circular Cylinders Subjected to a Uniform Crossflow," Trans. ASME, *Journal of Mechanical Design* (c. 1982).
- [16.7.18] Chen, S. S., "Design Guide for Calculating the Instability Flow Velocity of Tube Arrays in Cross Flow," Argonne National Laboratory, Report No. ANL-CT-81-40 (Dec. 1981).
- [16.7.19] Ishigai, S., Nishikawa, E., and Yagi, E., "Structure of Gas Flow and Vibration in Tube Bank with Tube Axes Normal to Flow," Int. Symp. on Marine Engineering, Tokyo, pp. 1–5–23 to 1–5–33 (1973).
- [16.7.20] Tanaka, H., "A Study on Fluid Elastic Vibration of a Circular Cylinder Array (One-row Cylinder Array)," Trans. of the Japan Society of Mechanical Engineers 46 408) (Section B), pp. 1398–1407 (1980).
- [16.7.21] Connors, H. J., "Fluidelastic Vibration of Heat Exchanger

- Tube Arrays,” *Trans. ASME, J. Mech. Design*, 100, pp. 347–353 (1978).
- [16.7.22] Hartlen, R. T., “Wind Tunnel Determination of Fluidelastic Vibration Thresholds for Typical Heat Exchanger Tube Patterns,” 74-309-K, Ontario Hydro, Toronto, Canada (Aug. 1974).
- [16.7.23] Halle, H., and Lawrence, W. P., “Crossflow-Induced Vibration of a Row of Circular Cylinders in Water,” presented at the ASME-IEEE Joint Power Generation Conference, Long Beach, CA, ASME Paper No. 77-JPGG-NE-4 (1977).
- [16.7.24] Gross, H., “Investigations in Aeroelastic Vibration Mechanisms and Their Application in Design of Tubular Heat Exchangers,” Technical University of Hanover, Ph.D. dissertation (1975).
- [16.7.25] Southworth, P. J., and Zdravkovich, M. M., “Effect of Grid-Turbulence on the Fluid-Elastic Vibrations of In-Line Tube Banks in Cross Flow,” *Journal of Sound and Vibration* 39(4), pp. 461–469 (1975).
- [16.7.26] Blevins, R. D., Gilbert, R. J., and Villiard, B., “Experiments on Vibration of Heat Exchanger Tube Arrays in Cross Flow,” 6th SMiRT, Paper No. B6/9 (1981).
- [16.7.27] Heilker, W. J., and Vincent, R. Q., “Vibration in Nuclear Heat Exchangers Due to Liquid and Two-Phase Flow,” presented at the Century 2 Nuclear Engineering Conference, San Francisco, CA, ASME Paper No. 80-C2/NE-4 (Aug. 19–21, 1980).
- [16.7.28] Gorman, D. J., “Experimental Developments of Design Criteria to Limit Liquid Cross-Flow-Induced Vibration in Nuclear Reactor Heat Exchange Equipment,” *Nucl. Sci. Eng.* 61, pp. 324–336 (1976).
- [16.7.29] Zukauskas, A., and Katinas, V., “Flow-Induced Vibration in Heat Exchanger Tube Banks,” *Symp. on Practical Experiences with Flow-Induced Vibration*, Karlsruhe, Germany (Sept. 3–6, 1979).
- [16.7.30] Yeung, H., and Weaver, D. S., “The Effect of Approach Flow Direction on the Flow Induced Vibrations of a Triangular Tube Array,” ASME Paper No. 81-DET-25, *Journal of Mechanical Design* (c. 1982).
- [16.7.31] Pettigrew, M. J., and Gorman, D. J., “Vibration of Heat Exchange Components in Liquid and Two-Phase Cross Flow,” Paper 2.3, *Proc. Vibration in Nuclear Plants*, Keswick (1978).
- [16.7.32] Owen, P. R., “Buffeting Excitation of Boiler Tube Vibration,” *Journal of Mechanical Engineering Science*, 7, pp. 431–439 (1965).
- [16.7.33] Pettigrew, M. J., “Flow Induced Vibration Phenomena in Nuclear Power Station Components,” *Power Industry Research*, 1, pp. 97–133 (1981).
- [16.7.34] Grotz, B. J., and Arnold, F. R., “Flow Induced Vibration in

- Heat Exchangers,” Stanford University, Department of Mechanical Engineering, Report No. 31, (August 1956).
- [16.7.35] Chen, Y. N., “Excitation Sources of the Flow-Induced Vibrations and Noise in Tube Bank Heat Exchangers,” in *Noise and Fluid Engineering*, ed. R. Hickling, pp. 239–246, ASME, New York, (1977).
- [16.7.36] Bryce, W. B., Wharmby, J. S., and Fitzpatrick, J., “Duct Acoustic Resonances Induced by Flow Over Coiled and Rectangular Heat Exchanger Test Banks of Plain and Finned Tubes,” Proc. BNES International Conference on Vibration in Nuclear Plant, Keswick, U.K. (1978).
- [16.8.1] Fritz, R. J., “Effect of Liquids on the Dynamic Motions of Immersed Solids,” *Journal of Engineering for Industry*, Trans. of the ASME, pp. 167–173, (Feb. 1972).
- [16.8.2] Soler, A. I., and Singh, K. P., “Dynamic Coupling in a Closely Spaced Two-Body System Vibrating in a Liquid Medium”: The Case of Fuel Racks,” Proceedings of the Third International Conference on Vibration in Nuclear Plant, Keswick, U.K. (May. 1982).
- [16.8.3] Chen, S. S., and Chung, Ho, “Design Guide for Calculating Hydrodynamic Mass, Part I: Circular Cylindrical Structures,” Argonne National Laboratory, Report No. ANL-CT-76-45.
- [16.8.4] Chung, H., and Chen, S. S., “Design Guide for Calculating Hydrodynamic Mass Part II: Noncircular Cylindrical Structures,” Ibid, Report No. ANL-CT-78-49.
- [16.8.5] Moretti, P. M., and Lowery, R. L., “Hydrodynamic Inertia Coefficients for a Tube Surrounded by Rigid Tubes,” ASME Paper No. 75-PVP-47, Second National Congress on Pressure Vessel and Piping, San Francisco (June 1975).
- [16.9.1] Lowery, R. L., and Moretti, P. M., “Natural Frequencies and Damping of Tubes on Multiple Supports,” *Heat Transfer Research and Application*, ed. J. C. Chen, AIChE Symp. Series, 174, Vol. 74, pp. 1–5 (1978).
- [16.9.2] Pettigrew, M. J., Platten, J. L., and Sylvestre, Y., “International Symposium on Vibration Problems in the Industry,” paper 424, Keswick, United Kingdom (1973).
- [16.9.3] Stokes, G. G., “On the Effect of Internal Friction of Fluids on the Motion of Pendulums,” Trans. Cambridge Phil. Soc., Vol. XI, Part II, pp. 8–106 (1851).
- [16.9.4] Connors, H. J., Savorelli, S. J., and Kramer, F. A., “Hydrodynamic Damping of Rob Bundles in Axial Flow,” *Flow Induced Vibration of Circular Cylindrical Structures – 1982*, S.S. Chen, et al., (eds), The American Society of Mechanical Engineers, Book No. H00220, pp. 109–124 (1982).
- [16.9.5] Wambsganss, M. W., and Chen, S. S., “Tentative Design Guide

- for Calculating the Vibration Response of Flexible Cylindrical Elements in Axial Flow," ANL-ETD-71-07, (June, 1971).
- [16.9.6] Chen, S. S., and Jendrzeczyk, J. A., "Flow Velocity-Dependence of Damping in Tube Arrays Subjected to Liquid Cross Flow," Pressure Vessel and Piping Conference, Paper No. PVP-129, San Francisco (1980).
- [16.10.1] Tinker, T., "General Discussion on Heat Transfer," Institution of Mechanical Engineers, pp. 97-116, London (1951).
- [16.10.2] Sha, W. T., Yang, C. I., Kao, T. T., and Cho, S. M., "Multidimensional Numerical Modeling of Heat Exchangers," The American Society of Mechanical Engineers, *Journal of Heat Transfer*, Vol. 104, pp. 417-425, (August, 1982).
- [16.10.3] Wambsgness, M. W., Yang, C. I., and Halle, H., "Fluid Elastic Instability in Shell and Tube Heat Exchangers – A Framework for a Prediction Method," Argonne National Laboratory, Report No. ANL-83-8, Argonne, Illinois (1982).
- [16.10.4] Palen, J. W., and Taborek, J., "Solution of Shellside Flow Pressure Drop and Heat Transfer by Stream Analysis Method," Chemical Engineering Progress Symposium, Vol. 65, No. 92, pp. 53-63, Philadelphia (1969).
- [16.10.5] Singh, K. P., and Holtz, M., "A Method to Design Shellside Pressure Drop Constrained Tubular Heat Exchangers," Trans. ASME, *Journal of Engineering for Power*, Vol. 99, No. 3 (1977).
- [16.10.6] Connors, H. J., "Fluidelastic Vibration of Heat Exchanger Tube Arrays," Trans. ASME, *Journal of Mechanical Design*, Vol. 10, pp. 347-353 (1978).
- [16.10.7] Kissel, J., "Flow Induced Vibration in a Heat Exchanger with Seal Strips," ASME publication HTD, Vol. 9 (1980).
- [16.10.8] Bell, K. J., "Final Report of the Cooperative Research Program on Shell and Tube Heat Exchangers," Bulletin No. 5, Univ. of Delaware Eng. Experiment Station (1963).
- [16.10.9] Singh, K. P., "Predicting Flow Induced Vibration in U-bend Regions of Heat Exchangers: An Engineering Solution," *Journal of the Franklin Institute*, Vol. 302, No. 2, pp. 195-205 (1976).
- [16.10.10] Kays, W. M., "Loss Coefficients for Abrupt Changes in Flow Cross-sections with Low Reynolds Number Flow in Single or Multiple Tube Systems," Trans. ASME, Vol. 72, pp. 1067-1074 (1950).
- [16.11.1] Reavis, J. R., "Vibration Correlation for Maximum Fuel Element Displacement in Parallel Turbulent Flow," *Nuclear Science and Engineering*, Vol. 38, pp. 63-69 (1969).
- [16.11.2] Gorman, D. J., "Analytical and Experimental Investigation of the Vibration of Cylindrical Reactor Fuel Element in Two-Phase

- Parallel Flow," *Nuclear Science and Engineering*, Vol. 44, pp. 277-290 (1971).
- [16.11.3] Chen, S. S., and Wambsganss, M. W., "Parallel Flow Induced Vibration of Fuel Rods," *Ibid*, 18, pp. 253-278 (1972).
- [16.11.4] Cedolin, L., Hassid, A., Rossini, T., and Solieri, R., "Vibration Induced by the Two-Phase (Gas and Liquid) Coolant Flow in the Power Channels of a Pressure Tube Type Nuclear Reactor," *Trans. First International Conference Structural Mechanics in Reactor Tech.*, Berlin, Paper E4/5 (1971).
- [16.11.5] Ohlmer, E., Russo, S., and Schwemmler, R., "Investigation of an Analytical Model for Parallel Flow Induced Rod Vibrations," *Nuclear Engineering and Design*, Vol. 22, pp. 272-259 (1972).
- [16.11.6] Paidoussis, M. P., "Dynamics of Cylindrical Structures Subject to Axial Flow," *Journal of Sound and Vibration*, Vol. 29, pp. 365-385 (1973).
- [16.11.7] Paidoussis, M. P., "An Experimental Study of Vibration of Flexible Cylinders Induced by Parallel Flow," *Nuclear Science and Engineering*, Vol. 35, pp. 127-138 (1969).
- [16.11.8] Chen, Y. N., "Turbulence Induced Vibration on Tube Bundle Heat Exchangers with Cross and Parallel Flow, Part I: Parallel Flow," in *Flow Induced Vibration in Heat Exchangers*, D.D. Reiff (ed.) pp. 57-66 (1970).
- [16.11.9] Chenoweth, J. M., "Flow Induced Vibrations in Shell and Tube Heat Exchangers," Report No. SAN/1273-1, National Technical Information Service, (February, 1977).
- [16.12.1] Eisinger, F. L., "Prevention and Cure of Flow-Induced Vibration in Tubular Heat Exchangers," *Trans. of the ASME*, Vol. 102, *Journal of Pressure Vessel Technology*, pp. 138-145 (May 1980).
- [16.12.2] Eisinger, F. L., "Helical Spacer for Heat Exchanger Tube Bundle," U.S. Patent No. 4, 204, 570, (May 1980).
- [16.12.3] Eisinger, F. L., "Prevention and Cure of Flow-Induced Vibration Problems in Tubular Heat Exchangers," *The Third National Congress on Pressure Vessel and Piping Technology*, *Flow Induced Vibration*, S. S. Chen and M. D. Bernstein (eds), pp. 47-55.
- [16.12.4] Walker, W. M., and Reisling, G. F. S., "Flow Induced Vibrations in Cross Flow Heat Exchangers," *Chemical and Process Engineering*, Vol. 49, pp. 95-103, (November 1968).
- [16.12.5] Zdravkovich, M. M., and Nuttal, J. A., "On the Elimination of Aerodynamic Noise in a Staggered Tube Tank," *Journal of Sound and Vibration*, Vol. 34, 1974, pp. 173-177.
- [16.B.1] Oden, J. T., and Ripperger, E. A., "Mechanics of Elastic Structures," second edition, Hemisphere (1981).

APPENDIX 16.A

COMPUTER PROGRAM MULTSPAN

This program computes the natural frequencies and mode shapes for a uniform beam with its two extremities fixed (built-in) and $(N-1)$ intermediate supports (Fig. 16.6.2). There are N spans. Numbering the spans from left to right, the length of span i is l_i . The solution for span i is assumed to have the form of Eq. (16.6.17). Using the boundary and interface conditions, namely Eqs. (16.6.18)–(16.6.22), $3N$ linear algebraic equations in $3N$ unknowns are assembled. Equation (16.6.18) yields $C_1 = 0$. The remaining integration constants can be arranged in a vector $\{x\}$ with $(2N-1)$ elements.

The following definitions apply:

$$\begin{aligned} B_i &= x_{1+(i-1)3}; & i &= 1, \dots, N \\ D_i &= x_{2+(i-1)3}; & i &= 1, \dots, N \\ C_i &= x_{(i-1)3}; & i &= 2, \dots, N \end{aligned} \quad (16.A.1)$$

The computer program provides the solution for vector $\{x\}$ and the corresponding natural frequencies.

Input Data (all input is in free field format)

Line 1: Tube material and inertia properties

Quantity	Fortran Symbol	Data for the example Problem
Young's modulus, E	YM	18×10^6 psi
Moment of inertia of tube cross section, I	AMOM	0.0037 in.^4
Reference mass of tube per unit length, m_0	VM	84.75×10^{-6} lb-sec ² /in. ²

Line 2: Span Data

Number of spans, N (input zero to terminate the run)	N	3
---	---	---

Line 3:

Length of span i ($i=1,2, \dots, N$), l_i ; (enter one value if all spans are equal)	ELL(I)	20 in.
--	--------	--------

The program reproduces the input data in its entirety. The values of the natural frequency and the corresponding mode shape for the first N frequencies are printed out. The mode shape is written out as values of the lateral deflection of the tube for 50 discrete equidistant points within each span.

In order to get a “physical feel” of the mode shape, it is useful to normalize it in some manner. One convenient approach is to scale each mode shape such that the maximum displacement is unity. Figure 16.A.1 shows the first three mode shapes normalized in this manner.

The following observations are apparent from these plots:

- (i) The displacement in the central span is the maximum in the first mode; the maximum displacement in the end spans is less than 1/2 of that in the central span.
- (ii) The second mode registers maximum displacement in the end span. The corresponding displacements in the central span are relatively small.
- (iii) The displacements are generally the same in the third mode in all three spans.

In performing a span-by-span flow induced vibration check, it is recommended to use for f the lowest frequency for which the maximum normalized displacement in that span is at least 40% of the maximum, normalized displacement anywhere in the tube for the corresponding mode shape. The normalized maximum displacement for a span is defined as the maximum displacement divided by the span length. This frequency is denoted as the “significant span frequency” for the tube span under consideration. This rule is more pragmatic than rigorous. It is consistent with the overall approach to flow induced vibration analysis presented in this book.

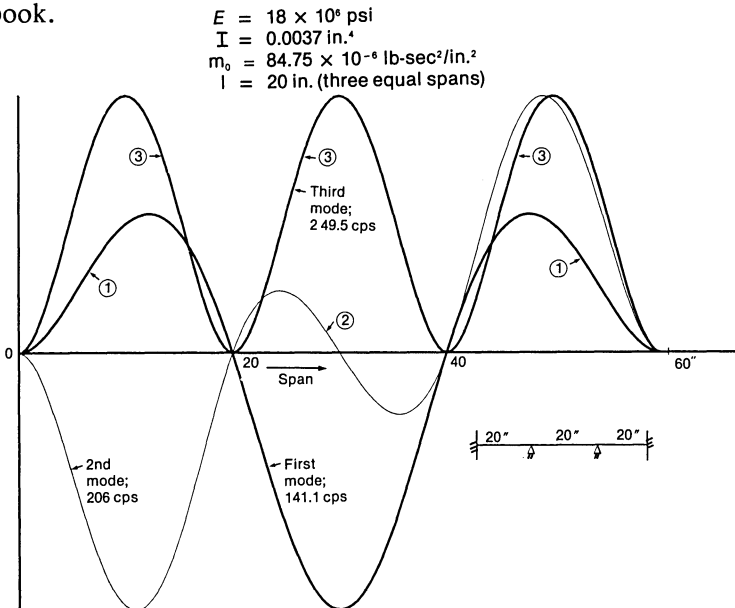


Fig. 16.A.1. First three mode shapes of three span beam with clamped ends.

PROGRAM MULTSPAN

```

DIMENSION ELL(10),X(30)
COMMON ELL,N,X
C
C INPUT ***** INPUT ***** INPUT ***** INPUT
C   CARD 1 - YM,AMOM,VM
C           YM=YOUNG'S MODULUS (PSI)
C           AMOM=MOMENT OF INERTIA OF TUBE CROSS SECTION (IN**4)
C           VM=TUBE VIRTUAL MASS (*(SEC/INCH)**2)
C
C   CARD 2 - N=NUMBER OF SPANS (ENTER 0 TO END PROGRAM)
C
C   CARD 3 - ELL(I)=LENGTH OF EACH SPAN I (IN)
C           IF ALL SPANS ARE EQUAL,ENTER ONLY ONE VALUE
C
C INPUT ***** INPUT ***** INPUT ***** INPUT
C
ACCEPT YM,AMOM,VM
DISPLAY "YOUNG'S MODULUS =",YM
DISPLAY "MOMENT OF INERTIA OF TUBE CROSS SECTION=",AMOM
EIV=SQRT(YM*AMOM/VM)
1 CONTINUE
ACCEPT N
IF(N.EQ.0) STOP
ISCL=0
HIGHELL=0.0
ELL(2)=0.0
DISPLAY "NUMBER OF SPANS=",N
PI=3.1415926
ACCEPT (ELL(I),I=1,N)
IF(N .EQ. 1) GO TO 10
IF(ABS(ELL(2)).GT. 1.0E-06) GOTO 10
DO 100 I=2,N
100 ELL(I)=ELL(1)
10 DO 101 I=1,N
101 HIGHELL=AMAX1(HIGHELL,ELL(I))
X1=3.0/HIGHELL
X2=1.01*X1
Y1=CALC(X1,0)
DO 150 I=1,1000
Y2=CALC(X2,0)
IF(Y1*Y2) 105,105,110
105 X3=.5*(X2+X1)
IF(ABS(X3-X2).LT. 5.0E-06) GOTO 130
Y3=CALC(X3,0)
IF(Y2*Y3) 115,115,120
115 X1=X2
120 X2=X3

```

```

      Y2=Y3
      GOTO 105
130 ISOL=ISOL+1
      AKAP=X3
      F=AKAP*AKAP*EIV/(2.*PI)
      DISPLAY " "
      DISPLAY " "
      WRITE(6,*) "FREQ=",F,"CYCLES/SEC"
      Y=CALC(X3,1)
      CALL MODESHAPE(AKAP)
      IF (ISOL.EQ.N) GOTO 160
      X2=AMAX1(X1,X2)
110 X1=X2
      X2=1.01*X2
      Y1=CALC(X1,0)
150 CONTINUE
160 STOP
      END
$CONTROL INIT
      FUNCTION CALC(AKAP,ISOLV)
      DIMENSION A(30,30),ELL(10),G(900),X(30)
      DIMENSION B(30,30),XS(30)
      COMMON ELL,N,X
      C(I) =COS(AKAP*ELL(I)) + COSH(AKAP*ELL(I))
      CS(I)=COS(AKAP*ELL(I)) - COSH(AKAP*ELL(I))
      S(I) =SIN(AKAP*ELL(I)) + SINH(AKAP*ELL(I))
      SS(I)=SIN(AKAP*ELL(I)) - SINH(AKAP*ELL(I))
C COEFFICIENTS OF A-MATRIX
      IF (N .EQ. 1) GO TO 220
      DO 120 I=1,N-1
      J=1+(I-1)*3
      A(J,J)=CS(I)
      A(J,J+1)=SS(I)
      A(J+1,J+1)=-S(I)
      A(J+1,J)=-C(I)
      A(J+1,J+3)=2.
      A(J+2,J+2)=-2.
      A(J+2,J)=-S(I)
      A(J+2,J+1)=CS(I)
120 CONTINUE
      IF(N.LT.3)GOTO 210
C DEFINE COEFFICIENT OF Ci
      DO 130 I=2,(N-1)
      J=1+(I-1)*3
      A(J,J-1)=S(I)
      A(J+1,J-1)=-SS(I)
      A(J+2,J-1)=C(I)
130 CONTINUE
210 CONTINUE
C LAST INTERMEDIATE PROP
      A(3*N-1,3*N-3)=C(N)
      A(3*N-2,3*N-3)=S(N)

```

```

220     N3=3*N
        N3M=N3-1-ISOLV
        A(N3-1,N3-1)=CS(N)
        A(N3-1,N3-2)=-S(N)
        A(N3-2,N3-2)=CS(N)
        A(N3-2,N3-1)=SS(N)
C
        DO 30 J=1,N3M
        DO 30 I= 1,N3M
        NDEX=(N3M*(J-1)+I)
30     G(NDEX)=A(I,J)
        N3M2=N3M**2
        CALL MINV(G,N3M,N3M*N3M,CALC)
        IF (ISOLV.EQ.0) RETURN
        DO 40 J=1,N3M
        DO 40 I=1,N3M
        NDEX=N3M*(J-1)+I
40     A(I,J)=G(NDEX)
        F=-SS(N)
        DO 300 I=2,N3M+1
        X(I)=A(I-1,N3M)*F
300    CONTINUE
        X(1)=0.0
        X(N3)=1.0
        RETURN
        END
        SUBROUTINE MODESHAPE(AKAP)
        DIMENSION ELL(10),X(30)
        DIMENSION YY(50),ZZ(50)
        COMMON ELL,N,X
        CS(Z)=COS(AKAP*Z) - COSH(AKAP*Z)
        S(Z) =SIN(AKAP*Z) + SINH(AKAP*Z)
        SS(Z)=SIN(AKAP*Z) - SINH(AKAP*Z)
        T=0.0
701    FORMAT(5X,10E12.4)
        DO 100 I=1,N
        I3=3*I
        DO 200 J=1,50
        W=ELL(I)*.02*J
        Y=X(I3-1)*CS(W)+X(I3-2)*S(W)+X(I3)*SS(W)
        T=T+.02*ELL(I)
        ZZ(J)=T
        YY(J)=Y
200    CONTINUE
        WRITE(6,702)
702    FORMAT(/,10(2H**),"MODE SHAPE",5(2H**),/,5(12X,"X",10X,"Y",3X))
        WRITE(6,700) (ZZ(J),YY(J),J=1,50)
700    FORMAT(5(6X,F9.3,2X,E10.3))
100    CONTINUE
        RETURN
        END

```

```

SUBROUTINE MINV(A,N,N2,D)
C
  DIMENSION L(N),M(N),A(N2)
  D=1.0
  NK=-N
  DO 80 K=1,N
    NK=NK+N
    L(K)=K
    M(K)=K
    KK=NK+K
    BIGA=A(KK)
    DO 20 J=K,N
      IZ=N*(J-1)
      DO 20 I=K,N
        IJ=IZ+I
10      IF(ABS(BIGA)-ABS(A(IJ))) 15,20,20
15      BIGA=A(IJ)
        L(K)=I
        M(K)=J
20      CONTINUE
        J=L(K)
        IF(J-K) 35,35,25
25      KI=K-N
        DO 30 I=1,N
          KI=KI+N
          HOLD=-A(KI)
          JI=KI-K+J
          A(KI)=A(JI)
30      A(JI) =HOLD
35      I=M(K)
        IF(I-K) 45,45,38
38      JP=N*(I-1)
        DO 40 J=1,N
          JK=NK+J
          JI=JP+J
          HOLD=-A(JK)
          A(JK)=A(JI)
40      A(JI) =HOLD
45      IF(BIGA) 48,46,48
46      D=0.0
        RETURN
48      DO 55 I=1,N
        IF(I-K) 50,55,50
50      IK=NK+I
        A(IK)=A(IK)/(-BIGA)
55      CONTINUE
        DO 65 I=1,N
          IK=NK+I
          HOLD=A(IK)
          IJ=I-N
          DO 65 J=1,N
            IJ=IJ+N

```

```

      IF(I-K) 60,65,60
60  IF(J-K) 62,65,62
62  KJ=IJ-I+K
      A(IJ)=HOLD*A(KJ)+A(IJ)
65  CONTINUE
      KJ=K-N
      DO 75 J=1,N
      KJ=KJ+N
      IF(J-K) 70,75,70
70  A(KJ)=A(KJ)/BIGA
75  CONTINUE
      D=D*BIGA
      A(KK)=1.0/BIGA
80  CONTINUE
      K=N
100 K=(K-1)
      IF(K) 150,150,105
105 I=L(K)
      IF(I-K) 120,120,108
108 JQ=N*(K-1)
      JR=N*(I-1)
      DO 110 J=1,N
      JK=JQ+J
      HOLD=A(JK)
      JI=JR+J
      A(JK)=-A(JI)
110 A(JI) =HOLD
120 J=M(K)
      IF(J-K) 100,100,125
125 KI=K-N
      DO 130 I=1,N
      -=KI+N
      HOLD=A(KI)
      JI=KI-K+J
      A(KI)=-A(JI)
130 A(JI) =HOLD
      GO TO 100
150  CONTINUE
      RETURN
      END

```

Note: Subroutine MINV is adapted from The “Scientific Subroutine Package”, System 360, by the Courtesy of IBM Corporation, White Plains, N.Y.

30.400	.161E+01	30.800	.159E+01	31.200	.157E+01	31.600	.153E+01	32.000	.149E+01
32.400	.163E+01	32.800	.161E+01	33.200	.159E+01	33.600	.155E+01	34.000	.151E+01
34.400	.165E+01	34.800	.163E+01	35.200	.161E+01	35.600	.157E+01	36.000	.153E+01
36.400	.167E+01	36.800	.165E+01	37.200	.163E+01	37.600	.159E+01	38.000	.155E+01
38.400	.128E+00	38.800	.745E-01	39.200	.343E-01	39.600	.887E-02	40.000	.009E+00
*****MODE SHAPE*****									
40.400	.880E-02	40.800	.341E-01	41.200	.743E-01	41.600	.128E+00	42.000	.192E+00
42.400	.267E+00	42.800	.350E+00	43.200	.439E+00	43.600	.533E+00	44.000	.630E+00
44.400	.729E+00	44.800	.829E+00	45.200	.927E+00	45.600	.102E+01	46.000	.112E+01
48.400	.153E+01	48.800	.159E+01	49.200	.168E+01	49.600	.182E+01	50.000	.198E+01
50.400	.161E+01	50.800	.159E+01	51.200	.157E+01	51.600	.153E+01	52.000	.148E+01
52.400	.142E+01	52.800	.136E+01	53.200	.128E+01	53.600	.120E+01	54.000	.112E+01
54.400	.102E+01	54.800	.928E+00	55.200	.829E+00	55.600	.730E+00	56.000	.631E+00
56.400	.533E+00	56.800	.439E+00	57.200	.350E+00	57.600	.267E+00	58.000	.193E+00
58.400	.128E+00	58.800	.745E-01	59.200	.343E-01	59.600	.887E-02	60.000	-.763E-05

APPENDIX 16.B

NATURAL FREQUENCY OF U-BENDS – COMPUTER PROGRAM UVIB

In this appendix, we derive expressions for the significant natural frequency of the U-bend region. We will concern ourselves with the out-of-plane vibration of U-bends, since the lowest frequencies significant to flow induced vibration occur in this mode. Fortunately, the in-plane and the out-of-plane vibrations of U-bends are dynamically uncoupled; i.e., the equations of motion characterizing out-of-plane motion do not contain in-plane motion terms and vice versa. As shown in sub-section 16.6.5, the equations for out-of-plane motion are characterized by transverse displacement v , and by twist β . Assuming harmonic motion, the amplitudes of v , and β are given by $V(\theta)$ and $W(\theta)/R$, respectively. $W(\theta)$ is defined by Eq. (16.6.45) as

$$W(\theta) = \sum_{i=1}^6 G_i e^{\lambda_i \theta} \quad (16.6.45)$$

where $\lambda_1, \lambda_2, \lambda_3$, etc. are given by solving the sixth order polynomial of Eq. (16.6.44). Depending on the value of q and k some of the λ_i can be complex numbers. Substituting for W and its derivatives, Eq. (16.6.42) furnishes the expression for V

$$V = - \frac{1}{(1+k)q} \left[\sum_{i=1}^6 (\lambda_i^4 + 2\lambda_i^2 + 1) G_i e^{\lambda_i \theta} \right] \quad (16.B.1)$$

The general problem treated herein is shown in Fig. 16.6.4. As shown in this figure, the 180° U-bend, together with the straight leg projections up to the U-bend baffles (denoted as tangent line baffles in Chapter 14), are modelled. The effect of the remainder of the tube span is included in the analysis by including equivalent bending springs K_1 and K_2 . The formulas to estimate K_1 and K_2 were derived in Chapter 14. These are

$$K_i = \frac{EI}{\frac{(2b_i + l_i)}{3} - \frac{(3l_i - a_i)(2l_i + b_i)}{12l_i}}; \quad i=1,2 \quad (16.B.2)$$

where a_i, b_i, l_i , etc. are defined in Fig. 14.2.3.

Finally, the resistance offered to the U-bend against twist is simulated by twist springs (Fig. 16.B.1) located at the ends of the U (nodes B and D). The stiffness of the twist spring, K_T , is given in terms of the straight leg length l_s from the elementary theory of torsion of circular shafts:

$$K_T = \frac{EIk}{l_s}; \quad k = 1/(1 + \nu) \quad (16.B.3)$$

The U-bend support is simulated by placing a support spring of stiffness K_s at angle θ_1 . By making K_s large, we can simulate a typical U-bend support. On the other hand, making K_s infinitesimally small effectively removes the U-bend support. In this manner both supported and unsupported U-bends can be treated.

The model presented in Fig. 16.B.1 involves 4 discrete regions, which are consecutively labelled as such. Regions 2 and 3 constitute the U-bend, and regions 1 and 4 cover the straight segments. The mode shapes for the straight spans (spans 1 and 4) were shown to have the general form (Section 16.6.3).

$$\begin{aligned} \psi_i(x) = & B_i (\cos(\kappa x_i) - \cosh(\kappa x_i)) \\ & + C_i (\sin(\kappa x_i) + \sinh(\kappa x_i)) \\ & + D_i (\sin(\kappa x_i) - \sinh(\kappa x_i)); \quad i = 1 \text{ and } 4 \end{aligned} \quad (16.6.17)$$

where

$$\kappa^4 = \omega^2 m_0 / EI \quad (16.6.5)$$

From classical beam theory, the expressions for the amplitudes of the bending moment (positive if the center of curvature is above the centerline in Fig. 16.B.2) and the shear force (positive if upward on the face with positive x -axis normal) are given as

$$M_s = EI \frac{d^2 \psi}{dx^2} \quad (16. B.4)$$

$$Q_s = -EI \frac{d^3 \psi}{dx^3} \quad (16.B.5)$$

Similarly, in the U-bend region, the shear Q_y , the moment M_x and the twisting couple M_z are related to the displacement variables V and W/R by the following equations (see Ref. 16.B.1 for development of these relationships).

$$M_x = \frac{EI}{R^2} \left(W - \frac{d^2 V}{d\theta^2} \right) \quad (16.B.6)$$

$$M_z = \frac{EI k}{R^2} \left(\frac{dW}{d\theta} + \frac{dV}{d\theta} \right) \quad (16.B.7)$$

$$Q_y = \frac{dM_x}{ds} + \frac{M_z}{R} = \frac{EI}{R^3} \left((1+k) \frac{dW}{d\theta} - (1-k) \frac{d^3 V}{d\theta^3} \right) \quad (16.B.8)$$

where $k = 1/(1+\nu)$. Assumed positive directions for W , V , M_x , M_z and Q_y are shown in Fig. 16.B.2.

The mode shape for each straight span ($i=1$ and 4) involves three unknown constants (Eq. 16.6.17). The mode shape for a U-bend span involves 6 undetermined constants per Eq. (16.6.45). Therefore, regions 2 and 3 are defined in terms of 12 undetermined constants. To keep track of

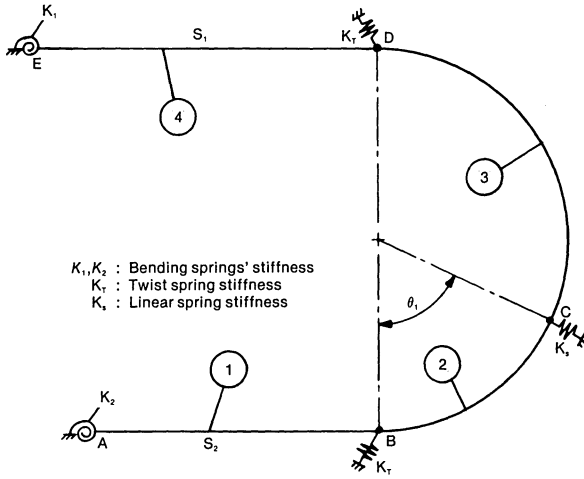


Fig. 16.B.1. Model for computer code UVIB

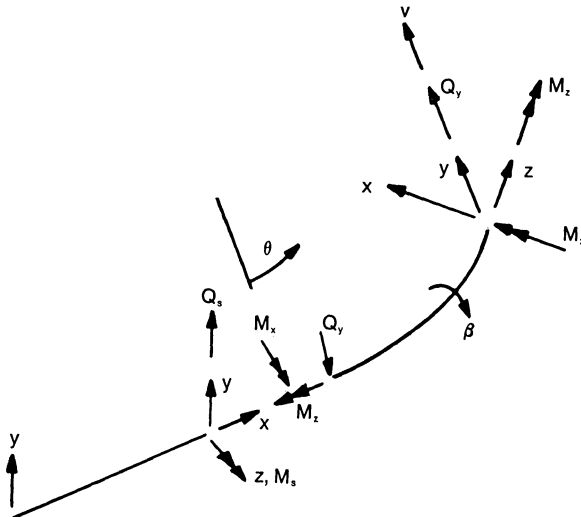


Fig. 16.B.2. Sign convention for moment, shear and twist in straight and U-bend region.

the terms we will use G_{ij} to denote the j th constant for the i th span ($i=2,3; j=1,2, \dots, 6$). Thus, we have a total of 18 constants to be determined by the boundary and interface conditions. These are assembled as follows:

(i) Conditions at node A (Fig. 16.B.1):

The rotation $d\psi/dx$ is opposed by the spring moment $K_2 d\psi_1/dx$, therefore

$$K_2 \frac{d\psi_1}{dx} = EI \frac{d^2 \psi_1}{dx^2} \tag{16.B.9}$$

where ψ_1 is given by Eq. (16.6.17) and the evaluation is at $x=0$.

(ii) Conditions at node *B* (Fig. 16.B.1):

Displacement continuity, referring to the sign convention of Fig. 16.B.2 gives:

$$\psi_1 (@x=S_2) = V_2 @\theta=0 \quad (16.B.10)$$

where V_2 is defined by Eq. (16.B.1) with G_i replaced by G_{2i} . Similarly, slope moment and shear continuity give

$$\frac{d\psi_1}{dx} (@x=S_2) = \frac{1}{R} \frac{dV_2}{d\theta} @\theta=0 \quad (16.B.11)$$

$$EI \frac{d^2 \psi_1}{dx^2} (@x=S_2) = \frac{EI}{R^2} \left(W_2 - \frac{d^2 V_2}{d\theta^2} \right) @\theta=0 \quad (16.B.12)$$

$$-EI \frac{d^3 \psi_1}{dx^3} (@x=S_2) = \frac{EI}{R^3} \left[(1+k) \frac{dW_2}{d\theta} - \frac{d^3 V_2}{d\theta^3} (1-k) \right] @\theta=0 \quad (16.B.13)$$

Finally, the twist of point *C* in the U-bend region (rotation about the *z*-axis) is resisted by the rotational spring K_T

$$K_T \beta (@\theta=0) = M_z \text{ in Eq. (16.B.7)}$$

or

$$\frac{K_T W_2}{R} (@\theta=0) = \frac{EI k}{R^2} \left(\frac{dW_2}{d\theta} + \frac{dV_2}{d\theta} \right) @\theta=0 \quad (16.B.14)$$

(iii) Conditions at node *C* (Fig. 16.B.1):

Displacement, slope, moment, shear and twist relations are written by reference to Eq. (16.6.45), (16.B.1) and (16.B.6–8):

$$V_2 (@\theta=\theta_1) = V_3 @\theta=0 \quad (16.B.15)$$

$$\frac{dV_2}{d\theta} (@\theta=\theta_1) = \frac{dV_3}{d\theta} @\theta=0 \quad (16.B.16)$$

$$\left(W_2 - \frac{d^2 V_2}{d\theta^2} \right)_{\theta=\theta_1} = \left(W_3 - \frac{d^2 V_3}{d\theta^2} \right) \Big|_{\theta=0} \quad (16.B.17)$$

Q_y (in region 3 solution) – Q_y (in region 2 solution) = support reaction = $K_s V_2 @\theta = \theta_1$

or

$$\left[(1+k) \frac{dW_3}{d\theta} - (1-k) \frac{d^3 V_3}{d\theta^3} \right] \Big|_{\theta=0} - \left[(1+k) \frac{dW_2}{d\theta} - \frac{d^3 V_2}{d\theta^3} (1-k) \right] \Big|_{\theta=\theta_1}$$

$$= K_s V_2 \Big|_{\theta=\theta_1} \quad (16.B.18)$$

$$W_2 (@ \theta=\theta_1) = W_3 @ \theta=0 \quad (16.B.19)$$

$$\left(\frac{dW_2}{d\theta} + \frac{dV_2}{d\theta} \right) \Big|_{\theta=\theta_1} = \left(\frac{dW_3}{d\theta} + \frac{dV_3}{d\theta} \right) \Big|_{\theta=0} \quad (16.B.20)$$

(iv) Conditions at node *D*:

Node *D* is the junction of the straight span (region 4) and the curved span (region 3). The expression for the mode shape in region 4, ψ_4 , given by Eq. (16.6.17), assumes the origin of the coordinate system at point *E* in Eq. 16.B.1. The displacement, slope, bending, shear and twist compatibilities yield:

$$\psi_4 (@ x=S_1) = V_3 @ \theta=\pi-\theta_1 \quad (16.B.21)$$

$$-\frac{d\psi_4}{dx} (@ x=S_1) = \frac{1}{R} \frac{dV_3}{d\theta} @ \theta=\pi-\theta_1 \quad (16.B.22)$$

$$EI \frac{d^2 \psi_4}{dx^2} (@ x=S_1) = -\frac{EI}{R^2} \left(W_3 - \frac{d^2 V_3}{d\theta^2} \right) @ \theta=\pi-\theta_1 \quad (16.B.23)$$

$$-EI \frac{d^3 \psi_4}{dx^3} (@ x=S_1) = -\frac{EI}{R^3} \left[(1+k) \frac{dW_3}{d\theta} - \frac{d^3 V_3}{d\theta^3} (1-k) \right] \Big|_{\theta=\pi-\theta_1} \quad (16.B.24)$$

$$K_s \frac{W_3}{R} (@ \theta=\pi-\theta_1) = \frac{-EI k}{R^2} \left(\frac{dW_3}{d\theta} + \frac{dV_3}{d\theta} \right) @ \theta=\pi-\theta_1 \quad (16.B.25)$$

(v) Condition at node *E*:

$$K_2 \frac{d\psi_4}{dx} = EI \frac{d^2 \psi_4}{dx^2} \quad (16.B.26)$$

Substituting for ψ_i , V_i and W_i and their derivatives in Eq. (16.B.9–26) furnishes 18 linear algebraic homogeneous equations in 18 unknown constants. The coefficient determinant is a function of ω , the natural frequency term. The smallest value of ω which makes the determinant vanish is the desired natural frequency.

To start the solution process, a suitable value of ω is assumed. Thus κ (Eq. (16.6.5, $n=1$)) and q in Eq. (16.6.41) become known. All terms of the coefficient matrix are now defined. The corresponding determinant is evaluated using standard procedures. An iterative procedure to arrive at the correct ω is implemented in computer program UVIB. The listing of this code, and the user manual with worked out examples, is given in ref. [16.6.9].

APPENDIX 16.C

COMPUTER PROGRAM UFLOW

UFLOW provides the vehicle to evaluate the quantities needed to describe the flow field in the U-bend region of a heat exchanger possessing the geometry of Figs. 16.10.5-6. The equations are derived in Sub-Section 16.10.4. The input for the program consists of one heading line, and one line of data in free field format. For each term in the input data, the equation in the text defining it, and its mathematical and FORTRAN symbols are identified.

Item	Equation Number	Mathematical Symbol	Fortran Symbol
Largest U-bend radius		R_L	R
Smallest U-bend radius		r_s	RS
Number of tube rows at the equator (at $x=0$ in Fig. 16.10.6)		N	RN
Total volumetric flow rate	(16.10.20)	Q	Q
Perforation coefficient of the bundle	(16.10.21)	η'	ETA
Ratio of loss coefficients	(16.10.14)	ω^*	OMEGA
Inside Radius of the shell		R_s	RSHEL

The program reprints the input data, and computes the value of the flow velocity $V(y,r)$ for stratum of outer radius y for 11 equidistance radii. The quadrant of the bundle is subdivided into 11 strata. The output for the example problem of Sub-Section 16.10.4 follows the code listing presented here.

PROGRAM U FLOW

```

C BY KRISHNA P. SINGH AND TEIK-LEE NG, REV 0, JANUARY 1984
C THIS PROGRAM EVALUATES THE QUANTITIES NEEDED TO DESCRIBE THE
C FLOW FIELD IN THE U-BEND REGION OF A HEAT EXCHANGER
C (POSSESSING THE GEOMETRY OF FIGS. 16.10.5-6). THE PROGRAM
C COMPUTES THE VALUE OF THE FLOW VELOCITY V(Y,R) FOR STRATUM
C OF OUTER RADIUS Y FOR 11 EQUIDISTANCE RADII.
C
C *****
C
C .....DEFINITIONS OF FORTRAN VARIABLES.....
C
C .....INPUT DATA.....
    
```



```

C R      : LARGEST U-BEND RADIUS
C RS     : SMALLEST U-BEND RADIUS
C RN     : NUMBER OF TUBE ROWS AT THE EQUATOR
C Q      : TOTAL VOLUMETRIC FLOW RATE
C ETA    : PERFORATION COEFFICIENT OF THE BUNDLE
C OMEGA  : RATIO OF LOSS COEFFICIENTS
C RSHEL  : INSIDE RADIUS OF SHELL
C
C .....OUTPUT.....
C VSTAR  : AVERAGE BUNDLE APPROACH VELOCITY
C TABULATED VELOCITY FIELD V(Y,R) FOR STRATUM OF OUTER
C RADIUS Y FOR 11 EQUIDISTANCE RADII. THE QUADRANT OF THE
C BUNDLE IS SUBDIVIDED INTO 11 STRATA.
C
C *****
      DIMENSION Y(12) ,V(12),TITLE(20)
      F(X) = 1./ SQRT(ZI*ZI + OM* (ZI-1./SQRT(1.-X*X)) + .5*OMEGA*
1      (ZI*ZI + (1./(1.+X*X))))
      N=100
      N2=N-2
1      READ(5,500,END=1000)(TITLE(I),I=1,20)
500  FORMAT(20A4)
      WRITE(6,510)(TITLE(I),I=1,20)
510  FORMAT (1H1,////////,25(1H*),1X,20A4,1X,28(1H*),/)
      READ(5,*) R,RS,RN,Q,ETA,OMEGA,RSHEL
      WRITE(6,704) R,RS,RN,Q,ETA,OMEGA,RSHEL
      RAT= RSHEL/R
      ZI=R/RS
      OM= ZI*OMEGA*(RN-1.)/(ZI-1.)
      RHO= SQRT (1.0-1.0/(ZI*ZI))
      FN=RHO/FLOAT(N)
      W=F(0.0) + F(RHO) + 4.*F(FN)
      DO 100 I=2,N2,2
100  W=W+2.*F(FN*I)+4.*F(FN*(I+1))
      W=RHO*W/(N*3.)
      C= .5*Q/ (R*R*((RAT-RHO) / (ZI*SQRT(1.+OMEGA)) + ETA*W))
      ALFA=ASIN(RHC)
      VSTAR=Q/(6.28*R*R*(.5*ETA*(ALFA+.5*SIN(2.*ALFA)) + (RAT-RHO)/ZI) )
      WRITE(6,700) VSTAR
      DO 250 I=1,11
250  Y(I) =(I-1)*.1*(R-RS) + RS
      WRITE(6,703) (I,I=1,11), (Y(I),I=1,11)
      DO 300 I=1,11
      DO 400 J=1,I
      V(J) = C/(3.14159*Y(J) *SQRT((1./(RS*RS)) + (OM*((1./RS) -
      (1./Y(I))/R)+ .5*OMEGA*(RS**(-2)+Y(I)**(-2)))) )
400  CONTINUE
      WRITE(6,701) Y(I),(V(J),J=1,I)
300  CONTINUE
      GOTO1
1000 STOP
700  FORMAT(1H0,15X,"*****RESULTS*****"//

```

```

+10X,"AVERAGE BUNDLE APPROACH VELOCITY ..... =",F10.2///
+35X,"*****TABULATED FLOW VELOCITY FIELD V(Y,R)*****")
701 FORMAT(5X, F10.4,3X, "I", 3X, 11F10.4)
703 FORMAT(26X, 11("R",I2,7X),/,11X,"Y",11X,11F10.4,/, 3X, "-----
1-----
2-----")
704 FORMAT(1H0,15X,"*****INPUT DATA*****")//
16X,"LARGEST U-BEND RADIUS .....=",F10.3/
+6X,"SMALLEST U-BEND RADIUS .....=",F10.3/
+6X,"NUMBER OF TUBE ROWS AT THE EQUATOR .....=",F10.0/
+6X,"TOTAL VOLUMETRIC FLOWRATE .....=",F10.0/
+6X,"PERFORATION COEFFICIENT OF THE BUNDLE .....=",F10.3/
+6X,"RATIO OF LOSS COEFFICIENTS .....=",F10.3/
+6X,"INSIDE RADIUS OF THE SHELL .....=",F10.4/)
END
FUNCTION ASIN(X)
PI=3.1415926
R=SQRT(1.-X*X)
IF(X) 1,2,3
3 IF(X.EQ.1.)GOTO 30
ASIN=ATAN(X/R)
RETURN
30 ASIN=.5*PI
RETURN
2 ASIN=0.0
RETURN
1 IF(X.EQ. -1.) GOTO 10
ASIN=ATAN(X/R)-PI
RETURN
10 ASIN=-.5*PI
RETURN
END

```

```

***** SAMPLE PROBLEM FOR PROGRAM UFLWD *****
0
***** INPUT DATA *****
LARGEST U-BEND RADIUS ..... = 11.800
SMALLEST U-BEND RADIUS ..... = 3.690
NUMBER OF TUBE ROWS AT THE EQUATOR ..... = 9
TOTAL VOLUMETRIC FLOWRATE ..... = 21732.
PERFORATION COEFFICIENT OF THE BUNDLE ..... = 1.200
RATIO OF LOSS COEFFICIENTS ..... = 1.000
INSIDE RADIUS OF THE SHELL ..... = 12.3740
***** RESULTS *****
0
AVERAGE BUNDLE APPROACH VELOCITY ..... = 133.69

*****TABULATED FLOW VELOCITY FIELD V(X,R)*****
-----
Y      R 1      R 2      R 3      R 4      R 5      R 6      R 7      R 8      R 9      R 10      R 11
3.6900 I 330.5599
4.5010 I 296.1415 242.7821
5.3120 I 276.7806 226.9097 192.2666
6.1230 I 264.3235 216.6971 183.6133 159.2935
6.9340 I 255.6223 209.5637 177.5690 154.0487 139.6121
7.7450 I 249.1956 204.2950 173.0197 151.1978 129.9815 116.3708 105.3403
8.5560 I 244.2525 197.6279 166.9470 144.8347 127.8948 114.5026 103.6492
9.3670 I 241.1443 194.4151 164.7331 142.9140 126.1988 112.9842 102.2747 94.6752
10.1780 I 237.1143 192.2493 162.8980 141.3219 124.7929 111.7255 101.1354 93.4197 85.9759
10.9890 I 234.5025 192.2493 162.8980 141.3219 124.7929 111.7255 101.1354 92.3790 85.0181
11.8000 I 232.2769 190.4247 161.3520 139.9807 123.6095 110.6652 100.1755 91.5023 84.2112 78.7437 72.6357
-----

```



17. SUPPORT DESIGN AND EXTERNAL LOADS

17.1 INTRODUCTION

Supports for heat exchangers and pressure vessels have remained largely beyond the pale of any governing codes. Whereas detailed rules for the design of the pressure parts have been available in the ASME Boiler and Pressure Vessel Codes for several decades [17.1.1–2], support design has received scant attention. Until recently, sizing of supports was generally left to the empirical judgement of the vessel designer. Since stresses due to dead weight, in most situations, amount to only a fraction of pressure-induced stress in the vessel, the effect of dead weight stress was deemed not critical. This situation changed radically with the advent of the commercial nuclear power industry. Equipment supports designed for use in nuclear power plants had to be checked for seismic loads, mechanical loads from attached piping, etc. Increased concerns about equipment reliability have resulted in the spillover of some of the nuclear power industry analysis requirements [17.1.3] into other sectors viz. fossil power, chemical, petrochemical and pharmaceutical industries. This chapter presents some introductory material and design data on sizing pressure vessel supports. Detailed treatment of specific support styles are found in subsequent chapters.

A brief description of common support styles is given in this chapter with some guidelines on their design. In the following sections, a brief account of the types of loadings and required analyses is also presented with special reference to equipment supports. Finally, available methods for evaluation of local stresses are summarized. In what follows, the term pressure vessel is used to indicate all pressure retaining equipment including tubular heat exchangers.

17.2 TYPES OF SUPPORTS—DESIGN DATA

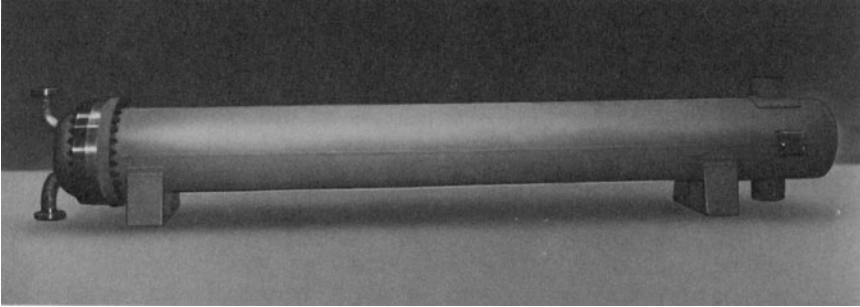
Pressure vessel supports take a variety of forms. The most common styles of supports may be divided into the following categories:

- (i) Saddle
- (ii) Lug
- (iii) Annular ring
- (iv) Skirt
- (v) Trapeze

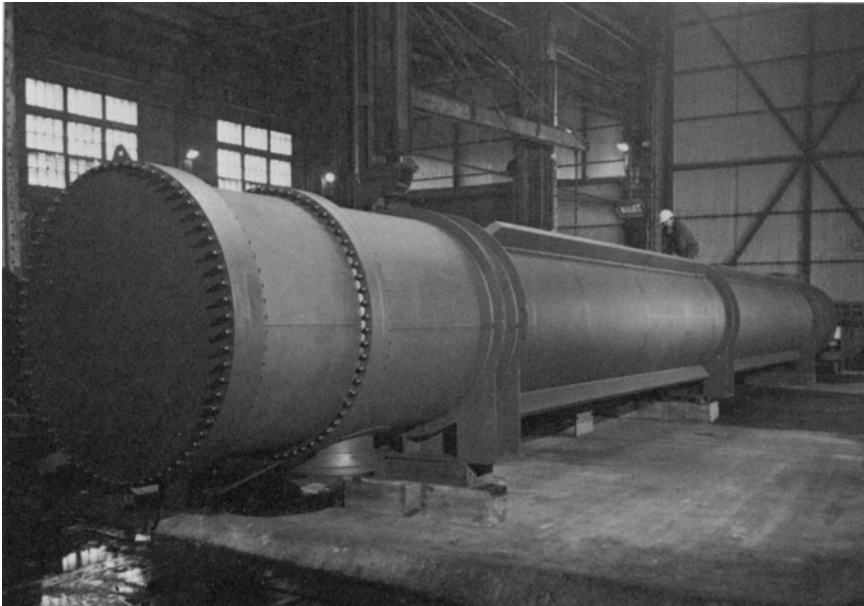
(i) *Saddle Supports*: Saddle supports are the most common means of

supporting horizontal pressure vessels. Two saddles are common (see Photograph 17.a), although three or more have been used in long units (Photographs 17.b) Figure 17.2.1 shows a typical saddle support cross section, along with standard welding symbols.

Tables 17.2.1 and 17.2.2 give typical dimensions for plate and gusset members and for weld dimensions. These dimensions are merely suitable for preliminary design purposes; the final design must be qualified for the external loads acting on the particular unit.



Photograph 17.a. Heat exchanger on two saddle supports.



Photograph 17.b. Heat exchanger on three saddle supports. (Courtesy Joseph Oat Corporation, Camden, N.J.)

Table 17.2.1. Saddle Support Member Dimensions*

Vessel Diameter, D	t_b	t_r	t_g	t_w	W_t	W_l	θ
24	1/2	3/8	1/4			6	120°
30	5/8	7/16	3/8	1/4	D-2	6	
36	5/8	1/2	3/8			6	
42	3/4	1/2	1/2				
48	3/4	9/16	1/2	5/16	D-3	8	
54	3/4	9/16	1/2			8	
60	1	5/8	9/16				
66	1	5/8	9/16	3/8	D-4	12	

Table 17.2.2. Weld Size (all supports)*

	Thickness of Thinner of the two parts being joined						
	1/4	1/4 to 3/8	7/16 to 5/8	11/16 to 1	1 1/16 to 1 1/4	1 5/16 to 1 1/2	1 9/16 to 2
w_b with penetration weld	1/8	3/16	1/4	5/16	3/8	1/2	1/2
w_b Fillet one side	3/16	3/8	5/8	3/4	13/16	7/8	1
w_b Fillet both sides	3/16	1/4	5/16	3/8	7/16	1/2	1/2
w_g	1/8	1/4	3/8	1/2	9/16	5/8	3/4
w_s		3/8			1/2		

*All dimensions are in inches unless otherwise indicated.

Legend for Tables 17.2.1-2

- t_b = Recommended thickness for base plate
- t_r = Recommended thickness for rib plate
- t_s = Shell thickness
- t_g = Recommended thickness for gusset plate
- t_w = Recommended thickness for wear plate
- w_b = Recommended weld size base plate
- w_g = Recommended weld size gusset plate
- w_s = Recommended weld size wear plate
- W_l = Longitudinal width
- W_t = Transverse width

One of the two saddles is equipped with slotted holes in the base plate to accommodate the variation in axial length of the unit under operating

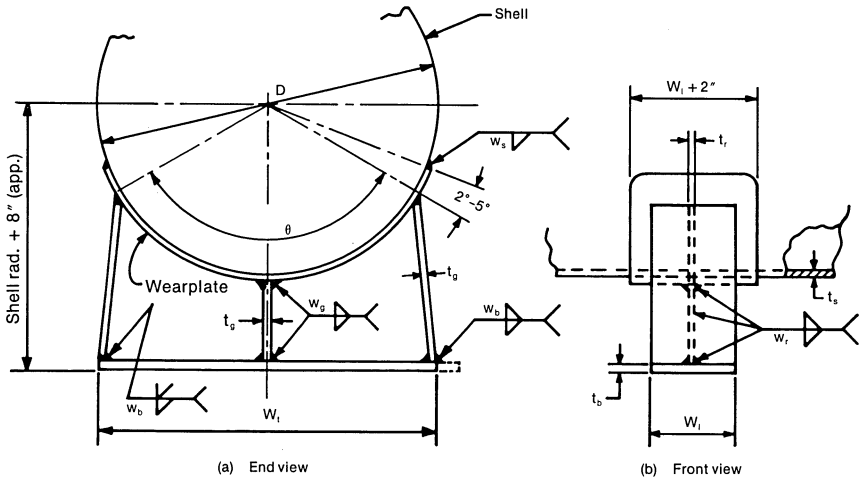


Fig. 17.2.1. Horizontal saddle type support.

conditions. In large diameter units (over 60"), slotted holes are required to accommodate lateral dimensional changes as well. The anchor bolts on the slotted holes should not be prestressed so that the saddle can slide over the concrete pedestal. Anti-friction interface plates are used where immunity from the uncertain coefficient of the friction value at the base plate-pedestal contact surface is desired. A number of anti-friction plates are commercially available. Among them are:

Lubrite:

A product of Merriman (Litton) Corporation, Hingham, Massachusetts. This plate is made from brass with blind recesses for accommodating special lubricants. The type of lubricant used is selected to match the operating condition.

Fluoroloc, Fluorotemp:

Products of Fluorocarbon Corporation, Pine Brook, New Jersey. This is a composite plate construction, where a highly polished teflon layer is embedded on one or both sides of a metallic backing plate. This not only provides a well defined range of friction coefficient, but also introduces an insulating barrier between the support structures and the heat exchanger support. This is helpful in concrete pedestal mounted units, where the pedestal temperature must be controlled to protect the concrete.†

(ii) *Lugs:* Lugs are commonly used for supporting units which have a vertical orientation and are mounted on structural members, such as I-

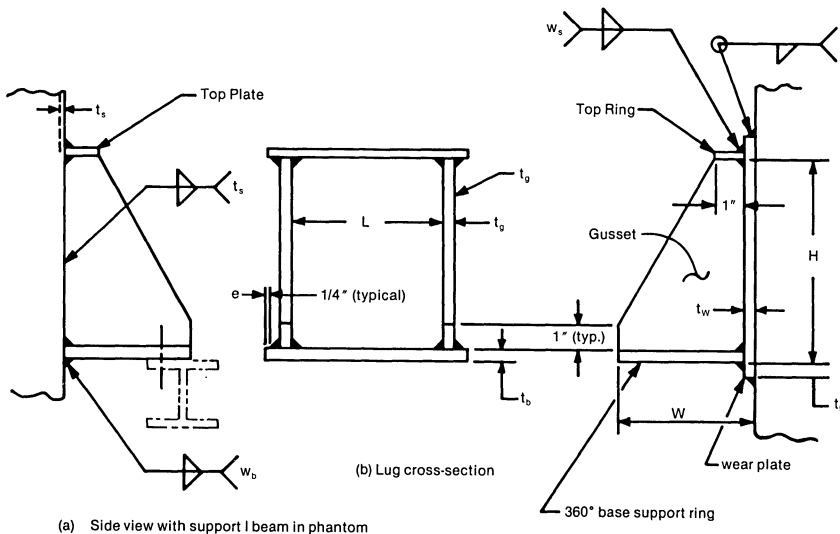
†Most concrete design codes limit the sustained surface temperature of reinforced concrete slabs to 150°F.

beams (Fig. 17.2.2). A lug may be manufactured from carbon steel stock and welded directly to the pressure vessel wall if the latter is also made from carbon steel. An intermediate wear plate may be added if direct welding of the lug to the vessel wall is not acceptable due to material incompatibility, or if weld contamination of one material by another is feared. A wear plate is also sometimes added to increase the local rigidity of the shell. The radial extent of the lug is determined by the clearance required for torquing the hold-down bolts, and by structural code requirements on the required edge dimension e (see Fig. 17.2.2.a). Appendix XVII of Section III of the ASME Boiler and Pressure Vessel Code gives rules for establishing the minimum edge distance. Table 17.2.3 gives typical values used in the industry.

The height of the lug is determined by the local stress calculations as discussed in Section 17.6.

Table 17.2.4 gives preliminary data on lug sizing and Table 17.2.2 gives weld size data. These tables may be used as the starting point for developing the lug design. Final dimensions, of course, should be determined from the results of a stress analysis.

(iii) *Annular Ring*: The annular ring type of support (Fig. 17.2.3) is also used to support vertically mounted units. This design consists of a full 360° base ring buttressed by suitably spaced vertical gussets. It is advisable to also include the top ring, although it is sometimes deleted to effect economy of construction. Preliminary design data on annular ring sizing is given in Tables 17.2.2 and 17.2.4. Edge distance data may be found in Table 17.2.3.



(a) Side view with support I beam in phantom

Fig. 17.2.2. Lug support.

Fig. 17.2.3. Ring type support.

Table 17.2.3. Minimum Edge Distance for Punched, Reamed or Drilled Holes

Bolt nominal diameter (in.)	Sheared edges (in.)	Minimum Value of e^*	
		Rolled edges of plates, shapes, bars, or gas cut edges (in.)	
1/2	7/8	3/4	
5/8	1 1/8	7/8	
3/4	1 1/4	1	
7/8	1 1/2	1 1/8	
1	1 3/4	1 1/4	
1 1/8	2	1 1/2	
1 1/4	2 1/4	1 5/8	
over 1/4	1 3/4 × bolt dia.	1 1/4 × bolt dia.	

* e is the minimum distance between the edge of the bolt hole and the *support member* edge (e.g. the I-beam in Fig. 17.2.2a).

Table 17.2.4. Preliminary Vertical Support Sizing Data

Nominal Vessel Diameter	t_b			Quan.*	H	L	W (Radial Projection)		
	Lug	Ring	Skirt		Height	Length	Lug	Ring	Skirt
24	5/8	1/2	5/8	3	6	4	6	6	6
30	3/4	9/16	3/4	4	6	6	6	6	6
36	3/4	5/8	3/4	4	6	6	8	6	6
42	7/8	3/4	7/8	4	8	6	10	8	8
48	1	7/8	1	4	8	6	10	8	8
54	1 1/4	1	1 1/4	6	8	8	12	10	10
60	1 1/2	1 1/4	1 1/2	6	10	8	12	12	12
66	2	1 1/2	2	6	10	8	16	12	12

*Indicates number of lugs for lug type supports, or number of pairs of gussets for skirt or ring type supports.

(iv) *Skirt*: The skirt support (Fig. 17.2.4) is used mostly with column type units. At times it is also used for supporting vertical heat exchangers. Evidently, skirt type support can only be employed with Bonnet (TEMA Type "B") construction. "Chairs" are frequently utilized (Fig. 17.2.5) to add free length to the anchor bolts. Table 17.2.4 also gives some preliminary data on skirt type support design. The skirt thickness t_{sk} is set equal to the smaller of t_h or t_s .

(v) *Trapeze*: A trapeze is an inverted saddle support. The saddles are bolted to a support member. Dead load of the unit places the support bolts in tension. The use of a trapeze type of support is confined to light vessels and to plants where the necessary floor space is unavailable for use of regular saddle supports.

17.3 LOADINGS

Typical pressure vessels and heat exchangers are subject to the following external loadings:

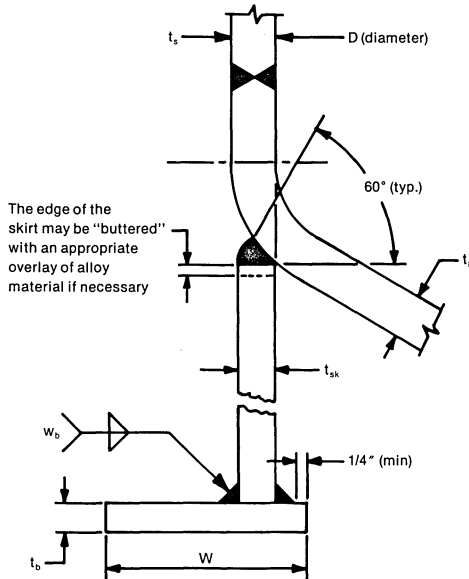


Fig. 17.2.4. Skirt type support.

- (i) Dead loads of the vessel including its inventory of contained fluid.
- (ii) Thermal expansion loads from attached piping, and from restraint of its own supports.
- (iii) Seismic loads (and wind loads).
- (iv) Handling loads.

(i) *Dead load*: The pressure vessel supports should be capable of withstanding the dead load of the equipment, including its internals, and the contained fluid, without experiencing permanent deformation at any location. The most critical location is the portion of the shell between the supports. A popular semi-empirical method for computing the stresses in saddle support is due to Zick [17.3.1]. More rigorous techniques are described later in this chapter. The local stresses at the support to shell junction are particularly important in the design of removable bundle heat exchangers (Fig. 4.1.1), since large deformations may hinder tube bundle removal. However, we note that the shell deformation due to welding between the supports and the shell is usually the cause for more concern in this respect.

(ii) *Thermal Expansion Loads*: The metal temperature of the pressure vessel under operating conditions is usually different from the ambient conditions during its installation. The consequent change in the distance between the supports, due to temperature change, should be considered in support design. As discussed before, designers are usually able to eliminate this source of loading by simple expedients such as the slotting of certain support holes in saddle supports and the use of unidirectional auxiliary

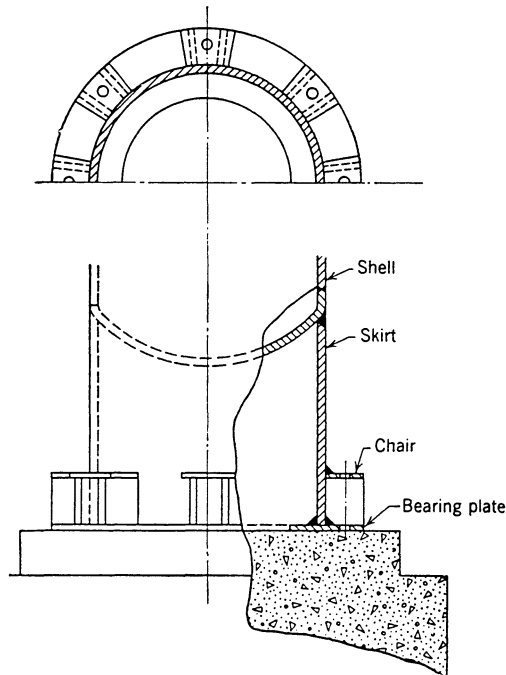


Fig. 17.2.5. Skirt type support with chairs.

supports in vertically mounted units. The other source of thermal loading arises from thermal expansion/contraction of interconnecting pipings. These loads are hard to obviate and the pressure vessel must be designed to withstand these loads. Unfortunately, precise data on these loads is usually not available at the time of the equipment design. Therefore, the equipment designer must consider various combinations of piping loads on the equipment to determine the most severe load combinations. In Chapter 20, we will discuss the question of finding the most severe load combination in some detail.

(iii) *Seismic Loads*: Seismic loads are usually specified in terms of multiples of “g”^{*} in three orthogonal directions. The orthogonal directions are normally taken to be along the natural axes of symmetry of the equipment. In some support configurations, such as the “four leg support”, to be discussed in Chapter 18, selection of the axes can have a substantial effect on the computed stresses.

The equipment is also subject to mechanical loadings due to the action of seismic accelerations on the attached piping. Common practice lumps these loads with the piping thermal expansion loads, and the total load is designated as the “nozzle load” in the common terminology of the pressure vessel industry.

^{*}Acceleration due to gravity.

Seismic loading is usually the controlling component among all mechanical loads. In large vessels containing liquids one must also consider the effect of “sloshing”. Reference [17.3.2] gives appropriate design information on sloshing. Wind loads are important in the design of tall towers.

(iv) *Handling Loads*: Loads due to lifting and maneuvering of vessels during installation should be carefully considered in the design stage. The main area of concern here is the local region around the lifting lugs. The ANSI Standards [17.3.3] for nuclear components require an impact factor of five on the lifting load. This means that the apparent weight to be utilized in static stress analysis of the lifting lugs should be six times the transportation weight of the hardware. The limit on the sum of local and primary stresses in this region is taken as 90% of the ultimate strength of the pressure vessel material. In addition to the local vessel stresses, the nominal stresses in the lug, specially at the lifting eye section, must be evaluated. Appendix XVII to Section III of the ASME code gives stress limits for bearing, tension, shear, etc. in support member design. These limits are summarized later in Section 18.7.

17.4 ANALYSIS FOR EXTERNAL LOADS

The following regions are commonly analyzed in heat exchangers and pressure vessels subject to external loadings.

(i) *Support-shell Junction*: The load transfer between the support and the shell produces local membrane and bending stresses (Chapter 2). In this respect the skirt type support is most desirable since it entails a minimum amount of geometric discontinuity. A method to evaluate skirt, head, and shell junction stresses due to internal pressure is given in Chapter 2. In the case of lug supports, some practical methods for computing the local stresses at lug-shell junctions are indicated in later sections of this chapter.

(ii) *Support-foundation Interaction*: The stresses in the support hold-down bolts, and the surface pressure on concrete pedestals (where used) do not concern designers where dead load (other than pressure) is the only loading. In fact, older books on this subject [17.4.1] treat support interaction analysis only in the context of tall columns subject to wind loads. Mechanical loadings, specially nozzle loads and seismic inertia loads, are often found to control anchor bolt number and size, and govern support/foundation interface design. Methods to estimate foundation/support interaction are presented in Section 17.7 and also in Chapters 19 and 20.

(iii) *Bending Stresses in the Shell*: “Beam-type” bending induced in the shell due to mechanical inertia or thermal loadings is usually quite small if the unit is properly supported. As a rule-of-thumb, the fundamental natural frequency, f_n , of the unit modelled as a beam simply supported at the support locations should be over 30 Hz. Since the natural frequency varies inversely with the square of the unsupported length, requiring a relatively high natural frequency implies that the support spacing must be limited.

This limiting of support spacing places a natural limit on beam bending stresses in the shell. The full expression for f_n is:

$$f_n = \frac{\pi}{2 l_s^2} \left(\frac{EI}{\mu} \right)^{1/2}$$

where

- E = Young's modulus of shell material at its design temperature.
- I = Moment of inertia of shell excluding corrosion allowance $I \approx \pi r^3 t$, where r is shell mean radius, and t is the corroded wall thickness.
- μ = Mass of the shell plus any contained metal and fluid per unit length.
- l_s = Distance between the support centerlines.

The above criterion is strictly judgemental and is intended to be no more than a design guide. The stiffening effect of tubes in fixed tubesheet exchangers, the presence of shell overhangs beyond supports are, among other factors, not included in the above formula.

In vertically mounted units, it is advisable to consider lateral restraints to eliminate cantilever type response of the shell to external loads. It is important to limit the "beam-type" stress to a fairly low value because the design codes place it in the primary "membrane stress" (Chapter 2) category.

(iv) *Nozzle-shell Junction*: Load transfer from the nozzle to the shell produces local membrane and bending stresses. Due to the non-symmetry in the geometry, even finite element solutions are quite expensive to obtain. The charts given in WRC-107 [17.4.2] have become the mainstay of the industry in this area. Simplified charts are also provided by the feedwater heater standards [17.4.3]. The use of these design charts has become quite routine and appears adequate in most normal applications.

(v) *Flanged Sections*: Flanged sections subject to bending moments and axial force due to external loadings should be examined for gasket relaxation and joint leakage. The ASME Code gives the following formula for computing the equivalent pressure, p_{eq} at flanged sections subject to bending moments.

$$p_{eq} = p + \frac{8 \Lambda M}{\pi G^3}$$

M is the total bending moment at the flanged section, and G is the effective gasket diameter (ref. Chapter 3). The parameter Λ is 2 if the moment is due only to sustained external loads, and is unity if the moment includes both sustained and short term loads. This formula is specifically given for flanges in piping runs. We feel that there is little reason why it cannot be used to make similar checks for vessels and heat exchanger joints. The reader is referred to the ASME Boiler and Pressure Vessel Code, Section III, Sub-

section ND, paragraph ND-3600 for further details on the use of this formula.

17.5 STRESSES IN AN ANNULAR RING SUPPORT DUE TO VERTICAL LOADS

In this section, expressions for stresses in the shell and in the annular ring support due to vertical loads are derived. We assume that the support ring transfers the load to the foundation in a symmetrical manner. This permits us to treat the deformations of the ring and shell as axisymmetric; hence, classical equations for edge loaded shells (Appendix A) can be employed to obtain the solution. The support system is modelled as an annular ring sitting on a surrounding foundation. The axial forces in the portion of the shell above and below the support ring are generally known from equilibrium. In some situations, notably fixed tubesheet heat exchangers (Chapter 9, Fig. 9.1.1) the axial forces are obtained from a detailed stress analysis. It is important to note that in this section we are assuming that the support ring is far removed from any tubesheet, or from any other component which would yield local stresses in the shell due to enforcement of compatibility. The lineal reaction of the foundation support system is assumed to act at radius c (Figs. 17.5.1-2). For the sake of conservatism, c is often taken to coincide with the bolt circle radius, even though bending of the support tends to move the foundation reaction resultant towards the inner edge of the ring/foundation annular patch. Referring to Fig. 17.5.3, we note that the offset of the support reaction F with respect to the shell centerline, produces a distributed couple on the support ring structure. The resultant rotation of the support, ϕ , must be compatible with radial movements of points A and B on the edges of the two shell halves. The

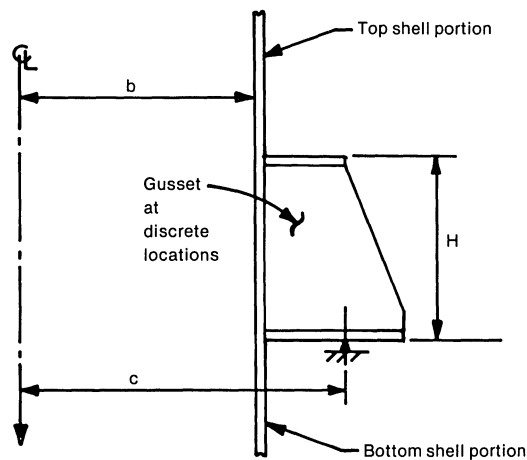


Fig. 17.5.1. Undeformed ring support/shell section.

expression for thin rings under distributed couples derived in Section 3.9 can be used to characterize the ring behavior. A standard discontinuity analysis performed in this manner give the complete solution. Details of the solution are presented below and computerized in the program "RINGSUP" listed in Appendix 17.A.

Equilibrium in the x -direction (axial) yields (Fig. 17.5.2)

$$F = (N'_{11} - N'_{21}) \frac{b}{c} \quad (17.5.1)$$

where F , N'_{11} and N'_{21} are the shell axial loads, per unit circumference, shown in Fig. 17.5.2.

Figure 17.5.3 shows the free bodies of the top and bottom shells, labelled as shells #2 and #1, respectively. Moment M_i and shear Q_i denote the edge discontinuity moment and shear of shell i . Referring to shell #2, displacement due to pressure p alone, δ_2 is given by

$$\delta_2 = \frac{pb^2}{E t_s} \left(1 - \frac{\nu N'_{21}}{p b} \right) \quad (17.5.2)$$

where E and t_s denote the Young's modulus and the shell thickness, respectively, ν denotes the Poisson's ratio and p is the applied internal pressure. Referring to the top shell (#2), the radial displacement of point B is given by the sum of the displacements due to pressure, and the displacements due to the discontinuity moment M_2 and shear Q_2 (see Appendix A for details):

$$W_2 = \delta_2 + \frac{1}{2 \beta^3 D} (\beta M_2 + Q_2) \quad (17.5.3)$$

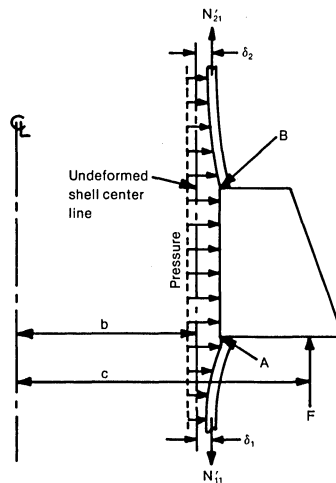


Fig. 17.5.2. Deformed shape of ring support/shell section.

where β and D are defined in Appendix A. Hence, the total outward displacement of point B of shell #2 is

$$W_2 = \frac{pb^2}{E t_s} \left(1 - \nu \frac{N'_{21}}{p b}\right) + \frac{1}{2 \beta^3 D} (\beta M_2 + Q_2) \quad (17.5.4)$$

Similarly, the total edge rotation of the top shell (shell #2 in Fig. 17.5.3) is:

$$\phi = \frac{1}{2 \beta^2 D} (2 \beta M_2 + Q_2) \quad (17.5.5)$$

where ϕ is the rotation of the support ring cross section. Referring to the lower shell (shell #1), we can write

$$\phi = -\frac{1}{2 \beta^2 D} (2 \beta M_1 + Q_1) \quad (17.5.6)$$

and we can also obtain expressions for the total outward deflection of point A :

$$W_1 = \delta_1 + \frac{1}{2 \beta^3 D} (\beta M_1 + Q_1)$$

$$\delta_1 = \frac{p b^2}{E t_s} \left(1 - \frac{\nu N'_{11}}{p b}\right)$$

Therefore, the outward deflection at point A is

$$W_1 = \frac{p b^2}{E t_s} \left(1 - \frac{\nu N'_{11}}{p b}\right) + \frac{1}{2 \beta^3 D} (\beta M_1 + Q_1) \quad (17.5.7)$$

Finally, we note that since the ring is assumed to undergo only a rigid body rotation under the applied loading,

$$W_1 = W_2 + H\phi \quad (17.5.8)$$

Hence Eqs. (17.5.4), (17.5.7) and (17.5.8) yield

$$\begin{aligned} & \frac{p b^2}{E t_s} \left(1 - \frac{\nu N'_{11}}{p b}\right) + \frac{1}{2 \beta^3 D} (\beta M_1 + Q_1) \\ &= \frac{p b^2}{E t_s} \left(1 - \frac{\nu N'_{21}}{p b}\right) + \frac{1}{2 \beta^3 D} (\beta M_2 + Q_2) + H \phi \end{aligned}$$

or

$$\beta M_1 + Q_1 - \beta M_2 - Q_2 = 2 \beta^3 D \left[\frac{\nu b}{E t_s} (N'_{11} - N'_{21}) + H \phi \right] \quad (17.5.9)$$

After using Eq. (17.5.1) to eliminate $N'_{11} - N'_{21}$, we obtain

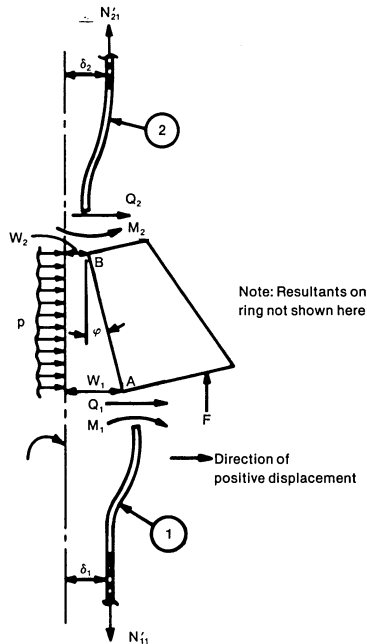


Fig. 17.5.3. Freebody of top and bottom shells.

$$\beta M_1 + Q_1 - \beta M_2 - Q_2 = 2 \beta^3 D \left[\frac{\nu F c}{E t_s} + H \phi \right] \quad (17.5.10)$$

Hence

$$\beta M_1 + Q_1 - \beta M_2 - Q_2 - \frac{2\nu\beta^3 D}{E t_s} F c = 2 \beta^3 D \phi H \quad (17.5.11)$$

We now require the resistance properties of the support ring. Treating the support as a thin ring, the following relationships are readily observed:

- (a) Force equilibrium: If R denotes the inward directed radial force circumference, then (Fig. 17.5.4):

$$2Rb \sin(d\theta/2) = 2F_\theta \sin(d\theta/2) \quad (17.5.12)$$

or, for small $d\theta$

$$F_\theta = Rb \quad (17.5.13)$$

where F_θ is the compressive hoop force.

- (b) Moment equilibrium: If m denotes the radial applied moment per unit circumference then, by writing moment equilibrium, we have

$$M d\theta = -m b d\theta$$

or $M = -m b$ (17.5.14)

where M is the resultant internal moment (see Section 3.9 for a detailed treatment of this subject matter).

Referring to Fig. 17.5.5, the radial deflection of a point located at axial coordinate η is $W_2 + \eta\phi$; therefore, the circumferential strain is:

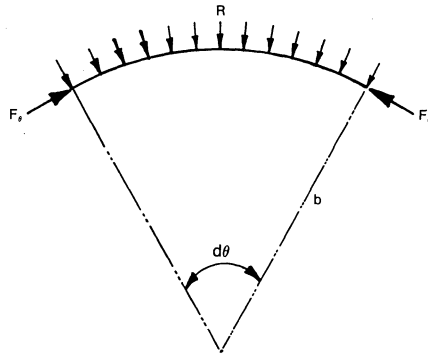
$$\epsilon_\theta = \frac{W_2 + \eta \phi}{r}$$

where r is the radial coordinate of the point. The hoop stress, σ_θ in the ring is

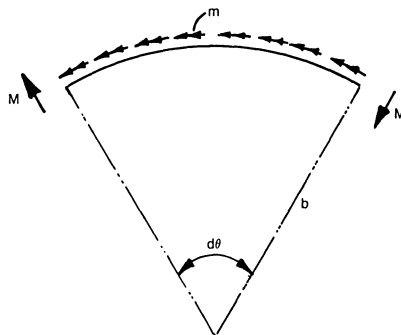
$$\sigma_\theta = E \epsilon_\theta = \frac{(W_2 + \eta \phi) E}{r}$$

Therefore, the hoop force F_θ is obtained in terms of W_2 and ϕ by forming:

$$F_\theta = - \int \sigma_\theta d A = - \int \frac{(W_2 + \eta \phi) E d A}{r}$$



(a) Hoop force F_θ in equilibrium with radial lineal load R



(b) Internal moment M in equilibrium with external moment m

Fig. 17.5.4. Freebody of a symmetrically loaded ring element.

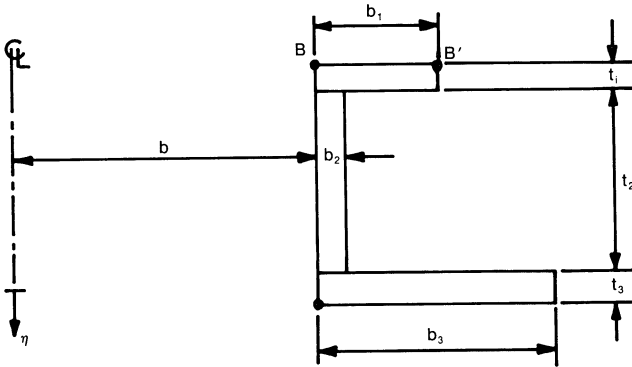


Fig. 17.5.5. Ring support (gussets not shown).

$$= -E W_2 \int \frac{d A}{r} - E \phi \int \frac{\eta d A}{r}$$

Hence

$$F_0 = -E W_2 I_1 - E \phi I_2 \quad (17.5.15)$$

where

$$I_1 = \int \frac{d A}{r} \quad (17.5.16)$$

$$I_2 = \int \frac{\eta d A}{r} \quad (17.5.17)$$

Taking moments about the BB' axis in Fig. 17.5.5 yields:

$$\begin{aligned} M &= \int \sigma_0 \eta d A \\ &= \int E \left[\frac{W_2 + \eta \phi}{r} \right] \eta d A \\ &= W_2 E I_2 + E \phi I_3 = -m b \end{aligned} \quad (17.5.18)$$

where

$$I_3 = \int \frac{\eta^2 d A}{r} \quad (17.5.19)$$

Hence, we can write m and R in terms of W_2 , ϕ :

$$m = -\frac{E}{b} [W_2 I_2 + \phi I_3] \quad (17.5.20)$$

$$R = -\frac{E}{b} [W_2 I_1 + \phi I_2] \quad (17.5.21)$$

We point out that the coupling terms involving I_2 appear because we have chosen not to introduce the radial ring displacement as an additional variable. In terms of the external shell resultants, and the pressure, we can also write R and m in the form

$$R = Q_1 + Q_2 - p H$$

$$m = -\left(M_1 - M_2 + F(c-b) \frac{c}{b} + Q_1 H + \frac{p H^2}{2} \right) \quad (17.5.22)$$

where m has been taken as the moment about point B .

We redefine the unknowns in dimensionless form below:

$$M'_2 = \frac{M_2}{\beta D}$$

$$M'_1 = \frac{M_1}{\beta D}$$

$$Q'_2 = \frac{Q_2}{\beta^2 D}$$

$$Q'_1 = \frac{Q_1}{\beta^2 D}$$

$$W'_2 = \frac{W_2}{b}$$

(17.5.23)

In terms of dimensionless variables, we can rewrite the two defining equations for ϕ (Eqs. (17.5.5), (17.5.6)), as

$$\phi = M'_2 + 0.5 Q'_2 \quad (17.5.24)$$

$$\phi = -M'_1 - 0.5 Q'_1 \quad (17.5.25)$$

Equation (17.5.4), for W_2 , and Eq. (17.5.11), can also be rewritten, along with Eqs. (17.5.20–22); the resulting equations are expressible as:

$$W'_2 = \frac{pb}{E t_s} \left(1 - \nu \frac{N'_{21}}{pb} \right) + \frac{1}{2 b \beta} (M'_2 + Q'_2) \quad (17.5.26)$$

$$M'_1 + Q'_1 - M'_2 - Q'_2 - \frac{2 \beta \nu F c}{E t_s} = 2 \beta H \phi \quad (17.5.27)$$

$$Q'_1 + Q'_2 - \frac{p H}{\beta^2 D} = - \frac{E}{\beta^2 D} \left(W'_2 I_1 + \phi \frac{I_2}{b} \right) \quad (17.5.28)$$

$$-M'_1 + M'_2 + Q'_1 \beta H - \frac{F c (c-b)}{b \beta D} - \frac{p H^2}{2 \beta D} = - \frac{E}{D} \left(W'_2 I_2 + \phi \frac{I_3}{b} \right) \quad (17.5.29)$$

We note that in the above six linear algebraic equations (Eqs. (17.5.24–29)), p , N'_{21} , and F are known quantities, and we desire to obtain solutions for W_2 , ϕ , M_1 , Q_1 , M_2 and Q_2 . These equations can be solved for any ring geometry using a standard linear equation solver subroutine.

Having determined W_2 , ϕ , M_1 , Q_1 , M_2 , and Q_2 , the stresses at location A and B in the shell follow immediately. We can classify these stresses as follows:

(a) Longitudinal stresses in the shell:

$$\text{Membrane: } \begin{cases} \text{Location B: } \sigma_{2m} = \frac{N'_{21}}{t_s} \\ \text{Location A: } \sigma_{1m} = \frac{N'_{11}}{t_s} \end{cases} \quad (17.5.30)$$

$$\text{Bending: } \begin{cases} \text{Location B: } \sigma_{2b} = \frac{6M_2}{t_s^2} \\ \text{Location A: } \sigma_{1b} = \frac{6M_1}{t_s^2} \end{cases}$$

(b) Circumferential stresses:

$$\text{Membrane: } \begin{cases} \text{Location B: } \sigma_{1m} = \frac{E W_2}{b} + \frac{\nu N'_{21}}{t_s} \\ \text{Location A: } \sigma_{1m} = \frac{E W_1}{b} + \frac{\nu N'_{11}}{t_s} \end{cases} \quad (17.5.31)$$

$$\text{Bending: } \begin{cases} \text{Location B: } \sigma_{1b} = \frac{6\nu M_2}{t_s^2} \\ \text{Location A: } \sigma_{1b} = \frac{6\nu M_1}{t_s^2} \end{cases}$$

For completeness, the expressions for the integrals I_1 , I_2 and I_3 , defined by Eqs. (17.5.16), (17.5.17), (17.5.19), are worked out below.

Referring to Fig. 17.5.5, we have

$$I_1 = \int \frac{dA}{r} = t_1 \ln\left(1 + \frac{b_1}{b}\right) + t_2 \ln\left(1 + \frac{b_2}{b}\right) + t_3 \ln\left(1 + \frac{b_3}{b}\right) \quad (17.5.32)$$

$$I_2 = \int \frac{\eta dA}{r} = \frac{1}{2} \left[t_1^2 \ln\left(1 + \frac{b_1}{b}\right) + t_2(t_2 + 2t_1) \ln\left(1 + \frac{b_2}{b}\right) + t_3(t_3 + 2t_2 + 2t_1) \ln\left(1 + \frac{b_3}{b}\right) \right] \quad (17.5.33)$$

$$I_3 = \int \frac{\eta^2 dA}{r} = \frac{1}{3} \left[t_1^3 \ln\left(1 + \frac{b_1}{b}\right) + \{ (t_1 + t_2)^3 - t_1^3 \} \ln\left(1 + \frac{b_2}{b}\right) + \{ (t_1 + t_2 + t_3)^3 - (t_1 + t_2)^3 \} \ln\left(1 + \frac{b_3}{b}\right) \right] \quad (17.5.34)$$

The solution just presented is computerized in program "RINGSUP" described in Appendix 17.A and enables the user to determine the stress state in the vicinity of an annular ring support structure.

17.6 LUG DESIGN

A milestone paper dealing with the evaluation of local stresses in shells, due to loadings on an attached lug, was published by Professor P. R. Bijlaard [17.6.1]. The Welding Research Council sponsored a program towards experimental verification of Bijlaard's analysis which culminated in the publication of WRC-107 [17.4.2]. WRC-107 has been extensively used in the design of lug attachments on pressure vessels and pipes. The stress coefficients required are presented in graphical form which facilitates rapid manual computation. More simplified variants of WRC-107 have appeared in the industry standards [17.4.3]. WRC-107 plots have been curve fitted in some commercial computer programs to eliminate the need for a manual look-up. Recognizing the need for further work in the field of lug attachment stresses, the Welding Research Council sponsored another project in 1974, which led to the publication of WRC-198 [17.6.2]. This bulletin formed the basis of ASME Code Cases N-122, [17.6.3] and N-318 [17.6.4] which are widely used in piping support design.

The intent of WRC-198 is to simplify the task of local shell stress evaluation. A brief synopsis of The WRC-198 method, as presented in the aforementioned code cases, is given in the following.

The external loads and lug dimensions are shown in Fig. 17.6.1. The following terms are defined:

b = Mean shell radius

- t_s = Shell wall thickness
- β_1 = L_1/D
- β_2 = L_2/b
- L_a = $\text{Min}(L_2, t_s)$
- L_b = $\text{Min}(L_1, t_s)$
- L_c = $\text{Min}(L_1, L_2)$
- L_d = $\text{Max}(L_1, L_2)$
- γ = b/t_s

Lug cross-sectional area, $A_l = 4L_1L_2$

Lug section modulus about its longitudinal axis, $z_L = 4L_1L_2^2/3$

Lug section modulus about its circumferential axis, $z_c = 4L_1^2L_2/3$

The stress coefficients for radial thrust W , for circumferential moment M_c , and for longitudinal moment M_L , are defined as C_T , C_c , and C_L , respectively, and can be written in the form:

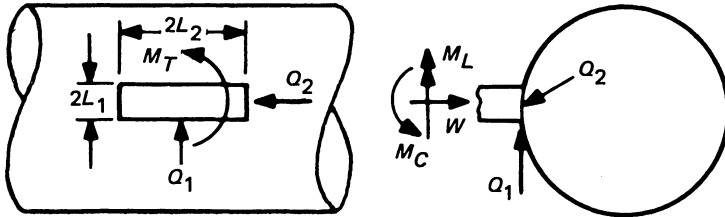


Fig. 17.6.1. Graphic representation of L_1 , L_2 , W , M_L , Q_1 , Q_2 , and M_T . L_1 and L_2 are to be measured along the surface of the shell. Welds or fillet radii between attachment and shell are not to be included.

$$C_T = 7.64 \gamma^{1.64} \beta_1 \beta_2 \eta^{1.54} \geq 1.0 \tag{17.6.1}$$

$$C_L = 0.51 \gamma^{1.74} \beta_1 \beta_2^2 \eta^{4.74} \geq 1.0 \tag{17.6.2}$$

$$C_c = 0.76 \gamma^{1.90} \beta_1^2 \beta_2 \eta^{3.40} \geq 1.0 \tag{17.6.3}$$

In Eqs. (17.6.1-3)

$$\eta = - (x_1 \cos\theta + y_1 \sin\theta) - \frac{1}{A_0} (x_1 \sin\theta - y_1 \cos\theta)^2$$

$$x_1 = x_0 + \log_{10} \beta_1$$

$$y_1 = y_0 + \log_{10} \beta_2$$

A_0 , θ , x_0 and y_0 are defined for each load case in the table below

Load	A_0	θ	x_0	y_0
Thrust	2.2	40°	0	0.05
Longitudinal Moment	2.0	50°	-0.45	-0.55
Circumferential Moment	1.8	40°	-0.75	-0.60

All terms are assumed to be expressed in lb-in. units. The maximum primary plus secondary stress in the shell wall is then given by

$$\sigma = \frac{C_T W}{A_l} + \frac{C_L M_L}{z_L} + \frac{C_c M_c}{z_c} + \frac{Q_1}{2L_1 L_a} + \frac{Q_2}{2L_2 L_b} + \bar{M}_T \quad (17.6.4)$$

where

$$\bar{M}_T = \text{Max} \left[\frac{M_T}{L_c L_d t_s \left(1 + \frac{L_c}{L_d}\right)}, \frac{M_T}{\left[0.8 + 0.05 \left(\frac{L_d}{L_c}\right)\right] L_c^2 L_d} \right] \quad (17.6.5)$$

The maximum value of primary plus local membrane stress is also given by Eq. (17.6.4) except that the stress coefficients C_T , C_c , and C_L are reduced to 2/3 of their values, the loadings do not include any thermal effects, and only sustained load amplitudes are considered.

The above formulas are intended for rapid design work. Readers interested in a detailed stress analysis technique are referred to WRC-198. These formulas are subject to certain dimensional restrictions on the lug and shell; these are:

$$\beta_1 \leq 0.5, \quad \beta_2 \leq 0.5$$

$$\beta_1 \beta_2 \leq 0.075$$

$$b/t_s \leq 50$$

In Section 17.8, we show how to obtain the loads on an individual lug.

17.7 STRESSES IN THE SHELL AT SADDLE SUPPORTS

The paper by Zick [17.3.1] has been extensively used as the conventional design procedure for estimating stresses in the vicinity of saddle supports on horizontal vessels. However, its semi-empirical nature was always recognized. Many other investigators have considered the saddle-shell support problem, notably Krupka [17.7.1], Brandes [17.7.2], Forbes and Tooth [17.7.3], Wilson and Tooth [17.7.4], and Vinet and Doré [17.7.5]. Krupka [17.7.1] uses a semi-bending theory of shells to predict saddle/shell interface pressure. Forbes and Tooth [17.7.3] consider the variation of shell stress resultants in both axial and circumferential directions consistent with a treatment of the saddle as a rigid member. Wilson and Tooth [17.7.4] extend this previous solution to include saddle flexibility. Vinet and Doré [17.7.5] solve the problem of a continuous saddle unwelded to the

pipe/vessel. Their solution is presented in an abbreviated form in the following:

Vinet and Doré Solution

Vinet, et al., consider a pipe under nominal pressure p containing a fluid of density ρ , and supported on a continuous rigid saddle. They use Flugge's shell equations and neglect the axial force due to header pressure. They show that the type of saddle/shell contact depends on the angle of opening $2\phi_0$ of the support and the parameters $p/b\rho$ and b/t_s . For a small angle of opening, contact takes place at each end of the support (see Fig. 17.7.1). Figure 17.7.2 gives the limiting half angle, θ_1 , for two line loads as a function of $p/b\rho$ and b/t_s . As the semi-saddle angle ϕ_0 is increased, a new line loads at the central vertical plane of support develops (Fig. 17.7.3). Figure 17.7.4 gives the limiting half angle, θ_2 , for the three line load condition. As ϕ_0 is increased even further, a surface of contact in the central part of the support is developed with line loads at the extremities of the surface of contact, and line loads at the horns of the saddle (Fig. 17.7.5). It is shown in [17.7.5] that for $\phi_0 > 43^\circ$, an interior contact patch will always develop. Since $\phi_0 > 43^\circ$ is the most common case of saddle geometry, it is appropriate to succinctly summarize the key results of interest. The semi-angle, α , of the surface of contact is found by solving the transcendental equation

$$C_{01} - 2C_{31} \sin\alpha + 2 C_{41} \cos\alpha + \frac{b^4 \rho}{4D} (\cos\alpha - 2\alpha \sin\alpha) = 0 \quad (17.7.1)$$

$$\text{where } D = Et_s^3 / 12 (1 - \nu^2) \quad (17.7.2)$$

The coefficients C_{01} , C_{31} , and C_{41} are given by the following expressions:

$$C_{31} = \frac{\text{Num}}{\text{Deno}} \quad (17.7.3)$$

$$C_{41} = \frac{C_{31}}{F^*} \{ \cos \phi_0 ((\phi_0 - \alpha) \cos \phi_0 \sin \alpha + \cos \alpha (\cos \phi_0 - \cos \alpha)) - (\cos(\phi_0 - \alpha) - 1)(\cos \phi_0 + (\phi_0 - \pi) \sin \phi_0) \} - \frac{b^4 \rho}{8DF^*} \{ \cos \phi_0 ((\alpha^2 - \phi_0^2) \cos \phi_0 \sin \alpha + 2\alpha \cos \alpha (\cos \alpha - \cos \phi_0)) + 2\pi(\cos(\phi_0 - \alpha) - 1)(\cos \phi_0 + (\phi_0 - \pi) \sin \phi) \} \quad (17.7.4)$$

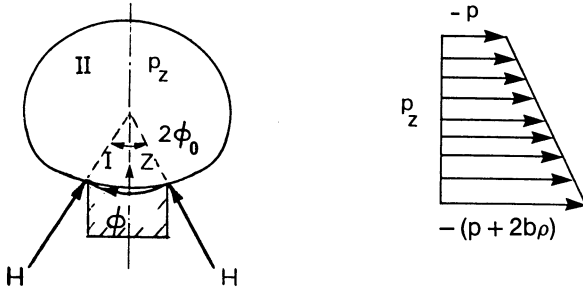


Fig. 17.7.1. Contact on two lines and internal pressure distribution.

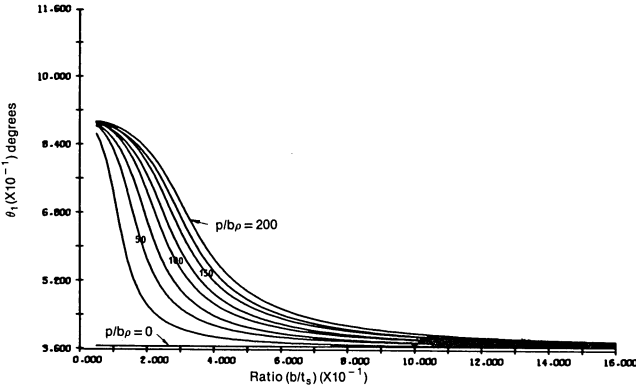


Fig. 17.7.2. Limiting half angle of opening for two line loads.

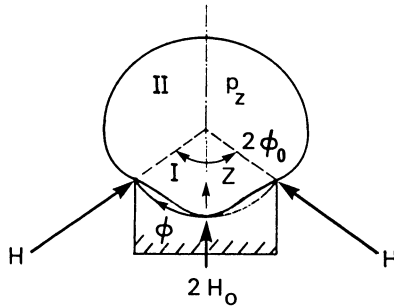


Fig. 17.7.3. Contact on three lines.

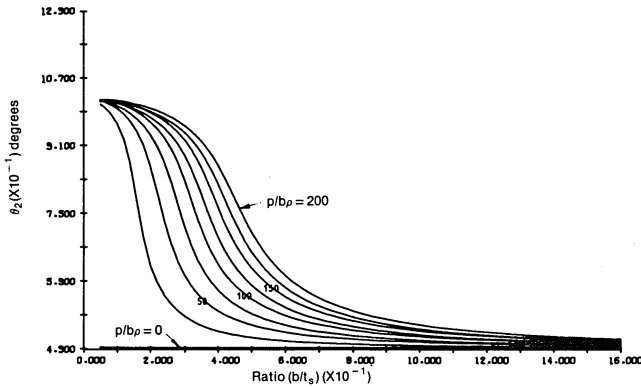


Fig. 17.7.4. Limiting half angle of opening for three line loads.

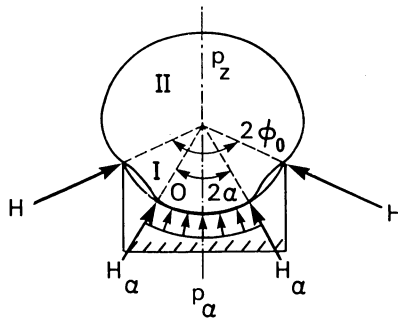


Fig. 17.7.5. Contact area with line loads.

$$\begin{aligned}
 C_{01} = & C_{31} \left\{ \frac{(\phi_0 - \alpha) \cos \phi_0 + \cos \alpha \sin(\alpha - \phi_0)}{\cos(\phi_0 - \alpha) - 1} \right\} \\
 & + C_{41} \left\{ \frac{(\phi_0 - \alpha) \sin \phi_0 + \sin \alpha \sin(\alpha - \phi_0)}{\cos(\phi_0 - \alpha) - 1} \right\} - \frac{b^4 \rho}{8D} \\
 & \left\{ \frac{(\alpha^2 - \phi_0^2) \cos \phi_0 + 2\alpha \cos \alpha \sin(\phi_0 - \alpha)}{\cos(\phi_0 - \alpha) - 1} \right\} \tag{17.7.5}
 \end{aligned}$$

In the above equations,

$$\begin{aligned}
 Num = & \{ \cos(\phi_0 - \alpha) - 1 \} \{ (\pi - \alpha)(\cos(\phi_0 - \alpha) - 1) \\
 & - ((\phi_0 - \alpha) \sin \phi_0 \sin \alpha + \sin \alpha (\cos \phi_0 - \cos \alpha)) \}
 \end{aligned}$$

$$\left\{ -\frac{b}{D'} (p + b\rho) \pi \cos \phi_0 - \frac{b^4 \rho \pi}{2D} + \frac{b^4 \rho}{4D} \cos \phi_0 (\alpha \cos \alpha (2 + k^2) - (1 + 2k^2 \alpha^2) \sin \alpha) \right\} + \frac{b^4 \rho}{8D} \left[\{ (\pi - \alpha) (1 + k^2) \cos \phi_0 ((\alpha^2 - \phi_0^2) \cos \phi_0 + 2\alpha \cos \alpha \sin(\phi_0 - \alpha)) \} \{ (\pi - \alpha) (\cos(\phi_0 - \alpha) - 1) - \sin \alpha ((\phi_0 - \alpha) \sin \phi_0 + \cos \phi_0 - \cos \alpha) \} + \{ (\pi - \alpha) (1 + k^2) ((\phi_0 - \alpha) \sin \phi_0 + \sin \alpha \sin(\alpha - \phi_0)) - 2(\cos(\phi_0 - \alpha) - 1) (\sin \alpha + \alpha k^2 \cos \alpha) \} \{ \cos \phi_0 ((\alpha^2 - \phi_0^2) \cos \phi_0 \sin \alpha + 2\alpha \cos \alpha (\cos \alpha - \cos \phi_0)) + 2\pi (\cos(\phi_0 - \alpha) - 1) (\cos \phi_0 + (\phi_0 - \pi) \sin \phi_0) \} \right]$$

where

$$D' = \frac{Et_s}{1 - \nu^2}$$

and

$$k = \frac{t_s}{2\sqrt{3}b}$$

$$\begin{aligned} Deno = & \{ (\pi - \alpha) (1 + k^2) \cos \phi_0 ((\phi_0 - \alpha) \cos \phi_0 \\ & + \cos \alpha \sin(\alpha - \phi_0)) + 2(\cos(\phi_0 - \alpha) - 1) (1 \\ & - \cos \phi_0 (\cos \alpha - \alpha k^2 \sin \alpha)) \} \{ (\pi - \alpha) (\cos(\phi_0 - \alpha) \\ & - 1) - \sin \alpha ((\phi_0 - \alpha) \sin \phi_0 + \cos \phi_0 - \cos \phi) \} \\ & + \{ (\pi - \alpha) (1 + k^2) ((\phi_0 - \alpha) \sin \phi_0 + \sin \alpha \sin(\alpha \\ & - \phi_0)) - 2(\cos(\phi_0 - \alpha) - 1) (\sin \alpha + \alpha k^2 \cos \alpha) \} \\ & \{ \cos \phi_0 ((\phi_0 - \alpha) \cos \phi_0 \sin \alpha + \cos \alpha (\cos \phi_0 \\ & - \cos \alpha)) - (\cos(\phi_0 - \alpha) - 1) (\cos \phi_0 + (\phi_0 - \pi) \sin \phi_0) \} \end{aligned}$$

and

$$F^* = \cos \phi_0 ((\pi - \alpha) (\cos(\phi_0 - \alpha) - 1) - \sin \alpha ((\phi_0 - \alpha) \sin \phi_0 + \cos \phi_0 - \cos \alpha)).$$

The line load intensities are (see Fig. 17.7.5):

$$H = \frac{\pi b^2 \rho}{2 \cos \phi_0} + \frac{2DC_{31}}{b^2 \cos \phi_0} \tag{17.7.6}$$

$$H_\alpha = -\frac{2D}{b^2} (C_{31} \cos \alpha + C_{41} \sin \alpha) - \frac{b^2 \rho}{4} (3 \sin \alpha + 2\alpha \cos \alpha) \tag{17.7.7}$$

The bending moment M_ϕ in region 1 (the region defined by $\alpha < \phi < \phi_0$ (see Fig. 17.7.5) is given by

$$M_\phi = -\frac{D}{b} \left[C_{01} - 2 C_{31} \sin \phi + 2 C_{41} \cos \phi + \frac{b^4 \rho}{4D} (\cos \phi - 2 \phi \sin \phi) \right] \tag{17.7.8}$$

The reader is referred to Wilson and Tooth [17.7.4] for the solution of the finite welded saddle problem.

17.8 ELEMENTARY SOLUTIONS FOR ANCHOR BOLT LOADS

If the foundation and the equipment support structure are relatively rigid, then the stresses in the anchor bolts can be assessed from equilibrium considerations alone. Two examples given below illustrate the procedure.

17.8.1 Bolt Load Distribution in a Three Lug Support System

Consider a shell supported at three equispaced lugs. A bending moment M and a vertically upward force F_{ax} act at the support circle location. The upward force F_{ax} includes the bolt pre-tension load, if any.

The three support locations around the support circle are idealized by point locations which we refer to as ‘‘anchor points’’ (Fig. 17.8.1). The moment vector M is assumed to make an angle θ with the y axis. The y axis is assumed to coincide with the radial line directed toward ‘‘anchor point’’ 1. The radial distance of all anchor points from the axis of symmetry is r .

Force equilibrium in the vessel axis direction yields

$$F_1 + F_2 + F_3 = F_{ax} \tag{17.8.1}$$

where F_i is defined as the tensile force at anchor point i . F_i positive implies tension in the bolts. F_i negative means that the lug and the structural support are in contact. In Fig. 17.8.1, F_{ax} is directed out of the paper, and F_i are directed into the paper.

Moment equilibrium about line AB yields the equation:

$$M = -F_1 r \sin \theta + F_2 r \sin \left(\frac{\pi}{2} - \theta + \omega \right) - F_3 r \sin \left(\frac{\pi}{2} - \theta - \omega \right)$$

or

$$\frac{M}{r} = -F_1 \sin \theta + F_2 \cos(\theta - \omega) - F_3 \cos(\theta + \omega) \quad (17.8.2)$$

where $\omega = 30^\circ$ for a 3 point support system.

Similarly, writing moment equilibrium about line CD (perpendicular to AB) yields:

$$0 = F_1 r \cos \theta + F_2 r \cos\left(\frac{\pi}{2} - \theta + \omega\right) - F_3 r \cos\left(\frac{\pi}{2} - \theta - \omega\right)$$

or

$$0 = F_1 \cos \theta + F_2 \sin(\theta - \omega) - F_3 \sin(\theta + \omega) \quad (17.8.3)$$

We now define Φ_i and μ by the relations

$$\Phi_i = \frac{F_i}{F_{ax}} \quad (17.8.4)$$

$$\mu = \frac{M}{F_{ax} r} \quad (17.8.5)$$

Then Eqs. (17.8.1-3) become

$$\Phi_1 + \Phi_2 + \Phi_3 = 0 \quad (17.8.6)$$

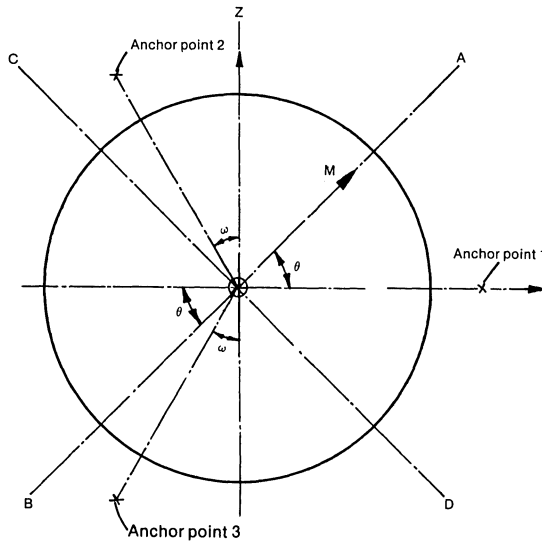


Fig. 17.8.1. Anchor points for a three lug support system.

$$-\Phi_1 \sin \theta + \Phi_2 \cos(\theta - \omega) - \Phi_3 \cos(\theta + \omega) = \mu \quad (17.8.7)$$

$$\Phi_1 \cos \theta + \Phi_2 \sin(\theta - \omega) - \Phi_3 \sin(\theta + \omega) = 0 \quad (17.8.8)$$

Writing Eqs. (17.8.6)–(17.8.8) in matrix form, we have

$$\begin{bmatrix} 1 & 1 & 1 \\ -\sin \theta & \cos(\theta - \omega) & -\cos(\theta + \omega) \\ \cos \theta & \sin(\theta - \omega) & -\sin(\theta + \omega) \end{bmatrix} \begin{Bmatrix} \Phi_1 \\ \Phi_2 \\ \Phi_3 \end{Bmatrix} = \begin{Bmatrix} 1 \\ \mu \\ 0 \end{Bmatrix} \quad (17.8.9)$$

The coefficient determinant of the left-hand side of Eq. (17.8.9) is given by

$$\begin{aligned} \Delta &= \{ -\cos(\theta - \omega) \sin(\theta + \omega) + \cos(\theta + \omega) \sin(\theta - \omega) \} \\ &\quad + \sin \theta \{ -\sin(\theta + \omega) - \sin(\theta - \omega) \} \\ &\quad + \cos \theta \{ -\cos(\theta + \omega) - \cos(\theta - \omega) \} \\ &= -\sin 2\alpha - \sin \theta \{ 2 \sin \theta \cos \omega \} \\ &\quad - \cos \theta \{ 2 \cos \theta \cos \omega \} \end{aligned}$$

or

$$\Delta = -\sin 2\alpha - 2 \cos \omega \quad (17.8.10)$$

$$\begin{aligned} \Phi_1 &= \frac{1}{\Delta} \begin{vmatrix} 1 & 1 & 1 \\ \mu \cos(\theta - \alpha) & -\cos(\theta + \omega) & 0 \\ 0 & \sin(\theta - \omega) & -\sin(\theta + \omega) \end{vmatrix} \\ &= \frac{1}{\Delta} [-\sin 2\omega + \mu(2 \sin \theta \cos \omega)] \end{aligned}$$

Therefore,

$$\Phi_1 = \frac{-\sin 2\omega + 2\mu \sin \theta \cos \omega}{-\sin 2\alpha - 2 \cos \omega} \quad (17.8.11)$$

Similarly, Φ_2 is given by

$$\Phi_2 = \frac{1}{\Delta} \begin{vmatrix} 1 & 1 & 1 \\ -\sin \theta & \mu & -\cos(\theta + \omega) \\ \cos \theta & 0 & -\sin(\theta + \omega) \end{vmatrix}$$

so that

$$\Phi_2 = \frac{1}{\Delta} [-\{\sin \theta \sin(\theta + \omega) + \cos \theta \cos(\theta + \omega)\} + \mu\{-\sin(\theta + \omega) - \cos \theta\}]$$

which simplifies to

$$\Phi_2 = \frac{1}{\Delta} [-\cos \omega + \mu\{-\sin(\theta + \omega) - \cos \theta\}]$$

Hence,

$$\Phi_2 = \frac{-\mu[\sin(\theta + \omega) + \cos \theta] - \cos \omega}{-\sin 2\alpha - 2 \cos \omega} \quad (17.8.12)$$

Finally, Φ_3 follows from Eq. (17.8.6).

Thus, we have seen how the reactions at all three support locations can be determined. The method given in the preceding Section 17.6 for lug design can now be used to compute the local shell stresses.

17.8.2 Foundation Response of Ring Type Supports Mounted on Rigid Foundations

We assume that there are n bolts arranged on a bolt circle of radius c . The outer radius of the support ring is d . The bolts are assumed to be pre-stressed and develop σ_0 psi tensile stress in each bolt. The effective tensile area of each bolt is defined as A . The object is to find the maximum stress in the bolts when the foundation is subject to a bending moment M , and to an axial force F_{ax} . The foundation is assumed to be rigid, and the ring support is assumed to undergo only rigid body rotation and translation. We let l denote the “free length” of the foundation bolts.

The bolts may be modeled as a cylindrical spring of stiffness Γ #/in./in. circumference, where

$$\Gamma = \frac{E n A}{2 \pi c l} \quad (17.8.13)$$

and E is the Young’s modulus of the bolt material.

Furthermore, the equivalent thickness of the ring of springs that replace the discrete foundation bolts may be defined as

$$t = \frac{n A}{2 \pi c} \quad (17.8.14)$$

From symmetry of the cross-section (Fig. 17.8.2), it is apparent that the ring will “edge” about point A (located at the diameter normal to the axis of M), since the configuration is oriented so that M is always positive. We will assume that F_{ax} is positive when directed vertically upward.

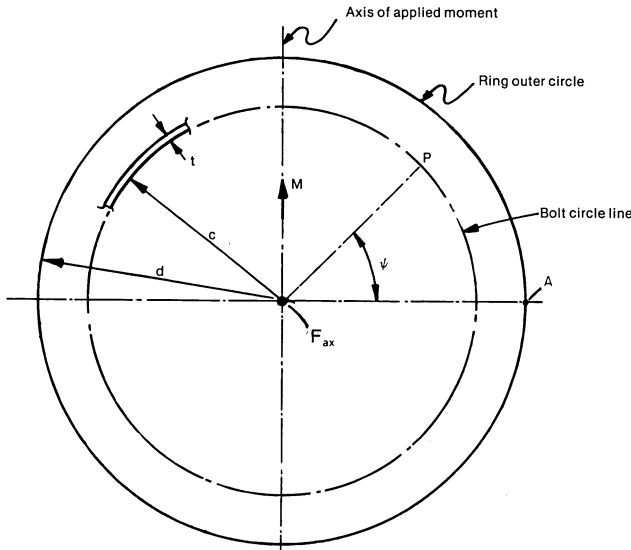


Fig. 17.8.2. Foundation geometry.

Taking moments about point A so as to eliminate the contribution of the edging force, we have (let χ be the angle of rotation of the support about point A)

$$M + F_{ax}^* d = \sigma_0 t \int_0^{2\pi} (d - c \cos\psi) c d\psi + \Gamma \chi \int_0^{2\pi} (d - c \cos\psi)^2 c d\psi$$

Performing the necessary integrations yields

$$\frac{M + F_{ax} d}{2} = \sigma_0 t c \pi d + \Gamma c \chi \pi (d^2 + c^2 / 2) \tag{17.8.15}$$

Hence, the support rotation can be written as

$$\chi = \frac{0.5[M + F_{ax} d] - \sigma_0 \pi t c d}{\Gamma c \pi \{d^2 + 0.5 c^2\}} \tag{17.8.16}$$

as long as Eq. (17.8.16) predicts $\chi > 0$.

However, $\chi = 0$ if

$$0.5[M + F_{ax} d] < \sigma_0 \pi t c d \tag{17.8.17}$$

The maximum bolt stress σ_{max} is given by

$$\sigma_{max} = \sigma_0 + \frac{\Gamma(d + c)\chi}{t} \tag{17.8.18}$$

Some allowable stress limits on anchor bolts are given in Chapter 19.

* F_{ax} is positive when directed vertically upwards.

NOMENCLATURE

- A = Tensile area of each bolt
 b = Mean shell radius
 c = Radius of action of support reaction
 d = Outer radius of support ring (Fig. 17.8.2)
 D = Flexural rigidity of the shell
 E = Young's modulus of shell material
 F = Support reaction per unit circumference acting at radius c
 F_{ax} = Axial load (Fig. 17.8.1)
 M_1, M_2, Q_1, Q_2 = Discontinuity moments and shear at support ring/shell junction
 N'_{11}, N'_{21} = Axial force per unit circumference in the shell (Fig. 17.5.3)
 n = Number of bolts (Section 17.8)
 p = Pressure
 t_s = Shell thickness
 δ_1, δ_2 = Radial displacements of lower and upper portions of the shell (Fig. 17.5.1) due to pressure and header load
 β = Shell attenuation coefficient
 ν = Poisson's ratio of shell material
 ϕ = Rotation of support ring structure (Fig. 17.5.1)

REFERENCES

- [17.1.1] The American Society of Mechanical Engineers, Boiler and Pressure Vessel Code, Section VIII, Div. 1 (1983), Div. 2 (1983).
 [17.1.2] Ibid, Section III, Div. 1, Subsections NB, NC, ND (1983).
 [17.1.3] Ibid, Section III, Div. 1, Subsection NF (1983).
 [17.3.1] Zick, L. P., "Stresses in Large Horizontal Cylindrical Pressure Vessels on Two Saddle Supports," *Pressure Vessel and Piping; Design & Analysis*, Vol. 2, pp. 959-970, The American Society of Mechanical Engineers (1972).
 [17.3.2] U.S. Department of Commerce, "Nuclear Reactors and Earthquakes," National Technical Information Service, TID-7024 (1963).
 [17.3.3] American National Standards Institute, "American National Standard for Special Lifting Devices for Shipping Containers . . .," ANSI N 14.6 (1978).
 [17.4.1] Brownell, L. E., and Young, E. H., "Process Equipment Design," Wiley (1959).
 [17.4.2] Wichman, K. R., Hopper, A. G., and Mershon, J. L., "Local Stresses in Spherical and Cylindrical Shells due to External Loadings," Welding Research Council, Bulletin No. 107, Rev. 1, (March 1979).

- [17.4.3] "Standards for Feedwater Heaters," 3rd Edition, Heat Exchange Institute, 1230 Keith Building, Cleveland, Ohio (1979).
- [17.6.1] Bijlaard, P. P., "Stresses from Local Loadings in Cylindrical Pressure Vessels," *Trans. ASME*, Vol. 77, No. 6 (August, 1955).
- [17.6.2] Rodabaugh, E. C., Dodge, W. G., and Moore, S. E., "Stress Indices at Lug Supports on Piping Systems," Welding Research Council Bulletin No. 198 (1974).
- [17.6.3] The American Society of Mechanical Engineers, Boiler and Pressure Vessel Code, Code Case N-122 (1979).
- [17.6.4] Ibid, Code Case N-318 (1981).
- [17.7.1] Krupka, V., "An Analysis for Lug or Saddle-Supported Cylindrical Pressure Vessels," Proceedings of the First International Conference on Pressure Vessel Technology, Delft, pp. 491-500 (1969).
- [17.7.2] Brandes, K., "Die Lagerung des Kreiszyylinderrohres auf einem Starren Linienlager," *Der Stahlbau* 10, pp. 298-310 (1971).
- [17.7.3] Forbes, P. D., and Tooth, A. S., "An Analysis for Twin Saddle Supported Unstiffened Cylindrical Vessels," Conference on Recent Advances in Stress Analysis, Royal Aeronautical Society, London, pp. 47-58 (1968).
- [17.7.4] Wilson, J. D., and Tooth, A. S., "The Support of Unstiffened Cylindrical Vessels," Proceedings of the Second International Conference on Pressure Vessel Technology, pp. 67-83, San Antonio, Texas (1973).
- [17.7.5] Vinet, R., and Doré, R., "Stresses and Deformations in a Cylindrical Shell Lying on a Continuous Rigid Support," Paper No. 75-AM-1, *Journal of Applied Mechanics, Trans. ASME*, (c, 1976).

APPENDIX 17.A

COMPUTER PROGRAM RINGSUP

Computer program RINGSUP is based on the analysis presented in Section 17.5. It calculates the total membrane and bending stress at the junction of the annular ring type support and the shell (denoted as A and B in Fig. 17.5.3). The input data is free field. Table 17.A.1 provides the required instructions for data preparation.

Table 17.A.1. Data for RINGSUP

Line 1: (Fig. 17.5.1 and Fig. 17.5.2)	Item	Fortran Symbol
	Internal pressure in the shell at the support location, p	P
	Shell mean radius, b	U

Young's Modulus of shell material, E	E
Poisson's ratio, ν	PR
Axial pull per unit circumference in the shell above the support, location B, N'_{21}	FN2
Axial pull per unit circumference in the shell below the support, location A, N'_{11}	FN1
Radius of action of support reaction, c	C
Height of Support, H	H
Thickness of shell, t_s	HS
<i>Line 2: (Fig. 17.5.5)</i>	
Thickness of top ring, t_1	T1
Distance between the two rings, t_2	T2
Radial width of top ring, b_1	B1
Thickness of the shell joining the two rings, b_2	B2
Radial width of bottom ring, b_3	B3

COMPUTER PROGRAM RINGSUP

```

C BY K. P. SINGH AND T. L. NG, REV 0, JANUARY 1984.
C THIS PROGRAM CALCULATES THE TOTAL MEMBRANE AND BENDING
C STRESS AT THE JUNCTION OF THE ANNULAR RING TYPE SUPPORT
C AND THE SHELL.
C
C *****
C
C .....DEFINITIONS OF FORTRAN VARIABLES.....
C
C .....INPUT DATA.....
C P : INTERNAL PRESSURE IN THE SHELL AT THE SUPPORT LOCATION
C U : SHELL MEAN RADIUS
C E : YOUNG'S MODULUS
C PR : POISSONS RATIO
C FN2 : AXIAL PULL PER UNIT CIRCUMFERENCE IN THE SHELL ABOVE THE
C SUPPORT, LOCATION B
C FN1 : " " " " " " " " " " " " , LOCATION A
C C : RADIUS OF ACTION OF SUPPORT REACTION
C H : HEIGHT OF SUPPORT
C HS : THICKNESS OF SHELL
C
C T1 : " " TOP RING
C T2 : DISTANCE BETWEEN THE TWO RINGS
C B1 : RADIAL WIDTH OF TOP RING
C B2 : THICKNESS OF THE SHELL JOINING THE TWO RINGS (IF ANY)
C B3 : RADIAL WIDTH OF BOTTOM RING

```

```

C
C .....OUTPUT.....
C BETA : ATTENUATION COEFFICIENT
C D : SHELL RIGIDITY MODULUS
  DIMENSION A(37),B(7),TITLE(20)
  READ(5,5) (TITLE(I),I=1,20)
  5 FORMAT(20A4)
  WRITE(6,6) (TITLE(I),I=1,20)
  6 FORMAT(1H1,20A4)
  READ(5,*) P,U,E,PR,FN2,FN1,C,H,HS
  WRITE(6,700)P,U,E,PR,FN2,FN1,C,H,HS
  PR2=PR*PR
  BETA=SQRT(SQRT(3.*(1.0-PR2)) / (U*HS))
  D=E*HS**3/(12.*(1.0-PR2) )
  F= (FN1-FN2)*U/C
  1 READ(5,*,END=1000)T1,T2,B1,B2,B3
  WRITE(6,704) T1,T2,B1,B2,B3
  WRITE(6,701) BETA,D
  T3=H-T1-T2
C SOLVE INTEGRALS
  FLOG1=ALOG(1.+B1/U)
  FLOG2=ALOG(1.+B2/U)
  FLOG3=ALOG(1.+B3/U)
  FI1=T1*FLOG1 + T2*FLOG2 + T3*FLOG3
  FI2=.5* (T1*T1*FLOG1 + T2*(T2+2.*T1) * FLOG2 + T3*(T3 + 2.*T2 + 2.
  1*T1)*FLOG3)
  FI3=.3333333*( T1**3*FLOG1 + ((T1+T2)**3 - T2**3) * FLOG2 + ((T1+T
  12+T3)**3 - (T1+T2)**3) * FLOG3)
  WRITE(6,702) FI1,FI2,FI3
C DEVELOP MATRIX
  DO 100 I=1,36
    A(I)=0.0
  100 CONTINUE
    A(3)=1.0
    A(5)=E*FI1/(BETA*BETA*D)
    A(6)=E*FI2/(BETA*D)
    A(7)=1.0
    A(8)=1.0
    A(10) = -2.*BETA*H
    A(11)=E*FI2/(BETA*BETA*D*U)
    A(12)=E*FI3/(BETA*D*U)
    A(14) =1.0
    A(16) =1.0
    A(18)=-1.0
    A(20)=.5
    A(22)=1.0
    A(23)=1.0
    A(24)= BETA*H
    A(25)=-1.
    A(27)=-.5/(U*BETA)
    A(28)=-1.
    A(30)= 1.

```

```

A(31)=-.5
A(33)=A(27)
A(34)=-1.
A(35)=1.
B(1)=0.0
B(2)=0.0
B(3)=P*U*(1.0-PR*FN2/(P*U))/(E*HS)
B(4)=(2.*BETA*PR*F*C)/(E*HS)
B(5)=P*H/(BETA*BETA*D)
B(6)= F*C/U*(C-U)/(BETA*D) + P*H*H/(2.*BETA*D)
N=6
CALL SIMQ(A,B,N,KS)
FM2=B(5)*BETA*D
FM1= B(3)*BETA*D
Q2=B(6)*BETA*BETA*D
Q1=B(4)*BETA*BETA*D
W2=B(1)*U
W1=W2+H*B(2)
W1P=W1/U
WRITE(6,703) W1P,(B(I),I=1,6),W1, W2, B(2),FM1,Q1,FM2, Q2
SLMA=FN1/HS
SLMB=FN2/HS
SLBA=6.*FM1/(HS*HS)
SLBB=6.*FM2/(HS*HS)
SCMA=E*W1/U + PR*FN1/HS
SCMB=E*W2/U + PR*FN2/HS
SCBA=PR*6.*FM1/(HS*HS)
SCBB=PR*6.*FM2/(HS*HS)
WRITE(6,705) SLMA,SCMA,SLBA,SCBA,SLMB,SCMB,SLBB,SCBB
GOTO1

```

```

600 FORMAT(7F10.0,2F5.0)
700 FORMAT(1H0///,6X,"PRESSURE",6X,"SHELL RADIUS",5X,"YOUNG MOD    PO
ISSON RATIO AXIAL FORCE UP AXIAL FORCE LOW",
1 /,5X,2F15.0,E15.4,F15.4,2F14.0, //,6X," BOLT CIRC
1LE SUPPORT HT SHELL THK",/,5X,3F15.4)
701 FORMAT(//,6X,"ATTENUATION COEF = ",F6.4 ,5X,"SHELL RIGITY MOD =",F
110.2)
702 FORMAT(//,6X,"INTEGRALS 1,2,3 =",3E15.4)
703 FORMAT(//,22X,"W1",10X,
1 "W2",9X,"PHI",9X,"M1",9X,"Q1",9X,"M2",9X,"Q2",/,
1 " DIMENSIONLESS",7E12.3,/, " DIMENSIONED ",3E12.4, 4F12.2)
704 FORMAT(/,9X,"T1",8X,"T2",8X,"B1",8X,"B2",8X,"B3",/,3X,5F10.3)
705 FORMAT(5X,60("-"),//,40X, " S T R E S S E S", /,10X, "LOCATION"
1 ,15X,"MEMBRANE STRESS", 15X, "BENDING STRESS", /, 33X,
2 "LONG", 8X,"CIRC", 15X,"LONG", 8X, "CIRC",/,
312X, "A", 20X, F7.0, 3X, F7.0,15X, F7.0, 3X,F7.0,/,
412X, "B", 20X, F7.0, 3X, F7.0,15X, F7.0, 3X,F7.0)
1000 STOP
END
SUBROUTINE SIMQ(A,B,N,KS)
DIMENSION A(400),B(20)

```

```

TOL=0.0
KS=0
JJ=-N
DO 65 J=1,N
JY=J+1
JJ=JJ+N+1
BIGA=0.
IT=JJ-J
DO 30 I=J,N
IJ=IT+I
IF (ABS(BIGA)-ABS(A(IJ))) 20,30,30
20 BIGA=A(IJ)
IMAX=I
30 CONTINUE
IF (ABS(BIGA)-TOL) 35,35,40
35 KS=1
RETURN
40 I1=J+N*(J-2)
IT=IMAX-J
DO 50 K=J,N
I1=I1+N
I2=I1+IT
SAVE=A(I1)
A(I1)=A(I2)
A(I2)=SAVE
50 A(I1)=A(I1)/BIGA
SAVE=B(IMAX)
B(IMAX)=B(J)
B(J)=SAVE/BIGA
IF (J-N) 55,70,55
55 IQS=N*(J-1)
DO 65 IX=JY,N
IXJ=IQS+IX
IT=J-IX
DO 60 JX=JY,N
IXJX=N*(JX-1)+IX
JJX=IXJX+IT
60 A(IXJX)=A(IXJX)-(A(IXJ)*A(JJX))
65 B(IX)=B(IX)-(B(J)*A(IXJ))
70 NY=N-1
IT=N*N
DO 80 J=1,NY
IA=IT-J
IB=N-J
IC=N
80 K=1,J
B(IB)=B(IB)-A(IA)*B(IC)
IA=IA-N
80 IC=IC-1
RETURN
END

```

***** SAMPLE PROBLEM FOR PROGRAM RINGSUP ***** 00001000

PRESSURE 250. SHELL RADIUS 17. YOUNG MOD .3000E+08 POISSON RATIO .3000 AXIAL FORCE UP 1457. AXIAL FORCE LOW 304.

BOLT CIRCLE 23.0000 SUPPORT HT 22.0000 SHELL THK .3750
 T1 1.000 T2 19.750 R1 4.938 R2 .375 R3 9.000

ATTENUATION COEF = .5091 SHELL RIGIDITY MOD = 144874.66

INTEGRALS 1,2,3 = .1217E+01 .1617E+02 .2518E+03

	W1	W2	PHI	M1	O1	M2	O2
DIMENSIONLESS	.451E-04	.340E-03	-.228E-03	.607E-02	-.117E-01	-.433E-03	.510E-03
DIMENSIONED	.7669E-03	.5788E-02	-.2282E-03	448.01	-439.03	-35.64	19.15

LOCATION*	MEMBRANE STRESS		BENDING STRESS	
	LONG	CIRC	LONG	CIRC
A	811.	1597.	19115.	5735.
R	3885.	11380.	-1521.	-456.

*Refers to the locations shown in Figs. 17.5.2-3.

18 FOUR-LEG SUPPORTS FOR PRESSURE VESSELS

18.1 INTRODUCTION

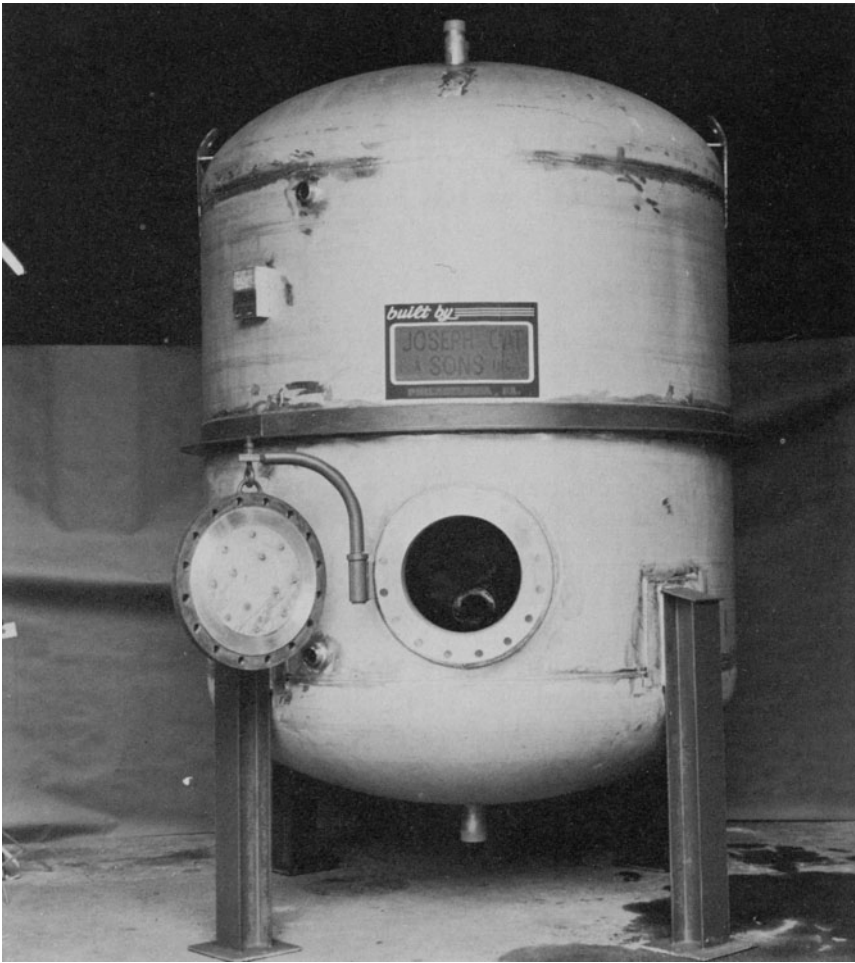
Pressure vessels are frequently mounted on four equispaced legs (Photographs 18.a–b). These legs are typically made out of “channel” or “I” sections available in product form in the industry. Such a support system is relatively inexpensive, and often quite adequate from a structural standpoint. In addition to simplicity, the four leg support system affords the added advantage of permitting nearly complete access to the underside of the vessel. This means, for example, that all welded joints in the bottom head are available for a complete in-service inspection. Also, drainage and instrumentation connections are easily installed with this class of support system.

These advantages, among others, have made the so-called “four leg” construction quite popular among pressure vessel designers. However, heightened considerations of plant safety require the evaluation of support leg stresses in the presence of mechanical loads (from interconnecting piping), seismic acceleration induced inertia loads, wind loads, etc. Since the stress level in the legs is often highly dependent on the direction of the loading and on its type (moment or transverse force), a proper stress analysis requires determination of the “optimal plane” of loading. The optimal plane of loading is defined as the plane which maximizes the maximum stress in at least one of the support legs.

Figure 18.1.1 shows a typical pressure vessel mounted on four legs. The design of this support system entails the following tasks:

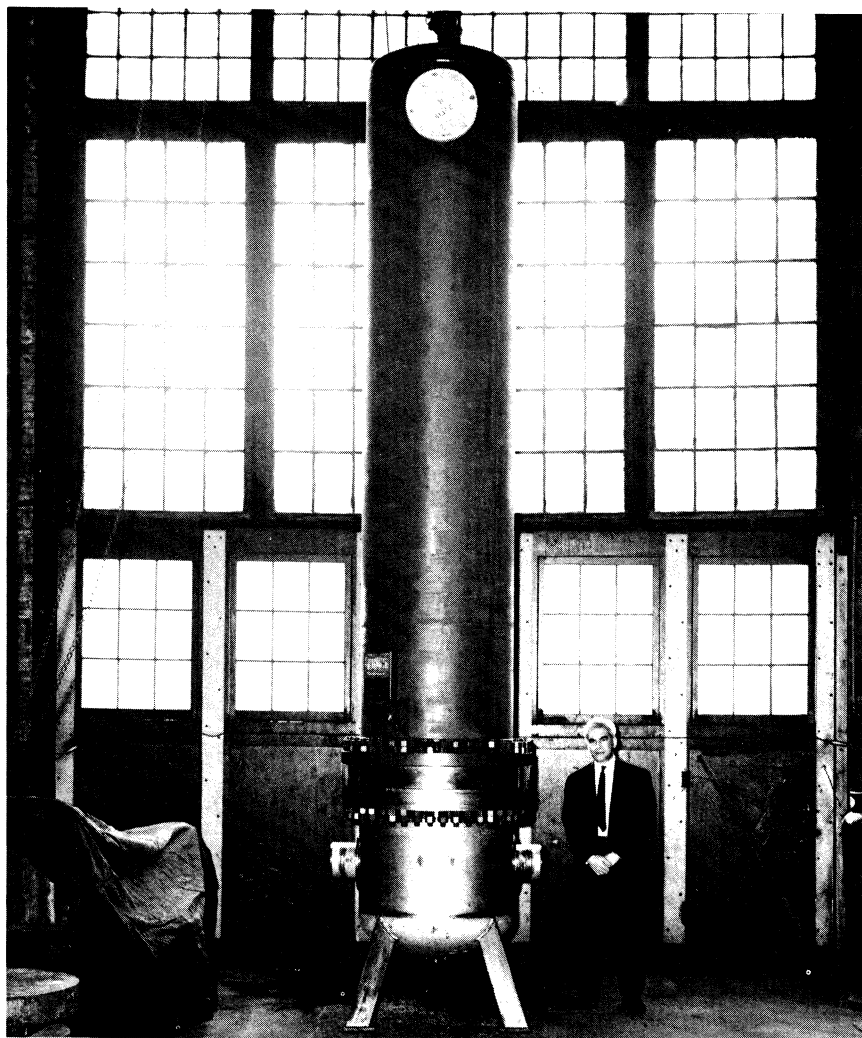
- (i) Establish all externally applied loads.
- (ii) Select a suitable leg cross-section.
- (iii) Select a suitable support height. Ordinarily, process and other considerations set the vessel height.
- (iv) Design the base plate (the plate, usually of rectangular shape, is welded to the upright legs and transfers the load from the legs to the foundation).
- (v) Size the foundation bolt.
- (vi) Determine the stresses in the support legs and base plate for the specified loadings.
- (vii) Evaluate stresses at the support/vessel junction.

Unfortunately, the direction of action of many of the externally applied



Photograph 18.a. A tank mounted on four legs.

loads is not known in advance. For example, wind loads and seismic loads can act in any arbitrary direction. Therefore, it is necessary to establish the most *vulnerable* direction of loading for the vessel in order to obtain conservative results from any subsequent stress analysis. Therefore, in what follows, we pay considerable attention to the establishment of the optimal loading plane. Referring to Fig. 18.1.1, a transverse load P is shown applied at a reference elevation (Level A). All forces and moments acting on the vessel can be transformed to a suitable reference elevation using standard load transformation techniques. In our analysis, we use the horizontal plane where the support legs meet the pressure vessel, denoted as Level A in Fig. 18.1.1, as the reference elevation. A moment M is also assumed to act in the



Photograph 18.b. Vertically mounted heat exchanger on four legs (Courtesy Joseph Oat Corporation, Camden, N.J.)

vertical plane perpendicular to the line of action of P . The object is to determine ω such that the maximum stress in at least one leg (say leg #1) reaches an absolute maximum. It is shown in the following that closed-form expressions can be derived within the spirit of a strength-of-materials approach. Thus, the solution presented herein can be utilized as an effective and expedient design tool in support design. After the support reactions are determined, the local vessel stresses can be computed in the manner described in Chapter 17. The base plate stresses can be computed using the

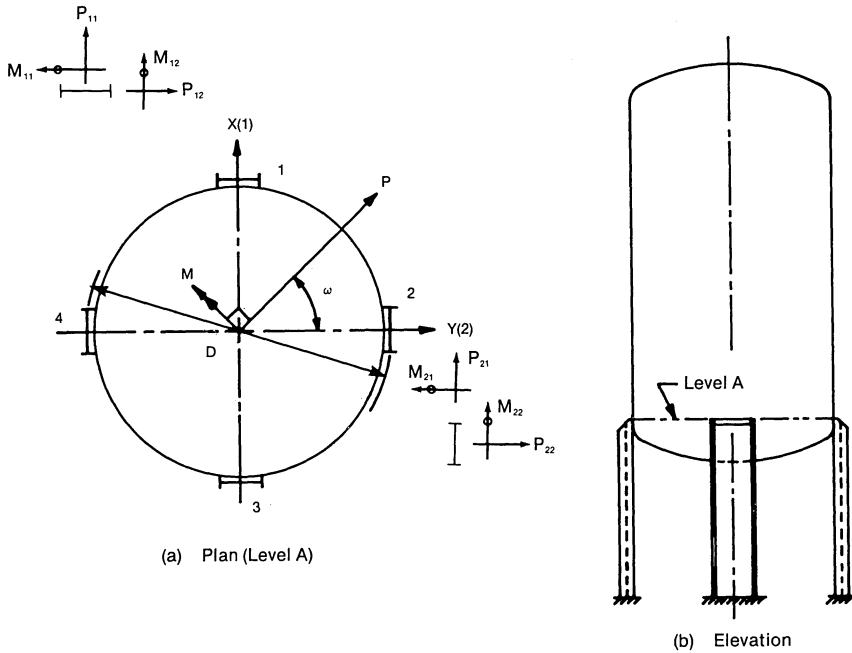


Fig. 18.1.1. 4-leg support system.

method given in Section 19.3.

The following assumptions are fundamental to the simplified analysis presented in the following:

- (i) The legs are assumed to be of symmetrical sections such as I beams and channels. Unsymmetrical sections, such as “angles” and “zee” shapes, fall beyond the purview of this treatment.
- (ii) The legs are assumed to be unbraced. Bracing the legs, however, is certainly an effective means for increasing the structural stiffness of the leg type of support system.
- (iii) Buckling in the support legs is assumed not to be incipient at the specified loading. Having determined the stresses, however, this assumption can be verified by comparing the developed axial loads with the buckling limit load for the leg configuration.
- (iv) All four supports are assumed to have identical cross section properties. There is little reason in practice to make them different.

18.2 PROBLEM DEFINITION

In Fig. 18.1.1, for the four-leg support structure under discussion here, the support legs are labelled 1 through 4 for convenience of reference. A

planar cartesian (x,y) coordinate system, with its origin at the tank geometric center, is located such that support 1 and 2, respectively, lie on the x and y axes. The tank will in general be subject to a variety of loads. The support system is symmetrical with respect to vertical load (e.g. dead load), and to axial torque. As mentioned earlier, the lateral load P and the moment M will induce stresses in the support legs which are dependent on their direction of action. As stated before, since many structural loadings encountered in practice have no a priori direction of action (e.g. horizontal seismic loads), it is necessary for us to determine the angle ω which will maximize the support leg stress. To fix our ideas, we will focus our attention on support 1, and seek to maximize the combined stress in that support due to P and M . The moment vector M is shown perpendicular to the P vector, which means that the force P lies in the plane of action of M . Load P is assumed to act at Level A. In general the applied loads will act at various elevations on the pressure vessel, and there will be several loads acting simultaneously. These loads are assumed to be transformed to Level A by appropriate transformations. For the purpose of this derivation, we assume one lateral load P and moment M oriented as shown in Fig. 18.1.1. The case of multiple loads can be treated in an identical manner as described in Appendix 18.A.

The support legs are modelled as end loaded "beam type" members mounted on rotational springs which simulate the effect of anchor bolts and foundation characteristics. (Fig. 18.2.1). Let D denote the distance between central planes of opposite supports (Fig. 18.1.1). We let E and l denote the Young's modulus and the "beam length" of the support legs. I_{ij} and Z_{ij} represent the moment of inertia and the section modulus of leg i pertinent to bending in the vertical plane containing the j -axis. M_{ij} , F_i , and P_{ij} are the associated bending moment, axial load and lateral shear (at Level A) in leg i . τ_{ij} is the rotational stiffness of the foundation/tank interface.

The appropriate expression for the combined stress in beam 1 at Level A as a function of ω is derived in the next section. For those not interested in the details of the manipulation, Section 18.4 presents a summary of the relevant calculations required.

18.3 DETERMINATION OF THE MOST VULNERABLE DIRECTION OF EXTERNAL LOADING

It can be shown using elementary beam theory that the end deflection δ and the slope ϕ of an end loaded beam (Fig. 18.2.1) is given by

$$\delta = \frac{M_0 l^2}{2EI} + \frac{P_0 l^3}{3EI} + \frac{(P_0 l + M_0)l}{\tau}$$

$$\phi = \frac{M_0 l}{EI} + \frac{P_0 l^2}{2EI} + \frac{P_0 l + M_0}{\tau}$$
(18.3.1)

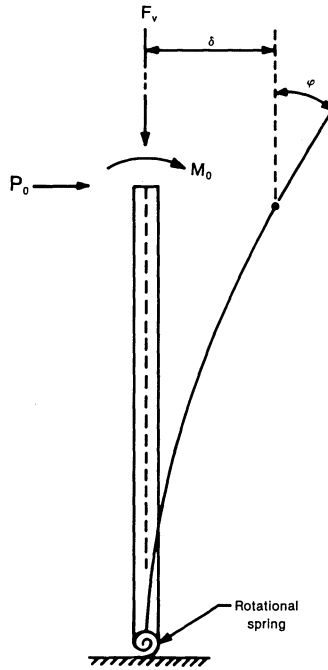


Fig. 18.2.1. End loaded cantilever.

In the spirit of our previous definitions, l , E , and I denote the length, the Young's modulus, and the plane moment of inertia (about the neutral axis) of the beam. τ is the rotational stiffness of the foundation modeled as a linear spring. Equations (18.3.1) are valid for any of the four support legs as long as we assign the proper values to M_0 , P_0 , corresponding to the specific orientation.

The axial load F_v causes an axial displacement δ_v , given by

$$\delta_v = \frac{F_v l}{AE} \tag{18.3.2}$$

where δ_v is positive if the leg is compressed.

The mutual interaction of axial and lateral loads in producing deflections has been neglected here for simplicity.

Returning to Fig. 18.1.1, force and moment equilibrium yields

$$\begin{aligned} P \sin \omega &= 2P_{21} + 2P_{11} \\ P \cos \omega &= 2P_{22} + 2P_{12} \\ M \sin \omega &= 2M_{21} + 2M_{11} + F_1 D \\ M \cos \omega &= 2M_{22} + 2M_{12} + F_2 D \end{aligned} \tag{18.3.3}$$

In the above equations P_{ij} denotes the horizontal reaction at support i in the j direction ($j, i = 1, 2$). M_{ij} denotes the moment at support i in the vertical plane perpendicular to the j direction ($j = 1$ is the x -direction, $j = 2$ is the y direction). D is the distance between central planes of Supports 1 and 3.

Let ϕ_{11} denote the slope of the tank (from the vertical) in the vertical plane containing the global x axis.

$$\phi_{11} = \frac{2\delta_{v1}}{D} = \frac{2F_1 l}{AED} \quad (18.3.4)$$

Equating slopes at beam ends at supports 1 and 2 yields

$$\begin{aligned} \phi_{11} &= M_{11} \left(\frac{l}{EI_{11}} + \frac{1}{\tau_{11}} \right) + P_{11} \left(\frac{l^2}{2EI_{11}} + \frac{l}{\tau_{11}} \right) \\ &= M_{21} \left(\frac{l}{EI_{21}} + \frac{1}{\tau_{21}} \right) + P_{21} \left(\frac{l^2}{2EI_{21}} + \frac{l}{\tau_{21}} \right) \end{aligned} \quad (18.3.5)$$

which can be rewritten succinctly as

$$\phi_{11} = a_{11}M_{11} + b_{11}P_{11} = a_{21}M_{21} + b_{21}P_{21}$$

where

$$\begin{aligned} a_{ij} &= \frac{l}{EI_{ij}} + \frac{1}{\tau_{ij}} \\ b_{ij} &= \frac{l^2}{2EI_{ij}} + \frac{l}{\tau_{ij}} \end{aligned} \quad (18.3.5a)$$

Similarly, if ϕ_{22} denotes the slope of the tank (from the vertical) in the vertical plane containing the global y axis, then

$$\phi_{22} = a_{22}M_{22} + b_{22}P_{22} = a_{12}M_{12} + b_{12}P_{12} = \frac{2\delta_{v2}}{D} \quad (18.3.6)$$

Equating the lateral displacements at beam ends (Level A) of beams 1 and 2, in the global x direction, we have, using Eq. (18.3.1) for each leg

$$b_{11}M_{11} + c_{11}P_{11} = b_{21}M_{21} + c_{21}P_{21} \quad (18.3.7)$$

where

$$c_{ij} = \frac{l^3}{3EI_{ij}} + \frac{l^2}{\tau_{ij}} \quad (18.3.8)$$

*In this derivation, since there is no external twisting moment applied, supports 1 and 3, and supports 2 and 4 will develop identical reactions, except for their axial loads which are equal and opposite.

From Eqs. (18.3.4), (18.3.5), and (18.3.6), we obtain

$$F_1 = \frac{AED}{2l} (a_{11}M_{11} + b_{11}P_{11})$$

$$F_2 = \frac{AED}{2l} (a_{22}M_{22} + b_{22}P_{22})$$
(18.3.9)

Rearranging the first and third equilibrium equations (Eq. (18.3.3)) so as to solve for P_{21} and M_{21} gives

$$P_{21} = 0.5P \sin \omega - P_{11} \quad (18.3.10)$$

$$M_{21} = 0.5M \sin \omega - M_{11} - \frac{F_1 D}{2}$$

$$= 0.5M \sin \omega - M_{11} - \frac{AED^2}{4l} (a_{11}M_{11} + b_{11}P_{11})$$

or

$$M_{21} = 0.5M \sin \omega - M_{11}(1 + a_{11}d) - b_{11}dP_{11} \quad (18.3.11)$$

where

$$d = \frac{AED^2}{4l} \quad (18.3.12)$$

Substituting for M_{21} and P_{21} in Eq. (18.3.5) yields

$$a_{11}M_{11} + b_{11}P_{11} = a_{21} \{ 0.5M \sin \omega - M_{11}(1 + a_{11}d) - b_{11}dP_{11} \} + b_{21} \{ 0.5P \sin \omega - P_{11} \}$$

or, after collecting terms,

$$\{ a_{11} + a_{21}(1 + a_{11}d) \} M_{11} + \{ b_{11} + a_{21}b_{11}d + b_{21} \} P_{11}$$

$$= 0.5a_{21}M \sin \omega + 0.5b_{21}P \sin \omega \quad (18.3.13)$$

Substituting for M_{21} and P_{21} in Eq. (18.3.7) yields

$$b_{11}M_{11} + c_{11}P_{11} = b_{21} \{ 0.5M \sin \omega - M_{11}(1 + a_{11}d) - b_{11}dP_{11} \} + c_{21} \{ 0.5P \sin \omega - P_{11} \}$$

Collecting appropriate terms together gives

$$\{ b_{11} + b_{21}(1 + a_{11}d) \} M_{11} + \{ c_{11} + b_{21}b_{11}d + c_{21} \} P_{11}$$

$$= 0.5b_{21}M \sin \omega + 0.5c_{21}P \sin \omega \quad (18.3.14)$$

For ease in manipulation, we define the following new geometric parameters:

$$\begin{aligned}
 \rho &= a_{11} + a_{21}(1 + a_{11}d) \\
 \alpha &= b_{11} + a_{21}b_{11}d + b_{21} \\
 \psi &= b_{11} + b_{21}(1 + a_{11}d) \\
 \theta &= c_{11} + b_{21}b_{11}d + c_{21}
 \end{aligned}
 \tag{18.3.15}$$

Then Eqs. (18.3.13), (18.3.14) take the simplified form

$$\begin{aligned}
 \rho M_{11} + \alpha P_{11} &= f \sin \omega \\
 \psi M_{11} + \theta P_{11} &= g \sin \omega
 \end{aligned}
 \tag{18.3.16}$$

where

$$\begin{aligned}
 f &= 0.5a_{21}M + 0.5b_{21}P \\
 g &= 0.5b_{21}M + 0.5c_{21}P
 \end{aligned}
 \tag{18.3.17}$$

Noting that $a_{11} = a_{22}$, $b_{11} = b_{22}$, and $a_{12} = a_{21}$, $b_{12} = b_{21}$, we can repeat the entire set of previous manipulations, using the equations involving P_{12} , P_{22} , M_{12} , M_{22} , F_2 . We obtain the analog of Eq. (18.3.16) as

$$\begin{aligned}
 \rho M_{22} + \alpha P_{22} &= f \cos \omega \\
 \psi M_{22} + \theta P_{22} &= g \cos \omega
 \end{aligned}
 \tag{18.3.18}$$

Let us define the determinant of the coefficients as

$$\Delta = \rho\theta - \alpha\psi
 \tag{18.3.19}$$

then, from Eq. (18.3.16), we can solve for M_{11} , P_{11} as

$$\begin{aligned}
 M_{11} &= \frac{1}{\Delta} (f\theta - g\alpha) \sin \omega = \chi \sin \omega \\
 P_{11} &= \frac{1}{\Delta} (\rho g - f\psi) \sin \omega = \xi \sin \omega
 \end{aligned}
 \tag{18.3.20}$$

Similarly, solving Eq. (18.3.18) for M_{22} , P_{22} yields

$$\begin{aligned}
 M_{22} &= \chi \cos \omega \\
 P_{22} &= \xi \cos \omega
 \end{aligned}
 \tag{18.3.21}$$

The maximum stress in support #1 is given by:

$$\sigma = \left| \frac{M_{11}}{Z_{11}} \right| + \left| \frac{M_{12}}{Z_{12}} \right| + \left| \frac{F_1}{A} \right|
 \tag{18.3.21a}$$

We recall the equilibrium equation (18.3.3)

$$2M_{12} + 2M_{22} + F_2 D = M \cos \omega$$

and the representation of F_2 given in Eq. (18.3.9)

$$F_2 = \frac{AED}{2l} (a_{11}M_{22} + b_{11}P_{22})$$

Solving the above for M_{12} yields

$$M_{12} = 0.5M \cos\omega - M_{22} - \frac{AED^2}{4l} (a_{11}M_{22} + b_{11}P_{22}) \quad (18.3.21b)$$

Hence, we can eliminate M_{12} and F_1 in the expression for σ by using Eqs. (18.3.21b) and (18.3.9), respectively

$$\sigma = \left| \frac{M_{11}}{Z_{11}} \right| + \frac{1}{Z_{12}} \left| \{0.5M \cos\omega - M_{22} - d(a_{11}M_{22} + b_{11}P_{22})\} \right| + \frac{ED}{2l} |(a_{11}M_{11} + b_{11}P_{11})|$$

or

$$\sigma = \left| \frac{\chi \sin\omega}{Z_{11}} \right| + \frac{1}{Z_{12}} \left| \{0.5M \cos\omega - \chi \cos\omega - da_{11}\chi \cos\omega - db_{11}\xi \cos\omega\} \right| + |(ea_{11}\chi \sin\omega + eb_{11}\xi \sin\omega)| \quad (18.3.22)$$

where

$$e = \frac{ED}{2l} \quad (18.3.23)$$

With no loss in generality, the expression for σ becomes

$$\sigma = \sin\omega \left[\left| \frac{\chi}{Z_{11}} \right| + e |(a_{11}\chi + b_{11}\xi)| \right] + \cos\omega \left[\left| \frac{1}{Z_{12}} \{0.5M - \chi - d(a_{11}\chi + b_{11}\xi)\} \right| \right]$$

For a maximum,

$$\frac{\partial \sigma}{\partial \omega} = 0$$

which yields the equation

$$\cos\omega \left\{ \left| \frac{\chi}{Z_{11}} \right| + e |(a_{11}\chi + b_{11}\xi)| \right\} = \frac{1}{Z_{12}} \left| \{0.5M - \chi - da_{11}\chi - db_{11}\xi\} \right| \sin\omega$$

For computation purposes, we can solve the above for $\tan \omega$ and obtain

$$\tan \omega = \frac{\frac{\chi |Z_{12}|}{Z_{11}} + eZ_{12} |(a_{11}\chi + b_{11}\xi)|}{|(0.5M - \chi - d(a_{11}\chi + b_{11}\xi))|} \quad (18.3.24)$$

Equation (18.3.24) determines the optimal angle ω .

18.4 COMPUTATION PROCEDURE

The foregoing analysis lends itself to rapid calculation on a hand calculator. For the convenience of the reader disinclined to wade through the details of the analysis, sequential steps to perform the computations are given in the following:

- (i) Required data: $l, D, E, A, I_{11}, I_{12}, Z_{11}, Z_{12}, \tau_{11}, \tau_{12}, M$ and P .
- (ii) Evaluate a_{ij}, b_{ij}, c_{ij} (Eqs. (18.3.5a) and (18.3.8)); d (Eq. (18.3.12)) and e (Eq. (18.3.23)).
- (iii) Evaluate $\rho, \alpha, \psi, \theta$ (Eq. (18.3.15)); f and g (Eq. (18.3.17)); Δ (Eq. (18.3.19)).
- (iv) Determine χ and ξ using Eq. (18.3.20)

$$\chi = \frac{1}{\Delta} (f\theta - g\alpha)$$

$$\xi = \frac{1}{\Delta} (\rho g - f\psi)$$

- (v) Compute the optimal ω (Eq. (18.3.24)).
- (vi) Compute M_{11}, P_{11} (Eq. (18.3.20)); M_{22} (Eq. (18.3.21)); M_{12} (Eq. (18.3.21b)); F_1 (Eq. 18.3.9)); and, finally, σ (Eq. (18.3.22)).

Computer program FORLEG, described in Appendix 18.B performs this analysis in an efficient manner.

18.5 AN EXAMPLE

A practical problem is examined in detail in this section to illustrate the application of the analysis presented in this chapter. The geometric and physical data for the problem is given in Fig. 18.5.1, wherein the maximum stress in leg #1 as a function of ω is shown for three loading cases; namely

- Case 1: Lateral load $P = 20,000$ lb.
- Case 2: Moment, $M = 20 \times 10^6$ lb.-in.
- Case 3: $P = 20,000$ lb and $M = 20 \times 10^6$ lb.-in.
(cases 1 and 2 combined)

It is of some interest to note that even though the beam sections are equal

and symmetrical ($I_{ij} = I_{ji}$) about the principal bending planes, the maximum stress does not occur when the loading is applied in the principal plane of symmetry of the equipment ($\omega = 0$ or 90°). For case 1, the optimal ω , ω_{op} , is 46.94° , and for case 2 it is 88.23° . Since case 3 is a combination of cases 1 and 2, its ω_{op} ($=69.28^\circ$) lies between the two optimal values of the individual loadings. Obviously, the relative magnitudes of P and M are important in the location of ω_{op} .

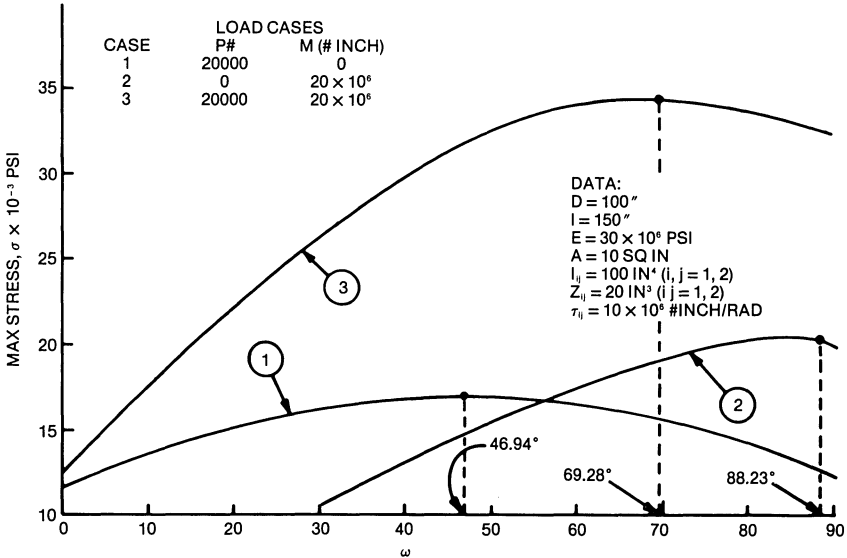


Fig. 18.5.1. Max. support stress vs. angle ω .

Figure 18.5.2 shows the important reactions, namely M_{11} , M_{12} , and F_1 for leg #1 as a function of ω for loading case 2. The strong dependence of these reactions on ω is evident from this figure.

Perhaps the most illustrative information is in Fig. 18.5.3, which shows the absolute maximum stress σ_{max} (maximum stress in any leg) as a function of ω for case 1. It is seen that the maximum stress is increased by over 36% when the direction of action of P is changed from a principal direction of symmetry ($\omega = 0$) to ω_{op} .

Sometimes the direct stress in the leg, due to F_i alone, is specified as the quantity to be limited in certain codes. Figure 18.5.3 also gives the maximum axial load (higher of the two leg axial loads) as a function of ω . The variation in F_i (maximum) is even greater – over 40% – between $\omega = 0$ to $\omega = 45^\circ$.

18.6 OBSERVATIONS ON THE OPTIMIZATION METHOD

A method to determine the worst angular orientation for applied lateral loads and for overturning moments on four leg supports has been

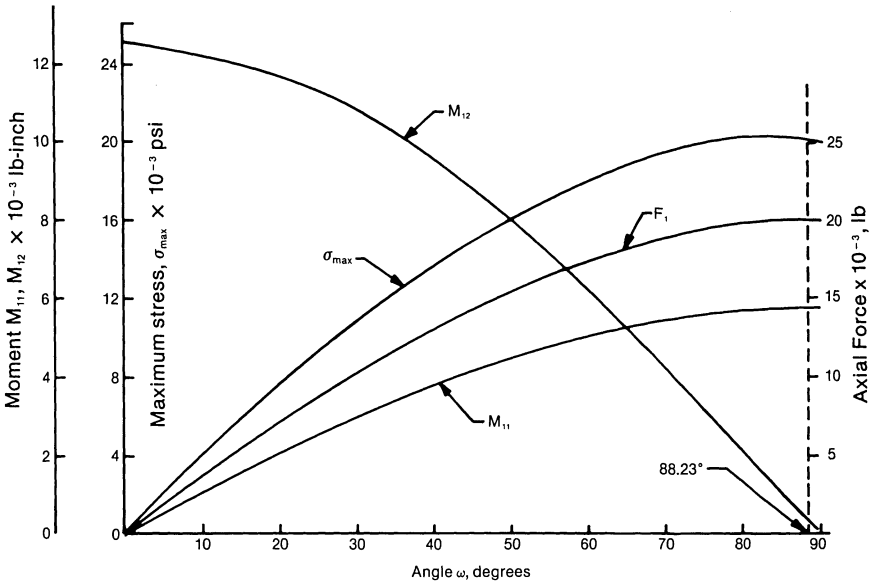


Fig. 18.5.2. Maximum stress, bending moment and axial force vs. ω .

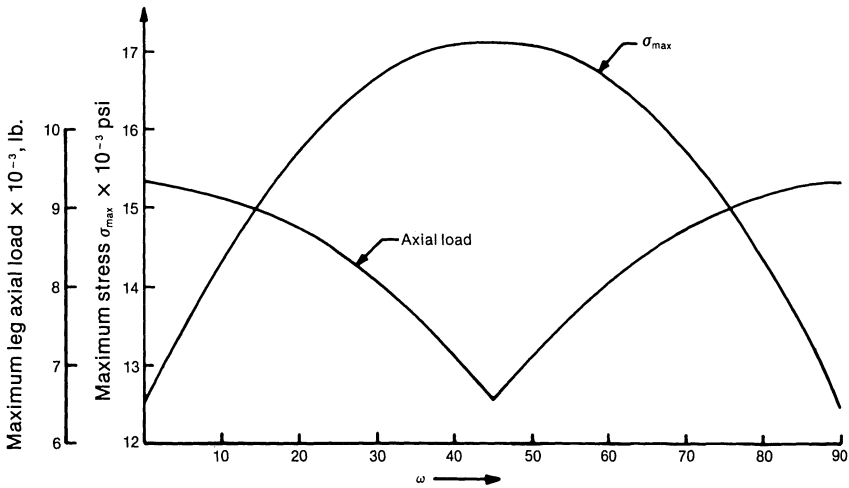


Fig. 18.5.3. Absolute maximum stress σ_{max} and axial reaction F_{max} vs. ω .

presented. The formulas are derived for a given lateral load P and moment M . If several sets of mutually independent loadings are present, then the

optimal orientation for each set can be found independently following the steps summarized in a preceding section. On the other hand, the governing equations are more complex if multiple loads are fixed in angular orientation relative to each other, but not with respect to the tank. Important results for this case are presented in concise form in Appendix 18.A.

The optimal value of ω derived here (Eq. (18.3.24)) is the value which maximizes the combined stress in one of the support legs. Some design codes require specific limits on direct stress. The value of optimal ω maximizing the direct stress can be found by differentiating only the term F_1/A in the expression for σ . This yields, after performing the required algebra, $\omega = \pi/2$. Thus, the peak value of direct stress corresponds to the loading applied along an axis of symmetry. Figure 18.5.3 confirms this fact through the numerical example.

The equations derived in this chapter determine the maximum beam stress in the support legs. Thus, local stresses at the leg-vessel junction are also maximized. The method to compute such local stresses are available in the literature and are outlined in Chapter 17. To complete this chapter, the next section sets forth the appropriate stress limits for the support legs.

18.7 STRESS LIMITS

Leg type supports are referred to as “linear type” supports in the ASME Boiler and Pressure Vessel Code [18.7.1]. A linear type support is defined as a support which resists applied loading in the manner of a beam, a column, or a shaft. Originally, the stress limits on this class of supports appeared in the Manual of Steel Construction published by the American Iron and Steel Institute [18.7.2]. The current edition of the ASME Code (nuclear component section) also recommends the same limits. These stress limits amount to six distinct bounds that the stress levels in the support must meet. These are:

(i) The average tension stress on a net cross section is limited by $F_t = 0.6S_y$, where S_y is the nominal yield stress at the design temperature.

(ii) Allowable shear stress is limited by $F_s = 0.4S_y$.

(iii) Allowable stress in compression is limited to F_a

(a) When kl/r is less than C_c .

$$F_a = \frac{\left[1 - \left(\frac{kl}{r}\right)^2 / 2C_c^2\right] S_y}{\left[\left(\frac{5}{3}\right) + \left[3\left(\frac{kl}{r}\right) / 8C_c\right] - \left[\left(\frac{kl}{r}\right)^3 / 8C_c^3\right]}\right.} \quad (18.7.1)$$

where kl is the “effective leg length” and r is the radius of gyration. k may be taken as 1.2 in practical design work.

$$C_c = \left[\frac{(2\pi^2 E)}{S_y}\right]^{1/2} \quad (18.7.2)$$

(b) When kl/r is greater than C_c

$$F_a = \frac{12\pi^2 E}{23} \left/ \left(\frac{kl}{r} \right)^2 \right. \quad (18.7.3)$$

(c) When kl/r exceeds 120:

$$F_a = \frac{F_a \text{ [from case (a) or (b)]}}{1.6 - \frac{l}{200r}} \quad (18.7.4)$$

(iv) Maximum bending stress at the outermost fiber due to flexure about one plane of symmetry is limited to $F_b = 0.60 S_y$. Reference [18.7.1] gives certain restrictions on the support leg geometry and dimensions for this formula to be applicable.

(v) Combined flexure and compression:

$$\frac{f_a}{F_a} + \frac{C_{mx} f_{bx}}{D_x F_{bx}} + \frac{C_{my} f_{by}}{D_y F_{by}} < 1 \quad (18.7.5)$$

where

f_a = Direct compressive stress in the section
 f_{bx} = Maximum flexural stress along x -axis
 f_{by} = Maximum flexural stress along y -axis
 $C_{mx} = C_{my} = 0.85$

$$D_x = 1 - \frac{f_a}{F'_{ex}} \quad (18.7.6)$$

$$D_y = 1 - \frac{f_a}{F'_{ey}}$$

where F'_e (x or y) is

$$F'_e = \frac{12\pi^2 E}{23 \left(\frac{kl_b}{r_b} \right)^2} \quad (18.7.7)$$

The length l_b is the unbraced leg length in the plane of bending and r_b is the corresponding radius of gyration.

(vi) Combined flexure and compression (or tension)

$$\frac{f_a}{0.6S_y} + \frac{f_{bx}}{F_{bx}} + \frac{f_{by}}{F_{by}} < 1.0 \quad (18.7.8)$$

The above requirement should be met for both the direct tension or compression case.

These limits are recommended for external loads of infrequent occurrence, defined as the “upset condition” in the ASME Code. In the event of an external load of extremely rare occurrence, F-1370 (Section III, Appendix F of the ASME code), states that the limits for the so called “faulted condition” are $1.2 (S_y/F_t)$ times the corresponding limits for normal or upset condition.

Reference [18.7.1] permits increasing the limit in the right-hand side of Eq. (18.7.8) by 1.5 if both primary and secondary stresses are included in the calculation of the numerators.

The foregoing stress limits constitute a rational set of design guides. Readers interested in learning more about the detailed industry practice and the ASME Code position in this area should consult Refs. [18.7.1–3].

NOMENCLATURE

- A = Cross sectional area of one support leg
- D = Equivalent support system diameter
- E = Young’s modulus of support material
- F_i = Axial load (compressive) in beam i
- I_{ij} = Plane moment of inertia of beam i for rotation in the vertical plane containing the j axis
- k = Effective length multiplier factor (Section 18.7)
- l = “Beam length” of support leg
- M_{ij} = Bending moment vector at the top of support beam i perpendicular to the j axis*
- P_{ij} = Lateral reaction at the top of beam (support) i in j direction
- r = Radius of gyration of the support cross section
- Z_{ij} = Section modulus of support beam associated with I_{ij}
- δ_v = Axial deflection of support (Eq. (18.3.2))
- τ_{ij} = Rotational spring constant at the root of beam i for rotation in the vertical plane containing the j axis
- ω = Optimal angle which maximizes total fiber stress in leg #1.
- ϕ_{ij} = Top end slope of beam i in the vertical plane containing the j axis

REFERENCES

- [18.7.1] ASME Boiler and Pressure Vessel Code, Section III, Division I, Appendix XVII, pp. 393–434, ASME, New York (1983).
- [18.7.2] “Manual of Steel Construction,” American Institute of Steel Construction, Eighth edition, AISC, Inc. Chicago (1980).
- [18.7.3] “Guide to Design Criteria for Metal Compression Members,” Second Edition, The Column Research Council (1966).

* $j = 1$ is the x direction, $j = 2$ is the y direction.

APPENDIX 18.A

MULTIPLE LOADINGS ON THE PRESSURE VESSEL

Let us assume that there are n applied overturning moments M_j ($j=1, \dots, n$) such that the moment M_j makes an angle $(\omega + \delta_j)$ with the x axis (Fig. 18.1.1). δ_i ($i=1, 2, \dots, n$) are constant angles which fix the angular orientation of various moments with respect to each other. ω is a variable reference angle which we seek to determine so as to maximize σ . Similarly, let us assume that there are m lateral loads P_j ($j=1, 2, \dots, m$) such that load P_j makes an angle $(\gamma_j + \omega)$ with the y axis. γ_j ($i=1, 2, \dots, m$) are known quantities.

Proceedings in the manner described in Chapter 18, the following expressions for M_{ij} and P_{ij} are obtained.

$$M_{11} = \chi \sum_{i=1}^n M_i \sin(\omega + \delta_i) + \xi \sum_{i=1}^m P_i \sin(\omega + \gamma_i) \quad (18.A.1)$$

$$P_{11} = \Omega \sum_{i=1}^n M_i \sin(\omega + \delta_i) + \zeta \sum_{i=1}^m P_i \sin(\omega + \gamma_i) \quad (18.A.2)$$

where

$$\begin{aligned} \chi &= \frac{1}{2\Delta} (a_{21}\theta - b_{21}\alpha) \\ \xi &= \frac{1}{2\Delta} (b_{21}\theta - c_{21}\alpha) \\ \Omega &= \frac{1}{2\Delta} (b_{21}\rho - a_{21}\psi) \\ \zeta &= \frac{1}{2\Delta} (\rho c_{21} - \psi b_{21}) \end{aligned} \quad (18.A.3)$$

Similarly,

$$M_{22} = \chi \sum_{i=1}^n M_i \cos(\omega + \delta_i) + \xi \sum_{i=1}^m P_i \cos(\omega + \gamma_i) \quad (18.A.4)$$

$$P_{22} = \Omega \sum_{i=1}^n M_i \cos(\omega + \delta_i) + \zeta \sum_{i=1}^m P_i \cos(\omega + \gamma_i) \quad (18.A.5)$$

Equilibrium requires (generalize the last of Eq. (18.3.3))

$$2M_{12} + 2M_{22} + F_2 D = \sum_{i=1}^n M_i \cos(\omega + \delta_i)$$

Substituting for F_2 from Eq. (18.3.9), we have

$$M_{12} = 0.5 \sum_{i=1}^n M_i \cos(\omega + \delta_i) - (1 + a_{11} d) M_{22} - b_{11} d P_{22} \quad (18.A.6)$$

The combined stress σ in leg #1 is given by

$$\sigma = \left| \frac{M_{11}}{Z_{11}} \right| + \left| \frac{M_{12}}{Z_{12}} \right| + \left| \frac{F_1}{A} \right|$$

Substituting for F_1 from Eq. (18.3.9); and for M_{11} , M_{12} and P_{11} from the foregoing equations we have

$$\begin{aligned} \sigma = & \frac{1}{Z_{11}} \left| \chi \sum_{i=1}^n M_i \sin(\omega + \delta_i) + \xi \sum_{i=1}^m P_i \sin(\omega + \gamma_i) \right| \\ & + \frac{1}{Z_{12}} \left\{ 0.5 \sum_{i=1}^n M_i \cos(\omega + \delta_i) - (1 + a_{11} d) \right. \\ & \left. \left\{ \chi \sum_{i=1}^n M_i \cos(\omega + \delta_i) + \xi \sum_{i=1}^m P_i \cos(\omega + \gamma_i) \right\} - b_{11} d \right. \\ & \left. \left\{ \Omega \sum_{i=1}^n M_i \cos(\omega + \delta_i) + \zeta \sum_{i=1}^m P_i \cos(\omega + \gamma_i) \right\} \right| \\ & + e \left| a_{11} \left\{ \chi \sum_{i=1}^m M_i \sin(\omega + \delta_i) + \xi \sum_{i=1}^m P_i \sin(\omega + \gamma_i) \right\} \right. \\ & \left. + b_{11} \left\{ \Omega \sum_{i=1}^n M_i \sin(\omega + \delta_i) + \zeta \sum_{i=1}^m P_i \sin(\omega + \gamma_i) \right\} \right| \quad (18.A.7) \end{aligned}$$

Assuming that the geometry and the loading values are known, this expression for σ is a nonlinear function of ω , which can be formally differentiated to obtain optimal ω . However, it is relatively straightforward to compute σ for incremental values of α (from 0 to 90) from Eq. (18.A.7); and determine the ω corresponding to the maximum value of σ in that manner.

APPENDIX 18.B

COMPUTER PROGRAM FORLEG

Program FORLEG automates the computational procedure outlined in Section 18.4. The input data for FORLEG is presented in Table 18.B.1 below. The data used in the example problem of Section 18.5 is also presented in Table 18.B.1 to illustrate data preparation.

Table 18.B.1.* Input Data for FORLEG*Line 1:* Heading (any 80 alphanumeric title)*Line 2:* Support leg data

Item	Fortran Symbol	Sample Problem Value
Height of support leg	L	50 in.
Outer diameter of the vessel	D	100 in.
Young's Modulus of Support Material	E	30×10^6 psi
Cross sectional area of support leg	A	10 sq. in.

Line 3: Section Properties of Support leg

Moment of inertia of leg 1 for bending in x - z plane (Fig. 18.1.1), I_{11}	I11	100 in. ⁴
Moment of inertia of leg 1 for bending in y - z plane (Fig. 18.1.1), I_{12}	I12	100 in. ⁴
Section Modulus corresponding to I_{11} , (Z_{11})	Z11	20 in. ³
Section Modulus corresponding to I_{12} , (Z_{12})	Z12	20 in. ³

Line 4: Support stiffness

Stiffness of the rotational spring for the root of leg 1 for rotation in x - z plane (Figs. 18.1.1 and 18.2.1)	τ_{11}	10×10^6 lb-in./rad
Stiffness of the rotational spring for the root of leg 1 for rotation in the y - z plane (Figs. 18.1.1 and 18.2.1)	τ_{12}	10×10^6 lb-in./rad

Line 5: Loads at Level A (Fig. 18.1.1)

Applied moment, M	20,000 lb	} case 3
Applied Force, P	20×10^6 lb-in.	

The program determines the optimal value of ω and the corresponding stress in leg #1. It gives all associated reactions, viz. M_{ij} , P_{ij} and F_i for supports 1 and 2. Results for these reactions for incremental values of ω (in increments of 5°) are also printed out. The Fortran labels in the output corresponding to the mathematical symbols are as follows:

$w \rightarrow W_j$; $M_{ij} \rightarrow MP(I,J)$; $P_{ij} \rightarrow PP(I,J)$; $F_i \rightarrow FP(I,J)$. The total stresses (membrane plus bending) in supports 1 and 2 are labelled as SIGMA (1) and SIGMA (2), respectively.

*All data is input using free field format.

PROGRAM FORLEG

```

C BY KRISHNA P. SINGH AND TEIK-LEE NG, REV. 0, JANUARY 1984
C THIS PROGRAM DETERMINES THE ANGLE W WHICH MAXIMIZES THE
C COMBINATION OF FLEXURAL AND DIRECT STRESSES IN BEAM 1, LOCATED
C ON THE GLOBAL X-AXIS, FOR A TANK (OR PRESSURE VESSEL) SUPPORTED
C ON FOUR EQUI-SPACED BEAMS. THE PROGRAM ALSO COMPUTES THE
C REACTIONS AND BEAM STRESSES AS A FUNCTION OF ANGLE W.
C
C *****DEFINITIONS OF FORTRAN VARIABLES*****
C
C .....INPUT.....
C L= HEIGHT OF SUPPORT LEG(BEAM)
C D= DIAMETER OF TANK
C E= YOUNG'S MODULUS OF BEAM
C A= CROSS-SECTIONAL AREA OF BEAM
C I(1,1)= PLANE M.I. OF BEAM 1 FOR BENDING IN X-Z PLANE
C I(1,2)= MOMENT OF INERTIA OF BEAM 1 FOR BENDING IN Y-Z PLANE
C Z(1,1)= SECTION MODULUS ASSOC. WITH I(1,1).
C Z(1,2)= SECTION MODULUS ASSOC. WITH I(1,2).
C TAU(1,1)= ROTATIONAL SPRING CONSTANT OF BEAM 1 FOR
C ROTATION IN X-Z PLANE
C TAU(1,2)= ROTATIONAL SPRING CONSTANT OF BEAM 1 FOR
C ROTATION IN Y-Z PLANE
C M= APPLIED MOMENT
C P= APPLIED HORIZONTAL FORCE
C
C .....OUTPUT.....
C W(DEG.)= OPTIMAL ANGLE WHICH MAXIMIZES TOTAL FIBER STRESS IN LEG 1
C DSDW2= MAX. BEAM STRESS
C REACTIONS ARE PP(I,J), MP(I,J), FP(I,J)
C SIGMA(1), SIGMA(2) =BEAM STRESSES
C
C *****
C DIMENSION TAU(2,2),STOR(13,40),CS(2,2),AS(2,2),BS(2,2),PP(2,2),
C $FP(2,2),Z(2,2),SIGMA(2),TITLE(20)
C REAL L,M,I(2,2),MP(2,2)
C CHARACTER*8 ANAM(13)
C PI=3.14159
C ANAM(1)="W"
C ANAM(2)="PP(1,1)"
C ANAM(3)="PP(1,2)"
C ANAM(4)="MP(1,1)"
C ANAM(5)="MP(1,2)"
C ANAM(6)="FP(1,1)"
C ANAM(7)="PP(2,1)"
C ANAM(8)="PP(2,2)"
C ANAM(9)="MP(2,1)"
C ANAM(10)=" MP(2,2)"
C ANAM(11)=" FP(2,2)"

```

```

      ANAM(12)="SIGMA(1)"
      ANAM(13)="SIGMA(2)"
C
      READ(5,999) (TITLE(K),K=1,18)
      READ(5,*) L,D,E,A
      READ(5,*) I(1,1),I(1,2),Z(1,1),Z(1,2)
      READ(5,*) TAU(1,1),TAU(1,2)
C
C
1      READ(5,*) M,P
      IF(ABS(M).LT..0001.AND.ABS(P).LT..0001) GO TO 500
C
C INPUT REPRINT
C
      WRITE(6,2000) (TITLE(K),K=1,18)
      WRITE(6,2005)M,P,L,D,E,A,I(1,1),I(1,2),Z(1,1),Z(1,2),TAU(1,1),
      $ TAU(1,2)
C
C VARIOUS TENSOR COMPONENT TERM EQUIVALENCES
C
      I(2,2)=I(1,1)
      I(2,1)=I(1,2)
      TAU(2,2)=TAU(1,1)
      TAU(2,1)=TAU(1,2)
C
C CALCULATE OTHER TENSOR COMPONENTS
C
      DO 10 K=1,2
      DO 10 J=1,2
          CS(K,J)=L**3/3./E/I(K,J) + L**2/TAU(K,J)
          AS(K,J)=L/E/I(K,J) + 1./TAU(K,J)
          BS(K,J)=L**2/2./E/I(K,J) + L/TAU(K,J)
10      CONTINUE
C
C CALCULATE MISCELLANEOUS PARAMETERS
C
      DS=A*E*D*D/4./L
      ES=E*D/2./L
C
      ROW=AS(1,1) + AS(2,1) *(1.+AS(1,1)*DS)
      ALPHA=BS(1,1)+AS(2,1)*BS(1,1)*DS + BS(2,1)
      PSI=BS(1,1)+BS(2,1)*(AS(1,1)*DS + 1.)
      THETA=CS(1,1)+BS(2,1)*BS(1,1)*DS + CS(2,1)
      F=.5*(AS(2,1)*M+BS(2,1)*P)
      G=.5*(BS(2,1)*M+CS(2,1)*P)
      DEL=ROW*THETA - ALPHA*PSI
      X=1./DEL*(F*THETA - G*ALPHA)
      ZETA=1./DEL *(ROW*G-F*PSI)
      AP=ABS(X/Z(1,1))+ES*ABS((AS(1,1)*X + BS(1,1)*ZETA))
      B=1./Z(1,2)*ABS((.5*M-X-DS*(AS(1,1)*X + BS(1,1)*ZETA)))
      W=ATAN(AP/B)
      WDEG=W/PI*180.

```

```

DSDW2= -AP*SIN(W) - B*COS(W)
WRITE(6,2015)WDEG,DSDW2
C
C COMPUTE THE BEAM STRESSES AS A FUNCTION OF ANGLE , WHICH IS ALLOWED
C TO VARY BETWEEN 0 AND 90 DEGREES IN INCREMENT STEP SIZE OF WINC DEG
C
WINC=5.
NST=90./WINC + 2
DO 30 NS=1,NST
  IF(NS.NE.1) W=(WINC/180.*PI) * (NS-2)
  MP(1,1)=X*SIN(W)
  PP(1,1)=ZETA*SIN(W)
  MP(2,2)=X*COS(W)
  PP(2,2)=ZETA*COS(W)
  PP(2,1)=.5*P*SIN(W)-PP(1,1)
  MP(2,1)=.5*M*SIN(W) -MP(1,1)*(1.+AS(1,1)*DS)-BS(1,1)*DS*PP(1,1)
  FP(1,1)=A*ES*(AS(1,1)*MP(1,1)+BS(1,1)*PP(1,1))
  FP(2,2)=A*ES*(AS(1,1)*MP(2,2)+BS(1,1)*PP(2,2))
  PP(1,2)=.5*P*COS(W)-PP(2,2)
  MP(1,2)=.5*M*COS(W) - MP(2,2)*(1.+AS(1,1)*DS)
  $ -BS(1,1)*DS*PP(2,2)
C
C
C MOMENT AND FORCE CONTRIBUTIONS TO STRESS ARE ALWAYS ADDITIVE IN
C MAGNITUDE AND HAVE THE SAME SIGN AS THE FORCE CONTRIBUTION
C
AMA=ABS(MP(1,1)/Z(1,1)) + ABS(MP(1,2)/Z(1,2))
AMB=ABS(MP(2,1)/Z(1,2) ) + ABS(MP(2,2)/Z(1,1))
ISA=1
IF(FP(1,1).NE.0.) ISA=FP(1,1)/ABS(FP(1,1))
ISB=1
IF(FP(2,2).NE.0.) ISB=FP(2,2)/ABS(FP(2,2))
SIGMA(1)=ISA*AMA + FP(1,1)/A
SIGMA(2)=ISB*AMB + FP(2,2)/A
C
C
C
C
C TEMPORARY DATA STORAGE
C
STOR(1,NS)=W/PI*180.
STOR(2,NS)=PP(1,1)
STOR(3,NS)=PP(1,2)
STOR(4,NS)=MP(1,1)
STOR(5,NS)=MP(1,2)
STOR(6,NS)=FP(1,1)
STOR(7,NS)=PP(2,1)
STOR(8,NS)=PP(2,2)
STOR(9,NS)=MP(2,1)
STOR(10,NS)=MP(2,2)
STOR(11,NS)=FP(2,2)

```

```

        STOR(12,NS)=SIGMA(1)
        STOR(13,NS)=SIGMA(2)
30    CONTINUE
C
C
C    OUTPUT PRINTOUT
C
        IT=NST/5.
        DO 40 IL=1,IT
            IZ1=5*IL-4
            IZ2=IL*5
            IF(IL.EQ.IT) IZ2=NST
            DO 38 ILF=1,13
                WRITE(6,2010)ANAM(ILF),(STOR(ILF,IZ),IZ=IZ1,IZ2)
38    CONTINUE
        WRITE(6,2020)
40    CONTINUE
        GO TO 1
999   FORMAT(20A4)
2000  FORMAT(1H1,5X," - PROGRAM FORLEG - (VERSION 0)//1H ,18A4//)
2005  FORMAT(1H0/15X,"*****INPUT DATA*****"/
$6X,"M, APPLIED MOMENT .....=",E16.8/
$6X,"P, APPLIED HORIZONTAL FORCE .....=",E16.8/
$6X,"L, HEIGHT OF SUPPORT LEG(BEAM) .....=",E16.8/
$6X,"D, OUTER DIAMETER OF TANK .....=",E16.8/
$6X,"E, YOUNG'S MODULUS OF BEAM .....=",E16.8/
$6X,"A, CROSS-SECTIONAL AREA OF BEAM .....=",E16.8/
$6X,"I(1,1), MOMENT OF INERTIA OF BEAM 1 FOR BENDING "/
$6X,"      IN X-Z PLANE ..... =" ,E16.8/
$6X,"I(1,2), MOMENT OF INERTIA OF BEAM 1 FOR BENDING "/
$6X,"      IN Y-Z PLANE ..... =" ,E16.8/
$6X,"Z(1,1), SECTION MODULUS ASSOC. WITH I(1,1)..... =" ,E16.8/
$6X,"Z(1,2), SECTION MODULUS ASSOC. WITH I(1,2)..... =" ,E16.8/
$6X,"TAU(1,1), ROTATIONAL SPRING CONSTANT OF BEAM 1 FOR"/
$6X,"      ROTATION IN X-Z PLANE .....=" ,E16.8/
$6X,"TAU(1,2), ROTATIONAL SPRING CONSTANT OF BEAM 1 FOR"/
$6X,"      ROTATION IN Y-Z PLANE .....=" ,E16.8)
2010  FORMAT(1H ,5X,A8,5E12.4)
2015  FORMAT(1H0//15X,"*****RESULTS*****"/
$6X,"W(DEG.), OPTIMAL ANGLE WHICH MAXIMIZES TOTAL FIBER STRESS"/
$6X,"      IN LEG 1 ..... =" ,E16.4/
$6X,"MAX. BEAM STRESS .....=",E16.4/1H0//
$5X,"***REACTIONS AND BEAM STRESSES AS A FUNCTION OF ANGLE W***")
2020  FORMAT(1H0/)
500   STOP
        END

```

*** SAMPLE PROBLEM FOR PROGRAM FORLEG ***

*****INPUT DATA*****

M, APPLIED MOMENT= .2000000E+05
 P, APPLIED HGRIXONTAL FORCE= .2000000E+08
 L, HEIGHT OF SUPPORT LEG(BEAM)= .5000000E+02
 D, OUTER DIAMETER OF TANK= .1000000E+03
 E, YOUNG'S MODULUS OF BEAM= .3000000E+08
 A, CROSS-SECTIONAL AREA OF BEAM= .1000000E+02
 I(1,1), MOMENT OF INERTIA OF BEAM 1 FOR BENDING
 IN X-Z PLANE = .1000000E+03
 I(1,2), MOMENT OF INERTIA OF BEAM 1 FOR BENDING
 IN Y-Z PLANE = .1000000E+03
 Z(1,1), SECTION MODULUS ASSOC. WITH I(1,1)..... = .2000000E+02
 Z(1,2), SECTION MODULUS ASSOC. WITH I(1,2)..... = .2000000E+02
 TAU(1,1), ROTATIONAL SPRING CONSTANT OF BEAM 1 FOR
 ROTATION IN X-Z PLANE= .1000000E+08
 TAU(1,2), ROTATIONAL SPRING CONSTANT OF BEAM 1 FOR
 ROTATION IN Y-Z PLANE= .1000000E+08

*****RESULTS*****

W(DEG.), OPTIMAL ANGLE WHICH MAXIMIZES TOTAL FIBER STRESS
 IN LEG 1 = .4701E+02
 MAX. BEAM STRESS= -.1709E+08

REACTIONS AND BEAM STRESSES AS A FUNCTION OF ANGLE W

W	.4701E+02	.0000E+00	.5000E+01	.1000E+02	.1500E+02
PP(1,1)	.3651E+07	.0000E+00	.4350E+06	.8667E+06	.1292E+07
PP(1,2)	.3416E+07	.5009E+07	.4990E+07	.4933E+07	.4838E+07
MP(1,1)	-.1693E+09	.0000E+00	-.2017E+08	-.4019E+08	-.5991E+08
MP(1,2)	-.1590E+09	-.2332E+09	-.2323E+09	-.2296E+09	-.2252E+09
FP(1,1)	.6797E+07	.0000E+00	.8098E+06	.1614E+07	.2405E+07
PP(2,1)	.3664E+07	.0000E+00	.4366E+06	.8698E+06	.1296E+07
PP(2,2)	.3403E+07	.4991E+07	.4972E+07	.4915E+07	.4821E+07
MP(2,1)	-.1705E+09	.0000E+00	-.2032E+08	-.4048E+08	-.6034E+08
MP(2,2)	-.1578E+09	-.2315E+09	-.2306E+09	-.2279E+09	-.2236E+09
FP(2,2)	.6337E+07	.9291E+07	.9257E+07	.9151E+07	.8976E+07
SIGMA(1)	.1709E+08	.1166E+08	.1270E+08	.1365E+08	.1449E+08
SIGMA(2)	.1705E+08	.1250E+08	.1347E+08	.1434E+08	.1509E+08

W	.2000E+02	.2500E+02	.3000E+02	.3500E+02	.4000E+02
PP(1,1)	.1707E+07	.2109E+07	.2495E+07	.2863E+07	.3208E+07
PP(1,2)	.4707E+07	.4540E+07	.4338E+07	.4103E+07	.3837E+07
MP(1,1)	-.7916E+08	-.9782E+08	-.1157E+09	-.1328E+09	-.1488E+09

MP(1,2)	-.2190E+09	-.2114E+09	-.2019E+09	-.1910E+09	-.1787E+09
FP(1,1)	.3178E+07	.3927E+07	.4646E+07	.5330E+07	.5974E+07
PP(2,1)	.1713E+07	.2117E+07	.2505E+07	.2873E+07	.3220E+07
PP(2,2)	.4690E+07	.4523E+07	.4322E+07	.4088E+07	.3823E+07
MP(2,1)	-.7976E+08	-.9853E+08	-.1166E+09	-.1337E+09	-.1499E+09
MP(2,2)	-.2175E+09	-.2098E+09	-.2004E+09	-.1896E+09	-.1773E+09
FP(2,2)	.8732E+07	.8422E+07	.8049E+07	.7611E+07	.7118E+07
SIGMA(1)	.1523E+08	.1585E+08	.1635E+08	.1672E+08	.1697E+08
SIGMA(2)	.1574E+08	.1626E+08	.1666E+08	.1693E+08	.1707E+08

W	.4500E+02	.5000E+02	.5500E+02	.6000E+02	.6500E+02
PP(1,1)	.3529E+07	.3823E+07	.4088E+07	.4322E+07	.4523E+07
PP(1,2)	.3542E+07	.3220E+07	.2873E+07	.2505E+07	.2117E+07
MP(1,1)	-.1637E+09	-.1773E+09	-.1896E+09	-.2004E+09	-.2098E+09
MP(1,2)	-.1649E+09	-.1499E+09	-.1337E+09	-.1166E+09	-.9857E+08
FP(1,1)	.6570E+07	.7118E+07	.7611E+07	.8047E+07	.8421E+07
PP(2,1)	.3542E+07	.3837E+07	.4103E+07	.4338E+07	.4540E+07
PP(2,2)	.3529E+07	.3208E+07	.2863E+07	.2495E+07	.2109E+07
MP(2,1)	-.1648E+09	-.1786E+09	-.1910E+09	-.2020E+09	-.2112E+09
MP(2,2)	-.1637E+09	-.1488E+09	-.1328E+09	-.1157E+09	-.9782E+08
FP(2,2)	.6571E+07	.5974E+07	.5329E+07	.4646E+07	.3928E+07
SIGMA(1)	.1708E+08	.1707E+08	.1693E+08	.1666E+08	.1626E+08
SIGMA(2)	.1708E+08	.1697E+08	.1672E+08	.1635E+08	.1584E+08

W	.7000E+02	.7500E+02	.8000E+02	.8500E+02	.9000E+02
PP(1,1)	.4690E+07	.4821E+07	.4915E+07	.4972E+07	.4991E+07
PP(1,2)	.1713E+07	.1296E+07	.8698E+06	.4366E+06	.5628E+01
MP(1,1)	-.2175E+09	-.2236E+09	-.2279E+09	-.2306E+09	-.2315E+09
MP(1,2)	-.7972E+08	-.6036E+08	-.4048E+08	-.2032E+08	-.2619E+03
FP(1,1)	.8731E+07	.8977E+07	.9152E+07	.9256E+07	.9291E+07
PP(2,1)	.4707E+07	.4838E+07	.4933E+07	.4990E+07	.5009E+07
PP(2,2)	.1707E+07	.1292E+07	.8667E+06	.4350E+06	.5607E+01
MP(2,1)	-.2191E+09	-.2253E+09	-.2296E+09	-.2323E+09	-.2332E+09
MP(2,2)	-.7916E+08	-.5991E+08	-.4019E+08	-.2017E+08	-.2600E+03
FP(2,2)	.3178E+07	.2405E+07	.1614E+07	.8100E+06	.1044E+02
SIGMA(1)	.1573E+08	.1509E+08	.1434E+08	.1347E+08	.1250E+08
SIGMA(2)	.1523E+08	.1450E+08	.1365E+08	.1270E+08	.1166E+08

19. SADDLE MOUNTED EQUIPMENT

19.1 INTRODUCTION

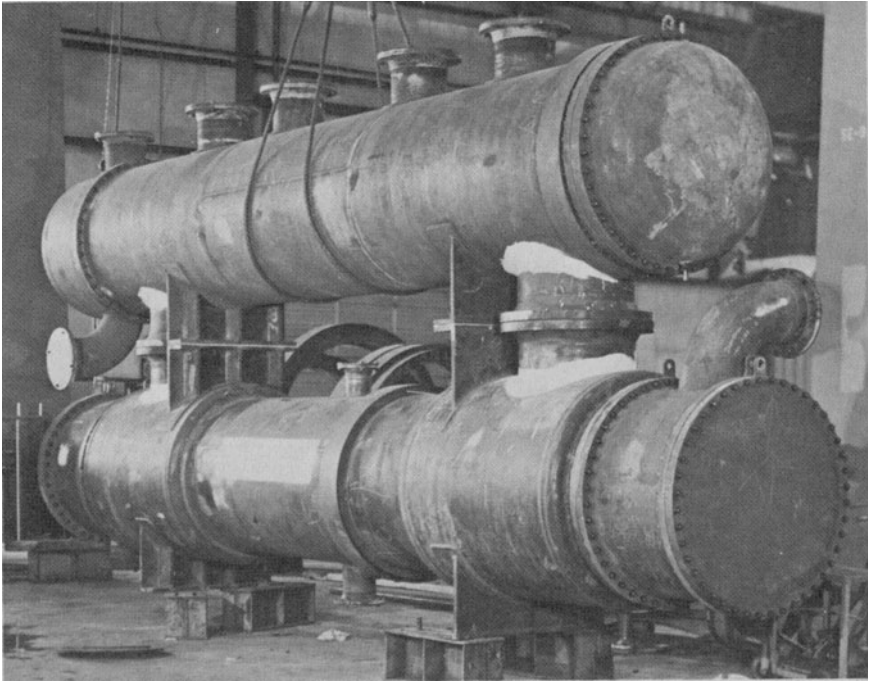
Design data for preliminary sizing of saddles for heat exchangers and pressure vessels was presented in Chapter 17. Saddle mounting is particularly preferable for heat exchangers where frequent tube replacement, or bundle or shell removal, is necessary. Horizontal mounting of the unit, however, suffers from the drawback of requiring additional “tube pull out” space at one end of the heat exchanger. Some of this loss of the available equipment mounting space can be made by stacking the units as shown in Photograph 19.a.

Usually, mounting on two saddles is the common and most favored practice. With only two supports, post-installation settlement of one of the support pedestals does not redistribute the vertical load between the two saddles. Three or more supports do not have this feature; settlement of any one support will cause load re-distribution. However, three supports have been used in long vessels with large length to diameter ratio (over 15). Photograph 19.b shows a fixed tubesheet exchanger on three supports, with longitudinally welded ribs to increase the flexural rigidity of the shell. This is a rather exceptional situation. Most exchangers and pressure vessels are mounted on two saddles and require no axial stiffening. The shell structure near the saddle, however, is sometimes buttressed with one (or two) rings to increase its circumferential stiffness. In general, a saddle supported heat exchanger has a sufficiently high fundamental natural frequency such that it behaves as a rigid body to external disturbances, such as earthquakes. The most critical region usually turns out to be located at the saddle-foundation interface.

Therefore, in this chapter we will develop a simplified method to determine the interfacial concrete pressure, and the foundation bolt stresses for saddle supported pressure vessels. The wide variety of loads acting on a vessel during its operating life may be broadly divided into two categories; namely,

- (i) Time invariant loads; e.g., the operating weight of the equipment and its attached appurtenances.
- (ii) Time variant loads; e.g., wind loads, inertia loads, forces due to seismic disturbances, reactions transmitted through the nozzles from constrained thermal expansion (contraction) of connecting pipe lines, etc.

“Invariant loads” are fairly simple to analyze because they are directed



Photograph 19.a. Stacked recycle condenser for a Gulf Coast petrochemical complex. (Courtesy Industrial Fabricating Co., Tulsa, Okla.)



Photograph 19.b. Fixed tubesheet exchanger mounted on three horizontal saddle supports. (Courtesy Joseph Oat Corporation, Camden, N.J.)

vertically downwards and hence produce only a uniform compressive stress on the foundation. Zick [19.1.1] gives a semi-empirical design procedure for saddle supports under invariant loads. "Time variant loads," on the other hand, are more difficult to treat. These loads arise from a number of effects, and may act coincidentally in numerous combinations. Hence, it is necessary to develop a general method for solution which may be computerized to examine the stresses resulting from each conceivable combination. As stated before, the main consequence of these loads seems to be in modifying the pressure vessel support detail (i.e., the shell is generally designed by dead weight plus pressure loading). Therefore, our attention is focused here on determining the stresses in the foundation bolts, and determining the peak concrete bearing pressure due to an arbitrary set of loadings applied to the pressure vessel. The solution procedure is programmed in the computer code "HORSUP," which is presented in Section 19.6.

A typical pressure vessel supported on two saddles is shown in Fig. 19.1.1. As discussed in Chapter 17, one of the two support base plates has slotted holes to accommodate thermal expansion of the shell. We will identify the two supports as the "fixed support" and the "slotted support", respectively.

In Section 19.2, the support reactions are expressed in terms of the imposed loads. Explicit formulas to correlate the foundation stresses to the support reactions are given in Sections 19.3 and 19.4. Section 19.5 includes an illustrative example and a brief discussion of the method of analysis.

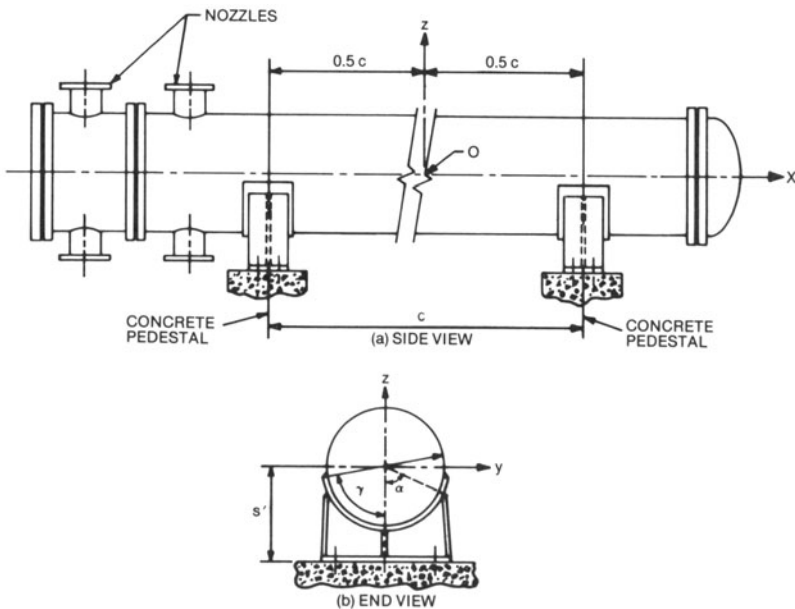


Fig. 19.1.1. A saddle supported heat exchanger.

19.2 DETERMINATION OF SUPPORT REACTIONS

To facilitate analysis, all imposed loads are resolved along the three coordinate axes shown in Fig. 19.1.1. The origin of the coordinate system, O , is located at the vessel centerline midway between the supports. One saddle has slotted holes (elongated in the x -direction) to accommodate longitudinal thermal expansion of the vessel. To fix ideas here, we assume that the “slotted support” is located on the positive x -axis and that the fixed support is located on the negative x -axis. The slotted support is idealized as a frictionless roller in the x -direction that can support moment about the y axis. The fixed support is assumed to be built-in at the foundation.

The first step in the analysis is to transform all loads (forces and moments from nozzle reactions and from seismic acceleration) to the origin of the coordinate system. Program “HORSUP” has the necessary logic to effect such a transformation.

The resulting loads are identified as F_x , F_y , and F_z acting along the x , y and z directions, respectively. The moments are similarly identified as M_x , M_y , and M_z , respectively, with the subscripts indicating their axes in accordance with the conventional “right hand screw rule.” The next step in the analysis lies in obtaining expressions for the foundation reactions due to these applied loads.

Let R_{ij} denote the forces and M_{ij} denote the moments applied on the foundation by the saddle base plate. The first subscript $i = 1$ (or 2) indicates that the reaction acts at the fixed (or slotted) support; and the second subscript, j (1, 2 or 3) indicates the direction of the reactions (x , y or z). Finally, $s + h$ is the height of the x - y plane (Fig. 19.2.1); α is the semi-saddle angle, a is the shell outer radius, and c is the distance between support centerlines.

In most cases of loading, approximate expressions for the reactions on the foundation can be obtained from static equilibrium alone. The results for reactions due to each load is given below.

- (i) Reactions due to F_x : Since support 2 is a frictionless roller, $R_{21} = 0$, therefore, static equilibrium in the x direction yields

$$R_{11} = F_x \quad (19.2.1)$$

The moments M_{12} , M_{22} and the vertical reactions R_{13} , R_{23} due to F_x are also obtained by modeling the heat exchanger as shown in Fig. 19.2.1. The shell is modeled as a rigid beam connected to the saddle support “beams” through rigid links. The saddle support beam extends from the support base plate to the center of gravity of the saddle/shell junction arc. Both supports are assumed to be restrained from rotation (about the y -axis) at the base plate level. These assumptions permit the derivation of the following reactions due to the load F_x .

$$R_{13} = -R_{23} = \frac{\chi h}{c} F_x \left[\frac{0.5 + \beta}{1 + \chi} \right] \quad (19.2.2)$$

$$M_{12} = \frac{F_x h}{2} \left[\frac{1.5 + \chi + \beta}{1 + \chi} \right] \quad (19.2.3)$$

$$M_{22} = \frac{F_x h}{2} \left[\frac{0.5 + \beta}{1 + \chi} \right] \quad (19.2.4)$$

where

$$\beta = s/h \quad (19.2.5)$$

$$\chi = \frac{kc^2 h}{4EI} \quad (19.2.6)$$

In the above results, k is the axial stiffness of the saddle supports. If the axial compliance of the bolts and any “shell pinching” effects are neglected, then

$$k = \frac{A_s E}{h} \quad (19.2.7)$$

A_s is the cross-sectional area of a support and I is the area moment of inertia of the support cross section, considered as a beam bending in the x - z plane. Equations (19.2.2-6) are derived under the assumption that the supports deform as guided cantilever beams under the action of the horizontal loading, and that the shell rotates as a rigid body.

(ii) Reactions due to F_y :

$$R_{12} = R_{22} = 0.5 F_y \quad (a)$$

$$M_{11} = M_{21} = 0.5 F_y (s + h) \quad (b) \quad (19.2.8)$$

(iii) Reactions due to F_z :

$$R_{13} = R_{23} = 0.5 F_z \quad (19.2.9)$$

(iv) Reactions due to M_x :

$$M_{11} = M_{21} = 0.5 M_x \quad (19.2.10)$$

(v) Reactions due to M_y : (Uses the same assumptions as in determining the effect of F_x .)

$$R_{13} = -R_{23} = \frac{\chi M_y}{c(1 + \chi)} \quad (a)$$

$$M_{12} = M_{22} = 0.5 M_y / (1 + \chi) \quad (b) \quad (19.2.11)$$

(vi) Reactions due to M_z :

$$R_{12} = -R_{22} = -\frac{M_z}{c} \quad (19.2.12)$$

The simple expressions for foundation loads derived above belie the true complexity of the problem. They do, however, provide a practical alternative to an otherwise difficult problem. We can also start with a different

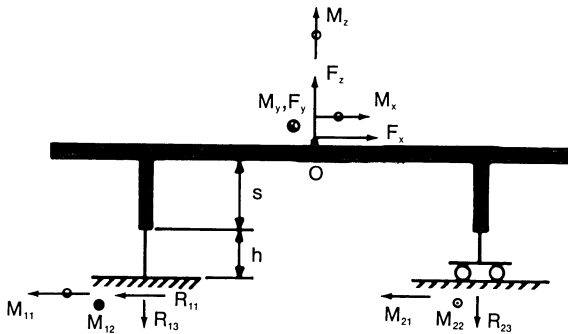


Fig. 19.2.1. “Stick model” for saddle mounted heat exchangers (external load vectors and opposing reactions by the foundation are shown).

set of assumptions, say, rigid saddles and flexible shell beams and arrive at somewhat different results. Similarly, the quality of the results can be improved by taking into account the elasticity of the rotational restraint at saddle supports, and the z -direction flexibility of the support shell junction, and the support-foundation. In most cases, such modifications will produce marginal improvement in the accuracy of the solution which is inherently approximate in nature.

Once we have determined the support reactions as explicit functions of the imposed loads, the next step in our analysis is to develop the relationship between these reactions and the foundation interfacial concrete pressure and bolt stresses.

In the next section, we develop an approximate two dimensional solution for the concrete pressure and associated bolt loads. That is, we restrict our analysis to the foundation response under loads R_{13} and moment M_{12} , for example. The foundation solution for this case can be obtained by examining its behavior in the x - z plane. We could similarly examine the effects of loadings M_{11} and R_{13} causing foundation deformation in the y - z plane. The true solution for foundation pressure under simultaneous application of R_{13} , M_{11} , and M_{12} is not obtained by superposing two 2-D solutions because of the nonlinearity of the problem. Nevertheless, adding the maximum concrete pressures obtained from two 2-D solutions provides a conservative estimate for the true maximum concrete pressure. A similar conservative estimate for the bolt pull can be obtained from the superposition of two 2-D solutions.

19.3 FOUNDATION STRESSES

A typical base plate is shown in Fig. 19.3.1. The base plate is of rectangular shape with a number of bolt lines. We assume that there are n bolt lines parallel to the y -axis. The distance of the i th bolt line from the right edge of the plate is denoted by b_i , $i=1,n$. We assume that a moment M_{12} ($=M$) and vertical thrust R_{13} ($= -W$) are applied on the foundation. The concrete base is assumed to be simulated as a bed of linear springs. Noting

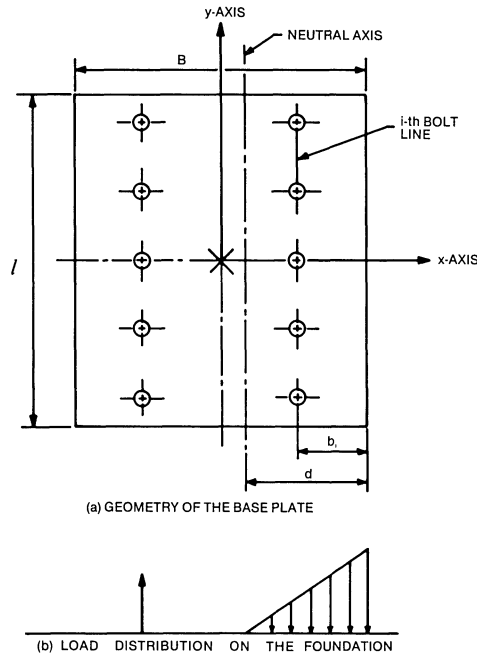


Fig. 19.3.1. Base plate and foundation with applied loads.

that the concrete surface is tensionless, and that the bolts are effective only in tension, we see that it is necessary to determine a neutral axis. Assuming the support base plate to be rigid, the load distribution on the foundation typically looks like Fig. 19.3.1b. Let d denote the distance of the neutral axis from the right edge and p denote the maximum pressure on the concrete. Then, if the location of the bolt lines b_j satisfy the relation

$$b_{j+1} \geq d > b_j, \quad j=0, n \tag{19.3.1}$$

where

$$b_0 = 0 \text{ and } b_{n+1} = B$$

then vertical equilibrium of the loads on the base plate requires that

$$W = \frac{pdl}{2} - \frac{pNA}{d} \sum_{i=j+1}^n (b_i - d) \tag{19.3.2}$$

Furthermore, moment equilibrium requires

$$M + W(d - 0.5B) = \frac{pld^2}{3} + \frac{pNA}{d} \sum_{i=j+1}^n (b_i - d)^2 \tag{19.3.3}$$

In the preceding equations, A is the total tensile stress area available in one bolt line, † and N is the ratio of the Young's modulus of the bolt material to that of the concrete. For common structural bolting material, e.g., A325 or A307, and common grades of concrete, N varies from 10 to 15. We note that to obtain Eqs. (19.3.2), (19.3.3), we have assumed that the bolts behave as linear elastic tension members and that the movement of the baseplate is characterized by a rigid body rotation about the y -axis. The following dimensionless quantities are introduced:

$$\rho_i = \frac{b_i}{B} \quad (a)$$

$$\rho = \frac{d}{B} \quad (b)$$

$$\theta = \frac{NA}{lB} \quad (c)$$

$$p^* = \frac{p}{\Lambda} \quad (d) \quad (19.3.4)$$

$$W^* = \frac{W}{\Lambda l B} \quad (e)$$

$$M^* = \frac{M}{\Lambda l B^2} \quad (f)$$

We note that all parameters in Eq. (19.3.4) are known save for ρ and p^* .

In Eqs. (19.3.4) we have introduced Λ as an arbitrary non-dimensionalizing pressure. Equations (19.3.2) and (19.3.3) cast in terms of the above dimensionless variables, become:

$$W^* = \frac{\rho p^*}{2} - \theta p^* \sum_{i=j+1}^n \frac{1}{\rho} (\rho_i - \rho) \quad (19.3.5)$$

$$M^* + W^*(\rho - 0.5) = \frac{\rho^2}{3} p^* + \theta p^* \sum_{i=j+1}^n \frac{1}{\rho} (\rho_i - \rho)^2 \quad (19.3.6)$$

where

$$\rho_j \leq \rho \leq \rho_{j+1}, \quad j=0, n \quad (19.3.7)$$

†Tensile stress area, A' , of a bolt of nominal diameter D , is defined in the Manual of Steel Construction [19.3.1] as

$$A' = \frac{\pi}{4} \left(D - \frac{0.9743}{n'} \right)^2$$

where n' = number of threads per inch.

Equations (19.3.5), (19.3.6) are two non-linear equations involving the unknown concrete pressure parameter p^* and the unknown location of the neutral axis (here characterized by the parameter ρ). Once we determine the neutral axis, the bolt load in line i is determined from the relation

$$T_i = \frac{pNA}{d} (b_i - d)$$

for values of i such that $b_i > d$.

Equations (19.3.5) and (19.3.6) can be combined to yield the single following non-linear equation in terms of ρ only:

$$(0.5 \rho^2 - \theta\omega) [M^* + W^*(\rho - 0.5)] - W^* \left(\frac{1}{3} \rho^3 + \theta\beta \right) = 0 \quad (19.3.8)$$

where the parameters ω , β are defined as

$$\omega = \sum_{i=j+1}^n (\rho_i - \rho) \quad (19.3.9)$$

$$\beta = \sum_{i=j+1}^n (\rho_i - \rho)^2 \quad (19.3.10)$$

Equation (19.3.8) is solved for ρ subject to the inequality (19.3.7).

The value of Λ used seems to directly affect the convergence of the solutions. As a general rule, keeping Λ below the anticipated value of peak concrete pressure ensures convergence.

Having thus determined the location of the neutral axis (ρ), the peak interfacial concrete pressure p is directly obtained from Eq. (19.3.6). The maximum bolt tensile stress is given by

$$\sigma_n = \frac{1}{d} Np (b_n - d) \quad (19.3.11)$$

It is obvious from physical considerations that the solution of Eq. (19.3.8), within the physically meaningful range ($0 < \rho < 1$), can be found only for a limited range of values W and M . Beyond this range, a neutral axis may not exist. Instead, one of the following two conditions may obtain

- (i) *Edging*: For large values of M , and relatively small W , the entire base plate lifts off the foundation and presses the concrete on one of its edges. This situation will occur when ρ in Eq. (19.3.8) approaches zero. Accordingly, the following relation between M and W will correspond to the onset of edging:

$$M = \frac{W(0.5B\sum b_i - \sum b_i^2)}{\sum b_i} \quad (19.3.12)$$

It should be realized that the above equation is a necessary, but not a sufficient, condition for the edging occurrence.

We can show that the maximum stress in the bolts for the edging condition is given by

$$\sigma_n = \frac{b_n (M - 0.5WB)}{A \Sigma b_i^2} \quad (19.3.13)$$

The maximum concrete pressure is mathematically infinite for the edging case.

- (ii) *Complete compression:* This case exists when the overturning moment is small relative to the vertical load W . In this case, it is clear that the pressure distribution is trapezoidal; we can show that the extremal magnitudes of the trapezoidal distribution are given by

$$p = \frac{W}{Bl} \pm \frac{6M}{lB^2} \quad (19.3.14)$$

We note from Eq. (19.3.13) that, in order that tension may exist in all the bolts, the following dimensionless conditions must be satisfied,

$$W^* < 2M^* \quad (19.3.15)$$

Furthermore, in order that some concrete be in compression, it is required that (via Eq. (19.3.14)), the dimensionless parameters W^* , M^* , must satisfy

$$W^* > 6M^* \quad (19.3.16)$$

It turns out that Eq. (19.3.16) is both a necessary and sufficient condition for complete compression.

19.4 AN EXAMPLE

We consider the case of a foundation base plate with an applied vertical load $W = 5,000$ lb. and a variable overturning moment which ranges from 50,000 lb. inch to 110,000 lb. inch. The geometric parameters are

$$B = 10''; \quad l = 40''; \quad n = 2; \quad b_1 = 2''; \quad b_2 = 8''; \quad A = 2 \text{ sq. in.}$$

The above information is all that is needed to be input to run the subroutine FOUND in the code HORSUP. The maximum concrete pressure p , and the neutral axis parameter ρ are calculated, and are plotted as functions of the applied moment in Fig. 19.4.1. In Section 19.6, we present complete details of "HORSUP." The application of HORSUP to seismic analysis of saddle mounted pressure vessels is presented in [19.4.1].

19.5 BOLT LOAD – RIGID FOUNDATION

If we make the assumption that the concrete is rigid, so that edging always occurs, then simple algebraic expressions for the pull on the anchor bolts can be derived. With the additional assumption of a rigid foundation, we can directly treat the 3-D problem. Figure 19.5.1 shows a rigid rectangular plate of dimensions B and l , subject to a vertical force F , and two

orthogonal moments M_1 and M_2 . Suppose physical reasoning establishes A as the anchor point. We assume that there are m identical anchor bolts where the coordinates of bolt i , with respect to the coordinate system of Fig. 19.5.1 (which has A as origin), are given by (x_i, y_i) . If we now assume that the bolts behave as linear elastic springs, the pull in bolt i is given by

$$P_i = \alpha_1 x_i + \alpha_2 y_i \quad (19.5.1)$$

where α_1 and α_2 are unknown constants to be determined from equilibrium.

Moment equilibrium about the x -axis yields

$$M_1 + \frac{Fl}{2} = \sum_m P_i y_i$$

Substituting for P_i from Eq. (19.5.1), we have

$$M_1 + \frac{Fl}{2} = \alpha_1 a_2 + \alpha_2 a_3 \quad (19.5.2)$$

where we have used the abbreviation

$$a_2 = \sum_m x_i y_i$$

$$a_3 = \sum_m y_i^2 \quad (19.5.3)$$

Similarly, moment equilibrium about the y -axis yields

$$M_2 + F \frac{B}{2} = \sum P_i x_i$$

$$\text{or } M_2 + \frac{FB}{2} = \alpha_1 a_1 + \alpha_2 a_2 \quad (19.5.4)$$

where

$$a_1 = \sum_m x_i^2 \quad (19.5.5)$$

From Eq. (19.5.2) and (19.5.4), we can solve for α_1, α_2 , and obtain

$$\alpha_1 = \frac{M_2 a_3 - M_1 a_2 + 0.5F(a_3 B - a_2 l)}{(a_1 a_3 - a_2^2)} \quad (19.5.6)$$

$$\alpha_2 = \frac{M_1 a_1 - M_2 a_2 + 0.5F(a_1 l - a_2 B)}{(a_1 a_3 - a_2^2)} \quad (19.5.7)$$

Thus the tension in all bolts is determined using Eqs. (19.5.6), (19.5.7), in Eq. (19.5.1).

The contact load, F_c , at the anchor point is then given by the z force equilibrium relation

$$F_c = \Sigma P_i = \alpha_1 \Sigma x_i + \alpha_2 \Sigma y_i \tag{19.5.8}$$

We see that the assumption of both a rigid baseplate and a rigid foundation permits the problem to be reduced to a linear form. The inclusion of foundation elasticity (Section 19.3) makes the problem inherently non-linear.

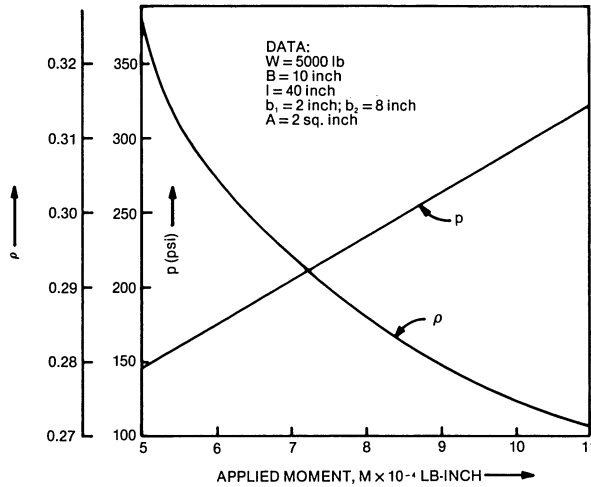


Fig. 19.4.1. Variation of neutral axis location and maximum concrete pressure with the applied loads.

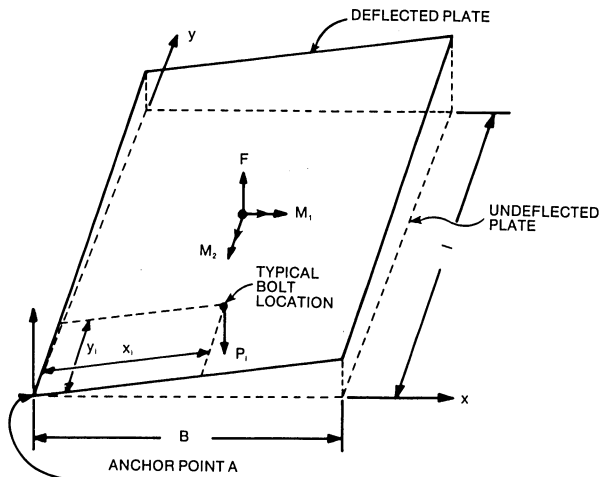


Fig. 19.5.1. Rigid base plate subject to bi-planar loading.

19.6 COMPUTER CODE HORSUP

HORSUP computerizes the analyses presented in the preceding sections. The nozzle loads are assumed to act at N discrete locations. The loading on each nozzle consists of six components; three forces and three shears. These loads are specified in the local coordinate system of each nozzle. Angle BETA in Fig. 19.6.1 characterizes the included angle between the local coordinate system (axis y') and the global system (axis y). The axes of all nozzles are assumed to lie in planes perpendicular to the shell axis (x -axis). "ALPHA" denotes the angle that the radial coordinate to the root of the local coordinate system makes with the x - y plane.

The seismic loads can be treated as another "nozzle load" by inputting as a set of orthogonal loads located at the origin of the coordinate system.

The program computes the overturning moment and axial force at both supports and determines the maximum concrete pressure and bolt stress. The maximum stress in the support is also printed out.

The subroutine FOUND in HORSUP computes the maximum pedestal bearing pressure and the maximum bolt stress for a vertical load and moment loading in one principal plane only. Therefore, the subroutine is called with R_{13} and M_{12} as the applied loads on the support. Next the subroutine computes the maximum bolt pull due to M_{11} alone. The total concrete peak pressure and bolt stress are obtained by adding the results from the two loadings. This procedure gives a fair estimate of the unit support/foundation interface response.

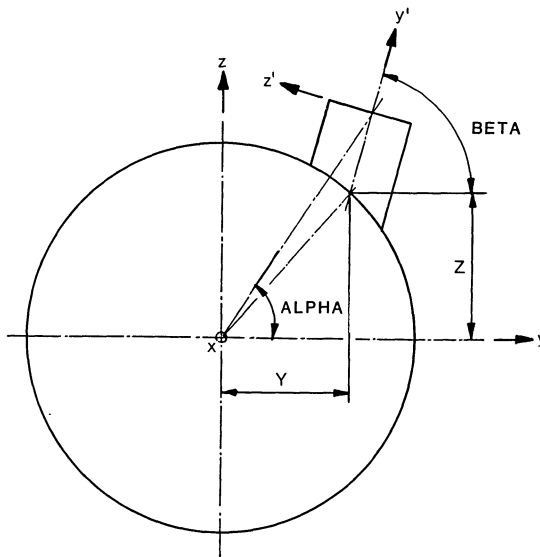


Fig. 19.6.1. Notation for HORSUP.

Table 19.6.1. Input Data for HORSUP (All input is in free field format)

Line 1: Heading card (any 80 alpha-numeric)

Line 2:

Item	Fortran Symbol
Distance between support center lines	C
Height of shell axis	H
Outer radius of shell	A
Semi-saddle angle	GAMMA
Number of discrete load locations	N
Index (equal to 0; terminate program equal to 1, continue with the next run)	K
Young's Modulus times the moment of inertia of the support beam cross section for bending about <i>y</i> -axis	EI
Axial flexibility of the root of the support (assumed to be equal for both supports)	SUPFLEX
<i>Line 3:</i> (Refer to Fig. 19.6.1 for this line)	
<i>x</i> -coordinate of applied load	X
<i>y</i> -coordinate of applied load	Y
<i>z</i> -coordinate of applied load	Z
Inclination of local load axis	BETA
<i>x</i> -local force vector (shear force)	FX
<i>y</i> -local force vector	FY
<i>z</i> -local force vector	FZ
<i>x</i> -local moment vector	AMX
<i>y</i> -local moment vector	AMY
<i>z</i> -local moment vector	AMZ
Repeat line 3 N times; one line for each nozzle.	
<i>Line 4</i>	
Data for bending of support due to <i>y</i> -moment vector and vertical load	
Axial width of support base	B
Lateral width of support base	L
Tensile stress area of bolts in one load line (Fig. 19.3.1)	AREA
Number of bolt lines perpendicular to the plane of rotation (i.e. in <i>x</i> direction)	NN
Distance of bolt line <i>i</i> from the edge, <i>i</i> = 1,2, . . . NN, (<i>b_i</i> in Fig. 19.3.1)	BB(I)
<i>Line 5</i>	
Data for rotation in <i>y-z</i> plane. (<i>x</i> -moment vector)	
Lateral width (<i>y</i> -direction) of support baseplate	B
Axial width (<i>x</i> -direction) of support baseplate	L
Total stress area of one bolt line	AREA
Number of bolt lines in <i>y</i> -direction	NN
Distance of bolt line <i>i</i> from the edge of rotation, <i>i</i> = 1,2 . . . NN	BB(I)

A Listing of HORSUP is given at the end of the chapter.

19.7 STRESS LIMITS FOR THE CONCRETE PEDESTAL AND ANCHOR BOLTS

The stress limits of the Manual of Steel Construction [19.3.1] are widely used in prescribing the value of bearing stress on the concrete pedestal, and anchor bolt direct and shear stresses.

(i) *Concrete pedestal:*

The maximum bearing stress p_{\max} should meet the inequality

$$p_{\max} \leq 0.35f_c' (A_2/A_1)^{1/2} \leq 0.7f_c' \quad (19.7.1)$$

where

- f_c' = Specified compressive strength of concrete, psi
 A_2 = Full cross-sectional area of the pedestal, sq. in.
 A_1 = Bearing area, sq. in.

(ii) *Anchor Bolts:*

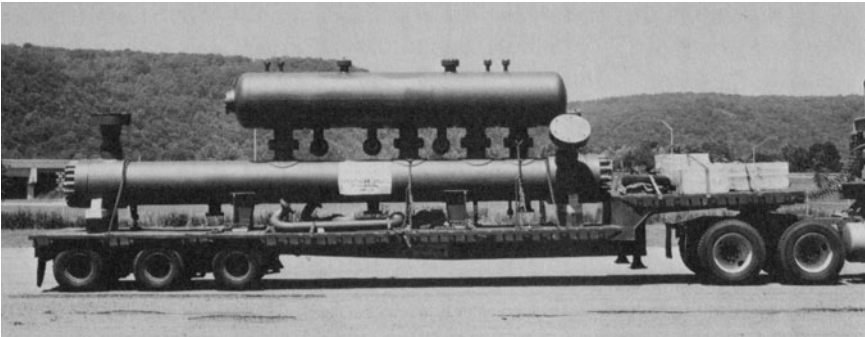
The most common anchor bolt material is ASTM-A307. The limits on bending stress σ_b and shear stress σ_s for A307 bolts are:

$$\sigma_b \leq 26000 - 1.8 \sigma_s \leq 20,000 \quad (19.7.2)$$

$$\sigma_s \leq 10,000 \text{ psi} \quad (19.7.3)$$

Sometimes higher strength bolts, e.g., A325 or A490 are also used. The reader is referred to the Manual of Steel Construction [19.3.1] for design stress data and restriction on their use.

The above stress limits for bolts and concrete are intended for design and live loads, but exclude wind and seismic loads. The code permits increasing the allowables by 33% when wind and seismic loads are present.



Photograph 19.c. Ammonia synthesis loop steam generator with a stack mounted de-entrainment vessel; 5000 psig channel pressure. Stacked saddle mounting of this unit is dictated by performance considerations. (Courtesy Struthers Wells Corp., Warren Pa.)

NOMENCLATURE

- a = Shell outer radius
 A = Tensile stress area in one bolt line (Fig. 19.3.1)
 B = Width of base plate
 b_i = Distance of i th bolt line (Fig. 19.3.1)
 c = Distance between support centerlines
 d = Distance of the neutral axis from edge of plate

- F_x, F_y, F_z = Applied load vectors at the origin of the coordinate system (Fig. 19.2.1)
 h = Length of rigid link (Fig. 19.2.1)
 l = Length of saddle base plate
 M = Applied moment
 M_x, M_y, M_z = Applied moment vectors
 M_{ij} = Moment at i th support in the j th direction
 M^* = Dimensionless moment
 N = Ratio of Young's moduli of anchor bolts to that of concrete
 n = Number of bolt lines
 p = Peak concrete pressure
 R_{ij} = Reaction at i th support in the j th direction
 s = Length of rigid link (Fig. 19.2.1)
 W = Vertical load
 W^* = Dimensionless vertical load
 ρ = Dimensionless distance of neutral axis
 Λ = Non-dimensional pressure parameter
 α = Semi-saddle angle (Fig. 19.1.1)

REFERENCES

- [19.1.1] Zick, L. P., "Stresses in Large Horizontal Cylindrical Pressure Vessels on Two Saddle Supports," *Pressure Vessel and Piping; Design and Analysis*, Vol. 2, pp. 959-970, ASME, New York (1972).
 [19.3.1] "Manual of Steel Construction," American Institute of Steel Construction, Eighth Edition, Chicago (1980).
 [19.4.1] Singh, K. P., and Soler, A. I., "HEXDES User Manual," Arc-turus Publishers Inc., Cherry Hill, N.J. (1984).

PROGRAM HORSUP

```

C   BY K.P. SINGH AND V. LUK, REV 0 (DECEMBER 1983)
C
C   *****
C   OBJECTIVE:
C     TO CALCULATE STRESSES AT SUPPORTS OF HORIZONTAL HEAT EXCHANGERS
C
C   DEFINITIONS:
C     C       : DISTANCE BETWEEN SUPPORT CENTERLINES
C     H       : HEIGHT OF THE CENTERLINE OF SHELL ABOVE GROUND
C     A       : SHELL OUTER RADIUS
C     GAMMA   : SEMI-SADDLE ANGLE
C     FX, FY, FZ : APPLIED LOAD VECTORS
C     MX, MY, MZ : APPLIED MOMENT VECTORS
C     MIJ     : REACTION MOMENT AT I-TH SUPPORT IN J-TH DIRECTION
C               (I=1 FOR FIXED SUPPORT AND I=2 FOR SLOTTED SUPPORT)
C     RIJ     : REACTION LOAD AT I-TH SUPPORT IN J-TH DIRECTION
  
```

```

C      X,Y,Z      : LOCATION OF THE APPLIED LOAD OR MOMENT
C      ALPHA      : ANGLE OF INCLINATION OF LOAD LOCATION
C      BETA       : PHASE ANGLE OF LOCAL COORDINATE SYSTEM
C      N          : NO. OF LOCATIONS FOR APPLICATION OF LOAD AND MOMENT
C      K          : INDEX COUNT
C                  ( K=0: TERMINATE THE PROGRAM
C                  K=1: CONTINUE WITH ANOTHER RUN )
C      EI         : YOUNG'S MODULUS TIMES THE MOMENT OF INERTIA OF THE
C                  SUPPORT BEAM CROSS SECTION FOR BENDING ABOUT Y-AXIS
C      SUPFLEX    : AXIAL FLEXIBILITY OF THE ROOT OF THE SUPPORT
C                  (ASSUMED TO BE EQUAL FOR BOTH SUPPORTS)
C      *****
C
C      REAL M11,M12,M21,M22
C      REAL L,M
C      DIMENSION HEAD(20),BBI(10)
C
C      ***INPUT JOB TITLE***
C
C      20 READ(5,100) (HEAD(I),I=1,20)
C
C      ***DISPLAY TITLE AND DATE***
C
C      WRITE(6,110) (HEAD(I),I=1,20)
C
C      ***INPUT PHYSICAL DIMENSIONS, LOADS AND MOMENTS***
C
C      READ(5,*) C,H,A,GAMMA,N,K,EI,SUPFLEX
C      WRITE(6,130) C,H,A,GAMMA,EI,SUPFLEX
C      SS=A*SIN(GAMMA)/GAMMA
C      HH=H-SS
C      WRITE(6,140)
C      SFX=0.
C      SFY=0.
C      SFZ=0.
C      SMX=0.
C      SMY=0.
C      SMZ=0.
C      BET=SS/HH
C      CHAI=C*C*HH*SUPFLEX/(4.*EI)
C      DO 10 I=1,N
C          READ(5,*) X,Y,Z,BETA,FX,FY,FZ,AMX,AMY,AMZ
C          WRITE(6,150) I,X,Y,Z,BETA,FX,FY,FZ,AMX,AMY,AMZ
C          D=SQRT(Y*Y+Z*Z)
C          IF (D.EQ.0) GO TO 30
C          ALPHA=ASIN(Z/D)
C          GO TO 35
C      30 ALPHA=0.
C
C      ***TRANSFER LOCAL LOADS TO THE SHELL CENTERLINE***
C
C      35 CALL TRANS (D,ALPHA,BETA,FX,FY,FZ,AMX,AMY,AMZ)

```

```

C
C   ***TRANSFER ALL LOADS TO THE ORIGIN OF COODINATE SYSTEM***
C
      SFX=SFX+FX
      SFY=SFY+FY
      SFZ=SFZ+FZ
      SMX=SMX+AMX
      SMY=SMY+AMY-FZ*X
10   SMZ=SMZ+AMZ+FY*X
      WRITE(6,160)

C
C   ***CALCULATE REACTIONS AT SUPPORTS***
C
      H1=H-A*SIN(GAMMA)/GAMMA
      R11=SFX
      R12=0.5*SFY-SMZ/C
      R13=0.5*SFZ+SFX*HH*CHAI*(0.5+BET)/(C*(1.+CHAI))+SMY*CHAI
1    /(C*(1.+CHAI))
      R21=0.
      R22=0.5*SFY+SMZ/C
      R23=-R13
      M11=-0.5*(SFY*H-SMX)
      M12=0.5*SMY/(1.+CHAI)+0.5*SFX*HH*(1.5+BET+CHAI)/(1.+CHAI)
      M21=M11
      M22=(0.5*SMY/(1.+CHAI))+0.5*SFX*HH*(0.5+BET)/(1.+CHAI)
      WRITE(6,170) R11,R12,R13,M11,M12
      WRITE(6,180) R21,R22,R23,M21,M22
      WRITE(6,190)
      SUMP=0.
      SSIGMA=0.
      DO 50 I=1,2
      READ(5,*) B,L,AREA,NN,(BBI(J),J=1,NN)
      IF (1.EQ.2) GO TO 40
      WD=-R13
      AM=ABS(M12)
      GO TO 45
40   WD=0.
      AM=ABS(M11)
45   CALL FOUND (B,L,AREA,NN,BBI,WD,AM,P,SIGMA)
      SUMP=SUMP+P
50   SSIGMA=SSIGMA+SIGMA
      WRITE(6,200) SUMP,SSIGMA

C
C   ***FORMATS FOR INPUT AND OUTPUT STATEMENTS***
C
100  FORMAT(20A4)
110  FORMAT(1H1,5X,20A4)
120  FORMAT(//,5X,A27)
130  FORMAT(//,5X,"I N P U T   D A T A",/,5X,30("--"),//,
      1 5X,"DISTANCE BETWEEN SUPPORT CENTERLINES (C) =",F7.2," (IN)",/,
      2 5X,"HEIGHT OF SHELL CENTERLINE ABOVE GROUND (H) =",F6.2,
      3 " (IN)",/,5X,"SHELL OUTER RADIUS (A) =",F6.2," (IN)",/,

```

```

4 5X,"SEMI-SADDLE ANGLE (GAMMA) =",F6.3," (RAD)",/,5X,
5 "PRODUCT OF YOUNG'S MODULUS AND M.I. OF SUPPORT",/,5X,
6 "BEAM CROSS-SECTION FOR BENDING ABOUT Y-AXIS      =",E12.4,
7 " (LB-IN*IN)",/,5X,"AXIAL FLEXIBILITY OF ROOT OF SUPPORT =",
8 E12.4," (LB/IN)"//)
140 FORMAT(/,5X,"1",4X,"X",5X,"Y",5X,"Z",3X,"BETA",6X,"FX",7X,"FY",
1 7X,"FZ",7X,"MX",7X,"MY",7X,"MZ",/,9X,"(IN)",2X,"(IN)",2X,
2 "(IN)",1X,"(RAD)",4X,"(LB)",5X,"(LB)",5X,"(LB)",3X,"(IN-LB)",
3 2X,"(IN-LB)",2X,"(IN-LB)"//)
150 FORMAT(/,4X,I2,1X,F6.1,1X,F5.1,1X,F5.3,1X,F8.0,5(1X,F8.0))
160 FORMAT(/,5X,30("--"),//)
170 FORMAT(/,5X,"REACTIONS AT THE FIXED SUPPORT:",//,
1 5X,"RX =",F10.1," (LB)",/,5X,"RY =",F10.1," (LB)",/,
2 5X,"RZ =",F10.1," (LB)",/,5X,"MX =",F10.1," (IN-LB)",/,
3 5X,"MY =",F10.1," (IN-LB)"//)
180 FORMAT(/,5X,"REACTIONS AT THE SLOTTED SUPPGRT:",//,
1 5X,"RX =",F10.1," (LB)",/,5X,"RY =",F10.1," (LB)",/,
2 5X,"RZ =",F10.1," (LB)",/,5X,"MX =",F10.1," (IN-LB)",/,
3 5X,"MY =",F10.1," (IN-LB)"//)
190 FORMAT(/,5X,"** THE STRESSES AT THE FIXED SUPPORT ARE TABULATED IN
1 THE FOLLOWING **")
200 FORMAT(/,5X,"** TOTAL CONCRETE PRESSURE =",F8.2," (PSI)",
1 //,5X,"** TOTAL BOLT STRESS =",F8.2," (PSI)")

```

C

```

IF(K.EQ.1) GO TO 20
STOP
END

```

C

C

C

```

SUBROUTINE TRANS (D,ALPHA,BETA,FX,FY,FZ,AMX,AMY,AMZ)
THETA=ALPHA-BETA
FYP=FY*COS(BETA)-FZ*SIN(BETA)
FZP=FY*SIN(BETA)+FZ*COS(BETA)
AMX=AMX-D*(FY*SIN(THETA)-FZ*COS(THETA))
AMYP=AMY*COS(BETA)-AMZ*SIN(BETA)+D*FX*SIN(ALPHA)
AMZ=AMY*SIN(BETA)+AMZ*COS(BETA)-D*FX*COS(ALPHA)
FY=FYP
FZ=FZP
AMY=AMYP
RETURN
END

```

C

C

C

```

SUBROUTINE FOUND (B,L,A,N,BBI,WD,AM,P,SIGMA)
REAL L,M
DIMENSION BI(10),BBI(10)
COMMON NA1,NA2,RHO,RHOI(10),ALPHA,BETA,M,W,FUN,THETA
W=WD
M=AM

```

```

NA1=N+1
NA2=N+2
BI(1)=0.
DO 5 I=2,NA1
J=I-1
5 BI(I)=BBI(J)
BI(NA2)=B
S=10.
EN=10.
THETA=EN*A/(L*B)
DO 100 I=1,NA2
100 RHOI(I)=BI(I)/B
WRITE(6,700) B,L,A,W,M,(BI(I),I=2,NA1)
C ***NON-DIMENSIONAL TERMS***
W=W/(S*L*B)
M=M/(S*L*B*B)
C ***CHECK FOR COMPLETE COMPRESSION***
IF(W.LE.0.) GO TO 120
IF(W-3.*M) 120,110,110
110 WRITE(6,705)
P=S*(W+3.*M)
SIGMA=0.
WRITE(6,706) P,SIGMA
GO TO 900
C ***SEARCH FOR POSSIBLE ROOTS***
120 CONTINUE
RHO=0.005
CALL FSUM
CALL FUNCT
FCTOLD=FUN
RHO=-0.005
DO 300 I=1,20
RHO=RHO+0.05
CALL FSUM
CALL FUNCT
FCT=FUN
IF(FCT*FCTOLD) 350,450,300
300 FCTOLD=FCT
C ***EDGING OCCURS HERE***
WRITE(6,707)
SUM=0.
DO 330 I=1,N
330 SUM=SUM+BBI(I)**2
P=0.
SIGMA=S*L*RHOI(NA1)*B**3*(M-0.5*W)/(A*SUM)
WRITE(6,706) P,SIGMA
GO TO 900
C ***APPLY METHOD OF SECANTS***
350 R1=RHO-0.05
R2=RHO
F1=FCTOLD
F2=FCT

```

```

DO 400 I=1,30
RHO=R2-F2*(R2-R1)/(F2-F1)
CALL FSUM
CALL FUNCT
IF(ABS(FUN-F2).LT.1.0E-6) GO TO 450
R1=R2
R2=RHO
F1=F2
400 F2=FUN
450 D=RHO*B
P=S*RHO*(M+W*(RHO-0.5))/((RHO**3)/3.+THETA*BETA)
SIGMA=EN*P*(RHOI(NA1)*B/D-1.)
WRITE(6,704) D,P,SIGMA,FUN
C ***FORMATS FOR OUTPUT STATEMENTS***
700 FORMAT(/,5X,"BASE PLATE WIDTH =",F8.3," (IN)",/,5X,
1 "BASE PLATE LENGTH =",F8.3," (IN)",/,5X,
2 "BOLT TENSILE STRESS AREA =",F7.3," (SQ IN)",/,5X,
3 "VERTICAL DOWNWARD FORCE =",F11.2," (LB)",/,5X,
4 "BENDING MOMENT =",F11.2," (IN-LB)",/,5X,
5 "BOLT LINES AT (IN) :",10(F7.3,3X))
704 FORMAT(/,5X,"NEUTRAL AXIS AT",F7.3," (IN)",/,5X,
1 "MAXIMUM CONCRETE PRESSURE =",F8.2," (PSI)",/,5X,
2 "MAXIMUM BOLT STRESS =",F8.2," (PSI)",/,5X,
3 "RESIDUAL =",E11.3,/, "-----",/)
705 FORMAT(/,5X,"COMPLETE COMPRESSION")
706 FORMAT(/,5X,"NO NEUTRAL AXIS",/,5X,
1 "MAXIMUM CONCRETE PRESSURE =",F8.2," (PSI)",/,5X,
2 "MAXIMUM BOLT STRESS =",F8.2," (PSI)",/,
3 "-----",/)
707 FORMAT(/,5X,"EDGING OCCURS")
900 RETURN
END
C
C *****
C
SUBROUTINE FSUM
REAL M
COMMON NA1,NA2,RHO,RHOI(10),ALPHA,BETA,M,W,FUN,THETA
DO 100 J=1,NA2
IF(RHO.LT.RHOI(J)) GO TO 110
100 CONTINUE
RETURN
110 SUM1=0.
SUM2=0.
DO 200 I=J,NA1
DIF=RHOI(I)-RHO
SUM1=SUM1+DIF
200 SUM2=SUM2+DIF*DIF
ALPHA=SUM1
BETA=SUM2
RETURN
END

```

C
C
C

```
      SUBROUTINE FUNCT
      REAL M
      COMMON NA1,NA2,RHO,RHOI(10),ALPHA,BETA,M,W,FUN,THETA
      FUN=(0.5*RHO*RHO-THETA*ALPHA)*(M+W*(RHO-0.5))
1     -W*((RHO**3)/3.+THETA*BETA)
      RETURN
      END
```

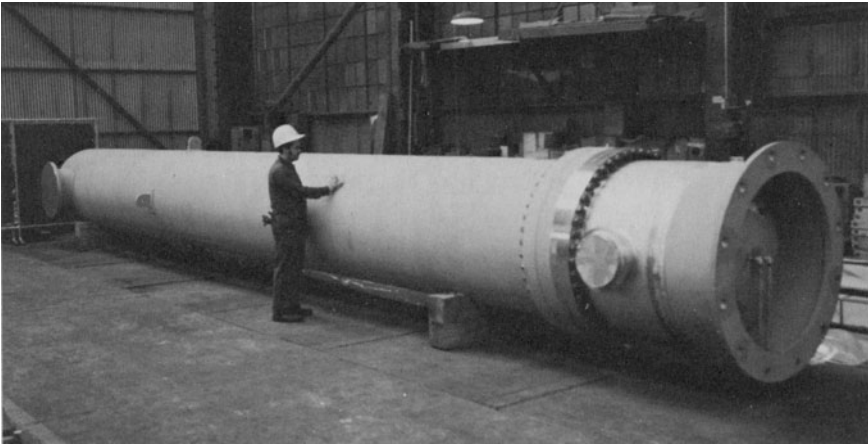
20. EXTERNAL LOADS ON VERTICALLY MOUNTED EQUIPMENT

20.1 INTRODUCTION

Heat exchangers and pressure vessels are frequently mounted vertically to economize plant floor space. In some cases, the process function of the hardware requires vertical installation. For example, gravity driven boiling in a thermosiphon reboiler, or fractionation in a distillation column, can proceed only if the equipment is vertically installed. As discussed in Chapter 17, the supports may consist of a skirt, a set of lugs, or a ring-type structure at (or near) the bottom and a lateral restraint near the top. Photograph 20.a shows a skirt mounted unit with a lateral support at the top. Figure 20.1.1 shows a skirt mounted unit without a top lug. Preliminary design data on sizing supports for vertical mounting is given in Chapter 17. However, it is subsequently necessary to determine the adequacy of the preliminary design for external loads. The external loadings on such equipment arise from various sources such as from wind load, from seismic motion, and from reactions due to attached piping. In its most simplified form, a seismic loading is specified as a set of static inertial accelerations in three orthogonal directions (two horizontal and one vertical). A precise specification of loads on the vessel nozzles from inter-connecting piping is more problematic, since piping design is usually not complete at the time of equipment procurement. This problem is usually circumvented by postulating a set of loads for each nozzle and by requiring that the plant designer route the piping to maintain the loads on the equipment-piping interface to within these limits. Thus the process of equipment and piping design can proceed concurrently. The piping load can be prescribed in terms of six vectorial components; three forces and three moments. The sense of action of these loads is not specified.

Our first task, therefore, is to determine the sense of action of these loads such that the applied loading on the equipment to be designed is maximized. The support reactions serve as meaningful references for this purpose. In the next section, a method to maximize the support response is symbolically described. The solution procedure is built into a computer program "VERSUP" which is also presented in this chapter.

Of course, the problem of incompletely defined nozzle reactions is not confined to skirt or lug mounted vessels. Horizontally mounted equipment (Chapter 19) or vessels supported on four-legs (Chapter 18) also suffer from the same lack of precise load information at the design stage. The method of maximization of support reactions presented here in the context of skirt



Photograph 20.a. Heat exchanger with skirt mounting, and lateral seismic lugs. (Courtesy Joseph Oat Corporation, Camden, N.J.)

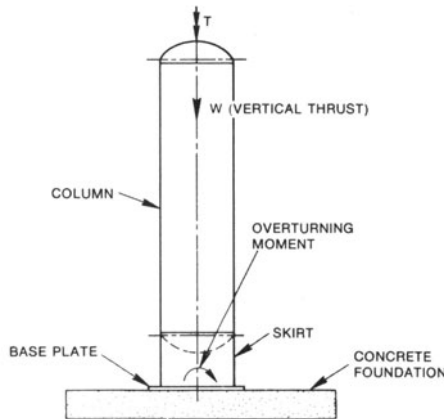


Fig. 20.1.1. Vertically mounted equipment under vertical load and overturning moment.

mounted equipment is also valid for other support configurations. The actual “influence coefficients” (defined later), however, will be different.

External load analysis of pressure vessels follows a two track approach: The support reactions are determined by modeling the pressure vessel as a beam; subsequently, the support-shell interaction is studied by examining the local shell-like behavior of the vessel. Thus, away from support/shell junctions, the pressure vessel is assumed to respond as a “beam”. The beam flexural stresses induced in the shell are classified as “primary membrane stress” (see Chapter 2). The stresses developed at the support/shell junction are classified as local membrane and bending stresses. Local bending stress

is often referred to as a secondary stress. Some common techniques for evaluating these local effects have been presented in Chapter 17. Therefore, our task in this chapter consists of devising suitable analytical techniques to express the maximum support reactions in terms of specified external loads, including nozzle loads, seismic loads, and wind loads.

Finally, we point out that the state of stress at the interface between the equipment support and the external support structure is a matter of design interest to both the equipment designer and the architect/engineer. This subject has been considered in Chapter 17 for some typical support configurations. The problem of interface loads has also been taken up in Chapter 19 for the case of saddle supports. In this chapter, similar results for skirt supports are derived assuming reinforced concrete support. The case of an annular (skirts or ring-type supports) bearing surface on a less pliable material such as one built from structural steel has been treated in Chapter 17.

In the next section, the methodology to maximize *one* component of the support reaction by determining the required *sense of action* of the applied nozzle loads is described. The vertical equipment is assumed to have two supports; one located near the bottom of the vessel, and the other one located near the top. The vessel may project beyond the top support, and there may be an arbitrary number of nozzles located along the vessel. We will model each support with a linear and a rotational spring. By varying the spring constants of these springs, a variety of cases can be treated. For example, setting the support springs at location B in Fig. 20.1.2 to be very small simulates the case of a vessel cantilevered from its base (location A). The skirt-lug combination is usually associated with a vertical orientation of the vessel centerline.

A heat exchanger or a pressure vessel mounted on a lower skirt, and having upper lug or ring type supports satisfying the mathematical model of Fig. 20.1.2, can be analyzed using the computer program “VERSUP”. The use of this program will be illustrated later by considering a typical design configuration.

20.2 MAXIMIZATION OF SUPPORT REACTION

The vertical equipment is modeled as a uniform beam having two supports (Fig. 20.1.2). Supports at locations A and B have linear and rotational springs. The spring constants, K_1 , C_1 (at support A) and K_2 , C_2 , (at support B) can be varied to simulate a wide variety of support conditions. The equipment is assumed to have n nozzles located at elevations d_k , $k = 1, 2, \dots, n$. As shown in Fig. 20.2.1, the nozzle axis lies in the horizontal plane at elevation d_k . The location of the nozzle intersection with the vessel wall is specified by the angle θ_k , measured from the global y axis, while the orientation of the nozzle axis is set by the angle ϕ_k also measured with respect to the global y axis.

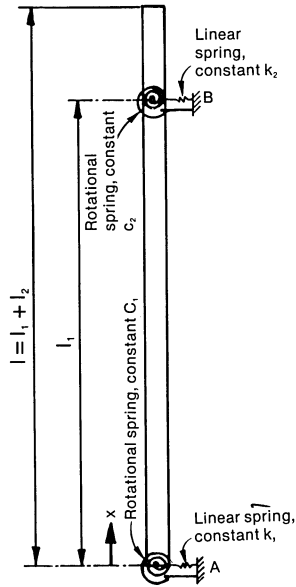


Fig. 20.1.2. Beam model of pressure vessel analyzed by VERSUP.

Each nozzle is assumed to have three forces and three moments applied in three orthogonal planes. Referring to Fig. 20.2.1 for typical nozzle k , we set up a local coordinate system (x'' , y'' , z''), such that x'' is vertical, y'' is directed along the axis of the nozzle, and z'' follows from the right-hand rule. Local nozzle loads P_x'' , P_y'' and P_z'' are assumed to act along the three axes at a distance r_k from the centerline of the equipment. Similarly, Moments M_x'' , M_y'' , and M_z'' act with their vectorial directions along the three local coordinate axes.

In common terminology, these loads are defined as follows:

- P_x'' = Longitudinal shear
- P_y'' = Axial force
- P_z'' = Circumferential shear
- M_x'' = Circumferential moment
- M_y'' = Axial twist
- M_z'' = Longitudinal moment

We have set up a global coordinate system (x , y , z) at the location of the bottom support as shown in Fig. 20.2.1. We also define an intermediate coordinate system (x' , y' , z'), located at the root of the nozzle, whose axes are parallel to the global axes, but whose origin is such that

$$\begin{aligned} y &= y' + r_k \cos\theta_k \\ z &= z' + r_k \sin\theta_k \\ x &= x' + d_k \end{aligned} \quad (20.2.1)$$

We recognize from Fig. 20.2.1, that nozzle loads can be expressed in terms of their components along the intermediate coordinate system axes as

$$\begin{aligned}
 P_x' &= P_x'' \\
 P_y' &= P_y'' \cos\phi_k - P_z'' \sin\phi_k \\
 P_z' &= P_z'' \cos\phi_k + P_y'' \sin\phi_k \\
 M_x' &= M_x'' \\
 M_y' &= M_y'' \cos\phi_k - M_z'' \sin\phi_k \\
 M_z' &= M_z'' \cos\phi_k + M_y'' \sin\phi_k
 \end{aligned}
 \tag{20.2.2}$$

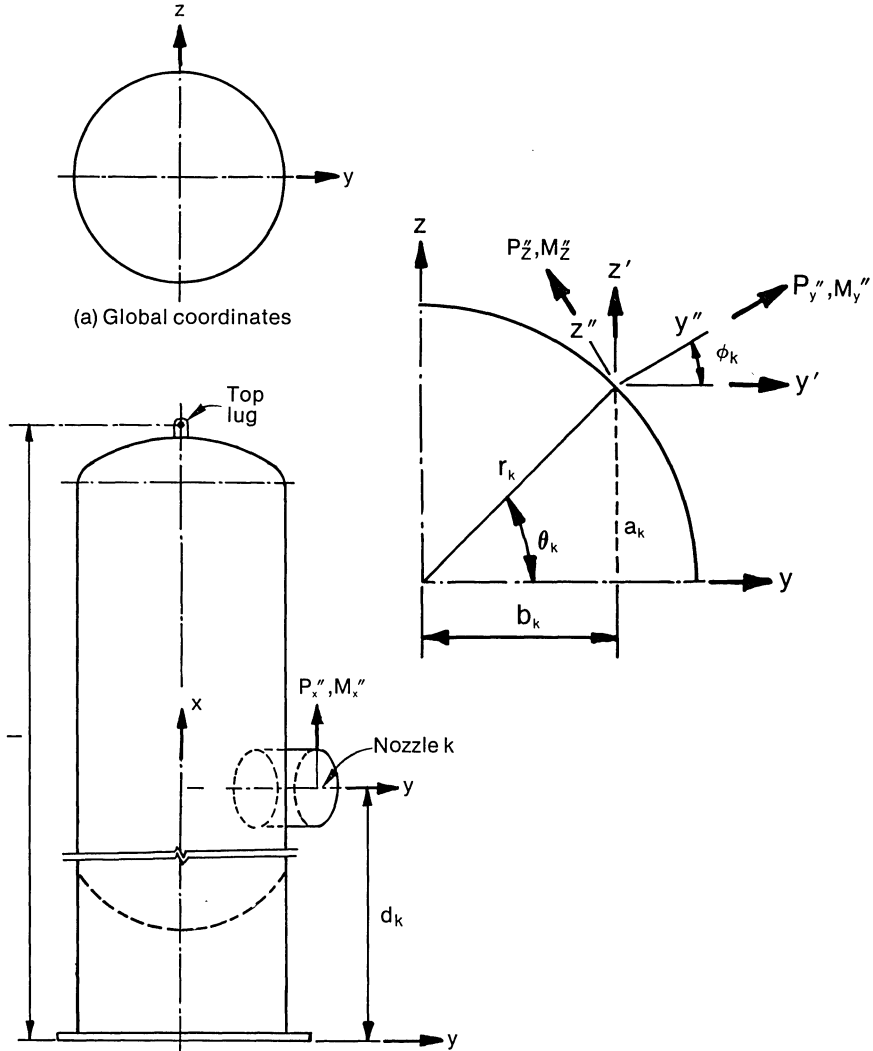


Fig. 20.2.1. Vertical tank coordinate system and nozzle loads.

Translating these loads to the projection of the global x, y, z coordinate system at level d_k yields

$$P_x = P_x' = P_x'' \quad (20.2.3)$$

$$P_y = P_y' = P_y'' \cos \phi_k - P_z'' \sin \phi_k \quad (20.2.4)$$

$$P_z = P_z' = P_z'' \cos \phi_k + P_y'' \sin \phi_k \quad (20.2.5)$$

$$M_x = M_x' - P_y' a_k + P_z' b_k$$

or

$$M_x = M_x'' - a_k (P_y'' \cos \phi_k - P_z'' \sin \phi_k) + b_k (P_z'' \cos \phi_k + P_y'' \sin \phi_k) \quad (20.2.6)$$

$$M_y = M_y' + a_k P_x'$$

or

$$M_y = M_y'' \cos \phi_k - M_z'' \sin \phi_k + P_x'' a_k \quad (20.2.7)$$

$$M_z = M_z' - b_k P_x'$$

or

$$M_z = M_z'' \cos \phi_k + M_y'' \sin \phi_k - P_x'' b_k \quad (20.2.8)$$

Hence, the loads referred to the axes of the beam coordinate system at level d_k with respect to the bottom support are given, via Eqs. (20.2.3–8), in matrix notation as follows:

$$\begin{Bmatrix} P_x \\ P_y \\ P_z \\ M_x \\ M_y \\ M_z \end{Bmatrix} = \begin{bmatrix} 1 & 0 & 0 & 0 & 0 & 0 \\ 0 & \cos \phi_k & -\sin \phi_k & 0 & 0 & 0 \\ 0 & \sin \phi_k & \cos \phi_k & 0 & 0 & 0 \\ 0 & -a_k \cos \phi_k & a_k \sin \phi_k & 1 & 0 & 0 \\ a_k & 0 & 0 & 0 & \cos \phi_k & -\sin \phi_k \\ -b_k & 0 & 0 & 0 & \sin \phi_k & \cos \phi_k \end{bmatrix} \begin{Bmatrix} P_x'' \\ P_y'' \\ P_z'' \\ M_x'' \\ M_y'' \\ M_z'' \end{Bmatrix} \quad (20.2.9)$$

The $\{P_x \dots\}$, $\{P_x'', \dots\}$ vectors in Eq. (20.2.9) are now rewritten with numeric subscripts in what follows. The equivalence of the two notations is defined by equality (20.2.10). The redefining of our notation is done simply to facilitate the subsequent manipulation.

$$\begin{bmatrix} P_x, P_x'' \\ P_y, P_y'' \\ P_z, P_z'' \\ M_x, M_x'' \\ M_y, M_y'' \\ M_z, M_z'' \end{bmatrix} \equiv \begin{bmatrix} F_{1k}, P_{1k} \\ F_{2k}, P_{2k} \\ F_{3k}, P_{3k} \\ F_{4k}, P_{4k} \\ F_{5k}, P_{5k} \\ F_{6k}, P_{6k} \end{bmatrix} \quad (20.2.10)$$

Denoting the coefficient matrix in Eq. (20.2.9) by A_{ijk} , we can now rewrite Eq. (20.2.9) in subscript notation, using the new definitions, in the compact form

$$F_{ik} = \sum_{j=1}^6 A_{ijk} P_{jk}; \quad k=1,2, \dots, q \quad (20.2.11)$$

where q = number of nozzles, and the generalized loadings are acting at location $x=d_k$, with respect to the global coordinate system defined at the vessel base.

Loads F_{ik} induce reactions at the base and the top lug. These reaction components R_i are defined as follows:

R_{1k} = Axial force at the lower support due to k th nozzle loads.

R_{2k} = Twisting moment (x vector) at the lower support due to the k th nozzle loads.

R_{3k} = Shear force at the base in the y -direction due to the k th nozzle.

R_{4k} = Bending moment in the x - y plane (z vector) at the base due to the k th nozzle.

R_{5k} = Shear force in the y -direction at the top lug due to the k th nozzle.

R_{6k} = Shear force at the base in the z -direction due to the k th nozzle.

R_{7k} = Bending moment in the x - z plane (y vector) at the base due to the k th nozzle.

R_{8k} = Shear force at the top lug in the z -direction due to the k th nozzle.

R_{9k} = Bending moment in the x - z plane (y vector) at the top lug.

R_{10k} = Bending moment in the x - y plane (z vector) at the top lug.

We assume that the vertical uplift and the axial twisting moment (R_{1k} , R_{2k}) are resisted only by the lower support.

The reactions at A and B (Fig. 20.1.2) can be expressed in terms of the applied loads F_{ij} using beam flexure equations. Classical strength of materials principles can be used to express the support reactions in terms of F_{jk} and the support spring rates. It can be shown that the results are expressible in the linear form

$$R_{ik} = \sum_{j=1}^6 B_{ijk} F_{jk} \quad i=1,2,3 \dots 10 \quad (20.2.12)$$

where the matrix B_{ijk} for k th nozzle is defined as follows:

$$[B] = \begin{bmatrix} -1 & 0 & 0 & 0 & 0 & 0 \\ 0 & 0 & 0 & -1 & 0 & 0 \\ 0 & -\rho_{11} & 0 & 0 & 0 & -\rho_{12} \\ 0 & \mu_{11} & 0 & 0 & 0 & \mu_{12} \\ 0 & -\rho_{21} & 0 & 0 & 0 & -\rho_{22} \\ 0 & 0 & -\rho_{11} & 0 & \rho_{12} & 0 \\ 0 & 0 & -\mu_{11} & 0 & \mu_{12} & 0 \\ 0 & 0 & -\rho_{21} & 0 & \rho_{22} & 0 \\ 0 & -\mu_{21} & 0 & 0 & 0 & -\mu_{22} \\ 0 & 0 & \mu_{21} & 0 & -\mu_{22} & 0 \end{bmatrix} \quad (20.2.13)$$

In Eq. (20.2.13) the influence coefficients ρ_{ij} and μ_{ij} are defined as follows:

- ρ_{11} = Reaction at base due to unit lateral force at height d_k .
- ρ_{21} = Reaction at top lug due to unit lateral force at height d_k .
- μ_{11} = Moment at base due to unit lateral force at height d_k .
- μ_{21} = Moment at top lug due to unit lateral force at height d_k .
- ρ_{12} = Reaction at base due to unit moment loading at height d_k .
- ρ_{22} = Reaction at top lug due to unit moment loading at height d_k .
- μ_{12} = Moment at base due to unit moment loading at height d_k .
- μ_{22} = Moment at top lug due to unit moment loading at height d_k .

Expressions for ρ_{ij} and μ_{ij} can be derived using classical beam theory and involve the spring rates for each support. The results of such derivations are implemented in computer program "VERSUP". The negative signs in Eq. (20.2.13) reflect the differences in sign convention between the positive directions assumed for R_{ik} and the sign conventions used to obtain the influence coefficients found in "VERSUP".

The combined reaction due to all nozzles is given by S_i where

$$S_i = \sum_{k=1}^q R_{ik} = \sum_{k=1}^q \sum_{j=1}^6 B_{ijk} F_{jk} \quad (20.2.14)$$

The subscript i ($i=1 \dots 10$) has the same meaning for the combined reaction as the subscript i in R_{ik} defined in the foregoing.

Substituting from Eq. (20.2.11) for F_{jk} so as to express the results in terms of the local nozzle loads, we have

$$S_i = \sum_{k=1}^q \sum_{j=1}^6 B_{ijk} \sum_{m=1}^6 A_{jmk} P_{mk} \quad (20.2.15)$$

OR

$$S_i = \sum_{j=1}^6 \sum_{k=1}^q \sum_{m=1}^6 B_{ijk} A_{jmk} P_{mk}$$

OR

$$S_i = \sum_{k=1}^q \sum_{m=1}^6 D_{imk} P_{mk} \quad (20.2.16)$$

where we have defined the elements of the transformation matrix D_{imk} as:

$$D_{imk} = \sum_{j=1}^6 B_{ijk} A_{jmk} \quad (20.2.17)$$

The matrix D_{imk} is readily computed because the matrices $[B]$ and $[A]$ are known from the physics of the problem. The next step is to maximize the reaction S_i , for a given i , (say i^*) by suitably choosing the sense of action of the components of P_{mk} . This is accomplished by selecting the signs of P_{mk}

such that the product $D_{imk} P_{mk}$ is positive for all m and k . Since all terms in the summation have the same sign, this will maximize S_i . Consistent values of other reaction components S_i ($i \neq i^*$) are obtained by performing the matrix multiplication in Eq. (20.2.16) where the terms of the P_{mk} matrix have the determined sign to maximize S_i . The same procedure is carried out for each reaction component in sequence beginning with $i^* = 1$.

In some cases, the sense of action of the applied nozzle loads is known, and therefore no optimization is required. This is accomplished in the analysis by simply omitting the foregoing step wherein the signs of P_{mk} are determined.

20.3 FOUNDATION RESPONSE

The support reactions due to all nozzle loads are maximized using the technique outlined in the preceding section and coded in "VERSUP". Each component of support reaction is maximized individually. These maximized reaction components are added to the corresponding components due to seismic loads. Having determined the maximized support response, the next step in the equipment qualification is to determine the foundation reactions. A simplified technique to determine the maximum concrete pressure and the bolt pull in a "skirt" or a "ring" type support on reinforced concrete pedestals is given in the following. We recall that a similar evaluation of rectangular foundations has been presented in the previous chapter.

We first develop a solution for the maximum interfacial concrete pressure p and the maximum bolt tensile stress, σ , when subject to the combined action of an axial thrust W and an overturning moment M . Subsequently, we consider a twisting torque and a shear force.

- (i) Axial Thrust W (tending to compress the foundation) and overturning moment M :

Depending on the magnitudes of W and M , either of the following two conditions will exist:

- (a) Complete compression:

The concrete is in compression over the entire base plate region. This case will correspond to a large W and a relatively small M .

- (b) Partial Compression:

Part of the base plate (in the negative x -quadrants in Fig. 20.3.1 will lift up, resulting in the formation of a neutral axis.

Equations relating the peak concrete pressure p to the applied M and W are found for the above two conditions in the following:

- (a) Complete Compression:

Assuming that the ring like foundation is composed of linearly elastic springs, the linearly varying component of concrete pressure $p = (p_m/r_0)x$ can be obtained as a function of the applied moment M . p_m is defined as the maximum value of the pressure at $x=r_0$ in Fig. 20.3.1 due to M . By appealing to moment equilibrium about the diametral axis (y -axis in Fig. 20.3.1), we obtain the equation

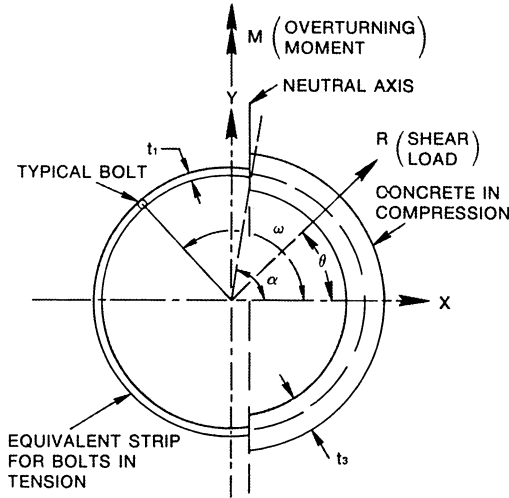


Fig. 20.3.1. Pressure distribution under base plate.

$$M = 4 \int_0^{\pi/2} \int_{r_i}^{r_o} x dF(r, \theta) \tag{20.3.1}$$

where

$$dF(r, \theta) = \left(p_m \frac{x}{r_o} \right) (r dr d\theta) \tag{20.3.2}$$

$x = r \cos \theta$, and θ here represents an angle measured from the x axis to an arbitrary radial line. r_o, r_i, M are defined as

- r_o = Base plate outer radius
- r_i = Base plate inner radius
- M = Applied overturning moment

Using Eqs. (20.3.1) and (20.3.2), and integrating over the limits of r and θ yields the following expression for the applied moment in terms of p_m .

$$M = \frac{\pi (r_o^4 - r_i^4) p_m}{4 r_o} \tag{20.3.3}$$

The maximum concrete pressure p , due to both M and W , is given as

$$p = p_m + p_0 \tag{20.3.4}$$

where the constant pressure term p_0 is defined as

$$p_0 = \frac{W}{\pi (r_o^2 - r_i^2)} \tag{20.3.5}$$

and p_m is calculated from Eq. (20.3.3). It is obvious that the bolts are unstressed in this case.

Commonly, the width of the foundation ring base plate is small compared to its radii, i.e.,

$$t_3 = (r_0 - r_i) < < \frac{1}{2} (r_0 + r_i) \quad (20.3.6)$$

The condition of a narrow base plate ring, expressed by inequality (20.3.6), translated in terms of numerical bounds, is recommended as

$$t_3 / (r_0 + r_i) < 0.2 \quad (20.3.6a)$$

Inequality (20.3.6) justifies simplifying Eqs. (20.3.3) and (20.3.5) even further.

Let

$$c = (r_0 + r_i) \quad (20.3.7)$$

Then

$$r_0 = 0.5c + 0.5t_3$$

$$r_i = 0.5c - 0.5t_3$$

Substituting Eq. (20.3.7) into Eq. (20.3.3) and (20.3.5), and neglecting terms of higher order, we have

$$M = \frac{\pi c^2 t_3 p_m}{4} \quad (20.3.8)$$

$$p_0 = \frac{W}{\pi c t_3} \quad (20.3.9)$$

Equations (20.3.8) and (20.3.9) may be used to compute p_m and p_0 instead of Eqs. (20.3.3) and (20.3.5), respectively, whenever inequality (20.3.6) holds.

The peak concrete pressure p is obtained using Eq. (20.3.4).

Finally, complete compression requires that

$$p_0 \geq p_m \quad (20.3.10)$$

If the above condition is not satisfied then “partial compression” exists, for which we outline the solution in the following:

(b) Partial Compression:

In this case, as mentioned above, a neutral axis parallel to the y axis (see Fig. 20.3.1) exists. The location of the neutral axis is identified by the angle α . The object is to determine the peak concrete pressure p and the angle α .

For narrow base plate rings where Eq. (20.3.6a) is satisfied, an approximate solution may be constructed using numerical iteration. It is assumed that the concrete annulus under the base plate may be treated as a thin ring of mean diameter c . Assuming the foundation to be linearly elastic, and the base plate to be relatively rigid, Brownell and Young [20.3.1] have developed an approximate solution which, with some modification, is summarized here and cast in a form suitable for numerical solution.

Let the total net tensile stress area* of all foundation bolts be A . Within the limits of accuracy sought, it is permissible to replace the bolts by a thin shell of thickness t and mean diameter equal to the bolt circle diameter c , such that

$$t = \frac{A}{\pi c} \tag{20.3.11}$$

We assume that the discrete tensile bolt loads, acting around the ring, are replaced by a line load, varying in intensity with distance from the neutral plane.

Let n be the ratio of the Young's moduli of the bolt material to that of the concrete; n normally varies between 10 to 15. Assuming that the concrete can take only compression (non-adhesive surface) and that the bolts are effective only in tension (untapped holes in base plate), an analysis similar to case (a) above yields the following results:

$$p = \frac{2W + \rho_2 tc\sigma}{\rho_1(t_3 - t)c} \tag{20.3.12}$$

$$\sigma = \frac{2(M - W\rho_4 c)}{\rho_2 \rho_3 tc^2} \tag{20.3.13}$$

where the dimensionless quantities ρ_1, ρ_2, ρ_3 and ρ_4 are defined as follows:

$$\rho_1 = \frac{2(\sin\alpha - \alpha\cos\alpha)}{(1 - \cos\alpha)} \tag{20.3.14}$$

$$\rho_2 = \frac{2}{1 + \cos\alpha} [(\pi - \alpha)\cos\alpha + \sin\alpha] \tag{20.3.15}$$

$$\rho_3 = \frac{1}{2} \left[\frac{(\pi - \alpha)\cos^2\alpha + \frac{\pi - \alpha}{2} + \frac{3\sin 2\alpha}{4}}{(\pi - \alpha)\cos\alpha + \sin\alpha} \right] + \frac{1}{2} \left[\frac{\frac{\alpha}{2} + \alpha\cos^2\alpha - \frac{3\sin 2\alpha}{4}}{\sin\alpha - \alpha\cos\alpha} \right] \tag{20.3.16}$$

*Tensile stress area A_t of a bolt of nominal material d and n' threads per in. is given by (see Ref. [20.3.2]).

$$A_t = \frac{\pi}{4} \left(d - \frac{0.9743}{n'} \right)^2$$

$$\rho_4 = \frac{1}{8} \left[\frac{2\alpha - \sin 2\alpha}{\sin\alpha - \alpha\cos\alpha} \right] \quad (20.3.17)$$

The angle which defines the location of the neutral axis, is given as

$$\alpha = \cos^{-1} \left[\frac{\sigma - np}{\sigma + np} \right] \quad (20.3.18)$$

Equations (20.3.12)–(20.3.18) give the required 7 non-linear equations to solve for 7 unknowns; namely p , σ , α , and the ρ_i ($i=1,4$) parameters. The simple iteration scheme described below converges rapidly. The iterative solution is started with assumed values of σ and p ; say σ_0 and p_0 . Then α is determined via Eq. (20.3.18). Knowing α , the dimensionless parameters ρ_1 , ρ_2 , ρ_3 , and ρ_4 are computed. This enables computation of corrected values of p and σ (say p_0' and σ_0') by Eqs. (20.3.12) and (20.3.13). The next iteration is started with σ_1 and p_1 where we choose

$$\begin{aligned} \sigma_1 &= 0.5(\sigma_0 + \sigma_0') \\ p_1 &= 0.5(p_0 + p_0') \end{aligned} \quad (20.3.19)$$

This process is continued until the errors e_i and ϵ_i at the i th iteration stage are within specified tolerances. ($e_i = \epsilon_i = 0.005$ is a practical value), where

$$\begin{aligned} e_i &= \left| \frac{\sigma_i' - \sigma_i}{\sigma_i} \right| \\ \epsilon_i &= \left| \frac{p_i' - p_i}{p_i} \right| \end{aligned} \quad (20.3.20)$$

Actual numerical tests show that the convergence is uniform and rapid regardless of the choice of starting values σ_0 and p_0 .

In Appendix 20.A, we present the development of a solution for the concrete pressure p and the neutral axis location d for the case of partial compression when the width of the base plate ring does not satisfy inequality (20.3.6a).

(ii) Axial Torque T and Lateral Shear R :

An axial torque and/or a lateral shear induces pure shear in the foundation bolts. Idealizing the foundation bolts by a thin shell of thickness t' as before, such that

$$t' = \frac{A'}{\pi c} \quad (20.3.21)$$

where A' = total gross area of bolting, an expression for shear stress can be readily developed. Referring to Fig. 20.3.1 leads us to express the shear stress in the x and y directions, τ_x and τ_y , for a bolt located at angle ω^* , as:

* T is assumed to be positive when the twist vector is directed vertically downward.

$$\begin{aligned}\tau_x &= \frac{2T}{cA'} \sin\omega + \frac{R}{A'} \cos\theta \\ \tau_y &= \frac{2T}{cA'} \cos\omega + \frac{R}{A'} \sin\theta\end{aligned}\quad (20.3.22)$$

Hence, the combined shear stress τ is given by

$$\tau = (\tau_x^2 + \tau_y^2)^{1/2} \quad (20.3.23)$$

20.4 COMPUTER PROGRAM VERSUP

20.4.1 Overview of the Code

Computer program VERSUP determines the support reactions in a vertically mounted unit supported at two locations. The lower support is assumed to be at (near) the bottom of the equipment. The upper support may be at any point in the span. Both top and bottom supports have the ability to resist lateral (horizontal) loads, and to resist bending moments. Only the bottom support is assumed to carry axial torque or vertical force. It is assumed that the nozzle loads are specified in a local nozzle coordinate system. The magnitude of the loads, but not their sense of action, is defined. The equipment is assumed to have uniformly distributed mass such that the effect of horizontal seismic acceleration can be simulated by solving a uniformly loaded beam problem. The horizontal seismic acceleration can be specified to act in two orthogonal directions (y and z in Fig. 20.2.1), or in one horizontal direction. In the latter case, the horizontal acceleration is assumed to act at 45° from the y and z axes. Setting NODIM = 3 in the input data file (described later) implies that equal value of horizontal acceleration are to be applied in both y and z directions. Any other value of NODIM means that the horizontal acceleration vector is at 45° from y and z axes. The vertical acceleration is also specified as a multiple of g (g = acceleration due to gravity).

The loads on the nozzles are input in the local nozzle coordinate systems (x'' , y'' and z'' axes in Fig. 20.2.1).

Coordinates r_k and θ_k define the origin of this local coordinate system. ϕ_k defines the nozzle orientation. We note that nozzles are required to lie in a horizontal plane; however, they do not have to be radial. Nozzles oriented out of a horizontal plane are rather rare and therefore such oblique nozzles axes are not covered in this version of the program.

The orientation of the y and z (global axes) are chosen to coincide with the direction of the horizontal accelerations (NODIM = 3); or to be equally inclined to the horizontal acceleration vector. The x -direction coincides with the vessel axis (vertical).

The program determines the sense of action of all components of the nozzle loads such that each one of the ten reaction components (six reactions at the base; and four reactions at the top lug – two lateral forces and

two bending moments) is maximized in turn. We recall that the top lug is assumed to provide no torsional or axial resistance (as is common in practical designs). These maximized reactions are combined with the seismic load induced reactions such that the maximax of each reaction component is obtained in turn. Thus 10 lines of reactions are printed; each line giving the maximax value of one reaction component. The program also affords the option of inputting the nozzle loads with specified sense of action. Setting IOPT = 0 in the input data file eliminates the optimization step in the program logic. IOPT > 0 implies that the sense of action of the nozzle loads will be selected to maximize the reaction component, as described above.

The program requires the input of support spring stiffnesses at both locations (Fig. 20.1.2). By suitably selecting these stiffnesses, most cases of skirt mounted equipment of practical interest can be solved.

The input data instructions are given below along with the data for an example problem. The output for this problem follows the program listing. The output is self-explanatory and therefore is not described here any further.

20.4.2 Input Data for Program VERSUP: All Input is in Free Field Format

Line 1: Title card; any alphanumeric heading of 80 characters or less

Line 2:

<u>Quantity</u>	<u>Fortran Symbol</u>	<u>Input for the example problem</u>
Distance between top and bottom lugs	EL	400 in.
Number of nozzle load locations	N	2
Weight of the vessel	W	10,000 lb
Overhang beyond top lug	OVER	0.0
Vertical acceleration as a multiple of "g"	VA	1.0
Horizontal acceleration as a multiple of g	HA	1.5
Support type (ISTYP = 0, lug type > 0, skirt with baseplate)	ISTYP	1
Indicate whether the horizontal seismic acceleration is to be applied in two or one direction	NODIM	3
Optimization option Skip to Line 4 if ISTYP = 0 in line 2.	IOPT	1

Line 3: Skirt type support data:

Width of base plate	WIDTH	7 in.
Outer radius of skirt	RS	20 in.
Diameter of the bolt circle	DBC	45 in.

Tensile stress area of anchor bolts	AB	10 in. ²
Gross area of anchor bolts	AGROS	11 in. ²
Skirt thickness	TS	1.0 in.

Line 4:

Linear stiffness of bottom support	AK1	40 × 10 ⁶ lb/in.
Linear stiffness of top support	AK2	40 × 10 ⁶ lb/in.
Rotational stiffness of bottom support	C1	40 × 10 ¹² lb-in./rad
Rotational stiffness of top support	C2	4.0 lb-in./rad
Flexural rigidity of the shell	EI	40 × 10 ¹⁰ lb-in. ²

Lines 5 and 6 are to be repeated *n* times (*n* = number of sets of nozzle loads)

Line 5: (Refer to Fig. 20.2.1 for further explanation)

	Fortran Symbol	Input Data	
		Nozzle 1	Nozzle 2
Radius of the point where the nozzle load (nozzle <i>k</i>) is applied, <i>r_k</i>	R(K)	20 in.	20 in.
Angular orientation of nozzle <i>k</i> with respect to the global axis <i>θ_k</i>	THETA(K)	0	π/2
Angular orientation of nozzle axis with respect to the global axis, <i>φ_k</i>	FI(K)	0	π/2
Height of nozzle <i>k</i> , <i>d_k</i>	DIS(K)	100 in.	300 in.

Line 6: Nozzle Loads:

Longitudinal shear	P(1,K)	5000 lb	5000 lb
Radial force	P(2,K)	5000 lb	5000 lb
Circumferential shear	P(3,K)	5000 lb	5000 lb
Circumferential bending moment	P(4,K)	10 ⁵ lb-in.	10 ⁵ lb-in.
Torsional moment	P(5,K)	10 ⁵ lb-in.	10 ⁵ lb-in.
Longitudinal bending moment	P(6,K)	10 ⁵ lb-in.	10 ⁵ lb-in.

PROGRAM VERSUP

C BY KRISHNA P. SINGH AND TEIK-LEE NG, REV 0, JANUARY 1984
 C *****
 C PROGRAM VERSUP EVALUATES SUPPORT REACTIONS DUE TO NOZZLE LOADS
 C AND SEISMIC LOADS ON VERT. VESSELS WITH 1 OR 2 SUPPORTS. BY VARYING
 C THE LINEAR AND ROTATIONAL STIFFNESSES OF THE SUPPORTS, EITHER SUPPORT
 C MAY BE MODELED AS FIXED, PINNED OR FREE. THE VESSEL MAY THEN HAVE
 C 1 OR 2 SPANS.
 C HORIZONTAL SEISMIC ACC. IS APPLIED IN TWO DIRECTIONS. THE WEIGHT IS



```

C ASSUMED TO BE UNIFORMLY DISTRIBUTED. THE BOTTOM AND UPPER SUPPORTS
C HAVE ROTATIONAL AND LINEAR SPRINGS.
C BY VARYING SENSE OF ACTION OF NOZZLE LOADS, EACH REACTION COM-
C PONENT IS MAXIMIZED IN TURN
C -----
C *****INPUT VARIABLES*****
C
C ..... LINE #1 .....
C TITLE : ANY ALPHANUMERIC STRING - 80 CHARACTERS LONG
C ..... LINE #2 .....
C EL : =ELL=L1=DISTANCE BETWEEN TOP AND BOTTOM LUGS (IN.)
C N : NO. OF NOZZLES
C W : WEIGHT OF VESSEL
C OVER : VESSEL OVERHANG PAST UPPER SUPPORT (=L2)
C VA : VERTICAL ACCELERATION AS A MULTIPLE OF G
C HA : HORIZONTAL ACCELERATION AS A MULTIPLE OF G
C ISTYP : IF =0 LOWER SUPPORT IS LUG TYPE; SKIP TO LINE #4
C        IF >0 LOWER SUPPORT IS SKIRT TYPE WITH BASEPLATE
C NODIM : NO. OF DIMENSIONS OF ANALYSIS
C IOPT : IF =0 PROGRAM DOES NOT MAXIMIZE REACTIONS
C        IF >0 PROGRAM LOOKS FOR DIRECTIONS TO MAXIMIZE REACTIONS
C
C ..... LINE #3 .....
C WIDTH : BASE RING WIDTH (IN.)
C RS : SKIRT OUTER RADIUS (IN.)
C DBC : DIAMETER OF BOLT CIRCLE (IN.)
C AB : TENSILE AREA OF BOLTS (SQ. INS.)
C AGROS : GROSS AREA OF BOLTS (SQ. INS.)
C TS : SKIRT THICKNESS (IN.)
C
C ..... LINE #4 .....
C AK1 : BASE LINEAR STIFFNESS
C AK2 : LUG LINEAR STIFFNESS
C C1 : BASE ROTATIONAL STIFFNESS
C C2 : LUG ROTATIONAL STIFFNESS
C EI : PRODUCT OF YOUNG'S MODULUS AND MOMENT OF INERTIA
C
C ----- INPUT A SET OF LINES #5 & #6 FOR EACH OF N NOZZLES -----
C ..... LINE #5 .....
C R(K) : RADIUS OF THE POINT WHERE THE KTH NOZZLE LOAD IS APPLIED
C THETA(K): ANGULAR ORIENTATION OF NOZZLE K WITH RESPECT TO THE
C          GLOBAL AXIS
C FI(K) : ANGULAR ORIENTATION OF KTH NOZZLE AXIS WITH RESPECT TO
C          THE GLOBAL AXIS
C DIS(K) : DISTANCE OR HEIGHT OF NOZZLE K FROM BOTTOM OF LOWER
C          SUPPORT OR BASE PLATE
C
C ..... LINE #6 .....
C P(J,K) : NOZZLE LOADS (J=1,2,...6) FOR KTH NOZZLE
C P(1,K)= LONG.SHEAR FORCE F(X) P(2,K)= RADIAL FORCE F(Y)
C P(3,K)= CIRC.SHEAR FORCE F(Z) P(4,K)= CIRC.BEND.MOMENT M(X)
C P(5,K)= TORSIONAL MOMENT M(Y) P(6,K)= LONG.BEND.MOMENT M(Z)

```

```

C *****
C
COMMON/ONE/EL,W,VA,HA,CG
COMMON/TWO/DBC,AB,WIDTH,AROOT,S
COMMON/THREE/RS,OR,TS
COMMON/FOUR/AK1,AK2,C1,C2,EI
DIMENSION THETA(7),FI(7),DIS(7),P(6,7),A(6,6,7),B(10,6,7),R(7),
*D(10,6,7),BETA(6,7),S(10,10),TITLE(20),SSIGN(10)
REAL MU11,MU12,MU21,MU22
DATA BEND/3HEND/
PI=3.1415927
IPAGE=1
5 READ (5,11)(TITLE(I),I=1,20)
11 FORMAT(20A4)
IF(TITLE(1).EQ.BEND)GO TO 1001
WRITE(6,14)(TITLE(I),I=1,20),IPAGE
14 FORMAT (1H1,/28(1H*),1X,20A4,1X,18(1H*)," PAGE ",I2)
READ(5,*) EL,N,W,OVER,VA,HA,ISTYP,NODIM,IOPT
IF (ISTYP.EQ.0) GO TO 6

C
C READ AND WRITE DATA FOR LUG TYPE SUPPORT (NO BASE PLATE)
C
READ(5,*) WIDTH,RS,DBC,AB,AGROS,TS
READ(5,*) AK1,AK2,C1,C2,EI
WRITE(6,12) EL, WIDTH, AK1, W, DBC, AK2, N, AGROS, C1, RS,
*OVER, AB, C2,TS,VA,EI,HA,NODIM,IOPT
12 FORMAT(1H," INPUT DATA ="/5X,
+"HT. OF SEIS.LUG(IN.)=",F8.2,6X,"BASE RING WIDTH (IN.)=",F6.2,8X,
+"BASE LIN.STIFF.,K1=", E9.3/5X,"WT. OF VESSEL (LBS.)=",F8.0,6X,
+"BOLT CIRCLE DIA.(IN.)=",F7.2, 7X,"LUG LIN.STIFF.,K2=",E9.3,4X/
+5X,"NO. OF NOZZLES =",I3,16X,"GROS AREA OF BOLTS(SQ.IN.)=",F6.2,
+3X,"BASE ROT.STIFF.,C1=",E9.3,4X,"SKIRT OUT. RAD.(IN.)=",F8.3/
+5X, "VESSEL OVERHANG(IN.)=",F8.2, 6X,"TENSILE AREA OF BOLTS =",
+F6.2,7X, "LUG ROT.STIFF.,C2=", E9.3,
+4X,"SKIRT THICKNESS(IN.)=",F8.3/5X,"VERT. ACCEL.(G)=",F5.2,50X,
+4HE*I=,E9.4 / 5X,"HORIZ. ACCEL. =", F5.2,
+14X,I1,"-D ANALYSIS",24X,"IOPT =",I3//
+ " NOZZ. R THETA FI NOZZ.HT. LG.SHE
1AR RAD.FORCE CIR.SHEAR CIR.MOM. TOR.MOM. LONG.MOM.")
GO TO 19

C
C READ AND WRITE INPUT DATA FOR SKIRT TYPE SUPPORT WITH BASE PLATE
C
6 READ(5,*) AK1,AK2,C1,C2,EI
WRITE (6,15) EL,VA,AK1,OVER,HA,AK2,W, C1, N, EI,C2
15 FORMAT (1H," INPUT DATA ="/, 13X, "HT. OF SEIS.LUG(IN.)=", F8.2,
*6X, "VERT. ACCEL.(G) =", F5.2, 6X, "BASE LIN. STIFF.(K1)=", E9.3,/
*13X, "VESSEL OVERHANG(IN.)=", F8.2, 6X, "HORIZ. ACCEL.(G)=", F5.2
*, 6X, "LUG LIN. STIFF.(K2)=",E9.3 / 13X, "WT. OF VESSEL (LBS.)="
*, F8.0, 34X,"BASE ROT. STIFF.(C1)=", E9.3 / 13X,"NO. OF NOZZLES =
*", 5X,I3, 16X,5HE*I =,3X, E9.4, 6X, "LUG ROT. STIFF.(C2)=", E9.3,
1//, " NOZZ. R THETA FI NOZZ.HT. LG.SHE

```

```

1AR RAD.FORCE CIR.SHEAR CIR.MOM. TOR.MOM. LONG.MOM."/)
19 DO 30 K=1,N
  READ(5,*) R(K),THETA(K),FI(K),DIS(K)
  READ(5,*) (P(J,K),J=1,6)
20 FORMAT(6F10.3)
  WRITE(6,21)K,R(K),THETA(K),FI(K),DIS(K),(P(J,K),J=1,6)
21 FORMAT(1H ,2X,I2,4(2X,F8.3),2(2X,F8.0),5X,F8.0,3(2X,F9.0))
30 CONTINUE
C
C GENERATE A MATRIX
C
  AROOT=AGROS
  DO 40 K=1,N
  DO 40 I=1,6
  DO 40 J=1,6
40 A(I,J,K)=0.0
  DO 50 K=1,N
  A(1,1,K)=1.
  X=THETA(K)
  Y=FI(K)
  A(5,1,K)=R(K)*SIN(X)
  A(6,1,K)=-R(K)*COS(X)
  A(2,2,K)=COS(Y)
  A(3,2,K)=SIN(Y)
  A(4,2,K)=-R(K)*SIN(X)*COS(Y)+R(K)*COS(X)*SIN(Y)
  A(2,3,K)=-A(3,2,K)
  A(3,3,K)=A(2,2,K)
  A(4,3,K)=R(K)*SIN(X)*SIN(Y)+R(K)*COS(X)*COS(Y)
  A(4,4,K)=1.0
  A(5,5,K)=COS(Y)
  A(6,5,K)=SIN(Y)
  A(5,6,K)=-A(6,5,K)
  A(6,6,K)=A(5,5,K)
50 CONTINUE
  DO 60 K=1,N
  DO 60 I=1,10
  DO 60 J=1,6
  B(I,J,K)=0.0
60 D(I,J,K)=0.0
  DO 65 K=1,N
  RO =(EL+OVER-DIS(K))/EL
  ETA =OVER/EL
  ITYP=1
C WHEN ITYP = 1, CALC. COEF FOR FORCE LOADING
  CALL COEF (ITYP,ETA,RO,RHO11,RHO21,MU11,MU21,EL)
  ITYP=0
C WHEN ITYP = 0, CALC. COEF FOR MOMENT LOADING
  CALL COEF (ITYP,ETA,RO,RHO12,RHO22,MU12,MU22,EL)
  B(1,1,K)=-1.
  B(3,2,K)=-RHO11
  B(4,2,K)=MU11

```

```

B(5,2,K)=-RH021
B(9,2,K)=-MU21
B(6,3,K)=-RH011
B(7,3,K)=-MU11
B(8,3,K)=-RH021
B(10,3,K)=MU21
B(2,4,K)=-1.
B(6,5,K)= RH012
B(7,5,K)= MU12
B(8,5,K)= RH022
B(10,5,K)= -MU22
B(3,6,K)= -RH012
      (4,6,K)= MU12
B(5,6,K)=-RH022
B(9,6,K)=-MU22

```

```
65 CONTINUE
```

```
C
```

```
C CREATE D MATRIX
```

```
C
```

```

DO 80 K=1,N
DO 80 I=1,10
DO 80 M=1,6
DO 70 J=1,6

```

```
70 D(I,M,K)=D(I,M,K)+B(I,J,K)*A(J,M,K)
```

```
80 CONTINUE
```

```
C
```

```
C MAXIMIZE RESULTANTS S(I) IF IOPT >0
```

```
C
```

```
WRITE(6,119)
```

```

119 FORMAT(1H ,136("-"),////," REACTIONS DUE TO NOZZLE LOADS ONLY"//
1" MAXIMIZED",2X,"AXIAL LOAD",4X,"TORSIONAL",3X,"SHEAR FORCE",3X,
1" OVERTURNING SEIS. LUG SHEAR FORCE OVERTURNING SEIS. LUG
1",2X,"MOMENT AT",2X,"MOMENT AT",/," (IF IOPT >0)",2X,
1"
1" F(X)",6X,"MOMENT M(X) F(Y)",6X,"MOME
1NT M(Z) LOAD N(Y) F(Z) MOMENT M(Y) LOAD N(Z)",
12X,"LUG MP(Z)",2X,"LUG MP(Y)",/," REACTION"/)

```

```
IS=1
```

```
85 DO 100 I=1,10
```

```
S(IS,I)=0.0
```

```
DO 90 K=1,N
```

```
DO 90 M=1,6
```

```
BETA(M,K)=1.0
```

```
IF(D(IS,M,K).LT.0..AND.IOPT .GT.0) BETA(M,K)=-1.
```

```
S(IS,I)=S(IS,I)+D(I,M,K)*BETA(M,K)*P(M,K)
```

```
90 CONTINUE
```

```
100 CONTINUE
```

```
WRITE(6,120)IS,(S(IS,I),I=1,10)
```

```
IF(IOPT .EQ.0) GO TO 130
```

```
IS=IS+1
```

```
IF (IS.GT.10) GO TO 130
```

```
GO TO 85
```

```
120 FORMAT (1H ,3X,I2,4X,F11.0,3X,F11.0,1X,F11.0,4X,F11.0,2X,F9.0,3X,
1F9.0,4X,F11.0,2X,F9.0,3X,F9.0,2X,F9.0)
```

```

C
C FIND COMBINATION OF SEISMIC AND NOZZLE LOADS FOR EACH MAX. LOAD CASE
C REACTIONS DUE TO SEISMIC LOADS
130 FH=W*HA
    FV=(1.+VA)*W
    FV2= (1.-VA)*W
    QDIST=FH/(EL+OVER)
    CALL UNIF(EL,OVER,QDIST,AVS,ACS,ANS,ACSS)
    WRITE (6,38) FV ,FV2,ACS,AVS,ACSS,ANS,FH
138 FORMAT(1X,136("-")////," REACTIONS DUE TO SEISMIC ACCELERATIONS
"ONLY"/28X,"DOWNWARD",6X,"UPWARD",16X,"REACTIONS DUE TO HORIZONTAL
" ACCELERATIONS",
" /,28X,"VERT.ACCEL.",3X,"VERT.ACCEL.
",5X,"OVERTURNING",5X, "SHEAR", 5X,"SEIS.LUG",4X,"SEIS.LUG", 3X,
" "TOT.HOR." / 28X,
" "AXIAL LOAD", 4X,"AXIAL LOAD",8X,"MOMENT",8X,"FORCE",5X," MOMENT
" ",6X,"LOAD", 5X,"LOADING",
* //,28X,F8.0,6X,F8.0,8X,E10.4,4X,F8.0,4X,F8.0,5X,F8.0,
* 2X, F8.0)
    IF (IOPT .EQ.0) GO TO 138
    IPAGE=IPAGE+1
    WRITE(6,14)(TITLE(I),I=1,20),IPAGE
138 WRITE(6,139)
139 FORMAT(1X,136("-")////," REACTIONS DUE TO SEISMIC,DEAD WEIGHT
1 AND NOZZLE LOADS"//
1" MAXIMIZED",2X,"AXIAL LOAD",4X,"TORSIONAL",3X,"SHEAR FORCE",3X,
1 "OVERTURNING SEIS. LUG SHEAR FORCE OVERTURNING SEIS. LUG
1",2X,"MOMENT AT",2X,"MOMENT AT",/, "(IF IOPT >0)",2X,
1 "F(X)", 6X,"MOMENT M(X) F(Y)",6X, "MOME
INT M(Z) LOAD N(Y) F(Z) MOMENT M(Y) LOAD N(Z)",
12X,"LUG MP(Z)",2X,"LUG MP(Y)",/, " REACTION"/)

C
C COMBINE SEISMIC LOADS WITH NOZZLE LOAD REACTIONS
C
DO 144 I=1,10
144 SSIGN(1)=1.0
    IF (IOPT .EQ.0) GO TO 146
145 SSIGN(1)=1.0
    SSIGN(2)=1.0
    SSIGN(3)=ABS(ANS)/ANS
    SSIGN(4)=ABS(ACS)/ACS
    SSIGN(5)=ABS(AVS)/AVS
    SSIGN(6)=SSIGN(3)
    SSIGN(7)=SSIGN(4)
    SSIGN(8)=SSIGN(5)
    SSIGN(9)=ABS(ACSS)/ACSS
    SSIGN(10)=SSIGN(9)
146 IF(NODIM.EQ.3) GO TO 147
    SEISFAC= .707
    GO TO 148
147 SEISFAC = 1.0
148 IF (IOPT .EQ.0) ISLAST=1

```

```

IF (IOPT .GT.0) ISLAST=10
DO 125 IS=1,ISLAST
S(IS,1)=S(IS,1)+FV
S(IS,3)=S(IS,3)+AVS*SSIGN(IS)*SEISFAC
S(IS,4)=S(IS,4)+ACS*SSIGN(IS)*SEISFAC
S(IS,5)=S(IS,5)+ANS*SSIGN(IS)*SEISFAC
S(IS,6)=S(IS,6)+AVS*SSIGN(IS)*SEISFAC
S(IS,7)=S(IS,7)+ACS*SSIGN(IS)*SEISFAC
S(IS,8)=S(IS,8)+ANS*SSIGN(IS)*SEISFAC
S(IS,9)=S(IS,9)+ACSS*SSIGN(IS)*SEISFAC
S(IS,10)=S(IS,10)+ACSS*SSIGN(IS)*SEISFAC
125 WRITE (6,120)IS,(S(IS,I),I=1,10)
IF(ISTYP.EQ.0) GO TO 136
CALL SKIRT(IOPT ,FV,FV2)
136 IPAGE=IPAGE+1
GO TO 5
1001 WRITE(6,1002)
1002 FORMAT(1HO,5X," ALL CASES FINISHED")
STOP
END
SUBROUTINE UNIF(L1,L2,Q,R1,AM1,R2,AM2)
REAL L1,L2,L,K1,K2
COMMON/FOUR/K1,K2,C1,C2,EI
2 L=L1+L2
A= C1+C2+C1*C2*L1/EI
-K1*L1 - C2*K1*L1*L1 /(2.*EI)
C = C1*L1*L1*.5 + EI*L1
D= EI*(1.+K1/K2) - K1*(L1**3)/ 6.
G = (Q*L*.5 - Q*L*L2 + Q*C2*(L1**3) / (6.*EI))
F= Q*(L1**4)/24. - EI*Q*L/K2
DEL= A*D-B*C
DEL1=(A*F-C*G ) /DEL
R1=-K1*DEL1
THE1 =(G*D-B*F)/DEL
AM1 =C1*THE1
A1= EI*THE1
A2= EI*DEL1
THE2=(-K1*L1*L1*DEL1/(2.*EI))+((C1*THE1*L1)/EI) -(Q*L1**3/(6.*EI)
/) +THE1
A3= EI*THE1-C2*THE2*L1
A4= EI*DEL1+C2*THE2*L1*L1*.5
DEL2=- (Q*L+K1*DEL1)/K2
R2=-K2*DEL2
AM2=C2*THE2
RETURN
END
SUBROUTINE COEF(TYP,ETA,RO,RHO1,RHO2,MU1,MU2,ELL)
COMMON/FOUR/AK1,AK2,C1,C2,EI
INTEGER TYP
REAL MU1,MU2
A1=AK1*ELL**3/EI
A2= AK2*ELL**3/EI

```

```

B=C2*ELL/EI
ATERM=AK2*ELL*ELL/C1
OMCAP=C2/C1
OM= AK2/AK1
AX=-(1+OM+.3333333*A2+ ATERM)
BX=0.50*B +OMCAP
CX=0.5*A2-1.-OM -ATERM
DX=-(1.+B -OMCAP)
IF(TYP.EQ.0) GO TO 50
P=1.0
FACT=P*ELL*ELL/EI
IF(RO .LT. ETA) GO TO 20
EX=-FACT*((1./A1)+.3333333*((1+ETA)**3-RO**3)-.50*(ETA+RO)*
/( (1+ETA)**2-RO*RO)+RO*ETA*(1.0+ETA-RO)) -P*ELL*(1.+ETA-RO)/C1
FX=FACT*(0.5*(1.+ETA-RO)**2-(1.0/A1)) -P*ELL*(1.+ETA-RO)/C1
GO TO 30
20 EX=-FACT*((1./A1)+.3333333*((1.+ETA)**3 -ETA**3)-.5*(ETA+RO)*
/ ((1.+ETA)**2 -ETA*ETA) + RO * ETA)-P*ELL*(1+ETA-RO)/C1
FX = FACT*(.5 +ETA-RO -(1./A1))-P*ELL*(1.+ETA-RO)/C1
30 DET=AX*DX-BX*CX
DP=(EX*DX-BX*FX)/DET
TH=(AX*FX-CX*EX)/DET
RH02=DP*A2*EI/(ELL**2)
MU2=B*EI*TH/ELL
RH01=P-RH02
IF (TYP.EQ.1) GO TO 39
MU1=MU2-RH02*ELL-TAU
RETURN
39 MU1=ELL*(P*(1.+ETA-RO)-RH02+MU2/ELL)
RETURN
50 B1=B/OMCAP
TAU=1.0
=TAU*ELL/EI
P=0.
IF (RO.GE.ETA) GO TO 60
EX= AZ*(.5+1./B1)
FX=-AZ*(1.-1./B1)
GO TO 30
60 EX= AZ*(.5*(1.-(RO-ETA)**2)+1./B1)
FX=-AZ*(1.+ETA-RO-1./B1)
GO TO 30
END
C
C
C
SUBROUTINE SKIRT(IOPT ,FV,FV2)
COMMON/TWO/DBC,AB,WIDTH,AROOT,S
COMMON/THREE/RS,OR,TS
DIMENSION S(10,10)
WRITE (6,39)
39 FORMAT(1H , 136("-"), ///, " SUPPORT REACTIONS DUE TO SEISMIC AN
1D NOZZLE LOADS VECTORIAL RESULTANTS",//, " MAXIMIZED ",3X,3("+"),

```

```

1 " DOWNWARD / UPWARD VERTICAL ACCELERATION ",3("+"),8X,"BOLT",5X,
1 13("+"), " RESULTANT LOADS ",11("+"),3X,"SKIRT"/" (IF IOPT >0)",
1 3X,"BOLT",11X,"CONCRETE", 7X,"RESULTANT",9X,"MAX SHEAR",2X,
1" SHEAR",5X,"BENDING",3X,"TORSIONAL",3X,"SEIS.LUG",2X,"COMPRESS."/,
1" REACTION",6X,"STRESS",11X,"STRESS",7X,"AXIAL LOAD",10X,
1 "STRESS",4X,"FORCE",5X,"MOMENT",6X,"MOMENT",6X,"LOAD",5X,"STRESS"
1,/)

```

```

IF (IOPT .EQ.0) ISLAST=1
IF (IOPT .GT.0) ISLAST=10
DC 135 IS=1,ISLAST
AXN=S(IS,1) -FV

```

C AX =AXIAL LOAD

```
AX1=AXN+FV
```

```
AX2=AXN+FV2
```

```
ANZ= (S(IS,8))
```

```
ANY= (S(IS,5))
```

C AN= LOAD AT SUPPT. LUG

```
AN=SQRT(ANZ**2+ANY**2)
```

```
ACSY= S(IS,10)
```

```
ACSZ= S(IS,9)
```

C ACS= MOMENT AT SUPPT. LUG

```
ACS= SQRT(ACSY**2+ACSZ**2)
```

```
AVZ= (S(IS,6))
```

```
AVY= (S(IS,3))
```

C AV= SHEAR AT BASE

```
AV=SQRT(AVZ**2+AVY**2)
```

```
ACZ= (S(IS,4))
```

```
ACY= (S(IS,7))
```

C AC= MOMENT AT BASE

```
AC=SQRT(ACZ**2+ACY**2)
```

```
TWIST=ABS(S(IS,2))
```

```
CALL BEAR(AX2,AC,SB2,SC2)
```

```
CALL BEAR(AX1,AC,SB1,SC1)
```

```
TAU=(2.*TWIST/(DBC*AROOT))+(AV/AROOT)
```

```
PI= 3.14159
```

```
SECMOD = PI* (RS-TS/2.))**2*TS
```

```
CROSEC = PI*(RS**2 -(RS-TS)**2)
```

```
COMP = AC/SECMOD + AX1/CROSEC
```

```
WRITE(6,45) IS,SB1,SB2,SC1,SC2,AX1,AX2,TAU,AV,AC,TWIST,
```

```
1 AN,COMP
```

```
45 FORMAT(1H ,3X,I2,5X,2(F6.0,"/",F6.0,4X),(F7.0,"/",F7.0,2X),F8.0,
```

```
1 1X,3(E9.3,2X) ,E9.3,2X,F9.0)
```

```
135 CONTINUE
```

```
RETURN
```

```
END
```

C

C

C

C

```
SUBRGUTINE COF (A,CT,CC,Z,AJ)
```

```
00520 SA=SIN(A)
```

```

00510 PI=3.14159
00530 CA=COS(A)
00540 CB=.5*A-1.5*SA*CA+A*CA*CA
00550 DB=SA-A*CA
00560 CC=2.*DB/(1.-CA)
00570 AJ=((.5*((P1-A)*CA*CA+.5*(P1-A)+1.5*SA*CA))/((P1-A)*CA+SA))
      ++(.5*CB/DB)
00590 Z=.5*(CA+(CB/DB))
00600 CT=2.*((P1-A)*CA+SA)/(1.+CA)
00610 RETURN
      END
      SUBROUTINE BEAR(WD,AM,FSU,FC)
      COMMON/TWO/DBC,AB,T3,AROOT,S
      COMMON/THREE/RS,OR,TS
      DIMENSION S(10,10)
      AN=10.
      PI=3.14159
      PO=WD/(PI*DBC*T3)
      PM=4.*AM/(PI*DBC*DBC*T3)
      IF(PO/PM.GT..99) GO TO 50
      T1=AB/(PI*DBC)
      T2=T3-T1
      I=0
      ALF2=0.25*PI
10  I=I+1
      CALL COF(ALF2,CT,CC,Z,AJ)
      FSU=(AM-WD*Z*DBC)/(0.5*DBC*DBC*CT*AJ*T1)
      FC = (WD+CT*FSU*.5*DBC *T1)/(T2*CC*.5*DBC)
      R = (FSU-AN*FC)/ (FSU+AN*FC)
      ALF1=ACOS(R)
      IF(R.LT.0.0) ALF1=PI-ACOS(ABS(R))
      ALFC=0.5*(ALF1+ALF2)
      IF(ABS(ALF2-ALF1).LT.1.E-04) GO TO 79
      ALF2=ALFC
      GO TO 10
75  WRITE(6,76)
76  FORMAT(" TRIAL DID NOT CONVERGE")
      STOP
50  FSU=0.
      FC=PM+PO
79  CONTINUE
      RETURN
      END

```


***** **SAMPLING PROBLEMS FOR VERSUP:MAXIMIZED REACTIONS:IMPDT=1** * 000061000 ***** PAGE 2

REACTIONS DUE TO SEISMIC, DEAD WEIGHT AND NOZZLE LOADS

REACTION	MAXIMIZED AXIAL LOAD (IF IOPT > 0) F(X)	TORSIONAL MOMENT M(X)	SHEAR FORCE F(Y)	OVERTURNING MOMENT M(Z)	SEIS. UUT LOAD M(Y)	SHARP FORCE F(Z)	OVERTURNING MOMENT M(Y)	SEIS. UUG LOAD M(Z)	MOMENT AT LUG MP(Z)	MOVEMT AT LUG MP(Y)
1	30000.	-400000.	5963.	-684964.	9039.	2430.	-1426547.	2571.	0.	0.
2	10000.	-400000.	2617.	-146868.	2384.	12268.	-691012.	2731.	0.	0.
3	20000.	-400000.	16458.	-1282959.	8544.	2430.	-1426531.	2571.	0.	0.
4	10000.	-200000.	-15802.	1420595.	-9199.	-11239.	703013.	-3762.	-0.	-0.
5	20000.	-400000.	15099.	-1339581.	9402.	3935.	-1264586.	1166.	0.	0.
6	10000.	-200000.	6992.	-684948.	8007.	16645.	-140708.	8356.	0.	0.
7	10000.	-200000.	-11754.	801534.	-3247.	-2429.	1426643.	-2570.	-0.	-0.
8	20000.	-400000.	6240.	-616001.	8709.	14912.	-233817.	10089.	0.	0.
9	30000.	-400000.	15802.	-1420595.	9199.	2430.	-1426531.	2571.	0.	0.
10	20000.	-200000.	2618.	-146884.	2383.	2429.	-1426643.	2570.	0.	0.

SUPPORT REACTIONS DUE TO SEISMIC AND NOZZLE LOADS VECTORIAL RESULTS

MAXIMIZED (IF IOPT > 0) REACTION	ROU STRESS	CONCRETE STRESS	ACCELERATION AXIAL LOAD	PFSULTANT AXIAL LOAD	MAX STRESS	ROU STRESS	SHARP FORCE	BENDING MOMENT	RESULTANT LOADS TORSIONAL MOMENT	SEIS.UUG LOAD	SKIRT COMPRESS. STRESS
1	6472./ 8620.	255./ 746.	30000./ 10000.	1614.	6445*04	1585*07	4000*06	940F*04	1570.		
2	3249./ 5459.	113./ 99.	10000./ -10000.	2021.	1255*05	7065*06	4000*06	400E*04	673.		
3	9593./ 11787.	303./ 291.	20000./ 0.	2294.	1665*05	1925*07	4000*06	842E*04	1769.		
4	8636./ 10852.	247./ 233.	10000./ -10000.	1885.	1945*05	1595*07	2000*06	984F*04	1408.		
5	9125./ 11318.	291./ 280.	20000./ 0.	2224.	1565*05	1845*07	4000*06	997E*04	1705.		
6	3277./ 5487.	113./ 100.	10000./ -10000.	1796.	1815*05	7115*06	2000*06	116E*05	677.		
7	8951./ 11167.	255./ 241.	10000./ -10000.	1393.	1205*05	1645*07	2000*06	114E*04	1451.		
8	1933./ 4048.	104./ 100.	20000./ 0.	1672.	1625*05	6595*06	2000*06	113E*05	715.		
9	9098./ 11265.	322./ 312.	30000./ 10000.	2251.	1605*05	2015*07	4000*06	955E*04	1930.		
10	6628./ 8811.	229./ 218.	20000./ 0.	831.	3575*04	1435*07	2000*06	350E*04	1364.		

ALL CASES FINISHED

NOMENCLATURE

- A = Gross tensile stress area of foundation bolts
 A' = Gross area of anchor bolts
 c = Mean diameter of annular base plate (also bolt circle diameter)
 C_1, C_2 = Rotational stiffness of bottom and top supports, respectively (Fig. 20.1.2)
 e_i = Error at iteration i (Eq. (20.3.20))
 F_{ik} = i th nozzle load vector (in the global coordinate system) for the k th nozzle
 K_1, K_2 = Linear stiffness of bottom and top supports, respectively (Fig. 20.1.2)
 M = Overturning moment (Fig. 20.1.1)
 M_x'', M_y'', M_z'' = Nozzle moments in the local coordinate system
 n = Ratio of Young's moduli of bolt material to that of concrete
 n' = Number of threads per in. in foundation bolts
 n_b = Number of anchor bolts
 P_x, P_y, P_z , etc. = Nozzle loads transformed to the global coordinate system (Fig. 20.2.1)
 P_{ik} = i th nozzle load vector for k th nozzle (Eq. (20.2.10)) in the local coordinate system
 p = Maximum concrete pressure
 p_m = Maximum pressure on concrete due to M
 p_0 = Uniform pressure due to W (Eq. (20.3.5))
 P_x'', P_y'', P_z'' = Nozzle loads in the local coordinate system
 q = Number of sets of nozzle loads
 R = Lateral shear force (Fig. 20.3.1)
 r = Bolt circle radius
 r_i = Inner radius of base plate
 r_0 = Outer radius of base plate
 r_s = Outer radius of skirt
 S_i = Support reaction component i
 t_3 = Width of base plate ($t_3 = r_0 - r_i$)
 T = Axial torque (Fig. 20.1.1)
 t = Thickness of fictitious shell based on bolting tensile stress area
 t' = Thickness of fictitious shell based on the gross area of the bolts
 σ = Maximum anchor bolt tensile stress
 ϵ_i = Error at iteration i (Eq. (20.3.20))
 τ = Combined shear stress in a bolt at angle ω

REFERENCES

- [20.3.1] Brownell, L. E., and Young, E. H., "Process Equipment

- Design," Wiley, pp. 183–197, New York (1959).
- [20.3.2] American Institute of Steel Construction, "Manual of Steel Construction," 8th edition, Chicago (1980).
- [20.A.1] Gradshteyn, I. S., and Ryzhik, I. M., "Table of Integrals, Series and Products," 4th edition, p. 86, Academic Press, New York (1965).

APPENDIX 20.A

PARTIAL COMPRESSION – WIDE RING BASE

A set of equations to determine the peak concrete pressure, p , the distance of the neutral plane from the y -axis, d , and the maximum bolt tensile stress for the case of partial compression on a ring base plate which does not satisfy ineq. (20.3.6) (see Fig. 20.3.1) is developed below.

We assume a linearly elastic spring foundation, linearly elastic bolts, and a rigid ring base plate. We let $r=0.5c$, and think of the bolt load as a "smeared" tensile pressure whose magnitude varies linearly with distance from the neutral axis. Then, using the nomenclature associated with Fig. 20.3.1, and noting that the base plate can only execute a rigid body rotation about the neutral axis, we obtain the following relation between peak compressive concrete pressure p (at $x=r_0$), and the peak bolt tensile pressure p_b (at $x = -r$)

$$p_b = |p| \frac{(r+d)}{(r_0-d)} n \quad (20.A.1)$$

In some of the integrals to follow, we use the angle ψ to denote an angle between the y axis and a radial line to an arbitrary location on the ring pad. Vertical force equilibrium requires that:

$$F_t + W = F_c \quad (20.A.2)$$

where F_t and F_c are the total tensile and compressive forces developed in the bolts and in the concrete, respectively. Since the bolt load per unit area is a linear function of distance from the neutral axis, and bearing in mind Eq. (20.A.1), we have

$$F_t = \frac{2npt(r+d)}{r_0-d} \int_{\alpha}^{\pi} (d-r\cos\psi) d\psi \quad (20.A.3a)$$

where $\alpha = \cos^{-1} d/r$ and r_0 is the outside radius of the concrete pad. Performing the integration yields

$$F_t = \frac{2npt(r+d)}{(r_0-d)} [(\pi-\alpha)d + r\sin\alpha] \quad (20.A.3b)$$

Similarly

$$F_c = 2p \int_d^{r_0} \left[\frac{(x-d)(r_0^2 - x^2)^{1/2}}{(r_0 - d)} \right] dx \tag{20.A.4}$$

$$- 2pH(r_i - d) \int_d^{r_i} \frac{(x-d)(r_i^2 - x^2)^{1/2}}{(r_0 - d)} dx$$

where $H(r_i - d)$ is the Heaviside unit function, defined as

$$H(r_i - d) = 1 \text{ when } r_i \geq d$$

$$H(r_i - d) = 0 \text{ when } r_i < d \tag{20.A.5}$$

The following results can be obtained by elementary integration:

$$\int (z^2 - x^2)^{1/2} dx = \frac{z^2}{2} \left(\theta + \frac{\sin 2\theta}{2} \right) \tag{20.A.6}$$

$$\int x(z^2 - x^2)^{1/2} dx = -\frac{z^3}{3} \cos^3 \theta \tag{20.A.7}$$

where

$$\theta = \sin^{-1} \frac{x}{z} \tag{20.A.8}$$

Using Eq. (20.A.6) and Eq. (20.A.7), the quadratures in Eq. (20.A.4) can be performed, which yields:

$$F_c = \frac{2p}{(r_0 - d)} \left[\frac{r_0^3 \cos^3 \theta_1}{3} - \frac{r_0^2 d}{2} \left(\frac{\pi}{2} - \theta_1 - \frac{\sin 2\theta_1}{2} \right) \right.$$

$$\left. - H(r_i - d) \left\{ \frac{r_i^3 \cos^3 \theta_2}{3} + \frac{r_i^2 d}{2} \left(\frac{\pi}{2} - \theta_2 - \frac{\sin 2\theta_2}{2} \right) \right\} \right] \tag{20.A.9}$$

where

$$\theta_1 = \sin^{-1} \frac{d}{r_0}$$

$$\theta_2 = \sin^{-1} \frac{d}{r_i} \tag{20.A.10}$$

Combining Eqs. (20.A.1), (20.A.3b), and (20.A.9), we have

$$\frac{2npt(r+d)}{(r_0 - d)} [(\pi - \alpha)d + r \sin \alpha] + W$$

$$= \frac{2p}{(r_0 - d)} \left[\frac{r_0^3 \cos^3 \theta_1}{3} - \frac{r_0^2 d}{2} \left(\frac{\pi}{2} - \theta_1 - \frac{\sin 2\theta_1}{2} \right) \right]$$

$$-H(r_i-d) \left\{ \frac{r_i^3 \cos^3 \theta_2}{3} + \frac{r_i^2 d}{2} \left(\frac{\pi}{2} - \theta_2 - \frac{\sin 2\theta_2}{2} \right) \right\} \quad (20.A.11)$$

Next, taking moments of concrete pressure and bolt tension stresses about the y -axis, and requiring moment equilibrium, we have

$$2 \int_d^{r_0} \frac{p(x-d)}{(r_0-d)} (r_0^2 - x^2)^{1/2} x dx - 2H(r_i-d) \int_d^{r_i} \frac{p(x-d) (r_i^2 - x^2)^{1/2} x dx}{(r_0-d)} - 2 \int_\alpha^\pi \frac{np(d-r \cos \psi) tr(r+d) \cos \psi d\psi}{(r_0-d)} = M \quad (20.A.12)$$

The integrations in Eq. (20.A.12) can be carried out by making use of Eqs. (20.A.7) and Eq. (20.A.13) given below:

$$\int x^2 (r^2 - x^2)^{1/2} dx = \frac{-x(r^2 - x^2)^{3/2}}{4} + \frac{r^2 (r^2 - x^2)^{1/2} x}{8} + \frac{r^4 \sin^{-1}(x/r)}{8} \quad (20.A.13)$$

The result given as Eq. (20.A.13) can be found in Ref. [20.A.1]. Performing the necessary algebra yields the final equation.

$$\begin{aligned} \frac{2p}{r_0-d} \left[\frac{\pi r_0^4}{8} + \frac{d(r_0^2 - d^2)^{3/2}}{4} - \frac{dr_0^2 (r_0^2 - d^2)^{1/2}}{8} - \frac{r_0^4}{8} \sin^{-1} \frac{d}{r_0} - \frac{dr_0^3}{3} \cos^3 \theta_1 \right. \\ \left. - H(r_i-d) \left\{ \frac{\pi r_i^4}{8} + \frac{d(r_i^2 - d^2)^{3/2}}{4} - \frac{dr_i^2 (r_i^2 - d^2)^{1/2}}{8} - \frac{r_i^4}{8} \sin^{-1} \frac{d}{r_i} - \frac{dr_i^3}{3} \cos^3 \theta_2 \right\} \right] \\ + \frac{2r(r+d)npt}{(r_0-d)} \left[d \sin \alpha + \frac{r}{2} \left(\pi - \alpha - \frac{\sin 2\alpha}{2} \right) \right] = M \quad (20.A.14) \end{aligned}$$

Equation (20.A.11) and Eq. (20.A.14) are the two required non-linear equations in p and d . Solution of these equations in closed form cannot be obtained. However, numerical answers may be obtained using well-known procedures such as the Newton-Raphson technique.

21. RESPONSE SPECTRUM

21.1 INTRODUCTION

The motion of pressure vessel supports during an earthquake is usually characterized by a zigzag plot of acceleration vs. time such as the one shown in Fig. 21.1.1. A comprehensive analysis for the stresses in the pressure vessel would require modeling the vessel as a multi-degree of freedom elastic system and formulating the equations of motion for each degree-of-freedom. These equations are thereafter integrated in time to obtain the response of the simulated structure as a function of time [21.1.1]. Such an analysis, called a “time history” analysis, is prohibitively expensive for the usual industrial hardware, and is therefore seldom employed. Designers often utilize static analysis methods wherein the dynamic problem is reduced to one of statics by replacing the actual dynamic loading by an appropriate static inertia load, usually expressed as a fraction (or multiple) of g .^{*} Unless chosen wisely, the static load applied can be unduly conservative and thus lead to fictitiously high values of computed vessel stresses and foundation reactions. The cumulative effect of such conservatism in all the equipment on a plant floor results in grossly exaggerated floor loadings. This has a direct effect on plant construction costs.

Modal analysis methods, which utilize the so-called “Earthquake Response Spectrum”, are a compromise between the tedium of direct time integration (time history) methods, and the oftentimes unaffordable conservatism of static analysis methods. Indeed, the modal analysis method involves little more computational effort than a purely static analysis. It has been widely used in the design of buildings, factories, bridges and other installations which must be built to be earthquake resistant. Recently, it has found extensive use in the design of piping systems in nuclear power plants.

In this section, a self-contained exposition of the modal analysis technique is given. After familiarizing the reader with the physical significance of the “response spectrum”, the mathematical concepts for its construction are derived from first principles. Application of the response spectrum to perform a modal analysis on a heat exchanger is next illustrated. An example problem is used to demonstrate the effectiveness of this method.

21.2 PHYSICAL MEANING OF RESPONSE SPECTRUM

“Response Spectrum” is the footprint of an earthquake. It is constructed by evaluating the maximum response of a simple oscillator (Fig. 21.2.1)

^{*}Acceleration due to gravity = 386.4 in./sec^2 .

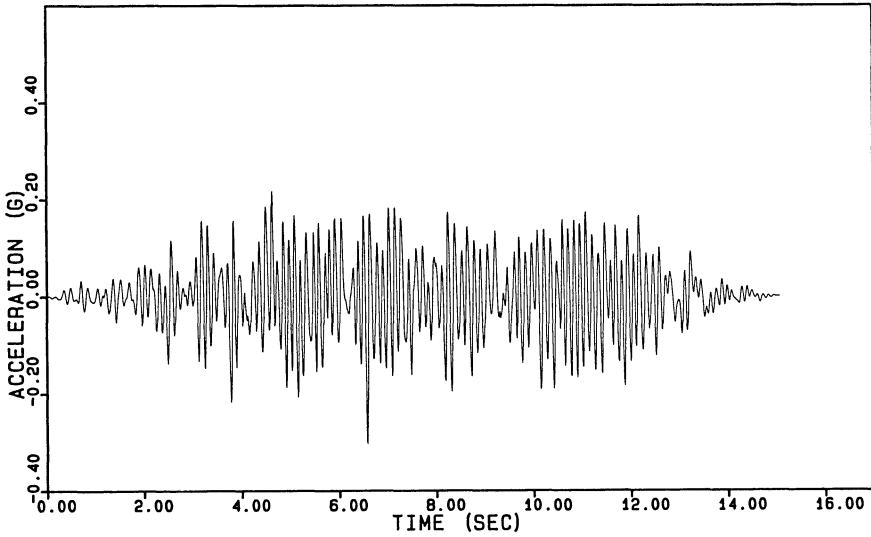


Fig. 21.1.1. Typical acceleration – time plot of an earthquake

when subjected to the earthquake. The single degree of freedom system shown in Fig. 21.2.1, is characterized by two basic parameters: (i), its undamped frequency ω_0 [$\omega_0 = (k/m)^{1/2}$]; and (ii), its damping coefficient, commonly expressed as a fraction of critical damping, ζ . In Section 16.9.2, we have shown that ζ is related to the damping coefficient c by the relationship

$$\zeta = c/2(km)^{1/2} = c/2m\omega_0$$

For a given value of ζ the maximum absolute acceleration of the mass m , denoted by a_m , can be computed for various values of ω_0 . The plot of a_m as a function of ω_0 is known as the “acceleration response spectrum”. Similarly, if the “maximum relative velocity of the mass with respect to the support”, henceforth called the pseudo-velocity, V , is plotted as a function of ω_0 with ζ as the parameter, such a plot is known as the “velocity response spectrum”. Alternatively, the maximum deformation of the spring (or the relative displacement of the mass), D can be plotted to produce the “displacement response spectrum”. As we will see in the next section, the absolute acceleration a_m , the pseudo-velocity V , and the pseudo-displacement, D are related as follows:

$$a_m = \omega_0 V \quad (21.2.1)$$

$$D = V/\omega_0 \quad (21.2.2)$$

This relationship permits plotting all three spectra on one tripartite logarithmic plot as shown in Fig. 21.2.2. The pseudo-velocity and the

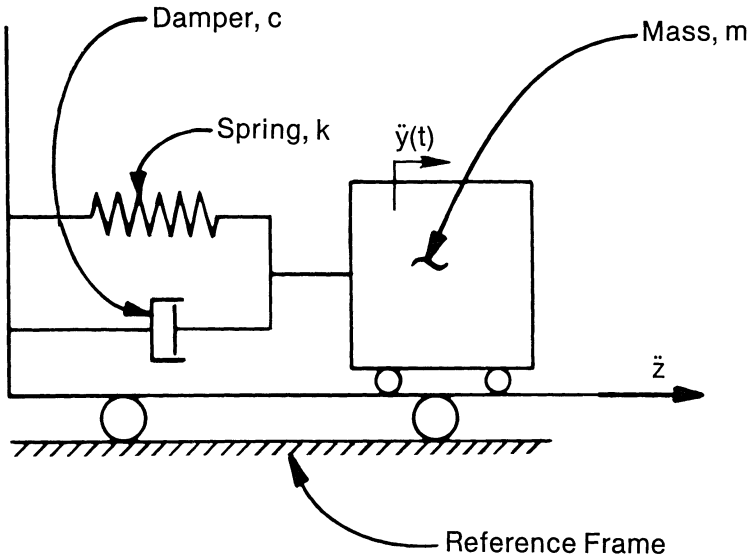


Fig. 21.2.1. Single oscillator model.

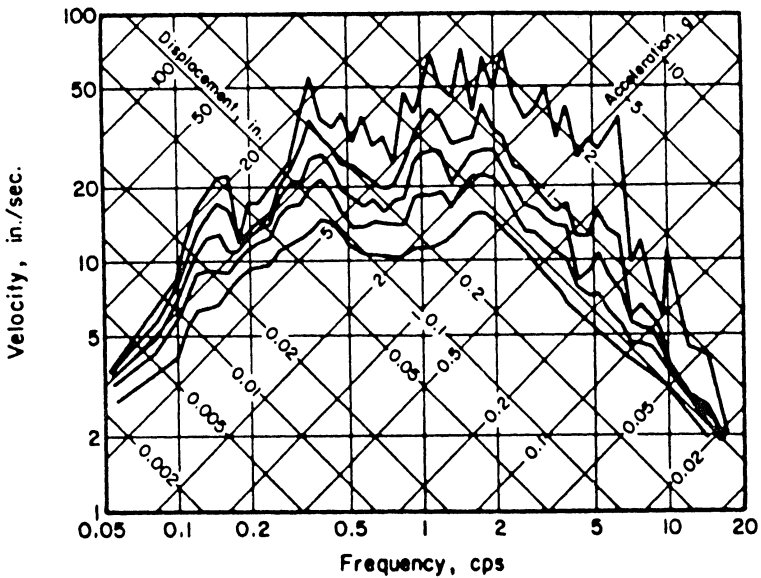


Fig. 21.2.2. Response spectrum, El Centro earthquake, May 18, 1940, North-South direction for 0, 2, 5, 10, 20 percent of critical damping.

frequency are plotted along the logarithmic vertical scale and logarithmic horizontal scale, respectively. On logarithmic diagonal scales along an axis that extends upwards at 45° from lower right to upper left are plotted values of pseudo-displacement. Absolute acceleration is plotted on diagonal scales along the axis which extends upwards at 45° from lower left to upper right. This type of plot shows the extreme values of D , V and a_m for the complete frequency range of interest. Furthermore, since the period of vibration is the reciprocal of frequency, the logarithmic scale for the period will have the same spacing between points; in fact, the scale for the period will be a mirror image of that corresponding to frequency.

The scheme of plotting the velocity, the acceleration, and the displacement versus the frequency on one plot is at once ingenious and intriguing. Texts on structural mechanics usually define the axes for reading these four quantities without explaining the underlying concepts. We will examine the basis of this remarkably compact representation scheme in what follows so as to provide the reader with an insight into its construction and use.

Taking natural logarithms on both sides of Eqs. (21.2.1) and (21.2.2) yields

$$\ln a_m = \ln \omega_0 + \ln V$$

$$\ln D = \ln V - \ln \omega_0$$

or, solving both expressions for $\ln V$,

$$\ln V = -\ln \omega_0 + \ln a_m \quad (21.2.3)$$

$$\ln V = \ln \omega_0 + \ln D \quad (21.2.4)$$

Ascribing $\ln V$ and $\ln \omega_0$ to the y - and x -axes of a graphical plot, we note from Eq. (21.2.3) that lines of constant acceleration ($\ln a_m = \text{constant}$) are straight lines with negative unit slope; i.e., these lines will make an angle of -45° with the positive x -axis. Since the acceleration axis has to be perpendicular to the lines of constant a_m , it will be directed along positive 45° slope to the x -axis ($\ln \omega_0$ -axis). Figure 21.2.3 illustrates these facts.

Similarly, Eq. (21.2.4) shows that lines of constant $\ln D$ have unit positive slope and the displacement axis will therefore have unit negative slope. It remains for us to prove that the acceleration and displacement axes, drawn in this manner, can be defined with consistent scaling factors such that all points on a curve on the chart correspond to appropriate values for the four quantities— ω_0 , D , a_m , and V —while satisfying Eqs. (21.2.1-2). A logarithmic plot of ω_0 implies that its value ω_1 at point 1 on the x -axis, at a distance x_1 from the intersection of the x and y axis, is

$$\omega_1 = e^{(x_1+c)r} \quad (21.2.5)$$

where c is the location of the origin (not shown) somewhere to the left of point 0 in Fig. 21.2.2, and r is the scaling factor chosen for the plot. Similarly, the value of ω_1 at point 2, ω_2 , is given by the expression

$$\omega_2 = e^{(x_2+c)r} \quad (21.2.6)$$

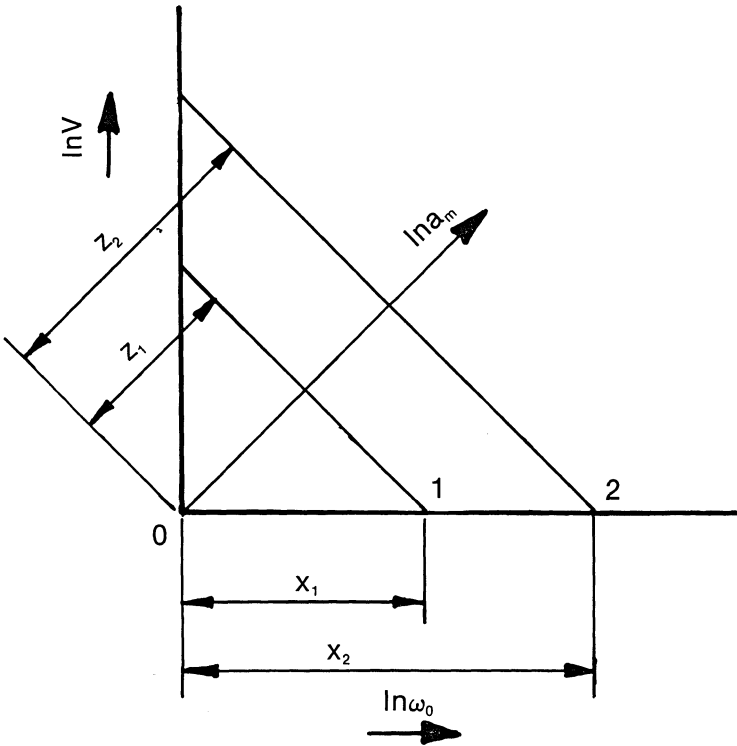


Fig. 21.2.3. Logarithmic plot of response spectra.

Let the logarithmic scale for the acceleration a_m be defined by scaling factor n , and origin offset d , i.e.,

$$a_m = e^{(z+d)n}$$

where z is a distance measured along the inclined acceleration axis. Therefore, the values of acceleration on the two lines of constant acceleration are

$$a_1 = e^{(z_1+d)n}$$

$$a_2 = e^{(z_2+d)n}$$

Hence,

$$\frac{a_2}{a_1} = e^{(z_2-z_1)n}$$

or

$$\ln a_2 - \ln a_1 = n(z_2 - z_1)$$

Since $z_2 - z_1 = (x_2 - x_1) \cos 45^\circ$, it follows that

$$\ln a_2 - \ln a_1 = \frac{n(x_2 - x_1)}{\sqrt{2}} \quad (21.2.7)$$

Denoting the value of velocity V as V_1 at the x -axis, satisfaction of Eq. (21.2.1) requires that

$$\begin{aligned} a_1 &= \omega_1 V_1 = V_1 e^{(x_1+c)r} \\ a_2 &= \omega_2 V_1 = V_1 e^{(x_2+c)r} \end{aligned}$$

Therefore,

$$\frac{a_2}{a_1} = e^{(x_2-x_1)r}$$

or

$$\ln a_2 - \ln a_1 = r(x_2 - x_1) \quad (21.2.8)$$

Comparing Eqs. (21.2.7) and (21.2.8), we find that Eq. (21.2.1) will be satisfied if

$$n = \sqrt{2}r$$

Since point 2 is arbitrarily chosen, it follows that setting the scaling factor of the acceleration scale to be $\sqrt{2}$ times that of the frequency scale satisfies Eq. (21.2.1) identically.

Similarly, we can prove that the scaling factor for the velocity axis must be r , and that the factor for the inclined displacement axis must be $\sqrt{2}r$. Therefore, meeting Eqs. (21.2.1-2) requires only that a consistent set of scaling factors be chosen for the ω_0 , V , a_m and D axes.

The most severe recorded earthquake in the U.S. is the El Centro earthquake of May 18, 1940 which in its N-S direction registered a maximum ground acceleration of 0.32 g, a maximum ground velocity of 13.7 in./sec, and a maximum ground displacement of 8.3 in. The acceleration, velocity, and displacement versus time plots of this earthquake, originally made by Newmark et al., are shown in Fig. 21.2.4. The corresponding response spectra are shown in Fig. 21.2.2.

Referring to Fig. 21.2.2, we note that the spectra cluster at the two extremes of frequency. On the extreme left corresponding to very small oscillator frequency, the value of D for all values of damping, ζ , approaches an asymptote corresponding to the value of maximum ground displacement. Since very small oscillator frequency implies a very weak spring and a relatively large mass, the mass behaves as though it were disconnected from the ground; thus its relative displacement is almost equal to the ground displacement. On the other end of the scale, at high frequencies, the acceleration spectra tend to the asymptote corresponding to the maximum ground acceleration. This, too, is logical, since high oscillator frequency implies a relatively stiff spring and light mass. The spring behaves like a rigid link making the mass move synchronously with the ground.

The El Centro response spectrum is quite typical of earthquake spectra. In fact, the response spectra of ground motions from other sources of

disturbances, such as quarry blasting, and underground nuclear detonation, have similar characteristics. Some fundamental features of earthquake spectra listed below are at the heart of the techniques for constructing artificial earthquake spectra for regions for which hard seismic data are not available.

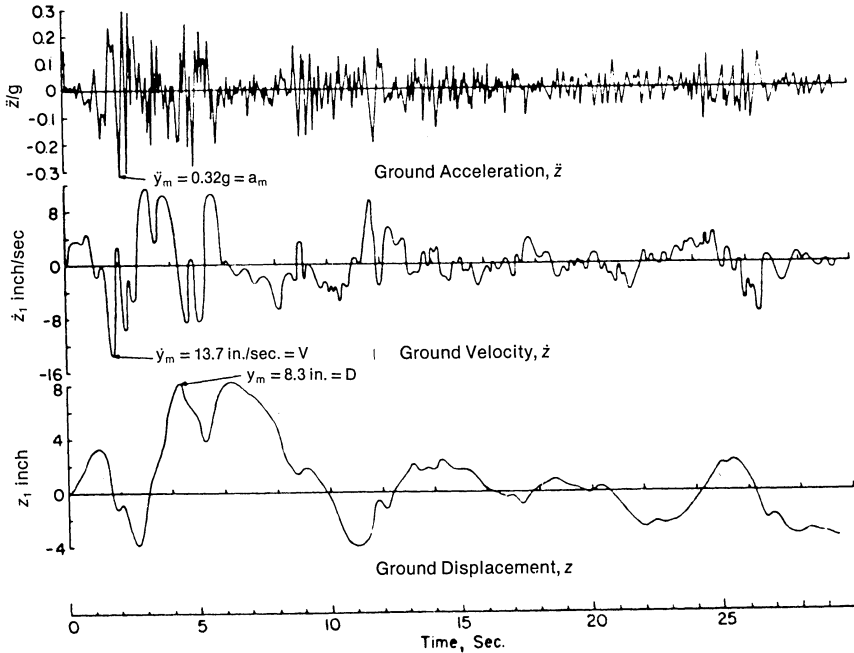


Fig. 21.2.4. El Centro, California earthquake of May 18, 1940, N-S component.

- i. For very low frequency systems, less than 0.05 cps, the maximum displacement is constant and equal to the maximum ground displacement, regardless of the amount of damping in the system.
- ii. For relatively low frequency systems, less than 0.3 cps, the maximum displacement shows a slight amplification over the maximum ground displacement. The amount of damping has a moderate influence.
- iii. In the intermediate range of 0.3 to 3 cps, the maximum velocity is nearly constant. Its magnitude is strongly influenced by damping. Since the kinetic energy of the oscillator is proportional to the square of its velocity, constant maximum velocity indicates that the oscillator absorbs a constant amount of energy in this frequency range.
- iv. In the medium-high frequency range (3 cps to 25 cps), the maximum acceleration shows a slight amplification over the maximum ground acceleration. The amount of damping has a moderate influence.

- v. In the high frequency range, over 25 Hertz, the maximum acceleration a_m is equal to the maximum ground acceleration. The amount of damping has no influence.
- vi. The local peaks and valleys in the response spectra are of inconsequential import in characterizing the ground motion. Since a small shift in the frequency would change the response significantly; and since the frequency cannot be ascertained with great accuracy, the spectrum should be smoothed out so that the modified spectrum envelopes the generated spectrum.

The above properties of the response spectrum permit the development of “design spectra” for a site if the values of maximum ground displacement, pseudo-velocity, and acceleration are specified. The procedure for obtaining the design spectrum was first proposed by Newmark, et al., [21.2.1]. It consists of the following steps:

- i. The maximum values of ground acceleration, velocity and displacement are sketched out on a tripartite logarithmic chart as shown in Fig. 21.2.5. These plots give a polygonal curve on the plot.
- ii. The design response spectrum is delineated by straight line bounds.

Depending on the value of the damping factor, amplification factors to the ground motion are applied to the constant displacement, velocity and acceleration segments of the ground motion spectra. For velocity, the bound is parallel to the ground velocity plot. The acceleration plot is parallel to the ground acceleration from f_1 to $4f_1$, where f_1 is the intersection point of constant velocity and constant acceleration segments. A straight line is drawn from the acceleration point at frequency $4f_1$ to the point on the ground acceleration line at $10f_1$. Beyond $10f_1$, the spectrum bound is the same as the maximum ground acceleration line.

Figure 21.2.5 also gives the amplification factor for different values of the damping parameters. The smoothed response spectrum for 2% damping is illustrated. The U.S. Nuclear Regulatory Commission’s recommended procedure for generating design response spectra is based on the foregoing concepts [21.2.2].

It follows from the above discussion that equipment having fundamental frequencies above a certain value will not experience any amplification of ground acceleration. The datum value for this so-called “rigid range” is 25–33 Hz. If the fundamental frequency of the hardware is above datum, then its seismic analysis can be conducted by using static analysis methods (see Chapters 18–20). However, if the fundamental frequency of the equipment lies below the datum frequency, then the equipment response sustains some amplification. It is then necessary to estimate the amount of damping available in the equipment. The exact amount of damping is hard to establish; however, empirical guidelines in this matter are available in the published literature [21.2.3].

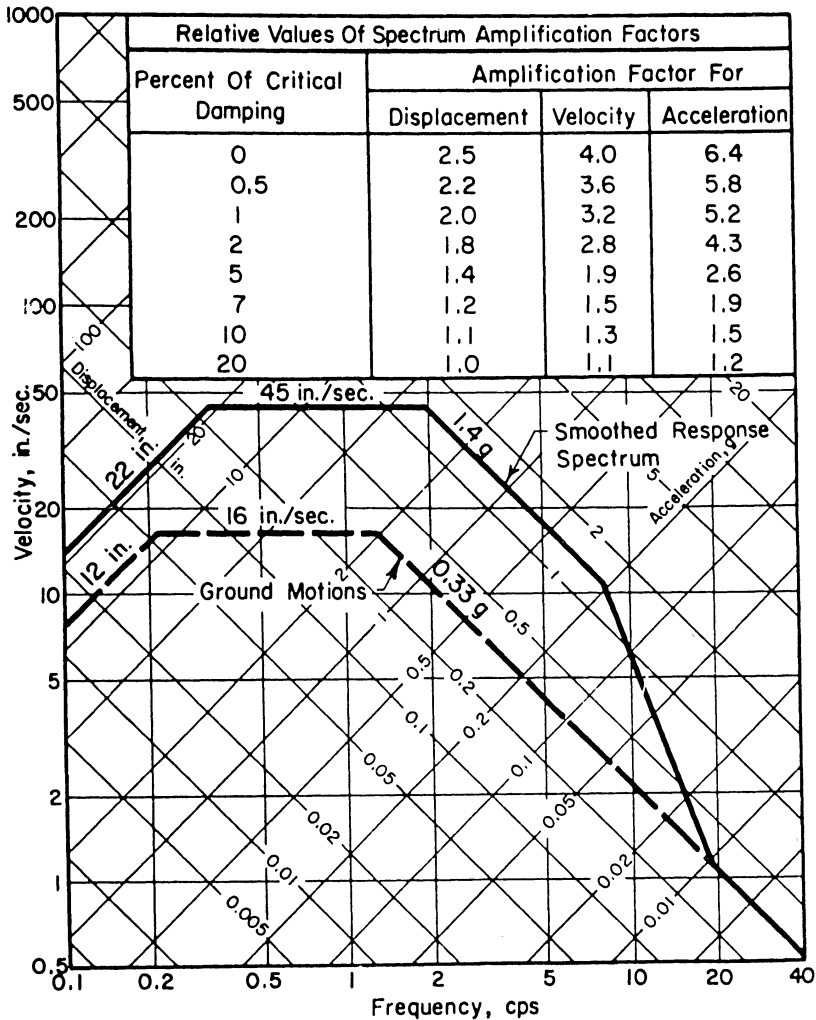


Fig. 21.2.5. Smoothed tripartite logarithmic response spectrum for 0.33 g earthquake, 2 percent critical damping.

Before proceeding to demonstrate the application of the response spectrum to determine equipment response, it is necessary to develop the mathematical basis for its construction. This mathematical basis is presented in the next section.

21.3 RESPONSE OF A SIMPLE OSCILLATOR TO SEISMIC MOTION

The single degree-of-freedom system shown in Fig. 21.2.1 consists of a mass m attached to the support via a linear spring of stiffness k and a

damper of damping coefficient c . *Relative displacement* of the mass with respect to the support, y , and its relative velocity dy/dt produce opposing forces ky and $c dy/dt$ in the spring and damper, respectively. If \ddot{z} denotes the acceleration of the support with respect to the inertial reference plane, then the absolute acceleration of the mass is $(\ddot{y} + \ddot{z})$.* Newton's second law gives:

$$m(\ddot{y} + \ddot{z}) + c\dot{y} + ky = 0$$

$$\text{or} \quad m\ddot{y} + c\dot{y} + ky = -m\ddot{z} \quad (21.3.1)$$

The left-hand side of Eq. (21.3.1) is recognized as the equation for free vibration of the oscillator. Thus, the net effect of the ground motion is equivalent to an external force $-m\ddot{z}$ applied on the mass. Dividing throughout by m , and using the definitions

$$\eta = \frac{c}{2m}, \quad \omega_0 = (k/m)^{1/2}$$

we have

$$\ddot{y} + 2\eta\dot{y} + \omega_0^2 y = -\ddot{z} \quad (21.3.2)$$

ω_0 is the undamped natural frequency of the system, and η is equal to $\zeta\omega_0$ where ζ is the fraction of critical damping (see Section 16.9.2 or Ref. [21.3.1]).

The solution of the free vibration problem (with \ddot{z} set equal to zero), defined by Eq. (21.3.2), is given by

$$y = e^{-\eta t} \left[y_0 \cos \omega t + \frac{\dot{y}_0 + \eta y_0}{\omega} \sin \omega t \right] \quad (21.3.3)$$

where

$$\omega = (\omega_0^2 - \eta^2)^{1/2} = \omega_0(1 - \zeta^2)^{1/2} \quad (21.3.4)$$

ω is known as the "damped frequency" of the system. y_0 and \dot{y}_0 are the displacement and velocity at $t=0$ (initial conditions).

The particular solution for $-\ddot{z}$ is constructed from first principles in the following.

If the mass is initially at rest and if at time $t=0$, the base is given an acceleration \ddot{z} that lasts for an infinitesimal time dt , the base will attain a velocity $\dot{z}dt$. Since the mass is initially at rest, it follows that at time dt , the mass will have a relative velocity $-\dot{z}dt$, and zero relative displacement. The subsequent response, dy , of the mass is given by setting $y_0 = 0$, and $\dot{y}_0 = -\dot{z}dt$ in Eq. (21.3.3). We obtain:

$$dy = -\frac{1}{\omega} e^{-\eta t} \dot{z} \sin \omega t dt \quad (21.3.5)$$

The continuous seismic acceleration function can be thought of as a succession of increments of $\dot{z}dt$ as shown in Fig. 21.3.1. The response at

*Dot ($\dot{}$) denotes differentiation with respect to time.

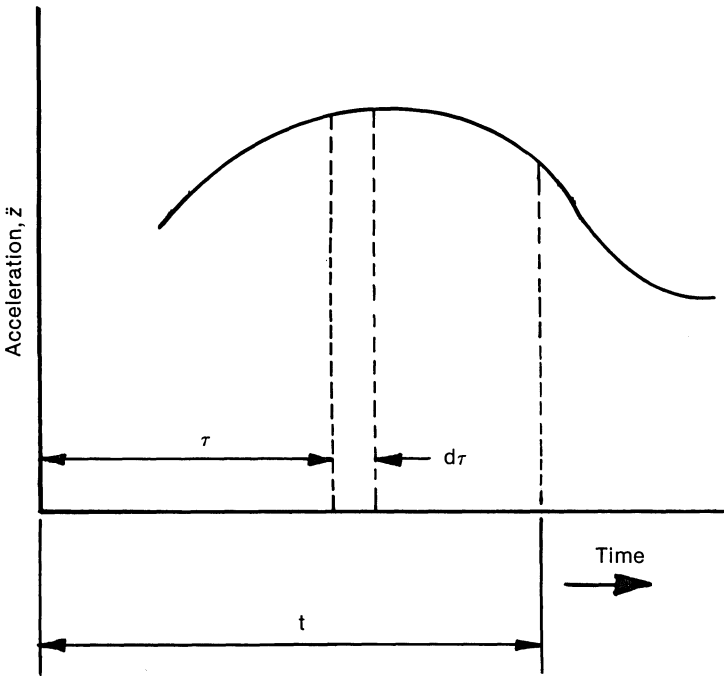


Fig. 21.3.1. Velocity impulse at τ .

time t due to the increment at time $\tau < t$ is given by Eq. (21.3.5) if t is replaced by $(t - \tau)$.

$$dy = \frac{-\ddot{z}}{\omega} e^{-\eta(t-\tau)} \sin \omega(t-\tau) d\tau; \quad t > \tau \tag{21.3.6}$$

Therefore, the response to a continuous \ddot{z} is given by summing up the response produced by all the increments.

$$y = -\frac{1}{\omega} \int_0^t e^{-\eta(t-\tau)} \ddot{z}(\tau) \sin \omega(t-\tau) d\tau \tag{21.3.7}$$

Equation (21.3.7) gives the displacement response of the single degree-of-freedom system mass to the seismic forcing motion assuming that the system starts from rest. The function $y(t)$ can be plotted as a function of time t ; the maximum value of y (called D in the preceding section) is referred to as the displacement response at frequency ω_0 for fractional damping ζ . Values of D , the maximum value of $y(t)$, can be obtained for different values of ω_0 ($\omega = \omega_0(1 - \zeta^2)^{1/2}$) and thus the “displacement response spectrum” can be constructed for a given fractional damping.

The expression for relative velocity, dy/dt can be obtained by differentiating Eq. (21.3.7) with respect to t .

$$\begin{aligned} \frac{dy}{dt} = & - \int_0^t \ddot{z} e^{-\eta(t-\tau)} \cos \omega(t-\tau) d\tau \\ & + \frac{\eta}{\omega} \int_0^t \ddot{z} e^{-\eta(t-\tau)} \sin \omega(t-\tau) d\tau \end{aligned} \quad (21.3.8)$$

Equations (21.3.7-8) can be recast in a more convenient form by defining the integrals:

$$A = \int_0^t \ddot{z} e^{-\eta(t-\tau)} \cos \omega \tau d\tau \quad (21.3.9)$$

$$B = \int_0^t \ddot{z} e^{-\eta(t-\tau)} \sin \omega \tau d\tau \quad (21.3.10)$$

Note that A and B are functions of time t , ω_0 , and ζ .

Expanding the trigonometric functions in Eqs. (21.3.7-8) and rearranging terms, we have:

$$y = - \frac{1}{\omega} (A \sin \omega t - B \cos \omega t) = - \frac{1}{\omega} (A^2 + B^2)^{1/2} \sin(\omega t - \alpha) \quad (21.3.11)$$

$$\begin{aligned} \dot{y} = & - \left(A + \frac{\eta}{\omega} B \right) \cos \omega t - \left(B - \frac{\eta A}{\omega} \right) \sin \omega t = \\ & - \left(1 + \frac{\eta^2}{\omega^2} \right)^{1/2} (A^2 + B^2)^{1/2} \cos(\omega t - \beta) \end{aligned} \quad (21.3.12)$$

where

$$\alpha = \tan^{-1} \frac{B}{A} \quad (21.3.13)$$

$$\beta = \tan^{-1} \frac{B - \frac{\eta}{\omega} A}{A + \frac{\eta}{\omega} B}$$

The expression for absolute acceleration ($\ddot{y} + \ddot{z}$) is conveniently obtained using Eq. (21.3.2)

$$\ddot{y} + \ddot{z} = -2\eta \dot{y} - \omega_0^2 y$$

Substituting for y and \dot{y} from Eqs. (21.3.11-12) and rearranging terms, we obtain

$$(\ddot{y} + \ddot{z}) = \omega \left(1 + \frac{\eta^2}{\omega^2} \right) (A^2 + B^2)^{1/2} \sin(\omega t - \gamma) \quad (21.3.14)$$

where the phase angle γ is defined as

$$\gamma = \tan^{-1} \frac{\left(1 - \frac{\eta^2}{\omega^2}\right)B - \frac{2\eta A}{\omega}}{\left(1 - \frac{\eta^2}{\omega^2}\right)A + \frac{2\eta B}{\omega}} \quad (21.3.15)$$

The response of the system can be expressed in concise terms by setting

$$\frac{1}{2} (A^2 + B^2) \left(1 + \frac{\eta^2}{\omega^2}\right) = \epsilon \quad (21.3.16)$$

so that

$$y = -\frac{1}{\omega_0} (2\epsilon)^{1/2} \sin(\omega t - \alpha) \quad (21.3.17)$$

$$\dot{y} = - (2\epsilon)^{1/2} \cos(\omega t - \beta) \quad (21.3.18)$$

$$\ddot{y} + \ddot{z} = \omega_0 (2\epsilon)^{1/2} \sin(\omega t - \gamma) \quad (21.3.19)$$

The functions A and B turn out to be approximately equal for earthquake ground motions; hence for small damping ($\eta^2/\omega^2 \ll 1$) α , β , and γ are approximately equal. Therefore, the maximum relative displacement, the maximum relative velocity, and the maximum absolute acceleration are related in the manner of a simple oscillator—a remarkable happenstance of nature.

It is noted that for each earthquake, the displacement, velocity and acceleration spectra need be generated only once. Housner and his co-workers [21.3.2] pioneered the generation of such spectra for a large number of earthquakes. As stated in the preceding section, even when detailed information on the earthquake is not available, the design response spectrum can be constructed with relative ease. Once the spectra are available, the task of seismic analysis of multiple degree-of-freedom becomes quite straightforward, as is shown in the next section.

21.4 APPLICATION TO HEAT EXCHANGER TYPE STRUCTURES

As noted in the previous chapters, most heat exchangers can be modeled as beam-like structures for seismic analysis purposes. Therefore, application of the response spectrum method to heat exchangers is developed herein with direct reference only to beams. For application to other multi-degree of freedom models, the reader is directed to [21.2.1] which are focused toward seismic analysis of general structures. As noted in Chapter 16, beams are known as continuous systems. They possess infinite degrees-of-freedom. As such they have an infinite number of frequencies of vibration. The free vibration deflection shape of the beam corresponding to a natural frequency is known as the “normal mode” for the beam. In Chapter 16, expressions for normal modes and for free vibration

frequencies for some common beam end support conditions have been derived. The normal modes possess the important property of ‘‘orthogonality’’ which is mathematically stated here, without proof, as

$$\int_0^l \mu \psi_m^2 dx = M_m = \text{generalized mass for the } m\text{th mode of vibration;}$$

$\mu = \text{mass per unit length}$

$$\int_0^l \mu \psi_n(x) \psi_m(x) dx = 0; \quad n \neq m \tag{21.4.1}$$

where ψ_i indicates the i th normal mode and l is the length of the beam. Another useful theorem on normal modes states that all forced vibrations of the beam can be expressed as a linear combination of the beam normal modes. Therefore, we can assume the relative displacement response of a beam under seismic excitation \ddot{z} and starting from rest as

$$y(x,t) = \sum C_n \psi_n(x) e^{-\eta t} \sin \omega_n t \tag{21.4.2}$$

where ω_n , $\psi_n(x)$, C_n are the damped circular frequency, the characteristic shape function, and the amplitude coefficient for the n th mode, respectively. We recall that $\psi_n(x)$ can be considered as determined to within an arbitrary constant. We will find it convenient to relate this arbitrary constant to the total beam mass.

As shown in the preceding section, for a simple oscillator, the base excitation is equivalent to a lateral force $-m\ddot{z}$ acting on each element of the mass. The effect of \ddot{z} acting from an infinitesimal time dt is to produce an incremental relative velocity $v_0 = -\ddot{z}dt$ at each point in the structure at time = 0. From Eq. (21.4.2), we obtain

$$\dot{y}(x,t) = \sum C_n \psi_n [-\eta e^{-\eta t} \sin \omega_n t + \omega_n e^{-\eta t} \cos \omega_n t] \tag{21.4.3}$$

Therefore, evaluating Eq. (21.4.3) at $t = 0$, we have

$$\dot{y}(x,t) \Big|_{t=0} = -\ddot{z}dt = \sum C_n \omega_n \psi_n(x)$$

Pre-multiplying both sides by $\mu \psi_m$ and integrating over the length of the beam yields

$$-\ddot{z}dt \int_0^l \mu \psi_m dx = C_m \omega_m \int_0^l \mu \psi_m^2 dx$$

Note that the orthogonality condition (Eq. (21.4.1)) enables us to reduce the summation on the right-hand side to a single term.

Therefore, we obtain

$$C_m = -\ddot{z} \frac{\Gamma_m}{\omega_m} dt \quad (21.4.4)$$

where

$$\Gamma_m = \frac{\int_0^l \mu \psi_m dx}{\int_0^l \mu \psi_m^2 dx} \quad (21.4.5)$$

The parameter Γ_m , which is a function of the mode shape $\psi_m(x)$, is known as the “participation factor” for mode m .

The quantity in the denominator in the r.h.s. of Eq. (21.4.5) is often referred to as the “modal mass” or “generalized mass” for mode m , i.e.

$$M_m = \int_0^l \mu \psi_m^2 dx$$

Substituting for C_m in Eq. (21.4.2) gives the result

$$y(x,t) = - \sum \frac{\ddot{z} \Gamma_m}{\omega_m} \psi_m(x) e^{-\eta t} \sin \omega_m t dt$$

where the sum is over all modes that are important to an accurate representation of y .

As in the case of the simple oscillator, the response due to \ddot{z} acting over a continuous time period is:

$$y(t) = \sum_m \Gamma_m \psi_m \left[-\frac{1}{\omega_m} \int_0^t \ddot{z}(\tau) e^{-\eta(t-\tau)} \sin \omega_m(t-\tau) d\tau \right] \quad (21.4.6)$$

Comparing the quantity in the square brackets with Eq. (21.3.7), it is seen that it is identical to the response of a single degree-of-freedom system of frequency ω_m ; say ϕ_m . Then

$$y(x,t) = \sum \Gamma_m \psi_m(x) \phi_m(t) \quad (21.4.7)$$

Thus, the total response of the beam is equal to the sum of the product of the participation factor, the mode shape, and the simple oscillator response corresponding to the natural frequency of each mode.

For different ω_m , the maximum value of ϕ_m would normally occur at different time instants. Therefore, if D_m represents the maximum relative displacement response (available from the response spectrum for the

earthquake) for ω_m , then a usually very conservative estimate for the maximum displacement at any x is

$$y_{\max}(x) \leq \sum |\Gamma_m \psi_m| D_m \quad (21.4.8)$$

The value of the response, y_{\max} , is often approximated by square-root-of-sum of the squares (SRSS) of the individual maxima of modal responses, i.e.,

$$y_{\max}(x) \doteq \left[\sum_m |\Gamma_m \psi_m D_m|^2 \right]^{1/2} \quad (21.4.9)$$

This usually yields a more realistic estimate of y_{\max} for the case when none of the modal frequencies are closely spaced.

From Eq. (21.4.7), we have

$$\frac{\partial y}{\partial x} = \sum \Gamma_m \frac{d\psi_m}{dx} \phi_m(t)$$

$$\frac{\partial^2 y}{\partial x^2} = \sum \Gamma_m \frac{d^2 \psi_m}{dx^2} \phi_m(t)$$

The bending moment at any section in the beam is given by

$$M = EI \frac{\partial^2 y}{\partial x^2} = EI \sum \Gamma_m \psi_m'' \phi_m(t)$$

where prime (') indicates differentiation with respect to the length coordinate.

Following similar logic as above, the maximum value of the bending moment, at any x , over the time interval of the seismic loading, is

$$M_{\max} \doteq EI \left[\sum_m |\Gamma_m \psi_m'' D_m|^2 \right]^{1/2} \quad (21.4.10)$$

Similarly, the maximum shear distribution is given by

$$Q_{\max} \doteq EI \left[\sum_{m=1} |\Gamma_m \psi_m''' D_m|^2 \right]^{1/2} \quad (21.4.11)$$

The mode shape of a prismatic beam is strictly a function of its boundary conditions. Therefore, the participation factor for a given mode shape is uniquely defined. Since the mode shapes are generally transcendental functions of x , analytical evaluation of the integrals in Eq. (21.4.5) is not always possible. However, numerical values are readily obtained using a computer. The participation factors corresponding to the first three modes for beams, subject to some common boundary conditions, are given in Table 21.4.1.

Table 21.4.1.* Participation Factors for Single Span Beams for Some Common Boundary Conditions

Boundary Condition	Mode	Participation Factor
Fixed-fixed	1	0.8308
	2	0
	3	0.3640
Fixed-pinned	1	0.8604
	2	0.0829
	3	0.3343
Fixed-free (cantilever)	1	0.7830
	2	0.4340
	3	0.2544

*Mode shape functions defined such that $\int_0^l \mu \psi_m^2 dx = \mu l$ for all modes.

We note from Table 21.4.1 that the participation factor for the fundamental mode is always the largest. In general, as m increases, the higher the mode number, the lower the participation factor. For single span beam type structures, it is usually sufficient to consider the first three modes.

We also note that in Table 21.4.1, the participation factors have been calculated by assuming that the generalized mass $M_m =$ total beam mass, μl , for all values of m . As we noted earlier, the mode shapes $\psi_m(x) = A_m F_m(x)$, and A_m may be set to any convenient value with no loss of generality. For example, A_m may be set to unity for all modes, may be adjusted so that

$$\int_0^l \mu \psi_m^2(x) dx = 1$$

or, as we suggest here, may be determined so that the generalized mass $M_m = \mu l$. Note that for the uniform beam considered here, our choice for normalization is the same as requiring that

$$\int_0^l \psi_m^2(x) dx = l$$

To summarize, the response spectrum analysis of heat exchangers consists of the following steps:

- (i) Perform a free vibration analysis, and determine the mode shapes and corresponding natural frequencies which lie in the range of 0 to 40 Hz. The mode shapes and frequencies for single span beams with classical boundary conditions are obtained using standard techniques and are available in books on vibration theory [21.4.1-3].
- (ii) Compute the participation factor Γ_m for mode m using Eq. (21.4.5). Table 21.4.1 gives the values for the first three modes for single span beams for some common boundary conditions.

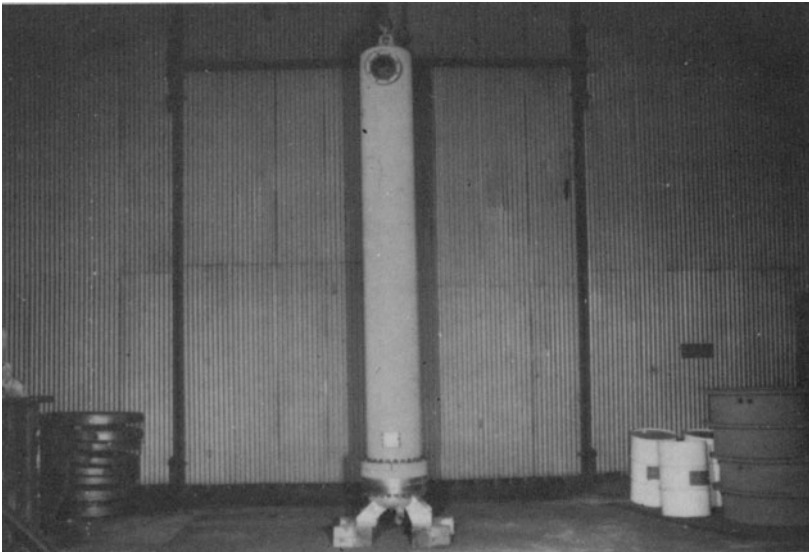
- (iii) Read-off the maximum relative displacement D_m corresponding to each natural frequency ω_m from the displacement response spectrum for the earthquake. We note that Eqs. (21.2.1-2) provide the displacement if the response spectrum for the pseudo-velocity or acceleration is provided instead of the relative displacement spectrum.
- (iv) The maximum relative displacement of a point of coordinate x is then given by Eq. (21.4.9). The maximum flexural moment M_{\max} and Q_{\max} follow from Eqs. (21.4.10) and (21.4.11), respectively. We note that the derivatives of the mode shape functions are required for this purpose.

21.5 AN EXAMPLE

To illustrate the application of the response spectrum method, let us consider a vertically mounted heat exchanger (viz. Photograph 21.a). The exchanger will be modeled as a uniform beam of constant EI which is built-in at the foundation. Therefore, the mode shapes and frequencies are available from the classical solutions for a cantilever. We will assume that the seismic loading acts only in one direction directed transverse to the axis of the unit. The exchanger barrel has the dimensions 23.88" O.D. \times 0.25" effective wall \times 20' long, and is constructed of an alloy steel material ($E = 30 \times 10^6$ psi). Its operating weight is assumed as 40,000 lbs.

The smoothed response spectrum of a horizontal earthquake for the assumed damping factor is shown in Fig. 21.5.1.

The natural frequencies of a cantilever are given by (see Eq. (16.6.16) in Section 16.6).



Photograph 21.a. Vertically mounted heat exchanger with no top support.

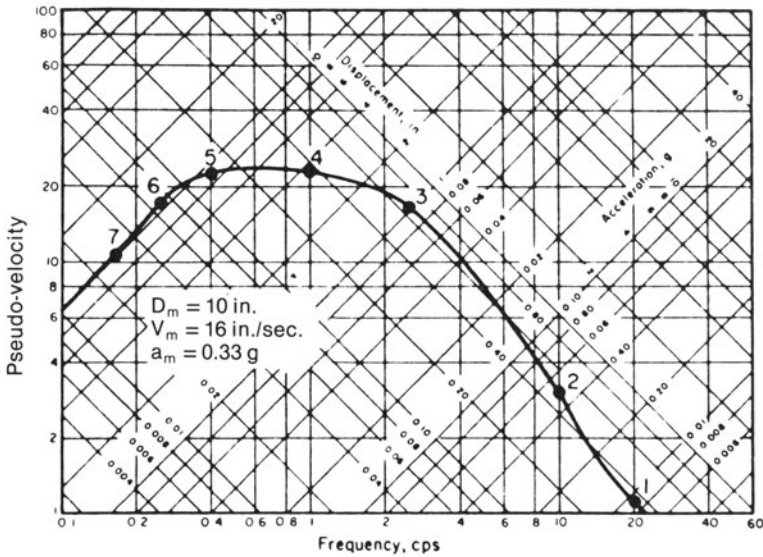


Fig. 21.5.1. Response spectrum for the earthquake of the example problem.

$$\omega_n = \frac{\lambda_n^2}{l^2} \left(\frac{EI}{\mu} \right)^{1/2}$$

where I is the moment of inertia of the beam (heat exchanger section), μ is the mass per unit length, and l is the length of the exchanger. The eigenvalue λ_n^2 depends on the boundary conditions. Values for λ_n and the corresponding mode shapes are given in Table 16.6.1. Some details of the numerical computations are shown below:

$$I = \pi r_m^3 t$$

$$r_m = \text{average radius} = \frac{23.88 - 0.25}{2} = 11.81''$$

$$t = \text{thickness} = 0.25''$$

Hence, $I = (\pi)(11.81)^3(0.25) = 1295 \text{ in.}^4$

$$\mu = \frac{40,000}{(20)(12)(386.4)} = 0.43 \text{ lb-sec}^2/\text{in.}^2$$

Therefore,

$$\omega_n = \frac{\lambda_n^2}{(240)^2} \left[\frac{(30 \times 10^6)(1295)}{0.43} \right]^{1/2}$$

$$\omega_n = 5.22 \lambda_n^2$$

Using the values of λ_n given in Table 16.6.1, for a cantilever beam, Table 21.5.1 can be prepared. The values of the maximum relative displacement corresponding to each of the first three frequencies are read-off from Fig. 21.5.1 and provided in Table 21.5.1. The participation factors reported in Table 21.4.1 are also copied in this table for completeness.

Table 21.5.1. Frequency and Response Data for the Example Problem

Mode No., n	Circular frequency, ω_n (rad/sec)	Natural* frequency, f_n cps	Maximum relative displacement for mode n , (in.)	Participation Factor, Γ_n
1	18.4	2.9	0.09	0.783
2	115.0	18.3	0.01	0.434
3	322.1	51.3	$(0.33)(386.4)/322.1^2$ $= 1.23 \times 10^{-3}$	0.254

* $f_n = \omega_n/2\pi$

We note that the response plot for the earthquake in Fig. 21.5.1 does not extend beyond 22 cps. Therefore, to determine the relative displacement for ω_3 , we used Eqs. (21.2.1-2) along with the fact that the response acceleration a_m is equal to the ground acceleration at high frequencies.

Table 21.5.2 gives the values of the mode shape function ψ , and its derivatives at six equidistant points on the heat exchanger axis ($x=0$ is the base). The mode shapes have been normalized, such that

$$\int_0^l \psi_n^2 dx = l$$

Table 21.5.2. Values of ψ_n , and its Derivatives for the First Three Modes

x/l	First Mode			Second Mode			Third Mode		
	ψ_1	$l^2 \psi_1''$	$l^3 \psi_1'''$	ψ_2	$l^2 \psi_2''$	$l^3 \psi_2'''$	ψ_3	$l^2 \psi_3''$	$l^3 \psi_3'''$
0	0	7.031	-9.677	0	44.07	-210.7	0	123.4	-969.1
0.2	0.128	5.101	-9.571	0.602	3.085	-189.	1.209	-48.74	-584.7
0.4	0.460	6.757	-8.879	1.367	-25.98	-88.95	1.052	-58.49	467.8
0.6	0.922	1.617	-7.192	1.179	-30.12	44.58	-0.948	64.91	632.2
0.8	1.451	0.450	-4.265	-0.140	-13.26	102.4	-0.79	74.60	-384.9
1.0	0	0	0	-2.000	0	0	2.000	0	0

The equipment response at these points can be obtained by straightforward computation following Eqs. (21.4.9-11).

For example, the maximum displacement in the beam, which occurs at the top ($x=l$), is given by:

$$y_{\max}(l) = [|\Gamma_1 \psi_1 D_1|^2 + |\Gamma_2 \psi_2 D_2|^2 + |\Gamma_3 \psi_3 D_3|^2]^{1/2}$$



or

$$\begin{aligned}
 y_{\max} &= \{ [(0.783)(2)(0.09)]^2 + [(0.434)(2)(0.01)]^2 \\
 &\quad + [(0.254)(2)(1.23 \times 10^{-3})]^2 \}^{1/2} \\
 &= [1.986 \times 10^{-2} + 7.534 \times 10^{-5} + 3.904 \times 10^{-7}]^{1/2} \\
 &= 0.141''
 \end{aligned}$$

We note that the first mode dominates the displacement response. Similarly, the maximum bending moment at the root of cantilever ($x=0$) is given by:

$$\begin{aligned}
 M_{\max} &= \frac{EI}{l^2} \{ [(0.783)(7.031)(0.09)]^2 + [(0.434)(44.07)(0.01)]^2 \\
 &\quad + [(0.254)(123.4)(1.23 \times 10^{-3})]^2 \}^{1/2} \\
 &= \frac{EI}{l^2} [2.455 \times 10^{-1} + 3.658 \times 10^{-2} + 1.486 \times 10^{-3}]^{1/2} \\
 &= \frac{(0.5325)(30 \times 10^6)(1295)}{(240)^2} \\
 &= 3.592 \times 10^5 \text{ lb-in.}
 \end{aligned}$$

We note that a uniformly distributed load along the beam, giving rise to a total resultant F , will produce the moment $Fl/2$ at the root. Thus we can see that M_{\max} corresponds to a total lateral load F , where

$$F = \frac{2M_{\max}}{l} = \frac{(2)(3.59 \times 10^5)}{240} = 2993 \text{ lb.}$$

This corresponds to an equivalent static acceleration a_e

$$a_e = \frac{2993g}{40,000} = 0.075g$$

Similarly, the maximum shear at the root of the cantilever is given by

$$\begin{aligned}
 Q_{\max} &= \frac{EI}{l^3} \{ [(0.783)(9.677)(0.09)]^2 + [(0.434)(210.7)(0.01)]^2 \\
 &\quad + [(0.254)(969.1)(1.23 \times 10^{-3})]^2 \}^{1/2} \\
 &= \frac{EI}{l^3} [0.465 + 0.836 + 0.0917]^{1/2} \\
 &= \frac{(1.18)(30 \times 10^6)(1295)}{(240)^3} = 3317 \text{ lb}
 \end{aligned}$$

This corresponds to a static acceleration of

$$\frac{3317g}{40,000} = 0.083g$$

The response at other values of x can be computed in a similar manner. It is apparent from the foregoing algebra that response spectrum calculations are best performed on a digital computer. The results are well worth the effort since the reduction in computed response over static analysis methods, using the maximum expected “ g ” level acceleration, can be considerable.

The equivalent static acceleration obtained for the sample problem here is on the order of $0.08 g$. Comparing this to the $0.33g$ maximum ground acceleration of the earthquake, it appears that a static seismic analysis using the maximum ground acceleration would be unduly conservative for this case.

21.6 SYSTEM RESPONSE WHEN THE NATURAL FREQUENCIES ARE CLOSELY SPACED

In the beam example considered in Section 21.4, we suggested that an estimate of the maximum value of any response during the period of time covered by the seismic loading could be obtained by combining the peak values for each mode using either an absolute value sum or by using a square root of the sum of the squares (SSRS) combination. (See Eqs. (21.4.8) and (21.4.9)). The use of the absolute value sum presumes that all modal contributions act in phase with each other, while the employment of the SRSS combination assumes that all modes do not act in phase, and therefore, a statistical summation is adequate to predict the equipment response.

It is quite clear that when some of the system natural frequencies are closely spaced, then it is likely that the contributions to the response from these modes will be directly additive. Hence, for closely spaced modes, prudence dictates the use of an absolute sum combination, while for the modes which are not closely spaced, the SRSS combination remains valid. The usual definition for “closely spaced” is summarized as follows:

Ascending sequentially from the lowest frequency, modes $i, i+1, \dots, j$, having characteristic frequencies f_i, \dots, f_j , are considered closely spaced if $f_i/f_j > \alpha$. α , known as the closeness ratio is usually set in the range 0.9–1.0.

If closely spaced modes are present, then the SRSS combination given by Eq. (21.4.9) is replaced by the grouping procedure outlined below. We let q_i be any peak result for the i th mode, i.e., displacement, moment, shear, etc. For example, if q_i is a displacement, then

$$q_i = \Gamma_i \psi_i D_i \quad (21.6.1)$$

Let us suppose that modes $k-m$ and $s-t$ are closely spaced, and that all other modes are not to be considered closely spaced. Then a popular generalization of the SRSS combination, which accounts for closely spaced modes, is given symbolically as

$$q = \left[\sum_{i=1}^{k-1} q_i^2 + \left(\sum_{i=k}^m |q_i| \right)^2 + \sum_{i=m+1}^{s-1} q_i^2 + \left(\sum_{i=s}^t |q_i| \right)^2 + \dots \right]^{1/2} \quad (21.6.2)$$

In Eq. (21.6.2), q represents the maximum value of the physical quantity desired, after combining all of the individual modes. We see that if all modes are closely spaced, Eq. (21.6.2) reduces to the absolute sum combination, while if no modes are closely spaced, Eq. (21.6.2) reduces to the square root of the sum of squares combination.

Usually, the design specifications governing the equipment will specify the combination method to be used, and the value for α if closely spaced modes are to be accounted for.

21.7 SYSTEM RESPONSE WHEN MULTI-DIRECTION SEISMIC LOADS ARE IMPOSED

In our discussion to this point, we have considered only seismic excitation in a single direction. However, in many practical situations, the designer is confronted with a seismic qualification task on equipment which is simultaneously acted upon by seismic loads in three orthogonal directions. Under these conditions, the user of the Response Spectrum method of seismic analyses not only must consider how to combine the modal responses from a single excitation direction, but must consider how to combine the results from each direction so as to evolve a realistic result for the maximum response due to simultaneous application of the loadings.

In this section, we consider a general multi-degree of freedom system subject to simultaneous excitations in two or three orthogonal directions. We presume that the response spectrum for each direction is known. For our given system, we assume that the characteristic frequencies f_i and the mode shapes ψ_i are available. Note that ψ_i may be a function of the spatial coordinates describing the systems (as in our beam example), or it may simply be a matrix of amplitudes if we have chosen to use a lumped spring mass model of our system. In any case, given the mode shapes (eigenvectors), and the location of the excitation points, we can obtain the participation factors for each mode for each of the directions of seismic input. We denote these participation factors as Γ_m^k where $k = 1,2,3$ represents the seismic load direction. Generalizing our previous discussions, the peak response in each mode, from each seismic loading, can be written in the following form:

$$q_m^k = \psi_m \Gamma_m^k D_m^k \quad (21.7.1)$$

Note that the modal parameters ψ_m are a function of the system being considered and not of the excitation direction. In general, we will find that the participation factors will be different for each excitation direction.

For the moment, let us disregard the possibility of closely spaced modes, and assume that we will combine the response in each direction using the same method used to combine the modes in any given direction. Therefore, if Q^* represents a total peak response, considering all modes and all directions, then using the absolute sum method, we have, for the k th seismic direction

$$q^k = \sum_m |\psi_m \Gamma_m^k D_m^k| \quad (21.7.2)$$

and

$$Q^* = |q^1| + |q^2| + |q^3|$$

or

$$Q^* = \sum_m |\psi_m| (|\Gamma_m^1 D_m^1| + |\Gamma_m^2 D_m^2| + |\Gamma_m^3 D_m^3|) \quad (21.7.3)$$

We see from Eq. (21.7.3) that it is immaterial in which order we do the absolute sum combination. We may combine the modes for one direction first and then combine the directions, or we may combine the directions for each mode first and then combine the resultant modes.

If we combine the effects in accordance with the SRSS method, then

$$q^k = \left[\sum_m (\psi_m \Gamma_m^k D_m^k)^2 \right]^{1/2} \quad (21.7.4)$$

and

$$Q^* = [(q^1)^2 + (q^2)^2 + (q^3)^2]^{1/2}$$

or

$$Q^* = \left[\sum_m \psi_m^2 \{ (\Gamma_m^1 D_m^1)^2 + (\Gamma_m^2 D_m^2)^2 + (\Gamma_m^3 D_m^3)^2 \} \right]^{1/2} \quad (21.7.5)$$

Again, it makes no difference in which order we do the combination.

It is, of course, possible to use the absolute sum method to combine the results from each direction at the modal level and then use the SRSS method to combine the modal responses, or vice versa. In this case, the order in which the combinations are carried out certainly affects the final results. Similarly, if we impose the criteria for closely spaced modes to combine the results, then the order of combination is also not interchangeable. This can be illustrated by the following example. Suppose we order the N modes so that the first S modes are closely spaced. If we first combine the modes for a given direction, and then combine the directions, we have

$$q^k = \left[\left(\sum_{m=1}^S |\psi_m \Gamma_m^k D_m^k| \right)^2 + \sum_{m=S+1}^N (\psi_m \Gamma_m^k D_m^k)^2 \right]^{1/2} \quad (21.7.6)$$

and if we use the SRSS method to combine directions

$$Q^{*2} = \{ (q^1)^2 + (q^2)^2 + (q^3)^2 \}$$

or

$$\begin{aligned} Q^{*2} = & \left(\sum_{m=1}^S |\psi_m \Gamma_m^1 D_m^1| \right)^2 + \left(\sum_{m=1}^S |\psi_m \Gamma_m^2 D_m^2| \right)^2 \\ & + \left(\sum_{m=1}^S |\psi_m \Gamma_m^3 D_m^3| \right)^2 + \sum_{m=S+1}^N \psi_m^2 [(\Gamma_m^1 D_m^1)^2 \\ & + (\Gamma_m^2 D_m^2)^2 + (\Gamma_m^3 D_m^3)^2] \end{aligned} \quad (21.7.7)$$

Alternatively, if we combine directions first, at the model level, and define the result as q_m , then

$$q_m^2 = \psi_m^2 [(\Gamma_m^1 D_m^1)^2 + (\Gamma_m^2 D_m^2)^2 + (\Gamma_m^3 D_m^3)^2] \quad (21.7.8)$$

If we now combine the modes, taking into account the closely spaced contributions, we obtain

$$\begin{aligned} Q^{*2} = & \left(\sum_{m=1}^S |q_m| \right)^2 + \sum_{m=S+1}^N \left[\psi_m^2 (\Gamma_m^1 D_m^1)^2 + (\Gamma_m^2 D_m^2)^2 \right. \\ & \left. + (\Gamma_m^3 D_m^3)^2 \right] \end{aligned} \quad (21.7.9)$$

The results obtained for Q^* using Eqs. (21.7.7) and (21.7.9) will, in general, be different. We emphasize, again, that the method of combination is usually spelled out in the specification, but the order of combination may not be. The user should use good engineering judgment when specific instructions are lacking.

21.8 FINITE ELEMENT METHOD FOR RESPONSE SPECTRUM ANALYSIS

There are many general purpose finite element codes available in the commercial marketplace that can do a response spectrum analysis of a given structure under a general seismic excitation. Typical of these are the general purpose programs ANSYS [21.8.1] and EASE2 [21.8.2]. To do a complete analysis of a structure, say a vertically or a horizontally mounted shell and tube exchanger, the user simply models the structure with series of nodes and elements. The input required is the usual geometry of the structure, the material characteristics, and the various mass densities. The response spectrum option of these general purpose codes requires specification of

excitation direction, and the frequency and amplitude level of the seismic spectra.

The finite element code generates the characteristic frequencies and mode shapes and computes the appropriate participation factors. The combination of modes and seismic directional response is also carried out automatically with the user required only to input the type of combinations desired. For example, the EASE2 code always combines the directional responses at each modal level first, and then performs the modal combination to obtain the desired result. The user may specify either an absolute sum, a square root of the sum of the squares combination, or an algebraic sum when combining directions at the modal level. When the final modal combination is carried out, the user can specify either an absolute sum, a SRSS combination, or one of six different methods to account for closely spaced modes. The ANSYS code takes a somewhat different approach; namely, the order and type of combination is almost entirely left up to the user. The combinations are carried out in a post-processing section of the code which permits complete user control over the summation methods.

We close this section by noting that the use of these general purpose finite element codes for response spectrum analysis is quite cost effective as it permits the user to define the structure in as detailed a manner as called for by the nature of the service, and by the requirements of the specification. The same overall model can be used for certain static analyses required for design, so that the total effect of static and seismic loads on the entire vessel may be examined.

NOMENCLATURE

- a_e = Equivalent static acceleration
- a_m = Maximum spectral acceleration
- A, B = Response integrals (Eqs. (21.3.9–10))
- c = Damping coefficient
- D = Maximum relative displacement of a single D.O.F. system under a given seismic loading
- E = Young's modulus of beam material
- I = Moment of inertia of beam section
- k = Spring constant (Fig. 21.2.1)
- l = Beam length
- M = Bending moment on beam
- m = Oscillator mass (Fig. 21.2.1)
- n = Scaling factor for the acceleration axis
- Q = Shear force on beam
- q_i = Peak value of response in the i th mode
- q = Summation of all peak modal responses (Eq. (21.6.2))
- Q^* = Total response combining all modal contributions and three earthquakes
- r = Scaling factor for the pseudo-velocity and frequency axes
- t = Wall thickness

- V = Maximum pseudo-velocity (spectral velocity)
 x = Coordinate along beam axis
 y_0, \dot{y}_0 = Initial displacement and velocity (Eq. (21.3.3))
 \ddot{z} = Ground acceleration
 α, β, γ = Response phase angles (Eqs. (21.3.13–15))
 ϵ = Response integral (Eq. (21.3.16))
 ζ = Fraction of critical damping
 η = Damping coefficient ($\eta = c/2m$)
 λ_n = Mode frequency coefficient
 μ = Mass per unit length
 $\psi_m(x)$ = m th mode shape
 ω_0 = Natural frequency of a single D.O.F. undamped system
 ω_n = Natural (damped) frequency of a continuous system in the n th mode
 $\phi_m(t)$ = Relative displacement of a single degree-of-freedom system of frequency ω_m
 Γ_m = Participation factor for the m th mode

Superscript

- k = Denotes the response to k th seismic loading ($k = 1, 2, 3$)

REFERENCES

- [21.1.1] Levy, S., and Wilkinson, J. P. D., "The Component Element Method in Dynamics," McGraw-Hill (1976).
 [21.2.1] Newmark, N. M., and Rosenbluth, "Fundamentals of Earthquake Engineering," Prentice-Hall, Inc., Englewood Cliffs, NJ (1971).
 [21.2.2] "Design Response Spectra for Seismic Design of Nuclear Power Plants," Reg. Guide 1.60, United States Nuclear Regulatory Commission, Washington, D.C. (1973).
 [21.2.3] "Damping Values for Seismic Design of Nuclear Power Plants," USNRC - Reg. Guide 1-61, Washington, D.C. (Oct. 1973).
 [21.3.1] Thomson, W. T., "Vibration Theory and Applications," Prentice-Hall (1965).
 [21.3.2] Housner, G. W., Martel, R. R., and Alford, J. L., "Spectrum Analysis of Strong Motion Earthquakes," Bulletin Seismological Society of America, 43 (1953).
 [21.4.1] Harris, C. M., and Crede, C. E., "Shock and Vibration Handbook," Second Edition, McGraw-Hill (1976).
 [21.4.2] Blevins, R. D., "Formulas for Natural Frequency and Mode Shape," Van Nostrand Reinhold (1979).
 [21.4.3] Gorman, D. J., "Free Vibration Analysis of Beams and Shafts," Wiley (1975).
 [21.8.1] ANSYS User's Manual, Revision 4, Swanson Analysis Corporation, Houston, PA (1983).
 [21.8.2] "EASE2 Manual", Engineering Analysis Corporation, Redondo Beach, CA (1979).

22. PRACTICAL CONSIDERATIONS IN HEAT EXCHANGER DESIGN AND USE

22.1 INTRODUCTION

Discussion of the detailed anatomy of the heat exchanger and the methods to devise analysis-aided designs have been the primary focus of the material presented up to this point in the book. The evolution of a high quality design, however, requires the interplay of practical considerations with mathematical analysis. The designer must give sufficient thought and consideration to practical matters such as integration of the equipment in the available plant space, equipment maintenance, in-service inspection, handling, and repair. While the equipment design specification prepared by the owner/user seeks to serve the function of familiarizing the designer with the overall plant needs, the breadth and depth of information found in the “specs” varies considerably. The material provided in this chapter is aimed to provide the designer with an overview of these “trans-design” topics. Engineers engaged in specification development, and plant personnel responsible for heat exchanger inspection and maintenance, will also find the information presented here useful in their work.

22.2 DESIGN FOR MAINTENANCE

Designing a heat exchanger to facilitate its maintenance and upkeep requires considerations beyond the “heat exchanger data sheet”. Broad provisions for maintenance, of course, must evolve from the design specification prepared by the system/equipment engineers. The specification alone, however, cannot catalog all salient features for convenient maintenance that the equipment designer can incorporate in the hardware with little additional cost. Approaching equipment design from the plant perspective is an essential element to reach the goal of a maintainable heat exchanger. Similarly, the system engineer responsible for developing the equipment specification should also view the plant layout from the vantage point of the heat exchanger designer. Some items behoving consideration by both the specifier and the designer are listed below:

- (i) Degree of dismemberment of the heat exchanger
- (ii) Plant layout and work space
- (iii) Facilities for handling
- (iv) Working environment

- (v) Process hazards
- (vi) In-service inspection
- (vii) Provision for isolation

In the following, we discuss each of these in detail.

(i) Degree of dismemberment of the heat exchanger:

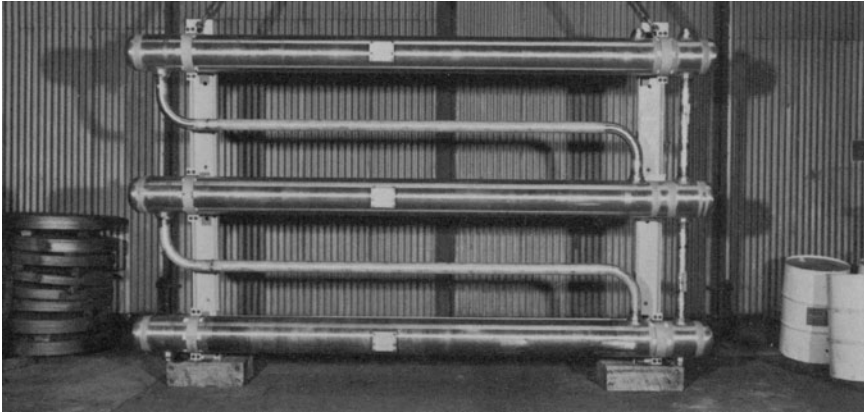
The designer has wide latitude in deciding the number of parts into which a heat exchanger can be separated. For example, Photograph 22.a shows an all welded construction; the degree of dismemberment is nil here. On the other hand, Photograph 22.b shows a U-bundle heat exchanger which can be separated into three parts: the bonnet; the tubesheet/tube bundle; and the shell.

The designer of the latter heat exchanger could have replaced the welded bonnet by a flanged flat cover to permit inspection and plugging of tube ends without breaking the tubesheet-to-channel flanged joint. He could have added a flanged joint at the shell head to shell junction to permit inspection of the U-bends without the inconvenience of removing the entire shell. He could also have elected to weld the shell to the tubesheet, and to introduce a flanged joint a short distance from the tubesheet in the shell. In general, the removability of a part is accomplished by adding a flanged or a packed joint (see Chapter 1 for details on packed joints). Both are more expensive than a welded joint. Therefore, a cost-benefit analysis is required in order to make an informed choice. In addition to commercial considerations, the designer must ensure that the flanged joint is compatible with the remainder of the exchanger design, and with the plant layout. Making a channel removable accomplishes little if the channel nozzles are welded to the plant piping. Making a shell removable would serve little purpose if the support saddles are welded to it, and these saddles are the sole means of supporting the equipment. In a similar vein, the physical removal space must exist in the plant to permit removal of the intended part.

Finally, the hazards of the process fluid must be considered in introducing flanged or packed joints, since these locations of removability are also sites of potential leakage. The designer can use a hybrid flanged joint where the joint is liable to be opened only two or three times in the unit life, and where complete immunity against leakage is desired. This construction is shown in Fig. 22.2.1. The specially shaped “joint rings” are edge welded to affect the seal so that no gasket is needed. Use of a sealing diaphragm is a similar contrivance for increasing flat cover to flanged joint reliability at the cost of some loss in ease of dismemberment.

(ii) Plant Layout and Workspace:

Ease of maintenance calls for permanent access areas, ladders, platforms, stairs, and ample work space. The increase in plant cost due to the added space requirements must be weighed against the tangible and intangible benefits of easier access.



Photograph 22.a. All welded construction.

It is often possible to provide the necessary work space while economizing in the total plant space.

Some common strategies are:

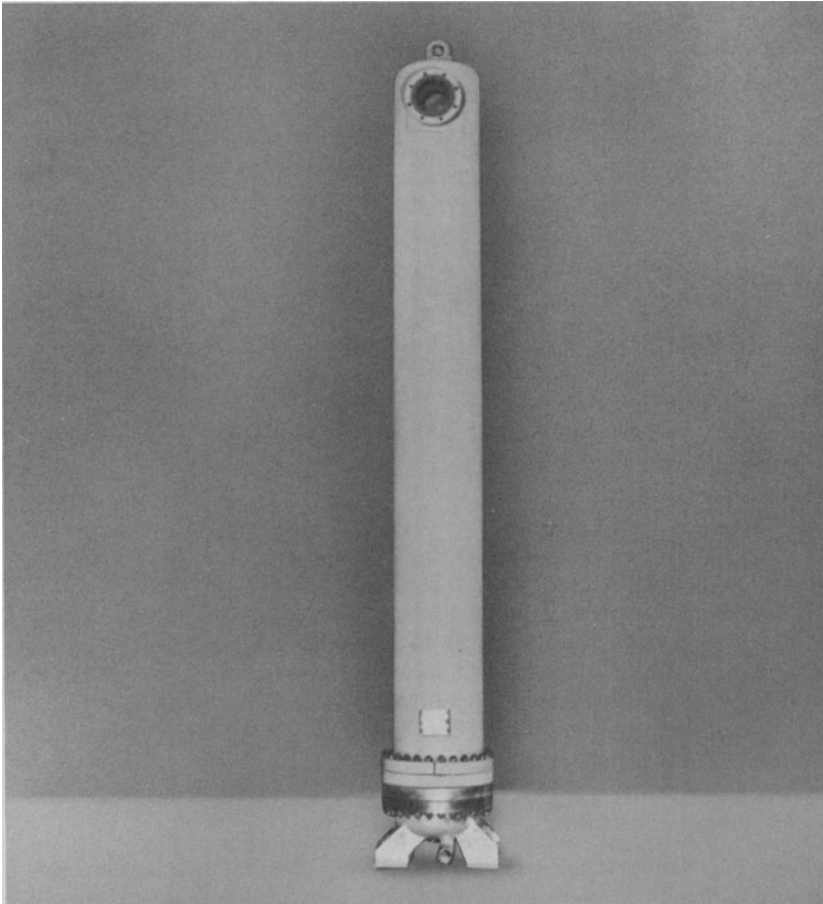
- (a) Stack the horizontal heat exchangers such that they share the same floor plan for parts removal and maintenance (see Chapters 17 and 19 for additional information on stacked designs).
- (b) Arrange the heat exchanger such that two or more units share the same floor space for bundle removal and maintenance work.
- (c) Provide removable spool pieces in piping runs that intrude into the heat exchanger work space.

(iii) Facilities for handling:

A heat exchanger is usually far heavier than other pressure vessels of comparable size. A preliminary estimate of the equipment weight should be made at the plant layout stage to enable the design of proper handling facilities. The plant designer can provide crane rails and trolleys for future use with a hoist, eye bolts at strategic locations for direct lift of relatively light parts such as the channel cover or the bonnets, tracks in the floor for moving dollies to carry the bundle, anchorage points for chain hoists, and the like. On the other hand, the equipment designer should incorporate tracks and bundle runners in the shell for long bundles which would be removed using dollies on rails. Vertical bundle insertion and removal (see Photograph 22.c) does not require bundle runners; instead, adequate overhead space, and bundle upending space, is needed.

(iv) Working environment:

Proper execution of the maintenance operation requires a number of ancillary provisions such as: (a), sufficient lighting and ventilation; (b),



Photograph 22.b. Vertically mounted TEMA type BEU heat exchanger with a top seismic lug.

utilities for electric and pneumatic tools and for electric welding machines; (c), a demineralized water supply for equipment wash-down or tube clean up; (d), floor drains, etc.

(v) Process hazards:

The heat exchanger design and plant support facilities can sometimes be equipped with features to provide a measure of protection to the maintenance and inspection personnel when the unit contains potentially hazardous fluids. For example, heat exchangers containing reactor coolant water in a nuclear power plant can have potentially radioactive material in that stream. Placing the reactor coolant stream inside the tubes and the other stream (with much less probability of contamination) in the shellside

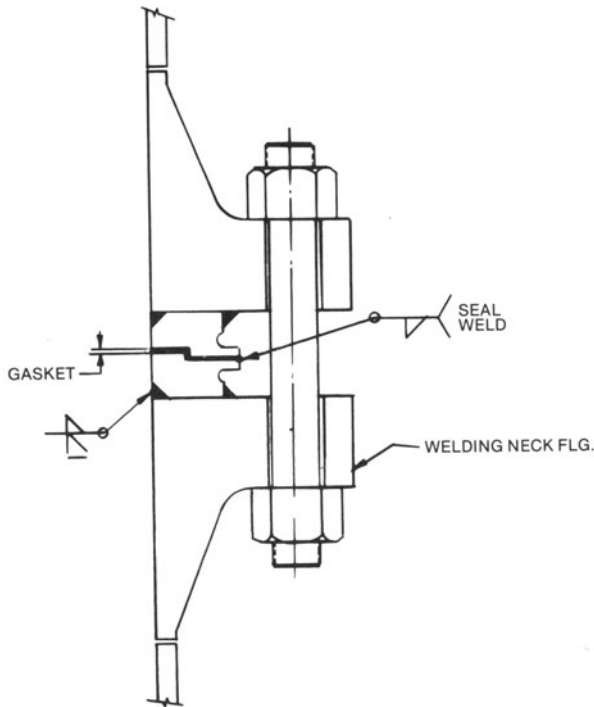


Fig. 22.2.1 Hybrid flanged joint.

provides a measure of self-shielding, since most of the heat exchanger exterior walls are in contact with the shellside fluid. Double tubesheet designs (see Chapter 10 for details) are found to enhance personnel safety in many process applications.

(vi) In-service inspection:

Section XI of the ASME Boiler and Pressure Vessel Code provides detailed requirements for in-service inspection of heat exchangers used in nuclear power plants. This inspection program is mainly focussed on the pressure parts and on the support welds. The design of the heat exchanger for nuclear power plant service must ensure that the welds subject to in-service inspection are accessible, and are capable of being examined in accordance with code rules. In particular, welds required to be volumetrically examined should have calibration blocks made upon completion of manufacturing, and shipped to the site with the heat exchanger, for the purpose of interpreting the results of future volumetric examinations.



Photograph 22.c. Vertical bundle insertion. (Courtesy Joseph Oat Corporation, Camden, NJ)

(vii) Provision for isolation:

Providing isolation valves on both sides of the heat exchanger permits repairing the unit without draining the entire system. Isolation valves are a must where several heat exchangers operate in parallel. Some exchangers are provided with flow bypass lines, such that system operation may be continued while the heat exchanger is being repaired. In most cases, it is possible to design each exchanger in a parallel network containing several of them, such that it can withstand the additional flow resulting from isolation of one unit in the network. Typically, the tubeside of a heat exchanger can accept flows two or three times above normal (sometimes even greater) for short durations without structural damage. It is seldom possible to design the shellside to accept flows in excess of 200% of the design flow without undue sacrifices in compactness and economy of construction. Designing the capability for added flow through each heat exchanger in a parallel batch eliminates the need for bypass lines and associated valves. This can mean significant savings in plant cost and elimination of a potential maintenance nuisance; viz. isolation valves.

22.3 SELECTING THE RIGHT TUBE

Selecting the tube material and the tube size is perhaps the most crucial decision in heat exchanger design. The tube wall must be thin enough to act as an efficient transport medium for heat. Therefore, the designer cannot provide a liberal “corrosion allowance” on the tube wall. In most cases involving alloy materials, no corrosion allowance is provided. The selection of tube material is usually made by the owner who is best familiar with the chemical and metallurgical effects of the process fluids on the candidate tubing materials. The selection of the tubing material is of significant import to the heat exchanger design. For example, U-tubes made from ferrite alloys cannot be bent to as tight a radius as austenitic stainless tubes. Welding of ferritic alloy tubing is also more difficult; the welding surface must be extremely clean and the welded zone must be thoroughly purged. For this reason, welding of tube-to-tubesheet joints involving ferritic alloys is done under a heavy argon purge after roller expanding the tube. The purging requirement for welding austenitic stainless tubing is not as severe; in fact, the tubes are routinely welded before roller expansion. The sequence of tube expanding after welding is preferable in as much as it enables a suitable leak test of the weld joint before the roller expansion is carried out.

Section II of the ASME Boiler and Pressure Vessel Code is usually a good guide for material specification. However, it cannot address individual process requirements. For example, admiralty brass tubing in the straightened condition is known to be prone to stress cracking [22.3.1]. Annealing of admiralty brass tubing as the last operation should be added in those applications where the danger of stress corrosion exists.

The selection of the tube material has consequences beyond the reliability of the heat exchanger itself. Failure of condenser tubes in one power plant installation led to intrusion of sea water into the condensate stream which actuated massive stress corrosion failure of high pressure feedwater heater tubes [22.3.2]. The use of copper-nickel tubes in surface condensers has been held at least partly responsible for widely reported failure of tubes in steam generators of Westinghouse designed pressurized water reactor plants [22.3.3]. Clearly, the choice of tube material is not one of casual selection.

Determination of the tube diameter is usually left up to the heat exchanger designer. Tube diameter is an important variable in optimizing the thermal performance of the heat exchanger. However, too small a tube diameter makes tube cleaning difficult. Tubes under 1/2" diameter should not be used unless strong arguments for their use can be shown to exist in a particular case.

Tubes with a variety of fins are now available. Heat transfer considerations will nearly always dictate the choice of the finning geometry used.

22.4 HANDLING

Handling of a heat exchanger takes place during: (i), unit fabrication,

and shipment of the completed unit from the manufacturer's shop; (ii), removal from the carrier and installation in the plant; (iii), scheduled and unscheduled inspection of the internals; (iv) repair of internals; and (v), shipment to an outside facility for major repairs such as retubing of the bundle, remachining of flanges, replacement of the baffle case, etc.

The handling considerations in each of these operations are somewhat different. The tube bundle is liable to be lifted and moved a few times during the course of fabrication in the manufacturer's shop. It is not advisable to lift a heavy tube bundle (over 20,000 lb) using slings or straps, especially if the bundle is for an unstayed tubesheet type (e.g., U-bundle). Photograph 22.d shows a multiple-tube pass bundle being lifted with a specially designed "bellyband" near the U-bend end, and a special adapter plate bolted to the tubesheet. Light bundles, however, can be lifted using straps in the manner shown in Photograph 22.e.

The height of the lower-most projection from the heat exchanger (usually the nozzle ends or the support attachments) should be no more than 6" to 12" off the floor during the movement of the equipment. ANSI publications [22.4.1-2] are excellent sources of information on guidelines for cranes, slings, chains, and other accessories in the handling operation. NUREG-0612 [22.4.3] is also an excellent handling instruction document even though it is specially written for nuclear plants.

Handling operations during receipt, during removal from the carrier, and during plant installation, are usually performed by site personnel. The heat exchanger is in an assembled condition when it arrives at the site. The heat exchanger may have several ostensible "lift points," of which only two are meant for lifting the entire unit. Other "lift points" may be intended for lifting the channel cover, shell head, etc., *alone*. In some instances, they may not be lift locations at all (such as the seismic restraint lug shown in Photograph 22.b). Needless to say, lifting from an unintended location can be hazardous both to the equipment and to the personnel in the vicinity of the hardware.

Every heat exchanger part intended for possible removal should be equipped with appropriate attachments, such as lugs, eye bolts, trunnions, and the like. The shackles, eye bolts, swivel connections, etc., to be used should be specified, preferably by brand name and rating.

Handling during inspection and routine maintenance usually entails removal of a part such as the channel cover, shell, or both the channel and cover as an assembly. Handling of a part requires care in protecting fragile regions such as the gasket bearing surfaces and the butt weld preparations on nozzle ends.

Handling during shipment of the unit for repairs at an outside facility should be preferably carried out with the unit in the assembled condition. Shipping the bare tube bundle or even the shell individually runs the risk of damage during transit. Moreover, it is prudent to establish the fitup of the replaced part with the remainder of the unit before the replaced item is brought back into the plant.



Photograph 22.d U-tube bundle being lifted with special “belly band” rig. (Courtesy Joseph Oat Corporation, Camden, NJ)



Photograph 22.e. Lifting a U-bundle using straps.

22.5 INSTALLATION

Heat exchanger installation is usually a quite straightforward procedure. However, the following observations are intended to alert the reader to some commonplace errors:

(i) Slotted holes:

Slotted holes in heat exchanger supports are intended to provide unrestrained axial thermal expansion/contraction for the shell (see Chapter 17 for details). A misaligned anchor bolt or support hole may defeat this design objective.

(ii) Vents and drains:

Both shellside and tubeside chambers of heat exchangers are provided with vents and drains. The number of drain connections in the channel depends on the number of tube passes in the tubeside. Similarly, heat exchanger shells containing longitudinal baffles (multi-shell pass designs) may require more than one drain connection. Each drain connection should be routed to the discharge point in such a manner that flow from one to the other is not possible. Connecting all drain connections to a manifold would set up an interpass flow path which would derate the heat exchanger.

Some heat exchangers, especially those involved with steam condensation, have operating vents for the purpose of continuous venting of non-condensibles. It is important to correctly identify “start-up” and “operating” vents and pipe them up accordingly.

(iii) Nozzle connections:

Typically, a heat exchanger has four nozzles, although units with multiple inlet and outlet nozzles (e.g., TEMA J and H shells; Table 1.3.1) are not uncommon. In some exchanger configurations, switching of the inlet and outlet nozzles in the shell or the tubesides does not have any heat transfer consequences; however in other units, switching may result in a serious loss of heat duty. Similarly, switching of the shellside and tubeside fluids is of no heat transfer import in some heat exchanger designs (known as “stream symmetric” designs [22.5.1] in the literature).

Interchanging of inlet and outlet nozzles in flow stream, or switching of fluids between shell and tubesides should not be done without a careful design review. In most cases, material selection, impingement considerations [Section 1.7], operating pressure, etc. would inhibit such a switch.

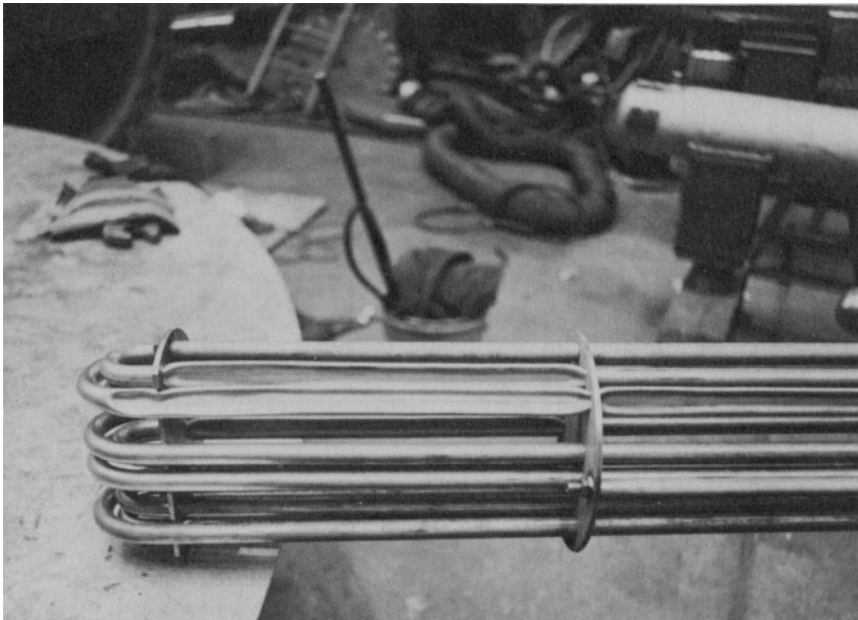
22.6 OPERATION

Normal operation of heat exchangers usually requires little operator attention. However, operating life of a heat exchanger can be drastically

curtailed by improper start-up and shutdown practices. Some common problems are: (i), tube failure due to “water hammer” effect caused by opening the shell inlet valve too quickly; (ii), bending of the pass partition plates in the channel due to “slug flow” from the tube inlet nozzle caused by rapid opening of the channel inlet valve; (iii), introduction of tubeside fluid in a fixed tubesheet heat exchanger with the shellside empty (since the resulting change in the tube metal temperature may overstress the tube-to-tubesheet joint resulting in joint failure); and (iv), thermal stress induced cracking of thick sections in regions of gross structural discontinuity (see Chapter 2), such as tubesheet/channel junction in integral designs, due to rapid changes in the fluid temperature. In order to avoid such problems, start-up and shut-down of the equipment should be carried out in a manner consistent with the original design basis.

At times, heat exchangers are designed to operate under differential pressure; i.e., the shell and tubeside pressures are always present simultaneously. The operator should ensure that the design assumption of differential pressure is never violated, including the periods of start-up and shut-down, or the period of system pressure testing. Photograph 22.f shows the consequence of operator’s disregard of this important fact.

Other operational problems in heat exchangers are: flow induced vibration, rapid tube fouling, corrosion and erosion of tube wall, tube joint failure, fluid level control difficulties, and flanged joint leakage. These are discussed in the context of exchanger maintenance in the next section.



Photograph 22.f. Buckled tube due to shellside overpressure.

22.7 MAINTENANCE AND TROUBLE-SHOOTING

Operating problems in heat exchangers may be broadly classified into three groups:

- (i) Structural problems
- (ii) Performance problems
- (iii) Metallurgical problems

(i) Structural problems:

Structural problems are the most insidious; failure is often swift and irreversible. Failures caused by flow induced vibration of heat exchanger tubes overshadow all other structural failures. Since flow induced vibration has been treated in depth in Chapter 16, we will not discuss it further here. Tube-to-tubesheet joint failure is also a frequent operational problem. Methods to repair or plug leaking joints are described in Chapter 7.

The other type of structural failure encountered in heat exchanger operation is leakage from bolted joints. Leaks frequently occur at nozzle flanges due to moment loading of the joint caused by thermal expansion of inter-connecting piping. These loads may not have been considered in the sizing of the joint. The flanged joints in the body of the heat exchanger may also experience leakage. These joints are tested at pressures which are normally at least 50% greater than the design pressure. Thus, the hydrostatic test pressure often exceeds the operating pressure by as much as 100%. Despite such a large factor of safety, some joints still leak. The most recurrent reason for this is over-bolting of the joint. In some cases, non-symmetrical temperature distribution in the tubesheet or cover in multiple pass designs induces joint leakage. Replacement of the leaking gasket with one having more appropriate loading and relaxation properties is usually the panacea for such problems. Tightening the bolts beyond specified limits may deform the flange, and can further aggravate the joint leakage.

(ii) Performance problems:

Performance problems are usually caused by excessive tube fouling. Deposition of foulants on the inside of the tube surface reduces the available flow area and increases the skin friction, causing an increase in pressure loss and decrease in heat transfer. Uneven rates of fouling of tubes usually occur in units with low flow velocity designs. Uneven fouling may occur on the shellside of the tubes due to a poor baffling scheme which leads to a flow maldistribution. Highly non-uniform fouling can severely modify the metal temperature profile in some tubes resulting in large tube-to-tubesheet joint loads. Deposits of adherent fouling material in the crevices of the shellside, particularly in the baffle-tube annuli, can eliminate the A-stream (see Chapter 16) of the shellside flow and lead to a modification (usually reduction) in the average shellside film coefficient.

Thermal stresses in the internals of the heat exchanger can cause serious degradation of heat duty. The most obvious example is failure of welds joining pass partition plates to each other, and to the channel. These welds are “non-pressure part” welds, and therefore usually do not undergo the kind of close scrutiny accorded to the “pressure part welds”. These welds are not tested during final hydrotest. Moreover, they are completely immersed in the process fluids which often accelerates their corrosion rate. Failure of these internal welds can produce large internal flow bypass resulting in drastic heat duty reductions.

(iii) Metallurgical problems:

Stress corrosion, galvanic corrosion, and erosion are the most frequently reported metallurgical problems. Care in the selection of materials can eliminate most of these problems. Where galvanic action cannot be completely eliminated, the use of “waster” anodes is recommended.

Examination of tube failure is usually carried out by removing the channels and by subjecting the shellside to a hydrostatic test. In some exchanger styles, particularly TEMA S and T, the shellside of the heat exchanger cannot be sealed against pressure with the channel removed unless other provisions are made. The common strategy is to use specially fabricated test rings (see Fig. 22.7.1). The user should purchase the “test ring” with such units and require that their soundness be proved during the shop hydrostatic test.

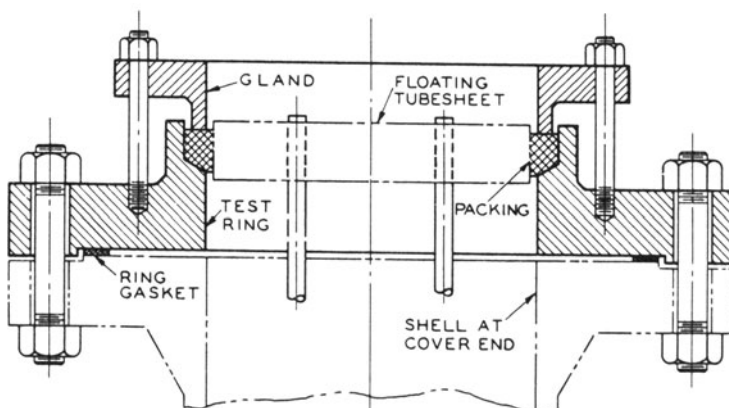


Fig. 22.7.1. Test ring (reprinted from TEMA standards with the courtesy of the publisher).

REFERENCES

- [22.3.1] Goetchens, D. F., “Criteria for Tube Materials Selection for Heat Exchangers in the Power Generation Industry,” Second Symposium on Shell and Tube Heat Exchangers, American Society for Metals, Metals Park, Ohio (1982).

- [22.3.2] Lunt, H. E., Bredder, R. E., and Weilhranch, P. E., "Failure of High Pressure Feedwater Heater Tubes following Seawater Intrusion," American Society for Metals, Metals Park, Ohio, (1982).
- [22.3.3] Electric Power Research Institute, reports NP-2703, NP-2704-SR, NP-2706, NP-2711, Palo Alto, California (1982).
- [22.4.1] "American National Standard for Special Lifting Devices for Shipping Containers Weighing 10,000 Pounds or More for Nuclear Materials," ANSI N14.6-1978.
- [22.4.2] American National Standard, "Safety Standards for Cranes, Derricks, Hoists, Hooks, Jacks and Slings," ANSI-B30.9-1971.
- [22.4.3] "Control of Heavy Loads at Nuclear Power Plants – Resolution of Generic Technical Activity A-36," NUREG-0612, USNRC, Washington, D.C. (July 1980).
- [22.5.1] Singh, K. P., "On the Necessary Criteria for Stream-Symmetric Heat Exchanger Geometries," Heat Transfer Engineering, Vol. 3, No. 1, pp. 19–22 (1981).

APPENDIX A

Classical Plate and Shell Theory and its Application to Pressure Vessels

A.1 INTRODUCTION

The study of the structural behavior of heat exchanger and pressure vessel components under mechanical and thermal loads inevitably requires use of the so-called “plate and shell theory.” Classical plate and shell theory is over a century old, and well documented in a number of excellent books. The pressure vessel designer, however, does not need to master the extensive body of information in this field to conduct his work. In order to understand and implement the analyses presented in this book, it is sufficient to acquire an understanding of axisymmetric loading of circular plates and of cylindrical shells. Axisymmetric loading implies that the stresses and displacements are rotationally symmetric. Internal pressure loading, or edge loading of the shell by the flange ring (Section 3.10) are examples of axisymmetric loads. Classical plate and shell theory permits a straightforward analysis of such loadings. In this Appendix, the necessary concepts of plate and shell theory are capsulized to foster concise comprehension of the subject matter without the peripheral material found in exhaustive treatises on this subject. We demonstrate the underlying unity between the general laws of elasticity and the theories derived herein by evolving the plate and shell equations from the 3-D theory of linear elasticity.

Specific solutions to some plate and shell problems required in this book are also presented to illustrate the solution technique and to supplement the analysis presented in various chapters.

A.2 BASIC ELASTICITY EQUATIONS

Figure A.2.1 shows a differential element of a rotationally symmetric three-dimensional body in the cylindrical coordinate system. The differential element has subtended angle $\Delta\theta$ and thickness Δz . z is the axis of geometric symmetry. If the applied loading is also symmetrical about the z -axis, one would expect the internal stresses to be independent of θ . Figure A.2.1 also shows the internal stresses under the assumption of symmetry of loading and geometry. It is noted that allowing Δr to become *small* (equal to h in Fig. A.2.2) would permit the differential element to simulate a sector of a cylindrical shell wherein the curved surfaces defined by $r = r$, and $r = r + \Delta r$

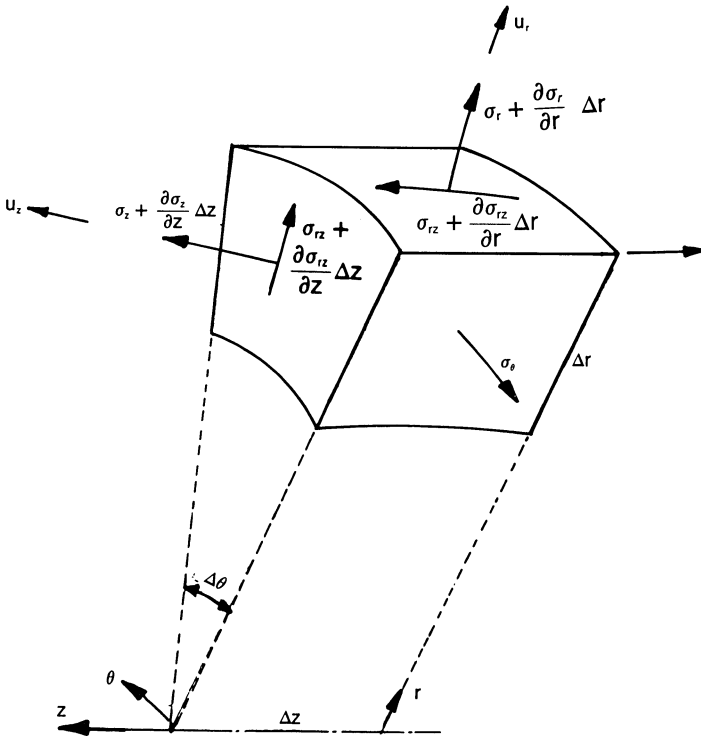


Fig. A.2.1. Freebody of an axisymmetric element under axisymmetric loadings.

represent inner and outer surfaces of the shell. Therefore, the stresses on this surface (viz., σ_r and σ_{rz} at $r=r$) will equal the applied external loads. For the case of internal pressure as the only load, $\sigma_r = -p$; $\sigma_{rz} = 0$ at $r=r$. Similarly, setting Δz small (equal to h in Fig. A.2.3) makes the two flat faces of the element coincide with those of a circular plate. In this case σ_z , σ_{rz} at $z=z_{\text{face}}$ must equal the applied surface loads on that face. Thus, by shrinking the appropriate dimension in the element of Fig. A.2.1, we can elicit the characteristic of a shell or a plate element. The equilibrium relations for the element in r and z directions can be written by direct inspection. These are:

$$\frac{1}{r} \frac{\partial}{\partial r}(r\sigma_r) + \frac{\partial \sigma_{rz}}{\partial z} - \frac{\sigma_\theta}{r} = 0 \tag{A.2.1}$$

$$\frac{1}{r} \frac{\partial}{\partial z}(r\sigma_{rz}) + \frac{\partial \sigma_z}{\partial z} = 0 \tag{A.2.2}$$

The stress-strain (or displacement) relations, however, require some assumptions on the nature of the elastic material. We will assume (for reasons which will become clear later) that the material is orthotropic; i.e.,

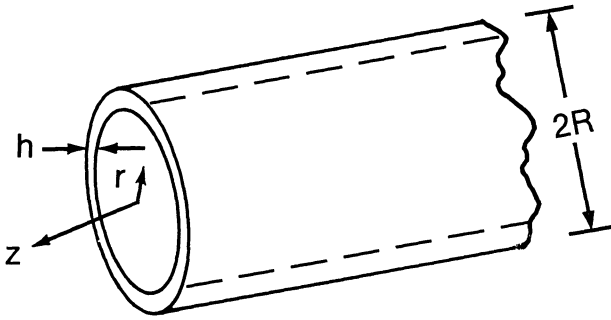


Fig. A.2.2. Shell

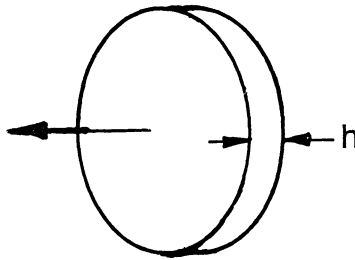


Fig. A.2.3. Plate.

that it requires six discrete elastic constants to characterize the stress-strain system. These elastic constants are $E_r, E_\theta, E_z, \nu_{r\theta}, \nu_{rz}, \nu_{\theta z}$. In terms of these elastic constants, the stress displacement relations (i.e., the 3-D version of Hooke's Law) are:

$$\frac{\partial u_r}{\partial r} - \alpha_r T = \frac{\sigma_r}{E_r} - \frac{\nu_{r\theta}}{E_\theta} \sigma_\theta - \frac{\nu_{rz}}{E_z} \sigma_z \tag{A.2.3}$$

$$\frac{u_r}{r} - \alpha_\theta T = \frac{-\nu_{\theta r}}{E_r} \sigma_r + \frac{\sigma_\theta}{E_\theta} - \frac{\nu_{\theta z}}{E_z} \sigma_z \tag{A.2.4}$$

$$\frac{\partial u_z}{\partial z} - \alpha_z T = \frac{-\nu_{zr}}{E_r} \sigma_r - \frac{\nu_{z\theta}}{E_\theta} \sigma_\theta + \frac{\sigma_z}{E_z} \tag{A.2.5}$$

$$\frac{\partial u_r}{\partial z} + \frac{\partial u_z}{\partial r} = \frac{\sigma_{rz}}{G_{rz}} \tag{A.2.6}$$

T denotes the temperature rise, also assumed to be a function of r and z only (axisymmetric), and α_r, α_θ and α_z denote coefficients of thermal expansion

of the material in radial, circumferential, and axial directions, respectively. The quantities $\nu_{r\theta}$, $\nu_{\theta r}$, etc., are related as follows:

$$\begin{aligned}\frac{\nu_{r\theta}}{E_\theta} &= \frac{\nu_{\theta r}}{E_r} \\ \frac{\nu_{\theta z}}{E_z} &= \frac{\nu_{z\theta}}{E_\theta} \\ \frac{\nu_{zr}}{E_r} &= \frac{\nu_{rz}}{E_z}\end{aligned}\tag{A.2.7}$$

Use of the stress-displacement relations for a general orthotropic material permits us to make “rigidity assumptions” in a certain coordinate direction without affecting the properties in others. For example, simplification to “plate” theory requires the assumption of infinite E_z (material rigid in the through-thickness direction). This concept will become clearer in subsequent sections.

A.3 SPECIALIZATION TO THE BENDING AND EXTENSION OF THIN WALLED CYLINDRICAL SHELLS

A thin cylindrical shell is characterized by $h/R \ll 1$ where h is the shell thickness, and R is the mean radius of the shell. This permits further simplification of the elasticity equations of the preceding section. It is intuitively obvious that the radial stress σ_r will be small compared to the circumferential stress σ_θ . Furthermore, the variation of all stresses across the shell thickness can be *approximated* by the sum of an average stress and a linearly varying component. The averaged stress is the so-called membrane stress component. The linearly varying component produces the cross-sectional bending moment. This *á priori* approximation on the stress distribution is the essence of the classical thin shell theory.

To carry out the simplification, we introduce a new variable in the r direction so that

$$r = R + \eta \tag{A.3.1}$$

R is the mean radius of the shell and $-0.5h < \eta < 0.5h$, h being the shell thickness. Restricting consideration to thin shells such that $h/R \ll 1$, and recognizing that σ_r and its derivatives are quantities of smaller order than σ_θ , the equations of equilibrium take the form

$$\frac{\partial}{\partial \eta}(\sigma_r) + \frac{\partial \sigma_{rz}}{\partial z} - \frac{\sigma_\theta}{R} \approx 0 \tag{A.3.2}$$

$$\frac{\partial}{\partial \eta}(\sigma_{rz}) + \frac{\partial \sigma_z}{\partial z} \approx 0 \tag{A.3.3}$$

As stated before, since the element is “thin” in the η direction, we content ourselves with solving the equilibrium equations only in an

“averaged” manner. That is, we replace Eqs. (A.3.2.), (A.3.3) by a set of equations involving force and moment resultants, acting on the shell cross section, rather than attempt to solve the equations for the detailed stress distribution.

We multiply Eq. (A.3.2) by $d\eta$ and integrate over the shell thickness to obtain

$$\int_{-0.5h}^{0.5h} \frac{\partial \sigma_r}{\partial \eta} d\eta + \frac{d}{dz} \int_{-0.5h}^{0.5h} \sigma_{rz} d\eta - \frac{1}{R} \int_{-0.5h}^{0.5h} \sigma_\theta d\eta \approx 0 \quad (\text{A.3.4})$$

Note that the integration through the thickness eliminates the r -coordinate from the equation and permits replacement of partial derivatives with total derivatives with the z -coordinate as the only independent variable left in the equations. Equation (A.3.4) suggests the introduction of the force resultants N_θ , Q_z , where

$$N_\theta = \int_{-0.5h}^{0.5h} \sigma_\theta d\eta; \quad Q_z = \int_{-0.5h}^{0.5h} \sigma_{rz} d\eta \quad (\text{A.3.5})$$

N_θ is the circumferential tension per unit length and Q_z is the sectional shear per unit width. We also introduce the concept of the net lateral pressure $p(z)$ defined as

$$p(z) = \sigma_r(0.5h) - \sigma_r(-0.5h) \quad (\text{A.3.6})$$

where σ_r at $0.5h$ and at $-0.5h$ are dependent on the applied pressures on the respective surfaces.

With the above definitions, Eq. (A.3.4) becomes

$$p(z) + \frac{d}{dz} Q_z - \frac{N_\theta}{R} \approx 0 \quad (\text{A.3.7})$$

We perform the same averaging operation on Eq. (A.3.3) to obtain

$$\tau(z) + \frac{dN_z}{dz} \approx 0 \quad (\text{A.3.8})$$

where $\tau(z) = \sigma_{rz}(0.5h) - \sigma_{rz}(-0.5h)$, and

$$N_z = \int_{-0.5h}^{0.5h} \sigma_z d\eta \quad (\text{A.3.9})$$

This completes averaging of the stresses over the shell section thickness. The effect of the linearly varying component is washed out in the averaging process. To obtain the moment resultant due to the linearly varying component, it is necessary to evaluate the moment of the stress with respect to the neutral axis. The neutral axis is assumed to lie on the mid-surface of the shell section.

Returning to Eq. (A.3.3), multiplying each term by $\eta d\eta$, and integrating across the shell thickness, we obtain

$$\int_{-0.5h}^{0.5h} \eta \frac{\partial}{\partial \eta} (\sigma_{rz}) d\eta + \int_{-0.5h}^{0.5h} \frac{\partial}{\partial z} (\eta \sigma_z) d\eta \approx 0 \quad (\text{A.3.10})$$

which can be rewritten as

$$\int_{-0.5h}^{0.5h} \left[\frac{\partial}{\partial \eta} (\eta \sigma_{rz}) - \sigma_{rz} \right] d\eta + \frac{d}{dz} \int_{-0.5h}^{0.5h} \eta \sigma_z d\eta \approx 0 \quad (\text{A.3.11})$$

Introducing the moment resultant

$$M_z = \int_{-0.5h}^{0.5h} \eta \sigma_z d\eta \quad (\text{A.3.12})$$

then yields the final equilibrium equation as

$$\frac{d}{dz} M_z - Q_z + 0.5h[\sigma_{rz}(0.5h) + \sigma_{rz}(-0.5h)] \approx 0 \quad (\text{A.3.13})$$

Equations (A.3.7), (A.3.8), (A.3.13) are the desired three equilibrium equations involving the four stress resultants N_z , M_z , Q_z , N_θ . It is assumed that the surface values of σ_r , σ_{rz} on $\pm h/2$ are known functions of z .

We now intend to specialize the constitutive Eqs. (A.2.3)–(A.2.6) to thin shell theory, and by proper averaging, relate the force and moment resultants to certain displacement variables. We begin by assuming a material with $E_r \rightarrow \infty$. From Eq. (A.2.7) we see that $\nu_{rz} = \nu_{r\theta} \rightarrow 0$. We also assume $\alpha_r = 0$ and $E_z = E_\theta = E$; $\nu_{\theta z} = \nu_{z\theta} = \nu$ and $\alpha_\theta = \alpha_z = \alpha$. Under this assumption of an effectively rigid material in the r direction, the strain-stress relations (A.2.3)–(A.2.5) reduce to the form

$$\frac{\partial u_r}{\partial r} \approx 0 \quad (\text{A.3.14})$$

$$\frac{u_r}{R} - \alpha T \approx \frac{1}{E} (\sigma_\theta - \nu \sigma_z) \quad (\text{A.3.15})$$

$$\frac{\partial u_z}{\partial z} - \alpha T \approx \frac{1}{E} (-\nu \sigma_\theta + \sigma_z) \quad (\text{A.3.16})$$

The above results indicate that

$$u_r = U(z) \quad (\text{A.3.17})$$

$$\sigma_\theta = \frac{E}{1-\nu^2} \left[\frac{u_r}{R} + \nu \frac{\partial u_z}{\partial z} - (1+\nu)\alpha T \right] \quad (\text{A.3.18})$$

$$\sigma_z = \frac{E}{1-\nu^2} \left[\frac{\partial u_z}{\partial z} + \nu \frac{u_r}{R} - (1+\nu)\alpha T \right] \quad (\text{A.3.19})$$

We now average Eqs. (A.3.18)–(A.3.19) through the shell wall thickness. We assume that the deformation $u_z(r,z)$ can be approximated by a linear function of η .

$$u_z(r,z) = w(z) + \eta\Theta(z) \quad (\text{A.3.20})$$

Using the previously defined stress resultants N_θ , N_z , and introducing a thermal force resultant

$$N^* = N^*(z) = \frac{E}{1-\nu} \int_{-0.5h}^{0.5h} \alpha T(\eta,z) d\eta \quad (\text{A.3.21})$$

yields

$$N_\theta = K \left[\frac{U}{R} + \nu \frac{dw}{dz} \right] - N^*; \quad K = \frac{Eh}{1-\nu^2} \quad (\text{A.3.22})$$

$$N_z = K \left[\frac{dw}{dz} + \nu \frac{U}{R} \right] - N^* \quad (\text{A.3.23})$$

We note that the result

$$\int_{-0.5h}^{0.5h} \eta d\eta = 0$$

has been used in obtaining Eqs. (A.3.22), (A.3.23). If we multiply the same two equations by $\eta d\eta$ and integrate across the shell thickness, we obtain

$$M_\theta = \nu \frac{Kh^2}{12} \frac{d\Theta}{dz} - M^* \quad (\text{A.3.24})$$

$$M_z = \frac{Kh^2}{12} \frac{d\Theta}{dz} - M^* \quad (\text{A.3.25})$$

where we use the result

$$\int_{-0.5h}^{0.5h} \eta^2 d\eta = \frac{h^3}{12}$$

and introduce the new moment resultants

$$M_\theta = \int_{-0.5h}^{0.5h} \eta \sigma_\theta d\eta; \quad M^* = \frac{E}{1-\nu} \int_{-0.5h}^{0.5h} \alpha \eta T d\eta \quad (\text{A.3.26})$$

The term

$$\frac{Kh^2}{12} = \frac{Eh^3}{12(1-\nu^2)}$$

is often referred to as the ‘‘flexural rigidity’’ D of the shell

$$D = \frac{Eh^3}{12(1-\nu^2)} \quad (\text{A.3.27})$$

We have averaged all of the equations except (A.2.6). Here, we assume that shear deformation is neglected; this is equivalent to setting the shear modulus G_{rz} to a very large value. Using Eqs. (A.3.1), (A.3.17), and (A.3.20) yields the result

$$\frac{dU}{dz} + \Theta \approx 0 \quad (\text{A.3.28})$$

We have now developed the equations governing the behavior of a symmetrically loaded cylindrical shell. The equations are the three equilibrium equations (A.3.7), (A.3.8), and (A.3.13), the four constitutive equations (A.3.22)–(A.3.25) and the kinematic relation (A.3.28). The eight equations involve eight unknown functions of z : N_z , M_z , N_θ , M_θ , Q_z , U , w , Θ .

These equations can be further simplified for special cases. Let us consider the case where the shell is subject to only normal surface loadings (e.g., pressure). Equation (A.3.8) yields $\tau(z) = 0$ so that $N_z = \text{constant}$. The header load N_z follows from equilibrium. For a thin cylindrical shell of radius of inner radius R_i subject to internal pressure p , the header load is

$$N_z = \frac{\pi R_i^2 p}{2\pi R} = \frac{R_i^2 p}{2R} \quad (\text{A.3.29})$$

Equations (A.3.13) and (A.3.25) become

$$\frac{dM_z}{dz} = Q_z \quad (\text{A.3.30})$$

$$M_z = \frac{Kh^2}{12} \frac{d\Theta}{dz} = D \frac{d\Theta}{dz}$$

Since $\Theta = -dU/dz$ (from Eq. (A.3.28)),

$$M_z = -D \frac{d^2 U}{dz^2} \quad (\text{A.3.31})$$

$$Q_z = -D \frac{d^3 U}{dz^3} \quad (\text{A.3.32})$$

Equation (A.3.7) can be recast, with Q_z substituted from above, as

$$p - D \frac{d^4 U}{dz^4} - \frac{N_\theta}{R} = 0 \quad (\text{A.3.33})$$

Note, from Eq. (A.3.22–23), in the absence of thermal loading, that

$$N_\theta = K \frac{U}{R} + \nu N_z - \nu^2 K \frac{U}{R} \quad (\text{A.3.34})$$

Substituting for N_θ in Eq. (A.3.33), we have

$$\frac{d^4 U}{dz^4} + 4\beta^4 U = \frac{1}{D} \left[p - \frac{\nu N_z}{R} \right] \quad (\text{A.3.35})$$

where

$$\beta = [3(1 - \nu^2)/h^2 R^2]^{1/4} \quad (\text{A.3.36})$$

For a thin cylinder with closed ends, N_z is given by Eq. (A.3.29). For an open ended cylinder, $N_z = 0$.

Equation (A.3.35) is a fourth order ordinary differential equation with constant coefficients. The general solution of this equation can be written as

$$U = e^{\beta z} (c_1 \cos \beta z + c_2 \sin \beta z) + e^{-\beta z} (c_3 \cos \beta z + c_4 \sin \beta z) + f_p(z) \quad (\text{A.3.37})$$

where $f_p(z)$ is a particular solution. The four constants of integration c_i ($i = 1, 2, \dots, 4$) must be determined by considering the boundary conditions at the two ends of the shell. In the above derivation, we assumed that the shell thickness h is constant. For a shell of varying thickness, the same process yields the following equation in lieu of Eq. (A.3.35).

$$\frac{d^2}{dz^2} \left(D \frac{d^2 U}{dz^2} \right) + \frac{Eh}{R^2} U = p - \frac{\nu N_z}{R}$$

This form is required in the analysis of the hub of the welding neck flange in Chapters 3 and 4.

The quantity β defined by Eq. (A.3.36) is an important parameter in shell theory. It is referred to as the ‘‘attenuation coefficient’’ or the ‘‘decay parameter’’ for reasons which become clear in the next section.

A.4 SOME APPLICATIONS OF THIN SHELL THEORY RESULTS

In this section, we illustrate the application of the equations derived in the preceding section.

(a) *Long circular shell subject to an edge moment M_0 and shear Q_0 at one end:*

Referring to Eq. (A.3.37) and Fig. A.4.1, we see that $f_p = 0$, since there is no distributed loading on the shell. Constants c_1 and c_2 must vanish identically since U must remain finite for large z . Therefore, the displacement solution reduces to

$$U = e^{-\beta z} (c_3 \cos \beta z + c_4 \sin \beta z) \quad (\text{A.4.1})$$

The constants c_3 and c_4 are computed by the conditions at the edge $z = 0$.

$$\begin{aligned} @z=0; \quad M_z = M_0 &= -D \frac{d^2 U}{dz^2} \quad (\text{Eq. (A.3.31)}) \\ @z=0; \quad Q_z = Q_0 &= -D \frac{d^3 U}{dz^3} \quad (\text{Eq. (A.3.32)}) \end{aligned} \quad (\text{A.4.2})$$

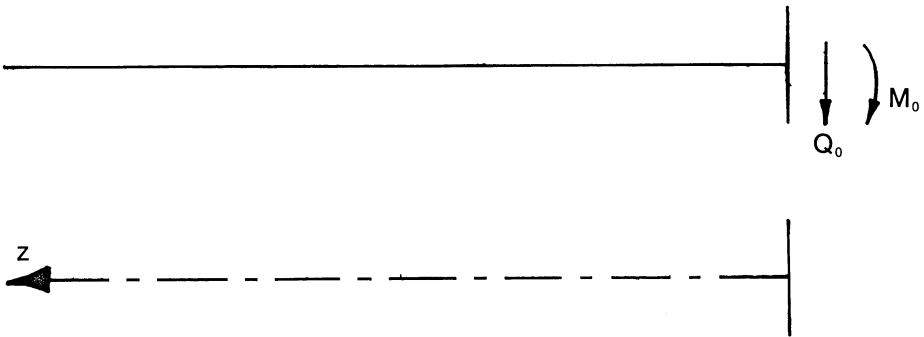


Fig. A.4.1. Edge loaded shell.

Substituting for the derivatives of U (from Eq. (A.4.1)) in the above, and solving for c_3 and c_4 yields

$$c_3 = -\frac{1}{2\beta^3 D} (Q_0 + \beta M_0) \quad (\text{a}) \quad (\text{A.4.3})$$

$$c_4 = \frac{M_0}{2\beta^2 D} \quad (\text{b})$$

Therefore

$$U(z) = \frac{e^{-\beta z}}{2\beta^3 D} [\beta M_0 (\sin \beta z - \cos \beta z) - Q_0 \cos \beta z] \quad (\text{A.4.4})$$

At the loaded end, the displacement is

$$U \Big|_{z=0} = -\frac{1}{2\beta^3 D} (\beta M_0 + Q_0) \quad (\text{A.4.5})$$

The negative sign results from the fact that U is taken positive for deflection away from the shell axis. Equation (A.4.4) also shows that the deflection U attenuates exponentially as $e^{-\beta z}$. Thus the ratio of deflection at the loaded end to that at distance $l = 2\pi/\beta$ is $e^{2\pi} \approx 536$.

Note

$$l = \frac{2\pi}{\beta} = \frac{2\pi(Rh)^{1/2}}{[3(1-\nu^2)]^{1/4}}$$

For $\nu = 0.3$, $l = 4.89 (Rh)^{1/2}$

This demonstrates that the deformation due to edge loading is of a local character and a shell of length $4.89 (Rh)^{1/2}$ simulates an infinitely long shell in so far as edge loadings are concerned.

We introduce the following notations to simplify the presentation for the expressions for U and its derivatives.

$$\phi(\beta z) = e^{-\beta z} (\cos \beta z + \sin \beta z)$$

$$\psi(\beta z) = e^{-\beta z} (\cos \beta z - \sin \beta z)$$

$$\lambda(\beta z) = e^{-\beta z} \cos \beta z$$

$$\zeta(\beta z) = e^{-\beta z} \sin \beta z$$

The expression for deflection U and its consecutive derivatives may be written as

$$U = -\frac{1}{2\beta^3 D} [\beta M_0 \psi + Q_0 \lambda]$$

$$\frac{dU}{dz} = \frac{1}{2\beta^2 D} [2\beta M_0 \lambda + Q_0 \phi]$$

$$\frac{d^2 U}{dz^2} = -\frac{1}{2\beta D} [2\beta M_0 \phi + 2Q_0 \zeta]$$

$$\frac{d^3 U}{dz^3} = \frac{1}{D} [2\beta M_0 \zeta - Q_0 \psi]$$

The bending moment, shear force, and deflection are expressed in terms of U and its derivatives, as was seen in the foregoing.

(b) *Uniformly distributed line load around a circular section:*

Figure A.4.2 shows a cylindrical shell under a circumferentially

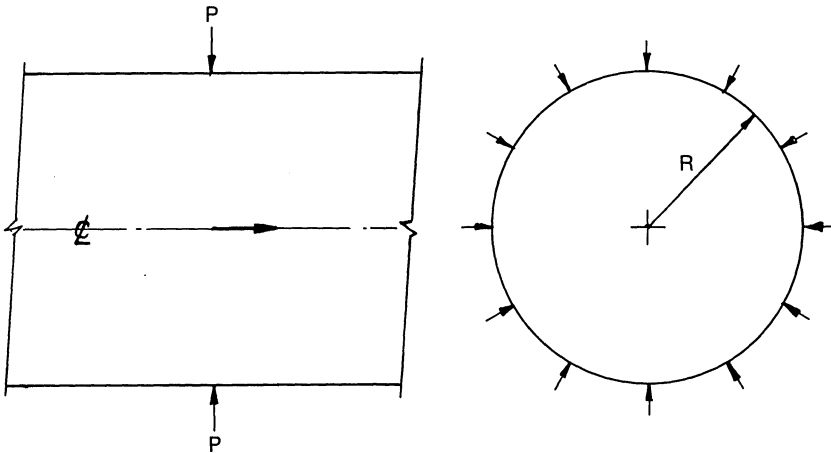


Fig. A.4.2 Cylindrical shell under line load

distributed load P per unit length. If the ends of the shell are far enough removed from the load line, then the previous solution can be used for each half of the shell. From symmetry, the slope dU/dz is zero under the load line, and the edge shear equals $P/2$. Thus, we have

$$U = \frac{e^{-\beta z}}{2\beta^3 D} \left[\beta M_0 (\sin\beta z - \cos\beta z) - \frac{P}{2} \cos\beta z \right] \quad (\text{A.4.6})$$

where z is measured from the cross section of the load line.

The moment, M_0 , in the above equation must be of such a magnitude that the condition of zero slope at $z=0$ is satisfied:

$$\frac{dU}{dz} = \frac{e^{-\beta z}}{2\beta^2 D} \left[2\beta M_0 \cos\beta z + \frac{P}{2} (\sin\beta z + \cos\beta z) \right] \quad (\text{A.4.7})$$

Hence,

$$\begin{aligned} \left. \frac{dU}{dz} \right|_{z=0} = 0 &= \frac{1}{2\beta^2 D} \left[2\beta M_0 + \frac{P}{2} \right] \\ \text{or } M_0 &= -\frac{P}{4\beta} \end{aligned} \quad (\text{A.4.8})$$

Substituting for M_0 in Eq. (A.4.6), the expression for the radial deflection of the shell becomes:

$$U = -\frac{Pe^{-\beta z}}{8\beta^3 D} (\sin\beta z + \cos\beta z) = \frac{-P\phi(\beta z)}{8\beta^3 D} \quad (\text{A.4.9})$$

Expressions for moment M_z and shear Q_z , can be obtained by using Eqs. (A.3.31–32).

(c) *Distributed load of intensity $q(z)$ over a certain length of the shell:*

It is assumed that the loaded patch is sufficiently removed from the shell ends and that it is substantially shorter than the shell length. The solution for this case can be obtained by the principle of superposition using the concentrated load results derived in (b) above.

Figure A.4.3 shows a uniformly loaded patch of length $l = b + c$. The deflection at point A , dU_A , due to a ring load $qd\xi$ per unit length located at a distance ξ is given by Eq. (A.4.9):

$$dU_A = \frac{-qe^{-\beta\xi}}{8\beta^3 D} (\sin\beta\xi + \cos\beta\xi) d\xi \quad (\text{A.4.10})$$

Therefore, the deflection produced by the total load is given by

$$U_A = -\int_0^b \frac{q}{8\beta^3 D} \phi(\xi) d\xi - \int_0^c \frac{q}{8\beta^3 D} \phi(\xi) d\xi \quad (\text{A.4.11})$$

where

$$\phi(\xi) = e^{-\beta\xi} (\sin\beta\xi + \cos\beta\xi) \tag{A.4.12}$$

Performing the integrations and simplifying, we have:

$$U_A = -\frac{qR^2}{2Eh} (2 - e^{-\beta b} \cos\beta b - e^{-\beta c} \cos\beta c) \tag{A.4.13}$$

The bending moment and shear at *A* can be determined in a similar manner.

As another example, let us consider a linearly varying load of peak intensity *p* over length *2b* (Fig. A.4.4). This loading can simulate a bending

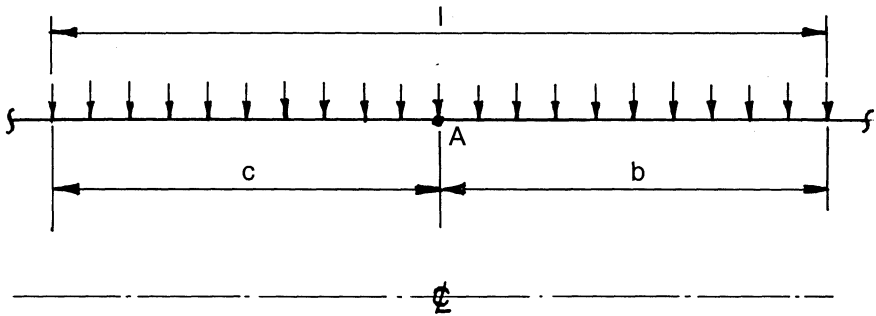


Fig. A.4.3. Uniform pressure over a patch of length *l*.

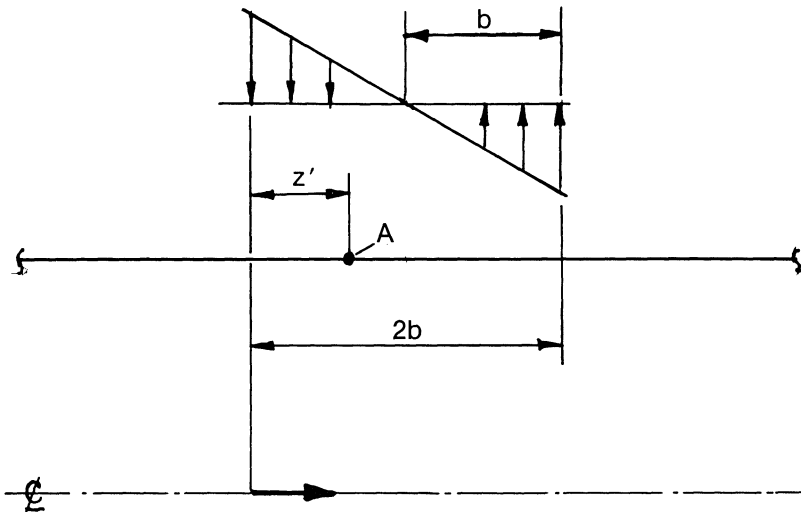


Fig. A.4.4. Linearly varying loading.

Moment or shear distributions can be found in a similar manner.

(d) *Short shell under internal pressure and edge loads:*

We consider now a short shell of length l subjected to internal pressure p , and edge loadings, F , M and Q , as shown in Fig. (A.4.5). The governing differential equation (Eq. (A.3.35)) takes the form

$$\frac{d^4 U}{dz^4} + 4\beta^4 U = \frac{1}{D} \left(p - \frac{\nu F}{R} \right) \tag{A.4.17}$$

The particular solution of this equation is

$$U_p = \frac{1}{4\beta^4 D} \left(p - \frac{\nu F}{R} \right)$$

or

$$U_p = \frac{R^2}{Eh} \left(p - \frac{\nu F}{R} \right) \tag{A.4.18}$$

The complementary solution can be written in the exponential form presented in Eq. (A.3.37). It is more convenient here to write the solution in terms of hyperbolic functions:

$$U_c = c_1 \sin\beta z \sinh\beta z + c_2 \sin\beta z \cosh\beta z + c_3 \cos\beta z \sinh\beta z + c_4 \cos\beta z \cosh\beta z \tag{A.4.19}$$

If the origin of the coordinate system is set at the mid-length of the shell, then symmetry considerations require that $c_2 = c_3 = 0$. The remaining two constants of integration are found using the edge conditions, as shown in Section 15.5.

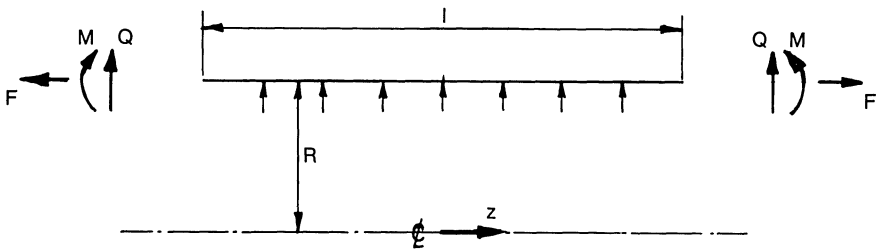


Fig. A.4.5. Short shell under internal pressure and edge loadings.

A.5 SPECIALIZATION TO THE BENDING AND EXTENSION OF CIRCULAR PLATES

Referring again to Fig. A.2.1, we now assume that $a < r < b$, where a, b are the inner and outer radius of the plate, respectively, and that the variable z satisfies the condition $-0.5h < z < 0.5h$, h being the plate thickness. In

Moment or shear distributions can be found in a similar manner.

(d) Short shell under internal pressure and edge loads:

We consider now a short shell of length l subjected to internal pressure p , and edge loadings, F , M and Q , as shown in Fig. (A.4.5). The governing differential equation (Eq. (A.3.35)) takes the form

$$\frac{d^4 U}{dz^4} + 4\beta^4 U = \frac{1}{D} \left(p - \frac{\nu F}{R} \right) \tag{A.4.17}$$

The particular solution of this equation is

$$U_p = \frac{1}{4\beta^4 D} \left(p - \frac{\nu F}{R} \right)$$

or

$$U_p = \frac{R^2}{Eh} \left(p - \frac{\nu F}{R} \right) \tag{A.4.18}$$

The complementary solution can be written in the exponential form presented in Eq. (A.3.37). It is more convenient here to write the solution in terms of hyperbolic functions:

$$U_c = c_1 \sin\beta z \sinh\beta z + c_2 \sin\beta z \cosh\beta z + c_3 \cos\beta z \sinh\beta z + c_4 \cos\beta z \cosh\beta z \tag{A.4.19}$$

If the origin of the coordinate system is set at the mid-length of the shell, then symmetry considerations require that $c_2 = c_3 = 0$. The remaining two constants of integration are found using the edge conditions, as shown in Section 15.5.

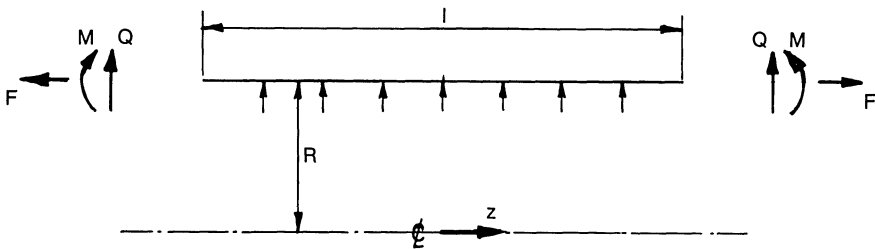


Fig. A.4.5. Short shell under internal pressure and edge loadings.

A.5 SPECIALIZATION TO THE BENDING AND EXTENSION OF CIRCULAR PLATES

Referring again to Fig. A.2.1, we now assume that $a < r < b$, where a, b are the inner and outer radius of the plate, respectively, and that the variable z satisfies the condition $-0.5h < z < 0.5h$, h being the plate thickness. In

contrast to Section A.3 where we performed equation averaging in the radial direction, we seek now to obtain a set of equations based on averaging in the z direction; i.e., in both of these sections, the field equations are derived by averaging the elasticity equations in the thickness direction of the structure. The following force and moment resultants are of interest in the study of circular plates:

$$\begin{aligned} N_r &= \int_{-0.5h}^{0.5h} \sigma_r dz; & M_r &= \int_{-0.5h}^{0.5h} z \sigma_r dz \\ N_\theta &= \int_{-0.5h}^{0.5h} \sigma_\theta dz; & M_\theta &= \int_{-0.5h}^{0.5h} z \sigma_\theta dz \\ Q_r &= \int_{-0.5h}^{0.5h} \sigma_{rz} dz \end{aligned} \quad (\text{A.5.1})$$

If we average Eqs. (A.2.1), (A.2.2) over the thickness of the plate (i.e., multiply by dz and integrate over the z region), we obtain the equations

$$\frac{1}{r} \frac{d}{dr} (rN_r) - \frac{N_\theta}{r} + \sigma_{rz}(0.5h) - \sigma_{rz}(-0.5h) = 0 \quad (\text{A.5.2})$$

$$\frac{1}{r} \frac{d}{dr} (rQ_r) + \sigma_z(0.5h) - \sigma_z(-0.5h) = 0 \quad (\text{A.5.3})$$

If we multiply Eq. (A.2.1) by zdz and integrate over the thickness, we obtain

$$\frac{1}{r} \frac{d}{dr} (rM_r) - \frac{M_\theta}{r} - Q_r + (z\sigma_{rz}) \Big|_{-0.5h}^{0.5h} = 0 \quad (\text{A.5.4})$$

Following the procedure set forth in detail in Section A.3, we now seek appropriately averaged constitutive equations for the plate element. To evolve the appropriate thin plate structural theory, we assume a material such that

$$E_z = G_{rz} \rightarrow \infty; \quad \alpha_z = 0 \quad (\text{A.5.5})$$

Therefore, from Eq. (A.2.7), $\nu_{z\theta} = \nu_{zr} = 0$. We also assume that $E_r = E_\theta = E$, $\nu_{r\theta} = \nu_{\theta r} = \nu$, and $\alpha_r = \alpha_\theta = \alpha$. With these assumptions the constitutive Eqs. (A.2.3)–(A.2.5) reduce to the forms:

$$\frac{\partial u_r}{\partial r} - \alpha T = \frac{1}{E} (\sigma_r - \nu \sigma_\theta) \quad (\text{A.5.6})$$

$$\frac{u_r}{r} - \alpha T = \frac{1}{E} (\sigma_\theta - \nu \sigma_r) \quad (\text{A.5.7})$$

$$\frac{\partial u_z}{\partial z} = 0 \quad (\text{A.5.8})$$

Thus, we find for thin circular plates under symmetric loading that

$$u_z(r,z) = W(r) \quad (\text{A.5.9})$$

$$\sigma_r = \frac{E}{1-\nu^2} \left[\frac{\partial u_r}{\partial r} + \nu \frac{u_r}{r} - (1+\nu)\alpha T \right] \quad (\text{A.5.10})$$

$$\sigma_\theta = \frac{E}{1-\nu^2} \left[\frac{u_r}{r} + \nu \frac{\partial u_r}{\partial r} - (1+\nu)\alpha T \right] \quad (\text{A.5.11})$$

If we now assume that the radial deformation $u_r(r,z)$ is linear through the plate thickness, so that

$$u_r(r,z) = U(r) + z\Theta(r) \quad (\text{A.5.12})$$

then the constitutive equations, averaged through the thickness of the plate are

$$N_r = K \left[\frac{dU}{dr} + \nu \frac{U}{r} \right] - N^* \quad (\text{A.5.13})$$

$$N_\theta = K \left[\frac{U}{r} + \nu \frac{dU}{dr} \right] - N^* \quad (\text{A.5.14})$$

where we have used the result

$$\int_{-0.5h}^{0.5h} z dz = 0.$$

Continuing as in Section A.3, and multiplying Eq. (A.5.10), (A.5.11) by zdz and averaging through the thickness yields

$$M_r = \frac{Kh^2}{12} \left[\frac{d\Theta}{dr} + \nu \frac{\Theta}{r} \right] - M^* \quad (\text{A.5.15})$$

$$M_\theta = \frac{Kh^2}{12} \left[\frac{\Theta}{r} + \nu \frac{d\Theta}{dr} \right] - M^* \quad (\text{A.5.16})$$

M^* , N^* in the above are given by Eqs. (A.3.21), (A.3.26) with z replaced by r and η replaced by z .

With the neglect of shear deformation in the plate section, Eq. (A.2.6) becomes

$$\Theta + \frac{dW}{dr} = 0 \quad (\text{A.5.17})$$

The governing equations for the radial extension of the plate are Eqs. (A.5.2), (A.5.13), and (A.5.14) which involve the unknown functions N_r , N_θ , U . The equations governing lateral bending of plates are Eqs. (A.5.3), (A.5.4), and (A.5.15)–(A.5.17) involving the five unknown functions M_r , M_θ , Q_r , Θ , and W . Note that in contrast to the shell equations, where ex-

tension of the shell and bending of the shell are coupled, the plate equations de-couple into a set of three equations for extension, and five equations for plate bending. The above remarks presume that the surface stresses $\sigma_{rz}(\pm 0.5h)$, and $\sigma_z(\pm 0.5h)$ are known functions of r .

We now investigate the solution to the plate bending problem, assuming that a lateral pressure $\sigma_z(0.5h) - \sigma_z(-0.5h) = p(r)$ is given and that $\sigma_{rz}(\pm 0.5h) = 0$.

Solving Eq. (A.5.4) for Q_r yields

$$Q_r = \frac{dM_r}{dr} + \frac{M_r - M_\theta}{r} \quad (\text{A.5.18})$$

Using Eqs. (A.5.15), (A.5.16), we can express Q_r in terms of $\Theta(r)$. For simplicity, we assume that M^* is independent of radial position. The resulting equation is

$$Q_r = \frac{Kh^2}{12} \left[\frac{d^2 \Theta}{dr^2} + \frac{1}{r} \frac{d\Theta}{dr} - \frac{\Theta}{r^2} \right] \quad (\text{A.5.19})$$

Substituting Eq. (A.5.19) into Eq. (A.5.3) yields

$$\frac{Kh^2}{12} \left[\frac{d^3 \Theta}{dr^3} + \frac{2}{r} \frac{d^2 \Theta}{dr^2} - \frac{1}{r^2} \frac{d\Theta}{dr} + \frac{\Theta}{r^3} \right] = -p(r) \quad (\text{A.5.20})$$

Finally, using Eq. (A.5.17), we obtain the differential equation for $W(r)$ in the form

$$\frac{d^4 W}{dr^4} + \frac{2}{r} \frac{d^3 W}{dr^3} - \frac{1}{r^2} \frac{d^2 W}{dr^2} + \frac{1}{r^3} \frac{dW}{dr} = \frac{p(r)}{D} \quad (\text{A.5.21})$$

where we have again introduced the flexural rigidity term $D = Kh^2/12$. Equation (A.5.21) may be written in the familiar form

$$\nabla^2(\nabla^2 W) = \nabla^4 W = \frac{p(r)}{D} \quad (\text{A.5.22})$$

where the Laplacian operator ∇^2 is given as

$$\nabla^2 = \frac{d^2}{dr^2} + \frac{1}{r} \frac{d}{dr} \quad (\text{A.5.23})$$

and $\nabla^4(\)$ is the biharmonic operator.

For the case where $p(r)$ is independent of r , say $p(r) = p_0$, a solution of Eq. (A.5.22) is easily effected by first considering

$$\frac{d^2 W}{dr^2} + \frac{1}{r} \frac{dW}{dr} = \psi \quad (\text{A.5.24})$$

so that Eq. (A.5.22) becomes

$$\frac{d^2 \psi}{dr^2} + \frac{1}{r} \frac{d\psi}{dr} = \frac{1}{r} \frac{d}{dr} \left(r \frac{d\psi}{dr} \right) = \frac{p_0}{D} \quad (\text{A.5.25})$$

Therefore

$$\psi(r) = A_0 \ln r + \frac{p_0 r^2}{4D} + A_1 \quad (\text{A.5.26})$$

Thus, the solution for $W(r)$ satisfies the differential equation

$$\frac{1}{r} \frac{d}{dr} \left(r \frac{dW}{dr} \right) = A_0 \ln r + \frac{p_0 r^2}{4D} + A_1 \quad (\text{A.5.27})$$

After appropriate integrations and combinations of constants of integration, we obtain

$$W(r) = c_0 + c_1 r^2 + c_2 \ln r + c_3 r^2 \ln r \quad (\text{A.5.28})$$

If the plate is solid (i.e., the inside radius limit $a=0$), then $c_2 = c_3 = 0$ in order that the solution remains finite at the center. The remaining constants c_0, c_1 are determined by applying appropriate boundary conditions at $r=b$. For the case of an annular plate with $b > a > 0$, then all four integration constants in Eq. (A.5.28) are determined by applying a pair of boundary conditions at each edge of the plate $r=a, r=b$.

Returning to Eq. (A.5.22), we now assume that the plate is resting on an elastic foundation which exerts an opposing pressure $K_f W$ corresponding to deflection W . Then the net pressure is $(p_0 - K_f W)$, and Eq. (A.5.22) becomes

$$\nabla^4 W + \frac{K_f}{D} W = \frac{p_0}{D} \quad (\text{A.5.29})$$

The solution of this equation is in the form of Kelvin functions, as noted in Chapter 9.

Numerous solutions of circular plate equations have been constructed and compiled in the literature. Roark and Young [A.5.1], Timoshenko, et al. [A.5.2] and Flugge [A.5.3] are excellent sources of reference in this matter. A computationally efficient procedure to solve the problem of a symmetrically loaded circular plate on multiple support locations has been given by Paul, et al. [A.5.4, A.5.5].

NOMENCLATURE

- c_1, c_2 , etc. = Constants of integration
- D = Flexural rigidity (Eq. (A.3.27))
- E = Young's modulus
- E_r, E_θ, E_z = Young's modulus of an orthotropic material in r, θ , and z directions, respectively
- F = Axial force (Eq. (A.4.17))

- G_{rz} = Shear modulus of an orthotropic material in r - z plane
 h = Thickness of plate or shell
 K = Membrane rigidity parameter (Eq. (A.3.22))
 M^* = Thermal moment (Eq. (A.3.26))
 M_z = Longitudinal bending moment
 M_θ = Circumferential bending moment
 N_θ, N_z = Membrane direct stress resultant in θ and z directions, respectively
 Θ = Rotation of $r-\theta$ plane (shell); of $z-\theta$ plane (plate)
 p = Net pressure
 Q_z = Shear stress resultant on $z = \text{constant}$ plane
 r = Radial coordinate (Fig. A.2.1)
 R = Mean shell radius
 T = Temperature rise above the zero stress state
 u_r, u_θ, u_z = Displacement of a material point in r , θ , and z directions, respectively
 U = Deflection of mid-plane of shell in r direction
 W = Deflection of mid-plane of plate in z -direction
 z = Coordinate along the axis of shell (Fig. A.2.2), or thickness of plate (Fig. A.2.3)
 α = Coefficient of the linear thermal expansion
 $\alpha_r, \alpha_\theta, \alpha_z$ = Coefficient of linear thermal expansion in r , θ , and z directions, respectively
 β = Attenuation coefficient or decay parameter
 $\sigma_r, \sigma_\theta, \sigma_z$ = Normal stresses on $\theta-z$, $r-z$, and $r-\theta$ planes (Fig. A.2.1)
 σ_{rz} = Shear stress (Fig. A.2.1)
 θ = Circumferential direction
 η = Thickness coordinate in shell equations (Eq. (A.3.1))
 $\tau(z)$ = Net surface shear stress (Eq. (A.3.8))
 ν = Poisson's ratio
 $\nu_{r\theta}, \nu_{rz}$, etc. = Elastic constants to characterize an orthotropic material.

REFERENCES

- [A.5.1] Roark, R., and Young, W. C., "*Formulas for Stress and Strain*," fifth edition, McGraw-Hill (1975).
- [A.5.2] Timoshenko, S., and Woinowsky-Krieger, S., "*Theory of Plates and Shells*," second edition, McGraw-Hill (1959).
- [A.5.3] Flugge, W. (ed), "*Handbook of Engineering Mechanics*," McGraw-Hill (1962).
- [A.5.4] Paul, B., and Sikarskie, D. L., "Explicit Solutions for Circular Plates with Discontinuous Supports," *Trans. ASME, Vol. 90, Series B, Journal of Engineering for Industry*, pp. (513-518) (1968).
- [A.5.5] Paul, B., and Singh, B., "Efficient Design of Axisymmetric Plates," *Trans. ASME, Vol. 96, Series B, Journal of Engineering for Industry*, pp. 210-216 (1974).

KEY WORD INDEX

- Acoustic Frequency 778
Acoustic Resonance 740, 748, 820
Acoustic Resonance
 Correlations 778
Acoustic Velocity 830
Anchor Bolts 938, 939
Anchor Bolt Loads 886
 Elementary Solution 886
Angle of Attack 740
Annular Ring 865
Area 31, 99
 Bolt Root 99
 Bundle Entrance 31
 Frontal 31
 Lateral 31
 Shell Entrance 31
ASME Code Formula for the Large
 End of a Reducer 647
Attenuation Coefficient 429, 657,
 696, 1029
Axially Locked Closure 289
Axisymmetric Loadings on Shell or
 Plate 1021
AXISTRESS (See Under Computer
 Codes)
Backing Ring 4, 48, 54, 83
Baffle, Tangent Line 672
Baffles 20
 Double Segmental 20
 Single Segmental 20
 Triple Segmental 20
Base Plate 863, 899
Beam Strip Analogy 57
Beam Strip Method 570
Bellows, Squirm 692, 709
Bending Stresses 948
Ber and Bei Kelvin Functions 424
Bessel Function Expansions 476
Bessel Functions 113
Biach Pre-Tensioner 97
Biharmonic Operator 1038
Bi-Planar Loading 936
Bolt 932, 958
 Nominal Diameter 932
 Tensile Stress Area 932, 958
Bolt Load—Rigid Foundation 934
Bolt Pre-Tensioning 95
Bolt Spacing, Normal 128
Bolt Stiffness 623
Bolt Tightening 101
Bolted Joint 81
Bolted Joint Length 175
Bolted Joint Stiffness 173
Bolted Joints 81
Boltless Flange 289
Bolting Data 100
Bredtschneider Closure 291
Breech Block 293
Bridgeman Principle 297
Bundle Entrance Area 31
Butt Welding 307, 315
Casale Joint 290
Castiglano's First Theorem 666
Castigliano's Theorem 712
Channel 5, 7
Circular Ring 102
Circumferential Radius of
 Curvature 639
Closely Spaced Modes 1000
Complete Compression
 Condition 934
Computer Codes
 AXISTRESS xx
 DOUBLESHEET 530, 534, 541,
 544
 EJMAREC 713, 726
 EXJOINT 700, 719, 729
 FIXFLOAT 454, 504
 FIXSHEET 427, 431, 490, 493
 FLANFLUE 707
 FLANGE 126, 131
 FORLEG 916, 918
 GENFLANGE 239, 244
 GENROLL 368
 HEADSKIRT 77
 HORSUP 927, 937, 940
 LAPCOV 595, 612, 615
 LIGTEM 338
 MICROFIXFLOAT 480, 514
 MULTSPAN 762, 841, 843
 POSTSHEET xx
 PRESHEET xx
 RINGSUP 872, 892

- ST4 796
 TBROLL 350
 TRIEL 164, 188, 190, 204, 595,
 614
 UBAX 666, 674, 681
 UFLOW 800, 856
 UTUBE 412
 UVIB 767, 851
 VERSUP 949, 960, 962
 Concrete Bearing Pressure 927
 Concrete Pedestal 927, 938
 Condenser Waterbox 567
 Conical Expander 26
 Conical Head 654
 Contact Circle on Flange Face 605
 Continuous System 756
 Contraction 177
 Controlled Compression Joint 144
 Controlled Metal-to-Metal Con-
 tact 164, 605, 613
 Corrosion 107
 Cramer's Rule 117
 Critical Damping 789
 Cross Baffles 24, 38
 Cross Flow Velocity 795
 Cumulative Damage Factor 714

 Damping 779, 788
 Fluid 788
 Internal 788
 Structural 788
 Damping Coefficient 788, 980
 Decay Parameter 1029
 Deformation Theory 317
 Design Spectra 986
 Differential Equation 1029
 Complementary Solution 1035
 Particular Solution 1029
 Differential Thermal Expansion 431
 Discontinuity
 Moment 61, 72, 872
 Shear 61, 72
 Discontinuity Stress Resultants 649
 Displacement Response Spectrum
 980, 989
 Distillation Column 947
 Double Casale Joint 291
 Double Segmental Baffles 20
 DOUBLESHEET 530, 534, 541, 544
 Double Tubesheets 12, 330, 517,
 1011

 Drag Force 740
 Drains 41, 43, 1016

 Earthquake Response Spectrum 979
 Edge Welding 307, 312
 Edging 933
 Effective Elastic Constants 390
 Effective Elastic Constants-Square
 Pattern 391
 Effective Gasket Diameter 166
 Effective Pressure 477
 Effective Random Excitation
 Coefficient 775
 Effective Tube Mass 782
 Effective Velocity 796, 825, 828
 EJMAREC 713, 726, 729
 Elastic Foundation 1039
 El Centro Earthquake 984
 Elementary Solutions 886
 Ellipsoidal Shell 653
 Elliptical Orbit of Whirling 742
 Endurance Limit 715
 Endurance Stress 826
 Erosion 1017
 Exciting Frequency 779
 EXJOINT 700, 719
 Expanding Methods 307
 Expansion Joints 5, 430, 689, 714
 Bellows 692
 Fatigue Life 714
 Formed Head 690
 Formed Membrane 692
 Expansion Loss 177

 Facings 83
 Confined and Pre-Stressed 84
 Self-Equalizing 84
 Semi-Confined and Pre-
 Stressed 84
 Unconfined and Pre-Stressed 83
 Fatigue Life 713
 Faulted Condition 914
 Feedwater Heater 39
 Finish, Flange Face 86
 Finite Element Method 1003
 Finite Element Method in Tubesheet
 Analysis 534
 Fixed Support 927
 Fixed Tubesheet 2
 Fixed Tubesheet Exchanger 925
 FIXFLOAT 454, 504

- FIXSHEET 427, 431, 490, 493
 FLANGE 126, 131
 Flange 101, 170
 Calculation of Stresses 225
 Hubbed Lap Joint 83, 127
 Lap Joint 101, 127
 Moments 101
 Ring Joint 101, 127
 Welding Neck 101, 127, 141
 Flange-Cover Interaction 598
 Flange Facing Finish 86
 Flange Ring Stress 609
 Flange Stress Analysis 171
 Flanged and Flued Heads 693
 Flanged Joint 1008
 Flat Cover 593
 Conventional Design
 Formulas 596
 Flexibility Factor 669
 Flexural Efficiency 399
 Flexural Rigidity 113, 429, 657, 696,
 1027
 Floating Head 10
 Outside Packed 10
 Packed with Lantern Ring 10
 With Backing Device 10
 Floating Head Exchangers 439
 Floating Tubesheet 10, 11
 Flow Bypass 609
 Flow Induced Vibration 1018
 Flow Straightener 26
 Fluid-Elastic Correlations 768
 Fluid-Elastic Excitation 740
 Fluid-Elastic Stability 825, 828
 Fluid Inertia Model 749
 Fluoroloc, Fluorotemp 864
 FORLEG 916, 918
 Fouling Factors 336, 735
 Fouling Resistance 432
 Foundation Response 955
 Compete Compression 955
 Partial Compression 955, 957
 Foundation Stresses 930
 Four-Leg Supports 899
 Fraction of Critical Damping 980
 Fractional Damping 810, 828
 Friction 96
 Between Nut and Flange 96
 Between Turning Nut and Stud 96
 Friction Loss 177
 Full Face Gasket-Two Element
 Joint 233
 Full Face Gaskets 209
 Fundamental Frequency 757
 Gasket Factor 612
 Gasket Relaxation 604
 Gasket Spring Rate 604
 Gasket Stiffness 623
 Gasketed Joint Model 227
 Gaskets 87, 596
 Actual Seating Stress 88
 Decompression Modulus 89
 Effective Circle 596
 Gross Area Seating Stress 89
 Initial Gasket Compressive
 Strain 89
 Minimum Seating Stresses 612
 O-Ring 94, 95
 Reaction Circle 596
 Recovery 89
 Ring 88
 Gaussian Elimination
 Subroutine 334, 335
 Generalized Mass 992, 995
 GENFLANGE 239, 244
 GENROLL 368
 Gross Structural Discontinuity 61,
 649
 Handling of Heat Exchangers 1009
 HEADSKIRT 77
 Head 625
 ASME Flanged and Dished
 Heads 625
 Crown Radius 625
 Inside Depth of Dish 625
 Knuckle Radius 625
 Straight Flange 625
 Torispherical 625
 Heat Capacity Rate Ratio 611
 Heat Exchange Institute 14, 45
 Heat Exchangers 1, 14, 415, 1012
 Degree of Dismemberment 1007
 Fixed 415
 Floating 415
 Handling 1007, 1013
 In-Service Inspection 1008
 Internals 14
 Isolation 1012
 Maintenance 1007

- Parts and Nomenclature 14
- Provision for Isolation 1008
- Tube 1013
- Working Environment 1007
- Heliflow Exchanger 663
- Hinged Davit 593
- Hooke's Law 322, 418, 649
- Hoop Stress 641
- HORSUP 927, 937, 940
- Hub Modulus 113
- Hydraulic Diameter 810
- Hydraulic Expansion 307, 310
- Hydrodynamic Mass 770, 783, 784, 827
- Hydrostatic Test 5
- Impact Welding 307, 311
- Impingement Plate
 - Circular 31
 - Square 31
- Incremental Procedure 211
- Inertia Loads 925
- Influence Coefficients 948
- In-Service Inspection 1011
- Instability Constant 747
- Inter-pass Leakage 610
- Jet Switching 741, 743, 747
- Joint Temperature 330
- Joints for High Pressure
 - Closures 289
- Kelvin Functions 142
- Kettle Reboiler 12
- Kirchoff's Plate Theory 420
- Kopp and Sayre Method 694
- Lamé's Equation 635
- Lamé's Formula 69
- Land 92, 93
- Lantern Ring 10, 12
- Lap Joint Flange 83
- LAPCOV 595, 612, 615
- Laplacian Operator 1038
- Layout Angle 23
- Layout Pitch 23
- Leakage Area 176, 181, 182
- Leakage Rate 88, 89
- Lift Force 740, 829
- Lift Points 1014
- Ligament Efficiency 166, 389, 390, 421, 422
- LIGTEM 338
- Linear Supports 912
 - Allowable Average Stress in Compression 912
 - Allowable Average Tension 912
 - Allowable Shear 912
 - Stress Limits 912
- Loadings 866
 - Dead 867
 - Handling 867
 - Seismic 867
 - Thermal Expansion 867
 - Wind 867
- Local Membrane 948
- Log Mean Temperature Difference (LMTD) 162, 432
- Logarithmic Decrement 788, 791, 825, 828
- Longitudinal Baffle 25
- Longitudinal Pitch 23
- Longitudinal Stress 641
- Lubrite 864
- Lugs 864, 879
- Mass Ratio 811
- Maximum Allowable Working Pressure 164
- Maximum Concrete Pressure 936
- Membrane Displacement 649
- Membrane Stress 701, 870
- Membrane Theory 629
- Meridian Curve 626
- Meridional Stress Concentration Factor 674
- MICROFIXFLOAT 480, 514
- Mode Shape 747, 825, 827
 - Orthogonality Condition 992
- Modified Bessel Functions 784
- Mohr's Diagram 68
- Moment 880
 - Circumferential 880
 - Longitudinal 880
- Multiple Beam Strip Design
 - Method 573
- Multiple Shell Pass 18, 19
- Multiple Span Tube 761
- Multiple Tube Pass 25
- MULTSPAN 762, 841, 843
- Nut 95
- Natural Frequency 827, 869

- Natural Frequency Coefficient 763
 Neoprene Gasket Stress Strain Relation 220
 Neutral Axis 933
 Newton-Raphson Technique 977
 Nomenclature, Heat Exchanger 14
 Non-Linear Gasket Behavior 219
 Non-Pressure Part Welds 1019
 Normal Modes 761
 No-Tubes-In-Window Concept 819
 Nozzle Loads 947, 950
 Axial Force 950
 Axial Twist 950
 Circumferential Moment 950
 Circumferential Shear 950
 Longitudinal Moment 950
 Longitudinal Shear 950
 Nozzle-Shell Junction 870
 Nozzles 11, 26
 Number of Transfer Units (NTU) 610

 O-Ring 94, 95
 Orthogonality Condition 992
 Orthotropic 1022
 Elastic Constants 1023
 Material 1023
 Outside Packed Floating Head 10
 Overall Heat Transfer Coefficient 433
 Overlay, Weld 867

 Packed Floating Head with Lantern Ring 10, 12
 Packed Joint 1008
 Parallel Curve 627
 Parallel Flow Induced Vibration 810
 Participation Factor 993, 1001
 Pass Partition Grooves 598
 Pass Partition Plates 19, 25
 Shellside 18
 Tubeside 19, 25
 Peak Stresses 329, 337
 Percentage of Critical Damping 788
 Perforated Radius 389
 Perforated Region 390
 Period of Damped Vibrations 790
 Periodic Wake Shedding 777
 Plate and Shell Theory 1021
 Poisson's Ratio 418
 "Pop"-a-plug 343

 POSTSHEET xx
 PRESHEET xx
 Potential Energy 114, 115
 Power Spectral Density 775
 Pressure Actuated Closure 295
 Pressure Actuated Joints 81, 289
 Pressure Areas 643
 Pressure Part Welds 1019
 Pre-Tensioning 95
 Mechanical 96
 Thermal 95
 Primary Membrane Stress 948
 Principal Planes 57
 Proportionality Parameter, Plasticity 318
 Pseudo-Velocity 980

 Radius of Curvature 627, 636
 Circumferential (Parallels) 627, 637
 Meridional 627, 636
 Radius of Gyration 912
 Rectangular Tubesheets 565
 Reference Mass Per Unit Length 824
 Removable Spool Pieces 1009
 Resonance 739
 Response Spectrum 979
 Retainer Ring 84
 Reynolds Number 178, 738
 Rigid Base Plate 936
 Ring Factors, Flange 123
 Ring Flange 82, 105
 Ring Gasketed Joint 235
 Ring Gasketed Joint with Compression Stop 236
 Ring Type Support 889
 Foundation Response 889
 RINGSUP 872, 892
 Roller Expansion 307, 308
 Rotational Springs 903

 Saddle Mounted Equipment 925
 Sand Pushing Method 342
 Schleicher Functions 142
 Seal Strips 799
 Secondary Stresses 337, 694
 Seismic Acceleration 437
 Seismic Motion 947
 Semi-Saddle Angle 882
 Service Bolt Stress 180
 Shape Functions 534

- Shear 872
- Shear Band Design for High Pressure Closure 294
- Shear Deformation 523
- Shear Pin Design for High Pressure Closure 292
- Shear Stud Closure 292
- Shell 2, 4, 635
 - Conical 635
 - Cylindrical 2
 - Ellipsoidal 635
- Shell Theory 124
- Shells 634
 - Cylindrical 634
 - Ellipsoidal 634
 - Toroidal 638
- Single Beam Strip Method 575
- Single Span Tube 757
 - Governing Equation 757
 - Mode Shapes 759
- Singly-Connected Curve 633
- Skirt, Support 866
- Slotted Holes 1016
- Slotted Support 927, 928
- Spacer 37
- Spherical Shell 653
- Spiral Wound Gasket 88
- Split Flanges 11
- Split Flow Shells 39
- Square Root-of-Sum-of-the-Squares (SRSS) 994
- Squirm 692, 709
- SRSS Method 1002
- ST4 796
- Stacked Heat Exchangers 1009
- Staggered Tube Layout 527
- Stagnation Pressure 738
- Stick Model for Seismic Analysis 930
- Stiffness Matrix 217
- Strain Energy 115, 212, 667
- Stream Analysis Method 798
- Stream Symmetric Design 1016
- Stress 57, 609, 703, 869, 878
 - Bending 869, 878
 - Circumferential 878
 - Circumferential Bending 72, 703
 - Hoop 703
 - Local Membrane 65
 - Longitudinal 878
 - Longitudinal Bending 72, 703
 - Longitudinal Membrane 69
 - Membrane 703, 869, 878
 - Peak 67
 - Primary Bending 64
 - Primary Membrane 63
 - Principal 57
 - Secondary 66
 - Stress Efficiency 402
 - Stress Intensity 68, 714
 - Stress Multiplier 170
 - Strouhal Number 738, 777
 - Support 861, 864, 949
 - Annular Ring 861, 949
 - Dimensions 863
 - Horizontal Saddle 864
 - Lug 861, 865
 - Ring Type 865
 - Skirt Type 861, 867, 949
 - Skirt Type With Chairs 868
 - Slotted 863
 - Trapeze 861
 - Weld Size 863
 - Support Reaction 928, 949
 - Maximization 949
 - Tapered Hub Flange 82
 - TBROLL, Computer Program 350
 - TEMA 14
 - TEMA Standards 415
 - Temperature Effectiveness 610
 - Tensile Stress Area 939, 958
 - Test Ring 1019
 - Theorem of Minimum Potential Energy 212
 - Thermal Capacitance 342
 - Thermal Performance 610
 - Thermal Skin Effect 329
 - Thermal Transients 36
 - Thermosiphon Reboiler 947
 - Threaded Joint 289
 - Three Element Bolted Joints 161
 - Three Element Joint 164, 237
 - Three Lug Support System 886
 - Threshold Instability Constant 769, 770
 - Tie Rods 34, 36
 - Time History Analysis 979
 - Time Invariant Loads 925
 - Time Variant Loads 925
 - Toroidal Shell 638
 - Transverse Pitch 23

- Trapeze 866
 Tresca Yield Condition 317, 350
 Triangular Pattern 390
 TRIEL 164, 188, 190, 204, 595, 614
 Tripanned Tubesheet Fillet Weld 314
 Tripartite Logarithmic Plot 980
 Tube Fouling 1018
 Tube Plugging 342
 Tube Pull-Out Load 325
 Tube Removal 342
 Tube Supports 19
 Tubesheet Sandwiched Between Two Flanges 161
 Tubing 1013
 Austenitic 1013
 Copper-Nickel 1013
 Ferritic 1013
 Finned 1013
 Turbulent Buffeting 748, 773
 Two Side Gasketed Construction 395
 Typical Ligament Region 331
- UBAX 666, 674, 681
 U-Bend Thermal Stresses 663
 UFLOW 800, 856
 Undamped Frequency 980
 Uniform Beams 760
 Mode Shapes 760
 Natural Frequency 760
 Universal Gas Constant 779
 Unsupported Area Principle 295, 296, 644, 648
- Upset Condition 914
 Usage Factor 714
 UTUBE 412
 U-Tube Heat Exchanger 5
 U-Tubesheet
 One Side Integral
 Construction 394
 Two Side Integral
 Construction 394
 UVIB 767, 851
- Velocity Response Spectrum 980
 Velocity of Sound 779
 Vents 12, 13, 1016
 VERSUP 949, 960, 962
 Vertically Mounted Equipment 947
 Virtual Mass Coefficient 784
 Volumetric Examination 1011
 von Kármán Streets 740
 von Mises Yield Criterion 329, 354
 Vortex Shedding 738, 748
- Wake Shedding 828
 Waster Anodes 1019
 Water Hammer 1017
 Wear Plate 863
 Wedge Seal Ring Closure 297, 298
 Weld Joint Efficiency 597, 647
 Welding Neck Flange 614, 1029
 Hub 1019
 Wind Load 925, 947
- Yoke Ring 294
 Young's Modulus 418